# The geology, timing of mineralisation, and genesis of the Menninnie Dam Zn–Pb–Ag deposit, Eyre Peninsula, South Australia

Michael W. Roache MSc (Hons)

Submitted in fulfilment of the requirements
for the degree of
Doctor of Philosophy

University of Tasmania
December 1996

*This thesis contains no material which has been accepted for the award of any other higher degree or graduate diploma in any tertiary institution and, to the best of the author's knowledge and belief, contains no material previously published or written by another person, except where due reference is made in the text of the thesis.*

Michael W Roache

**CONFIDENTIAL THESIS**

**Restricted access only. Embargo applies till 22nd November 1998**

This thesis shall not be made available for consultation, loan, or photocopying for a period of eighteen months starting May 22nd 1997 without the written consent of the author and in accordance with the laws of copyright.

Frontispiece: View looking south along the 10000 mE base line of the Menninnie Dam Pb - Zn - Ag prospect. The road to riches, or the road to nowhere?

## Abstract

The Menninnie Dam Pb - Zn - Ag deposit is located on the northern Eyre Peninsula of South Australia, approximately 1- 2 km south of the main mass of the Gawler Range Volcanics. The deposit has no surface expression and was located by drilling of aeromagnetic anomalies in deeply weathered, flat lying terrain. Mineralisation occurs over ≈ 3 km strike and is hosted by upper amphibolite facies (≈ 700°C and 7 kbars) marbles and diopside-rich calc-silicate lithologies, correlated with the Katunga Dolomite and lower units of the Cook Gap Schist of the Middleback Subgroup, a subdivision of the Hutchison Group (1964 - 1845 Ma.). The Katunga Dolomite is bound to the west by a shear zone (> 50 m wide) formed during the latter stages of the Kimban Orogeny (1740 - 1710 Ma.). Syn-deformation granite dykes intruded into the shear zone, and, to a lesser extent, into the Katunga Dolomite and Cook Gap Schist. Late tectonic pegmatite dykes intruded into the Katunga Dolomite and lower units of the Cook Gap Schist, where they produced zones of K-feldspar - calc-silicate metasomatism.

Previous researchers have incorrectly suggested that the Menninnie Dam Pb - Zn - Ag deposit is a Broken Hill-type. However, Pb - Zn - Ag mineralisation post-dates metamorphism, deformation and metasomatism and has replaced the host marble, and to a lesser extent, diopside-rich calc-silicate lithologies. On the basis of lithologic relationships, most mineralisation formed within 100 - 600m of the palaeosurface, and resulted in a central zone of stockwork and matrix to marble and calc-silicate breccias, flanked by veins. Sulphide and gangue minerals consist of a simple assemblage of pyrite, quartz, sphalerite, galena and Ca-Mn-Mg-Fe carbonate, with accessory chalcopyrite, chlorite, adularia, sericite, fluorite, rhodonite, talc, phlogopite, dolomite, hematite and matildite. Three paragenetic stages of mineralisation are present with an early pyrite stage, followed by a sphalerite galena, and late pyrite stages. Metal abundances have a bell-shaped distribution along the length of the deposit and the highest values are associated with the zone of stockwork and breccia mineralisation.

Post metamorphic, porphyritic rhyolite intruded the Hutchison Group, and interacted with (heated?) groundwater resulting in explosive fragmentation of the host rocks and formation of polymictic breccia pipes. Some of these erupted onto the palaeosurface and formed layered polymictic breccias. Rhyolite continued to intrude through polymictic breccia pipes, and resulted in formation of peperite at the margins. Some rhyolite intrusions erupted onto the palaeosurface and formed volcanic breccias and rhyolite lavas. Polymictic breccias contain clasts of paragenetically early sulphide and gangue minerals, and have an altered matrix that includes paragenetically late sulphide minerals, indicative of syn-mineralisation emplacement. U-Pb zircon dating of the rhyolite intrusions constrains the timing of mineralisation to 1594 ± 7 Ma. which is indistinguishable from that determined for the Hiltaba Suite granitoids and co-magmatic Gawler Range Volcanics.

Modelling of regional gravity and aeromagnetic data indicates the Menninnie Dam deposit lies near the north-western margin of a ≈ 20 km diameter Hiltaba Suite granite that intruded to within 1 - 3 km of the palaeo-surface. Lead was derived from the underlying Hiltaba Suite granite and leached from Cook Gap Schist. Lead isotope ratios have a spatial distribution on a prospect scale, and the least radiogenic ratios correspond with the highest metal values and the central zone of stockwork and breccia style mineralisation, consistent with a single zone of fluid up-flow. Carbonate gangue is interpreted to have precipitated via interaction of the mineralising fluid ($\delta^{18}O$ = -2.0‰; $\delta^{13}C$ = -6.9‰) in equilibrium with $H_2CO_{3(aq)}$ (> 0.01 molal) and the host marbles ($\delta^{18}O$ = 15.5 to 21.09‰; $\delta^{13}C$ = -1.1 to 1.6‰) between 200° and 125°C. Hydrous phyllosilicates associated with mineralisation have calculated fluid values of $\delta^{18}O$ = -0.7 to -2.0‰ and $\delta D$ = -43 to -48‰, indicative of a mixed meteoric - magmatic origin for the mineralising fluids. Sulphide $\delta^{34}S$ values range from -3.0 to 8.2‰, with most between 4 to 6‰. The lack of evidence for sulphur isotope fractionation between different sulphide minerals is consistent with non-equilibrium precipitation of sulphides from a reduced fluid, low temperature kinetic effects and / or a $H_2S$ : metal ratio ≥ 1. Sulphur was sourced from either the magma, the country rocks, or a combination of both.

Primary fluid inclusions hosted by sphalerite and quartz have a range of trapping temperatures and salinities interpreted to have resulted from mixing of ≈ 140°C and ≈ 27 wt.% NaCl equivalent Na-Ca-K-Cl brine with a ≈ 180°C dilute chloride water. Thermodynamic modelling has shown that sufficient concentrations of Pb and Zn (> 1 ppm) can be transported together with reduced sulphur ($\sum S$ = 0.002 molal) in a low temperature (150°C) saline brine (≈ 6 molal) to form the Menninnie Dam deposit. The physiochemical attributes of the mineralising fluid at 150°C are estimated to have been log $fO_2$ = -46 and pH = 4.6. Dilution through mixing with heated groundwater was a possible base metal depositional mechanism but is predicted to have been less effective than the pH increase that resulted from dissolution of the host marbles.

Soon after cessation of the mineralising event, the stratigraphy was mantled by a single cooling unit > 260 m thick of lithic-rich (≈ 45% and up to 20 m across) welded ignimbrite (MD ignimbrite). The thickness, abundance and size of lithic clasts in the MD ignimbrite, and shallow intrusion of granite are consistent with an intracaldera setting. Following welding and cooling of the MD ignimbrite, the lower part of the MD ignimbrite and the Hutchison Group near the southern end of the Menninnie Dam deposit were partially altered to a texturally destructive quartz - chlorite - carbonate - calc-silicate assemblage by a hot, low salinity water (190 - 356°C and 0 - 3 wt. % NaCl equiv.). Carbon, hydrogen, and oxygen isotopes are consistent with a meteoric water that had undergone partial isotopic exchange with igneous rocks. Mineral textures, whole rock geochemistry, lead and sulphur isotope data are consistent with the Menninnie Dam Pb - Zn - Ag mineralisation being partially dissolved and reprecipitated by this event, with no addition of metals or sulphur.

## Acknowledgements

My thanks go to my partner, Margaret for her love, patience and support throughout the course of this thesis.

Research on the Menninnie Dam prospect would not have been possible without logistical and financial support by Aberfoyle Resources Ltd. and Acacia Resources Ltd. In particular I would like to thank John Anderson, Dr. Bob Beeson, Dave Borton and Chris Young who helped established this research project and who provided encouragement throughout. I would like to point out that although Dr Beeson has previously published papers concerning the similarity of the Menninnie Dam mineralisation to Broken Hill-type, he always listened to my findings with an unbiased ear and provided constructive comments. It is this ability to move forward in research rather than pursue a model that is the hallmark of a competent scientist.

Without the guidance, support, enthusiasm, and patience of my supervisors, Dr Bruce Gemmell, Dr David Cooke and Prof. Ross Large, completion of this thesis would probably have been significantly delayed. Dr. Bruce Gemmell and Prof. Ross Large also contributed useful advice to the organisation of early drafts, but the crown has to go to Dr David Cooke for his valiant efforts in correcting my grammar, and to whom I owe a debt of numerous red pens. In addition, I extend my gratitude to others who also laboured through early drafts of chapters and the ensuing discussions including: Dr Paul Kitto, Dr Ron Berry, Dr Garry Davidson, Dr Mike Solomon, Dr Jocelyn McPhie, Dr Michael J. Roach, Dr Khin Zaw, Dr Joe Stolz, Mark Doyle, Dr Graham Carr and Dr Peter McGoldrick.

Dr. Graham Carr (CSIRO) is thanked for his discussions regarding the lead isotope data from Menninnie Dam, and for reviewing a wild and woolly early draft of Chapter 7. Dr. Carr's assistance in organising additional lead isotope analyses is gratefully appreciated. Dr. Judy Dean (CSIRO) is thanked for her efforts in locating early lead isotope data from Menninnie Dam, and allowing some of her unpublished data to be used for this study. Dr. Anita Andrew (CSIRO) analysed the Menninnie Dam samples for hydrogen isotopes and her contribution to discussions regarding sample preparation and isotopic fractionation are appreciated. Anita Andrew is also thanked for allowing her unpublished sulphur isotope data to be used for this study.

I extend my thanks to numerous people from the Mines and Energy Department of South Australia (MESA) for their willing assistance in locating samples and reports. Particular thanks go to Dr. John Parker who freely gave his time to guide a group of us on a very enjoyable excursion examining the geology of the Eyre Peninsula. Dr Parker was

instrumental in organising MESA funding for U-Pb zircon dating of Menninnie Dam samples. Thanks to Dr. Mark Fanning (A.N.U.) for his time and efforts in determination of U-Pb zircon dates, and for the constructive discussions that followed.

Chris Drown, Dr. Steve Toteff, Mark Teakle, Brett Rava, Nicki, Bowden, Cathy Curran, Rick Elson, Banantyne (Ben) Coutts, Robert (Beags) Appleby, Roger Wilmer and Russell (Ferd) Durdin from Aberfoyle's Adelaide office are thanked for their friendship, support and interesting discussions. Chris Drown's considerable knowledge of the Menninnie Dam project, his unflagging interest and contribution to discussions were of great benefit. There were numerous instances where conception of credible solutions to complex lithological textures required a little lubrication, and although sometimes teetotal, Chris always willingly contributed to these occasions... Cheers!

I am grateful for the technical help and administrative assistance provided by numerous people including: Ralph Botteril, Peter Cornish, Lynn Davies, Marilyn Feast, Jeanette Hankin, Christine Higgins, Neila Hlaing, Dr Wieslaw Jablonski, Fred Koolhof, Gerrit Kuipers, June Pongratz, Mike Power, Phil Robinson, Kathi Stait, Simon Stevens, Richard Woolly.

Throughout the period of this thesis I have enjoyed the company and friendship of numerous staff and students at CODES and in the Scitech Library, to all of you ..... Cheers!

# Table of Contents


Frontispiece ..... i
Title Page ..... ii
Statement ..... iii
Abstract ..... iv
Acknowledgments ..... vi
Table of contents ..... viii
List of figures ..... xiii
List of tables ..... xvi
List of appendices ..... xviii

**Chapter 1: Introduction**
1.1 Introduction ..... 1.1
1.2 Location ..... 1.2
1.3 Previous work ..... 1.3
1.4 Menninnie Dam project history ..... 1.3
1.5 General statement of aims and methods ..... 1.4

**Chapter 2: Physiography and regional geology**
2.1 Introduction ..... 2.1
2.2 Physiography ..... 2.1
2.3 Regional Geology ..... 2.4
2.3.1 Stratigraphy ..... 2.5
Archaean ..... 2.5
Palaeoproterozoic ..... 2.9
Mesoproterozoic ..... 2.14
2.3.2 Mineralisation ..... 2.20
2.4 Summary ..... 2.21

**Chapter 3: Prospect geology: The Palaeoproterozoic**
3.1 Introduction ..... 3.1
3.2 Palaeoproterozoic stratigraphy ..... 3.1
3.2.1 Western suite ..... 3.5
3.2.2 The central suite ..... 3.7
3.2.3 Eastern suite ..... 3.10
3.3 Determination of the metamorphic history at Menninnie ..... 3.12
3.3.1 Methods ..... 3.12
3.3.2 Analytical results ..... 3.13
3.3.3 Thermobarometric calculations ..... 3.16
3.4 Granite dykes ..... 3.22
3.4.1 MD granite dyke description ..... 3.22
3.4.2 Granite dyke geochemistry ..... 3.24
3.5 Deformation ..... 3.28
3.5.1 Deformation of the western suite ..... 3.30
3.5.2 Deformation of the central suite ..... 3.32
3.5.3 Eastern suite ..... 3.32
3.6 Pegmatite dykes ..... 3.32
3.7 Metasomatism ..... 3.34
3.7.1 Mineralogy ..... 3.36
3.7.2 Metasomatic mineral textures ..... 3.36
3.8 Discussion ..... 3.39
3.8.1 Origin of the central suite calc-silicates ..... 3.39
3.8.2 Regional correlations and implications for the Menninnie Dam stratigraphy ..... 3.40
3.8.3 Timing of deformation and MD granite dyke emplacement ..... 3.44
3.8.4 Timing of metasomatism ..... 3.46
3.9 Summary ..... 3.47

**Table of contents cont.**

**Chapter 4: Local geology: The Mesoproterozoic**

4.1 Introduction ..... 4.1
4.2 Geological setting ..... 4.1
4.3 Prospect geology ..... 4.4
4.3.1 Rhyolite intrusions ..... 4.4
Description ..... 4.6
4.3.2 Polymictic breccia units ..... 4.7
DP breccia units ..... 4.9
Fiamme-bearing DP breccia units ..... 4.11
Alteration of DP breccias ..... 4.12
Association of DP breccias and faults ..... 4.12
Rhyolite-bearing DP breccias ..... 4.12
Interpretation of rhyolite-bearing DP breccias ..... 4.16
LP breccia units ..... 4.17
Rhyolite-bearing LP breccia ..... 4.20
4.3.3 Coherent rhyolite ..... 4.26
4.3.4 Muddy sandstone and pumice breccia units ..... 4.26
4.3.5 Geochemistry of rhyolite intrusions, peperites and coherent rhyolite ..... 4.28
4.3.6 Menninnie Dam Ignimbrite (MD ignimbrite) ..... 4.32
Description ..... 4.32
MD ignimbrite in the basal 34m of drill hole PD0032 ..... 4.40
4.4 Discussion ..... 4.43
4.4.1 Rhyolite intrusions elsewhere in the Gawler Range Volcanic Province ..... 4.43
4.4.2 Interpretation of DP breccias ..... 4.44
Fluidisation ..... 4.47
4.4.3 Interpretation of LP breccias ..... 4.48
4.4.4 Interpretation of the rhyolite-bearing LP breccia ..... 4.49
4.4.5 Interpretation of fiamme-bearing DP breccias ..... 4.50
4.4.6 Interpretation of muddy sandstone and pumice breccia ..... 4.50
4.4.7 Genetic model for the formation of polymictic breccias, coherent rhyolite, muddy sandstone and pumice breccia units 4.51
4.4.8 Interpretation of the MD ignimbrite ..... 4.53
Origin of lithic clasts in the MD ignimbrite ..... 4.54
4.4.9 Genetic model for the MD ignimbrite ..... 4.57
4.4.10 Distribution of lithic clasts in the MD ignimbrite ..... 4.57
4.4.11 Timing and duration of Mesoproterozoic intrusive and volcanic events at Menninnie Dam ..... 4.57
4.4.12 Timing of metasomatism ..... 4.57
4.5 Summary ..... 4.58

**Chapter 5: Sulphide mineralisation**

5.1 Introduction and previous work ..... 5.1
5.2 Mineralisation in the northern and central zones ..... 5.2
5.2.1 Relationship between sulphides and host rocks ..... 5.4
5.2.2 Sulphide and gangue mineralogy ..... 5.5
5.2.3 Sulphide and gangue mineral textures and their paragenesis ..... 5.5
Sulphides hosted by marbles ..... 5.7
Sulphides hosted by diopsidic rocks ..... 5.17
Sulphides hosted by marbles and diopsidic rocks ..... 5.19
Mineralisation hosted by DP and LP breccias ..... 5.19
Mineralisation hosted by granite dykes, graphitic schist, eastern and western suite schists. ..... 5.21
5.3 Mineralisation in the southern zone ..... 5.21
Distribution of sulphides ..... 5.21
Late alteration overprint ..... 5.22
5.3.1 Relationship between sulphides and host rocks ..... 5.22

**Table of contents cont.**


5.3.2 Sulphide and gangue mineralogy and textures ..... 5.23
MD ignimbrite hosted mineralisation ..... 5.29
5.4 Chemical analysis of mineralised zones ..... 5.31
5.4.1 Spatial variations in mineralisation chemistry ..... 5.32
5.5 Mineral chemistry ..... 5.34
5.5.1 Method ..... 5.34
5.5.2 Results ..... 5.34
5.6 Discussion ..... 5.40
5.6.1 Sulphide textures ..... 5.40
5.6.2 Paragenetic stages ..... 5.41
5.6.3 Association of mineralisation with fractures and brittle faults ..... 5.42
5.6.4 Inclusions of chalcopyrite in sphalerite ..... 5.43
5.6.5 Spatial distribution of metals ..... 5.45
5.6.6 Mineral chemistry ..... 5.45
5.6.7 Relative timing of DP breccias and rhyolite dykes ..... 5.46
5.6.8 Relative timing of mineralisation, the MD ignimbrite and the late alteration overprint ..... 5.46
5.7 Summary ..... 5.47

**Chapter 6: Gravity and magnetic modelling**
6.1 Introduction ..... 6.1
6.2 Methods ..... 6.2
6.3 Gravity and magnetic data ..... 6.2
6.4 Transect lines ..... 6.2
6.5 Nature and distribution of lithologies ..... 6.3
6.6 Rock Densities ..... 6.7
6.7 magnetics susceptibility ..... 6.9
6.8 Results of geophysical modelling ..... 6.11
6.9 Discussion ..... 6.16
6.10 Conclusions ..... 6.19

**Chapter 7: Lead isotopes**
7.1 Introduction ..... 7.1
7.2 Lead isotope data ..... 7.1
7.3 Analytical methods ..... 7.2
7.4 Results ..... 7.2
7.4.1 Lead isotope ratio plots ..... 7.3
7.4.2 Feldspar analyses ..... 7.4
7.4.3 Galena analyses ..... 7.7
7.4.4 Whole rock analyses ..... 7.10
7.4.5 Isotopic ratios versus lead assay ..... 7.12
7.5 Discussion ..... 7.12
7.5.1 Range of Pb isotopic determinations for the Hiltaba Suite granites 7.12
7.5.2 Isotopic ratios versus lead assay ..... 7.12
7.5.3 Source of the lead ..... 7.14
7.5.4 Spatial distribution of lead isotope ratios ..... 7.19
7.5.5 Interpretation of lead isotopes from the rhyolite intrusion ..... 7.21
7.5.6 isotopic ratios of the southern zone ..... 7.23
7.5.7 Lead model age for the Menninnie Dam mineralisation ..... 7.23
7.5.8 Mixing of granite derived lead and host rock derived lead ..... 7.25
7.6 Summary ..... 7.28

**Chapter 8: Timing of mineralisation**
8.1 Introduction ..... 8.1
8.2 Interpretation of geological constraints for the timing of mineralisation .. 8.1
8.3 U -Pb zircon dating of the rhyolite intrusions ..... 8.3
8.3.1 Introduction ..... 8.3
8.3.2 Ion - microprobe procedures ..... 8.4

**Table of contents cont.**


8.3.3 Results ..... 8.5
8.4 Timing of the late alteration overprint ..... 8.9
8.5 Discussion ..... 8.10
8.6 Summary ..... 8.10

**Chapter 9: Fluid inclusions**
9.1 Introduction ..... 9.1
9.2 Method of studies ..... 9.1
9.3 Classification of fluid inclusion types ..... 9.2
9.4 Fluid inclusion petrography and microthermometric measurements ..... 9.4
9.4.1 Type P2, P3, S1, S2, and S2a fluid inclusions hosted by sphalerite 2 9.4
9.4.2 Type S1, P2 and P3 fluid inclusions hosted by quartz 1 ..... 9.9
9.4.3 Type S2 and S3 fluid inclusions in SA rhyolite intrusions ..... 9.12
9.4.4 Type P2 and P3 fluid inclusions hosted by quartz 3 ..... 9.14
9.5 Fluid inclusion salt compositions ..... 9.16
9.6 Discussion ..... 9.19
9.6.1 Fluid inclusions hosted by sphalerite 2 ..... 9.19
9.6.2 Fluid inclusion salinities ..... 9.20
9.6.3 Fluid inclusion trapping temperatures ..... 9.20
9.6.4 Trapping temperature vs salinity diagrams and fluid mixing..... 9.27
9.6.5 Mineral inclusions in primary and secondary fluid inclusions - .. daughter minerals or accidentals? ..... 9.29
9.6.6 Comparison of fluid inclusions in the rhyolite intrusion, quartz 1 and sphalerite 2..... 9.30
9.6.7 Composition of the mineralising fluid..... 9.32
9.6.8 Composition of the late alteration overprint fluid ..... 9.33
9.7 Summary ..... 9.36

**Chapter 10: Stable isotopes**
10.1 Introduction ..... 10.1
10.2 Oxygen and carbon isotopes ..... 10.1
10.2.1 Sample selection ..... 10.2
10.2.2 Analytical methods ..... 10.3
10.2.3 Results ..... 10.4
10.2.4 Discussion ..... 10.4
10.2.4.1 Host rock carbonates ..... 10.6
10.2.4.2 Hydrothermal carbonates ..... 10.6
Interpretation of isotopic values from intra-mineralisation carbonates ..... 10.9
Interpretation of margin carbonates ..... 10.17
Isotopic halos to mineralisation ..... 10.18
Late alteration overprint carbonate ..... 10.20
10.2.5 Summary ..... 10.22
10.3 Silicate oxygen and hydrogen - deuterium isotopes ..... 10.23
10.3.1 Samples ..... 10.23
10.3.2 Methods ..... 10.23
10.3.4 Discussion ..... 10.26
10.3.4.1 Calculation of fluid isotopic values..... 10.26
10.3.4.2 Source of the mineralising fluids..... 10.29
10.3.4.3 Source of the late alteration overprint fluids ..... 10.32
10.3.5 Summary ..... 10.32
10.4 Sulphur isotopes ..... 10.33
10.4.1 Previous work ..... 10.33
10.4.2 Method and samples ..... 10.34
10.4.3 Results ..... 10.35
10.4.4 Discussion ..... 10.39
10.4.4.1 Sulphur isotopes from northern and central zones mineralisation..... 10.39

**Table of contents cont.**

10.4.4.2 Sulphur isotopes from southern zone mineralisation ..... 10.44
10.4.4.3 Source of sulphur ..... 10.45
10.4.5 Summary ..... 10.49
10.5 Conclusions ..... 10.49

**Chapter 11: Thermodynamic modelling**
11.1 Introduction ..... 11.1
11.2 Transport of Pb, Zn, Fe, Cu and Ag in hydrothermal fluids ..... 11.1
11.3 Mineral deposition ..... 11.3
11.4 Hydrothermal modelling ..... 11.4
11.5 Results and discussion ..... 11.6
11.5.1 Composition of the mineralising fluid ..... 11.6
11.5.2 Effects of variations in $\Sigma S$ content ..... 11.8
11.5.3 Deposition of sulphides at Menninnie Dam ..... 11.10
11.5.4 Temporal zonation of Zn and Pb ..... 11.12
11.5.5 Review of the mineral paragenesis and fluid evolution at Menninnie Dam ..... 11.14
11.6 Conclusions ..... 11.15

**Chapter 12: Conclusions: A genetic model for the Menninnie Dam deposit and implications for exploration**
12.1 Introduction ..... 12.1
12.2 Genesis of the Menninnie Dam deposit ..... 12.1
12.3 Comparison to other carbonate hosted Pb - Zn - Ag deposits ..... 12.7
12.4 Implications for exploration of Pb - Zn - Ag deposits on the Eyre Peninsula of South Australia ..... 12.8

**References**
**Appendices**

# List of Figures


| Figure | | |
|---|---|---|
| 1.1 | Location of the Menninnie Dam prospect | 1.2 |
| 2.1 | Geologic time scale | 2.2 |
| 2.2 | Tectonic provinces of South Australia | |
| 2.3 | Stratigraphy of the Cleve sub domain and Gawler Range Volcanic Province | 2.6 |
| 2.4 | Simplified Geology of the eastern Eyre Peninsula | 2.7 |
| 2.5 | Distribution of the Gawler Range Volcanics | 2.15 |
| 2.6 | Subdivision of the Gawler Range Volcanics | 2.16 |
| 3.1 | Geological plan of the Menninnie Dam prospect | 3.2 |
| 3.2 | Cross section through the Menninnie Dam prospect | 3.3 |
| 3.3 | Aeromagnetic image of the Wilcherry hill exploration lease | 3.4 |
| 3.4 | Lithologies of the western and central suites | 3.6 |
| 3.5 | Lithologies of the central and eastern suites | 3.11 |
| 3.6 | Element zonation in garnet | 3.15 |
| 3.7 | Mineral inclusions in garnet | 3.17 |
| 3.8 | Metamorphic conditions for the Palaeoproterozoic at Menninnie Dam | 3.19 |
| 3.9 | Metamorphic conditions for the Eyre Peninsula | 3.21 |
| 3.10 | Distribution of Lincoln Complex granitoids | 3.23 |
| 3.11 | Plutonic igneous rock classification scheme | 3.26 |
| 3.12 | Variation diagrams for granites and the granite dykes | 3.27 |
| 3.13 | Fault rock classification scheme | 3.29 |
| 3.14 | Deformation textures of the Western suite | 3.31 |
| 3.15 | Deformation textures of the central suite | 3.33 |
| 3.16 | Pegmatite dyke and metasomatic textures | 3.35 |
| 3.17 | Metasomatic textures | 3.37 |
| 3.18 | Alteration halo surrounding a pegmatite dyke | 3.38 |
| 3.19 | Regional correlation of lithologies at Menninnie Dam | 3.41 |
| 3.20 | Fault repetition of the eastern suite | 3.43 |
| 4.1 | Simplified stratigraphy of the southern Gawler Range Volcanics | 4.2 |
| 4.2 | Simplified geologic map of the southern Gawler Range Volcanics | 4.3 |
| 4.3 | Rhyolite intrusion textures | 4.5 |
| 4.4 | DP breccia textures | 4.8 |
| 4.5 | Width and occurrence of DP breccias | 4.10 |
| 4.6 | DP breccia host rock contacts | 4.13 |
| 4.7 | Rhyolite-bearing DP breccias | 4.15 |
| 4.8 | Cross section of the Menninnie Dam | 4.18 |
| 4.9 | LP breccia textures | 4.19 |
| 4.10 | Graphic logs of LP breccia units | 4.21 |
| 4.11 | Rhyolite-bearing LP breccia textures (Lower) | 4.24 |
| 4.12 | Rhyolite-bearing LP breccia and coherent rhyolite-textures | 4.25 |
| 4.13 | Muddy sandstone and pumice breccia textures | 4.27 |
| 4.14 | Volcanic rock classification | 4.30 |
| 4.15 | Gawler Range Volcanics, Hiltaba Suite and rhyolite geochemical variation diagrams | 4.31 |
| 4.16 | Basal contact of the MD ignimbrite, and rind on a large lithic clast | 4.33 |
| 4.17 | Basal surface of the MD ignimbrite | 4.34 |
| 4.18 | Summary log and textures of MD ignimbrite in drill hole PD0021 | 4.35-36 |
| 4.19 | Distribution of lithic clasts in the MD ignimbrite | 4.38 |
| 4.20 | Summary log and textures of MD ignimbrite in drill hole PD0032 | 4.41-42 |
| 4.21 | Genetic model for Mesoproterozoic units at Menninnie Dam | 4.52 |
| 5.1 | Vein, stockwork and breccia mineralisation | 5.3 |
| 5.2 | Paragenesis of sulphide and gangue minerals in the northern and central zones | 5.6 |

**List of Figures cont.**


| | | |
|---|---|---|
| 5.3 | Textures of Dolomite and pyrite 1 hosted by marble | 5.8 |
| 5.4 | Adularia and sericite textures - marble host | 5.10 |
| 5.5 | Sphalerite 1, 2, 3 and chalcopyrite 1, 2, and 3 textures - marble host | 5.11 |
| 5.6 | Ca-Mn-Mg-Fe carbonate 1, and quartz 1 textures - marble host | 5.14 |
| 5.7 | Galena 1 textures - marble host | 5.14 |
| 5.8 | Sericite 2, chlorite 2 and rhodonite textures - marble host | 5.14 |
| 5.9 | Pyrite 2 textures - marble host | 5.16 |
| 5.10 | Fluorite textures - marble host | 5.16 |
| 5.11 | Sulphide and gangue minerals that have replaced diopside | 5.18 |
| 5.12 | Sulphides in DP breccias, granite dykes and mylonites | 5.20 |
| 5.13 | Alteration of a granite dyke | 5.20 |
| 5.14 | Mineralisation in the southern zone | 5.20 |
| 5.15 | Paragenesis of sulphide and gangue minerals in the southern zone | 5.24 |
| 5.16 | Sphalerite textures, southern zone | 5.25 |
| 5.17 | Galena 1 textures, southern zone | 5.27 |
| 5.18 | Chlorite 3 and Ca-Mn-Mg-Fe carbonate 3 textures | 5.27 |
| 5.19 | Sphalerite 4, chalcopyrite 4, pyrite 3 veinlet | 5.27 |
| 5.20 | Replacement of galena 1 by sphalerite 4 | 5.27 |
| 5.21 | Tremolite and quartz 3 textures | 5.30 |
| 5.22 | Epidote, garnet and rhodochrosite textures | 5.30 |
| 5.23 | Haematite 2 textures | 5.30 |
| 5.24 | Mineralisation in the MD ignimbrite | 5.30 |
| 5.25 | Spatial variations in mineralisation chemistry | 5.33 |
| 5.26 | Copper to zinc ratios | 5.35 |
| 5.27 | Metal variation plots | 5.35 |
| 5.28 | Ca-Mn-Mg-Fe carbonate 2 composition diagrams | 5.38 |
| 5.29 | Tungsten versus zinc variation diagram | 5.39 |
| 6.1 | Aeromagnetic image of the region surrounding Menninnie Dam | 6.4 |
| 6.2 | Geology of the region surrounding Menninnie Dam | 6.5 |
| 6.3 | Transect line A-A' | 6.12 |
| 6.4 | Transect line B-B' | 6.13 |
| 6.5 | Transect line C-C' | 6.14 |
| 6.6 | Transect line D-D' | 6.15 |
| 7.1 | Lead isotope plots of all Menninnie Dam data | 7.5 |
| 7.2 | The target lead isotope population | 7.6 |
| 7.3 | Lead isotope plots of data from feldspar | 7.8 |
| 7.4 | Lead isotope data for galena samples | 7.9 |
| 7.5 | Lead isotope data for whole rock samples | 7.11 |
| 7.6 | Lead assay versus lead isotope ratios | 7.13 |
| 7.7 | Menninnie Dam data and the Plumbotectonics model | 7.16 |
| 7.8 | Host rock source for lead | 7.18 |
| 7.9 | Spatial variation of lead isotope ratios | 7.20 |
| 7.10 | Hiltaba Suite source for the rhyolite intrusion | 7.22 |
| 7.11 | Lead model age for Menninnie Dam mineralisation | 7.26 |
| 8.1 | U-Pb zircon age for the weakly altered rhyolite intrusion | 8.6 |
| 8.2 | U-Pb zircon age for the strongly altered rhyolite intrusion | 8.7 |
| 8.3 | All U-Pb zircon age for the weakly and strongly altered rhyolite intrusions | 8.8 |
| 9.1 | Type P1, P2, P3 fluid inclusions | 9.3 |
| 9.2 | Type S2, S3, P2 and P3 fluid inclusions, and hematite inclusions in sphalerite 2 | 9.5 |
| 9.3 | Type P2 and P3 fluid inclusions hosted by sphalerite 2 | 9.8 |
| 9.4 | Type P2 and P3 fluid inclusions hosted by Quartz 1 | 9.11 |
| 9.5 | Type S2 and S3 fluid inclusions hosted by quartz phenocrysts | 9.13 |
| 9.6 | Type P2 and P3 fluid inclusions hosted by quartz 3 | 9.15 |

**List of Figures cont.**


| | | |
|---|---|---|
| 9.7 | X-ray map of fluid inclusion decrepitate | 9.18 |
| 9.8 | Fluid inclusion salinity histograms | 9.21 |
| 9.10 | Spatial variations in fluid inclusion salinities and trapping temperatures | 9.24 |
| 9.11 | Depth variations in fluid inclusion salinities and trapping temperatures | 9.25 |
| 9.12 | Trapping temperature versus salinity diagrams | 9.28 |
| 9.13 | Fluid inclusion area versus mineral inclusion area | 9.31 |
| 9.14 | Fluid inclusion decrepitate compositions | 9.31 |
| 9.15 | Hydrohalite melting versus ice melting temperatures | 9.34 |
| 9.16 | Fluid inclusion trapping temperatures in drill hole PD0032 | 9.35 |
| 9.17 | Trapping temperature versus salinity for all fluid inclusions from Menninnie Dam | 9.37 |
| 10.1 | Location of carbonates for isotopic analysis | 10.3 |
| 10.2 | Isotopic composition of Menninnie Dam carbonates | 10.5 |
| 10.3 | Water - rock interaction in marbles | 10.12 |
| 10.4 | Water - rock interaction in metasomatic marbles | 10.13 |
| 10.5 | Fluid mixing | 10.16 |
| 10.6 | Water - rock interaction for an $HCO_3^-$ predominant fluid | 10.19 |
| 10.7 | Water - rock interaction for LAO carbonates | 10.21 |
| 10.8 | Source of the mineralising and LAO fluids | 10.31 |
| 10.9 | Laser and conventional sulphur isotope data | 10.36 |
| 10.10 | Sulphur isotope composition of sulphide minerals | 10.37 |
| 10.11 | Sulphur isotope composition of the country rock | 10.38 |
| 10.12 | Spatial variation of sulphur isotopes | 10.40 |
| 10.13 | Depth variation of sulphur isotopes | 10.41 |
| 11.1 | Log $fO_2$ -pH diagram | 11.7 |
| 11.2 | Pb and Zn solubility in mixed fluids | 11.9 |
| 11.3 | Pb and Zn solubility in mixed fluids | 11.11 |
| 12.1 | Genetic model for the Menninnie Dam mineralisation | 12.3 |

# List of Tables


| Table | | |
|---|---|---|
| 2.1 | Syn tectonic granitoids of the Lincoln complex | 2.13 |
| 3.1 | Subdivision of the Menninnie Dam stratigraphy | 3.5 |
| 3.2 | Eastern suite schist bulk rock composition | 3.13 |
| 3.3 | Range of garnet compositions | 3.14 |
| 3.4 | Biotite compositions | 3.14 |
| 3.5 | Plagioclase and K-feldspar compositions | 3.14 |
| 3.6 | P-T for peak and final metamorphic conditions at Menninnie Dam | 3.20 |
| 3.7 | Granite and granite dyke compositions | 3.25 |
| 4.1 | Rhyolite intrusion occurrences | 4.4 |
| 4.2 | DP breccia occurrences | 4.9 |
| 4.3 | Rhyolite-bearing DP breccia occurrences | 4.12 |
| 4.4 | LP breccia occurrences | 4.17 |
| 4.5 | Rhyolite-bearing LP breccia occurrences | 4.20 |
| 4.6 | Characteristics of Rhyolite-bearing LP breccias | 4.23 |
| 4.7 | Muddy sandstone and pumice breccia occurrences | 4.26 |
| 4.8 | Rhyolite samples used for geochemical analyses | 4.29 |
| 4.9 | MD ignimbrite occurrences | 4.32 |
| 4.10 | Lithic rich zones in the MD ignimbrite | 4.39 |
| 4.11 | Lithology of clasts >10 cm across in the MD ignimbrite | 4.39 |
| 4.12 | Characteristics of hydrothermal breccias | 4.45 |
| 4.13 | Coarse lithic breccias in pyroclastic flows | 4.54 |
| 5.1 | Adularia composition | 5.9 |
| 5.2 | Composition of sulphide mineralisation in the northern and central zones | 5.32 |
| 5.3 | Composition of sulphide mineralisation in the southern zone | 5.32 |
| 5.4 | Trace element compositions of galena 1 and 2 | 5.37 |
| 5.5 | Minor and trace element compositions of sphalerite 2 | 5.37 |
| 6.1 | Transect lines for geophysical modelling | 6.3 |
| 6.2 | Density of Hutchison Group units | 6.8 |
| 6.3 | Density values used for geophysical modelling | 6.9 |
| 6.4 | Magnetic susceptibility values used for geophysical modelling | 6.10 |
| 7.1 | Range of Pb isotope ratios for feldspar | 7.7 |
| 7.2 | Range of Pb isotope ratios for galena | 7.7 |
| 7.3 | Range of Pb isotope ratios for whole rock samples | 7.10 |
| 7.4 | Pb isotope composition of the eastern suite schist | 7.17 |
| 7.5 | Lead model ages for 3 granites of the Hiltiba Suite | 7.24 |
| 9.1 | Microthermometric measurements of fluid inclusions hosted by sphalerite 2 | 9.7 |
| 9.2 | Microthermometric measurements of fluid inclusions hosted by quartz 1 | 9.10 |
| 9.3 | Microthermometric measurements of fluid inclusions hosted by quartz phenocrysts | 9.14 |
| 9.4 | Microthermometric measurements of fluid inclusions hosted by quartz 3 | 9.16 |
| 9.5 | Composition of fluid inclusion decrepitates | 9.17 |
| 9.6 | Na,K,Ca,Ma ratios of fluid inclusions | 9.32 |
| 9.7 | Eutectic temperatures for various water-salt systems | 9.32 |
| 10.1 | Carbonate samples used for isotope analyses | 10.2 |
| 10.2 | Range of carbonate isotopic compositions for Menninnie Dam | 10.4 |
| 10.3 | Isotopic fractionation equations | 10.7 |
| 10.4 | Carbon and oxygen isotope fluid compositions | 10.9 |

**List of tables cont.**


| | | |
|---|---|---|
| 10.5 | Samples used for hydrogen and oxygen isotope analyses | 10.24 |
| 10.6 | Results of hydrogen and oxygen isotope analyses | 10.26 |
| 10.7 | Hydrogen and oxygen isotope fluid compositions | 10.28 |
| 10.8 | Sulphur isotope compositions of sulphide minerals | 10.39 |
| 11.1 | Total sulphur content of geothermal fluids | 11.5 |

# List of Appendices

Appendix
3.1 Summary drill logs and cross sections

3.2 XRF procedures and machine settings
3.3 Mineral compositions used for thermobarometric calculations
3.4 Lincoln Complex, Hiltaba Suite, St. Peters Suite, MD granite dykes, and Menninnie Dam rhyolite compositions
3.5 XRD equipment, techniques, and results of analyses

4.1 Lithic clasts in the MD ignimbrite

5.1 Adularia compositions
5.2 Geochemical compositions of mineralised zones
5.3 Electron microprobe analyses of trace elements in galena
5.4 Electron microprobe analyses of sphalerite
5.5 Electron microprobe analyses of Ca-Mn-Mg-Fe carbonates

6.1 Field acquisition parameters used for aeromagnetic surveys
6.2 Bouguer gravity and magnetic intensity data for transects A - A' to D - D'
6.3 Rock density measurements

7.1 Summary of the methods used for Pb isotope determinations
7.2 Pb isotope determinations

8.1 Results of U-Pb zircon analyses

9.1 Fluid inclusion microthermometric data

10.1 Oxygen and carbon isotope analyses of carbonate minerals
10.2 XRD diffractograms of silicate minerals used for hydrogen and oxygen isotope analyses
10.3 Results of sulphur isotope analyses and standards

11.1 Thermodynamic data used to construct models

# Chapter one
# Introduction

## 1.1 Introduction

Australia's major lead-zinc deposits can be subdivided into four groups;

- Mississippi Valley type. Typically 2-10 million tonnes (eg. Cadjebut, W.A; Murphy, 1990).
- Volcanic-hosted massive sulphides. Typically 5-15 million tonnes (eg. Hellyer, Tasmania; Large, 1992).
- Sediment hosted stratiform deposits of Middle Proterozoic age. Typically up to 200 million tonnes. (eg. HYC, McArthur River, N.T; Logan et al., 1990).
- Sediment hosted stratiform deposits of Lower Proterozoic age. (eg. Broken Hill; 280 million tonnes; Parr and Plimer, 1993).

Australian Lower to Middle Proterozoic, sediment hosted, metamorphosed, Broken Hill-type (Beeson, 1990a) deposits have accounted for a considerable proportion of the worlds past production of lead, zinc and silver, however, as reserves of this deposit type are depleted, renewed emphasis is being placed on additional discoveries. The genesis and timing of mineralisation in relation to the host rocks has been debated since the discovery of the Broken Hill deposit and is still poorly understood (Walters, 1996). Research and documentation of Broken Hill-type deposits, particularly in the area of genesis and timing of mineralisation, will greatly improve our understanding of the geological environment in which these deposits were formed and contribute significantly to the success of exploration programs.

The Menninnie Dam prospect is a sub-economic Pb - Zn - Ag deposit hosted by Lower Proterozoic rocks of the Eyre Peninsula, South Australia (Fig. 1.1). The deposit was interpreted to have a number of similarities to Broken Hill-type mineralisation including;

- Lower Proterozoic carbonate and calc-silicate host rock lithologies (Higgins et al., 1990)
- Stratabound, and possibly stratiform, mineralisation (Higgins et al., 1990)
- High metamorphic grade (Higgins et al., 1990)
- Associated carbonate-facies banded iron formations (Higgins et al., 1990)
- Broad geochemical similarities (Beeson, 1990b)

Early in the project's history, Billiton Australia Ltd, and joint venture partner, Aberfoyle Resources Ltd, recognised the need to determine the paragenesis of the host rocks and the mineralisation, and undertook intensive in-house research. However, the genetic relationship between the mineralisation and host rocks remained unresolved.

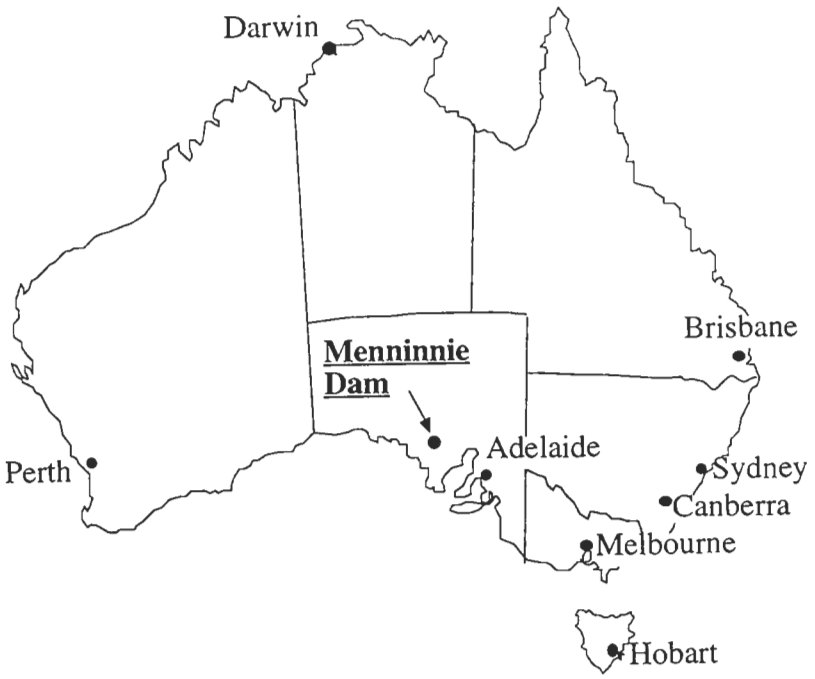


Fig. 1.1 location of the Menninnie Dam prospect

From a company point of view, the selection of specific mineral belts for the application of advanced exploration techniques requires confidence that economic deposits may exist in that belt. While most exploration investment is directed towards mineral belts known to contain large viable deposits with a recognised style of mineralisation, the mineral potential of Lower Proterozoic rocks (≈ 20,000 $km^2$) of the Eyre Peninsula, South Australia is reliant on the significance of the only known large Pb - Zn - Ag occurrence at Menninnie Dam. The genetic model arrived at for the Menninnie Dam deposit could initiate interest in a major 'new' mineral belt close to existing rail, smelting and shipping facilities at Port Pirie.

To ensure continued investment in this substantial portion of South Australia, the genetic style of the Menninnie Dam mineralisation requires formal research on the geologic setting, mineralogy, paragenesis, geochemical and isotopic signatures, nature of the mineralising fluids, deposit halos, and effect of metamorphism, in order to format genetic concepts that will contribute to useful exploration models. Positive results will enhance the confidence of present and future explorers in the area.

## 1.2 Location

The Menninnie Dam prospect is one of a number of base metal prospects on the Wilcherry Hill exploration lease, located 50 km north of the small township of Kimba and 130 km west-south-west of Port Augusta on the northern Eyre Peninsula of South Australia (Fig. 1.1). The geographic co-ordinates of Menninnie Dam are; latitude 32°38'S and longitude 136°26'E. The Australian map grid co-ordinates are; 632850E, 6386986N. The local

geology is covered by the Yardea (SI 53-4) 1:250,000 and the Buckleboo (6132) 1:100,000 scale geological map sheets.

## 1.3 Previous work

The Menninnie Dam prospect has been the subject of ongoing exploration since its discovery in 1981. The history of exploration is detailed in numerous confidential reports held by the Mines and Energy Department of South Australia.

The first public domain information on the Menninnie Dam project was published by Higgins and Hellsten (1986). They briefly described the local geology as part of the Hutchison Group lithologies and subdivided the host rocks into 4 suites. Higgins et al. (1990) gave a more detailed account of the discovery, mineralisation, host rocks, and recognised a fifth rock suite. An inferred resource, based on widely spaced drilling, was estimated as 1.7 million tonnes grading 5% Pb, 8% Zn and 100 grams per tonne Ag. Beeson (1990b) analysed 212 host rock samples from three prospects on the Wilcherry Hill exploration lease, including Menninnie Dam.

Beeson (1990b) used litho-geochemistry to:

- test for geochemical halos which may exist around known mineralisation.
- to compare the composition of marble and calc-silicate associated with mineralisation with that from non-mineralised parts.
- characterise the deposition environment for the three prospects.

The Menninnie Dam prospect was considered to have many similarities to the Northern Australian SEDEX deposits (Beeson, 1990b).

## 1.4 Menninnie Dam project history

Billiton Australia Ltd (now Acacia Resources Ltd) began exploring for sedimentary-exhalative Broken Hill-type mineralisation in the Eyre Peninsula of South Australia in the early 1980's. Metasediments of the Lower Proterozoic Middleback Subgroup were considered to have a number of attributes in common with the host sequences to major base metal deposits including Aggeneys and Gamsberg in South Africa and Broken Hill in Australia (Higgins et al., 1990). The Middleback Subgroup was considered comparable to lithologies in the Broken Hill area on the basis of a Lower Proterozoic age, mixed clastic and chemical sedimentary lithologies and high metamorphic grade.

Aero-magnetics were used to define initial exploration targets. Targets were defined as positive linear magnetic features parallel to stratigraphy, interpreted as banded iron formations (Higgins et al., 1990). In 1981, drill testing of a series of isolated magnetic highs on the Wilcherry Hill exploration lease intersected a number of zones of base metal mineralisation. Disseminated and massive base metal sulphides intersected at a prospect near the Menninnie stock watering dam subsequently became known as the Menninnie Dam

prospect. By 1989, six percussion holes and fourteen diamond holes had outlined an area of anomalous Pb and Zn over a 3 km by 1 km area (Higgins et al., 1990).

In 1989, Aberfoyle Resources Ltd. joint ventured into the Wilcherry Hill exploration lease acquiring a 60% share and project management. Aberfoyle Resources Ltd drilled a further 18 diamond holes and 13 percussion holes between 1989 and 1993, extending the known area of mineralisation. Because of the wide spacing of drill holes and the complex nature of the mineralisation, no new resource figure was calculated.

Given the unusual nature of the Pb - Zn - Ag mineralisation, the joint venture partners decided more detailed research was required to investigate the deposit genesis. It was around this time that I approached the joint venture partners and suggested they offer the Menninnie Dam prospect as a PhD research topic examining the timing and genesis of mineralisation. Mr John Anderson (then; Regional Manager of Aberfoyle Resources Ltd., South Australia) and Dr. Bob Beeson (then; Senior Research Scientist, Billiton Resources Ltd) were instrumental in supporting a PhD research project, and in mid 1992 final approval was given. Since establishment of this research project, negligible additional exploration has been undertaken by the joint venture partners. In the latter half of 1995, Aberfoyle Resources Ltd diluted its interest in the Wilcherry Hill exploration lease below 50% and passed management to Acacia Resources Ltd.

## 1.5 General statement of aims and methods

This research project was established to unravel the genesis of the Menninnie Dam Pb - Zn - Ag deposit. A thorough study of all aspects of the deposit is considered to be beyond the limits of this PhD, and three topics were selected for in-depth research:

- Geologic setting of mineralisation
- The timing of mineralisation
- The nature of the ore forming fluids

The decision to target these topics was based on the belief that they would contribute significantly to understanding the processes involved in formation of the deposit.

The local geology has been briefly described by Higgins and Hellsten (1986), Higgins et al. (1990) and Beeson (1990). Since publication of their work, additional drilling has been undertaken, enlarging the zone of known mineralisation and contributing significant new information on the local geology. It was therefore necessary to review and revise the prospect geology so that the contribution of the various geologic processes that controlled the mineralising event could be better appreciated.

The following data has been made available by the Joint Venture Partners and by Dr Graham Carr, Dr. Anita Andrew, and Dr. Judy Dean (CSIRO) for the purposes of this research project:

- Core from the 32 diamond drill holes (11,639m total).
- Percussion drill chips.
- Geochemical assay results from drilling (elements analysed: Mn, Fe, Zn, Cu, Pb, Ag and, rarely, W, Sn, As, Hg and Au).
- Whole rock geochemistry for drill holes PD0001-PD0008 as used by Beeson (1990b).
- Collection of 210 thin and polished sections.
- Airborne magnetic survey results for the Menninnie Dam prospect and surrounds.
- Lead isotope database for the Menninnie Dam prospect (228 analyses).
- Sulphur isotope database (14 analyses).

The prolonged period of exploration at Menninnie Dam (1981 - present), with the involvement of a number of companies and numerous geologists, has resulted in a lack of uniformity of drill hole logging techniques. In order to overcome this problem, the diamond drill core has been re-logged, with emphasis on documenting the relationship between the host rocks and mineralisation. The percussion pre-collars to diamond drill holes have not been re-logged.

Establishment of the relationship between the host rocks, various tectonic events and mineralisation is fundamental to determining the timing of mineralisation. The ages of the host rocks and major tectonic events can be constrained within reasonable limits by comparison to similar units elsewhere on the Eyre Peninsula for which there are well-established ages. In this thesis, constraining the timing of mineralisation is attempted using a number of independent techniques including; stratigraphic relationships, model lead isotope ages and U-Pb zircon dating.

The nature and composition of the mineralising fluids have been investigated through examination of; sulphide and gangue mineralogy, mineral paragenesis, fluid inclusions, sulphur, lead, oxygen, deuterium and carbon isotope data and thermodynamic modelling.

# Chapter two
# Physiography and regional geology

## 2.1 Introduction

This chapter provides a review of the physiography and regional geologic setting of the Eyre Peninsula of South Australia. Drexel et al. (1993) reviewed and collated publications on the Precambrian geology of South Australia, as well as contributing a significant amount of new data compiled by the Geological Survey of South Australia. Much of the regional geology summary is taken from their publication. The geologic time scale adopted in this study is based on the IUGS, 1989, Global Stratigraphic Chart (Fig. 2.1).

## 2.2 Physiography

Much of the Eyre Peninsula has low topographic relief, rising gently from the coast to form extended flat plains. On the eastern Eyre Peninsula, the plains are dissected by ranges of low hills, such as those inland from Cowell, north of Cleve and the extensive Gawler Ranges which form the northern margin of the Eyre Peninsula (Fig. 2.2). Elsewhere, the plains are broken by isolated hills and ridges of more resistant granite and sedimentary formations. The Middleback Ranges, Darke Peak, Uno and Corunna are examples of prominent, resistant sedimentary formations while Carappee Hill and Minnipa Hill are examples of resistant granite bodies. The highest peak on the Eyre Peninsula is Mount Kolendo in the Gawler Ranges (488 m A.S.L).

The morphology of the Gawler Ranges was described by Campbell and Twidale (1991) as "ordered rows of bornhardts" formed by differential weathering along fracture systems including orthogonal fractures, sheet fractures and columnar jointing. Bornhardts were interpreted to have been initiated by weathering in the Jurassic or earlier Mesozoic, and then exposed by erosion in the Late Cretaceous to Early Tertiary (Campbell and Twidale, 1991).

Outcrop over much of the Eyre Peninsula is poor, and Quaternary aeolian sands and silts form an extensive cover sequence. Inland, rock exposures are restricted to isolated ridges, creeks, quarries and road cuts. This contrasts with the eastern coast line of the Eyre Peninsula which probably has some of the better coastal exposure in Australia.

Much of the central and southern Eyre Peninsula is cropped for wheat, however some 20 km south of the Gawler Ranges, land use changes from wheat to sheep. The Menninnie Dam prospect is about 20 km north of the northern margin of the wheat belt and immediately south of the Gawler Ranges in an area dominated by mallee scrub and salt bush. The terrain rises gently from the edge of the wheat belt to the low hills of the Gawler Range Volcanics.

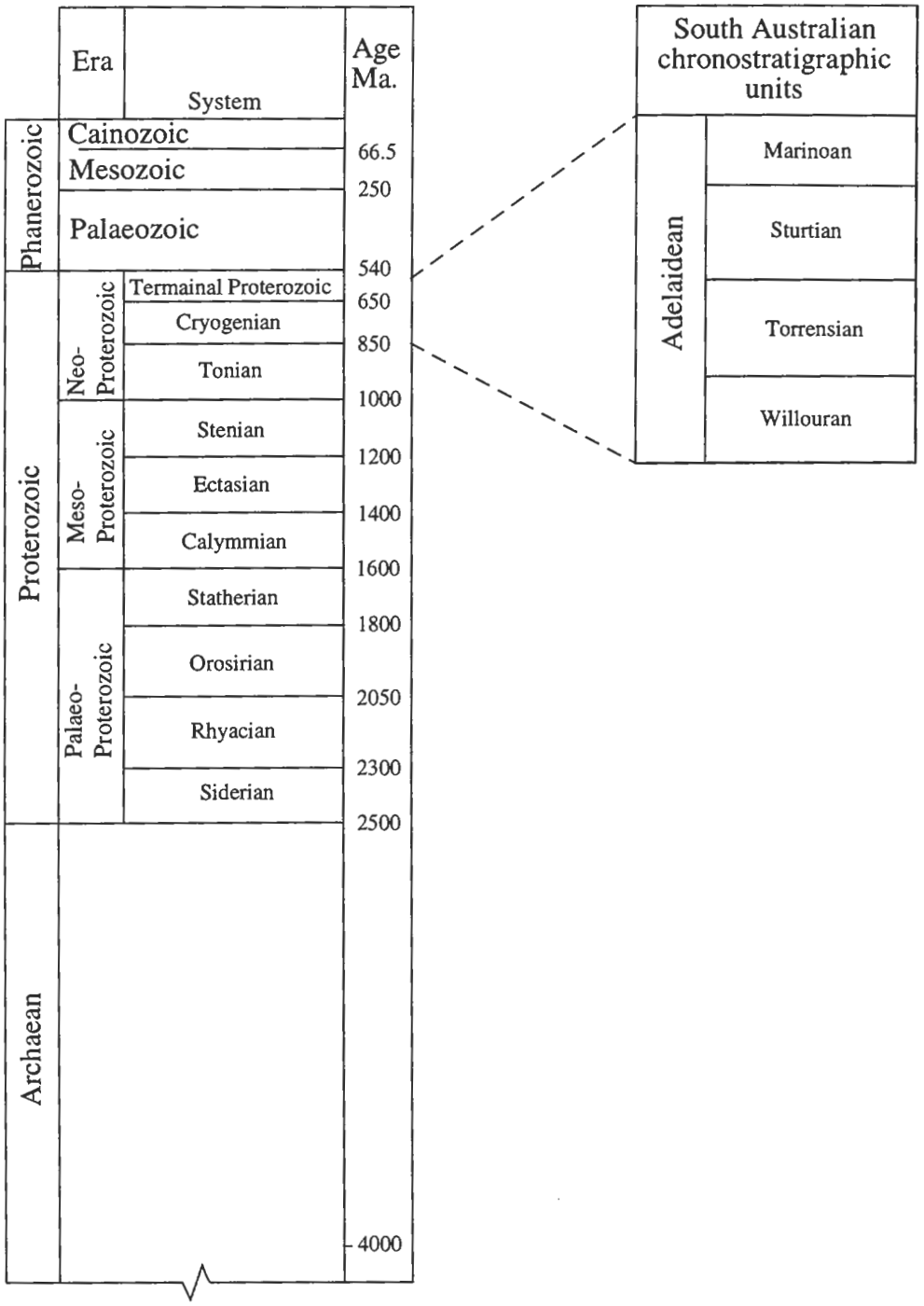


Fig. 2.1. Geologic time scale based on the IUGS 1989 Global Stratigraphic Chart. The Neoproterozoic Adelaidean subdivisions follow usage by Preiss (1987).

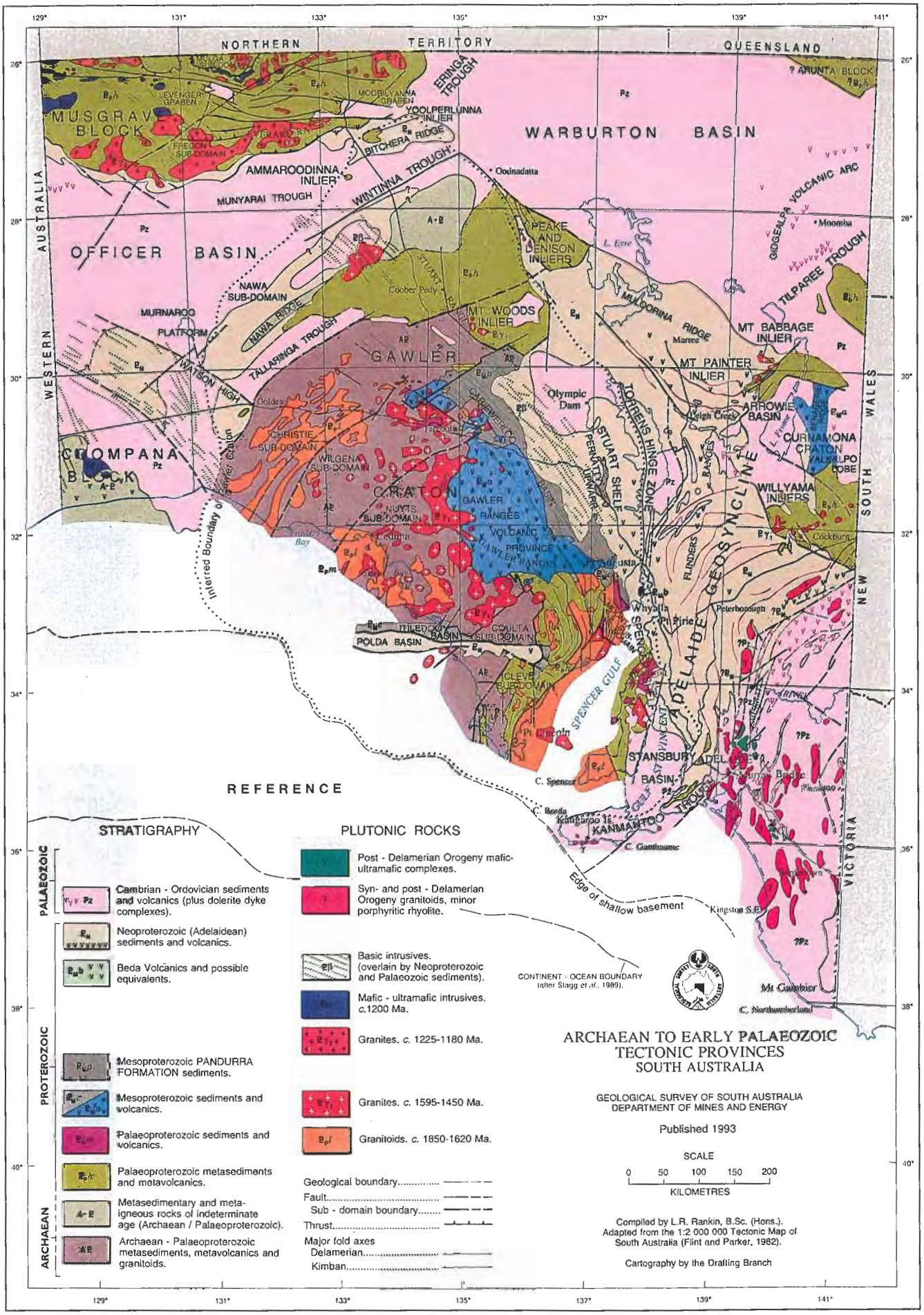


Fig. 2.2 Tectonic provinces, and summarised stratigraphy of South Australia (after Parker et al., 1993). The approximate margin of the Gawler Craton is indicated by a dotted line.

The Menninnie Dam prospect area is covered by a variable thickness of Quaternary reddish brown and yellowish brown gravelly and sandy clay, silt and sand with soft earthy carbonates and hard calcrete nodules (Blissett et al., 1988). Within a kilometre to the east and south of the prospect, breakaways of terrazzo type silcrete form small scarps a few metres high. Widely scattered outcrop of low lying Gawler Range Volcanics surround the prospect area and increase in abundance and profile to the west and north where they have formed the foothills of the Gawler Ranges. Areas of no outcrop are commonly weathered to depths of > 60 m.

## 2.3 Regional Geology

*Gawler Craton*

The Gawler Craton is a stable block of late Archaean and Early Proterozoic gneisses, granites and metasediments, Middle Proterozoic sedimentary rocks and extensive acid volcanics (Fig. 2.2). Parker et al. (1993) defined the Gawler Craton as that region of crystalline basement that has not been substantially deformed or remobilised, except by minor epiorogenic movements since approximately 1450 Ma. The Gawler Craton is bound to the north-west by the Musgrave Orogenic Domain, although the contact zone is concealed by sediments of the Officer Basin. The western boundary is also indistinct, and has been placed along a distinct gravity and aeromagnetic feature, interpreted to define the western edge of shallow crystalline basement (Parker et al., 1993).

The Torrens Hinge Zone forms the eastern margin of the Gawler Craton, with the boundary mantled by sedimentary lithologies of the Adelaide Geosyncline. The south-eastern margin of the Gawler Craton was interpreted by Belperio and Flint (1993) to extend to the eastern margin of the Torrens Hinge Zone and to the northern margin of Kangaroo Island. The south-western margin of the Gawler Craton is interpreted to be a faulted contact associated with the break up of Gondwana and separation of Antarctica during the Mesozoic (Willcox and Stagg, 1990).

*Subdomains*

The Gawler Craton has been subdivided into a number of discrete tectonic subdomains based on structural, metamorphic, and stratigraphic differences. Boundaries are separated by major aeromagnetic linears interpreted as significant crustal sutures (Parker et al., 1993; Fig. 2.2). The Nawa Subdomain crops out in the north-west of the craton and is of mixed or complex character incorporating late Archaean - Paleoproterozoic rocks, Mesoproterozoic granites, Neoproterozoic sediments and Cambrian - Ordovician sediments and volcanics. The Christie and Coulta subdomains (Fig. 2.2) contain most of the exposed Archaean rocks, and some of the Paleoproterozoic granitoids, but are largely free of younger Proterozoic metasediments, volcanics, or intrusives. The Wilgena and Nuyts subdomains (Fig. 2.2) contain Archaean metasediments intruded by Mesoproterozoic granites.

The Cleve Subdomain crops out in the south east of the Eyre Peninsula (Fig. 2.2) and is a Paleoproterozoic fold belt containing both clastic and chemical sediments (eg. Hutchison Group 1950-1840 Ma.), and voluminous granitoids (eg. Lincoln Complex) associated with closure of the basin and deformation (eg. Kimban Orogeny, KM - $D_1$ to KM - $D_3$). The Moonta Subdomain crops out in the north-eastern Eyre Peninsula (Fig. 2.2) and is considered to be a younger extension of the Cleve Subdomain (Parker et al., 1993). Much of the deformation and emplacement of granitoids in the Cleve Subdomain ceased by ≈1740 Ma., when sequences in the Moonta Subdomain were being deposited or erupted. Later deformation was manifested as shear zones in the Cleve Subdomain and extensive folding in the Moonta Subdomain.

The Mesoproterozoic Gawler Ranges Volcanic Province in the central Gawler Craton formed during voluminous out-pouring of acid to intermediate lavas and pyroclastics. Whereas other sub-domains have north-east trending boundaries, the Gawler Range Volcanics Province has poorly defined boundaries and no clear underlying tectonic control. Unlike other subdomains, the Gawler Range Volcanic Province is relatively undeformed. Co-magmatic Mesoproterozoic, granitoids of the Hiltaba Suite crop out in a broad belt along the southern and western margins of the Gawler Range Volcanic Province (Fig. 2.2).

Mesoproterozoic and late Paleoproterozoic sediments (eg. Tarcoola Formation and Corunna Conglomerate) have not been assigned to basins, except for the Blue Range Beds (Itiledoo Basin of Flint and Rankin, 1989), and the Pandurra Formation which was deposited in the Midproterozoic Cariewerloo Basin (Cowley, 1993).

### 2.3.1 Stratigraphy

This section focuses on the Archaean and Proterozoic units of the Cleve and Coulta Sub-domains and the Gawler Range Volcanics Province. The occurence of Archaean and Proterozoic rocks is detailed in the relative geological maps produced by the South Australian Department of Mines and Energy and has been summarised by Parker et al. (1988). A more detailed account, which includes recent data, was given by Drexel et al. (1993). The following summary is largely derived from these two publications. The stratigraphy of the Eyre Peninsula is summarised in Figures 2.3. and 2.4.

#### Archaean

*Sleaford Complex*

The Sleaford Complex are the basement rocks of the Gawler Craton and are more abundant in the western half of the Eyre Peninsula. Outcrop is excellent along the southern and south-western coastlines, however, inland exposure is restricted to scattered outcrops surrounded by Cainozoic cover.

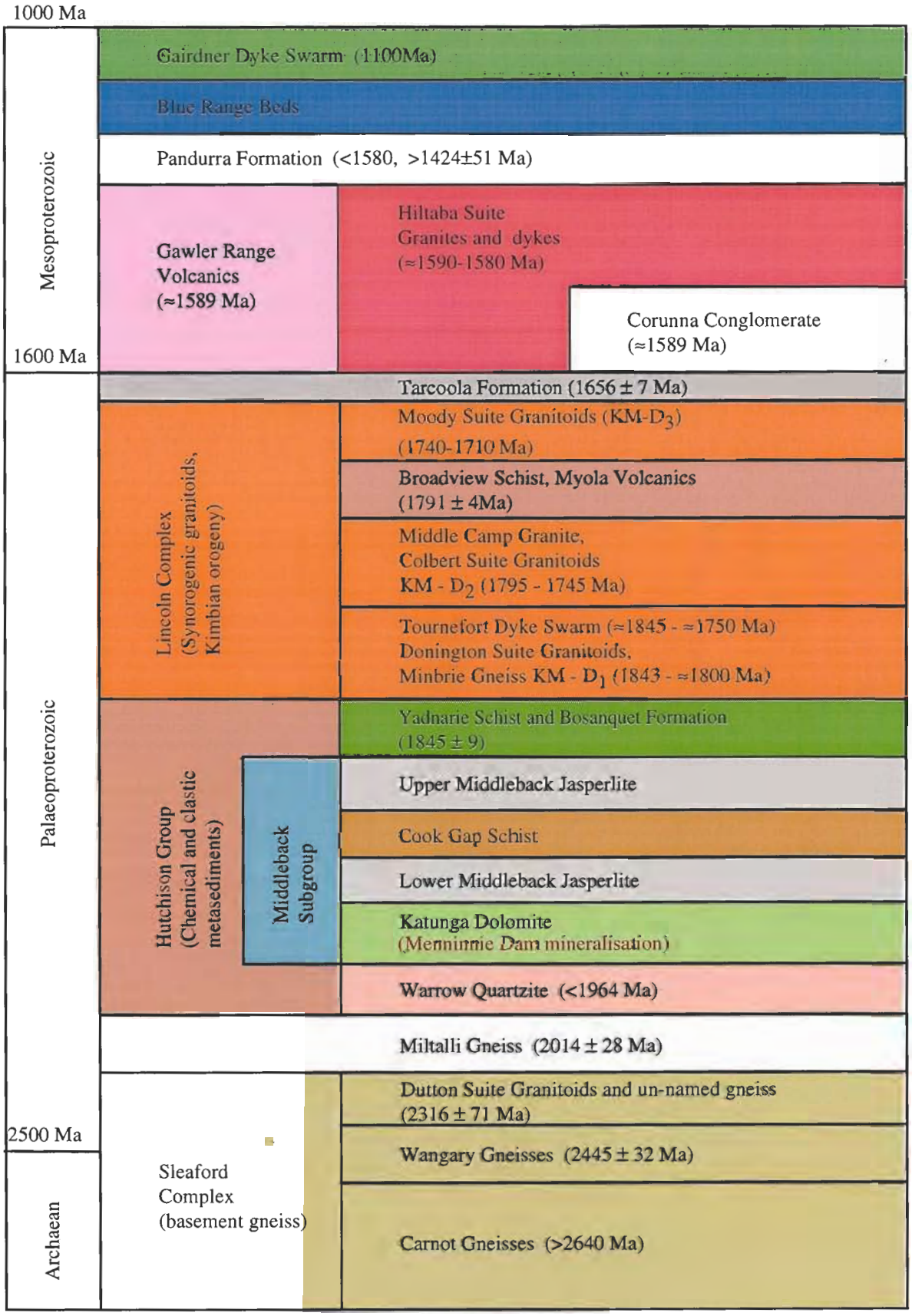


Figure 2.3 Stratigraphic colomn of the Archaean and Proterozoic rocks of the Cleve Subdomain and Gawler Range Volcanic Province. (Modified from Parker et al., 1988; Drexel et al., 1993).

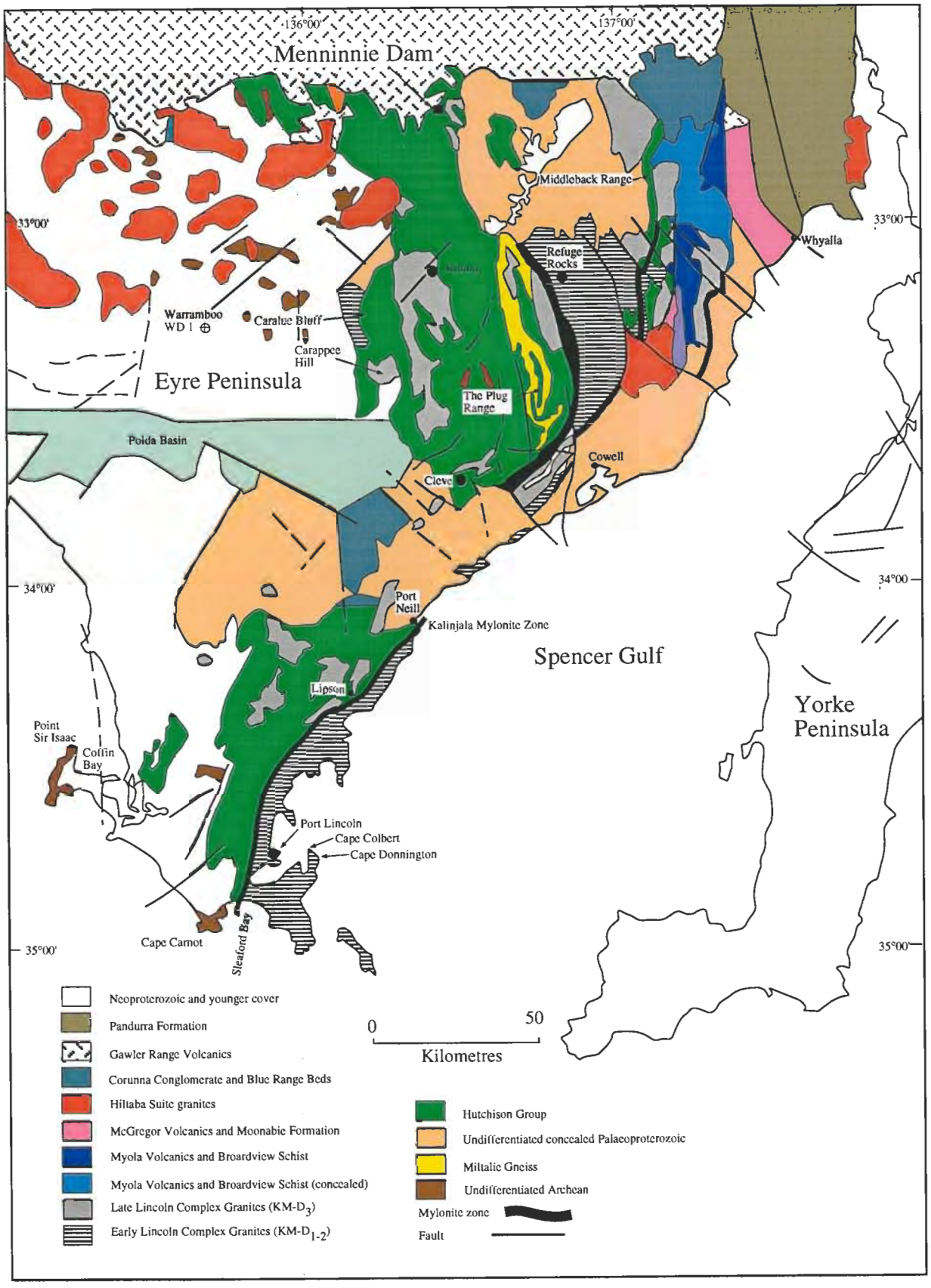


Fig. 2.4 Simplified geology of the eastern Eyre Peninsula of South Australia (modified after Parker, 1993b).

The Sleaford Complex consists of gneissic metasediments deposited in a shallow water platform sequence, possibly with associated contemporaneous tholeiitic basalt sills and flows. The age of sedimentation was interpreted to be older than 2640 Ma., based on U-Pb zircon dating by Fanning et al. (1986).

The Sleaford Complex is divided into four units:

- Dutton Suite granitoids youngest
- unnamed gneiss
- Wangary Gneiss
- Carnot Gneisses oldest

*Carnot Gneiss*

The Carnot Gneiss has been subdivided into ortho and para-gneisses and consists of compositionally banded metasediment, concordant sheets of tholeiitic metabasalts, (flows, sills or dykes), and synorogenic felsic intrusions.

Fanning et al. (1980) described a compositionally layered garnetiferous quartzo-feldspathic ortho-gneiss cropping out on a wave-cut platform at the southern-most tip of the Eyre Peninsula (Cape Carnot; Fig. 2.4), and applied the name 'Carnot Gneiss' to them. The Carnot Gneiss consists of plagioclase, K-feldspar, quartz, biotite and garnet with accessory spinel, magnetite, ilmenite and rutile and rounded zircons. Geochemically, the gneisses contain normative corundum, indicating excess $Al_2O_3$, consistant with a sedimentary origin.

The para-gneisses consist of concordant 1-2 m thick bands of tholeiitic composition interpreted to have been emplaced as sills and / or dykes prior to, or during peak metamorphic conditions (Daly and Fanning, 1993).

The Carnot Gneiss also crops out in the Warramboo-Waddikee area of the central Eyre Peninsula, where it consists of compositionally banded, to homogenous, quartz, garnet, feldspar gneiss. Whole rock Rb-Sr geochronology of felsic gneiss from a North Broken Hill Ltd and CRA Exploration drill hole (Warramboo WD1; Fig. 2.4) gives an age of 2520 ± 163 Ma. (Webb et al., 1986).

*Wangary Gneiss*

The Wangary Gneiss is exposed 13 km southwest of Point Sir Isaac on the Coffin Bay Peninsula and along the coast for ≈ 60 km north of Coffin Bay (Fig 2.4). The Wangary Gneiss is a compositionally layered microcline-plagioclase-quartz-biotite-muscovite gneiss interpreted as a metasediment and interpreted to be a lower grade equivalent of the Carnot Gneiss (Daly and Fanning, 1993). Whole rock Rb-Sr dating by Webb et al. (1986) gives an age of 2380 ± 60 Ma. A poorly defined U - Pb zircon age of 2445 ± 32 Ma. was obtained by Fanning (1987).

*Sleaford Orogeny*

The earliest recorded orogenic episode on the Eyre Peninsula spans the period 2300 - 2637 Ma., and is known as the Sleaford Orogeny (Webb, 1980; Fanning et al., 1986). The Sleaford Orogeny is interpreted to have consisted of three and possibly four deformational events. U - Pb zircon dating of an intrusive hypersthene granulite facies gneiss at Cape Carnot gave a concordant age of 2637 ± 21 Ma. (Fanning et al., 1986), which has been interpreted as the maximum age for the onset of metamorphism (Daly and Fanning, 1993). The minimum age for peak granulite facies metamorphism has been interpreted at 2436 ± 137 Ma. based on whole rock Rb-Sr dating (Fanning et al., 1986). Prograde mineral assemblages for the Sleaford Complex indicate temperatures of 700 - 800°C and pressures of 7 - 9 kb (Bradley, 1980). Two pyroxene geothermometry by Fanning (in Parker et al., 1988) for the basic granulites give comparable calculated temperatures of 800 - 860°C.

## Paleoproterozoic

Paleoproterozoic rocks in the Gawler Craton are widespread, forming a broad belt across the eastern Eyre Peninsula (Fig 2.4).

*Dutton Suite*

The Dutton Suite consists of synorogenic granitoids emplaced during the Sleaford Orogeny, exposed in the southwest of the Eyre Peninsula, and on nearby islands. The timing of the later stages of the Sleaford Orogeny are interpreted from whole rock Rb-Sr dating of the Dutton Suite granitoids at 2316 ± 71 and 2334 ± 109 Ma. (Webb et al., 1986).

*Palaeoproterozoic gneisses*

In a number of localities, there is a sequence of gneisses separating the Archaean Sleaford Complex from the overlying Palaeoproterozoic Hutchison Group metasediments. An unnamed gneiss underlying the Warrow Quartzite at Ullabidinie Creek and at 'Minbrie Springs' (≈ 20 km north of Cleve on the eastern Eyre Peninsula) has a Rb-Sr age of 2315 ± 175 Ma., which is indistinguishable from the age obtained for the Dutton Suite Granites.

The Miltalie Gneiss underlies the Warrow Quartzite at Plug Range (Fig. 2.4), and consists of a medium grained, well foliated quartz-microcline-plagioclase-biotite gneiss with pink pegmatitic segregations. U - Pb geochronology by Fanning et al. (1988), gave a zircon crystallisation age of 2014 ± 28 Ma., with metamorphism at ≈ 1964 Ma. The 1964 Ma. age provides a constraint on the maximum age of the overlying Hutchison Group.

*Hutchison Group*

Unconformably overlying the Sleaford Complex, or Miltalie Gneiss (and equivalents), is the Paleoproterozoic Hutchison Group. The Hutchison Group consists of high metamorphic grade rocks derived from shallow clastic and chemical marine sediments, and minor acid and

mafic volcanics (Parker, 1993b). Corbett (1987) estimated the total thickness of the Hutchison Group to be about 10 km. The Hutchison Group has been intruded by numerous synorogenic granitoids, known as the Lincoln Complex, associated with the Kimban Orogeny. The Hutchison Group is host to Pb-Zn-Ag mineralisation at Menninnie Dam. Parker (1980b) subdivided the Hutchison Group into three main sequences:

- A basal quartzite sequence equated with the Warrow Quartzite of the southern Eyre Peninsula.
- A mixed chemical and clastic sequence equated to the Middleback Group of the Middleback Ranges, re-defined as the Middleback Subgroup.
- An upper pelitic unit known as the Yadnarie Schist.

The Warrow Quartzite consists of a massive flaggy, quartz-feldspar quartzite with rare bedding and cross stratified layering. It overlies the Sleaford Complex in the southern Eyre Peninsula and has a locally developed basal conglomerate and / or pelitic schist unit. In the eastern Eyre Peninsula, complex deformation and intrusion of synorogenic granitoids of the Lincoln Complex has obscured the base and, locally, the top of the Warrow Quartzite. The thickness of the Warrow Quartzite is not known, although quartzite units up to 1000 m thick are exposed at Caralue Bluff in the central Eyre Peninsula (Fig. 2.4).

Trough cross bedding in the Warrow Quartzite at Caralue Bluff has been interpreted to indicate fluviatile to marginal marine deposition. In the Cleve and Lipson regions, the Warrow Quartzite shows a upwards transition from massive flaggy quartzite to interbedded pelitic schist. The transition is interpreted to be a lateral facies change from shallow marine to a more distal marine environment of deposition associated with landward or westerly transgression which immediately preceeded deposition of the Middleback Subgroup (Parker and Lemon, 1982).

*The Middleback Subgroup*

The Middleback Subgroup conformably overlies the Warrow Quartzite. The thickness of the Middleback Subgroup has been estimated at 2000-2500 m, based on a section northwest of Cleve (Parker, 1993b). Based on the stratigraphy in the Middleback Ranges west of Whyalla (Fig. 2.4), Lemon (1980) subdivided the Middleback Subgroup into a basal dolomite unit overlain by two iron formations that are separated by a schist unit of clastic origin. The Katunga Dolomite lies unconformably on the Warrow Quartzite (Lemon, 1980). Parker (1993b) described the Katunga Dolomite as "a generally massive to poorly layered, white to pale grey dolomitic marble which is mostly medium grained and holocrystalline. Layering (when present) is defined by bands of serpentine (± forsterite relics) and calcite ± diopside ± tremolite alternating with massive dolomite ... pale yellow-green serpentine nodules and diopside characterise high grade metamorphic zones whereas tremolite, actinolite and talc are common in lower grade areas".

The Katunga Dolomite contains minor bands of schist, and becomes more Fe-rich up stratigraphy, and grades into the overlying 'Lower Middleback Jaspilite'. Pyrite occurs at the dolomite / iron formation boundary (Lemon, 1980). Iron silicate minerals in the Lower Middleback Jasperlite include iron-rich talc, grunerite, cummingtonite and anthophyllite, diopside / hedenbergite, with rare hypersthene present at higher metamorphic grades. Magnetite is the dominant iron oxide at depth, with more oxidised minerals such as haematite and iron oxyhydroxides occuring in the near surface environment. Parker (1993b) stated that "the iron formations are well banded with alternating 0.5 - 20 mm thick bands of quartz, carbonate or iron oxides ± iron silicates ± carbonate. Accessory minerals include garnet, biotite, tremolite and occasionally microcline. Original chert has been variably recrystallised to form fine to medium, and locally coarse, grained quartz. Strong crystallographic and grain-shape fabrics are ubiquitous and define axial planar foliations in early fold generations". The prominent banding and local cyclic banding in carbonate facies iron formations were interpreted to be relict primary layering (Parker and Lemon, 1982).

The Lower Middleback Jaspilite increases in clastic content and grades upwards into the Cook Gap Schist. The Cook Gap Schist is estimated to have an apparent thickness of >1500 m, and consists of predominantly semi-pelitic, quartz-veined garnet-mica schist and gneiss with minor calc-silicate gneiss, magnetite-bearing gneiss, and concordant amphibolites (Parker, 1993b). The origin of the amphibolites is uncertain; they may either be concordant volcanics of quartz tholeiite composition, or metamorphosed sills and dykes rotated into structural concordance.

The Cook Gap Schist grades upwards into a mixed carbonate-silicate facies iron formation that forms the basal section of the Upper Middleback Jaspilite. The Upper Middleback Jaspilite is chemically and mineralogically similar to the Lower Middleback Jaspilite, and Yeates (1990) argued tectonic repetition, an interpretation disputed by Parker (1993b). The top of the Middleback Subgroup is defined as the top of the Upper Middleback Jaspilite.

In the Cleve region (Fig. 2.4), the Upper Middleback Jaspilite is overlain by the Yadnarie Schist which consists of a fine to medium grained pelitic to semipelitic, quartz-veined mica schist that contains quartz, muscovite and biotite with minor opaque minerals, plagioclase, sillimanite, garnet and tourmaline. Amphibolites are rare or absent. Near Carappee Hill, in the central Eyre Peninsula (Fig. 2.4), the Middleback Subgroup is overlain by mixed acid volcanics and calc-silicates of the Bosanquet Formation (Rankin et al., 1988) which was considered to be a lateral equivalent of the Yadnarie Schist (Parker, 1993b). The volcanics consist of recrystallised rhyodacite with distinctive relict phenocrysts of microcline and bluish coloured quartz. U - Pb dating of zircons from the Bosanquet Formation give a zircon crystallisation age of 1845 ± 9 Ma. (Rankin et al., 1988), and provides a minimum age for deposition of the Hutchison Group.

Lemon (1980) interpreted the changes in lithofacies within the Middleback Subgroup to have resulted from deposition in a shallow sea with a north-south trending shoreline. Initial transgressive chemical deposition of the dolomite was succeeded by sulphide, carbonate-silicate, and oxide facies iron formations. This was terminated by a period of shoreline progradation and a change to clastic sedimentation (Cook Gap Schist) followed by a return to transgression and chemical sedimentation (Upper Middleback Iron Formation). This was probably terminated once more by clastic sedimentation, (Yadnarie Schist).

*Myola Volcanics and Broadview Schist*

The Myola Volcanics and Broadview Schist crop out in the north-east Eyre Peninsula (Fig. 2.4), east of the Middleback Ranges (Moonta Subdomain). While their relationship to the Hutchison Group is uncertain, U - Pb zircon dates for the Myola Volcanics of 1791 ± 4 Ma. indicate they are younger than both the Bosanquet Formation and the Hutchison Group (Fanning et al.,1988).

*Kimbian Orogeny*

The Hutchison Group metasediments underwent a period of orogenic activity between ≈ 1845 and 1710 Ma. known as the Kimban Orogeny. Parker (1978) recognised three major tectonic events preserved in rocks of the Cowell-Cleve area, north-eastern Eyre Peninsula that he ascribed to the Kimban Orogeny. The metamorphic events and the associated deformations are referred to as KM-$D_1$, KM-$D_2$ and KM-$D_3$ respectively.

Peak metamorphic conditions for KM-$D_1$ and KM-$D_2$ attained >8 kbar and 800 - 900°C (granulite facies) in the southern Eyre Peninsula (Mortimer et al., 1980; Bradley, 1980) and 5 - 7 kbar and 600 - 675°C (amphibolite facies) in the central Eyre Peninsula (Parker et al, 1988). KM-$D_1$ produced a layer parallel fabric and KM-$D_2$ is characterised by tight to isoclinal folding and an axial planar fabric (Parker, 1993a).

KM-$D_3$ was a retrograde event, with pressures of ≈ 1.5 - 2 kbar and temperatures of ≈ 450 - 550°C corresponding to the greenschist - amphibolite boundary (Parker, 1993a). KM-$D_3$ resulted in formation of broad, open folds and major north to northeast-trending mylonitic shear zones. The Kalinjala Mylonite Zone is a major linear zone of intense ductile deformation (3 km wide at Port Neill) extending the length of the eastern Eyre Peninsula from Sleaford Bay in the south to the Middleback Ranges in the north (Parker, 1980a; Fig.2.4). The Kalinjala Mylonite Zone consists of mylonite with minor ultramylonite, remnants of protomylonite and scattered boudins of amphibolite. The mylonites at Port Neill were interpreted by Parker (1993a) to have a major component of dextral shear, which is consistent with their regional sigmoidal distribution. Rb-Sr dating of a weakly deformed pegmatite intruding the mylonite at Port Neill places an upper age limit on KM-$D_3$ of 1710 Ma. (Fanning, 1984).

*Lincoln Complex*

Each deformation phase of the Kimbian Orogeny was accompanied by the intrusion of (syn-orogenic) granitoids collectively known as the Lincoln Complex (Fig. 2.4). Radiometric age determinations of the granites has helped to constrain the timing of each deformation event (Table 2.1).

Table 2.1 Syn-tectonic granitoids of the Lincoln Complex .

| Deformation event | Granite Suite | Age | Reference |
|---|---|---|---|
| $KD_3$ | Moody Suite | ≈1740-1710 Ma.** | 5 and 6 |
| $KD_2$ | Middle Camp Granite | 1738 ± 68 Ma.* | 4 |
| | Colbert Suite (late $KD_2$ to pre $KD_3$) | 1757 ± 14 Ma.** | 2 |
| $KD_1$ | Minbrie Gneiss | >1800 Ma.** | 3 |
| | Donington Suite | 1818 ± 13 Ma.* and | 2 |
| | | 1843 ± 2 Ma.* | 1 |

*U-Pb zircon; **Rb-Sr

References; 1) Mortimer et al., (1988). 2) Mortimer et al., (1986). 3) Webb et al., (1986). 4) Fanning, (1987). 5) Parker, (1993a). 6) Fanning, (1984).

The Donington Suite Granites are I-type, Sr-depleted, Y-undepleted, fractionated granites low in incompatible elements (Wyborn et al., 1992). The Moody Suite Granites are considered to be a sub-group of this granite suite, with F enrichment and variable Y, Zr and Nb. Moody Suite Granites with high $SiO_2$ contents are enriched in $K_2O$, F, Th, U, Rb and K/Rb (Wyborn et al., 1992). Detailed petrochemistry for the Colbert Suite and MiddleCamp Granite has not been published.

Multiply deformed mafic dolerite to gabbronorite dykes of the Tournefort Dyke Swarm comprise up to 25% of the Donington Granitoid Suite (Parker, 1993a), and were interpreted to have been emplaced between 1845 - 1750 Ma. (Parker, 1989).

*Tarcoola Formation*

The Tarcoola Formation consists of fluvial to marginal-marine clastic sediments deposited in grabens and half grabens (Daly, 1993a) along the north-western margin of the GRV (Fig 2.2). Daly (1985) subdivided the Tarcoola Formation into three members. The basal Peela Conglomerate Member comprises conglomerate, arkosic quartzite and green lithic and volcaniclastic sandstone. The Fabian Quartzite Member overlies the Peela Conglomerate Member and consists of micaceous quartzite. At Tarcoola, quartzite is interbedded with laminated carbonaceous shale and pyritic siltstone of the Sullivan Shale Member which includes minor water-laid tuffs. U - Pb zircon dating of the tuffs indicates and age of 1656 ± 7 Ma. for volcanism and sedimentation (Fanning, 1990). The Tarcoola Formation has undergone lower greenschist facies metamorphism and is folded about broard, open, fold axis (Daly, 1993a).

*Wartakan Event*

Throughout most of the Eyre Peninsula, there is evidence of a later deformation event named the Wartakan Event by Thomson (1969) and abbreviated here to $WD_1$. Deformation is more

pronounced in the Cowell-Cleve area and the southern Eyre Peninsula where late stage crenulations, kink bands and fractures associated with $WD_1$ occur. Emplacement of granitoids of the St. Peters Suite in the Streaky Bay region are interpreted to have been associated with $WD_1$. Granitoids of the St. Peters Suite are deformed, and characterised by intermingling of felsic and mafic magma. phases. The granitoids have U - Pb zircon dates of 1630 - 1620 Ma. (Flint et al., 1990), which constrains the timing of $WD_1$.

**Mesoproterozoic**

*Gawler Range Volcanics (GRV)*

Thomson (1966) introduced the name Gawler Range Volcanics (GRV) for the ellipsoidal mass of acid to intermediate volcanics exposed in the north-central Eyre Peninsula (Fig. 2.2; Fig. 2.5). The GRV Province covers an area of at least 25,000 $km^2$, and was presumably more extensive prior to being reduced to their current extent by weathering. When scattered outcrops and drill intersections are taken into account, Campbell and Twidale (1991) estimated the original extent of the GRV to be of the order of 60,000 $km^2$.

Most of the mapping and interpretation of the GRV has been undertaken by the Mines and Energy Department of South Australia and postgraduate students of the University of Adelaide and La Trobe University. Blissett (1975; 1986) formally described and named many of the units of the GRV. Detailed studies of the Kokatha area (Fig. 2.5) were undertaken by Branch (1978) and Robertson (1989). Giles (1977) undertook a detailed study of the Lake Everard area. Jagodzinski (1985) described the geology of the Toondulya Bluff area (Fig. 2.5). Creaser and White (1991) described the geology, geochemistry, geothermometry and possible origins of the Yardea Dacite (Fig. 2.5). Giles (1980), Stewart (1992) and Creaser (1995) undertook detailed studies of the petrogenesis of the GRV. A summary compilation of previous work up until 1993 (excluding Stewart, 1992) was presented by Blissett et al. (1993).

Blissett and Radke (1980) subdivided the GRV into 'older' and 'younger' sequences based partly on the attitude of more steeply dipping older beds and flat lying younger beds. Blissett et al. (1993) adopted the terms 'lower' and 'upper', and put the division at the base of the Yardea dacite and equivalents. Stewart (1992) divided the GRV into an earlier 'developmental phase' and a later 'mature phase' on the basis of geochemical and isotopic differences, and placed the boundary at the base of the Nonning Rhyodacite. The developmental phase includes all volcanics in the Lake Everard, Tarcoola, Kokatha areas in the west, and units which lie below and including the Bittali Rhyolite in the south of the GRV province. Subdivision of the GRV into the developmental and mature phases of Stewart (1992) is presented in Figures 2.5 and 2.6.

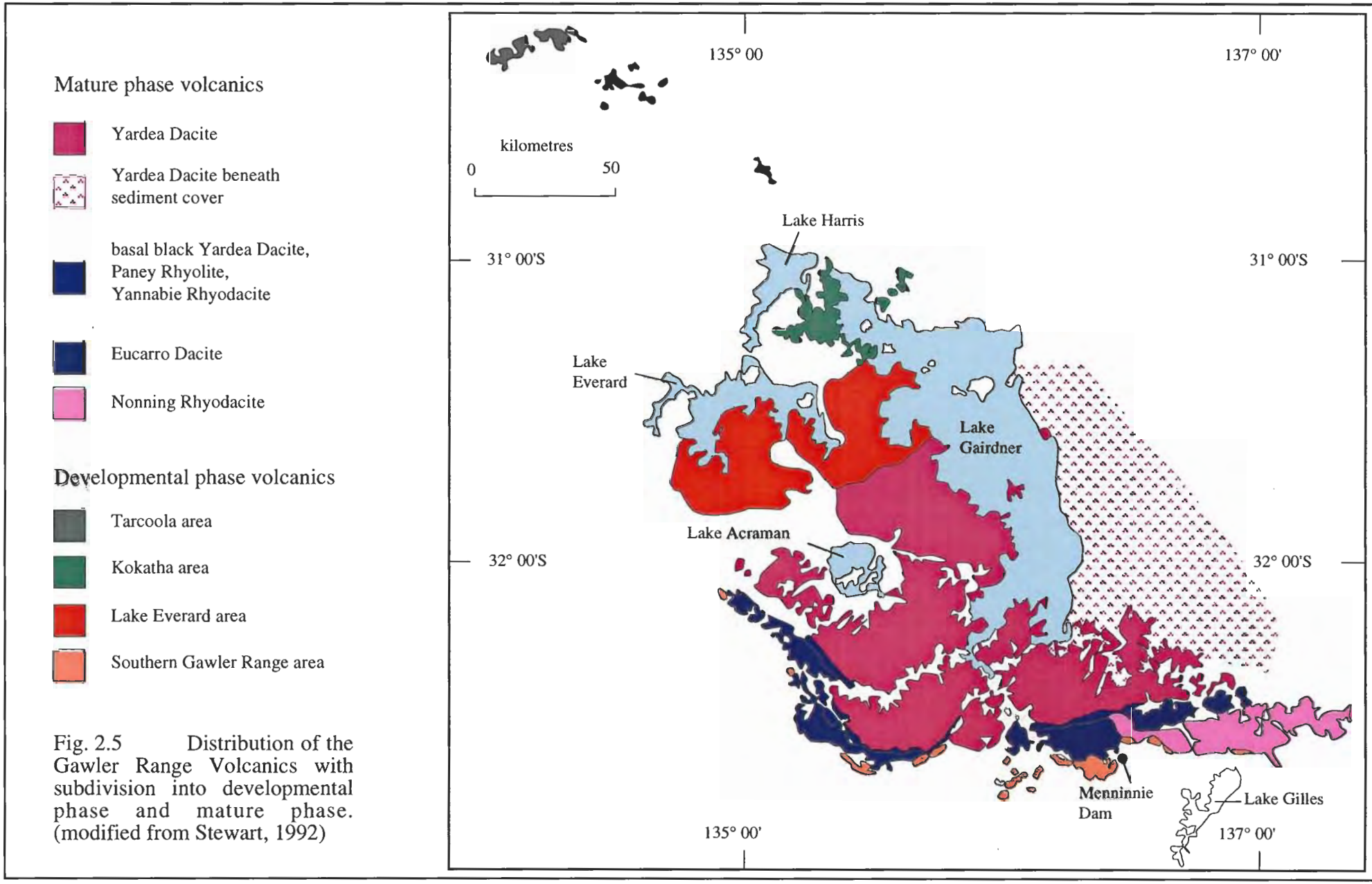


Fig. 2.5 Distribution of the Gawler Range Volcanics with subdivision into developmental phase and mature phase. (modified from Stewart, 1992)

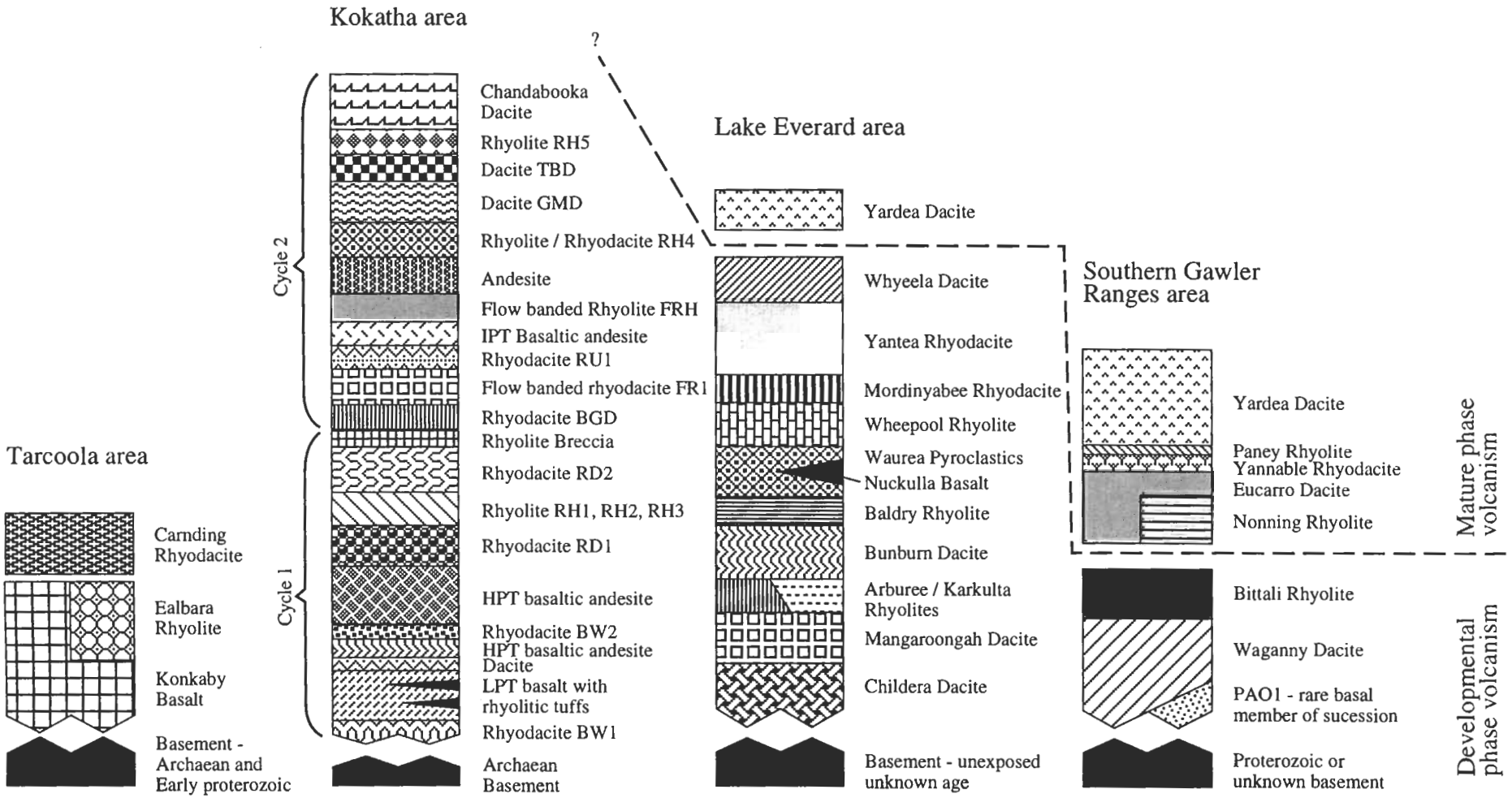


Fig. 2.6 Subdivision of the Developmental phase and mature phase of the Gawler Range Volcanics (after Stewart, 1992)

The developmental phase occurs as smaller more scattered volcanic centres along the western and southern margins of the GRV Province (eg. the Tarcoola, Kokatha, Lake Everard centres in the west and the Bittali Rhyolite along the southern margin; Stewart, 1992) The later, more voluminous units of the mature phase cannot be attributed to any particular volcanic centre.

Units of the GRV comprise variably welded ignimbrites with minor localised lava flows, domes and dykes. Volcanic breccias and air fall tuffs form only a small component. Restricted flows of basalts and andesites are present in the lower part of the succession. Many of the units resemble lavas and show little evidence of a pyroclastic origin. However, Turner (1975), Blissett (1975), Blissett and Radke (1980), Giles (1977 and 1980), Giles et al. (1980), Creaser and White (1991), Stewart (1992) and others, have demonstrated that the GRV consists of composite layers of welded ignimbrite and rheoignimbrite. The Yardea Dacite is the most voluminous unit, covering an area of 12000 $km^2$ to an estimated thickness of > 250 m with little textural or compositional variation (Blissett, 1975). The lava-like appearance of the Yardea Dacite may be due to the high emplacement temperature (900 - 1100°C) and rheomorphic behaviour (Creaser and White, 1991; Stewart, 1992).

U - Pb zircon dating of oldest unit, the Waganny Dacite, and youngest unit, the Yardea Dacite, give ages of 1591 ± 3Ma. and 1592 ± 3 Ma. These ages are statistically indistinguishable (Fanning et al., 1988), and are interpreted to indicate eruption of a large volume of felsic magMa. in a geologically short space of time.

The GRV comprise a calc-alkaline assemblage of dacites, rhyodacites and rhyolites with minor potassic andesites and tholeiitic basalts erupted in a subaerial continental environment (Blissett et al., 1993). The entire Gawler Range Volcanic Province is high in K and enriched in Ba, Th, Zr, Y, Rb, and light rare earth elements (Stewart and Foden, 1990; Stewart, 1992). In a study of the geochemistry of the Lake Everard area, Giles (1980) demonstrated a compositional break in the $SiO_2$ content from 52 to 58 wt%, which could not be satisfactorily explained by crystal fractionation. Giles (1980) demonstrated that the parental andesites and low silica dacites can be closely matched by invoking 20-30% partial melting of a lower crustal, basic granulitic source in which plagioclase, clinopyroxene, orthopyroxene and magnetite are residual. Giles (1980) suggests primitive basalts in the province originated from a relatively shallow (< 60 km) mantle source, and separated from a rising mantle diapir or plume, ultimately providing the heat source for melting of the crust, from which the acid magmas were generated.

By contrast, Stewart (1992) suggested the developmental phase was formed by fractional crystallisation of a mantle-derived magma. and assimilation of up to 43% Archaean and / or Proterozoic crustal material in a series of isolated magma. chambers. These isolated magma.

chambers later coalesced to form a single large chamber which gave rise to the mature phase volcanics. The gravity high underlying much of the GRV was interpreted by Stewart (1992) as a major mafic intrusive whose upper surface is at approximately 5 km depth.
The GRV have undergone little deformation since emplacement, except for epiorogenic faulting. Low temperature oxidation of iron, associated with devitrification, has resulted in a characteristic brick red colour of the GRV (Blissett et al., 1993).

*Hiltaba Suite*
The Hiltaba Suite comprises anorogenic granitoids that have formed large batholiths and smaller plutons prevalent around the north-western, western and southern margins of the Gawler Ranges (Figs. 2.2 and 2.4). Granites are the most abundant rock type but the suite is bimodal and more mafic lithologies (quartz monzonite and granodiorite) occur as scattered plutons in the north-east of the craton. Granitoids of the Hiltaba Suite commonly have a distinctive brick red colour due to abundant minute inclusions of haematite in plagioclase and K-feldspar. The Hiltaba Suite was co-magmatic with the GRV, and is both overlain by, and intruded into the GRV. Granitoids of the Hiltaba Suite have intruded the Corunna Conglomerate and the Tarcoola Formation but not the Pandurra Formation. A mean weighted age for all U - Pb zircon dates of the GRV and Hiltaba Suite is 1589 ± 2 Ma., with a peak at 1590 Ma. (Creaser and Cooper, 1993).

The Hiltaba Granite and Charleston Granite of the Hiltaba Suite are considered to be a sub-group of I-type, Sr-depleted, Y-undepleted granites, (anorogenic), enriched in incompatible elements and characterised by high $Fe_2O_3$ / ($FeO$+$Fe_2O_3$) levels compared to all other Australian Proterozoic granites (Wyborn et al., 1992).

*Dykes*
Blissett et al. (1993) described the occurance of numerous dykes around the margin of the central GRV mass. Dykes vary in length up to 18 km (Moonamby Dyke Suite; Giles, 1977), and vary in width from a few metres up to 1 km northwest of Corunna (Blissett et al., 1993). The dykes vary in composition from rhyolitic to andesitic. Rhyolitic dykes are commonly porphyritic. Blissett et al. (1993) suggested that the dykes in the Kokatha and Lake Everard areas may have been either feeder dykes to overlying volcanics, or slightly younger and co-magmatic with the Hiltaba Suite.

*Sediments associated with the GRV*
The Corunna Conglomerate occurs as scattered outcrops around the south and north-west margin of the GRV and east of Whyalla (Fig. 2.4). It consists of an interbedded thick sequences of coarse conglomerate, fine siltstone and sandstone (Daly, 1993b). Conglomerate clasts include Hutchison Group metasediments and GRV. Finer sediments include siltstones, sandstones, carbonaceous siltstone and silicified dolomite with common

tuffaceous horizons. The age of the Corunna Conglomerate is estimated to be between 1740 - 1585 Ma. and deposition was probably synchronous with the GRV (Daly, 1993b). The Corunna Conglomerate is interpreted to be of fluvial origin although the fine grained carbonaceous siltstone and sandstone at the top of the sequence were probably deposited in a shallow to moderately restricted marine basin (Lemon, 1972; Lemon and Gostin, 1983).

*Pandurra Formation*

The Pandurra Formation is a thick (>950 m) monotonous sequence of flat lying arenaceous redbed sediments confined to the Cariewerloo Basin on the north-east margin of the Gawler Ranges (Fig 2.2). It consists of medium to coarse grained, poorly sorted quartz and lithic sandstone with minor medium grained sandstone, pebble conglomerate and shale. The Pandurra Formation is interpreted as a continental, dominantly fluvial sequence (Cowley, 1993) although alluvial fan, aeolian and possible deltaic environments have been suggested for some of the formation (Lemon and Gostin, 1983; Lemon, 1972) and a shallow marine environment has also been interpreted (Curtis, 1977; O'Shea, 1982). The age of the Pandurra Formation is uncertain, however it clearly postdates the GRV. Rb - Sr geochronology of interbedded shale and siltstone indicate the unit is pre-Adelaidian, with a minimum age of 1424 ± 51Ma. (Fanning et al., 1983).

*Blue Range Beds*

The Itiledoo Basin is a elongate, east-west basin in the central Eyre Peninsula (Fig. 2.2). Up to 2500 m of sediments have filled the basin and are assigned to the Blue Range Beds (Flint, 1993a). Sediments were deposited in a braided stream - alluvial fan environment, and are dominated by sandy conglomerates with clasts of Hutchison Group lithologies and GRV (Flint, 1993a).

*Cratonisation*

The Gawler Craton was cratonised at about 1450 Ma. and has not been subject to significant deformation or remobilisation since, except for minor epiorogenic movement and intrusion of the Gairdner Dyke Swarm.

*Gairdner Dyke Swarm*

Much of the north-eastern Gawler Craton is cut by a suite of north - north-west and north-west orientated mafic dykes known as the Gairdner Dyke Swarm (Fig. 2.2). Widths of composite dykes probably exceed 50 m and are commonly 30 km or more in length (Cowley and Flint, 1993). Dykes were emplaced around 1100 Ma., at approximately the same time as rifting of the Adelaide Geosyncline (Parker, 1989). The Gairdner Dyke Swarm produces a strong, positive, magnetic response, clearly visible on aeromagnetic maps. These magnetic features crosscut all older units of the Gawler Craton.

### 2.3.2 Mineralisation

*Iron ore*

Iron ore has been mined from the Middleback Ranges for nearly 100 years (Fig. 2.4). The following summary has been taken from various informal publications produced by the Public Affairs Department of BHP Steel. The explorer credited with discovering iron ore in the Eyre Peninsula was Edward John Eyre, and an entry in Eyres' journal, dated 18th September 1840, reports the presence of an ironstone formation atop a hill at the northern end of the Middleback Ranges (probably what is now the Iron Baron or Iron Princess mine). However, it was not until 1897 that the leases were acquired by BHP. The iron ore was initially used as a flux in the smelters across the Spencer Gulf at Port Pirie before being shipped to the Newcastle steel works in 1915, signifying the start of the nation's steel production. Iron ore is still being mined some 80 years later with a number of producing mines along a > 40 km strike length of the Middleback Ranges. Total production of iron ore for each of the principal mining areas up to the end of 1990 stood at:

| | |
|---|---|
| Iron Knob | 130 Mt |
| Iron Baron | 56 Mt |
| Iron Duke | <1 Mt |

*Uranium - copper - gold mineralisation*

The Olympic Dam U - Cu - Au - Ag deposit was discovered in 1975 by Western Mining Corporation and is one of the largest copper and uranium mines in the world. It is located 520 km north-northwest of Adelaide at the northern end of the Stuart Shelf (Fig. 2.2) In 1987 the measured and indicated resource stood at 32 Mt contained copper, 1.2 Mt contained $U_3O_8$, 1200 t contained gold and 7000 t contained silver (Scott, 1987). The orebody occurs beneath 300 m of younger, flat lying sediments, within the Olympic Dam Breccia Complex, a large hydrothermal breccia system. The breccia complex is fully enclosed within the Roxby Downs Granite of the Hiltaba Suite, dated at 1598 ± 2 Ma. to 1588 ± 4 Ma. (Mortimer et al., 1988; Creaser and Cooper, 1993). Detailed descriptions of the history, mineralisation and geology are contained within publications by Scott, (1987), Lalor, (1986), Reeve, (1990a and b), Reeve et al., (1990), Smith, (1993), Creaser, (1989), Johnson and Cross, (1991), Roberts and Hudson, (1983, 1984), Conan-Davies, (1987), Oreskes and Einaudi, (1990, 1992), Bradbury, (1988), Esdale et al., (1987) and Johnson and McCulloch, (1995).

Sub-economic deposits of Fe-Cu-(U-Au) occur 20 km southwest of Olympic Dam at the Acropolis and Wirrda Well prospects (Cross, 1993) and at Oak Dam East, 39 km west of Lake Torrens (Davidson and Paterson, 1993).

*Gold mineralisation*

Quartz-vein hosted gold mineralisation has been mined at the Earea Dam, Glenloth and Tarcoola Goldfields in the north and north-west of the Gawler Range Volcanics Province (Fig. 2.2). Quartz veins in the Earea Dam and Glenloth Goldfields are hosted by Archaean gneiss, whereas those of the Tarcoola Goldfields are hosted by siltstones and quartzites of the Tarcoola Formation (1656 ± 7 Ma., Fanning, 1990). Mineralisation in all three goldfields is interpreted to be related to granitoids of the Hiltaba Suite (Daly, 1993c). Detailed accounts of the mineralisation and geology are presented by Hein et al. (1994), Daly et al. (1990), Blissett, (1985), Fradd, (1988), Circosta and Gum, (1988).

*Base metal mineralisation*

The Menninnie Dam Pb-Zn-Ag deposit is the most significant discovery of base metal mineralisation in the Gawler Craton (Fig. 2.4). Smaller deposits within Hutchison Group sediments have been mined at the Atkinson's Silver Mine and Miltalie Mine 20 km northwest of Cowell (Parker, 1993b), however their relationship to the host metasediments has not been resolved.

## 2.4 Summary

The Gawler Craton is a stable block of late Archaean and Early Proterozoic gneisses, granites and metasediments, Middle Proterozoic sedimentary rocks and extensive acid volcanics. Archaean metasedimentary and volcanic rocks of the Sleaford Complex are more prevalent in the north and west of the craton whereas Palaeoproterozoic rocks are more prevalent in the south-eastern Gawler Craton. The earliest recorded orogenic episode on the Eyre Peninsula, the Sleaford Orogeny, spans the period 2300 - 2637 Ma., and attained upper amphibolite to granulite facies metamorphism. Dutton Suite granitoids were emplaced during the Sleaford Orogeny in the southwest of the Eyre Peninsula.

The Miltali Gneiss and other unnamed gneisses locally separate the Archaean Sleaford Complex from the overlying Palaeoproterozoic Hutchison Group. The Hutchison Group (≈ 1964 - 1845 Ma.) has been divided into three main sequences; the basal Warrow Quartzite, a mixed chemical and clastic sequence (Middleback Subgroup), and an upper pelitic unit (Yadnarie Schist). The depositional environment is interpreted to have been a shallow sea with a north-south trending shoreline with the periods of shoreline progradation and marine transgression.

The Kimban Orogeny (≈ 1845 to 1710) Ma. consisted of three major tectonic events. Peak metamorphic conditions during KM-$D_{1-2}$ attained upper amphibolite facies followed by retrograde upper greenschist facies during KM-$D_3$ (Parker, 1993a). The Wartakan Event (Thomson, 1969) is a later unrelated minor deformation event interpreted to have been related to emplacement of granitoids of the St. Peters Suite (1630 - 1620 Ma., Flint et al.,

1990). The Tarcoola formation (1656 ± 7 Ma.) in the north-west of the GRV province consists of a fluvial to marginal-marine clastic sequence. The Gawler range Volcanics (GRV) consists of an ellipsoidal mass of acid to intermediate variably welded ignimbrites with minor localised lava flows, domes and dykes exposed in the north-central Eyre Peninsula. Two phases of volcanic activity are recognised termed the 'developmental phase' and 'mature phase' by Stewart (1992). The Hiltaba Suite comprises anorogenic granitoids that have formed large batholiths and smaller plutons prevalent around the north-western, western and southern margins of the Gawler Ranges. A mean weighted age of 1589 ± 2 Ma. is obtained for the GRV and Hiltaba Suite (Creaser and Cooper, 1993).

The Corunna Conglomerate occurs as scattered outcrops around the margin of the GRV and is considered to have been deposited in a fluvial to shallow marine environment synchronous with emplacement of the GRV (Daly, 1993b). The Pandurra Formation, Blue range beds, and Gairdner dyke swarm all post date the GRV. The Pandurra Formation consists of redbed sediments of fluvial origin and is confined to the Cariewerloo Basin on the northern side of the Gawler Ranges (Cowley, 1993). The Blue Range Beds are confined to the Itiledoo Basin in the central Eyre Peninsula and consist of sandy conglomerates interpreted to have been deposited in a braided stream - alluvial fan environment (Flint, 1993a). The Gawler Craton was cratonised at about 1450 Ma. and has not been subject to significant deformation or remobilisation since, except for minor epiorogenic movement and intrusion of the Gairdner Dyke Swarm around 1100 Ma.

Units of the Middleback Subgroup in the north-eastern Eyre Peninsula hosts iron ore bodies on which the Australian steel industry was founded over eighty years ago. In the northeast of the Gawler Craton the world class Olympic Dam Cu-Ag-U-Ag deposit is hosted by a hydrothermal breccia developed in a granite of the Hiltaba Suite. The Menninnie Dam Pb-Zn-Ag deposit is the most significant discovery of lead and zinc mineralisation in the Gawler Craton.

# Chapter three
# Prospect geology: The Palaeoproterozoic

## 3.1 Introduction

For the purposes of this thesis, descriptions of the Menninnie Dam prospect geology have been subdivided into the Palaeoproterozoic and the Mesoproterozoic and are reviewed in Chapters three and four respectively. Chapter three incorporates descriptions of:

- Palaeoproterozoic stratigraphy
- Metamorphism
- Deformation
- Intrusions
- Pegmatite veins
- Metasomatism

A local north - south, east - west metric grid was established over the Menninnie Dam prospect by Billiton Australia Ltd. and all local features are referenced to this grid throughout this thesis (Fig. 3.1).

The prospect geology has been interpreted from relogging of all diamond drill holes drilled prior to 1996 (drill holes PD0001 to PD0032), and investigation of more than 300 petrographic sections. Unfortunately, attempts to orientate the drill core during drilling were mostly unsuccessful, and a detailed structural interpretation of the Menninnie Dam prospect is not possible. The orientation of individual rock units has been interpreted from their intersection in two or more drill holes, and on two or more cross sections. Summary drill hole logs and cross sections are presented in Appendix 3.1. An interpretative geological plan, and the 9400 mN cross section are presented as Figures 3.1 and 3.2 respectively. The geology could only be accurately constrained in the immediate vicinity of drill holes and where drill holes are widely spaced, interpretation of the geology has been based on interpolation between drill holes and adjacent east - west sections.

## 3.2 Paleoproterozoic stratigraphy

The Menninnie Dam prospect occurs within a NNE-oriented linear band of magnetic rocks (approximately 5 km long by < 1 km wide), flanked by less magnetic rocks to the east and west (Fig. 3.3). Examination of drill core from the prospect has revealed that the magnetic response is to due to magnetite-bearing marbles, calc-silicate lithologies and iron formations. The non-magnetic rocks to the east and west comprise schist and leucogranite.

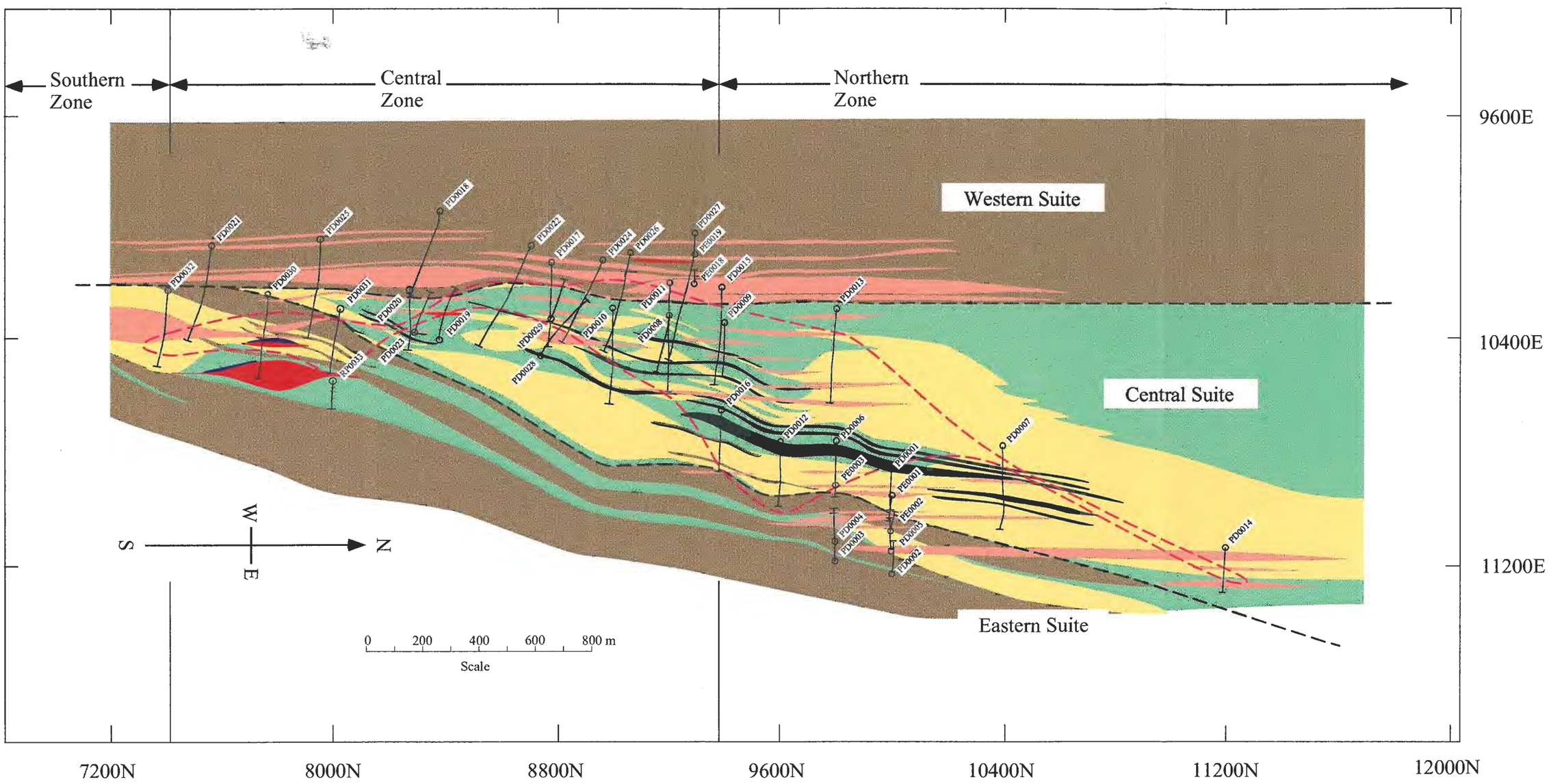


Figure 3.1 Menninnie Dam prospect geology plan (schematic interpretation)

plan view at -65m R.L (approx -280m below ground level). Structure, alteration and mineralisation are not shown.
Local grid scale is in metres

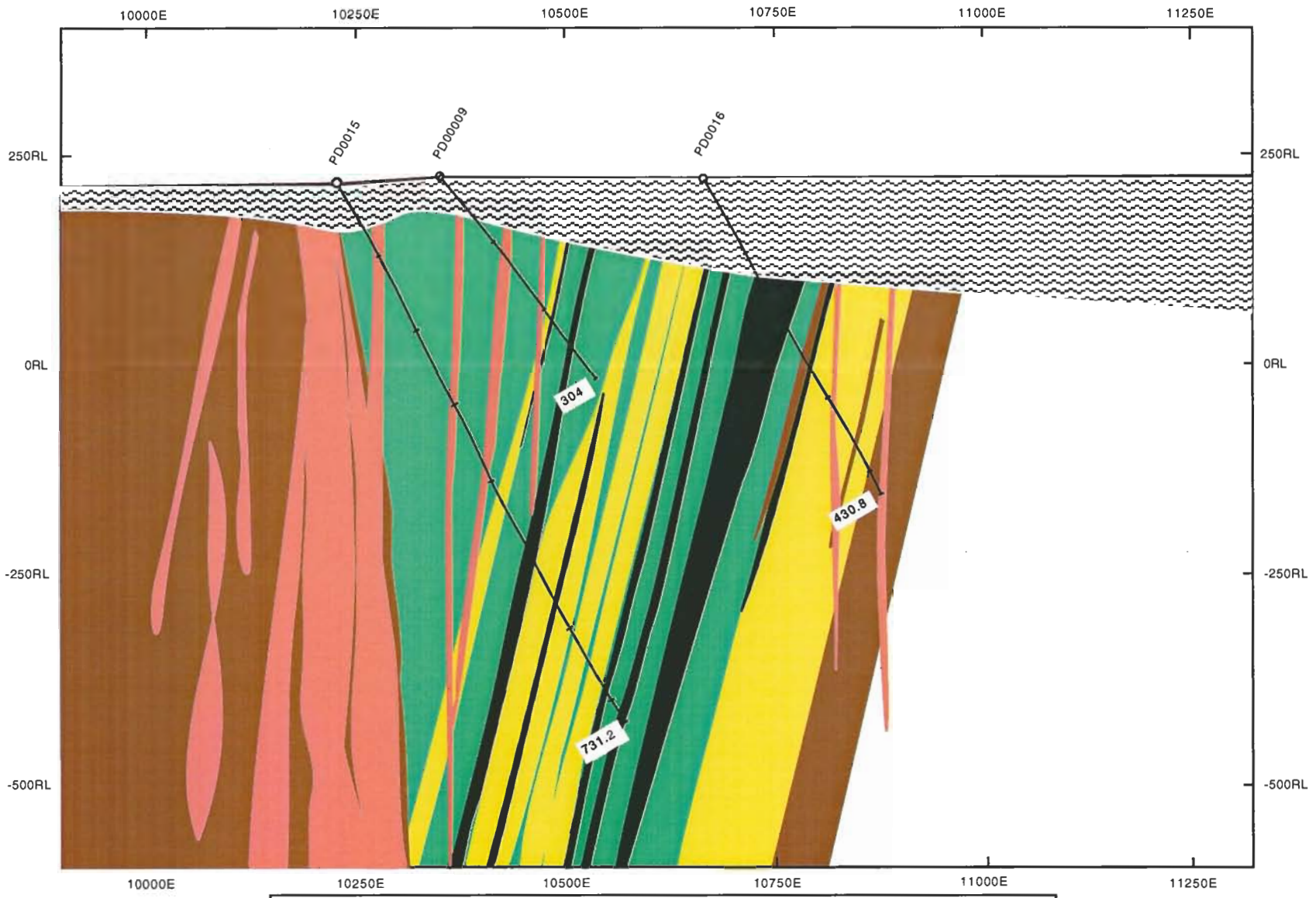


Menninnie Dam, South Australia

Figure 3.2. Section 9400 mN. Schematic geological interpretation
Maximum forward and back extrapolation ± 100m. Drill hole ticks are 100m intervals

## Key to interpretative geology plan and 9400 mN cross section

### Quaternary

Surficial, transported clays and sand. Minor ferricrete and silcrete.

### Mesoproterozoic

Lithic rich Menninnie Dam ignimbrite.

Discordant polymictic breccia

Rhyolitic intrusions.

### Palaeoproterozoic

Granite dykes.

Eastern and western suites. Quartz - feldspar - biotite - muscovite - sillimanite - garnet schist.

Central suite. Carbonate - calc-silicate facies, and silicate facies iron formations.

Central suite. Chaotically banded quartz - diopside rock, massive diopside, and diopside - marble rock with minor disseminated magnetite. Includes minor retrograde metamorphic calc-silicates.

Central suite, dolomitic and calcitic marbles. Minor disseminated and chaotically banded magnetite.

Approximate maximum lateral extent of known mineralisation

Western, central and eastern suite boundaries

Horizontal projection of drill holes

prefix 'PD' = diamond drill hole with percussion precollar
prefix 'PE' = reverse circulation percussion drill hole
prefix 'RP' = rotary air blast percussion drill hole

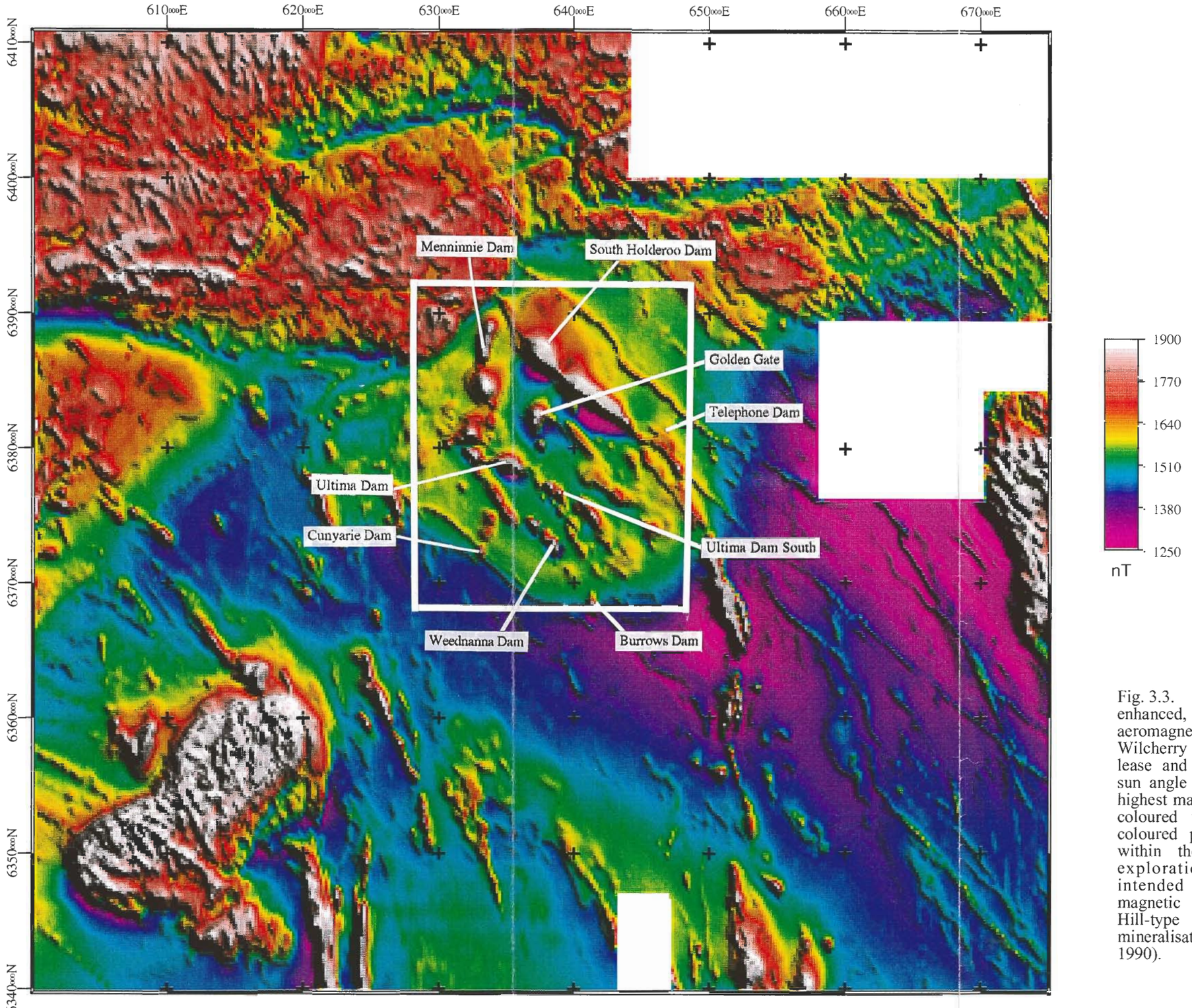


Fig. 3.3. False colour, enhanced, 1:300,000 scale aeromagnetic image of the Wilcherry Hill exploration lease and surrounds. False sun angle is 090°. Units of highest magnetic intensity are coloured white; lowest are coloured purple. Prospects within the Wilcherry Hill exploration lease were intended to test small magnetic highs for Broken Hill-type Pb - Zn - Ag mineralisation (Higgins et al., 1990).

Subdivision of the schists, marble and calc-silicate lithologies into five suites by Higgins and Hellsten (1986) and Higgins et al. (1990) was based on distinct mineralogical and textural characteristics. Since the publication of Higgins et al. (1990), an additional 18 diamond drill holes have been drilled into the prospect, enabling further refinement of the stratigraphy. As a consequence, the original subdivisions have been discarded, and a new subdivision is proposed which divides the prospect geology into western, central and eastern suites. Correlation between the proposed subdivisions and those of Higgins and Hellsten (1986) and Higgins et al. (1990) is presented in Table 3.1.

Table 3.1. Correlation between the proposed subdivisions and those of Higgins and Hellsten (1986) and Higgins et al. (1990)

| Proposed subdivision (this study) | Subdivision of Higgins and Hellsten (1986) and Higgins et al. (1990) |
|---|---|
| Western suite | Suite 5 |
| Central suite | Suites 3 and 4 |
| Eastern suite | Suites 1 and 2 |

The Warrow Quartzite was interpreted by previous authors to occur to the immediate east of the prospect, directly underlying 'suite 1' rocks (Higgins and Hellsten, 1986; Higgins et al., 1990; Beeson, 1990). Warrow Quartzite is also shown in this region on the 1:250,000 scale Yardea geological sheet (Blissett et al., 1988). However, exposures that could be unequivocally assigned to the Warrow Quartzite could not be located within the vicinity of the prospect, and have not been intersected by drilling. Hellsten (1985) observed garnet in weathered surficial rubble to the east of the prospect that had previously been interpreted as Warrow Quartzite sub-crop. Hellsten (1985) suggested the rubble may have been weathered, silicified, impure marble or calc-silicate lithologies rather than Warrow Quartzite.

### 3.2.1 Western suite

The western suite correlates with 'suite 5' of Higgins et al. (1990). The western suite consists of variably sheared and retrograde schist that has been intruded by north - south trending granite dykes. Detailed descriptions of the metamorphism, granite dykes, and deformation are presented in Sections 3.3, 3.4 and 3.5 respectively.

Unaltered schist is preserved as clasts in a protocataclasite (Fig. 3.4a). Clasts consist of dark brown, medium to fine grained, quartz - feldspar - biotite - muscovite - sillimanite - garnet schist. Garnet is rare, constituting less than one percent of the rock. Garnet-rich layers are uncommon, although a one metre wide band with ≈ 12 % disseminated, 1 - 2 mm diameter, garnets was observed in drill hole PD0018. The garnet-rich band is orientated parallel to the metamorphic foliation.

A single 5 m wide zone of migmatite occurs near the end of drill hole PD0023. Pale quartzo-feldspathic segregations ('neosome'; Mehnert, 1968) comprise ≈ 30% of the rock and are separated by medium grey - green schist relicts ('mesosome'; Mehnert, 1968).

Fig. 3.4a. Drill hole PD0018, 256.65 m. Deformed western suite schist. Augen, to elongated clasts of schist (1) are separated by thin zones (2) of sericite and chlorite-altered, brecciated, schist matrix (≈ 10 - 15%). The schistose fabric of protolith clasts is variably orientated indicating clasts have been rotated during deformation. Grain size reduction resulted from brittle fragmentation, and the resultant texture is that of a protocataclasite.

Fig. 3.4b. Drill hole PD0027, 510.6 m. Quartz - diopside rock of the central suite. Quartz (Q) has formed bands and isolated domains in pale green diopside (D). The dark green fine bands near the right hand side of Fig. 3.4b is a fine grained mix of quartz and rod shaped diopside. At the left hand side of Fig. 3.4b, a 3 mm wide, contorted, dark green band of talc and tremolite (T) separates diopside - quartz rock from marble (M).

Fig. 3.4c. Drill hole PD0026, 599.1 m (upper) and 433.9 m (lower). Massive diopside of the central suite.
Upper: light green diopside with dispersed inclusions of magnetite (M). Epidote (E) is interpreted to have formed during retrograde metamorphism.
Lower: light green diopside with minor retrograde minerals including chlorite (C) and garnet (G).

Fig. 3.4d. Drill hole PD0013, 153.5 m. Diopside - marble rock of the central suite. Chaotically banded light green diopside (D) and white marble (M) separated by thin, dark green rinds (T) of tremolite, talc ± serpentine, actinolite and magnetite. Dark flecks of magnetite are dispersed throughout the marble.

Fig. 3.4e. Drill hole PD0008, 277 m. Diopside - marble rock of the central suite. Whitish quartz (Q) is separated from magnetite and serpentine-bearing marble (M) by a halo of light green diopside (D) and dark green intergrown tremolite, talc and serpentinite (T).

Fig. 3.4f. Drill hole PD0027, 483.4 m. Massive, white, dolomitic marble.

Fig. 3.4g. Drill hole PD0015, 509.6 m. Calcitic marble of the central suite with thin biotite-rich metapelitic bands and dispersed flecks of biotite. Some of the metapelitic bands adjacent to the white and pink carbonate-bearing vein (V) have been partially altered to K-feldspar by metasomatic processes (eg. M).

Fig. 3.4h. Drill hole PD0007, 255.2 m. Rock type 5. Calcitic marble with dispersed flecks of dark brown biotite, some of which is altered to dark green chlorite.

3.4a

2 cm

3.4b

2 cm

3.4c

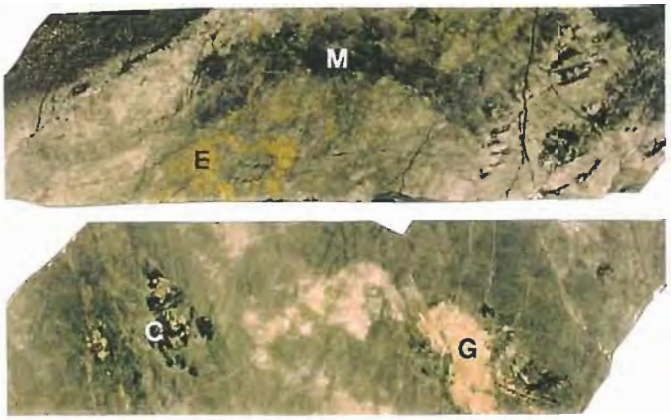


2 cm

3.4d

2 cm

3.4e

2 cm

3.4f

2 cm

3.4g

2 cm

3.4h

2 cm

Most of the schist has been altered, with biotite altered to chlorite, and plagioclase feldspar altered to calcite and sericite.

A fine grained amphibolite unit was encountered near the end of drill hole PD0028. The amphibolite contains hornblende (≈ 38%), plagioclase (≈ 30%), biotite (≈ 15%), quartz (≈ 15%), apatite (≈ 1%) and magnetite (≈ 1%). Minerals have textures typical of high grade metamorphism (Turner, 1980), and a schistose fabric parallel to that of the enclosing schist. The amphibolite does not appear to have been affected by later tectonic deformation (Section 3.5) or by mineralogical changes associated with retrograde alteration (Section 3.3).

### 3.2.2 The central suite

The contact between the central and western suites has a north - south strike and dips steeply to the east. The central suite is characterised by marble and calc-silicate lithologies, iron formations and minor graphitic and meta-pelitic schists. Central suite rocks strike north-northeast and dip between 65° and 80° to the west (Figs. 3.1 and 3.2). The orientation of units has been deduced from drill hole intersections of probable primary sedimentary lithologies, such as iron formations. Iron formations (and by inference, other lithologies) have been deformed into open folds with a ≈ 400 m wavelength and ENE trending fold axes (Fig. 3.1). The central suite is wedge-shaped in plan view and has a minimum present thickness of ≈ 650 m in the north of the prospect, and is absent in the south of the prospect over a distance of ≈ 4 km (Fig. 3.1).

Diopside is the most abundant mineral in calc-silicate lithologies. Tremolite is a minor component (< 5% of the total calc-silicate minerals). Grossular garnet and epidote (< 1%) locally occur in marble and calc-silicate lithologies. Marbles and calc-silicate lithologies can be subdivided into five rock types, based on variations in the ratios of dolomite or calcite, calc-silicate minerals, quartz, and other silicate minerals. These rock types are described in the following sections. Rock types 1 - 4, including the iron formations and the graphitic schists, correspond to suite 4 of Higgins et al. (1990).

*1) Quartz - diopside rock*

Quartz - diopside rock constitutes a few percent of the central suite. The rock is characterised by the presence of quartz with undulose extinction and diopside, and the absence of dolomite or calcite (Fig. 3.4b). Interlayered quartz and diopside bands are a few centimetres to several tens of centimetres thick and have irregular contacts. Dispersed magnetite (< 5%) occurs in some diopside bands. Retrograde mineral assemblages are rare or absent. Small rod-shaped diopside aggregates occur within many of the quartz-rich layers and commonly have long axes that are parallel to quartz - diopside banding, but appear to be discordant to nearby iron formations. Where quartz - diopside rock is in contact with

marble-bearing rock types, quartz-rich layers not occur in contact with marble and are invariably separated by an intervening layer of diopside ± tremolite ± talc (Fig. 3.4b).

The quartz - diopside rock cannot be easily correlated between drill holes or between adjacent sections in a manner that conforms to the interpreted orientation of stratigraphy (Fig. 3.1).

*2) Massive diopside*

Massive diopside is characterised by greater than 70% equigranular, medium to coarsely crystalline diopside (Fig. 3.4c). Magnetite (< 5%), quartz (< 10%), Ca - Mg carbonate (< 10%) and tremolite (< 5%) are accessory minerals in massive diopside units. Where present, magnetite occurs dispersed throughout diopside crystals (Fig. 3.4c), and as thin, highly contorted bands. Accessory quartz and Ca - Mg carbonate are invariably separated by a layer of tremolite or diopside.

Massive diopside units are commonly several metres, to several tens of metres thick, and are commonly discordant to stratigraphic layering. Massive diopside locally has an intense fracture pattern or jig-saw fit breccia texture with light brown garnet, epidote and hematite - dusted albite or microcline as the breccia matrix.

*3) Diopside - marble*

Diopside - marble rock is characterised by variable proportions of equigranular, medium to coarsely crystalline diopside and calcitic or dolomitic marble. Accessory minerals include tremolite, talc, serpentine, actinolite, magnetite and rare quartz. Diopside and marble bands of variable thickness (commonly < 5 cm) are complexly interlayered, resulting in a chaotic banded texture with orientations that vary over distances of a few centimetres (Fig. 3.4d, e). Diopside - marble rock is distributed throughout the central suite and appears to be discordant to stratigraphic layering (Fig. 3.1).

Diopside bands occur as irregularly - shaped lenses that vary in width from tens of centimetres to less than 1 centimetre. Diopside bands of ≥ one metre wide are classified as massive diopside. The contact between diopside and calcitic or dolomitic marble bands typically has an intervening dark green rind of silicate minerals, including tremolite, talc, actinolite, chlorite and serpentine (Fig. 3.4d). Magnetite is locally concentrated in this zone, and also occurs dispersed throughout marble bands, and to a lesser extent, diopside bands. Rock types 2 and 3 together comprise between 50 and 70% of the central suite.

*4) Marble*

This rock type consists of white, off - white, and pale grey, massive, coarsely crystalline dolomitic, and calcitic marble devoid of quartz (Fig. 3.4f). Drill intersections of marble range from 1m to > 100 m. Accessory minerals constitute less than 10% and include

diopside, serpentine, talc, graphite and magnetite. When present, trace amounts of dispersed graphite impart a pale grey colour to the marble. Accessory minerals are more common in calcitic marbles compared to dolomitic marbles and calcitic marble commonly contain between 2 - 10% disseminated (Fig. 3.4g) or chaotically - banded magnetite.

*5) Impure marble*

The impure marble unit correlates with suite 3 of Higgins et al. (1990). This rock type occurs near the eastern extent of the central suite, bounded by iron formations* to the west, and by schists to the east. Impure marble is characterised by calcite with minor biotite, the common presence of thin pelitic schist bands, and little, or no diopside (Fig. 3.4h). Small aligned, biotite flakes (typically < 0.5 mm) occur dispersed throughout the impure marble, resulting in a mottled brownish-green colour. Schist bands comprise less than 10% of impure marble units and are typically 0.3 - 3 cm thick. Biotite (partially altered to chlorite) is the most common silicate mineral in schist bands with minor plagioclase, hornblende, quartz and accessory apatite.

Impure marble units are interpreted to be gradational between the marble, calc-silicate lithologies, and iron formations of the central suite and the meta-pelitic schists of the eastern suite. To the west, the impure marble unit is locally separated from iron formations by several metres of massive diopside rock or diopside - marble rock. However, where these rock types are absent (eg. drill holes PD0001 and PD0007; Appendix 3.1), the contact between the iron formations and impure marble is gradational over several metres (Fig. 3.5a). The gradation from iron formations to impure marble is marked by a progressive decrease in the thickness of iron formation bands from several tens of centimetres, down to less than one centimetre, and the common occurrence of a 1 - 5 mm wide hedenbergite ± diopside ± tremolite band between marble and iron formation bands.

Within 20 m of the eastern suite contact, the amount of dispersed biotite increases gradationally to around 20%, and schist bands become progressively more common and thicker, eventually grading into the eastern suite schists. Near the eastern suite contact, the quartz and feldspar content of schist bands increases, and bands > 0.2 m thick are mineralogically zoned with quartz and minor feldspar occurring in the western portions and biotite in the eastern portions (Fig. 3.5b). This is interpreted to be the metamorphosed equivalent of graded argillaceous sandstone beds and is used to propose an eastward younging direction.

A significant proportion of impure marble rock has a mottled pale pinkish and pale apple green colour interpreted to be a result of metasomatism. Mineral changes associated with metasomatism are described in Section 3.7.

---

* Iron formations are described in more detail on Page 3.6

*Iron formations*

In this study, iron formations are considered to be sedimentary units containing greater than 15 wt.% total iron in accordance with the definitions of James (1954) and Gross (1991). Packets of banded, iron-rich metasediments (iron formations) are a minor component of the central suite. Iron formations appear to be lenticular, with individual lenses ranging from several hundred metres to several kilometres in length (Fig. 3.1). Iron formations in the western half of the central suite are less than a few metres thick, whereas those in the eastern part of the central suite reach 20m in thickness.

Iron formations consist of 0.5 cm to 10 cm thick bands rich in iron silicate and oxide minerals including hastingsite / ferrohastingsite, grunerite, hedenbergite, biotite, magnetite ± almandine garnet, alternating with 0.3 to 5 cm thick layers of either quartz, marble, or diopside (Fig. 3.5c). The proportions of amphibole, pyroxene, biotite, magnetite and garnet vary widely, but not systematically, between iron formations, and in many iron formations, garnet and quartz are absent. Iron formations and the intervening quartz, diopside or marble bands have granoblastic textures (Turner, 1980), and a foliation formed by the preferred orientation of amphibole and biotite (Fig. 3.5d). Iron formations hosted by marble are commonly surrounded by a halo of calc-silicate minerals including hedenbergite, diopside, tremolite, garnet and epidote.

*Graphitic Units*

Minor graphitic schist units occur in the central suite (eg. drill holes PD0008 and PD0031; Appendix 3.1). Graphitic schists range from 0.5 - 10 m thick and are probably lenticular in shape, rarely exceeding a few hundred metres in maximum lateral extent. They consist of dark grey to black meta-pelitic schist with a graphite content between 5 and 10% (Fig. 3.5e). Traces amounts of pyrite, sphalerite and galena are locally present, and typically occur in thin veins and segregations that crosscut the metamorphic fabric (Fig. 3.5e). Sulphides textures are described in Chapter 5.

### 3.2.3 Eastern suite

The contact between the carbonate and calc-silicate lithologies of the central suite and the schists of the eastern suite is gradational over several metres. The boundary between the central and eastern suites is arbitrarily placed at the first occurrence of a schist band more than 5 m thick. The eastern suite consists of dark brown, biotite - quartz - feldspar - muscovite - sillimanite - almandine garnet schist with trace amounts of graphite and pyrite (Fig. 3.5f). Graphite and pyrite are part of the prograde mineral assemblage and commonly occur intergrown with garnet and biotite. Plagioclase has been partially altered to sericite and fine grained calcite and biotite has been partially altered to chlorite.

Fig. 3.5a. Drill hole PD0006, 382 m. The contact between iron formations and marble is gradational over several metres. Iron formation bands (IF) comprise intergrown hastingsite, biotite and magnetite, commonly with an outer rind of hedenbergite or diopside ± tremolite. Metapelitic bands (MP) comprise disseminated biotite with accessory magnetite, hornblende, and apatite. Biotite is commonly partially altered to dark green chlorite.

Fig. 3.5b. Drill hole PD0016, 400.6 m. The contact between impure marble and eastern suite schist is gradational and the metapelitic component increases towards the east. Some metapelitic bands are mineralogically zoned with quartz and feldspar-rich bases (B) and biotite-rich tops (T), interpreted as metamorphosed graded beds. Metapelitic bands are separated by calcitic marble with disseminated biotite (C).

Fig. 3.5c. Upper: drill hole PD0026, 524 m. Silicate facies iron formation, with bands of greyish quartz (Q) separated by darker bands (IF) of hastingsite / ferrohastingsite, grunerite, hedenbergite, biotite ± magnetite ± almandine garnet.
Lower: Drill hole PD0006, 179 m. Carbonate facies iron formation with bands of whitish marble, disseminated biotite and hedenbergite (1), separated by dark bands of hastingsite / ferrohastingsite, grunerite, hedenbergite, biotite almandine garnet ± diopside ± magnetite (2).

Fig. 3.5d. Drill hole PD0016, 254.5 m. Transmitted light photomicrograph of a silicate facies iron formation band consisting of intergrown, aligned, biotite flakes (B), olive green hastingsite (H), magnetite (M), garnet (G), and quartz (Q).

Fig. 3.5e. Drill hole PD0008, 192 m. Graphitic schist with cross-cutting veinlets of sphalerite, galena and pyrite (S). Graphitic schist has a metamorphic schistosity, whereas sulphide veinlets do not appear to have been metamorphosed.

Fig. 3.5f. Drill hole PD0006, 410.6 m. Transmitted light photomicrograph (x nicols) of eastern suite quartz - K-feldspar (K) - biotite (B)- plagioclase (P) - sericite - muscovite (M)- sillimanite - calcite - garnet (G) schist.

3.5a

3.5b

3.5c

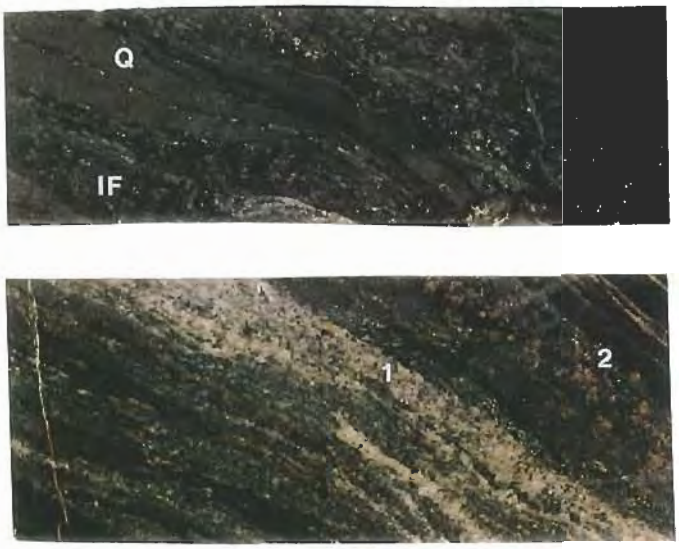


3.5d

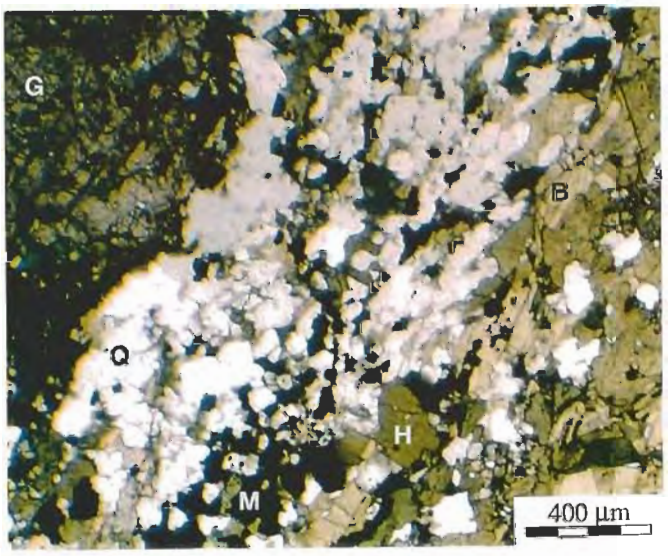


3.5e

3.5f

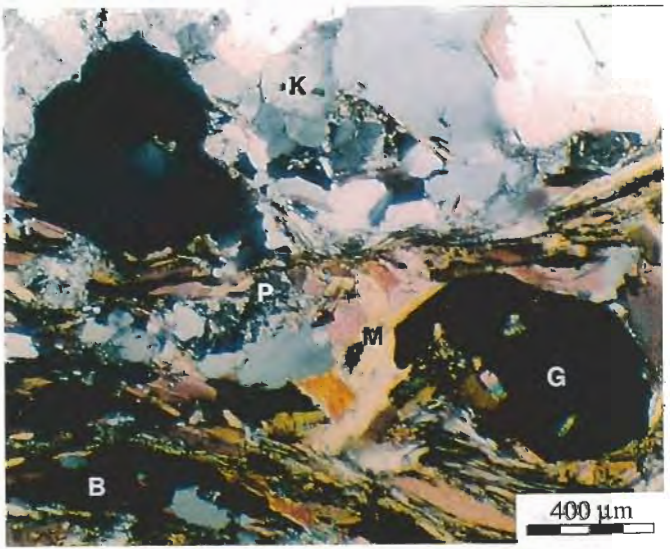

A 2 - 3 m thick, medium grained, hornblende amphibolite with trace amounts of quartz was intersected in the south of the prospect (ie. drill hole PD0031 at 525 m; Appendix 3.1). Lithologic contacts between the amphibolite and schist are sharp and parallel to the schistose fabric. The mineralogy and texture of the amphibolite is similar to the amphibolite intersected in the western suite schists (Section 3.2.1).

Calc-silicate, marble and graphitic schist units several metres thick occur as lenticular, to continuous, units within the eastern suite schist, particularly near the contact of the eastern and central suites and is interpreted as a transitional assemblage between the central and eastern suites. The calc-silicate and marble units within the eastern suite equate to 'suite 1' of Higgins and Hellsten (1986) and Higgins et al. (1990). Suite 1 was previously interpreted to directly overly the Warrow Quartzite (Higgins and Hellsten, 1986). However, subsequent drilling has shown that meta-pelitic schist of the eastern suite lie to the east of 'suite 1'. The thickness of the eastern suite schist is not known. A minimum thickness of 50 m has been defined by drilling although aero-magnetic data is interpreted to indicate a substantially greater thickness (Chapter 6).

## 3.3 Determination of the metamorphic history at Menninnie Dam

Higgins and Hellsten (1986) and Lee (1989) used mineral assemblages to interpret the host rocks *and* mineralisation at Menninnie Dam to have been subjected to amphibolite facies regional metamorphism (650 - 700°C; 3 - 5 kbars). A retrograde metamorphic event was also recognised. Parker (1993a) estimated similar peak metamorphic temperatures of 600 - 700°C, but higher pressures (5 - 8 kbars) for the central Eyre Peninsula.

In this section, the peak and retrograde metamorphic conditions that the Menninnie Dam host rocks were subjected have been established using the compositions of biotite, garnet and plagioclase for thermobarometric calculations. Comprehensive reviews of mineral thermobarometry have been presented by Ferry, (1982), Spear (1993) and Kretz, (1994).

### 3.3.1 Methods

A sample of schist from 410.6 m in drill hole PD0006 comprised the least altered or deformed* portion of eastern suite schist encountered during drilling at Menninnie Dam. Mineral abundances for this sample have been visually estimated at; 29% quartz, 27% K-feldspar, 22% biotite, 7% plagioclase, 5% sericite, 4% muscovite, 3% fibrous sillimanite, 2% calcite, 1% garnet, and trace amounts of chlorite, graphite, Fe-Ti oxides (ilmenite?), pyrite, apatite and zircon (Fig. 3.5f). Retrograde alteration is minimal, with partial replacement of plagioclase by a fine grained mixture of sericite, calcite and quartz, local alteration of biotite to chlorite and minor alteration of sillimanite margins.

---

* Deformation and alteration of lithologies at Menninnie Dam are introduced in Section 3.5.

The bulk rock composition was determined by XRF analysis at the Geology Department, University of Tasmania. Mineral compositions were determined using a Cameca SX50 electron microprobe in the Central Science Laboratory, University of Tasmania under the supervision of W. Jablonski. Details of the procedures and machine settings for XRF analysis and microprobe analysis are included in Appendices 3.2.

Garnet porphyroblasts were analysed at spacings of ≈ 50 μm along a line bisecting the garnet using a beam diameter of 10 μm. The outer-most spot analysed was situated as close as possible to the edge of the garnet. Eight additional analyses from within 20 μm of the margins of garnet and biotite crystals in mutual contact were also obtained.

Only visually unaltered biotite crystals were selected for microprobe analysis. Biotite was analysed with a beam current of 10 nA, to avoid volatilisation of lighter elements. In addition to the eight biotite microprobe analyses mentioned above, three analyses were obtained from the cores of large biotites crystals well away from contacts with other Fe or Mg bearing minerals.

Plagioclase compositions are required for a number of geobarometers. Unaltered plagioclase crystals were analysed from one margin to the next at ≈ 50 μm intervals in order to examine element zoning. K-feldspar was analysed in order to compare the composition with that of plagioclase.

### 3.3.2 Analytical results

Results of XRF analyses are presented in Table 3.2. This sample of the eastern suite schist has a high potassium content, which is consistent with the high potassium content for most rock suites at Menninnie Dam (Beeson, 1990b).

Table 3.2. XRF bulk rock analysis of eastern suite schist from 410.6 m in drill hole PD0006.

| Major elements | (wt.%) | Trace elements | (ppm) |
|---|---|---|---|
| $SiO_2$ (wt.%) | 57.46 | Y | 35 |
| $TiO_2$ | 0.78 | Rb | 283 |
| $Al_2O_3$ | 17.83 | Cu | 36 |
| $Fe_2O_3$* | 9.51 | Pb | 52 |
| MnO | 0.39 | Zn | 173 |
| MgO | 3.08 | Ni | 43 |
| CaO | 0.79 | U | 4 |
| $Na_2O$ | 0.89 | Th | 21 |
| $K_2O$ | 5.55 | Nb | 18 |
| $P_2O_5$ | 0.14 | Zr | 213 |
| LOI | 2.58 | Sr | 74 |
| | | Ba | 864 |
| | | Sc | 19 |
| Total | 99.05 | V | 110 |

*total iron is calculated as $Fe_2O_3$

Results of garnet, biotite, K-feldspar and plagioclase electron microprobe analyses are summarised in Tables 3.3 - 3.7 and detailed in Appendix 3.3. Element variations associated with zoning in garnets are illustrated in Figures 3.6a -d.

Table 3.3 Compositional range of 75 garnet analyses (wt. %). Complete analyses are listed in Appendix 3.3

| Element oxide* | Range (wt.%) |
|---|---|
| CaO | 0.912 - 4.543 |
| MgO | 1.125 - 2.764 |
| FeO | 25.667 - 29.270 |
| MnO | 7.632 - 12.814 |

*Garnet compositions have been recalculated on the basis of 8 cations and 12 oxygens using MinTab version 1.1 (Rock and Corroll, 1990), which uses the procedures of Droop (1987). Iron, analysed as FeO, was not recalculated as FeO + $Fe_2O_3$ as $Fe^{3+}$ is unlikely to have been significant in this graphite-bearing assemblage. The mean garnet end member composition was calculated as: 8.5% andradite, 61.6% almandine, 8.5% pyrope, 21.4% spessartine.

Manganese concentrations are elevated in the margins and weakly elevated in the core of garnets (Fig. 3.6d). Almandine garnets with elevated Mn concentrations in their cores are common in many metapelites (Turner, 1980; Spear, 1993) due to the high affinity of garnet for $Mn^{2+}$ (Sturt, 1962). Later overgrowths of garnet resulted in isolation of the garnet core, and the higher Mn signature of the core was retained due to unfavourable diffusion kinetics (Turner, 1980). Decreased Fe, Ca and Mg concentrations at garnet margins (Figs. 3.6a - c) are interpreted to have resulted from depletion of Fe, Ca and Mg and their preferential inclusion in other minerals such as biotite and plagioclase during a decompressional cooling path. The corresponding rise in Mn content at garnet margins (Fig. 3.6d) is a result of Fe, Ca and Mg consumption during this stage.

Table 3.4. Average biotite analyses (wt.%). N = number of analyses. The composition of biotite cores is similar to that of biotite rims. Complete analyses are listed in Appendix 3.3.

| | N | MgO | $Al_2O_3$ | $SiO_2$ | $K_2O$ | $TiO_2$ | MnO | FeO |
|---|---|---|---|---|---|---|---|---|
| Biotite margins | 17 | 8.09 | 19.74 | 33.85 | 9.36 | 2.52 | 0.31 | 19.65 |
| Biotite cores | 3 | 7.88 | 19.65 | 34.00 | 9.64 | 2.34 | 0.36 | 19.77 |

Table 3.5 Average analyses (wt.%) of K-feldspar and plagioclase. N = number of analyses. Complete analyses are listed in Appendix 3.3.

| | N | $Na_2O$ | $Al_2O_3$ | $SiO_2$ | $K_2O$ | CaO |
|---|---|---|---|---|---|---|
| K-feldspar | 9 | 1.12 | 19.00 | 62.94 | 14.86 | 0.03 |
| Plagioclase | 8 | 7.54 | 25.24 | 59.1 | 0.31 | 6.32 |

Element zoning in K-feldspar, plagioclase or biotite was not detected and may have resulted from metamorphic homogenisation.

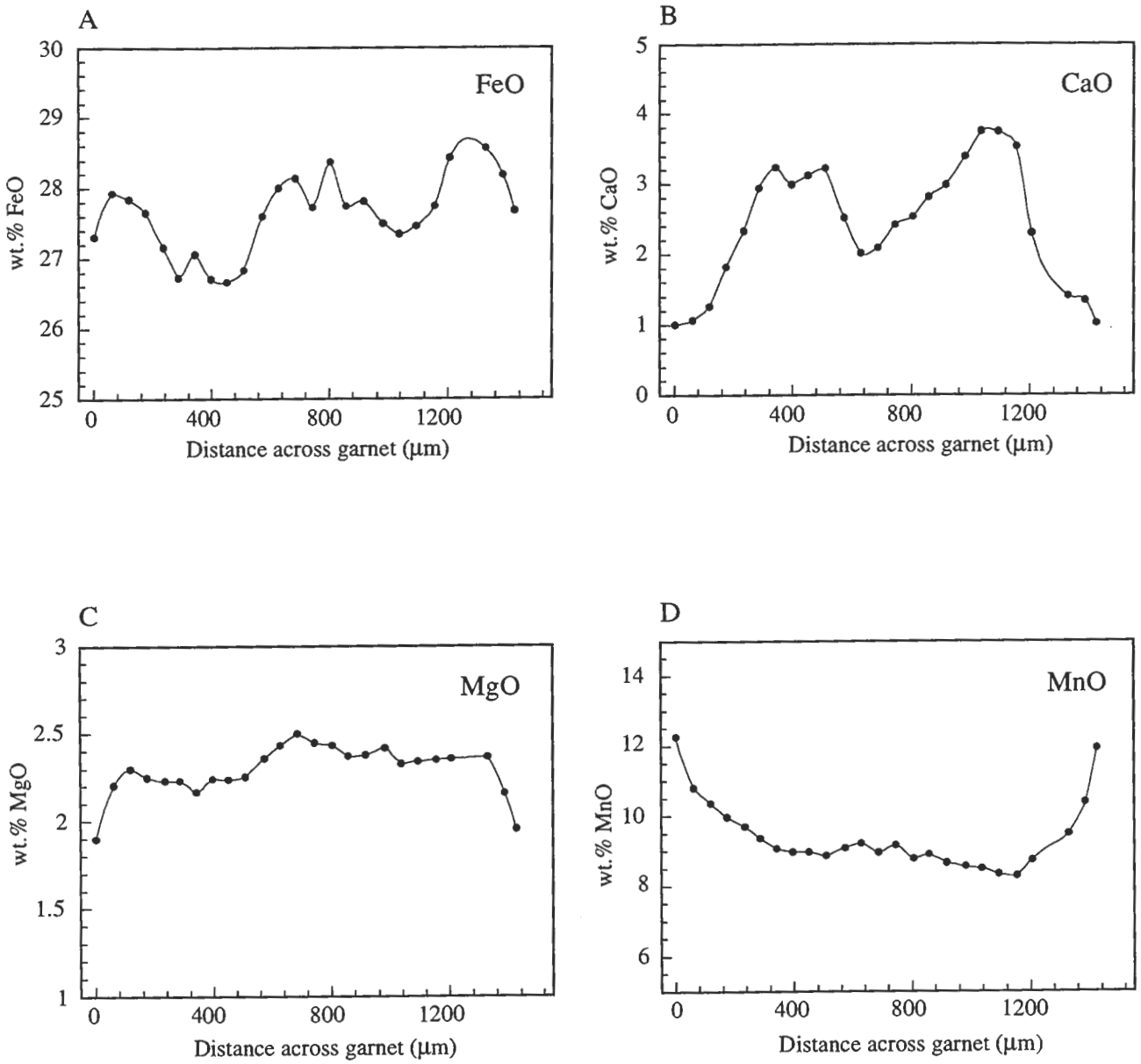


Fig. 3.6. Oxide variations across a zoned almandine garnet (garnet 1A; Appendix 3.3). Refer to the text for interpretation.

### 3.3.3 Thermobarometric calculations

Frost and Tracy (1991) outline minimum criteria for calculation of P - T - time paths from zoned garnets, which include:

1) The equilibrium mineral assemblage or assemblages present at all stages of garnet growth must be known
2) The changes in composition of phases participating in the garnet-producing reaction, particularly biotite and plagioclase, must be known.
3) Any modification of growth zoning by post-crystallisation diffusive processes must be understood.
4) Any P-T changes must be corroborated by textural or structural evidence.

Garnets in the eastern suite schist commonly contain inclusions of other minerals (Figs. 3.7a, b). Quartz and biotite are present as inclusions throughout garnet crystals. Muscovite inclusions have only been observed in garnet cores. Fe-Ti - oxides (ilmenite?) are disseminated throughout garnet crystals, commonly in association with an unknown fine grained, high relief, mineral with high interference colours (sphene?). Trace amounts of graphite are also present. Rare, fine-grained mica ± chlorite pseudomorphs of an unknown mineral are present in the mid zones of some garnets. Rare inclusions of feldspar have been observed but are not present in sufficient quantities to determine their distribution. Sillimanite inclusions have not been observed in garnet.

As biotite inclusions are present at all stages of garnet crystal growth, determination of the temperature range over which metamorphism occurred can be attempted using biotite - garnet geothermometers (eg. Ferry and Spear, 1978; Berman, 1990) providing the composition of biotite is known at all stages of garnet growth. However, due to the small number of biotite inclusions in garnet crystals, their compositions have not been systematically analysed. An approximation of the biotite composition can be estimated based on the following argument: The amount of garnet in eastern suite schists (≈ 1 wt.%) is significantly less than that of biotite (≈ 25 wt.%), and the diffusion rate in garnet is slow (Turner 1980). Therefore, assuming a closed system in which the abundance of other Fe - Mg minerals was insignificant (probably reasonable for peak and post-peak metamorphic conditions), any changes in the bulk iron or magnesium content of biotite due to changes in P - T conditions are likely to have been insignificant compared to changes preserved in garnet. Analyses of biotite cores are similar to those of biotite in contact with garnet (Table 3.4), probably indicative of homogenisation during peak and retrograde metamorphism. As there is little variation in biotite compositions, an average composition must be assumed.

The composition of garnets in the eastern suite schist are significantly higher in Mn and Ca than those used by Ferry and Spear (1978) to develop their garnet - biotite geothermometer.

Fig. 3.7a, b. Drill hole PD0006, 410 m. Fig 3.7a Transmitted light photomicrograph, Fig. 3.7b reflected light photomicrograph. Garnets contain inclusions of quartz, biotite, muscovite, rare plagioclase, oxides (ilmenite?), sphene, mica ± chlorite pseudomorphs of an unknown precursor, and trace amounts of graphite. Not all mineral inclusions are present in all garnets. The garnet shown, contains inclusions of quartz (Q), biotite (B), oxides (FT), and partially altered plagioclase (P).

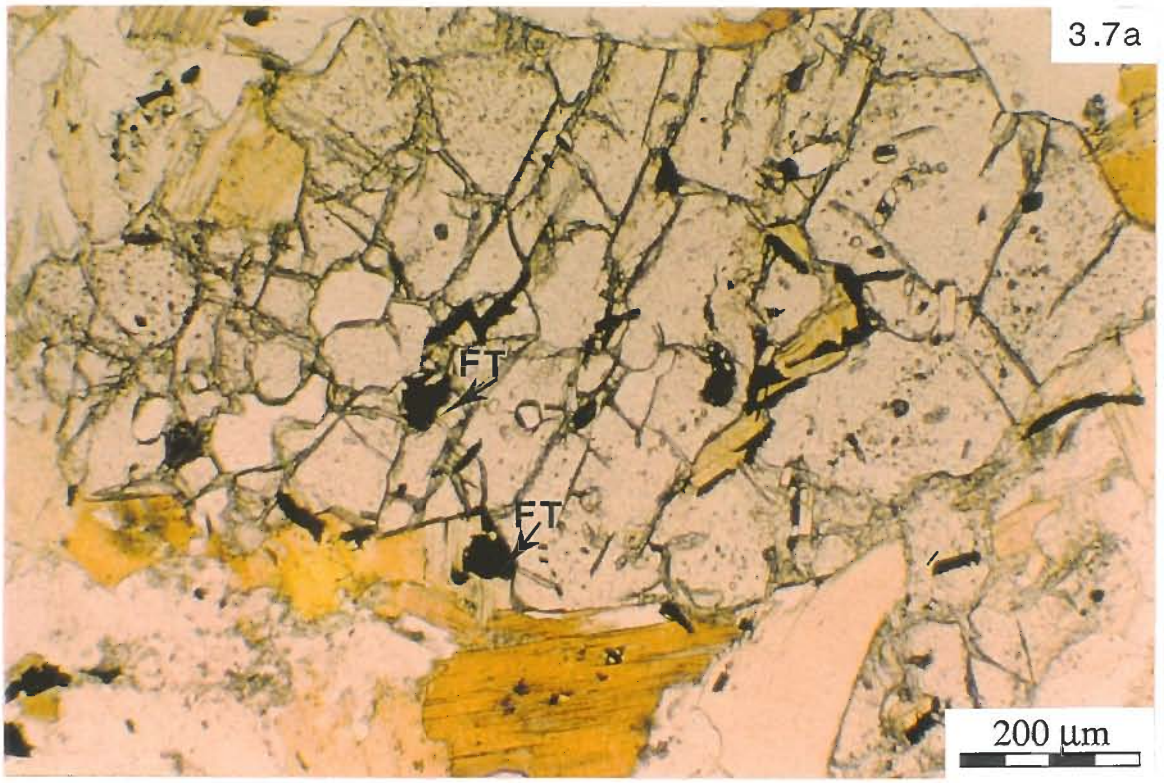
3.7a
FT
FT
200 µm

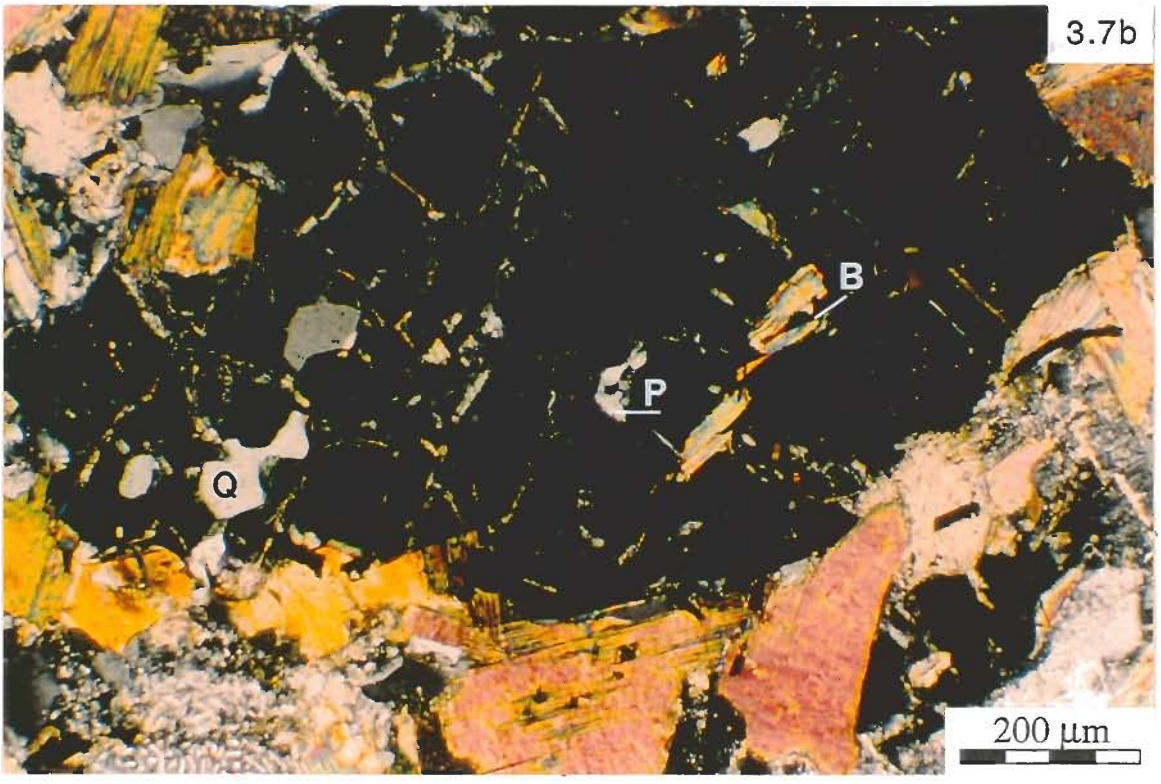
3.7b
B
P
Q
200 µm

Berman (1990) developed a mixing model for quaternary Ca-Mg-Fe-Mn garnets intended to compensate for the effects of Mn and Ca. The calibrations of Ferry and Spear (1978) and Berman (1990) have been combined in the computer program by Spear and Peacock (1990) and used for this study.

Quartz is present as inclusions throughout garnet crystals and is interpreted to have been stable throughout the metamorphic event. Preservation of muscovite inclusions in the cores of garnet crystals and the common occurrence of K-feldspar throughout the rock is consistent with reaction between muscovite and quartz to form sillimanite and K-feldspar at higher metamorphic grades (Turner, 1980). Geobarometers involving muscovite are therefore unlikely to result in realistic pressure estimates. Geobarometers involving sillimanite are likely to be applicable to peak metamorphism only.

Plagioclase is likely to have been a stable phase above upper greenschist facies (Turner, 1980) although its composition is likely to have varied throughout the metamorphic event. As plagioclase comprises only ≈ 7% of the rock and has an average composition of ≈ $An_{31}$, use of an average composition as representative of all stages of metamorphic growth is unlikely to be valid. Application of average plagioclase compositions for geobarometric calculations commonly results in an over estimate of the pressure conditions for all but the final stages of metamorphism . This is due to an increase in the calcium content of garnet and a corresponding decrease in the calcium content of plagioclase at higher metamorphic conditions (Frost and Tracey, 1991; Figs. 3.8a, b). If the plagioclase is assumed to comprise $An_{100}$ (ie. retained all of its calcium) then a lower limit of peak pressure and temperature conditions can be calculated (Figs. 3.8c, d).

Garnet, biotite, quartz and plagioclase are likely to have been stable phases throughout the period of garnet growth, and with the caveat of assumed compositions for biotite and plagioclase, criteria 1 - 3 of Frost and Tracey (1991) are satisfied within the limitations of these data. A garnet which had the most symmetrical element zonation pattern was chosen for thermobarometric calculations (Figs. 3.6a - d; Appendix 3.3, 'garnet 1A'). Garnet compositions with the highest calcium contents have been used for determination of peak metamorphic conditions using the biotite - garnet geothermometer of Ferry and Spear (1978), and Berman (1990) in combination with the garnet - plagioclase - sillimanite - quartz geobarometer of Koziol (1989) and the garnet - plagioclase - quartz - biotite geobarometer of Hoisch (1990). Garnet and biotite margins in mutual contact have been used to calculate the final metamorphic conditions at which these minerals attained equilibrium using an average biotite composition and the biotite - garnet geothermometer of Ferry and Spear (1978), and Berman (1990), and the garnet - plagioclase - quartz - biotite geobarometer of Hoisch (1990). Results are illustrated in Figure 3.8e and summarised in Table 3.6.

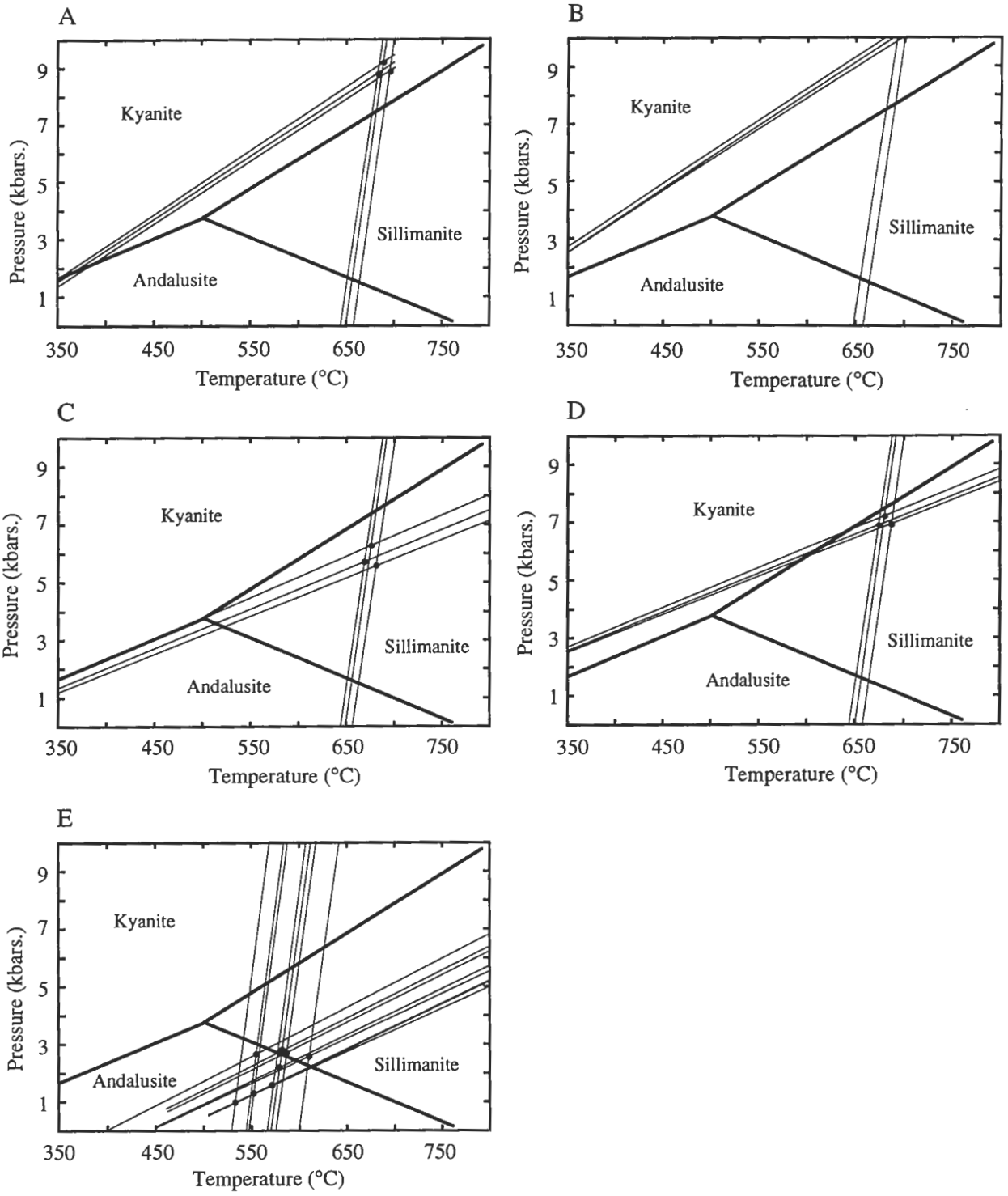


Fig. 3.8. Pressure vs temperature plots for calculated peak (A - D) and final (E) metamorphic conditions at Menninnie Dam using the garnet biotite geothermometer calibrations of Ferry and Spear (1978) and Berman (1990) and various geobarometers and plagioclase compositions. A) Garnet - biotite - quartz - plagioclase geobarometer (Hoisch, 1990) and plagioclase composition of $An_{31}$. B) Garnet - silimanite - quartz - plagioclase geobarometer (Koziol, 1989) and plagioclase composition of $An_{31}$. C) Garnet - biotite - quartz - plagioclase geobarometer (Hoisch, 1990) and plagioclase composition of $An_{100}$. D) Garnet - silimanite - quartz - plagioclase geobarometer (Koziol, 1989) and plagioclase composition of $An_{100}$. Garnet - biotite - quartz - plagioclase geobarometer (Hoisch, 1990) and plagioclase composition of $An_{31}$.

Table 3.6. Summary of calculated peak and final metamorphic conditions.

| Metamorphism | Thermometer | Barometer | Plagioclase | Temperature (°C) | Pressure (kbar) |
|---|---|---|---|---|---|
| Peak | Gnt - bio | Gnt - plag - qz - bio | $An_{31}$ | 650 - 700 | 9 |
| | Gnt - bio | Gnt - plag - sill - qz | $An_{31}$ | ≈ 700 | 10 |
| | Gnt - bio | Gnt - plag - qz - bio | $An_{100}$ | ≈ 650 | 6 |
| | Gnt - bio | Gnt - plag - sill - qz | $An_{100}$ | ≈ 650 | 7 |
| Final | Gnt - bio | Gnt - plag - qz - bio | $An_{31}$ | 500 - 600 | 1 - 3 |

In accordance with criteria 4 of Frost and Tracy (1991), the application of this technique can be tested by comparison between calculated values, mineral textures and previously determined P - T conditions. Calculations of peak metamorphic conditions that include plagioclase = $An_{31}$, result in pressure estimates that are inconsistent with the presence of sillimanite. More realistic estimates are obtained by constraining metamorphic conditions to the sillimanite stability field and using geobarometer calculations that include plagioclase = $An_{100}$, to give minimum pressure. The final metamorphic conditions at which biotite and garnet attained equilibrium are near the sillimanite - andalusite boundary, or, within the andalusite field. Estimates near the sillimanite - boundary are more consistent with the absence of andalusite, however, the absence of andalusite at lower pressures and temperatures probably reflects the bulk rock composition (Table 3.2) which is too K-rich for $Al_2SiO_5$ stability, except above the quartz - muscovite breakdown reaction.

Estimated peak and final pressure and temperature conditions for rocks at Menninnie Dam are illustrated as fields in pressure - temperature space (Fig. 3.9) with inclusion of the geobarometer error limits estimated by Kohn and Spear, (1991a, b), and the geothermometer error limits estimated by Ferry and Spear (1978). Peak metamorphic conditions calculated for Menninnie Dam rocks lie to the left of the quartz - muscovite break-down curve estimated by Spear and Cheney (1989; Fig. 3.9), The occurrence of sillimanite and K-feldspar is interpreted to indicate that the activity of water was less than 1.0 (Spear and Cheney 1989). Relatively dry conditions are consistent with calculated pressure and temperature conditions which lie to the right of the minimum melting curve for common granite (wet solidus; after Turner, 1980).

Peak pressure and temperature conditions calculated for Menninnie Dam (5 - 7 kbar and 600 - 700°C) are lower than those estimated for KM-$D_{1-2}$ in the southern Eyre Peninsula (> 8 kbar and 800 - 900°C; Mortimer et al., 1980; Bradley, 1980; Fig. 3.9) but comparable to KM-$D_{1-2}$ estimated for the Cowell Cleve area of the central Eyre Peninsula (7 kbar and 700°C, Parker, 1978; Fig. 3.9). Parker (1993a) described KM-$D_3$ as a retrograde metamorphic event (KM-$D_3$ = 1.5 - 2 kbars and 450 - 550°C), with pressure and temperature conditions that peaked below the andalusite - sillimanite - kyanite triple point (Fig. 3.9).

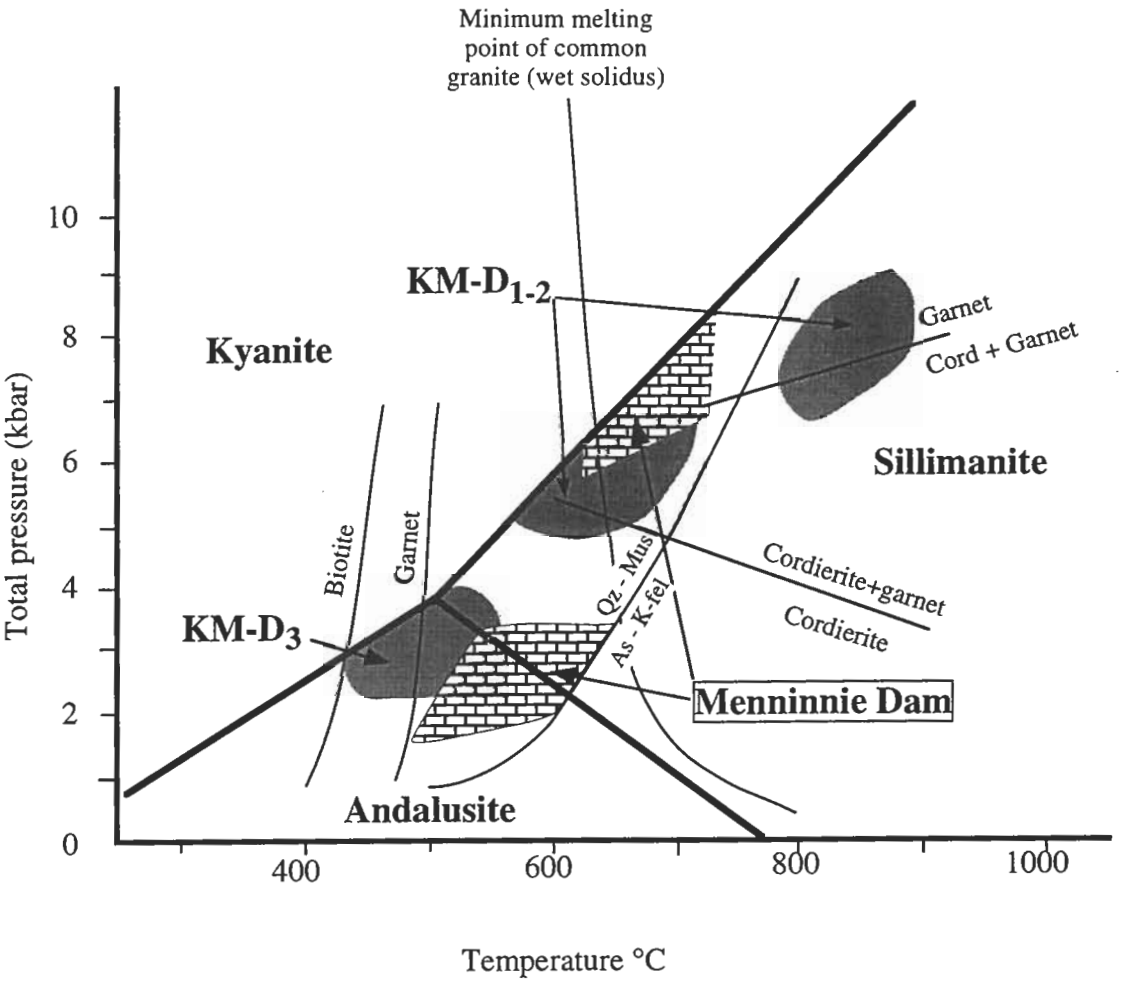


Figure 3.9 Metamorphic grade of the Kimban Orogeny events on the eastern Eyre Peninsula (modified from Parker, 1993a). Higher metamorphic conditions during KM-$D_{1-2}$ are recorded for the southern Eyre Peninsula compared to the central Eyre Peninsula. Peak and retrograde metamorphic conditions at Menninnie Dam overlap those estimated for the central Eyre Peninsula. $Al_2SiO_5$ polymorph curves after Holdaway, (1971), lower stability limit for biotite after Winkler, (1976), lower stability limit for almandine after Winkler, (1976), stability field for bulk Fe/(FeO + MgO) ratio of 0.6 (cordierite + garnet) after Currie, (1971). Muscovite - quartz / aluminium silicate - K-feldspar curve after Spear and Cheney (1989). Minimum melting point of common granite (wet solidus) after Turner (1980).

Calculated pressure and temperature conditions for the final metamorphic event at Menninnie Dam (≈ 1 - 3 kbars and 450 - 650°C) are similar to those estimated by Parker (1988) for KM-$D_3$. The Menninnie Dam host lithologies have undergone a similar metamorphic history to that of the Central Eyre Peninsula.

## 3.4 Granite dykes

The western, central and eastern suites at Menninnie Dam have been intruded by numerous granite dykes ('MD granite dykes'). MD granite dykes are more common in the western suite schists (≈ 40%) than in either the central or eastern suites (≈ 5%). Beeson (1990b) noted the occurrence of granitoids at Menninnie Dam but did not resolve whether they were intrusions or "metamorphosed tuffaceous units". Scattered exposures of granite of the Lincoln Complex occur ≈ 5 km to the east of the Menninnie Dam prospect (Blissett et al., 1988). This granite was interpreted by Parker (1993a) to be a late, syntectonic granite, associated with KM-$D_3$ (Moody Suite correlative, Fig. 3.10).

The aim of this section is to:

- Describe the morphology and mineralogy of the MD granite dykes.
- Compare the major and trace element geochemistry of the MD granite dykes with those of other granite bodies from the Eyre Peninsula.

### 3.4.1 MD granite dyke description

The width of MD granite dykes vary in drill intersection from 10 cm to in excess of 60 m (Figs. 3.1, 3.2; Appendix 3.1). MD granite dykes within the western suite schists strike north - south and have been traced through drilling over distances ≈ 2 km whereas those in the central and eastern suites cannot be easily correlated between sections spaced 200 m apart. MD granite dykes in the central suite locally crosscut iron formations, typically at angles of 5 - 30°, which is considered to be evidence for an intrusive origin.

MD granite dykes in the eastern, central and western suites have similar textures and mineralogy. They do not have chilled margins and comprise uniform, medium-grained, leucogranites with less than 5% mafic minerals . The granite dykes are composed of 20 - 35% quartz (0.5 - 3 mm), 30 - 65% orthoclase and microcline (0.5 - 5 mm), 5 - 20% albite (0.1 - 2 mm), 1 - 7% muscovite (< 2 mm), < 2% biotite (< 0.5 mm), < 2% chlorite, < 2% calcite, < 3% sericite, and trace amounts of zircon, apatite, hematite, magnetite, leucoxene, pyrite, chalcopyrite and sphalerite.

Two types of quartz have been recognised. Quartz is present as 20 - 200 μm rounded inclusions within orthoclase and, rarely, albite. Quartz also occurs as discrete grains or clusters up to several mm in diameter interstitial to feldspar crystals. Poikilitic orthoclase contains inclusions of quartz, albite and biotite.

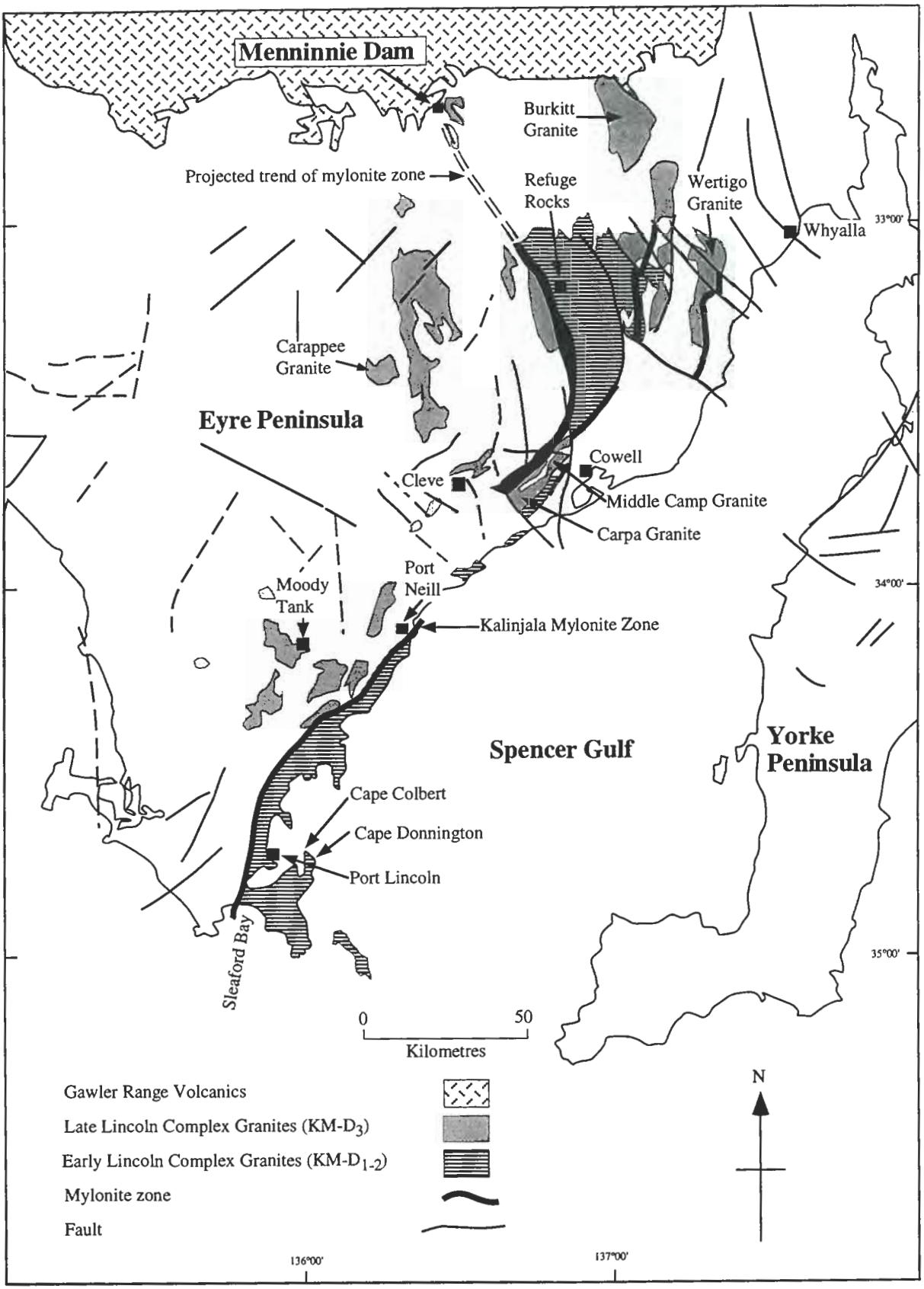


Fig. 3.10 Distribution of Lincoln Complex granitoids and mylonite zones on the eastern Eyre Peninsula (modified after Parker, 1993b).

Orthoclase also occurs as non-poikilitic euhedral crystals that locally have graphic intergrowths with quartz. Most of the orthoclase is microperthitic and some orthoclase has partially reverted to microcline. Muscovite and biotite occur interstitial to large quartz and feldspar crystals. Apatite occurs as small sub-rounded crystals within quartz and feldspar, and as fine euhedral needles at the boundaries of other minerals. Rare, sub-rounded, zoned zircon crystals were probably derived from an earlier source. Chlorite, calcite and sericite are alteration products of biotite, albite and K-feldspar respectively. Every MD granite dyke examined contains evidence of varying degrees of deformation. Deformation textures are described in Section 3.5.

### 3.4.2 Granite dyke geochemistry

MD granite dykes were analysed for major and selected trace element compositions to enable geochemical classification, and to attempt correlations with granites occurring elsewhere in the Eyre Peninsula (eg. the Lincoln Complex; 1845 - 1710 Ma., Parker, 1993a; St. Peters Suite; 1630 - 1620 Ma.; Flint et al., 1990; Hiltaba Suite; 1589 Ma., Creaser and Cooper, 1993).

Approximately one kilogram portions of those MD granite dykes that had undergone minimal hydrothermal alteration were selected for geochemical analyses. Major and trace elements were analysed using a Phillips PW1480 X-ray fluorescence (XRF) spectrometer at the Geology Department, University of Tasmania. The granites were analysed for, $SiO_2$, $TiO_2$, $Al_2O_3$, $Fe_2O_3$, MnO, MgO, CaO, $Na_2O$, $K_2O$, $P_2O_5$, loss on ignition (L.O.I.), Y, Rb, Cu, Pb, Zn, Ni, U, Th, Nb, Zr, Sr, Ba, Sc, V. Total iron is expressed as $Fe_2O_3$. Preparation methods and XRF. settings are presented in Appendix 3.2.

*Analytical results*

MD granite dyke analyses, analyses of granitoids and associated mafic intrusions of the Lincoln Complex, graintoids and granodiorite dykes of the St Peter Suite (Parker, 1993a), and granitoids of the Hiltaba Suite (Flint, 1993b), are summarised in Table 3.7 and detailed in Appendix 3.4.

MD granite dykes plot in the granite field defined by Le Maitre (1989; Fig. 3.11). Their chemistry, mineralogy and textures are consistent with crystallisation from a melt rather than pegmatite, or as products of metamorphic reactions. The granite dyke compositions plot as a cluster on $Al_2O_3$ vs $SiO_2$, $TiO_2$ vs $SiO_2$, $TiO_2$/Nb vs $SiO_2$ and Y vs $TiO_2$ variation diagrams (Fig. 3.12a - f), interpreted to indicate that the MD granite dykes were co-genetic, and probably coeval. MD granite dykes can be differentiated from granitoids of the Hiltaba Suite on $P_2O_5$ vs $SiO_2$ and $TiO_2$ vs $SiO_2$ variation diagrams (Fig. 3.12e, f). At similar $SiO_2$ levels, MD granite dykes are enriched in $P_2O_5$ and depleted in $TiO_2$ relative to the granitoids of the Hiltaba Suite. Insufficient analyses of granitoids of the St. Peters Suite are available to test for differences to MD granite dykes.

Table 3.7. Range and average analyses of the granite dykes from Menninnie Dam, selected analyses of granites of the Hiltaba Suite (Flint, 1993b) and Lincoln Complex (Moody Suite; Parker, 1993a) that occur close to the Menninnie Dam prospect, and a granite of the St. Peters Suite (Parker, 1993a).

| | Granite dykes | | St Peters Suite Granite - adamellite | Lincoln Complex Carappee Granite | Lincoln Complex Burkitt Granite | Hiltaba Suite Buckleboo Granite | Hiltaba Suite Charleston Granite |
|---|---|---|---|---|---|---|---|
| | Composition range | Average composition | | | | | |
| $SiO_2$ (wt.%) | 63.84 - 76.17 | 71.94 | 71.45 | 72.68 | 64.78 | 76.60 | 72.93 |
| $TiO_2$ (wt.%) | 0.04 - 0.52 | 0.16 | 0.34 | 0.20 | 0.36 | 0.16 | 0.34 |
| $Al_2O_3$ (wt.%) | 13.33 - 16.58 | 14.25 | 13.45 | 8.03 | 16.02 | 12.40 | 12.87 |
| $Fe_2O_3$ (wt.%) | 0.67 - 4.28 | 1.64 | 2.29 | 0.78 | 4.09 | 0.44 | 2.00 |
| FeO (wt.%) | - | - | 1.07 | 1.14 | - | 0.74 | 1.50 |
| MnO (wt.%) | 0.01 - 0.09 | 0.05 | 0.07 | 0.03 | 0.09 | 0.02 | 0.06 |
| MgO (wt.%) | 0.24 - 1.70 | 0.66 | 0.83 | 0.24 | 1.07 | 0.15 | 0.38 |
| CaO (wt.%) | 0.45 - 1.62 | 0.91 | 1.61 | 0.74 | 2.29 | 0.57 | 1.26 |
| $Na_2O$ (wt.%) | 1.85 - 6.92 | 3.67 | 3.88 | 3.42 | 4.51 | 3.15 | 3.14 |
| $K_2O$ (wt.%) | 0.61 - 7.30 | 4.96 | 4.13 | 5.35 | 5.86 | 5.22 | 5.21 |
| $P_2O_5$ (wt.%) | 0.03 - 0.23 | 0.15 | 0.08 | 0.19 | 0.21 | 0.02 | 0.09 |
| $H_2O^+$ (wt.%) | - | - | - | 0.10 | - | 0.29 | 0.24 |
| $H_2O^-$ (wt.%) | - | - | - | 0.62 | - | 0.15 | 0.25 |
| $CO_2$ (wt.%) | - | - | - | - | - | 0.04 | 0.03 |
| L.O.I. (wt.%) | 0.87 - 2.39 | 1.49 | 0.99 | 0.96 | 0.68 | - | 0.65 |
| Total (wt.%) | - | 99.88 | 100.19 | 94.48 | 99.96 | 99.95 | 100.95 |
| Ba (ppm) | 47 - 1131 | 382.56 | 945 | 210 | 1737 | - | 626 |
| Ce (ppm) | - | - | 73 | 95 | 200 | - | 142 |
| Co (ppm) | - | - | 126 | 80 | 27 | - | 102 |
| Cr (ppm) | - | - | 14 | 20 | 13 | - | 25 |
| Cu (ppm) | 2 - 47 | 8 | 19 | 200 | 7 | - | - |
| La (ppm) | - | - | 43 | 60 | 85 | - | - |
| Li (ppm) | - | - | - | - | - | - | - |
| Nb (ppm) | 4 - 40 | 12.75 | 15 | 26 | 26 | - | 22 |
| Ni (ppm) | 5 - 11 | 7.94 | 11 | 40 | 10 | - | - |
| Pb (ppm) | 24 - 119 | 59.06 | 5 | 170 | 66 | - | - |
| Rb (ppm) | 46 - 367 | 201.38 | 179 | 420 | 280 | - | - |
| Sc (ppm) | 2 - 8 | 4.31 | - | - | - | - | - |
| Sr (ppm) | 21 - 394 | 89.06 | 281 | 50 | 591 | - | 120 |
| Th (ppm) | 8 - 60 | 19.63 | 11 | 36 | 93 | - | 70 |
| U (ppm) | 5 - 49 | 20.44 | 3 | 8 | 30 | - | 12 |
| V (ppm) | 3 - 48 | 11.81 | 25 | 20 | 50 | - | - |
| W (ppm) | - | - | - | 10 | - | - | - |
| Y (ppm) | 7 - 26 | 15.50 | 31 | 34 | 18 | - | 20 |
| Zn (ppm) | 23 - 74 | 44.06 | 58 | 80 | 54 | - | - |
| Zr (ppm) | 38 - 244 | 104.69 | 190 | 170 | 261 | - | 192 |
| Number of analyses | 15 | 15 | 4 | 2 | 6 | 2 | 8 |

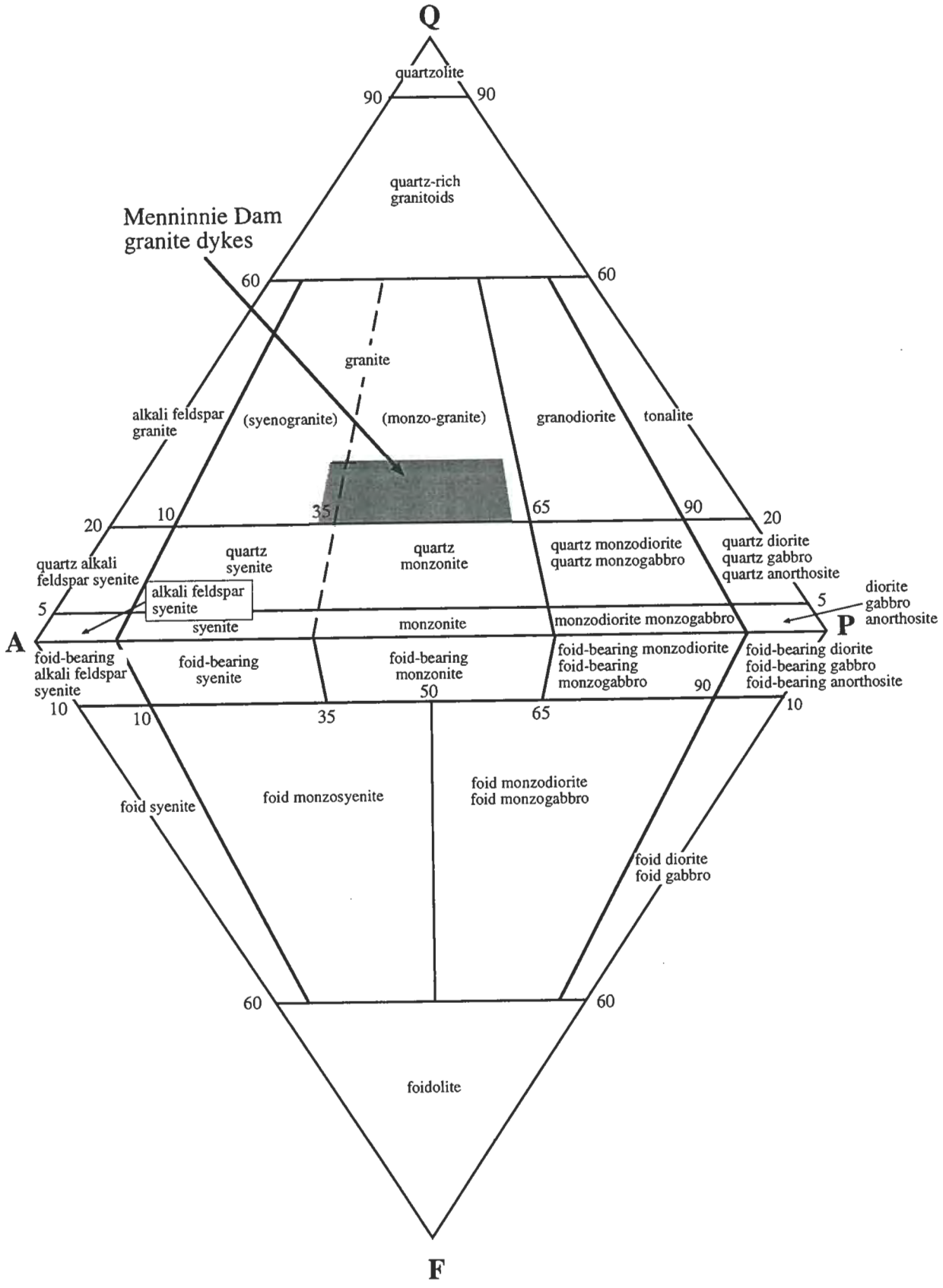


Figure 3.11 Plutonic igneous rock classification scheme of Le Maitre (1989). Assuming albite is altered calcic plagioclase, data for the granite dykes at Menninnie Dam plot in the granite field.

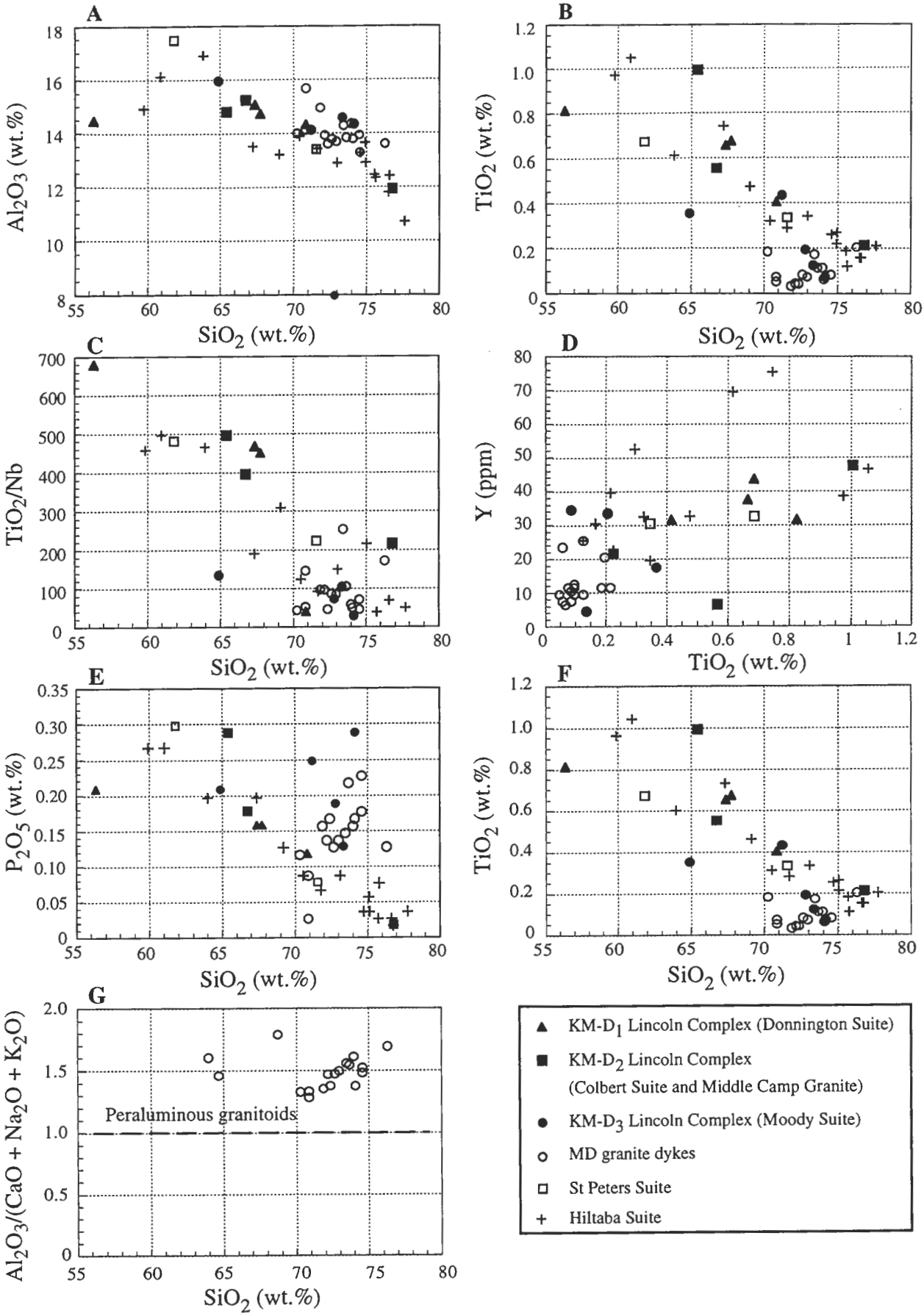


Figures 3.12A - G. Variation diagrams for Granites of the Eyre Peninsula and the granite dykes from Menninnie Dam. MD granite dykes plot as a cluster, consistent with a co-genetic and possibly coeval relationship. The MD granite dykes can be differentiated from other granite suites of the Gawler Craton by their higher $P_2O_5$ contents and lower $TiO_2$ contents at equivalent $SiO_2$ contents. Data for the MD granite dykes plot in the field for peraluminous granitoids (Shand, 1927).

Granitoids of the Lincoln Complex have been subdivided into:

- Donington Granitoid Suite associated with KM-$D_1$ (≈ 1843 - 1818 Ma., Mortimer et al., 1986; Mortimer et al., 1988; Webb et al., 1986).
- Colbert Suite and Middle Camp Granite associated with KM-$D_2$ (≈ 1757 - 1738 Ma., Mortimer et al., 1986; Fanning, 1987, )
- Moody Suite, Carpa Granite, Wertigo Granite, Burkitt Granite and Carappee Granite associated with KM-$D_3$ (≈ 1740 - 1710 Ma., Parker, 1993a; Fanning, 1984).

The MD granite dykes and granitoids of the Moody Suite both have high $P_2O_5$ contents (Fig. 3.12e). The MD granite dyke compositions have a positive correlation between $P_2O_5$ and $SiO_2$. The correlation between $P_2O_5$ and $SiO_2$ does not appear to be due to alteration and when loss on ignition (L.O.I.) is excluded and the granite dyke compositions recalculated, the positive correlation between $P_2O_5$ and $SiO_2$ remains. The granite dykes are strongly peraluminous (Fig. 3.12g), with an average aluminium saturation index of 1.50 (The aluminium saturation index = $Al_2O_3$ / (CaO + $Na_2O$ + $K_2O$); Shand 1927). The correlation between $P_2O_5$ and $SiO_2$ is interpreted to have been caused by the magma not having achieved apatite saturation prior to emplacement as dykes. Apatite solubility in a melt increases linearly with the aluminium saturation index, although for many L.C.T. granites, feldspar is the principal reservoir for phosphorous (London, 1995; L.C.T. granites are defined as granites with Li, Cs and Ta as their signature elements, Cerny, 1991 a, b).

## 3.5 Deformation

The aim of this section is to:

- Describe the deformation textures of the MD granite dykes and metasediments at Menninnie Dam.
- Compare the effects of deformation at Menninnie Dam with the effects of regional tectonic events.

The textural classification of fault rocks adopted in this study follows that of Sibson (1977; Fig. 3.13). The definition of mylonite is modified from that proposed by Sibson (1977) to included the criteria of White et al. (1980), who defined mylonite as the rock produced in a ductile shear zone or fault in which the rock matrix was deformed by crystal-plastic processes. In addition, Lister and Snoke (1984) considered the presence of strong crystallographic orientations (eg. quartz c-axis fabrics) to be important in the definition of mylonites. While cataclasis may occur within mylonites with subsidiary brittle deformation of harder mineral phases such as feldspar (Lister and Snoke, 1984), the dominant deformation process in mylonites is by crystal-plastic processes.

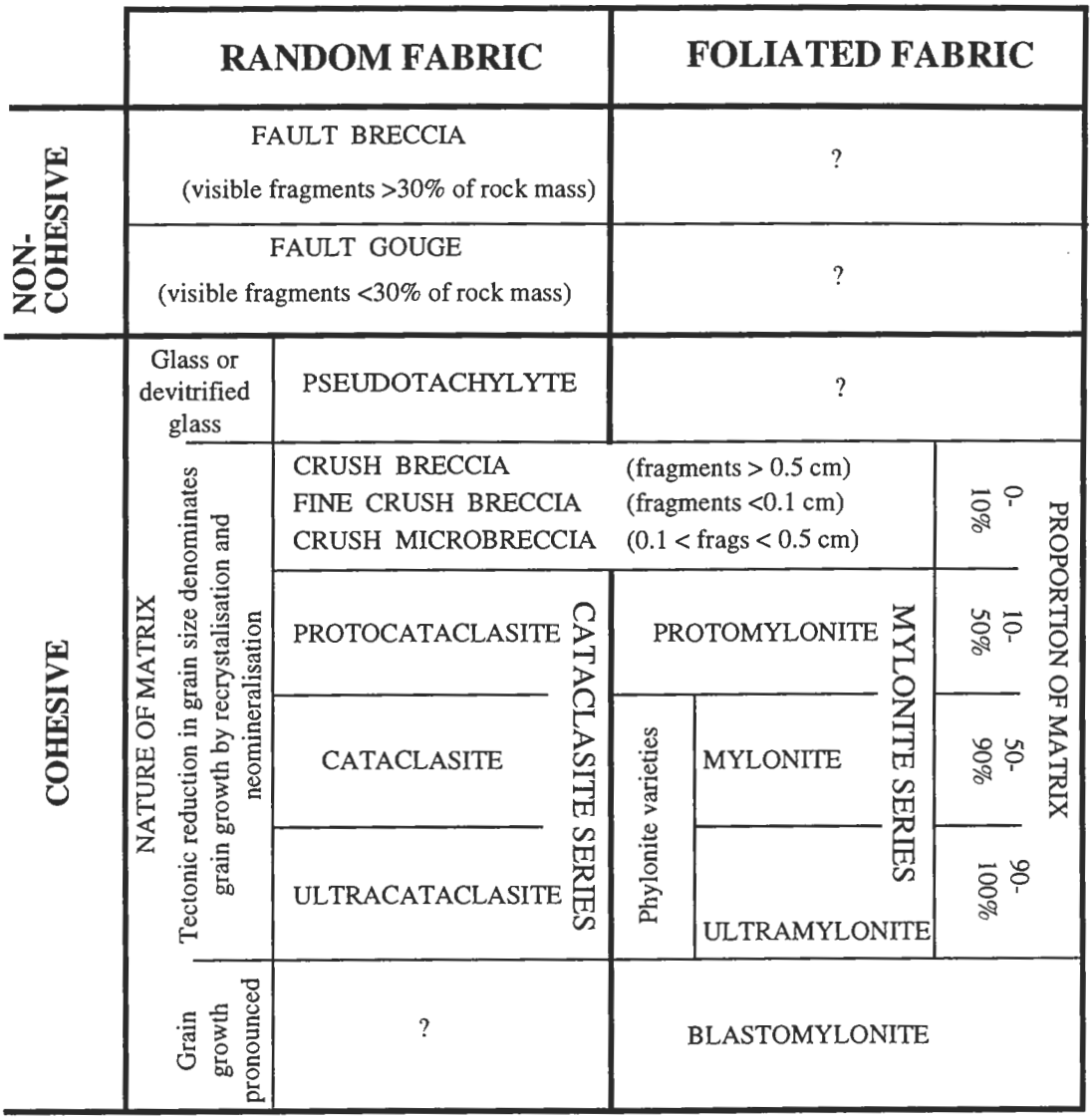


Figure 3.13 Textural classification of fault rocks (modified after Sibson, 1977).

Deformation textures in each of the rock suites will be described in turn, starting with the western suite. It was not possible to conduct a structural analysis of lithologies at the Menninnie Dam prospect due to the absence of orientated drill core or a consistent 'marker fabric' such as cleavage which could be used as a reference plane for structural studies.

### 3.5.1 Deformation of the western suite

The western suite was recognised as being problematic by Higgins et al. (1990) and Beeson (1990b), in that it did not easily correlate with the Hutchison Group stratigraphy as proposed by Parker et al., (1985; Fig 2.3). Drilling carried out after 1990, has confirmed the north-south trend, and steep easterly dip of the western suite - central suite contact. This contrasts with the steep westerly dip and NNE strike of the central and eastern suites. The discordant boundary between the western and the central suites is therefore interpreted to be a major north - south trending shear zone.

The western suite is cut by a number of sub-parallel faults which collectively form a deformation zone several hundred metres wide. Deformation styles form a continuum from brittle, to intense ductile deformation, which has resulted in substantial changes to rock textures and, to a lesser extent, mineralogy. In most of the deformed schist, the schistose protolith is easily identifiable and the texture is typical of a protocataclasite (Fig. 3.4a). Increased deformation was associated with retrograde alteration of biotite and feldspar to sericite and chlorite, which has produced dark green, or yellow green schists (Fig. 3.14a).

Intense deformation is typically confined to zones up to a few tens of meters wide in drill intersection. Deformation is heterogenous within these zones, with less deformed clasts in a fine grained, highly deformed matrix. Matrix material, which comprises $\approx$ 10 - 15% of deformed zones, consists of fine grained quartz and rare feldspar fragments, and abundant chlorite and sericite. The matrix formed mostly by brittle processes, resulting in grain size reduction of quartz and, to lesser extent, feldspar. The resultant texture is that of a cataclasite (Fig. 3.14a).

Apart from local zones of cataclastic deformation, most of the schists have protocataclastic textures. By contrast, granite dykes in the western suite have a wider range of deformation textures, from weakly deformed granite to mylonite. The interior of the granite dykes is typically weakly deformed, with more intense deformation concentrated in a narrow band within dykes, near the contact with the enclosing schist (typically less than 1m wide). It appears that strain has been partitioned into granite dyke margins, rather than the enclosing schist (Fig. 3.14b). Intense deformation is invariably associated with retrograde alteration of feldspar and biotite to sericite $\pm$ chlorite $\pm$ pyrite, resulting in a characteristic light yellow green colour.

Fig. 3.14a. Drill hole PD0021, 331.4 m. Deformed western suite schist with a cataclastic texture. Biotite and feldspar have been altered to sericite and chlorite, resulting in a yellow - green or dark green colour.

Fig. 3.14b. Drill hole PD0027, 179.8 m. Deformed margin of a granite dyke intruded into the shear zone bounding the central and western suites. Deformation and alteration are most intense at the outer margin of the dyke (RHS). In more deformed zones, feldspar is altered to yellow - green sericite. Towards the interior of granite dyke (LHS), deformation is less intense.

Figs. 3.14c - e. are from drill hole PD0027 at ≈ 179 m. They illustrate the progressive textural and mineralogical changes that have occurred over a 2 m interval near the margin of a granite dyke. Fig. 3.14c is from towards the interior of the granite dyke and is least deformed, and Fig. 3.14e is near the granite dyke margin and is most deformed.

Fig. 3.14c. Transmitted light photomicrograph (x nicols). ≈ 2 m from the granite dyke margin. Less deformed granite has a sub-gneissic foliation. Quartz crystals in contact with each other (Q) have serrated grain contacts typical of grain margin migration.

Fig. 3.14d. Transmitted light photomicrograph (x nicols). ≈ 20 cm from the granite dyke margin. More deformed granite has a higher proportion of matrix and ductile processes are dominant. Most of the larger porphyroclasts are comprised of feldspar (F) of < 8 mm diameter, although quartz + feldspar ± muscovite clasts, and rare quartz are locally present. The matrix is dominated by quartz ribbons (Q), with minor feldspar and muscovite (M) fragments, and interstitial fine grained sericite and calcite (C). Most tabular - elongate quartz grains and quartz ribbons have a consistent crystallographic orientation, typical of dynamic recrystallisation. Pressure shadows of fine grained quartz and mica are common in the lee of porphyroclasts (P). Quartz in pressure shadows has recrystallised with polygonal grain boundaries and no consistent crystallographic orientation.

Fig. 3.14e. Transmitted light photomicrograph (x nicols). ≈ 5 cm from the granite dyke margin. The most intensely deformed granite is fine grained and contains pervasive sericite alteration and trace amounts of finely disseminated pyrite. The frequency and size of porphyroclasts has diminished, and most are commonly ovate to augen and comprised of feldspar (F). Fine grained matrix comprises 80% of the rock. Quartz ribbons make up an estimated 5% of the matrix and the size of sub-grains within ribbons is typically less than 200 μm (Q). The remainder of the matrix has an average grain size of < 50 μm and the abundance of sericite appears to be inversely proportional to the abundance of feldspar porphyroclasts and is typical of 'reaction softening' (ref. Section 3.8.3)

3.14a

3.14b

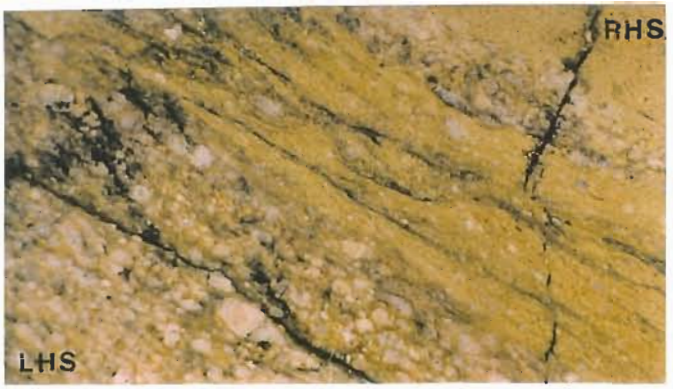


3.14c

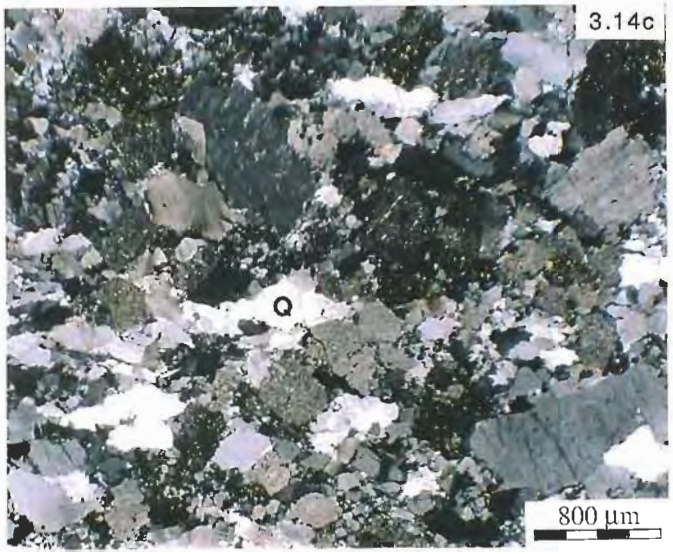


3.14d

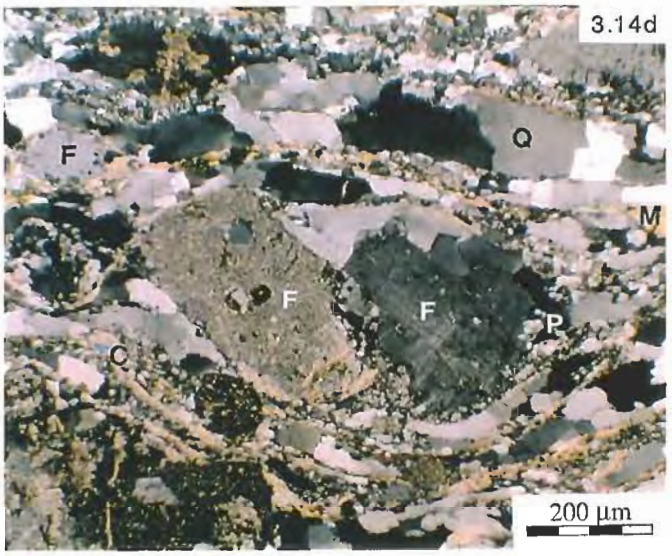


3.14e

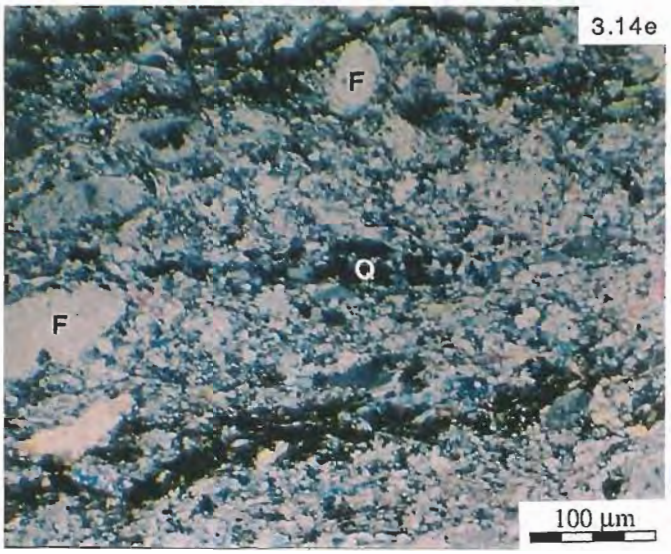

Progressive textural changes in the granite dyke can be compared due to the textural homogeneity of the granite protolith. Figures 3.14c - e illustrate changes in the intensity of deformation over a 1m interval, starting with weakly deformed granite (Fig. 3.14c) and progressing to more intensely deformed granite at the dyke margin (Fig. 3.14e).

### 3.5.2 Deformation of the central suite

Deformation is much less pronounced in rocks of the central suite compared to the western suite, and appears to be restricted to narrow zones that become less common away from the western - central suite boundary. Massive diopside zones are locally brecciated over intervals of up to 30 m wide. The degree of brecciation is highly variable, ranging from closed framework jigsaw fit (< 10% matrix), to open framework with more dispersed clasts and ≤ 40% matrix. The matrix consists of finer clasts of diopside with minor secondary carbonate and / or chlorite. The overall texture varies from crush breccia to protocataclasite.

A 17 m wide zone of diopside - quartz - dolomite in drill hole PD0017 contains both ductile and brittle deformation textures. The zone has a central core of banded quartz - diopside rock flanked by massive diopside, which grades outwards into diopside - marble rock. Throughout the 17 m wide zone, diopside clasts have a jigsaw fit, clast-supported breccia texture typical of those produced by brittle deformation processes (Ramsay and Huber, 1987). By contrast, quartz bands in the quartz - diopside core are intensely deformed, and have ultramylonite textures (Fig. 3.15a, b) due to competency contrasts between the two minerals.

Marbles of the central suite were probably also deformed, however, mylonitic deformation textures cannot be determined unequivocally due to recrystallisation (Fig. 3.15c, d).

All of the granite dykes in the central suite are deformed. The intensity of deformation varies from serrated quartz grain boundaries and thin zones of crush microbreccia to rare mylonites.

### 3.5.3 Eastern suite

Deformation in eastern suite schists is much less pervasive than in western suite schists. Deformation zones are typically less than a few metres wide and are concentrated within the schists, rather than at granite dyke margins. Brittle deformation textures are generally more common than the ductile deformation textures shown in Figure 3.15e.

## 3.6 Pegmatite dykes

Pegmatites occur as dykes up to 1m wide in close spatial association with granite dykes in rocks of the western, central, and eastern suites. Pegmatite dykes consist of hematite-dusted K-feldspar (usually microcline), quartz and, locally, minor tourmaline.

Fig. 3.15a. Drill hole PD0017, 286 m. Transmitted light photomicrograph (x nicols). Quartz bands in quartz - diopside rock, consist of quartz ribbons, and ribbon fragments (typically 0.5 - 1 cm long) in a fine grained mosaic of 20 - 100 μm polygonal quartz. The margins of quartz ribbons have a mortar texture of recrystallised, polygonal quartz, and most ribbons have been partially recrystallised to fine grained polygonal quartz.

Fig. 3.15b. Transmitted light photomicrograph. Rotated view of Fig. 3.15a with insertion of a gypsum plate. Fine grained polygonal quartz has a consistent crystallographic orientation that is commonly discordant to the crystallographic orientation of ribbon quartz. All of the quartz has recrystallised by ductile processes and this quartz band has an ultramylonitic texture.

Fig. 3.15c. Drill hole PD0010, 229.9 m, central suite. Finely laminated textures with relict 'porphyroclasts' apparent in hand specimen (P), are interpreted to have resulted from deformation of some 'marbles'.

Fig. 3.15d. Transmitted light photomicrograph of the sample shown in Fig. 3.15c. Fine grained dolomite (clear) and trace amounts of fine grained graphite (dark). Deformation textures interpreted from the hand specimen are not apparent in thin section possibly due to recrystallisation.

Fig. 3.15e. Drill hole PD0031, 241.5 m. Transmitted light photomicrograph. A 2 - 3 m wide deformed zone in the eastern suite schist has a 0.5 m wide core of mylonitic deformation, flanked by cataclasites and protocataclasites. The mylonite has well developed quartz ribbons (Q) wrapped around small feldspar porphyroclasts (F), a classical mylonitic texture.

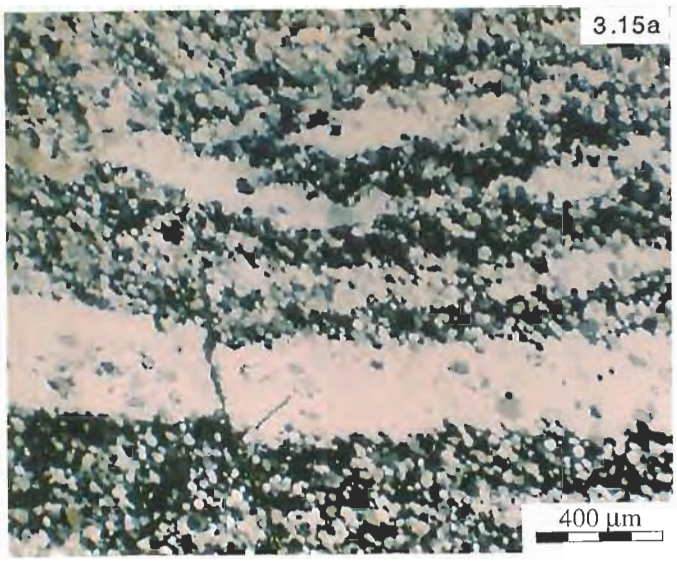
3.15a
400 µm

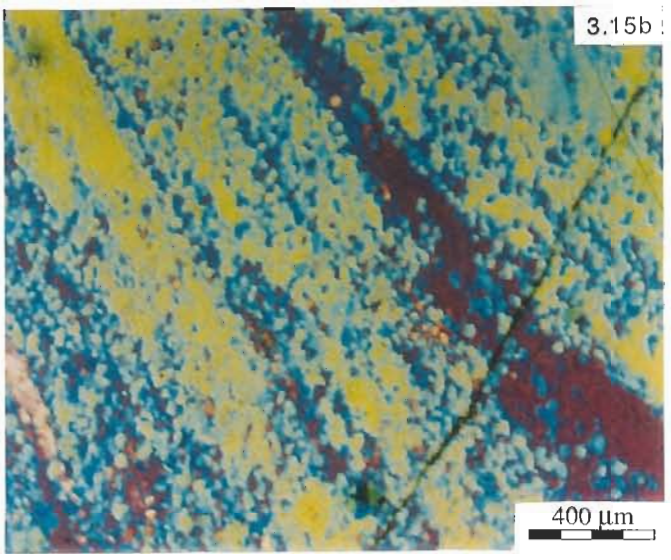
3.15b
400 µm

3.15c
P
2 cm

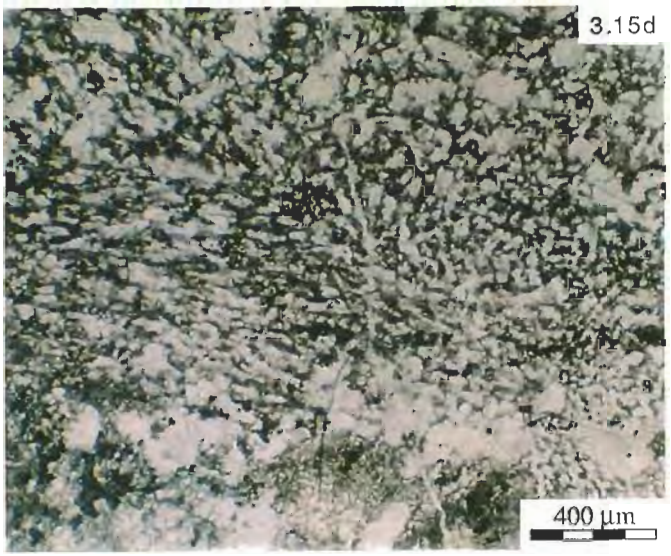
3.15d
400 µm

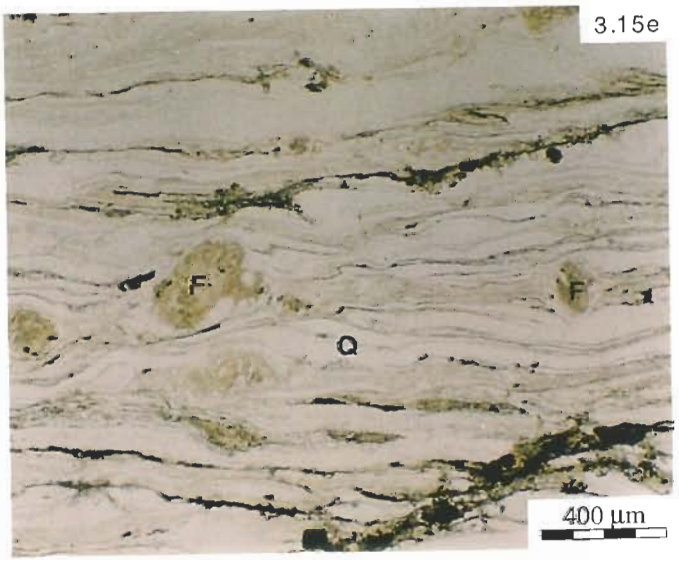
3.15e
F
F
Q
400 µm

Whereas all of the granite dykes are medium grained and deformed, the pegmatite dykes are coarse grained and either undeformed or weakly deformed. On the basis of the contrasting deformation styles, pegmatite dykes are considered to be younger than the granite dykes (Fig. 3.16a - d). Whereas granite dykes do not have alteration halos, larger pegmatite dykes typically have an extensive alteration halo which can extend for several metres into the enclosing country rock (described in Section 3.7.2).

## 3.7 Metasomatism

Naumann (1826) described metasomatism as the process by which one mineral is replaced by another of different chemical composition due to reactions caused by the introduction of material from external sources. Lindgren (1912) described metasomatic rocks as those whose chemical composition has been substantially changed by metasomatic alteration of the original constituents.

Some of the central suite calc-silicates and marbles have a distinct pinkish colouration that is interpreted to have resulted from metasomatic alteration. Marble that contains thin bands and disseminations of metapelitic material and / or thin iron formation bands has been more affected by metasomatism than other lithologies (Fig. 3.16e).

Higgins et al. (1990) described the metasomatised marbles of the central suite as being "vaguely banded marble", that contained small grains or aggregates of quartz, feldspar, diopside, amphibole and rare garnet, talc, forsterite and epidote. "Large porphyroblasts (up to 3 cm) and irregular layers and blebs of microcline may comprise 10% of the mineralised host rock". Higgins et al. (1990) interpreted this to be related to a tuffaceous component within the calcitic marble. Beeson (1990b) used whole rock geochemistry to calculated the average modal mineral composition of the metasomatised marbles as 65% calcite, 20% K-feldspar and 15% quartz. Beeson (1990b) considered that a primary volcanic component or authigenic K-feldspar contributed to modal K-feldspar. The positive correlation between K and other rock-forming elements such as Ti and variations in the Al : K ratios between nearby prospects led Beeson (1990b) to favour an authigenic origin.

In this study, interpretation of the origin of K-feldspar in the marbles of rock type 5 has centred around careful examination of the mineralogy and mineral textures. The whole rock geochemical database used by Beeson (1990b) was kindly made available by Dr. Beeson (then; Chief Geologist, Acacia Resources Ltd.). An attempt was made to utilise the whole rock geochemical data in Gresens (1967) type mass balance calculations, however, due to the nature of the sampling, intervals of similar rock types could not be unequivocally assigned to 'altered' and 'unaltered' groups. Mass balance calculations were therefore abandoned.

Fig. 3.16a. Drill hole PD0032, 294.8 m. Light, yellow - green, sericite altered, protomylonitic granite clasts (G) in an undeformed feldspar pegmatite (P). The clasts have alteration rinds of pink K-feldspar (K).

Fig. 3.16b. Transmitted light photomicrograph of the margin of an altered granite dyke clast illustrated in Fig. 3.16a. The contact between the altered margin of the granite clast and the unaltered interior is marked by a diffuse line (dashed line). Sericite that formed during deformation and alteration of the granite dyke is preserved in the interior of the clast (S). At the margin of the clast, sericite has been altered to K-feldspar (K). The relict texture of sericite is preserved by K-feldspar alteration.

Fig. 3.16c. Drill hole PD0007, 261.3 m. A 5 - 6 cm wide granite dyke hosted by metasomatically altered calcitic marble. The granite dyke has been brecciated, and hematite-dusted K-feldspar has formed the breccia matrix.

Fig. 3.16d. Drill hole PD0016, 281.4 m. Transmitted light photomicrograph (x nicols). A brecciated granite dyke adjacent to a pegmatite vein. Metasomatic microcline (M) occurs as overgrowths on granite breccia clasts (G).

Fig. 3.16e. Drill hole PD0020, 273.7 m. Metasomatic alteration of central suite marble has resulted in a mineralogical changes and a pinkish colouration due to finely disseminated hematite. Bands of silicate minerals (iron formation or schist) and segmented bands (SB), are intensely altered around their margins whereas the interior of bands and segments is typically less altered.

Fig. 3.16f. Drill hole PD0016, 310.5 m. Transmitted light photomicrograph (x nicols). Metasomatic alteration of thin iron-rich band hosted by pinkish, calcitic marble has resulted in alteration of iron silicate minerals to microcline (M) and phyllosilicates (P). Remnant magnetite (MG) in the iron-rich band has retained a metamorphic orientation. Metasomatic epidote (E) and garnet (G) form a halo around the iron-rich band and passes into metasomatically altered calcite (C).

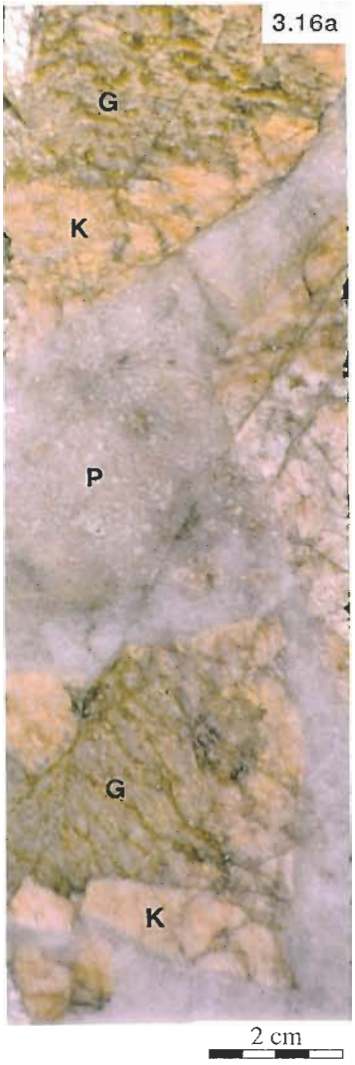
3.16a
G
K
P
G
K
2 cm

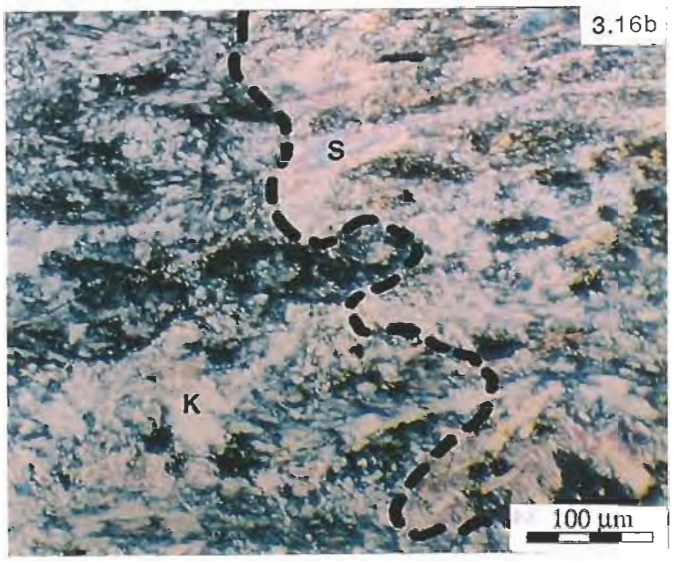
3.16b
S
K
100 µm

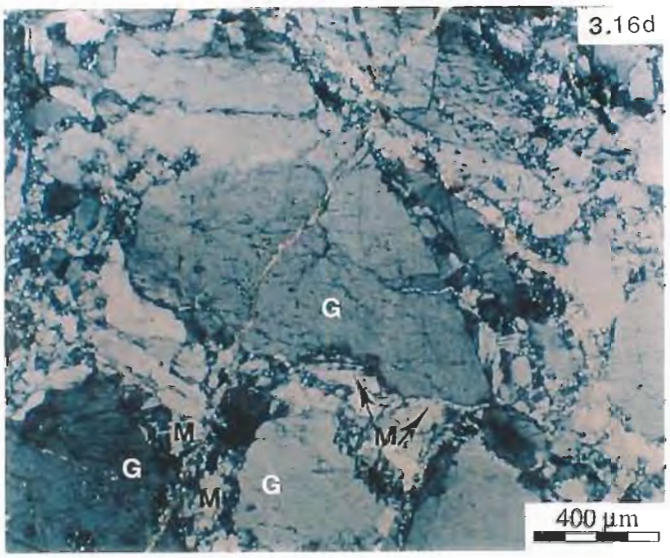
3.16d
G
M
M
G
M
G
400 µm

3.16c
2 cm

3.16e
SB
2 cm

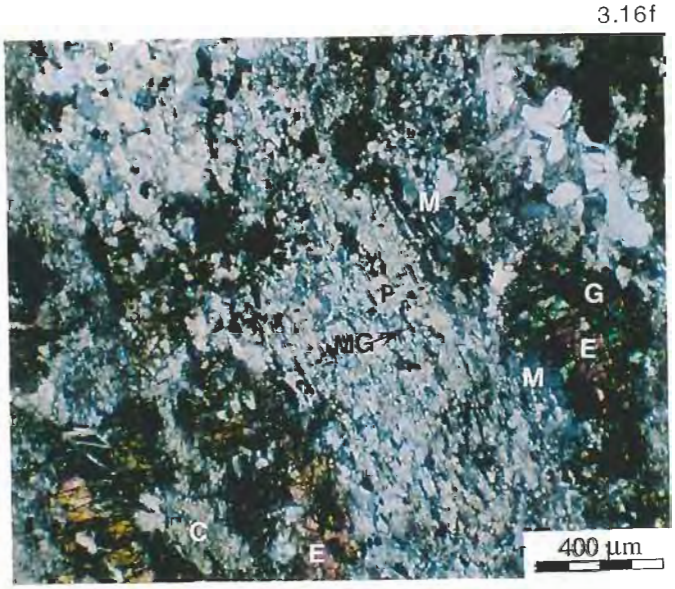
3.16f
M
P
G
E
M
MG
C
E
400 µm

### 3.7.1 Mineralogy

The mineralogy of metasomatised marbles and silicate rocks has been determined by a combination of standard optical techniques and X-ray diffraction (XRD). XRD samples were analysed both prior to, and after, treatment with HCl. All samples were analysed as randomly orientated powders using the standard pressed powder technique (Brindley and Brown, 1980). XRD results and a description of the equipment and techniques used are presented in Appendix 3.5. When there was some uncertainty as to the nature of the feldspar, discrimination was made on the basis of staining using the techniques of Norman (1974), or by electron microprobe analysis.

Metasomatised marbles are medium grained, calcitic marbles, with between 1 - 40% disseminated silicate minerals or thin bands of silicate minerals. The pinkish colouration is caused by the presence of disseminated hematite and hematite-dusted microcline, or, in some cases, hematite-dusted albite. Other mineral species, in order of decreasing abundance, include: brown to olive green andradite garnet, pale brown grossular garnet, epidote, chlorite, sericite / mica, wollastonite, leucoxene, apatite and sphene. Trace amounts of cuspidine ($Ca_4Si_2O_7(F,OH)_2$), vesuvianite and scapolite have been observed by commercial petrographers (Cowan, 1990) but have not been confirmed in this study . Siderite ± calcite occurs in conjunction with metasomatic silicate minerals.

### 3.7.2 Metasomatic mineral textures

Metasomatic calcite and siderite are texturally different to metamorphic marbles. Most of the metamorphic calcite crystals are 1 - 3 mm in diameter, and commonly have deformation twins and sutured grain contacts. By contrast, metasomatic carbonates are commonly calcitic and locally sideritic, are finer grained (1 - 10 μm), do not have stress twins, and have irregular diffuse grain contacts. The most intense metasomatism of metamorphic marbles occurs adjacent to metapelitic bands and iron formation bands (Fig. 3.16f).

Metasomatic alteration of iron formations has resulted in partial, to complete replacement of Fe and Mg-silicates (hastingsite, grunerite, biotite and diopside) by fine grained sericite, chlorite and leucoxene (Fig. 3.17a). Magnetite has been partially replaced by hematite. Metasomatic sericite and chlorite were subsequently partially replaced by hematite-dusted microcline (Fig. 3.17b). In some instances, chlorite (after metamorphic biotite) and magnetite were overgrown by, and preserved as remnants within microcline (Fig. 3.17c). The remnant metamorphic fabric of the precursor ferro-magnesian minerals has been partially preserved as lineated clots of leucoxene or sphene enclosed within metasomatic minerals.

Fig. 3.17a. Drill hole PD0001, 127.45 m, Hand specimen of altered thin iron-rich bands (IF) in metasomatically altered calcitic marble (M) adjacent to the a thick iron formation. The dark iron-rich bands consist of biotite, hastingsite, quartz and minor disseminated magnetite. Bands are surrounded by halos of sericite, hematite-dusted microcline, minor leucoxene, remnant quartz and magnetite, and outer bands of olive green garnet and apple green epidote (CS). Light green remnant diopside at the margins of iron-rich bands has been partially altered to fine grained chlorite + calcite.

Fig. 3.17b. Drill hole PD0001, 127.43 m. Transmitted light photomicrograph (x nicols) of the central portion of an iron-rich band. The left hand side of the diagram shows the core of the band (C), where the biotite and amphibole have been completely replaced by a fine grained sericite, quartz, microcline, chlorite and leucoxene. Relict grains of magnetite (MG) and trace amounts of chlorite-altered biotite are preserved, although most has been altered to sericite or microcline. Towards the margin of the iron-rich band (right hand side of the diagram), hematite-dusted microcline (M) has replaced metamorphic minerals. Some martitised magnetite (MG) has not been replaced and occurs as inclusions in microcline. All evidence of the original metamorphic fabric has been destroyed.

Fig. 3.17c. Drill hole PD0016, 278.4 m. Transmitted light photomicrograph (x nicols) of an altered iron-rich band. Remnant metamorphic biotite has been completely altered to dark green chlorite (C) and preserved as inclusions within metasomatic microcline (M). Disseminated magnetite (MG) and rare quartz have also been preserved within metasomatic microcline.

Fig. 3.17d. Drill hole PD0017, 549.9 m. Transmitted light photomicrograph (x nicols) of the outer portion of an altered iron formation band. The alteration assemblage includes pale brown, growth zoned grossular garnet (G). The central core of some garnets contains partially altered diopside relicts (D) which have locally been overgrown by opaque andraditic garnet and growth zoned grossular garnet. Calcite (C) has infilled between grossular garnet crystals.

Fig. 3.17e. Drill hole PD0001, 291.3 m. Transmitted light photomicrograph (x nicols) of rounded microcline 'grains' (M) produced through metasomatic alteration of disseminated biotite flakes in calcitic marble. Sphene (S) is a common accessory mineral.

3.17a

3.17b

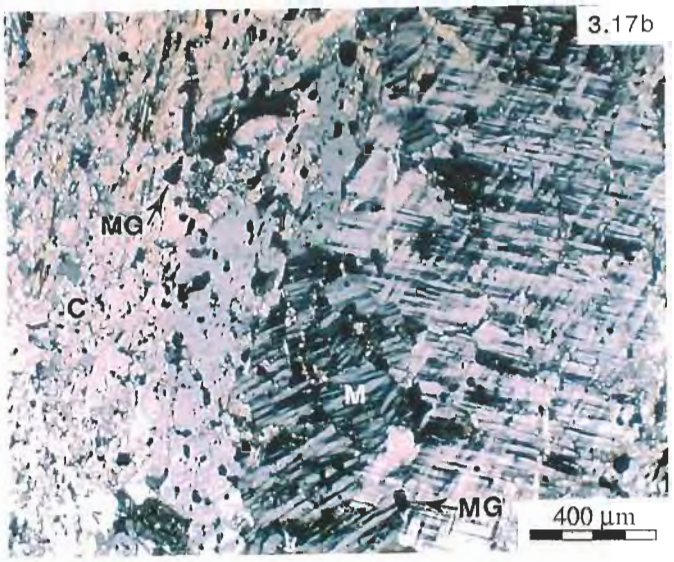


3.17c

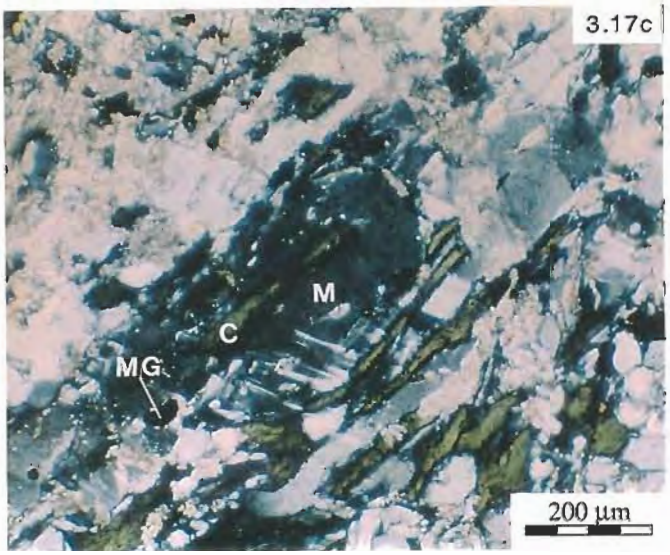


3.17d

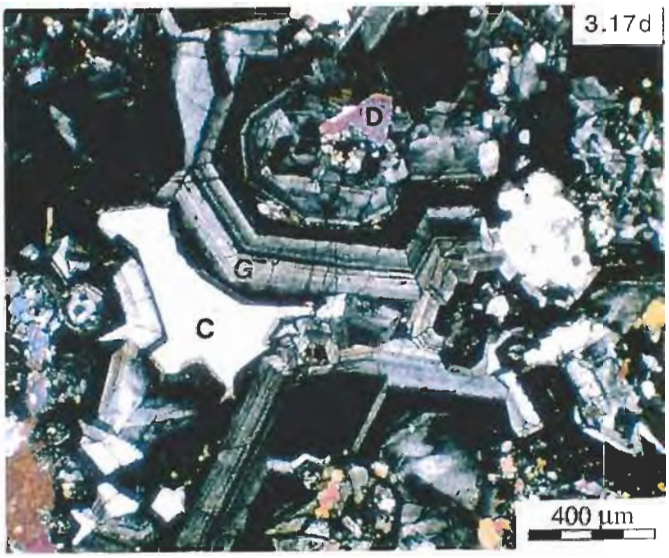


3.17e

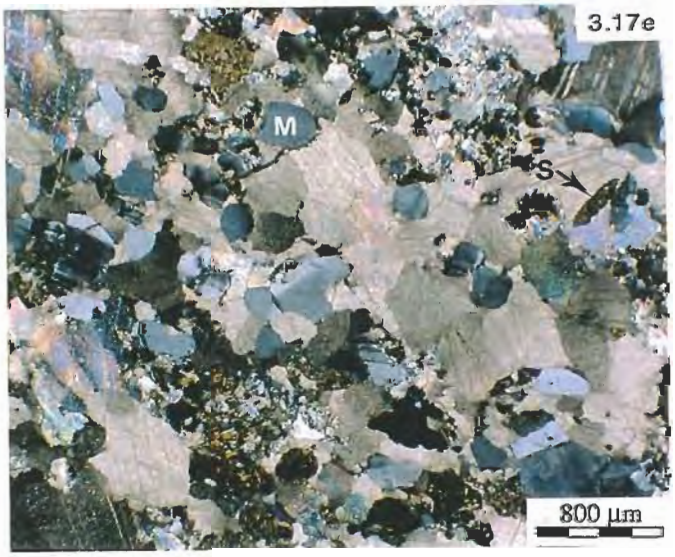

Figs. 3.18a - e. Drill hole PD0026. 395.8 m - 420.8 m. A series of photographs across the alteration halo surrounding a pegmatite dyke hosted by massive diopside. Figure. 3.18a is from near the margin of the alteration halo. Figure 3.18c is from near the centre of the dyke and Figure 3.18d - e are from the alteration halo on the opposite side of the pegmatite dyke.

Fig. 3.18a. 402.8 m. Massive diopsidic host rock (D) with minor calcite (C) and chlorite (CH) alteration.

Fig. 3.18b. 399.8 m. Near the margin of the pegmatite dyke. Brecciated diopside (LHS), has been altered to whitish calcite, dark green chlorite, epidote ± garnet and trace amounts of pyrite. The margin of the dyke (RHS), is indistinct due to partial to pervasive alteration of calcite, chlorite, epidote ± garnet to hematite-dusted K-feldspar.

Fig. 3.18c. 399 m. Core of the pegmatite dyke. Hematite-dusted K-feldspar and quartz have completely replaced diopside. Remnants of chlorite + calcite + epidote ± garnet alteration after diopside are preserved within feldspar + quartz alteration.

Fig. 3.18d. 395.8 m. The outer alteration zone (RHS) comprises dark green chlorite + calcite + epidote ± garnet alteration of breccia textured diopside.

Fig. 3.18e. 395.7 m. Transmitted light photomicrograph (x nicols) of Large epidote laths (E) with interstitial feldspar (F) from the outer alteration halo of a pegmatite vein hosted by massive diopside.

Figs. 3.18f - g. Drill hole PD0013, 129 - 134 m. Two diagrams of the alteration halo surrounding a pegmatite vein in the south of the prospect.

Fig. 3.18f. Diopside (D) has been brecciated and partially altered to epidote ± garnet (E).

Fig. 3.18g. Towards the centre of the pegmatite vein, hematite-dusted feldspar (red) has overprinted epidote + chlorite + calcite ± garnet alteration (green). The sulphide vein (S) cuts across the alteration and is interpreted to have post-dated metasomatic alteration.

3.18a

2 cm

3.18b

2 cm

3.18c

2 cm

3.18d

2 cm

3.18e

3.18f

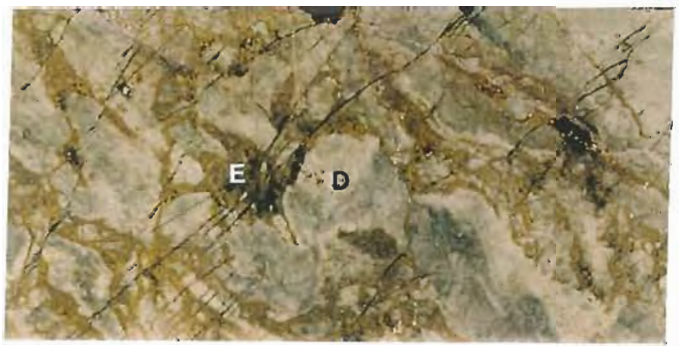


2 cm

3.18g

2 cm

Epidote and garnet form an outer halo to microcline (Fig. 3.17a). Epidote is present as irregular shaped crystals and locally, growth-zoned prisms. Some garnets have an irregular core of olive-green andradite overgrown by pale brown, growth-zoned grossular (Fig. 3.17d). Fine grained Fe-rich carbonate and finely dispersed hematite occurs as matrix fill. Diopside has been partially altered to a fine grained mix of carbonate ± talc ± chlorite.

Metasomatic alteration has also affected banded or disseminated aluminous minerals and dispersed biotite has been partially, to completely, replaced by small (10-100μm diameter), rounded 'grains' of hematite-dusted microcline and trace amounts of leucoxene or sphene (Fig. 3.17e). Although metasomatism has resulted in pervasive alteration of most impure marble units, it is most intense in proximity to pegmatite dykes, where the alteration assemblage locally includes wollastonite. Altered impure marble units are bound to the east by schist (eastern suite schist) and to the west by thick iron formations (Fig. 3.1). Marble and calc-silicate lithologies to the west of the iron formations have not been extensively altered by metasomatism.

Although not extensively altered, massive diopside is locally altered to feldspar + epidote + chlorite + calcite. A criteria for alteration of diopside appears to have been a pre-existing fracture network and proximity to pegmatite dykes. Pegmatite dykes in diopside have a zoned alteration pattern (Figs. 3.18a - g) with (i) a core of pinkish hematite-dusted feldspar, which grades outwards to the diopside host through zones of; (ii) hematite-dusted feldspar ± epidote ± garnet; (iii) epidote ± garnet + chlorite + calcite ± traces of disseminated pyrite; (iv) chlorite + calcite ± disseminated hematite with remnant diopside; (v) jig-saw fit brecciated massive diopside; (vi) massive diopside. In the absence of a biotite precursor, metasomatic feldspars in altered diopsidic host rocks are sodic rather than potassic (Fig. 3.18e).

## 3.8 Discussion

In this section, the Palaeoproterozoic stratigraphy at Menninnie Dam is compared with similar units that occur elsewhere on the Eyre Peninsula for the purposes of regional correlations. The timing of deformation, granite and pegmatite dyke emplacement, and metasomatism is discussed with reference to regional tectonic and intrusive events.

### 3.8.1 Origin of the central suite calc-silicates

Two hypotheses can be proposed for the origin of calc-silicate minerals in the central suite rocks.

- Prograde and retrograde metamorphism of a dolomite - calcite - quartz and iron oxide rich protolith.
- Metasomatism of a metamorphosed dolomite and / or limestone protolith.

Whereas isochemical regional metamorphism requires all the elements to be present prior to metamorphism, metasomatism can result in addition of Mg and $SiO_2$ into a carbonate rock with elemental and mineral zonation occurring over a large area around the heat or fluid source (eg. Bingham Canyon; Atkinson and Einaudi, 1978). No such zonation has been observed at Menninnie Dam. The lack of zonation is not considered to be due to the limited area of the Menninnie Dam prospect, as marble and calc-silicate rocks with similar mineralogy and textures are common elsewhere on the Eyre Peninsula in units correlated with the Katunga Dolomite (Parker, 1993b). The mineralogy and textures of the central suite at Menninnie Dam are therefore concluded to be a product of regional metamorphism of a dolomite, calcite, quartz and iron oxide rich protolith.

The mineralogy of the central suite rocks are consistent with the metamorphic grade determined for the eastern suite schist (Section 3.3). Forsterite is absent from the central suite rocks whereas tremolite is common. The appearance of forsterite as a stable phase coincides with the disappearance of tremolite during prograde metamorphism of calc-silicate rocks (Trommsdorff, 1966, 1972; Slaughter et al., 1975; Metz, 1976). The presence of talc in central suite rocks is inconsistent with calculated peak metamorphic conditions and talc most likely formed during retrograde metamorphism through the break-down and hydration of calc-silicate minerals and carbonates (Turner, 1980). Disseminated magnetite occurs in calcitic marbles, dolomitic marbles, mixed calc-silicate - marble rocks and in massive diopside. Magnetite occurs within diopside crystals in massive diopside units and is commonly concentrated along the contact between diopside and calcite, or tremolite and calcite, in marble - calc-silicate lithologies (Fig. 3.4d). If iron oxide was evenly dispersed throughout the carbonate protolith, magnetite concentration could have occurred through consumption of carbonate during formation of calc-silicate minerals.

### 3.8.2 Regional correlations and implications for the Menninnie Dam stratigraphy.

Lithologies at Menninnie Dam can be correlated with the Middleback Subgroup of the Hutchison Group (Fig. 3.19). The marbles, calc-silicate lithologies, graphitic schists and iron formations of the central suite at Menninnie Dam are interpreted to correlate with the Katunga Dolomite and Lower Middleback Jaspilite respectively, as proposed by Parker (1993b). Marbles and calc-silicate lithologies similar to those of the central suite at Menninnie Dam crop out west of Cowell and at Sleaford Bay, and are interpreted to be equivalent to the Katunga Dolomite or Lower Middleback Jaspilite (Parker, 1993b). Iron formations at Menninnie Dam are similar to those of the Upper and Lower Middleback Jaspilites of the Middleback Subgroup. The graphitic schists at Menninnie Dam are similar to graphitic schists described elsewhere on the Eyre Peninsula.

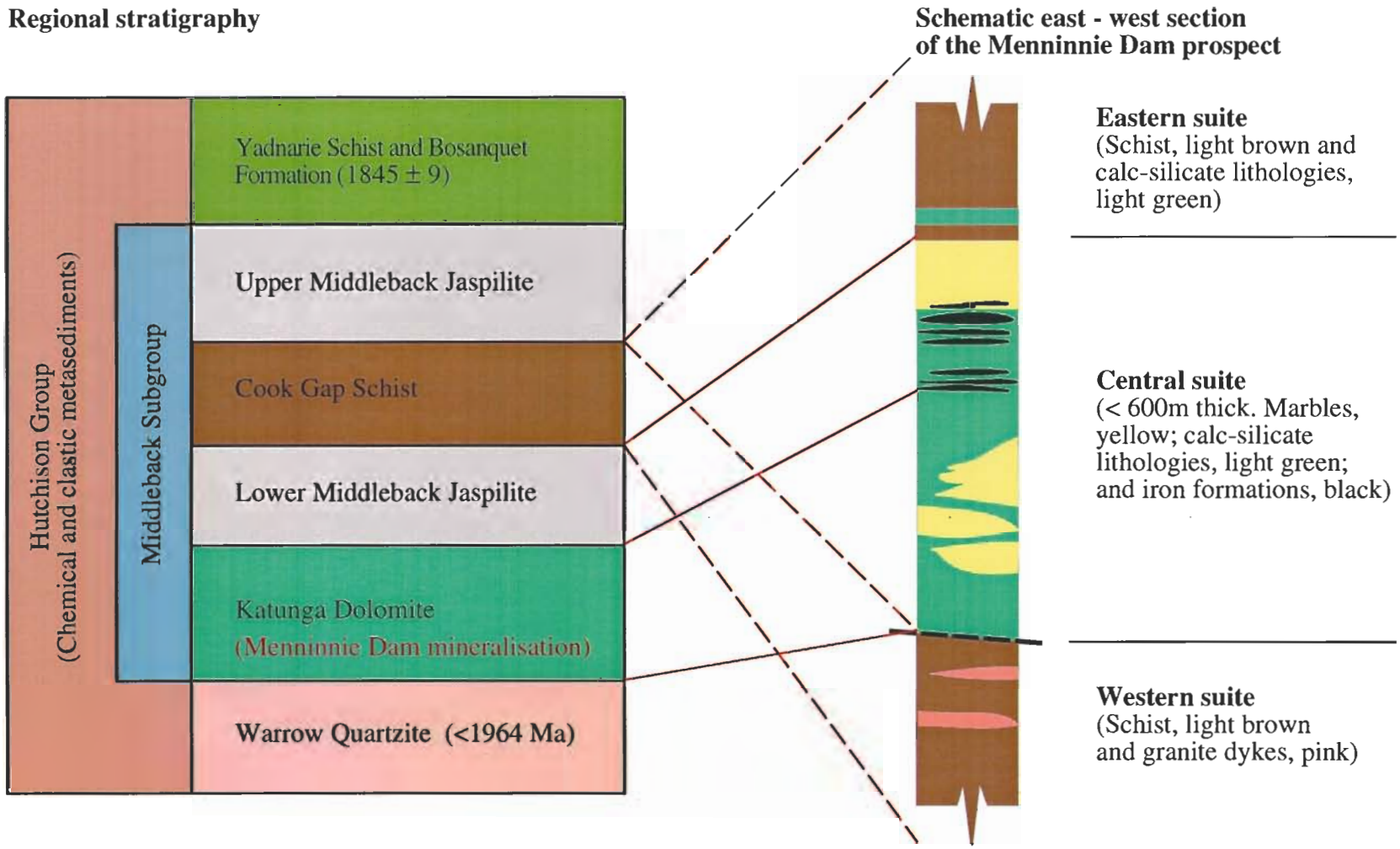


Figure 3.19 Correlation between the Menninnie Dam outcrop pattern (schematic interpretation, not to scale) and the regional stratigraphy of the Hutchison Group (modified from Parker et al., 1988 and Drexel et al., 1993). Red lines connect correlated lithologies. The heavy dashed line is the faulted contact between the central and western suites at Menninnie Dam.

Graphite is a minor component of some of the iron formations in the Middleback Ranges (Parker, 1993b) and a significant component of Middleback Subgroup schists in the Uley and Koppio regions of the southern Eyre Peninsula (Parker, 1993b).

The gradational contact between the central suite marble and calc-silicate lithologies and the eastern suite schist, along with the interpreted facing direction of metamorphosed graded beds, implies that the eastern suite is younger than the central suite. The eastern suite schist is interpreted to correlate with the Cook Gap Schist which is stratigraphically younger than the Katunga Dolomite and Lower Middleback Jaspilite (Fig. 2.3). The mineralogy, textures, occurrence of amphibolite layers, calc-silicate units, migmatites, and garnet-rich layers in the eastern suite schist are consistent with Parkers (1993b) description of the Cook Gap as "dominantly semipelitic, quartz-veined garnet-mica schist and gneiss with minor calc-silicate gneiss, magnetite-bearing gneiss, and concordant amphibolites ... the schists and gneisses are layered, comprising bands either rich or poor in mica (biotite or muscovite), garnet, feldspar, sillimanite, and quartzo-feldspathic or pegmatitic segregations". Garnetiferous bands were interpreted by Parker (1993b) to result from sedimentary layering. Migmatites are restricted to zones of higher metamorphic grade and concordant amphibolites occur throughout the lower part of the Cook Gap Schist (Parker, 1993b).

The Yadnarie Schist, interpreted to be younger than the Cook Gap Schist, is mineralogically and texturally similar to the Cook Gap Schist (Parker, 1993b), however, calc-silicate lithologies, garnetiferous bands and migmatites have not been described from the Yadnarie Schist and amphibolites are rare or absent (Parker, 1993b). Correlation of the eastern suite schist with the Cook Gap Schist is consistent with interpretation of the Menninnie Dam stratigraphy by Parker (1993b).

The contact between the western and central suites is discordant relative to stratigraphic layering in the central and eastern suites and is interpreted to be a sheared contact. In the Gawler Craton, KM-$D_3$ is associated with the formation of broad, northerly-trending mylonite zones, such as the Kalinjala Mylonite (Parker, 1978; Fig. 3.10). The sense of movement of the mylonites has been interpreted to include a major component of dextral shear (Parker, 1993a). Parker (1993a) mapped the trace of a major north-northwesterly trending mylonite zone near Refuge Rocks. If this mylonite zone was projected northwards along strike for a further 50 km, it would pass close to, or through the Menninnie Dam prospect (Fig. 3.10).

Recognition of the western suite / central suite contact as a major shear zone assists interpretation and correlation of the local stratigraphy at Menninnie Dam. The western suite schist is mineralogically and texturally similar to the eastern suite schist and the Cook Gap Schist.

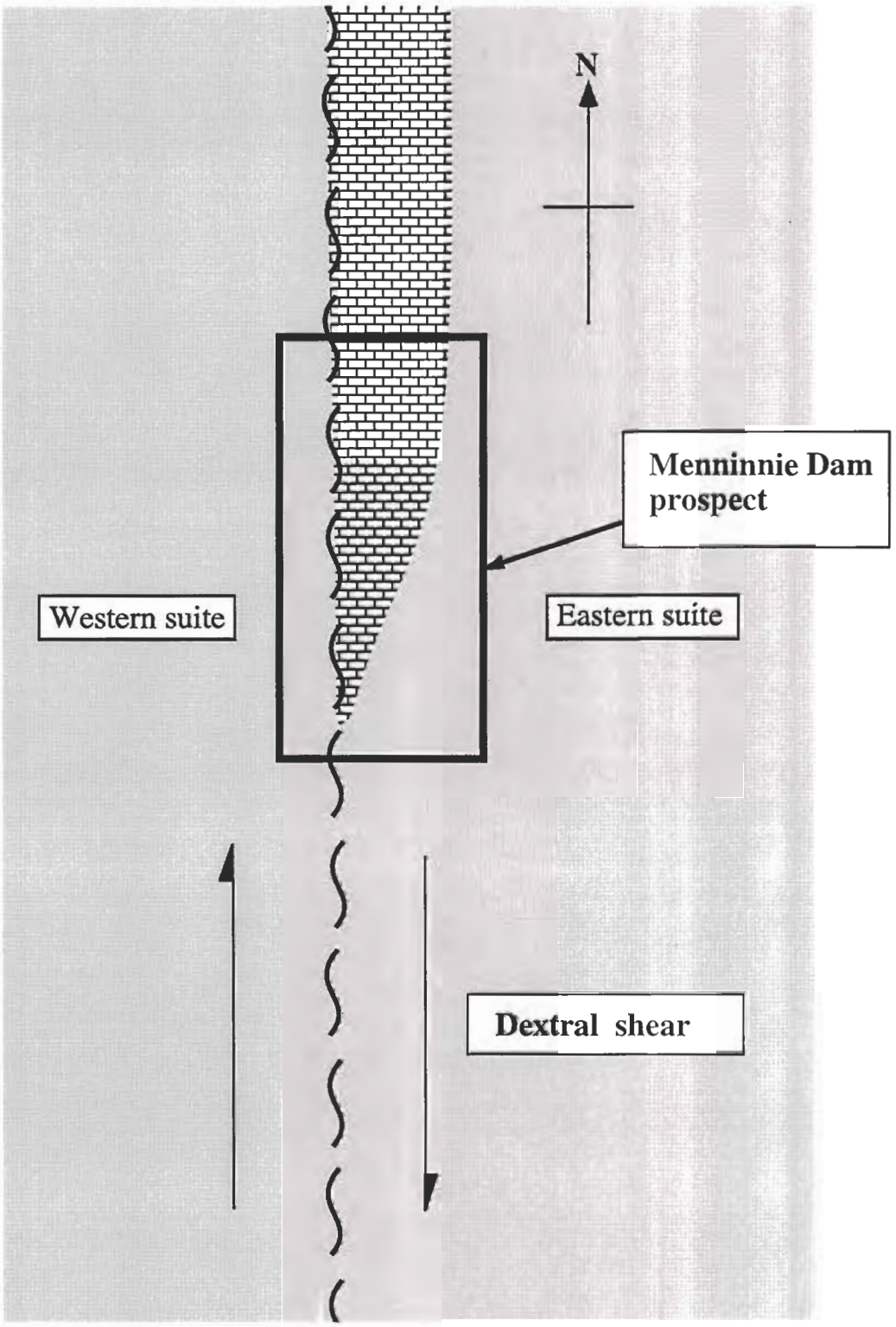


Fig. 3.20. Cartoon. The NNE trending central suite rocks (brick pattern) may have been truncated by a dextral shear bounding the central and western suites resulting in juxtoposition of the Cook Gap Schist (stippled pattern) against the lower part of the Katunga Dolomite.

Garnetiferous bands, migmatites and rare amphibolites in the western suite schist are similar to those described in the Cook Gap Schist by Parker (1993b). The western suite at Menninnie Dam is interpreted to be a structural repetition of the eastern suite that was emplaced during dextral movement along the bounding fault zone, and is therefore also correlated with the Cook Gap Schist (Fig. 3.20). Structural repetition is interpreted to have resulted in the juxtaposition of younger Cook Gap Schist against the lower units of the Katunga Dolomite (Fig. 3.2).

Higgins et al. (1990) noted the thickness of the Katunga Dolomite (central suite) at Menninnie Dam is greater than the same unit in the Middleback Ranges. Local deformation zones recognised within the central suite may have resulted in structural thickening of this unit, although this cannot be proved.

### 3.8.3 Timing of deformation and MD granite dyke emplacement

The common occurrence of deformed MD granite dykes in zones of intense deformation is consistent with a link between deformation and MD granite dyke emplacement. Factors which contribute to constraining the timing of dyke emplacement are:

- The granite dykes all have similar chemistry, and are interpreted to be co-genetic and coeval.
- Units containing abundant silicate minerals, such as iron formations and schist layers, that are enclosed in marble are commonly surrounded by a halo of calc-silicate minerals. This halo is interpreted to have formed at near peak-metamorphic conditions, and probably formed by element diffusion between silicate layers and marble. In contrast, MD granite dykes in contact with marbles have no such halo. Therefore, either the MD granite dykes did not react with the marbles, or, they were emplaced after peak-metamorphic conditions (KM-$D_{1-2}$), ie. sometime after 1745 Ma. (Parker, 1993a).
- MD granite dykes were probably intruded while the host rocks were at elevated temperatures. MD granite dykes less than a few tens of centimetres wide are not likely to have propagated any distance unless they maintained low viscosity through elevated temperatures. The absence of chilled margins to larger MD granite dykes is also consistent with hot host rocks. It therefore seems likely that the MD granite dykes were intruded prior to, or during, KM-$D_3$ (1745 - 1710 Ma., Parker 1993a), or within the thermal aureole of a granite pluton.
- Scattered outcrop of granite of the Lincoln Complex occurs ≈ 5 km to the east of the Menninnie Dam prospect and was considered by Parker (1993a) to have been emplaced during KM-$D_3$ (Moody Suite correlative; Fig. 3.10) .
- The MD granite dykes have similar geochemical compositions to granitoids of the Moody Suite. The Moody Suite and the MD granite dykes are elevated in $P_2O_5$ at

similar $SiO_2$ values (Section 3.4.2). The age of the Moody Suite is ≈ 1745 - 1710 Ma. (Parker, 1993a; Fanning, 1984).

- MD granite dykes are tectonically deformed, and have textural and geochemical attributes which distinguish them from granitoids of the Hiltaba Suite (1589 ± 2 Ma., Creaser and Cooper, 1993) which are not tectonically deformed. Therefore, MD granite dykes must have been intruded prior to 1589 Ma., and are likely to have been intruded prior to or during the previous deformation event ($KM\text{-}D_3$).

The style of MD granite dyke deformation can be used to help constrain the timing of granite dyke emplacement. Ductile deformation was more common at the margins of MD granite dykes, whereas deformation in the enclosing schist is characterised by cataclastic deformation. Strain may intuitively have been expected to partition into the phyllosilicate-rich schist, however, at Menninnie Dam, it has partitioned into the margins of granite dykes. Two mechanism could account for this:

1) Strain partitioning into MD granite dyke margins may have resulted from ductility contrasts, where the granite magma was more ductile than the enclosing schist. This situation may have arisen if hot, low viscosity granite magma was intruded into an active deformation zone in which the host rocks were cooler and less plastic.

2) Interaction of aqueous fluids with the margin of a hot MD granite dyke may have resulted in hydrothermal alteration of the MD granite dyke margin with destruction of feldspar and formation of fine grained phyllosilicates. The presence of abundant phyllosilicates may have enhanced strain partitioning. This process is similar to 'reaction softening', described by White et al. (1980).

The first mechanism requires that the MD granite dykes were intruded into an active deformation zone. If this was so, then MD granite dykes might be expected to show a lineation fabric due to both magmatic flow and solid state flow (Paterson et al., 1989). However, magmatic flow may be masked by rapid cooling and / or solid state flow in high strain environments (Miller and Paterson, 1994).

The second mechanism also requires MD granite dyke emplacement to have occurred either prior to, or during deformation. The fluid required for hydrothermal reactions and formation of chlorite and sericite at the MD granite dyke margin may have been derived from fluid entering the shear system. Beach (1980) discussed retrograde metamorphic mineral formation associated with shearing in the Lewisian Complex, NW Scotland. Hydration reactions converted feldspar to muscovite, amphibole to chlorite, and biotite to chlorite. The amount of fluid involved in such reactions can be considerable, although the source of the fluid was not known (Beach, 1980).

MD granite dykes that have intruded marbles and calc-silicate lithologies of the central suite do not show the same degree of deformation and alteration at their margins, nor are the host rocks pervasively altered to a retrograde mineral assemblage. It appears that most of the fluid flow which resulted in alteration of the MD granite dykes was focused into a zone of maximum deformation within the western suite.
The common association of hydrothermal alteration and more intense deformation at the margins of MD granite dykes in the western suite shear zone is interpreted as evidence for reaction softening as a mechanism of strain partitioning. However, strain partitioning due to ductility contrasts cannot be discounted and may have occurred prior to reaction softening.

When factors interpreted to constrain the timing of MD granite dyke are considered in conjunction, the MD granite dykes are most likely Moody Suite correlates that were emplaced during deformation associated with KM-$D_3$, and probably related to the exposed granite ≈ 5 km to the east of the Menninnie Dam prospect (Moody Suite correlative, Parker, 1993a). This constrains the timing of MD granite dyke emplacement to ≈ 1745 - 1710 Ma. (Parker, 1993a; Fanning, 1984). The pegmatite dykes (Section 3.6) are spatially associated with MD granite dykes, however the undeformed nature of pegmatite dykes is consistent with post-kinematic emplacement. Weakly deformed pegmatites intruded into the Kalinjala Mylonite Zone were dated at ≈ 1710 Ma. and were considered to have been emplaced during the latter phases of KM-$D_3$ (Fanning, 1984). A similar age of ≈ 1710 Ma. could be inferred for the pegmatite dykes at Menninnie Dam, however, on the basis of data presented in this study, the timing of the pegmatite dyke emplacement cannot be unequivocally determined.

### 3.8.4 Timing of metasomatism

None of the silicate minerals produced through metasomatic alteration have textures that are compatible with high grade metamorphism:

- Triple junctions are absent.
- There is no tendency towards metamorphic refining of minerals; for example, microcline is poikolitic (Section 3.7.1).
- Epidote, talc and chlorite are incompatible with the peak metamorphic conditions calculated for the Menninnie Dam rocks.
- Carbonate and talc are fine grained, and do not appear to have been recrystallised.
- Garnet and epidote contain well-preserved complex growth zoning.

Metasomatic alteration is spatially and genetically related to pegmatite dykes, if pegmatite dykes were associated with the latter stages of MD granite dyke emplacement, then metasomatism would also have occurred around 1710 Ma. The timing of pegmatite dykes and metasomatism is addressed again in Section 4.4.12 following presentation of data on the Mesoproterozoic stratigraphy at Menninnie Dam.

Impure marbles bound to the west by iron formations and to the east by schist (eastern suite) were pervasively altered during metasomatism. The iron formations and the schist may have acted as aquatards, impeding the passage of hydrothermal fluids.

## 3.9 Summary

The Palaeoproterozoic stratigraphy at the Menninnie Dam prospect has been subdivided into three suites, a western suite, a central suite and an eastern suite. Marbles, diopsidic calc-silicates, iron formations and minor graphitic schist bands of the central suite are correlated with the Katunga Dolomite and Lower Middleback Jaspilite of the Middleback Subgroup. The eastern suite biotite - quartz - feldspar - muscovite - sillimanite - garnet schist correlates with the Cook Gap Schist of the Middleback Subgroup. Deposition of the host rocks can therefore be constrained to ≈ 1964 - 1845 Ma.

Thermobarometric calculations indicate peak conditions corresponding to upper amphibolite facies followed by a retrograde greenschist event. Calculated P - T conditions correspond with those determined elsewhere on the Eyre Peninsula for peak-metamorphic (KM-$D_{1-2}$) and retrograde metamorphic (KM-$D_3$) phases of the Kimban Orogeny.

Regionally, the Warrow Quartzite underlies Katunga Dolomite. However, in contrast to earlier reports (Higgins and Hellsten, 1986; Higgins et al., 1990), the Warrow Quartzite is not known to occur in the immediate vicinity of Menninnie Dam. The contact between the central and western suites is interpreted to be a large protocataclastic to mylonitic shear zone. Assuming a dextral sense of movement, the western suite schist is probably a faulted repetition of the eastern suite. The shear zone was probably initiated during KM-$D_3$, synchronous with the formation of large, N-S trending, mylonite zones elsewhere on the Eyre Peninsula. Granite dykes are interpreted to have intruded the western suite protocataclastic to mylonitic schists during the deformation event with partitioning of ductile strain into the margin of the granite dykes. Granite dykes are tentatively considered to be Moody Suite correlates and have an inferred age of 1740 - 1710 Ma. Pegmatitic dykes are spatially associated with granite dykes but have textures consistent with post-kinematic emplacement. Pegmatite dykes may have been emplaced during the latter stages of KM-$D_3$ (≈ 1710 Ma.; Fanning, 1984), however the timing of emplacement is uncertain. Fluids associated with pegmatitic dykes resulted in pervasive metasomatism of central suite marbles, particularly those that contained a minor pelitic component.

# Chapter four
# Local geology: The Mesoproterozoic

## 4.1 Introduction

The Mesoproterozoic geology at Menninnie Dam is described in this chapter. Excluding a veneer of Quaternary cover, all rocks younger than Palaeoproterozoic at Menninnie Dam are interpreted to be of Mesoproterozoic age (1600 Ma. - 1000 Ma.). At Menninnie Dam, Mesoproterozoic rocks overlie Palaeoproterozoic rocks, however, unlike Palaeo-Proterozoic lithologies, they have not been metamorphosed, tectonically deformed or metasomatised. Mesoproterozoic rocks have been deeply weathered to depths commonly in excess of 100m and much of the weathered profile was percussion drilled, therefore, drill core of Mesoproterozoic rocks is less complete than that for Palaeoproterozoic rocks. All descriptions and interpretations are based on limited drill core and a few percussion holes.

The orientation of some Mesoproterozoic rock units at Menninnie Dam are poorly constrained due to their limited lateral extent and the wide spacing of drill holes (typically spaced 200m apart, Fig. 3.1). Where possible, the orientation of Mesoproterozoic rock units has been interpreted from their intersection in two or more drill holes, and on two or more sections. Summary drill hole logs and cross sections are presented in Appendix 3.1.

The aims of this chapter are to:

- Describe the regional geological setting.
- Describe the Mesoproterozoic rock units at Menninnie Dam.
- Compare the geochemistry of intrusive rocks to the geochemistry of the Gawler Range Volcanics (GRV) and co-magmatic Hiltaba Suite.
- Interpret the processes which resulted in formation of Mesoproterozoic rock units.

## 4.2 Geological setting

Mesoproterozoic rock units in the vicinity of the Menninnie Dam prospect comprise volcaniclastic lithologies, lavas, and dykes of the GRV. A simplified stratigraphy and outcrop map of the GRV in the southern Gawler Range area are illustrated in Figures 4.1 and 4.2 respectively. Two kilometres to the west of the Menninnie Dam prospect are low hills comprising Bittali Rhyolite. Scattered, low-lying, Bittali Rhyolite also crops out to the east and south of the Menninnie Dam prospect (Fig. 4.2). The Nonning Rhyodacite crops out ten kilometres to the northeast of the Menninnie Dam prospect and forms low lying, dissected foothills of the Gawler Ranges.

The Eucarro Dacite crops out two kilometres to the north of the Menninnie Dam prospect as low-lying dissected foothills of the Gawler Ranges.

Stratigraphy of the Southern Gawler Ranges area

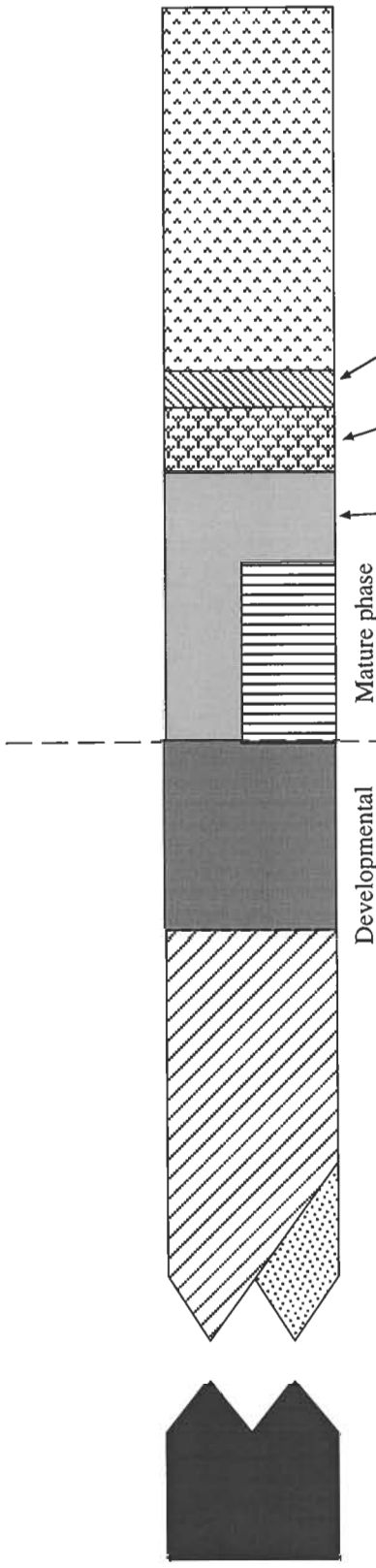


Yardea Dacite Massive porphyritic dacite and rhyodacite. Phenocrysts of plagioclase (≤1cm across), smaller K-feldspar and clinopyroxene set in a finely granular felsic matrix.

Paney Rhyolite. Fine grained to coarsely porphyritic rhyolite with phenocrysts of K-feldspar and spherical quartz set in a fine-grained felsic matrix. Common flow banding and fiamme. Grades into rhyodacite.

Yannabie Rhyodacite. Fine grained to porphyritic rhyodacite with phenocrysts of plagioclase, K-feldspar and some spherical quartz in tuffaceous, vesicular matrix. Grades into rhyolite with more abundant quartz phenocrysts.

Eucarro Dacite. Massive porphyritic dacite grading to rhyodacite with scattered plagioclase (≈ 5 mm across), spherical quartz, and minor K-feldspar, and clinopyroxene phenocrysts set in a finely-granular or granophyric matrix of K-feldspar and quartz.

Nonning Rhyolite. Massive porphyritic rhyodacite to dacite. Phenocrysts of plagioclase (≤ 1 cm across), smaller K-feldspar crystals, clinopyroxene and round quartz are set in a reddish-brown, granophyric or microgranular felsic matrix.

Bittali Rhyolite. Variable assemblage of rhyolitic to rhyodacitic lavas, intrusive feeder dykes and welded ash flows with flow banding, fiamme and pumiceous streaks. Texture ranges from fine-grained to porphyritic with phenocrysts of K-feldspar, plagioclase and round quartz.

Waganny Dacite. Porphyritic dacite to rhyodacite with phenocrysts of plagioclase and minor K-feldspar up to 2 mm across set in a aphanitic or microgranular matrix.

PAO1 - (rare basal member of sucession). Unnamed porphyritic rhyolite.

Proterozoic or unknown basement

Fig. 4.1 Schematic, simplified stratigraphy of the Gawler Range Volcanics in the southern Gawler Ranges area (not to scale; stratigraphy and descriptions modified after Blissett et al., 1988), with subdivision into the developmental and mature phases (after Stewart, 1992).

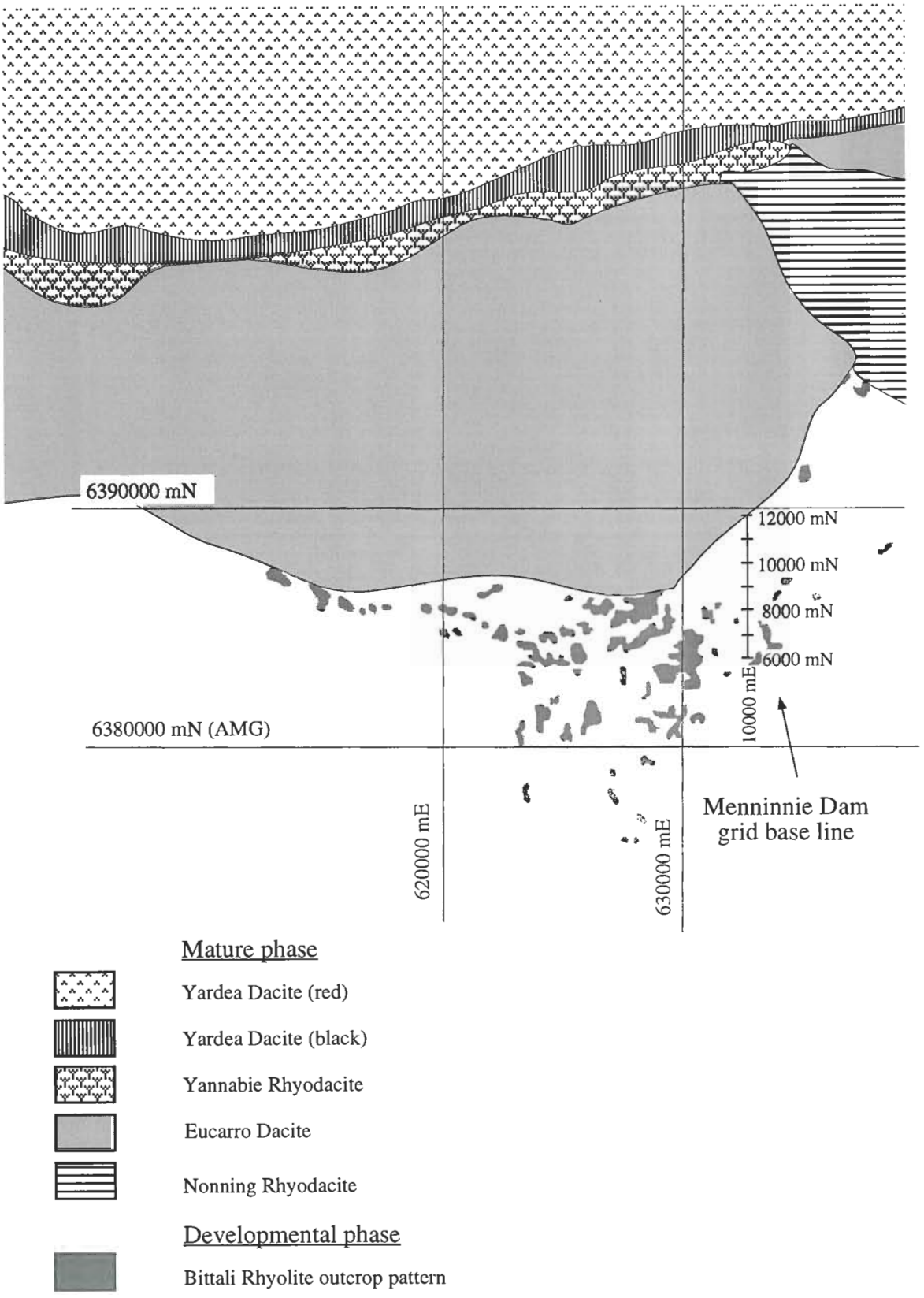


Figure 4.2 Location of the Menninnie Dam grid and simplified map of the Gawler Range Volcanics units in the southern area of the Gawler Ranges (modified after Blissett et al., 1988), with subdivision into the developmental and mature phases after Stewart (1992).

## 4.3 Prospect geology

Mesoproterozoic rock units encountered during drilling at Menninnie Dam are described starting with units interpreted to be the oldest followed by progressively younger units. These include:

- Rhyolite intrusions
- Discordant polymictic breccia units
- Fiamme-bearing discordant polymictic breccia units
- Rhyolite-bearing discordant polymictic breccia units
- Layered polymictic breccia units
- Rhyolite-bearing layered polymictic breccia units
- Coherent rhyolite
- Muddy sandstone and pumice breccia units
- Menninnie Dam ignimbrite

An interpretation of rhyolite-bearing discordant polymictic breccia units is presented immediately following the description, however all other units are interpreted in a later discussion section.

### 4.3.1 Rhyolite intrusions

Brick-red, quartz- and feldspar-phyric rhyolite intrusions were intersected in four drill holes in the south of the Menninnie Dam prospect (Table 4.1 and Fig. 4.3a). The lower contacts of two rhyolite intrusions (drill holes PD0030 and PD0031) were not intersected by drilling, and their extent is not known.

Table 4.1 Drill hole intersections of rhyolite intrusions. Northing and easting coordinates are for drill collars. 'From' and 'To' are down hole depths. The orientation of rhyolite intrusions is not known, therefore the width is equal to that intersected in drill holes.

| Drill hole | Northing | Easting | From(m) | To(m) | Width (m) | Type* |
|---|---|---|---|---|---|---|
| PD0019 | 8381 | 10408 | 283.5 | 296.5 | 13.0 | ? |
| PD0027 | 9293 | 10025 | 76 | 82 | 6 | ? |
| PD0027 | 9293 | 10025 | 86 | 116 | 30 | ? |
| PD0030 | 7764 | 10250 | 373.9 | 388.25 | 14.35 | W.A. |
| PD0030 | 7764 | 10250 | 395.00 | 417.00 | 22.0 | S.A. |
| PD0030 | 7764 | 10250 | 459.74 | >551.00 (EOH) | >91.26 | W.A. |
| PD0031 | 8023 | 10300 | 644.2 | >644.8 (EOH) | >0.6 | W.A. |

* W.A. = weakly hydrothermally altered; S.A. = strongly hydrothermally altered; ? = intensity of hydrothermal alteration unknown as masked by intense weathering. EOH = end of hole.

Rhyolite intrusions in drill holes PD0027 and PD0019 are intensely weathered and will not be considered further. With so few drill hole intersections, it is not possible to determine the dimensions or shape of rhyolite intrusions although lenticular or pipe-like shapes are considered likely (Fig. 3.1 and Appendix 3.1).

Fig. 4.3a. Drill hole PD0030, 471 m. Hand specimen of weakly altered, brick-red quartz- and feldspar-phyric rhyolite intrusion. A single 1.5 x 1 cm xenolith consisting of altered silicate minerals and pyrite occurs in the centre of the figure (X).

Fig. 4.3b. Drill hole PD0030, 471 m. Transmitted light photomicrograph (x-nicols) of the groundmass of a rhyolite intrusion. The groundmass consists of a mosaic of fine-grained quartz and feldspar with a granophyric texture.

Fig. 4.3c. Drill hole PD0030, 471 m. Photomicrograph (reflected light) of round and embayed pyrite from the 1.5 x 1 cm xenolith illustrated in Figure 4.3a.

Fig. 4.3d. Drill hole PD0030, 410 m. Hand specimen of strongly altered, light yellow-green, quartz- and feldspar-phyric rhyolite intrusion. Relict feldspar and ferro-magnesian phenocrysts have been pervasively altered to dark, fine grained sericite, quartz, calcite and chlorite. The groundmass is an alteration assemblage of fine grained, felted sericite, quartz, calcite and chlorite.

Fig. 4.3e. Drill hole PD0030, 410 m. Reflected light photomicrograph of irregularly shaped crystals of chalcopyrite (CP) have been enclosed by galena (G) in the strongly altered rhyolite intrusion.

4.3a

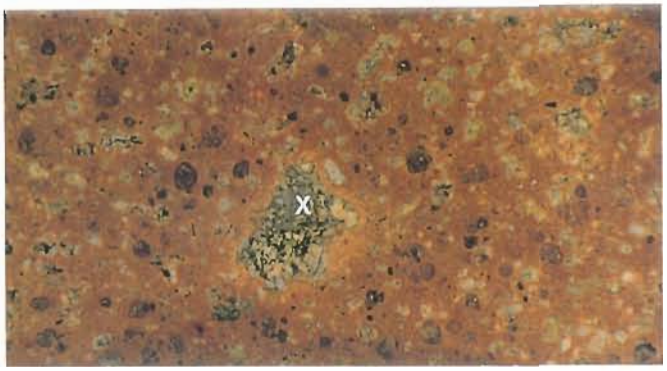


4.3b

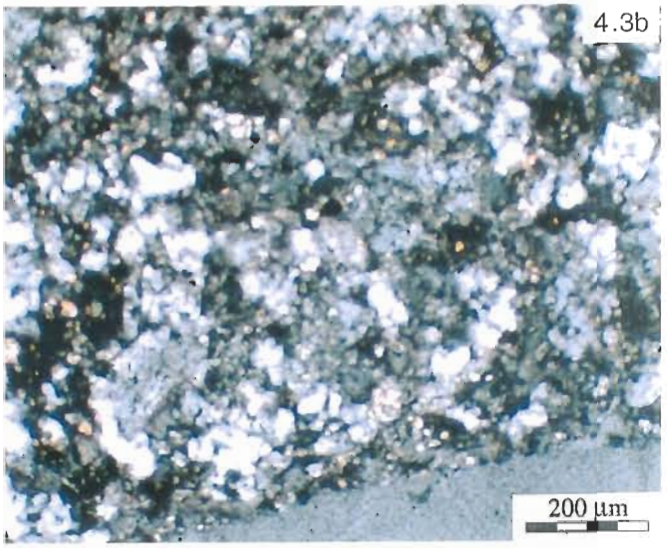


4.3c

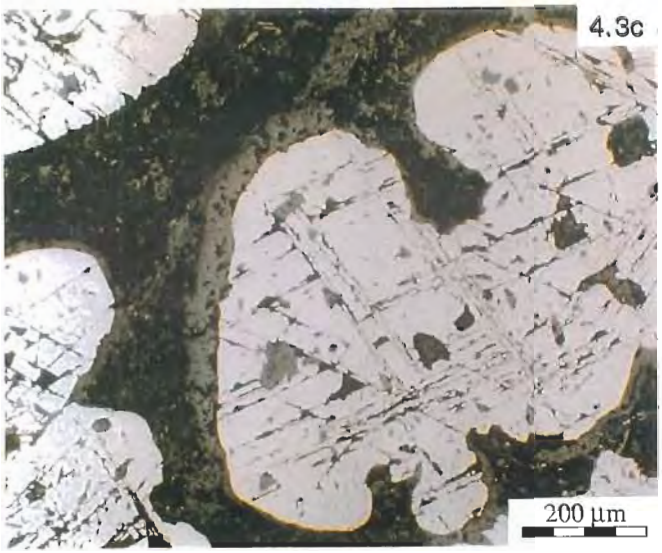


4.3d

4.3e

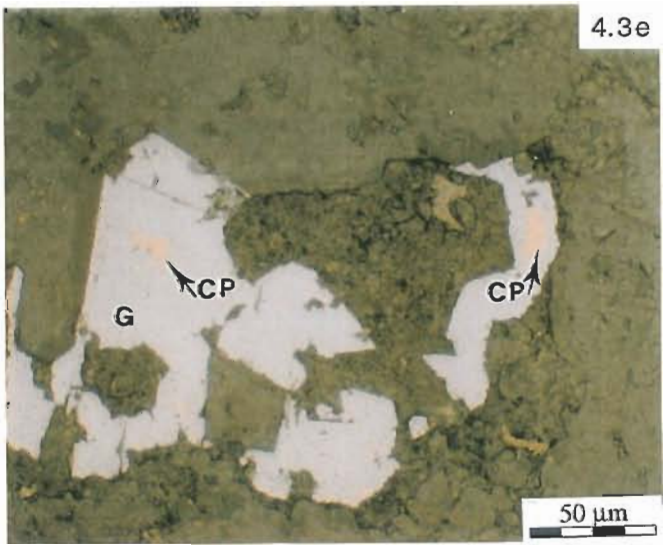

**Description**

All rhyolite intrusions are non-vesicular and have similar primary mineralogy and textures. Their mineralogy and mineral proportions have been visually estimated as: subhedral, round and embayed quartz phenocrysts, typically 0.5 - 4 mm across (15%); euhedral albite phenocrysts, typically 0.1 - 2 mm across (6%); euhedral K-feldspar, typically 0.1 - 4 mm across (10%), in a fine-grained groundmass. Altered remnants of ferro-magnesian phenocrysts comprise less than 1%. Rhyolite intrusions can be subdivided into two groups based on the intensity of hydrothermal alteration:

1) Weakly altered rhyolite intrusions
2) Strongly altered rhyolite intrusions

*Weakly altered rhyolite intrusions*

Weakly altered rhyolite intrusions are brick-red. The groundmass has a granophyric texture and consists of a fine grained mosaic of quartz and feldspar (Fig. 4.3b), a texture commonly attributed to primary crystallisation of relatively slowly cooled lavas, welded ignimbrites, and shallow intrusions (Lofgren 1971b).

Ferro-magnesian minerals have been altered to fine grained quartz, calcite, hematite and chlorite. Rare trace amounts of chalcopyrite are locally associated with relict ferro-magnesian phenocrysts. Albite phenocrysts have been partially, to pervasively, altered to sericite, quartz, minor calcite, trace amounts of chlorite and a dusting of hematite. K-feldspar phenocrysts are mostly unaltered, although locally, some have been partially altered to sericite, calcite, and quartz with traces of chlorite, and a dusting of hematite. Groundmass feldspar has been partially altered to sericite. The groundmass has a pervasive dusting of hematite which imparts a characteristic brick red colour to weakly altered rhyolite intrusions.

Trace amounts of pyrite (< 0.5 mm across) are sparsely, but evenly, dispersed throughout the groundmass. The shape of pyrite grains is irregular, to blebby, with rare subhedral grains. A single 1.5 x 1 cm clast comprising pyrite and altered silicate minerals occurs at 471 m in drill hole PD0030. Pyrite 'grains' within the clast are up to 3 mm across and have blebby and embayed shapes, similar to dispersed pyrite grains. The clast has distinct margins consistent with inclusion of a sulphide-rich xenolith (Figs. 4.3a, c).

The size of phenocrysts in the rhyolite intrusion intersected near the end of drill hole PD0030 has a zonal distribution. Within seven metres of the intrusion margin, quartz and feldspar phenocrysts are 0.5 -2 mm across. Greater than seven metres from the margin of the intrusion, quartz and feldspar phenocrysts are 1 - 4 mm across. Hutchison Group calc-silicate lithologies at the upper contact of the rhyolite intrusion are fractured over an interval of 1.3 m. 'Fingers' of rhyolite , typically a few centimetres thick, have intruded fractures in calc-silicate lithologies.

*Strongly altered intrusion(s)*

The rhyolite intrusion at 395.00 - 417.00 m in drill hole PD0030 is light yellow-green due to pervasive hydrothermal alteration (Fig. 4.3d). Quartz and relict feldspar phenocrysts are of similar size and abundance (≈ 31%) to those in the outer seven metres of weakly altered rhyolite intrusions. Relict feldspar phenocrysts have been pseudomorphed by fine grained sericite, quartz, calcite and chlorite. The former presence of ferro-magnesian phenocrysts cannot be determined due to the intensity of alteration. The groundmass has been altered to fine grained mosaic of sericite, quartz, calcite and chlorite. Some groundmass quartz micropoikilitically encloses fine grained sericite ± calcite ± chlorite and quartz pseudomorphs of feldspar microlites, similar to the weakly altered rhyolite intrusions.

Trace amounts of fine grained (< 0.2 mm) pyrite, sphalerite, galena and chalcopyrite are locally associated with relict feldspar and/or ferro-magnesian phenocrysts (Fig. 4.3e). Sphalerite, galena and chalcopyrite have highly irregular grain shapes. Most pyrite also has irregular grain shapes, with rare subhedral and cubic crystals, in contrast to the round and embayed shape of pyrite in the weakly altered rhyolite intrusion.

The upper margin of the intrusion is in contact with eastern suite schist which shows little evidence of disruption or alteration. The lower margin is in contact with brecciated and altered Hutchison Group marble.

### 4.3.2 Polymictic breccia units

Localised, polymictic breccia units have discordant contacts with Hutchison Group and MD granite dyke lithologies, and also occur as layered units overlying the Hutchison Group (discordant and layered polymictic breccias are abbreviated to 'DP breccia' and 'LP breccia' throughout the remainder of the text). DP and LP breccias consist of unsorted to poorly sorted, matrix supported, polymictic breccia (Fig. 4.4a). Clast are commonly randomly oriented, and range from angular to rounded. There is no correlation between clast lithology and the degree of rounding and angular and sub-rounded clasts of the same size and lithology are locally adjacent. A complete range of clast sizes is present. The largest clasts observed are ≈ 8 cm across and most clasts are generally ≤ 5 cm across. There is no lower clast size limit and clearly discernible clasts grade down to sub-millimetre size and form the matrix to larger clasts. For the purpose of this study, clasts < 2 mm diameter are considered to form the matrix. In order of decreasing abundance, clast lithologies include marbles and calc-silicate lithologies, granite dyke fragments, pegmatite dyke fragments, western and / or eastern suite schist, iron formation, graphitic schist, rhyolite intrusion fragments, rhyolite fiamme, and rare sulphide clasts.

Although DP and LP breccia units are composed of similar rock types and have textural similarities, sufficient differences are present to justify separate consideration.

Fig. 4.4a. Drill hole PD0010, 173.63 m. Hand specimen of a typical poorly sorted, matrix supported, discordant polymictic breccia (DP breccia). Angular to sub-rounded clasts of marble (M), pyrite (PY), sulphide-bearing marble (SM) and granite dyke fragments (G) are randomly orientated. The matrix (< 2 mm) consists of fragments of similar lithologies.

Fig. 4.4b. Drill hole PD0025. Upper: 544.6 m, Middle: 543.0 m, Lower: 539.2 m. Hand specimens sampled at different localities across a DP breccia unit that is graded from one margin to next. The upper sample contains coarser, more angular lithic clasts (L) and rhyolite clasts (R) with a distinct orientation. The middle sample is finer grained with minor rounded lithic clasts (L) and a moderately distinct fabric. The lower sample is the finest grained, all lithic clasts are well rounded and the breccia has a distinct fabric.

Fig. 4.4c. Drill hole PD0014, 207.7 m. Hand specimen near the centre of a graded DP breccia unit. Larger, rounded lithic clasts are more common near the centre of this DP breccia unit. Late calcite veins (C) have cross-cut the DP breccia.

Fig. 4.4d. Drill hole PD0031, 196 m. Hand specimen of a fiamme-bearing DP breccia unit. The DP breccia consists of small lithic clasts (L), rhyolite clasts (R) and rhyolite fiamme (F). Rhyolite clasts and rhyolite fiamme have a common orientation. The angle between the drill core axis and the orientation of fiamme is consistent with either a sub-horizontal or sub-vertical orientation.

Fig. 4.4e. Drill hole PD0031, 196 m. Transmitted light photomicrograph of sericite altered rhyolite fiamme (F) in a fiamme-bearing DP breccia unit. Fiamme commonly contain round and embayed quartz crystals (Q).

Fig. 4.4f. Drill hole PD0031, 196 m. Transmitted light photomicrograph of the groundmass of a rhyolite clast in a fiamme-bearing DP breccia unit. The groundmass consists of quartz that micropoikilitically encloses feldspar microlites.

4.4a
M
SM
SM
M
PY
M
G
2 cm

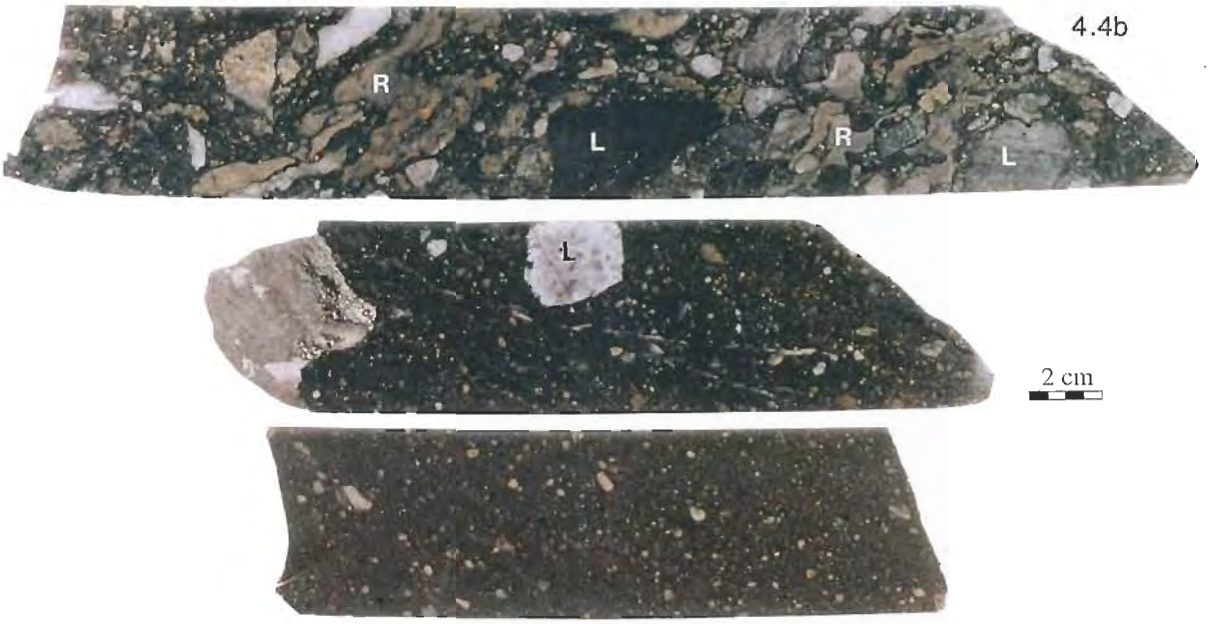
4.4b
R
L
R
L
L
2 cm

4.4c
C
2 cm

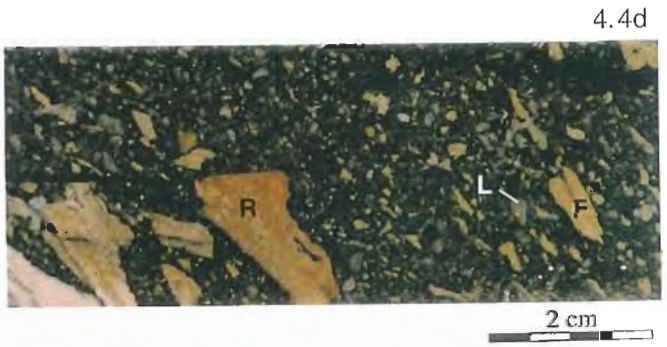
4.4d
R
L
F
2 cm

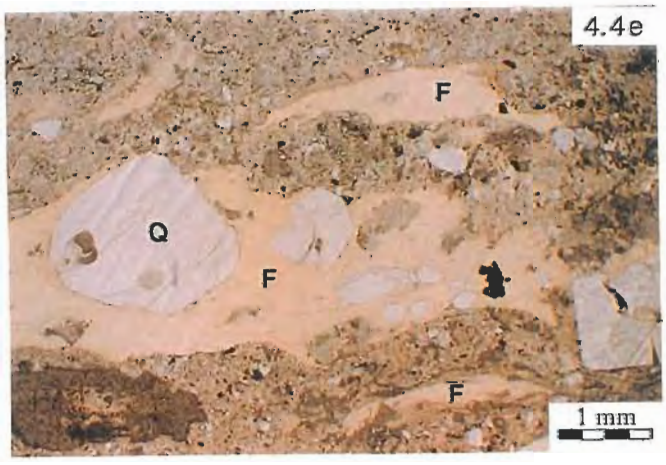
4.4e
F
Q
F
F
1 mm

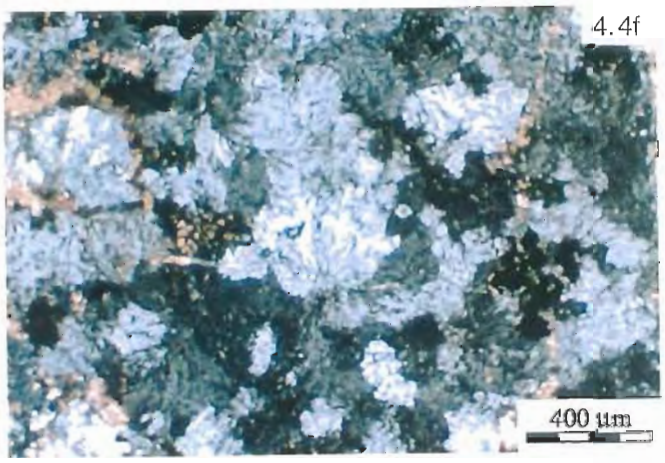
4.4f
400 µm

## DP breccia units

DP breccia units appear to be restricted to marble and calc-silicate lithologies of the central suite, and marble - calc-silicate lithologies of the eastern suite (Table 4.2), however this may be a function of the restricted location of drill holes.

Table 4.2 Drill hole intersections of DP breccia units. Northing and easting are drill collar coordinates. All depths are down hole depths. The orientation of DP breccia units is not known, therefore, the width is equal to that intersected in drill holes.

| Drill hole | Northing | Easting | DP breccia Interval (m) | DP breccia Width (m) | Fault zone interval (m) |
|---|---|---|---|---|---|
| PD0003 | 10000 | 11235 | 183.10 - 183.2 | 0.10 | 182.93 - 187.20 |
| PD0007 | 10400 | 10791 | 105.20 - 107.65 | 2.45 | |
| PD0007 | 10400 | 10791 | 215.30 - 215.55 | 0.25 | 214.2 - 220.50 |
| PD0008 | 9200 | 10314 | 223.65 - 223.85 | 0.20 | 223.33 - 224.13 |
| PD0009 | 9400 | 10350 | 231.00 - 231.40 | 0.40 | |
| PD0009 | 9400 | 10350 | 236.85 - 236.95 | 0.10 | |
| PD0010 | 9000 | 10300 | 153.60 - 153.66 | 0.06 | |
| PD0010 | 9000 | 10300 | 158.30 - 160.90 | 2.60 | |
| PD0010 | 9000 | 10300 | 167.80 - 179.18 | 11.38 | |
| PD0011 | 9200 | 10210 | 422.70 - 423.60 | 0.90 | 421.20 - 423.90 |
| PD0014 | 11200 | 11140 | 179.78 - 179.88 | 0.10 | 179.66 - 180.00 |
| PD0014 | 11200 | 11140 | 196.10 - 196.14 | 0.04 | |
| PD0014 | 11200 | 11140 | 207.47 - 207.86 | 0.39 | |
| PD0016 | 9392 | 10663 | 102.10 - 132.91 | 30.81* | |
| PD0021 | 7564 | 10073 | 379.24 - 379.96 | 0.72 | |
| PD0024 | 8961 | 10125 | 322.70 - 325.37 | 2.67 | |
| PD0024 | 8961 | 10125 | 385.25 - 385.85 | 0.60 | 384.50 - 385.85 |
| PD0025 | 7957 | 10051 | 536.73 - 545.30 | 8.57 | 531.00 - 545.80 |
| PD0026 | 9060 | 10104 | 299.80 - 302.75 | 2.95 | 296.13 - 303.74 |
| PD0027 | 9293 | 10025 | 460.33 - 461.53 | 1.20 | |
| PD0027 | 9293 | 10025 | 462.70 - 462.90 | 0.20 | |
| PD0027 | 9293 | 10025 | 465.00 - 465.50 | 0.50 | |
| PD0027 | 9293 | 10025 | 473.15 - 477.17 | 4.02 | 473.15 - 477.47 |
| PD0028 | 8746 | 10461 | 507.23 - 509.60 | 2.37 | 507.23 - 518.4 |
| PD0028 | 8746 | 10461 | 513.91 - 516.00 | 2.09 | 507.23 - 518.4 |
| PD0029 | 8776 | 10329 | 274.02 - 275.20 | 1.18 | 274.00 - 280.10 |
| PD0030 | 7764 | 10250 | 373.90 - 388.25 | 14.35 | |
| PD0031 | 8023 | 10300 | 195.5 - 197.35 | 1.85 | |
| PD0031 | 8023 | 10300 | 422.50 - 424.80 | 2.30 | 418.10 - 424.80 |

*DP breccia in drill hole PD0016 is intensely weathered and its thickness is uncertain.

DP breccia units vary greatly in drill intersection width from 0.04m to 14.35 m (and possibly 30.81 m) and occur from ≈ 100m to > 500m depth. The orientation and shape of DP breccia units is not known and they cannot be interpolated between adjacent drill holes, or adjacent sections. In general, DP breccia units are more common between 8500 mN and 9500 mN and their drill intersection width is greater to the south of 9500 mN compared to those north of 9500 mN (Fig. 4.5a). The drill intersection width of DP breccias does not show any systematic change with depth (Fig. 4.5b). Contacts between DP breccia units and the host rocks are sharp and curviplanar and fracturing of the host rock adjacent to DP breccia units is common.

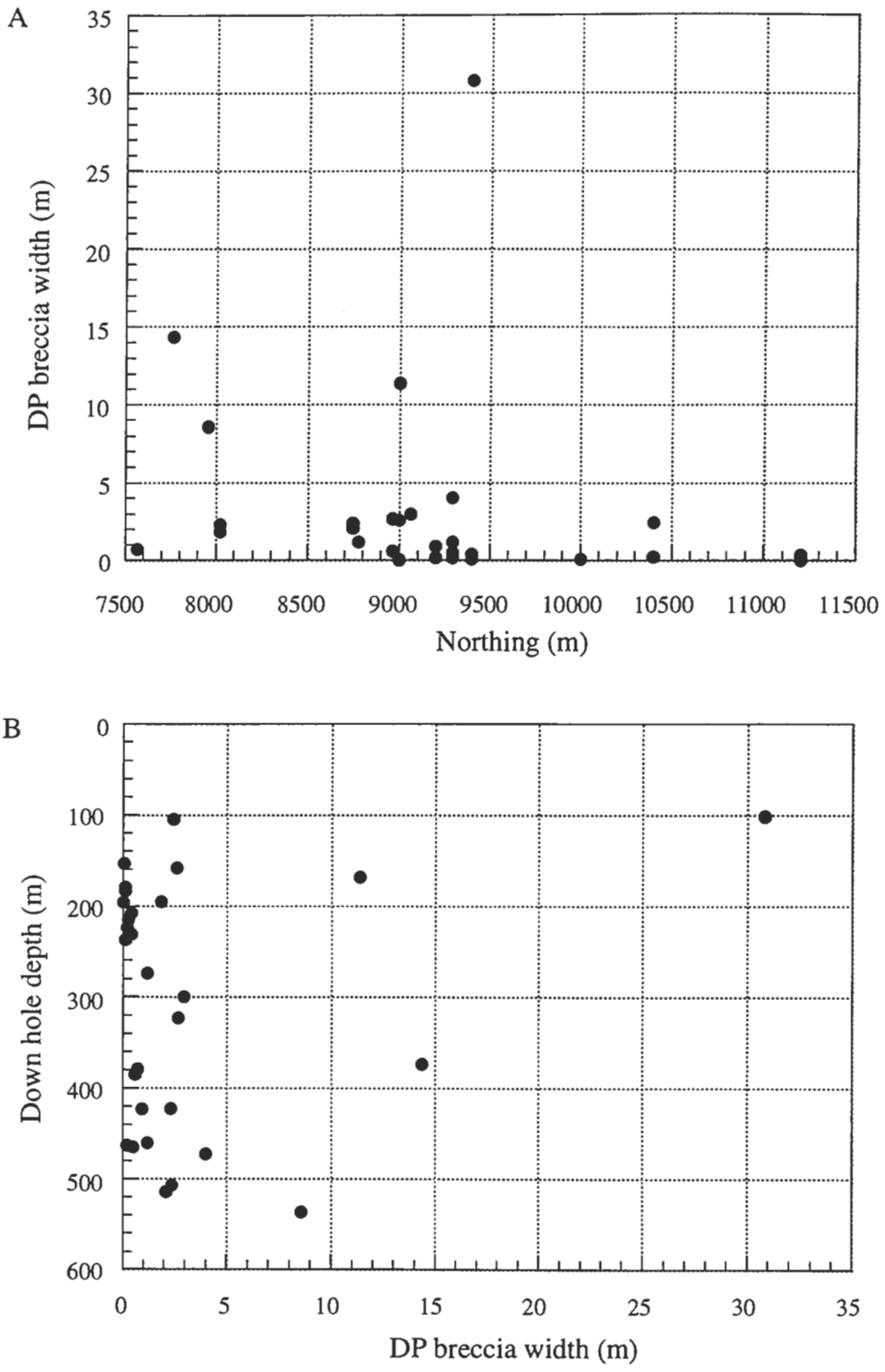


Fig. 4.5A - B Diagrams of the width of DP breccias vs northing (A), and down hole depth vs width of DP breccia (B). DP breccias are more common between 8500 mN and 9500 mN and commonly wider in the south of the Menninnie Dam prospect. DP breccias occur over a range of depths with no systematic relationship between depth and the width of DP breccia bodies.

Many of the clast lithologies present in DP breccias are not present in the adjacent wall rock. Where DP breccias are hosted by a thick sequence of a single rock type, clasts of the same lithology as the host rock are more abundant. Different drill intersections of DP breccia commonly have different proportions of clasts to matrix. DP breccias with ≥ 40% matrix commonly contain smaller, rounded clasts, and DP breccia with a < 40% matrix commonly contain larger, angular to rounded clasts. Clasts in some DP breccia units are laterally graded. Three different types of clast grading have been recognised:

- 'Double coarse margin grading': Smaller, rounded clasts with a higher proportion of matrix occur near the centre of the DP breccia unit and larger, more angular clasts with a diminished matrix content occur near the breccia margins.
- 'Single coarse margin grading': Gradational variation in the size and proportion of clasts to matrix from one margin to the next (Fig. 4.4b).
- 'Coarse centre grading': Small rounded clasts and a higher proportion of matrix occur near the margins of the DP breccia unit, and coarser well rounded clasts with a smaller proportion of matrix near the centre of the DP breccia unit (Figs. 4.4c).

The finer-grained portion of graded DP breccias commonly has a faint fabric with the long axis of clasts oriented parallel to the margin of the DP breccia unit (Fig. 4.4b).

**Fiamme-bearing DP breccia units**

DP breccias in drill holes PD0021 and PD0031 at 379.24 - 379.96m and 195.5 - 197.35m respectively contain rhyolite fiamme* and rhyolite clasts (Fig. 4.4d). Both units have a poorly defined layered fabric orientated ≈ 30 - 60° to the drill core axis (the drill hole is orientated ≈ 60° from horizontal). Layers are typically 0.5 - 5 cm wide and comprise layers of poorly sorted sand to mud sized matrix, and less commonly, layers of matrix supported clasts. Contacts between layers are diffuse but planar. Fiamme-bearing DP breccia units consist of 5 - 15% rounded lithic clasts, typically 2 - 10 mm across, 1 - 5% sub-rounded rhyolite clasts, typically 10 - 50 mm across, and 5 - 15% of light green, sericite altered rhyolite fiamme, typically 2 - 20 mm long, set in a fine grained altered matrix. The orientation of fiamme is consistently parallel to layering. Fiamme have ragged terminations and locally include round and embayed quartz crystals and crystal fragments (< 2 mm across) similar to those in the strongly and weakly altered rhyolite intrusions (Fig. 4.4e). The groundmass of fiamme comprises a fine grained mosaic of quartz, sericite, chlorite and calcite. The groundmass of rhyolite clasts commonly comprises quartz that micropoikilitically encloses partially altered feldspar microlites (Fig. 4.4f). Round and

* Fiamme is derived from the Italian 'fiamma' = flame, and relates to the ragged to wispy flame like shape of clasts. In this study, the term fiamme is used as purely descriptive term without genetic connotations or any implication of hot emplacement or welding. This is in recognition of near identical shapes derived from the sintering together of hot, juvenile pyroclasts and from burial-compaction flattening of cool diagenetically altered pumice lapilli as well as shapes which resemble clasts but are in-fact a product of hydrothermal alteration (Allen, 1988).

embayed quartz crystals and crystal fragments are also scattered throughout the matrix of the fiamme-bearing DP breccia.

### Alteration of DP breccias

The matrix of DP breccias is commonly pervasively hydrothermally altered and some clasts have an outer altered rind, typically < 3 mm wide. Alteration minerals in order of decreasing abundance are: chlorite, calcite, sericite, minor disseminated pyrite, rare quartz and galena, and trace amounts of fine grained hematite. Marble clasts are more commonly hydrothermally altered than other clast lithologies which are generally weakly altered, or unaltered.

### Association of DP breccias and faults

Nearly half of the DP breccia units are hosted by zones of fractured host rock or fault breccias (Table 4.2; and Fig. 4.6). Fault breccias are monomict and the clast lithology is identical to the surrounding host rock. Fault breccia clasts are angular and have either a jigsaw-fit texture or a more disrupted texture. Tabular clasts are rare or absent. The contact between DP breccia and fault breccia is typically sharp and curviplanar.

DP breccias not hosted by fault breccias also have sharp host rock contacts, although the host rock is commonly fractured. Tabular host rock clasts at the contact with DP breccias have not been observed, however this may be a function of the small sample size provided by drill core. The contact between DP breccia and fractured host rock is usually inclined to the drill hole axis at such an angle that the contact must be either subvertical or subhorizontal. A subvertical orientation is considered to be more likely as this conforms with the orientation of major faults, such as the faulted contact between the western and central suites (Fig. 3.1).

### Rhyolite-bearing DP breccias

DP breccias in the southern end of the prospect are spatially associated with rhyolite intrusions. Three of the DP breccia units either partially merge with a rhyolite intrusion or contain clasts derived from rhyolite intrusions (Table 4.3).

Table 4.3 Drill hole intersections of DP breccias that either merge with a rhyolite intrusion or contain clasts of rhyolite intrusion. Northing and easting are drill collar coordinates. 'From' and 'To' are down hole depths. The orientation of DP breccia units is not known, therefore, the width is equal to that intersected in drill holes.

| Drill hole | Northing | Easting | From (m) | To (m) | Width (m) |
|---|---|---|---|---|---|
| PD0025 | 7957 | 10051 | 536.73 | 545.3 | 8.57 |
| PD0030 | 7764 | 10250 | 373.9 | 388.25 | 14.35 |
| PD0031 | 8023 | 10300 | 422.5 | 424.8 | 2.30 |

*Descriptions*

The three DP breccia intersections listed in Table 4.3 have different textures and are described separately.

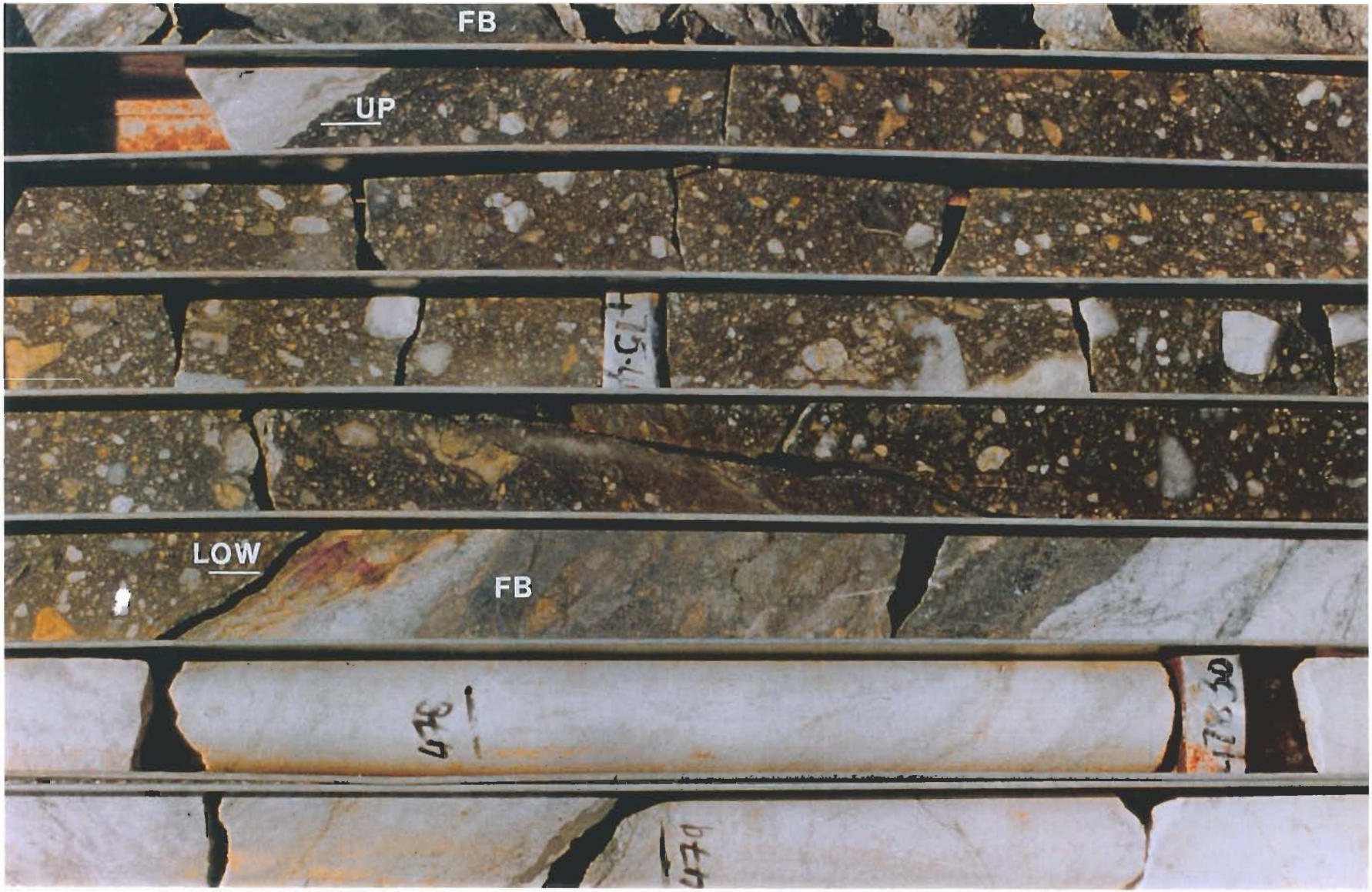


Fig. 4.6. Drill hole PD0027, 473 m (upper) - 479 m (lower). Drill core of a DP breccia unit hosted by a fault zone in dolomitic marble. The upper (UP) and lower (LOW) contacts between the DP breccia unit and brecciated marble are sharp. The fault breccia (FB) is monomict and consists of partially altered dolomite marble clasts. The angle between the host rock contact and the marble fabric is consistent with a sub-vertical orientation.

*Drill hole PD0030*

The DP breccia at 373.9 - 388.25m in drill hole PD0030 is partially merged with a rhyolite intrusion (Fig. 4.7a). The centre of rhyolite intrusion contains minor clots of DP breccia and ≈ 5% dispersed DP breccia clasts. The proportion of DP breccia clots and dispersed clasts increases in towards the margin of the rhyolite intrusion, and eventually grades into DP breccia devoid of rhyolite intrusion.

Near the outer margin of the rhyolite intrusion, rhyolite has formed a complex interpenetration into the DP breccia, partially surrounding portions of DP breccia and larger clasts (Fig. 4.7a). Unbroken, penetrating 'fingers' of rhyolite intrusion can be traced back to more coherent rhyolite intrusion. In the DP breccia-dominated outer zones, the rhyolite has formed isolated clots and globules with delicate, irregular, feathery margins (Fig. 4.7b). The feathery margins of rhyolite clots and globules contrast with the angular to sub-rounded shape of lithic clasts in the DP breccia. Quartz phenocrysts within rhyolite clots and globules are commonly intact, however, minor brecciated jigsaw-fit quartz phenocrysts locally occur.

The rhyolite intrusion has a devitrified groundmass of quartz which micropoikilitically encloses feldspar microlites. Feldspar microlites and feldspar phenocrysts have been partially altered to sericite ± calcite. Alteration of the DP breccia is more intense than that of the rhyolite intrusion, and rhyolite clots and globules. DP breccia included in the rhyolite intrusion is partially to pervasively altered to chlorite, sericite and calcite. DP breccia external to the rhyolite intrusion has been pervasively hydrothermally altered to chlorite, calcite, sericite and traces of disseminated pyrite.

*Drill hole PD0031*

DP breccia at 422.5 - 424.8m in drill hole PD0031 contains abundant, dispersed, randomly oriented, blocky rhyolite clasts that have similar mineralogy and textures to coherent rhyolite intrusions (Fig. 4.7c). Some rhyolite clasts have delicate feathery margins whereas others have more curviplanar margins. The delicate feathery margins of rhyolite clasts contrasts with the ubiquitous angular and sub-rounded shape of lithic clasts. Feldspar phenocrysts, and the groundmass of rhyolite clasts have been pervasively altered to light green sericite, quartz, calcite, disseminated pyrite ± chlorite (Fig. 4.7d). Alteration has destroyed former groundmass textures. The DP breccia matrix is similarly altered to dark green chlorite, calcite, sericite, quartz and disseminated pyrite.

Fig. 4.7a. Drill hole PD0030, 389.8 m (lower right) - 379 m (upper left). Drill core of rhyolite intrusion that has merged with DP breccia. DP breccia clasts and domains of DP breccia (DP) have been incorporated in the rhyolite intrusion.

Fig. 4.7b. Drill hole PD0030, 385.62 m. Hand specimen of peperite. Pinkish quartz- and feldspar-phyric rhyolite intrusion (R) has formed a network of interconnected, irregularly shaped, penetrations into DP breccia as well as isolated 'globules' of rhyolite with delicate margins.

Fig. 4.7c. Drill hole PD0031, 422.5 m. Hand specimen of peperite with yellow-green sericite, calcite, chlorite altered quartz- and feldspar-phyric rhyolite clasts (R). Most rhyolite clasts have curviplanar margins, however some have delicate, irregular margins which contrast with the angular to rounded shape of lithic clasts (eg. 'L').

Fig. 4.7d. Drill hole PD0031, 422.5 m. Reflected light photomicrograph of altered peperite with round to embayed quartz crystals (Q) in an altered matrix which includes trace amounts of galena (G) and pyrite (P).

Fig. 4.7e. Drill hole PD0025, 544.5 m. Hand specimen of peperitic quartz- and feldspar-phyric rhyolite clasts in a DP breccia. The rhyolite clasts (R) have delicate, fluidal shapes which contrasts with the angular to rounded shape of lithic clasts (L). The rhyolite clasts and the lithic clasts have a consistent preferred orientation.

4.7a
DP

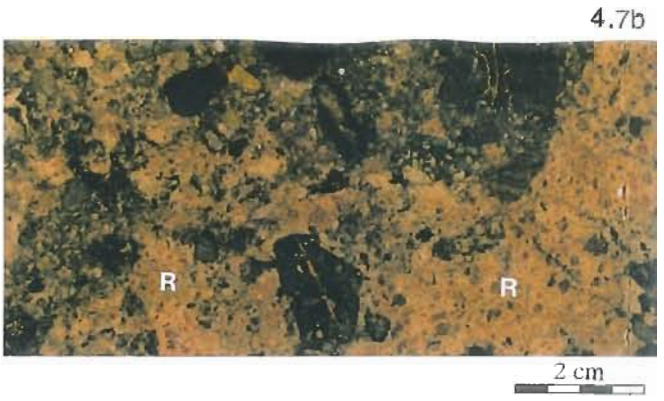
4.7b
R
R
2 cm

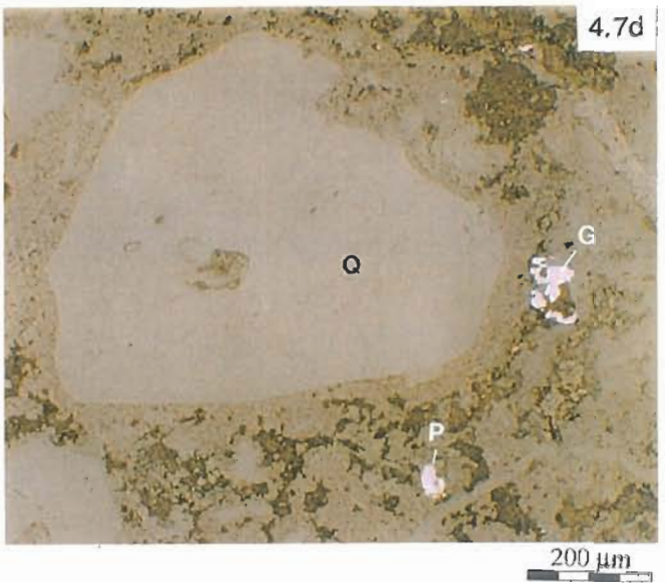
4.7d
Q
G
P
200 µm

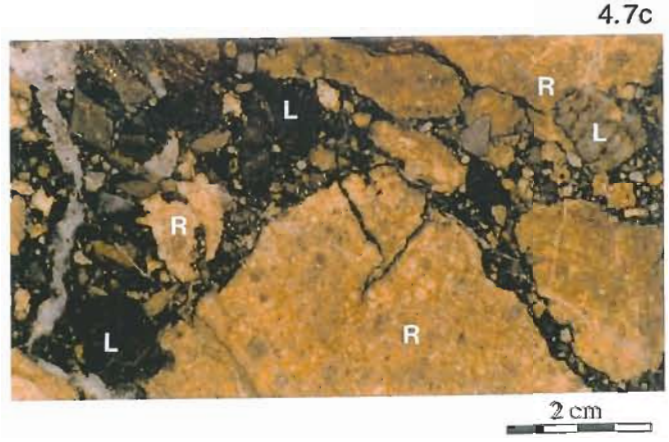
4.7c
L
R
L
R
R
L
2 cm

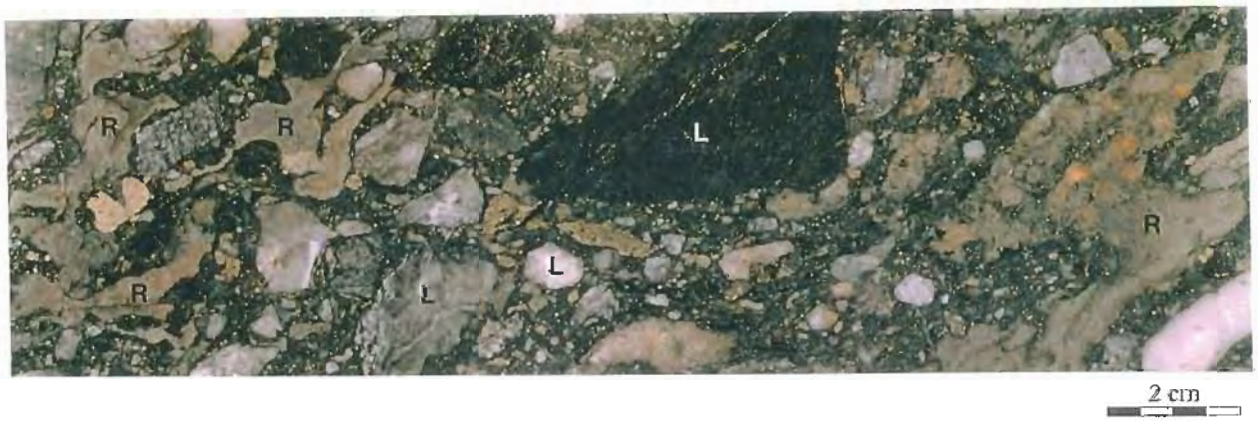
4.7e
R
R
L
R
L
L
R
2 cm

*Drill hole PD0025*

In contrast to the blocky rhyolite clasts described from drill hole PD0031, dispersed rhyolite clasts within DP breccia in drill hole PD0025 have fluidal shapes (Fig. 4.7e). Fluidally-shaped rhyolite clasts have delicate, elongated shapes, and an internal finely laminated fabric parallel to the elongation direction of the clast (flow banding?). Lithic clasts are also weakly aligned parallel to the orientation of fluidal rhyolite clasts, however the fluidal shape of rhyolite clasts contrast with the more angular to rounded shape of lithic clasts. The groundmass of fluidal rhyolite clasts and the matrix of DP breccia has been partially altered to calcite, sericite, chlorite and trace amounts of disseminated pyrite. Alteration is more intense in the outer ≈ 0.5 mm of fluidal rhyolite clasts.

**Interpretation of rhyolite-bearing DP breccias**

Rhyolite clasts have similar textures to the weakly and strongly altered rhyolite intrusions, and in one instance (373.9 - 388.25 m in drill hole PD0030), rhyolite clasts are connected to rhyolite intrusion that has merged with DP breccia. The contrasting shapes of rhyolite and lithic clasts is interpreted to indicate formation by different mechanisms. Inclusion of disaggregated and altered DP breccia into less altered rhyolite intrusion (Fig. 4.7a, b) is interpreted to indicate that the DP breccia was unconsolidated and wet at the time of rhyolite intrusion.

The rhyolite-bearing DP breccias have similarities to descriptions of peperite (Fisher, 1960; Williams and McBirney, 1979; Hanson and Schweickert, 1982; Hanson and Wilson, 1993). Busby-Spera and White (1987) described two textural types of peperite:

- Blocky peperite
- Globular (fluidal) peperite

The formation of one type over another was considered to be strongly influenced by the nature of the host sediment. Coarser-grained sediments were considered to give rise to blocky peperite whereas globular (fluidal) peperite was considered have formed in fine-grained sediment where an insulating vapour film formed between the magma and the sediment.

The rhyolite-bearing DP breccia at 422.5 - 424.8m in drill hole PD0031 is interpreted as blocky peperite, whereas that at 536.73 - 545.3m in drill hole PD0025 has a more fluidal shape than the globular peperite described by Busby-Spera and White (1987). Kokelaar (1982) and Brooks (1995) discussed the intrusion of magma into water-saturated, unconsolidated sediments, and suggested that as the water was heated, it expanded and locally vaporised, resulting in turbulent mixing of magma clasts and sediment. If rhyolite clasts at 536.73 - 545.3m in drill hole PD0025 were able to maintain a low viscosity, then fluidal shapes of magma clasts may have resulted through turbulent mixing with the sediment (cf. Branney and Suthren, 1988; Brooks, 1995). Heat retention could have been maintained

through an insulating vapour film if clasts were surrounded by sufficient fine grained DP breccia matrix (Busby-Spera and White, 1987), or, if sufficient space was generated by expansion of the mixture, clasts could have been mostly surrounded and insulated by steam. The consistent orientation of fluidal rhyolite clasts may have resulted from fluidisation and streaming of the vapour - sediment mix. Fluidisation of DP breccias is discussed in Section 4.4.2.

### LP breccia units

Intersections of LP breccias are restricted to the south of the Menninnie Dam prospect (Table 4.4).

Table 4.4 Drill hole intersections of LP breccia. Northing and easting are drill collar coordinates. 'From' and 'To' are down hole depths. The thickness of LP breccia is calculated assuming they are horizontal (drill holes are generally angled at between 50 - 70° from horizontal).

| Drill hole | Northing | Easting | From (m) | To (m) | Thickness (m) |
|---|---|---|---|---|---|
| PD0019 | 8380 | 10408 | 273.50 | 296.50 | 21.40 |
| PD0021 | 7564 | 10073 | 324.80 | 328.79 | 3.27 |
| PD0025 | 7957 | 10051 | 210.40 | 226.57 | 13.80 |
| PD0030 | 7764 | 10250 | 201.42 | 208.03 | 5.40 |
| PD0032 | 7406 | 10235 | 279.37 | 288.20 | 8.03 |

Some LP breccias can be correlated between drill holes and adjacent sections (Fig. 4.8). The contact between LP breccias and the underlying Hutchison Group is sharp and unconformable (Fig. 4.9a). Hutchison Group and granite dykes dip steeply to the west and steeply to the east respectively, whereas the orientation of LP breccia units is sub-horizontal (Fig. 4.8). Hutchison Group, metasomatised lithologies, and / or granite dykes directly beneath the LP breccia are extensively fractured with a jigsaw-fit breccia texture (Fig. 4.9a) and the intensity of fracturing diminishes with depth over several metres.

LP breccia clasts are typically angular to sub-rounded. Rounded clasts are uncommon in LP breccias, which contrasts to the rounded shape of many smaller DP breccia clasts. Angular and sub-rounded clasts of the same size and lithology are locally adjacent. As for DP breccias, the matrix of LP breccias is considered to be all clasts < 2 mm and consists of polymictic clasts from < 2 mm diameter to microscopic. The matrix of LP breccias has been partially altered to fine grained carbonate, sericite, minor chlorite and traces of pyrite. Galena has not been observed as an alteration mineral in LP breccias.

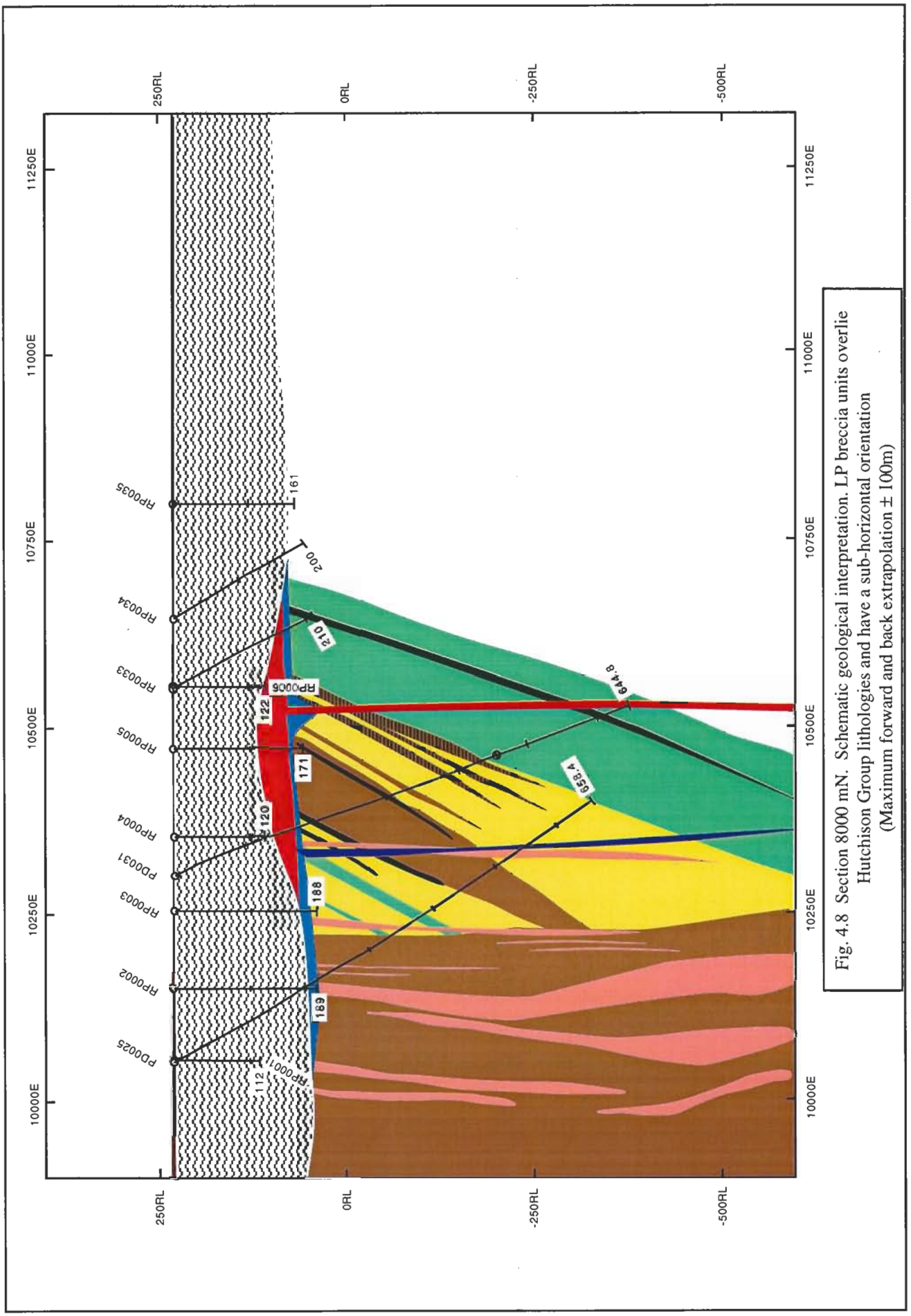


Fig. 4.8 Section 8000 mN. Schematic geological interpretation. LP breccia units overlie Hutchison Group lithologies and have a sub-horizontal orientation (Maximum forward and back extrapolation ± 100m)

Fig. 4.8 (cont.)

## Key to interpretative geology plan and 8000 mN cross section

### Quaternary

Surficial, transported clays and sand. Minor ferricrete and silcrete.

### Mesoproterozoic

Lithic rich Menninnie Dam ignimbrite.

Layered polymictic breccia (LP breccia)

Discordant polymictic breccia (DP breccia)

Rhyolitic intrusions and coherent rhyolite.

### Palaeoproterozoic

Granite dykes.

Central suite. Graphitic quartz - feldspar - biotite - muscovite - sillimanite - garnet schist.

Eastern and western suites. Quartz - feldspar - biotite - muscovite - sillimanite - garnet schist.

Central suite. Carbonate - calc-silicate facies, and silicate facies iron formations.

Central suite. Chaotically banded quartz - diopside rock, massive diopside, and diopside - marble rock with minor disseminated magnetite. Includes minor retrograde metamorphic calc-silicates.

Central suite, dolomitic and calcitic marbles. Minor disseminated and chaotically banded magnetite.

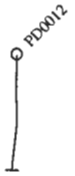


Horizontal projection of drill holes

prefix 'PD' = diamond drill hole with percussion precollar
prefix 'PE' = reverse circulation percussion drill hole
prefix 'RP' = rotary air blast percussion drill hole

Fig. 4.9a. Drill hole PD0025, 221.7 m (upper left) - 230.5 m (lower right). Contact (C) between a granite (G) dyke and LP breccia (LP). The granite dyke is strongly altered and fractured / brecciated with a jigsaw-fit texture. The contact between LP breccia and the granite dyke is sharp. The proportion of lithic clasts to matrix is higher near the base of the LP breccia and lithic clasts are commonly larger.

Fig. 4.9b. Drill hole PD0032, 282.0 m. Hand specimen of altered LP breccia. The matrix and some clasts have been pervasively altered to a quartz - carbonate - chlorite - calc-silicate ± hematite assemblage.

Fig. 4.9c. Drill hole PD0032, 280.4 m. Transmitted light photomicrograph of quartz - carbonate - chlorite - calc-silicate ± hematite altered LP breccia. Sphalerite (S) and galena (G)-bearing sulphide clasts in the LP breccia have undergone partial dissolution and have corroded margins. Sulphides also occur in trace amounts disseminated throughput the matrix (Small dark flecks).

Fig. 4.9d. Drill hole PD0025, 221.9 m (lower) - 209 m (upper). Drill core of LP breccia with the base of each layer marked by blue bars. Layers are defined by the abundance of coarse lithic clasts near the base and finer clasts near the top. The upper layer is altered to clays with minor relict lithic clasts of < 1 cm diameter. The contact between LP breccia and the overlying MD ignimbrite is also marked.

Fig. 4.9e. Drill hole PD0025, 226.1 m (LHS) and 218.8 m (RHS). The sample on the LHS is from near the base of a LP breccia layer and has a high lithic clast to matrix ratio. Note the rounded sulphide clast (S). The sample on the RHS straddles the contact (indicated by arrow) between two LP breccia layers. The top of the underlying layer is finer grained and incorporates more matrix than the base of the overlying layer.

4.9a

4.9b

2 cm

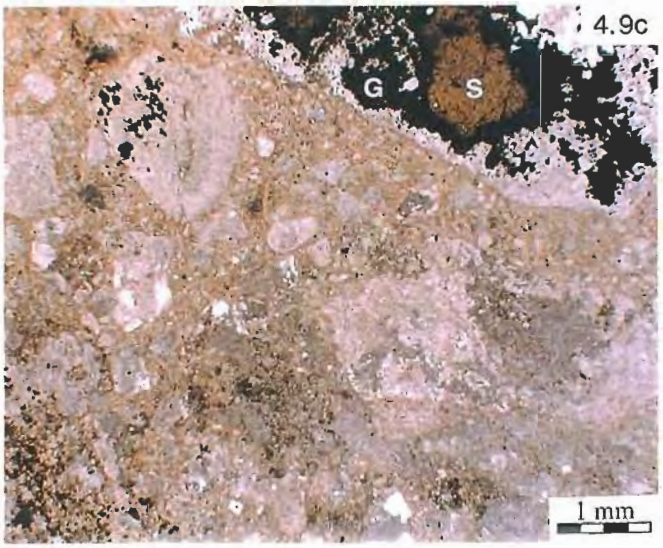


4.9c

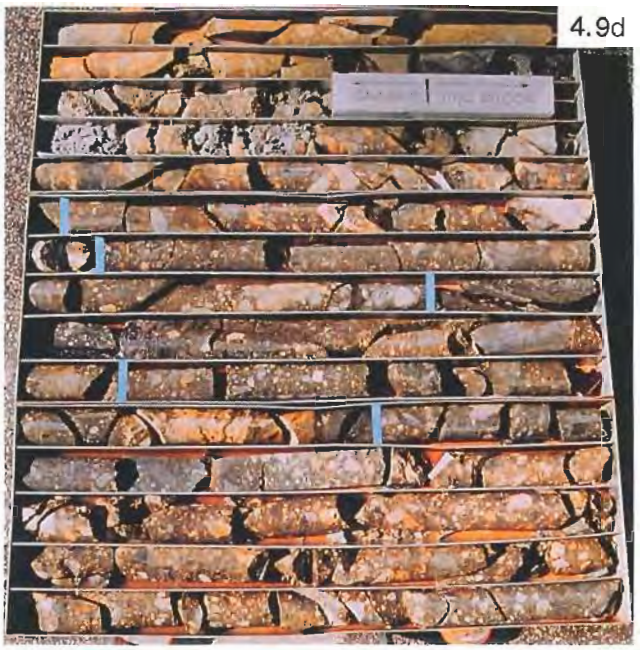

4.9d

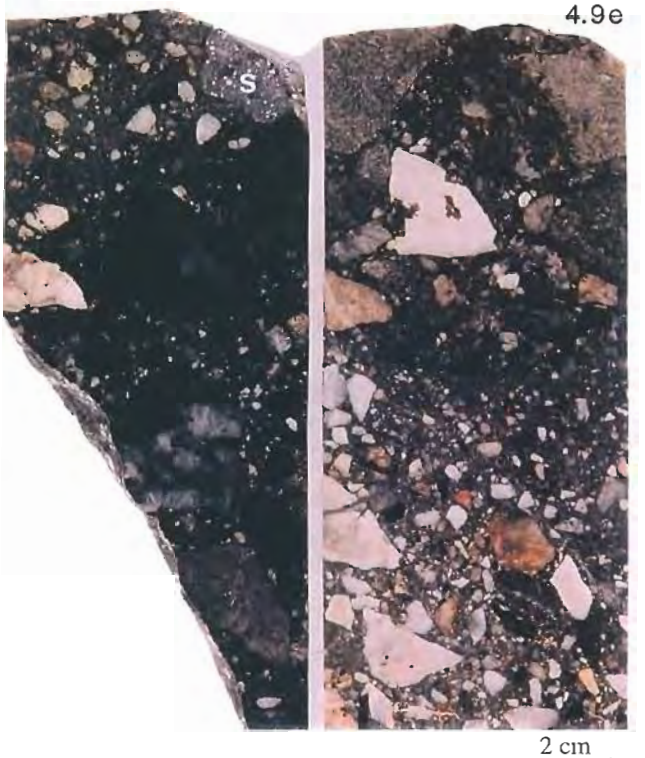


4.9e

2 cm

LP breccia in drill hole PD0032 is more intensely altered than other LP breccia intersections. The matrix, and some carbonate clasts, are pervasively altered to dark green chlorite, carbonate, epidote, sericite and tremolite with minor serpentine. Patches of hematite-dusted quartz locally overprint chlorite - carbonate - epidote - sericite - tremolite - serpentine alteration, particularly near the top of the LP breccia (Fig. 4.9b). Traces of galena, sphalerite, chalcopyrite and pyrite are scattered throughout the altered matrix (Fig. 4.9c). Alteration of marble clasts has resulted in a pattern of concentric rings of alteration minerals including epidote, tremolite, chlorite, calcite, locally overprinted by hematite-dusted quartz.

*Layering*

The LP breccia in drill hole PD0025 is layered (Fig. 4.9d, e). Layering is oriented approximately normal to the drill hole axis which corresponds to approximately 30° from horizontal. Layers range in thickness from 0.9 m to 8.5 m (Fig. 4.10). The tops and bases of layers are either irregular and diffuse, or sharp and near planar. Clasts of ≥ 5 cm diameter are more abundant in the basal 20 - 50 cm of layers, and are commonly clast supported with interstitial matrix. The interior of layers consists of matrix-supported LP breccia with ≈ 30 % clasts. The size of clasts decreases from ≈ 0.2 - 4 cm to ≈ 0.2 - 3 cm across towards the top of each layer with a corresponding increase in the amount of matrix. The tops of layers comprise a 1 - 4 cm thick interval with ≈ 60% matrix in which clasts are typically 0.2 - 1 cm across (Fig. 4.9e).

The uppermost layer in drill hole PD0025 contains ≈ 5 - 10% clasts, all of which are 0.2 - 1 cm across (Fig. 4.9d). The matrix and many of the clasts have been pervasively altered to light-grey, puggy clays and quartz fragments.

Layering is less well defined in other LP breccia intersections and correlation of layers between drill holes has not been attempted.

## Rhyolite-bearing LP breccia

Overlying the Hutchison Group in drill hole PD0031 is an LP breccia that contains fiamme and clasts of crystal-bearing rhyolite referred to as 'rhyolite-bearing LP breccia'. The rhyolite-bearing LP breccia is overlain by non-vesiculated coherent rhyolite whose upper contact was not cored (Table 4.5).

Table 4.5 Intersection of rhyolite-bearing LP breccia and coherent rhyolite in drill hole PD0031. 'From' and 'To' are down hole depths. The true width is calculated assuming the rhyolite-bearing LP breccia and the coherent rhyolite units are horizontal.

| | Drill hole | Northing | Easting | From (m) | To (m) | Width (m) |
|---|---|---|---|---|---|---|
| Coherent rhyolite | PD0031 | 8023 | 10300 | 171 | <146 | >22.8 |
| Rhyolite-bearing LP breccia | PD0031 | 8023 | 10300 | 180.7 | 171 | 9.17 |

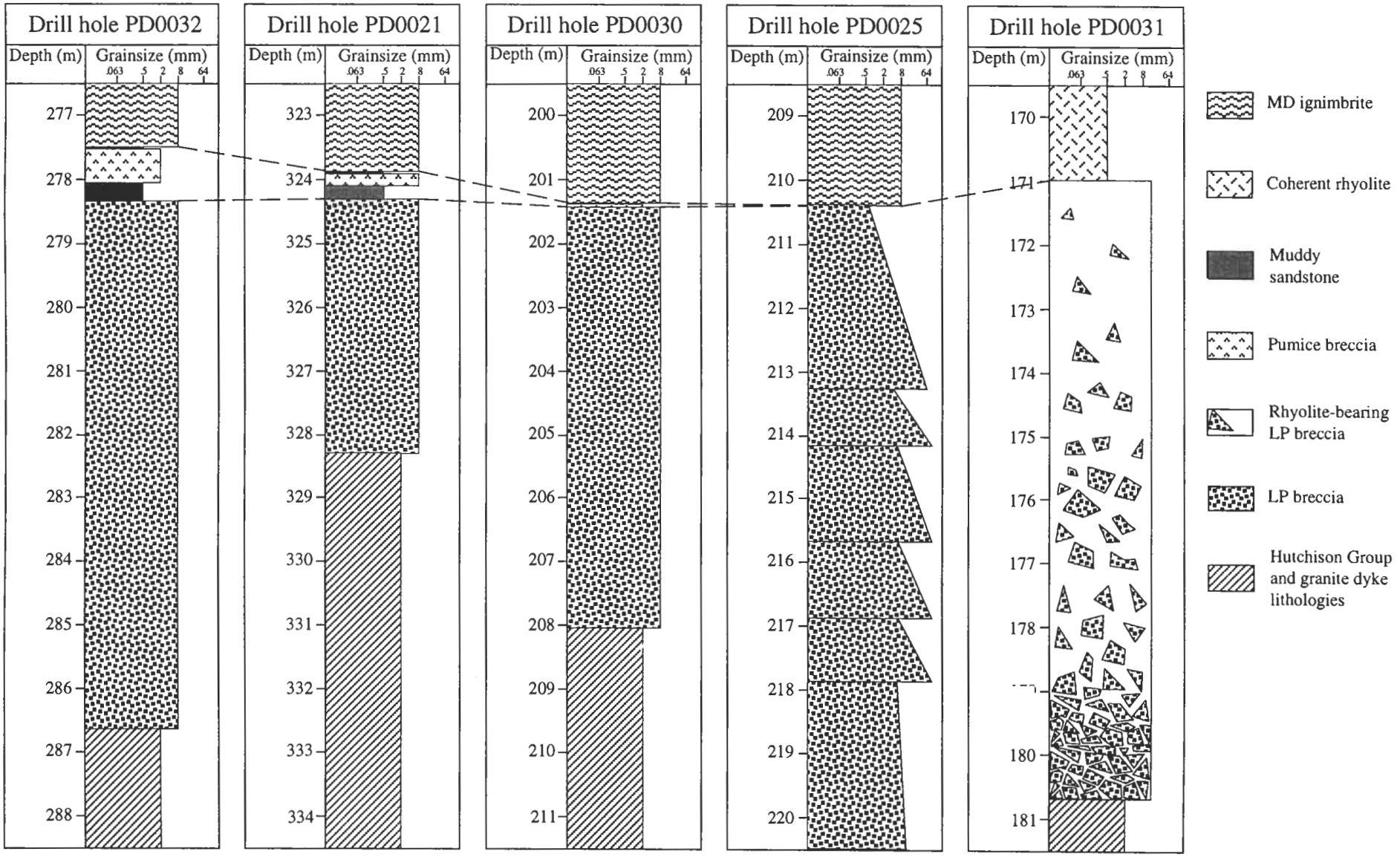


Fig. 4.10 Graphic logs of LP breccia, muddy sandstone, pumice breccia, rhyolite-bearing LP breccia, and coherent rhyolite in the five most southerly drill holes. PD0032 is the most southerly drill hole and PD0031 is the most northerly drill hole. Dotted lines connect units between drill holes.

There is a gradational variation in the abundance, size, and texture of rhyolite fiamme and clasts from the base to the top of the rhyolite-bearing LP breccia unit and a corresponding change in the nature of the matrix from lithic dominated near the base, to volcanic dominated near the top. (Fig. 4.11a and Table 4.6). The proportion and size of rhyolite fiamme and clasts increases from the base upwards from ≈ 30% at 1.8m from the base to > 95% above 5.39m (Figs. 4.11b - f, 4.12a - f). Rhyolite fiamme and clasts throughout the unit are consistently oriented sub-parallel to the basal contact with the Hutchison Group.

Nearer the base of the unit, rhyolite fiamme are typically < 5 cm long, < 1 cm wide and have ragged terminations. Fiamme contain crystals and crystal fragments of ≈ 2% quartz (0.2 - 2 mm) , ≈ 2% of 0.1 - 3 mm K-feldspar and ≈ 1% of 0.1 - 1.5 mm relict plagioclase. Intact quartz crystals are commonly round and embayed. Fragmented crystals are less common and where present, have a jigsaw-fit texture. The groundmass of fiamme comprises a fine grained mosaic of alteration minerals including quartz, calcite, sericite and chlorite.

Towards the top of the unit, fiamme become progressive larger and are typically longer than can be determined from drill core (> 8 cm). Those that are longer than the drill core are referred to as 'rhyolite clasts'. Rhyolite clasts contain a higher proportion of crystals than fiamme and crystal fragments are rare (ie. ≈ 4% quartz (0.2 - 2 mm), ≈ 4% of 0.1 - 3 mm K-feldspar and ≈ 3% of 0.1 - 1.5 mm relict plagioclase). Above 5.39m from the base, the groundmass of fiamme and rhyolite clasts comprises a fine grained mosaic quartz that micropoikilitically encloses sericite - calcite altered feldspar microlites. The matrix between clasts is predominantly fine grained volcanic fragments with a minor fine grained lithic content and comprises patches of quartz that micropoikilitically encloses sericite - calcite altered feldspar microlites. Due to the presence of a micropoikilitic texture in fiamme, rhyolite clasts and the matrix, the upper and lower margins of rhyolite clasts are not well defined but can be differentiated from matrix by their higher crystal content, and the occurrence of lithic fragments and crystal fragments in the matrix. Micropoikilitic texture is consistent with high temperature devitrification from a glassy precursor (Lofgren 1971a, b, 1974; Anderson, 1969).

An 8 cm wide composite clast of volcanic and lithic breccia is present in the centre of the example illustrated in Figure 4.11d. The upper and lower margins of the composite clast are irregular and feathery to cuspate. The composite clast comprises ≈ 30% attenuated fiamme (< 2 cm long) and ≈ 30% lithic clasts (0.2 - 3 cm across), in a fine grained groundmass. Fiamme in the clast have a consistent orientation parallel to the to the general fabric of the unit, and are commonly plastically deformed around lithic clasts. Fiamme contain micropoikilitic and rare spherulitic devitrification textures (Fig. 4.11e) consistent with welding and devitrification from a glassy precursor (Lofgren 1971a, b, 1974; Anderson, 1969).

Table 4.6. Summary of the rhyolite-bearing LP breccia at various depths above the Hutchison Group.

| Height above Hutchison Group (m) | Proportion of rhyolite clasts | Size of lithic clasts | Size of rhyolite clasts | Matrix | Shape of rhyolite clasts | Juvenile rhyolite clast devitrification textures | Breccia fabric | Alteration |
|---|---|---|---|---|---|---|---|---|
| 1.80 | ≈ 30% | 2 mm to 13 cm | Typically 2 mm to 2 cm long and locally up to 4 cm across | Lithic fragments, minor altered rhyolite fragments and quartz crystal fragments | Clasts of 2 mm to 2 cm have fiamme shapes with feathery margins. Clasts > 2 cm are equant. | None apparent | Lithic clasts are randomly orientated. Fiamme define weak planar fabric. | Rhyolite clasts and the breccia matrix partially altered to fine grained quartz, calcite, chlorite, sericite, and trace amounts of disseminated hematite |
| 5.01 | ≈ 60% | Typically < 1.5 cm across | 2 mm to 5 cm | Lithic fragments, minor altered rhyolite fragments and quartz crystal fragments | Fiamme with feathery ends weakly cuspate upper and lower margins | None apparent | Planar fabric defined by the orientation of fiamme | Rhyolite clasts and the breccia matrix partially altered to fine grained quartz, calcite, chlorite and sericite |
| 5.39 | ≈ 90% | Typically < 1 cm and rarely > 1.5 cm across | 40% are > 8 cm long (diameter of the drill core) and 1 - 2 cm wide | Altered rhyolite fragments, minor lithic fragments, quartz and feldspar crystal fragments | Fiamme with feathery ends weakly cuspate upper and lower margins | Rhyolite clasts have patches with a micropoikilitic texture | Pronounced planar fabric. Fiamme have a foliation fabric parallel to layering | Feldspar in rhyolite clasts and the breccia matrix partially altered to calcite, sericite and trace amounts of chlorite |
| 6.05 | ≈ 95% | Typically < 2 mm (matrix) and rarely up to 1 cm across | 60% are > 8 cm long and 1 - 7 cm wide | Altered rhyolite fragments?, quartz and feldspar crystal fragments and minor lithic fragments (1-2%) | Attenuated shapes | Rhyolite clasts and the matrix to clasts have a micropoikilitic texture. Clast boundaries are indistinct. | Weak planar fabric due to orientation of rhyolite clasts and trails of crystal within rhyolite clasts | Feldspar in the matrix of rhyolite clasts and the breccia partially altered to calcite, sericite and trace amounts of chlorite. K-feldspar crystals are less altered |
| 9.17 | Coherent rhyolite contact | | | | | Micropoikilitic textures | | Matrix partially altered to calcite and sericite. K-feldspar crystals are unaltered |

Fig. 4.11a. Drill hole PD0031, 181.6 m (lower right) - 168.8m (upper left). Drill core of altered carbonate facies iron formation (IF) overlain by rhyolite-bearing LP breccia at 180.7 m (LP) which is overlain by coherent rhyolite at 171.0 m (R). The contacts are marked by arrows.

Fig. 4.11b. Drill hole PD0031, 178.73 m. Hand specimen from near the base of the rhyolite-bearing LP breccia unit. Lithic clasts are (L) mostly angular to sub-rounded. Rhyolite clasts (R) are brick red and comprise smaller fiamme clasts and larger, more equidimensional quartz-feldspar phyric clasts. Both fiamme shaped clasts and larger rhyolite clasts have delicate feathery margins in contrast to the shape of lithic clasts.

Fig. 4.11c. Drill hole PD0031, 177.3 m. Transmitted light photomicrograph of rhyolite-bearing LP breccia from 3.4 m from the base of this unit. Fiamme have been altered to a fine grained mosaic of quartz, sericite, chlorite and carbonate. Round and embayed quartz crystals (Q) and are common throughout fiamme.

Fig. 4.11d. Drill hole PD0031, 175.5 m. Hand specimen of rhyolite-bearing LP breccia unit. Rhyolite clasts have fiamme shapes (F). The centre of the figure consists of an eight centimetre wide composite clast made up of lithic clasts and welded pyroclastics. The upper and lower margins of the composite clast are cuspate with embayments and small fine protrusions into LP breccia.

Fig. 4.11e. Drill hole PD0031, 175.5 m. Transmitted light photomicrograph of the composite clast illustrated in Figure 4.11d. The groundmass comprises fiamme (F) and relict shards that have a pronounced eutaxitic texture and have commonly been plastically deformed around lithic clasts (L).

Fig. 4.11f. Drill hole PD0031, 175.5 m. Transmitted light photomicrograph of the composite clast illustrated in Figures 4.11e. Relict shards (S) have a pronounced eutaxitic texture and have been plastically deformed around lithic clasts (L). Larger shards commonly have ragged terminations of former bubble walls (T).

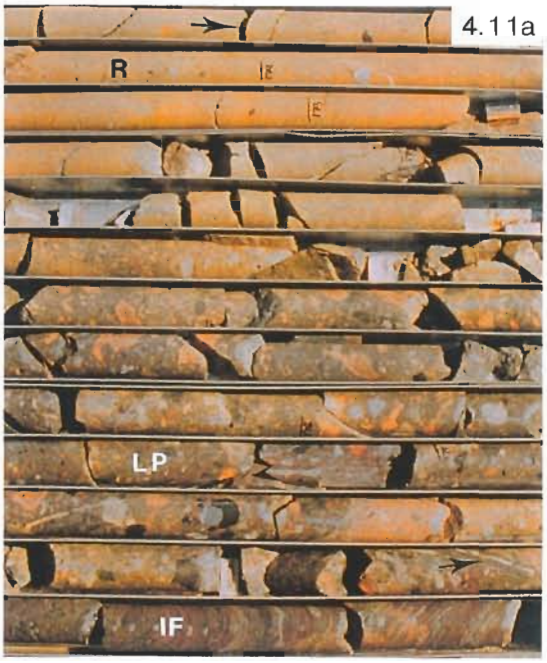
4.11a
R
LP
IF

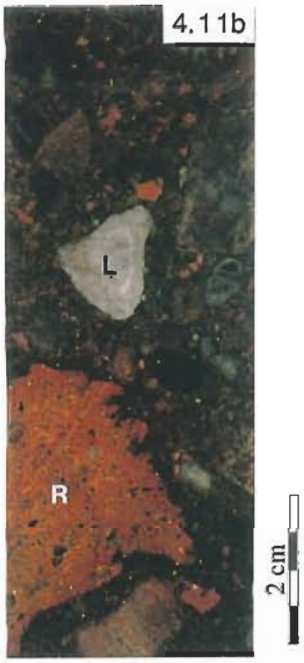
4.11b
L
R
2 cm

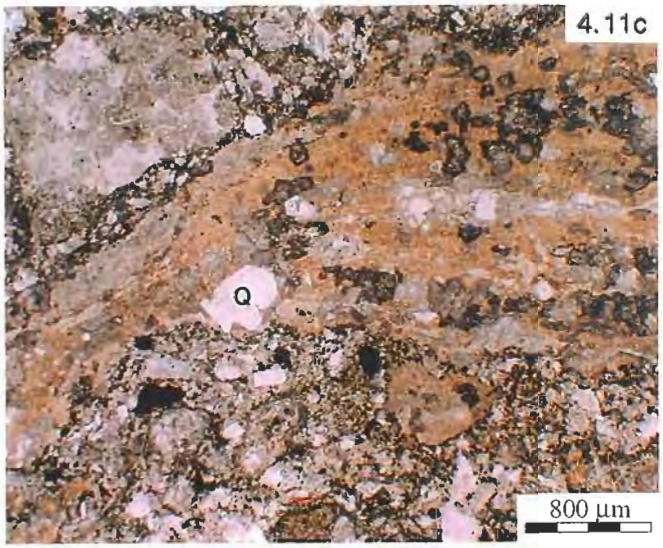
4.11c
Q
800 µm

4.11d
F
2 cm

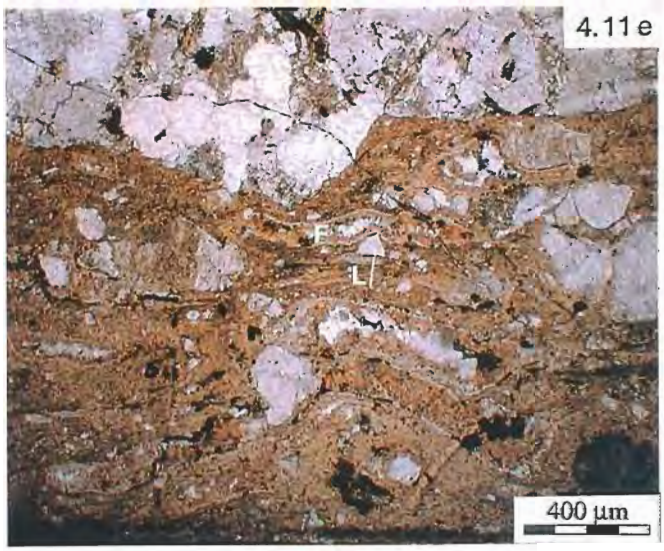
4.11e
F
L
400 µm

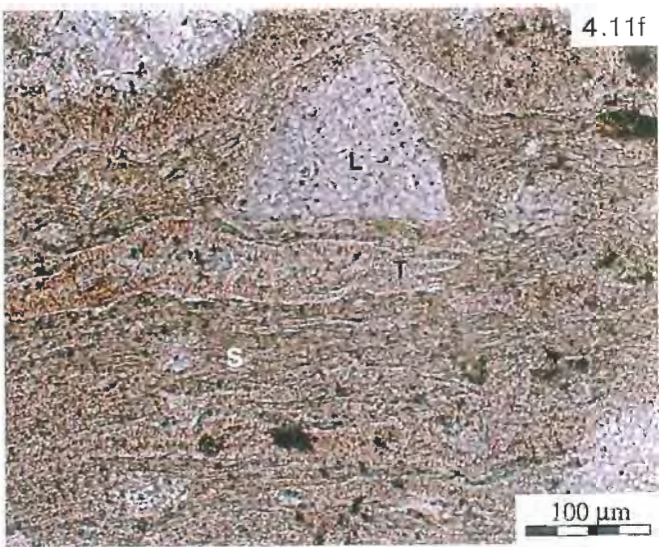
4.11f
L
T
S
100 µm

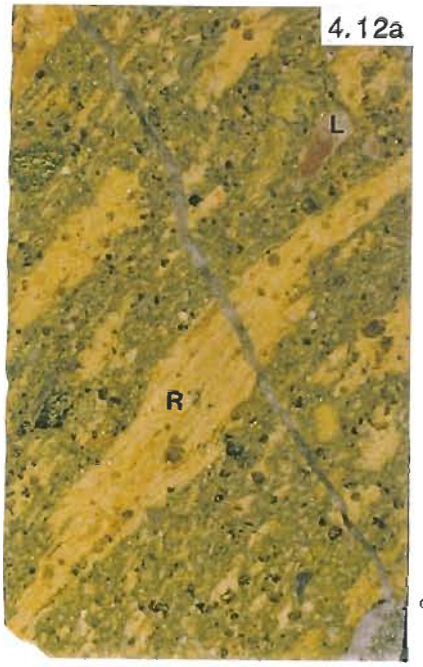
4.12a
L
R
2 cm

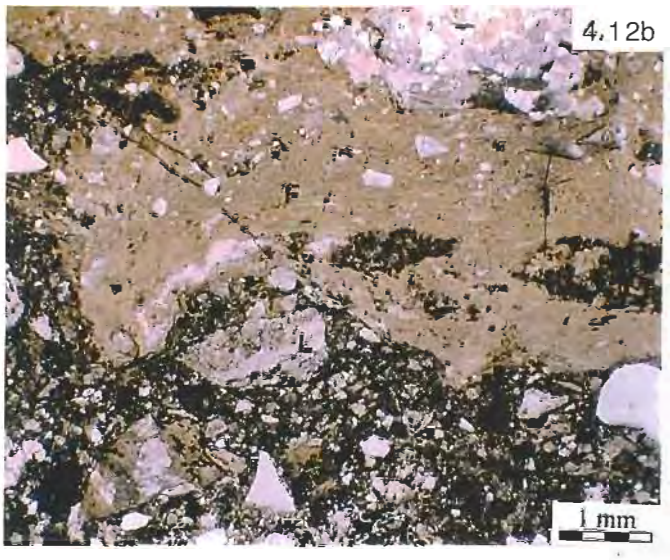
4.12b
F
L
1 mm

4.12c
F
L
R
2 cm

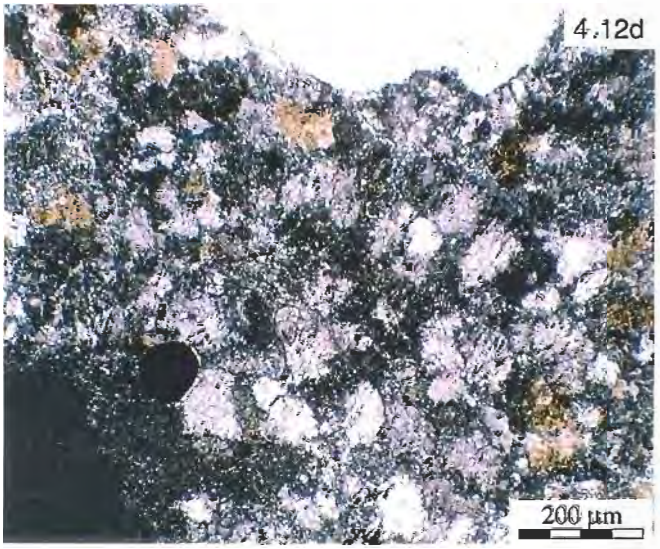
4.12d
200 µm

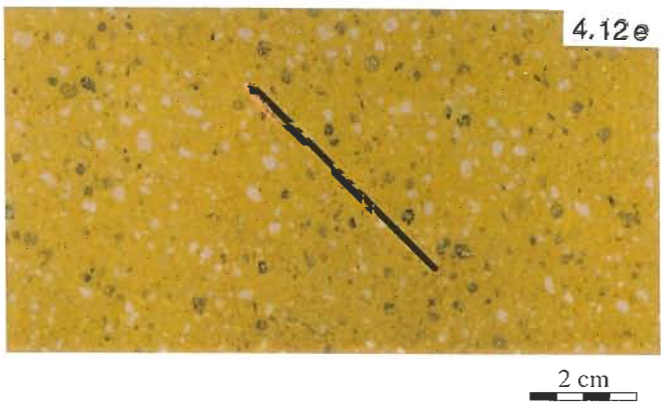
4.12e
2 cm

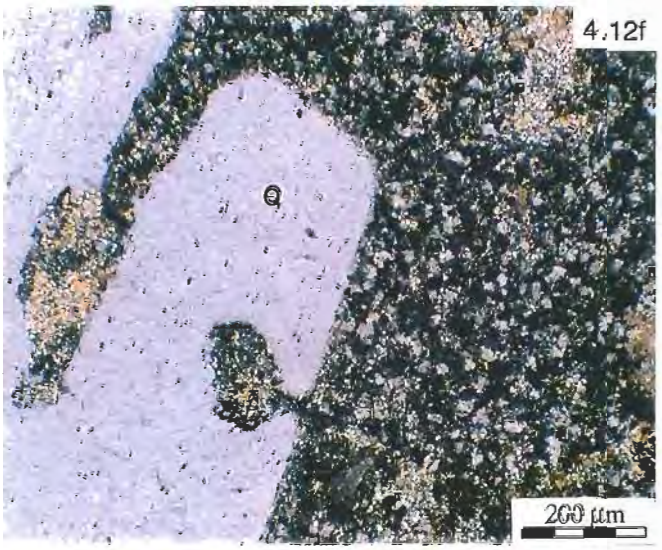
4.12f
Q
200 µm

The groundmass comprises attenuated and plastically deformed relict shards with a well developed compactional foliation parallel to fiamme (Fig. 4.11f). Lithic clasts are angular to rounded, poorly sorted, and consist of Hutchison Group lithologies and granite dyke fragments, similar to those in LP breccia.

At 9.17 m from the base, the rhyolite-bearing LP breccia has a sharp contact with overlying massive, coherent rhyolite (Fig. 4.12e, f).

### 4.3.3 Coherent rhyolite

Quartz and feldspar phenocrysts in the coherent rhyolite are mostly intact with rare fragmented phenocrysts. The coherent rhyolite has a weak fabric accentuated by trails of quartz and feldspar phenocrysts (Fig. 4.12f). The orientation of the fabric is parallel to that developed in the underlying rhyolite-bearing LP breccia. The upper surface of coherent rhyolite is not preserved in drill core, and the measured thickness of 22.9 m is a minimum thickness.

Coherent rhyolite was not intersected in drill holes 200 - 300m to the north, south and west. There is no drill hole control to the east. The rhyolite-bearing LP breccia unit and the coherent rhyolite occupy the same stratigraphic position as muddy sandstone, and pumice breccia units intersected in drill holes to the south (Fig. 4.10).

### 4.3.4 Muddy sandstone and pumice breccia units

Overlying the LP breccia is a thin sequence of interbedded, poorly sorted, lithic and muddy sandstone units and pumice breccia units referred to as 'muddy sandstone' and 'pumice breccia' respectively. Muddy sandstone and pumice breccia units were intersected in 5 drill holes in the southern end of the prospect (Table 4.7).

Table 4.7 Drill hole intersections of muddy sandstone and pumice breccia. All depths are down hole depths. The true width is calculated assuming muddy sandstone and pumice breccia units are horizontal.

| | Drill hole | From (m) | To (m) | Width (m) |
|---|---|---|---|---|
| Muddy sandstone | PD0021 | 324.37 | 324.41 | 0.03 |
| Pumice breccia | PD0021 | 324.41 | 324.59 | 0.18 |
| Muddy sandstone | PD0021 | 324.59 | 324.80 | 0.18 |
| Muddy sandstone | PD0030 | 201.36 | 201.38 | 0.02 |
| Pumice breccia | PD0030 | 201.38 | 201.42 | 0.04 |
| Muddy sandstone | PD0032 | 278.50 | 278.53 | 0.03 |
| Pumice breccia | PD0032 | 278.53 | 279.08 | 0.55 |
| Muddy sandstone | PD0032 | 279.08 | 279.37 | 0.25 |

*Muddy sandstone units*

Muddy sandstone units consist of laminated, to medium bedded, poorly sorted, non-graded beds that range in thickness from 2 cm to 29 cm (Fig. 4.13 a, b).

Fig. 4.13a. Drill hole PD0032, 279.15 m. Hand specimen of a thinly bedded to thickly laminated muddy sandstone unit.

Fig. 4.13b. Drill hole PD0032, 279.15 m. Transmitted light photomicrograph (x nicols) of poorly sorted muddy sandstone. This unit contains quartz fragments derived from the underlying Hutchison Group or granite dykes (Q1), and round and embayed quartz crystals (Q2).

Fig. 4.13c. Drill hole PD0032, 278.6 m. Hand specimen of pumice breccia unit. Most of this unit is comprised of rhyolite fiamme (F).

Fig. 4.13d. Drill hole PD0032, 279.15 m. Transmitted light photomicrograph of the pumice breccia unit with rhyolite fiamme (F) in a fine-grained finely-laminated matrix. Fiamme are commonly bent around lithic fragments (L), and fragments of round and embayed quartz (Q).

Fig. 4.13e. Drill hole PD0032, 279.15 m. Transmitted light photomicrograph (x nicols) of a rhyolite fiamme in the pumice breccia unit. The interior of fiamme consists of quartz that locally micropoikilitically encloses feldspar microlites and resembles a micropoikilitic texture.

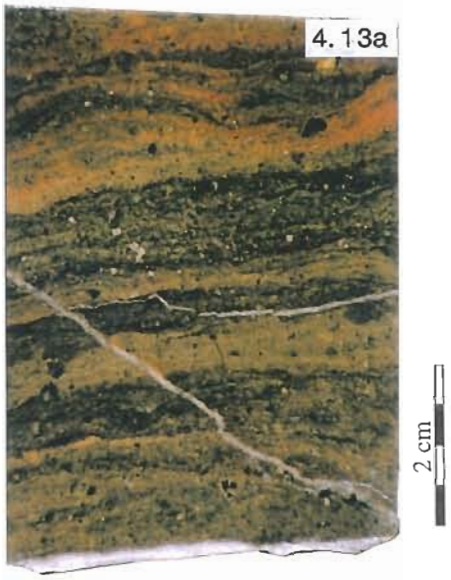
4.13a
2 cm

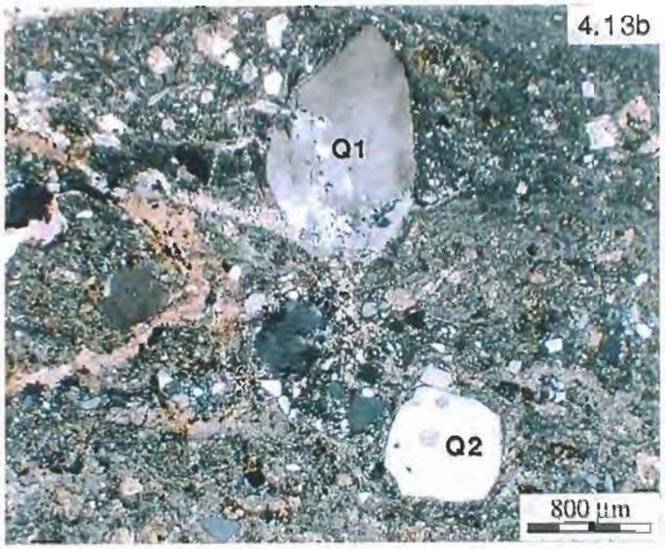
4.13b
Q1
Q2
800 µm

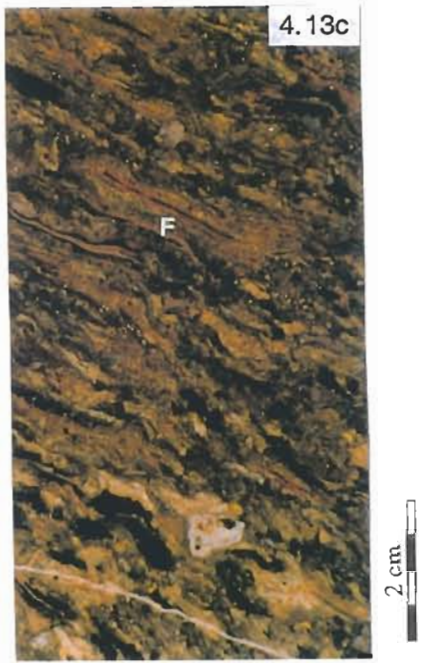
4.13c
F
2 cm

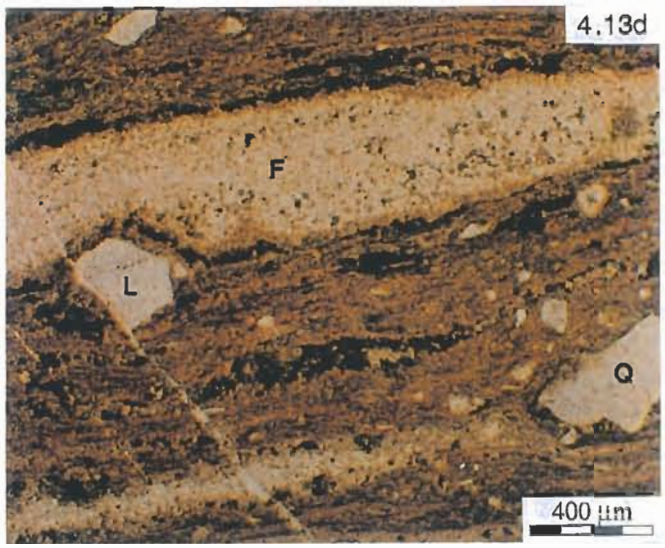
4.13d
F
L
Q
400 µm

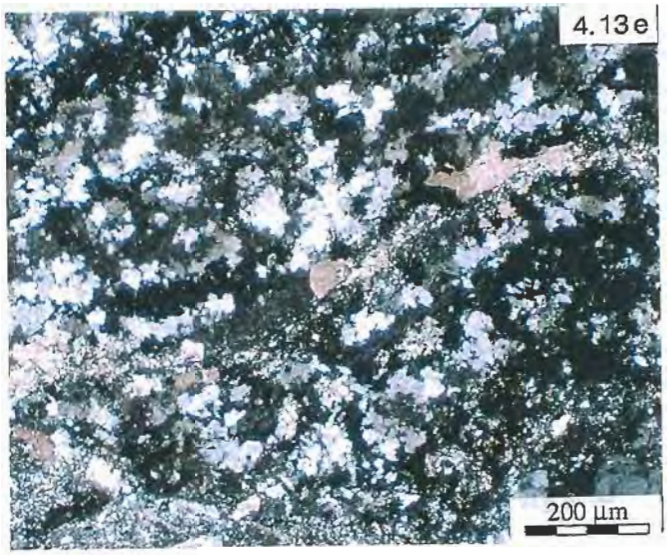
4.13e
200 µm

The tops and bases of beds are sharp, and planar to irregular. Clasts of 2 mm - 2 cm constitute ≈ 30% of the unit and consist of lithic fragments (≈ 19%), fiamme (≈ 9%), round and embayed quartz crystals and crystal fragments (1%), feldspar crystals and crystal fragments (< 1%). Fiamme are elongated parallel to bedding and contain < 3% round and embayed quartz crystals and crystal fragments of < 1.5 mm diameter, and sericite pseudomorphs of feldspar crystals, in a fine-grained felted intergrowth of quartz, sericite, chlorite and trace amounts of hematite. Quartz crystals and crystal fragments have straight extinction. Lithic fragments consist of quartz with undulose extinction, schist fragments and partially altered diopside and marble. The matrix to muddy sandstone units (≈ 70%) comprises fine grained felted quartz, carbonate, sericite, chlorite and traces of hematite.

*Pumice breccia units*

Pumice breccia units consist of thickly bedded, to very thinly-bedded, poorly sorted, non-graded beds (Fig. 4.13c) which comprise juvenile volcanogenic clasts (≈ 50%), lithic clasts (1 - 5%) and matrix ≈ 45%. Pumice breccia units range in thickness from 4 cm to 55 cm (Table 4.7). The tops and bases of pumice breccia beds are sharp, planar and conformable. Volcanogenic clasts have fiamme shapes (0.2 - 5 cm long) and comprise rare embayed to round quartz crystals and crystal fragments of < 2 mm diameter, rare K-feldspar crystals and crystal fragments of < 1 mm diameter in a fine-grained felted groundmass of quartz, sericite, calcite, chlorite and locally, K-feldspar (Fig. 4.13d). The groundmass of some fiamme contain zones of quartz which micropoikilitically encloses fine grained feldspar microlites, and rare spherulitic quartz and K-feldspar intergrowths (Fig. 4.13e), consistent with devitrification from a glassy precursor (Lofgren 1971a, b, 1974; Anderson, 1969). Lithic clasts consist of quartz fragments with undulose extinction and minor granite fragments and partially to pervasively altered grains (marble or calc-silicate ?).

### 4.3.5 Geochemistry of rhyolite intrusions, peperites and coherent rhyolite.

The rhyolite intrusions, the rhyolite component of peperite, and rhyolite clasts in the various LP and DP breccias have a common crystal / phenocryst population of K-feldspar, plagioclase, and embayed to round quartz in similar proportions. Direct physical links cannot be examined from drill core, however, comparison of their geochemistry is a means of testing the hypothesis that they were derived from the same batch of magma. In this section, the geochemistry of some of these units is examined and compared to published analyses of units of the GRV and granitoids of the Hiltaba Suite.

*Methods*

The samples listed in Table 4.8 were jaw crushed to less than 5 mm, and split to obtain a few hundred grams which was then ground in a chrome-steel ring mill. The resultant powder was made into pills and beads for X-ray fluorescence analyses (XRF) using the procedures of Norrish and Hutton (1969). Pills and beads were analysed using a Phillips PW1480

XRF spectrometer at the Geology Department, University of Tasmania. XRF analytical conditions are detailed in Appendix 3.2.

Table 4.8 Samples used for geochemical analysis.

| Sample | Drill hole | Depth |
|---|---|---|
| Strongly altered rhyolite intrusion | PD0031 | 644m |
| Strongly altered rhyolite intrusion | PD0030 | 403m |
| Weakly altered rhyolite intrusion | PD0030 | 471m |
| Coherent rhyolite | PD0031 | 157m |
| Rhyolite component of peperite | PD0030 | 385.6 |

*Results*

Detailed analytical results and are presented in Appendix 3.4 along with analyses of granitoids of the Hiltaba Suite (Flint, 1993b), and units of the GRV (Blissett et al., 1993, Stewart, 1992, and Jagodzinski, 1985). The degree of alkali ion mobility and exchange during cooling, devitrification and hydration of glassy rocks has been described as negligible (Lipman, 1965; Lipman et al., 1969) to variable and complex behaviour (Scott, 1971). Stewart (1992) considered the degree of alkali ion mobility in the Eucarro and Yardea Dacites of the GRV to be minimal and suggested that ion mobility may be lower in coherent lavas and densely welded ignimbrites due to lower porosity, resulting in restricted fluid movement. Assuming negligible alkali ion exchange occurred during cooling and devitrification of the weakly altered rhyolite intrusion, its composition plots in the field for rhyolite defined by Le Bas et al. (1986) on a $Na_2O + K_2O$ versus $SiO_2$ variation diagram (Fig. 4.14a).

Elements interpreted to have been immobile under most hydrothermal conditions (Rollinson, 1993) have been used to determine the composition of altered lithologies. Their compositions lie near the boundary of the rhyolite and trachyandesite fields defined by Winchester and Floyd, (1977; Fig. 4.14b). The concordance between alkali element and immobile trace element variation diagrams is consistent with interpretation as rhyolite.

Compositions of the rhyolite intrusions, coherent rhyolite and the rhyolite component of peperite plot as a cluster on various immobile element variation diagrams, interpreted to indicate derivation from the same batch of magma (Fig. 4.15a - f). Compositions of granitoids of the Hiltaba Suite, and units of the mature and developmental phases of the GRV plot as overlapping fields on a number of immobile element variation diagrams (Fig. 4.15a - f). Compositions of the rhyolite intrusions, igneous component of peperite and coherent rhyolite lie outside the fields for analyses of the mature and developmental phases of the GRV and close to, or within, the field for analyses of granitoids of the Hiltaba Suite.

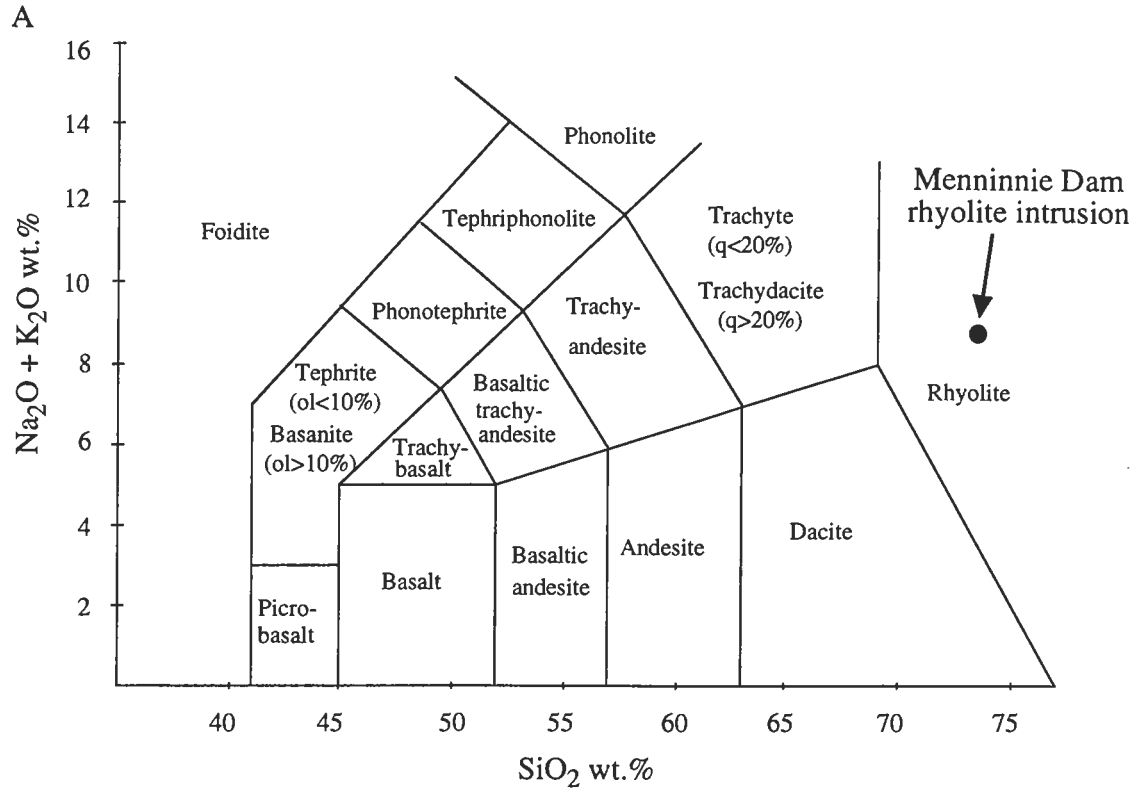


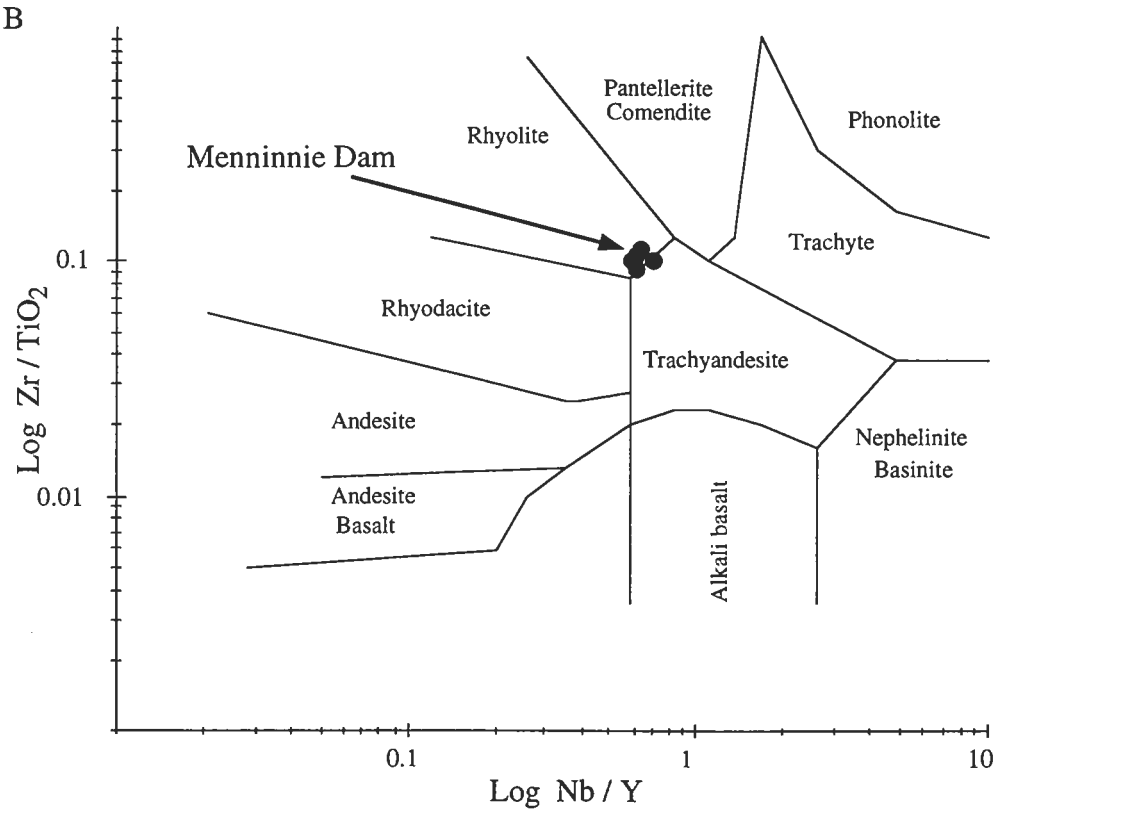


Fig. 4.14a Total alkali vs silica (TAS) variation diagram for classification of igneous rocks with least altered sample of rhyolite intrusion plotted (after Le Bas et al. 1986).

Fig. 4.14b Immobile trace element ratio variation diagram for the compositions of the strongly and weakly altered rhyolite intrusions, coherent rhyolite and the igneous component of peperite (after Winchester and Floyd, 1977).

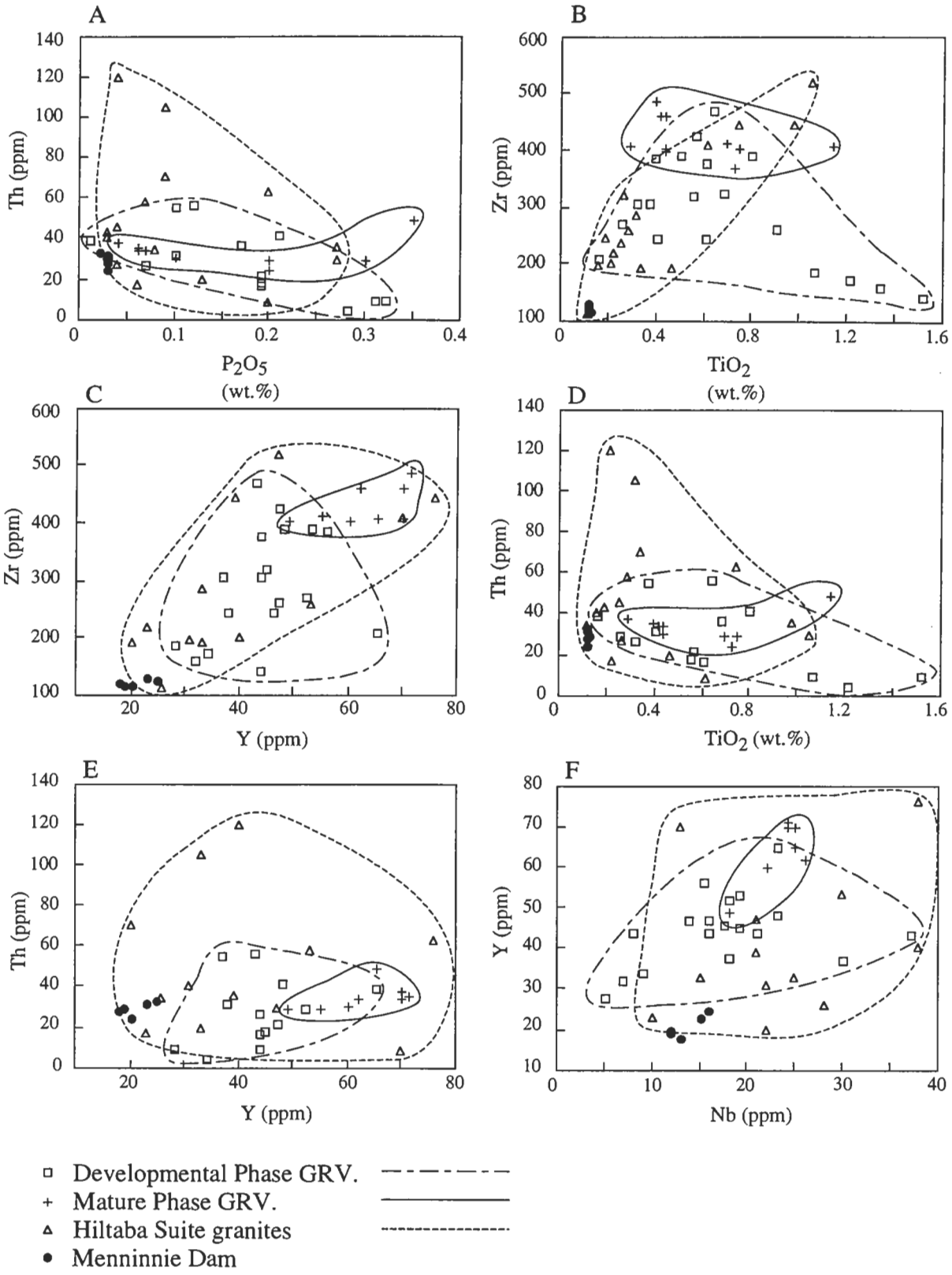


Figure 4.15 Immobile element variation diagrams with composition fields for Hiltaba Suite granite (Flint, 1993b), developmental, and mature phases of the GRV (Blissett et al., 1993; Stewart, 1992; Jagodzinski, 1985). The rhyolite intrusions, coherent rhyolite and igneous component of peperite from Menninnie Dam have compositions that lie close to, or within, the composition field for Hiltaba Suite granite and are distinct from the mature and developmental phases of the GRV.

| | | |

Fig. 4.16a. Drill hole PD0021, 266.1 m (vert.). Basal contact of the MD ignimbrite with a muddy sandstone unit. The muddy sandstone unit (M) is 3 cm thick and overlies a pumice breccia unit (P). The contact between the MD ignimbrite (MD) and the muddy sandstone is sharp and conformable. Fiamme in the pumice breccia are parallel to lithologic contacts. Fiamme within the lower 1 cm of the MD ignimbrite are parallel to the basal contact whereas those a few centimetres higher are at an angle to the contact.

Fig. 4.16b. Drill hole PD0021, 132.54 m (vert.). A thin rind (R) ≈ 8 mm wide comprised of fine relict ash and minor fine grained lithics has coated the margin of a brecciated and altered 16m diameter granite clast (G). The rind is differs from the enclosing MD ignimbrite (MD) which contains coarser pyroclastic and lithic clasts.

4.16a

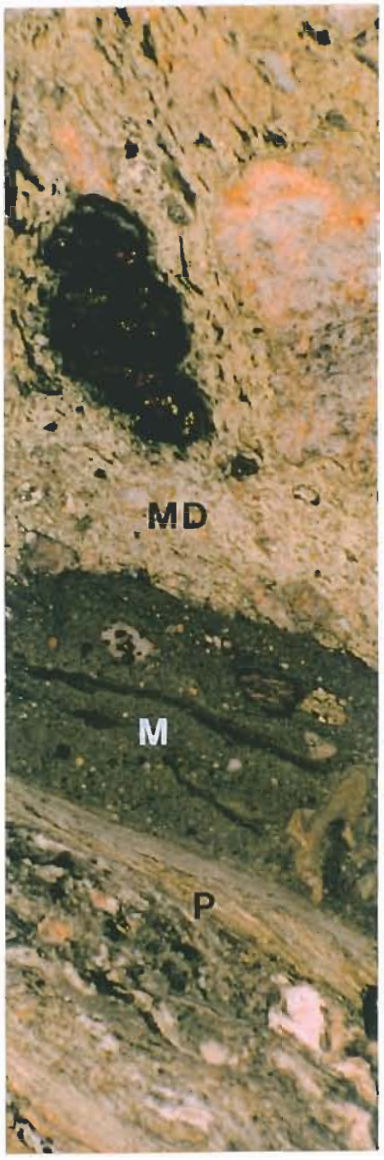


4.16b

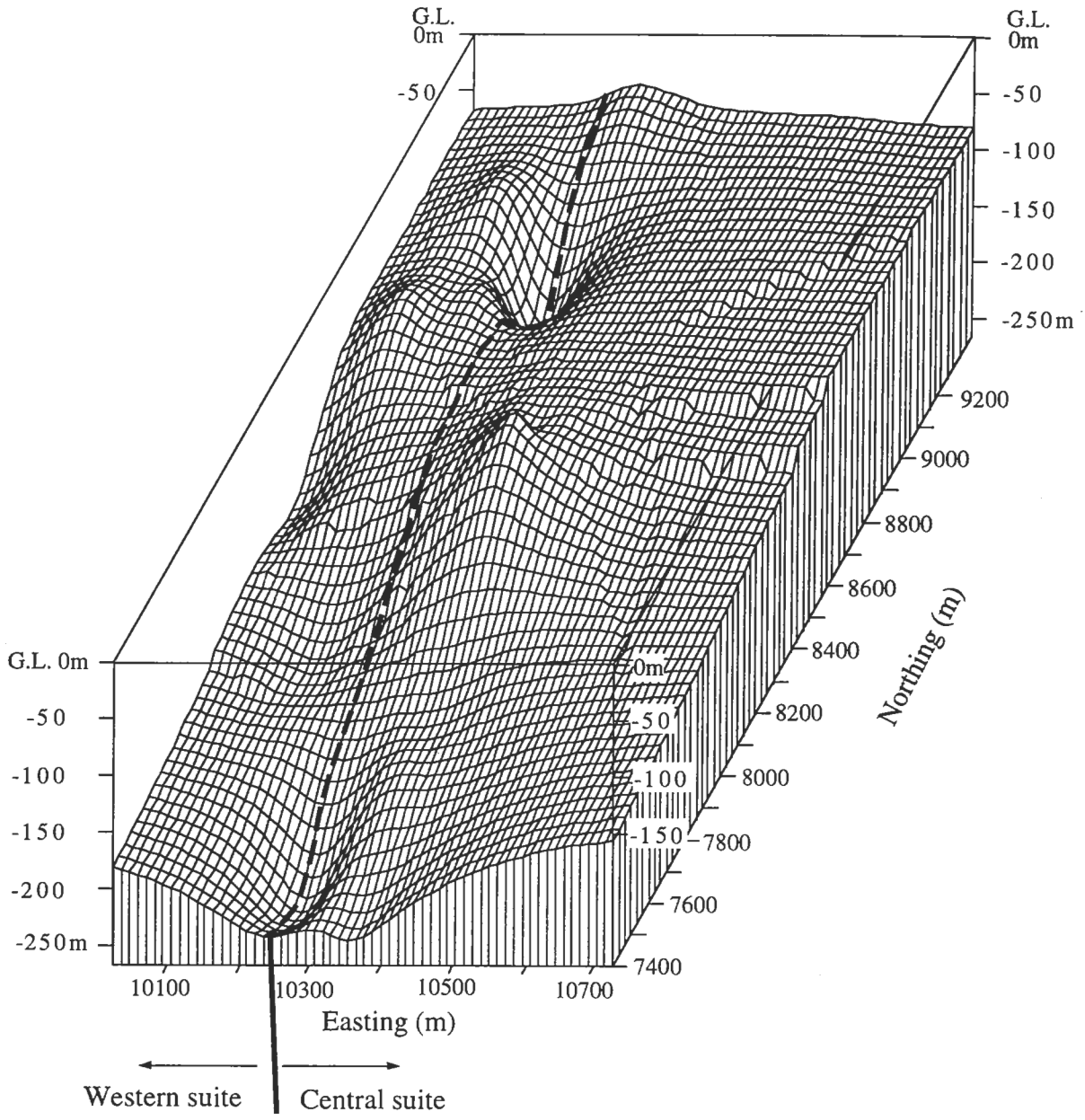


Fig 4.17 3D Wire mesh model of the basal surface of the Menninnie Dam ignibrite viewed from the south-east and looking to the north west. The greatest thickness of ignimbrite occurs in the south of the prospect close to the faulted contact between western and central suites (the trace of the fault is shown as a dashed line). The fault zone is interpreted to have been a valley at the time of ignimbrite deposition.

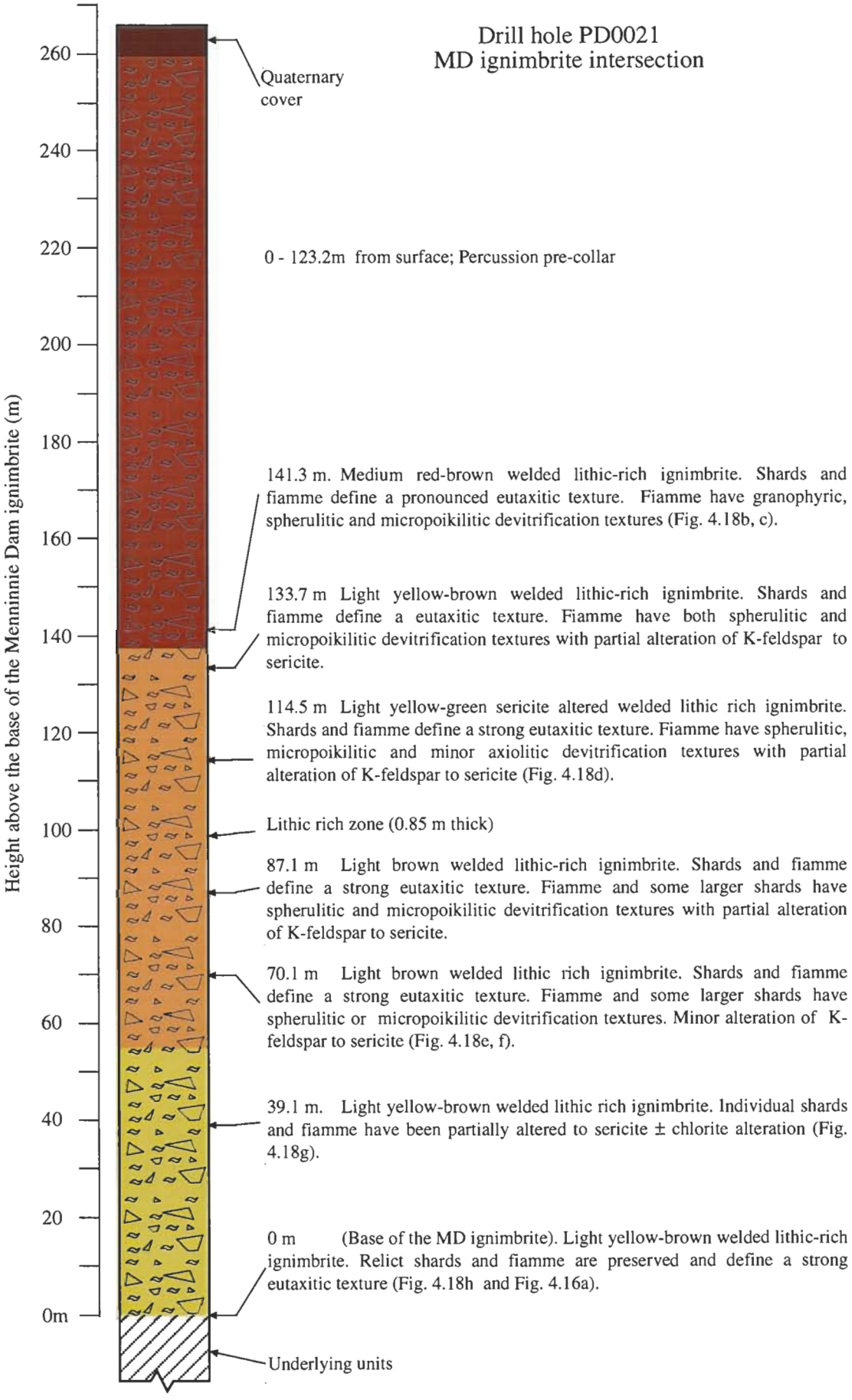


Fig. 4.18a Summary graphic log of textures and alteration mineralogy in the Menninnie Dam ignimbrite in drill hole PD0021.

Fig. 4.18b. Drill hole PD0021, 141.3 m from the base of the MD ignimbrite. Transmitted light photomicrograph of welded lithic-rich MD ignimbrite. Shards and fiamme define a pronounced eutaxitic texture. Many fiamme (F) are curved around lithic fragments (L).

Fig. 4.18c. Drill hole PD0021, 141.3 m from the base of the MD ignimbrite. Transmitted light photomicrograph of welded lithic-rich MD ignimbrite. Intensely flattened shards (S) are commonly bent around small lithic fragments (L).

Fig. 4.18d. Drill hole PD0021, 114.5 m from the base of the MD ignimbrite. Transmitted light photomicrograph (x nicols). The interior of a fiamme contains spherulites (SP) that have partially recrystallised (R). The groundmass has a layered fabric due to the orientation of compacted shards (S).

Fig. 4.18e. Drill hole PD0021, 70.1 m from the base of the MD ignimbrite. Hand specimen. Granite clasts (G) are the most common clast lithology throughout the MD ignimbrite. Fiamme (F) are clearly visible in hand specimen and define a eutaxitic texture.

Fig. 4.18f. Drill hole PD0021, 70.1 m from the base of the MD ignimbrite. Transmitted light photomicrograph (x nicols). Part of the interior of a fiamme. The fiamme has inner margins with a spherulitic texture (S) and a core of quartz and feldspar (C).

Fig. 4.18g. Drill hole PD0021, 39.1 m from the base of the MD ignimbrite. Transmitted light photomicrograph (x nicols). of quartz and sericite altered fiamme (F) contained with a fine grained matrix.

Fig. 4.18h. Drill hole PD0021, Transmitted light photomicrograph of MD ignimbrite from within 10 cm of the basal contact. Relict shards (S) have a pronounced eutaxitic texture and are commonly curved around lithic fragments (L).

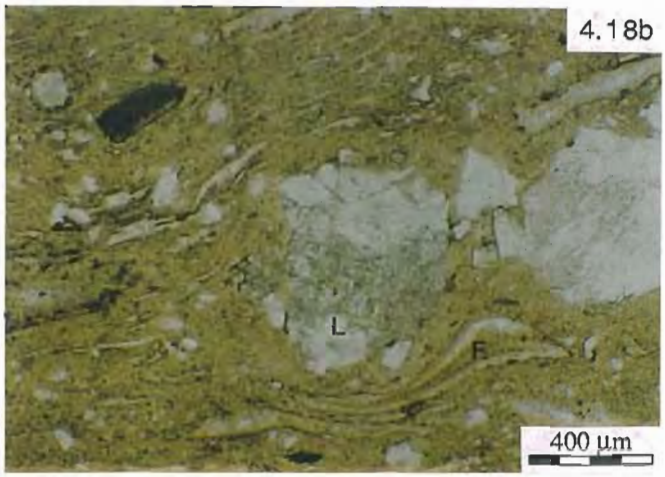
4.18b
L
F
400 µm

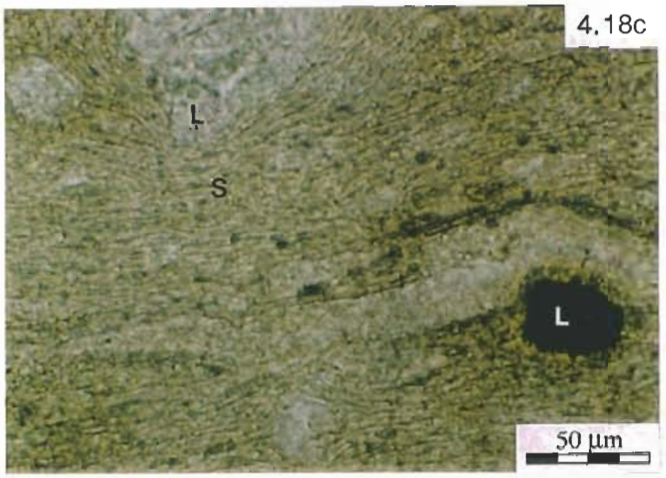
4.18c
L
S
L
50 µm

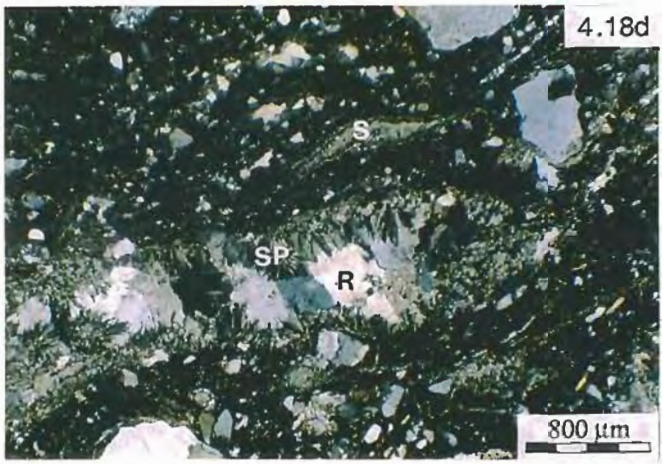
4.18d
S
SP
R
800 µm

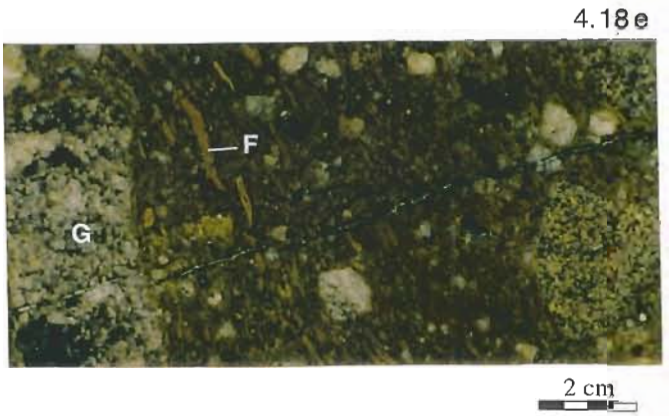
4.18e
F
G
2 cm

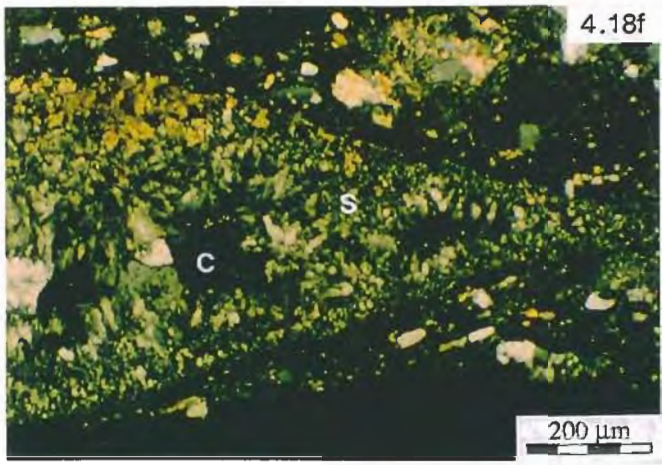
4.18f
S
C
200 µm

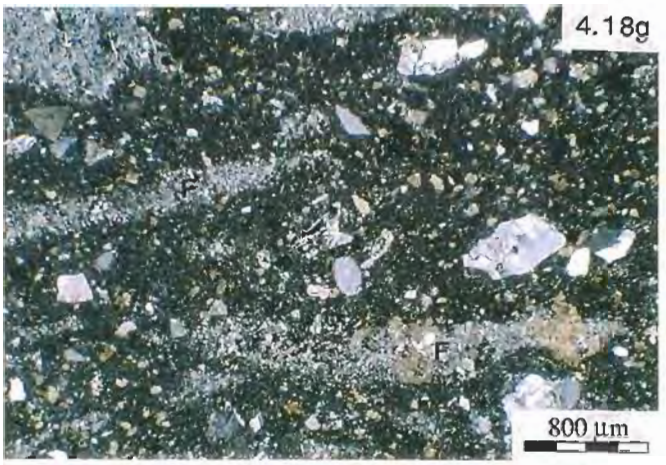
4.18g
F
F
800 µm

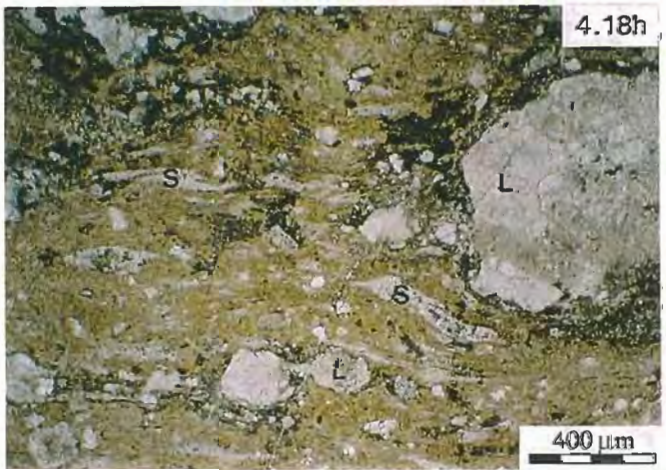
4.18h
S
L
S
L
400 µm

There is no apparent change in the length of fiamme throughout the drill core, although those higher up in the MD ignimbrite are commonly thinner and more attenuated (Figs. 4.18b, d, e, f, g, h). The orientation of fiamme varies locally over distances as small as 1 cm (Fig. 4.16a), however, the general orientation of fiamme is ≈ 25 - 45° to the drill core axis, which translates to either a sub-vertical or a sub-horizontal orientation (drill holes are inclined at ≈ 60° from horizontal). Given that the base of the MD ignimbrite is sub-horizontal (Fig. 4.17), and there has been little deformation since the late Palaeoproterozoic (Section 2.3.1), the orientation of fiamme is interpreted to indicate a sub-horizontal flattening orientation. Local perturbations in the orientation of fiamme commonly occur in proximity to lithic clasts with fiamme curving around the margins of lithic clasts.

*Lithic clasts*

Lithic clasts comprise Hutchison Group lithologies, including marble, calc-silicate lithologies, schist, iron formation, graphitic schist, as well as granite fragments, pegmatite fragments and fragments of metasomatised lithologies. Lithic clasts range in size from 2 mm to 19.85 m. Those smaller than 2 mm are considered to be part of the matrix. The shape of clasts varies from angular to sub-rounded with no correlation between the shape of clasts, size or lithology (as well as can be determined from drill core). The concentration of lithic clasts is not homogenous throughout the MD ignimbrite.

The lithic content of the MD ignimbrite in drill holes PD0021, PD0025 and PD0032 has been estimated with subdivision of clasts into two groups:

- Clasts greater than 10 cm
- Clasts between 2 mm and 10 cm

The position and size of lithic clasts greater than 10 cm have been recorded. The proportion of clasts less than 10 cm have been visually estimated at various depths by comparison with the 'grain percentage' diagrams of Terry and Chilingar (1955). The accuracy of visual estimates was periodically checked by sectioning the core length-ways, overlaying 1 mm square graph paper onto the flat surface of the core and tracing all clasts greater than 2 mm. Visual estimates were within 5% of the measured value. Estimated percentages of clasts < 10 cm and measurements of clasts > 10 cm are illustrated in Fig. 4.19 and detailed in Appendix 4.1.

The proportion of clasts 2 mm - 10 cm across ranges from 10 - 80% and systematically increases with depth to ≈ 234 m (drill holes PD0032 and PD0021; Fig. 4.19). Near 234m in drill hole PD0021 the clast size is diminished and again shows a systematic increase towards the base of the MD ignimbrite at 266 m. Clasts > 5m are more common above 214 m (Fig. 4.19). Interpretation of the variation in abundance and size of lithics is discussed in Section 4.4.8.

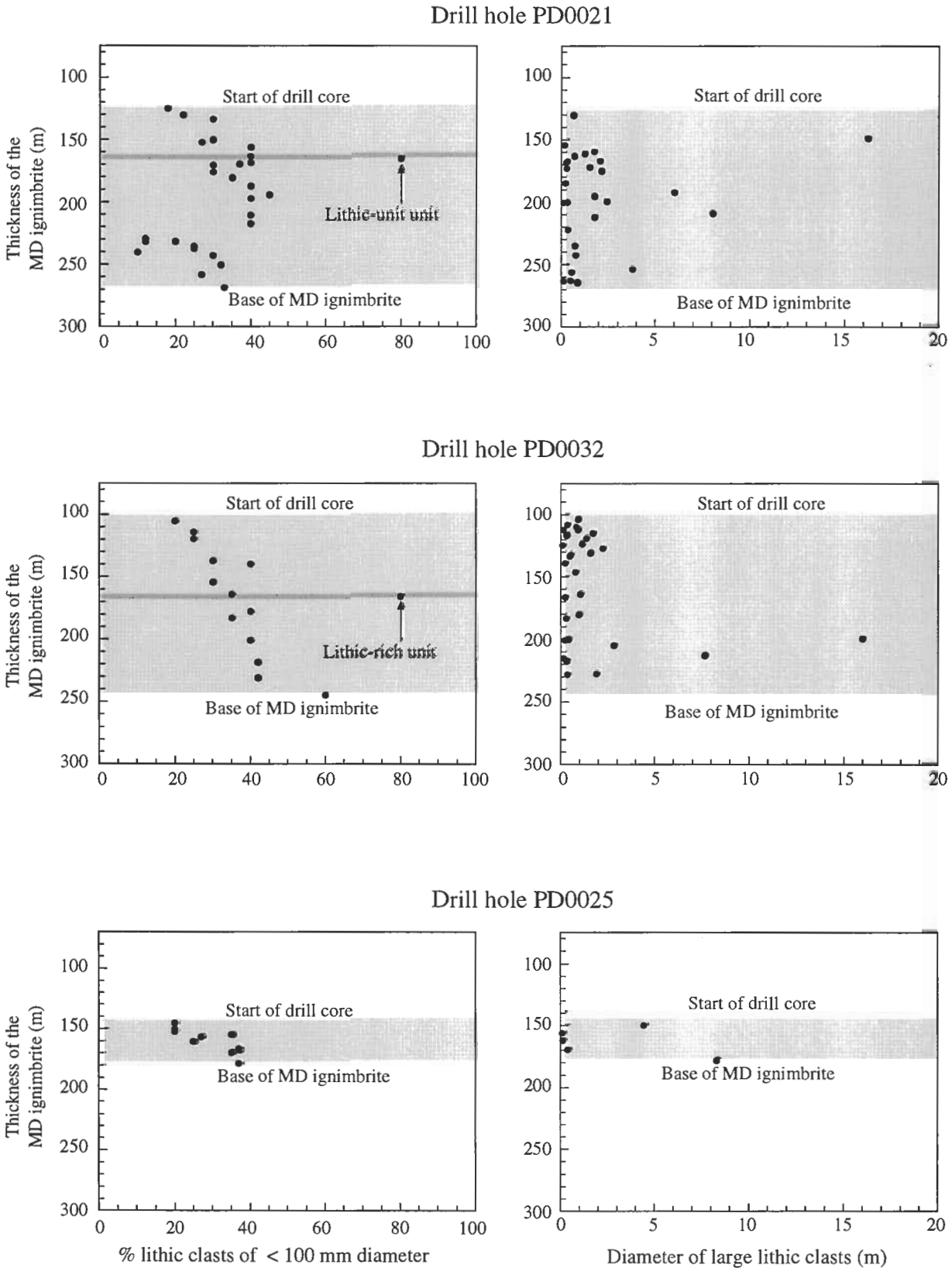


Fig. 4.19 Diagrams illustrating the percentage of lithic clasts < 100 mm across and lithic clast > 100 mm across throughout the MD ignimbrite for the three drill holes with significant intersections of MD ignimbrite. L ithic clasts < 100 mm diameter have a systematic increase in abundance with depth to ≈ 234 m. Lithic clasts > 5 m diameter are more common in zones that also have a higher percentage of lithic clasts < 100 mm diameter. The position of the lithic-rich unit is also illustrated.

Thin, lithic-rich zones are present in the two most southerly drill holes (Table 4.10 and Fig. 4.19).

Table 4.10 Lithic-rich zones in the MD ignimbrite. Northing and easting are drill collar coordinates. 'Depth' is the vertical depth below surface (the land surface is horizontal). Thickness is the vertical thickness.

| Drill hole | Northing | Easting | Depth (m) | Thickness (m) | Estimated % lithic clasts |
|---|---|---|---|---|---|
| PD0021 | 7564 | 10073.7 | 165.39 | 0.85 | 80 |
| PD0032 | 7406 | 10235 | 165.85 | 0.45 | 80 |

Both lithic-rich zones are at similar depths (the land surface is ≈ horizontal), have similar lithic clast contents, range of lithic clast types and sizes. The matrix to lithic-rich zones comprises fine lithic fragments devoid of a juvenile volcanic component. The bases of lithic-rich zones are irregular and diffuse over ≈ 20 cm and incorporate a juvenile volcanic component. The tops of lithic rich units are sharp, irregular and parallel to the orientation of fiamme in the overlying MD ignimbrite. A lithic-rich zone was not intersected at the same depth in drill hole PD0025, 390 m to the north. The corresponding interval in drill hole PD0030, 200m to the north was percussion drilled and the data cannot be evaluated as percussion samples are 2 m composites.

*Relationship between lithic clast lithology, abundance and size*

Granite clasts are mineralogically and texturally indistinguishable from the deformed granite dykes that locally intruded Hutchison Group and interpreted to be ≈ 1745 - 1710 Ma. (Section 3.8.3). Of the 64 clasts > 10 cm across in drill holes PD0021, PD0025 and PD0032, 73% are composed entirely of granite and 92% are composed entirely of granite, or, are composite clasts which included granite (Table 4.11). Granite clasts are also the most common lithology for clasts of 2 mm - 10 cm (Fig. 4.18e).

Table 4.11 Lithology of clasts > 10 cm across in drill holes PD0021, PD0025 and PD0032.

| Clast lithology | Number of clasts |
|---|---|
| Granite | 47 |
| Granite and schist | 10 |
| Granite and marble | 2 |
| Schist | 4 |
| Marble | 1 |

Some granite clasts > 10 cm across are moderately fractured and some contain zones of tight jigsaw-fit breccia. Fractures and breccia zones do not extend beyond clast margins. Clasts > 2m commonly have a thin rind separating the clast from the enclosing ignimbrite (Fig. 4.16b). The rind varies from 3 mm to 2 cm in width and consists of greyish tuff (< 2 mm), and minor lithic fragments (< 2 mm). Rinds commonly have a weak lineation fabric parallel to the clast margin and commonly discordant to layering of fiamme outside the rind.

*MD ignimbrite matrix*

Matrix is defined as all components < 2 mm. The matrix comprises various proportions of lithic fragments and relict glassy shards (excluding the two lithic rich zones, Table 4.10). Flattened, and plastically deformed relict glassy shards are present throughout the MD ignimbrite, including within a few millimetres of the basal contact. More attenuated relict, glassy-shards common occur at higher levels in the MD ignimbrite (Figs. 4.18b, c).

Fragments of round and embayed quartz crystals (with straight extinction) are present within a few metres of the base of the MD ignimbrite. These are identical to those in the underlying muddy sandstone and / or pumice breccia. Throughout the remainder of the MD ignimbrite, fragments of round and embayed quartz crystals are absent. The apparent absence of a juvenile crystal population in the MD ignimbrite matrix concurs with the absence of a crystal population within fiamme.

*Evidence for hot emplacement of the MD ignimbrite*

The MD ignimbrite has textures which are indicative of hot emplacement and welding (Fig. 4.18b - i). Fiamme are strongly attenuated and commonly plastically deformed around lithic clasts. The interior of fiamme commonly comprise spherulitic, or axiolitic textures, or quartz which micropoikilitically encloses feldspar microlites. Cuspate shards are plastically deformed around small lithic fragments. The presence of spherulites and micropoikilitic quartz and feldspar are interpreted to indicate high temperature devitrification from a glassy precursor of flattened, welded, pumice lapilli (Lofgren, 1971 a and b, Lofgren, 1974, Wright, 1915, Ross and Smith, 1961, Anderson, 1969).

**MD ignimbrite in the basal 34m of drill hole PD0032**

The basal 34m of drill hole PD0032 differs from other intersections of MD ignimbrite in that it is non-welded and selectively, to pervasively altered. The intensity of alteration increases with depth and the alteration minerals show a corresponding systematic change. A summary of the textures and alteration mineralogy of MD ignimbrite in drill hole PD0032 is illustrated in Figures 4.20a - i.

*Description (ref. Figs. 4.20a - i)*

The basal 34m of drill hole PD0032 contains a lithic clast content of ≈ 54% which is slightly higher than the average lithic clasts content determined for the remainder of the MD ignimbrite (≈ 47%). Above ≈ 58.5 m from the base of drill hole PD0032, the MD ignimbrite is welded with a strong eutaxitic texture. Between ≈ 58.5 - 33.5 m from the base, the MD ignimbrite consists of light greenish-brown, chlorite altered, lithic-rich, partly-welded ignimbrite with a moderate eutaxitic texture, and common micropoikilitic and spherulitic devitrification textures within fiamme.

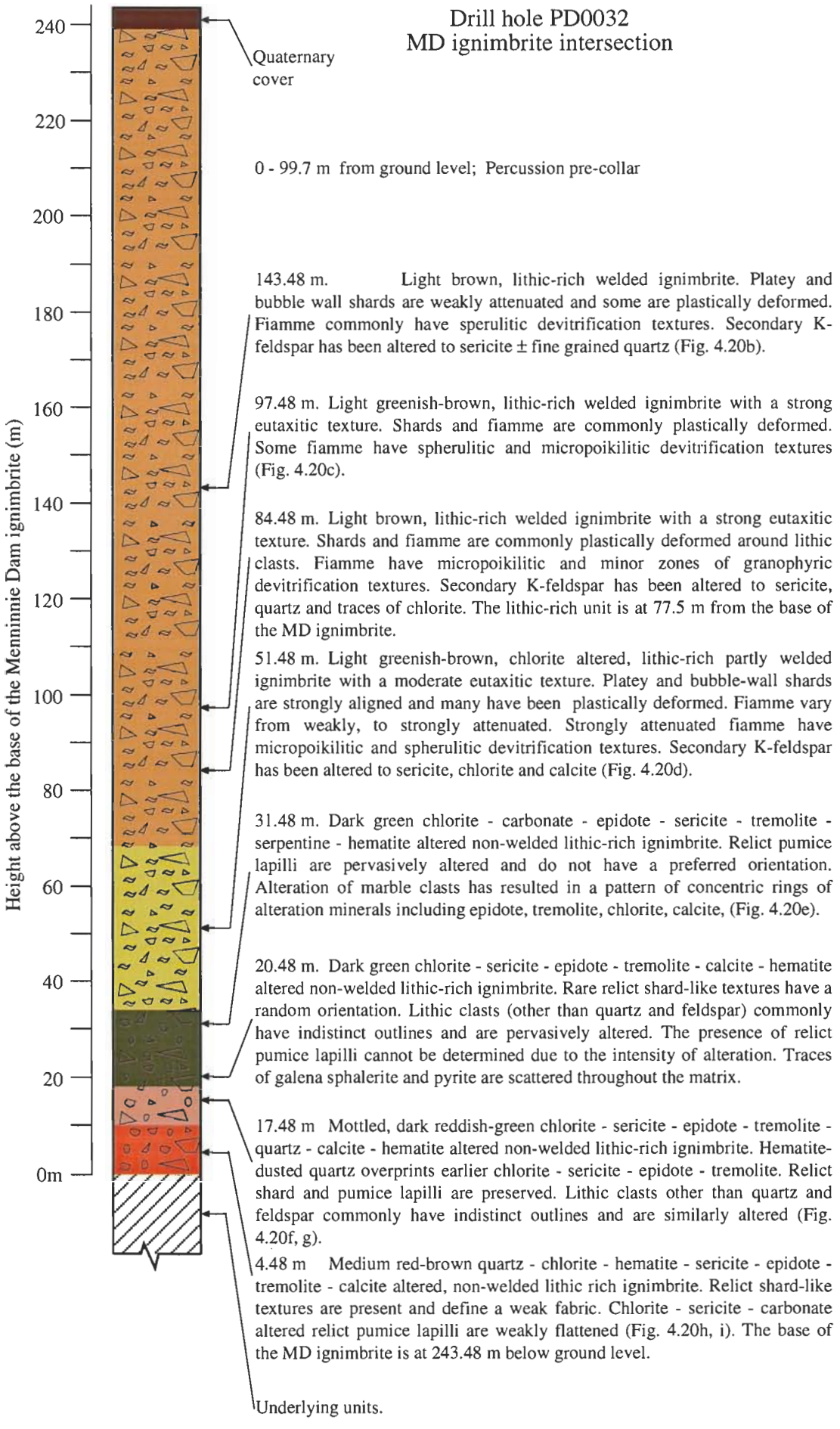


Fig. 4.20a Summary graphic log of textures and alteration mineralogy in the Menninnie Dam ignimbrite in drill hole PD0032.

Fig. 4.20b. Drill hole PD0032, 143.48 m from the base of the MD ignimbrite. Hand specimen. Fiamme are common, but not pronounced in hand specimen, and define a weak eutaxitic texture.

Fig. 4.20c. Drill hole PD0032, 97.48 m from the base of the MD ignimbrite. Transmitted light photomicrograph of fiamme (F) and relict shards (S) that are commonly curved around lithic clasts and fragments (L) and define a eutaxitic texture.

Fig. 4.20d. Drill hole PD0032, 51.48 m from the base of the MD ignimbrite. Hand specimen. Light greenish-brown, sericite, chlorite, calcite altered, lithic-rich partly welded ignimbrite with a moderate eutaxitic texture. Fiamme (F) are altered to yellow-green sericite, and minor chlorite and calcite.

Fig. 4.20e. Drill hole PD0032, Transmitted light photomicrograph. 31.48 m from the base of the MD ignimbrite. Fiamme (F) in the MD ignimbrite have been altered to sericite, chlorite and calcite.

Fig. 4.20f. Drill hole PD0032, 17.48 m from the base of the MD ignimbrite. Hand specimen. Mottled, dark reddish-green altered non-welded lithic-rich ignimbrite. Pumice lapilli (P) and some shards (S) are preserved as yellow-green sericite - chlorite - calcite altered relicts. Sericite - chlorite - calcite alteration of the MD ignimbrite matrix has mostly been overprinted by dark-green chlorite - sericite - epidote - tremolite - quartz - calcite - hematite alteration. Some marble clasts contain pyrite (PY) and galena (G) as alteration minerals.

Fig. 4.20g. Drill hole PD0032, 17.48 m from the base of the MD ignimbrite. Transmitted light photomicrograph. Pumice lapilli (within the dashed line) are commonly weakly flattened and have been altered to sericite, chlorite and calcite. Pumice lapilli are enclosed in a darker green, chlorite - sericite - epidote - tremolite - quartz - calcite - hematite altered groundmass.

Fig. 4.20h. Drill hole PD0032, 4.48 m from the base of the MD ignimbrite. Hand specimen. Medium red-brown non-welded lithic rich ignimbrite. Early sericite - chlorite - calcite alteration has been preserved in relict pumice lapilli (PL) whereas the MD ignimbrite matrix has been overprinted by dark green epidote -tremolite - chlorite - sericite - carbonate alteration which has been later partially overprinted by red-brown quartz - hematite alteration.

Fig. 4.20i. Drill hole PD0032, 4.48 m from the base of the MD ignimbrite. Transmitted light photomicrograph. Relict shard-like textures (S) are preserved and have been altered to quartz. Some relict pumice lapilli (PL) have been preserved as sericite - chlorite - calcite altered pseudomorphs.

4.20b

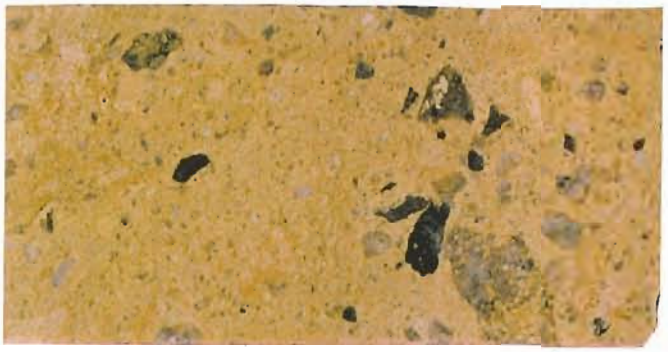

2 cm

4.20c

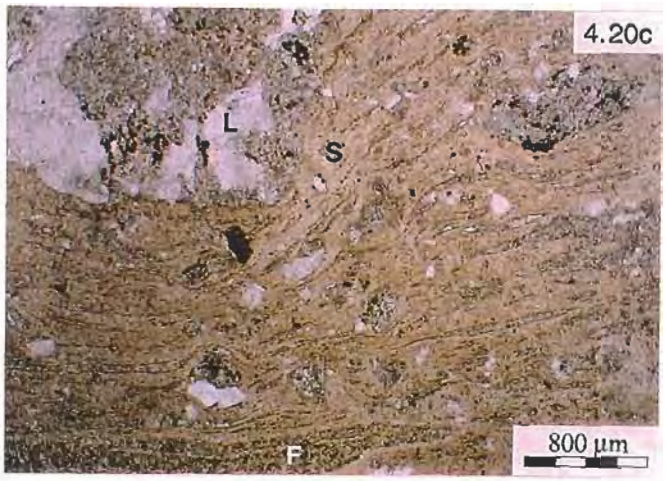


4.20d

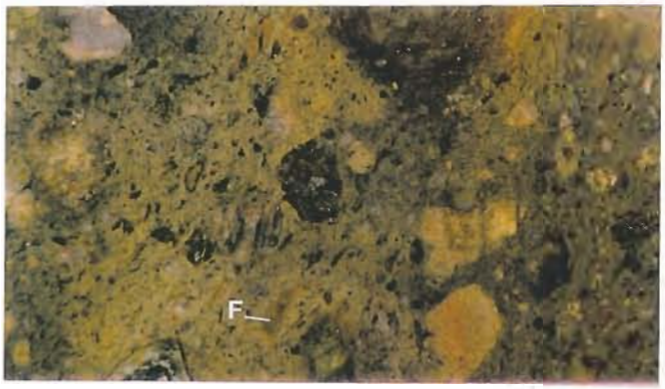


2 cm

4.20e

4.20f

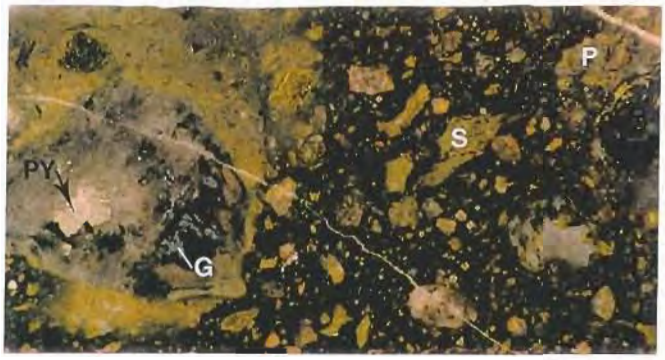


2 cm

4.20g

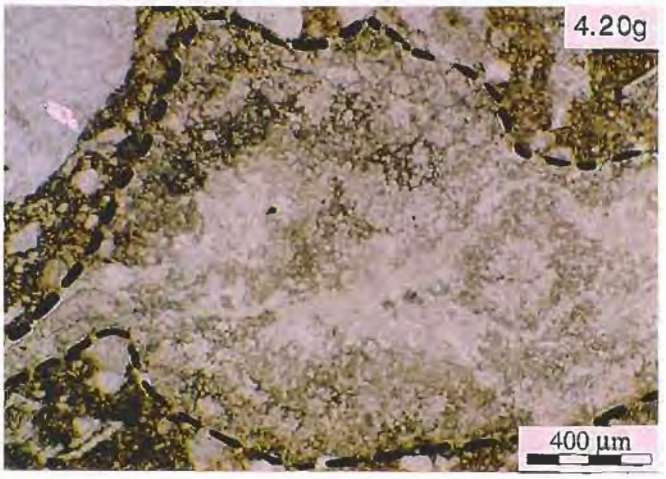


4.20h

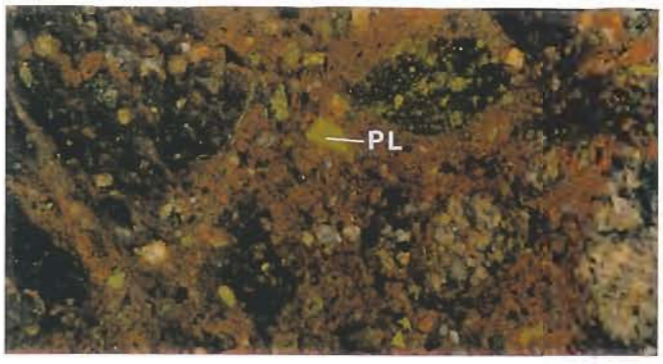


2 cm

4.20i

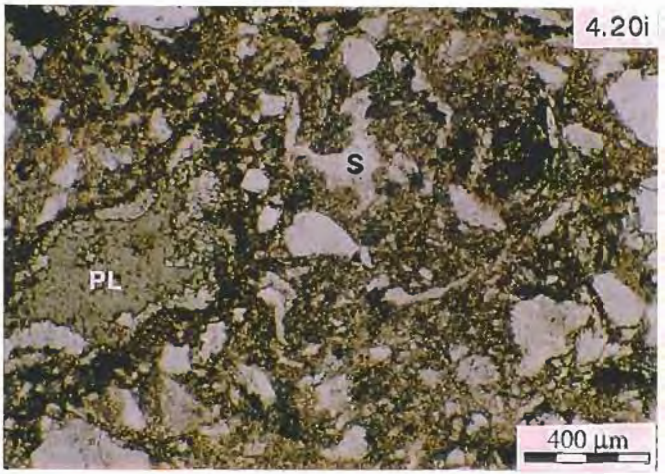

Between ≈ 33.5 - 18.5 m from the base, the MD ignimbrite consists of dark green chlorite - carbonate - epidote - sericite - tremolite - serpentine - hematite altered non-welded lithic-rich ignimbrite. Fiamme are absent and relict pumice lapilli are uncompacted and pervasively altered. Alteration of marble clasts has resulted in a pattern of concentric rings of alteration minerals including epidote, tremolite, chlorite and calcite. Trace amounts of galena, sphalerite and pyrite are scattered throughout the altered matrix. Between 18.5 - 10.5 m from the base, the MD ignimbrite is non-welded, dark reddish-green, and has been pervasively altered to chlorite, sericite, epidote, tremolite, quartz, calcite, serpentine and hematite. Hematite-dusted quartz has overprinted earlier chlorite - sericite - epidote - tremolite - serpentine alteration. Lithic clasts other than quartz and feldspar, commonly have indistinct margins and are similarly altered. Altered relict pumice lapilli (and shards?) are preserved within hematite dusted quartz. The basal ≈ 10.5 m of the MD ignimbrite comprises medium red-brown, non-welded lithic rich ignimbrite with more intense hematite-dusted quartz alteration.

## 4.4 Discussion

In this section an interpretation of the units described in Sections 4.31 - 4.34 is presented and a genetic model for their emplacement is proposed. This is followed by an interpretation of the MD ignimbrite and the volcanic architecture at the time of its emplacement.

### 4.4.1 Rhyolite intrusions elsewhere in the Gawler Range Volcanic Province

The geometry of the rhyolite intrusions at Menninnie Dam is uncertain, and they may be either sills, dykes or plugs of restricted extent. The rhyolite intrusions are texturally similar to rhyolite dykes described elsewhere in the Gawler Range Volcanic Province. Giles (1977) described brick-red, alkali-feldspar, quartz, and plagioclase-phyric, rhyolitic to dacitic dykes up to 80m wide (Moonamby Dyke Suite) in the Glyde Hill Volcanic Complex in the north-west of the GRV Province. Dykes were considered to have been co-magmatic with the GRV and emplacement of granitoids of the Hiltaba Suite. Watmuff (1973a and b) described similar dykes from the Glenloth Goldfield area in the far north-west of the GRV Province. Rhyolite dykes were described as containing small phenocrysts of euhedral, sericitised K-feldspar, and spherical quartz in a devitrified, fine-grained, reddish-brown matrix with a micropoikilitic texture. Similar dykes occur in the Tarcoola area (Wiltabbie Volcanics; Daly, 1985), and north-west of Corunna (Turner, 1975), and in the Kokatha area, (Blissett et al., 1993). With the exception of Wiltabbie Volcanics, most dykes were interpreted to have intruded units of the GRV and to have been co-magmatic with the Hiltaba Suite (Flint, 1993b). On the basis of their immobile element geochemistry (Section 4.3.5), rhyolite intrusions at Menninnie Dam are also interpreted to be genetically linked to the Hiltaba Suite which constrains their age to ≈ 1589 Ma. (Creaser and Cooper, 1993).

### 4.4.2 Interpretation of DP breccias.

DP breccias are hosted by and include clasts of Hutchison Group lithologies, deformed granite dykes, pegmatite dykes and metasomatised lithologies. Hutchison Group lithologies have been subjected to upper amphibolite facies metamorphism whereas DP breccias are neither deformed nor metamorphosed and therefore, cannot have been primary sedimentary breccias.

DP breccias are tentatively interpreted to be pipe-like bodies with a sub-vertical orientation ('breccia pipes') because:

- DP breccias have limited lateral extent and significant vertical extent.
- Many DP breccias occupy fault zones. Fault zones were interpreted to be sub-vertical (Section 3.5.1), therefore, DP breccias are also interpreted to be sub-vertical.

Reference to breccias pipes interpreted be related to collapse, or associated with volcanic or igneous activity is common in the literature (eg. Wenrich, 1985; Sillitoe, 1985; Hazlitt and Thompson, 1990). Baker et al. (1986) reviewed the processes proposed for formation of hydrothermal breccia pipes and suggested that the processes that gave rise to breccia pipes can be interpreted from a variety of breccia textures considered in combination. The major features of hydrothermal breccia pipes with emphasis on the characteristics relating to their recognition are summarised in Table 4.12 (modified after Baker et al., 1986).

Inverted cone or ellipsoidal-cylindrical shapes are common for breccias formed by different processes (Table 4.12). In the absence of exposure, or more detailed drilling, it cannot be determined as to whether DP breccia bodies flare towards the surface or not (inverted cone shape). McCallum (1985) conducted scaled experiments on breccia pipe formation. Smaller, less flared pipes were developed in less permeable hosts whereas larger diameter pipes formed in more permeable hosts. The competent and impermeable nature of the host rocks at Menninnie Dam may account for the *apparent* absence of an inverted cone shape of DP breccia pipes. DP breccias south of 8200 mN are spatially associated with rhyolite intrusions. Formation of peperite at the contact between rhyolite intrusions and DP breccia requires DP breccias to have been wet and unconsolidated at the time of rhyolite intrusion. It is therefore considered likely that DP breccias immediately preceded rhyolite intrusions and could have been genetically related to rhyolite intrusions.

DP breccias have many similarities to the maar / diatreme breccias described by Baker et al. (1986; Table 4.12). The sharp host rock contacts, polymict nature of DP breccias, and the angular to rounded shape of clasts distinguishes them from fault related breccia pipes. The matrix supported nature of DP breccias is similar to that for hydrothermal and maar / diatreme breccias but differs from the commonly clast supported nature of hypabyssal breccias.

Table 4.12 Summary of the major features of hydrothermal breccia pipes with emphasis on those characteristics relating to their recognition (modified after Baker et al., 1986).

| | Hypabyssal | Maar / Diatreme | Hydrothermal eruption | Fault related |
|---|---|---|---|---|
| **General form** | Steeply dipping cylindrical (in granitoid hosts), elongate (in metasediments). Often inverted cone shaped. Ovate | Inverted cones. Mostly circular, becoming cylindrical at depth. | Inverted cones, and irregular, pipe-like bodies. Relatively smaller scale. Irregular to ovate. | Pipes of irregular form. Ovate, cylindrical, linear to irregular, generally small scale. |
| **General environment** | Intrusive related | Volcanic related | Volcanic / geothermal | No specific environment |
| **Wallrock contact features** | Typically sharp, with sub-parallel sheeted veining. Upper sections encased by shatter zones | Sharp contacts. Margins commonly contain large, fractured blocks of host rocks. | Sharp complex finger-like contacts. | Irregular contacts, poorly defined. Strong relation to adjacent fault zones. |
| **Internal fragment characteristics** | Sections of the pipe show wide variation in clast type, size and angularity. Tendency for rounding. Pronounced in softer (granitic) and smaller clasts. Metasediments etc. less well rounded. Usually altered. | Fragments mixed, commonly rounded. Contain wall rocks from upper levels and rare carbonised wood. Usually altered. | Fragments mixed, of near surface wall rocks. Often rounded. Pervasively altered. | Fragments angular, monoclastic. Commonly large blocks only mildly shuffled. Commonly altered. Wide size range. |
| **Matrix** | Fine comminuted rock flour, matrix : clast ratio typically 20: 80. Often replaced. Clast supported. | Comminuted rock flour. Matrix commonly predominates over clasts, ie. matrix supported. | Comminuted rock flour, clays. Matrix variable in amount, often low in volume, usually replaced. Matrix supported. | Comminuted rock, relatively small in volume and relatively coarse-grained. Clast-supported. Usually altered. |
| **Hydrothermal components** | Replacement of fragments and matrix. Vugh component low and usually small size. Usually completely infilled. Vugh of similar mineralogy to the alteration. Mineralisation infill commonly in vughs and replaced matrix often peripheral. | Replacement of fragments and matrix, especially in upper levels. Mineralisation in breccia matrix and overprinting veins and fractures. | Pervasive mineralisation mostly as replacement of matrix and clasts. Also in overprinting veins. | Mineralisation usually restricted to irregular infill regions, veins, lenses, pods etc. Locally occurs as replacement of blocks. |
| **Examples** | Kidston, North Queensland, (Mustard, 1983; Baker, 1987, 1988, Wormald et al., 1991. Torquepala, Peru (Richard and Courtright, 1959). | Acupan, Philippines (Sawkins et al., 1979), Wau (Sillitoe et al., 1984). | Borealis, Nevada, Champagne Pool, New Zealand (Weissberg, 1969). Waiotapu geothermal system (Hedenquist and Henley, 1985) | Vulcan, Irvinebank, North Queensland (Mason, 1953) |
| **Formation depth** | 0.5 - 2.0 km, possibly deeper. | 500m to surface | 300m to surface | Any depth in brittle regime. |

NB: Some of the above types incorporate several breccia styles. All incorporate fault block shuffle / 'shatter breccia' style phenomena. Some areas of hypabyssal, maar / diatreme, and to a lesser extent eruption breccias contain areas of collapse. Fragments here are large tabular, clast supported with vugh / infill components. This summary does not include collapse of solution styles prevalent in carbonate / Mississippi Valley type regimes.

The depth extent of DP breccias (> 545 m, Table 4.2) is more than the maximum depth attributed to hydrothermal breccias, but similar to that for hypabyssal and maar / diatreme breccias. Sillitoe (1985) reviewed breccia pipes formed in volcano-plutonic arcs. The "phreatic breccias" described by Sillitoe (1985) are interpreted to be similar to the hydrothermal breccias of Baker et al. (1986). Sillitoe (1985) described the dominant feature that separated phreatic breccias from most magmatic hydrothermal breccias was the widespread occurrence of quartz as a cement and replacing the matrix and breccia fragments, as well as the common occurrence of argillic alteration in magmatic hydrothermal breccias. Quartz is not a pervasive alteration mineral or cement in DP breccias at Menninnie Dam and argillic alteration is absent.

Cas and Wright (1987) described diatreme breccias as a "pipe-like volcanic conduit filled with volcaniclastic debris". While DP breccias have many similarities to maar / diatreme breccias, they do not comply with the definition of Cas and Wright (1987) in that they are not obviously volcanic conduits and are not filled with volcanic debris. Other authors (eg. Wolfe, 1986) considered the definition of diatreme to be too restrictive and suggested it should be broadened to include structures such as kimberlite pipes and intrusive breccias.

Sillitoe (1985) applied the term 'porphyry-type breccias' to a group of pipe and dyke-like breccia bodies that are commonly associated with base metal mineralisation (eg. the breccias in the Leadville District, Colorado). Porphyry-type breccias were interpreted to be associated with a particular intrusive phase that commonly post-dated ore deposition. Hazlitt and Thompson (1990) described heterolithic breccia bodies from the Leadville District that locally crosscut manto and chimney* style Pb - Zn - Ag mineralisation. Breccias bodies locally exceed 600 m vertical extent and are localised by high angle faults. Breccias were interpreted to have been associated with rhyolite porphyry dykes and plugs and "to have formed much like diatremes by fluidisation of rock along hydrothermal fluid conduits as the ore-forming magmatic hydrothermal system collapsed and meteoric water encroached" (Hazlitt and Thompson, 1990). Of the four breccia stages identified by Hazlitt and Thompson (1990), stages 1 and 2 have many similarities to DP breccias at Menninnie Dam. Stage 1 breccias are polymict and incorporate angular and rounded clasts in a finer matrix of similar material. Stage 2 breccias have a distinct banding of fragments and matrix and commonly include wispy fragments of "flow banded material", considered to resemble a local flow banded porphyry unit. Breccia pipes and pebble dykes associated with Pb - Zn - Ag manto ore bodies have been observed in a number of other districts including; Tintic and Park City, Utah (Hazlitt and Thompson, 1990), the Potossi Mine, Santa Eulalia District, Chihuahua, Mexico (Miguel et al., 1986) and Butte, Montana (Meyer et al., 1968). On the

* manto' is Spanish for blanket and refers to the sub-horizontal shape of carbonate replacement style Pb - Zn - Ag mineralisation. Chimneys are sub-vertical equivalents.

basis of this discussion, a mechanism is proposed for the formation of DP breccias at Menninnie Dam and presented as part of a *genetic model* in Section 4.4.7.

**Fluidisation**

The term 'fluidisation' rather than 'gas or fluid streaming' (Wolfe, 1986) is used in this study in keeping with common usage. The polymict nature and lateral grading across some DP breccia bodies (Section 4.3.2) is interpreted to have resulted from fluidisation processes. Burnham (1985) attributed breccia formation in sub-volcanic environments to second boiling and subsequent decompression of the host rock, and calculated breccias could form by these processes at subsurface depths in excess of 1 km. Fracture-generated decompression of the host rocks was postulated to result in increased effervescence of the magma at depth (Burnham, 1985), possibly resulting in fluidisation of material in the lower part of the system and rafting of wall-rock fragments hundreds of metres upwards.

Alternatively, DP breccia formation and fluidisation may have resulted from rapid magmatic heating of ground water and conversion to a gaseous phase. Analytical and numerical solutions to ground water flow and pore pressure increases associated with rapid intrusion of magma into wet rock by Delaney (1982), were interpreted to indicate that greater *fluid* pressures were generated by rapid intrusion of magma into relatively impermeable rocks at depths of less than 1 km. Hydraulic fracturing of brittle rocks, or rapid migration of heated fluids along pre-existing fractures, faults or lithologic contacts open to the surface, could result in flashing of the fluid to steam above the boiling point - depth curve. Rapid expansion caused by conversion of the fluid to steam could result in brecciation of the host rock and possibly fluidisation of breccia clasts similar to that proposed by Burnham (1985).

Experimental simulation of fluidisation processes lead McCallum (1985) to attribute fluidisation by a gaseous fluid as a possible method of clast transport resulting in homogenous mixing of breccia clasts. McCallum (1985) attributed lateral grading of clasts within modelled breccia pipes to the duration of fluidisation. In short lived pipes, coarser clasts were concentrated near the centre of the pipe and finer clasts nearer the margins due to elutriation of finer particles (equivalent to 'coarse centre grading'; Section 4.3.2). Where fluidisation persisted for longer periods, the reverse grading pattern was found with coarser particles concentrated near the margins of pipes and finer, more rounded, clasts near the centre of the pipe in zones of higher gas velocity attributed to increased particle - particle interaction and clast milling (equivalent to 'double coarse margin grading'; Section 4.3.2).
The lateral grading observed in DP breccias at Menninnie Dam is interpreted to have resulted from processes similar to those observed by McCallum (1985).

### 4.4.3 Interpretation of LP breccias

LP breccias do not fulfil any of the criteria of Holland and Zbinden (1985) for the identification of Precambrian paleosols and there is no evidence of a subaqueous environment having been present during deposition, therefore, LP breccias are not considered to be products of weathering or sub-aqueous deposition.

The poor sorting and weak grading of individual LP breccia layers are common features of subaerial debris flow deposits (Schmincke, 1967; Ballance, 1984; Smith 1986). However, LP breccias have features that are not consistent with a debris flow origin. Pb - Zn - Ag sulphide mineralisation is interpreted to have been present only at depths of > 80 m below the palaeosurface at the time of LP breccia deposition and cannot have been incorporated as clasts in a debris flow (ref. Sections 5.6.7; 5.6.8; and 8.6).

Incorporation of lithic clasts of identical lithology to the underlying Hutchison Group, and Pb - Zn - Ag sulphide clasts, can be interpreted to indicate the LP breccias were locally derived. The local terrain at the time of LP breccia deposition has been established as gently sloping (Fig. 4.17). The rounded shape of many LP breccia clasts is typical of abrasion (Blatt et al., 1980) which is unlikely to have occurred during plug or laminar flow of a debris flow for short distances over gently sloping terrain (Johnson, 1970; Enos, 1977).

Most debris flows incorporate a significant clay component derived from weathering or hydrothermal alteration of the precursor lithologies (Voight et al., 1981; Scott et al, 1995). LP breccias do not appear to contain a clay component, and lithic clasts do not show any evidence of having been weathered prior to incorporation in LP breccia.

LP breccia bodies have many features in common with less fluidised DP breccias. They have the same clast compositions (including clasts of Pb - Zn - Ag sulphides), a similar clast : matrix ratio, similar matrix composition, and similar textures. Differences lie in the contrasting styles of clast grading, geometry of the units, and alteration mineralogy. Two of the more substantial thicknesses of LP breccia occur in drill holes that also intersected DP breccia bodies of > 8.5m thickness. McCallum (1985) observed that laboratory models of breccia pipes which broke through to the surface formed a bedded cone of ejecta immediately surrounding the pipe, which is similar to surficial deposits associated with maars (Lorenz, 1986; Cas and Wright, 1987; Self et al., 1980).

Although LP breccias are not interpreted to be associated with maar volcanoes or tuff rings, the eruptive mechanism involving interaction of magma and ground water (Kienle et al., 1980; Lorenz, 1986; White, 1991), may have been similar to that which resulted in the formation of the DP and LP breccias at Menninnie Dam. Cas and Wright (1987) noted that the first fragments ejected from maars and tuff rings comprise coarse angular fragments of

country rock. Lorenz (1973) described the ejecta from the Boos Maar, Eifel District, Germany, as constituting 60 - 80% country rock debris. Self et al. (1980) described a coarse grained, lithic fall deposit near the basal Ukinrek maar deposit. Kienle et al. (1980) cite two examples of maar deposits in which non-juvenile clasts were the only material ejected.

LP breccias are interpreted to have resulted from DP breccias stopping their way through to the surface and erupting onto the surface forming proximal breccia deposits with similarities to the basal lithic rich deposits associated with maars and tuff rings (Lorenz, 1973; Self et al., 1980; Kienle et al., 1980). The layering developed in LP breccia may have resulted from sequential eruptions or fluctuations in the intensity of eruptions of DP breccia, similar to deposits observed to have formed during eruptions at Taal volcano, Philippines (Wolfe, 1986). Layering has also been reported from a hydrothermal eruption breccia deposit, but is not common (Hedenquist and Henley, 1985a) The more intense alteration of DP breccias compared to LP breccias is interpreted to have resulted from a sub-surface hydrothermal fluid which did not interact with surficial LP breccias.

### 4.4.4 Interpretation of the rhyolite-bearing LP breccia

The rhyolite fiamme in the rhyolite-bearing LP breccia are interpreted to have been juvenile vesiculated clasts. The common occurrence of crystal fragments, evidence of high temperature devitrification textures, consistent compaction fabric parallel to the basal contact of the unit, curvature of fiamme around lithic fragments, and absence of evidence for a sub-aqueous depositional environment are interpreted to indicate a subaerial pyroclastic origin for rhyolite clasts. Formation of micropoikilitic textures in rhyolite clasts and fiamme as well as the matrix between clasts in the upper part of the unit is consistent with welding followed by devitrification (Lofgren 1971a, b, 1974; Anderson, 1969). The progressive increase in the size of fiamme and rhyolite clasts is consistent with a decrease in the degree of vesiculation of the parental melt (Fisher and Schmincke, 1984; Cas and Wright, 1987).

The apparent reverse grading of pyroclasts, poor sorting and absence of impact structures are not consistent with a conventional fallout origin (Cas and Wright, 1987). A pyroclastic flow origin is also considered unlikely. If the rhyolite-bearing LP breccia had resulted from a pyroclastic flow, it might be expected to have been laterally extensive and intersected in surrounding drill holes. It could be argued that the deposit generated by a pyroclastic flow was eroded and the rhyolite-bearing LP breccia is an isolated remnant. This is considered unlikely as it would require preferential erosion of a pyroclastic flow deposit with a welded upper surface and preservation of less consolidated (or most likely unconsolidated) LP breccia in drill holes PD0021, PD0030 and PD0032.

Feathery margins of the welded, composite clast at 175.4m in drill hole PD0031 (Fig. 4.11d), are interpreted to indicate the clast was re-fragmented and re-sedimented while still hot, plastic, and partially vesiculated. The composite clast has similarities to descriptions of spatter in felsic and intermediate pyroclastic deposits (Turbeville, 1992; Mellors and Sparks, 1991; Perrotta and Scarpati, 1994.). Most spatter deposits are considered to be vent proximal (Cas and Wright, 1987, Turbeville, 1992; Stevenson et al., 1993) or proximal facies of pyroclastic flow deposits (Turbeville, 1992, Mellors and Sparks, 1991; Perrotta and Scarpati, 1994).

On the basis of this discussion, a mechanism is proposed for the formation of rhyolite-bearing LP breccia and presented as part of a *genetic model* in Section 4.4.7.

### 4.4.5 Interpretation of fiamme-bearing DP breccias.

The fiamme-bearing DP breccia in drill hole PD0031 is ≈ 12.8 m (vert.) below the base of the rhyolite-bearing LP breccia in the same drill hole. The ragged terminations of fiamme are interpreted to have resulted from flattening of vesiculated volcanic clasts rather than shredding of magma. The fiamme-bearing DP breccia is interpreted to be the near surface equivalent of the overlying rhyolite-bearing LP breccia. The fiamme-bearing DP breccia in drill hole PD0021 is 43.7m (vert.) below an intersection of LP breccia in the same drill hole, although in this instance, rhyolite clasts are not present in the LP breccia. The absence of rhyolite pyroclasts in the LP breccia may relate to the greater depth at which fiamme-bearing DP breccia occurs in this drill hole and solidification of the magma prior to eruption.

### 4.4.6 Interpretation of muddy sandstone and pumice breccia

Rhyolite clasts in the rhyolite-bearing LP breccia, muddy sandstone unit and the pumice breccia all contain crystals or crystal fragments of feldspar, and round and embayed quartz. Rhyolite-bearing LP breccia occupies the same stratigraphic position as muddy sandstone and pumice breccia units in drill holes a few hundred metres to the south. These units are correlated, and the muddy sandstone and pumice breccia units are interpreted to be a primary distal facies equivalent of the rhyolite-bearing LP breccia.

The emplacement mechanism of pumice breccia and muddy sandstone units cannot be easily determined from drill core. They may have been deposited by fall out, pyroclastic flow (pumice breccia) or re-sedimentation of ash, pumice lapilli, and lithic fragments. Pyroclastic deposits immediately preceding rhyolite lava flows are a common phenomenon (Newhall and Melson, 1983; Heiken and Wohletz, 1987).

The local presence of micropoikilitic textures in some fiamme in the pumice breccia unit are interpreted to indicate high temperature devitrification of a glassy precursor (Lofgren 1971a, b, 1974, Anderson, 1969). If the pumice breccia unit was derived from a pyroclastic flow, it would be expected to have dissipated heat rapidly due to the small thickness (≤ 55 cm) and

unlikely to have resulted in micropoikilitic devitrification textures. If the pumice breccia was not partially welded, then the devitrification textures may have resulted from secondary welding due to transfer of heat from the considerable thickness of overlying MD ignimbrite. Many fiamme show extreme attenuation which is unlikely to have resulted from cold compactional process alone. The processes and effects of secondary welding have been described by Smith (1960), Christiansen and Lipman (1966), Schmincke (1967), McPhie and Hunns (1995).

### 4.4.7 Genetic model for the formation of polymictic breccias, coherent rhyolite, muddy sandstone and pumice breccia units

A genetic model is proposed for the rhyolite intrusions, peperite, DP breccias, fiamme-bearing DP breccias, LP breccias, rhyolite-bearing LP breccia, overlying coherent rhyolite, muddy sandstone units and pumice breccia units.

The rhyolite intrusions, rhyolite component of peperite and coherent rhyolite have mineralogical, textural and geochemical similarities and were probably derived from the same batch of magma, (possibly Hiltaba Suite?). DP breccias are interpreted to have formed near vertical pipe like bodies that resulted from interaction of rhyolite intrusions and fault hosted ground waters (Fig. 4.21a - b) similar to the mechanism proposed by Delaney (1982). Rapid expansion due to flashing of the ground water to steam may have brecciated the host rocks and resulted in fluidisation of the resultant breccia with formation of lateral grading (McCallum, 1985). DP breccia pipe formation post-dated early formed Pb - Zn - Ag mineralisation and locally included mineralised clasts (Fig. 4.21b). DP breccia pipes may have been a path of least resistance to the ascending rhyolite intrusion resulting in formation of peperite at the contact of wet DP breccia and the rhyolite intrusion.

Some DP breccia pipes are interpreted to have erupted onto the palaeo-surface resulting in proximal deposition of poorly sorted LP breccias. Repeated eruptions or changes in the intensity of eruptions resulted in crude layering of LP breccia deposits. Muddy sandstone units occupy the same stratigraphic position as LP breccia deposits and are interpreted to distal facies equivalents (Fig. 4.21c).

Some rhyolite intrusions continued to intrude along DP breccia pipes and as they neared the surface decompression of dissolved gas resulted in explosive fragmentation, formation of fiamme-bearing DP breccias followed by eruption of the breccia and rhyolite pyroclasts through earlier accumulations of LP breccia. The resultant deposit is interpreted to have been vent proximal rhyolite-bearing LP breccia (Fig. 4.21d). Pumice breccia is interpreted to be the distal facies equivalent of rhyolite-bearing LP breccia.

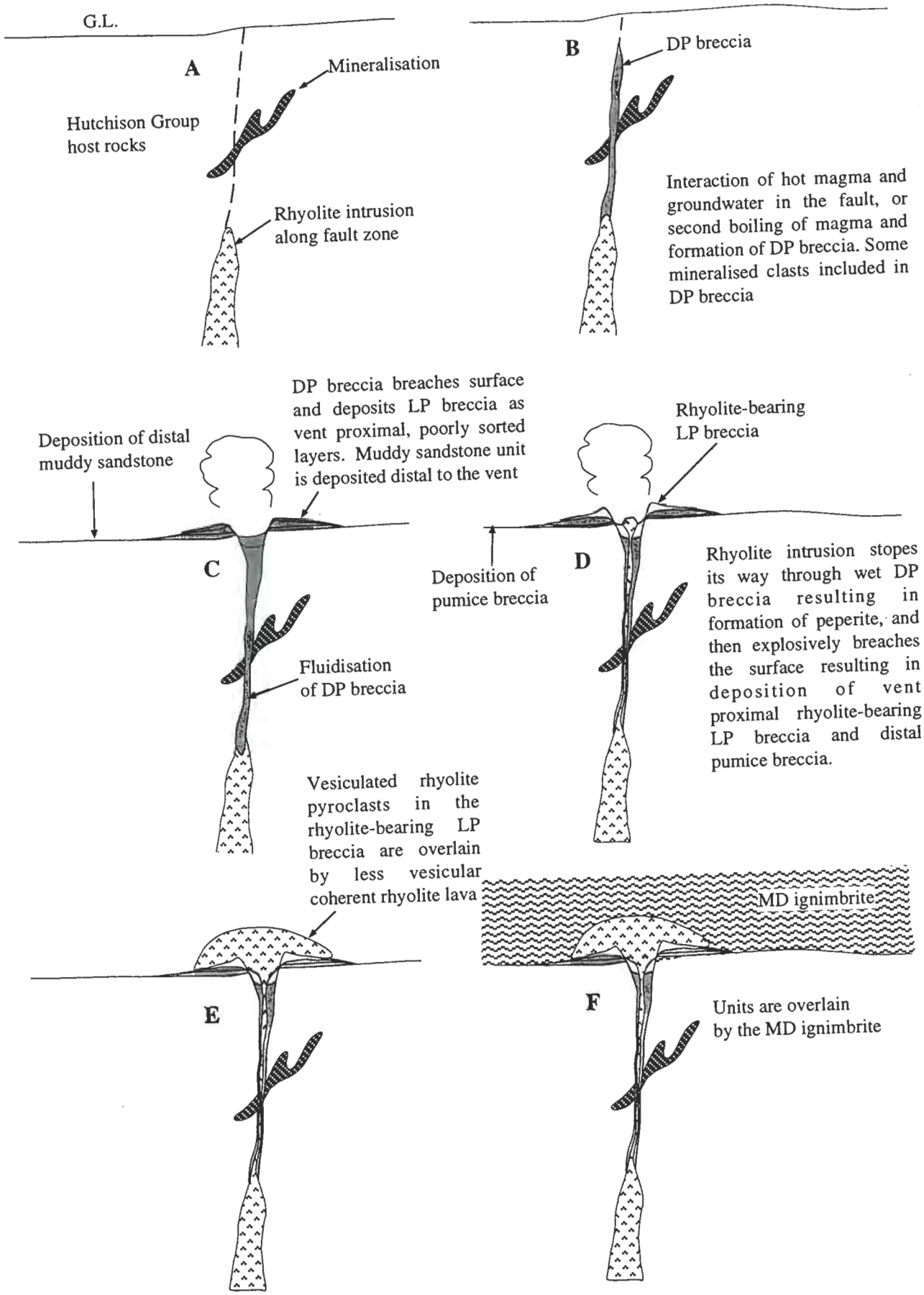


Fig. 4.21 Cartoon (not to scale) of a genetic model for the formation of DP breccia (B) and peperite (D), deposition of the LP breccia (C), muddy sandstone (C), formation of the rhyolite-bearing LP breccia (D), and coherent rhyolite (E).

As the upper vesiculated portion of the rhyolite intrusion was consumed, pyroclasts became less vesiculated forming agglutinated proximal spatter which eventually gave way to coherent rhyolite lava and formation of a restricted flow or dome (Fig. 4.21e). The rhyolite flow or dome, LP breccias and pumice breccias were later overlain by MD ignimbrite (Fig. 4.21f).

Although not interpreted to be a maar volcano, the proposed genetic model is consistent with formation of the DP breccia and deposition of the LP breccia by *similar processes* to those involved in the formation of maar volcanoes. Spatter, pyroclastic deposits, and coherent lava have been recognised from a number of maar deposits (eg. Hopi Buttes, Arizona, White, 1991; Tower Hill, Victoria, Cas and Wright, 1987; Ukinrek, Alaska, Self et al.). These are all of basaltic composition, however, similar deposits have been described from vent proximal settings of felsic volcanics (eg. Cas and Wright, 1987, Turbeville, 1992; Stevenson et al., 1993). The sequence of probable vent breccias (LP breccia and muddy sandstone units), pyroclastics (rhyolite-bearing LP breccia, and pumice breccia units) and rhyolite lava (coherent rhyolite) has similarities to the cycle of silicic dome emplacement described by Heiken and Wohletz (1987).

### 4.4.8 Interpretation of the MD ignimbrite

In this section, the thickness of the MD ignimbrite, source of lithic clasts realtionship between lithic clast content and welding and distribution of lithic clasts in the MD ignimbrite are discussed and used to interpret the environment of deposition in Section 4.4.9.

The absence of sediments of unequivocally marine or lacustrine origin at the base of the MD ignimbrite and the occurrence of welding to the base of the MD ignimbrite (Fig. 4.18i) are interpreted to be evidence for subaerial emplacement onto a dry landscape, which is consistent with interpretation of the palaeo-geographic setting for the GRV (Blissett et al, 1993).

The abundance of fiamme, relict glass shards, and evidence for hot emplacement are consistent with a pyroclastic origin for the MD ignimbrite. The absence of complete cooling breaks or other significant interruptions during deposition are interpreted to indicate a single cooling unit with a gradation from the base upwards in the degree of welding (Fig. 4.18a - i). The occurrence of unsorted lithic clasts throughout > 260 m of MD ignimbrite and absence of bedding, are not consistent with a fall-out origin. The evidence for dense welding is interpreted to indicate the MD ignimbrite was not deposited by a debris flow mechanism, and the most likely mode of emplacement for this unit is interpreted to be by pyroclastic flow.

Lipman and Christiansen (1964), noted a similar variation in the degree of welding in the basal section of the Yucca Mountain Tuff which they considered to be a thick ignimbrite unit. Sparks et al. (1978) explained the variable welding of ignimbrites using the column collapse model. Eruptions with low gas content, and low gas velocity, were interpreted to result in low collapse heights and little heat loss during collapse, which was interpreted to favour the formation of high emplacement temperatures and densely welded ignimbrites (Sparks et al., 1978). This condition was interpreted to have resulted in less expanded flows which lost only minor amounts of their vitric ash, as appears to be the case for many densely-welded intracaldera ignimbrites (Cas and Wright, 1987).

The original thickness of the MD ignimbrite is not known as it forms the current weathering surface, and a minimum thickness of > 260 m is interpreted from drill core (Table 4.9). Single ignimbrite thicknesses of > 500 m are commonly interpreted as ponded intra-caldera fill sequences (eg. Lipman, 1984; Sawyer and Lipman, 1983; Howells et al., 1991; Branney et al., 1992; Shawe and Snyder, 1988; Lipman et al., 1993). Single units of outflow facies ignimbrites rarely reach thickness comparable to the MD ignimbrite in all but the largest ignimbrite eruptions (eg. Fish Canyon Tuff up to 200m thick; Self and Wright, 1983). Thick outflow facies are likely to have been vent proximal, or ponded in depressions such as valleys or earlier calderas.

### Origin of lithic clasts in the MD ignimbrite

Lithic clasts in the MD ignimbrite may have either been derived from the surface through gravity in-sliding of country rock along a caldera margin, incorporation of surficial lithics into a pyroclastic flow, or, from the sub-surface as either ballistic particles or entrained in a pyroclastic eruption column. Attributes of coarse lithic breccia associated with pyroclastic flows are summarised in Table 4.13.

Table 4.13 Summary of coarse lithic breccias associated with pyroclastic flow deposits.

| *Surface derivation.* |
|---|
| Mesobreccia (Lipman, 1976)<br>Occur in intracaldera fill sequences and form tabular sheets of a few metres to a few 10's of metres thick which are typically thickest near the caldera margin and thin towards the centre. They comprise lithic clasts of < 1m and a matrix of lithic-rich micro-breccia of the same composition. Clasts do not have a preferred orientation and units have many similarities to debris flows. |
| Megabreccia (Lipman, 1976)<br>Occur in intracaldera fill sequences, form more bulbous deposits than mesobreccias and are commonly thickest at caldera margins. They comprise lithic clasts of ≥ 1m diameter and single clasts may approach 1 km in length. Minor pyroclastic material forms the matrix to clasts. Clasts are of similar composition to caldera walls and are interpreted to have resulted from syn-eruptive gravity insliding of over-steepened caldera margins. |

Table 4.13 cont.

| *Sub-surface derivation* |
|---|
| Proximal, coarse lithic breccia, co-ignimbrite lag breccia, and proximal layer 2bL breccia<br>Lithic segregation zones within ignimbrites (layer 2bL of Sparks et al., 1973) may be graded, lack internal stratification, are commonly matrix supported, but rarely exceed 1 m in thickness (Walker, 1985). Ground breccias (Druitt and Sparks, 1982) were interpreted to have segregated out from the strongly fluidised head of pyroclastic flows. They may be graded, lack internal stratification, are clast supported and fines depleted, and seldom more than 1 m thick. Lag breccias are characterised by their coarseness, fines depletion, presence of internal stratification, and are commonly between 1 - 20 m thick (Walker, 1985). |
| Co-ignimbrite lag-fall breccias<br>Co-ignimbrite lag-fall breccias formed at, or near, the site of continuous eruption column collapse through accumulation of clasts that were too large, or too heavy for the column to support. Pumice and fine pyroclasts were interpreted to have been transported away from the vent by flows (Wright and Walker, 1977, 1981; Druitt and Sparks, 1982). |
| Eruptive megabreccia<br>Shawe and Snyder (1988) described lithic breccias associated with the caldera fill sequence from the Manhattan and Mount Jefferson Calderas, Nye County, Nevada. They described breccia units of > 200 m thickness with a lithic clast content between 1 - 40%, and a matrix of poorly consolidated juvenile ash to lapilli size pyroclasts. Lithic clasts of all sizes (microscopic to > 200 m) and shapes, with varying degrees of rounding occur side by side in breccia units. Lithic clasts were interpreted to be derived from the vent or conduit, and entrained in the eruption column. Shawe and Snyder (1988) suggested that most (but not all) clasts were in thermal equilibrium with the tuff matrix. Some larger clasts interpreted to be from cooler parts of the vent and in thermal disequilibrium with the tuff have an indurated rind of a few centimetre thick composed of fine-grained, chilled glass shards. |

*Lithic clasts in the MD ignimbrite*

The matrix of the thin lithic-rich breccia lens at 165 m in drill holes PD0021 and PD0032 does not incorporate any juvenile pyroclasts and is similar to descriptions of surface derived mesobreccia units (Lipman 1976). Interpretation as mesobreccia implies a break in accumulation of the MD ignimbrite although cooling breaks are not evident. Mesobreccia emplacement is catastrophic and geologically instantaneous and may have occurred during a short break in deposition of the MD ignimbrite which was not sufficient to have resulted in significant cooling.

The distribution of lithic clasts throughout the remainder of the MD ignimbrite differs from coarse, proximal, lithic breccias described by Walker (1985), in that clasts are much coarser (up to 20 m diameter), the lithic clasts lack obvious stratification, lithic clasts are completely enclosed in a matrix of juvenile pyroclasts, and the lithic-bearing part of the MD ignimbrite (all of it) is considerably thicker. Lithic breccias in the MD ignimbrite are dissimilar to the lithic-rich portions of outflow facies ignimbrites (Ground layers, layer 2bL; Walker, 1985) but have some similarities to descriptions of surface-derived mega and meso breccias associated with caldera collapse (Lipman, 1976; Lipman et al., 1993; Fiske and Tobisch, 1994; Thompson, 1985; Branney and Kokelaar, 1992; Kokelaar et al., 1994; Howells et al., 1991). Lithic breccias in the MD ignimbrite also have similarities to descriptions of the sub-surface derived, proximal vent breccias described by Shawe and Snyder (1988) although differences lie in the welded and non-welded nature respectively of the juvenile volcanic component.

Lithologies similar to the lithic clasts in the MD ignimbrite are interpreted to have been present in both the sub-surface and at the palaeosurface immediately prior to deposition of the MD ignimbrite. Clasts of granitic composition are the most common clast type (Table 4.11) and granite dykes are more abundant in the fault zone separating the central and western suites (Fig. 3.2). Two possibilities are considered:

- Lithologies of the western suite formed a topographic high at the time of emplacement of the MD ignimbrite.
- Vent excavation and flaring occurred within a zone of abundant granite dykes. The fault zone may have been a favourable site for establishment of a vent.

Localised areas containing up to 30% lithic clasts between 5 cm to 50 m across, supported in a matrix of Eucarro or Yardea Dacites occur in the south-west and southern Gawler Range Volcanic Province (Garner, 1996). Granite clasts with metamorphic textures are the most common lithology, and many show effects of partial melting attributed to a sub-surface explosive origin (Garner, 1996). The sub-surface / surface derivation of lithic clasts in the MD ignimbrite cannot easily be determined. An average lithic content of 47% is determined for the MD ignimbrite (ie. 30% $\leq$ 10 cm + 17% > 10 cm). Incorporation of cool lithic clasts (surface derived) or hotter lithic clasts (sub-surface) may have resulted in differences in the extent of compaction and welding of the MD ignimbrite. For example, the lithic clast content of the basal 34m of drill hole PD0032 is estimated as 53% and this is the only part of the MD ignimbrite that was not welded.

Eichelberger and Koch (1978) demonstrated that the time required for 10% cool lithic fragments of $\leq$ 20 cm diameter to reach thermal equilibrium with a 100 m thick ignimbrite erupted at 750°C was around 1 hour which was insignificant compared to the time required to achieve welding ($\approx$ 1 year). Incorporation of cooler lithics was interpreted to have the same effect as a lower emplacement temperature of the ignimbrite.

Eichelberger and Koch (1979) used the welding model of Riehle (1973) which is based on the assumption that viscous strain occurs. Bierwirth (1982) considered this to be invalid for porous volcanic ash. Riehle et al (1995) re-evaluated earlier modelling, concluded the assumption of viscous strain was valid, and compiled a computer program for modelling of cooling, degassing and compaction of rhyolitic ignimbrites. Parameters necessary for modelling, such as the emplacement temperature, water content, thickness, permeability, and initial porosity of the MD ignimbrite are not known and approximations would invalidate interpretation of sub-surface versus surface derivation of the lithic clasts. A further complication is that welding may have been initiated during ignimbrite deposition and prior to attainment of thermal equilibrium with larger lithic clasts (ie rheomorphism; Branney and

Kokelaar, 1994). On the basis of this discussion, a surface or sub-surface origin for the lithic clasts in the MD ignimbrite cannot currently be determined.

### 4.4.9 Genetic model for the MD ignimbrite

The thickness of the MD ignimbrite is consistent with either an intracaldera ignimbrite or a large, ponded outflow facies. Lithic clasts within the MD ignimbrite are consistent with a an intracaldera facies ignimbrite irrespective of whether lithic clasts were derived from the surface or the sub-surface. The volcanic stratigraphy at Menninnie Dam of rhyolitic lava ('coherent rhyolite') followed by eruption of the MD ignimbrite is similar to the pre-caldera and main caldera forming events of the 'general caldera cycle' described by Lipman (1984). Based on the above discussion, the MD ignimbrite is interpreted to be the eroded remnant of a ponded, intracaldera ignimbrite.

### 4.4.10 Distribution of lithic clasts in the MD ignimbrite

Lithic clasts > 10 cm comprise two intervals, each of which has a systematic increase in the abundance and size of clasts with depth (Fig. 4.19). If lithic clasts are interpreted as caldera collapse breccia, then the two zones can be interpreted as distinct phases of caldera margin collapse that occurred during essentially uninterrupted pyroclastic deposition (the MD ignimbrite is a single cooling unit). If the lithic breccias were derived from the subsurface, they can be interpreted as distinct phases of vent excavation during otherwise uninterrupted pyroclastic deposition. Alternatively, a combination of the surface and sub-surface derivation may have contributed to the 'two phases' of lithic clasts.

### 4.4.11 Timing and duration of Mesoproterozoic intrusive and volcanic events at Menninnie Dam

Emplacement of the rhyolite intrusions, peperite, coherent rhyolite, DP and LP breccias, muddy sandstone and pumice breccia are interpreted to have occurred over a short space of time and were essentially coeval. The LP breccias, muddy sandstone, and possibly the pumice breccia, are interpreted to have been deposited as unconsolidated sediments. Their preservation probably resulted from deposition of the MD ignimbrite soon afterwards. It can be concluded that all of the Mesoproterozoic units preserved at Menninnie Dam were emplaced in a geologically short space of time. The interpretation of a genetic, and therefore temporal, association between the rhyolite intrusions at Menninnie Dam and granitoids of the Hiltaba Suite can be extended to encompass all Mesoproterozoic units at Menninnie Dam and an age of ≈ 1589 Ma. is inferred (Creaser and Cooper, 1993).

### 4.4.12 Timing of metasomatism

In Section 3.8.4, it was suggested that the timing of pegmatite dyke emplacement and metasomatic alteration of marble and calc-silicate lithologies at Menninnie Dam probably occurred during the final phase of KM-$D_3$ (≈ 1710 Ma., Fanning, 1984). Metasomatised

lithologies occur locally directly beneath LP breccia (Section 4.3.2) and have been incorporated as clasts in DP and LP breccia units and the MD ignimbrite. The LP breccias are interpreted to have been deposited onto the palaeosurface at ≈ 1589 Ma. and it is unlikely that metasomatic alteration occurred at the palaeosurface, therefore, an age for metasomatism of ≈ 1710 Ma. is considered to be consistent with available data.

## 4.5 Summary

At Menninnie Dam, rocks younger than 1600 Ma. consist of intrusive and volcanic rocks and breccias interpreted to be the remnants of a deeply eroded cauldron associated with eruption of the GRV and intrusion of the co-magmatic Hiltaba Suite. Rock units include:

- Quartz- and feldspar-phyric rhyolite intrusions ('rhyolite intrusions'), locally with peperitic margins into DP breccia.
- Discordant polymictic breccia dykes ('DP breccia') hosted by Hutchison Group lithologies.
- Layered polymictic breccia ('LP breccia'), deposited on top of Hutchison Group lithologies.
- Rhyolite-bearing LP breccia interpreted to be a mix of DP breccia, LP breccia, and subaerially deposited rhyolite pyroclastic deposits.
- Muddy sandstone, interpreted to be a distal facies correlative of LP breccia.
- Pumice breccia, interpreted to be a distal facies correlative of rhyolite-bearing LP breccia.
- Coherent rhyolite lava that overlies the rhyolite-bearing LP breccia.
- Lithic-rich Menninnie Dam ignimbrite ('MD ignimbrite') interpreted to be the eroded remnant of an intracaldera ignimbrite.

Rhyolite intrusions have textural and geochemical similarities to granitoids of the Hiltaba Suite and porphyritic dykes that occur elsewhere on the northern Eyre Peninsula. Interaction of the rhyolite intrusions with ground water resulted in subsurface explosive fragmentation of the host rocks and formation of near vertical, pipe-like bodies of DP breccia. Vaporisation of ground water adjacent to the rhyolite intrusions resulted in fluidisation, clast mixing, and upwards transport of DP breccia clasts. Locally, the rhyolite intrusion continued to migrate upwards, intruding into wet, unconsolidated DP breccia forming peperitic contacts. Some of the DP breccia pipes vented on to the palaeosurface forming proximal deposits of LP breccia and distal deposits of muddy sandstone. The rhyolite intrusion locally erupted through the same vent, resulting in mixed DP breccia, LP breccia and rhyolite pyroclasts (rhyolite-bearing LP breccia). Pumice breccia units are interpreted to be distal facies correlatives of rhyolite-bearing LP breccia. Following eruption of the upper vesiculated portion of the rhyolite intrusion, less vesiculated rhyolite lava was extruded and formed a small dome or restricted flow (coherent rhyolite).

Eruption of the lithic-rich Menninnie Dam ignimbrite mantled earlier deposited units to a depth in excess of 260 m. An intracaldera eruptive setting is interpreted for the MD ignimbrite and all of the intrusive and volcanic units at Menninnie Dam are interpreted to have been emplaced in a geologically short interval of time around 1589 Ma. Their present occurrence is consistent with a deeply eroded cauldron.

# Chapter five
# Sulphide mineralisation

## 5.1 Introduction and previous work

The aim of this chapter is to:

- describe the relationship between the sulphides and the host rocks,
- describe the mineralogy and textures of sulphide mineralisation,
- investigate paragenetic relationships of the sulphide and gangue minerals, and
- investigate the distribution of Pb, Zn, and other metals throughout the Menninnie Dam prospect.

Higgins and Hellsten (1986) described the sulphide mineralisation at Menninnie Dam as having formed clusters of 0.5m wide bands, comprising massive pyrite, sphalerite, galena and minor chalcopyrite. Higgins et al. (1990) briefly described the sulphide mineralogy and estimated an inferred resource to 300m depth, of 1.7 million tonnes containing 5% lead, 8% zinc and 100 grams per tonne silver. Sulphides were considered to show ample evidence for remobilisation and metamorphism including; exsolution of chalcopyrite along sphalerite cleavages and sub-grain boundaries, and curved cleavages of polygonal galena. Higgins and Hellsten (1986), Higgins et al. (1990) and Beeson (1990) considered the mineralisation to be syn-sedimentary having accumulated in a restricted basin. A 20 m wide zone of chert - dolomite - sulphide breccia near the geographic centre of the prospect was interpreted to have been a footwall stringer system to the mineralisation (Higgins et al., 1990).

The work by Higgins and Hellsten (1986), Higgins et al. (1990) and Beeson (1990), was based on interpretation of 6 percussion and 14 diamond drill holes. Since these publications, an additional 18 diamond drill holes have been drilled into the Menninnie Dam prospect, and a more comprehensive examination of the sulphide mineralisation can now be made.

Throughout this study, the sulphide mineralisation has been subdivided into three zones (Fig. 3.1):

*Northern zone.* The northern zone is defined as: north of, and including drill hole PD0015 (9391 mN).

*Cental zone.* The central zone is defined as: north of drill hole PD0032 (7406 mN) and south of drill hole PD0015 (9391 mN)

*Southern zone.* The southern zone is defined as: south of, and including drill hole PD0032 (7406 mN).

The basis for these subdivision relates to differences in the style of mineralisation, gangue mineral assemblage, and sulphide textures. Sulphide mineralisation which is not

incorporated in the above subdivisions includes; trace amounts of disseminated pyrite associated with sericite - chlorite - quartz alteration of deformed granite dykes in the shear system bounding the western and central suites (Section 3.5.1), trace amounts of disseminated pyrite in weakly altered rhyolite intrusions (Section 4.3.1), and trace amounts of pyrite associated with metasomatic alteration (Section 3.7.1). These occurrences are considered to be unrelated to Pb - Zn - Ag sulphide mineralisation at Menninnie Dam and will not be considered further in this chapter. The sulphide and gangue mineralogy in the northern and central zones, and the southern zone are described separately.

## 5.2 Mineralisation in the northern and central zones

The major occurrence of Pb - Zn - Ag sulphide mineralisation at Menninnie Dam is hosted by marble, calc-silicate lithologies, and mixed marble - calc-silicate lithologies of the central suite, and by similar units in the eastern suite. In the northern zone, four bands (0.1 - 2m wide) of galena - sphalerite - pyrite - chalcopyrite mineralisation hosted by metasomatised marble were intersected in drill holes PD0006 and PD0016 (Fig. 3.1; Appendix 3.1). Sulphide bands were not intersected at the same stratigraphic position in drill hole PD0012 which lies midway between drill holes PD0006 and PD0016. Most of the Pb - Zn - Ag mineralisation occurs in the central zone hosted by units of the central suite. South of 7600 mN, the central suite thins and pinches out against the fault bounding the western and central suites, and minor amounts of sulphide mineralisation are hosted by marble and calc-silicate lithologies of the eastern suite.

Pb - Zn - Ag sulphides appears to occupy a 'window' between 80 - 400m depth (vertical), however, this may be a function of the extent of drilling. The deepest mineralisation encountered is a 6 cm wide vein at 643m (vert.) in drill hole PD0015. The upper limit of the 'window' marks the average extent of weathering which ranges from 8m in drill holes PD0032 and PD0021 to 344m in drill hole PD0019. The base of weathering is often marked by a 1 - 20m thick zone of secondary Pb - Zn - Ag enrichment. Sulphides other than pyrite are absent in this zone and Zn, Pb and Ag are probably associated with iron and manganese oxides or adsorbed onto clay minerals. This zone of secondary Pb - Zn - Ag enrichment was percussion drilled and samples are not suitable for the purposes of this study.

Minor Pb - Zn - Ag sulphide mineralisation locally overprints cataclasites in the western suite (Fig. 5.1a) and contributes to the matrix of brecciated granite dykes in both the western and central suites. DP breccias contain minor amounts of Pb - Zn - Ag sulphide, either as discrete clasts of galena - sphalerite - pyrite - chalcopyrite mineralisation, or as pyrite, minor galena and traces of sphalerite and chalcopyrite associated with alteration of both lithic clasts and the matrix (Section 4.3.2). Rare clasts of galena - sphalerite - pyrite - chalcopyrite mineralisation occur in LP breccias. The matrix of LP breccias has locally been altered to an assemblage that includes trace amounts of pyrite (Section 4.3.2).

Fig. 5.1a. Drill hole PD0026, 197.3 m (central zone). Pyrite 1, sphalerite 2, galena 1 and quartz 1 have overprinted cataclasite in the western suite shear zone. Breccia fragments are comprised of metamorphic quartz (Q) veins.

Fig. 5.1b. Drill hole PD0013, 131.8 m (northern zone). Hand specimen of a 5 - 6 cm wide sulphide vein in massive diopside. The attitude of the vein is ≈ 90° to metamorphic layering developed in the diopsidic host rock.

Fig. 5.1c. Drill hole PD0016, 273.4 m (northern zone). Hand specimen of a sulphide vein in metasomatically altered marble. The vein has a 2 cm wide alteration halo with bands of pink hematite-dusted metasomatic microcline (M) surrounded by light yellow - green sericite 1 (SE). Pyrite 1 (P) is more abundant in the centre of the vein and galena 1 (G) is more abundant nearer the vein margin. Sphalerite 1 and 2 (S) have formed overgrowths on pyrite 1. Sphalerite 1 and 2 are more abundant in a zone between pyrite 1 and galena 1. The core of the vein has been infilled with Ca-Mn-Mg-Fe carbonate 1 (CA). Larger growth zoned sphalerite crystals have locally attained 9mm across (9MM).

Fig. 5.1d. Drill hole PD0008, 326.0 m (central zone). Breccia developed in stockwork mineralisation hosted by banded calc-silicate - marble - quartz rock. Marble and calc-silicate bands have been replaced by sulphide and gangue minerals. Metamorphic quartz (Q) bands are unaltered and form breccia fragments.

Fig. 5. 1e. Drill hole PD0006 (northern zone), Hand specimens. upper 257.62 m - 258.03m, lower 258.4 - 258.68 m. Upper (UH) and lower (DH) contacts of a sulphide vein (S) hosted by metasomatic marble (M). Dotted lines are drawn parallel to the metamorphic fabric of the host marble. The vein has a 2 - 3 cm alteration halo (AH) of fine-grained, altered metasomatic marble. Mineralising fluids have permeated a fracture (F) in metasomatic marble near the up hole contact of the sulphide vein.

5.1a

5.1b

5.1c

5.1d

5.1e

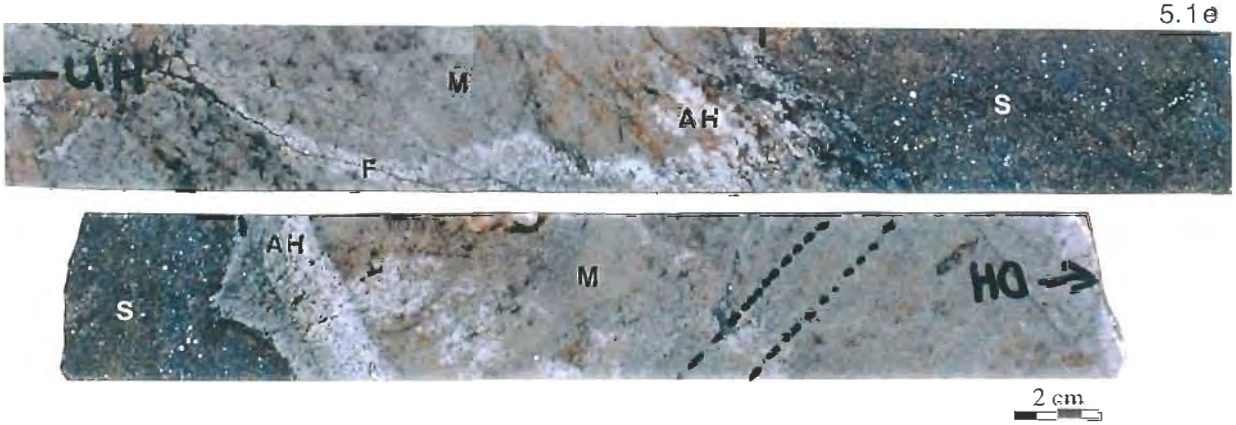

Strongly altered rhyolite intrusions and peperite contain trace amounts of disseminated pyrite, sphalerite, galena and chalcopyrite (Section 4.3.1).

Approximately one square metre of weathered, silicified marble subcrop (or calc-silicate lithology?) , with 1 - 3% finely disseminated pyrite and trace amounts of galena and sphalerite was uncovered during shallow excavations of a drill sump (<1m deep) at 9000 mN, 10250 mE which is close to the faulted contact between the western and central suites.

### 5.2.1 Relationship between sulphides and host rocks

Mineralisation is not confined to any particular lithological horizon, nor does it parallel stratigraphic layering. Mineralisation is not directly associated with the major north-south fault separating the central and western suites, however, there is a relationship between mineralisation and deformation which will be discussed in more detail on Section 5.6.3. It is not possible to define the shape, or lateral extent of mineralised zones as drill intersections cannot be meaningfully connected between adjacent drill holes and this may, in part, result from the wide spacing between drill holes (typically 200 m). The approximate extent of known mineralisation is indicated on Figure 3.1.

Sulphides have formed veins (Figs. 5.1b, c), anastomosing stockworks and breccias (Fig 5.1d) which crosscut marble, calc-silicate lithologies and mixed marble - calc-silicate lithologies. Vein mineralisation is more common north of 9300 mN and south of 8200 mN whereas stockwork, breccia and vein mineralisation occurs between 8200 mN and 9300 mN.

The width of veins varies between 1 cm to 2m. The orientation of individual sulphide veins cannot be accurately established due to the unorientated nature of drill core, however it is likely they have a wide variety of orientations as the angle between vein margins and the long axis of the drill core varies from parallel to 90°. The contact between veins and the host rock is sharp and defines an irregularly shaped horizon with an alteration halo that rarely extends beyond a few centimetres into the host rock (Fig. 5.1e). Sulphide and gangue minerals within veins are mostly intimately intergrown and veins do not have crustiform banding or cockscomb textures. Some veins hosted by massive diopsidic units have poorly developed banding that comprises irregularly shaped, millimetre to centimetre wide lenses of sulphide and minor gangue minerals, alternating with similarly shaped lenses in which gangue minerals are more abundant than sulphide minerals (Fig. 5.1b). Some marble hosted veins also have a poorly developed mineralogical banding (Fig. 5.1c).

Stockwork and breccia zones extend vertically for tens of metres and are commonly better developed in host rocks of calc-silicate lithology (mostly diopside, or diopside - quartz) and mixed marble - calc-silicate lithology compared to marble (Fig. 5.1d). The host rock

surrounding stockwork zones has a well developed fracture pattern, and locally, a breccia texture. The network of veins in stockwork zones are commonly poorly defined as the host rock in between veins has undergone selectively-pervasive alteration with preferential alteration of marble followed by calc-silicate lithologies, whereas quartz bands have remained unaltered (Fig. 5.1d).

Alteration of the host rock between stockwork veins has resulted in breccia textures (Fig. 5.1d). Breccias are poorly sorted, non-graded, and matrix supported. The proportion of clasts to matrix is variable and ranges between 10 and 80%. Some clasts have a weak preferred orientation, commonly orientated 45 - 70° to the drill core axis, which translates to either a sub-vertical or sub-horizontal orientation (drill holes are commonly inclined 60° from horizontal). Breccia clasts range from angular to sub-rounded and consist of metamorphic quartz, and minor marble and calc-silicate lithologies identical to that of the surrounding unaltered host rock (Fig. 5.1d). Clasts of marble and calc-silicate lithologies have diffuse corroded margins that 'blend' into the matrix and are more likely to be sub-rounded, whereas metamorphic quartz clasts have sharp margins and are invariably angular. The breccia matrix comprises abundant, small remnant clasts of highly corroded marble and calc-silicate lithology (< 2 mm across), angular quartz fragments, and sulphide and gangue minerals. Unlike vein mineralisation, the matrix to stockwork mineralisation hosted by calc-silicate lithologies commonly has a significant proportion of cryptocrystalline quartz which locally comprises up to 95% of the rock.

### 5.2.2 Sulphide and gangue mineralogy

Sulphides consist of a simple assemblage of pyrite, sphalerite, galena and chalcopyrite. Pyrrhotite has been described as a minor phase by Higgins et al. (1990) but has not been identified from this study following examination of 167 polished thin sections covering all diamond drill holes. No sulphate minerals have been identified throughout the Menninnie Dam prospect. Gangue minerals include; dolomite, phlogopite, talc, chlorite, adularia, sericite, quartz, rhodonite, fluorite, Ca-Mn-Mg-Fe carbonate, hematite and calcite.

### 5.2.3 Sulphide and gangue mineral textures and their paragenesis

Sulphides hosted by marbles have different textures to those hosted by calc-silicate lithologies, therefore, mineralisation hosted by different rock types is described separately. Descriptions of sulphide and gangue minerals follows a paragenetic sequence, starting at the first formed mineral. Minerals of the same composition that appear to have formed at different times during the mineralising event are assigned a number following the mineral name with '1' representing the first formed phase and 2, 3 ... representing progressively later phases. A summary of the sulphide and gangue mineral paragenesis applicable to the northern and central zones is illustrated in Figure 5.2

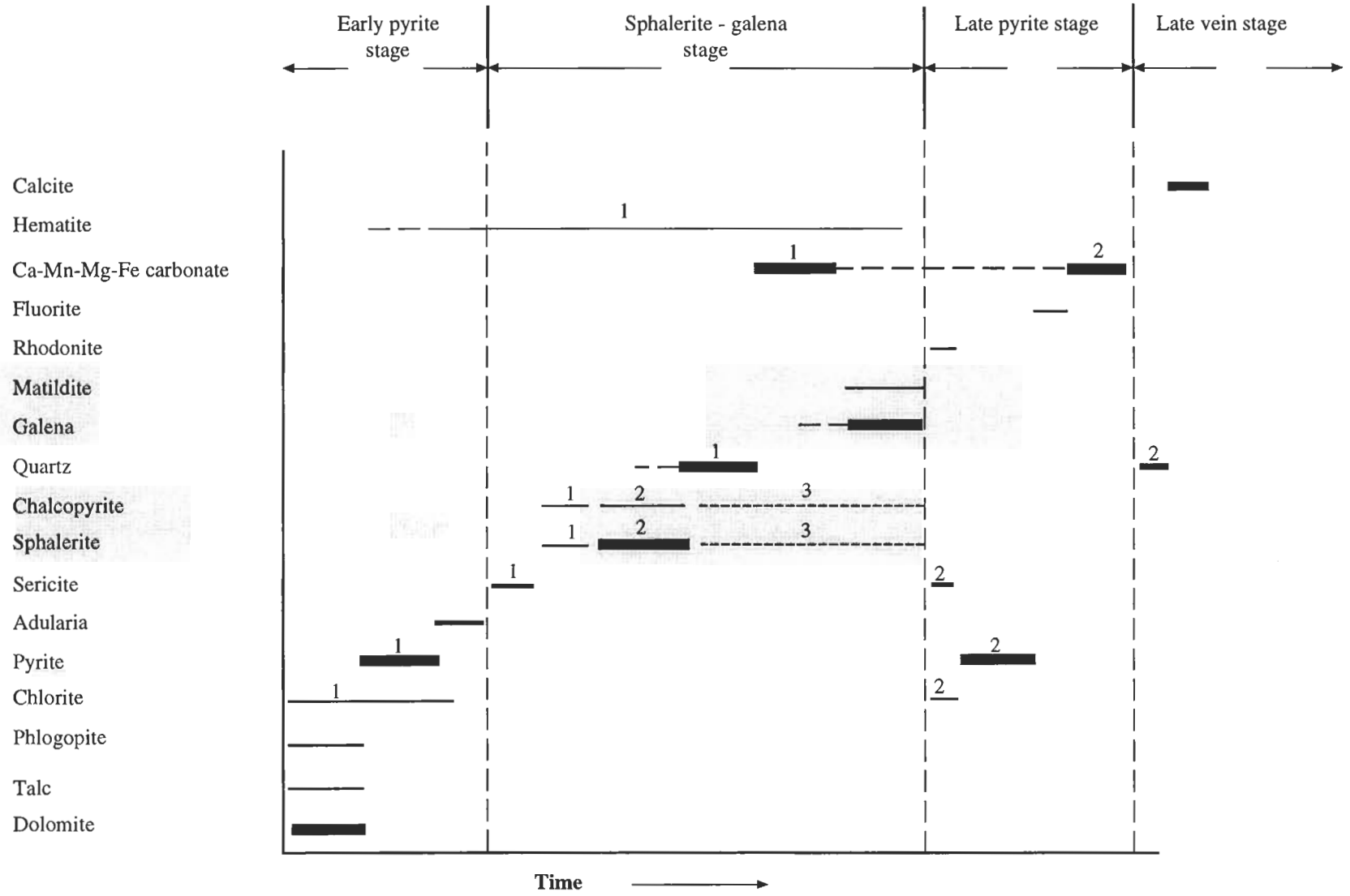


Fig. 5.2 Paragenesis of sulphide and gangue minerals in the northern and central zones. Thicker lines represent more abundant minerals, and dotted lines represent trace amounts of minerals of uncertain paragenesis. The grey bars have no significance other than to assist the reader.

## Sulphides hosted by marbles

*Dolomite*

Within 1 - 2 cm of the margin of sulphide veins hosted by calcitic marble, the marble has been altered along crystal margins, and to a lesser extent along twin planes and replaced by finely crystalline dolomite rhombs, typically 10 - 50 μm across (Fig. 5.3a). The size of dolomite rhombs is increased closer to the centre of the sulphide vein, and locally attains 0.5 mm across. Replacement by finely crystalline dolomite has not occurred in dolomitic marbles.

*Pyrite 1*

Pyrite 1 consists of disseminated subhedral to euhedral crystals, typically 1 - 20 μm across and larger aggregates. In calcitic marble host rocks, deposition of finely crystalline pyrite 1 followed, and commonly replaced finely crystalline dolomite (Figs. 5.3b, c). In dolomitic host rocks, finely crystalline pyrite 1 replaced the host dolomitic marble along crystal margins. Pyrite 1 locally forms small atoll structures with cores of later sulphide minerals (Fig. 5.3d), many of which have relict rhombic shapes inherited from replacement of finely crystalline dolomite. Replacement of dolomite by pyrite 1 is illustrated in Figures 5.3e, f where replacement has been halted by replacement of dolomite by finely crystalline quartz 1.

Small pyrite 1 crystals have locally coalesced forming randomly oriented, irregularly shaped aggregates and larger, euhedral pyrite crystals. Contacts between coalesced crystals of pyrite 1 are rounded to irregular with no evidence of polygonal crystal contacts or 120° triple junctions. Some larger pyrite 1 aggregates and euhedra have been fractured or have a jigsaw-fit breccia textures with a matrix of paragenetically later sulphide minerals (Fig. 5.3h). Pyrite 1 crystals hosted by metasomatically altered marble commonly either overgrow and / or contain inclusions of metasomatic minerals such as andraditic garnet, epidote and microcline (Fig. 5.3g).

*Chlorite 1*

Trace amounts of light green chlorite 1 locally occurs as overgrowths on pyrite 1. Chlorite 1 has only been observed near the contact between sulphide minerals and the host rocks and is not present within the central part of veins or stockwork breccias.

*Adularia and hematite*

Adularia has been identified by its rhombic shape, common finely crystalline inclusions of hematite and other unidentified minerals (typically < 1.0 μm), and by electron microprobe analysis (Table 5.1 and Appendix 5.1). Adularia typically forms rhombic crystals of 0.1 - 1 mm across, and rarely exceeds 1 - 2% of mineralised zones.

Fig. 5.3a. Drill hole PD0017, 319.5 m (central zone). Photomicrograph, crossed nicols. Calcitic marble (M) in the outer margin of a 2 cm wide alteration halo surrounding a sulphide vein has been altered along grain boundaries to fine-grained dolomite (D).

Figs. 5.3b, c. Drill hole PD0017, 319.5 m (central zone). Photomicrographs; (5.3b) transmitted light, (5.3c) reflected light. Fine-grained pyrite 1 (P) has replaced fine-grained dolomite and surrounds corroded marble crystals (M).

Fig. 5.3d. Drill hole PD0008, 311.4 m (central zone). Photomicrograph, reflected light. Pyrite 1 (P) has locally formed small atoll structures with cores of later sulphides including galena (G). Some of the larger atolls have a relict rhombic shape and have pseudomorphed dolomite.

Figs. 5.3e, f. Drill hole PD0019, 298.2 m (central zone). Photomicrographs, (5.3e) transmitted light, (5.3f) reflected light. Relict dolomite has been partially replaced along cleavage planes by pyrite 1, and resulted in formation of pyrite atoll structures (A). Not all of the fine pyrite grains are at the surface, and visible in Fig. 5.3f. Some scattered pyrite 1 grains have retained the relict rhombic shape of dolomite (A). Quartz 1 (Q) has replaced remaining dolomite and overgrown pyrite 1.

Fig. 5.3g. Drill hole PD0015, 731 m. Photomicrograph, combination of reflected and transmitted light. Pyrite 1 (P) has overgrown andraditic garnet (G) and hematite-dusted microcline (M). Andradite garnet and microcline formed by metasomatic alteration of marble and calc-silicate lithologies.

Fig. 5.3h. Drill hole PD0011, 452.2 m (central zone). Photomicrograph, reflected light. Fractures in brecciated pyrite 1 (P) have been infilled with sphalerite 2 (S), galena 1 (G) and Ca-Mn-Mg-Fe carbonate 1 (C). Galena 1 has a straight cleavage pattern and has not been deformed.

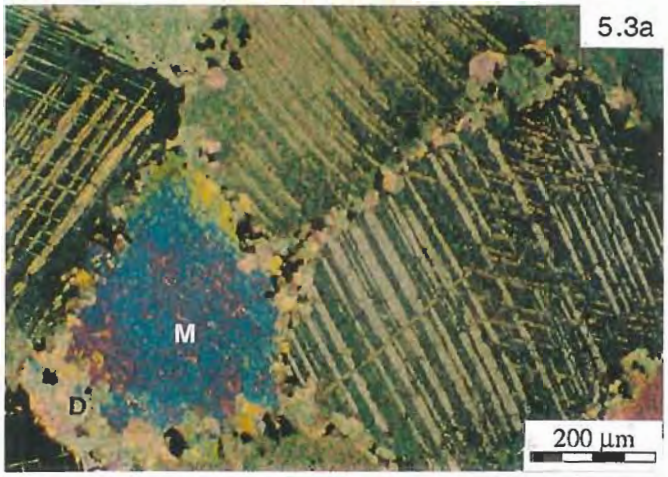
5.3a
M
D
200 µm

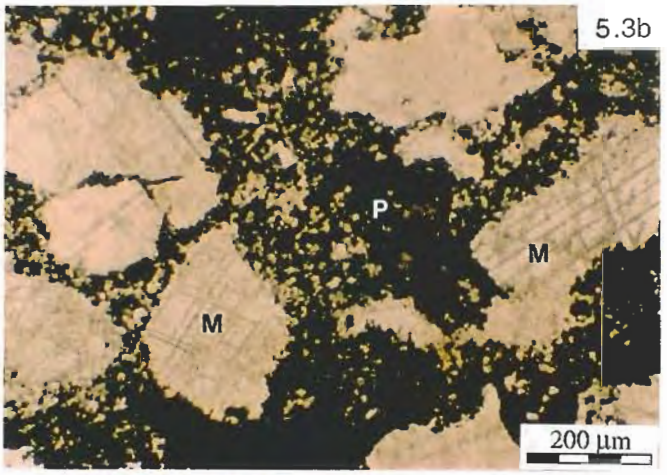
5.3b
P
M
M
200 µm

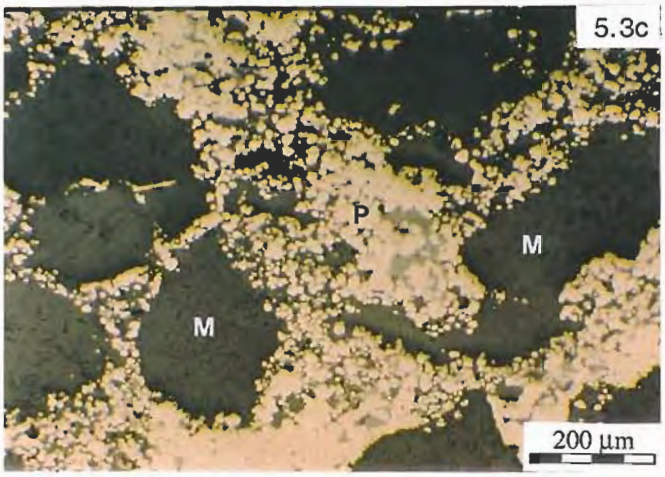
5.3c
P
M
M
200 µm

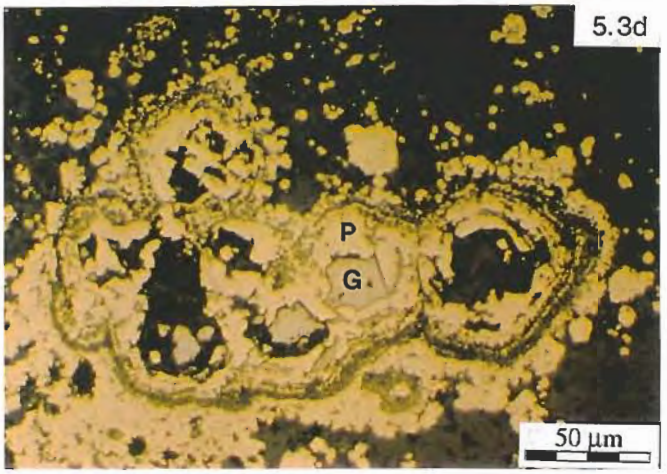
5.3d
P
G
50 µm

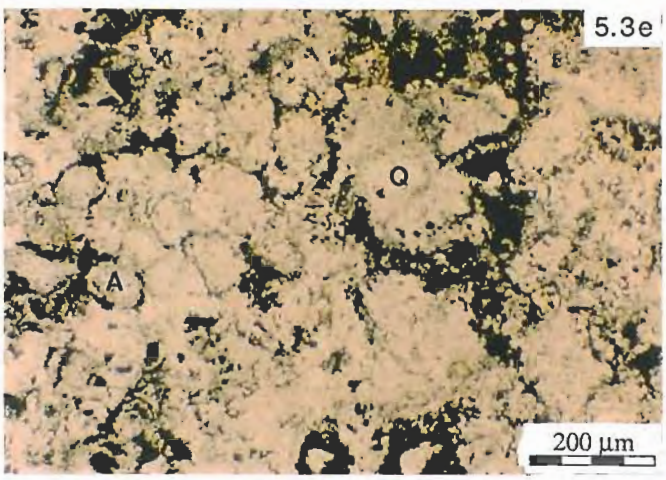
5.3e
Q
A
200 µm

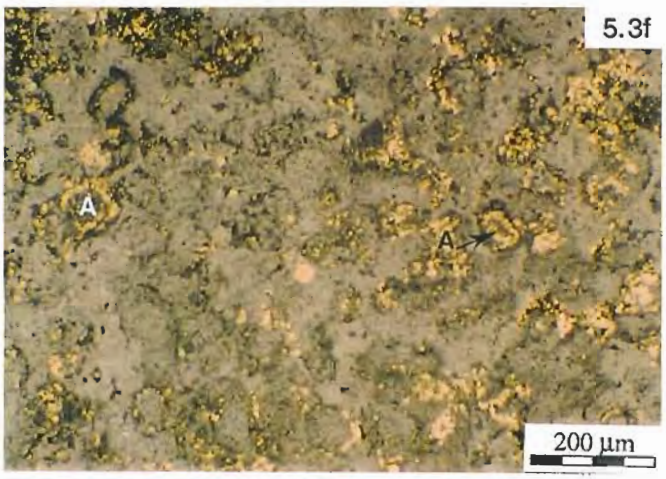
5.3f
A
A
200 µm

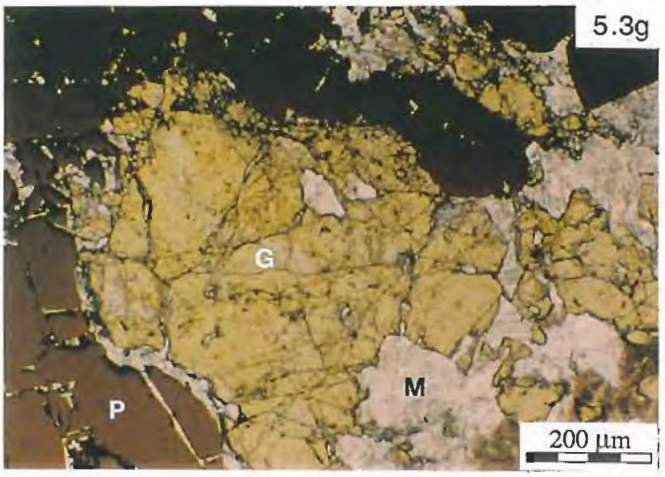
5.3g
G
P
M
200 µm

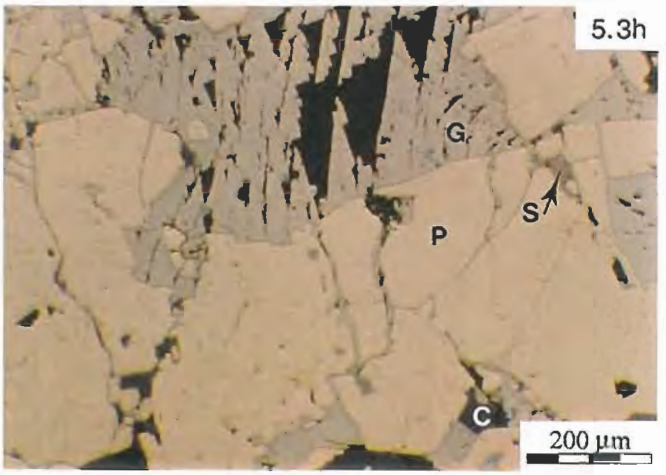
5.3h
G
S
P
C
200 µm

Contact relationships between chlorite 1 and adularia have not been observed and adularia locally occurs as overgrowths on pyrite 1 or as overgrowths on rounded microcline 'grains' formed by metasomatic alteration of disseminated biotite (Fig. 5.4a, b and Section 3.7.2). Although trace amounts of finely disseminated hematite occurs throughout adularia, hematite alteration of pyrite 1 has not been observed.

Table 5.1 Average of 21 analyses of adularia from Menninnie Dam. An adularia analysis from Switzerland is listed for comparison. All oxide values are wt.%.

| | $SiO_2$ | $Al_2O_3$ | $K_2O$ | $Na_2O$ | CaO | $Fe_2O_3$ | SrO | BaO |
|---|---|---|---|---|---|---|---|---|
| *1 | 64.18 | 18.64 | 15.19 | 0.25 | 0.01 | 0.04 | 0.20 | 0.10 |
| *2 | 64.28 | 19.19 | 15.30 | 0.92 | 0.11 | 0.09 | | 0.11 |

*1 Menninnie Dam
*2 Analysis of adularia from St. Gotthard, Switzerland (Spencer, 1937)

*Sericite 1*

Adularia has been partially altered to sericite 1 and in many instances, sericite 1 forms an outer rind on adularia crystals (Fig. 5.4c). Sericite 1 comprises < 1% of mineralised zones and is locally more abundant (1 - 5%) in the 0.5 - 3 cm wide alteration halo that surrounds veins hosted by metasomatically altered marble (Fig. 5.1c). Sericite flakes are typically less than 4 $\mu$m long and can easily be distinguished from muscovite flakes present prior to the mineralising event that occur as 20 - 100 $\mu$m long platelets overgrown by all sulphide minerals, including pyrite 1 (Figs. 5.4d, e).

*Sphalerite 1 and chalcopyrite 1*

Three phases of sphalerite are present in the northern and central zones at Menninnie Dam referred to as sphalerite 1 - 3. Sphalerite 1 commonly occurs as a dark, corroded, growth zoned core to later sphalerite 2 (Fig. 5.5a). The dark colour of sphalerite 1 relates to a high proportion of small chalcopyrite 1 and minor pyrite 1 inclusions (typically < 5 $\mu$m across) in light yellow - brown sphalerite. Inclusions of chalcopyrite 1 define growth zones whereas the small inclusions of pyrite 1 are randomly distributed throughout sphalerite 1. Sphalerite 1 is rarely in contact with earlier minerals but has locally mantled sericite 1 rims on adularia or in the absence of sericite 1, sphalerite 1 has mantled corroded crystals of adularia (Fig. 5.5a). Sphalerite 1 constitutes less than 5% of the sphalerite present at Menninnie Dam.

*Sphalerite 2 and chalcopyrite 2*

Sphalerite 2 forms pale to light yellow - brown isolated, and more commonly, coalesced growth zoned crystals that typically range in size from 50 $\mu$m to 2 mm across (Fig. 5.5a, b). Crystals of up to 9 mm across are locally present with growth zoning clearly visible in hand specimen (Fig. 5.1c). Growth zoning is well developed in most sphalerite 2 crystals and defined by slight colour variations and finely crystalline inclusions chalcopyrite 2 (typically < 5 $\mu$m; Fig. 5.5b). Inclusions of chalcopyrite 2 also occur along cleavage planes in sphalerite 2 and as randomly scattered crystals (Fig. 5.5c).

Figs. 5.4a, b. Drill hole PD0016, 262.77 m (northern zone). Photomicrograph; (5.4a) transmitted light, crossed nicols, (5.4b) reflected light. Subrounded 'grains' of metasomatic microcline (M) have been overgrown by adularia (A). Microcline grains in contact with pyrite 1 (P) do not have an intervening overgrowth of adularia. Adularia and pyrite 1 are enclosed within sphalerite 2 (S). Adularia in contact with sphalerite 2 has corroded margins.

Fig. 5.4c. Drill hole PD0016, 262.77 m (northern zone). Photomicrograph transmitted light, crossed nicols. Subrounded 'grains' of metasomatic microcline (M) have been overgrown by adularia (A) and enclosed within sphalerite 2 (S). The margins of adularia have been partially altered to sericite 1 (SE) prior to being overgrown by sphalerite 2.

Figs. 5.4d, e. Drill hole PD0016, 262.77 m (northern zone). Photomicrograph; (5.4d) transmitted light, crossed nicols, (5.4e) reflected light. Metamorphic muscovite (M) locally occurs as inclusions in pyrite 1 (P), sphalerite 2 (S) and galena 1 (G). Metamorphic muscovite has a consistent orientation which is not present in sulphide minerals.

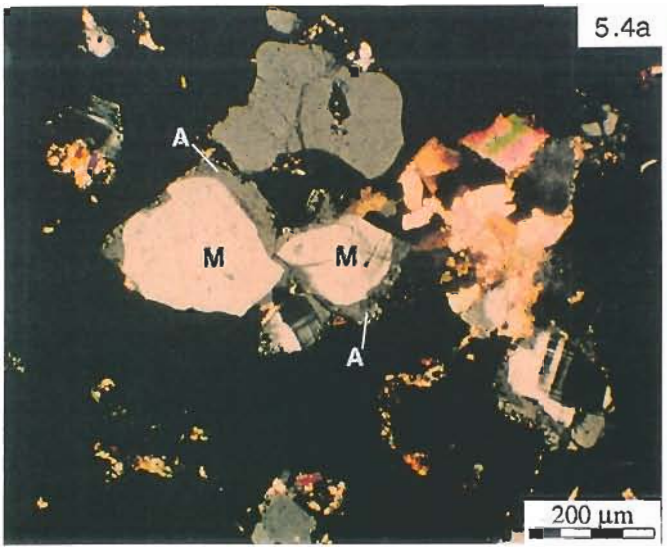
5.4a
A
M
M
A
200 µm

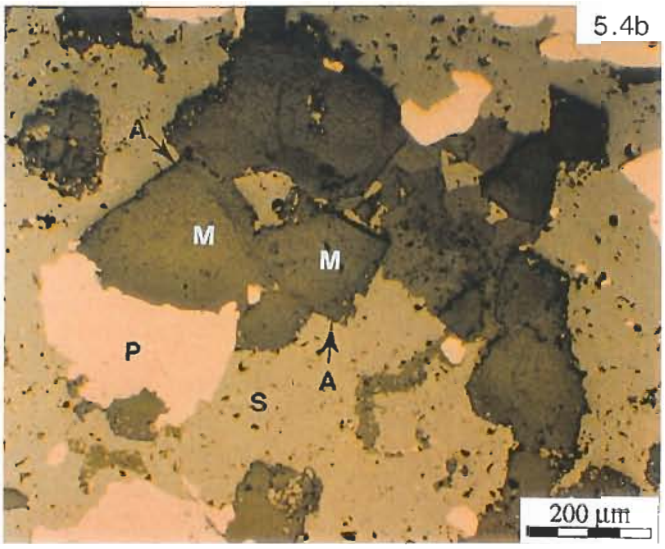
5.4b
A
M
M
P
A
S
200 µm

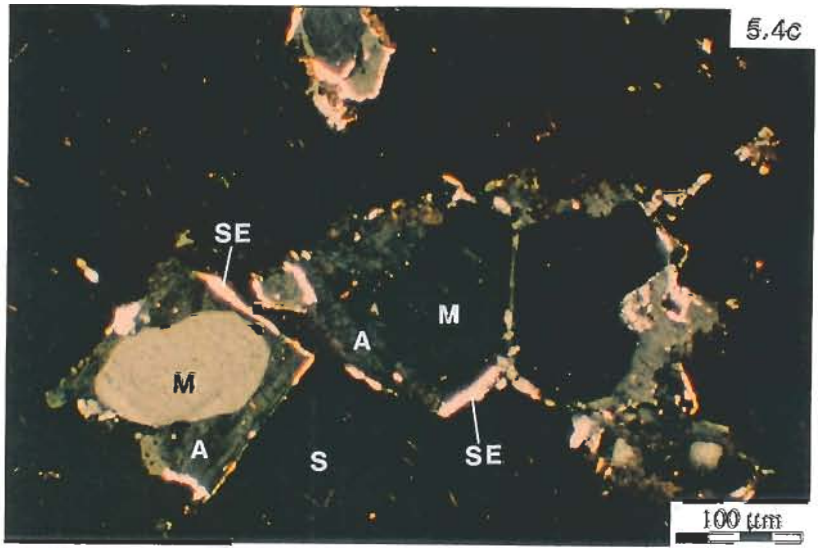
5.4c
SE
M
A
M
A
S
SE
100 µm

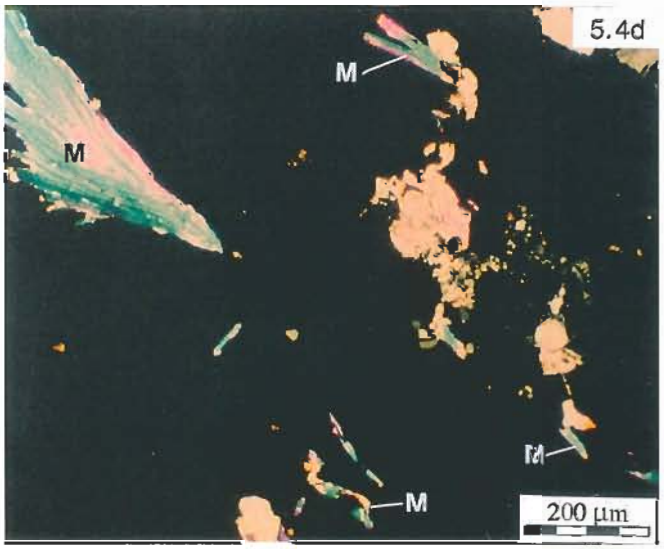
5.4d
M
M
M
M
200 µm

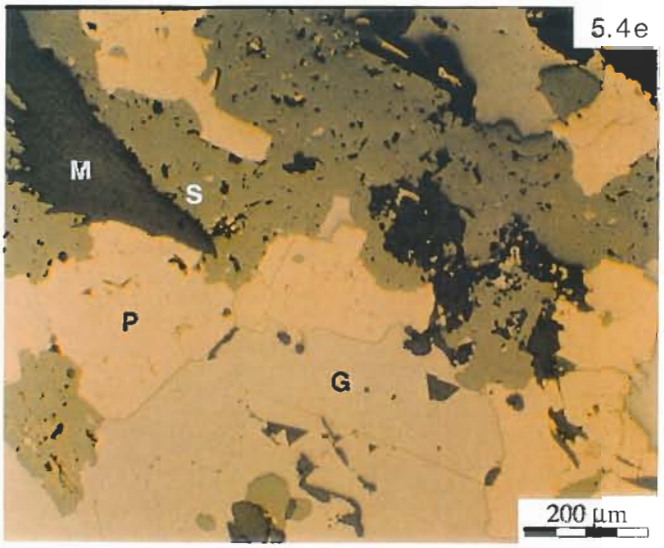
5.4e
M
S
P
G
200 µm

Fig. 5.5a. Drill hole PD0016, 262.77 m (northern zone). Photomicrograph, transmitted light. Adularia rims (A) formed on metasomatic microcline (M) have been corroded and overgrown by sphalerite 1 (S1) which contains abundant inclusions of opaque, fine-grained chalcopyrite 1. Sphalerite 1 forms corroded cores to light yellow - brown sphalerite 2 (S2). Sphalerite 2 forms coalescing growth zoned crystals defined by inclusions of chalcopyrite 2 (C2).

Fig. 5.5b. Drill hole PD0006, 258 m, (northern zone). Photomicrograph, transmitted light. Growth zones in sphalerite 2 (S2) are defined by inclusions of fine-grained chalcopyrite 2 (opaque) which commonly have a gradational distribution across growth zones, and a higher proportion of inclusions occurs near the outer margin of each growth zone (arrow).

Fig. 5.5c. Drill hole PD0011, 452.2 m, (central zone). Photomicrograph, transmitted light. Small opaque inclusions of chalcopyrite 2 are scattered throughout sphalerite 2 (S2) as well as concentrated along cleavage planes. A small flake of hematite (H) has been included in sphalerite 2.

Fig. 5.5d. Drill hole PD0016, 262.77 m, (northern zone). Reflected light photomicrograph of an etched thin section. Sphalerite 2 commonly has broad growth twins (GT) with little evidence of deformation. Grain boundaries between coalesced grains of sphalerite 2 are commonly rounded to irregular (arrow).

Fig. 5.5e. Drill hole PD0011, 452.2 m, (central zone). Reflected light photomicrograph of an etched thin section. Sphalerite 2 (S2) overgrown by quartz 1 (Q). Sphalerite 2 near sphalerite 3 commonly has curved stress twins (ST). Broad growth twins are rare or absent.

Fig. 5.5f. Drill hole PD0029, 258.9 m, (central zone). Reflected light photomicrograph. Sphalerite 2 (S2) has been overgrown by chalcopyrite 3 (C3) which is overgrown by galena 1 (G). Chalcopyrite 3 results from explusion of chalcopyrite 2 inclusions during dynamic recrystallisation of sphalerite 2 to form sphalerite 3. Chalcopyrite 3 and galena 1 have infilled fractures in sphalerite 2. Galena 1 is not obviously deformed and has straight cleavage planes.

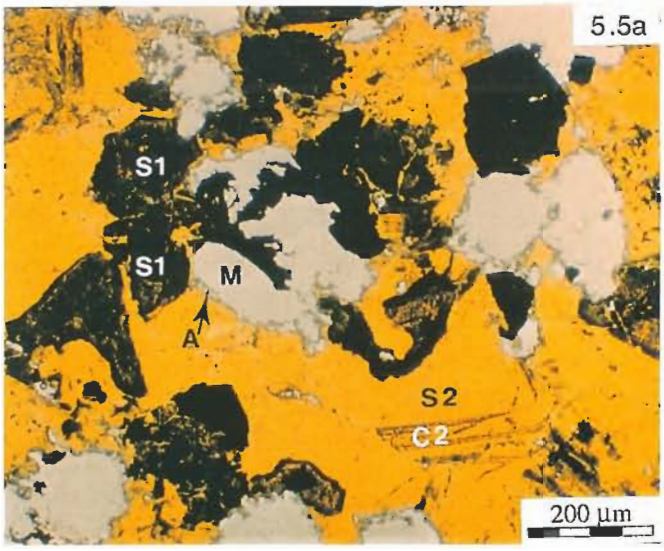
5.5a
S1
S1
M
A
S2
C2
200 µm

5.5b
S2
400 µm

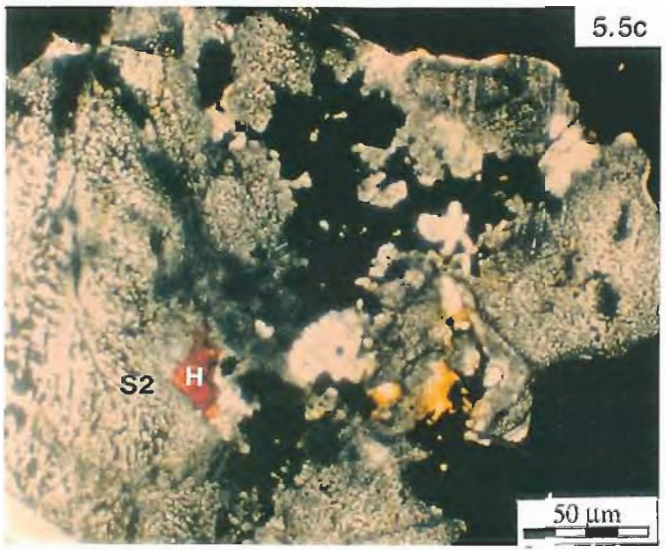
5.5c
S2
H
50 µm

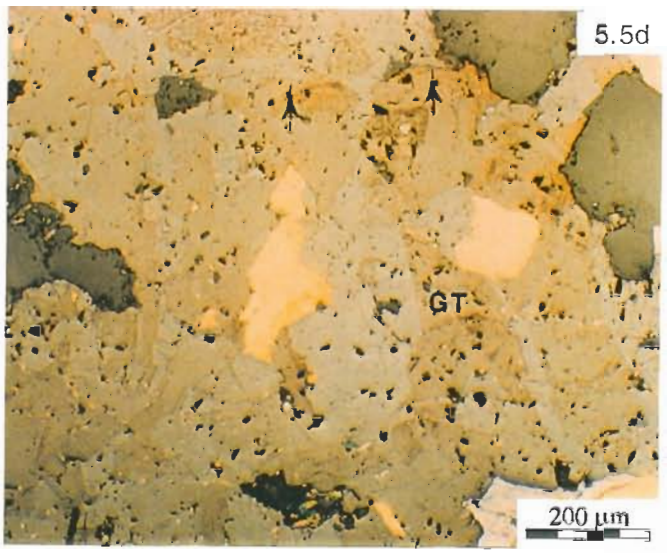
5.5d
GT
200 µm

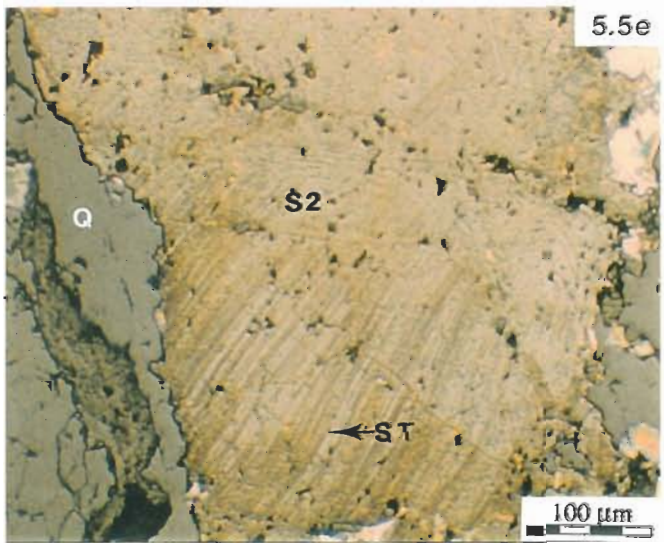
5.5e
Q
S2
ST
100 µm

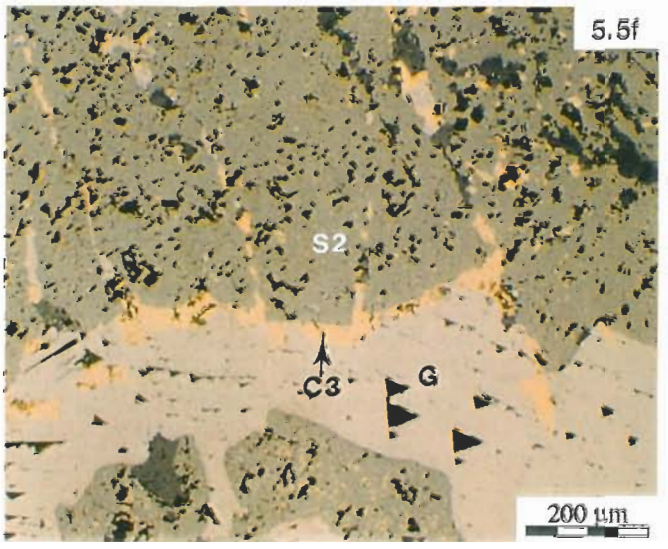
5.5f
S2
C3
G
200 µm

The abundance of chalcopyrite 2 inclusions is gradational across individual growth zones (Fig. 5.5b). The inner margin of a growth zone typically has < 1% of small (< 5 μm), scattered, rounded blebs of chalcopyrite 2. Towards the outer margin of a growth zone, the proportion of chalcopyrite 2 inclusions is increased to ≈ 20% resulting in a near opaque band typically < 20 μm wide. The outer most margin of a growth zone is defined by a sudden drop in the abundance of chalcopyrite 2 inclusions to < 1% which marks the start of the next growth zone.

Sphalerite 2 typically occurs without a core of earlier minerals but has locally overgrown sphalerite 1, sericite 1 or adularia (Figs. 5.4c, 5.4a). Some sphalerite 2 contains trace amounts of pyrite 1 inclusions (typically 5 - 70 μm across) and rare hematite flakes (typically < 20 μm across; Fig. 5.5c). In metasomatised marbles sphalerite 2 locally contains small inclusions of epidote, garnet, microcline, and remnants of carbonate - quartz - chlorite altered diopside. Sphalerite 2 constitutes ≈ 94% of the sphalerite present at Menninnie Dam.

*Etching*

Sphalerite 2 was etched to assess the nature of the contact between coalescing sphalerite crystals and possible strain effects within sphalerite crystals. The etch consisted of a $H_2SO_4$ - $KMnO_4$ solution prepared as follows:

- Dissolve 1.0 grams of $KMnO_4$ in 40 ml of distilled water.
- Add 40 ml of 25% $H_2SO_4$. (after: Ramdohr, 1969)

Polished thin sections were immersed in the etch solution for between 35 - 45 seconds, then flushed with distilled water.

Coalescing sphalerite 2 crystals have sub-rounded to irregular margins, and polygonal crystal contacts and triple junctions are absent (Fig. 5.5d). Ramdohr (1969), Clark and Kelly (1973) and Cox (1987) described growth twins in etched, undeformed sphalerite and also fabrics that resulted from deformation of sphalerite. Growth twins formed broad, parallel sided, or stepped and bluntly terminated bands (Cox, 1987). Deformational twinning was formed by dislocation glide and can be distinguished from growth twins on the basis of their fine, tapering and discontinuous habit (Cox, 1987). Sphalerite 2 has well developed broad growth twins (Fig. 5.5d).

*Sphalerite 3*

Sphalerite 3 occurs in zones of sulphide mineralisation that and contain brecciated crystals of pyrite 1. Sphalerite 3 consists of coalesced, polygonal crystals (typically 10 - 30 μm across) of homogenous, light brown sphalerite, devoid of micron size chalcopyrite inclusions. Sphalerite 3 is intimately intergrown with the margin of sphalerite 2 and locally crosscuts sphalerite 2 growth zones. Etched sphalerite 2 adjacent to sphalerite 3 has well developed

deformational twins (Fig. 5.5e). The texture of sphalerite 3 is similar to a mortar texture that results from dynamic recrystallisation (White, 1976; Brown et al., 1980; Cox, 1987).

*Chalcopyrite 3*

Chalcopyrite 3 has only been observed in the presence of dynamically recrystallised sphalerite 3. Chalcopyrite 3 commonly mantles sphalerite 3 and has in-filled fractures developed in sphalerite 2 (Fig. 5.5f). Where chalcopyrite 3 has infilled fractures in sphalerite 2, the margins of sphalerite 2 fragments are nearly opaque due to abundant micron size inclusions of chalcopyrite 3.

*Quartz 1*

The outer margins of sphalerite 2 locally incorporate small inclusions of euhedral quartz 1, but more commonly quartz 1 rims sphalerite 2 and forms euhedral growth zoned crystals, and crystal aggregates (Fig. 5.6a, b). Quartz 1 contains abundant small fluid inclusions (typically < 1 μm and rarely up to several μm diameter) and a dusting of hematite 1 which collectively, define growth zones. Quartz 1 locally infills fractures developed in sphalerite 2 and mantles adjacent dynamically recrystallised sphalerite 3 and chalcopyrite 3. Some quartz 1 adjacent to sphalerite 3 and chalcopyrite 3 has undulose extinction and is also deformed.

*Ca-Mn-Mg-Fe carbonate 1*

Ca-Mn-Mg-Fe carbonate 1* forms overgrowths on quartz 1 (Figs. 5.6a, b), sphalerite 2, and locally, sphalerite 3. Ca-Mn-Mg-Fe carbonate 1 forms both poorly crystalline, pale brownish aggregates, and euhedral rhombic crystals, and crystal aggregates, locally with a radiating fan texture, attributed to open space growth (Ineson, 1989).

*Galena 1*

Galena 1 forms overgrowths on Ca-Mn-Mg-Fe carbonate 1 and paragenetically earlier minerals. Galena 1 forms irregularly shaped crystals whose margins are dictated by the shape of earlier minerals (Figs. 5.3h, 5.4e, 5.5f). Deposition of galena 1 has not resulted in corrosion of dolomite or sphalerite 2 and 3, however, it has corroded euhedral pyrite 1 along growth zones or cleavage planes (Fig. 5.7). Most galena 1 has straight cleavage planes, however, curved cleavage planes are locally present.

*Sericite 2, chlorite 2 and rhodonite*

Some mineralised zones contain trace amounts of a second phase of sericite (sericite 2) which occurs in association with trace amounts of chlorite and rhodonite rimming galena 1. Some sericite flakes are up to 10 μm long and are more correctly termed muscovite, however to avoid confusion it is referred to as sericite 2.

---

* The composition of Ca-Mn-Mg-Fe carbonates were determined using the electron microprobe (ref. Section 5.5.2).

Figs. 5.6a, b. Drill hole PD0011, 452.2 m, (central zone). Photomicrograph; (5.6a) transmitted light, (5.6b) transmitted light, crossed nicols. Sphalerite 2 (S2) has been overgrown by growth zoned quartz 1 (Q) with later, interstitial Ca-Mn-Mg-Fe carbonate 1 (C). Ca-Mn-Mg-Fe carbonate 1 has been partially altered to chlorite 2 (CH).

Fig. 5.7. Drill hole PD0024, 401.31 m, (central zone). Photomicrograph, reflected light. Pyrite 1 (P) overgrown by sphalerite 2 (S2) and later galena 1 (G). Galena 1 has corroded and replaced pyrite 1 crystals along cleavage planes (arrow).

Figs. 5.8a, b. Drill hole PD0017, 234.15 m, (central zone). Photomicrograph; (5.8a) reflected light, (5.8b) transmitted light, crossed nicols. The outer margin of galena 1 (G) locally contains small laths of sericite 2 (SE) giving the appearance of 'spines'. Sericite 2 has been overgrown by pyrite 2 (P2) which is overgrown by Ca-Mn-Mg-Fe carbonate 2 (C2).

Fig. 5.8c. Drill hole PD0011, 452.2 m, (central zone). Photomicrograph, combination of reflected and transmitted light. Pyrite 1 (P) has been overgrown by Ca-Mn-Mg-Fe carbonate 1 (C) which has later been altered and locally pseudomorphed by chlorite 2 (CH) and overgrown by fluorite (F).

Fig. 5.8d. Drill hole PD0017, 367 m, (central zone). Photomicrograph, transmitted light. Sphalerite 2 (S2) and quartz 1 (Q) with interstitial rhodonite (R).

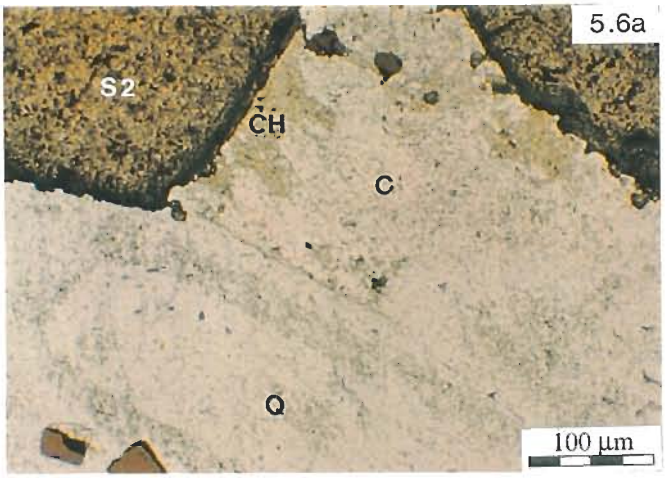
5.6a
S2
CH
C
Q
100 µm

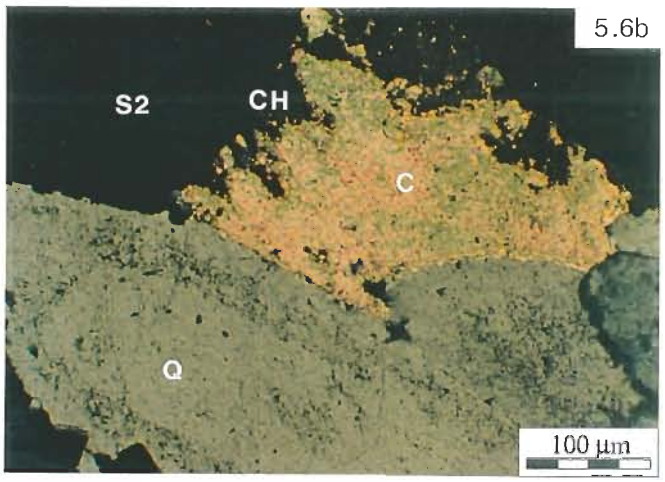
5.6b
S2
CH
C
Q
100 µm

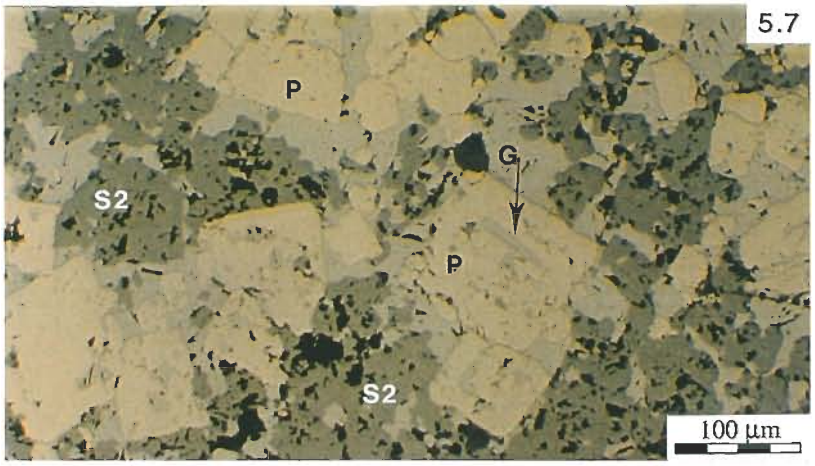
5.7
P
G
S2
P
S2
100 µm

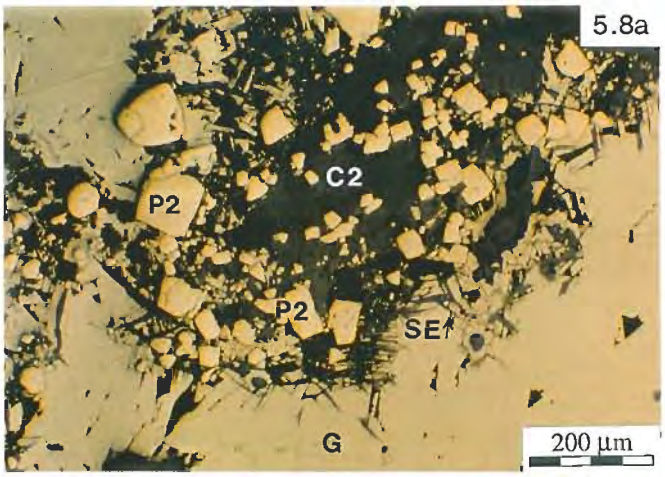
5.8a
C2
P2
P2
SE
G
200 µm

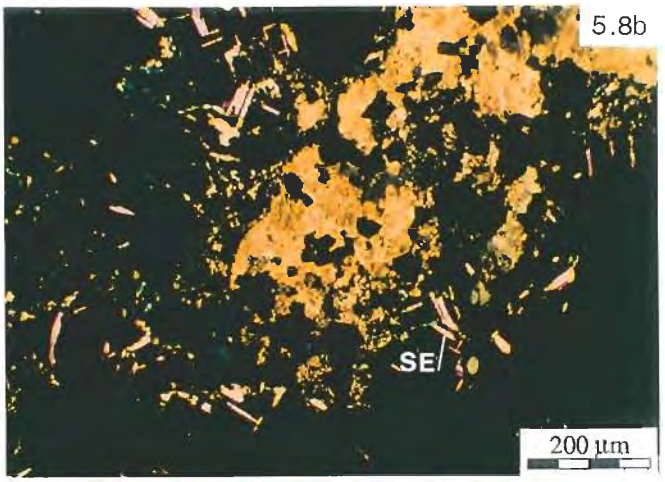
5.8b
SE
200 µm

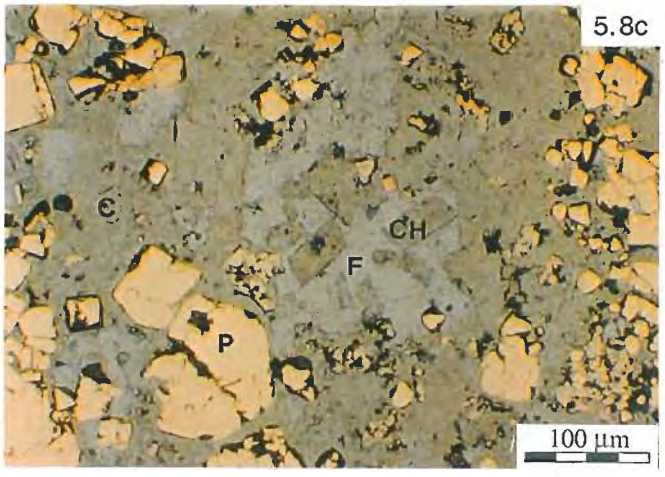
5.8c
C
CH
F
P
100 µm

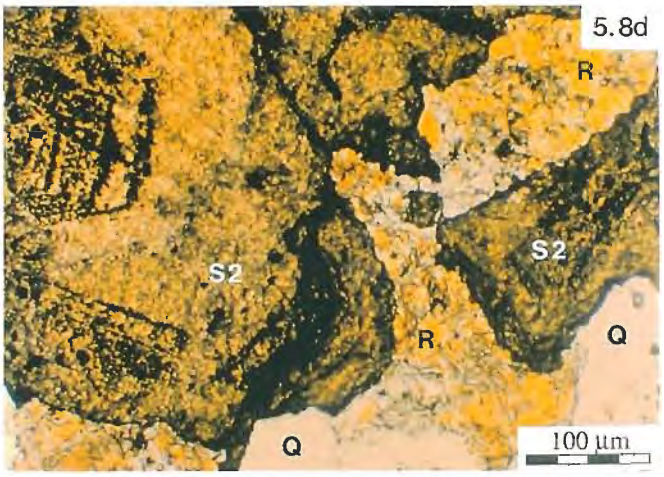
5.8d
R
S2
S2
R
Q
Q
100 µm

Sericite 2 forms finely crystalline aggregates surrounding earlier formed minerals and has locally formed radiating elongated laths around the margin of galena 1, giving the appearance of 'spines' (Figs. 5.8a, b). Trace amounts of finely crystalline chlorite 2 are intergrown with sericite 2 and also occur as pseudomorphs after euhedral Ca-Mn-Mg-Fe carbonate 1 (Fig. 5.8c). Trace amounts of rhodonite occur in some sulphide veins in drill hole PD0017 as scattered, poorly crystalline, irregularly shaped straw coloured aggregates of up to 50 μm across (Fig. 5.8d). Due to the trace amounts of chlorite 2, sericite 2 and rhodonite, a paragenetic sequence for the three minerals cannot be established, therefore, they are tentatively considered coeval and paragenetically later than galena 1.

*Pyrite 2*

Pyrite 2 forms overgrowths on sericite 2, galena 1, and locally sphalerite 2. Pyrite 2 forms small (typically 20 - 50 μm across), subhedral to euhedral crystals and larger crystal aggregates around the margins of earlier minerals (Fig. 5.9). Undeformed pyrite 2 has locally overgrown brecciated pyrite 1.

*Fluorite and Ca-Mn-Mg-Fe carbonate 2*

Clear, to purplish fluorite occurs in minor to trace amounts interstitial to galena 1 and pyrite 2 crystals (Fig. 5.10). The shape of fluorite crystals was dictated by earlier formed minerals. Fluorite has been overgrown by Ca-Mn-Mg-Fe carbonate 2 or in the absence of fluorite, Ca-Mn-Mg-Fe carbonate 2 has overgrown earlier minerals. Ca-Mn-Mg-Fe carbonate 2 forms clear, to pale brown, poorly crystalline aggregates as well as isolated euhedral crystals, and crystal aggregates.

*Quartz 2*

Rare veinlets of quartz 2 cut across all earlier formed minerals. Veinlets are typically a few millimetres long and < 0.5 mm wide. Quartz 2 veinlets appear to be restricted to zones of sulphide mineralisation and have not been observed in the adjacent host rocks.

*Late calcite veins*

White calcite veins referred to as 'late calcite veins' have crosscut all earlier minerals and are equally abundant in mineralisation, the host rocks, and DP breccia units. Late calcite veins are typically a few millimetres wide and locally exceed 1 cm. Their length is not known as they extend beyond the confines of drill core. Their relationship to sulphide mineralisation (if any) is uncertain.

Fig. 5.9. Drill hole PD0017, 351.7 m, (central zone). Reflected light photomicrograph. Pyrite 1 (P1) has been overgrown by sphalerite 2 (S2). Both pyrite 1 and sphalerite 2 have been brecciated and overgrown by non-brecciated pyrite 2 (P2).

Fig. 5.10. Drill hole PD0016, 305.6 m, (northern zone). Transmitted light photomicrograph. Pyrite 1 (P) with interstitial sphalerite 2 (S2) have been overgrown by clear to purple fluorite (F). A 'grain' of microcline (M) adjacent to a crystal of pyrite 1 has been overgrown by adularia (A) which is also overgrown by fluorite.

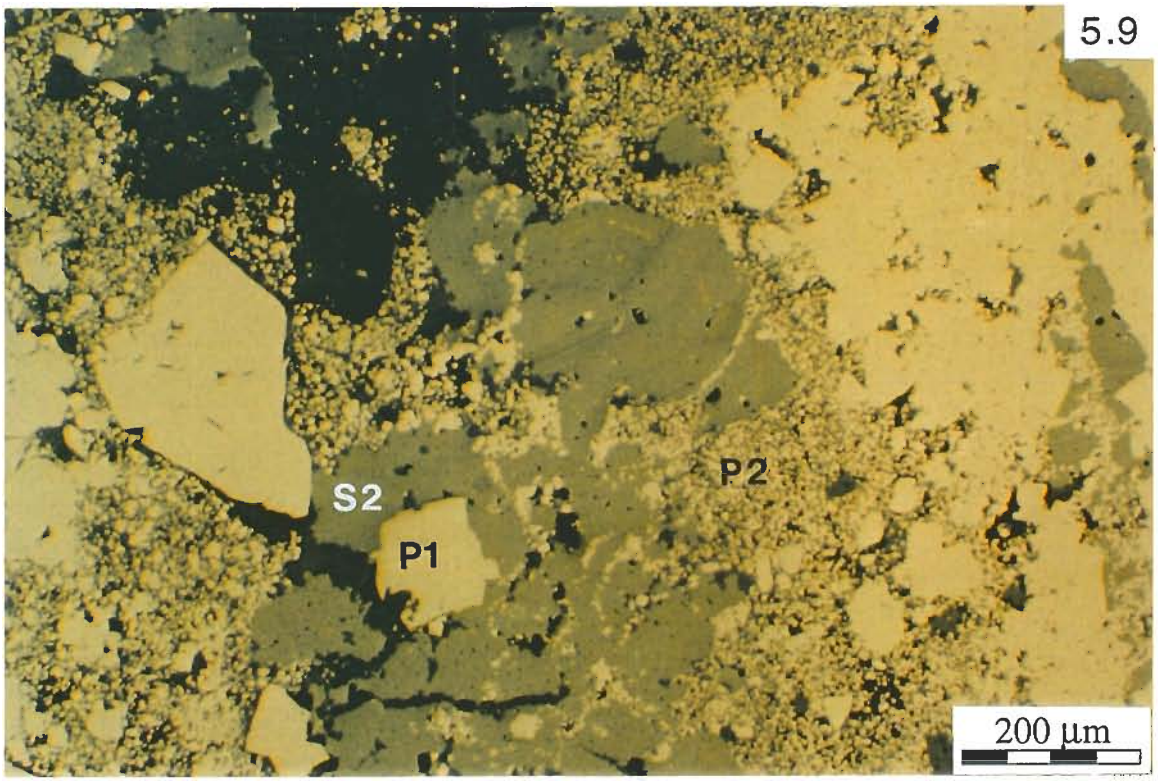
5.9
S2
P1
P2
200 µm

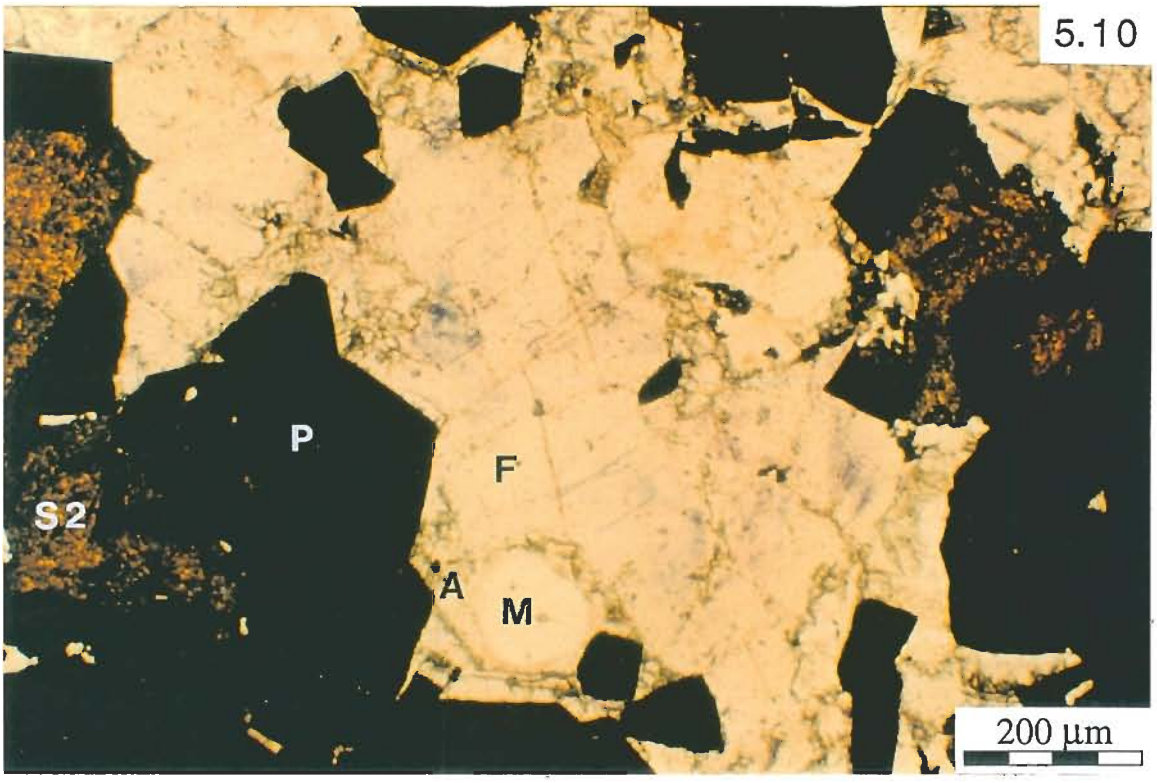
5.10
P
S2
F
A
M
200 µm

**Sulphides hosted by quartz - diopside and massive diopside rock types**

Only the diopside component of quartz - diopside rock and massive diopside has been replaced by sulphide mineralisation. Metamorphic quartz is commonly brecciated in stockwork zones, but remains unaltered and is not host to sulphide mineralisation. Sulphides and gangue minerals hosted by quartz - diopside and massive diopside rock types have a similar paragenesis to sulphides and gangue minerals hosted by marbles, however, there are pronounced textural differences and minor mineralogical differences. Description of the sulphide and gangue mineralogy and textures will follow a paragenetic sequence starting with the first formed minerals.

*Dolomite, talc 1, phlogopite and chlorite 1*

Alteration and mineralisation developed in diopside units has preferentially occurred along fractures and in breccia zones. Mineralising fluids have preferentially permeated along fractures resulting in a series of lobate alteration 'fronts' (Fig. 5.11a). Fronts comprise discontinuous laminations of finely crystalline sulphide and gangue minerals (Fig. 5.11b). On a microscopic scale, alteration has occurred along diopside cleavage planes resulting in a finely crystalline, felted mix of dolomite, talc 1, phlogopite and chlorite 1 (Fig. 5.11c). The matrix to brecciated diopside and the margins of diopside breccia clasts have been similarly altered. Alteration has resulted in chemical rounding and a reduction in the size of diopside clasts.

*Pyrite 1, sphalerite 1, sphalerite 2, chalcopyrite 1 and chalcopyrite 2*

Pyrite 1 forms lobate bands and isolated euhedral to subhedral crystals of 2 - 100 μm across, and locally, small atoll structures and rare framboids (Fig. 5.11d). Adularia and sericite 1 are uncommon alteration minerals in diopside-bearing host rocks and pyrite 1 is commonly over grown by sphalerite 1 or in the absence of sphalerite 1, pyrite 1 is overgrown by sphalerite 2. Sphalerite 1 and 2 have formed isolated anhedral to subhedral crystals of 40 - 240 μm diameter and appear to have nucleated on small crystals of pyrite 1 (Fig. 5.11e). In addition to pyrite 1 inclusions, sphalerite 1 and 2 commonly contain micron sized inclusions of chalcopyrite 1 and 2 respectively. The fine banding of sulphide and gangue minerals produced through alteration of diopside are typically spaced 600 microns apart (Fig. 5.11b). Some pyrite 1 crystals in bands further away from the diopsidic host rock are coarser (5 - 70 μm diameter) compared to those in bands closer to the diopsidic host rock (5 - 10 μm diameter). Sphalerite 1 and 2 crystals are similarly larger further away from the unaltered diopsidic host rock.

*Quartz 1*

Quartz 1 is significantly more abundant in mineralisation hosted by diopside-bearing lithologies compared to mineralisation hosted by marble.

Fig. 5.11a. Drill hole PD0008, 289.83 m, (central zone). Hand specimen from near the contact between mineralisation and diopsidic host rock. The diopside has been altered along fractures (F) resulting in lobate 'fronts' of sulphide and gangue minerals. The direction of front migration is towards the top of the diagram.

Fig. 5.11b. Drill hole PD0017, 377 m, (central zone). Transmitted light photomicrograph of alteration 'fronts' similar to those in Figure 5.11a with bands of fine-grained pyrite 1 (opaque) and dolomite, chlorite ± phlogopite ± talc (mottled light brown). Less altered diopside is towards the top of the diagram. Larger crystals of pyrite 1 are more common near the rear of each front.

Fig. 5.11c. Drill hole PD0017, 377 m, (central zone). Transmitted light photomicrograph. Diopsidic host rock (D) has been preferentially altered along grain boundaries and cleavage planes to fine grained dolomite ± chlorite ± phlogopite ± talc. Fronts that contain fine-grained pyrite 1 (small black flecks) are further from the diopsidic host rock.

Fig. 5.11d. Drill hole PD0017, 377 m, (central zone). Reflected light photomicrograph. Small pyrite 1 framboids (P) in cryptocrystalline quartz 1 (Q) that have resulted from alteration of diopsidic host rock.

Fig. 5.11e. Drill hole PD0017, 377 m, (central zone). Transmitted light photomicrograph from near the contact between mineralisation and diopsidic host rock. Small sphalerite 1 crystals (S1) have been enclosed in fine grained dolomite ± chlorite ± phlogopite ± talc gangue (G). Sphalerite 1 has nucleated on pyrite 1 (P1) crystals which form dark cores to sphalerite 1 crystals.

Fig. 5.11f. Drill hole PD0019, 317.7 m, (central zone). Photomicrograph, transmitted light, crossed nicols. Cryptocrystalline quartz 1 (almost all of Figure 5.11f) is common in mineralised diopsidic units. Minor amounts of sulphides dispersed throughout cryptocrystalline quartz 1 has resulted in a fine-grained dark grey silicic rock.

5.11a

5.11b

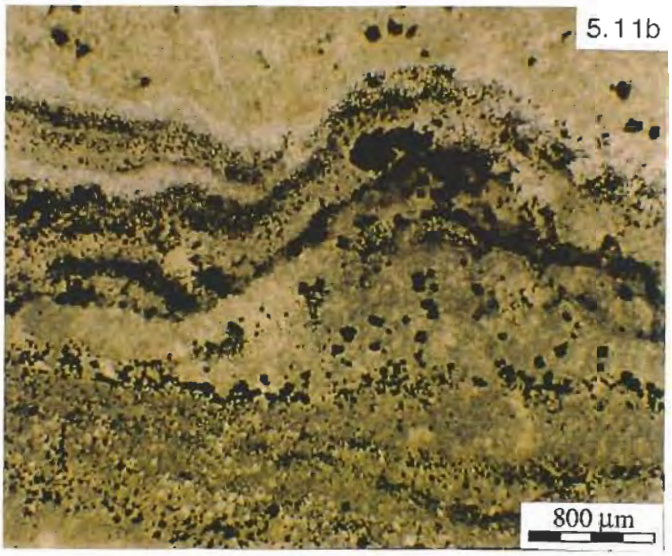


5.11c

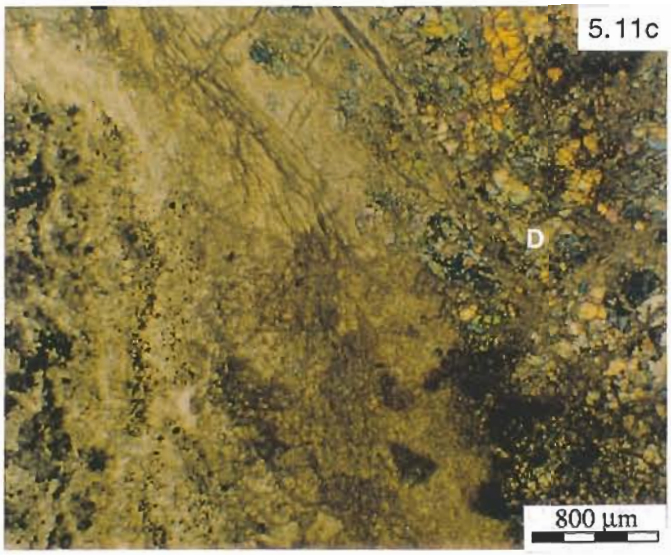


5.11d

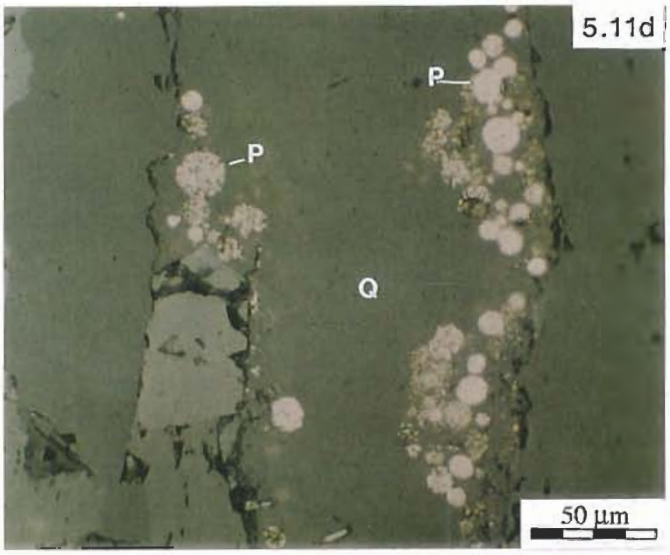


5.11e

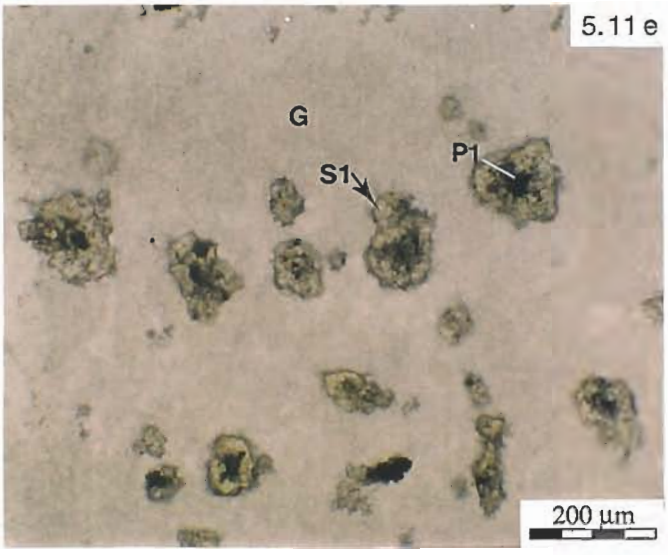


5.11f

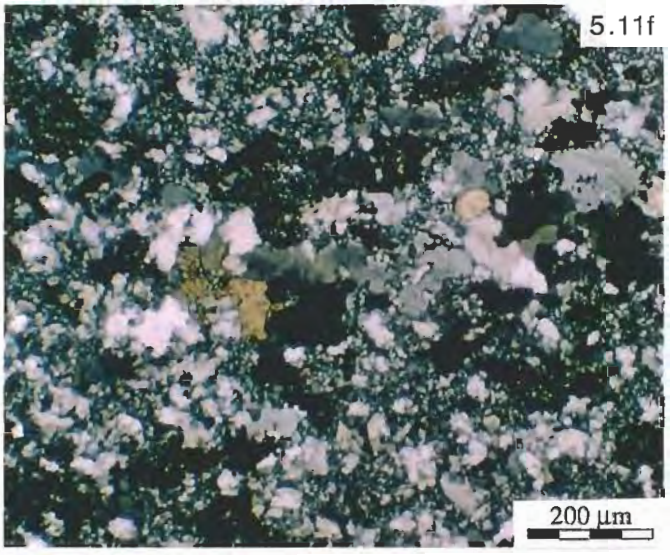

Quartz 1 commonly forms an interlocking mosaic of fine euhedral and rare anhedral crystals that appear to have nucleated on pyrite 1 sphalerite 1 and sphalerite 2 crystals and have replaced dolomite, talc 1 and chlorite 1 (Fig. 5.11f). Pyrite 1, sphalerite 1 and sphalerite 2 crystals that have been overgrown by quartz 1 are generally smaller compared to those that have not been overgrown by quartz 1. Quartz 1 contains diffuse hematite-dusted patches, however, the presence of hematite does not appear to have had any affect on pyrite 1. Quartz 1 was commonly the last mineral to have formed in diopsidic host rocks, resulting in a medium to dark grey, finely crystalline, siliceous rock with disseminations of finely crystalline pyrite 1 and trace amounts of sphalerite 1 and 2. The abundance of quartz 1 appears to have inhibited the formation of paragenetically later minerals such as Ca-Mn-Mg-Fe calcite 1 and 2, galena 1, sericite 2, chlorite 2, pyrite 2 and fluorite and these minerals locally occur as infill minerals in millimetre sized veins that crosscut the finely crystalline mosaic of interlocking quartz 1 crystals.

**Sulphides hosted by marble - calc-silicate lithologies**

Alteration of mixed marble and calc-silicate lithologies has resulted in a combination of textures described for marble hosted mineralisation and diopside - quartz rock or massive diopside hosted mineralisation.

**Mineralisation hosted by DP and LP breccias**

Both DP and LP breccias contain discrete sulphide clasts and composite sulphide - host rock clasts whose sulphide mineralogy consists of pyrite 1, sphalerite 1 and 2, chalcopyrite 1 and 2, and galena 1 (Fig. 4.9e and 5.12a). The matrix of most DP breccias and some marble and diopside clasts in DP breccias have been altered to various proportions of finely crystalline galena 1, pyrite 2, Ca-Mn-Mg-Fe carbonate 2, chlorite 2, sericite 2, and rarely, trace amounts of sphalerite 2. The matrix of some LP breccias is altered to an assemblage which contains disseminated pyrite of unknown paragenesis. The sulphide-bearing clasts in both LP and DP breccias can be subdivided into three types on the basis of their sulphide and gangue mineralogy and textures. These are referred to as clast types 1, 2 and 3, and described below.

*Clast type 1*

Clast type 1 consists of various combinations and proportions of pyrite 1, adularia, sericite 1, sphalerite 1 and 2, chalcopyrite 1 and 2, quartz 1, Ca-Mn-Mg-Fe carbonate 1 galena 1 ± marble (Fig. 5.12a). Clasts typically range from 2 mm to 5 cm across and have a range of shapes from angular to rounded. The paragenesis and textures of the sulphides and gangue minerals are identical to those of mineralisation hosted by marble except that sulphide and gangue minerals paragenetically later than galena 1 are absent.

Fig. 5.12a. Drill hole PD0031, 178.8 m, (central zone). hand specimen of LP breccia. LP breccia consists of lithic clasts (LC), rhyolite pyroclasts (R) and rare sulphide clasts (S) in a matrix of lithic fragments and fine pyroclastics. Sulphide clasts have similar mineralogy and textures to sulphide mineralisation hosted by the underlying Hutchison Group.

Fig. 5.12b. Drill hole PD0008, 179.92 m, (central zone). Hand specimen of a deformed and brecciated granite dyke with undeformed sulphide (S) and gangue mineral (GA) overgrowths on breccia clasts (G). Sulphide and gangue minerals have similar mineralogy and textures to those hosted by marble and calc-silicate lithologies.

Fig. 5.12c. Drill hole PD0031, 241.5 m, (central zone). Transmitted light photomicrograph. A vein comprised of undeformed, growth zoned sphalerite 2 (S2) with abundant fine-grained inclusions of chalcopyrite 2 (opaque), has cross-cut a mylonite (M) formed in eastern suite schist.

Fig. 5.13. Drill hole PD0032, 331.5 m, (southern zone). Hand specimen of brecciated granite dyke (G) that has been pervasively altered to fine-grained, dark green chlorite, carbonate, quartz and light yellow green sericite (LAO). This style of pervasive, texturally destructive alteration is typical of the 'late alteration overprint'.

Fig. 5.14. Drill hole PD0032, 437.5 m, (southern zone). Hand specimen of a sulphide vein hosted by dolomitic marble (M). The sulphide vein comprises sphalerite 2 and 4 (S), chalcopyrite 4 (CP4), pyrite 1 (P1) and trace amounts of galena 1 or 2 (G) and hematite 2. The dark green alteration halo (AH) comprises, chlorite 3, Ca-Mn-Mg-Fe carbonate 3, and minor calc-silicate minerals.

5.12a
R
LC
S
2 cm

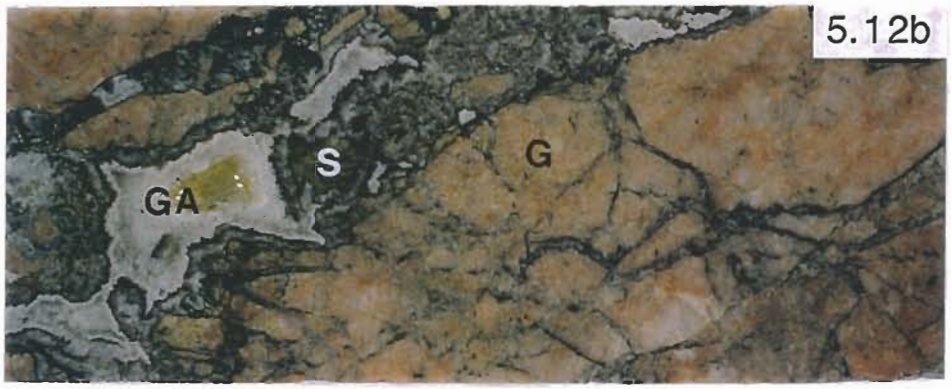
5.12b
GA
S
G
2 cm

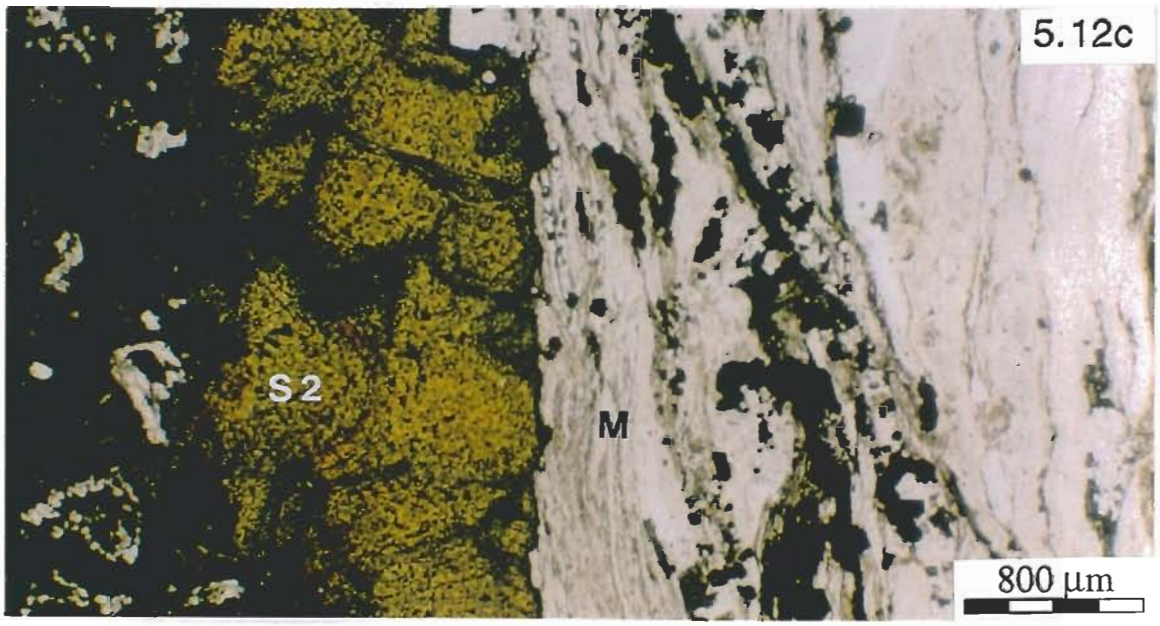
5.12c
S2
M
800 µm

5.13
LAO
G
2 cm

5.14
S
AH
M
G
CP4
P1
2 cm

*Clast type 2*

Clast type 2 consists of finely crystalline, disseminations of pyrite 1 in a finely crystalline matrix of quartz 1. Trace amounts of sphalerite 1 and 2, chalcopyrite 1 and 2, Ca-Mn-Mg-Fe carbonate 1 and galena 1 are present in some clasts. Clasts typically range from 1 mm to 5 cm across and have a range of shapes from angular to rounded. Sulphide and gangue minerals paragenetically later than galena 1 have not been observed. Partially altered remnants of diopside are present in some clasts. The sulphide and gangue paragenesis and textures are similar to mineralisation hosted by massive diopside and diopside bands.

*Clast type 3*

Clast type 3 consists of angular fragments of pyrite 1 aggregates and typically range from 1 mm to 1 cm across. The size range of clasts type 3 is similar to pyrite 1 aggregates hosted by marble units.

**Mineralisation hosted by granite dykes, graphitic schist, eastern and western suite schists.**

Minor amounts of sulphide mineralisation are locally hosted by granite dykes, graphitic schists (Fig. 3.14g), and eastern and western suite schists. Mineralisation hosted by granite dykes invariably occurs in the matrix of brecciated granite dykes (Fig. 5.12b). Mineralisation hosted by graphitic schist occurs as thin veinlets typically 0.5 - 2 mm wide which crosscut the schistose fabric (Fig. 3.5e). Mineralisation hosted by eastern and western suite schists is commonly associated with fault zones but crosscuts the fault zone fabric and locally crosscuts mylonitic fabrics (Figs. 3.15e, 5.12c). Sulphide and some gangue minerals have primary mineral zoning and have not been deformed (Fig. 5.12c). The mineralogy, textures and paragenesis of sulphide and gangue minerals hosted by brecciated granite dykes, graphitic schist, and eastern and western suite schists are similar to those of marble hosted mineralisation.

## 5.3 Mineralisation in the southern zone

Interpretation of mineralisation and alteration in the southern zone is based on a single diamond drill hole (drill hole PD0032; Fig. 3.1) and a few percussion drill holes to the south of drill hole PD0032. Summary geological logs for drill hole PD0032 and the southern percussion drill holes are illustrated in Appendix 3.1.

**Distribution of sulphides**

Most sulphide mineralisation in the southern zone is hosted by marbles and calc-silicate lithologies of the eastern suite, interpreted to be part of a transition zone between the marbles and calc-silicate lithologies of the central, and schist of the eastern suite (Section 3.2.3). Minor amounts of disseminated sulphides are hosted by brecciated granite dykes and altered eastern suite schist. LP breccia and the lower 34m of the MD ignimbrite (Section 4.3.2)

contain trace amounts of disseminated sulphides. Marble clasts scattered throughout the remainder of the MD ignimbrite are locally altered, and some contain trace amounts of sulphide mineralisation. Rare sulphide-bearing veins crosscut the eutaxitic texture of the MD ignimbrite. Due to the absence of outcrop and the limited number of drill holes, it is not possible to further define the shape or lateral extent of mineralisation in the southern zone.

**Late alteration overprint**

A significant difference between rock units and mineralisation in the southern zone compared to those in the northern and central zones, is the occurrence of pervasive chlorite - carbonate - quartz - calc-silicate - hematite alteration that has affected both the host rocks and mineralisation. Pervasive chlorite - carbonate - quartz - calc-silicate - hematite alteration is referred to as the '*late alteration overprint*' throughout the remainder of this thesis. The late alteration overprint has resulted in significant mineralogical and textural modifications of all rock units with both selective and pervasive alteration and destruction of metamorphic textures. Marble and calc-silicate lithologies have been altered to chlorite, calcite, epidote, tremolite ± garnet ± talc ± serpentine ± graphite ± rhodochrosite ± hematite. Schist units have been partially altered to quartz, chlorite, calcite, epidote, tremolite and sericite with partial destruction of metamorphic textures. Feldspar in granite dykes has been selectively altered to sericite, chlorite, calcite, quartz and minor epidote. Locally, granite dykes have been brecciated and pervasively altered to chlorite, calcite, sericite, quartz and minor epidote with total destruction of primary textures (Fig. 5.13).

### 5.3.1 Relationship between sulphides and host rocks

The style of mineralisation in the percussion holes cannot easily be determined due to the nature of the drilling process and interpretation of the relationship between mineralisation and the host rocks is based solely on diamond drill hole PD0032.

Mineralisation in the southern zone occurs as veins and less commonly as disseminations throughout the host rock (Fig. 5.14). Veins vary from 1 - 10 cm wide and are generally less common, and thinner, than veins in the northern and central zones. Veins are commonly associated with a zone of host rock alteration several centimetres to several metres wide zone which is significantly more extensive than the alteration halo surrounding veins in the northern and central zones (Fig. 5.14). Unlike mineralisation in the northern and central zones, the relationship between mineralisation and fractured or brecciated host rock is not obvious. This may have resulted from destruction of host rock textures by the late alteration overprint.

### 5.3.2 Sulphide and gangue mineralogy and textures

The sulphide and gangue mineralogy and textures are described in paragenetic order starting with the first formed mineral. Minerals in the southern zone that have a similar label to those in the northern and central zones are paragenetically equivalent.

eg. Sphalerite $2_{\text{southern zone}}$ = Sphalerite $2_{\text{northern and central zones}}$

A summary of the sulphide and gangue mineral paragenesis applicable to the southern zone is illustrated in Figure 5.15.

*Pyrite 1 and sphalerite 2*

Pyrite 1 was the earliest formed mineral, present as euhedral to subhedral crystals and aggregates of 5 μm - 1 mm diameter. Sphalerite 1 has not been observed in the southern zone and 5 - 100 μm crystals of pyrite 1 are commonly overgrown by sphalerite 2. Sphalerite 2 forms corroded and embayed crystals and aggregates of 0.1 - 3 mm diameter and rare, isolated, rounded to subhedral crystals (Fig. 5.16a). Euhedral crystal margins are locally preserved where sphalerite 2 is in contact with pyrite 1, quartz 1, Ca-Mn-Mg-Fe carbonate 1, or galena 1 (Figs. 5.16c, d, 5.17).

Sphalerite 2 commonly comprises two, and locally, three sectors, referred to as the 'inner sector', the 'mid sector' and the 'outer sector' (Fig. 5.16a). The inner sector of sphalerite 2 is light to medium yellow - brown with well developed growth zoning. Trace amounts of hematite 1 locally occur as < 20 μm diameter inclusions scattered throughout the inner sector of sphalerite 2. The inner sector is surrounded by the mid sector which consists of light yellow - brown sphalerite 2 typically devoid of growth zoning, or locally with a remnant, partially corroded, outermost growth zone (Figs. 5.16a, c). The contact between the darker coloured inner sector and the lighter coloured mid sector is irregular and diffuse and cuts across growth zoning developed in the inner sector. The width of the mid sector is variable and ranges from 50 microns to almost 1 mm. The mid sector (or in its absence, the inner sector) is mantled by an outer sector of pale brown sphalerite 2 devoid of growth zoning. The contact between the mid sector and the outer sector is either abrupt, occurring at the single outer growth zone of the mid sector (Figs. 5.16a, c), or transgresses the outer growth zone and is diffuse.

Growth zoning in the inner sector of sphalerite 2 is defined by micron sized inclusions of chalcopyrite 2. As with sphalerite 2 in the northern and central zones, individual growth zones often show a gradation in the intensity of micron sized inclusions of chalcopyrite 2. The inner part of a growth zone has < 1% scattered small (< 5 μm) rounded blebs of chalcopyrite 2. As the outer margin of the growth zone is approached, the proportion of chalcopyrite 2 inclusions is increased to ≈ 20%.

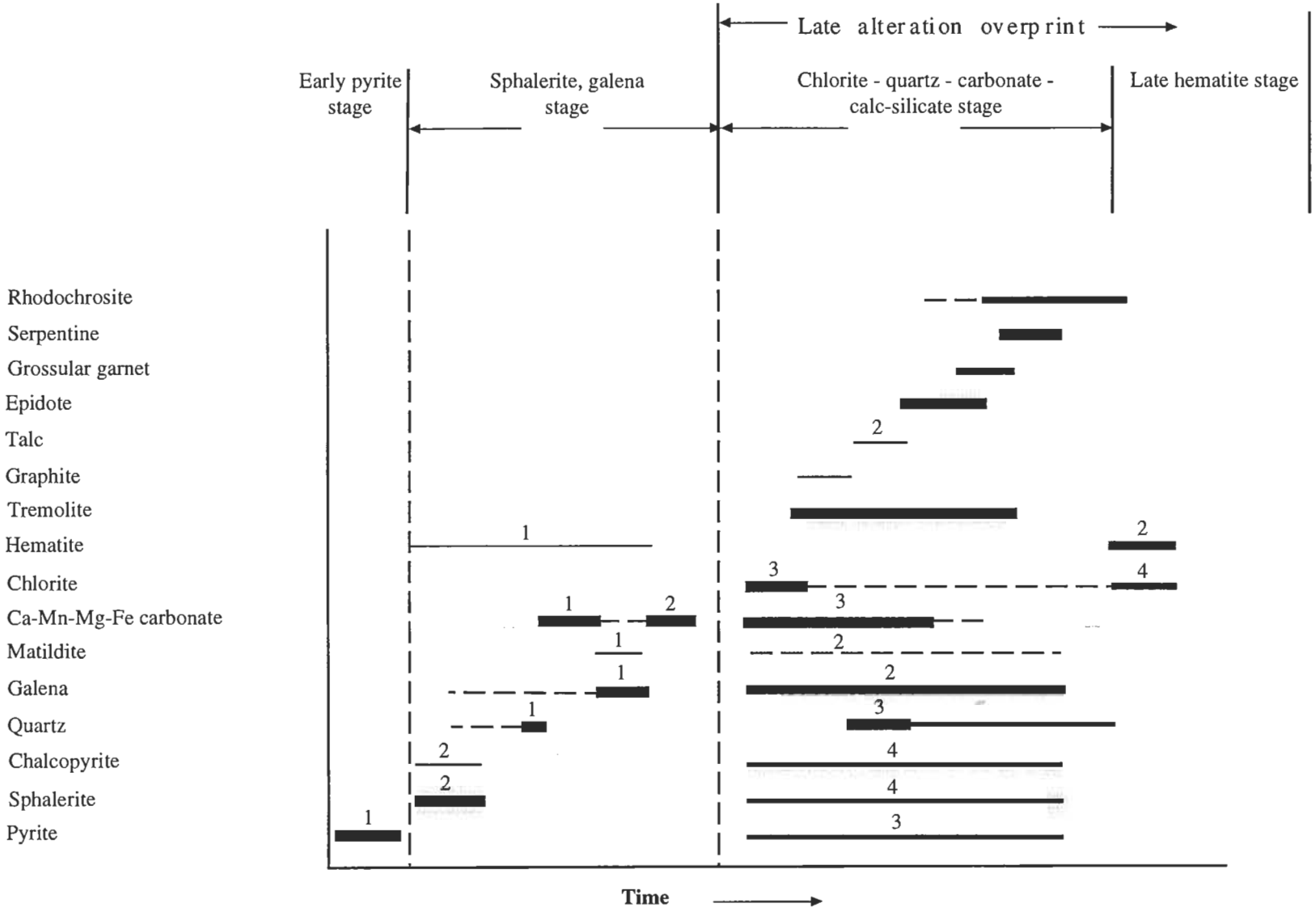


Fig. 5.15 Paragenesis of sulphide and gangue minerals in the southern zone. Thicker lines represent more abundant minerals, and dotted lines represent trace amounts of minerals of uncertain paragenesis. The grey bars have no significance other than to assist the reader.

Figs. 5.16a, b. Drill hole PD0032, 245.7 m, (southern zone). Photomicrograph, (5.16a) transmitted light (5.16b) reflected light. Light yellow - brown sphalerite 2 with inner (I), mid (M) and outer (O) sectors. The outer margin of the outer sector has a dark rind of abundant fine grained chalcopyrite 4 (CP4). The dark rind is also present at the boundary between sphalerite 2 grains in mutual contact and along fractures in sphalerite 2. Sphalerite 2 in contact with galena 1 (G) and Ca-Mn-Mg-Fe carbonate 2 (C2) has euhedral crystal margins whereas sphalerite 2 in contact with Ca-Mn-Mg-Fe carbonate 3 and chlorite 3 (C3) has corroded crystal margins.

Figs. 5.16c, d. Drill hole PD0032, 245.7 m, (southern zone). Photomicrograph, transmitted light, (5.16c) reflected light (5.16d). Mid (M) and outer (O) sectors of pale yellow - brown sphalerite 2 with dark chalcopyrite rich outer margins. Sphalerite 2 has euhedral margins in contact with Ca-Mn-Mg-Fe carbonate 2 (C2) and corroded margins in contact with tremolite (T), Ca-Mn-Mg-Fe carbonate 3 (C3) and trace amounts of graphite (opaque flecks). Corroded sphalerite 2 (S2) crystals have been mantled by a thin rim of galena 2 (G2).

Fig. 5.16e. Drill hole PD0032, 245.7m, (southern zone). Reflected light photomicrograph of an etched thin section. Sphalerite 2 grains in mutual contact have round to irregular shapes (arrow) and broad growth twins (GT).

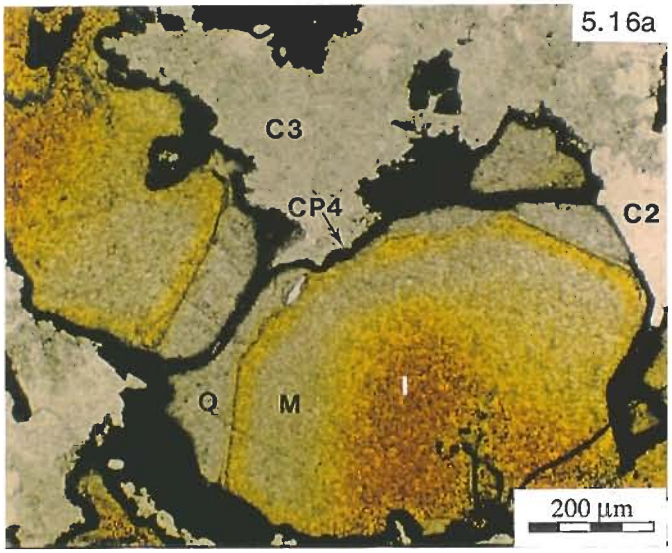
5.16a
C3
CP4
C2
Q
M
I
200 µm

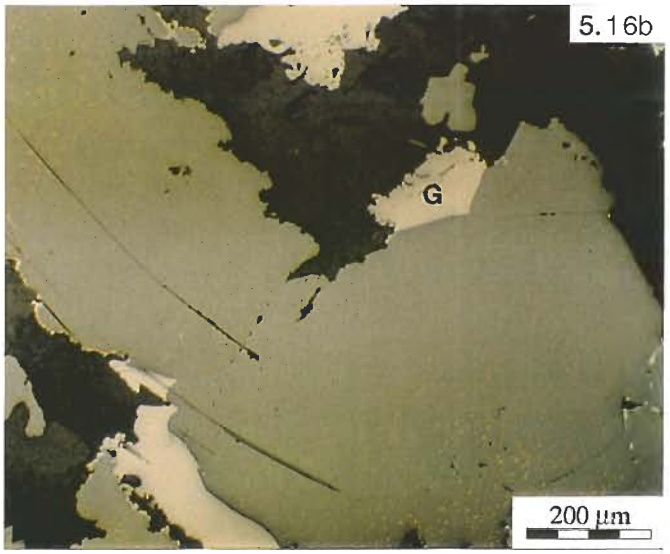
5.16b
G
200 µm

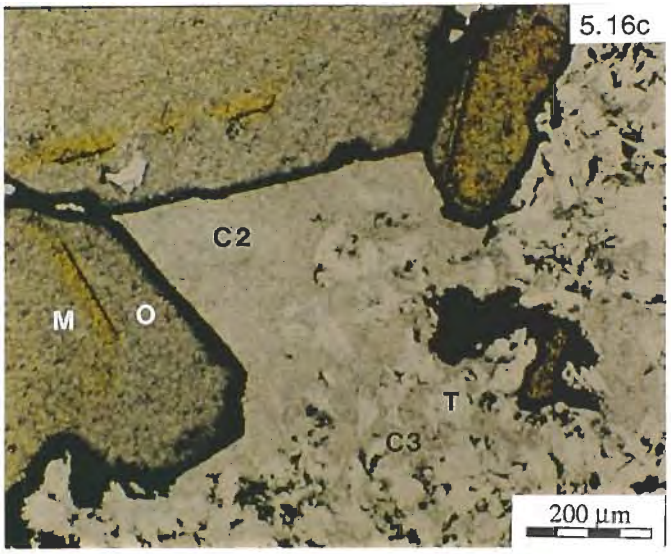
5.16c
C2
M
O
T
C3
200 µm

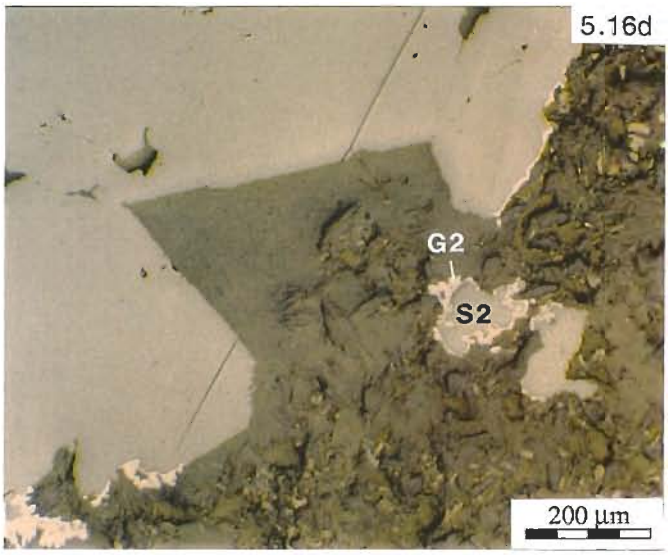
5.16d
G2
S2
200 µm

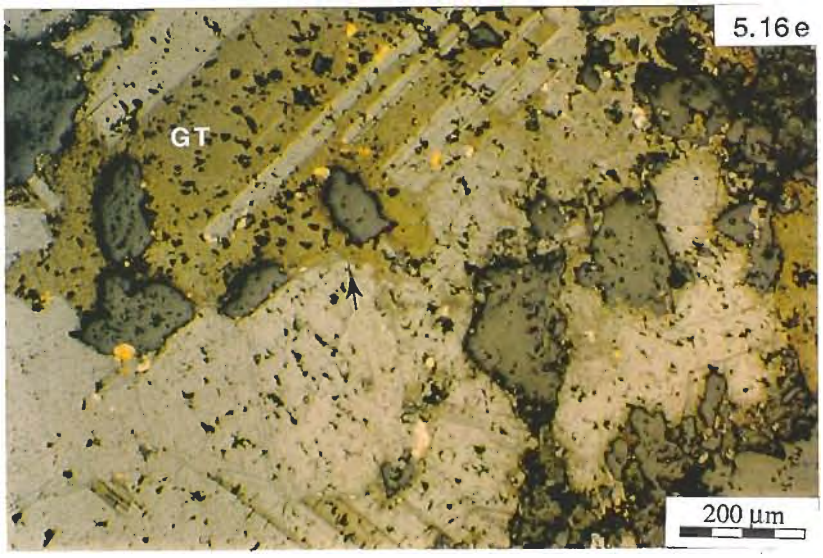
5.16e
GT
200 µm

The outer-most margin of a growth zones is defined by a sudden decrease in the proportion of chalcopyrite 2 inclusions to < 1% which also marks the inner-most boundary of the next growth zone.

The mid sector of sphalerite 2 is either devoid of chalcopyrite 2 inclusions or contains scattered inclusions of chalcopyrite 2 and a concentration of chalcopyrite 2 inclusions along a single outer-most growth zone. Chalcopyrite 2 inclusions in the mid sector are commonly smaller than those in the inner sector. The outer margin of the outer sector is corroded and is commonly packed with fine chalcopyrite 2 inclusions of < 1 μm diameter that are smaller than those in either the mid sector or the inner sector. The abundance of fine chalcopyrite 2 inclusions along the outer margin of the outer sector forms a dark, opaque rind of ≈ 40 μm wide on most sphalerite 2 crystals. (Figs. 5.16a, c). The boundaries of sphalerite 2 crystals in mutual contact and sphalerite 2 adjacent to fractures have a similar dark rind of sub-micron chalcopyrite 2 inclusions (Fig. 5.16a).

Broad growth twins and irregular crystal boundaries are apparent in etched sphalerite 2 (Fig. 5.16e). Deformation twins have not been observed in sphalerite 2 in the southern zone.

*Quartz 1*

The outer margin of sphalerite 2 locally contains small euhedral crystals of quartz 1. More commonly, quartz 1 forms euhedral growth zoned crystals and crystal aggregates that overgrow sphalerite 2. Growth zoning is defined by abundant fluid inclusions and mineral inclusions typically < 1 μm across, and rarely up to several microns.

*Ca-Mn-Mg-Fe carbonate 1*

Ca-Mn-Mg-Fe carbonate 1 has overgrown quartz 1, sphalerite 2, or pyrite 1 (Fig. 5.16c, d). Trace amounts of small hematite 1 flakes (< 5 μm diameter) are locally scattered throughout Ca-Mn-Mg-Fe carbonate 1.

*Galena 1 and Ca-Mn-Mg-Fe carbonate 2*

Galena 1 has overgrown Ca-Mn-Mg-Fe carbonate 1, quartz 1 and sphalerite 2 (Fig. 5.17) and forms coarse crystal aggregates with irregular corroded margins. In the northern and central zones, galena 1 locally corroded pyrite 1, however, the nature of the contact between pyrite 1 and galena 1 has not been established in the southern zone. Galena 1 has locally been overgrown by Ca-Mn-Mg-Fe carbonate 2.

Up to this point, descriptions of the mineralogy and mineral paragenesis of the southern zone are similar to those of the northern and central zones, however, minerals paragenetically later than Ca-Mn-Mg-Fe carbonate 2 in the southern zone are significantly different from those of the northern and central zones.

Fig. 5.17. Drill hole PD0032, 245.7 m, (southern zone). Reflected light photomicrograph. Sphalerite 2 (S2) contains small inclusions of chalcopyrite 2 (yellow). Sphalerite 2 adjacent to galena 1 (G1) has euhedral crystal margins. Galena 1 has a straight cleavage pattern. Galena 2 (G2) has resulted from remobilisation of galena 1 and forms rims on corroded crystals of sphalerite 2.

Fig. 5.18. Drill hole PD0032, 245.7 m, (southern zone). Transmitted light photomicrograph. Sphalerite 2 (S2) has been overgrown by Ca-Mn-Mg-Fe carbonate 1 (C1). Ca-Mn-Mg-Fe carbonate 1 has been partially replaced by a Ca-Mn-Mg-Fe carbonate 3 and chlorite 3 (C3). The contact between Ca-Mn-Mg-Fe carbonate 1, and Ca-Mn-Mg-Fe carbonate 3 and chlorite 3 is an irregular front (arrow).

Figs. 5.19a, b. Drill hole PD0032, 383.25 m, (southern zone). Photomicrograph, transmitted light (5.19a), reflected light (5.19b). Corroded sphalerite 2 crystals (S2) have been cross-cut by a thin vein of sphalerite 4 (S4), chalcopyrite 4 (CP4), galena 2 (G2), and Ca-Mn-Mg-Fe carbonate 3 (C3). Sphalerite 4 is devoid of chalcopyrite inclusions.

Figs. 5.20a, b. Drill hole PD0032, 392.95 m, (southern zone). Photomicrograph, transmitted light (5.20a), reflected light (5.20b). Sphalerite 2 (S2) contains abundant small inclusions of chalcopyrite 2 (CP2; yellow flecks in Fig. 5.2Ob). Sphalerite 4 (S4) adjacent to sphalerite 2 is devoid of chalcopyrite 2 inclusions and contains small inclusions of remnant galena 1 (G1; white flecks in Fig. 5.20b). A rind of hematite 2 (H2) has partially encompassed sphalerite 2 and 3.

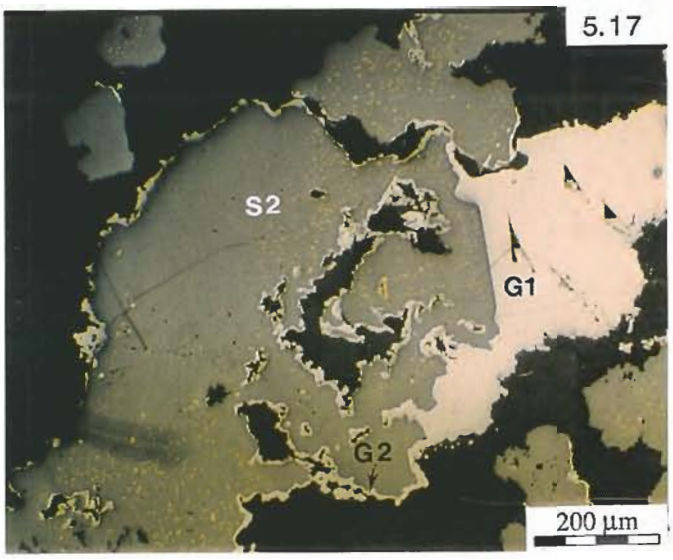
5.17
S2
G1
G2
200 µm

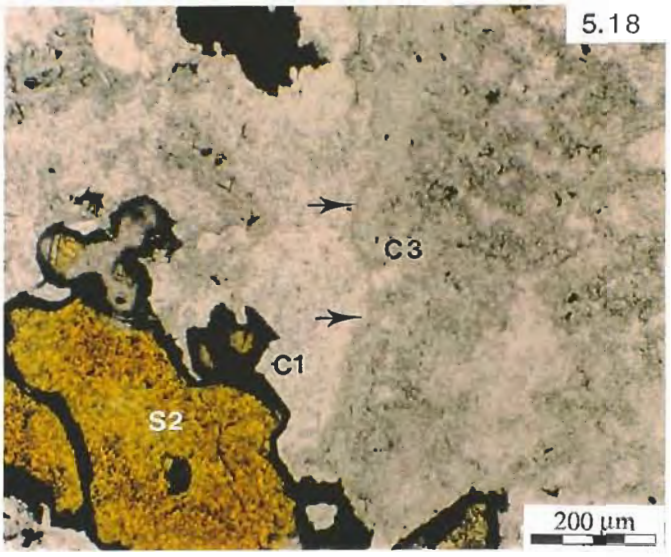
5.18
C3
C1
S2
200 µm

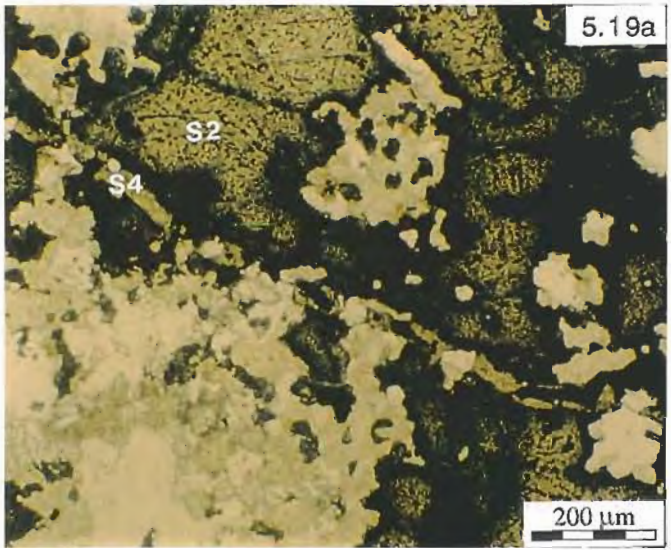
5.19a
S2
S4
200 µm

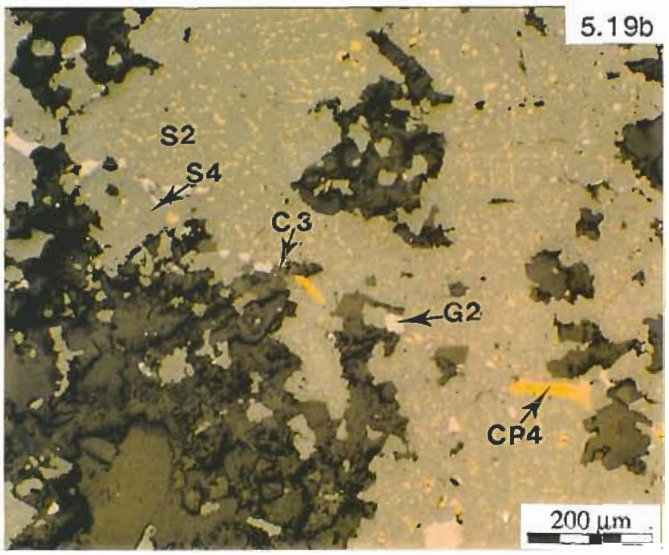
5.19b
S2
S4
C3
G2
CP4
200 µm

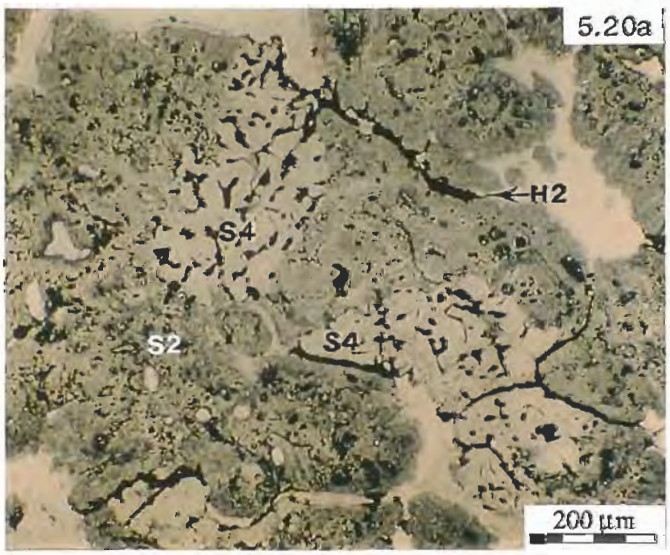
5.20a
H2
S4
S2
S4
200 µm

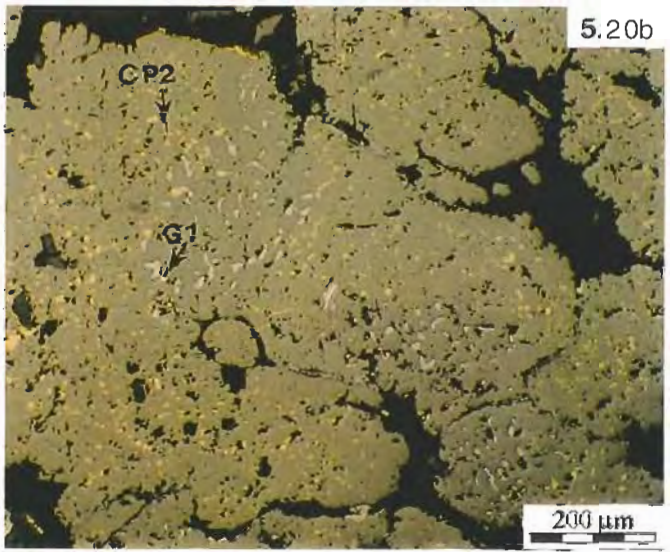
5.20b
CP2
G1
200 µm

Pervasive chlorite - carbonate - quartz - calc-silicate - hematite alteration ('late alteration overprint') of the host rocks and mineralisation has occurred irrespective of the nature of the host rocks. The paragenetic sequence of late alteration overprint minerals is not always clear and the following descriptions follow a paragenetic sequence as closely as could be determined (Fig. 5.15).

*Chlorite 3 and Ca-Mn-Mg-Fe carbonate 3*

In mineralised zones hosted by marble, pervasive, finely crystalline, chlorite 3 and Ca-Mn-Mg-Fe carbonate 3 alteration has corroded and replaced earlier Ca-Mn-Mg-Fe carbonate 1 and 2 (Fig. 5.16a, 5.18).

*Galena 2, sphalerite 4, chalcopyrite 4 and pyrite 3*

Galena 1, sphalerite 2, chalcopyrite 2 and pyrite 1 have undergone partial dissolution, and have been locally re-precipitated, or more commonly re-precipitated elsewhere as galena 2, sphalerite 4, chalcopyrite 4 and pyrite 3 respectively. Dissolution of sulphides is evidenced by rare veinlets of sphalerite 4, chalcopyrite 4, galena 2 and pyrite 3 that crosscut sphalerite 2 (Fig. 5.19a, b). Dissolution of sphalerite 2 resulted in corrosion and embayment of sphalerite 2 crystal margins and leaching of iron and micron sized inclusions of chalcopyrite 2. This resulted in the lighter colour, and the diminished content and smaller size of chalcopyrite 2 inclusions in the mid and outer sectors of sphalerite 2 (Fig. 5.16a, c).

Partial dissolution of galena 1 has resulted in highly corroded crystal shapes and the outer ≈ 50 μm of galena 1 crystals is devoid of the characteristic, well defined, cleavage pattern, of galena 1. Galena 2 also forms 10 - 50 μm wide overgrowths on corroded sphalerite 2 crystals immediately adjacent to the dark rind of sub-micron chalcopyrite 2 inclusions (Fig. 5.17). Galena 1 adjacent to sphalerite 2 has locally been mostly replaced by pale yellow brown sphalerite 4. Small irregular to elongated, rounded 'globs' of remnant galena 1 (10 - 60 μm long) remain randomly scattered throughout sphalerite 4 (Fig. 5.20a, b).

*Tremolite, talc 2 and graphite*

Tremolite, talc 2, and locally, trace amounts of graphite, have overprinted chlorite 3 and partially replaced Ca-Mn-Mg-Fe carbonate 3 (Fig. 5.16c, d). Tremolite has formed randomly orientated, scattered laths (typically 80 μm, and locally up to 5 mm long) and radiating aggregates. Talc 2 is present as a finely crystalline mosaic interstitial to tremolite laths. Graphite has only been observed in a single polished thin section where it forms small randomly orientated disseminated flakes (< 5 μm length) dispersed between tremolite laths. Remnant Ca-Mn-Mg-Fe carbonate 3 has a mottled pinkish colour.

*Quartz 3*

Euhedral growth zoned quartz 3 has partially replaced Ca-Mn-Mg-Fe carbonate 3 and locally, overprinted tremolite (Fig. 5.21). Quartz 3 locally forms a mosaic of finely crystalline, irregularly shaped, interlocking crystals with poorly defined crystal margins. Chlorite 3 does not appear to have been replaced by quartz 3 and is locally present as inclusions in quartz 3.

*Epidote and garnet*

Epidote appears to have formed in association with tremolite and has locally replaced quartz 3, Ca-Mn-Mg-Fe carbonate 3 and chlorite 3 (Fig. 5.22). Epidote is present as isolated, randomly orientated, light yellow - green and colourless prismatic crystals, up to 2 mm in length as well as larger crystal aggregates. Locally, grossular garnet is present as scattered, pale coloured, euhedral crystals, typically 100 - 300 μm across and appears to be paragenetically later than epidote (Fig. 5.22).

*Serpentine and rhodochrosite*

Minor amounts of serpentine locally occur in association with epidote and garnet. In zones that contain epidote and garnet, remnant Ca-Mn-Mg-Fe carbonate 3 has been converted to rhodochrosite (Fig. 5.22).

*Chlorite 4 and hematite 2*

Chlorite 4 and hematite 2 are the latest minerals in the paragenetic sequence. Hematite 2 forms irregular shaped clusters up to 500 μm diameter, that infills fractures in sphalerite and epidote as well as overgrowths on garnet (Fig. 5.23). Hematite also occurs as small needle shaped laths within chlorite 4.

**MD ignimbrite hosted mineralisation**

The basal 34m (vert.) of the MD ignimbrite in drill hole PD0032 and the underlying LP breccia have been pervasively altered to a mineral assemblage similar to that described for the southern zone. Alteration of the MD ignimbrite has been described in Section 4.3.6 and is summarised below. This description applies equally to the underlying LP breccia. Minor sulphide mineralisation also occurs in thin veins at higher levels in the MD ignimbrite.

*Basal 34m of the MD ignimbrite in drill hole PD0032*

Marble clasts in the LP breccia and overlying MD ignimbrite have been altered to tremolite ± epidote ± Ca-Mn-Mg-Fe carbonate 3 ± trace amounts of pyrite 3, chalcopyrite 4, sphalerite 4 and galena 2. Lithic clasts have been partially altered to sericite, chlorite and Ca-Mn-Mg-Fe carbonate 3. The groundmass has been pervasively altered to finely crystalline, felted, sericite, chlorite, quartz, serpentinite, Ca-Mn-Mg-Fe carbonate 3 and trace amounts of pyrite 3, chalcopyrite 4, sphalerite 4, galena 2, and hematite 2 (Figs. 4.20a - i).

Fig. 5.21. Drill hole PD0032, 383.25 m, (southern zone). Transmitted light photomicrograph. Crystals of sphalerite 2 (S2) have been corroded, and overgrown by Ca-Mn-Mg-Fe carbonate 3 (C3), chlorite 3 (CH3) and tremolite (T). Chlorite 3 and tremolite have been overgrown by quartz 3 (Q3). Quartz 3 has partially replaced tremolite but not chlorite 3. Ca-Mn-Mg-Fe carbonate 3 has a pale brownish colour with a pinkish hue.

Fig. 5.22. Drill hole PD0032, 392.6 m, (southern zone). Transmitted light photomicrograph. Corroded remnants of sphalerite 2 (S2), galena 1 (and 2?; GN) have been overgrown by later epidote (E), garnet (G) and rhodochrosite (R).

Fig. 5.23. Drill hole PD0032, 392.6 m, (southern zone). Photomicrograph, transmitted light. Sphalerite 2 (S2) and garnet (G) have been overgrown by hematite 2 (H2).

Fig. 5.24a. Drill hole PD0032, 120.65 m (105 m vert.), southern zone. Hand specimen of an altered marble clast within the MD ignimbrite. The marble clast has been altered to concentric bands with variable amounts of disseminated fine-grained pyrite calcite and sericite.

Fig. 5.24b. Drill hole PD0032, 170m (148 m vert.), southern zone. Photomicrograph, low level transmitted light. A quartz (Q'), sphalerite (S), galena (G), chlorite, carbonate (C) vein has cross-cut welded MD ignimbrite (MD). Euhedral quartz crystals have later quartz overgrowths (Q''). The MD ignimbrite has a well developed eutaxitic texture.

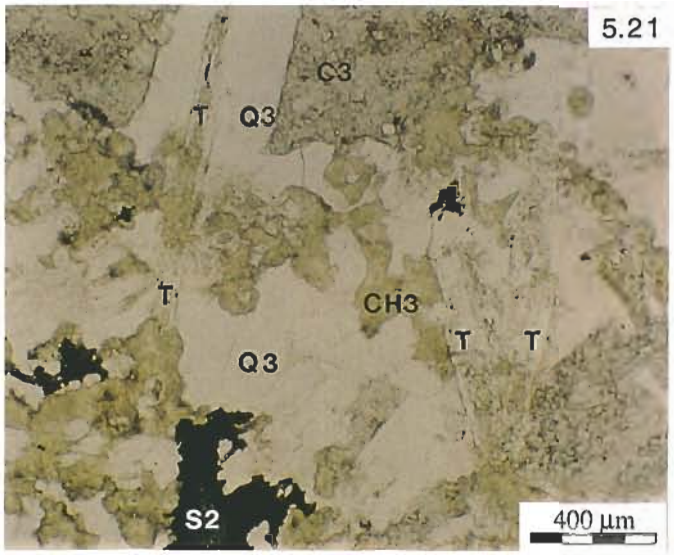
5.21
C3
T
Q3
T
CH3
T
T
Q3
S2
400 µm

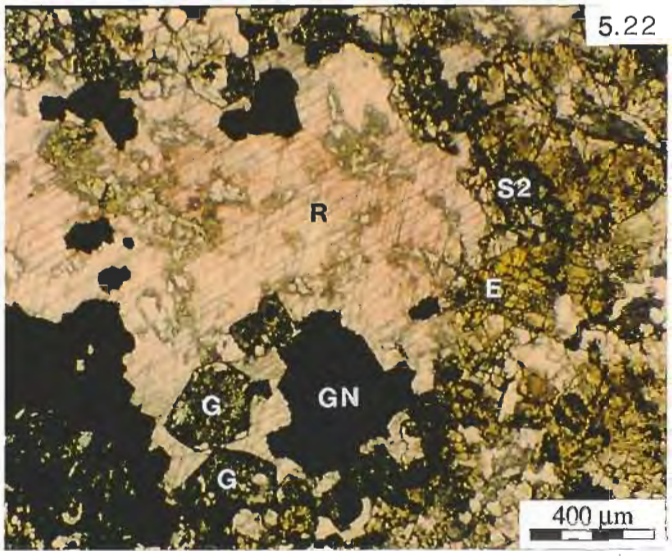
5.22
S2
R
E
G
GN
G
400 µm

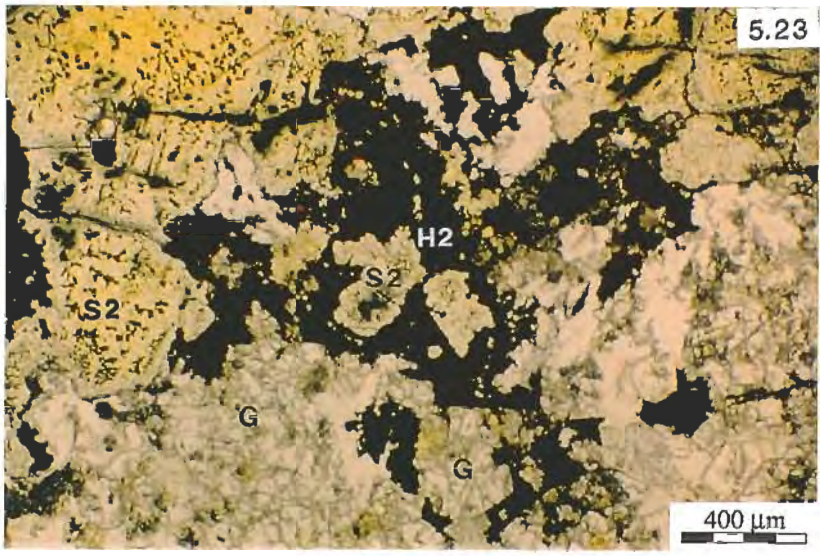
5.23
H2
S2
S2
G
G
400 µm

5.24a
2 cm

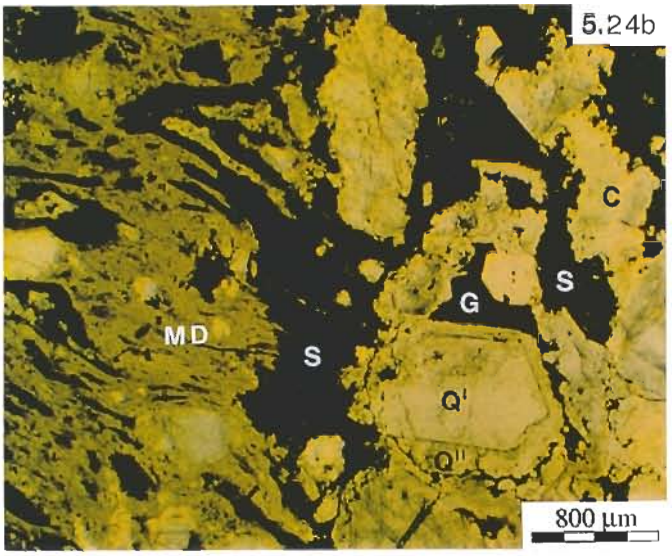
5.24b
C
S
G
MD
S
Q'
Q''
800 µm

The paragenesis of sericite, chlorite, quartz and some carbonate in the MD ignimbrite is uncertain as they may equally have been associated with either the late alteration overprint or with devitrification of the volcaniclastics.

A 30 cm marble clasts occurs completely enclosed within altered MD ignimbrite at 245.7m (30.8m from the base) in drill hole PD0032. The marble clast has been crosscut by a sulphide-bearing vein that does not extend beyond the clast margin. The sulphide minerals have identical mineralogy, textures and paragenesis to southern zone, marble-hosted mineralisation (Section 5.2.3). Both the enclosing ignimbrite, marble clast, and mineralisation have been partially altered to chlorite 3, Ca-Mn-Mg-Fe carbonate 3, and quartz 3 with minor amounts of epidote, tremolite, talc, pyrite 3, sphalerite 4, chalcopyrite 4 and galena 2 and trace amounts of graphite.

*Higher levels in the MD ignimbrite*

Some marble clasts > 34m from the base of the MD ignimbrite have been altered to a pattern of concentric, alternating bands of finely crystalline pyrite 3, carbonate and sericite (Fig. 5.24a). The alteration bands approach a sub-spherical or ellipsoidal shape irrespective of the angularity of the original marble clast.

A 5 mm wide quartz 3 - calcite - sphalerite 4 - galena 2 - pyrite 3 - chlorite 3 vein crosscuts welded MD ignimbrite at 96.5m (vert.) from the base of the MD ignimbrite in drill hole PD0032 (Fig. 5.24b).

*Sulphides in percussion drill holes*

Percussion drill holes to the south of drill hole PD0032 intersected either MD ignimbrite, granite dyke or rhyolite intrusion (Appendix 3.1). MD ignimbrite from these drill holes has been pervasively altered to chlorite 3, quartz 3, carbonate ± epidote ± tremolite with traces of disseminated pyrite 3, chalcopyrite 4, sphalerite 4 and galena 2.

## 5.4 Chemical analysis of mineralised zones

Many ore bodies have a vertical and / or lateral zonation in their mineralogy and the abundance of sulphide and gangue minerals (eg. Gilman, Colorado, Beaty and Merchant, 1990; VHMS deposits, Large, 1992; porphyry copper deposits, Beane and Titley, 1981) Variations in mineral abundances have a corresponding variation in their constituent elements, therefore, examination of the whole rock chemistry can be used to examine mineralogical abundances. The aim of this section is to examine prospect scale mineral variations using the existing geochemical database.

With the exception of drill hole PD0018 and the upper part of drill hole PD0021, all drill holes have been assayed throughout their length for a range of elements including Pb, Zn,

Cu, Ag, Mn, Fe and less commonly, Au, Hg, As, Sn, W and Ba. Samples for analysis were collected by grinding a strip along the length of non-mineralised core and collecting the powder for each interval of between 2 - 6 m. Core which contained visible sulphides was quartered. Samples were submitted to commercial laboratories for analysis using either atomic absorption spectrometry (AAS) or X-ray fluorescence (XRF). Summary geochemical logs for each of the 32 diamond drill holes are illustrated in Appendix 3.1. Analyses of mineralised core intervals, below the zone of weathering are presented in table format in Appendix 5.2.

Only assays from samples below the zone of weathering that have either Pb or Zn greater than 1000 ppm (0.10 wt.%) are used throughout this section. Assay values for the northern and central zone, and the southern zone are summarised in Tables 5.2 and 5.3 respectively.

Table 5.2 Summary of chemical analyses of mineralisation from the northern and southern zones. Only samples that have Pb or Zn > 0.10 wt.% have been included.

| Element | Number of analyses | Range | Median | Average |
|---|---|---|---|---|
| Pb (wt.%) | 878 | 0 - 44.60 | 0.24 | 1.36 |
| Zn (wt.%) | 878 | 0.0046 - 40.00 | 0.38 | 1.82 |
| Cu (ppm) | 878 | 0 - 6950 | 46 | 244 |
| Ag ppm | 878 | 0 - 900 | 4 | 16 |
| Mn (wt.%) | 877 | 0 - 16.00 | 0.43 | 0.86 |
| Fe (wt.%) | 878 | 0 - 24.70 | 2.82 | 3.84 |
| Au (ppm) | 81 | 0 - 0.450 | 0.019 | 0.046 |
| Hg (ppm) | 85 | 0 - 0.390 | 0.025 | 0.053 |
| As (ppm) | 49 | 0 - 569 | 54 | 110 |
| Sn (ppm) | 31 | 0 - 22 | 5 | 6 |
| W (ppm) | 55 | 0 - 3240 | 184 | 509 |
| Ba (ppm) | 38 | 10 - 793 | 142 | 200 |

Table 5.3 Summary of chemical analyses of mineralisation from the southern zone. Only samples that have Pb or Zn > 0.10 wt.% have been included. Hg, As, Sn, W, and Ba were not analysed.

| Element | Number | Range | Median | Average |
|---|---|---|---|---|
| Pb (wt.%) | 79 | 0.007 - 3.46 | 0.16 | 0.51 |
| Zn (wt.%) | 79 | 0.0026 - 13.25 | 0.26 | 1.76 |
| Cu (ppm) | 79 | 10 - 5470 | 86 | 459 |
| Ag ppm | 79 | 0 - 154 | 1 | 11 |
| Mn (wt.%) | 79 | 0.002 - 1.73 | 0.45 | 0.59 |
| Fe (wt.%) | 79 | 0.7 - 25.73 | 4.34 | 4.85 |
| Au (ppm) | 3 | 0.010 - 0.036 | 0.021 | 0.022 |

### 5.4.1 Spatial variations in mineralisation chemistry

Variations in metal abundances over the length of the prospect are illustrated in Figures 5.25a - g. Diagrams have a bell shaped distribution with the highest analyses in the vicinity of 9000 mN and tailing off to both the north and south. The absence of data in the vicinity of 8500 mN does not necessarily represent an absence of mineralisation, but rather the paucity of drilling and the extreme depth of weathering.

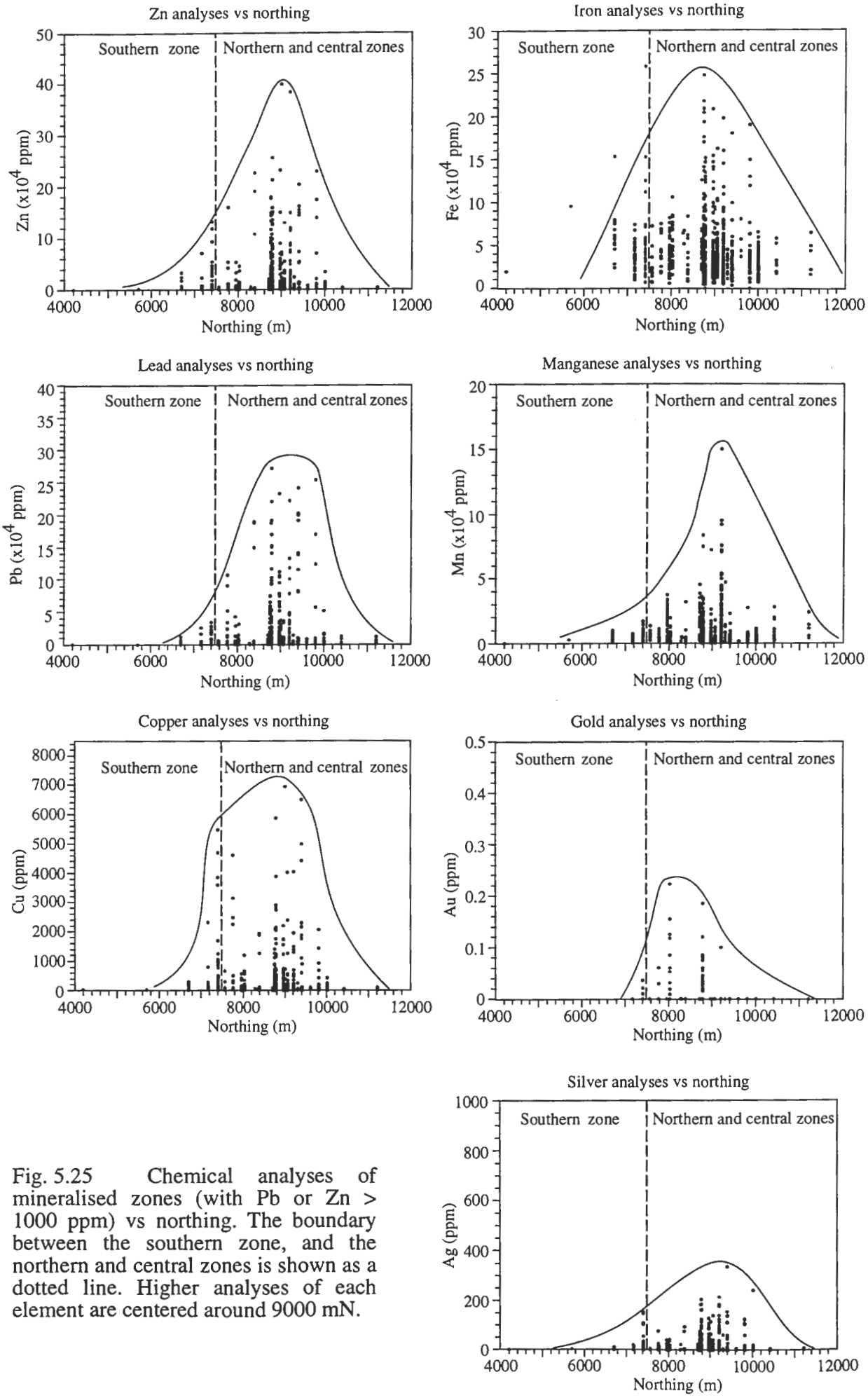


Fig. 5.25 Chemical analyses of mineralised zones (with Pb or Zn > 1000 ppm) vs northing. The boundary between the southern zone, and the northern and central zones is shown as a dotted line. Higher analyses of each element are centered around 9000 mN.

There is no systematic variation between metal values or metal ratios with depth below the zone of weathering. Insufficient analyses for As, W and Sn are available for investigation of spatial variances.

*Copper to zinc ratios*

Copper to zinc ratios (100 Cu / Cu + Zn) for the southern zone and the combined northern and central zones are illustrated in Figure 5.26. Copper ratios are commonly higher in the southern zone compared to the combined northern and central zones.

## 5.5 Mineral chemistry

Sulphide mineralisation at Menninnie Dam averages ≈ 0.84 wt.% manganese with a maximum of 16 wt.%. Silver is present in concentrations up to 900 ppm and typically ≈ 16 ppm. Analyses of up to 3240 ppm tungsten have been recorded from mineralisation in the northern and central zones. Up to 3% of rhodochrosite ($MnCO_3$) is present in the southern zone and may account for analyses with elevated Mn. The only obvious Mn-bearing mineral in the northern and central zones is trace amounts of rhodonite [$(Mn,Ca,Fe)SiO_3$] which cannot account for the high Mn analyses of mineralised zones. Similarly, no silver or tungsten-bearing minerals have been observed throughout the Menninnie Dam prospect. The aim of this section is to identify the host minerals to Mn, Ag and W using the electron microprobe.

### 5.5.1 Method

Variation diagrams with Ag, W, or Mn plotted against other elements were used to establish element correlations. Elements with a significant correlation were then related to a likely host mineral (eg. Pb and galena). The likely host mineral was analysed for either Ag, Mn or W using the electron microprobe in the Central Science Laboratory, University of Tasmania under the supervision of W. Jablonski. Analytical results are detailed in Appendicies 5.3 - 5.5.

### 5.5.2 Results

*Silver*

Pb and Ag analyses from mineralisation in the northern and central zones have a positive correlation with a correlation coefficient of 0.50 (Fig. 5.27a). Pb and Ag analyses from mineralisation in the southern zone do not have an obvious correlation (Fig. 5.27b). Bismuth and silver were identified by electron microprobe analysis of galena 1 from the northern and central zones and galena 1 and 2 from the southern zone (Table 5.4 and Appendix 5.3). Silver and bismuth from analyses of galena 1 in the northern and central zones have a positive correlation (correlation coefficient of 0.77; Fig. 5.27c).

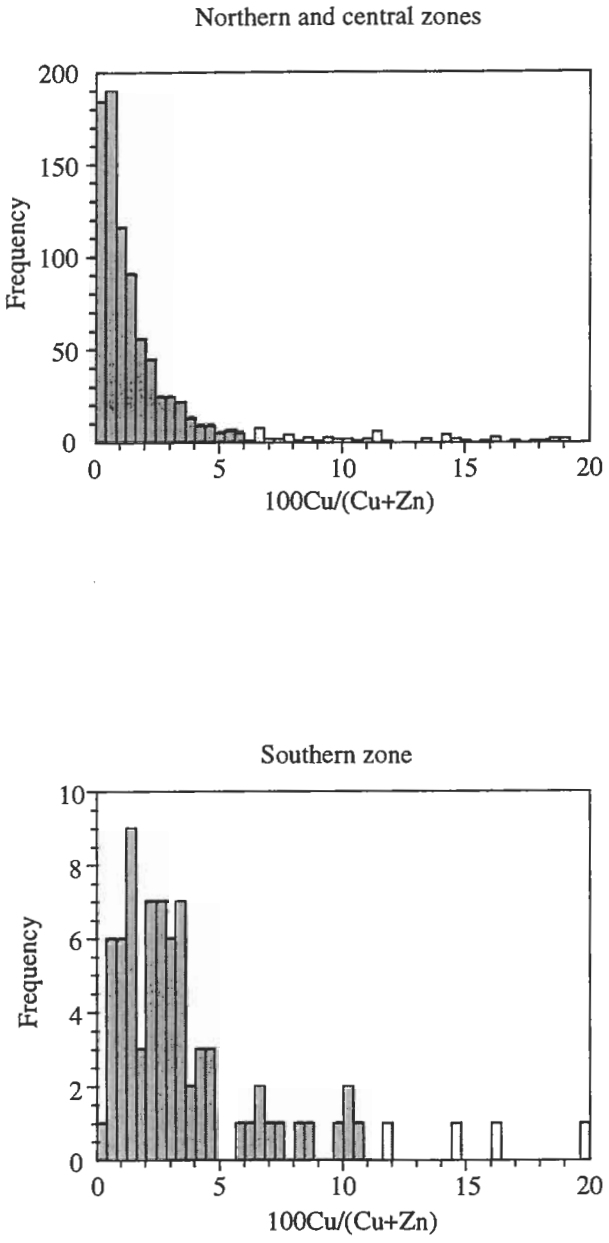


Fig. 5.26 Frequency diagrams of copper : zinc ratios for the northern and central zones, and for the southern zone.

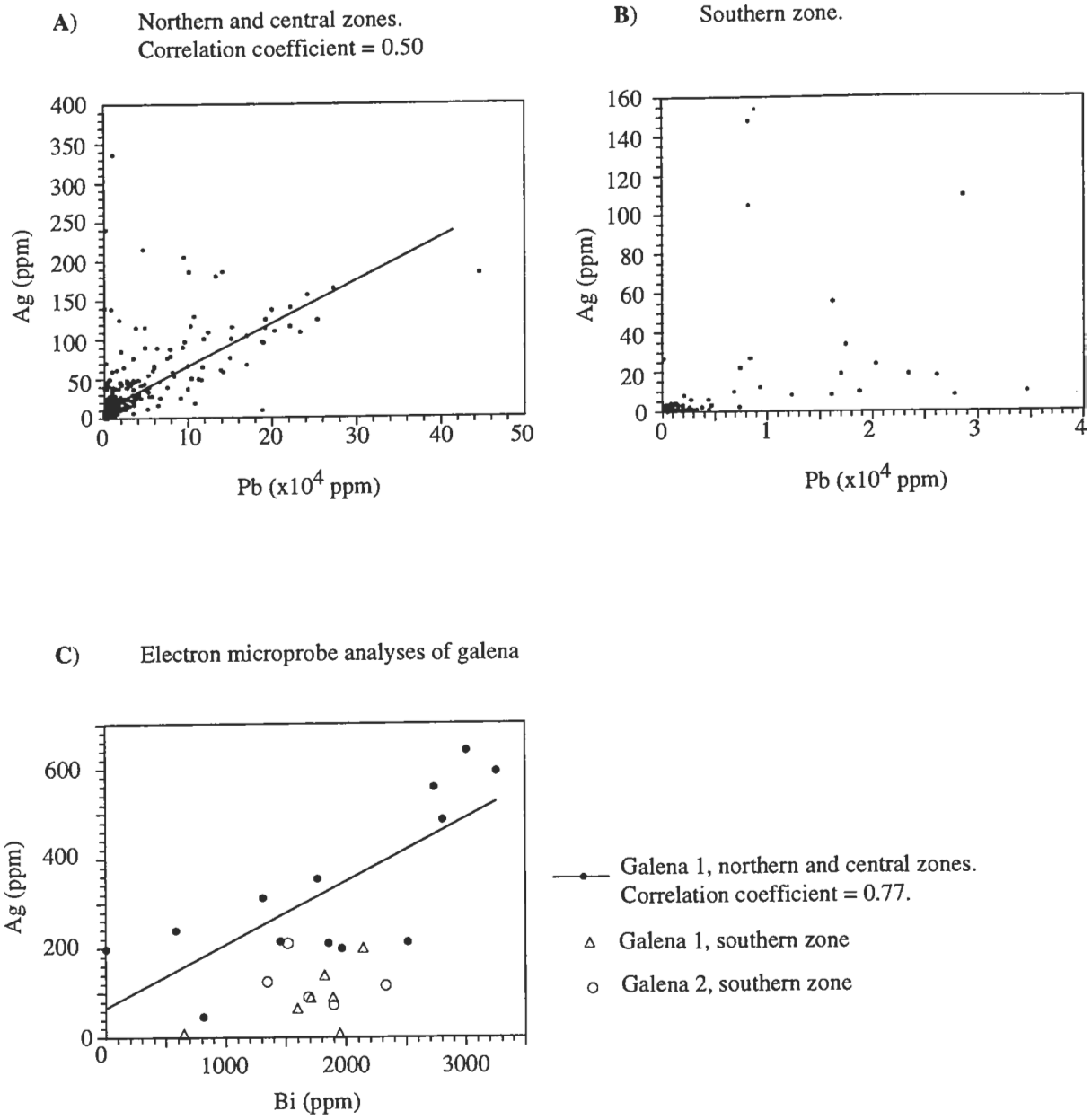


Fig. 5.27 A) Drill hole analyses for lead and silver in the northern and central zones. B) Drill hole analyses for lead and silver in the southern zone. C) Electron microprobe analytical results for silver and bismuth in galena 1 and 2 from the northern and central zones, and the southern zone.

Insufficient data are presented to enable assessment of a correlation between Bi and Ag in galena 1 and 2 from the southern zone. The trace element chemistry of galena 1 and galena 2 from all three zones is similar and they cannot be distinguished on the basis of the data presented.

Table 5.4 Trace element compositions of galena 1 and 2

| Zone | Mineral paragenesis | Element | Detection limit (ppm) | Number of analyses | Range (ppm) | Median (ppm) |
|---|---|---|---|---|---|---|
| Northern and central | galena 1 | Ag | 62 | 13 | 46 - 639 | 238 |
| " | | Bi | 283 | 13 | 0 - 3253 | 1857 |
| " | | Sb | 300 | 13 | below dectn. | |
| Southern | galena 1 | Ag | 62 | 7 | 0 - 203 | 91 |
| " | | Bi | 283 | 7 | 651 - 2136 | 1810 |
| " | | Sb | 300 | 7 | below dectn. | |
| Southern | galena 2 | Ag | 62 | 5 | 75 - 214 | 120 |
| " | | Bi | 283 | 5 | 1331 - 2316 | 1674 |
| " | | Sb | 300 | 5 | below dectn. | |

*Manganese*

Variation diagrams involving Mn and other elements produce a scatter with no obvious correlations. Pyrite rarely contains significant Mn, however, sphalerite can accommodate up to a few percent of Mn (Deer et al. 1978). Electron microprobe analyses of sphalerite 2 from the northern, central and southern zones shows significant quantities of iron, manganese and cadmium. There is no appreciable difference in Cd and Mn contents of sphalerite 2 from the northern and central zone, and sphalerite 2 from the southern zone (Table 5.5 and Appendix 5.4).

Table 5.5. Mn, Cd and Fe contents of sphalerite 2 from the northern, central and southern zones.

| Zone | Element | Detection limit (ppm) | Number of analyses | Range (ppm) | Median (ppm) |
|---|---|---|---|---|---|
| Northern and central | Mn | 202 | 21 | 410 - 6449 | 2990 |
| " | Cd | 290 | 24 | 1160 - 2436 | 1760 |
| " | Fe | 0.020 wt.% | 29 | 1.14 - 4.32 wt.% | 4.08 wt.% |
| Southern | Mn | 202 | 4 | 2019 - 3703 | 2811 |
| " | Cd | 290 | 4 | 1769 - 2237 | 1953 |

A small number dolomite, Ca-Mn-Mg-Fe carbonate 2 and late calcite veins were analysed using the electron microprobe. Results are illustrated in Figure 5.28 and detailed in Appendix 5.5. Dolomites and late calcite veins are close to end member dolomite and calcite compositions respectively. Ca-Mn-Mg-Fe carbonate 2 has a range of compositions that lie between kutnahorite, calcite, ankerite and dolomite and constitutes a significant reservoir of manganese. The compositional variations in Ca-Mn-Mg-Fe carbonate 1, 2 and 3 have not systematically been investigated, and although such a study has merit, it is not consistent with the aims of this thesis.

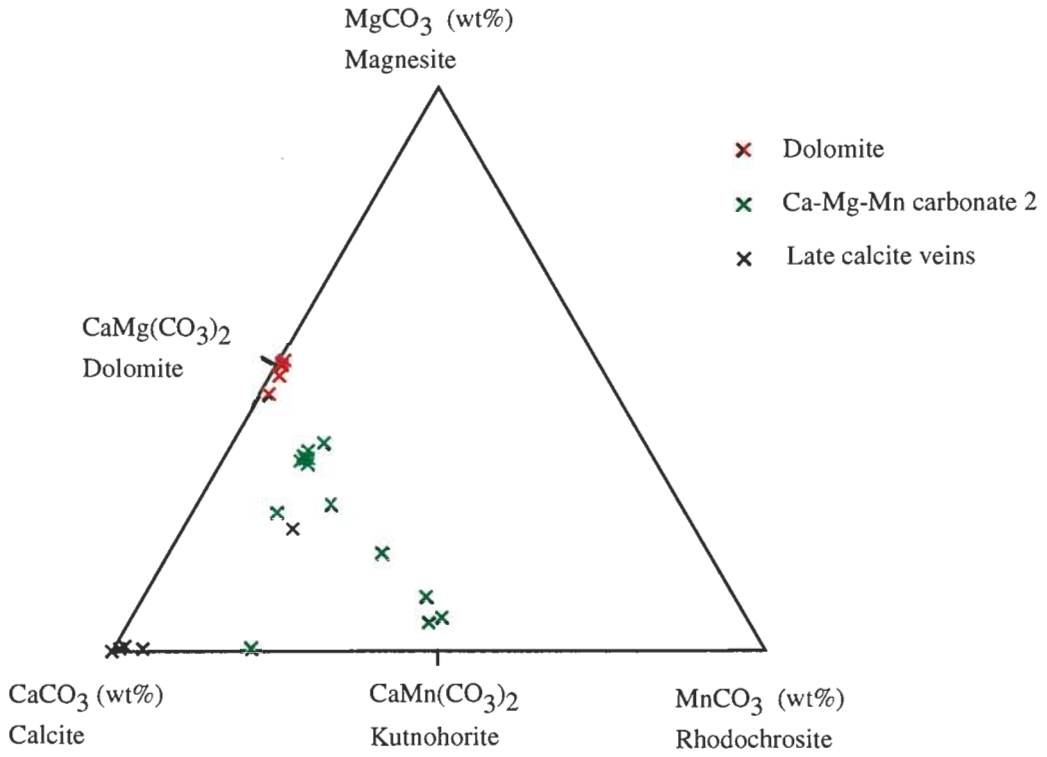


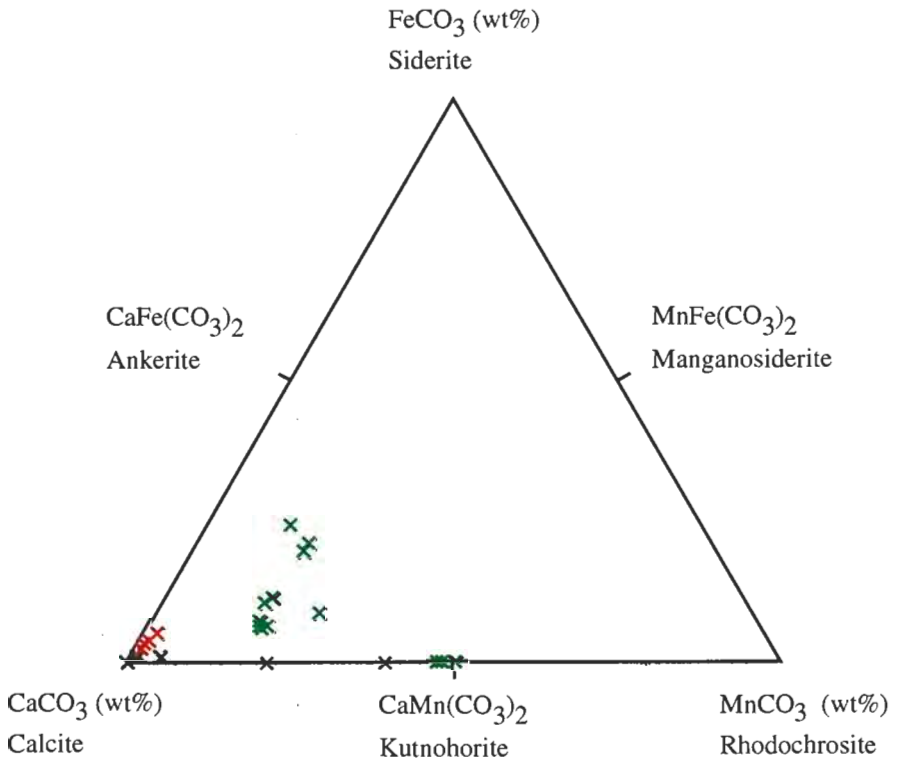


Fig. 5.28 Electron microprobe analysis of dolomite, Ca-Mn-Mg-Fe carbonate 2 and the late vein calcite.

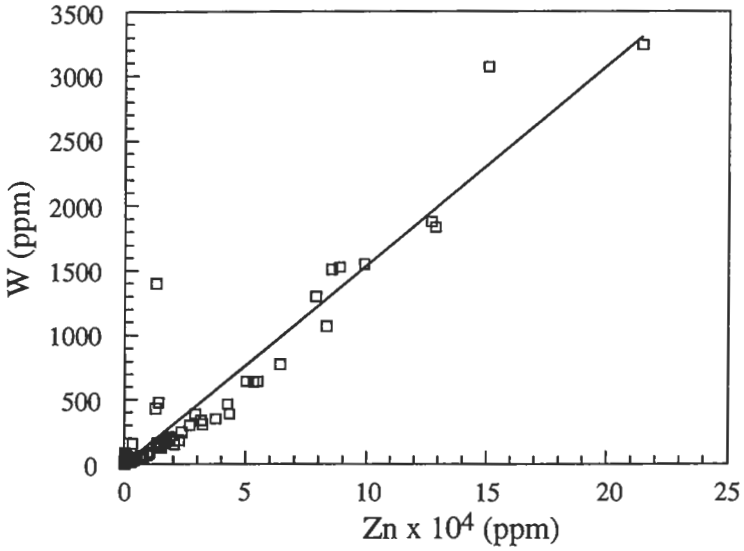


Fig. 5.29. Tungsten vs Zinc variation diagram of drill core analyses from the northern and central zones. Tungsten and zinc have a positive correlation with a correlation coefficient of 0.96.

*Tungsten*

W and Zn analyses from mineralisation in the northern and central zones have a positive correlation with a correlation coefficient of 0.96 (Fig. 5.29). No tungsten bearing minerals have been detected despite examination of 167 thin sections and ultraviolet light irradiation of both thin sections and core. Sphalerite and all other minerals from samples with high tungsten contents were analysed using the electron microprobe to produce back scattered element maps. No tungsten was detected.

## 5.6 Discussion

In this section, the relative timing of sulphide mineralisation and the host rocks, metamorphic events, rhyolite intrusions and the MD ignimbrite are interpreted from mineral textures. The association of mineralisation and brittle deformation, the spatial distribution of mineralisation, and attributes of the mineral chemistry are also discussed.

### 5.6.1 Sulphide textures

The host rocks to mineralisation have undergone upper amphibolite facies metamorphism (Section 3.3.3). Sulphide and gangue mineral textures in the northern, central and southern zones are not consistent with those expected in high grade metamorphic terrains. Inconsistencies include:

- Sulphide and gangue minerals form veins, stockwork and breccias and have clearly replaced the host marble and calc-silicate lithologies (Figs. 5.1b - e and 5.3a, 5.3a, b, 5.11a -c)
- Adjacent sulphide or gangue minerals have not formed polygonal contacts (most Figs. from 5.3a - 5.24b).
- Growth zoning in sphalerite 1, sphalerite 2, and quartz 1 is preserved and unlikely to have survived upper amphibolite facies metamorphism (Figs. 5.5a, b, 5.6a, b, 5.16a, c).
- Sphalerite 2 contains broad growth twins which are unlikely to have survived upper amphibolite facies metamorphism (Figs. 5.5d and 5.16e).
- Some sulphide and gangue minerals contain abundant inclusions of other minerals (eg. inclusions of chalcopyrite 2 in sphalerite 2; Figs. 5.5a - c, 5.16a -c). High grade metamorphism commonly results in 'refining' of minerals and 'expulsion' of inclusions (Turner, 1980).
- Finely crystalline minerals such as dolomite, talc 1 and 2, phlogopite, sericite 1 and 2, quartz 1 and Ca-Mn-Mg-Fe carbonate 1, 2 and 3 and chlorite 1, 2 and 3 have not been recrystallised as might be expected at higher metamorphic grades (Figs. 5.3a, b, 5.11b, c).
- Adularia is a disordered form of K-feldspar more commonly associated with low temperature epithermal systems (Henley et al. 1984; Figs. 5.4a - c).

- The gangue minerals talc 1 and 2, chlorite 1, 2 and 3, and epidote are not stable under the peak P - T conditions interpreted for the Menninnie Dam host rocks (Turner 1980 and Section 3.3.3).
- Sulphides have post dated deformation and locally, veins containing growth zoned sphalerite 2 have crosscut mylonitic textures (Fig. 5.12c).
- Sulphides have post dated emplacement of granite dykes which were interpreted to postdate upper amphibolite facies metamorphism (Section 3.8.3; Fig. 5.12b)
- Sulphide minerals have locally overprinted minerals interpreted to have formed during metasomatism (Fig. 5.3g).

Based on the interpretation of sulphide and gangue mineral textures, mineralisation cannot have been deposited at the same time as the host rocks and clearly post-dated peak metamorphism (KM-$D_{1-2}$), retrograde metamorphism (KM-$D_3$), granite dyke emplacement, and metasomatism.

### 5.6.2 Paragenetic stages

*Northern and central zones*

The sulphide and gangue mineral paragenesis has been divided into four stages (Fig. 5.2):

- An early pyrite stage
- A sphalerite - galena stage
- A late pyrite stage
- A late vein stage.

The early pyrite stage is associated with the dissolution of marble or diopside and the initial precipitation of dolomite, chlorite 1 ± talc 1 ± phlogopite, pyrite 1, and adularia. The start of the sphalerite - galena stage is marked by partial alteration of adularia to finely crystalline sericite 1. Sericite 1 was followed by sphalerite 1 and chalcopyrite 1, sphalerite 2 and chalcopyrite 2, quartz 1, Ca-Mn-Mg-Fe carbonate 1 and galena 1. The late pyrite stage is marked by the re-appearance of sericite (sericite 2) as well as chlorite 2 ± rhodonite + pyrite 2 followed by fluorite and Ca-Mn-Mg-Fe carbonate 2 respectively. The late vein stage consists of rare crosscutting veins of quartz 2 and common calcite veins (late calcite veins). The relationship between mineralisation and the late calcite veins is uncertain.

*Southern zone*

The sulphide and gangue mineral paragenesis in the southern zone is subdivided into four stages (Fig. 5.15):

- An early pyrite stage
- A sphalerite - galena stage
- A chlorite - quartz - carbonate - calc-silicate stage
- A late hematite stage

The early pyrite, and sphalerite - galena stages have similar mineralogy, textures and paragenesis to the early pyrite, and sphalerite - galena stages of the northern and central zones. The chlorite - quartz - carbonate - calc-silicate stage and the late hematite stage have been collectively termed the 'late alteration overprint'.

The apparent absence of chlorite 1 and sericite 1 in the early pyrite and galena - sphalerite stages of the southern zone is interpreted to have resulted from overprinting of these minerals by the late alteration overprint. The apparent absence of adularia in the southern zone is interpreted to have resulted from either local non-deposition of adularia or alteration of adularia during the late alteration overprint. Feldspar does not appear to have been a stable phase throughout the late alteration overprint, and feldspar in granite dykes has been altered to felted, finely crystalline chlorite, sericite, calcite and quartz (Fig. 5.13).

### 5.6.3 Association of mineralisation with fractures and brittle faults

Mineralisation and gangue textures are not typical of open space vein-fill and are interpreted to have resulted from replacement of host rock marble or diopside. Textures are interpreted to be consistent with replacement of marble along crystal margins and twin planes (Figs. 5.3a, 5.3b, c) and replacement of diopside along fractures and cleavage planes (Figs. 5.11a - c). In many hydrothermal systems such as skarns, Mississippi Valley Type deposits and carbonate replacement Pb - Zn - Ag bodies, carbonate is a reactive rock type and commonly host to mineralisation. While marble is commonly hosts mineralisation at Menninnie Dam, a significant amount of mineralisation is hosted by diopsidic units.

Diopsidic units that are host to mineralisation are invariably fractured or brecciated, and mineralising fluids are interpreted to have preferentially permeated along fractured or brecciated zones (Figs. 5.11a). Brittle deformation of diopside is interpreted to have resulted from competency contrasts between diopside and adjacent marbles or quartz units during deformation associated with KM-$D_3$ (Section 3.5.2), or following KM-$D_3$.

Marbles do not have a well developed network of fractures or breccia zones similar to that of diopsidic units and this may be due to recrystallisation of marble units. Rarely, fracturing of marbles has been observed (Fig. 5.1e) and in such instances, fracturing is interpreted to have post-dated KM-$D_3$. Despite the apparent absence of a fracture network in marble units, mineralisation hosted by marbles is interpreted to have been associated with faulting.

Some sulphide textures are consistent with post-depositional deformation and others are interpreted to have resulted from syn-depositional deformation. Pyrite 1 locally has a jigsaw-fit breccia texture and has been overgrown by galena 1 that has a straight cleavage pattern (Fig. 5.3h). The margins of sphalerite 2 have locally undergone dynamic recrystallisation resulting in formation of sphalerite 3. Growth twins in sphalerite 2 adjacent

to sphalerite 3 have been replaced by stress twins (Fig. 5.5e). Recrystallised sphalerite 3 does not contain chalcopyrite inclusions and is locally overgrown by chalcopyrite 3, interpreted to have been expelled from sphalerite 2 during dynamic recrystallisation. Chalcopyrite 3 is overgrown by galena 1 with a straight cleavage pattern (Fig. 5.5f). Brecciated pyrite 1 and sphalerite 2 fragments are locally overgrown by undeformed pyrite 3 (Fig. 5.9). Fractures and brittle fault structures may have been important fluid conduits during the mineralising event with permeability maintained through syn-mineralisation faulting.

### 5.6.4 Inclusions of chalcopyrite in sphalerite

Mechanisms that result in small inclusions of chalcopyrite in sphalerite are contentious and a variety of processes have been proposed including:

- Recrystallisation or exsolution of copper and iron-bearing sphalerite (Ramdohr 1969).
- Replacement of FeS in sphalerite by a hot copper-bearing solution ('chalcopyrite disease'; Barton, 1978; Eldridge et al., 1983; Barton and Bethke, 1987; Eldridge et al., 1988; Kojima and Sugaki, 1987).
- Co-precipitation of sphalerite and chalcopyrite (Kojima, 1990; Bortnikov et al., 1991)
- Replacement of sphalerite by chalcopyrite with introduction of both copper and iron (Bortnikov et al., 1991)
- Solid state diffusion (Bente and Doering, 1993).

Barton and Bethke (1987) described a number of different textures of chalcopyrite inclusions in sphalerite. 'Watermelon', 'dusting' and 'bimodal' textures were attributed to replacement of FeS by copper rich fluids. 'Bead chain' textures were attributed to exsolution and 'orchard textures' were tentatively attributed to co-precipitation. Chalcopyrite diseased sphalerite was produced experimentally by Kojima and Sugaki (1987) and Eldridge et al. (1988) by reacting hot copper-bearing solutions with natural sphalerite. Chalcopyrite was demonstrated to have replaced FeS in sphalerite. Experiments by Kojima (1990) demonstrated that some chalcopyrite disease textures could be produced by co-precipitation of chalcopyrite and sphalerite by cooling of a solution supersaturated with respect to both sphalerite and chalcopyrite.

Bortnikov et al. (1991) suggested that replacement of FeS by copper-rich fluids may have occurred in some cases, but was not the sole cause of chalcopyrite disease. Either co-precipitation of sphalerite and chalcopyrite, or replacement of ZnS by chalcopyrite were interpreted to have occurred in a number of Russian deposits. Bortnikov et al. (1991) suggested in the absence of volume changes, the replacement of ZnS and FeS in sphalerite by copper rich solutions should be associated with evidence for zinc mobility. Bortnikov et al. (1991) also suggested that in many deposits where chalcopyrite inclusions were attributed

to co-precipitation, there was little correlation between the iron content of sphalerite and the occurrence of chalcopyrite inclusions.

Solid state diffusion experiments by Bente and Doering (1993) produced many of the chalcopyrite - sphalerite textures seen in nature and they proposed the term "diffusion induced segregations" (DIS) to replace the term chalcopyrite disease. There findings included (among others):

- Significant DIS reactions can occur at temperatures below 300°C.
- There is a minimum Fe content below which no DIS are produced.
- Following precipitation of an Fe-bearing sphalerite, an increase in the sulphur fugacity of the fluid is required for the formation of DIS.
- DIS textures depend on the Fe content of sphalerite, time , temperature, the Cu : Fe ratio in the diffusing source and the sulphur fugacity.
- During formation of DIS, the Fe content of sphalerite is not only used to form DIS-phases, but Fe is also removed from sphalerite resulting in depletion of Fe in sphalerite.

*Inclusions of chalcopyrite in sphalerite in the northern and central zones*

Chalcopyrite disease (or DIS) is ubiquitous in sphalerite 1 and 2 throughout the northern and central zones of the Menninnie Dam prospect and has similar textures to the orchard texture described by Barton and Bethke (1987; Figs. 5.5a - c), however there is no evidence for a later, hotter, Cu rich fluid having overprinted sphalerite 2. Apart from local dynamic recrystallisation around the margin of sphalerite 2, there is no evidence for zinc mobility after deposition of sphalerite 2. Dynamic recrystallisation of sphalerite 2 has resulted in local segregation of chalcopyrite 3 from sphalerite 3 (Fig. 5.5f). Sphalerite 2 with chalcopyrite disease (or DIS) is commonly completely enclosed within quartz 1 or galena 1 interpreted to indicate either co-precipitation of sphalerite 2 and chalcopyrite 2, or, introduction of chalcopyrite 2 immediately after deposition of sphalerite 2 and prior to deposition of quartz 1 and galena 1. On the basis of textural evidence, chalcopyrite 1 and 2 are interpreted to be part of the sphalerite - galena stage and not related to a later, hot copper-bearing fluid.

*Inclusions of chalcopyrite 2 in sphalerite 2 in the southern zone at Menninnie Dam*

The late alteration overprint is interpreted to have resulted in dissolution, and re-deposition of pre-existing sulphides, particularly sphalerite 2, galena 1 and chalcopyrite 2 (Figs. 5.16a, c, 5.19a, b, 5.17, 5.20a, b). The lighter colours of the mid and outer sectors of sphalerite 2 in the southern zone compared to sphalerite 2 in the northern and central zones is interpreted to have resulted from removal of iron by fluids associated with the late alteration overprint (Figs. 5.16a, c). Chalcopyrite 2 inclusions in the mid and outer sectors of sphalerite 2 in the southern zone are commonly absent or smaller than those in the inner sector (Figs. 5.16a, c). The distribution and size of chalcopyrite 2 inclusions in sphalerite 2 is interpreted to have

resulted from partial, or complete, dissolution of chalcopyrite 2 in the mid and outer sectors of sphalerite 2 and local re-deposition as chalcopyrite 4 at the margins of sphalerite crystals. Veins of sphalerite 4, chalcopyrite 4 and pyrite 3 that crosscut sphalerite 2, rinds of galena 1 on sphalerite 2, and replacement of galena 1 by sphalerite 4 are interpreted as evidence for sulphide dissolution and re-precipitation (Figs. 5.16a - d; 5.17; 5.19a, b; 5.20a, b).

### 5.6.5 Spatial distribution of metals

Analytical values of lead, zinc, manganese, iron, copper, silver and gold commonly have a maxima centred around 9000 mN and progressively lower values to the north and south. The bell shaped distribution of analytical values (Fig. 5.25) is interpreted to have resulted from a single mineralising system whose conduit zone was centred around 9000 mN. A single mineralising system is also interpreted to account for the spatial distribution of mineralisation styles with stockwork and vein style mineralisation between 8200 mN and 9200 mN, flanked by vein style mineralisation to the north and south.

The copper to zinc ratio of the southern zone is higher than that of the northern and central zones (Fig. 5.26) and is interpreted to have resulted from either introduction of minor amounts of copper during the late alteration overprint, or local dissolution and removal of zinc. In the absence of unequivocal evidence for the introduction of copper during the late alteration overprint, removal of zinc is considered more likely.

### 5.6.6 Mineral chemistry

*Silver*

Van Hook (1960) demonstrated that argentite ($Ag_2S$) has a maximum solubility in PbS of 0.4 mole % at 700°C, which is probably close to the assumed maximum solubility at the binary eutectic temperature of 615°C in the PbS-AgS system. The solubility of AgS in galena is negligible below 455°C which is near the upper limit for most ore fluid temperatures (Van Hook, 1960). Assuming the mineralisation at Menninnie Dam formed from a fluid of < 455°C, then, if argentite was present in galena, it would be present as an exsolved phase. However, argentite has not been observed in galena from Menninnie Dam.

The solubility of AgS in galena increases dramatically in the presence of bismuth and antimony with coupled substitution of $Ag^{1+} + Bi^{3+}$ for $2Pb^{2+}$, or $Ag^{1+} + Sb^{3+}$ for $2Pb^{2+}$ (Van Hook, 1960). PbS forms a series of solid solutions with $AgBiS_2$ (matildite) or $AgSbS_2$ (miargyrite) above 215°C. At lower temperatures, matildite is commonly exsolved, although about 8 mole % of matildite may remain dissolved within the galena structure at room temperature (Van Hook 1960; Craig, 1967). The apparent absence of specific silver bearing minerals at Menninnie Dam and the occurrence of silver and bismuth in galena is best explained by solid solution of matildite in galena.

Galena from the Menninnie Dam prospect contains much more bismuth than can be accommodated in matildite alone. Van Hook (1960) noted the composition range of galena was not confined to the PbS-$AgBiS_2$ join line, and considerable amounts of $Bi_2S_3$ (up to 9 mole % outside the PbS-$AgBiS_2$ join line) could be accommodated.

*Tungsten*

The presence of tungsten in mineralised zones is questionable. No tungsten bearing minerals have been detected and tungsten could not be located within other minerals. The nature of the sample preparation techniques used by commercial laboratories prior to analysis of tungsten are unknown. Tungsten values of > 3000 ppm are considered unlikely to have been derived from contamination if a tungsten carbide mill was used for sample preparation. Tungsten and zinc have a positive, linear relationship and a correlation coefficient of 0.96 (Fig. 5.29). 'Tungsten-bearing samples' were analysed at Analabs, Perth, W.A., by XRF using the 1st order L beta and K beta peaks for tungsten and zinc respectively (pers. comm. A. Ronald, Analabs, Perth, W.A.). In the presence of significant amounts of zinc, the zinc K beta and the tungsten L beta peaks cannot be resolved. It seems likely that the presence of tungsten may have been misinterpreted in the presence of abundant zinc.

### 5.6.7 Relative timing of DP breccias and rhyolite dykes

The sulphide and gangue paragenesis established for the northern and central zones can be used to interpret a relative timing for formation of DP breccias. Sulphide and gangue minerals in sulphide clasts are paragenetically earlier than the late pyrite stage of mineralisation. The presence of pyrite 2 and trace amounts of galena 1 and sphalerite 2 as part of the alteration assemblage that affected the matrix of DP breccia is interpreted to indicate DP breccias formed near the end of the sphalerite - galena stage of mineralisation. DP breccias are interpreted to be temporally and genetically related to emplacement of rhyolite intrusions (Section 4.4.7), therefore, the timing of rhyolite intrusions is also interpreted to have occurred near the end of the sphalerite - galena stage of the mineralising event.

### 5.6.8 Relative timing of mineralisation, the MD ignimbrite and the late alteration overprint.

The relative timing of the mineralising event, deposition of the MD ignimbrite and the late alteration overprint can be established. LP breccias are interpreted as surficial deposits that resulted from DP breccia bodies erupting onto the palaeosurface (Section 4.4.7) and therefore also formed near the end of the sphalerite - galena stage of mineralisation. Sulphide mineralisation in the southern zone is interpreted to have been overprinted by the late alteration overprint. LP breccia and the basal 34m of the MD ignimbrite in drill hole PD0032 have been altered by the late alteration overprint (Section 5.3.2) and sulphide-bearing veins crosscut welded MD ignimbrite (Fig. 5.24b). The pattern of concentric

alteration bands in marble clasts in the MD ignimbrite is interpreted to have resulted from in-situ alteration (Fig. 5.24a). Therefore, the late alteration overprint is interpreted to have post dated both the mineralising event and emplacement, welding and cooling of the MD ignimbrite. The time period between the mineralising event and the late alteration overprint cannot be established from geological associations alone.

## 5.7 Summary

Sulphides in the northern and central zones have replaced marbles and calc-silicate lithologies of the central suite. Sulphides in the southern zone have replaced marble and calc-silicate lithologies of the eastern suite. Sulphide and gangue minerals form veins and stockwork style mineralisation. Stockwork and vein style mineralisation is more common between 8200 mN and 9300 mN flanked by vein style mineralisation to the north and south. Mineralisation in marbles is interpreted to have been associated with both pre-mineralisation and syn-depositional brittle faulting. Calc-silicate lithologies have been preferentially replaced along fractures and breccia zones. Sulphide clasts occur scattered throughout DP breccias and LP breccias and minor sulphides occur throughout the matrix of DP breccias and to a lesser extent, the matrix of LP breccias.

Sulphide and gangue minerals in the northern and central zones consist of a simple assemblage of pyrite, quartz, sphalerite, galena and Ca-Mn-Mg-Fe carbonate with minor amounts of chalcopyrite and chlorite and trace amounts of adularia, sericite, fluorite, rhodonite, talc, phlogopite, dolomite, hematite and matildite. Chalcopyrite occurs as inclusions in sphalerite and is interpreted to have resulted from either co-precipitation or was included immediately after sphalerite deposition. Sulphide and gangue minerals have not been metamorphosed and most primary textures are preserved. The sulphide and gangue mineral paragenesis has been used to interpret the a syn-mineralisation timing for rhyolite intrusion, and DP and LP breccia formation.

Pb, Zn, Mn, Fe, Cu, Ag and Au analytical values have bell shaped distributions that have a maxima at ≈ 9000 mN and decrease to both the north and south. Maximum assay values correspond with the zone of stockwork and vein style mineralisation. In the northern and central zones, manganese is incorporated in Ca-Mn-Mg-Fe carbonate 1 and 2 with minor amounts in sphalerite and rhodonite. In the southern zone manganese is incorporated in Ca-Mn-Mg-Fe carbonate 1 and 2 and rhodochrosite with minor amounts in sphalerite. Silver is present as matildite dissolved in galena. Tungsten analyses reported by commercial laboratories resulted from mis-interpretation of XRF analyses and significant tungsten is absent in the Menninnie Dam mineralisation.

The southern zone is the southern periphery of the mineralised system and has been overprinted by a later hydrothermal event ('late alteration overprint'). The late alteration

overprint resulted in pervasive calcite - chlorite - quartz - carbonate - calc-silicate - hematite alteration of the Hutchison Group, granite dykes, mineralisation and the basal 34m of the MD ignimbrite. Pre-existing sulphide and gangue mineralisation was partially dissolved by the late alteration overprint and re-precipitated both locally and distally. The late alteration overprint postdates emplacement of the MD ignimbrite.

# Chapter six
# Gravity and magnetic modelling

## 6.1 Introduction

The volcanic architecture of units overlying the Hutchison Group lithologies at Menninnie Dam is similar to that of a deeply eroded cauldron (Section 4.4.9). In many caldera and cauldron settings, the volcanic pile has been interpreted to have been genetically, and temporally, related to an underlying, shallow igneous intrusion (Smith and Bailey, 1968; Goff, 1983; Smith and Braile, 1994). The small rhyolite intrusions at Menninnie Dam are interpreted to have similar immobile element geochemistry to granitoids of the Hiltaba Suite (Section 4.3.5). In this chapter, regional geophysical data has been used to assess the possible presence of a large igneous intrusive, such as a granitoid of the Hiltaba Suite, beneath the Menninnie Dam prospect.

The Menninnie Dam prospect is associated with two short wavelength, north-northeast trending magnetic highs which lie on the north-western flank of a long wavelength, sub-circular, magnetic high of lower magnetic intensity (Fig. 6.1). This long wavelength, sub-circular, magnetic feature is associated with a near coincident, long wavelength, gravity low.

## 6.2 Methods

Interpretation of regional gravity and magnetic data was selected as an appropriate method for assessment of the presence or absence of a granitoid body beneath the Menninnie Dam prospect for the following reasons:

- Gravity data covering the appropriate area of the Eyre Peninsula was already available.
- Aeromagnetic data extending in all directions for at least 30 km beyond the Menninnie Dam prospect was available through various sources including; Mines and Energy department of South Australia, Billiton Australia Ltd. and Aberfoyle Resources Ltd.
- The rock types likely to be present (as determined from 1 : 250,000 geological maps) were considered to have sufficient density and magnetic contrast to facilitate discrimination.
- Modelling of magnetic lithologies is most effective in the upper few kilometres of the crust. If an intrusive body with a magnetic response is present at shallow depths it may have a magnetic signature (eg. magnetite series granite; Ishihara, 1981).
- While the top of an intrusive body may be within a few kilometres of the present surface, it may have considerable vertical extent. Bouguer gravity is an effective means of deciphering upper crustal components, providing units have sufficient density contrast (Vigneresse, 1990).
- When used in combination, magnetic and gravity methods are considerably more informative than either method used individually.

Vigneresse (1990) suggested criteria for using gravity data to model the sub-surface shape of granitoid bodies, which included:

- A sample density of one gravity station per 1 $km^2$.
- Using 3D modelling rather than 2D modelling techniques.
- Data should extend a few kilometres beyond the margin of the pluton.
- Geological observations have shown that granites are not homogeneous and may consist of different intrusive phases with different facies within each intrusion. Geological mapping and representative density sampling of the various intrusive phases and facies is required.

## 6.3 Gravity and magnetic data

*Gravity data*

The gravity data used in this study was made available by the Australian Geological Survey Organisation (AGSO). The gravity data was collected by AGSO in 1966 and 1969 (Rowan, 1970; Gerdes, 1972). Gravity stations were acquired on a nominal four mile (6.44 km) grid with an average station density of 1 per 41.4 square kilometres. Bouguer gravity values were calculated using a reduction density of 2.67 $tm^{-3}$. The r.m.s. error in the Bouguer gravity was considered to be less than ± 0.6 mGal (Rowan, 1970; Gerdes, 1972).

*Aeromagnetic data*

Aeromagnetic data covering the Menninnie Dam prospect and to the west was flown specifically for Billiton Australia Ltd. in 1981. Aeromagnetic data to the east of the Menninnie Dam prospect was acquired by the Mines and Energy Department of South Australia and released in 1993 (DME, 1993). The acquisition parameters for the two data sets are summarised in Appendix 6.1. The two data sets were merged by Acacia Resources Ltd and made available for the purposes of this study. Profiles of the magnetic intensity along selected transect lines (Section 6.4) were extracted from the gridded data. The magnetic intensity data along each of the transect lines is presented in Appendix 6.2.

The paucity of surface outcrop, and the coarse spacing of gravity data does not satisfy the strict criteria of Vigneresse (1990) for interpretation of the shape of sub-surface granitoid bodies. However, in the absence of other geological information, interpretation of the geophysical data is considered the only viable method of assessing the presence or absence of a sub-surface granite body in the Menninnie Dam area.

## 6.4 Transect lines

Three transects lines were selected to examine the main anomalies present in the regional geophysical data sets using two dimensional modelling (lines A-A', B-B' and C-C': Fig. 6.1). The transect lines intersect at a point approximately 10 km to the south of the

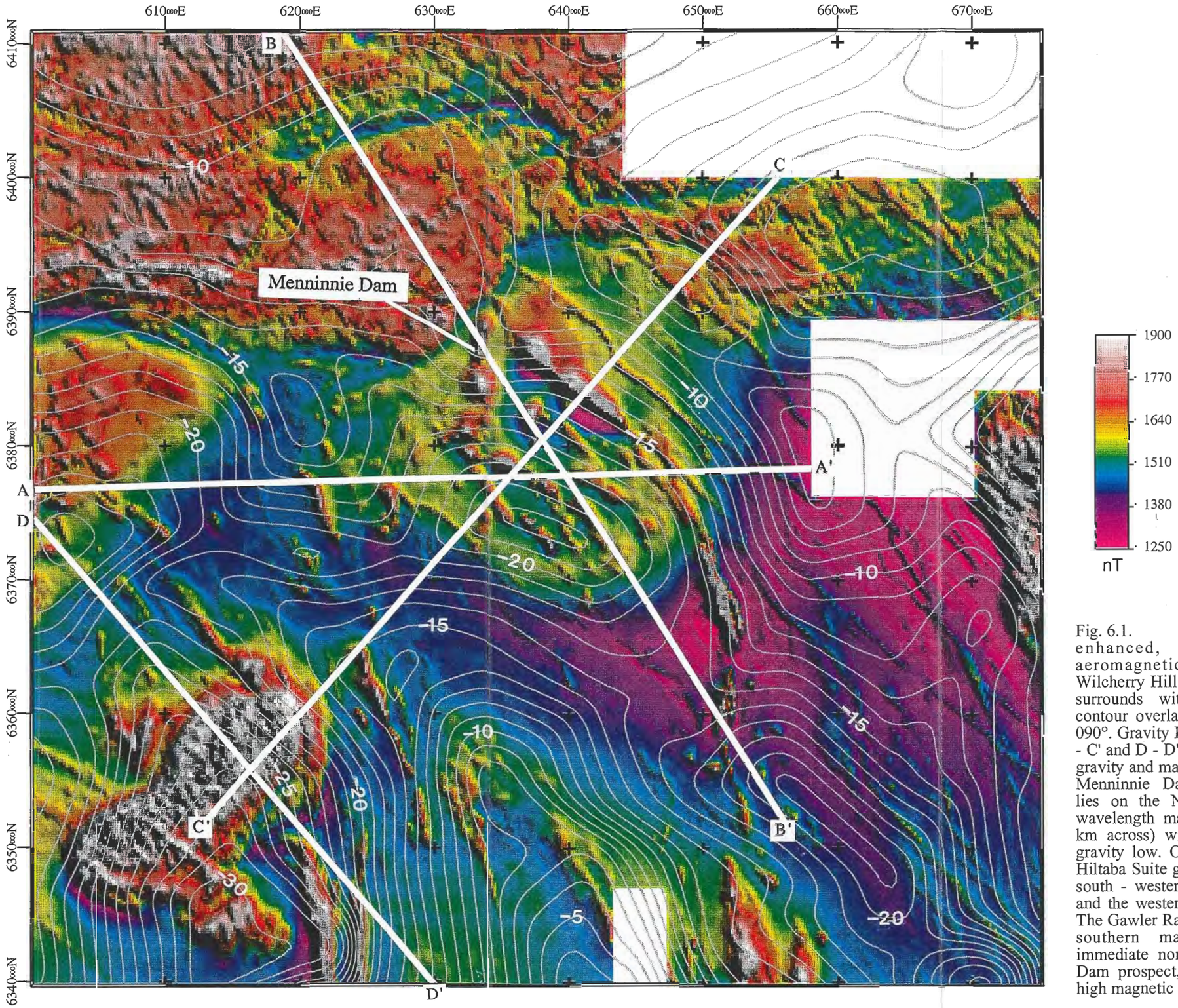


Fig. 6.1. False colour, enhanced, 1:300,000 scale aeromagnetic image of the Wilcherry Hill exploration lease and surrounds with 1 mGal gravity contour overlay. False sun angle is 090°. Gravity Lines A - A', B - B', C - C' and D - D' are transects used for gravity and magnetic modelling. The Menninnie Dam magnetic feature lies on the NW flank of a long wavelength magnetic feature (≈ 20 km across) with a near coincident gravity low. Outcrop or subcrop of Hiltaba Suite granite occurs near the south - western end of line C - C' and the western end of line A - A'. The Gawler Range Volcanics, whose southern margin lies to the immediate north of the Menninnie Dam prospect, have a moderate to high magnetic response.

Menninnie Dam prospect. The western end of transect line A - A' intersects a sub-cropping granite of the Hiltaba Suite near Buckleboo, referred to as the 'Buckleboo Granite'.

A fourth transect line with a north-westerly orientation (line D-D') was selected across a granite of the Hiltaba Suite cropping out at Cunyarie Rocks, referred to as the 'Cunyarie Granite' (Fig. 6.1). The north-western end of transect line D - D' joins the western end of the transect line A - A'. The transect across the 'Cunyarie Granite' was chosen to help constrain the density and magnetic parameters used for modelling of granites of the Hiltaba Suite and provides two additional transect line intersections as checks of the internal consistency of models. The location, orientation and length of transect lines are detailed in Table 6.1.

Table 6.1 Transect lines.

| Transect line | Line A - A' | Line B - B' | Line C - C' | Line D - D' |
|---|---|---|---|---|
| Start (A.M.G.*) | 600000 mE<br>6376800 mN | 618800 mE<br>6410900 mN | 655350 mE<br>6400000 mN | 600000 mE<br>6375000 mN |
| Finish (A.M.G.*) | 657900 mE<br>6378400 mN | 655400 mE<br>6352000 mN | 612500 mE<br>6352000 mN | 630000 mE<br>6340000 mN |
| Length | 58 km | 69.5 km | 64.5 km | 46 km |
| Orientation** | 089° | 148° | 222° | 133° |

*Australian map grid. **Orientation measured with respect to true north.

Bouguer gravity values for each traverse were manually interpolated at 3 km intervals from the gravity contour map. Magnetic intensity values were interpolated at 1 kilometre intervals from magnetic intensity profiles supplied by Acacia Resources Ltd. Individual values were estimated to the nearest 10 nT (Appendix 6.2).

Gravity and magnetic profiles were modelled using an interactive, two dimensional, forward modelling program 'Model 2D, version 3.1a' (Roach, 1993). The program uses the algorithms of Talwani et al. (1959) and Talwani (1965) to calculate the gravity and magnetic fields resulting from bodies of polygonal cross-section and infinite extent perpendicular to the model section. The calculated anomalies were then compared to the observed gravity and magnetic response and the shape of model polygons adjusted accordingly (within the bounds of reasonable geological constraints) until the resultant calculated response matched the observed response.

## 6.5 Nature and distribution of lithologies

Modelling of the gravity and magnetic fields requires certain assumptions about the spatial distribution and physical properties of the lithologies which give rise to the fields. The spatial distribution can be constrained in two dimensions through surface outcrop.

The surface outcrop geology, and the position of the Menninnie Dam prospect are presented in Figure 6.2. The surface geology is taken directly from the Kimba, (Flint and Rankin, 1989), Port Augusta, (Dalgarno et al., 1968), Yardea, (Blissett, et al., 1988) and Whyalla, (Parker, 1983), 1 : 250,000 scale geological map sheets. Much of the area of interest is covered by a veneer of Quaternary cover with only scattered outcrop of older lithologies. Interpretation of the geology beneath Quaternary cover is subject to considerable lateral extrapolation of outcropping units. Interpretation of the three dimensional shape of lithological packages is even more complex due to the highly deformed nature of Archaean and Palaeoproterozoic rocks (Daly and Fanning, 1993, Parker, 1993a).

The closest Archaean rocks to the Menninnie Dam prospect (Sleaford Complex, Coulta Subdomain) occur as an arcuate band of scattered outcrop approximately 40 km to the south-west and south of the Menninnie Dam Prospect. South of the Gawler Ranges in the Wudinna - Kyancutta - Kimba region, the Sleaford Complex forms the basement to the Gawler Volcanics without any intervening Hutchison Group lithologies (Webb, 1980). Rocks of the Sleaford Complex that crop out in the area covered by the Yardea 1 : 250,000 geological map sheet were described by Blissett et al. (1988) as "foliated quartzo-felspathic gneisses and gneissic granitoids with deformed veins and pods of milky quartz and pegmatite, quartz, feldspar, biotite gneiss, augen gneiss with garnet locally, and migmatitic garnetiferous gneiss".

Palaeoproterozoic age rocks of the Hutchison Group crop out to the south, west and east of the Menninnie Dam prospect where they are almost entirely represented by Warrow Quartzite (Dalgarno et al., 1968; Blissett et al., 1988). Outcrop and subcrop of the Middleback Subgroup units and Yadnarie Schist are known to occur near Menninnie Dam and Ultima Dam. The absence of outcrop elsewhere in the area of interest may relate to either non-occurrence or to preferential weathering. In the Cleve Subdomain, the Hutchison Group has been interpreted to thicken towards the east (Parker 1993b). The thickness of individual units of the Hutchison Group is not well known and units vary significantly from one locality to the next (Parker, 1993b). Thickness variations may have been related to either deformation processes or primary sedimentary thickness variations (Parker, 1993b).

Granite of the Lincoln Complex occurs as scattered outcrop to the south and east of the Menninnie Dam prospect. A more substantial mass of Lincoln Complex granite has formed a north-south trending arcuate band to the south-southeast of the Menninnie Dam prospect. Older granites of the Lincoln Complex, associated with KM-$D_{1-2}$, have a strong north-south lineation. Younger granites of the Lincoln Complex commonly have a north-south lineation although less pronounced than for older granites of the Lincoln Complex (Parker 1993a). North-south trending mylonite zones formed during KM-$D_3$ commonly have a near vertical dip (Parker 1993a). Deformation associated with the formation of mylonite zones has

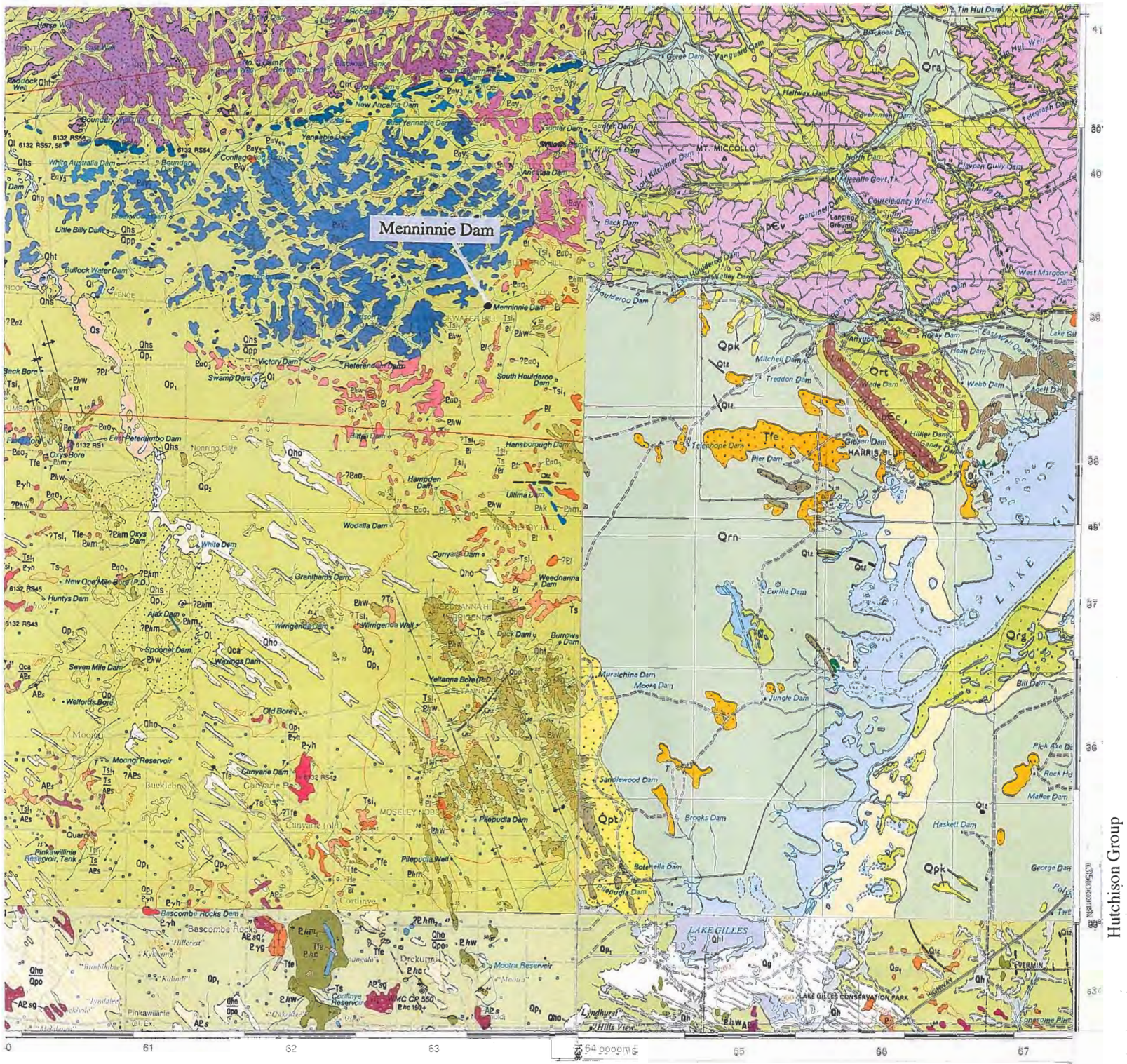
Menninnie Dam
MT. MICCOLLO
LAKE GILLES
HARRIS BLUFF
SLAKE
Qra
Qrn
Qpk
Qpt
Qrg
Qrt
Tfe
pEv
Qtz
Qh
Qha
Qpo
Qp1
Qp2
Qha
Qhs
Qpp
Qi
Ql
Qs
Qca
Qo
Bhw
Bhm
Bhc
Bhk
Bpk
Bpt
Bpy
Bpa
Bpx
Bpo
Byh
Bay
Bay1
Bay2
Bay3
Bay4
Bay5
Bay6
Bay7
Bay8
Bay9
Bay10
Bay11
Bay12
Bay13
Bay14
Bay15
Bay16
Bay17
Bay18
Bay19
Bay20
Bay21
Bay22
Bay23
Bay24
Bay25
Bay26
Bay27
Bay28
Bay29
Bay30
Bay31
Bay32
Bay33
Bay34
Bay35
Bay36
Bay37
Bay38
Bay39
Bay40

probably contributed to the north-south elongated shape of some granites of the Lincoln Complex.

Granitoids of the Hiltaba Suite comprise massive, anorogenic granites, that formed large batholiths and smaller plutons (Flint, 1993b). Compositionally, granites predominate but the suite is distinctly bimodal with both mafic lithologies and felsic lithologies (Flint, 1993b). Granitoids of the Hiltaba Suite were interpreted to have formed flat topped intrusions of considerable lateral extent (Turner, 1975).

The Gawler Range Volcanics (GRV) have been intersected on transect lines B - B' and C - C'. All of the more substantial intersections are of the mature phase GRV (Stewart, 1992) whereas the developmental phase (Stewart, 1992) occurs as scattered outcrop and is not volumetrically significant. Units of the mature phase GRV have been interpreted to be a series of near flat lying rheoignimbrites with more steeply inwards dipping margins (Blissett et al., 1993; Giles, 1988; Creaser and White, 1991). The Yardea Dacite is volumetrically the most significant unit of the mature phase GRV and is remarkably homogenous, both mineralogically and chemically, over a considerable lateral extent (Giles, 1988; Creaser and White, 1991).

## 6.6 Rock Densities

Knowledge of the density of lithologic bodies is required for modelling their contribution to the regional gravitational field. Unfortunately there is a paucity of published density data for the rock units of the Eyre Peninsula. Therefore, density measurements were conducted on a suite of lithologies to provide control for models. Where possible, unweathered drill core was used for density measurements. If drill core was not available, surface samples were collected and every effort made to collect unweathered or least weathered samples. Densities were determined from water saturated samples using Archimedes principle. Density measurements are summarised in Table 6.3 and detailed in Appendix 6.3. Because of poor surface exposure in the area of interest, it cannot be determined how well the measured densities approximate the true densities of Proterozoic and Archaean lithologies.

A veneer of Quaternary cover locally mantles weathered Archaean or Proterozoic rocks in the area of interest. As the depth extent of weathering or the thickness of Quaternary cover is not uniform and has not been quantified during the course of this, or previous studies, the net effect of these units has not been incorporated in modelling. Local variations in the depth of weathering and the thickness of Quaternary cover generally results in high frequency gravitational responses and such variations are unlikely to have been adequately sampled. Despite their high density contrast, weathering profiles and Quaternary sediments are volumetrically insignificant and unlikely to have had any effect on regional gravity measurements.

An averaged density of 2.76 $tm^{-3}$ was determined for the Sleaford Complex based on density measurements of outcropping Sleaford Complex 42 km to the south-west of the Menninnie Dam prospect (A.M.G. 603500 mE, 6355550 mN).

Corbett (1987) estimated the total thickness of the Hutchison Group to be about 10 km. The thickness and distribution of individual units of the Hutchison Group in the vicinity of transect lines cannot be established due to poor outcrop. Therefore, all Hutchison Group lithologies have been grouped and the contribution of each unit to the overall density has been calculated from the relative thickness of each unit from a section near Cleve (Parker, 1993b). Results are summarised in Table 6.2. Warrow Quartzite from Caralue Bluff (A.M.G. 610000 mE, 6316500 mN) has an average density of 2.63 $tm^{-3}$. Yadnarie Schist from Poolalalie Creek, north-east of Karkarook (A.M.G. 633620mE, 6277000 mN) has an average density of 2.75 $tm^{-3}$. Twelve samples of marbles, magnetite bearing marbles, calc-silicate lithologies, and iron formations from Menninnie Dam drill core have an average density of 3.01 $tm^{-3}$. Cook Gap Schist from the Wangaraleednie area (A.M.G. 650800 mE, 6273350 mN) has an average density of 2.73 $tm^{-3}$. Using the proportions shown in Table 6.2, the average density calculated for the Hutchison Group is 2.74 $tm^{-3}$. In a study of geophysical modelling of granites of the Hiltaba Suite and associated cauldrons of the Stuart Shelf area, Gow et al. (1993) used a density of 2.73 $tm^{-3}$ for Hutchison Group rocks. The density calculated in this study is comparable to that determined by Gow et al. (1993).

Table 6.2 Density values for units of the Hutchison Group and their contribution to determination of an average density value for the Hutchison Group.

| Rock unit | Density $tm^{-3}$ | Contribution |
|---|---|---|
| Warrow Quartzite | 2.63 | 16% |
| Lower Middleback Jaspilite and Katunga dolomite | 3.01 | 3% |
| Cook Gap Schist | 2.73 | 55% |
| Upper Middleback Jaspilite | 3.01 | 4% |
| Yadnarie Schist | 2.75 | 22% |
| Average density for the Hutchison Group | 2.74 | |

Determination of an average density value for granitoids of the Lincoln Complex is problematic due to the wide compositional range from leucogranite, (Yunta Well Leucogranite, Moody Suite) to quartz gabbronorite, (Cape Donington, Donington Granitoid Suite). Scattered granite outcrop of the Lincoln Complex in the vicinity of the Menninnie Dam prospect was interpreted as a member of the Moody Suite (Parker, 1993a). Density measurements of samples from the Carpa Granite (Moody Suite), Burkitt Granite (Moody Suite) and the Carappee Granite (Moody Suite) ranged from 2.61 to 2.65 $tm^{-3}$. Density values for granites of the Lincoln Complex obtained from Paterson and Muir, (1986), Gow (pers. comm.) and Gow et al. (1993) are slightly denser than those measured in this study (Appendix 6.3). By combining the data from Paterson and Muir, (1986), Gow (pers. comm.) and Gow et al. (1993) with data obtained in this study, an average value of 2.66 $tm^{-3}$ has been estimated for granites of the Lincoln Complex.

The closest granite of the Hiltaba Suite to the Menninnie Dam prospect are the 'Cunyarie Granite' to the south-west, the 'Buckleboo Granite' to the west and the Charleston Granite to the east. Samples of granite from the 'Cunyarie Granite', the Charleston Granite, the 'Buckleboo Granite', Calca Granite, and from Pildappa Rock and Willauka Hill (Gow et al., 1993) have an averaged density of 2.62 $tm^{-3}$. The Calca Granite is quarried for decorative stone and the density is well constrained at 2.61 $tm^{-3}$ (pers. comm. J. Craghan, 1994). Gow et al. (1993) used an average value of 2.64 $tm^{-3}$ for gravity modelling of granites of the Hiltaba Suite. The more dense value used by Gow et al. (1993) probably resulted from measurements of granitoids with more mafic compositions than those used for determination in this study. The lower density of granites measured as part of this study may relate to their chemical composition, as density is mainly dependant on the ferromagnesian mineral content (Henkel, 1976; Bateman and Chapell, 1979; Kanaya et al., 1984). The 'Cunyarie Granite', Charleston Granite and the 'Buckleboo Granite' have average ($Fe_2O_3$ + FeO + MgO) contents of 1.33 wt.%, 3.88 wt.% and 1.60 wt.% respectively whereas the average ($Fe_2O_3$ + FeO + MgO) content of 16 different granitoids of the Hiltaba Suite is 3.99 wt.% (110 analyses; Flint, 1993b).

Density measurements of the various units of the GRV are summarised in Table 6.3 and detailed in Appendix 6.3. Density values were obtained from measurement of samples collected as part of this study, from Gow (pers. comm.), and Paterson and Muir (1986). For comparison, Gow et al. (1993) used an average density of 2.63 $tm^{-3}$ for all felsic GRV in their models.

Table 6.3 Summary of averaged density data for rock units used for modelling in this study. The density contrast is the measured density minus the averaged density of 2.67 $tm^{-3}$ used for calculation of the Bouguer gravity.

| Rock Type | Number | Range ($tm^{-3}$) | Average ($tm^{-3}$) | Density contrast ($tm^{-3}$) |
|---|---|---|---|---|
| Granites of the Lincoln Complex | 25 | 2.55 - 2.82 | 2.66 | -0.01 |
| Granites of the Hiltaba Suite | 37 | 2.58 - 2.65 | 2.62 | -0.05 |
| Hutchison Group | 20 | 2.63 - 3.38 | 2.74 | +0.07 |
| Sleaford Complex (basement) | 8 | 2.76 | 2.76 | +0.09 |
| Eucarro Dacite (GRV) | 3 | 2.53 | 2.53 | -0.14 |
| Nonning Rhyodacite (GRV) | 2 | 2.56 | 2.56 | -0.11 |
| Black Yardea Dacite (GRV) | 2 | 2.65 | 2.65 | -0.02 |
| Yardea Dacite (GRV) | 2 | 2.61 | 2.61 | -0.06 |

## 6.7 Magnetics susceptibility

The observed magnetic responses from the 1988 aeromagnetic survey of the Gawler Craton were interpreted to have resulted from bedrock sources and not flat lying Tertiary sediments (Tucker and Nelson, 1991). Positive magnetic anomalies with circular to elliptical shapes of 5 - 30 km diameter were attributed to plutons, plugs or stocks mostly associated with granitoids of the Hiltaba Suite (Tucker and Nelson, 1991).Units of the GRV have a distinct magnetic pattern described as a "mottled and / or granular pattern" by Tucker and Nelson (1991). Both the older and younger GRV rocks contain magnetite and exhibit high magnetic

susceptibility. Regional aeromagnetic maps of the GRV commonly show a high level of 'noise' which may have resulted from variations in topography, weathering, and to a lesser extent, variations in the magnetic mineral content of different units (Rajagopalan et al., 1993).

Magnetic susceptibility was measured on the same samples used for density measurements. Measurements were made using a Exploranium KT - 5 susceptibility meter. All susceptibility values were corrected for geometric effects including surface unevenness, specimen size and drill core diameter, in accordance with the correction factors listed in the instruction manual for the susceptibility meter. Additional magnetic susceptibility values were obtained from Gow (pers. comm.). Magnetic susceptibility measurements for the Sleaford Complex, Hiltaba Suite and units of the Gawler Range Volcanics were generally low and do not appear to fully correspond with the large range of magnetic susceptibilities inferred from the aeromagnetic data. Most of these samples were collected from surface outcrop and the low measured values have probably resulted from partial destruction of magnetite through weathering. The magnetic susceptibility values used for construction of the models were inferred from qualitative evaluation of the aeromagnetic data and all fall within average limits for similar rock types world wide (Sharma, 1986). Measured values and the values used of the construction of models are listed in Table 6.4.

Table 6.4 The range of measured magnetic susceptibility values for rock types from Menninnie Dam and values of the assumed magnetic susceptibility used for construction of models.

| Lithology | Measured mag. sus. range ($x10^{-3}$ SI)* | Mag. sus. used for models ($x10^{-3}$ SI) |
|---|---|---|
| Granites of the Lincoln Complex | 0.04 - 34.77 | 12.57 |
| Granites of the Hiltaba Suite | 0.16 - 10.11 | 37.70 - 62.83 |
| Hutchison Group | 0.05 - 5.33 | 0.63 |
| Sleaford Complex | 0.15 - 0.30 | 12.57 |
| Eucarro Dacite (GRV) | 2.03 | 37.70 |
| Nonning Rhyodacite (GRV) | 1.64 - 34.77 | 37.70 |
| Black Yardea Dacite (GRV) | 7.68 - 13.36 | 37.70 |
| Yardea Dacite (GRV) | 2.52 - 6.47 | 37.70 |

*Data obtained from this study and from Gow (pers. comm.)

Associated with the long wavelength magnetic high and coincident gravity low which encompasses the Menninnie Dam prospect, are a number of high amplitude, high frequency magnetic anomalies with half wavelengths commonly less than 1 km indicative of a shallow source. North-south trending linear features have been interpreted as iron formations of the Middleback Subgroup (Ragagopalan et al. 1993). North - north-west to north-west trending linear features have been interpreted as mafic dykes of the Gairdner Dyke Suite (Ragagopalan et al. 1993). In addition to these linear magnetic anomalies, there are a number of isolated magnetic features that have formed a 10 - 18 km diameter arcuate zone coincident with the long wavelength magnetic high (Fig. 6.1). These local, high frequency, magnetic highs may be similar to magnetite skarn zones described by Gow et al. (1993) and

interpreted to have formed in the roof pendants of Hiltaba Suite plutons, or as part of a contact metamorphic aureole (Vigneresse, 1990). As the purpose of this exercise to determine the presence or absence of a sub-surface granite body, likely to have resulted in a long wavelength magnetic response, the effect of these smaller magnetic features has been ignored. There is no gravimetric expression of these bodies due to their small size and the wide spacing of gravity stations.

## 6.8 Results

The results of modelling are illustrated in Figures 6.3 - 6.6. Three models are presented for transects A - A', B - B' and C - C'.

1) The first is based on the assumption that there is no granite body beneath the Menninnie Dam prospect.
2) The second models the presence of a granite of the Lincoln Complex.
3) The third models the presence of a granite of the Hiltaba Suite.

The first model assumes the scattered outcrop of Hutchison Group rocks are the surface expression of a coherent mass, several kilometres thick which are underlain by an unknown thickness of Sleaford Complex rocks extending to at least 10 kilometres depth. The 'Buckleboo' and 'Cunyarie Granites' of the Hiltaba Suite have been modelled as irregular shaped bodies at the western end of transect lines A - A' and C - C' respectively. A large, steep sided mass of granite of the Lincoln Complex is modelled at the eastern end of transect line B - B', consistent with scattered surface outcrop and the interpreted distribution of the Lincoln Complex (Parker, 1993a). The Hutchison Group and Sleaford Complex have been intensely folded and deformed (Parker, 1993a). However, the nature of the deformation in the area of interest cannot be quantified from existing data and the contact between the Hutchison Group and the Sleaford Complex has been modelled as planar and tilted to the east, in accordance with the general variation in thickness of the Hutchison Group across the Eyre Peninsula (Parker, 1993b).

*Models with no sub-surface granite (model 1)*

The gravity and magnetic profiles for models without a sub-surface granite do not fit the observed data (Figs. 6.3a, 6.4a and 6.5a). The modelled gravity profiles are significantly higher than the observed values. This contrasts with the gravity low present in the observed data. Modelled magnetic profiles are generally flat and do not correspond to the long wavelength magnetic high present in the observed data. Variations in the relative thickness of the Hutchison Group and Sleaford Complex have little effect on the modelled gravity and magnetic profiles due to the similarity in physical properties of the two units.

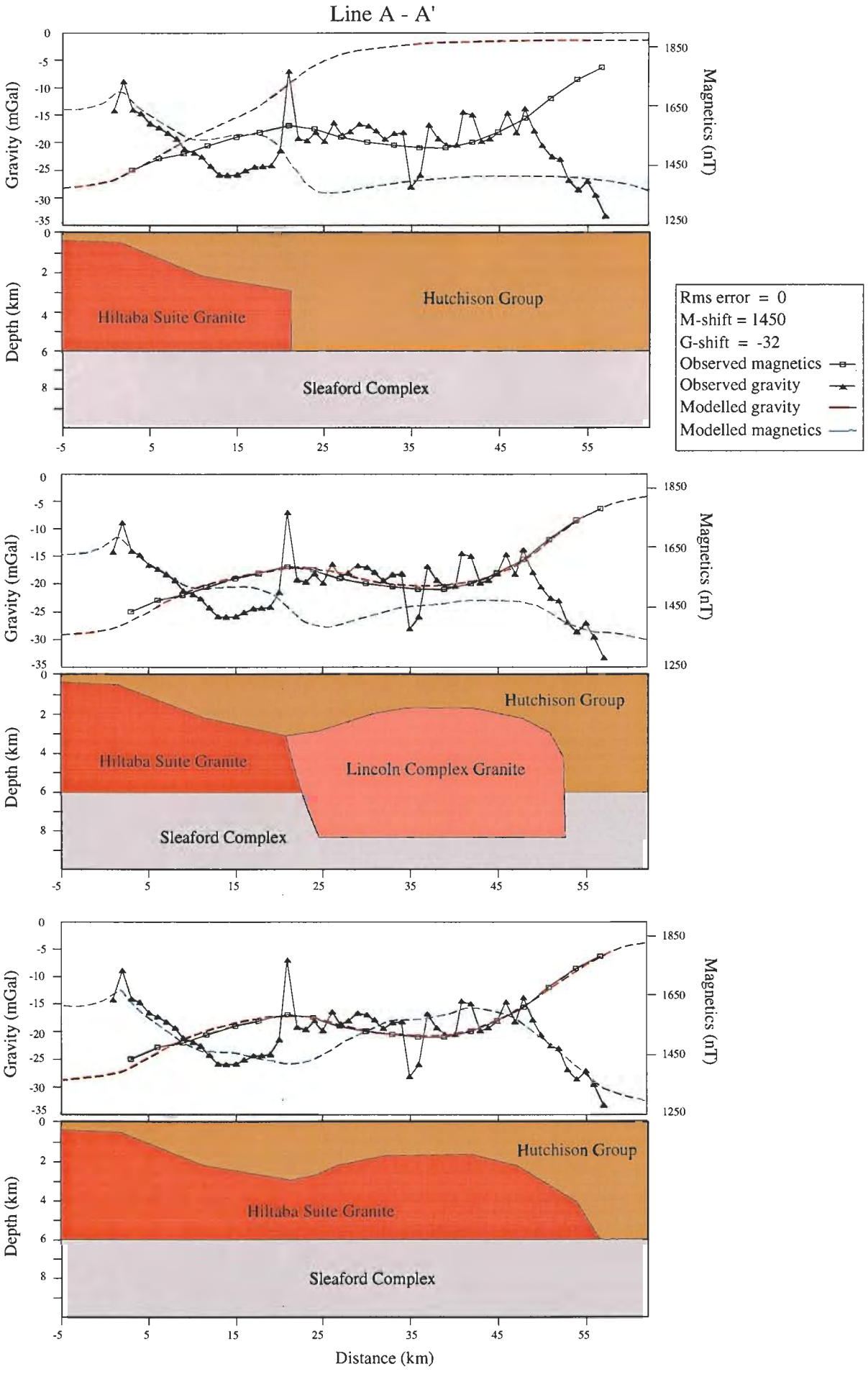


Fig. 6.3 Gravity and magnetic models for transect line A - A'. Upper; no granite. Middle; Lincoln Complex granite. Lower; Hiltaba Suite granite.

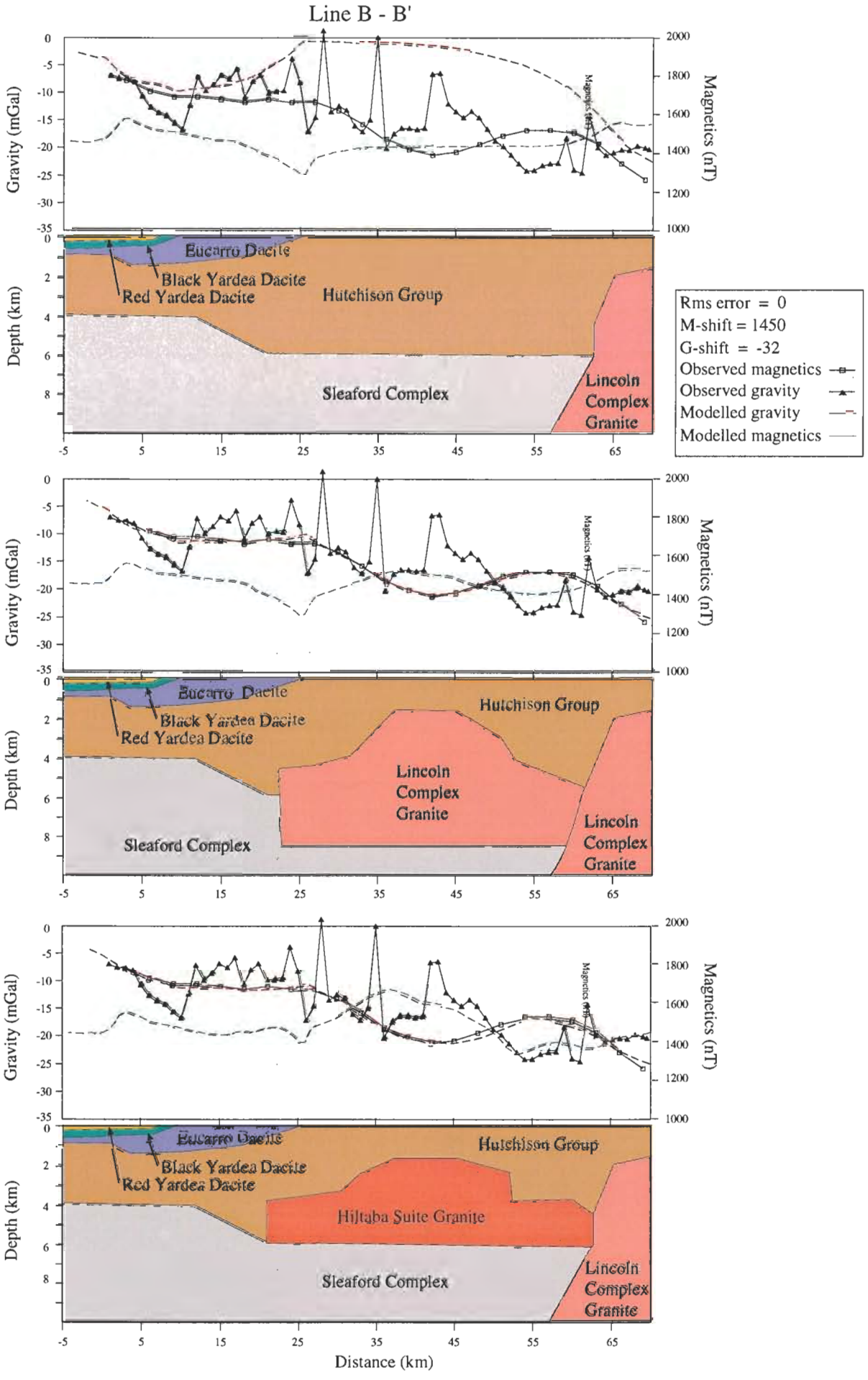


Fig. 6.4 Gravity and magnetic models for transect line A - A'. Upper; no granite. Middle; Lincoln Complex granite. Lower; Hiltaba Suite granite.

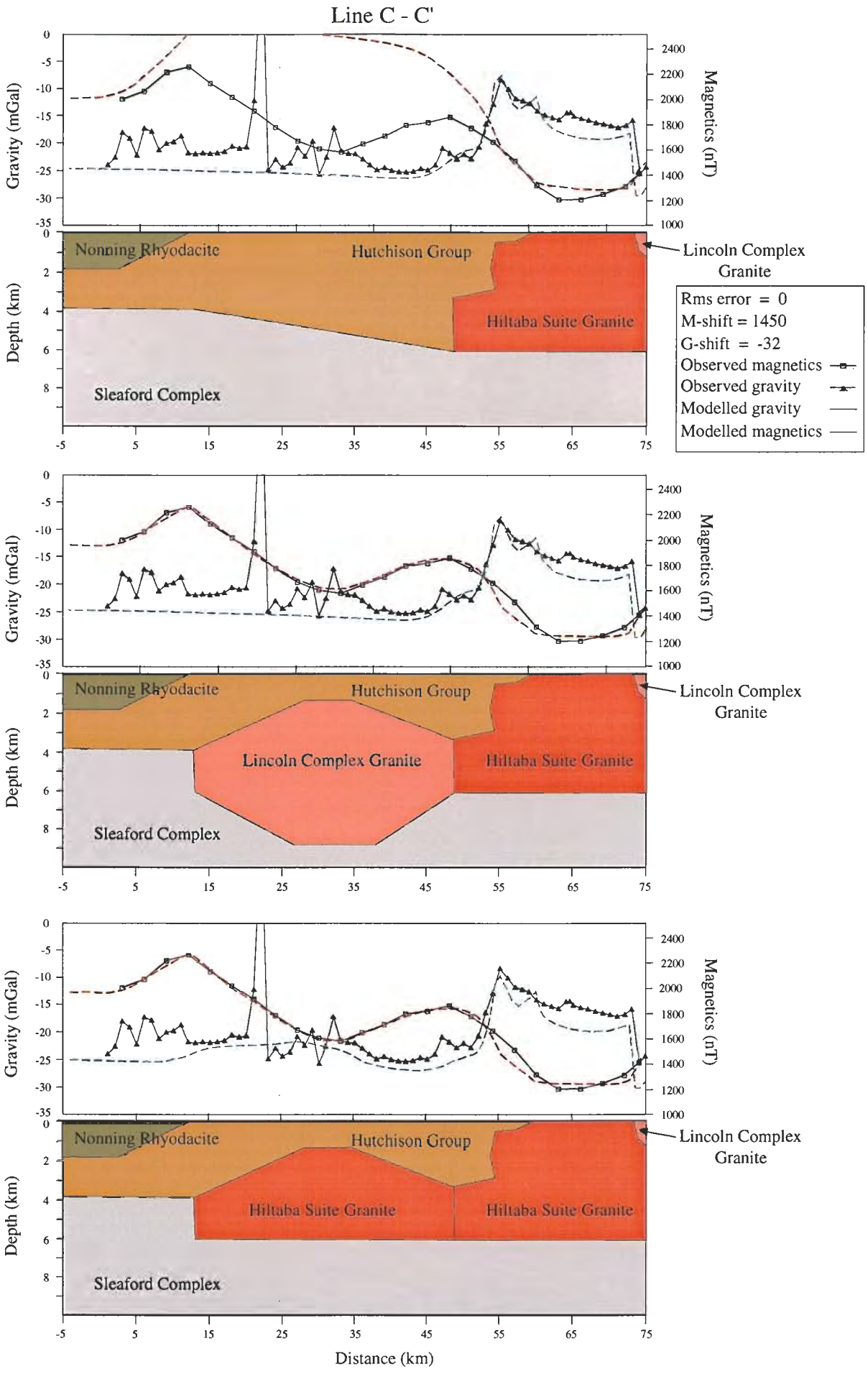


Fig. 6.5 Gravity and magnetic models for transect line A - A'. Upper; no granite. Middle; Lincoln Complex granite. Lower; Hiltaba Suite granite.

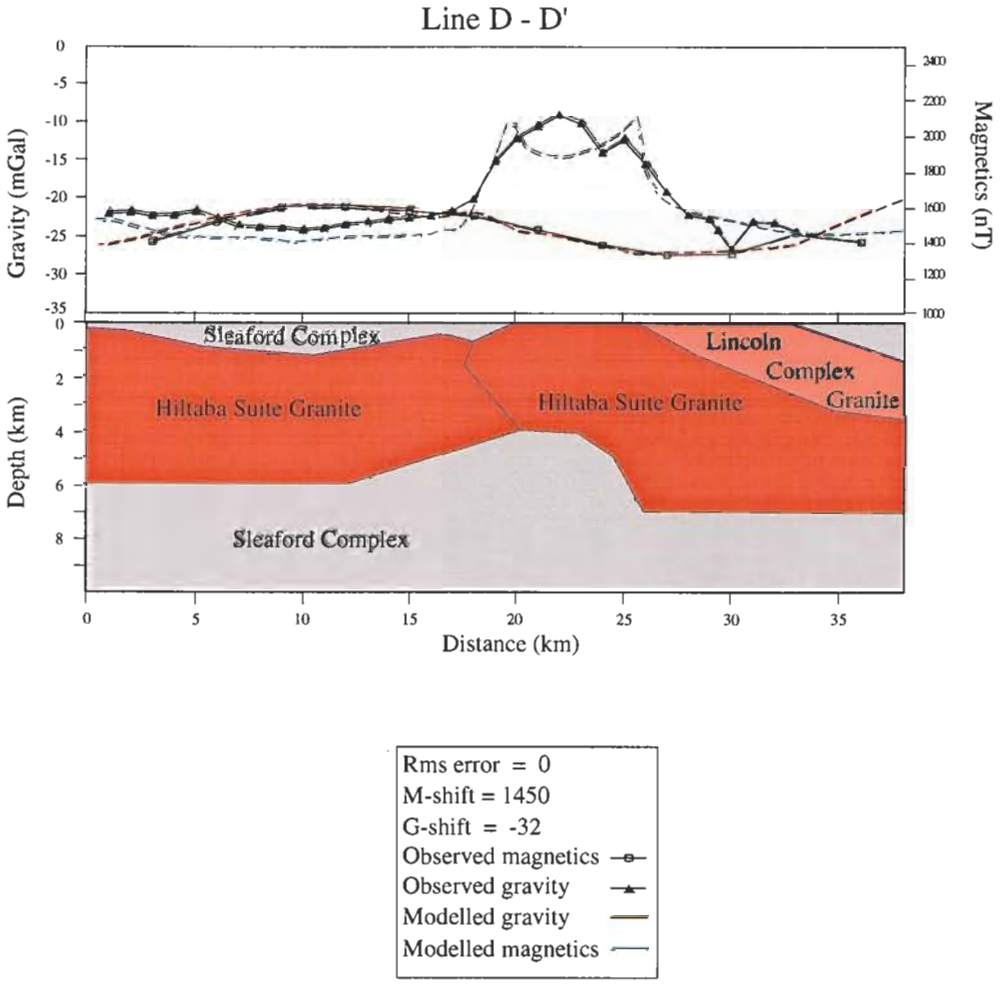


Fig. 6.6 Gravity and magnetic models for transect line D - D' which traverses the 'Cunyarie granite' (Hiltaba Suite).

*Models incorporating a sub-surface granite (models 2 and 3).*

For ease of reference, the hypothetical granite beneath the Menninnie Dam prospect will be referred to as the 'MD granite'. Gravity and magnetic profiles for models that incorporate the 'MD granite' more closely correspond with the observed data compared to models that do not incorporate a sub-surface granite (Figs. 6.3b, c; 6.4b, c; and 6.5b, c). As density values are better constrained than magnetic susceptibility, the shape and depth of the 'MD granite' has been adjusted so that the modelled gravity profiles correspond with the observed data. The top of the 'MD granite' has been modelled at ≈ 1.5 km below the surface, however, this is not well constrained. The 'MD granite' has not been intersected by drilling at the Menninnie Dam prospect and nearby prospects on the Wilcherry Hill exploration lease (Fig. 6.1). Therefore, the minimum depth to the top of the 'MD granite' must exceed the maximum extent of drilling (0.64 km).

The match between the modelled magnetic profiles and the observed data for a 'MD granite' with properties similar to a granite of the Lincoln Complex can be improved by reduction of the depth to the top of the 'MD granite'. In order to achieve a reasonable match it is necessary to raise the body to a depth less than 0.64 km. An increased depth to the top of the MD granite (greater than ≈ 1.5 km) results in broadening of the modelled gravity profile and diminishes the intensity of the modelled magnetic profile.

The magnetic profiles for a 'MD granite' with properties similar to a granite of the Hiltaba Suite more closely match the observed data compared to models incorporating a granite with properties similar to those of the Lincoln Complex. Transect Line D - D' straddles two outcropping granites of the Hiltaba Suite. The modelled gravity and magnetic profiles for transect line D - D' correspond reasonably well to the observed data.

## 6.9 Discussion

Leaman (1994) discussed potential field interpretations and suggested the following criteria for their evaluation:

1) Does the model honour geological or other control?
2) Does the model contain discontinuities in either properties or geometry which are not sustainable?
3) Are the properties used within ranges measured or which can be inferred from the data?
4) Is the solution based on several, preferably interlocking, profiles across the data set? A direct map match for the entire area is an alternative.
5) Has a consistent (or correct) base level been derived for the entire data set from the modelling? Uniform acquisition and processing, as well as interpretation, assumptions are required.

As outcrop is poor across much of the area of interest, only volumetrically significant units have been included in the models. Localised scattered outcrop of the Bittali Rhyolite has not been incorporated in the models, nor has the veneer of Tertiary and Quaternary cover or the weathering profile developed over older rocks. The effects of small volume units is likely to have been under sampled in both the gravity and magnetic data. The shape and position of lithological units in the upper few kilometres of the crust can be reasonably modelled due to the constraints imposed by limited surface outcrop and simultaneous modelling of both the magnetics and Bouguer gravity. The anomaly due to magnetic rock units buried more than a few kilometres is generally of long wavelength and low amplitude. Because of the diminished magnetic effect, modelling of deeper units is strongly dependant on their Bouguer gravity. Due to the poor quality of the gravity data, little attempt has been made to model realistic shapes for lithologic units at depth as they cannot be constrained by the data. The models are interpreted to satisfy the first criteria of Leaman (1994) within the constraints of the quality of the geophysical data and limited surface outcrop.

Intersecting transects are internally consistent with the same lithological units in similar positions and at similar depths. Small variations in depth for the same unit on different transects (up to a few hundred metres) have probably resulted from projection of three dimensional data onto a two dimensional format. Lithologic units have consistent gravity and magnetic properties with the exception of the granites of the Hiltaba Suite. The 'Buckleboo Granite' and the 'MD granite' have been modelled with a magnetic susceptibility of 37.70 SI whereas the 'Cunyarie Granite' has been modelled with a magnetic susceptibility of 62.83 SI. Attempts to model all three granites with similar magnetic susceptibility have resulted in significant mis-match between modelled profiles and observed data. As the Cunyarie Granite and the Buckleboo Granites outcrop and produce different aeromagnetic responses, use of different magnetic susceptibilities is considered reasonable. With the above proviso, the second criteria of Leaman (1994) is satisfied.

Leaman's (1994) third criteria is satisfied for the density properties of lithologic units, but not for the measured magnetic susceptibility values. This is most likely due to partial destruction of magnetite during weathering, although variations in the magnetic susceptibility within each rock type is a possibility. The inferred magnetic susceptibility values are within the range of average values for similar rock types world wide (Sharma, 1986), therefore, the models are considered reasonable.

The pattern of four intersecting transects satisfies the fourth criteria of Leaman (1994).

The 'M - shift' and 'G - shift' shown in Figures 6.2 - 6.5 are a measure of the amount by which the calculated Bouguer anomaly and magnetic base lines need to be shifted in order to coincide with the actual values. An explanation and justification for the M - shift and G -

shift are given by Leaman (1994) and the following is extracted from his article (with minor modifications). The zero in the observed magnetic data after removal of the International Geomagnetic Reference Field is dependant on the reference value chosen for the survey which is usually arbitrarily selected due to the time variance of the magnetic field. The resultant zero may vary considerably from the true value, however, the relativity of the magnetic responses are unaffected and merely require a scalar (M - shift) in order to adjust them to the true value. The Bouguer gravity data are normalised to a density of 2.67 $tm^{-3}$, however the actual values depend on regional effects and the geology to considerable depths. In the absence of correction for regional affects, a scalar (G - shift) is required to adjust the observed data to the true values. A residual gravity value has not been calculated for the Eyre Peninsula. All profiles have consistent M - shift and G - shift values satisfying Leaman's (1994) fifth criteria.

With all of the criteria established by Leaman (1994) satisfied within the limitations of the data, models incorporating a granite body of 20 - 40 km diameter beneath the Menninnie Dam prospect are considered to form a valid, geologically defensible solution to the long wavelength positive magnetic feature and coincident gravity low occurring near the Menninnie Dam prospect.

The 1 - 3 km depth to the upper surface of the 'MD granite' is compatible with the absence of substantial thicknesses of granite in drill intersections from the Menninnie Dam prospect and nearby prospects (maximum depth extent of drilling is 643 m vert.). The 'MD granite' has been modelled with a near flat to gently dipping upper surface. The apparent flat topped nature is consistent with the observations of Turner (1975) for granites of the Hiltaba Suite. The large lateral extent and smaller depth extent of the 'MD granite' is similar to dimensional relationships observed for granite plutons elsewhere, (Vigneresse, 1983; Lee, 1986; Hodge et al., 1982; Hutton, 1982), The shape of granite bodies has been interpreted to result from effects during intrusion and / or syn, or post, intrusive deformation (Vigneresse, 1990). A near equidimensional plan shape of the 'MD granite' is interpreted from geophysical modelling, compatible with post, or late, orogenic intrusion. On the basis of shape, the 'MD granite' can be differentiated from granites of the Lincoln Complex intruded during KM-$D_{1-2}$ which commonly have a pronounced north - south elongation. The shape of the 'MD granite' cannot be used as a discriminant to differentiate between a granite of the Lincoln Complex intruded during, or soon after KM-$D_3$ (Moody Suite; Parker, 1993a) and a granite of the Hiltaba Suite as the Moody Suite are commonly less deformed than granites of the Lincoln Complex interpreted to have intruded prior to, or during KM-$D_{1-2}$ (Parker, 1993a).

Rhyolite intrusions, and the coherent rhyolite unit at the Menninnie Dam prospect have textural similarities to rhyolite dykes of the Hiltaba Suite (Section 4.4.1). They also have geochemical similarities to granites of the Hiltaba Suite (Section 4.3.5). Granite dykes

intruded into the Hutchison Group at Menninnie Dam have been interpreted to be temporally and genetically related to granites of the Moody Suite (Section 3.8.3). It could be equally argued that the rhyolite intrusions and coherent rhyolite units are indicative of an underlying granite of the Hiltaba Suite, or, that the granite dykes are indicative of an underlying granite of the Moody Suite. Neither the rhyolite intrusions and coherent rhyolite units, or the granite dykes are definitive in resolving the nature of the 'MD granite'.

The MD ignimbrite, considered to represent an intracaldera ignimbrite can be interpreted to favour Hiltaba Suite affinities for the 'MD granite'. Scattered outcrop of Bittali Rhyolite forms a circular pattern of 8 - 10 km diameter with a poorly defined coincident circular magnetic pattern to the west of the Menninnie Dam prospect (Figs. 6.1 and 6.2). The position of the Bittali Rhyolite outcrop lies above the interpreted western flank of the 'MD granite' on transect A - A'. Scattered outcrop of Bittali Rhyolite is also associated with the eastern margin of the 'Buckleboo Granite' (Figs. 6.1 and 6.2). The outcrop pattern of the Bittali Rhyolite has formed a rough circular pattern and has a coincident circular magnetic pattern of approximately 10 km diameter. It can be speculated that the 'MD granite', MD ignimbrite, 'Buckleboo Granite' and the scattered outcrops of Bittali Rhyolite are genetically related, in which case, the MD granite would be a member of the Hiltaba Suite. If this speculation is true, then the interpreted 1 - 3 km depth to the top of the 'MD granite' would be within a few kilometres of the final crystallisation depth. As the rhyolite intrusions at Menninnie Dam are interpreted to have been associated with a granite of the Hiltaba Suite, and mineralisation is interpreted to be temporally associated with the rhyolite intrusions (Section 5.6.7), then it can be speculated that mineralisation is also temporally associated with a granite of the Hiltaba Suite.

## 6.10 Conclusions

Two dimensional gravity and magnetic modelling of existing regional geophysical data provides a means of testing the presence or absence of a granite body beneath the Menninnie Dam prospect using an interactive two dimensional modelling program. Measured densities of the different lithologies used for modelling are within the accepted range for similar rock types world wide (Sharma, 1986) and similar to densities used by Gow et al. (1993). Magnetic susceptibility measurements of the same rock samples are generally lower than values inferred from qualitative evaluation of the aeromagnetic data. By substituting average magnetic susceptibility values for similar rock types, meaningful models can be constructed.

The following points are concluded from gravity and magnetic modelling:

- The long wavelength, low order, magnetic high and the near coincident gravity low in the vicinity of the Menninnie Dam prospect are considered to have resulted from intrusion of a granite pluton ('MD granite') of between 20 and 40 km diameter.

- Gravity and magnetic modelling cannot be used as a 'stand alone method' to ascribe Moody Suite, or Hiltaba Suite affinities to the 'MD granite'.
- If the 'MD granite' is genetically related to the intracaldera MD ignimbrite then it must be a member of the Hiltaba Suite.
- The 'MD granite' is likely to be part of a much larger, laterally extensive, batholith which connects granites of the Hiltaba Suite of similar magnetic susceptibility and density outcropping near Buckleboo and Cunyarie Rocks ('Buckleboo Granite' and 'Cunyarie Granite' respectively).
- The 'MD granite' is interpreted to have crystallised as a flat topped, to gently dipping body. If the 'MD granite' is a member of the Hiltaba Suite, then a final crystallisation depth of 0.6 - 3 km is interpreted.
- The sub-circular ring of magnetic highs overtop the 'MD granite' may be due to magnetite produced in high temperature skarns associated with intrusion of the 'MD granite'.
- Weakly altered and strongly altered rhyolite intrusions at Menninnie Dam are interpreted to have intruded during the mineralising event. The rhyolite intrusions may be temporally and genetically linked to intrusion of the 'MD granite', in which case the mineralisation at Menninnie Dam may also be temporally related to intrusion of the 'MD granite'.

# Chapter seven
# Lead isotopes

## 7.1 Introduction

This chapter examines the lead isotope systematics of the Menninnie Dam mineralisation and attempts to answer the following questions:

- What is the lead isotopic signature of the mineralisation?
- Are there any spatial variations in the lead isotope values?
- Was the Menninnie Dam mineralisation produced by a single mineralising event or multiple episodes.
- Has the mineralisation resulted from remobilisation of a pre-existing sulphide deposit? (ie. Broken Hill - Type; Beeson, 1990).
- What was the source of the metals?
- Can a lead model age be calculated for the mineralisation and if so, is this compatible with other age constraints?

## 7.2 Lead isotope data

Lead isotope data from the Menninnie Dam prospect used in this study were compiled from unpublished reports of collaborative research projects between CSIRO, Billiton Australia, and Aberfoyle Resources Ltd., as well as later contract research undertaken by CSIRO for Aberfoyle Resources Ltd. Unpublished CSIRO data are considered to be co-owned by Aberfoyle Resources Ltd and CSIRO and used here with the permission of both organisations.

Samples from Menninnie Dam that were used for Pb isotope analysis were derived from either diamond drill core, reverse circulation percussion chips (RC), or rotary air blast percussion chips (RAB). Samples included extremely weathered rock and kaolinitic clays (commonly from RAB pulp samples), unweathered Hutchison Group rocks, sulphide mineralisation, rhyolite intrusions, and granite dykes. Samples of weathered rock were analysed as whole rock samples. A considerable number of unweathered, sulphide-bearing drill pulps were also analysed as whole rock samples. For other unweathered samples, galena was separated and analysed. Feldspar was extracted and analysed from samples of granite dykes.

Pb isotope determinations of feldspar from the Tarcoola Granite (Hiltaba Suite), located 280 km to the NW of Menninnie Dam were obtained from Fanning (1988). Samples of the Tarcoola Granite were obtained from diamond drill core submitted to AMDEL laboratories by MESA (Flintoft and Horn, 1989). Unpublished Pb isotope determinations of feldspar from

the Charleston Granite, 100 km to the SE of the Menninnie Dam prospect, were analysed at CSIRO by Dean (1994) and are presented here with her permission.

Five Pb isotope determinations were undertaken by Dr. Graham Carr, CSIRO, North Ryde, as part of this study. Four determinations were of sequential leachates of eastern suite schist from 410.62 m in drill hole PD0006. The fifth determination was a feldspar leach of an unnamed granite of the Hiltaba Suite outcropping at Cunyarie Rocks, 32.7 km to the SSW of Menninnie Dam. For ease of reference this unnamed granite is referred to as the 'Cunyarie granite'. Samples of the 'Cunyarie granite' were supplied by MESA and are from the same batch of material used for Rb - Sr dating (MESA sample No. 6132 RS42; Webb et al., 1986).

## 7.3 Analytical methods

With the exception of the Tarcoola Granite determination, all analyses were obtained over a 10 year period at the CSIRO, North Ryde, New South Wales, Australia using the same mass spectrometer under the supervision of either Dr. Gulson, Dr. Carr or Dr. Dean. (Appendix 7.1). Pb isotope determinations of the Tarcoola Granite were obtained by Dr. Mark Fanning at the Australian National University in Canberra.

The methods used for sample preparation and analyses are detailed in the various relevant reports. As some of the reports are unpublished and remain the property of the respective owners, a summary of the methods used is repeated in Appendix 7.1. A measure of the precision for each analysis is shown as two intersecting lines in the upper left corner of most Pb isotope ratio plots (eg. Fig. 7.1a - b). These lines are the axis of the precision ellipse and apply exclusively to analyses performed at CSIRO. Construction of the precision ellipse is based on over 1500 analyses of international standards (Dean, 1994).

## 7.4 Results

A total of 228 lead isotope determinations were undertaken including 224 from the Menninnie Dam prospect from 158 individual samples. The excess of determinations over samples relates to repeat analyses, or analyses of sequential leach solutions from the same sample. The range of determinations is summarised in Table 7.1 Detailed results of determinations are presented in Appendix 7.2 along with the sample source (drill hole number and depth), drill hole collar co-ordinates, drill hole interval, lead assay, uranium and thorium assay, type of analysis, lead content*, and the source of the data.

---

* The difference between 'lead assay' and 'lead content' is explained on page 7.3

The determinations have been subdivided into two groups which correspond to the sample location (Fig. 3.1):

Group 1) northern and central zones

Group 2) southern zone

The basis for this subdivision relates to differences in the style of mineralisation between the northern and central zones, and the southern zone. The southern zone was subjected to the 'late alteration overprint' described in Section 5.3. Of the 224 Pb isotope determinations from the Menninnie Dam prospect, 216 were derived from central and northern zones and 8 are derived from the southern zone.

The drill collar co-ordinate (local grid) does not correspond to the exact northing and easting of the down hole sample position as drill holes are inclined at around 60° from horizontal, and most deviated to the north or south. However, the drill collar coordinate is a useful parameter for assessing spatial variations in isotopic ratios on a prospect scale.

The 'drill hole interval' corresponds to an interval of drill core, or chips, (typically 0.5 - 5 m long) that was assayed for Pb and other elements. The lead assay for each drill hole interval is referred to as the 'lead assay'. The distribution of lead is not homogenous throughout drill hole intervals and a lead assay of 1000 ppm could result from a single sulphide vein only a few centimetres wide in 2 m of core, or alternatively, from more disseminated sulphide mineralisation. The lead assay value is useful for investigation of how the lead assay of the rock affects the lead isotope determination.

The lead content of the actual sample used for isotopic determination is presented for some determinations and is referred to as the 'lead content'. The lead content of whole rock, or feldspar separates, was measured by the 'lead isotope dilution technique' (Gulson, 1986; Carr and Dean, 1990). The lead content may vary substantially from the lead assay, particularly for determinations of galena which have a lead content of 86.6 wt.%, but may have been derived from a drill hole interval that has a low lead assay value.

Uranium and thorium assays of drill hole intervals were not routinely determined and are presented where applicable (Appendix 7.2). Beeson (1990) determined the average uranium content of the host rocks and mineralisation to be < 4 ppm with no appreciable variation between host rocks and mineralisation.

### 7.4.1 Lead isotope ratio plots

All Pb isotope ratio diagrams are presented in the standard format of $^{207}Pb$ / $^{204}Pb$ or $^{208}Pb$ / $^{204}Pb$ versus $^{206}Pb$ / $^{204}Pb$ and incorporate the Stacey and Kramers (1975) average crustal growth curve. The Stacey and Kramers (1975) average crustal growth curve was considered

by Gulson (1986) to be more conformable with stratigraphic ages for the Proterozoic of Australia compared to the Cumming and Richards (1975) growth curve.

Diagrams of lead isotope data from Menninnie Dam are illustrated in Figures 7.1a -b. These data form an elongated array with a cluster of less radiogenic determinations. Many of the less radiogenic determinations lie along the machine fractionation trend line and are contained within the precision ellipse. It is this least radiogenic population which Carr et al. (1986) termed the 'target population' which defined the 'target signature' (Fig. 7.2). The concept of a target signature was intended to define the isotopic signature of massive sulphide mineralisation at the Menninnie Dam prospect. This signature was then used as a discriminant to focus exploration towards more massive, and hence potentially more economic mineralisation. Pb isotope values that plot outside the target population were interpreted to have been derived from mineralisation that was less likely to be economic.

Carr et al. (1986) defined the target signature as encompassing a cluster of least radiogenic Pb isotope determinations with a mean $^{206}Pb$ / $^{204}Pb$ ratio of 16.063 and a standard deviation of 0.011. Dean and Carr (1990) redefined the target signature ($\pm$ 2 sigma) as:

$^{206}Pb$ / $^{204}Pb$ ratio of 16.063 $\pm$ 0.022
$^{207}Pb$ / $^{204}Pb$ ratio of 15.434 $\pm$ 0.028
$^{208}Pb$ / $^{204}Pb$ ratio of 35.913 $\pm$ 0.088

In defining the target signature, only galena separates, or sample pulps with a high lead content (and contained galena), were used. Some isotopic analyses from high lead samples fell outside the target population and were interpreted as probably derived from vein style mineralisation (Carr et al., 1986). The commonly radiogenic signature of low lead samples was attributed to in-situ decay of U and Th resulting in a higher proportion of radiogenic lead (Carr et al., 1986).

### 7.4.2 Feldspar Pb isotopes

Feldspar determinations have been separated into two groups:

- Three determinations from granite dykes. Granite dykes intrude Hutchison Group lithologies at Menninnie Dam and are interpreted to be Moody Suite correlatives intruded at $\approx$ 1745 - 1710 Ma. during KM-$D_3$ (Section 3.8.3).
- Three determinations from granites of the Hiltaba Suite located in the northern Eyre Peninsula. (eg. Tarcoola Granite, 'Cunyarie Granite' and the Charleston Granite.). The Hiltaba Suite has a mean weighted age of 1589 Ma. (Creaser and Cooper, 1993).

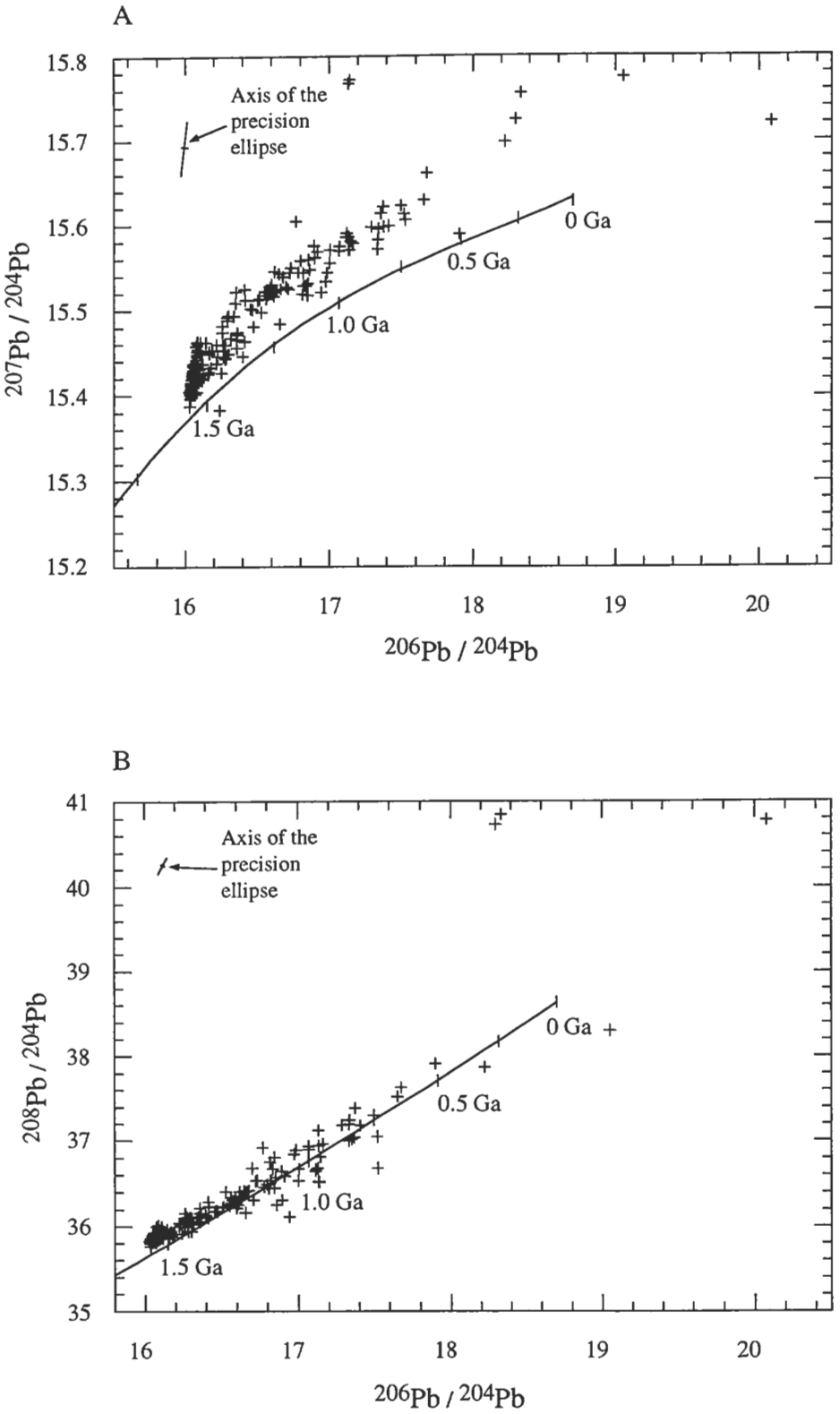


Fig. 7.1a and b. Pb isotope ratios of all of the Menninnie Dam galena and whole rock Pb isotope determinations (224) define a sub-linear array with a distinct cluster of determinations a at the least radiogenic end of the array which define the 'target population' (ref. text). Most of the determinations lie above a Stacey and Kramer (1975) average crustal growth curve. A measure of the precision of determinations is indicated by the error bars (top left of diagrams) which define the axis of the 'precision ellipse'.

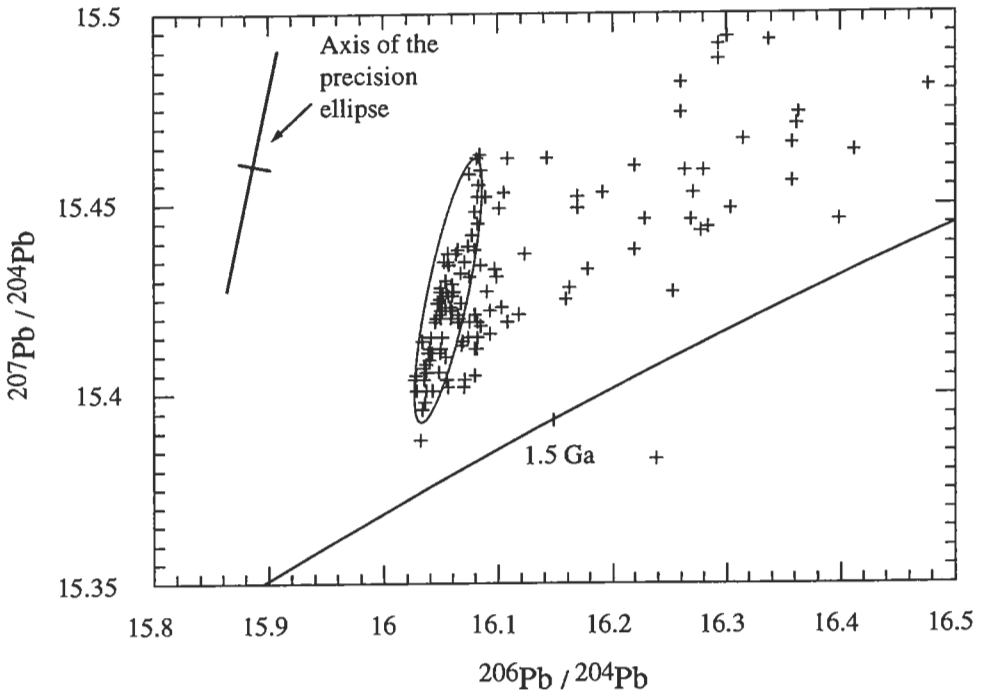


Fig. 7.2. An expanded view of the least radiogenic determinations, or 'target population' (circled) relative to the position of the Stacey and Kramer (1975) average crustal growth curve. The target population is elongated parallel to the long axis of the precision ellipse.

The Hiltaba Suite Pb isotope determinations are generally less radiogenic than granite dyke determinations (Table 7.1 and Figs. 7.3a - b).

Table 7.1 Range of the least radiogenic Pb isotopic determinations from analyses of feldspars from three granite dykes at Menninnie Dam and three granites of the Hiltaba Suite from the northern Eyre Peninsula.

| Isotopic ratio | Granite dykes | Granites of the Hiltaba Suite |
|---|---|---|
| $^{206}Pb / ^{204}Pb$ | 16.449 - 16.897 | 15.858 - 16.441 |
| $^{207}Pb / ^{204}Pb$ | 15.291 - 15.480 | 15.341 - 15.413 |
| $^{208}Pb / ^{204}Pb$ | 35.986 - 36.038 | 35.616 - 36.214 |

*Granite dykes*

Granite dyke determinations were derived from three samples, two of which are from granite dykes intruded into Hutchison Group lithologies at Menninnie Dam and the third is a ≈ 15 m diameter granite clast incorporated in the MD ignimbrite. Feldspar from the granite dykes is commonly unaltered or weakly altered (Section 3.4.1). Feldspar from the granite clast has been partially, to pervasively, altered to sericite, calcite and chlorite and Pb isotope determinations are unlikely to be representative of the unaltered material. The two granite dyke samples plot close to the Stacey and Kramers (1975) average crustal growth curve, and have higher $^{207}Pb / ^{204}Pb$ and $^{208}Pb / ^{204}Pb$ ratios than the target population (Figs. 7.3a - b). The granite clast included in the MD ignimbrite has a lower $^{207}Pb / ^{204}Pb$ ratio compared to the target population. Due to the effects of alteration, the Pb isotope determination of the granite clast is considered to be of little value for the purposes of this study and will not be considered further.

*Granites of the Hiltaba Suite*

Feldspars from the Tarcoola Granite (Fanning, 1988) and the 'Cunyarie granite' that were used for analyses were unaltered. The nature of feldspar from the Charleston Granite is not known. Determinations from granites of the Hiltaba Suite lie close to, but below the target population on a $^{207}Pb / ^{204}Pb$ vs $^{206}Pb / ^{204}Pb$ diagram (Fig. 7.3a).

### 7.4.3 Galena Pb isotopes

Lead isotope data derived for galena are shown in Figures 7.4a - b, and summarised in Table 7.2. Ninety seven determinations are presented in Figures 7.4a - b from 70 individual samples. The excess of determinations over samples relates to repeat analyses.

Table 7.2 Range of values for 97 Pb isotopic determinations of galena from Menninnie Dam.

| Isotopic ratio | Granite dykes |
|---|---|
| $^{206}Pb / ^{204}Pb$ | 16.027 - 17.159 |
| $^{207}Pb / ^{204}Pb$ | 15.398 - 15.587 |
| $^{208}Pb / ^{204}Pb$ | 35.804 - 36.962 |
| Lead assay values range from | 44.6 wt.% - 30 ppm Pb |

The galena Pb isotope data defines a near linear array with a cluster of less radiogenic values elongated along the machine fractionation trend (Figs. 7.4a - b).

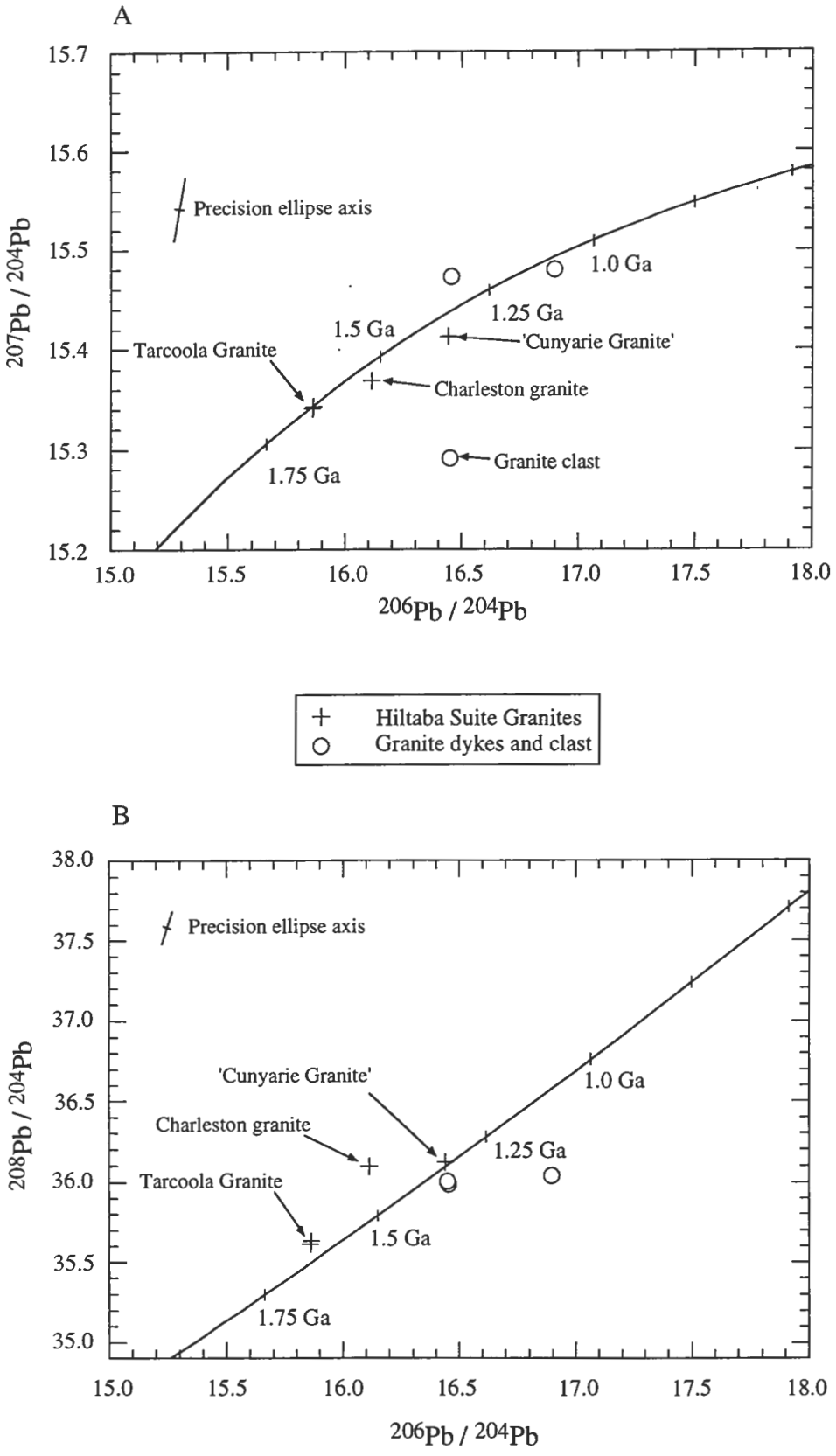


Fig. 7.3a -b. Lead isotope determinations from felspar leaches of 3 granites of the Hiltaba Suite, 2 granite dykes and 1 large granite clast from within the MD ignimbrite. Pb isotope determinations of granites of the Hiltaba Suite and the granite dykes lie close to the Stacey and Kramer (1975) average crustal growth curve. The granite clast lies well below the Stacey and Kramer (1975) average crustal growth curve in Fig. 7.3a.

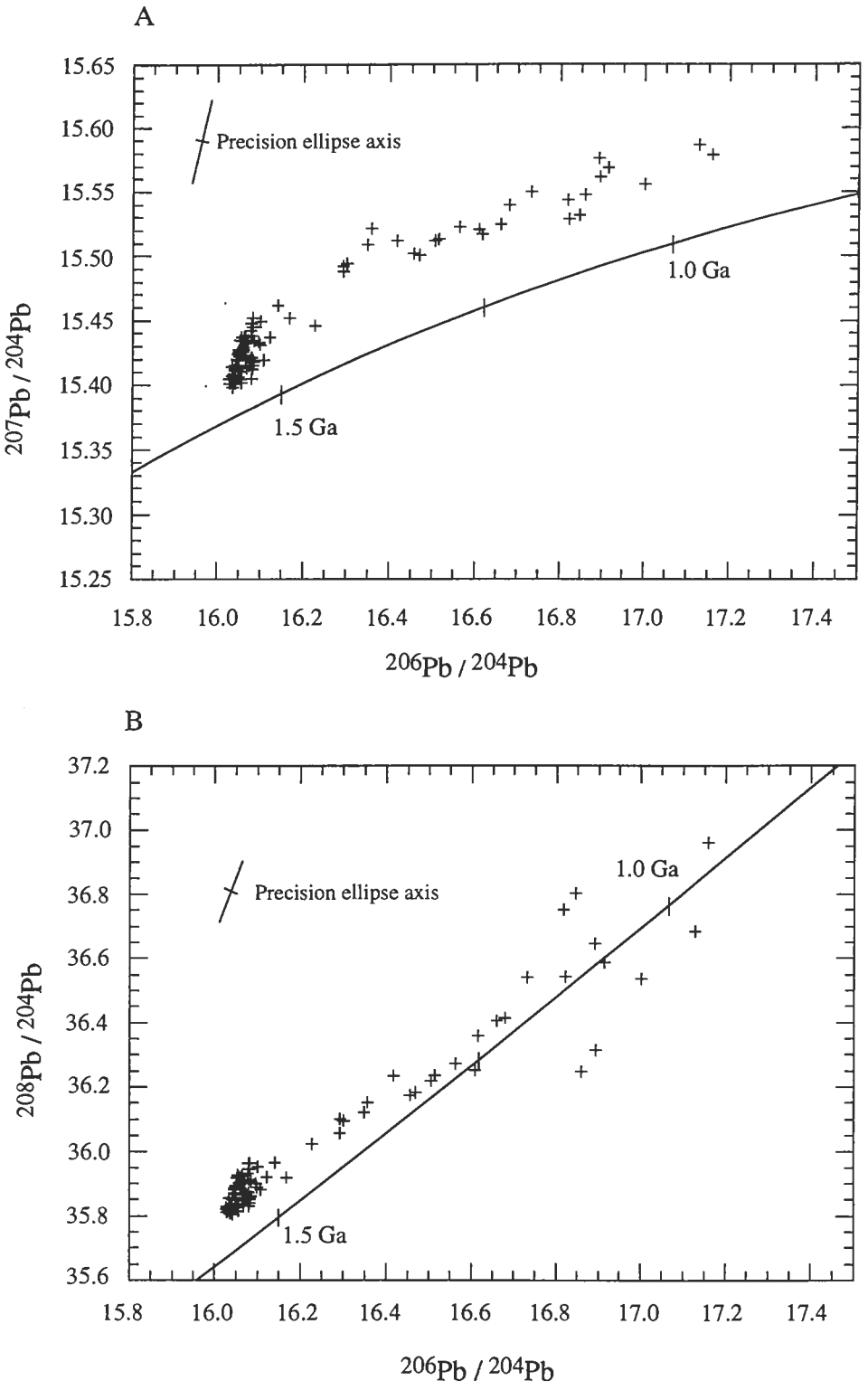


Figs. 7.4a - b. Lead isotope determinations from galena. Many of the least radiogenic determinations form a cluster that overlaps with the target population. A significant number of analyses lie outside the target population and form an array of more radiogenic values, most of which lie above the Stacey and Kramer (1975) average crustal growth curves.

This cluster corresponds to the target population defined by Dean and Carr (1990) and contains 45% of the galena determinations. The remaining 55% of determinations are more radiogenic. The high lead content and near zero U / Pb and Th / Pb ratios of galena assure that a negligible amount of radiogenic lead has been produced from the decay of either Th or U since formation of galena. Therefore, the measured $^{207}Pb$ / $^{204}Pb$, $^{206}Pb$ / $^{204}Pb$ and $^{208}Pb$ / $^{204}Pb$ ratios are initial ratios and any radiogenic Pb must have been incorporated at the time of galena formation.

### 7.4.4 Whole rock Pb isotopes

The whole rock data was derived from a variety of samples including:

- Pulps of unweathered, mineralised Hutchison Group lithologies. Pulps invariably contain galena.
- Pulps of unweathered, mineralised granite dykes, MD ignimbrite and DP breccias. Pulps commonly contain galena.
- Pulps of unweathered Hutchison Group lithologies, granite dykes and rhyolite intrusions that contain no visible mineralisation.
- Pulps of weathered lithologies with abundant clay minerals.

The range of Pb isotope ratios derived from whole rock samples is summarised in Table 7.3 and detailed in Appendix 7.2.

Table 7.3 Range of values for 119 Pb isotopic determinations of derived from whole rock samples from Menninnie Dam.

| Isotopic ratio | Granite dykes |
|---|---|
| $^{206}Pb$ / $^{204}Pb$ | 16.032 - 20.082 |
| $^{207}Pb$ / $^{204}Pb$ | 15.383 - 15.775 |
| $^{208}Pb$ / $^{204}Pb$ | 35.764 - 40.776 |
| Lead assay values range from | 25.4 wt.% - 75 ppm Pb |

As with the galena samples, the whole rock analyses define an elongated, near linear, array on a $^{207}Pb$ / $^{204}Pb$ vs $^{206}Pb$ / $^{204}Pb$ diagram (Fig. 7.5a). These data form a cluster of least radiogenic values many of which lie within the precision ellipse and overlap with the target population defined from galena samples and results from the galena-rich nature of some pulp samples.

Most determinations lie above the Stacey and Kramers (1975) average crustal growth curves on a $^{207}Pb$ / $^{204}Pb$ vs $^{206}Pb$ / $^{204}Pb$ diagram (Fig. 7.5a). Less radiogenic determinations lie above the Stacey and Kramers (1975) growth curve on a $^{208}Pb$ / $^{204}Pb$ vs $^{206}Pb$ / $^{204}Pb$ diagram, whereas more radiogenic samples commonly plot on or below the growth curve (Fig. 7.5b). The position of determinations relative to the Stacey and Kramers (1975) $^{207}Pb$ / $^{204}Pb$ vs $^{206}Pb$ / $^{204}Pb$ average crustal growth curve has significance as to the origin of the lead and is discussed on Section 7.9.

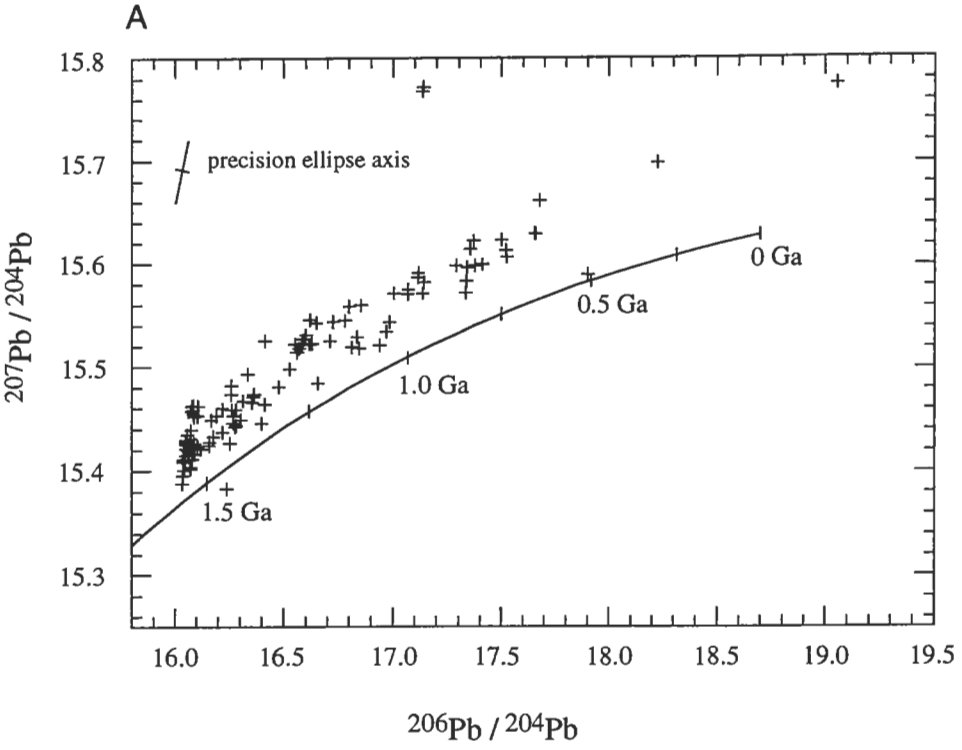


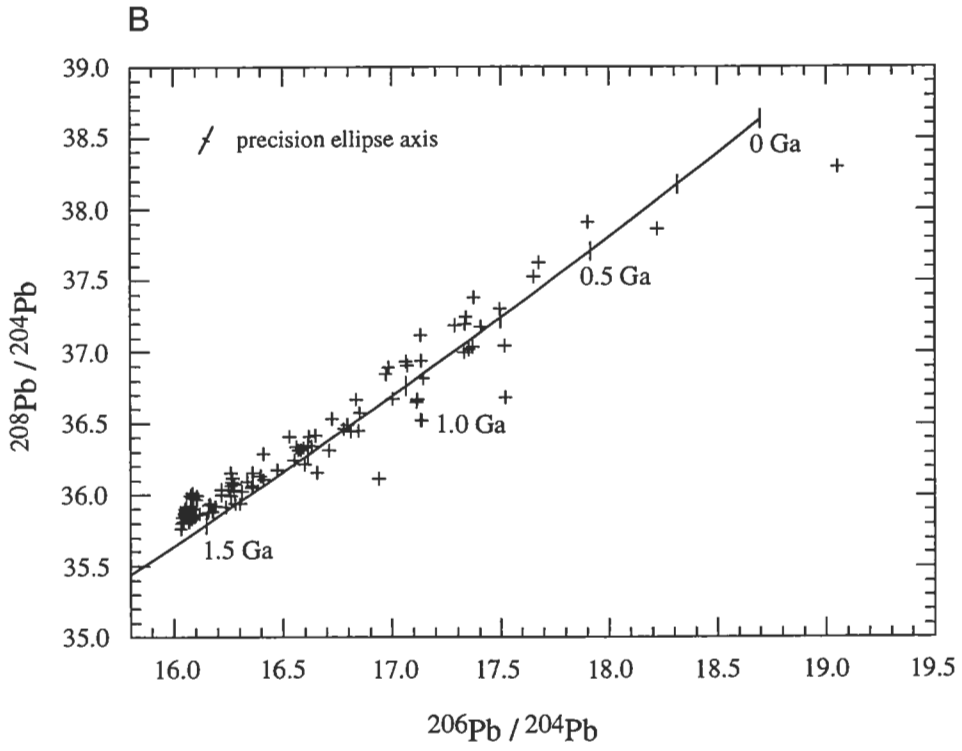


Figs. 7.5a - b. Lead isotope determinations from whole rock samples. Most determinations lie above the Stacey and Kramer (1975) average crustal growth curve and form an array with a cluster of least rediogenic determinations.

### 7.4.5 Isotopic ratios versus lead assay.

The relationship between the lead assay and the $^{207}Pb$ / $^{204}Pb$, $^{206}Pb$ / $^{204}Pb$ and $^{208}Pb$ / $^{204}Pb$ ratios for both galena and whole rock samples from the northern, central and southern zones is illustrated in Figures 7.6a - c. Lead assay values generally have an inverse relationship with isotopic ratios.

## 7.5 Discussion

### 7.5.1 Range of Pb isotopic determinations for granites of the Hiltaba Suite

Granites of the Hiltaba Suite were interpreted to have been emplaced over a geologically short time period between 1600 - 1585 Ma. (Flint, 1993b; Creaser and Cooper, 1993), yet Pb isotope determinations of three granites of the Hiltaba Suite have a range of values (Figs. 7.3a - b). Assuming the initial leach process used during sample preparation was 100% effective in removing all radiogenic lead produced by decay of uranium or thorium after crystallisation of the granite, and the samples consisted solely of unaltered feldspar, variations in the isotopic ratios for the three granites of the Hiltaba Suite may have resulted from:

- Local variations in the isotopic ratios of the source rocks to each of the granites.
- Local variations in the extent of partial melting, fractionation and crustal assimilation in producing the leach of the granites. The role of these processes in formation of the Hiltaba Suite and co-magmatic Gawler Range Volcanics has been discussed by Giles (1988), Stewart (1992) and Creaser (1995).

Alternatively, the leach processes involved in sample preparation may not have been 100% effective in removing all radiogenic lead produced by decay of uranium or thorium after crystallisation of the granite. Analysis of successive feldspar leachates commonly result in progressively less radiogenic isotopic ratios, however, in some instances, analysis of the final leachate results in a more radiogenic isotopic ratio than analyses of earlier leachates. The final leach results in total dissolution of all minerals, and the high uranium content may result from of microscopic inclusions of zircon. The least radiogenic determination from analyses of different leachates for the Tarcoola and Charleston Granites is reported, however only the final leach of the 'Cunyarie Granite' was analysed. This may explain the more radiogenic determination for the 'Cunyarie Granite'.

### 7.5.2 Isotopic ratios versus lead assay

An inverse relationship of lead content and radiogenic ratios is common for galena free samples with lead contents of less than a hundred parts per million from many lead bearing mineral deposits (Gulson, 1986; Gulson et al., 1987).

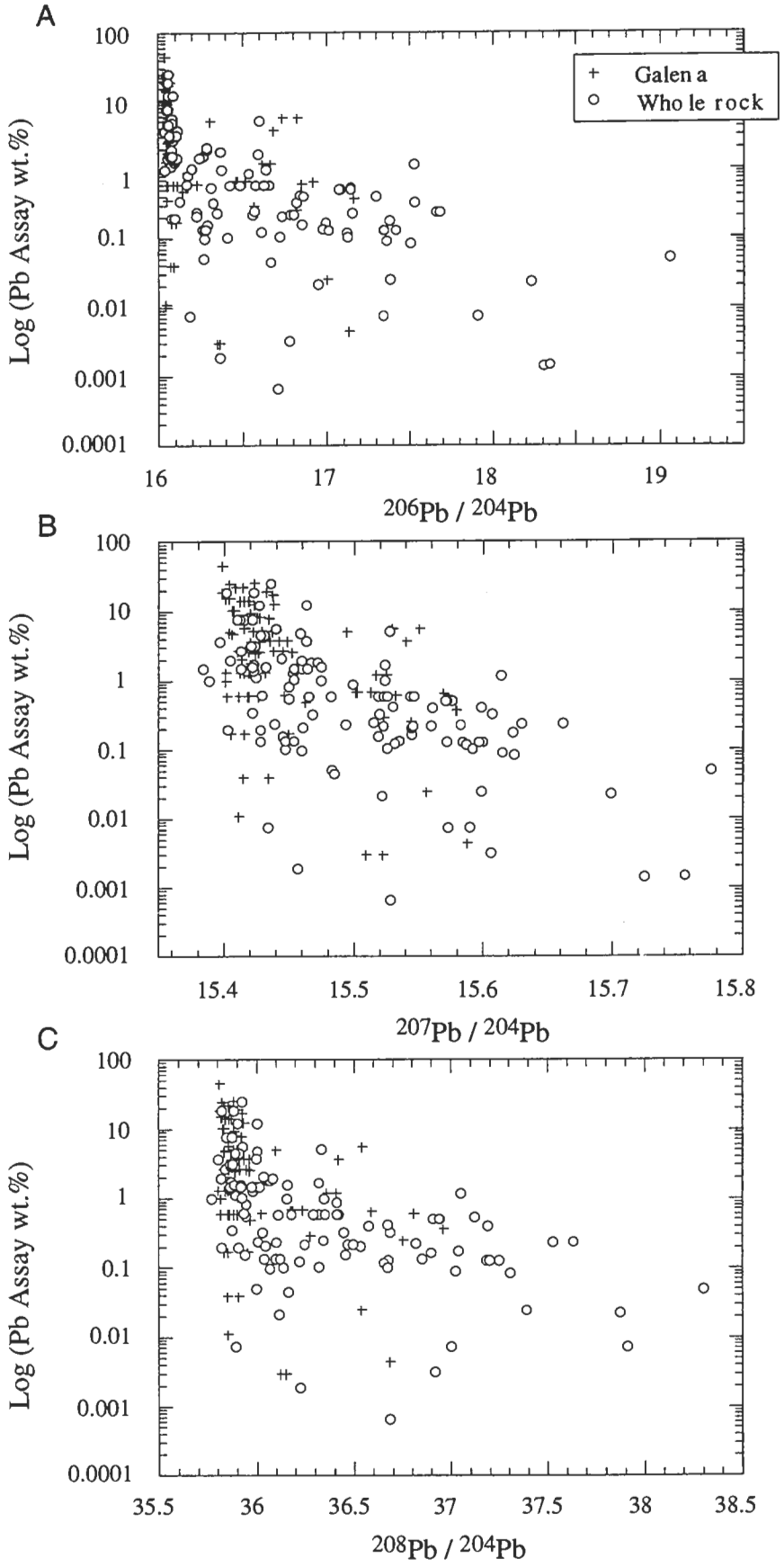


Figure 7.6a - c. Diagrams of log lead assay (wt.%) versus log 206Pb / 204Pb, log 207Pb / 204Pb and log 208Pb / 204 Pb. Lead assay is the Pb assay value of the drill hole sample interval from which the Pb isotope sample was derived. Lead isotope determinations derived from galena are shown as crosses and determinations derived from whole rock samples are shown as circles. Lead assay values have an inverse relationship with Pb isotope determinations derived from both galena and whole rock samples.

In older rocks, such as the Hutchison Group, an inverse relationship may have resulted from a low initial lead content, relatively high initial U / Pb and Th / Pb ratios, and the addition of radiogenic lead through decay of U and Th.

More radiogenic signatures associated with veins or more distal portions of mineral deposits are well known (eg. Russell and Farquhar 1960; Zartman and Stacey, 1971; Goodwin et al., 1982). For example, Thompson and Beaty (1990) found that vein galena from the Leadville district had a greater range of isotopic values than the manto galenas. They attributed this distribution to a greater influence of the wall rocks away from the main carbonate replacement bodies.

The association of more radiogenic lead isotope ratios with low lead assay values at Menninnie Dam is also interpreted to have resulted from greater interaction of the mineralising fluids with host rocks. Carr et al. (1986) arrived at a similar conclusion for the Menninnie Dam mineralisation. More radiogenic isotopic ratios of low lead samples result from the difference in availability of non-radiogenic versus radiogenic lead from the host minerals. Lead incorporated in the lattices of minerals, such as feldspar, is tightly held whereas uranium and thorium are often present as interstitial ions in mineral lattices, particularly in uranium-rich minerals such as zircon, and are commonly less tightly held. $^{206}Pb$, $^{207}Pb$ and $^{208}Pb$ produced by in-situ decay of uranium and thorium is also loosely held and more readily leached by hydrothermal fluids (Doe et al., 1972; Ludwig and Silver, 1977; Doe et al., 1979; Godwin et al., 1988). The availability of radiogenic lead produced by in-situ decay may be aided by radiation damage to the host mineral during the decay process (Godwin et al., 1988).

An alternative interpretation is that more radiogenic lead was associated with a younger mineralising event, however this can be discounted as the late alteration overprint is the only hydrothermal event interpreted to have post-dated mineralisation at Menninnie Dam, and is confined to the southern zone (Section 5.3). While there are in excess of 100 lead isotope determinations with values that are more radiogenic than the target signature, only nine determinations were derived from the southern zone.

### 7.5.3 Source of the lead

Doe and Zartman (1979) recognised a relationship between small deviations in the isotopic ratios of similar age ore bodies and their tectonic setting. Their model, which they named 'Plumbotectonics' contains four growth curves. Three of the growth curves relate to lead derived from three different lead reservoirs, namely 'upper crustal', 'mantle' and 'lower crustal'. The fourth growth curve results from a mix of the three lead reservoirs as might occur during orogenesis and is termed the 'orogene curve'.

The Menninnie Dam data for the northern, central and southern zones lies between the upper crust and the orogene growth curves (Fig. 7.7). More radiogenic determinations plot closer to the upper crustal growth curve and are interpreted to have incorporated a greater component of upper crustal lead compared to the target population. The target population lies mid-way between the orogene and upper crustal growth curves and is interpreted to contain a component of lead derived from orogene, mantle or lower crustal reservoirs.

The Hutchison Group lithologies are interpreted to be upper crustal rocks. The nature of the lower crust beneath the Menninnie Dam prospect is not known. Sleaford Complex rocks (≈ 2600 Ma.; Daly and Fanning, 1993) crop out ≈ 40 km to the SW of the Menninnie Dam prospect and probably underlie the Hutchison Group at Menninnie Dam (ref. Section 6.5). The presence of older crustal rocks in the Eyre Peninsula with depleted mantle model ages of ≤ 3200 Ma. was interpreted from Nd isotope analyses of some Archaean rocks (Daly and Fanning, 1990; Cowley and Fanning, 1991; Creaser and Fanning, 1993). No lead isotopic data was located for Archaean rocks of the Gawler Craton.

Rock types in the vicinity of Menninnie Dam that may have a mantle or orogene Pb isotope signature include the granite dykes and the granites of the Hiltaba Suite. Mineralisation is interpreted to have significantly post dated intrusion of the granite dykes (Section 5.6.1), therefore the granites dykes could not have provided the mineralising fluid. Later leaching of lead from granite dyke feldspars is interpreted to have been an unlikely lead source as the granite dykes have higher $^{206}Pb$ / $^{204}Pb$, $^{208}Pb$ / $^{204}Pb$ and variable $^{207}Pb$ / $^{204}Pb$ ratios compared to the target population (Fig. 7.7).

*Hiltaba Suite lead source*

Granites of the Hiltaba Suite have lower $^{207}Pb$ / $^{204}Pb$ ratios than the target population and comparable $^{208}Pb$ / $^{204}Pb$ and $^{206}Pb$ / $^{204}Pb$ ratios. Lead isotope determinations of granites of the Hiltaba Suite lie on, or close to, the orogene curve of Doe and Zartman (1979; Fig. 7.7). Formation of the mineralisation at Menninnie Dam and emplacement of the rhyolite intrusions are interpreted to have been coeval (Section 5.6.7). The rhyolite intrusions are interpreted to have similar geochemistry to granites of the Hiltaba Suite (Section 4.3.5) and a substantial body of granite with possible Hiltaba Suite affinities is interpreted to be present few kilometres beneath the Menninnie Dam mineralisation based on gravity and magnetic modelling (Section 6.9). It is conceivable that a granite of the Hiltaba Suite is one end member of a mixing trend which supplied lead with a lower $^{207}Pb$ / $^{204}Pb$ ratio that mixed with lead with higher a $^{207}Pb$ / $^{204}Pb$ ratio (upper crustal lead) to form the target population.

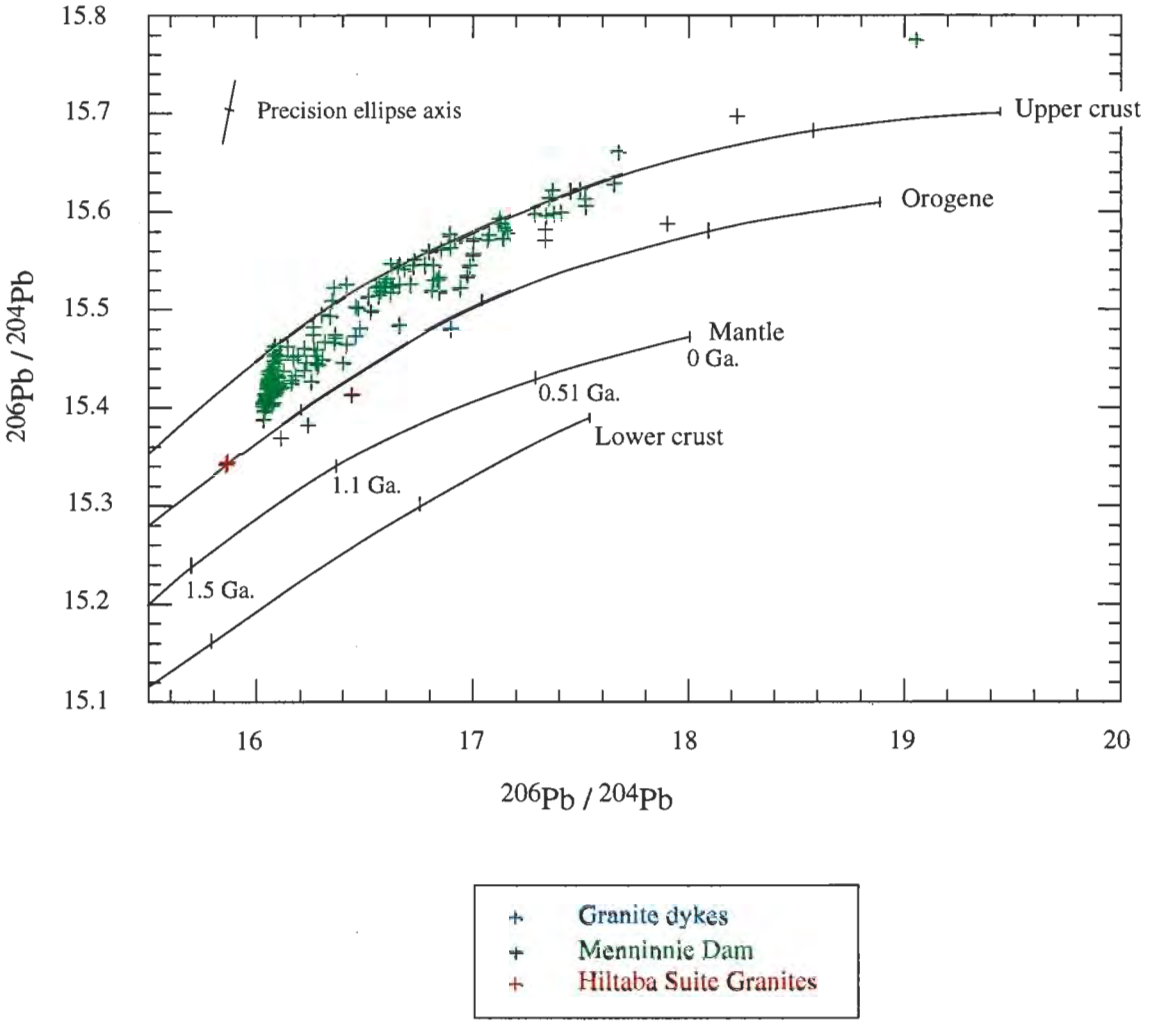


Fig. 7.7. Plumbotectonics model of Doe and Zartman (1979) with four growth curves that result from the evolution of three lead reservoirs: mantle, lower crustal and upper crustal, and a fourth growth curve, the orogene curve, that results from mixing of the three lead reservoirs. The Menninnie Dam target population lies midway between the orogene and upper crustal growth curves. More radiogenic determinations lie closer to the upper crustal growth curve. The Hiltaba Suite granites lie on or just below the orogene growth curve.

*Hutchison Group lead source*

The second end member of a mixing trend may have been lead sourced from the Hutchison Group rocks. Although the mineralisation is hosted by carbonates and calc-silicate lithologies, volumetrically, the most common lithology in the vicinity of the Menninnie Dam deposit is the schists of the western and eastern suites which have been correlated with the Cook Gap Schist (Sections 3.2.1 and 3.2.3). The average lead content of un-mineralised eastern suite schist and marble at Menninnie Dam is ≈ 30 ppm and ≈ 10 ppm respectively. The world wide average concentration of lead in carbonates and marbles, and schists / gneisses is 5 and 19.6 ppm respectively (Wedepohl 1978), therefore the schist was probably greater Pb reservoir than the carbonate rocks. The age of the Cook Gap Schist is constrained by the approximate timing of metamorphism of the Miltalie Gneiss at the base of the Hutchison Group (≈ 1964 Ma.; Fanning et al., 1988) and by uranium - lead zircon dating of the Bosanquet Formation at the top of the Hutchison Group (1845 Ma., Rankin et al., 1988).

In order to test the hypothesis that the eastern and western suite schists were the second end member of a mixing trend, a sample of eastern suite schist from 410.6m depth in drill hole PD0006 was jaw-crushed to < 4 mm and the 0.5 - 1.0 mm fraction separated and subjected to four sequential leaches (Table 7.4). The lead isotopic ratios of each of the leachates were determined by Dr. Graham Carr at CSIRO laboratories, North Ryde, NSW.

Table 7.4. Sequential acid leach treatment of a sample of the eastern suite schist. Detailed analyses are presented in Appendix 7.2

| Leach sequence | Solvent | $^{206}Pb$ / $^{204}Pb$ | $^{207}Pb$ / $^{204}Pb$ | $^{208}Pb$ / $^{204}Pb$ |
|---|---|---|---|---|
| First leach | HCl leach | 16.358 | 15.456 | 36.219 |
| Second leach | HCl leach | 16.701 | 15.528 | 36.681 |
| Third leach | HCl and $HNO_3$ leach | 16.769 | 15.605 | 36.916 |
| Fourth leach | $HNO_3$ and HF leach | 18.336 | 15.755 | 40.850 |
| Fourth leach | repeat analysis | 18.298 | 15.724 | 40.734 |

The first leach was intended to strip unbound lead contamination caused by a variety of geologic processes and for this reason is disregarded, however all results are reported in Appendix 7.2. Leachate from the final $HNO_3$ / HF leach has been analysed twice as a check of precision. Both analyses are within the limits of the precision ellipse (Fig. 7.8). Lead isotope ratio determinations of the leachates have a range of isotopic ratios interpreted to have resulted from variations in the solubility of different minerals in each of the different leach solutions and the differing proportions of radiogenic and non-radiogenic Pb in each of the minerals.

The isotopic determinations of the eastern and western suite schists plot above the Stacey and Kramers (1975) average crustal growth curve which has a $\mu$ value of 9.736 ($\mu = {}^{238}U / {}^{204}Pb$). Different leach solutions probably leached lead from different minerals to varying extents. The Pb isotope evolutionary paths for each of the minerals should lie on different growth curves with $\mu$ values of > 9.736.

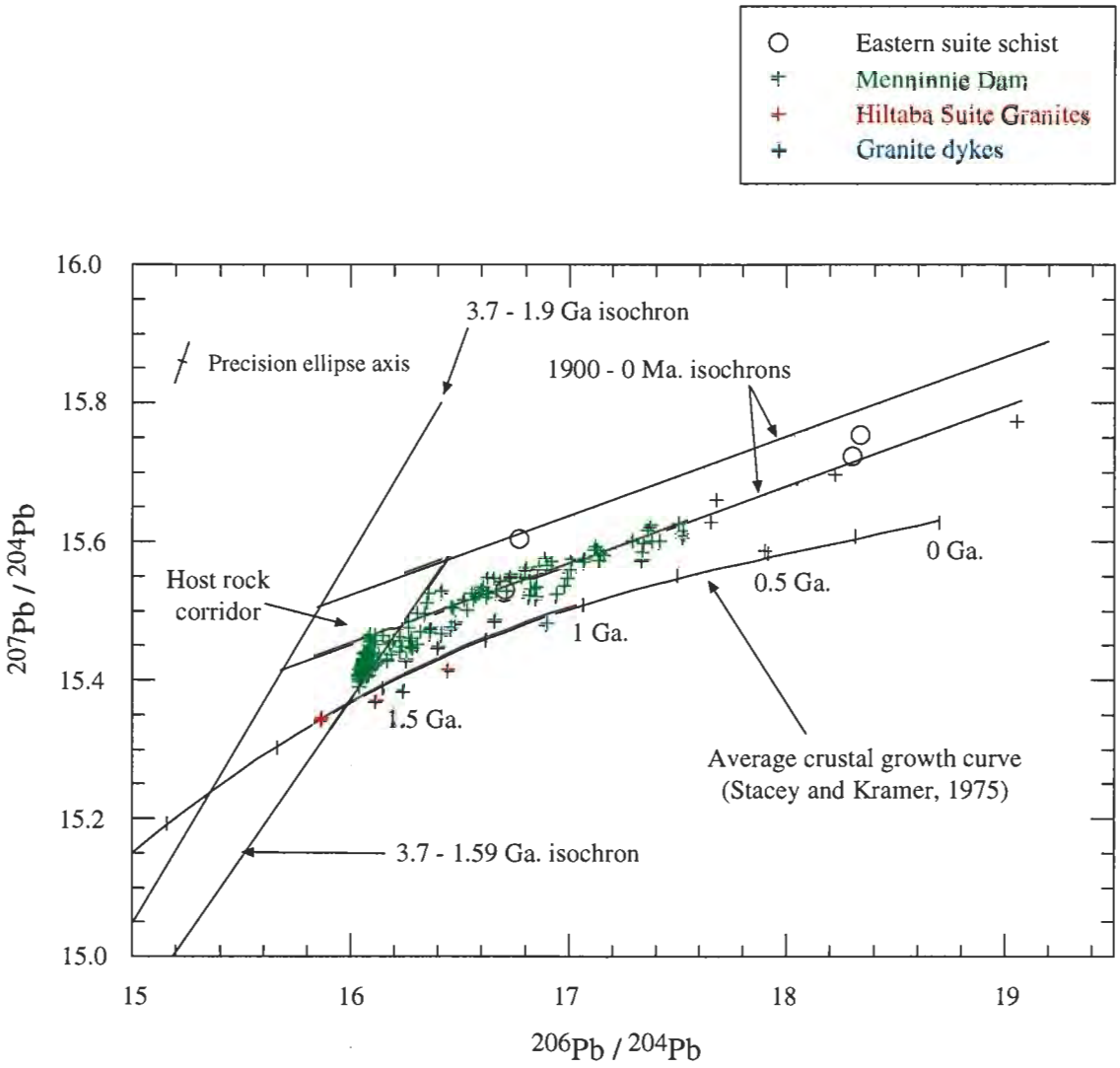


Figure 7.8 Sequential leaches of un-mineralised eastern suite schist have a range of lead isotope ratios. When these ratios are constrained within two 1900 - 0 Ma secondary isochrons (the approximate age of the Hutchison Group to present) they define the 'host rock corridor' that lies above the target population at 1590 Ma. The host rock corridor approximates the evolutionary trend of lead in Hutchison Group lithologies from 1900 Ma. to present. The host rock corridor incorporates a significant proportion of the more radiogenic Menninnie Dam whole rock and galena determinations.

The start of each growth curve is constrained by the initial Pb isotope ratio for the particular mineral, most of which should lie on a 3700 - 1900 Ma. isochron*, but cannot be quantified further. The Pb isotope evolutionary path for the eastern suite schist from the time of formation, ≈ 1900 Ma. ago to present, can be approximated by constraining the determinations to a 'corridor' defined by two 1900 - 0 Ma. isochrons constructed for two different initial $^{207}Pb$ / $^{204}Pb$ ratios of 15.442 and 15.373 (Fig. 7.8). This approximation is subject to the caveat that there has been no loss or gain of uranium or lead during this time period (closed system).

The age of the Hiltaba Suite is estimated as 1589 Ma. (Creaser and Cooper, 1993). When a 3700 - 1589 Ma. isochron is constructed, the target population lies in-between the interpreted 1589 Ma. ratio for the host rocks and the initial ratio for granites of the Hiltaba Suite (Fig. 7.8). Therefore, the target population can be interpreted to be the product of mixing of lead derived from these two sources.

The host rock corridor incorporates a significant proportion of the more radiogenic whole rock and galena analyses from Menninnie Dam, most of which have corresponding low lead assay values. Determinations outside the target population are interpreted to have resulted from a higher component of radiogenic lead derived from the host rocks through interaction with the mineralising fluids at low fluid : rock ratios. The correlation between low lead assay values and more radiogenic isotopic ratios is similarly interpreted to have resulted from interaction between the mineralising fluid and the host rock with a substantial proportion of the lead derived from the host rock.

### 7.5.4 Spatial distribution of lead isotope ratios

Diagrams of the spatial distribution of lead, silver, zinc, iron, manganese, copper and gold assay values versus northing have a crude bell shaped distribution centred around 9000 mN (Fig. 5.25). which is interpreted to have been close to the centre of the mineralising fluid conduits (Section 5.4.1). With the large number of lead isotope determinations, it is possible to investigate the spatial distribution of isotopic ratios and qualitatively assess the extent to which more radiogenic lead was acquired from the host rocks.

All of the galena and whole rock determinations of samples from the northern, central and southern zones have been used to assess the spatial distribution of lead isotope ratios. Feldspar determinations of the granite dykes and granites of the Hiltaba Suite have been excluded. Diagrams of Pb isotopic ratios versus northing are illustrated in Figure 7.9. At all northings, there is a range of isotopic ratios, interpreted to have resulted from variations in the fluid : host rock ratio.

---

* Detrital mineral grains that have survived metamorphism intact may have initial Pb isotope ratios that do not lie on a 3700 - 1900 Ma isochron.

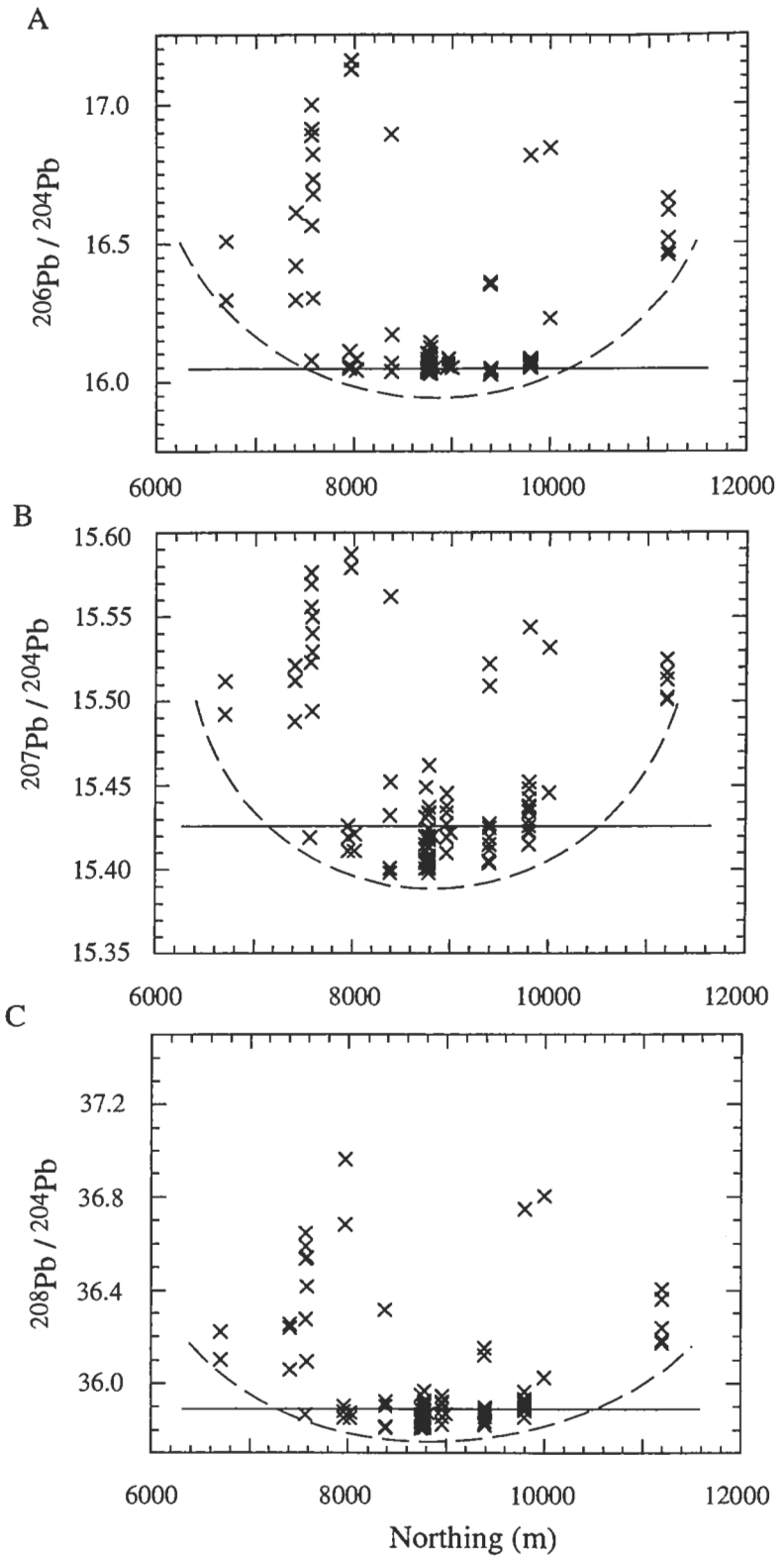


Figure 7.9a - c. The least radiogenic lead isotope ratios have a spatial distribution on over the length of the Menninnie Dam prospect. There is a trend towards more radiogenic values away from the central region (9000 mN). The upper limit of precision (2 sigma level) for the least radiogenic determination is shown as a horizontal line. The least radiogenic isotopic ratios in the north and south of the prospect lie outside the limit of error due to the precision of analyses.

The least radiogenic isotopic ratios occur around 9000 mN. The value of the least radiogenic Pb isotopic ratio at each northing increases with distance away from 9000 mN to both the north and south. The upper precision limit (2 sigma level) of machine fractionation has been illustrated as a horizontal line on Fig. 7.9. The least radiogenic analyses of the most northerly and southerly samples lie outside the precision limits of machine fractionation and are interpreted to indicate the trend towards more radiogenic values with distance away from 9000 mN is not an analytical artefact. The spatial distribution of lead isotope ratios can be interpreted to indicate that lead was derived from a single mineralising system with the main conduit zone centred around 9000 mN. More radiogenic values of lead in the periphery of the system are interpreted to have resulted from a greater degree of host rock interaction.

The relationship between isotopic ratios and depth has similarly been investigated and no trends have emerged.

### 7.5.5 Interpretation of lead isotopes from the rhyolite intrusion.

A single whole rock lead isotope determination was derived from the weakly altered rhyolite intrusion at 486.6 m in drill hole PD0030. Rhyolite intrusions are interpreted to have been coeval with mineralisation (Section 5.6.7), and have geochemical similarities to granitoids of the Hiltaba Suite (Section 4.3.5). In this section, the relationship between the Hiltaba Suite and the rhyolite intrusion is investigated using lead isotopes.

A whole rock sample of rhyolite intrusion was treated with HCl prior to dissolution in order to remove contamination and more radiogenic lead. Pb isotope ratios of the rhyolite intrusion are strongly radiogenic and lie below the array of Menninnie Dam mineralisation with a lead model age some time in the future (Fig. 7.10). The rhyolite intrusion has similar $^{207}Pb$ / $^{206}Pb$ ratios to granites of the Hiltaba Suite (Appendix 7.2), and lies close to the extension of a 1589 - 0 Ma. isochron which passes through the Hiltaba Suite determinations (Fig. 7.10). The isotopic ratios of the rhyolite intrusion do not lie exactly on the extended 1589 - 0 Ma. isochron, but are within the precision limits of machine fractionation. Construction of a 1589 - 0 Ma. isochron assumes that no lead or uranium has been added or removed from the rhyolite intrusion during since 1589 Ma. The apparent future age of the rhyolite intrusion is interpreted to have resulted from a high initial U / Pb ratio and formation of radiogenic lead between 1589 Ma. and the present. The similar $^{207}Pb$ / $^{206}Pb$ ratios of the granites of the Hiltaba Suite and the rhyolite intrusion can be interpreted to indicate (but does not prove), that both the rhyolite intrusion and granites of the Hiltaba Suite may have been derived from the same source rocks, or, that the rhyolite intrusion was derived from a granite of the Hiltaba Suite.

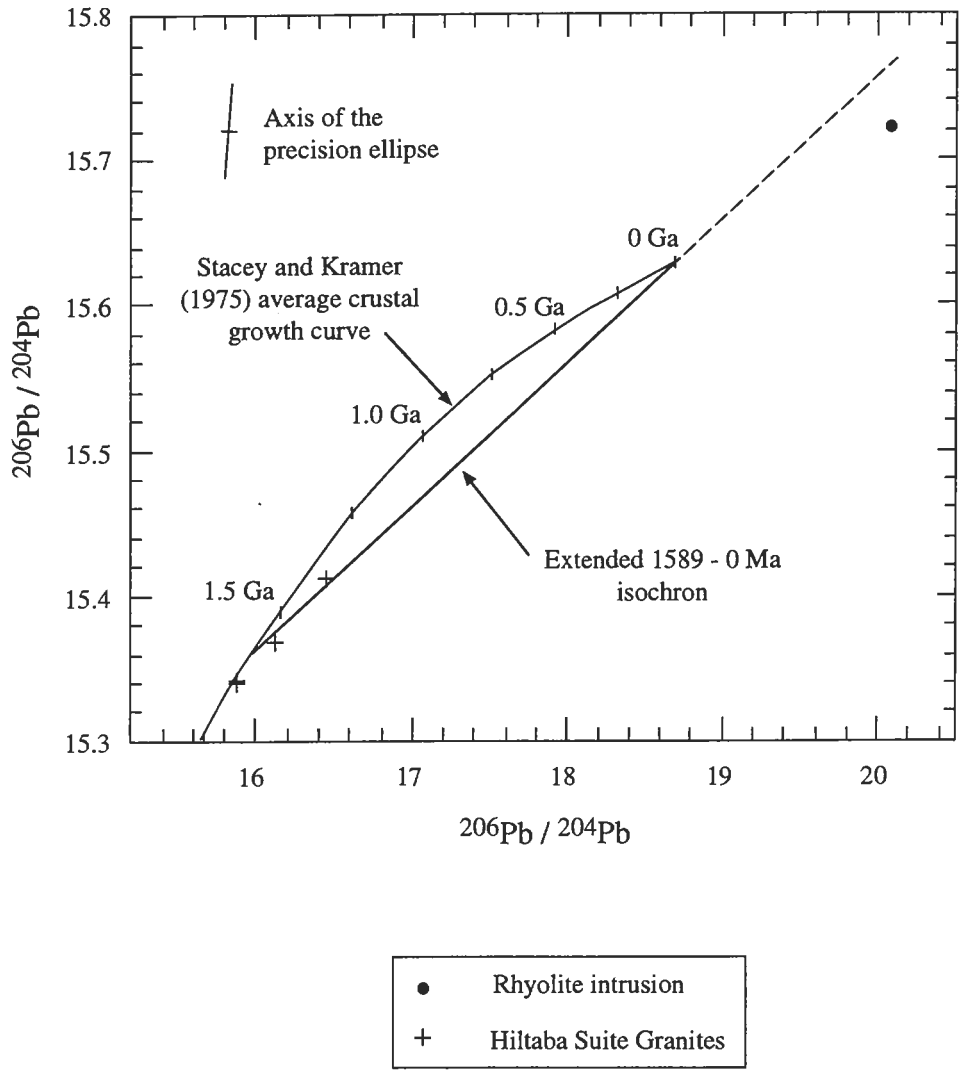


Fig. 7.10. A whole rock Pb isotope determination for the rhyolite intrusion lies within the precision limits of an extended 1589 - 0 Ma. isochron which passes through the Hiltaba Suite granite determinations.

### 7.5.6 Isotopic ratios of the southern zone

Eight lead isotope determinations were derived from samples of mineralisation from drills PE0025, PE0026 and PD0032 in the southern zone (Appendix 7.2). Six determinations were derived from galena separates and two from whole rock samples. The lead isotope determinations range from:

$^{206}Pb / ^{204}Pb$ 16.293 - 17.139
$^{207}Pb / ^{204}Pb$ 15.488 - 15.772
$^{208}Pb / ^{204}Pb$ 36.057 - 36.522

Lead isotope ratios of the southern zone are more radiogenic than the target population. Galena in the southern zone is interpreted to comprise galena 1 and galena 2 (Section 5.3.2). Galena 1 is paragenetically identical to galena 1 in the northern and central zones. Galena 2 is interpreted to have resulted from local dissolution and reprecipitation of galena 1 during the late alteration overprint. Local dissolution of galena 1 and reprecipitation as galena 2 should not significantly alter the isotopic ratios. Two possible explanations for the more radiogenic signature of isotopic ratios in the southern zone are:

- A low fluid : rock ratio during formation of the galena 1 resulting in a higher proportion of more radiogenic host rock derived lead compared to the target signature. The southern zone is ≥ 1.5 km from the interpreted centre of the mineralising system at 9000 mN.
- Contribution of more radiogenic lead through stripping of host rock lead by fluids associated with the late alteration overprint.

Without separate analysis of galena 1 and galena 2 from the southern zone it is not possible to resolve the contribution of lead from fluids associated with the late alteration overprint.

### 7.5.7 Lead model age for the Menninnie Dam mineralisation

The Menninnie Dam mineralisation has been interpreted as syn-sedimentary (Beeson, 1990; Higgins et al., 1990) although sulphide and gangue textures do not support this interpretation (Section 5.6.1). It is possible that the Menninnie Dam mineralisation has resulted from remobilisation of pre-existing stratiform sulphides and this hypothesis can be tested using lead isotopes. If galena (or some other high lead-bearing mineral) was remobilised without contribution of additional lead, then the isotopic signature of the initial lead rich mineral should be preserved and the approximate age of the initial mineralisation can be calculated from a lead model age.

Kanasewich (1962) and Kanasewich and Farquhar (1965) suggested criteria for judging the appropriateness of a single stage lead model age determination, and these criteria have equal relevance model lead age determinations based on the multiple stage evolutionary models currently in common usage.

These were summarised by Gulson (1986) as:

- The isotopic composition for a number of samples should be homogenous both within a deposit and within a metallogenic province.
- The isotopic data should plot on, or close to, accepted lead evolution or growth curves.
- The model age should agree with the proposed geologic age, possibly to within 150 Ma.

The Menninnie Dam data does not satisfy the first criteria of Kanasewich (1962) and Kanasewich and Farquhar (1965), however, if the target population alone is considered, and it is understood that the Menninnie Dam deposit is the only significant deposit in the district, then the first criteria is satisfied.

Stacey and Kramers (1975) and Cumming and Richards (1975) average crustal growth curves are the most popular for determination of lead model ages. Model lead ages determined using the Stacey and Kramers (1975) average crustal growth curve appear to be more conformable with stratigraphic ages for the Proterozoic of Australia compared to the Cumming and Richards (1975) growth curve (Gulson, 1986). An alternative is a terrain specific growth curve such as that developed for the Mid-Proterozoic sediment hosted Pb - Zn deposits in the Mount Isa Inlier (Sun and Page, 1994). Use of the terrain specific model developed for the Mount Isa Inlier is considered inappropriate as the Menninnie Dam deposit is contained within a different cratonic block, and hosted by rocks that are significantly older and have little lithological similarity to those of the Mount Isa inlier.

Analyses of granites of the Hiltaba Suite lie on, or close to the Stacey and Kramers (1975) average crustal growth curve, however the 1589 Ma. age determined for the Hiltaba Suite (Creaser and Cooper, 1993) does not correspond to the lead model ages determined from the Stacey and Kramers (1975) average crustal growth curve (Table 7.5). As the target population lies above the average crustal growth curve and is interpreted to have resulted by mixing with lead from a reservoir with an undefined growth curve, the second criteria of Kanasewich (1962) and Kanasewich and Farquhar (1965) is not satisfied.

Table 7.5. Lead model ages and corresponding radiometric ages for granites of the Hiltaba Suite. The model age is calculated using a Stacey and Kramers (1975) average crustal growth curve which uses a $\mu$ value of 9.736 ($\mu = {}^{238}U / {}^{204}Pb$). The $\mu$ value shown in Table 7.5 has been calculated from initial and final ${}^{206}Pb / {}^{204}Pb$ ratios assuming the age of the granites is 1589 Ma. (Creaser and Cooper, 1993).

| Hiltaba Suite granite | Lead model age (Ma.) with $\mu = 9.74$ | $\mu$ value when age = 1589 Ma. | Rb-Sr age* | U-Pb zircon age | Reference ** |
|---|---|---|---|---|---|
| Tarcoola | 1654 | 9.49 | 1474 ± 45 | | 1 |
| Charleston | 1497 | 10.01 | 1445 ± 39 | 1585±5 | 1, 2 |
| 'Cunyarie' | 1313 | 10.67 | 1477 ± 34 | | 1 |

* There is a disparity between the Rb - Sr age determinations and the U - Pb zircon age for the Charleston Granite. The Rb-Sr systematics of the Hiltaba Suite and the Gawler Range Volcanics are disturbed on local and regional scales and appear to be consistently around 100 Ma. too young (Creaser, 1989).
**References: 1) Webb et al., (1986). 2) Creaser and Fanning, (1993).

Although no general growth curve, or terrain specific growth curve, is strictly appropriate for determination of a model lead age of the Menninnie Dam mineralisation, an approximation can be attempted using the average crustal growth curve of Stacey and Kramers (1975) with the caveat that any estimation may be subject to substantial errors. An isochron passing through the mean of the target population (as defined by Dean and Carr, 1990) intersects a Stacey and Kramers (1975) average crustal growth curve at 1637 Ma. (Fig. 7.11). This approximate model lead age is closer to ages determined for granites of the Hiltaba Suite (1589 Ma.; Creaser and Cooper, 1993) than that determined for the Hutchison Group rocks (1964 - 1845 Ma.; Fanning et al., 1988; Rankin et al., 1988). When the lead model ages are considered in conjunction with the interpretation of a mixing between lead derived from a granite of the Hiltaba Suite and from the host rocks, it is unlikely that the Menninnie Dam mineralisation resulted from remobilisation of pre-existing stratiform sulphides.

### 7.5.8 Mixing of granite derived lead and host rock derived lead.

Volumetrically, most of the lead in the Menninnie Dam prospect has a isotopic signature approaching that of the target population. Lead which makes up the target population has higher $^{207}Pb$ / $^{204}Pb$ ratios than those of the hypothetical Hiltaba Suite granite source and lower $^{207}Pb$ / $^{204}Pb$ ratios than the host rock corridor (Fig. 7.8). The mechanism that resulted in deposition of galena with the target signature must account for the following:

- The homogenous signature of the target population.
- The absence of isotopic ratios in the mineralisation similar to that of the hypothetical Hiltaba Suite granite composition.
- The host rocks are interpreted to have been a significant source of lead, however there is no evidence from drill core of a substantial volume of hydrothermally altered host rock.

In the absence of data from the granite and adjacent host rocks, assessment of mechanisms which may account for these factors is speculative. Possible mechanisms may include:

1) All of the lead in the target population was derived from a Hiltaba Suite granite with the same signature as the target population. More radiogenic lead outside the target population was derived from host rock interaction during migration of the lead-bearing fluid to the deposition site.
2) All of the lead in the target population was derived from a Hiltaba Suite granite which assimilated sufficient host rock to adjust the lead isotopic signature to that of the target population.

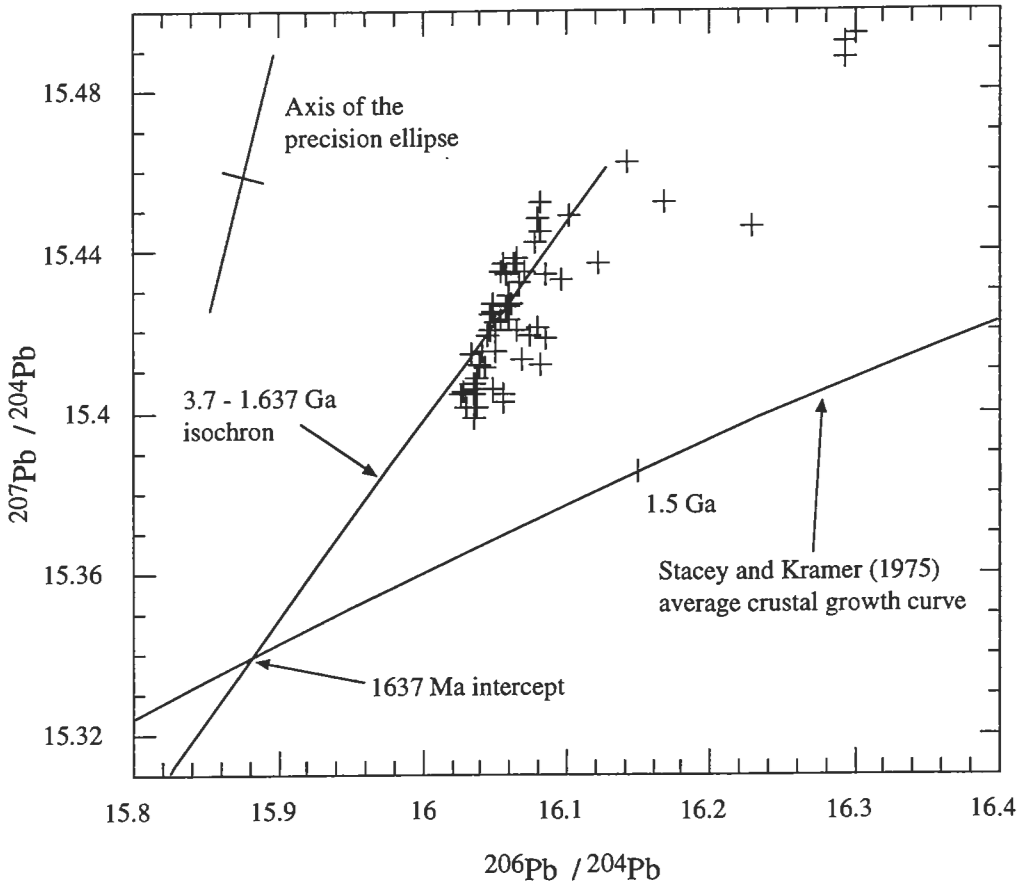


Fig. 7.11. A isochron passing through the mean of the target population for Pb isotopes determinations derived from galena intersects a Stacey and Kramer (1975) average crustal growth curve at 1637 Ma.

3) Lead in the target population was derived from mixing of lead leached from the host rocks with lead derived from a Hiltaba Suite granite. Most of the leaching and mixing occurred some distance from the site of lead deposition and resulted in isotopic homogenisation of the lead-bearing fluid prior to deposition. The more radiogenic signature of lead outside the target population may have resulted from continued leaching of host rock lead in zones with a lower fluid : rock ratio during fluid migration from the site of homogenisation to the site of deposition.

*Mechanism 1: 100% of the derived from a Hiltaba Suite granite*

If it is assumed that the Hiltaba Suite are I type granites (Wyborn et al., 1992) derived from fractionation of a more mafic magma at depth (Stewart, 1992) then a mechanism cannot be envisaged that would result in an a lead-bearing fluid separating from a granite of the Hiltaba Suite with isotopic ratios identical to the target population without involvement of host rock lead.

*Mechanism 2: Host rock assimilation*

A fluid derived from a granite of the Hiltaba Suite could have had an isotopic ratio identical to that of the target population if a suitable quantity of the appropriate host rock was assimilated by the granite. Stewart (1992) suggested that the source melt that gave rise to the felsic volcanics of the developmental phase Gawler Range Volcanics in the Lake Everard area (and by inference, the co-magmatic Hiltaba Suite) had assimilated up to 43% of Paleoproterozoic country rock. One of the complications in assessing isotopic modification through assimilation, is that the isotopic signatures of the Hiltaba Suite may have been modified by assimilation (eg. the Tarcoola, Charleston and 'Cunyarie Granites'), and therefore, an end member isotopic composition may be an unknown. Assessment of the processes involved in host rock assimilation and the resultant modification of the lead isotopic signature of the melt is beyond the scope of this study. However, based on the isotopic signature of other granites of the Hiltaba Suite (ie. Tarcoola, 'Cunyarie' and Charleston Granites), it is considered unlikely that a granite of the Hiltaba Suite beneath the Menninnie Dam prospect would have had a substantially different isotopic signature.

*Mechanism 3 (mixed granite and host rock source)*

Gravity and magnetic modelling was interpreted to indicate the presence of a granite body beneath the Menninnie Dam prospect intruded to within 3 km of the current land surface (Section 6.9). As there is no drill core evidence of pervasive leaching of the host rocks, pervasive leaching could have occurred at depth near the granite contact or below the level of drilling. A sufficient volume of host rock is interpreted to have been present between the top of the granite and the site of mineral deposition so that the zone of hydrothermally leached rock occurs well below the site of mineral deposition. Sufficient lead is unlikely to have been derived from vein margins to account for the radiogenic signature of some veins. A

possible explanation is that the mineralising fluids did not migrate up a single pipe like conduit, but rather a more substantial zone of complex fractures which had zones with both high and low fluid : rock ratios. The periphery of the conduit zone may have had the lowest fluid rock ratio which may contribute to the more radiogenic signature of more distal parts of the mineralisation.

It can be concluded that leaching of lead from the host rocks at depth by circulating hydrothermal fluids, and mixing with lead derived from a granite of the Hiltaba Suite is geologically reasonable and may account for the isotopic signature of the target population and the more radiogenic signature of some mineralisation.

## 7.6 Summary

Lead isotope determinations from the Menninnie Dam prospect were derived from whole rock samples, galena and feldspar separates. Pb isotope data derived from galena and whole rock samples form a sub-linear array on lead isotope ratio diagrams with a distinct cluster of least radiogenic values that lie within the precision ellipse of machine fractionation. Volumetrically, most of the Menninnie Dam mineralisation has Pb isotopic ratios that lie within this cluster. There is an inverse correlation between the amount of contained lead in a sample and its lead isotope ratios which is interpreted to have resulted from leaching of more radiogenic lead from the host rocks. Lead isotope data are interpreted to indicate mixing of two lead reservoirs. One reservoir was a fluid that emanated from a granite of the Hiltaba Suite intruded beneath the Menninnie Dam prospect. The second reservoir, which supplied more radiogenic lead, was the Hutchison Group host rocks. Mixing probably occurred at depth resulting in a fluid with a homogenous isotopic composition. More radiogenic Pb isotope signatures are interpreted to have resulted from continued fluid / host rock interaction during migration of the mixed fluid to the site of mineral deposition.

Lead isotope ratios have a spatial distribution with the least radiogenic ratios centred around 9000 mN and progressively more radiogenic ratios to both the north and south. This is interpreted to have resulted from a single mineralising system with the main zone of fluid conduits centred around 9000 mN.

Mineralisation in the southern zone is more radiogenic than the target population and is interpreted to have resulted from low fluid : rock ratios in a more distal part of the mineralising system. Lead isotope ratios from the southern zone mineralisation are interpreted to be consistent with a single mineralising event, and no addition of lead during the late alteration overprint, although separate analyses of galena 1 and galena 2 are required to more fully investigate the possibility of lead addition.

The evidence for mixing of lead from a granite of the Hiltaba Suite and a host rock source is consistent with an age of mineralisation equivalent to the age determined for the Hiltaba Suite. Although poorly constrained, a lead model age for mineralisation of ≈ 1637 Ma. is also consistent with an age of the mineralisation equivalent to the age of the Hiltaba Suite. Based on these timing constraints, formation of the Menninnie Dam mineralisation by remobilisation of pre-existing, stratiform mineralisation (ie. Broken Hill-type) is considered unlikely.

# Chapter eight
# Timing of mineralisation

## 8.1 Introduction

The aim of this chapter is to bring together all of the interpretations developed in previous chapters that contribute to constraining the timing of both the mineralising event, and the late alteration overprint. The results of U-Pb dating of zircons from the rhyolite intrusions are also presented.

## 8.2 Interpretation of geological constraints for the timing of mineralisation

Mineralisation is hosted by marbles and calc-silicates of the central suite that is equated with the Katunga Dolomite of the Middleback Subgroup (Sections 3.8.2 and 5.2.1). The calc-silicate lithologies have been interpreted to be the product of prograde metamorphism which regionally reached upper amphibolite facies during KM-$D_{1-2}$ (Section 3.8.1). Granite dykes have intruded the host rocks and are interpreted to have been associated with intense deformation during retrograde metamorphism (KM-$D_3$; Section 3.8.3). Pegmatitic dykes are interpreted to have been associated with the latter stages of KM-$D_3$ and are associated with pervasive metasomatic alteration of some marble units, and to a lesser extent, other rock types of the central suite (Sections 3.6; 3.7; 3.8.4; 4.4.12).

Mineralisation consists of a central zone of stockwork-breccia and vein mineralisation flanked by more distal veins. Mineralisation has replaced the host marbles and calc-silicate lithologies (Section 5.2.1). Sulphide textures are not consistent with having been subjected to either upper amphibolite facies metamorphism during KM-$D_{1-2}$ or retrograde metamorphism during KM-$D_3$, and therefore, sulphide mineral formation is interpreted to have post-dated both KM-$D_{1-2}$ and KM-$D_3$ (Section 5.6.1). Some sulphide textures are interpreted to have resulted from brittle deformation, and are overgrown by later, undeformed sulphides (Section 5.6.3). However, there is no evidence of the intense ductile deformation characteristic of the mylonite zones associated with KM-$D_3$. Locally, undeformed sulphide veins have formed the matrix to brecciated granite dykes (Fig. 5.12b) and pegmatite dykes, and sulphide deposition is interpreted to have post dated granite dyke intrusion and pegmatite dyke development. Sulphides have locally overprinted minerals interpreted to have formed during the pegmatite dyke - metasomatic event (Fig. 5.3g). The final phase of KM-$D_3$ has been determined as $\approx$ 1710 Ma. by Rb-Sr dating of a pegmatite intruding the Kalinjala Mylonite at Port Neill (Fanning, 1984). Mineralisation is interpreted to be younger than $\approx$ 1710 Ma. based on the absence of metamorphic and ductile deformation textures, and the crosscutting relationships between granite dykes and mineralisation, and pegmatite dykes and mineralisation.

Discordant polymictic breccias (DP breccias) are interpreted to have been genetically and temporally related to rhyolite intrusions (Section 4.4.7). DP breccias units are generally wider in the southern part of the prospect (Fig. 4.5). Rhyolite intrusions are also more common in the southern part of the prospect (Table 4.1). Locally, the rhyolite intrusions have either merged with DP breccia, or, have formed peperite near the contact with DP breccias (Section 4.3.2). Some DP breccias include rhyolite clasts with delicate, fiamme shapes surrounded by angular to rounded lithic clasts. Fiamme commonly have micropoikilitic devitrification textures (Fig. 4.4f). DP breccias are interpreted to have formed by phreatic interaction between rhyolite intrusions and ground waters, or by second boiling of shallow rhyolite intrusions (Fig. 4.21). The polymict nature of DP breccias, and the angular to rounded shape of clasts are interpreted to have resulted from fluidisation processes during rhyolite intrusion and DP breccia formation (Section 4.4.7). Some DP breccias are interpreted to have vented onto the Palaeosurface forming layered polymictic breccias (LP breccias; Section 4.4.7). LP breccias are overlain by the Menninnie Dam ignimbrite (MD ignimbrite; Section 4.3.6), or locally, by coherent, banded, rhyolite that is texturally and geochemically similar to rhyolite intrusions (Section 4.3.3).

DP breccias commonly contain clasts of sulphide mineralisation. Sulphide-bearing clasts comprise sulphide and gangue minerals that are generally paragenetically earlier than the late pyrite stage of mineralisation (Section 5.2.1). The matrix of DP breccias is commonly altered and includes sulphide and gangue minerals that occur in the sphalerite - galena and late pyrite stages of the mineralising event (Section 5.2.1). Based on the sulphide and gangue mineral paragenesis of sulphide-bearing clasts in DP breccias, and the sulphide and gangue mineral paragenesis of the matrix to DP breccias, DP breccias are interpreted to have formed during the mid to latter stages of the mineralising event (Section 5.6.7). As the DP breccias are interpreted to have been genetically and temporally related to rhyolite intrusions, then the mineralisation is also interpreted to have been temporally associated with rhyolite intrusions.

Rhyolite intrusions at Menninnie Dam have textural similarities to rhyolite intrusions elsewhere in the Eyre Peninsula that have been interpreted to be associated with intrusion of the Hiltaba Suite (Giles, 1977; Watmuff, 1973a and b; Daly, 1985; Turner, 1975; Blissett et al., 1993; Flint, 1993b). The rhyolite intrusions at Menninnie Dam have similar immobile element chemistry to granitoids of the Hiltaba Suite, and are interpreted to be genetically associated with a granite of the Hiltaba Suite (Section 4.3.5).

The MD ignimbrite consists of > 266 m of lithic rich, welded ignimbrite, interpreted as a ponded intracaldera ignimbrite (Section 4.4.9). The volcanic architecture of the Menninnie Dam prospect is interpreted to be that of a deeply eroded cauldron. For many caldera and cauldron settings, the volcanic pile has been interpreted to have been genetically, and

temporally, related to an underlying, shallow igneous intrusion (Smith and Bailey, 1968; Goff, 1983; Smith and Braile, 1994; and others). Two dimensional gravity and magnetic modelling is interpreted to indicate the presence of a 15 - 20 km diameter granite body (MD granite) intruded to within 0.64 - 3 kilometres beneath the current surface at the Menninnie Dam prospect (Section 6.9).

The array of lead isotope determinations for the Menninnie Dam mineralisation and host rocks is interpreted to have resulted from mixing of lead from two different lead reservoirs (Section 7.5.3). One source is interpreted to have been the Hutchison Group host rocks and a granite of the Hiltaba Suite was the second. An poorly constrained lead model age for the mineralisation is calculated as ≈ 1637 Ma., which is compatible with the age of the Hiltaba Suite (Section 7.5.7). Emplacement of the Hiltaba Suite is tightly constrained to a geologically short time period with a mean weighted age of 1589 ± 2 Ma. (Creaser and Cooper, 1993). A whole rock lead isotope determination from a rhyolite intrusion from the Menninnie Dam prospect lies on an extended 1589 - 0 Ma. secondary isochron and can be interpreted to indicate (but does not prove) that the rhyolite intrusion and a granite of the Hiltaba Suite had a similar source, or, that the rhyolite intrusion was sourced from a granite of the Hiltaba Suite (Section 7.5.5).

When the geological constraints and interpretations outlined above are considered collectively, there is a temporal and genetic association between the mineralisation at Menninnie Dam, the rhyolite intrusions, and a granite of the Hiltaba Suite. The timing of the mineralising event at Menninnie Dam can be further constrained by U-Pb zircon dating of the rhyolite intrusions.

## 8.3 U - Pb zircon dating of the rhyolite intrusions

### 8.3.1 Introduction

U - Pb zircon dating of the rhyolite intrusions was initiated as a result of discussions with Dr. John Parker* and Dr. Mark Fanning. Through the support of Dr. Parker and Dr. Fanning, it was agreed that Mines and Energy Department of South Australia (MESA) would fund a 'commercial - collaborative' project between MESA, Dr Mark Fanning and myself using the ion microprobe at ANU to date zircons from the rhyolite intrusions.

The rhyolite intrusions have been subdivided into 'strongly altered' and 'weakly altered' groups (Section 4.3.1). Strongly altered rhyolite intrusions have been altered to sericite, quartz, chlorite, calcite and trace amounts of galena, pyrite, sphalerite, chalcopyrite and hematite with a similar paragenesis a sulphide and gangue minerals associated with

* Dr J. Parker: previously from the Mines and Energy Department of South Australia, (MESA) and Dr Mark Fanning from the School of Earth Sciences, ANU.

mineralisation. Alteration is interpreted to have occurred during the mineralising event. Weakly altered rhyolite intrusions have a groundmass with micropoikilitic intergrowths of feldspar in quartz and partial alteration of plagioclase feldspars to chlorite, calcite ± sericite. Weakly altered rhyolite intrusions have intruded altered DP breccias. Alteration of DP breccias is interpreted to have been associated with the sphalerite - galena and late pyrite stages of mineralisation. The weakly altered rhyolite intrusions are not as intensely altered as the DP breccias they intrude, and commonly completely enclose clasts and patches of altered DP breccia. Based on the alteration mineralogy and paragenesis of strongly and weakly altered rhyolite intrusions, and DP breccias, the strongly altered and weakly altered rhyolite intrusions are interpreted to have been emplaced during the mineralising event and in the later stages of the mineralising event respectively of the mineralising event.

Two samples of rhyolite intrusion were submitted to Dr. Fanning for U - Pb zircon analysis:

- Strongly altered rhyolite intrusion from 403m in drill hole PD0030
- Weakly altered rhyolite intrusion from 506.2m in drill hole PD0030

With the exception of the discussion and summary sections, the remainder of this chapter has been summarised from a report, and a personal communication on the results of the U-Pb zircon analysis compiled by Fanning (Fanning, 1993, 1994). The report by Fanning (1993) details the procedures, results and an interpretation. The personal communication (Fanning, 1994) details the results and an interpretation of additional analyses from the same samples. A summary of the results and an interpretation was given in Roache and Fanning (1994).

### 8.3.2 Ion - microprobe procedures

Zircons from both the weakly, and strongly altered rhyolite intrusions, together with a chip of the standard zircon SL13, were mounted in epoxy, sectioned approximately in half and polished. The SL13 standard zircon was analysed 12 times in the course of a single analytical session on SHRIMP I. Nineteen "unknown" areas were analysed from nineteen zircon grains from the sample of weakly altered rhyolite intrusion, and fifteen "unknown" areas were analysed from thirteen zircon grains from the sample of strongly altered rhyolite intrusion. The data has been reduced and ages calculated in a manner similar to that described by Compston et al. (1984, 1986 and 1992) and Williams and Claesson (1987). Each analyses consist of 5 scans through the mass range. The observed coefficient of variation in the Pb / U ratio measured for the SL13 standard was 2.27%. The Pb / U ratio has been normalised to a value of 0.0928 for the $^{206}Pb$ / $^{238}U$ ratio for this standard, ie. equivalent to an age of 572 Ma. Th / U has been calculated from ThO / UO using a conversion factor of 1.11. The "unknowns" have been corrected for a slight isobaric interference at mass 204 (a total of 3 excess counts for a combined 50 second integration).

### 8.3.3 Results

The results, corrected for $^{204}Pb$, are illustrated in Figures 8.1 - 8.3 and detailed in Appendix 8.1. Uncertainties given in Appendix 8.1, and used for the concordia plots (Figs. 8.1 - 8.3), are at the one sigma level. Uncertainties given in age calculations are 95% confidence limits. Each analysis is illustrated as a box in Figures 8.1 - 8.3. The number '12.1' corresponds to the first analysis of the twelfth zircon from that sample. The dimensions of each box in Figures 8.1 - 8.3 correspond to the uncertainties associated with each analysis.

*Weakly altered intrusion*

An homogeneous population of equant, to elongate, euhedral zircons, or fragments of such zircons, were retrieved from the weakly altered intrusion. The grains are notably clear and colourless, with a few grains showing simple zonation from centre to rim consistent with igneous formation.

A notable feature of all areas analysed is the relatively high Th / U ratios, mostly greater than 1 with many greater than 1.5. The U contents are varied, ranging from about 50 ppm to 600 ppm, with most less than 150 ppm. The high Th / U ratios are therefore a result of relatively high Th contents of about 80 to 1200 ppm. The relatively low U contents, are consistent with those recorded for zircons analysed from the GRV (approximately 40 to 140 ppm U, Fanning et al., 1988).

Areas 3.1 and 10.1 in Figure 8.1 are significantly discordant, having lost 21% and 13% radiogenic Pb respectively, whilst analyses 2.1 and 13.1 are 10% and 8% discordant respectively. There is no simple relationship between discordance and U content, nor discordance and Th content or Th / U ratios.

Radiogenic ratios of analysis 7.1 (Fig. 8.1) have significantly higher uncertainties than other analyses. This is a consequence of a low U content (67 ppm) and relatively high measured $^{206}Pb$ / $^{204}Pb$ ratio (0.000359), therefore, the proportion of common Pb ($f_{206}$, Appendix 8.1) is similarly relatively high at 0.57% and the radiogenic ratios are not well constrained.

A weighted mean of the $^{207}Pb$ / $^{206}Pb$ ages for all 19 analyses has little excess scatter giving an age of 1590 ± 9 Ma. (MSWD of 2.0). The discordance noted above has resulted through loss of radiogenic Pb at the present day. There appears to be some slight dispersion of the analyses on the concordia plot and this may have resulted from non-zero age Pb loss, for example analyses 10.1, 13.1, 9.1, 7.1 and 12.1, however, the effects of such a hypothetical event on the age calculation are not significant.

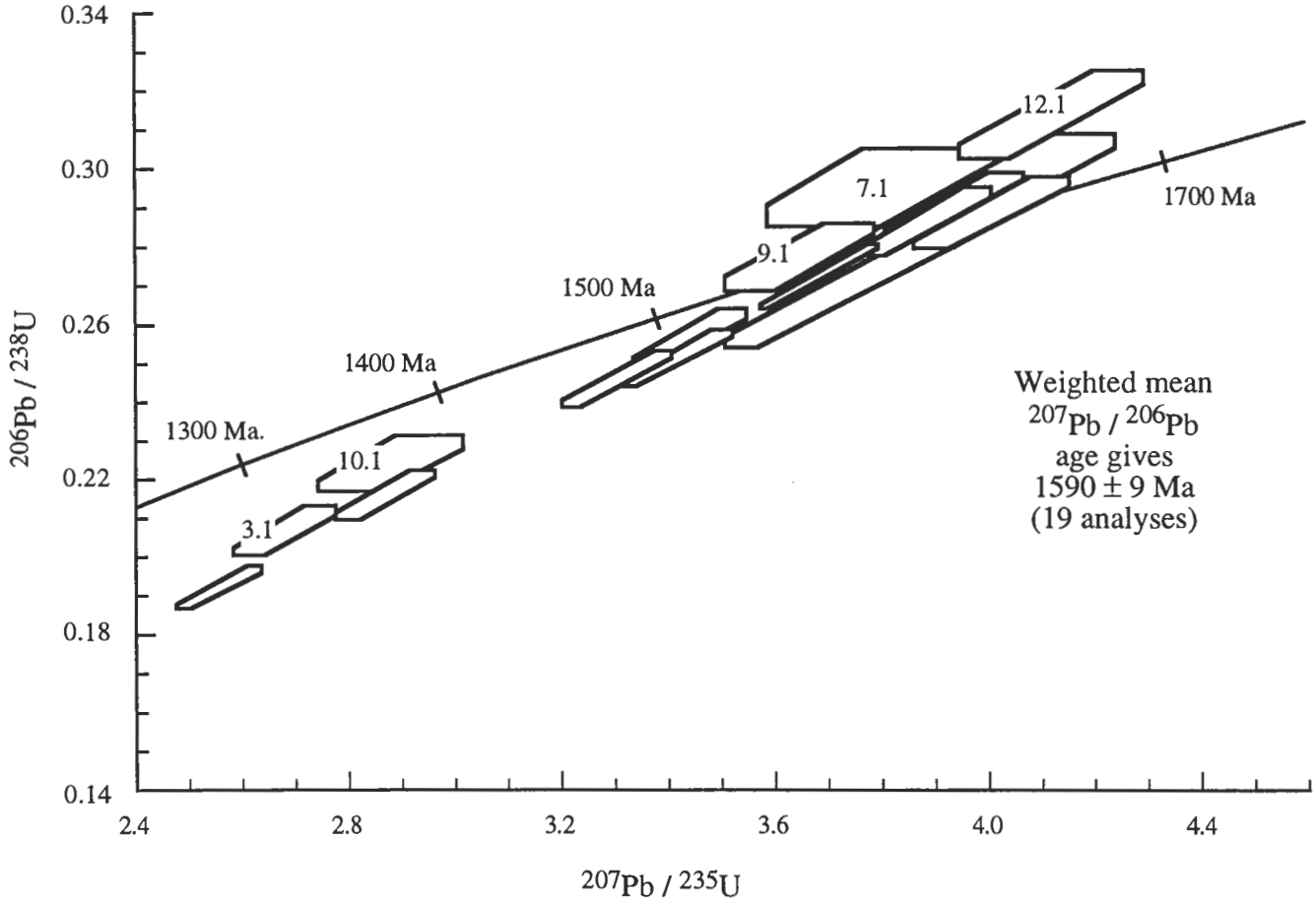


Fig. 8.1. Age determinations for the weakly altered rhyolite intrusion. Each analysis is illustrated as a box. Numbers (ie. '7.1') correspond to the first analysis of the 7th zircon grain. The dimensions of each box correspond to the uncertainties associated with each analysis. Uncertainties given in age calculations are 95% confidence limits.

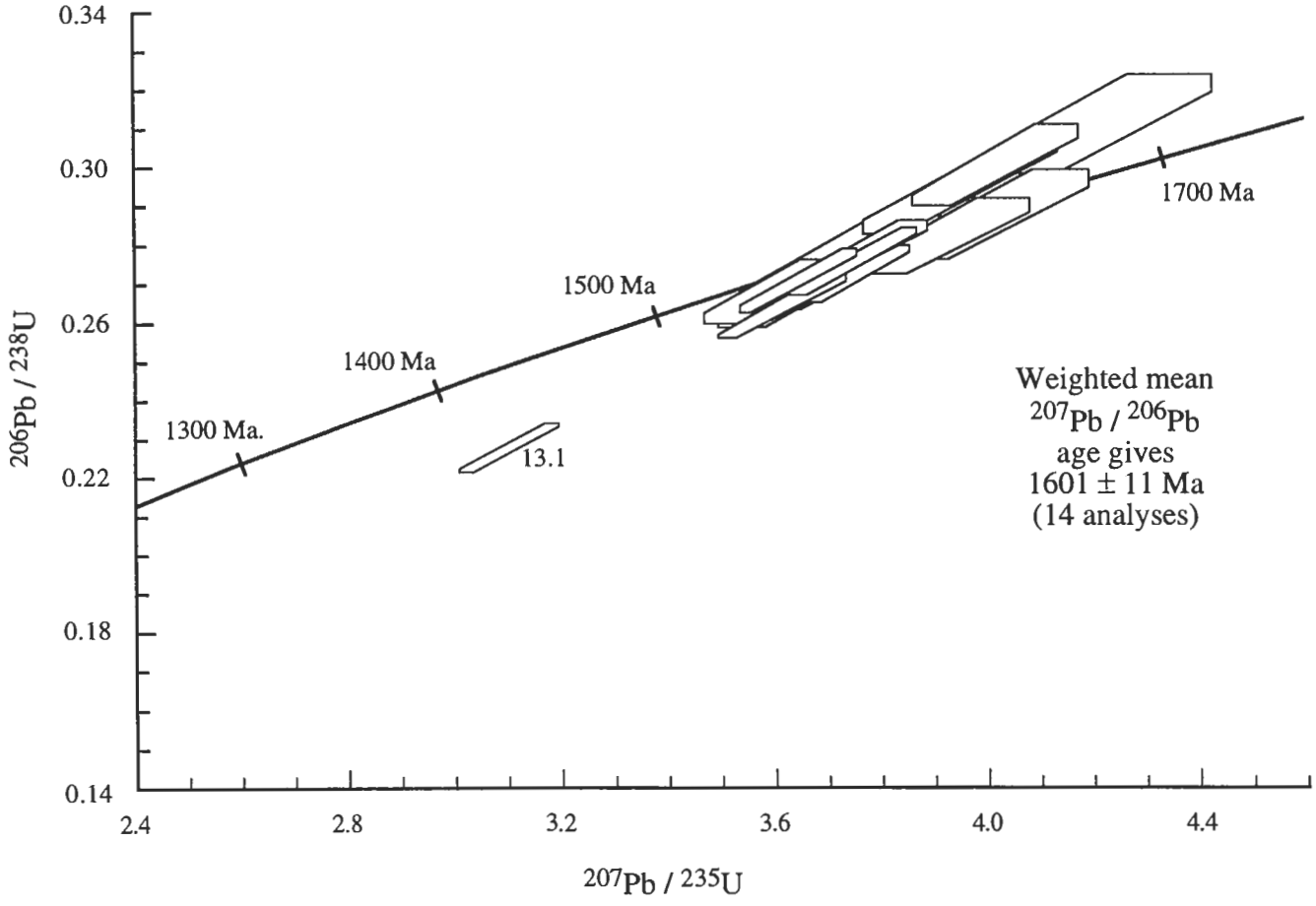


Fig. 8.2. Age determinations for the strongly altered rhyolite intrusion. Each analysis is illustrated as a box. The number 13.1 corresponds to the first analysis of the 13th zircon grain. The dimensions of each box correspond to the uncertainties associated with each analysis. Uncertainties given in age calculations are 95% confidence limits.

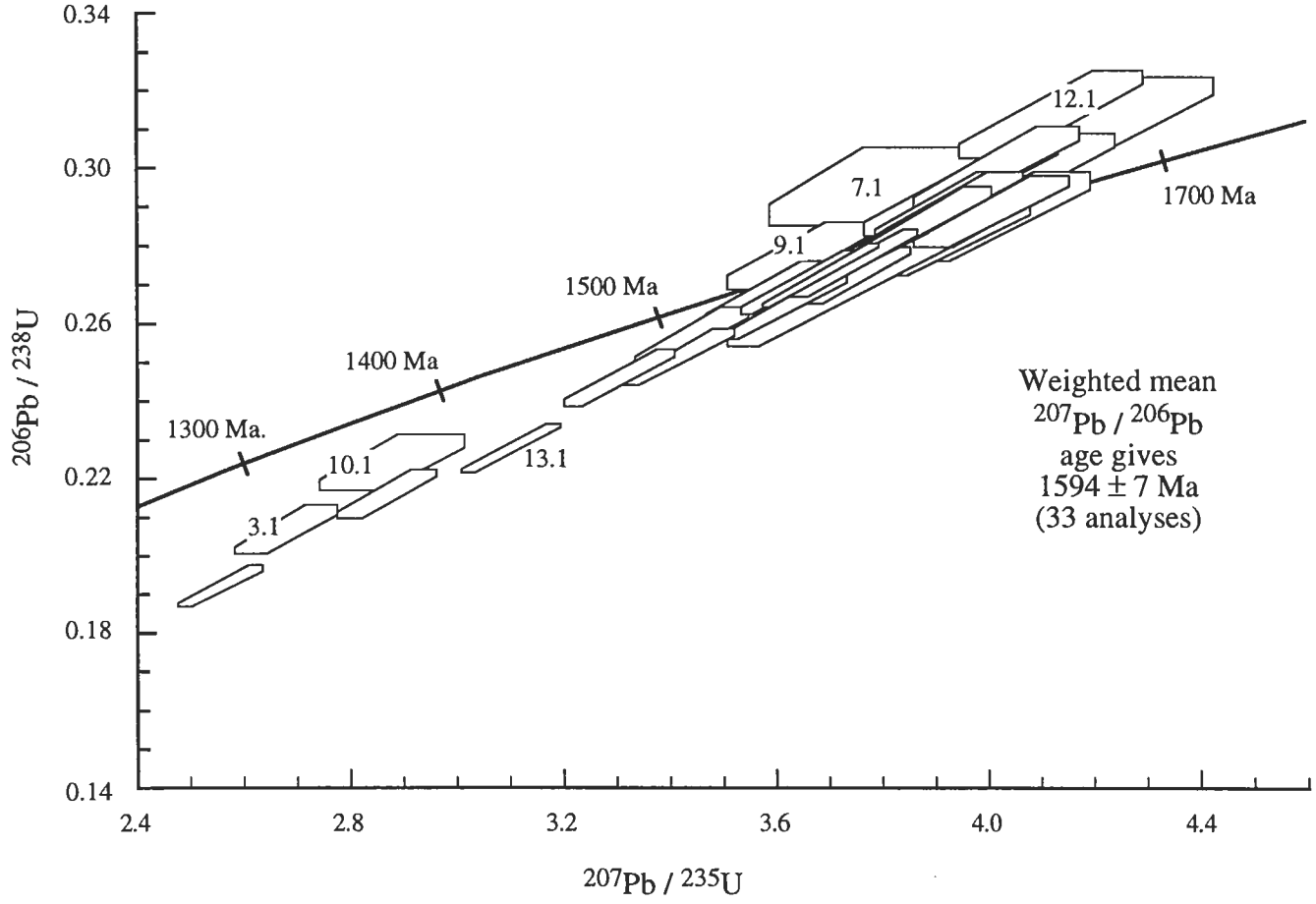


Fig. 8.3. Combined age determinations for weakly altered and strongly altered rhyolite intrusions. Each analysis is illustrated as a box. The numbers (ie.'12.1') corresponds to those shown in Figs. 8.1 and 8.2. The dimensions of each box correspond to the uncertainties associated with each analysis. Uncertainties given in age calculations are 95% confidence limits.

*Strongly altered intrusion*

Zircons separated from the strongly altered intrusion sample are identical to those from the weakly altered dyke sample. The zircons are homogeneous, equant to elongate, euhedral grains or fragments of such grains, notably clear with a few showing simple zonation from centre to rim. The zircon morphology is consistent with a simple igneous crystallisation.

Fifteen analyses were carried out on thirteen zircons (Fig. 8.2 and Appendix 8.1). As with the weakly altered intrusion, the areas analysed have high Th / U ratios, greater than 1.3, with low U contents ranging from about 40 to 160 ppm.

Fourteen of the fifteen analyses are within uncertainty of concordia (Fig. 8.2) and a weighted mean of the $^{207}Pb$ / $^{206}Pb$ ages has no excess scatter at 1601 ± 11 Ma. While there may be some significance in the 11 Ma. age difference between the strongly altered intrusion and the weakly altered intrusion, the ages are within analytical precision of each other. Excluding analysis 7.1 of the strongly altered intrusion, a weighted mean age for all 33 analyses gives 1594 ± 7 Ma. with a MSWD of 1.51 (Fig. 8.3). This age is well within the mean weighted age of 1589 ± 2 Ma. for the GRV and the Hiltaba Suite (Creaser and Cooper, 1993).

A single analysis of a zircon from the strongly altered intrusion (analysis 7.1; Appendix 8.1) has been excluded from Figures 8.2 and 8.3. This analysis is concordant at about 2000 Ma., which is significantly older than all of the other zircons. U - Pb zircon dating of the Miltalie Gneiss at the base of the Hutchison Group metasediments defines a minimum zircon crystallisation age of 2014 ± 28 Ma. (Fanning et al., 1988).

## 8.4 Timing of the late alteration overprint

Compared to mineralisation in the northern and central zones, there are fewer geological constraints on the timing of the late alteration overprint. The late alteration overprint is only present in the southern zone and interpretation of mineral textures has been based on a single drill hole (drill hole PD0032). Earlier sulphide mineralisation and some gangue minerals have similar textures and paragenesis to mineralisation in the northern and central zones. The late alteration overprint has resulted in pervasive chlorite, carbonate, calc-silicate, hematite alteration of both host rocks and earlier sulphide and gangue minerals. Pre-existing sulphide and gangue minerals have been partially dissolved and reprecipitated both locally (Fig. 5.19a, b) and some distance from earlier sulphide mineralisation (Section 5.3.2). The basal 34m of the MD ignimbrite and the underlying LP breccia have been pervasively altered by the late alteration overprint (Sections 4.3.6). Minor sulphide minerals are associated with altered MD ignimbrite and altered LP breccia (Section 5.3.2). Sulphide and gangue minerals that have a similar paragenesis to the late alteration overprint, occur as veins that have crosscut welded MD ignimbrite (Section 5.3.2).

Some marble clasts in welded MD ignimbrite have been altered in-situ to sulphide and gangue minerals with similar mineralogy and paragenesis to those of the late alteration overprint (Section 5.3.2). The late alteration is interpreted to have post-dated sulphide mineralisation, deposition of LP breccia, and emplacement, welding and cooling of the MD ignimbrite. The MD ignimbrite is tentatively interpreted to have been associated with emplacement of a granite of the Hiltaba Suite beneath the Menninnie Dam prospect (Section 6.9) which would constrain the age of the MD ignimbrite to ≈ 1589 Ma. The time taken for the MD ignimbrite to have welded and cooled has not been established and the the timing of the late alteration overprint and only be constrained to < 1589 Ma.

## 8.5 Discussion

*Older crustal source rocks*

It is conceivable that some of the Miltalie Gneiss was assimilated by the rhyolite intrusion or by the MD granite and later incorporated in the rhyolite intrusion. Alternatively, the MD granite may have resulted from partial melting of crustal rocks including the Miltalie Gneiss, or resulted from fractionation and assimilated crustal rocks including some of the Miltalie Gneiss. Magmatic zircons with older cores were also analysed from samples of the Charleston Granite (Hiltaba Suite; Creaser and Fanning, 1993).

## 8.6 Summary

Strongly altered and weakly altered rhyolite intrusions are interpreted to be synchronous with the timing of the mineralising event at Menninnie Dam. Identical, homogeneous populations of simple igneous zircons were separated from samples weakly altered and strongly altered rhyolite intrusions and analysed using an ion microprobe. Analyses of zircons from the weakly altered rhyolite intrusion have a weighted mean $^{207}Pb$ / $^{206}Pb$ age of 1590 ± 9 Ma. for all 19 analyses. Analyses of zircons from the strongly altered rhyolite intrusion have a weighted mean $^{207}Pb$ / $^{206}Pb$ age of 1601 ± 11 Ma. Although the 11 Ma. age difference may have some significance, the ion microprobe data is not sufficiently precise to resolve the two samples. A weighted mean $^{207}Pb$ / $^{206}Pb$ age for both the strongly altered intrusion and the weakly altered intrusion is 1594 ± 7 Ma. The results are interpreted to indicate that both the strongly altered, and weakly altered rhyolite intrusions crystallised simple igneous zircons at the same time as the zircon crystallisation age determined for the main mass of the GRV and the Hiltaba Suite.

Based on the interpretation that the rhyolite intrusions and the mineralisation formed at approximately the same time, the mean weighted age of 1594 ± 7 Ma. determined for the rhyolite intrusions is interpreted to be the age of the mineralisation at Menninnie Dam. The U - Pb zircon age interpreted for the Menninnie Dam mineralisation is consistent with interpretation of stratigraphic relationships, mineral paragenetic relationships, and the lead model age. It is concluded that the timing of the mineralising event at Menninnie Dam was

geologically synchronous with the mean weighted age for intrusion of the Hiltaba Suite and eruption of the co-magmatic GRV at 1589 ± 2 Ma. (Creaser and Cooper, 1993).

The timing of the late alteration overprint is less well constrained. The late alteration overprint is interpreted to have post dated welding and cooling of the MD ignimbrite. The MD ignimbrite is interpreted to have been co-magmatic with the Hiltaba Suite and GRV which places an lower limit on the timing of the late alteration overprint of < 1589 Ma.

# Chapter nine
# Fluid inclusions

## 9.1 Introduction

One of the more powerful techniques for determining the nature of mineralising fluids is through direct measurements of fluid inclusions (Roedder, 1984; Shepherd et al., 1985). No previous study of fluid inclusions has been undertaken of minerals from Menninnie Dam. The aim of this chapter is to:

- Describe fluid inclusions associated with mineralisation and the late alteration overprint.
- Attempt to establish the temperature and salinity of the fluids related to the mineralisation, and the late alteration overprint.

Subdivision of the Menninnie Dam deposit into northern, central and southern zones is used throughout this chapter (these zones are defined in Section 5.1).

## 9.2 Method of studies

*Petrographic observations and microthermometric measurements*

Petrographic observations, and microthermometric measurements of fluid inclusions were derived from unmounted, doubly polished, 150 μm thick thin sections using the procedures described by Roedder (1984). Fluid inclusions were analysed by means of a Fluid Inc. modified USGS, gas-flow, freezing - heating stage (Sterner and Bodnar, 1984; Bodnar and Sterner, 1985). The temperature was recorded using a chromel-constantan thermocouple attached to a digital display unit. The thermocouple was placed directly on the fluid inclusion wafer, as close as possible to the fluid inclusions being measured. The general methods and procedures for heating and freezing determinations are detailed elsewhere (eg. Roedder, 1984; Shepherd et al., 1985). In order to facilitate clearer observation of phase changes in sphalerite 2, the practical recommendations of Shepherd et al. (1985) were employed.

Equipment was calibrated at regular intervals using the triple point of $CO_2$ (-56.6°C), the freezing point of water (0.0°C), the critical point of water (374.1°C), and synthetic fluid inclusions manufactured by 'Syn Flinc', USA that had a range of salinities and homogenisation temperatures. The accuracy of temperature measurements was estimated as ± 0.3°C below +30°C rising to ± 3°C at > 300°C. The true accuracy of fluid inclusion microthermometric measurements is probably greater due to difficulty in distinguishing some phase changes, particularly at temperatures below -40°C. The precision of microthermometric measurements is less than ± 1°C for heating runs; less than 0.3°C for freezing runs at temperatures above -40°C; and ± 4°C at temperatures less than -40°C.

During heating runs, fluid inclusions that homogenised at lower temperatures were analysed prior to those that homogenised at higher temperatures in order to minimise any incorrect determinations that may have resulted from stretching and leakage (Bodnar and Bethke, 1984). All heating and freezing runs for individual fluid inclusions were duplicated, and in many cases triplicated, as an observational check. Only duplicate (or triplicate) measurements within acceptable limits of precision are used throughout this study.

*Determination of fluid inclusion salt compositions*

Analysis of fluid inclusion salts was achieved by heating the wafers to 400°C so as to decrepitate the contained fluid inclusions. Decrepitation invariably involved formation of a series of microfractures through which fluid inclusion leaked. As the fluid evaporated, a residual mound of salts (referred to as the 'decrepitate') accumulated and these salts were analysed. Samples were carbon coated immediately after decrepitation and analysed using a Cameca SX50 electron microprobe at the University of Tasmania under the supervision of W. Jablonski. Leakage of the fluid inclusion through microfractures too narrow for the passage of any contained mineral inclusions, assured that any mineral inclusions remained in the space vacated by the fluid inclusion, and therefore, did not contribute to the decrepitate analysis. A consequence of this technique was that it was not possible to analyse mineral inclusions.

## 9.3 Classification of fluid inclusion types

Fluid inclusions have been subdivided into different types based on their primary vs secondary character (Roedder, 1984), and the number of phases that were observed at room temperature. The first letter of the type term ('P' or 'S'), refers to the primary or secondary nature of fluid inclusions. The number refers to the number of phases present in fluid inclusions. For example, a type P3 fluid inclusion is a primary fluid inclusion with three phases (vapour, liquid and mineral inclusions). Three phase fluid inclusions may contain more than one mineral inclusion. The type term for three phase fluid inclusions is not intended to discriminate between daughter minerals or accidental mineral inclusions.

*Type P2 fluid inclusions*

Type P2 fluid inclusions are the most common type and constitute 75% of all primary fluid inclusions examined. Type P2 fluid inclusions are primary, two phase (liquid + vapour), with no mineral inclusion and occur in sphalerite 2, quartz 1 and quartz 3 in the northern, central and southern zones (Figs. 9.1a - c).

*Type P3 fluid inclusions*

Type P3 fluid inclusions are primary, three phase, with one or more mineral inclusions and occur in sphalerite 2, quartz 1 and quartz 3 in the northern, central and southern zones (Figs. 9.1d, e). Type P3 fluid inclusions are the second most abundant fluid inclusion type.

Fig. 9.1a. Drill hole PD0006, 258.2 m. Transmitted light photomicrograph. An isolated 25 $\mu$m long type P2 fluid inclusion hosted by sphalerite 2 (V = vapour bubble, L = liquid).

Fig. 9.1b. Drill hole PD0032, 380 m. Transmitted light photomicrograph. Type P2 fluid inclusions hosted by growth zoned quartz 3 formed during the late alteration overprint in the southern zone. Quartz 3 growth zones are defined by micron scale fluid and mineral inclusions (V = vapour bubble; L = liquid).

Fig. 9.1c. Drill hole PD0032, 170 m. Transmitted light photomicrograph. Type P2 and P3 fluid inclusions hosted by quartz 3 in a vein that cross cuts welded MD ignimbrite. The largest fluid inclusion is 14 $\mu$m long. (ref. Fig. 5.24b; V = vapour bubble, L = liquid, M = mineral inclusion).

Fig. 9.1d. Drill hole PD0016, 262.77 m. Transmitted light photomicrograph. An isolated, 60 $\mu$m long type P3 fluid inclusion hosted by sphalerite 2 with a carbonate mineral inclusion (V = vapour bubble, L = liquid, C = carbonate mineral inclusion).

Fig. 9.1e. Drill hole PD0021, 451.87 m. Transmitted light photomicrograph. An isolated, 22 $\mu$m long type P3 fluid inclusion hosted by quartz 1 with two opaque and one carbonate mineral inclusions (V = vapour bubble, L = liquid, C = carbonate mineral inclusion, O = opaque mineral inclusion).

Fig. 9.1f. Drill hole PD0032, 245.5 m. Transmitted light photomicrograph. A 40 $\mu$m long type P1 fluid inclusion (liquid only) hosted by sphalerite 2 in the southern zone. The inclusion is attached to a small crystal of pyrite 1 (P).

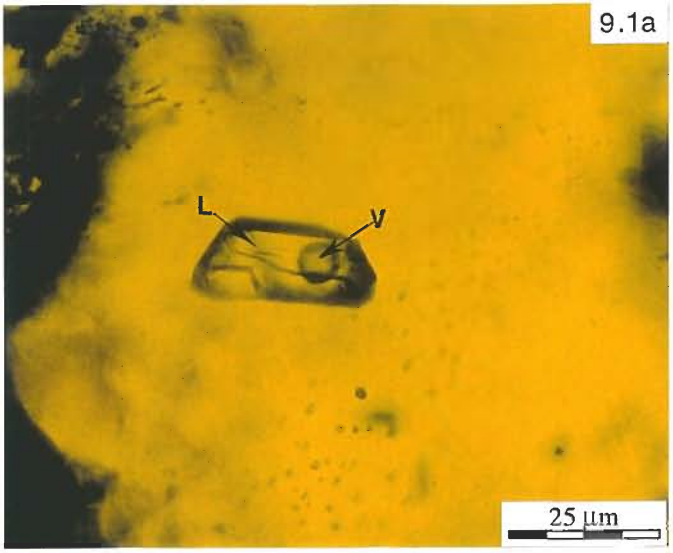
9.1a
L
V
25 µm

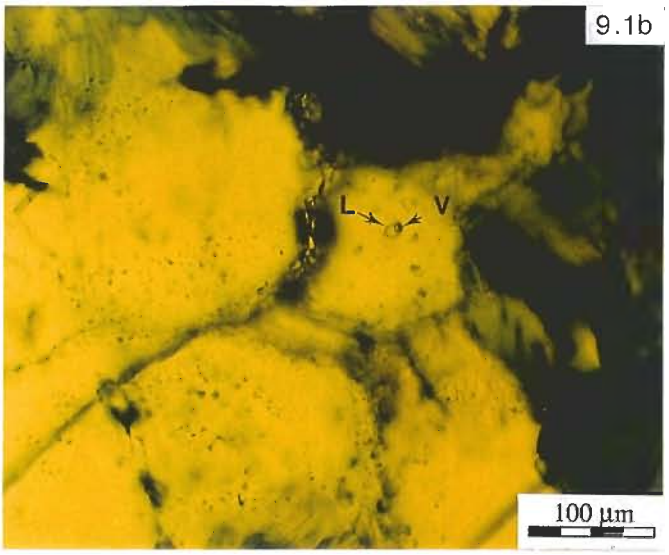
9.1b
L
V
100 µm

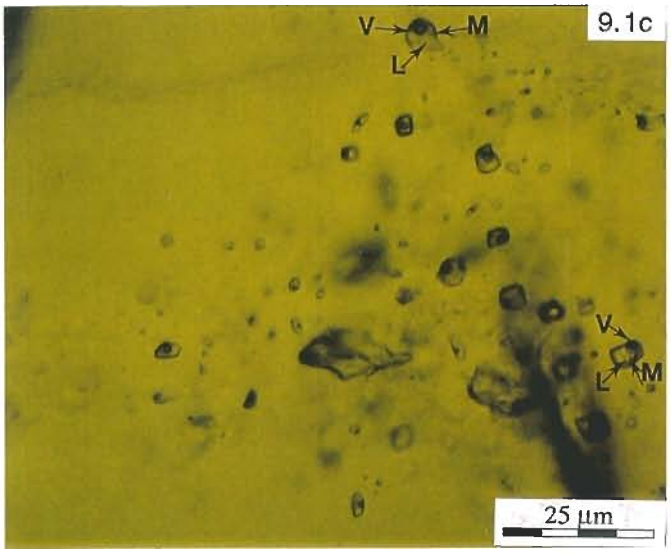
9.1c
V
M
L
V
L
M
25 µm

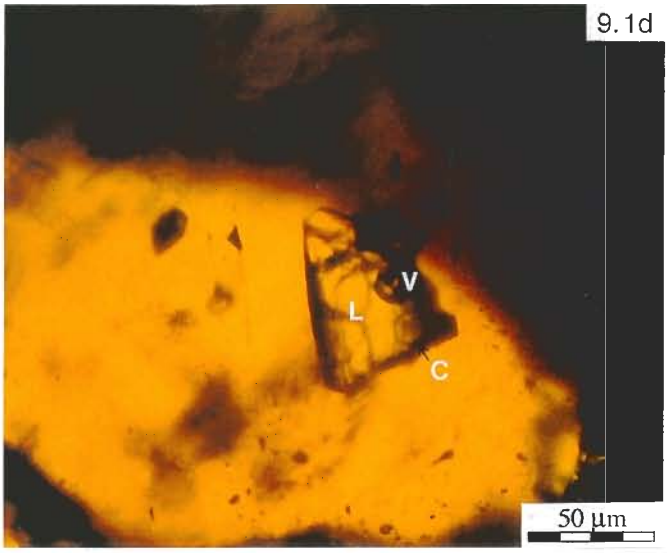
9.1d
V
L
C
50 µm

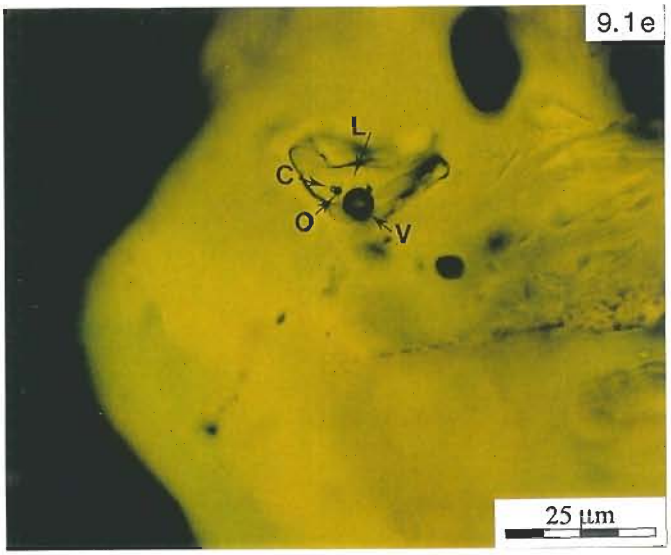
9.1e
L
C
O
V
25 µm

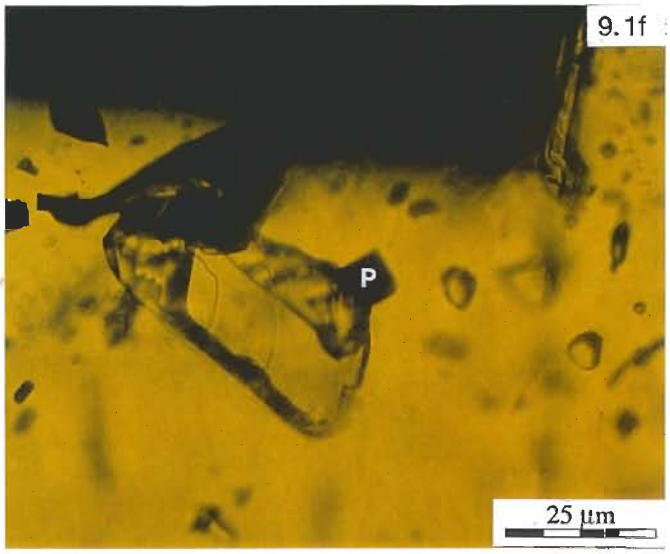
9.1f
P
25 µm

*Type S1 fluid inclusions*

Type S1 fluid inclusions are secondary, single phase, liquid or vapour-only and occur in trails along healed fractures in quartz phenocrysts in strongly altered rhyolite intrusions ('SA rhyolite intrusions') and in fractures in sphalerite 2 in the southern zone. Rare (< 1%) type S1 inclusions occur in sphalerite 2 and quartz 1 in the northern and central zones (Fig. 9.1f).

*Type S2 fluid inclusions*

Type S2 fluid inclusions are secondary, two phase (liquid + vapour), and occur in trails along healed fractures in quartz phenocrysts in SA rhyolite intrusions and as trails along fractures in sphalerite 2 in the southern zone (Figs. 9.2a, b). A variant of type S2 fluid inclusions, type S2a, occur in sphalerite 2 in the northern and central zones and comprises < 1% of all fluid inclusions. Type S2a fluid inclusions consist of liquid and a small mineral inclusion, devoid of a vapour phase.

*Type S3 fluid inclusions*

Type S3 fluid inclusions are secondary, three phase, with one or more mineral inclusions. They occur in trails along healed fractures in quartz phenocrysts in SA rhyolite intrusions (Fig. 9.2a).

## 9.4 Fluid inclusion petrography and microthermometric measurements

Single mineral crystals commonly contain populations of different fluid inclusion types. In this section the occurrence, description and microthermometric properties of fluid inclusions hosted by different minerals are described following the paragenetic sequence established for the host minerals (Figs. 5.2 and 5.15). Detailed micro-thermometric measurements are presented in Appendix 9.1 and summarised in Tables 9.1 - 9.5.

### 9.4.1 Type P2, P3, S1, S2 and S2a fluid inclusions hosted by sphalerite 2

Sphalerite 2 in the northern, central and southern zones is sufficiently light in colour to facilitate investigation of contained fluid inclusions.

*Type P2 and P3 fluid inclusions*

Type P2 and P3 fluid inclusions occur as isolated fluid inclusions and clusters in the growth zones of sphalerite 2 (Figs. 9.1a, d, 9.2c - d). They range in size from ≤ 1 $\mu$m to 75 $\mu$m in their longest dimension and typically have a negative crystal shape, or have one or more sides which are crystallographically controlled. Large fluid inclusions locally have more irregular shapes. The negative crystal shape of fluid inclusions may be a primary feature, or a result of modification of the fluid inclusion interior by continual dissolution and re-precipitation since formation (Roedder, 1984). Type P2 and P3 fluid inclusions locally occur side by side in the same growth zone of sphalerite 2.

Fig. 9.2a. Drill hole PD0030, 403 m. Transmitted light photomicrograph. Trails of secondary fluid inclusions (type S2 and S3) hosted by quartz phenocrysts in the strongly altered rhyolite intrusion. Type S2 fluid inclusions consist of liquid and a vapour bubble, type S3 fluid inclusions consist of liquid, vapour and one or more mineral inclusions (usually carbonate and rarely sericite?).

Fig. 9.2b. Drill hole PD0032, 223.33 m. Transmitted light photomicrograph of type S2 secondary fluid inclusions hosted by sphalerite 2 in the southern zone. Fluid inclusions have irregular shapes and occur as a planar array between two fractures (F). Microthermometric data was not obtained for these fluid inclusions as they invariably leaked during freezing and heating runs.

Fig. 9.2c. Drill hole PD0017, 223.95 m. Transmitted light photomicrograph. Abundant primary type P2 and P3 fluid inclusions hosted in a single growth zone of sphalerite 2. All bar one of these fluid inclusions had salinities of < 5 wt.% NaCl equivalent. The outer margin of the growth zone (M) contains abundant chalcopyrite inclusions. Fluid inclusions nearer the outer margin of the growth zone are generally smaller than those near the inner margin of the growth zone.

Fig. 9.2d. Drill hole PD0017, 223.95 m. Transmitted light photomicrograph. Enlarged view of Figure 9.2c. Fluid inclusions consist of liquid and vapour (type P2), or liquid, vapour and one or more mineral inclusions (type P3). Mineral inclusions mostly consist of anhedral and rarely euhedral carbonate (C) as well as rare halite (H). Many type P2 and P3 are attached to inclusions of chalcopyrite 2 or pyrite 1 and type P2 and P3 fluid inclusions occur side by side. With the exception of the halite-bearing fluid inclusion, all fluid inclusions in this figure had salinities of less than 5 wt.% NaCl equivalent (V = vapour bubble, L = liquid).

Fig. 9.2e. Drill hole PD0016, 462.77 m. Transmitted light photomicrograph. Type P2 and P3 fluid inclusions hosted by sphalerite 2. Most are attached to an inclusion of chalcopyrite 2. One type P3 fluid inclusion contains accidental mineral inclusions of carbonate and hematite (C = carbonate, H = hematite, V = vapour bubble, L = liquid).

Fig. 9.2f. Drill hole PD0032, 223.33 m. Transmitted light photomicrograph. Rare hematite inclusions (H) locally occur in sphalerite 2. Less than 30 such inclusions have been observed from inspection of 167 sphalerite-bearing thin sections.

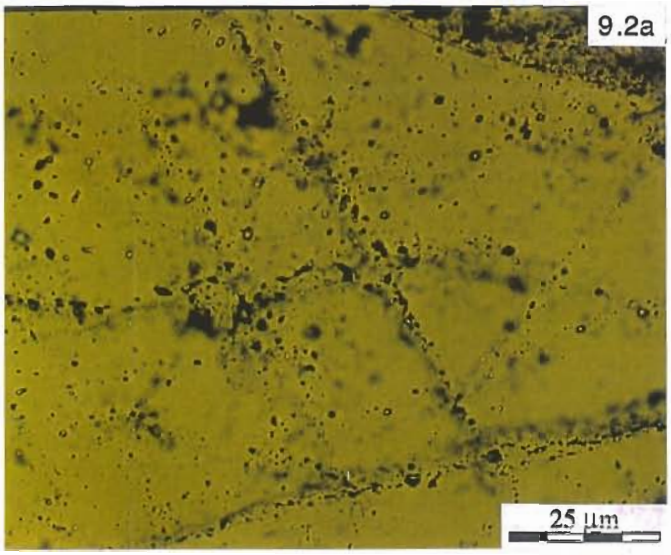
9.2a
25 µm

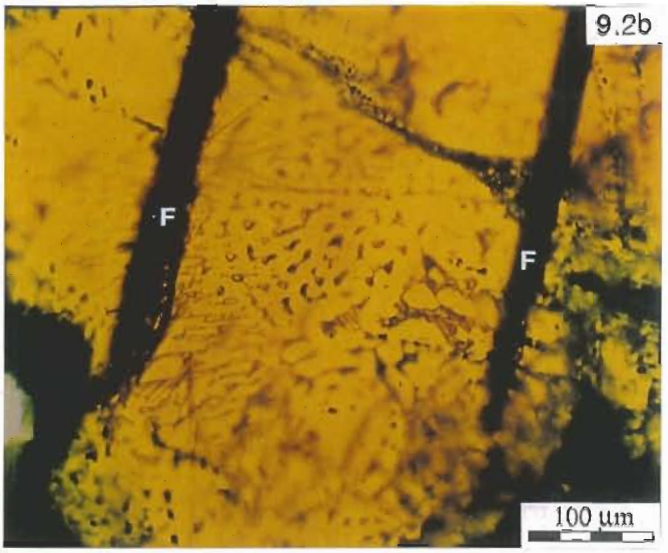
9.2b
F
F
100 µm

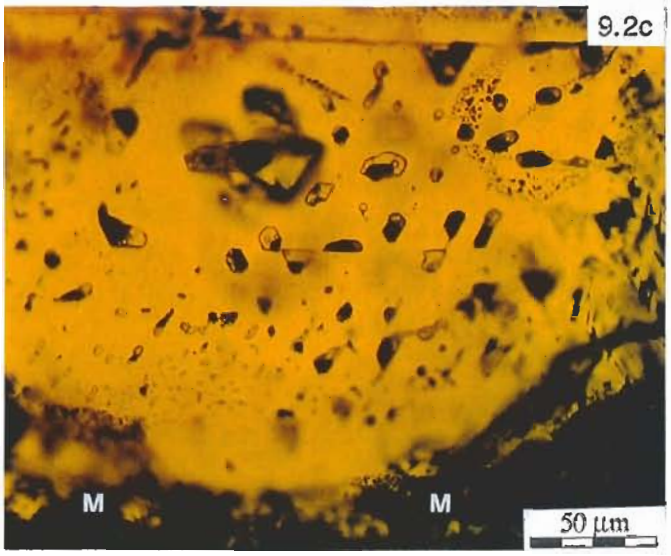
9.2c
M
M
50 µm

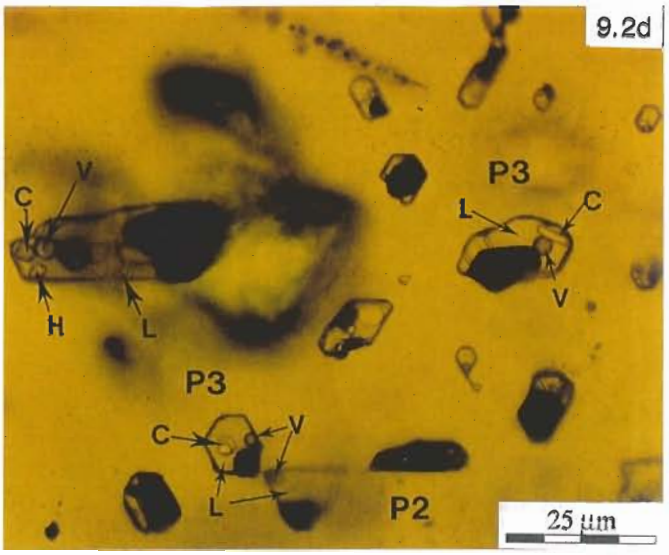
9.2d
P3
C
V
H
L
L
C
V
P3
C
V
L
P2
25 µm

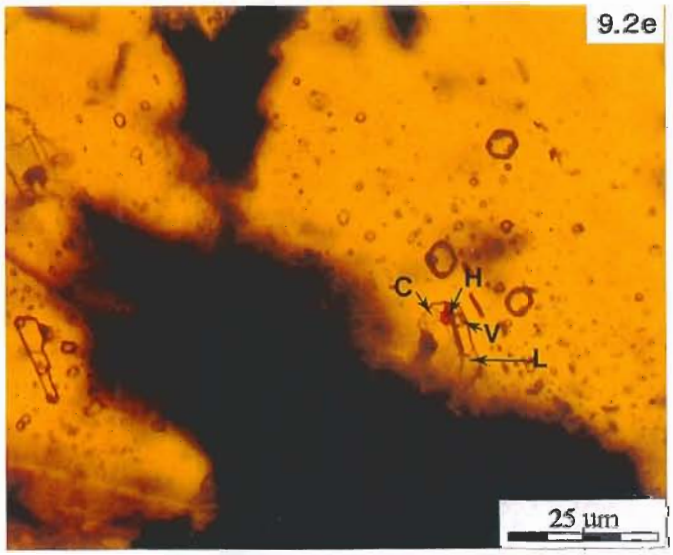
9.2e
C
H
V
L
25 µm

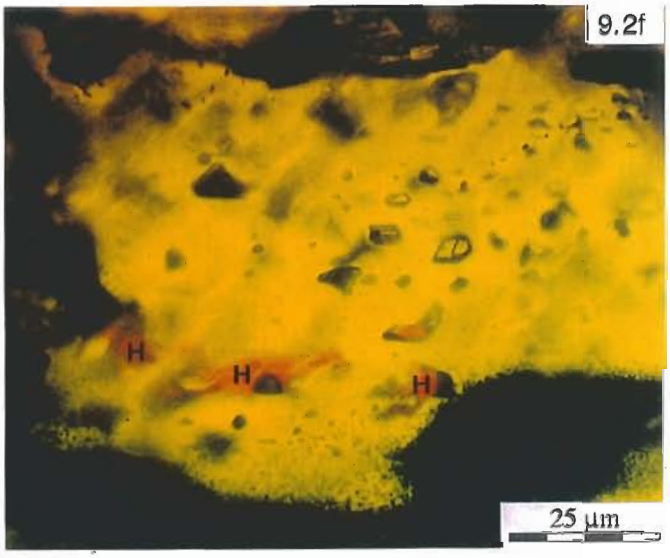
9.2f
H
H
H
25 µm

Of the 247 analysed fluid inclusions hosted by sphalerite 2, 161 are type P2 and 84 are type P3 (the other two are type S2). At room temperature, 74 type P3 fluid inclusions contained mineral inclusions interpreted to be calcite or dolomite (referred to as carbonate; Figs. 9.2c, d). Five contained carbonate and an unknown, non-opaque mineral inclusions; one contained halite and carbonate inclusions (Fig. 9.2d); one contained halite as the only mineral inclusion; one contained an opaque mineral, carbonate, and halite inclusions; one contained an opaque mineral as the only mineral inclusion; one contained carbonate and hematite inclusions (Fig. 9.2e); and one contained a sericite inclusion. Carbonate inclusions were identified by their high birefringence colours, rare rhombic shape, and double refraction of light (only locally observed). Although these are not definitive criteria for the identification of calcite or dolomite, given the circumstances, a calcite or dolomite composition was a best estimate. Hematite was identified by its distinctive red colour. Muscovite was differentiated from carbonate on the basis of its distinct plate-like morphology. Halite was identified by its cubic shape, isotropic character and dissolution upon heating.

The degree of fill (volume % liquid; Shepherd et al., 1985) in type P2 and P3 fluid inclusions was estimated to range from 70 - 99% with a median of 96% (Figs. 9.1a, d, 9.2c - e). Greater than 50% of type P2 and P3 fluid inclusions in sphalerite 2 are attached to an opaque solid mineral inclusion (Figs. 9.2c, d). The size of the opaque mineral is commonly crudely comparable to the size of the attached fluid inclusion, although there are a number of examples where there is a considerable disparity between the two. The shape of the opaque mineral appears to be unrelated to the size and shape of the attached fluid inclusion. In a few instances where the opaque mineral intersected the surface of the slide, it was identified as chalcopyrite 2 or pyrite 1. The overall size range of opaque minerals is consistent with the size range of chalcopyrite 2 and pyrite 1 inclusions in sphalerite 2, described in Section 5.2.3. Type P2 and P3 fluid inclusions that were not attached to an opaque mineral locally occur in the same growth zone of sphalerite 2, and adjacent to type P2 and P3 fluid inclusions attached to an opaque mineral (Figs. 9.2c, d).

*Type S1, S2 and S2a fluid inclusions*

Corroded remnants of sphalerite 2 in the southern zone have been overprinted by the late alteration overprint and locally contain secondary (Roedder, 1984) liquid, and liquid plus vapour filled fluid inclusions. Type S1 and S2 fluid inclusions are not attached to opaque mineral inclusions and form planar arrays that cut across growth zones in sphalerite 2. Type S1 inclusions contain either liquid or vapour, and appear to have resulted from necking of type S2 fluid inclusions. Type S1 and S2 fluid inclusions have irregular shapes and range in longest dimension from 1 - 20 μm. The irregular shape of type S1 and S2 fluid inclusions in the southern zone contrasts with the common negative crystal shape of type P2 and P3 fluid inclusions hosted by sphalerite 2 in the northern and central zones (Fig. 9.2b).

Rare (< 1%) type S2, S2a and S1 (liquid only) fluid inclusions occur in sphalerite 2 in the northern and central zones (Fig. 9.1f). Their morphology and occurrence is similar to that for type P2 and P3 fluid inclusions hosted by sphalerite 2. Type S2, S2a and S1 fluid inclusions occur within a few microns of the wafer surface, or are associated with microfractures, and are interpreted to have resulted from leakage of type P2 and P3 fluid inclusions.

*Microthermometry*

Microthermometric measurements of type P2, and P3 fluid inclusions hosted by sphalerite 2 have been summarised in Table 9.1 and illustrated in Figures 9.3a - f. Measurements are incomplete for many individual fluid inclusions due to inability to determine some phase changes within reasonable limits of precision. Microthermometric analyses of type S1 and S2 fluid inclusions hosted by sphalerite 2 in the southern zone were unsuccessful as they invariably leaked during freezing and / or heating cycles. Microthermometric measurements were obtained for only two type S2 fluid inclusion from the northern zone. Measurements of phase changes in type S1 (liquid only) fluid inclusions from the northern and central zones had poor precision and are not reported.

Table 9.1. Summary of microthermometric measurements of type P2, P3 and S2 fluid inclusions hosted by sphalerite 2. Detailed microthermometric results are presented in Appendix 9.1.

| | | Type P2 | Type P3 | Type S2 |
|---|---|---|---|---|
| Total number measured | | 161 | 84 | 2 |
| First melt temperature | number | 3 | 7 | |
| | range (°C) | -51.0 to -50.2 | -72.8 to -50.5 | |
| | median (°C) | -50.6 | -53.3 | |
| Hydrohalite final melt temperature | number | 35 | 31 | 1 |
| | range (°C) | -29.9 to -20.4 | -32.5 to -22.6 | -25.6 |
| | median (°C) | -24.3 | -24.8 | |
| Ice final melt temperature | number | 135 | 74 | 2 |
| | range (°C) | -25.2 to -0.1 | -23.8 to -0.3 | -20.7 and -9.5 |
| | median (°C) | -3.9 | -5.1 | |
| Clathrate final melt temperature | number | 5 | 7 | |
| | range (°C) | -3.6 to +6.8 | -5.0 to +19.8 | |
| | median (°C) | +4.5 | +4.6 | |
| Homogenisation temperature | number | 95 | 66 | |
| | range (°C) | +111.8 to +252.6 | +95.7 to +184.6 | |
| | median (°C) | 150.6 | 141.3 | |

A single large type P3 fluid inclusion (50 x 30 μm) had a reproducible first melting temperature of -72.8°C with melting into the vapour phase. This was the only fluid inclusion where this first melting phenomenon was observed, and no special significance was attached except to note its occurrence.

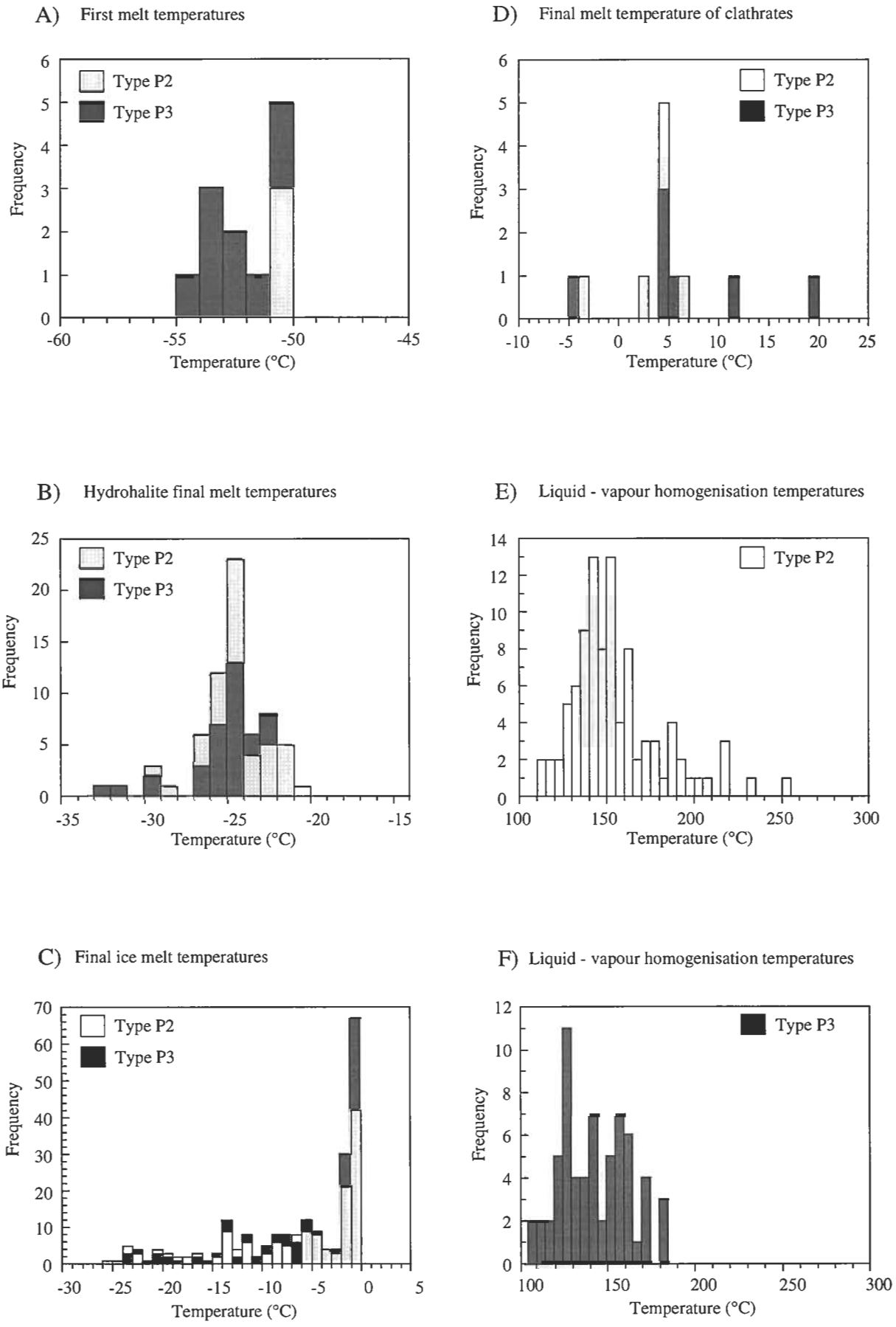


Fig. 9.3. Microthermometric measurements for type P2 and P3 fluid inclusions hosted by sphalerite 2.

Eighteen type P3 and 10 type P2 fluid inclusions froze to a distinct mottled brownish colour. Microthermometric data was obtained for 10 of these and all had a first melting phenomenon that occurred over the temperature range of -55.0 to -50.2°C (Fig. 9.3a). The median first melting temperatures for type P2 and P3 fluid inclusions are indistinguishable within the limits of precision.

Approximately 22% of type P2, and 37% of type P3 fluid inclusions had a hydrohalite final melting temperature between -32.5 and -20.4°C. The median hydrohalite final melting temperatures for type P2 and P3 fluid inclusions are similar (Fig. 9.3b). The one type S2 fluid inclusion that was analysed, had a hydrohalite final melt temperature within the range for type P2 and P3 fluid inclusions.

Final ice melting for type P2 and P3 fluid inclusions occurred over a range of temperatures between -25.2°C and -0.1°C with a cluster of analyses in the range 0 to -2°C (Fig. 9.3c). The two type S2 fluid inclusion analysed had ice final melt temperatures within the range for type P2 and P3 fluid inclusions.

Five type P2 and seven type P3 fluid inclusions formed clathrates with final melting in the temperature range -5.0 to +6.8°C (Fig. 9.3d). Clathrate temperatures are consistent with the presence of $CO_2$, although a $CO_2$ liquid phase was not observed in any fluid inclusion. Four of the type P3 fluid inclusions that formed clathrates, also froze to a distinct mottled brownish colour, and first melting temperatures between -51.2 and -53.3 were observed for two of these. Fluid inclusions that formed clathrates commonly had lower final ice melting temperatures in the range -5.0 to -26.2°C. Two type P3 fluid inclusions formed clathrates with final melt temperatures of 11.1 and 19.8°C (Fig. 9.3d) which is outside the range of $CO_2$ clathrate melting temperatures (Roedder, 1984), however, the gas composition of fluid inclusions was not analysed.

All type P2 and P3 fluid inclusions homogenised into the liquid phase over the temperature range 95.7 - 252.6°C (Figs. 9.3e, f). The median homogenisation temperature for type P2 fluid inclusions of 150.6°C is similar to that for type P3 fluid inclusions (141.3°C).

Type P2 and P3 fluid inclusions that had different first melting phenomenon, final hydrohalite melting temperatures, final ice melting temperatures and presence or absence of clathrates, commonly occur in the same growth zone of sphalerite 2 and are locally adjacent.

### 9.4.2 Type S1, P2 and P3 fluid inclusions hosted by quartz 1

Type S1, P2 and P3 fluid inclusions occur in growth zones of quartz 1 in conjunction with micron sized, non-opaque mineral inclusions. Fluid inclusions are abundant in quartz 1, however, only 36 of the observed fluid inclusions were of sufficient size for

microthermometric measurements (2 - 50 μm in longest dimension). Fluid inclusion shapes vary from equant to irregular, and negative crystals shapes are rare (Fig. 9.1e). Of the 36 fluid inclusions measured, 30 were type P2 fluid inclusions, 5 were type P3 and 1 was a type S1 liquid only fluid inclusion. No special significance is attached to the type S1 fluid inclusion and it is not considered further, other than to indicate its existence. The median degree of fill of type P2 and P3 fluid inclusions has been estimated as 95%. Four of the five type P3 fluid inclusions contained between 1 and 3 unidentified opaque mineral inclusions and three of these also contained an unidentified non-opaque mineral inclusion (Fig. 9.1e). The fifth type P3 fluid inclusion contained an unidentified non-opaque mineral inclusion.

*Microthermometry*

Microthermometric measurements of type P2 and P3 hosted by quartz 1 are summarised in Table 9.2 and illustrated in Figs. 9.4a - d. Microthermometric data is incomplete for many individual fluid inclusions due to inability to determine some phase changes within reasonable limits of precision.

Table 9.2. Summary of microthermometric measurements for type P2 and P3 hosted by quartz 1. Details of microthermometric measurements are presented in Appendix 9.1.

| | | Type P2 | Type P3 |
|---|---|---|---|
| Total number measured | | 31 | 5 |
| Hydrohalite final melt temperature | number | 2 | 3 |
| | range (°C) | -23.8 | -25.4 to -23.4 |
| | median (°C) | -23.8 | -23.5 |
| Ice final melt temperature | number | 26 | 5 |
| | range (°C) | -23.2 to -0.6 | -23.1 to -10.2 |
| | median (°C) | -1.1 | -21.6 |
| Clathrate final melt temperature | number | | 1 |
| | range (°C) | | +1.8 |
| | median (°C) | | |
| Homogenisation temperature | number | 18 | 4 |
| | range (°C) | +121.8 to +233.7 | +147.8 to +156.1 |
| | median (°C) | 178.0 | 153.2 |

Four type P2, and 2 type P3 fluid inclusions froze to a distinct mottled brownish colour, however, microthermometric data was not obtained for these. Type P2 and P3 fluid inclusions have a similar range of hydrohalite final melting temperatures between -25.4 and -23.4°C (Fig. 9.4a). Final ice melting occurred over the temperature range -23.2°C to -0.6°C (Fig. 9.4b) Type P2 fluid inclusions have a broader range of final ice melting temperatures compared to type P3 fluid inclusions with a population of final ice melting temperatures between 0 and -2°C, although this apparent difference between type P2 and P3 fluid inclusions may be due to the small number of measurements.

One type P3 fluid inclusion formed a clathrate with a final melting temperature of +1.8°C. This fluid inclusion had a final ice melting temperature of -23.1°C.

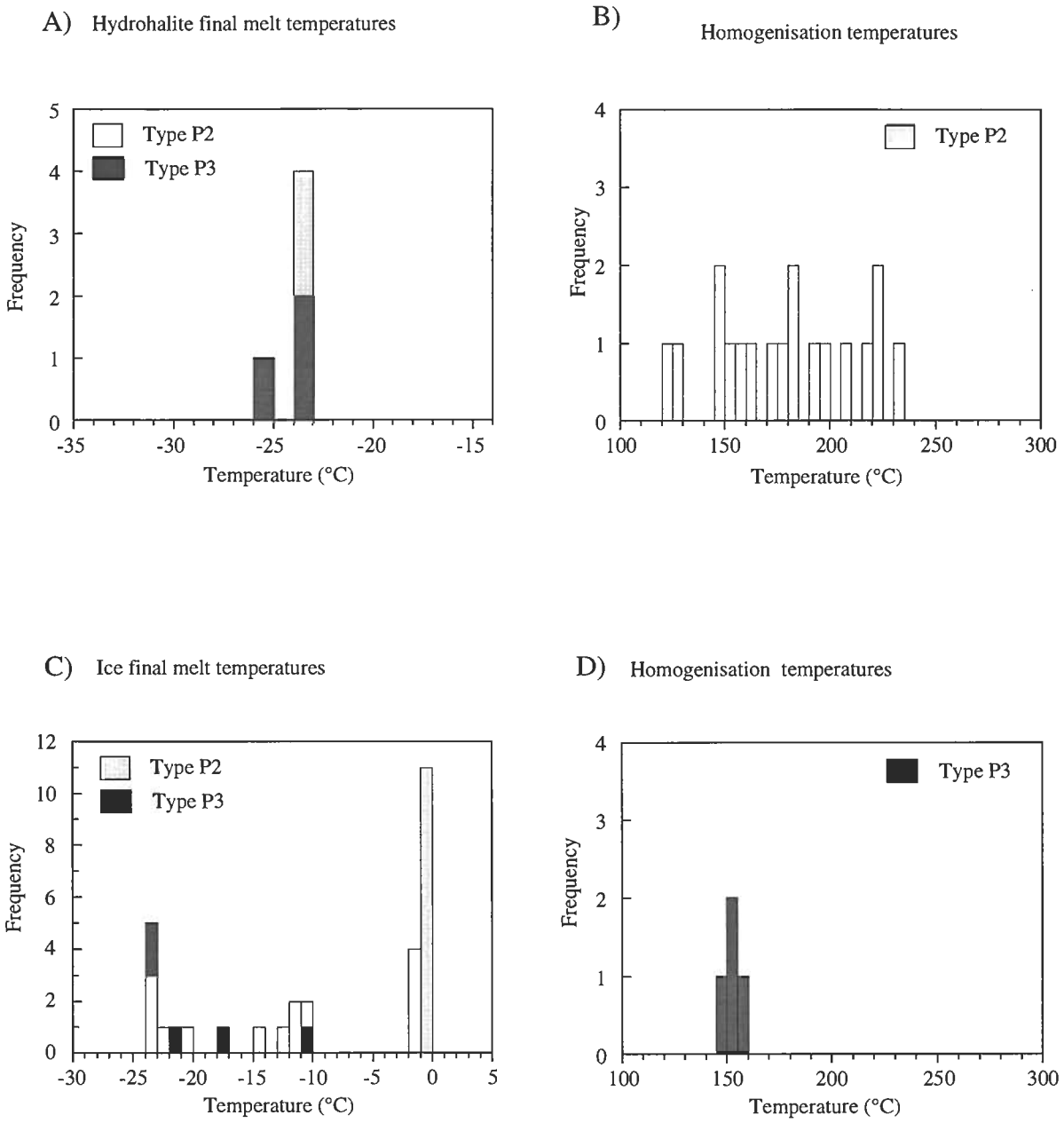


Fig. 9.4. Microthermometric measurements for type P2 and P3 fluid inclusions hosted by quartz 1.

Type P2 and P3 fluid inclusions homogenised into the liquid phase over the temperature range 121.8 - 233.7°C (Figs. 9.4c, d). Insufficient analyses are available to compare the homogenisation temperature populations for type P2 and P3 fluid inclusions, and the smaller range of homogenisation temperatures for type P3 fluid inclusions is attributed to the small number of analyses. Type P2 (and possibly type P3) fluid inclusions hosted by quartz 1 have a similar range of homogenisation temperatures to type P2 and type P3 fluid inclusions hosted by sphalerite 2.

Type P2 and P3 fluid inclusions with different hydrohalite final melting temperatures, final ice melting temperatures, and presence or absence of clathrates, commonly occur in the same growth zone of quartz 1 and are locally adjacent.

### 9.4.3 Type S2 and S3 fluid inclusions in SA rhyolite intrusions

Secondary fluid inclusions (Roedder, 1984) occur along healed fractures in quartz phenocrysts scattered throughout SA rhyolite intrusions (Fig. 9.2a). They range in size from ≤ 1 - 12 $\mu$m in longest dimension and have a median degree of fill of 95%. Fluid inclusion shapes vary from equant to irregular with elongated fluid inclusion shapes commonly orientated parallel to healed fracture surfaces. Of the 63 fluid inclusions measured, 54% are type S3 and the remainder comprise type S2 fluid inclusions. Carbonate is the most common mineral inclusion in type S3 fluid inclusions and 19 fluid inclusions contained carbonate as the only solid phase; 3 contained carbonate and halite; 3 contained halite only; 1 contained carbonate and an unidentified opaque mineral; 2 contained unidentified opaque minerals only; 5 contained an unidentified clear, anisotropic mineral, (possibly sericite?); and 1 contained both unidentified clear and opaque minerals.

*Microthermometry*

Microthermometric measurements of type S2 and S3 hosted by quartz phenocrysts in the SA rhyolite intrusion are summarised in Table 9.3 and illustrated in Figures 9.5a - e. Microthermometric data are incomplete for many individual fluid inclusions due to inability to determine some phase changes within reasonable limits of precision:

One type S2 and 7 type S3 fluid inclusions froze to a distinct mottled brownish colour. Microthermometric data were obtained for 5 of these fluid inclusions and all had a first melting phenomenon over the temperature range -50.2 to -45°C (Fig. 9.5a).

Eleven type S2 and S3 fluid inclusions had a hydrohalite final melting temperature between -35.7 and -22.8°C. Fluid inclusions for which a hydrohalite final melt temperature was recorded are commonly type S3 fluid inclusions (Fig. 9.5b). Fluid inclusions with low hydrohalite final melt temperatures commonly froze to a distinct mottled brownish colour.

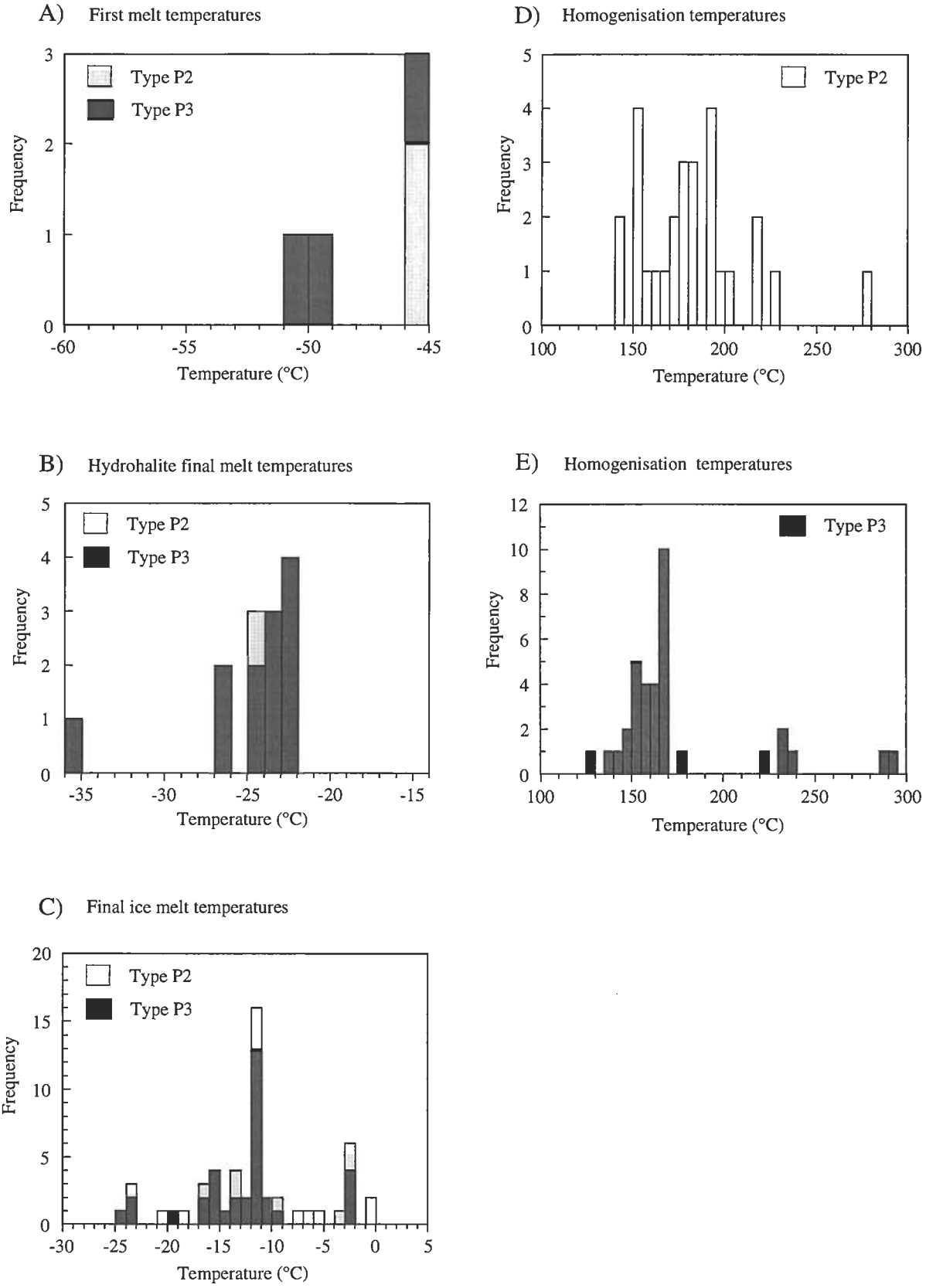


Fig. 9.5. Microthermometric measurements for type S2 and S3 fluid inclusions hosted by quartz phenocrysts in the strongly altered rhyolite intrusion.

Table 9.3. Summary of microthermometric measurements for type S2 and S3 fluid inclusions hosted by quartz phenocrysts in the SA rhyolite intrusion. Details of microthermometric measurements are presented in Appendix 9.1.

| | | Type S2 | Type S3 |
|---|---|---|---|
| Total number measured | | 29 | 34 |
| First melt temperatures | number | 2 | 3 |
| | range (°C) | -45.9 | -45.0 to -50.2 |
| | median (°C) | -45.9 | -49.9 |
| Hydrohalite final melt temperatures | number | 1 | 10 |
| | range (°C) | -24.4 | -35.7 to --22.8 |
| | median (°C) | -24.4 | -24.0 |
| Ice final melt temperatures | number | 15 | 29 |
| | range (°C) | -23.8 to -0.5 | -24.9 to -2.1 |
| | median (°C) | -11.9 | -12.9 |
| Homogenisation temperatures | number | 22 | 28 |
| | range (°C) | +142.3 to +276.1 | +128.3 to +291.6 |
| | median (°C) | 182.1 | 160.7 |

Type S2 and S3 fluid inclusions had final ice melting temperatures over the range -24.9°C and -0.5°C (Fig. 9.5c). Type S2 and S3 fluid inclusions homogenised into the liquid phase over the temperature range 140 - 240°C with most measurements within the range 140 - 200°C (Fig. 9.5d, e).Clathrates were not observed to have formed in type S2 and S3 inclusions.

### 9.4.4 Type P2 and P3 fluid inclusions hosted by quartz 3

Quartz 3 is associated with the late alteration overprint and commonly forms euhedral crystals of several millimetres diameter in altered Hutchison Group rocks, the basal part of the MD ignimbrite, and in veins higher up in the MD ignimbrite (Section 5.3.2). Type P2 and P3 fluid inclusions occur in the growth zones of quartz 3 in conjunction with micron sized inclusions of chlorite, and possibly tremolite (Fig. 9.1c). Type P2 and P3 fluid inclusion shapes vary from equant to irregular, and negative crystals shapes are rare. The maximum length of fluid inclusions ranges from ≤ 1 - 25 μm. Type P2 and P3 fluid inclusions have a similar degree of fill, estimated as 94%. Of the 165 type P2 and P3 fluid inclusions analysed, 146 were type P2 fluid inclusions and 19 are type P3 fluid inclusions. Fifteen type P3 fluid inclusions contained a clear, lath shaped, anisotropic mineral inclusion (possibly epidote?); 2 contained a clear, cubic or rhombic shaped, anisotropic mineral (possibly carbonate?); one contained an unidentified opaque mineral and one contained a small green, plate-like mineral with low birefringence, interpreted to be chlorite.

*Microthermometry*

Microthermometric measurements of type P2 and P3 hosted by quartz 3 are summarised in Table 9.4 and illustrated in Figures 9.6a - d. Microthermometric data is incomplete for many individual fluid inclusions due to inability to determine some phase changes within reasonable limits of precision.

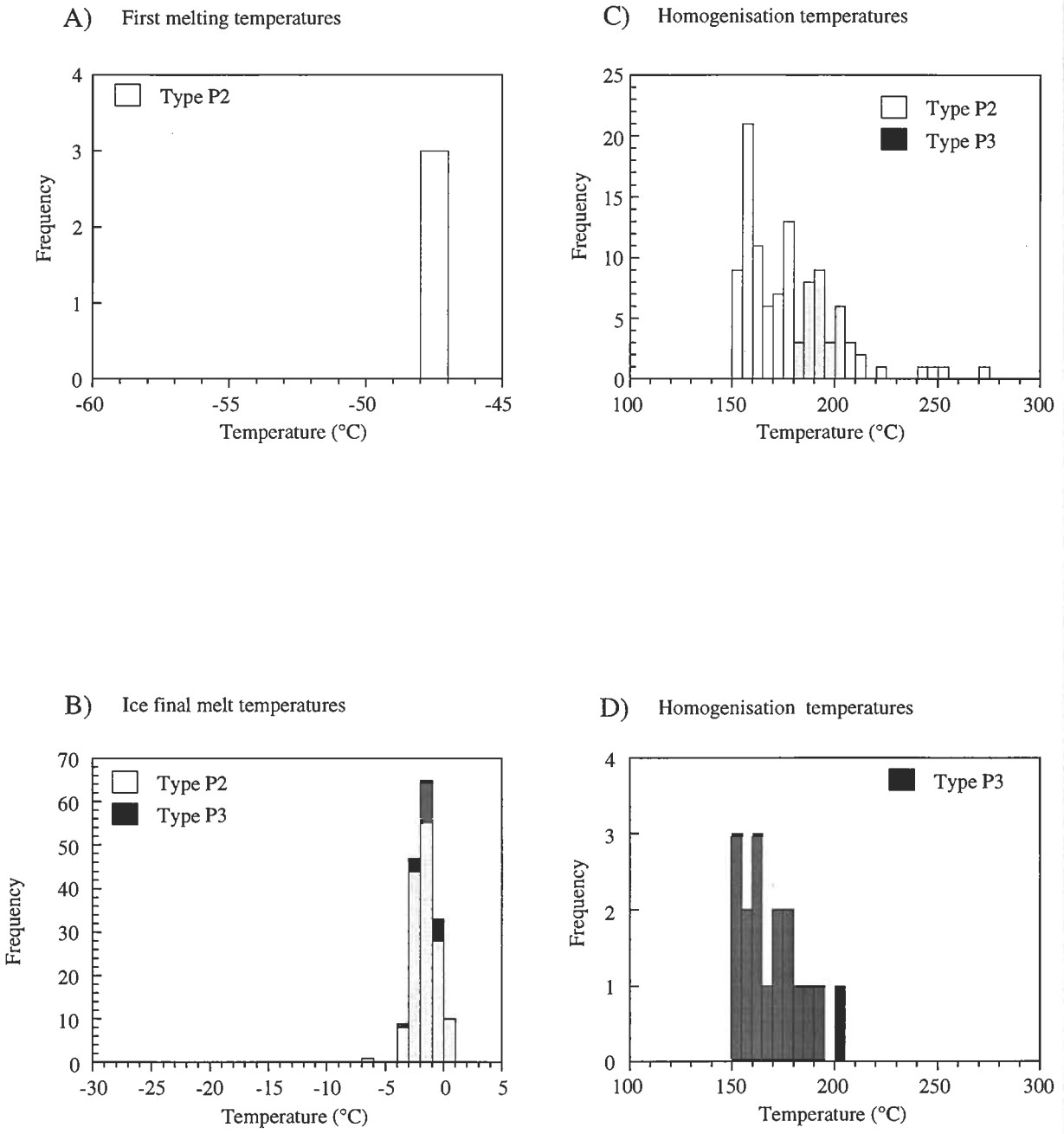


Fig. 9.6. Microthermometric measurements for type P2 and P3 fluid inclusions hosted by quartz 3.

Table 9.4. Summary of microthermometric measurements for type P2 and P3 fluid inclusions hosted by quartz 3. Details of microthermometric measurements are presented in Appendix 9.1.

| | | Type P2 | Type P3 |
|---|---|---|---|
| Total number measured | | 146 | 19 |
| First melt temperatures | number | 3 | |
| | range (°C) | -48.0 | |
| | median (°C) | -48.0 | |
| Ice final melt temperatures | number | 136 | 19 |
| | range (°C) | -6.6 to -0.6 | -3.8 to -0.6 |
| | median (°C) | -2.0 | -1.5 |
| Homogenisation temperatures | number | 108 | 17 |
| | range (°C) | +151.1 to +314.3 | +153.4 to 202.9 |
| | median (°C) | 174.5 | 169.5 |

Three type P2 fluid inclusions froze to a mottled brownish colour and had a first melting phenomenon at -48°C (Fig. 9.6a).

Hydrohalite final melting, or clathrate formation were not observed for any fluid inclusions hosted by quartz 3. Final ice melting for both P2 and P3 fluid inclusions occurred over a narrow range of values between -6.6°C to -0.6°C, with all except one fluid inclusion within the range -3.8 to -0.6°C (Fig. 9.6b). Type P2 and P3 fluid inclusions homogenised into the liquid phase over the temperature range 153.4 - 202.9°C. Median homogenisation temperatures for type P2 and type P3 fluid inclusions have similar distributions and median values of 174.5 and 169.5°C respectively (Figs. 9.6c, d).

## 9.5 Fluid inclusion salt compositions

Despite decrepitation of in excess of two hundred fluid inclusions, only nine were suitable for analysis. The paucity of suitably large decrepitates was attributed to a number of factors including:

- Non-decrepitation of fluid inclusions at 400°C
- The common small size of fluid inclusions.
- Decrepitation of low salinity fluid inclusions that resulted in formation of decrepitates too small for analysis.
- Leakage of fluids to the lower side of the wafer that then spread laterally between the wafer and the glass supporting slide.
- Evaporation of the fluid as a vapour through micro-cracks resulting in the residual salts remaining in the space evacuated by the fluid inclusion.

The shape of decrepitates varied from volcano shaped mounds with a halo of dispersed spatter, to a series of smaller mounds aligned along a microfracture. Analyses of fracture aligned decrepitates and single volcano shaped decrepitates of less than 4 μm diameter were discarded as element ratios were found to vary considerably from larger volcano shaped decrepitates in accordance with the observations of Haynes et al. (1988).

Electron microprobe analytical results are presented in Table 9.5. An X-ray map of a volcano shaped decrepitate showing the homogenous distribution of Cl, Na, Ca and K is illustrated in Figure 9.7.

Table 9.5 Electron microprobe analyses of nine decrepitates from primary fluid inclusions hosted by quartz 1 and sphalerite 2.

| Analysis No. | 1 | 2 | 3 | 4 | 5 | 6 | 7 | 8 | 9 |
|---|---|---|---|---|---|---|---|---|---|
| Drill hole | 21 | 21 | 30 | 21 | 21 | 17 | 6 | 17 | 16 |
| Depth (m) | 451.07 | 451.07 | 403 | 451.07 | 451.07 | 343.36 | 258.2 | 343.36 | 262.77 |
| Mineral | *qz 1 | qz 1 | qz 1 | qz 1 | qz 1 | sp 2 | sp 2 | sp 2 | sp 2 |
| Mg (ppm) | 96 | 853 | 209 | 112 | 102 | 155 | 21 | 0 | 208 |
| Ca (ppm) | 9703 | 37843 | 1422 | 7255 | 4712 | 12328 | 9631 | 9327 | 4068 |
| Mn (ppm) | 0 | 1447 | 379 | 149 | 0 | 2999 | 26940 | 4031 | 2941 |
| Fe (ppm) | 1548 | 468 | 183 | 535 | 414 | 19183 | 27725 | 57301 | 36656 |
| Na (ppm) | 24420 | 195038 | 7513 | 30697 | 72142 | 61651 | 81867 | 75398 | 96506 |
| K (ppm) | 158 | 13349 | 1089 | 231 | 359 | 395 | 9071 | 1013 | 4352 |
| F (ppm) | 1559 | 2554 | ***n/a | 3244 | n/a | n/a | 3764 | n/a | n/a |
| Cl (ppm) | 35177 | 298878 | 14095 | 56585 | 125776 | 67382 | 81980 | 86392 | 114424 |
| Anions / Cations** | 0.66 | 0.80 | 0.92 | 1.03 | 1.13 | 0.58 | 0.61 | 0.68 | 0.77 |

*qz 1 = quartz 1, sp 2 = sphalerite 2. **Total cations were calculated as the sum of (Na + K + 2x(Mg + Ca)). ***n/a = not analysed.

Haynes et al. (1988) conducted a series of decrepitation experiments on quartz hosted synthetic fluid inclusions of the three component systems NaCl - KCl - $H_2O$ and NaCl - $CaCl_2$ - $H_2O$ and the four component system NaCl - KCl - $CaCl_2$ - $H_2O$. Decrepitates were analysed using the scanning electron microscope and energy dispersive analysis (SEM / EDA). In each case analysis of the decrepitate fell within 6 wt.% of the original fluid chemistry, interpreted to indicate that the decrepitates were representative of the original fluid chemistry. Their results place a number of important constraints on use of this technique to obtain meaningful analytical results, including:

- Decrepitation temperatures in excess of 400°C were likely to lead to inaccurate results due to differences in the volatility of the solutes, particularly NaCl.
- A single volcano-shaped decrepitate was found to give more accurate results than fracture-aligned decrepitates above a single fluid inclusion. Electron mapping of fracture aligned decrepitates indicated Na and K formed discrete halite and sylvite crystals, whereas Ca appeared to have been dispersed peripheral the main decrepitate mass.
- Anion and cation totals were usually within 6% of each other. Those outside the 6% range were rejected.
- The accuracy of decrepitate analysis was dependant of the size on the decrepitate. Accuracy diminished for both small and large decrepitates and an optimum size of 8 - 30 μm diameter was interpreted. The lower limit is governed by the resolution of the raster mode method. Element mapping of larger decrepitates indicated chemical inhomogeneity.

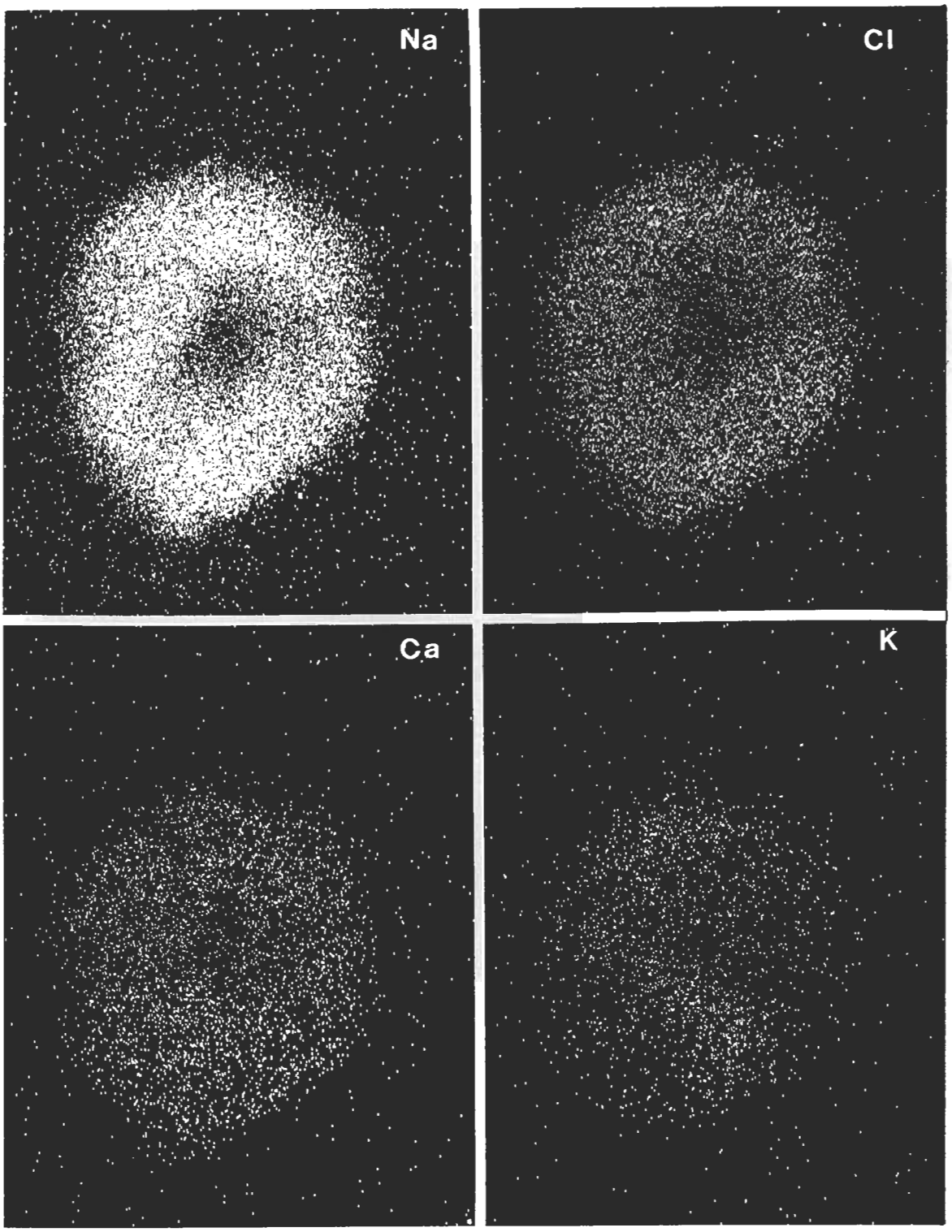


Fig. 9.7. X-ray map of the distribution of Na (top left), Cl (top right), Ca (bottom left) and K (bottom right) of a volcano-shaped decrepitate mound above a primary fluid inclusion hosted by quartz 1 in drill hole PD0021 at 452m. The diameter of the decrepitate mound is 7 μm.

Analyses of decrepitates from this study have a cation / anion ratio that is either greater or smaller than 1 (Table 9.5) which is interpreted to have resulted from volatilisation of chlorine, fluorine or sodium during electron microprobe analysis. Although the cation / anion ratio generally differs by more than 6 wt.% and does not fulfil one of the criteria established by Haynes et al. (1988), these data are considered suitable for the purposes of this study.

Fe and Mn were detected in analysis of decrepitates above fluid inclusions hosted by quartz 1, however, these could not be unequivocally assigned to the decrepitate due to the presence of disseminated sulphide minerals within quartz 1, close proximity ($< 2\ \mu m$) to sulphide minerals. Mn and Fe detected in analyses of decrepitates from fluid inclusions hosted by sphalerite 2 are attributed to their common occurrence in the host sphalerite (Section 5.5.2). Many decrepitates contained trace amounts of Fluorine. Fluorite occurs paragenetically later than sphalerite 2 (Section 5.2.3), and fluorine is interpreted to be an anionic species that was present in the mineralising fluid prior to fluorite saturation.

## 9.6 Discussion

### 9.6.1 Fluid inclusions hosted by sphalerite 2

Greater than 50% of fluid inclusions hosted by sphalerite 2 are attached to an opaque mineral inclusion, interpreted to be either pyrite 1 or chalcopyrite 2. Inclusions of pyrite 1 in sphalerite 2 are consistent with the interpreted paragenesis of pyrite 1 prior to deposition of sphalerite 2 (Section 5.2.3). The mechanism that resulted in inclusions of chalcopyrite 2 in sphalerite 2 has not been resolved, however, inclusions of chalcopyrite 2 in sphalerite 2 were interpreted to have formed either during, or immediately following, deposition of sphalerite 2, and prior to deposition of quartz 1 and galena 1 (Section 5.6.4). On the basis of this interpretation, fluid inclusions attached to either pyrite 1 or chalcopyrite 2 inclusions in sphalerite 2 are interpreted to have trapped a portion of the fluid from which the sphalerite - galena stage of mineralisation formed. The attachment of fluid inclusions to a pre-existing (pyrite 1) phase has been included as suitable criteria for identification of primary fluid inclusions by Roedder (1984).

Despite an absence of microthermometric data for type S1 and S2 fluid inclusions hosted by sphalerite 2, the genesis of these fluid inclusions can be postulated on the basis of their occurrence and morphology. Type S1 and S2 fluid inclusions form planar arrays that crosscut sphalerite growth zones. They have only been observed in the southern zone at Menninnie Dam in sulphide-bearing veins that have been altered by the late alteration overprint. Type S1 and S2 fluid inclusions hosted by sphalerite 2 are interpreted to have trapped a portion of the fluid associated with the late alteration overprint.

### 9.6.2 Fluid inclusion salinities

Salinities were calculated from ice final melting temperatures using the algorithm of Bodnar et al. (1989) and expressed as wt.% NaCl equivalent. For mixed Ca - Na - K - Mg chloride solutions, the error in estimating salinity using the depression of freezing point method of NaCl equivalents is generally assumed to be < 5% (Clynne and Potter, 1977). For the small number of fluid inclusions with a halite daughter, salinity was calculated by halite dissolution. Use of ice melting temperatures to calculate salinities for fluid inclusions in which clathrates formed results in an over-estimation of the salinity as formation of the clathrate consumes $H_2O$ and excludes salts, resulting in an increased salinity of the residual fluid (Collins, 1979). The equation of Bozzo et al. (1975) was used to calculate salinity for fluid inclusions in which clathrates formed.

Calculated salinities for type P2 and P3 fluid inclusions hosted by sphalerite 2 and quartz 1 are illustrated in Figures 9.8a - d. Salinity histograms for type P2 and P3 fluid inclusions hosted by sphalerite 2 have similar distributions with a low salinity fluid population (< 5 wt.% NaCl equivalent) and a higher salinity (5 - 28 wt.% NaCl equivalent). While there is a smaller number of microthermometric analyses for fluid inclusions hosted by quartz 1, and distinct populations are poorly defined, the salinity distributions are similar to those of type P2 and P3 fluid inclusions hosted by sphalerite 2.

Calculated salinities for type S2 and S3 fluid inclusions hosted by quartz phenocrysts in the SA rhyolite intrusion are illustrated in Figures 9.8e, f. Any difference in the salinity distributions of type S3 and type S2 fluid inclusions cannot be meaningfully distinguished from the limited number of measurements. The range and distribution of salinities for type S2 and S3 fluid inclusions is similar to that for type P2 and P3 fluid inclusions hosted by sphalerite 2.

Calculated salinities for type P2 and P3 fluid inclusions hosted by quartz 3 are illustrated in Figures 9.8g, h. Type P2 and P3 fluid inclusions hosted by quartz 3 have distinctly different distributions compared to type P2 and P3 fluid inclusions hosted by sphalerite 2 with only one analysis of > 7 wt.% NaCl equivalent.

### 9.6.3 Fluid inclusion trapping temperatures

In order to calculate the trapping temperature of fluid inclusions, an estimate of the pressure correction due to lithostatic or hydrostatic load is required (Roedder, 1984).

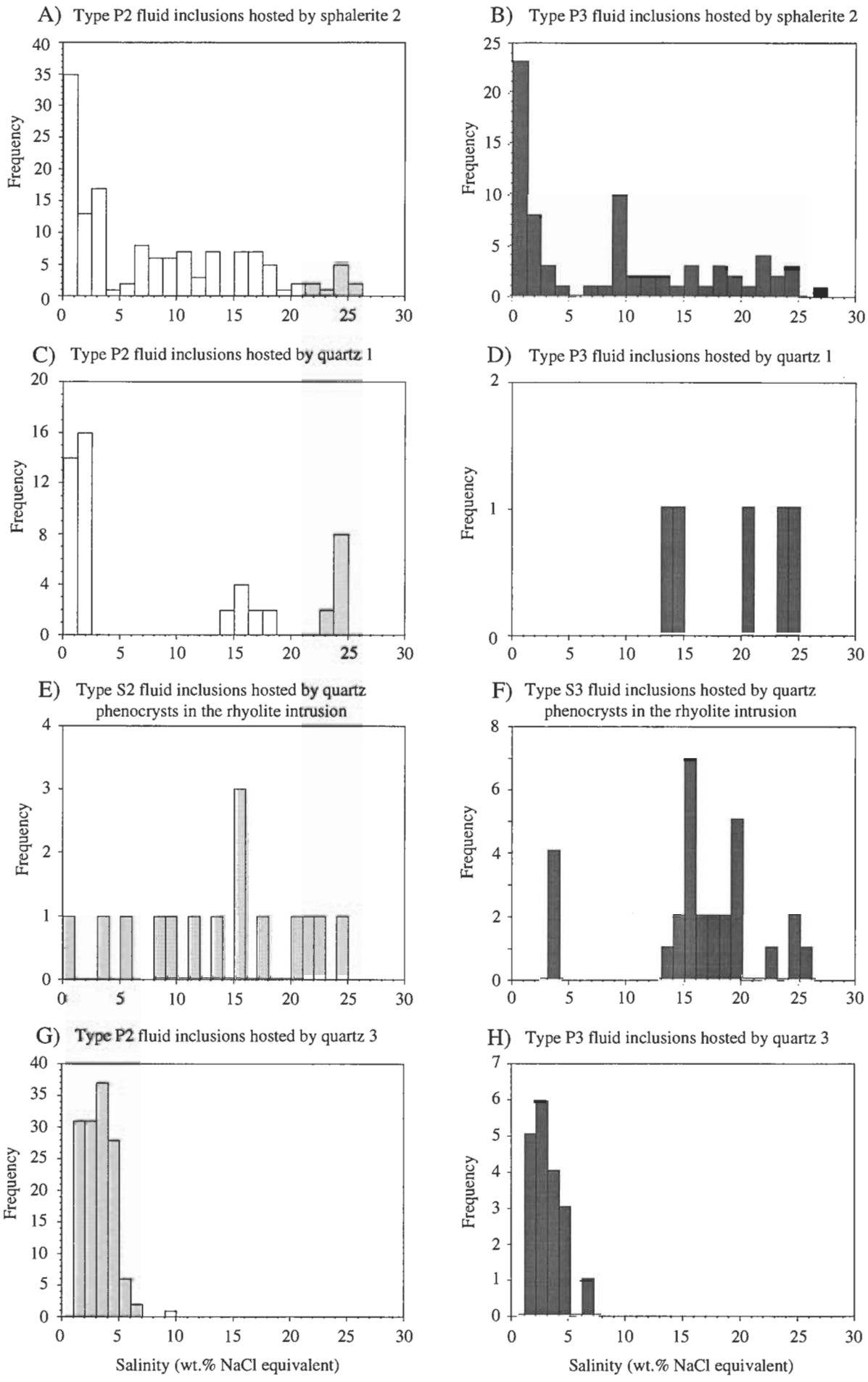


Fig. 9.8. Salinity histograms for type P2, P3, S2 and S3 fluid inclusions hosted by sphalerite 2, quartz 1, quartz 3 and quartz phenocrysts in the strongly altered rhyolite intrusion.

*Trapping temperatures of fluid inclusions hosted by sphalerite 2, quartz 1, and the SA rhyolite intrusion.*

Emplacement of rhyolite intrusions is interpreted to have been coeval with Pb - Zn - Ag mineralisation (Section 5.6.7). LP breccias are interpreted to have been erupted onto the palaeosurface (Section 4.4.7) and were overlain by MD ignimbrite soon after deposition (Section 4.4.11). Therefore the base of the MD ignimbrite (or LP breccia where present) is interpreted to approximate the palaeosurface soon after formation of the Menninnie Dam mineralisation (Fig. 4.17).

In the absence of evidence for fluid-filled channel ways that connected the mineralising fluids to the palaeo-surface, it is assumed that the mineralising fluids were under lithostatic, rather than hydrostatic pressure. For fluid inclusions hosted by sphalerite 2 and quartz 1, the lithostatic load has been calculated by measuring the vertical thickness of Hutchison Group rocks above the fluid inclusion trap site (82 - 316 m), and assuming a density of 3.01 $tm^{-3}$ (Table 6.2). The pressure correction was calculated using the curves of Potter (1977) and assuming an average fluid salinity of 15 wt.% NaCl equivalent. The resultant pressure correction has been added to the homogenisation temperature for each fluid inclusion to give the estimated fluid temperature at the time of entrapment ('trapping temperature'). Pressure corrections for primary fluid inclusions hosted by sphalerite 2, quartz 1, and secondary inclusions hosted by quartz phenocryst in the SA rhyolite intrusion, are between 1.6 and 14.2°C (Figs. 9.9a - f; Appendix 9.1).

The distribution of trapping temperatures for type P2 and P3 fluid inclusions hosted by quartz 1 is similar to that for type P2 and P3 fluid inclusion hosted by sphalerite 2. Differences in the distribution of trapping temperatures between type P2 and P3 fluid inclusions hosted by sphalerite 2 and quartz 1 (Figs. 9.9a - d) are interpreted to be an artefact of non-random sampling and they can be interpreted as a single population with a range of 104 - 266.8°C, and a median trapping temperature of 154°C. Type S2 and S3 fluid inclusions hosted by quartz phenocrysts in the SA rhyolite intrusions have similar, but not identical distributions with a range of trapping temperatures of 134.3 - 297.6°C and a median trapping temperature of 173°C (Figs. 9.9e, f). Only a few fluid inclusions have trapping temperatures less than 150°C.

Type P2, P3, S2 and S3 fluid inclusions hosted by sphalerite 2, quartz 1 and quartz phenocrysts in the SA rhyolite intrusion do not show any systematic variation in salinity or trapping temperature along the length of the deposit (Fig. 9.10a, b), nor is there any systematic relationship between salinity and depth (Fig. 9.11a). It could be argued that there is a trend towards higher trapping temperatures with depth (Fig. 9.11b), although these data are not conclusive.

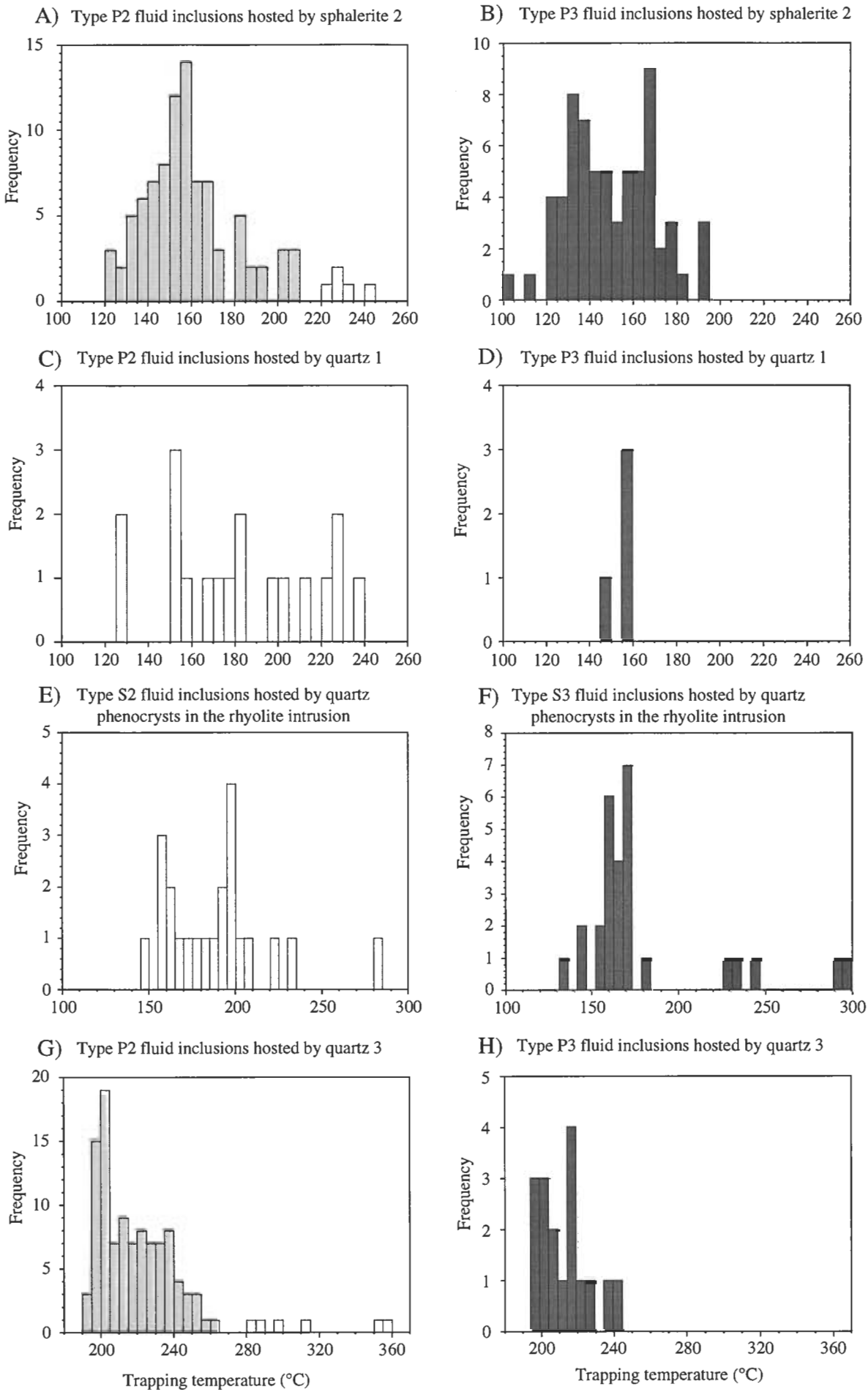


Fig. 9.9. Trapping temperature histograms for type P2, P3, S2 and S3 fluid inclusions hosted by sphalerite 2, quartz 1, quartz 3 and quartz phenocrysts in the strongly altered rhyolite intrusion.

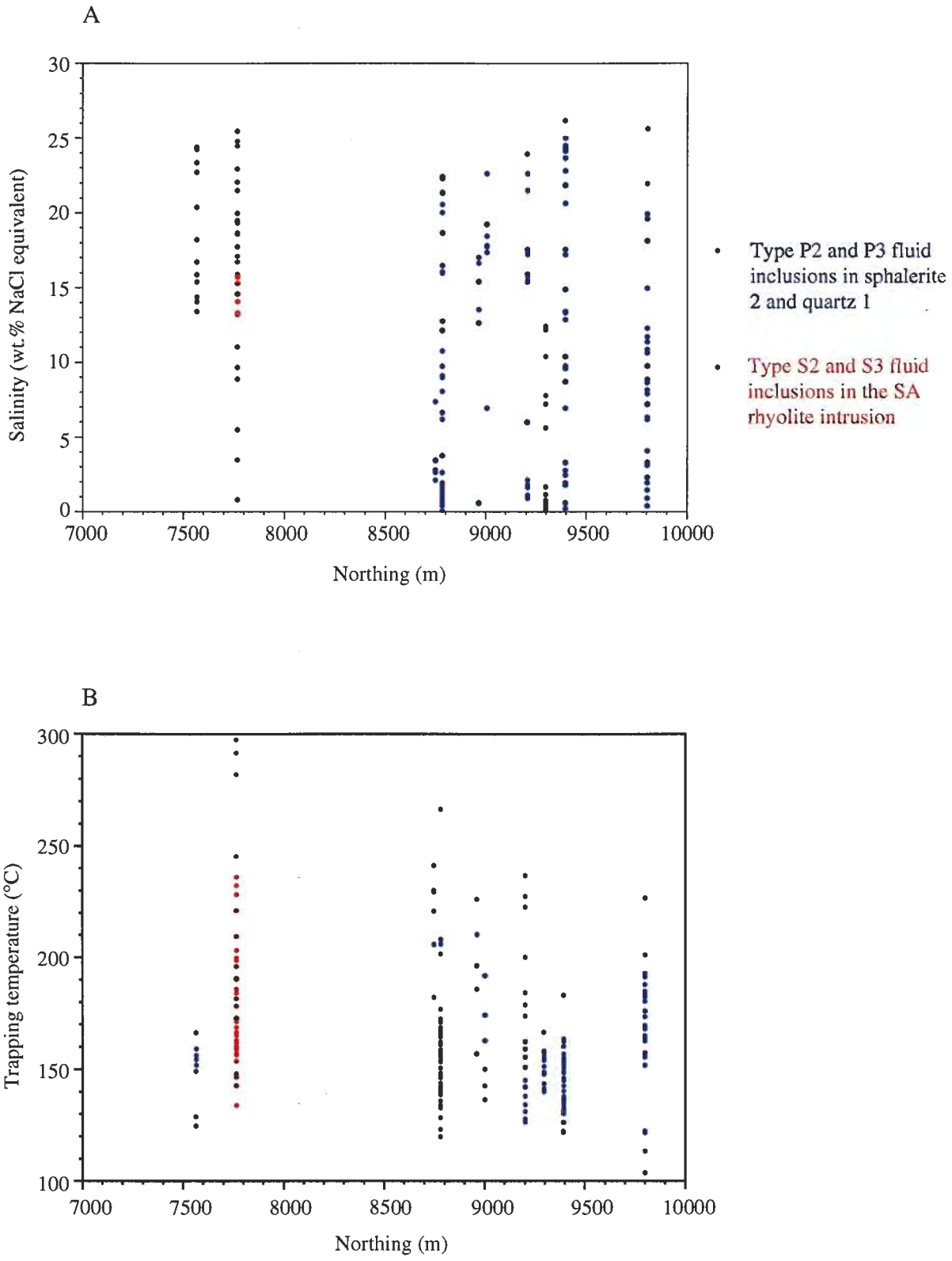


Fig. 9.10A - B. Salinity (A) and trapping temperature (B) vs northing for type P2, P3, S2 and S3 fluid inclusions hosted by sphalerite 2, quartz 1 and quartz phenocrysts in the strongly altered rhyolite intrusion.

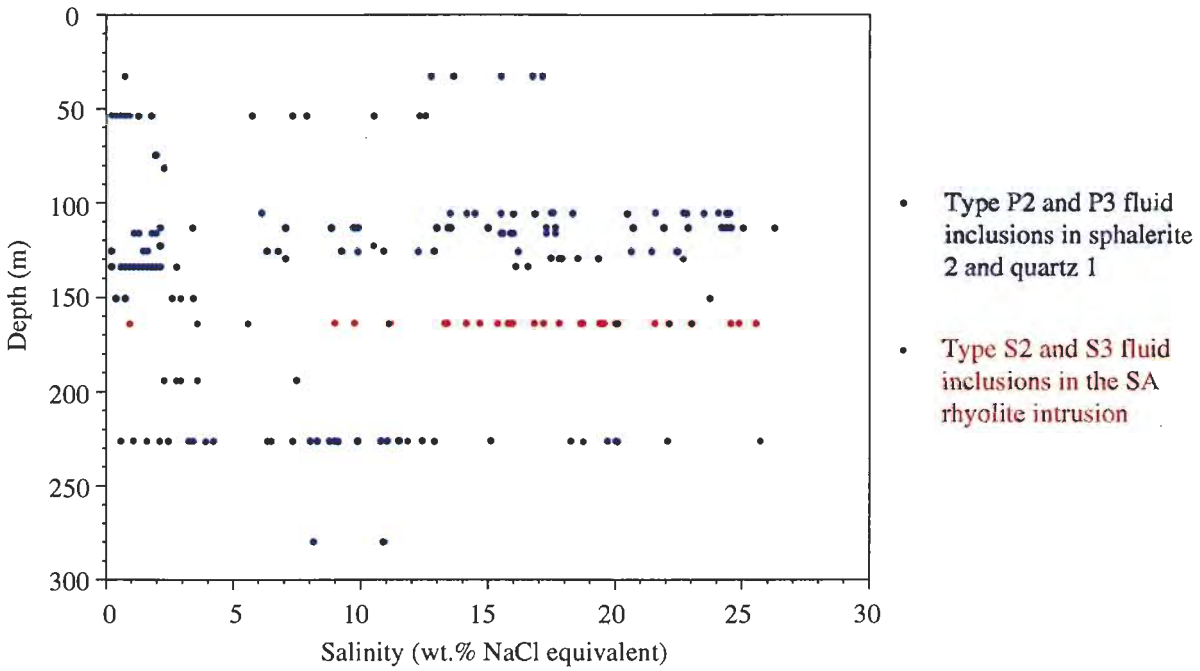


Fig. 9.11a The depth at which fluid inclusions occur plotted against their calculated salinity. There is no systematic relationship between depth and fluid inclusion salinity.

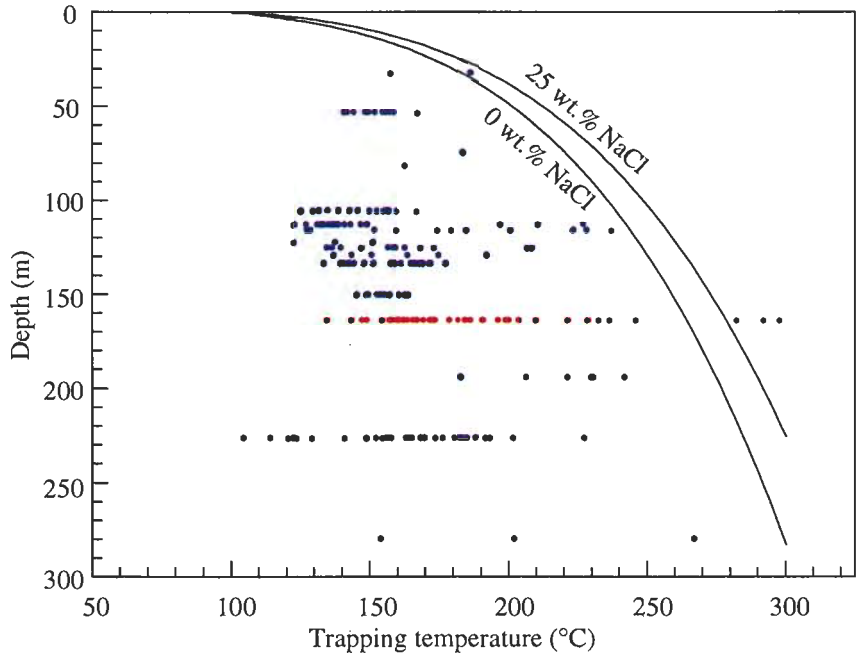


Fig. 9.11b The depth at which fluid inclusions occur plotted against their calculated trapping temperature. Also shown are boiling point curves for $H_2O$ with 0 wt.% dissolved NaCl and 25 wt.% dissolved NaCl (Haas, 1971). All except four fluid inclusions plot below the boiling point - depth curve for a fluid with 0 wt.% NaCl and all except three fluid inclusions plot below the boiling point - depth curve for a fluid with 25 wt.% NaCl.

With the exception of three fluid inclusions, all type P2, P3, S2 and S3 fluid inclusions hosted by sphalerite 2, quartz 1 and quartz phenocrysts in the SA rhyolite intrusion lie below the boiling point depth curve for a fluid with 25 wt.% dissolved NaCl that was subjected to lithostatic pressure due to Hutchison Group host rocks with a density of 3.006 $tm^{-3}$ (Fig. 9.11b). The three fluid inclusions that lie above, and to the right, of the boiling point depth curve are secondary inclusions hosted by quartz phenocrysts in the SA rhyolite intrusion and may have resulted from either necking or higher temperatures due to additional heat from the rhyolite intrusion. With the possible exception of fluid in the immediate vicinity of the rhyolite intrusions, it can be concluded that the mineralising fluids have not undergone phase separation which is consistent with the absence of variable liquid - vapour ratios in type P2 and P3 fluid inclusions, or co-existing vapour rich fluid inclusions.

*Trapping temperatures of fluid inclusions hosted by Quartz 3*

Trapping temperatures for type P2 and P3 fluid inclusions hosted by quartz 3 have been calculated differently to those for primary fluid inclusions hosted by sphalerite 2, quartz 1 and secondary fluid inclusions hosted by quartz phenocrysts in the SA rhyolite intrusion. Formation of quartz 3 post-dated emplacement of the MD ignimbrite (Section 5.3.2), therefore, the lithostatic load of the MD ignimbrite (and overlying units?) must be taken into account in estimating the pressure correction. The MD ignimbrite is interpreted to be the eroded remnant of a ponded intracaldera ignimbrite (Section 4.4.9), however, the true thickness of the MD ignimbrite is not known. The thickness of the MD ignimbrite and overlying units can be approximated by comparison to other well known intracaldera fill sequences.

Intracaldera fill sequences are commonly interpreted to have been of substantial thickness*. Assuming a total thickness of caldera fill sequence of 1.5 km, with a density of 2.62 $tm^{-3}$ (equivalent to granites of the Hiltaba Suite, Table 6.2), this would correspond to a lithostatic load of 39 MPa. Based on this assumption, the average trapping temperature for type P2 and P3 fluid inclusions hosted by quartz 3 is estimated as $\approx$ 42°C higher than the homogenisation temperature (Potter, 1977). The median trapping temperature is estimated as 214°C, with a peak trapping temperature of 356.3°C (Figs. 9.9g, h). The range of estimated trapping temperatures is consistent with the occurrence of epidote and garnet in the late alteration overprint, and the minimum temperatures of 200 °C and 320°C at which epidote and garnet respectively have been interpreted to occur in geothermal wells (Henley and Ellis, 1983).

---

* eg. Lake City Caldera, 1.5 km thick, Lipman, 1976; San Jaun Caldera, >1 km thick, Lipman, 1976; Job Canyon Caldera, 2 km thick, John, 1995; Poco Canyon Caldera, >4.5 km thick, John, 1995; Elevenmile Canyon Caldera, >4 km thick, John, 1995; Chegem River, >2 km thick, Lipman et al., 1993; Minarets Caldera, 2 km thick, Friske and Tobisch, 1994; La Garita Caldera, >1.4 km thick, Self and Wright, 1983; and others.

### 9.6.4 Trapping temperature vs salinity diagrams, and fluid mixing

*Sphalerite 2 and quartz 1*

Trapping temperatures plotted against salinity for type P2 and P3 fluid inclusions hosted by sphalerite 2 have negative correlations, with correlation coefficients of 0.22 (90% confidence level) and 0.47 (95% confidence level) respectively (Figs. 9.12a, b). Although a similar trend may exist for type P2 and P3 fluid inclusions hosted by quartz 1, there are too few analyses to assess the validity of a correlation (Figs. 9.12c, d).

*Strongly altered rhyolite intrusions*

Trapping temperature vs salinity diagrams for type S2 fluid inclusions hosted by quartz phenocrysts in the SA rhyolite intrusion have a negative correlation with a correlation coefficient of 0.81 (95% confidence level; Fig. 9.12e). Type S3 fluid inclusions can be separated into two populations with a lower temperature population (< 200°C) and a higher temperature population (200 - 300°C; Fig. 9.12f). The lower temperature population has a negative correlation with a correlation coefficient of 0.60 (99% confidence level) which is similar to that for P2 and P3 fluid inclusions hosted by sphalerite 2 and quartz 1. The higher temperature population consists of five, scattered analyses that may have resulted from necking, or addition of heat from the rhyolite intrusion discussed previously.

*Quartz 3*

Type P2 and P3 fluid inclusions hosted by quartz 3 do not show any linear trends and plot as a cluster of values (Figs. 9.12g, h) which contrasts to the distributions for primary fluid inclusions hosted by sphalerite 2, quartz 1 and secondary fluid inclusions hosted by quartz phenocrysts in the SA rhyolite intrusion.

*Fluid mixing*

The range of fluid inclusion salinities and the negative correlation between salinity and temperature for fluid inclusions hosted by sphalerite 2, quartz 1 and secondary fluid inclusions hosted by quartz phenocrysts in the SA rhyolite intrusion are interpreted to have resulted from mixing of a lower temperature, higher salinity fluid (≈ 140°C and ≈ 27 wt.% NaCl equivalent) with a higher temperature lower salinity fluid (≈ 180°C and ≈ 1 - 3 wt.% NaCl equivalent; Figs. 9.12a - f). Experimental studies by Henley and McNabb (1978) indicated that fluids which differ markedly in density (and hence salinity) are extremely slow to mix. This may account for the occurrence of fluid inclusions of different salinity side by side in the same mineral growth zone.

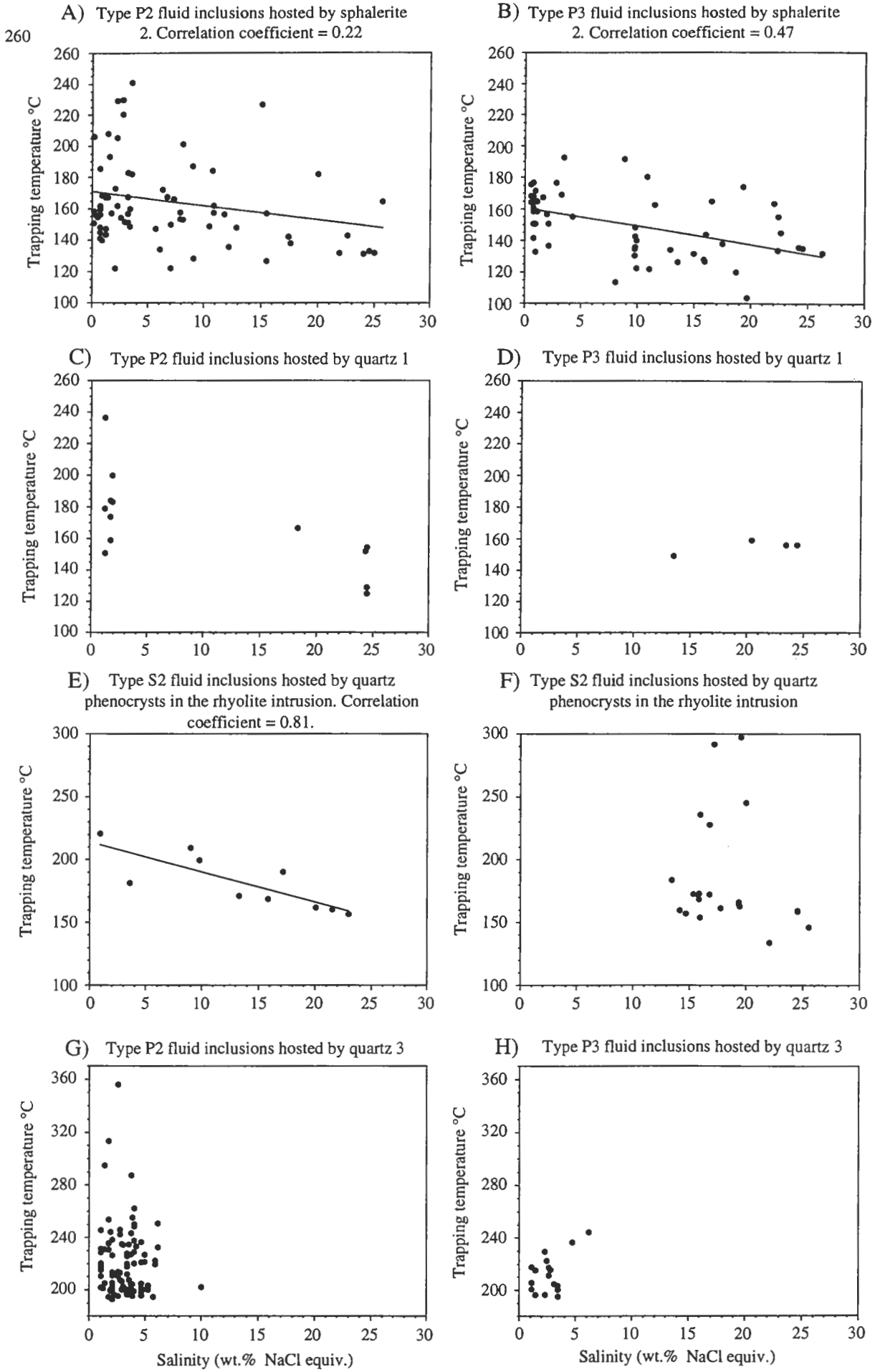


Fig. 9.12a - h. Trapping temperature versus salinity diagrams for fluid inclusions hosted by sphalerite 2, quartz 1, quartz 3 and quartz phenocrysts in the rhyolite intrusion.

### 9.6.5 Mineral inclusions in primary and secondary fluid inclusions - daughter minerals or accidentals?

Mineral inclusions (other than halite) present at room temperature in type P3 fluid inclusions did not homogenise during heating runs. Roedder (1984) suggested a number of reasons as to why mineral inclusions may not dissolve on heating including:

- Equilibrium was not attained in the given time
- Equilibrium was attained but the melting temperature of the solid inclusion lies above that of the vapour - liquid homogenisation temperature.
- The solid may be a accidental inclusion
- The fluid inclusion may have been necked.

There is no morphological or microthermometric evidence for necking of type P2 and P3 fluid inclusions. When fluid inclusions were maintained at temperatures of up to 400°C (well beyond that for vapour - liquid homogenisation) for in excess of 30 minutes, no change in the morphology of the solid phase was observed. Similarly, when fluid inclusions were maintained at temperatures just above the freezing temperature for in excess of 30 minutes, no change in the morphology of the solid phase was observed.

Roedder (1984) suggested the distinction between accidental fluid inclusions and daughter minerals should be made on the basis of:

- A mineral that occurs only in some of the fluid inclusions, in highly variable amounts (particularly if it also occurs as simple solid fluid inclusions in the host), is probably an accidental solid inclusion.
- Daughter minerals should be ubiquitous, and if present, they should occur in a regular ratio to other phases. The larger a fluid inclusion is, the more likely all phases which should be present are present. This is related to nucleation problems in small fluid inclusions.

Mineral inclusions, other than carbonate, are present in only a small number of primary fluid inclusions. As there is nothing to indicate these fluid inclusions (type P3) are genetically different from type P2 fluid inclusions hosted by the same mineral, the solid phase is interpreted as an accidental. One type P3 fluid inclusions hosted by sphalerite 2 contained a small hematite inclusion. Hematite is known to form in some fluid inclusions through later diffusive loss of hydrogen (Roedder, 1984), however, the occurrence of hematite as rare scattered inclusions throughout sphalerite 2 at Menninnie Dam is interpreted to be evidence in favour of accidental inclusion (Fig. 9.2f).

Carbonate is present as a mineral inclusion in 34% of measured fluid inclusions hosted by sphalerite 2. Within the constraints of two dimensional observations, the dimensions of the carbonate mineral inclusions are approximately proportional to the size of the fluid inclusions

(Fig. 9.13), and carbonate was not observed as a mineral inclusion in sphalerite 2 outside of fluid inclusions. However, there is no correlation between the occurrence of carbonate in fluid inclusions, the first melting phenomenon at around -52°C, salinity, clathrate formation or trapping temperatures. As carbonate-bearing fluid inclusions cannot be attributed to a separate fluid event, and occur side by side in the same sphalerite growth zone with non-carbonate bearing fluid inclusions, the non-ubiquitous occurrence of carbonate is interpreted to have resulted from accidental inclusion. As mineralisation is hosted by marbles, accidental carbonate inclusions may have resulted from incomplete dissolution of the host marble, or result from a fluid composition that was saturated with respect to carbonate at the time of trapping.

In a study of the structural and geochemical controls on tin mineralisation at the Renison Mine in Tasmania, Kitto (1994) noted an association between fluid inclusions with carbonate inclusions and dolomite horizons. Carbonate inclusions were absent in fluid inclusions hosted by minerals in non-dolomitic horizons. Whereas Kitto (1994) concluded the carbonate inclusions were daughter minerals derived from $CaCl_2$ saturation of a NaCl - KCl - $H_2O$ brine during interaction with the dolomite host rocks, their occurrence in fluid inclusions at Menninnie Dam is interpreted to be accidental. As eutectics of < -50°C were observed for only a small percentage of fluid inclusions from Menninnie Dam, saturation of the fluid with respect to carbonate is unlikely to have been the predominant mechanism that resulted in carbonate inclusions (ref. Section 9.6.7).

*Mineral inclusions in secondary fluid inclusions*

Thirty five percent of the measured secondary fluid inclusions hosted by quartz phenocrysts in the SA rhyolite intrusion contain carbonate inclusions. As with fluid inclusions hosted by sphalerite 2, there is no correlation between the occurrence of carbonate inclusions, first melting phenomenon at around -52°C, salinity, clathrate formation, or trapping temperature, and carbonate inclusions are also interpreted to be of accidental origin.

### 9.6.6 Comparison of fluid inclusions in the rhyolite intrusion, quartz 1 and sphalerite 2

Microthermometric characteristics of secondary fluid inclusions hosted by quartz 1 are similar to primary fluid inclusions of sphalerite 2 and quartz 1. Secondary fluid inclusions hosted by quartz phenocrysts in the SA rhyolite intrusion have a similar range of salinities (0 - 28 wt.% NaCl equivalent), accidental lithic population, first melting phenomenon near -50°C, hydrohalite final melting temperature, and ice final melting temperature to fluid inclusions hosted by sphalerite 2 and quartz 1. The proportion of secondary fluid inclusions hosted by quartz phenocrysts in the SA rhyolite intrusion that contain carbonate inclusions (≈ 37%) is similar to the proportion of fluid inclusions hosted by sphalerite 2 that contain carbonate inclusions (≈ 34%).

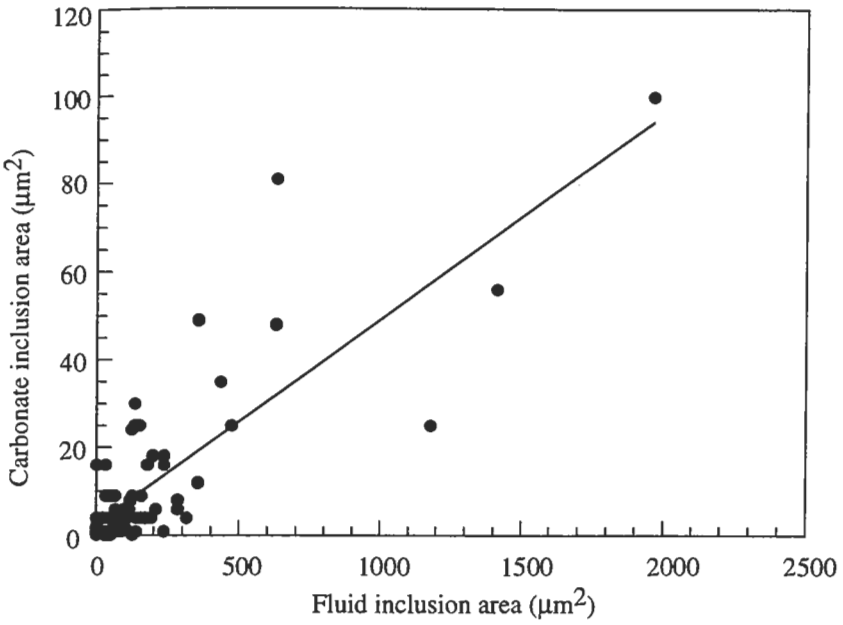


Fig. 9.13. Area of type P3 fluid inclusions hosted by sphalerite 2 versus the area of their contained carbonate mineral inclusions. The area of carbonate mineral inclusions is approximately proportional to the area of the host fluid inclusion (correlation coefficient = 0.81)

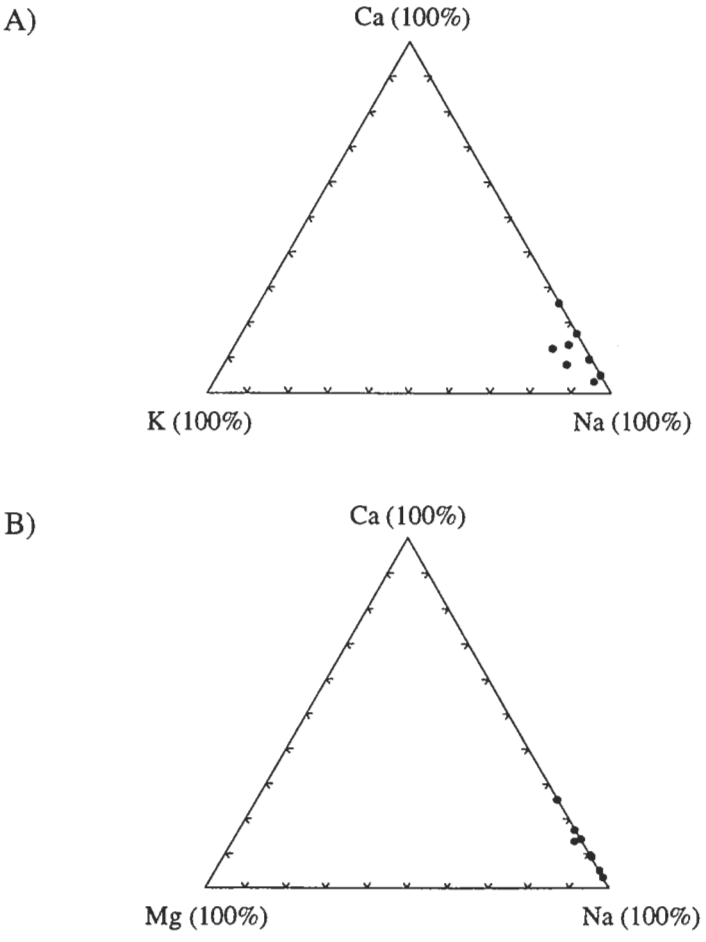


Fig. 9.14a, b. Triangular diagrams of salt compositions determined by electron microprobe analyses of primary fluid inclusion decrepitates.

Diagrams of trapping temperature versus salinity are also similar to those for quartz 1 and sphalerite 2 (Figs. 9.12e, f). Secondary fluid inclusions in the quartz phenocrysts are interpreted to have been derived from the same fluid from which the mineralisation formed. The slightly higher trapping temperatures (30 - 40°C) of secondary fluid inclusions in the SA rhyolite intrusion may have resulted from localised heating of fluids by the rhyolite intrusion.

### 9.6.7 Composition of the mineralising fluid

The composition of the mineralising fluid can be determined from consideration of decrepitate analyses and fluid inclusion freezing and heating characteristics. Total salinities cannot be calculated from analyses of decrepitates as the volatile component is lost through evaporation, however, element ratios can be calculated (Fig. 9.14a, b; Table 9.6). Some of the decrepitates analysed may have been derived from type P3 fluid inclusions that contained an accidental carbonate fluid inclusion. In such instances, the Ca component of the decrepitate may have been under-represented as the carbonate is likely to have acted as a nucleation site for any Ca and $CO_2$ present in the fluid inclusion.

Table 9.6. Average Na, K, Ca and Mg ratios of fluid decrepitate analyses

| | Element ratio |
|---|---|
| K / Na | 0.041 |
| Ca / Na | 0.155 |
| Mg / Na | 0.004 |

Based on the analyses of decrepitates, the mineralising fluid is interpreted to have comprised a predominantly NaCl - $CaCl_2$ - KCl - $H_2O$ fluid with minor $MgCl_2$ and aqueous fluorine species. The addition of salts such as $MgCl_2$, $CaCl_2$, KCl and $FeCl_2$ to the NaCl - $H_2O$ system has the effect of lowering the eutectic temperature below -21.2°C (Borisenko, 1977; Table 9.7).

Table 9.7 Eutectic temperatures for various water - salt systems.

| System | Eutectic (°C) | Reference |
|---|---|---|
| KCl - $H_2O$ | -10.8 | Schul'gina, et al., 1955 |
| NaCl - $H_2O$ | -21.2 | Borisenko, 1977 |
| KCl - NaCl - $H_2O$ | -23.5 | Borisenko, 1977 |
| $MgCl_2$ - $H_2O$ | -33.6 | Borisenko, 1977 |
| $FeCl_2$ - $H_2O$ | -35.0 | Borisenko, 1977 |
| $MgCl_2$ - NaCl - $H_2O$ | -35.0 | Crawford, 1981 |
| $FeCl_3$ - $H_2O$ | -36.5 | Borisenko, 1977 |
| $FeCl_2$ - NaCl - $H_2O$ | -37.0 | Borisenko, 1977 |
| $MgCl_2$ - KCl - $H_2O$ | -37.8 | Borisenko, 1977 |
| $CaCl_2$ - $H_2O$ | -49.8 | Yanatieva, 1946 |
| $CaCl_2$ - KCl - $H_2O$ | -50.5 | Borisenko, 1977 |
| $MgCl_2$ - $CaCl_2$ - $H_2O$ | -52.2 | Borisenko, 1977 |
| $CaCl_2$ - KCl - NaCl - $H_2O$ | -55.0 | Yanatieva, 1946 |
| $CaCl_2$ - NaCl - $H_2O$ | -55.0; -52.0 | Borisenko, 1977; Crawford, 1981 |
| $CaCl_2$ - $MgCl_2$ - NaCl - $H_2O$ | -58.0 | Luzhnaja and Vereshtchetina, 1946 |

The small number of observed eutectics between -55 and -50°C in fluid inclusions at Menninnie Dam are consistent with a $CaCl_2$ - KCl - NaCl - $H_2O$ system. Eutectics between -50 and -45°C probably resulted from observations after the eutectic point had been passed and highlights the difficulties of observing eutectics at low temperatures for fluid inclusions hosted by coloured sphalerite. Hydrohalite final melting temperatures were consistently lower than ice final melting temperatures which is compatible with a high NaCl : $CaCl_2$ ratio in a NaCl - $CaCl_2$ salt system (Fig. 9.15). If the $CaCl_2$ component of fluid inclusions was locally derived through dissolution of the host marbles and calc-silicate lithologies, the primary fluids would have had a composition in which the dominant salts were NaCl and KCl.

The formation of clathrates with final melt temperatures of less than 10°C are interpreted to indicate $CO_2$ is present in at least some fluid inclusions (Roedder, 1984). $CO_2$ may have been present in more fluid inclusions but not detected by clathrate formation, and could have been as high as 1.026 molal without formation of an immiscible $CO_2$ phase at room temperature in fluid inclusions with negligible salinity (Hedenquist and Henley, 1985b). The effect of undetected, dissolved $CO_2$ would result in an over-estimation of the salinity, which subsequently effects estimations of metal solubility (Hedenquist and Henley, 1985b). The $CO_2$ content of Menninnie Dam fluid inclusions has not been measured, however as $CO_2$ clathrate was not observed to form in most fluid inclusions, the concentration of $CO_2$ is interpreted to be generally less than 0.85 molal (Hedenquist and Henley, 1985b).

### 9.6.8 Composition of the late alteration overprint fluid

The composition of fluids associated with the late alteration overprint differ from those associated with mineralisation. Late alteration overprint fluids have a lower salinity and are interpreted to have had a higher trapping temperature. A eutectic temperature of -48°C was observed for only three fluid inclusions, all of which froze to a mottled brownish colour. This eutectic temperature is close to the eutectics for salt - water systems that contain $CaCl_2$. Electron microprobe analysis of decrepitates were not attempted for fluid inclusions associated with the late alteration overprint, as formation of a sufficient quantity of decrepitate for analysis was considered unlikely given the small size of fluid inclusions and their low salinity. The absence of clear eutectics, and the low salinity of fluid inclusions is interpreted to indicate a dilute NaCl - $H_2O$ fluid system that locally contained minor amounts of $CaCl_2$.

A diagram of trapping temperature versus depth for fluid inclusions hosted by quartz 3 in drill hole PD0032 (Fig. 9.16) shows the maximum fluid inclusion trapping temperature occurred in the non-welded basal portion of the MD ignimbrite and underlying LP breccia.

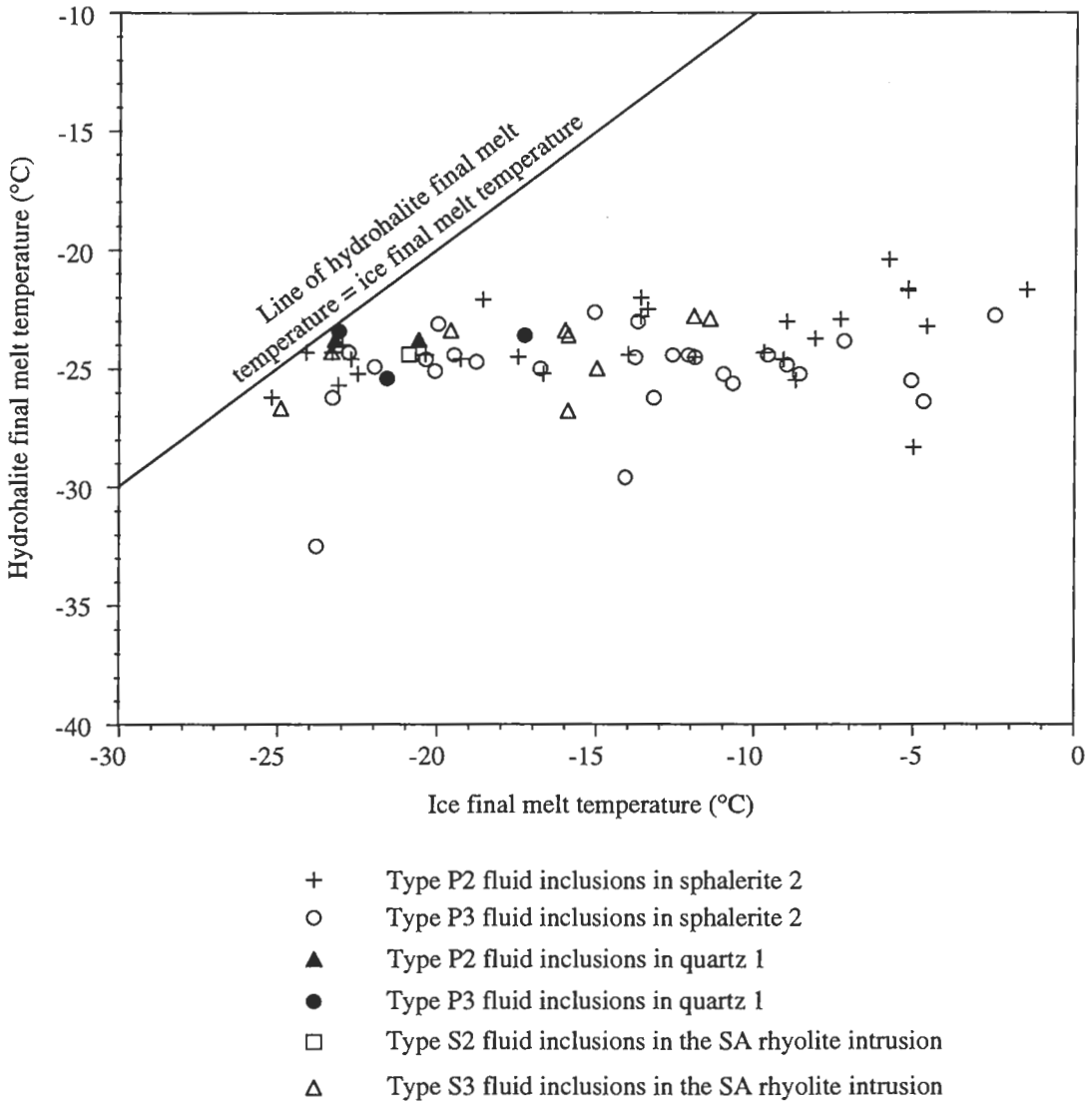


Fig. 9.15. Hydrohalite final melt temperature versus ice final melt temperature. Hydrohalite final melt temperatures are all lower than ice final melt temperatures.

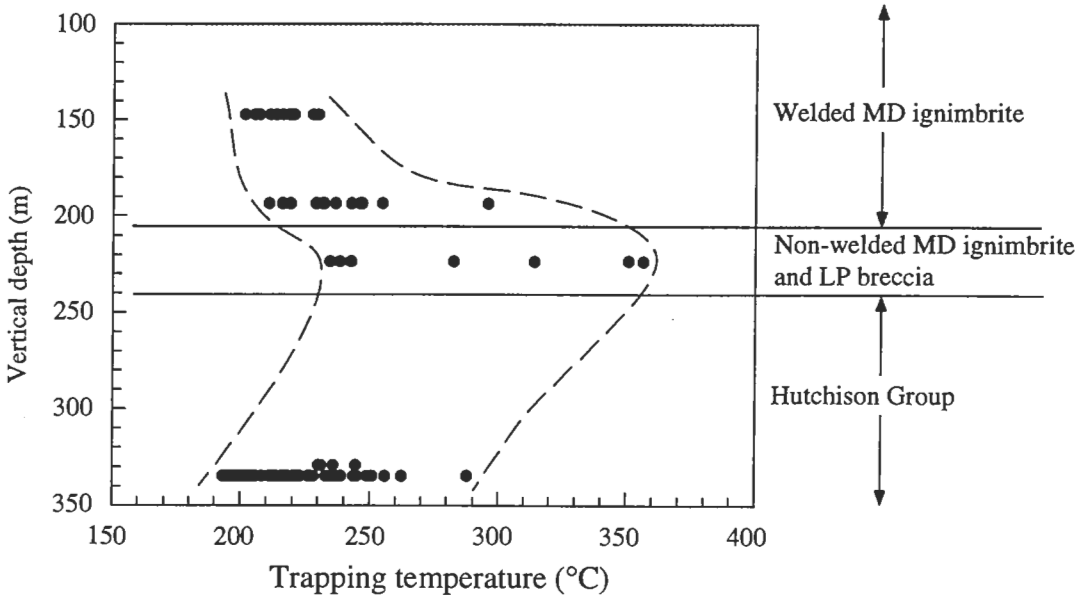


Fig. 9.16. Diagram showing the variation in trapping temperatures with depth in drill hole PD0032 for fluid inclusions hosted by quartz 3. Fluid inclusion tapping temperatures are highest in LP breccia and the non-welded part of the MD ignimbrite.

The non-welded portion of the MD ignimbrite and LP breccia may have acted as an aquifer sandwiched between an upper aquitard of welded ignimbrite and a lower aquitard of Hutchison Group lithologies. This interpretation is subject to the caveat that it is based on a small number of higher temperature fluid inclusions.

The lower trapping temperature of fluid inclusions higher up in the welded portion of the MD ignimbrite is interpreted to indicate the MD ignimbrite was welded and had cooled prior to infiltration of fluids associated with the late alteration overprint. This effectively excludes the MD ignimbrite as a heat source for fluids which gave rise to the late alteration overprint. If the cooling rate of the MD ignimbrite could be established, the maximum timing of the late alteration overprint could be established. However, the time taken for the MD ignimbrite to cool is dependant on a number of unknown factors including the thickness, the intensity of welding, degree of fracturing, rainfall, etc. (Kamata et al., 1993, Dzurisin et al., 1990).

Although the late alteration overprint paragenetically post-dates the mineralisation at Menninnie Dam, an earlier phase of a similar fluid could have formed the low salinity, end member of the mixing trend interpreted from fluid inclusions associated with mineralisation. This hypothesis can be evaluated by applying the pressure correction used for fluid inclusions hosted by sphalerite 2, quartz 1 and those in the SA rhyolite intrusions to fluid inclusions hosted by quartz 3 (Fig. 9.17). The data for quartz 3 fluid inclusions overlaps with the low salinity end of an array defined by fluid inclusions associated with mineralisation. This can be interpreted to indicate (but by no means proves) an earlier phase of a fluid similar to that associated with the late alteration overprint may have been one end member of a fluid mixing trend.

## 9.7 Summary

At Menninnie Dam, three distinct fluids have been interpreted from fluid inclusions, two are associated with the mineralisation and a third is associated with the late alteration overprint.

*Fluid inclusions associated with mineralisation.*

Primary fluid inclusions associated hosted by sphalerite 2 and quartz 1 comprise liquid + vapour fluid inclusions (type P2) and liquid + vapour + one or more mineral inclusions (type P3). Mineral inclusions consist of carbonate and less commonly, mica, halite, hematite or an opaque mineral. With the exception of halite, all mineral inclusions are interpreted to be accidental and type P2 and P3 fluid inclusions comprise a single population.

Fluid inclusion trapping temperatures range between 100 - 266°C with a median of ≈ 154°C and all lie below the a lithostatic boiling point - depth curve. Fluid inclusion salinities comprise a range of values between 0 - 27 wt.% NaCl equivalent and more saline fluid inclusions generally have lower trapping temperatures.

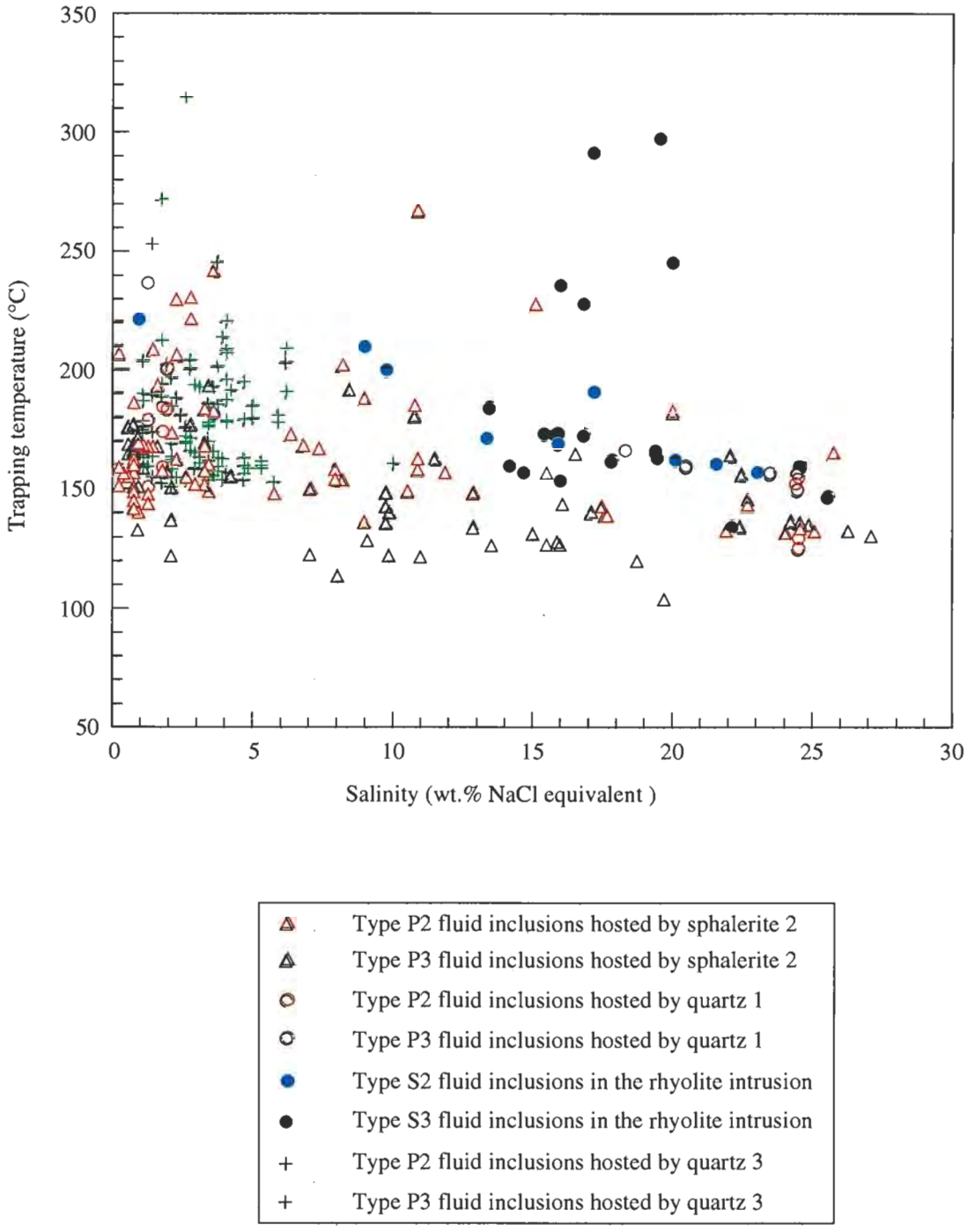


Fig. 9.17. Diagram of trapping temperature versus salinity for all measured fluid inclusions from Menninnie Dam. The array of data is interpreted to have resulted from mixing of a lower temperature, higher salinity fluid, with a higher temperature, lower salinity fluid. Fluid inclusions hosted by quartz 3 overlap with lower salinity, higher temperature fluid inclusions when the same pressure correction is applied to all fluid inclusions.

Higher trapping temperatures generally occur at greater depths although there is no systematic variation in either salinity or trapping temperature along the length of the Menninnie Dam deposit. The range of salinities and trapping temperatures is interpreted to have resulted from mixing between a fluid of ≈ 180°C and 0 - 3 wt.% NaCl equivalent, with a fluid of ≈ 140°C and ≥ 27 wt.% NaCl equivalent.

Fluid inclusion microthermometric data, and microprobe analyses of salt decrepitates are interpreted to indicate the fluids associated with the mineralising event can be approximated by the system NaCl - KCl - $CaCl_2$ - $H_2O$ with trace amounts of $MgCl_2$, in which NaCl was the most abundant salt. The $CaCl_2$ component may have been locally derived through dissolution of marble and calc-silicate lithologies.

Secondary fluid inclusions hosted by quartz phenocrysts in the SA rhyolite intrusion have similar microthermometric characteristics and accidental mineral inclusions to fluid inclusions associated with the mineralisation. A minimum timing for rhyolite intrusion can be interpreted from fluid inclusions, and when combined with previous mineral paragenetic relationships, a close temporal relationship between rhyolite intrusions and mineralisation is confirmed.

*Fluid associated with the late alteration overprint*

Fluid inclusions associated with the late alteration overprint and hosted by quartz 3 have salinities of < 5 wt.% NaCl equivalent. The late alteration overprint is interpreted to have post-dated both mineralisation and emplacement of the MD ignimbrite. Due to the presence of the overlying MD ignimbrite, fluids associated with the late alteration overprint are interpreted to have been subjected to higher lithostatic pressures resulting in trapping temperatures in the range 193 - 356°C with a median trapping temperature of 214°C. If the same pressure correction used for fluid inclusions associated with mineralisation is applied to fluid inclusions associated with the late alteration overprint, these data overlap with the higher temperature, lower salinity data derived from fluid inclusions associated with mineralisation.

# Chapter ten
# Stable isotopes

## 10.1 Introduction

Hydrothermal fluids commonly contain the elements H, C, O, N, and S. Stable isotopes provides a means of determining the source of these elements, studying the effects of fluid - rock interaction, and mixing of fluids. In some instances, stable isotopes can be used as palaeo-thermometers, and to assist with determination of the diffusion and reaction mechanisms in geological processes. Comprehensive reviews of the principals of stable isotope geochemistry are presented by numerous authors, including; Taylor (1979), Hoefs (1980), Valley et al. (1986), Kyser (1987), and Taylor et al. (1991).

Carbon and oxygen isotopes from carbonate minerals, and oxygen and deuterium / hydrogen isotope analyses of hydrous silicate minerals from Menninnie Dam have been used to assist with interpretation of the source of the fluids that produced the Pb - Zn - Ag mineralisation, the extent of fluid - rock interaction, and the speciation of aqueous carbon. Sulphur isotope analyses of sulphide minerals in the host rocks and mineralisation have been used to assist with interpretation of possible sulphur sources and to examine the likely speciation of sulphur in the mineralising fluids.

No previous study of carbon, oxygen, deuterium / hydrogen isotope study has been undertaken on the Menninnie Dam mineralisation or host rocks. Andrew (1992) undertook a pilot study of sulphur isotopes from samples of Menninnie Dam mineralisation to assess suitability for inclusion in a research project examining the genesis of a number of Australian Proterozoic mineral deposits. The Menninnie Dam deposit was not included in the research project for reasons unknown to the author.

## 10.2 Oxygen and carbon isotopes

Pb - Zn - Ag mineralisation at Menninnie Dam is hosted by marble and calc-silicate lithologies with minor graphitic schist units and metasomatised marble lithologies (Section 5.2.1). Pb - Zn - Ag mineralisation has replaced metamorphic marble and calc-silicate lithologies as well as metasomatic marble and resulted in formation of Ca-Mn-Mg-Fe carbonate as a common gangue mineral. Mineralisation has locally been overprinted by the 'late alteration overprint' (Section 5.3). Within the constraints of other geologic and geochemical data, carbon and oxygen isotope analysis of carbonate minerals provides a means of determining the extent of fluid - rock interaction during the mineralising event, and during the late alteration overprint. (eg. Taylor, 1974, 1977; Sverjensky, 1981; Zheng and Hoefs, 1993; Kitto, 1994).

Fluid inclusion studies of the Menninnie Dam mineralisation are interpreted to indicate mixing of two fluids (Section 9.6.4). Carbon and oxygen isotopes can be used to assess fluid mixing as a means of producing the carbonates associated with mineralisation (eg. Zheng and Hoefs, 1993; Taylor and Bucher-Nurminen, 1986), and can assist with determination of the source of both the mineralising fluids as well as the fluids which gave rise to the late alteration overprint (eg. Bethke and Rye, 1979; Rye and Williams, 1981; Shelton, 1983; Beaty and Landis 1990).

### 10.2.1 Sample selection

Samples of the host marbles were collected from drill core throughout the Menninnie Dam prospect and subdivided into 'marble', 'impure marble' and 'metasomatic marble'. (Table 10.1). Samples of carbonate associated with mineralisation were collected from various mineralised zones throughout the prospect and subdivided into two groups 'intra-mineralisation carbonates' (Fig. 10.1a) and 'margin carbonates' (Fig. 10.1b) dependant on their proximity to the contact between mineralisation and the host rocks (Table 10.1).

Table 10.1. Summary of carbonate samples used for carbon and oxygen isotope analyses.

| Sample Group | Subgroup | Number | Description |
|---|---|---|---|
| Host rock carbonate | Marble | 25 | Dolomitic marble ≥ 2m distant from silicate mineral-bearing units. |
| | Impure marble | 12 | Dolomitic or calcitic marble that either contains minor dispersed magnetite, graphite or calc-silicate minerals, or is within 30 cm of significant zones of calc-minerals such as diopside, talc and tremolite. |
| | Metasomatic marble | 19 | Calcitic marble with disseminated silicate minerals that have been overprinted by post-metamorphic metasomatic alteration. |
| Hydrothermal carbonate | intra-mineralisation carbonates | 28 | Ca-Mg-Mn-Fe 1 and 2 carbonate formed during the mineralising event (Section 5.2.3). These include samples from carbonate from sulphide veins, stockwork style mineralisation and carbonate from the matrix of altered DP breccias (Fig. 10.1a). |
| | margin carbonates | 4 | Ca-Mg-Mn-Fe 1 and 2 formed during the mineralising event (Section 5.2.3), and within 1 cm of the contact between mineralisation and host marble (Fig. 10.1b). |
| | halo carbonates | 7 | Samples at ≈ 4 cm intervals along a traverse from the contact between mineralisation and the host rocks and extending out into the host rocks for a distance of 25.5 cm (Fig. 10.1c). |
| Late alteration overprint carbonates | LAO carbonate | 5 | Ca-Mg-Mn-Fe 3 formed during the late alteration overprint (Section 5.3.2). Samples were selected from zones where an estimate of the temperature of alteration could be determined from either fluid inclusions or from the mineral assemblage. |

The extent of the alteration halo surrounding mineralisation was assessed through sampling and analysis of a traverse from the margin of a sulphide vein and extending out into the host rocks over a distance of 25.5 cm (Fig. 10.1c). These samples are treated separately and

referred to as 'halo carbonates' (Table 10.1). Samples of carbonate formed during the late alteration overprint of the southern zone (Section 5.3.2) are referred to as LAO carbonates.

Figure 10.1a - c. Cartoons of sample locations for intra-mineralisation carbonate, margin carbonate and halo carbonate.

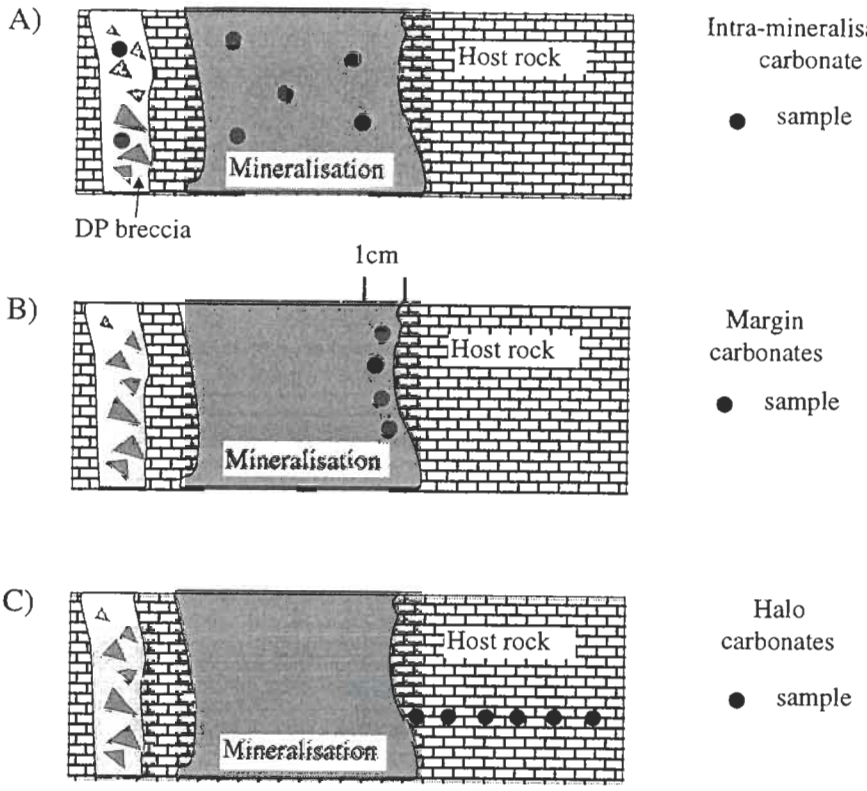


*Carbonate compositions*

Samples of the host rock marble and impure marble have dolomitic compositions. Metasomatic marble is calcitic. Intra-mineralisation carbonates and margin carbonates have a range of compositions, that have been collectively termed Ca-Mg-Mn-Fe carbonate 1 and 2 (Fig. 5.28). Ca-Mg-Mn-Fe carbonate 1 and 2 formed during sulphide deposition, immediately following deposition of sphalerite 2 and extending through to deposition of pyrite 2 (Fig. 5.2). Trace amounts of dolomite were associated with the early stages of marble and diopside alteration prior to the deposition of pyrite 1, but has not been sampled as part of this study. LAO carbonate has a range of compositions that have been collectively termed Ca-Mn-Mg-Fe carbonate 3 (Section 5.3.2).

### 10.2.2 Analytical methods

Carbonate minerals were sampled with a diamond tip dentists drill. Twenty five milligrams of sample was reacted with $H_3PO_4$ for 24 hours at 25°C using the method of McCrea (1950). The resultant $CO_2$ gas was analysed with a Micromass 602D stable isotope mass spectrometer in the Central Science laboratory, University of Tasmania. Weights of matrix sample were obtained in proportion to the modal abundance of calcite. Analytical precision has been established ± 0.06 ‰ for $\delta^{13}C$ and 0.1 ‰ for $\delta^{18}O$ using the international standard

'Biggenden calcite'. All results reported as part of this study are within the limits of precision. All $\delta^{18}O$ and $\delta^{13}C$ values are reported relative to V-SMOW and V-PDB standards respectively (Coplen et al., 1983; O'Neil, 1986).

### 10.2.3 Results

Analytical results are summarised in Table 10.2, illustrated in Figure 10.2 and detailed in **Appendix** 10.1.

Table 10.2. Range of $\delta^{18}O$ (V-SMOW) and $\delta^{13}C$ (V-PDB) for carbonates from Menninnie Dam.

| | $\delta^{18}O$ range (V-SMOW) | $\delta^{13}C$ range (V-PDB) |
|---|---|---|
| Marble | 15.52 to 21.09‰ | -1.08 to 1.63‰ |
| Impure marble | 9.65 to 17.73‰ | 0.48 to -4.21‰ |
| Metasomatic marble | 7.77 to 18.01‰ | -1.80 to 0.68‰ |
| Intra-mineralisation | 7.74 to 14.16‰ | -0.38 to -5.56‰ |
| Margin carbonates | 14.23 to 14.87‰ | -0.66 to -5.10‰ |
| Halo carbonates | 14.61 to 15.82‰ | 0.22 to -5.46‰ |
| LAO carbonates | 8.09 to 10.32‰ | 1.30 to -2.12‰ |

Marbles plot as a cluster, centred around $\delta^{18}O \approx 19.6$‰ and $\delta^{13}C \approx 0.5$ ‰ (Fig. 10.2). Impure marbles are consistently lighter in both $\delta^{13}C$ and $\delta^{18}O$ compared to samples of marble. Metasomatic marbles have an array of $\delta^{13}C$ and $\delta^{18}O$ values with a cluster of values that are lighter than marble samples, and a tail of lighter values that overlap with impure marble samples. Intra-mineralisation carbonates form a cluster of values which are generally lighter than the host marbles, impure marbles and metasomatic marbles. Margin carbonates have a narrow range of $\delta^{18}O$ and a wider range of $\delta^{13}C$ that lie between those of intra-mineralisation carbonates and the host marbles. Halo carbonates form a cluster of values which overlap with the host metasomatic marbles. A single halo carbonate analysis lies near the field for mineralisation carbonates and corresponds to the sample taken 1 cm away from sulphide mineralisation. Data for LAO carbonates form a cluster with $\delta^{18}O$ values that are generally lighter than all other carbonates (Fig. 10.2).

### 10.2.4 Discussion

In this section, the processes that may have resulted in the isotopic compositions of host carbonates (marble, impure marble, and metasomatic marble) are discussed, and the isotopic composition of the hydrothermal fluid from which the intra-mineralisation carbonates formed is established. Some of the more important mechanisms that may have effected the isotopic composition of the hydrothermal fluid, and the resultant carbonate minerals, are investigated including; local derivation of carbon from graphitic units, decarbonation reactions that occured during mineralisation, interaction of the hydrothermal fluid and the host marbles, and mixing of fluids with different isotopic compositions.

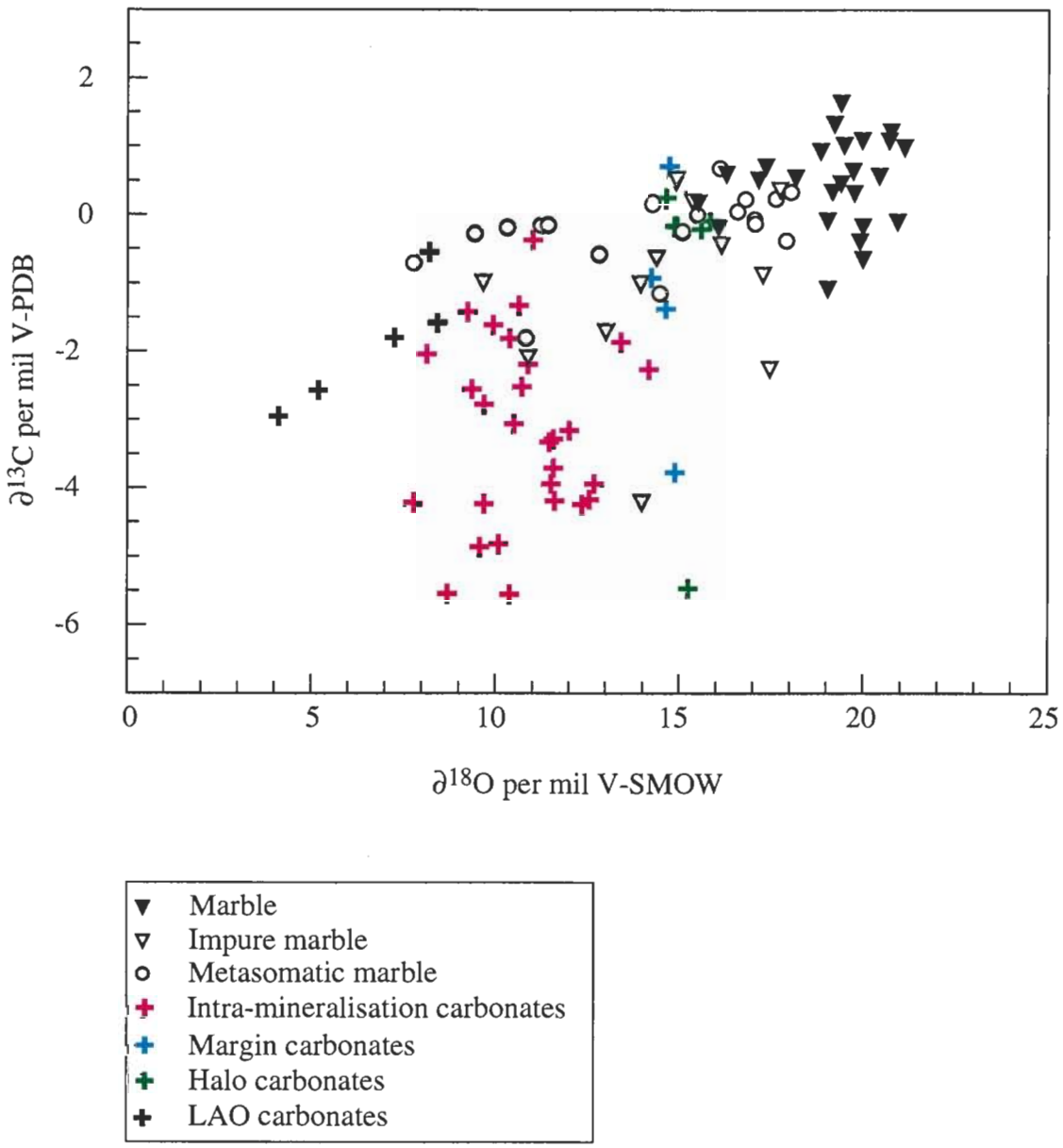


Figure 10.2 $\partial^{13}C$ ‰ V-PDB vs $\partial^{18}O$ ‰ V-SMOW isotopic values for carbonate minerals from Menninnie Dam, including: host rock marbles (marbles, impure marbles and metasomatic marbles), carbonates associated mineralisation (intra-mineralisation carbonates), carbonates associated with mineralisation and within 1 cm of the host rock contact (margin carbonates), carbonates from a traverse from the margin of mineralisation into the host metasomatic marbles (halo carbonates), and carbonates formed during the late alteration overprint (LAO carbonates).

### 10.2.4.1 Host rock carbonates

*Marble and impure marble*

The $\delta^{13}C$ and $\delta^{18}O$ isotopic composition of Proterozoic oceans is a contentious issue (Holland, 1984; Holser, 1984) and there are arguments supporting similar isotopic values to the modern oceans (Sheppard, 1986) and significant excursions towards heavier values in the Middle-Palaeoproterozoic (Baker and Fallick, 1989). Marbles devoid of silicate minerals are considered to be relatively impermeable in metamorphic terrains and commonly preserve their primary isotopic signature (Sheppard and Schwarcz, 1970; Rye et al., 1976; Griggs and Handlin, 1960; Turner, 1967). Marble samples from Menninnie Dam are all from > 2m distant from any silicate minerals and have isotopic values that are within the range for modern marine limestones and marbles (Rollinson, 1993).

Samples of impure marble either contain minor amounts of calc-silicate minerals or magnetite, trace amounts of dispersed graphite, or are in close proximity to significant zones of calc-silicate minerals (< 30 cm). They have $\delta^{13}C$ and $\delta^{18}O$ values which are generally lighter than those for marble (Fig. 10.2). Formation of calc-silicate minerals through reaction of quartz, or silicate minerals, with carbonate involves decarbonation reactions that result in fractionation of the lighter isotopes into the calc-silicate minerals and loss of the heavier isotopes (Valley, 1986). Formation of metamorphic magnetite and graphite results in a similar fractionation trend of oxygen and carbon isotopes (Valley, 1986).

*Metasomatic marbles*

The range of isotopic compositions for metasomatic marble probably results from a combination of factors including:

- Decarbonation reactions during prograde and retrograde metamorphism with loss of the heavy isotopes (Valley, 1986).
- Interaction between the host marble and a metasomatic fluid with a different isotopic composition (Gregory and Criss, 1986).
- Variations in the temperature of the metasomatic fluid (O'Neil, 1986).
- Decarbonation reactions through formation of calc-silicate minerals during metasomatism (Valley, 1986).
- Proximity to fluid channel ways either during metamorphic, or metasomatic processes (Valley, 1986).

### 10.2.4.2 Hydrothermal carbonates

Hydrothermal carbonates include intra-mineralisation carbonates, margin carbonates, halo carbonates and LAO carbonates.

*Isotopic composition of the hydrothermal fluids*

Hydrothermal carbonates have a range of compositions between kutnahorite, Mg-calcite, dolomite, and calcite (Section 5.5.2). Mineral - fluid isotopic fractionation equations for kutnahorite have not been published, therefore throughout the remainder of this chapter the composition of hydrothermal carbonates are collectively approximated by calcite. Application of calcite - water fractionation equations to the small number of dolomitic samples may result in calculated fluid values that vary by < 2‰ from those calculated from using dolomite - water fractionation equations (Ohmoto and Rye, 1979; Deines et al., 1974; O'Neil et al., 1969), and are therefore unlikely to significantly alter the results and interpretation of the Menninnie Dam data.

Ohmoto (1986) suggested that at temperatures greater than 100°C and under acid conditions the amount of aqueous $HCO_3^-$ is negligible compared to the amount of $H_2CO_3$ and therefore;

$$\delta^{13}C_{\Sigma CO2} = \delta^{13}C_{calcite} - \Delta_{(calcite - H2CO3)}.$$

(Ohmoto, 1986)

Fluid inclusion data from Menninnie Dam are interpreted to indicate a median trapping temperature of 154°C and based on association of sericite with mineralisation, the hydrothermal fluids were probably acidic (Barnes, 1979). Fluids are therefore interpreted to have been in equilibrium with $H_2CO_3$.

Temperature dependant fractionation equations (Equations 10.1 and 10.2; Table 10.3) are used to calculate fluid isotopic values for hydrothermal carbonates (Table 10.4).

Table 10.3. Isotopic fractionation equations used to calculate fluid compositions, water rock interaction, and fluid mixing.

**Equation 10.1**

$$\Delta^{13}C_{(calcite - CO2)} = 8.27+(-18.11x10^3 / T)+(8.557x10^6 / T^2) - (8.914x10^8 / T^3)$$

(Ohmoto and Rye, 1979)

**Equation 10.2**

$$\Delta^{18}O_{(calcite - H2O)} = (2.78x10^6 / T^2) - 2.89$$

(Friedman and O'Neil, 1977)

**Equation 10.3**

$$(F / R)X_{H2CO3} = (\delta^{13}C_{cc} - \delta^{13}C^{i}_{hr})/(\Delta^{13}C_{cc-H2CO3} + \delta^{13}C^{i}_{H2CO3} - \delta^{13}C_{cc})$$

(modified after Shelton, 1983, and Sverjensky, 1981)

Where $(F / R)X_{H2CO3}$ = mole ratio of mineralising fluid to host rock at a specified molality of $H_2CO_3$, $\delta^{13}C^{i}_{hr}$ is the initial carbon isotopic composition of the host rock carbonate, $\delta^{13}C_{cc}$ is the isotopic composition of hydrothermal calcite formed by cooling alone of the mineralising fluid, $\delta^{13}C^{i}_{H2CO3}$ is the initial carbon isotopic composition of $H_2CO_{3(aq)}$ in the mineralising fluid and $\Delta^{13}C_{cc-H2CO3}$ is the carbon isotopic fractionation between calcite and aqueous $H_2CO_3$ determined from Equation 10.1.

Table 10.3. cont.....

**Equation 10.4**

$$(F / R) / 3 = (\delta^{18}O_{cc} - \delta^{18}O^{i}_{hr})/(\Delta^{18}O_{cc\text{-}H2O} + \delta^{18}O^{i}_{H2O} - \delta^{18}O_{cc})$$

(modified after Shelton, 1983, and Sverjensky, 1981)

Where F / R = mole ratio of mineralising fluid to host rock, $\delta^{18}O^{i}_{hr}$ is the initial oxygen isotopic compositions of the host rock carbonate, $\delta^{18}O_{cc}$ is the isotopic composition of hydrothermal calcite formed by cooling alone of the mineralising fluid, $\delta^{18}O^{i}_{H2O}$ is the initial oxygen isotopic composition of the mineralising fluid, and $\Delta^{13}C_{cc\text{-}H2O}$ is the oxygen isotopic fractionation between calcite and water determined from Equation 10.2.

**Equation 10.5**

$$(F / R)_{open\ system} = \ln((F / R)_{closed\ system} + 1)$$

(Taylor, 1977)

A closed system is one from which none of the fluid is lost. An open system is one in which the fluid makes a single pass.

**Equation 10.6**

$$\delta^{13}C_{calcite} = (X_a(\delta^{13}C_a + \Delta^{13}C_{(calcite\text{-}CO2)a}) + Y(1-X_a)(\delta^{13}C_b + \Delta^{13}C_{(calcite\text{-}CO2)b}) \quad / (Y + X_a - YX_a)$$

(modified after Zheng and Hoefs, 1993)

Where, $\delta^{13}C_{calcite}$ is the isotopic composition of hydrothermal calcite formed by mixing of fluids A and B, $X_a$ is the mole fraction of fluid A, $\delta^{13}C_a$ and $\delta^{13}C_b$ are the carbon isotopic composition of fluids A and B respectively, $\Delta^{13}C_{(calcite\text{-}CO2)a}$ and $\Delta^{13}C_{(calcite\text{-}CO2)b}$ are the equilibrium fractionation factors between calcite and $CO_2$ for fluids A and B respectively determined using Equation 10.1 and temperatures of 180°C and 140°C respectively, Y is the proportion of carbon in fluid A compared to fluid B.

**Equation 10.7**

$$\delta^{18}O_{calcite} = \delta^{18}O_b + \Delta^{18}O_{(calcite\text{-}H2O)} + X_a(\delta^{18}O_a - \delta^{18}O_b)$$

(modified after Zheng and Hoefs, 1993)

Where, $\delta^{18}O_{calcite}$ is the isotopic composition of hydrothermal calcite formed by mixing of fluids A and B, $X_a$ is the mole fraction of fluid A, $\delta^{18}O_a$ and $\delta^{18}O_b$ are the carbon isotopic composition of fluids A and B respectively, $\Delta^{18}O_{(calcite\text{-}H2O)}$ is the equilibrium fractionation factors between calcite and $H_2O$ determined using Equation 10.2.

**Equation 10.8**

$$\Delta^{13}C_{(calcite\ -\ HCO3^-)} = 0.91 + (0.095 \times 10^6 / T^2)$$

(Deines et al., 1974)

**Equation 10.9**

$$(F / R)\ X_{HCO3^-} = (\delta^{13}C_{cc} - \delta^{13}C^{i}_{hr}) / (\Delta^{13}C_{cc\text{-}HCO3^-} + \delta^{13}C^{i}_{HCO3^-} - \delta^{13}C_{cc})$$

(modified after Shelton, 1983, and Sverjensky, 1981)

Where $(F / R)\ X_{HCO3^-}$ = mole ratio of mineralising fluid to host rock at a specified molality of $HCO_3^-$, $\delta^{13}C^{i}_{hr}$ is the initial carbon isotopic composition of the host rock carbonate, $\delta^{13}C_{cc}$ is the isotopic composition of hydrothermal calcite formed by cooling alone of the mineralising fluid, $\delta^{13}C^{i}_{HCO3^-}$ is the initial carbon isotopic composition of $HCO_{3(aq)}^-$ in the mineralising fluid and $\Delta^{13}C_{cc\text{-}HCO3^-}$ is the carbon isotopic fractionation between calcite and aqueous $HCO_3^-$ determined from Equation 10.8.

In the absence of direct fluid inclusion data for carbonate minerals, the median trapping temperature of 154°C for primary fluid inclusions hosted by sphalerite 2 and quartz 1 (type P2 and P3 fluid inclusions) is used to approximate the formation temperature of hydrothermal carbonates. Justification for using a temperature of 154°C lies in the close paragenetic association between sphalerite 2, quartz 1 and hydrothermal carbonates (Section 5.2.3). This is exclusive of LAO carbonates which formed at higher temperatures (Section 9.6.3).

Estimated formation temperatures of LAO carbonates vary for each sample. Temperatures were estimated from trapping temperatures of fluid inclusions hosted by quartz 3 which has a similar paragenesis to LAO carbonate. Where fluid inclusion data was not avaliable, the temperature was estimated by comparing the mineralogy of associated calc-silicate minerals with the temperature at which they occur in geothermal wells (Henley and Ellis, 1983).

Table 10.4 Range of calculated fluid isotopic values for hydrothermal carbonates. Fluid values are calculated using the fractionation equations of Friedman and O'Neil (1977) and Ohmoto and Rye (1979).

| | Fluid temp. (°C) | $\delta^{18}O$ ‰ (fluid) | $\delta^{13}C$ ‰ (fluid) |
|---|---|---|---|
| Intra-mineralisation carbonates | 154 | 1.81 to -4.61 | -3.21 to -6.90 |
| LAO carbonates | 200 to 282 | 0.13 to -2.36 | 0.39 to -1.47 |

**Interpretation of isotopic values from intra-mineralisation carbonates**

The array of carbon and oxygen isotope values for intra-mineralisation carbonates may have resulted from mixing between mineralising fluids, and other carbon and oxygen reservoirs with different isotopic compositions. Mixing may have occurred over a range of temperatures resulting in variations in the extent of fluid - mineral isotopic fractionation. Potential reservoirs, or modifiers, of carbon and oxygen isotopes include:

- Carbon derived from interaction between the mineralising fluid and graphitic units.
- Decarbonation reactions.
- Variations in the extent of interaction between the mineralising fluid and the host marbles and calc-silicate lithologies.
- Carbon and oxygen contributed through different degrees of mixing between two fluids of different isotopic composition.

This is by no means an exhaustive list of processes which may account for the observed array of isotopic values, and other processes may have been important. In the absence of evidence indicating the existence of other processes, each of the four processes listed above will be considered in turn.

*Graphite as a carbon source*

Graphite separates from graphitic schists at Menninnie Dam were not analysed. Taylor and Berry (1990), analysed carbon isotopes from Hutchison Group graphitic schists and adjacent marbles near the Uley and Koppio graphite mines, approximately 240 km SSW of Menninnie Dam. The units sampled by Taylor and Berry (1990), are interpreted to be stratigraphically similar to graphitic schists at Menninnie Dam. Taylor and Berry (1990), reported $\delta^{13}C_{graphite}$ values of ≈ -25 ‰, a value typical of organically derived carbon (Ohmoto, 1986).

It is conceivable that the range of $\delta^{13}C$ values from hydrothermal carbonates at Menninnie Dam resulted from derivation of isotopically lighter carbon from oxidation and hydration of graphite. However, this is considered unlikely, as graphitic schists at Menninnie Dam are

localised, volumetrically small in the context of the Menninnie Dam host rocks, rarely associated with mineralisation, and there is no evidence to support wide spread or local leaching of graphitic schists by the mineralising fluids.

*Decarbonation reactions*

Talc is interpreted to have formed early in the mineralisation paragenesis through interaction of the mineralising fluids and host dolomitic marbles (Section 5.2.3). Formation of talc probably liberated $CO_2$ into the fluid phase, eg:

$$3CaMg(CO_3)_2 + 4SiO_2 + 4H_2O = Mg_3Si_4O_{10}(OH)_2 + 3CaCO_3 + 3H_2CO_3$$

(3 dolomite + 4 quartz + 4 water = talc + 3 calcite + 3 $H_2CO_2$)

(modified after Turner, 1980)

Decarbonation reactions result in a fluid which is isotopically heavier than the original reactants (Valley, 1986). Decarbonation reactions could have provided a source of heavy carbon and oxygen for the formation of intra-mineralisation carbonates, however, talc occurs in trace amounts and cannot account for the $\delta^{13}C$ and $\delta^{18}O$ values the more voluminous intra-mineralisation carbonates.

*Fluid - rock interaction*

Mineralisation at Menninnie Dam replaces the host marbles and calc-silicate lithologies forming stockwork and vein style mineralisation (Section 5.2.1). Fluid - rock interaction during the replacement process may account for the array of carbon and oxygen isotope values of hydrothermal carbonates. Taylor (1974 , 1977) used isotopic mass balance equations to assess the extent of fluid - rock interaction in both open and closed systems. Kitto (1994) used a similar approach to Taylor (1974, 1977) in combination with cooling curves to assess the extent of fluid - rock interaction at the Renison tin mine in Tasmania. A similar approach is taken in this study (after Kitto, 1994) using Equations 10.3, 10.4 and 10.5 (Table 10.3) and stipulating various mineralising fluid : host rock ratios between 500 : 1 and 1 : 1 for closed systems.

The isotopic composition of the mineralising fluid was calculated as $\delta^{18}0 = -1.98$; $\delta^{13}C = -6.90$ ‰ using Equations 10.1 and 10.2, the isotopically lightest intra-mineralisation carbonate and the median trapping temperature for fluid inclusions hosted by sphalerite 1 and quartz 1 of 154°C. Mineralisation is hosted by marbles, impure marbles and metasomatic marbles which collectively, have a broad range of carbonate carbon and oxygen isotope values.

In order to assess the effect of a range of host rock compositions, two models have been constructed:

- Model 1 uses the median isotopic composition for marble of $\delta^{18}O$ = 19.60 and $\delta^{13}C$ = 0.50 ‰ as representative of the composition of the host rock (Fig. 10.3).
- Model 2 uses the median isotopic composition for metasomatic marble of $\delta^{18}O$ = 15.00 and $\delta^{13}C$ = 0.00 ‰ as representative of the composition of the host rock (Fig. 10.4).

Calcite precipitated from the mineralising fluid at temperatures between 250 - 100°C that did not interact with the host rocks would have isotopic compositions which lie along the calcite - fluid fractionation curve ('hydrothermal calcite' line, Figs. 10.3 and 10.4). Use of the calcite - mineralising fluid fractionation curve assumes that carbon in the mineralising fluid is present as $H_2CO_3$ and species such as $CH_4$ (-4 oxidation state) are absent. The absence of $CH_4$ is interpreted from fluid inclusion observations. Clathrates were observed to have formed in 13 out of 249 fluid inclusions hosted by sphalerite 1 and quartz 1. Eleven of these were interpreted as $CO_2$ clathrate formation with only two attributed to mixed gas systems (Section 9.4). In the absence of unequivocal evidence for the presence of $CH_4$ in fluid inclusions, the variation in $\delta^{13}C$ values of carbonate associated with mineralisation was considered to have resulted from other factors.

Fluid - host rock interaction has been modelled for fluids with a molal concentration of $H_2CO_3$ (X-$H_2CO_3$ in Figs. 10.3 and 10.4) equal to 0.01 and a range of fluid temperatures between 225 - 100°C. Higher $H_2CO_3$ molalities of 0.05 and 0.1 have been modelled for a fluid at 200°C, and the resultant fields encompass many of the hydrothermal carbonates but not all. Figures 10.3 and 10.4 can be interpreted to indicate a $H_2CO_3$ molality of 0.01 is a minimum value and many of the intra-mineralisation carbonates could have resulted from a fluid with a significantly higher molality of $H_2CO_3$.

Figures 10.3 and 10.4 show that the array of carbon and oxygen isotope values of mineralisation carbonates could have resulted from interaction between a fluid composition of $\delta^{18}0$ = -1.98 and $\delta^{13}C$ = -6.90 ‰ at X-$H_2CO_3$ = 0.01, and host rock compositions of $\delta^{18}O$ = 19.60 to 15.00 ‰ and $\delta^{13}C$ = 0.50 to 0.00 ‰ over the temperature range 200 - 125°C. Figures 10.3 and 10.4 also show that fluid - rock ratios were high, and generally > 3 for an open system and > 20 for a closed system (ref. Equation 10.5, Table 10.3).

It is considered significant that the 200 - 125°C temperature range indicated for formation of the intra-mineralisation carbonates from Figures 10.3 and 10.4 is consistent with trapping temperatures for 87% of fluid inclusions hosted by sphalerite 1 and quartz 1 (Sections 9.4.1 and 9.4.2).

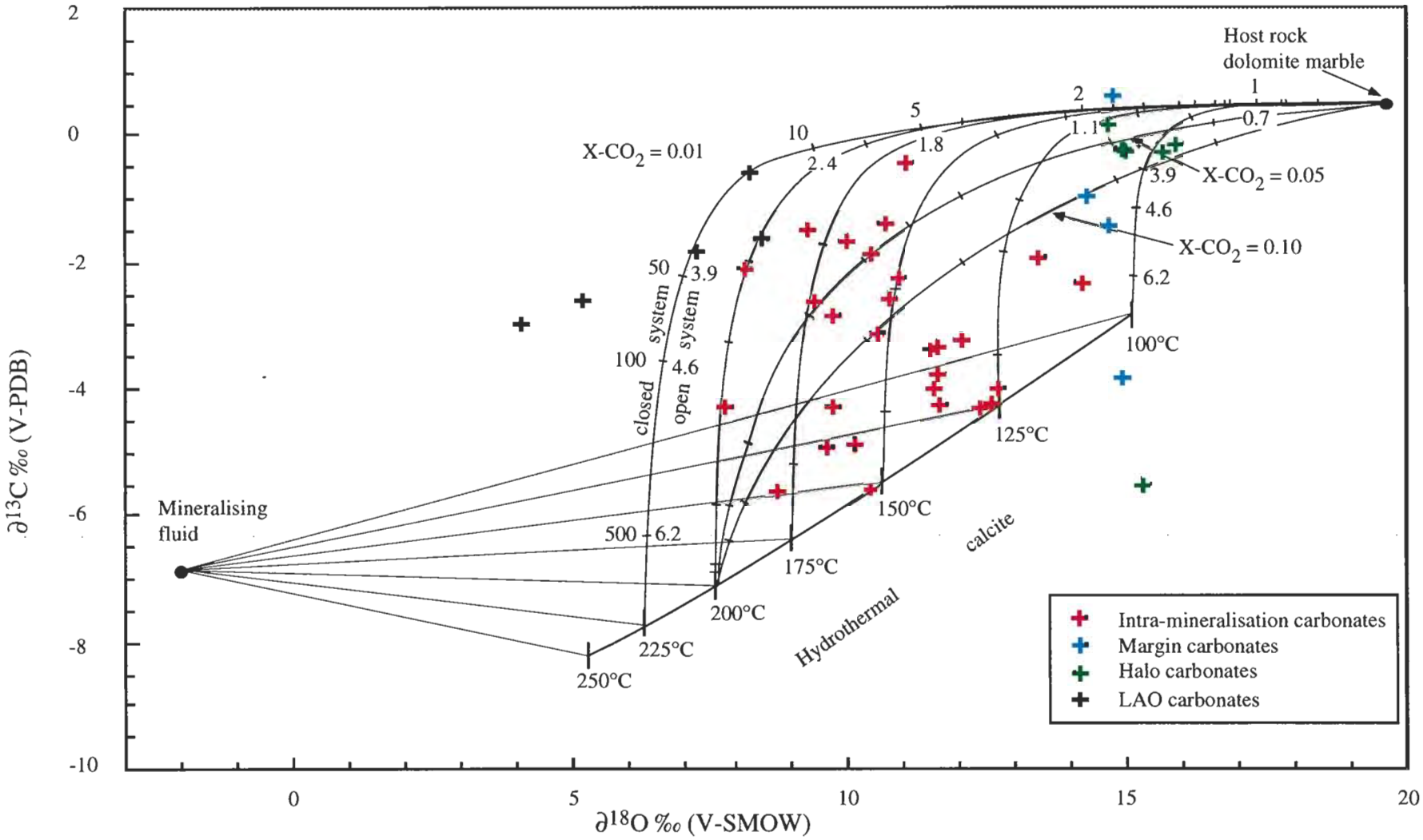


Figure 10.3 $\partial^{13}C_{(V\text{-}PDB)}$ vs $\partial^{18}O_{(V\text{-}SMOW)}$ plot of Menninnie Dam carbonates, assumed composition of the mineralising fluid and host rocks represented by marbles. Also shown is a curve for calcite in equilibrium with the mineralising fluid and isothermal mixing curves for specified X $CO_2$ values with fluid - rock mixing ratios for open and closed systems. Fluid : rock ratios for closed systems are shown on the outside of curves and corresponding values for open systems are shown on the inside of curves (after Kitto, 1994).

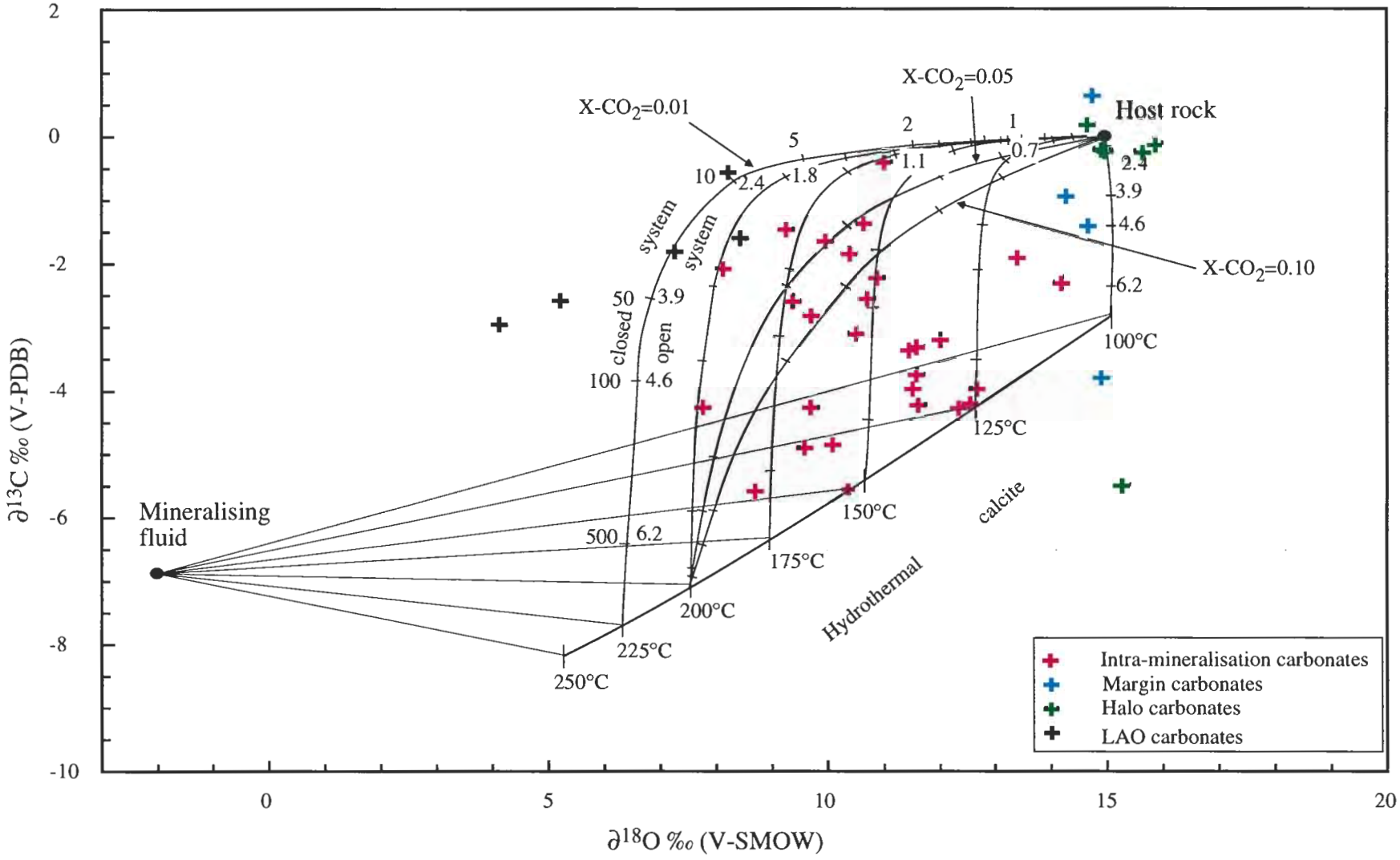


Figure 10.4 $\partial^{13}C$ ‰ (V-PDB) vs $\partial^{18}O$ ‰ (V-SMOW) plot of Menninnie Dam carbonates, assumed composition of the mineralising fluid and host rocks represented by metasomatic marbles. Also shown is a curve for calcite in equilibrium with the mineralising fluid and isothermal mixing curves for specified X $CO_2$ values with fluid - rock mixing ratios for open and closed systems. Fluid : rock ratios for closed systems are shown on the outside of curves and corresponding values for open systems are shown on the inside of curves (after Kitto, 1994).

The isotopic composition of the mineralising fluid used for models can therefore be interpreted to closely approximate the true isotopic composition with little change in the temperature of the fluid between precipitation of sphalerite 1 and precipitation of intra-mineralisation carbonates.

*Mixing of two fluids*

In the previous discussion of fluid rock interaction, it was assumed that only one fluid was involved in the formation of intra-mineralisation carbonates, however, fluid inclusions are interpreted to indicate mixing between a high salinity, low temperature fluid (≈ 140°C and 27 wt.% NaCl equivalent) and a low salinity, higher temperature fluid (≈ 180°C and 0 - 3 wt.% NaCl equivalent). This section will investigate whether the isotopic composition of intra-mineralisation carbonates could have resulted solely from mixing of two fluids, without any host rock interaction.

It can be argued that the two fluids were sourced from meteoric waters and / or magmatic waters. Fluids with isotopic compositions approximated by metamorphic and formational waters can be excluded as mineralisation clearly post dates metamorphism. Proterozoic seawater can be assessed as a fluid source by consideration of the palaeo-geographic setting. Mineralisation, eruption of the GRV, and intrusion of the Hiltaba Suite are interpreted to have been coeval (Section 8.5). The palaeo-geographic setting of the GRV has been established by previous authors and is summarised below.

The Corunna Conglomerate crops out to the south and north-west of the GRV, and was considered to have been of fluvial origin although the fine grained carbonaceous siltstone and sandstone at the top of the sequence was probably deposited in a shallow to moderately restricted marine basin (Lemon, 1972; Lemon and Gostin, 1983). The Tarcoola Formation to the north-west of the GRV was considered to have been a fluvial, to marginal marine, clastic succession (Daly, 1993a) and was interpreted to correlate with the Corunna Conglomerate (Daly, 1993b). The Pandurra Formation, which onlaps the northern GRV was interpreted to have been deposited as a continental, dominantly fluvial sequence (Cowley, 1993) although alluvial fan, aeolian and possibly deltaic environments have been suggested for some units of the formation (Lemon and Gostin, 1983; Lemon, 1972), and a shallow marine environment was interpreted by Curtis (1977) and O'Shea (1982). The Blue Range Beds to the south of the GRV, were considered have been deposited in a braided stream - alluvial fan environment (Flint, 1993a).

The GRV were considered to have been erupted sub-aerially over a landscape of late Archaean - Palaeoproterozoic metamorphic rocks in a mid-cratonic setting (Blissett et al., 1993). The depositional environments of sediments considered to either precede volcanism, or, to have been coincident with volcanism (ie. Tarcoola Formation and the Corunna

Conglomerate; Daly, 1993a, b), and those following volcanism (Blue Range Beds and the Pandurra Formation; Flint, 1993a; Cowley, 1993), are consistent with a continental eruption environment. Based on the above discussion, formational, metamorphic and seawater fluid sources are considered unlikely, therefore, magmatic fluids and meteoric fluids are considered to have been more likely sources for the two fluids associated with mineralisation at Menninnie Dam.

Isotopic compositions of hydrothermal calcite formed by mixing of two fluids with different isotopic compositions and different temperatures was evaluated for calcite in the Pb - Zn deposits in the Harz Mountains of Germany by Zheng and Hoefs (1993) and a similar approach is taken in this study using Equations 10.6 and 10.7 (Table 10.3) and the following assumptions:

- The isotopic composition of 'fluid A' is approximated by meteoric water with a composition of $\delta^{13}C = 0.0$ and $\delta^{18}O = -6.8$. The $\delta^{18}O$ value is derived from a later section (Section 10.3.4.3). Because of the dominance of $H_2O$ over $H_2CO_3$, fluid A is assumed to have interacted with the host marbles at a sufficiently high water rock ratio such that the $\delta^{13}C$ composition was inherited from the host marbles, but the $\delta^{18}O$ composition of the fluid was not significantly modified.
- The isotopic composition of 'fluid B' is approximated by a 'magmatic fluid' with $\delta^{13}C = -6.90$ ‰ and $\delta^{18}O = 6.0$ ‰. The $\delta^{13}C$ ‰ value is identical to that of the mineralising fluid used earlier for modelling of fluid - rock interaction. The $\delta^{18}O$ ‰ value is an average value for juvenile waters derived by Taylor (1979).
- Fluid A equates with the higher temperature, low salinity fluid (≈ 180°C and 0 - 3 wt.% NaCl equivalent), and fluid B equates with the lower temperature higher salinity fluid (≈ 140°C and 27 wt.% NaCl equivalent), interpreted from fluid inclusions (Section 9.6.4).
- Both fluids were in equilibrium with $H_2CO_3$ as the only aqueous carbon bearing species.
- No other processes operated which affected the isotopic composition of hydrothermal calcite.

Mixing between fluids A and B was modelled for mole fractions of fluid A between zero and one, and for variations in the proportion of carbon in fluid A compared to fluid B between 0.01 and 100. Results are illustrated in Figure 10.5.

Based on the results of modelling, it can be concluded that the range of hydrothermal carbonate isotopic compositions did not result from fluid mixing. If fluid mixing had been a significant process, the isotopic composition of hydrothermal carbonates would lie on, or between, mixing lines in illustrated Figure 10.5.

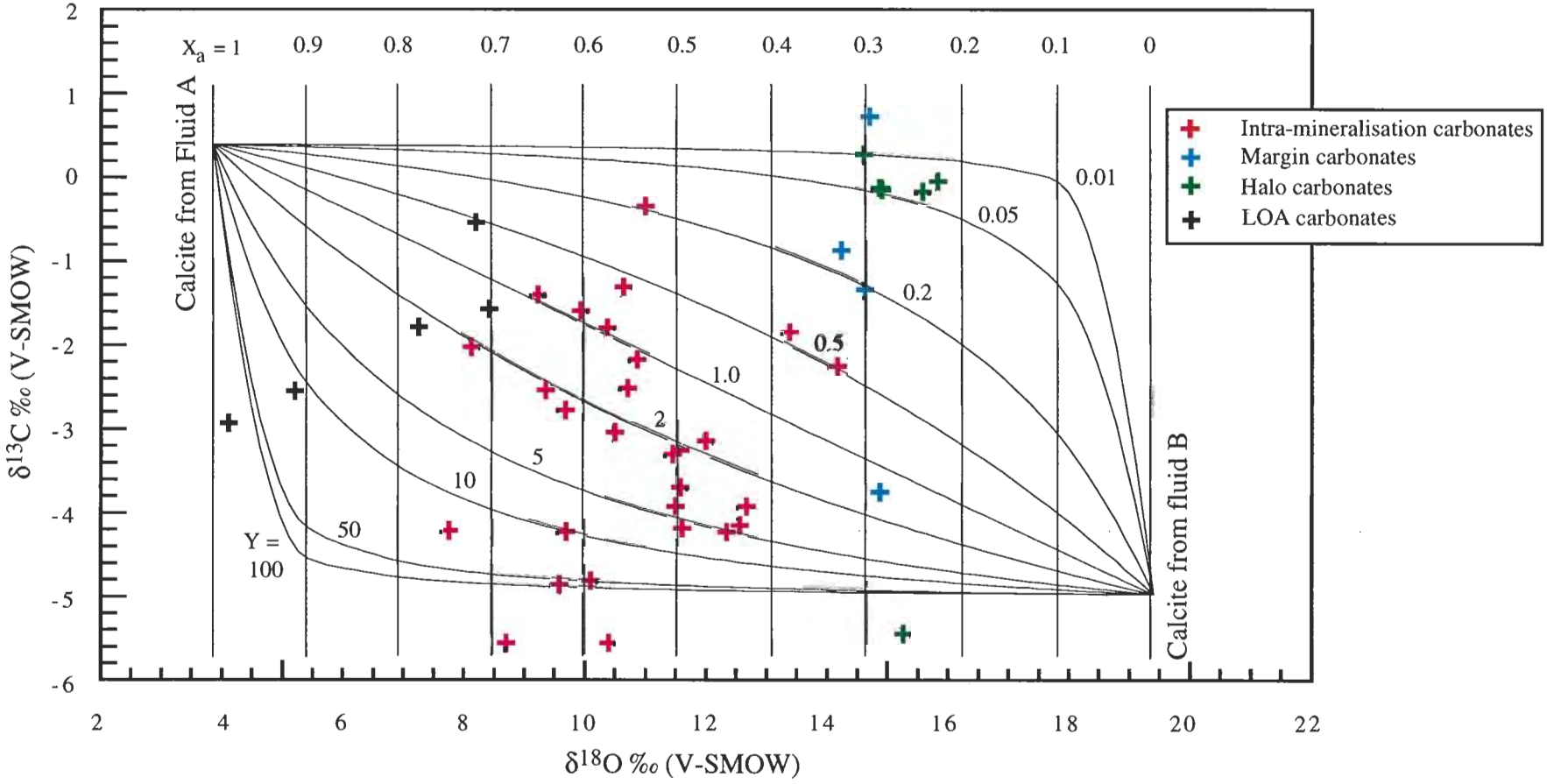


Figure 10.5. $\delta^{13}C$ ‰ (V-PDB) vs $\delta^{18}O$ ‰ (V-SMOW) modelling mixing of two fluids with different isotopic compositions at 154°C. Fluid A has an isotopic composition similar to meteoric waters with $\delta^{13}C$ = 0.00 ‰ and $\delta^{18}O$ = -6.80 ‰. Fluid B has an isotopic composition similar to magmatic fluids with $\delta^{13}C$ = 6.90 ‰ and $\delta^{18}O$ = 6.00 ‰. The lines between the two end member calcites are mixing lines for different proportions of aqueous carbon in fluid A compared to fluid B.

Fluids with isotopic compositions other than those used for modelling could be tested, and would result in changes to the position and shape of mixing curves, however, the scatter in the data for intra-mineralisation carbonates is unlikely to correspond to any fluid mixing line. Throughout the remainder of this chapter, the mixed fluid is approximated by a single fluid and referred to as the 'mineralising fluid'.

**Interpretation of margin carbonate isotopic values**

Margin carbonates have isotopic compositions that lie between those for intra-mineralisation carbonates and the host rocks (marbles, impure marbles, and metasomatic marbles). As margin carbonates were derived from mineralised zones within 1 cm of the host rock contact, their isotopic compositions can be interpreted to have resulted from isotopic mixing with variable mineralising fluid - host rock ratios at temperatures between 125°C and 100°C (Figs. 10.3 and 10.4).

One sample contains carbon which is ≈1 ‰ heavier than the field for calcites produced by cooling and interaction between the mineralising fluid and the host rocks (Figs. 10.3 and 10.4). This may have resulted from interaction of the mineralising fluid with host rock with a slightly heavier $\delta^{13}C$ value than that used for modelling. Another sample contains carbon which is ≈ 1 ‰ lighter than the calculated composition of hydrothermal calcite formed by cooling of the mineralising fluid without host rock interaction. As this sample corresponds to a calculated temperature marginally greater than 100°C, the fluid may have locally been in equilibrium with $HCO_3^-$ formed by either dissociation of $H_2CO_3$ or interaction between an acidic mineralising fluid and the host marbles. At temperatures less than 125°C and pH between ≈ 6.5 and 10, aqueous $HCO_3^-$ is likely to be the dominant aqueous carbon bearing species (Barnes, 1979; Ohmoto, 1986).

The significance of a localised fluid dominated by $HCO_3^-$ at the contact of mineralisation and the host marbles can be evaluated through construction of a cooling curve and modelling of the interaction between the host rocks and the mineralising fluid, similar to that used to construct Figures 10.3 and 10.4. The following parameters were applied:

- Initial fluid composition of $\delta^{18}0 = -1.98$ and $\delta^{13}C = -6.90$ ‰ determined in earlier.
- The host rocks have an isotopic composition of $\delta^{18}0 = 15.00$ and $\delta^{13}C = 0.00$ ‰ which approximates that of the host metasomatic marbles.
- The calcite - $HCO_3^-$ fractionation equation (Equation 10.8; Table 10.3)
- Calculation of F / R ratios for closed systems using Equations 10.4 and 10.9 (Table 10.3) and stipulating various mineralising fluid : host rock ratios between 500 : 1 and 1 : 1 for closed systems.
- Calculation of F / R ratios for open systems using Equation 10.5 (Table 10.3)

Carbon, and oxygen isotopic compositions for margin and halo carbonates are plotted on Figure 10.6. Isotopic values for intra-mineralisation carbonates, and LAO carbonates are also plotted for reference, although the fluid : rock mixing curves do not apply to these samples because of their higher formation temperatures. Calcite precipitated from a fluid in equilibrium with $HCO_3$- at temperatures between 125 - 75°C, which did not interact with the host rocks would have isotopic compositions which lie along the hydrothermal calcite line. The mineralisation margin carbonate with the lightest $\delta^{13}C$ value lies within the field defined for carbonates formed by interaction of the host rocks and an evolved mineralising fluid in equilibrium with $HCO_3^-$. It is concluded that the isotopic composition of at least this sample, and possibly others at the mineralisation - host rock contact, may have resulted from fluids with $HCO_3^-$ as the dominant aqueous carbon bearing species. The local predominance of $HCO_3^-{}_{(aq)}$ over $H_2CO_{3(aq)}$ is interpreted to have occurred where an acidic mineralising fluid approached neutral to alkaline conditions through interaction with the host rock marble at temperatures < 125°C (Barnes, 1979). This interpretation is based on a single data point which may simply have resulted from a combination of analytical scatter, the various assumptions used by previous authors in calculating isotopic fractionation, and the numerous assumptions used in this study. Therefore, the above interpretation should be considered with due regard.

**Isotopic halos to mineralisation**

Halo carbonates were sampled with the aim of establishing the extent to which the mineralising fluids penetrated the host marbles. In Section 5.2.1 it was suggested that the contact between mineralisation and the host rocks was sharp, or, transitional over a few centimetres at most.

Halo carbonate analyses can be subdivided into two groups:

- A group of 6 analyses sampled between 5 and 26 cm away from the mineralisation contact. Analyses plot as a cluster of values near the centre of the field for metasomatic carbonate ($\delta^{13}C \approx 0.00‰$ and $\delta^{18}O \approx 15.00$ ‰).
- A single analysis of a sample collected 1 cm from the margin of mineralisation from a thin band (0.5 - 2 cm wide) of fine grained spongy textured carbonate formed between mineralisation and the host rock. This sample contains significantly lighter carbon ($\delta^{13}C = -5.46$ ‰) than the first group.

The isotopic composition of the sample collected 1 cm away from the mineralisation contact plots well below the 'hydrothermal calcite' line on Figures 10.3 and 10.4 but almost on the hydrothermal calcite line in Figure 10.6. This sample may have formed from a low temperature fluid (≈ 100°C), in which $HCO_3^-$ was the dominant carbon species, and at high fluid : rock ratios.

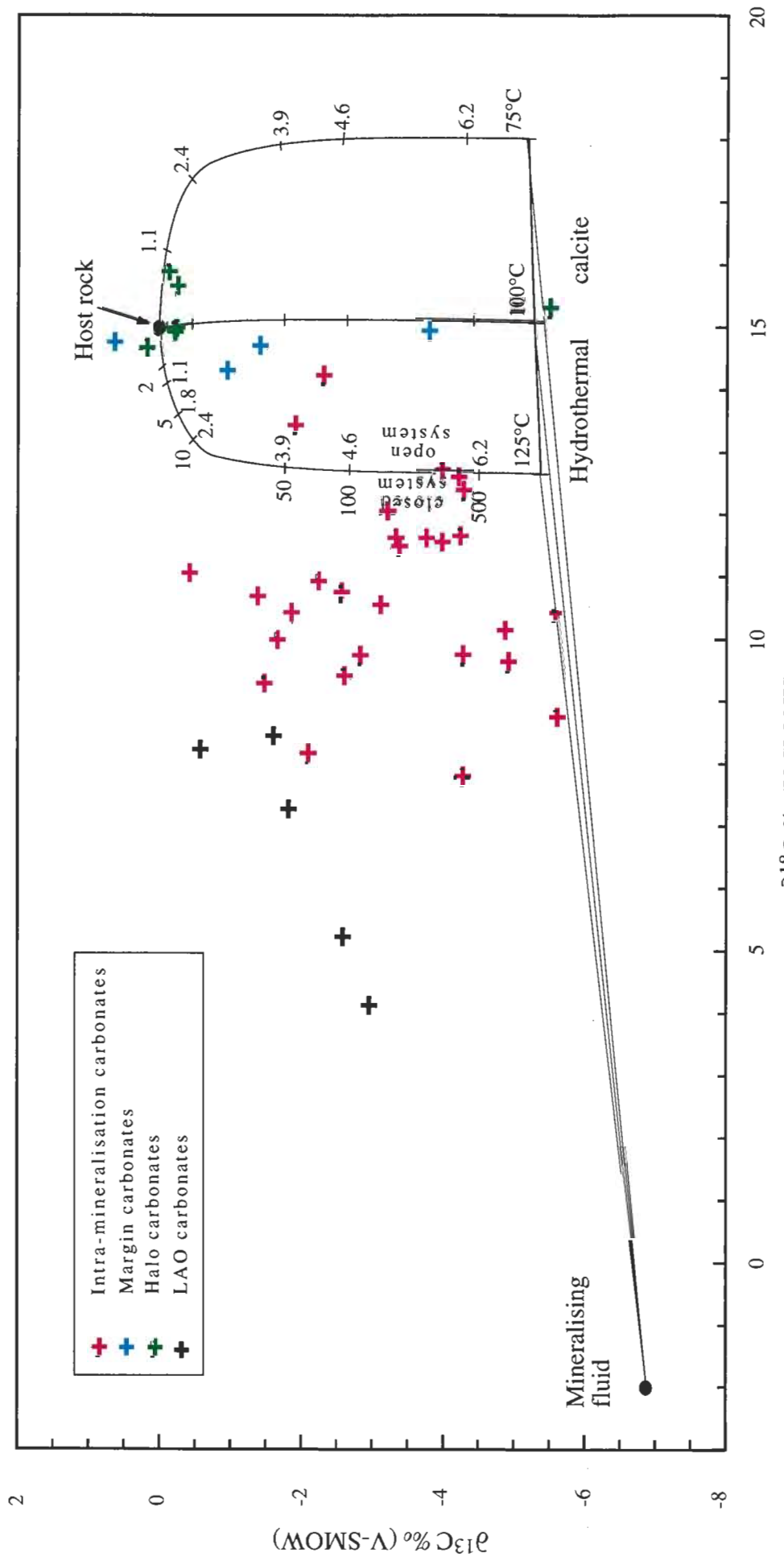


Figure 10.6 $\partial^{13}C$ ‰ (V-PDB) vs $\partial^{18}O$ ‰ (V-SMOW) plot of Menninnie Dam carbonates, associated with mineralisation, the assumed composition of the mineralising fluid and host rocks (metasomatic marbles). Also shown is a curve for hydrothermal calcite in equilibrium with an $HCO_3^-$ dominated fluid, isothermal mixing curves for an X-$CO_2$ value of 0.01, and fluid - rock mixing ratios for open and closed systems. A fluid in equilibrium with $HCO_3^-$ may have locally existed at low temperatures (< 125°C) near the mineralisation - host rock contact.

This second sample interpreted to have formed from a $HCO_3^-$ dominated fluid at the mineralisation - host rock contact adds a little more credibility to the interpretation, although, both isotopic compositions may have resulted from analytical scatter, or, the result of entirely different processes.

Host rock calcite, only 5 cm away from mineralisation, has an isotopic composition similar to that of metasomatic marble, and is interpreted to indicate that the mineralising fluid did not penetrate more than a few centimetres into the host marbles. This interpretation is consistent with the mineralogy and textures of unaltered host marble only centimetres away from mineralisation (Section 5.2.3). The presence of a narrow geochemical and mineralogical alteration halo surrounding mineralisation is interpreted to have resulted from the low permeability of the host rocks and further emphasises the importance of structurally generated fluid pathways (Section 5.6.3).

**Late alteration overprint carbonate**

The late alteration overprint (LAO) post-dates the mineralising event at Menninnie Dam (Section 5.3). The isotopic composition of the LAO fluid has been calculated as $\delta^{18}O$ = -1.12 and $\delta^{13}C$ = -1.39 using the LAO carbonate sample with the heaviest $\delta^{18}O$ composition, a temperature of 200°C derived from fluid inclusions hosted by quartz 3 intergrown with LAO carbonate, and Equations 10.1 and 10.2 (Table 10.3). Interaction between the mineralising fluid and the host rocks was modelled assuming a fluid in which $H_2CO_3$ was the only carbon bearing species, a host rock composition of $\delta^{18}O$ = 19.60 and $\delta^{13}C$ = 0.50 ‰, and Equations 10.3 - 10.5 (Table 10.3). Results are illustrated in Figure 10.7. The assumption that $H_2CO_3$ was the dominant aqueous carbon species is based on the high trapping temperature of fluid inclusions and the absence of gas clathrates in fluid inclusions. This assumption may not be entirely correct on a local scale as trace amounts of graphite were observed in a single thin section and interpreted to have formed early in the mineral paragenesis of the LAO.

LAO carbonates plot close to the calculated hydrothermal calcite line interpreted to indicate a high fluid : host rock ratio of ≈ 6 : 1 (open system). Deviation of > 1 ‰ from this trend for one sample may have resulted from scatter in the data caused by the compounded effect of analytical errors and errors associated with the various assumptions used in this study and those associated with calculation of isotopic fractionation. Estimation of such errors are beyond the scope of this study.

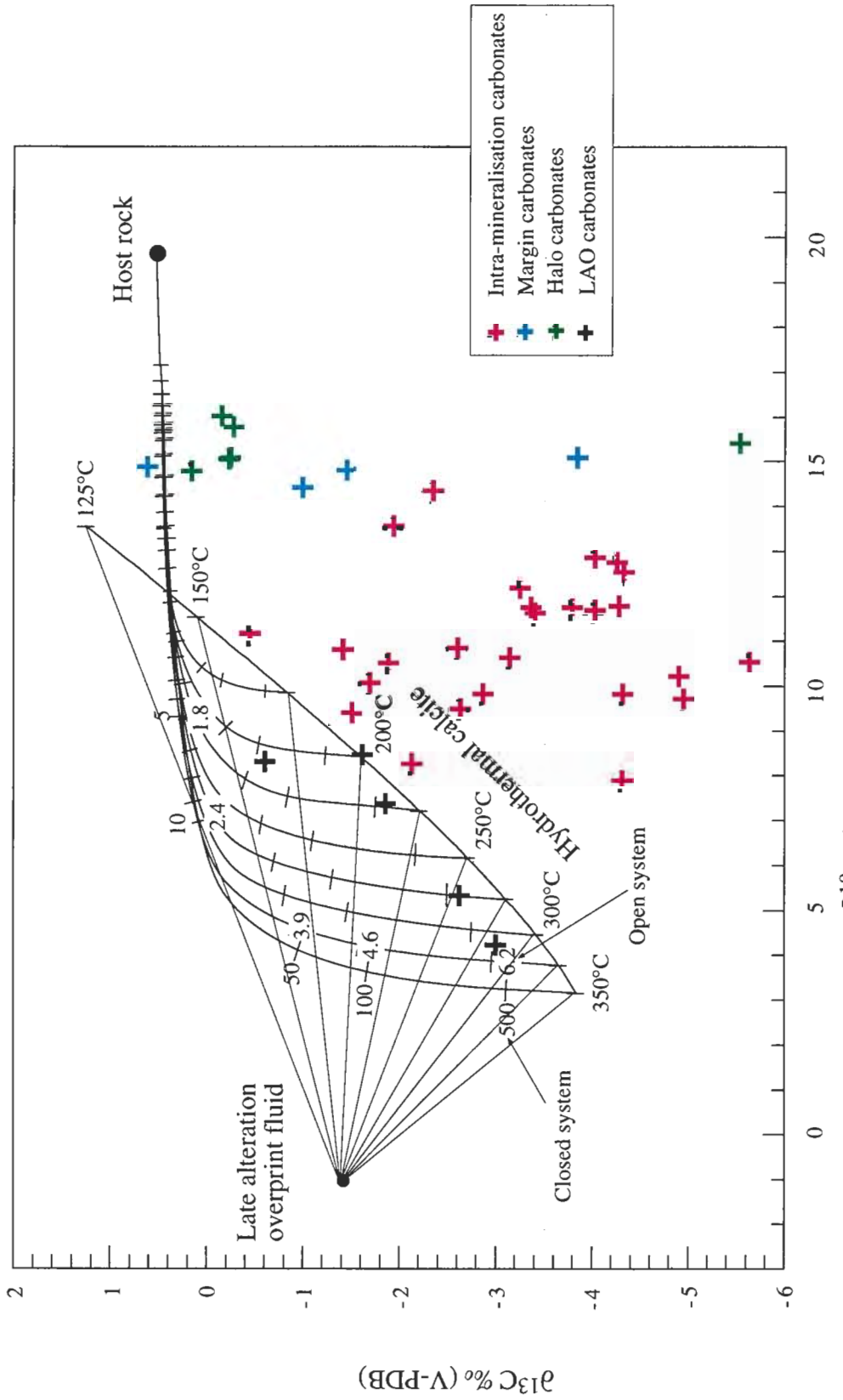


Figure 10.7 $\partial^{13}C$ ‰ (V-PDB) vs $\partial^{18}O$ ‰ (V-SMOW) diagram of Menninnie Dam carbonates, interpreted composition of the fluid which gave rise to the late alteration overprint, and host rocks (metasomatic marbles). Also shown is a curve for calcite in equilibrium with $H_2CO_3$ in the late alteration overprint fluid, isothermal mixing curves for an X-$CO_2$ value of 0.01, and fluid - rock mixing ratios for open and closed systems.

### 10.2.5 Summary

The following points are concluded from carbonate oxygen and carbon isotopes from Menninnie Dam:

- The host marbles that are devoid of calc-silicate minerals and haven't been metasomatised have carbon and oxygen isotope values of $\delta^{18}O$ = 15.52‰ to 21.09‰ and $\delta^{13}C$ = -1.08‰ to 1.63‰ which are similar to those of recent marine carbonates. Impure marbles that contain calc-silicate minerals are shifted to lighter $\delta^{13}C$ and $\delta^{18}O$ compositions through loss of heavy carbon during metamorphic decarbonation reactions or proximity to fluid channel ways. Metasomatic marbles are isotopically lighter than other marbles ($\delta^{18}O$ = 7.77‰ to 18.01‰ and $\delta^{13}C$ = -1.80‰ to 0.68‰), interpreted to have resulted from loss of heavy isotopes through decarbonation reactions either prior to or during metasomatism, or through interaction with metasomatic fluids.

- Carbonates associated with mineralisation (Intra-mineralisation carbonates) have isotopic compositions between $\delta^{18}O$ = 8.68‰ to 12.54 ‰ and $\delta^{13}C$ = -0.38‰ to -5.56‰ which are lighter than the host marbles. Carbon and oxygen produced by decarbonation reactions, and carbon derived from hydration of metamorphic graphite are not considered to have significantly contributed to the isotopic composition of intra-mineralisation carbonates. Mixing of two fluids is interpreted from fluid inclusion studies, but mixing alone did not result in the range of isotopic compositions for intra-mineralisation carbonates. The range in isotopic compositions is interpreted to have resulted from the predominant effects of interaction between the mixed fluids ('mineralising fluid') and the host marbles over a range of temperatures.

- Carbonates formed during the mineralising event and within 1 cm of the host rock contact ('margin carbonates') are interpreted to have formed at lower temperatures than intra-mineralisation carbonates and may have locally been in equilibrium with $HCO_3$-.

- The isotopic composition of host rock carbonate adjacent to mineralisation ('halo carbonates'), are interpreted to indicate that the mineralising fluid did not penetrate more than a few centimetres into the host marbles. This is consistent with mineralogical and textural observations detailed in Section 5.2.3 and emphasises the importance of faults in provision of permeable fluid pathways.

- The isotopic composition of carbonate formed during the LAO is interpreted to have resulted from interaction between the host rocks and a fluid with an isotopic composition of $\delta^{18}O$ = -1.12‰ and $\delta^{13}C$ = -1.39‰. The source of the mineralising fluid and late alteration overprint fluid is be investigated in the following section using oxygen and D/H isotopes from silicate minerals.

## 10.3 Silicate oxygen and hydrogen - deuterium isotopes

The aim of this section is to determine the source of each of the two fluids which collectively comprised the mineralising fluid, and the fluid which gave rise to the late alteration overprint. Deuterium - hydrogen (D / H), and oxygen isotope fluid values, were calculated from analyses of hydrothermal silicate minerals formed during mineralisation, and the late alteration overprint. The fluid isotopic values were then compared to established isotopic fields for waters from various sources, to infer fluid sources.

Application of D / H and oxygen isotope studies of hydrous minerals to obtain information about ancient fluids is subject to the caveat that no isotopic exchange has taken place between the time when the mineral was formed, and the time when it was analysed (ie. closed system). The Menninnie Dam mineralisation has not been subjected to alteration and deformation since formation, however, whether the minerals remained as closed systems since the Middle-Proterozoic is uncertain as the rate of D / H isotopic exchange between ground waters and hydrous phyllosilicate minerals is not well known. Existing data on exchange rates was summarised by Savin and Lee (1988).

### 10.3.1 Samples

Eleven silicate minerals were analysed for either D / H and oxygen, or, oxygen isotopes only. This small number of samples is due the paucity of suitable material, and the high cost of analyses. Where possible, monomineralic samples of hydrous phyllosilicate minerals analysed for both D / H and oxygen.

Samples have been subdivided into three groups which relate to the nature of the samples and their paragenesis (Table 10.5):

Group A) Samples of talc, phlogopite and sericite 1 associated with the early pyrite, and sphalerite galena stages of mineralisation in the northern and central zones (Section 5.2.3). The sericite sample was obtained from a 1 - 2 cm wide alteration halo surrounding marble hosted mineralisation.

Group B) Samples of chlorite 3 and quartz 3 associated with the late alteration overprint (Section 5.3.2).

Group C) Whole rock and quartz phenocryst separates of the weakly altered and strongly altered rhyolite intrusions used for U-Pb zircon dating (Section 8.3).

### 10.3.2 Methods

In order to obtain meaningful analytical results from group A and B samples, monomineralic samples of hydrous phyllosilicates were required. Phyllosilicate minerals were manually extracted from drill core with a stainless steel needle. The resultant chips (< 1.0 mm diameter) were scanned under 20x magnification and those which appeared to be monomineralic were separated and crushed to a powder with an agate mortar and pestle.

In most cases, the resultant powder totalled less than 200 mg. Powders were analysed by X-ray diffraction analysis (XRD).

Table 10.5 Samples used for D / H and oxygen isotope determinations.

| Group | Sample Number | Drill hole | Down hole depth (m) | Mineral |
|---|---|---|---|---|
| A | MR147 | PD0011 | 195.5 | talc |
| A | MR148 | PD0016 | 273 | sericite 1 |
| A | MR149 | PD0008 | 117 | phlogopite |
| B | MR144 | PD0032 | 245 | chlorite 3 |
| B | MR145 | PD0032 | 380 | chlorite 3 |
| B | MR146 | PD0032 | 170 | chlorite 3 |
| B | MR150 | PD0032 | 170 | quartz 3 |
| C | MR138 | PD0030* | 403 | quartz |
| C | MR139 | PD0030* | 403 | whole rock |
| C | MR140 | PD0030** | 471 | quartz |
| C | MR141 | PD0030** | 471 | whole rock |

*Strongly altered rhyolite intrusion
**Weakly altered rhyolite intrusion

Group C samples were jaw crushed and split in a riffle box into two equal portions. One portion was ground in a ring mill and the powder used for whole rock oxygen isotope analysis. The second portion was sieved to obtain a 1 - 0.5 mm fraction from which fragments of quartz phenocrysts were manually separated under 20x magnification to obtain ≈ 150 mg of quartz. The quartz separate was then washed in an ultrasonic cleaner for 30 minutes, rinsed with distilled water and dried prior to oxygen isotope analysis.

*XRD analyses*

Because of their small size, samples of groups A, B and C powders were mixed with a small amount of acetone and vigorously agitated to form a suspension. The suspension was placed on a standard aluminium XRD disk and the acetone allowed to evaporate. The rapid, turbulent, evaporation of acetone results in particles with a random orientation (Paterson et al., 1986) comparable to that achieved using the standard pressed powder technique (Brindley and Brown, 1980).

All samples were irradiated with copper K-alpha radiation at 39 kVA and 30 mA using a Phillips PW1729 X-ray generator operated in fully automated mode, at the Tasmania Department of Mines. The signal was filtered using a graphite monochronometer and input into a Phillips PW1710 diffractometer control unit coupled to a computer. Diffraction peaks were automatically matched with those of known minerals using software developed by the CSIRO. X-ray diffractograms are presented in Appendix 10.2.

Interpretation of X-ray diffractograms for group A and B samples indicate a single, hydrous, phyllosilicate mineral, minor carbonate, and in two samples, minor quartz. As carbonate and quartz are anhydrous minerals, they have no affect on the D / H isotopic determination of hydrous phyllosilicates, but contribute to the oxygen isotope determination and must either be removed, or their effect quantified.

Carbonate contamination was removed by chemical means using the sodium acetate pre-treatment technique of Jackson (1969). Brewster (1980) examined the effect of chemical pre-treatments on the XRD pattern of clays in a pedon and concluded that the sodium acetate pre-treatment technique (Jackson , 1969) had little affect on the XRD pattern of illite or chlorite. Huon et al. (1994) used the much harsher technique of 2N HCl under pH control at 4°C for separating carbonate from potassium white mica prior to using the pre-treated samples for oxygen, and D / H isotope analyses. Huon et al. (1994) demonstrated the mica was not unduly damaged by this technique and no isotopic exchange took place between $OH^-$ groups in hydrous minerals and the solvents. It can be concluded that the relatively mild sodium acetate pre-treatment technique (Jackson, 1969) is unlikely to affect the chemistry, structure, or isotopic composition of hydroxyl groups in phyllosilicates.

Two samples contained minor quartz contamination (samples MR149 and MR146). Quartz cannot be physically or chemically removed without damage to phyllosilicates. Samples MR149 and MR146 were only analysed for D / H isotopes and the fluid oxygen isotope compositions were calculated from analysis of intra-mineralisation carbonate from the same sample, and from quartz 3 (sample MR150) respectively.

Silicate oxygen isotope analyses were carried out at the Silicate Oxygen Isotope Laboratory, University of Tasmania by Dr. G. Kuipers. Samples were heated to 190°C under high vacuum for 24 hours prior to analysis to expel any loosely bound water which may have undergone isotopic exchange since mineral formation. Samples were then reacted with $BrF_5$ at 520°C in evacuated nickel reaction vessels using the technique of Clayton and Mayeda (1963). The oxygen gas liberated by this process was converted to $CO_2$ by reaction with heated graphite and analysed using a VG-Micromass 602D mass spectrometer in the Central Science Laboratory, University of Tasmania. D / H isotope analyses were carried out at the CSIRO Division of Petroleum Resources, NSW by Dr. Anita Andrew (Principal Research Scientist).

### 10.3.3 Results

Results of D / H and oxygen isotope analyses are presented in Table 10.6. D / H analyses of chlorite, sericite, talc and phlogopite associated with mineralisation (group A) and chlorite associate with the LAO (group B) have a small range of values between -85 to -72‰. Oxygen isotopes from group A minerals are heavier than those of group B minerals. Whole rock analyses of strongly altered and weakly altered rhyolite intrusions have $\delta^{18}O$ compositions of 7.2 and 9.9 respectively. Quartz phenocrysts from the strongly altered and weakly altered rhyolite intrusions have near identical $\delta^{18}O$ compositions of 9.1 and 9.4 respectively.

Table 10.6 Results of D/H and oxygen isotope determinations. Analytical error for oxygen is ± 0.20 ‰ (2 sigma). Analytical error for D / H is ± 1.0 ‰ (2 sigma).

| Group | Sample Number | Mineral | δD min (SMOW) | $\delta^{18}O$ min (SMOW) |
|---|---|---|---|---|
| A | MR147 | talc | -85 | +7.9 |
| A | MR148 | sericite 1 | -74 | +11.7 |
| A | MR149 | phlogopite | -74 | |
| B | MR144 | chlorite 3 | -74 | +1.3 |
| B | MR145 | chlorite 3 | -72 | -0.7 |
| B | MR146 | chlorite 3 | -74 | |
| B | MR150 | quartz 3 | | +8.2 |
| C | MR138 | quartz | | +9.1 |
| C | MR139 | whole rock | | +7.2 |
| C | MR140 | quartz | | +9.4 |
| C | MR141 | whole rock | | +9.9 |

### 10.3.4 Discussion

*Low temperature hydrothermal origin of phyllosilicate minerals*

Talc is commonly associated with either metamorphic rocks or alteration of basic rocks such as gabbros (Deer et al., 1978), or formed in a variety of hydrothermal environments at temperatures around 250 -350°C (Evans and Guggenheim, 1988). Talc has also been produced experimentally from Si - Mg gels at temperatures as low as 170°C (Mondesir, 1987; Decarreau et al., 1988) and reported to have formed diagenetically at temperatures of < 100°C from alteration of kerolite (Noack et al., 1989).

Phlogopite is commonly associated with ultrabasic rocks and metamorphosed impure limestones (Deer et al., 1978). However, hydrothermal phlogopite has been reported from the Latera geothermal field at temperatures above 200°C (Cavarretta et al., 1985) and at temperatures of 178°C from a hydrothermal well in the Sabatini volcanic district (Belkin et al., 1988).

The low formation temperatures of approximately 170 - 180°C described for talc and phlogopite (Mondesir, 1987; Decarreau et al., 1988; Belkin et al., 1988), are consistent with their occurrence at Menninnie Dam and formation from low temperature hydrothermal processes interpreted from fluid inclusions (median fluid inclusion trapping temperature of 154°C; range 104 - 227°C, Section 9.6.3). The XRD pattern for sericite (sample MR148) shows the presence of the 1M mica polymorph (Appendix 10.2). Velde (1965) demonstrated that the 1M or $1M_d$ polymorphs of muscovite are probably metastable phases that crystallise at lower temperatures than the $2M_1$ polymorph. The presence of the 1M muscovite polymorph is consistent with a low temperature hydrothermal origin rather than metamorphic formation.

#### 10.3.4.1 Calculation of fluid isotopic values.

*Sericite*

Oxygen isotopic fractionation between muscovite and water has been investigated at high temperatures (> 400°C) by O'Neil and Taylor (1967), Bottinga and Javoy (1973) and

Suzuoki and Epstein (1976). In the absence of low temperature data, sericite - water isotopic fractionation is calculated on the basis of bond types using the algorithm of Zheng (1993). The sericite-bearing sample (sample MR148) was collected from a 1 - 2 cm wide alteration halo between mineralisation and unaltered marble. Carbonate from a similar location (halo carbonate) was interpreted to have formed at lower temperatures than the mineralisation (Section 10.2.4.2) and a temperature of ≈ 100°C is interpreted from Figure 10.6. Using a fluid temperature of 100°C, the isotopic composition of the fluid that was in equilibrium with sericite is calculated as $\delta^{18}O = 0.04$ ‰.

D / H fractionation between muscovite and water over the temperature range of 800 - 400°C has been investigated experimentally by Suzuoki and Epstein (1976). For temperatures in the range 450 - 800°C the equilibrium fractionation factor vs $1 / T^2$ fits a straight line, however, at temperatures of ≤ 400°C the fraction factor deviates from a straight line and changes less with temperature. In a study of hydrogen isotopes from clay minerals in the Ohnuma Geothermal area, Murumo et al. (1980) found that sericite - water fractionation was not temperature dependant over the temperature range 130 - 250°C and had a near constant value of -23 to -27 ‰. The absence of temperature dependence for temperatures below 300°C was supported by Shimazaki and Kusakabe (1990) and Sheppard and Gilg, (1996). From the above argument, a sericite-water fractionation factor of -26 ‰ is considered appropriate for group A sericite from Menninnie Dam. Calculated $\delta^{18}O$ and D / H fluid values for sericite are presented in Table 10.7.

*Phlogopite*

Suzuoki and Epstein (1976) investigated the hydrogen isotope fractionation between phlogopite and water over the temperature range of 650 - 575°C. As for sericite, the fractionation factor was postulated to change less at lower temperatures. Phlogopite - water fractionation has not been investigated experimentally below 575°C. In the absence of low temperature data, the sericite - water fractionation value of -26 ‰ is used as a best guess.

Phlogopite oxygen isotopes ratios were not analysed due to the presence of minor amounts of quartz in the sample. A fluid isotope composition of $\delta^{18}O = -1.98$ ‰ was calculated from the intra-mineralisation carbonate from the same sample. Calculated $\delta^{18}O$ and D / H fluid values for phlogopite are presented in Table 10.7.

*Talc*

Experimental calibration of oxygen isotope fractionation between talc and water has not been published. Isotopic fractionation calculated on the basis of bond types is presented by Savin and Lee (1988) and by Zheng (1993). The algorithm of Zheng (1993) was used in this study.

Data for D / H talc - water fractionation has not been published and as a best guess, the low temperature data for serpentine was used. Wenner and Taylor (1973) developed a serpentine - water fractionation curve over the temperature range ≈ 25 - 235°C based on the isotopic composition of naturally occurring samples. Their curve shows more *negative* fractionation values with decreasing temperature. Suzuoki and Epstein (1976) reported a single serpentine - water fractionation value obtained at 400°C which lies close to the curve of Wenner and Taylor (1973). Sakai and Tsutsumi (1978) compared experimental data for D / H fractionation between serpentine and water over the range 100-500°C and 2 kbars. Their data agrees with the single point obtained by Suzuoki and Epstein (1976) but has a trend towards *positive* fractionation values with decreasing temperature which is opposite to that obtained by Wenner and Taylor (1973). Ikin and Harmon (1981) considered the partial exchange data of Sakai and Tsutsumi (1978) to be unreliable at temperatures of less than 400°C and preferred the fractionation curve of Wenner and Taylor (1973). Using the serpentine-water fractionation curve developed by Wenner and Taylor (1973) as a substitute for talc fractionation, a talc - water fractionation of ≈ -42 ‰ is obtained at 154°C. Calculated $\delta^{18}O$ and D / H fluid values for talc are presented in Table 10.7.

*Chlorite*

Oxygen isotope fractionation between chlorite and water has been investigated experimentally by Cole (1985) and empirically by Wenner and Taylor (1971). Savin and Lee (1988) and Zheng (1993) calculated the isotopic fractionation on the basis of bond types. The fractionation algorithm of Zheng (1993) was used in this study.

Investigation of D / H fractionation between chlorite - water has received more attention than the previous minerals (eg. Marumo et al., 1980; Heaton and Sheppard, 1977; Kuroda et al., 1976; Graham et al., 1987). Savin and Lee (1988) summarised previous fractionation data and proposed a best fit curve. Fluid inclusions hosted by quartz 3 from the same samples as those used for chlorite D / H isotope have trapping temperatures in the range 200°C - 282°C. Using the curve proposed by Savin and Lee (1988), D / H chlorite - water fractionation over the temperature range 200 - 282°C is approximately -34 to -37 ‰. Calculated $\delta^{18}O$ and D / H fluid values for chlorite are presented in Table 10.7.

Table 10.7. Calculated fluid isotopic compositions for group A and B minerals.

| Group | Sample Number | Mineral | Fluid temp °C | δD fluid (SMOW) | $\delta^{18}O$ fluid (SMOW) | Reference |
|---|---|---|---|---|---|---|
| A | MR147 | talc | 154 | -43 | -0.78 | 1, 3 |
| A | MR148 | sericite 1 | 100 | -48 | +0.04 | 1, 4 |
| A | MR149 | phlogopite | 154 | -48 | *-1.98* * | 1 |
| B | MR144 | chlorite 3 | 282 | -38 | 0.81 | 1, 5 |
| B | MR145 | chlorite 3 | 205 | -38 | -3.30 | 1, 5 |
| B | MR146 | chlorite 3 | 200 | -40 | | 5 |
| B | MR150 | quartz 3 | 200 | | -3.41 | 2 |

*Fluid $\delta^{18}O$ value for phlogopite calculated from group 1 carbonate from the same sample.
References: 1) Zheng, 1993 2) Matsuhisa et al., 1979 3) Wenner and Taylor, 1973
4) Murumo et al., 1980 5) Savin and Lee, 1988.

*Rhyolite intrusions*

Rhyolite intrusions at Menninnie Dam have previously been subdivided into strongly altered ('SA rhyolite intrusion') and weakly altered ('WA rhyolite intrusion'; Section 4.3.1). Both WA and SA rhyolite intrusions have a similar quartz phenocryst content of 15% (Section 4.3.1). SA rhyolite intrusions were interpreted to have been altered by the mineralising fluid during the latter stages of sulphide deposition (Section 9.6.6). Quartz phenocrysts in the SA rhyolite intrusion contain abundant secondary fluid inclusions which are interpreted to have formed during the mineralising event. The average temperature of the fluid that resulted in alteration of the rhyolite intrusion is estimated to have been ≈ 154 °C (Section 9.6.4).

Quartz phenocrysts are more resistant to isotopic exchange during hydrothermal processes than feldspars, and oxygen isotopes are commonly little modified from their original igneous values (Beaty, 1990). The $\delta^{18}O$ values for quartz phenocrysts in the SA and WA rhyolite intrusions are similar, and the difference of 0.30 ‰ is within the range of analytical error (analytical error is ± 0.20 ‰; 2 sigma level) and quartz phenocrysts from both the SA and WA rhyolite intrusions are interpreted to be isotopically identical.

Whole rock XRD analysis of the SA rhyolite intrusion show sericite is the major phyllosilicate with minor chlorite (Appendix 10.2). If sericite is assumed to be the only alteration mineral, and $\delta^{18}O$ of the quartz phenocrysts is assumed to be 9.40 ‰, then, sericite has a $\delta^{18}O$ value of 6.81 ‰.

ie; $^{18}O_{whole\ rock} = 15\%\ ^{18}O_{quartz} + 85\%\ ^{18}O_{sericite}$

where $^{18}O_{quartz} = 9.40$ ‰ and $^{18}O_{whole\ rock} = 7.2$ ‰

Using the equation of Zheng (1993) for $\delta^{18}O$ muscovite - fluid fractionation at 154°C, a value of $\delta^{18}O$ = -0.10 ‰ is calculated for the fluid that resulted in alteration of the SA rhyolite intrusion.

### 10.3.4.2 Source of the mineralising fluids

In this section, the source of the two fluids that mixed to form the 'mineralising fluid', and the source of the late alteration overprint fluid, are interpreted from the results of carbon, oxygen and D / H isotope analysis. Fluid isotopic compositions are compared to established D / H and oxygen isotope fields for waters from various sources.

Fluid inclusion studies (Section 9.6.4) indicate mixing between a high salinity, low temperature fluid (≈ 140°C and 25 wt.% NaCl equivalent) and a lower salinity, higher temperature fluid (≈ 180°C and 0 - 3 wt.% NaCl equivalent). The carbon and oxygen isotopic composition of intra-mineralisation carbonates are interpreted to have resulted from mixing of two fluids, and interaction between the resultant mixed fluids and the host

marbles. Therefore, three reservoirs are interpreted to have contributed to the oxygen and carbon isotope signature of intra-mineralisation carbonates (2 fluids and the host marbles). Hydrous phyllosilicates would also have derived oxygen from the three reservoirs, whereas D / H would have been derived from only two reservoirs.

The calculated D / H and oxygen isotopic composition of the mineralising fluid is summarised in Figure 10.8. This Figure also includes:

- The range of $\delta^{18}O$ ‰ fluid values calculated for intra-mineralisation carbonates.
- The estimated $\delta^{18}O$ fluid value used for modelling of fluid - host rock interaction.
- The range of $\delta^{18}O$ fluid values calculated from LAO carbonates.
- The $\delta^{18}O$ fluid value calculated for the SA rhyolite intrusion.

The $\delta^{18}O$ fluid value calculated for the strongly altered rhyolite intrusion lies within the range of $\delta^{18}O$ fluid values interpreted for the mineralisation. This adds additional weight to the argument developed in Chapters 5, 7 and 8 for a temporal relationship between the rhyolite intrusions and Pb - Zn - Ag mineralisation at Menninnie Dam.

The calculated D / H and oxygen isotope compositions of the mineralising fluid lie within the field for formation waters, and between the meteoric water line and the fields for magmatic waters and meteoric waters (Fig. 10.8). The D / H values clearly indicate that seawater can be discounted as a potential fluid source which is consistent with interpretation of a intracontinental setting for mineralisation (Section 10.2.4.2). Formational and metamorphic waters can be discounted as the Menninnie Dam mineralisation post-dates upper amphibolite facies metamorphism ($KM\text{-}D_{1\text{-}2}$) and later retrograde metamorphism ($KM\text{-}D_3$). This leaves meteoric waters and magmatic waters as potential fluid sources.

Trends away from the meteoric water line have been observed for a number of active geothermal systems. Criss and Taylor (1986) summarised D / H and oxygen isotope data from a number of active geothermal systems and epithermal ore deposits and demonstrated that source waters were of meteoric origin, although, a small component of magmatic water could not be ruled out (eg. Wairaki, Larderello, The Gysers, Hekla, Lassen Park, Niland and Steamboat Springs geothermal fields). Chloride-type geothermal waters from a single geothermal system commonly have similar $\delta D$ values and a range of $\delta^{18}O$ values. When the fluid values are plotted on a $\delta D$ vs $\delta^{18}O$ diagram, the resultant array defines a line which trends away from the meteoric water line, and in some cases, towards the field of magmatic waters. Numerous authors (summarised by Criss and Taylor, 1986) have attributed the $\delta D$ vs $\delta^{18}O$ trend line to interaction between circulating meteoric waters and country rock.

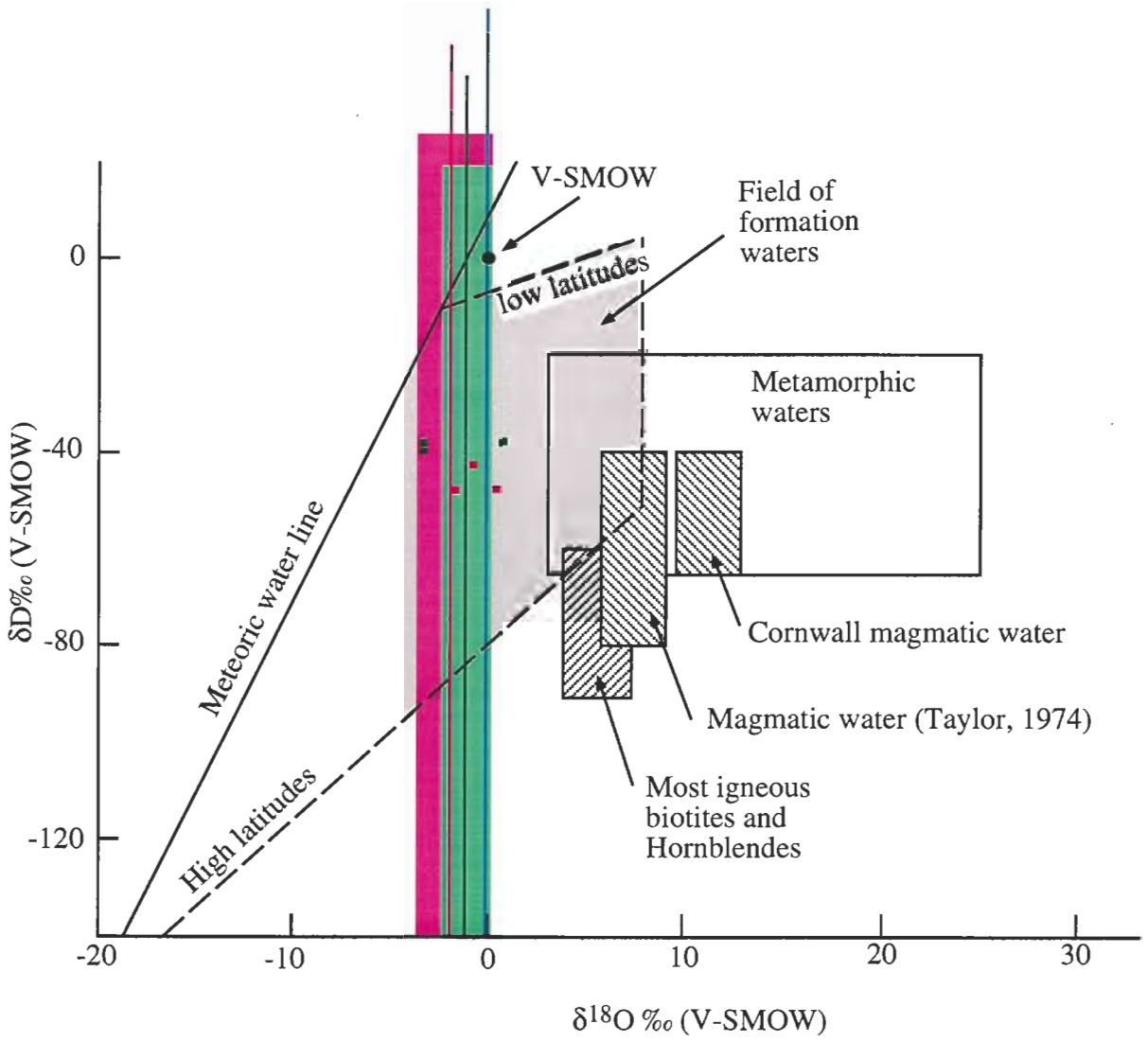


Figure 10.8. Summary δD ‰ vs $\delta^{18}O$ ‰ (V-SMOW) diagram with calculated $\delta^{18}O$ ‰ fluid values for intra-mineralisation carbonates, LAO carbonates, hydrous phyllosilicates, and the SA rhyolite intrusion. The calculated δD ‰ and $\delta^{18}O$ ‰ composition of the mineralising fluid and the late alteration overprint fluid lie between the meteoric water line and the magmatic water box.

In Section 10.2.4.2, it was noted that the initial $\delta^{13}C$ fluid value of = -6.90 ‰ calculated for intra-mineralisation carbonates was within the range of values attributed to magmatic carbon (mean of -6 ‰, Faure, 1977; Hoefs, 1980; Ohmoto, 1986; Exley et al., 1986; Taylor 1987). However, the interpreted $\delta^{18}O$ fluid value of -1.98 ‰ is too low for magmatic oxygen (+5.5 to +13.5 ‰, Taylor, 1974; Sheppard, 1977). A possible explanation is that the mineralising fluid consisted of mixed magmatic and meteoric waters with an oxygen isotope composition derived in proportion to the contribution from each fluid and a carbon isotopic composition predominantly derived from the magmatic fluid due to a higher dissolved carbon content.

Interpretation of a mineralising fluid with a magmatic component is consistent with geophysical modelling of a granite intrusion at 1 - 3 km beneath the Menninnie Dam prospect (Section 6.9) and a significant proportion of the lead derived from a granite of the Hiltaba Suite (Section 7.5.3) Providing the assumptions used throughout this section are appropriate, it can be concluded that the mineralising fluid consisted of a mixture of two fluids, one of which comprised of meteoric water and the other comprised magmatic water.

#### 10.3.4.3 Source of late alteration overprint fluids

A significant difference between the mineralising fluid and the fluid that gave rise to the late alteration overprint lies in their interpreted $\delta^{13}C$ compositions. The $\delta^{13}C$ composition of the mineralising fluid is interpreted to have been ≈ -6.90 ‰, compared to ≈ -1.39 ‰ for the late alteration overprint fluid. The $\delta^{13}C$ composition of the late alteration overprint fluid is similar to that of the host rocks ($\delta^{13}C$ ≈ 2 to -2 ‰; Table 10.2) and the late alteration overprint fluid may have been an evolved meteoric fluid with $\delta^{13}C$ and $\delta^{18}O$ compositions that had been modified from their original meteoric compositions through water - rock interaction. The isotopic composition of geothermal fluids are commonly interpreted to have been modified by similar processes (Criss and Taylor, 1986).

### 10.3.5 Summary

The composition of the mineralising fluid and the late alteration overprint fluid have been established through D / H and oxygen isotope analysis of hydrous phyllosilicate minerals. Calculated $\delta^{18}O$ fluid isotopic compositions overlap with those calculated for carbonate minerals formed during mineralisation (intra-mineralisation carbonates) and during the late alteration overprint. The isotopic composition of the mineralising fluid and the late alteration overprint fluid have been compared to established isotopic fields for waters from different sources (Fig. 10.8). The mineralising fluid and the late alteration overprint fluid have overlapping D / H and $\delta^{18}O$ compositions and lie between the meteoric water line and the field for magmatic fluids. A significant difference between the mineralising fluid and the late alteration overprint fluid lies in their $\delta^{13}C$ compositions. The isotopic composition of the mineralising fluid is interpreted to have resulted from mixing of two fluids, one of which was of meteoric origin and the second was of magmatic origin which is consistent with

interpretation of fluid inclusion measurements, lead isotopes and geophysical modelling. The source of fluids that produced that late alteration overprint are interpreted to have been evolved meteoric waters whose isotopic composition was modified through water - rock interaction.

## 10.4 Sulphur isotopes

With the proviso of isotopic equilibrium having been attained, fractionation between sulphur bearing minerals may provide information on the speciation of sulphur in the mineralising fluid, the temperature of deposition, and the source of the sulphur. The problem of establishing equilibrium - disequilibrium on an isotopic scale is commonly ambiguous, but may be assisted by other, independent means, such as interpretation of mineral textures and fluid inclusion trapping temperatures.

In this section, sulphur isotopes will be used to assist with the following:

- Metal abundancies show a zonal distribution on a prospect scale, centred around 9000 mN (Section 5.4.1). A similar zonation is interpreted from lead isotope ratios (Section 7.5.4). The possibility of spatial variations in sulphur isotopic values will be addressed by examining sulphides from various parts of the prospect and at various depths.

- Within the constraints imposed by sulphide textures and mineral paragenesis (Section 5.2.3), sulphur isotopes will be used to establish whether isotopic equilibrium was attained between sulphur species in the mineralising fluid and the sulphide minerals.

- Lead isotope systematics have previously been used to show that a significant proportion of lead, and by inference other metals, were derived from a Hiltaba Suite granite. The sulphur isotope characteristics of the mineralisation, host rocks, and granite will be examined in order to establish whether sulphur was also contributed from a Hiltaba Suite granite, or, if sulphur was acquired from a different source.

- In Section 5.3.2, it was suggested the late alteration overprint locally partially dissolved and reprecipitated existing sulphide minerals without appreciable addition of sulphur or metals. Sulphur isotopes may provide a means of testing this hypothesis.

### 10.4.1 Previous work

Andrew (1992) analysed 31 individual sulphide minerals from 14 samples of sulphide mineralisation spread over the length of the Menninnie Dam deposit. The analyses were conducted as a trial to assess the suitability of the Menninnie Dam mineralisation for inclusion in an AMIRA* project examining a number of Australian Proterozoic mineral

* Australian Mineral Industries Research Association Limited

deposits. Samples were obtained from polished drill core sections using a dentists drill which usually results in a minimum sample size of 0.5 - 2 mm diameter.

Where possible, Andrew (1992) analysed mineral pairs from adjacent grains in an attempt to determine the degree of isotopic fractionation between minerals. Andrew (1992) concluded that pyrite had been deposited in isotopic equilibrium with the other sulphides and equilibrium may have been reached between four of the five sphalerite - galena pairs with interpreted deposition temperatures of > 300°C.

Bird et al. (1989) undertook a sulphur and hydrogen isotope study of surficial alunite in Australia. Included in the study are two sulphur isotope values for sulphides contained within the Carnot Gneiss from drill hole WD/3 98-99m drilled into the Warramboo aeromagnetic anomaly in the northern-central Eyre Peninsula (Fig. 3.??). The $\delta^{34}S$ values reported by Bird et al. are used in this study and referred to as "Carnot Gneiss pyrite' (Table 10.8).

### 10.4.2 Method and samples

The laser ablation, sulphur isotope, microprobe technique, described by Huston et al. (1995) was used for this study (Central Science Laboratory, University of Tasmania). Briefly, samples were combusted in an oxygen atmosphere by ablation with a focused Nd-YAG laser. The $SO_2$ gas generated was automatically cleansed of contaminant gases and analysed by a VG Sira Series 2 mass spectrometer run in fully automated mode. Calibration of the equipment was checked daily against international, and well known local standards.

The advantage of laser ablation over conventional sampling techniques is that it permits analysis of much smaller samples. Isotopic variations in individual sulphide crystals can be determined from samples which might otherwise be homogenised into a single larger conventional sample (Huston et al., 1995). In practise, the sample size is dependant on the amount of contained sulphur, and therefore, on the sulphide mineralogy. An ablation pit of 60 μm diameter proved adequate for pyrite, whereas 200-300 μm ablation pits were required for galena.

126 analyses of sulphides from a range of locations throughout the Menninnie Dam prospect were undertaken. Samples analysed as part of this study include:

- Pyrite 1, sphalerite 2, galena 1, and chalcopyrite 3 hosted by units of the central suite in the northern, central and southern zones. Where possible, the margins of sulphide minerals in mutual contact were analysed for the purpose of evaluating attainment of isotopic equilibrium.
- Pyrite 1, sphalerite 2, galena 1, and chalcopyrite 3 hosted by sulphide clasts in DP breccias and LP breccias (Section 5.2.3).

- Pyrite 2 from the matrix of DP breccias (Section 5.2.3).
- Pyrite 3 and chalcopyrite 4 from the southern zone. These minerals are associated with the late alteration overprint. Sphalerite 4 and galena 2 are also associated with the late alteration overprint, but were not analysed as sufficiently large sample areas could not be clearly separated from sphalerite 2 and galena 1 respectively (Section 5.3.2).
- Pyrite from the eastern suite schists (Section 3.2.3). This shall be referred to as 'eastern suite pyrite'
- Pyrite associated with metasomatism of central suite calc-silicate lithologies (Section 3.7.2). This shall be referred to as 'metasomatic pyrite'.
- Pyrite formed during retrogressive alteration in the shear zone which separates the western and central suites (Section 3.5.1). This is referred to as 'KM-$D_3$ pyrite'.

All of Andrew's (1992) analyses were performed on samples from the northern and central zones. An appraisal of the samples used by Andrew (1992), shows that samples were obtained from sphalerite 2, galena 1, chalcopyrite 3, pyrite 1 and possibly pyrite 2 in some instances. Sphalerite 2 analyses undoubtedly contained minor chalcopyrite 2 due to the abundance of small inclusions of chalcopyrite 2 in sphalerite 2. By contrast, laser ablation was used to target zones of sphalerite 2 devoid of inclusions of chalcopyrite 2.

### 10.4.3 Results

Analytical results from this study, Andrew (1992), and Bird et al. (1989) are summarised in Table 10.8 and detailed in Appendix 10.3 as $\delta^{34}S$ ‰ variance from troilite in the Canyon Diablo meteorite (CDT). All analyses were corrected for machine fractionation factors. The precision of the laser technique was established by Huston et al. (1995) as ± 0.3 - 0.5 ‰. Andrew (1992) reported a precision of ± 0.2 ‰ for conventional analyses. A measure of the precision for the Carnot Gneiss pyrite was not reported by Bird et al. (1989) .

Analytical results obtained during this study (referred to as 'laser analyses') were compared with analyses obtained by Andrew (1992; referred to as 'conventional analyses'). Conventional analyses plot as two discrete populations whereas laser analyses of sulphides from the northern and central zones plot as a single population (Figs. 10.9a, b). The apparent difference between laser and conventional analyses is interpreted to be a result of the smaller number of conventional analyses rather than two populations. It is concluded that the agreement between the two laboratories is sufficient to allow meaningful comparison of analyses and the two data sets are combined throughout the remainder of this thesis. The combined data sets are illustrated in Figures 10.10a - g. Analyses of pyrite from the eastern suite schist, the shear zone separating the eastern and central suites, pyrite associated with metasomatic alteration and pyrite from the Carnot Gneiss are illustrated in Figure 10.11.

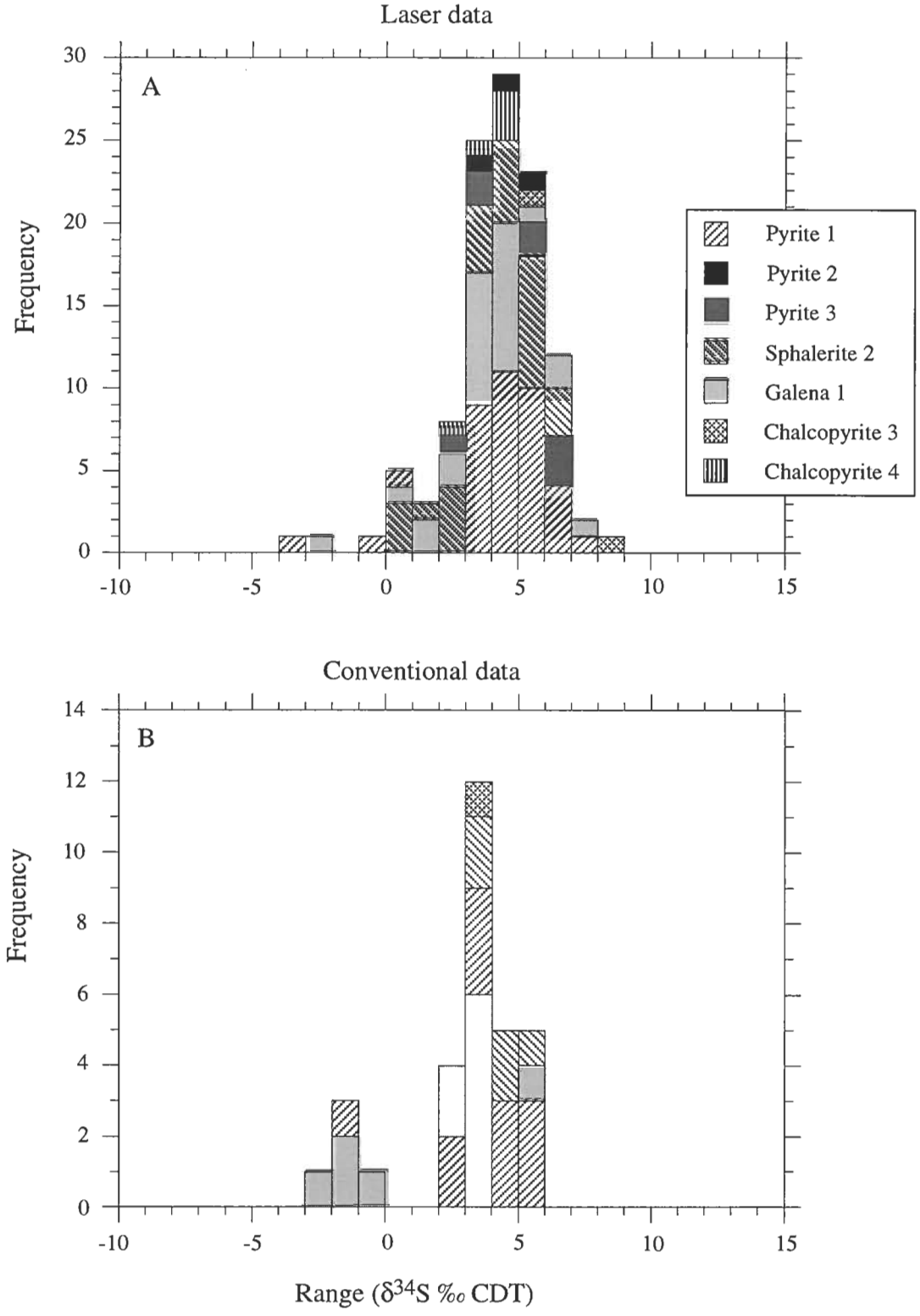


Figure 10.9A - B. Comparison of $\delta^{34}S$ ‰ values of sulphides from the northern, central and southern zones sampled by different methods and analysed at different laboratories. Sulphides sampled by laser ablation at the University of Tasmania as part of this study (A) and by Andrew (1992) at the CSIRO Division of Exploration of Geoscience, NSW, using conventional dentists drill sampling techniques (B) produce similar values and distributions.

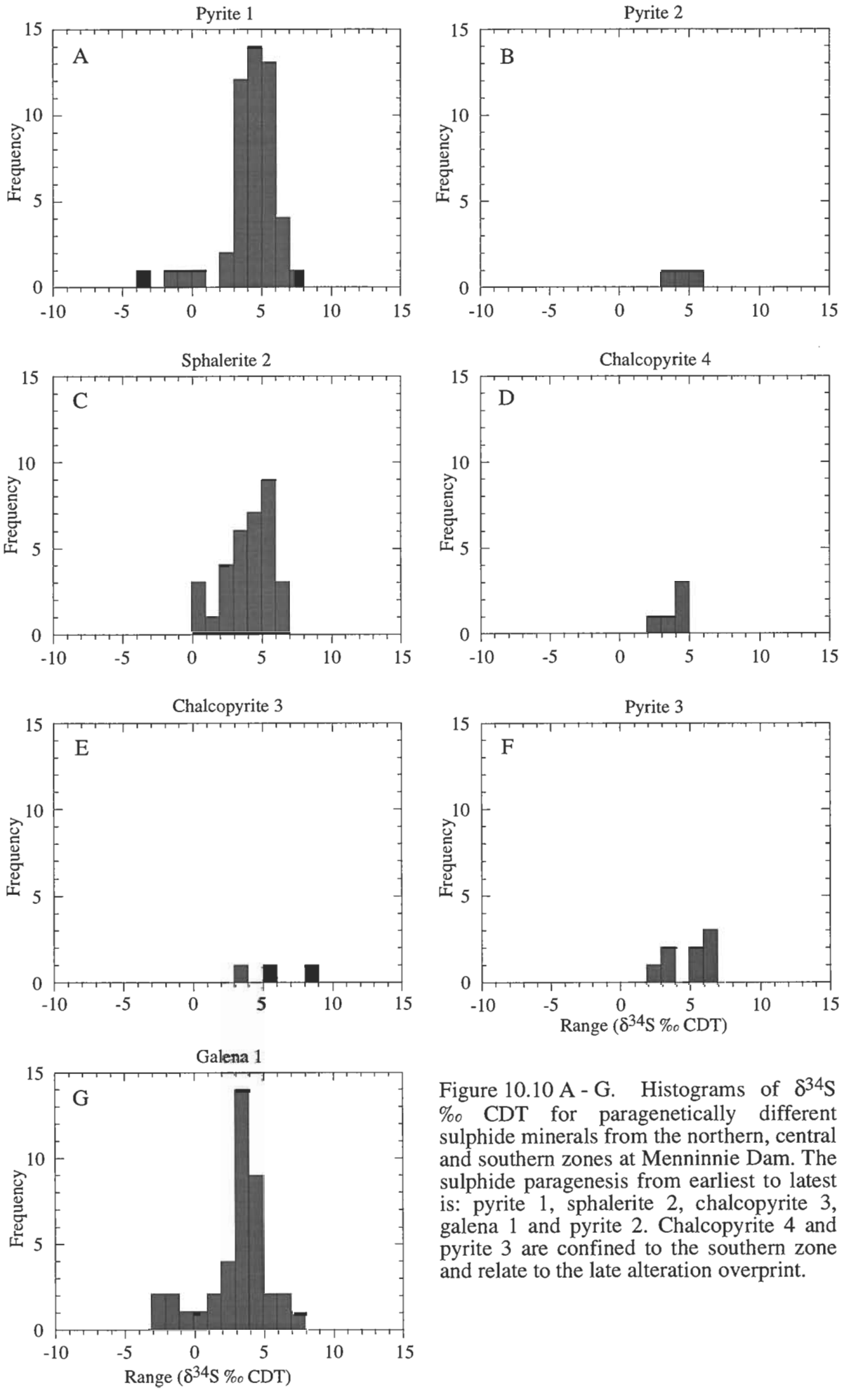


Figure 10.10 A - G. Histograms of $\delta^{34}S$ ‰ CDT for paragenetically different sulphide minerals from the northern, central and southern zones at Menninnie Dam. The sulphide paragenesis from earliest to latest is: pyrite 1, sphalerite 2, chalcopyrite 3, galena 1 and pyrite 2. Chalcopyrite 4 and pyrite 3 are confined to the southern zone and relate to the late alteration overprint.

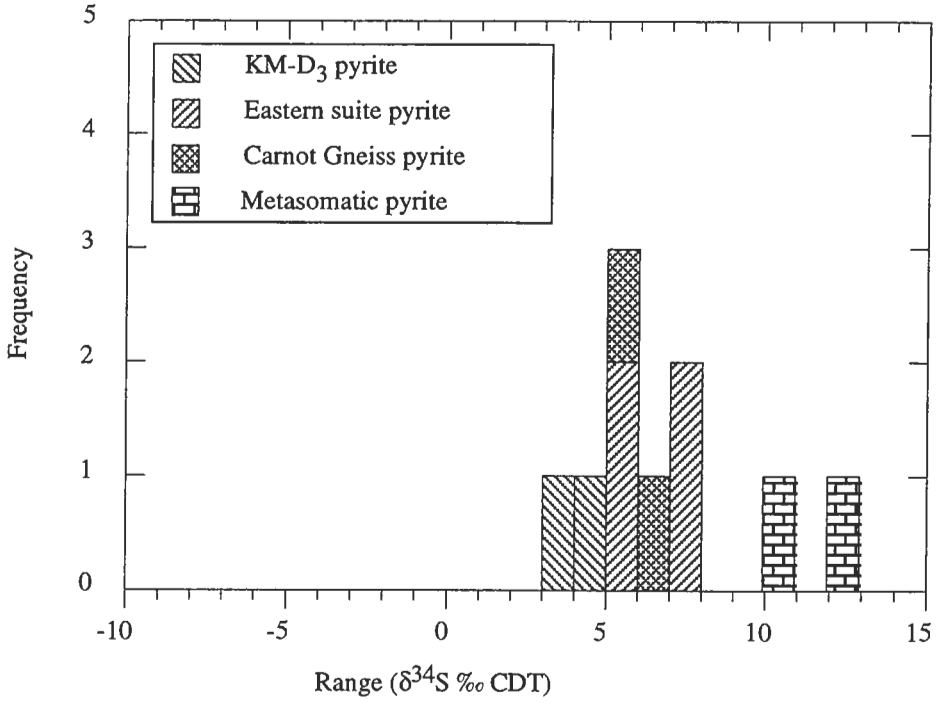


Figure 10.11. $\delta^{34}S$ ‰ (CDT) values of pyrite from the Archaean basement ('Carnot Gneiss pyrite', from Bird et al., 1989), the eastern suite schists at Menninnie Dam ('Eastern suite pyrite'), pyrite associated with retrogressive alteration in the shear system separating the western and central suites at Menninnie Dam ('KM-$D_3$ pyrite') and traces of pyrite associated with metasomatic alteration of central suite rocks at Menninnie Dam ('Metasomatic pyrite').

Table 10.8 Summary table of combined laser and conventional sulphur isotope analyses ($\delta^{34}S$ ‰ CDT). Sulphides associated with mineralisation (rows 1 - 7) are arranged in order with the paragenetically earlier minerals higher in table 10.8 and paragenetically later minerals lower in table 10.8.

| Mineral | Number of analyses | Range ($\delta^{34}S$ ‰ CDT) | Median | Average | Standard deviation |
|---|---|---|---|---|---|
| Pyrite 1 | 50 | -3.04 to +7.22 | 4.37 | 4.13 | 1.97 |
| Sphalerite 1 | 33 | +0.68 to 6.80 | 4.41 | 4.03 | 1.58 |
| Chalcopyrite 2 | 3 | +3.60 to +8.23 | 5.42 | 5.75 | |
| Galena 1 | 40 | -2.30 to +7.53 | 3.53 | 3.20 | 2.29 |
| Pyrite 2 | 3 | +3.96 to +5.81 | 4.96 | 4.91 | |
| Pyrite 3 | 8 | +2.98 to +6.54 | 5.36 | 5.00 | 1.52 |
| Chalcopyrite 3 | 5 | +2.87 to +4.99 | 4.03 | 4.08 | |
| Eastern suite pyrite | 4 | +5.43 to +7.38 | 6.54 | 6.47 | |
| Metasomatic pyrite | 2 | +10.87 to +12.76 | | | |
| KM-D3 pyrite | 2 | +3.82 to +4.79 | | | |
| Carnot Gneiss pyrite | 2 | +5.9 to +6.1 | | | |

## 10.4.4 Discussion

In this section, the spatial distribution of sulphur isotopes is investigated, the attainment of sulphur isotopic equilibrium between sulphide minerals is discussed and the source of sulphur in the northern and central zones and the southern zones is investigated.

### 10.4.4.1 Sulphur isotopes from northern and central zones mineralisation

$\delta^{34}S$ values are consistent along strike and at depth with no evidence of spatial variations (Figures 10.12a - c and 10.13a - c). The absence of spatial variations in $\delta^{34}S$ values for different sulphide minerals is interpreted to indicate sulphur isotopes were not fractionated in more distal parts of the prospect, or with depth, and that the chemical and physical attributes of the mineralising fluid did not significantly vary throughout the deposit.

Use of sulphur isotopes as geothermometers is dependant on kinetic and equilibrium fractionation of sulphur isotopes between co-existing sulphur bearing species. The principals behind stable isotope geothermometry are discussed by O'Neil (1986). In order to interpret fractionation of sulphur isotopes between adjacent mineral pairs for geothermometry, they must first satisfy the following conditions outlined by Ohmoto (1986):

1) The mineral species must have retained their isotopic composition since formation.
2) The co-efficient of fractionation is well calibrated and strongly temperature dependant.
3) The mineral species were in isotopic equilibrium at the time of deposition.

The first condition of Ohmoto (1986) is considered to be satisfied for sulphides in the northern and central zones as there is no evidence supporting later events which may have resulted in modification of the isotopic composition of sulphide minerals.

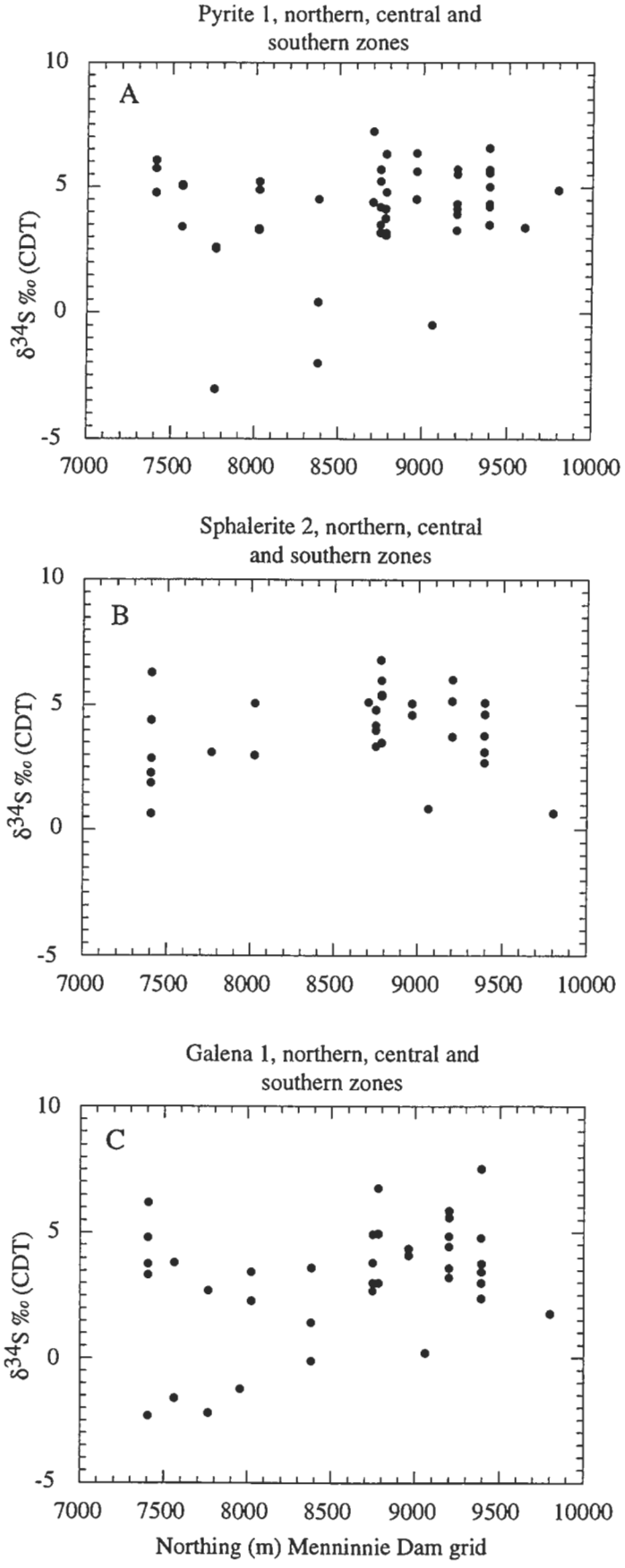


Figure 10.12A - C. Plots of $\delta^{34}$S ‰ (CDT) vs northing for pyrite 1, sphalerite 2 and galena 1 from the northern, central and southern zones. Sulphur isotopes do not show any systematic variation over the length of the deposit.

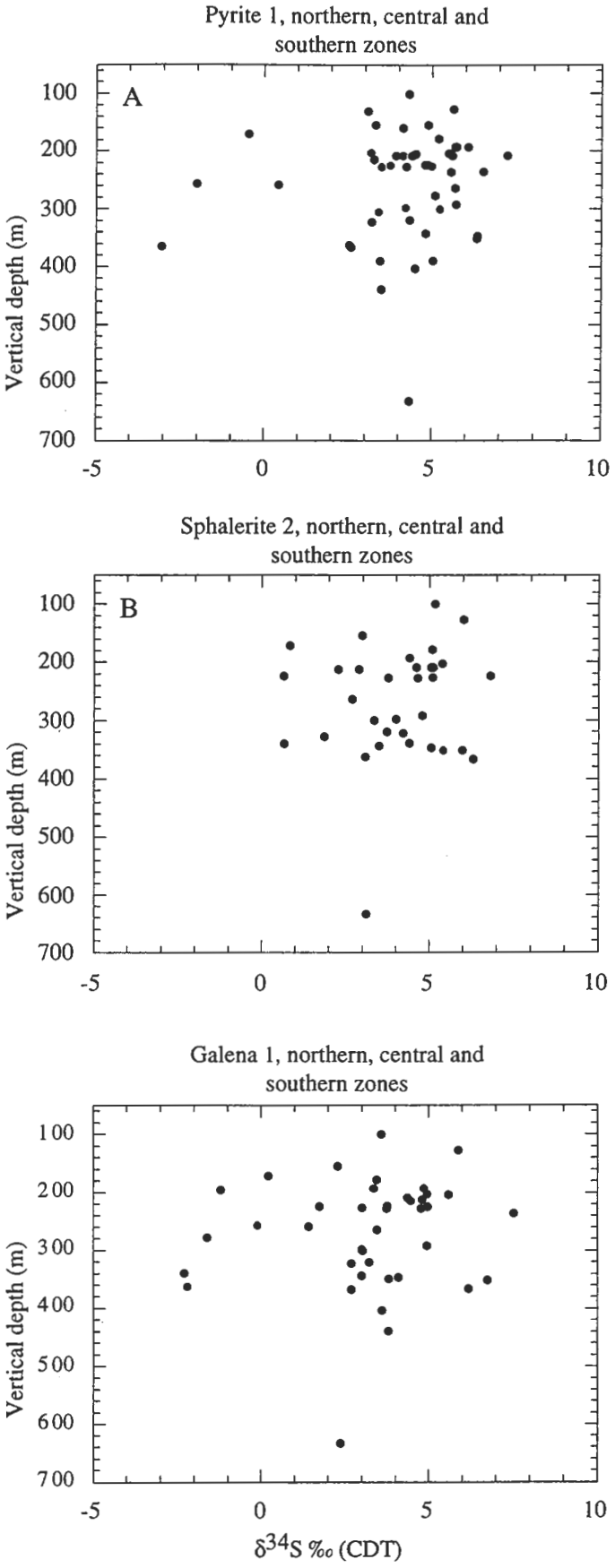


Figure 10.13A - C. Plots of $\delta^{34}S$ ‰ (CDT) versus vertical depth for pyrite 1, sphalerite 2 and galena 1 from the northern, central and southern zones. Sulphur isotopes do not show any systematic variation with depth.

The second condition of Ohmoto (1986) has been addressed by numerous authors (eg. Ohmoto and Rye, 1979; Taylor, 1987). The normal sequence of isotopic fractionation between an equilibrium assemblage of aqueous $H_2S$ and sulphides is:

$$\delta^{34}S_{pyrite} > \delta^{34}S_{sphalerite} > \delta^{34}S_{chalcopyrite} > \delta^{34}S_{galena}$$

(Ohmoto and Rye, 1979)

The extent of fractionation between co-precipitated mineral species is temperature dependant and decreases with increasing temperature (Ohmoto and Rye, 1979). In Section 9.6.3, the median temperature of the mineralising fluid was established to have been ≈ 154°C. Using the equations of Ohmoto and Rye (1979), the fractionation between sulphide pairs in isotopic equilibrium with aqueous $H_2S$ at 154°C are calculated to be:

$$\delta^{34}S_{pyrite} - \delta^{34}S_{sphalerite} \approx -1.7\ ‰$$
$$\delta^{34}S_{pyrite} - \delta^{34}S_{galena} \approx -5.7\ ‰$$
$$\delta^{34}S_{sphalerite} - \delta^{34}S_{galena} \approx -4.0\ ‰$$
$$\delta^{34}S_{pyrite} - \delta^{34}S_{chalcopyrite} \approx -2.5\ ‰$$

The third condition of Ohmoto (1986) addresses attainment of isotopic equilibrium during sulphide (or sulphate) deposition. Calculated fractionation values for adjacent sulphide mineral pairs at Menninnie Dam are less than that for equilibrium precipitation from a fluid at 154°C. This is also apparent from the mean $\delta^{34}S$ values for different sulphide minerals and the difference between the mean values for $\delta^{34}S_{pyrite\ 1}$ and $\delta^{34}S_{galena\ 1}$ is less than 1 ‰ (Table 10.8 and Figs. 10.10a - g). Calculation of fractionation values between the mean $\delta^{34}S$ values for the different sulphide minerals at Menninnie Dam results in:

$$\delta^{34}S_{pyrite\ 1} \approx \delta^{34}S_{sphalerite\ 2} \approx \delta^{34}S_{chalcopyrite\ 3} \approx \delta^{34}S_{galena\ 1}$$

This is interpreted to indicate that isotopic equilibrium was not attained between different sulphide minerals. Non-attainment of isotopic equilibrium could have resulted from a number of factors including:

- Sulphur could have been locally derived. Ohmoto (1986) suggested that at low temperatures, the local production of reduced sulphur probably takes place very slowly, so that the molar concentration of reduced sulphur remains below the molar concentration of metals. Therefore, if only one sulphide mineral was precipitated at a time, all of the reduced sulphur would be consumed resulting in similar $\delta^{34}S$ values for different sulphide minerals and the fluid.

- If sulphur and the metals were transported in the same fluid, but, the molar concentration of reduced sulphur in solution was less than the molar concentration of the metals, the first formed sulphide mineral would consume much of the sulphur resulting in erratic $\delta^{34}S$ values for paragenetically later sulphide minerals (Ohmoto, 1986).

- The sulphide minerals at Menninnie Dam were not co-precipitated. The sulphide and gangue paragenesis established in Section 5.2.3, is interpreted to indicate a hiatus between the deposition of pyrite 1 and sphalerite 1, with interceding deposition of chlorite 1, adularia and sericite 1. Hiatuses are also interpreted between deposition of sphalerite 2 and galena 1, with interceding quartz 1 and Ca-Mg-Mn carbonate 1, and between galena 1 and pyrite 2, with interceding chlorite 2, sericite 2 and rhodonite. As chalcopyrite 3 resulted from local remobilisation of chalcopyrite 2 during deformation, and all sulphide minerals have essentially identical $\delta^{34}S$ values, then the sulphur isotopic composition of chalcopyrite 3 would be expected to be similar to that of chalcopyrite 2.

There is no local sulphur source in the marbles and calc-silicate lithologies at Menninnie Dam, therefore, reduced sulphur was not sourced from the depositional site. Sulphur and the metals are interpreted to have been transported to the depositional site in either the same fluid or by different fluids. The concordance between the median $\delta^{34}S$ values of paragenetically later sulphide minerals at Menninnie Dam most likely resulted from the absence of isotopic equilibrium between different sulphide phases at Menninnie Dam is the sulphide minerals were not co-precipitated.

The presence of co-existing sulphides and trace amounts of haematite in the Menninnie Dam mineralisation places further constraints on the mineralising fluid(s). Co-precipitation of trace amounts of haematite throughout deposition of sphalerite 1, chalcopyrite 1, sphalerite 2, chalcopyrite 2 and galena 1 indicates the mineralising fluid(s) probably contained minor aqueous $SO_4^{2-}$. The concentration of $SO_4^{2-}$ must have been low as there is a marked absence of sulphate minerals and sulphides precipitated sequentially from a fluid containing both reduced and oxidised sulphur would be expected to have a wide range of $\delta^{34}S$ values (Ohmoto, 1986).

Ohmoto and Lasaga (1982) proposed that the rate at which aqueous sulphide - sulphate equilibria is attained is dependent on temperature, pH, and the total sulphur content of the fluid. For example, the time required to reach 90% equilibrium (ie, conditions indistinguishable from equilibrium) between aqueous sulphates and sulphides for a fluid at 150°C, with a pH of 4 - 7 (most hydrothermal fluids), and a total sulphur content of 0.1

molal, is in the order of 4000 years (Ohmoto and Lasaga 1982). A similar fluid at 350°C would be expected to attain isotopic equilibrium in 17 days (Ohmoto and Lasaga 1982).

The sulphides at Menninnie Dam are interpreted to have been deposited from a fluid with a median temperature of 154°C and less than 700 m from the palaeosurface. Therefore, the fluids are interpreted to have cooled rapidly and isotopic equilibrium between aqueous sulphide and sulphate would not have been achieved. Precipitation of early formed sulphide phases would be expected to have had negligible effect on $\delta^{34}S_{H2S}$ of the fluid or $\delta^{34}S$ of later precipitated sulphides. As precipitation sequence of sulphides is pyrite 1→ sphalerite 2 → galena 1, then any tendency towards equilibrium (ie. an increase in $\delta^{34}S_{H2S}$ of the fluid) would have been partially offset by mineral - fluid fractionation.

Sulphur isotopic disequilibrium has been noted in a number of sulphide deposits (eg. Creede, Colorado; Park City, Utah, Rye and Ohmoto, 1974). Rye and Ohmoto (1974) suggested that in shallow deposits such as Creede and Park City, boiling, fluid mixing and redox reactions probably occurred at the site of mineral deposition and the time period between deposition of sulphide minerals was insufficient for the fluid to attain isotopic equilibrium.

### 10.4.4.2 Sulphur isotopes from southern zone mineralisation

Mineralisation in the southern zone consists of an identical sulphide assemblage and paragenesis to the northern and central zones which is interpreted to have been partially dissolved and re-precipitated during the late alteration overprint (Section 5.3.2). Dissolution and re-precipitation probably involved hydration of pre-existing sulphides followed by co-precipitation of sphalerite 4, galena 2, pyrite 3 and chalcopyrite 4. There is no mineralogical evidence for sulphur in the form of sulphates or sulphides having been added during the late alteration overprint.

There is no appreciable difference in the $\delta^{34}S$ composition of pyrite 3 and chalcopyrite 4 formed during the late alteration overprint and earlier formed sulphides (Table 10.8 and Fig. 10.10a - g) and essentially:

$$\delta^{34}S_{\text{pyrite 3}} \approx \delta^{34}S_{\text{chalcopyrite 4}} \approx \delta^{34}S_{\text{sphalerite 2}} \approx \delta^{34}S_{\text{galena 1}} \approx \delta^{34}S_{\text{pyrite 1}}$$

This is interpreted to indicate pyrite 3 and chalcopyrite 4 did not attain isotopic equilibrium with aqueous $H_2S$ in the late alteration overprint fluid, even though they appear to have been co-precipitated (Section 5.3.2).

Factors which may have contributed to the absence of $\delta^{34}S$ fractionation between apparently co-precipitated pyrite 3 and chalcopyrite 4 include:

- A low sulphur concentration in the late alteration overprint fluids.
- The sulphur source had a similar isotopic composition to sulphides produced during the late alteration overprint. This could have resulted from derivation of sulphur by hydration of earlier sulphides as the $\delta^{34}S$ composition of $H_2S$ produced by hydration of pyrite (and by inference other sulphides) was essentially the same as that of pyrite (Ohmoto and Rye, 1979).
- The rate of local production of reduced sulphur through hydration of sulphides probably takes place slowly producing only small quantities at a time so that the molar concentration of reduced sulphur is low. Therefore, if only one sulphide mineral phase was saturated at any one time, all of the sulphur would be completely consumed, resulting in:

$$\delta^{34}S_{\text{sphalerite 4}} \approx \delta^{34}S_{\text{galena 2}} \approx \delta^{34}S_{\text{chalcopyrite 4}} \approx \delta^{34}S_{\text{pyrite 3}}$$

(Ohmoto, 1986)

### 10.4.4.3 Source of sulphur

The sources of sulphur are investigated in this section. Sulphur sources may have included:

- Proterozoic sea water.
- Hydration of pyrite within metasedimentary units in the vicinity of Menninnie Dam.
- Downwards percolating sulphur-bearing fluids from saline lakes or sulphur leached from surficial or lacustrine evaporites.
- Magmatic sulphur derived from an underlying Hiltaba Suite granite.

*Proterozoic sea water source.*

Seawater sulphate can be discounted as a sulphur source on the basis of:

- The intra-continental setting (Section 10.2.4.2).
- Hydrogen and oxygen isotope characteristics of the mineralising fluid indicate the involvement of meteoric and / or magmatic fluids and exclude seawater derived fluids (Section 10.3.4.2).

*Host rock sulphur source*

Possible host rock sources of sulphur include hydration of pyrite from; the Archaean basement (Carnot Gneiss pyrite), eastern suite schists (eastern suite pyrite), metasomatised lithologies (metasomatic pyrite), and from the shear zone separating the central and eastern suites (KM-$D_3$ pyrite).

Metasomatic pyrite will not be considered further as a sulphur reservoir due to its occurrence in trace amounts. Carnot Gneiss pyrite and eastern suite pyrite are isotopically heavier ($\delta^{34}S$

≈ 6 - 7 ‰, Table 10.8) than the mean $\delta^{34}S$ of the mineralisation (≈ 4 ‰). In order to achieve a 2 - 3 ‰ shift, a fractionation process is required such as oxidation as hydration of pyrite does not result in appreciable fractionation between pyrite and aqueous sulphur (Ohmoto, 1986). However, isotopic equilibrium between aqueous sulphide and sulphate species at Menninnie Dam is unlikely to have been achieved at the low temperatures interpreted for formation of sulphides. Therefore, oxidation could not have been an effective fractionation mechanism and hydration of Carnot Gneiss pyrite and eastern suite pyrite could not have been the sole source of sulphur for the Menninnie Dam mineralisation.

KM-$D_3$ pyrite and the Menninnie Dam mineralisation have near identical average $\delta^{34}S$ compositions. Hydration of KM-$D_3$ pyrite could have produced a fluid with an isotopic composition similar to that of the mineralisation.

*Surficial saline lake or evaporite source*

Carbon and oxygen isotopes from mineralisation carbonates, and D / H and oxygen isotopes of hydrous phyllosilicates and quartz associated with mineralisation are interpreted to indicate the mineralising fluid consisted of a mixture of magmatic and meteoric fluids. Heating - freezing measurements on fluid inclusions indicated a range in fluid inclusions salinities which is interpreted to have resulted from mixing of a more saline, lower temperature fluid (≈ 140°C and 27 wt.% NaCl equivalent) with a less saline higher temperature fluid (≈ 180°C and 0 - 3 wt.% NaCl equivalent). A source of saline meteoric fluids could have been deeply circulating saline brines derived from a proximal saline lake. Although there is no evidence of a saline lake environment having been present at Menninnie Dam, the very restricted nature of drilling does not preclude its prior existence. If high salinity fluids were derived from such a source, then it is possible that sulphur could also have been contributed from the same source.

Determination of the sulphur isotope composition of a hypothetical saline lake is problematic. In a study of surficial alunite from Australian inland salt lakes, Bird et al. (1989) suggested that the major sulphur source was wind blown marine sulphate rather than weathering of a continental landmass. If a similar process was to have operated in the Middle-Proterozoic, then saline lakes might be expected to have a sulphur composition not that far removed from Middle-Proterozoic seawater sulphate. Strauss (1993) interpreted the $\delta^{34}S$ composition of Middle-Proterozoic seawater to have been ≈ +15 to +25 ‰, similar to that of the modern oceans which is considerably heavier than the Menninnie Dam mineralisation. Alternatively, sulphur could have been leached from the country rocks during weathering, or contributed by circulating hydrothermal fluids. Without prior knowledge of the isotopic composition of the hypothetical saline lake, the $\delta^{34}S$ value of a circulating fluid derived from such a brine could lie within a wide range and would have been dependant on the interplay of biological activity, evaporite formation, fluid - rock interaction and others.

The oxygen isotopic composition of a fluid derived from a saline lake is likely to have been heavier than meteoric water through evaporative processes. The $\delta^{18}O$ composition of Middle-Proterozoic meteoric water is interpreted to have been ≈ -6.80 ‰ (Fig. 10.8), and the mineralising fluid was interpreted to have been approximately 5 ‰ heavier with $\delta^{18}O \approx$ -1.98 ‰ (Section 10.3.4.2). In summary, although a saline lake source of fluids and sulphur is intuitively considered unlikely, in the absence of independent evidence, it cannot be discounted on the basis of the geologic, geochemical and isotopic evidence presented in this thesis.

*Granite source*

A Hiltaba Suite granite is interpreted to underlie the Menninnie Dam prospect (referred to as the 'MD granite' Section 6.9) A significant proportion of the lead in the Menninnie Dam deposit (and by inference the other metals) is interpreted to have been derived from the MD granite (Section 7.5.3). It is considered possible that some, or all, of the sulphur was also derived from the MD granite. Unlike lead, there are a number of physical and chemical processes which fractionate sulphur isotopes. Without direct knowledge of the sulphur isotope composition of the granite and the pathway followed by a granite derived fluid, the task of assessing a granite source is difficult.

If the Menninnie Dam granite was derived by partial melting of crustal rocks (Giles, 1977), then, the sulphur isotope signature of the granite would probably be similar to the bulk sulphur isotope composition of the source rocks (Ohmoto and Rye, 1979). If the Carnot Gneiss and eastern suite schist ($\delta^{34}S \approx$ 6.0‰ and 6.5 ‰ respectively) are considered as possible source rocks for the Menninnie Dam granite, then the granite might also be expected to have a $\delta^{34}S$ value ≈ 6.0 ‰.

If the Menninnie Dam granite was derived from fractionation of a mantle derived magma and assimilation of crustal rocks (Stewart, 1992), it may have had a sulphur isotopic composition between that of mantle sulphur (≈ -3 to 3 ‰; Ohmoto, 1986) and the assimilated country rock. Assimilation of crustal sulphur has been suggested for some of the granitoid rocks in Japan which show a strong correlation with the sulphur isotopic composition of the enclosing country rocks (Ishihara, 1981). Similar observations were made from selected Caledonian granites of Britain and Ireland by Laouar et al. (1990) and by Recio et al. (1991) for granitoids from central Spain.

If the assimilated country rock comprised Carnot Gneiss or eastern suite schist then the sulphur isotopic composition of the granite would be expected to lie between -3 ‰ and +6 ‰. The sulphur isotopic composition of a fluid separating from a granite melt is dependant on temperature, $P_{H2O}$, and the nature of the sulphur species in the fluid, which in turn is largely controlled by the oxidation state of the magma (Ohmoto and Rye 1979). In more

reduced melts (high $Fe^{2+}$ / $Fe^{3+}$), $H_2S$ is the dominant sulphur species in the fluid phase. Fractionation between $H_2S$ and the sulphur species in the melt is negligible and the $\delta^{34}S$ of a magmatic fluid separating from such a melt is essentially identical to that of the melt.

For more oxidised melts (low $Fe^{2+}$ / $Fe^{3+}$), $SO_2$ is a significant sulphur species, and in some cases, $SO_2$ may exceed $H_2S$ (Ohmoto, 1986). The low solubility of $SO_2$ in oxidised hydrous melts (Burnham, 1979) may result in all of the sulphur in the melt being removed in a fluid phase as $SO_2$ and under these conditions, $\delta^{34}S$ of the separated fluid is similar to $\delta^{34}S$ of the melt (Ohmoto and Rye, 1979). However, when the volume ratio of fluid to melt is small, $SO_2$ in the fluid may be buffered by sulphur remaining in the melt (as $SH^-$), and the $\delta^{34}S$ of the fluid may be as much as 4 ‰ greater than the melt (Ohmoto and Rye, 1979).

From the above discussion, three options are considered possible for a fluid separating from the interpreted MD granite underlying the Menninnie Dam prospect:

1) If the MD granite was reduced, and derived by partial melting of the Carnot Gneiss and / or the eastern suite schist, then any sulphur-bearing fluid phase separating from the granite would be dominated by $H_2S$ with an isotopic composition of ≈ 6.0‰.

2) If the MD granite resulted from fractionation of a mantle melt and assimilation of country rock (Carnot Gneiss and / or eastern suite schist), and was oxidised, then a fluid separating from the melt with a high fluid to melt ratio would be dominated by oxidised sulphur with a $\delta^{34}S$ composition similar to that of the melt and lie between -3 and +6 ‰.

3) If the MD granite resulted from fractionation of a mantle melt and assimilation of country rock (Carnot Gneiss and / or eastern suite schist), and was oxidised with a small fluid to melt ratio, a fluid separating from the melt would be isotopically heavier than that of the melt (ie > -3 ‰).

Options 2 or 3 are favoured over option 1 for two reasons. A fluid with $\delta^{34}S$ = 6 ‰ is too heavy to have formed the Menninnie Dam mineralisation, and most of the Hiltaba Suite are oxidised with abundant minute iron oxide inclusions in plagioclase and K-feldspars (Flint 1993b). Discrimination between options 2 and 3 cannot easily be resolved from the available data.

An important consideration is that the sulphur isotopic composition of a magmatic fluid may have been modified during transportation through leaching and mixing with host rock sulphur. The resultant fluid might be expected to have a sulphur isotopic composition which

lay between that of the granite derived fluid and the country rocks and potentially equivalent to the $\delta^{34}S$ composition of the Menninnie Dam mineralisation.

### 10.4.5 Summary

Sulphur isotopes do not show any lateral or depth variation throughout the Menninnie Dam prospect. Sulphur isotope compositions of sulphides from the northern and central zone have a narrow range of values with an average of ≈ 4 ‰. The absence of fractionation between different sulphide minerals is attributed to sulphide minerals having been precipitated sequentially rather than co-precipitated, and low temperature kinetic effects.

Sulphur was not locally sourced, and both sulphur and metals were introduced. Seawater sulphate can be discounted as a sulphur source. The source of sulphur cannot be clearly discriminated, and possible sulphur sources include circulating saline ground-waters, hydration of pyrite in the shear zone separating the central and western suites (KM-$D_3$ pyrite), sulphur derived entirely from the Menninnie Dam granite, and sulphur derived from a combination of the Menninnie Dam granite and country rock sulphur sources.

Sulphides in the southern zone have a narrow range of $\delta^{34}S$ values with a mean around 4.7 ‰, which is indistinguishable from sulphides of the northern and central zone. The absence of $\delta^{34}S$ fractionation between seemingly co-precipitated sulphides (pyrite 3 and chalcopyrite 4) probably resulted from hydration of pre-existing sulphides and a molar aqueous sulphur to metal ratio near 1. The hypothesis that sulphur was added during the late alteration overprint cannot be unequivocally resolved using sulphur isotopes, although a molar aqueous sulphur to metal ratio near 1 is interpreted to indicate sulphur was not added during the late alteration overprint.

## 10.5 Conclusions

The aims of this chapter were to establish the following:

- The source of the fluids from which the Menninnie Dam mineralisation was formed
- The extent of fluid - rock interaction
- The source of sulphur in sulphide minerals
- The speciation of carbon and sulphur in the mineralising fluid

Each of these can now be addressed:

- The mineralising fluids at Menninnie Dam are interpreted to have resulted from mixing of two fluids, one of which was meteoric in origin and the second was of magmatic origin. The source of fluids which produced that late alteration overprint are interpreted to have been of meteoric origin.

- Carbonate produced during the mineralising event has isotopic compositions that resulted from the predominant effects of fluid - rock interaction. The mineralising fluids did not penetrate significantly into the host rocks resulting an isotopic alteration halo of only a few centimetres extent.

- Sulphur was not locally sourced and both sulphur and metals were introduced. Seawater sulphate can be discounted as a sulphur source. The source of sulphur cannot be clearly discriminated and possible sulphur sources include circulating saline ground-waters, hydration of KM-$D_3$ pyrite, sulphur derived entirely from the Menninnie Dam granite, and sulphur derived from a combination of the Menninnie Dam granite and country rock sources. Sulphides in the southern zone are isotopically similar to sulphides in the northern and central zones. The hypothesis that sulphur may have been added during the late alteration overprint cannot be unequivocally resolved from isotopic data alone because of the similarity between host rock sulphur and mineralisation sulphur.

- The carbon species present in the mineralising fluid was probably $H_2CO_3$ with a molar concentration of $\geq 0.01$. $HCO_3^-$ may have been locally present at the contact between the mineralising fluids and the host marbles but is interpreted to have been volumetrically insignificant.

- The ratio of reduced to oxidised sulphur species present in the mineralising fluid is thought to be high due to the absence of sulphate minerals but cannot be unequivocally determined from isotopic studies alone due to low temperatures kinetic effects and near surface environment in which the Menninnie Dam mineralisation is interpreted to have formed.

# Chapter eleven
# Thermodynamic modelling of mineralisation

## 11.1 Introduction

Formation of an economic Pb - Zn sulphide deposit requires an interplay between three factors:

- Source(s) of fluid, metals and sulphur.
- Fluids capable of transporting metals ± reduced sulphur.
- An efficient depositional mechanism that results in precipitation of ore grade quantities of galena and sphalerite.

The aim of this chapter is to use thermodynamic modelling to examine the physicochemical attributes of the mineralising fluid, and the mechanism of sulphide deposition that resulted in the Menninnie Dam Pb - Zn - Ag mineralisation.

The mineral paragenesis has been subdivided into an early pyrite stage, a sphalerite - galena stage, and a late pyrite stage (Section 5.6.2). Due to its economic importance, the sphalerite - galena stage is the focus of thermodynamic modelling. Data derived from attributes of the geological setting, mineralogy, mineral paragenesis, fluid inclusion, and isotopic data established in preceding chapters are used to construct a number of activity diagrams that illustrate some of the chemical parameters and processes fundamental to the transport and deposition of Pb - Zn sulphide at Menninnie Dam.

## 11.2 Transport of Pb, Zn, Fe, Cu and Ag in hydrothermal fluids

In general, lead, and the transition metals Fe, Ag, Cu, Zn and Ag, are transported in hydrothermal solutions as complex ions bound to, or coordinated by ligands (Barnes, 1979; Brimhall and Crerar, 1987). Ligands considered to be important for the transport of Fe, Ag, Cu, Zn and Ag in geologic environments include $Cl^-$, $OH^-$, $HS^-$, $H_2O$ and to a lesser extent organic acids, $NH_3$, $F^-$, $S_x^{2-}$, $S_2O_3^{2-}$ and $HCO_3^-$ (Barnes, 1979; Brimhall and Crerar, 1987; Baes and Mesmer, 1976; Smith and Martell, 1976; Wood et al., 1987; Bourcier and Barnes, 1987). In most geothermal systems, ligands such as $Cl^-$ (and to a significantly lesser extent, $HS^-$), are probably more important for the solution and transport of Pb, Fe, Cu, Ag and Zn at temperatures less than 350°C (Schwarzenbach and Widmer, 1966; Crerar and Barnes, 1976; Seward, 1976; Barrett and Anderson, 1982, 1988; Ruaya and Seward, 1986; Zotov et al., 1986; Gammons and Barnes, 1989; Hayashi et al., 1990; Hemley et al., 1992; Seyfried and Ding, 1993; Gammons and William-Jones, 1995).

The extent of dissociation of water and salts, and hence the formation of ligands, is dependant on temperature, pressure, ionic strength, and molecular vibration (Brimhall and

Crerar, 1987). At higher temperatures, ion pairs become more associated with a tendency to form electrically neutral, or low charge complexes whereas increases in pressure have the reverse effect;

eg. $Na^+ + Cl^- \rightarrow NaCl$ (high temperature and low pressure).

$Na^+ + Cl^- \leftarrow NaCl$ (low temperature and high pressure).

The tendency to form ion pairs at higher temperatures and lower pressures is partly countered by increased molecular vibration, which commonly results in a dissociation maxima (Helgeson, 1967).

*Zinc and lead*

Chloride complexes are the most common lead and zinc species in most natural hydrothermal fluids. The solubilities of chlorozinc and chlorolead complexes increase with increasing $\Sigma Cl^-$, $aH^+$, and temperature over the range 25 - 700°C (Ruaya and Seward, 1986; Barrett and Anderson, 1982, 1988; Wood et al., 1987; Bourcier and Barnes, 1987; Hemley et al., 1992). At temperatures of < 100°C, all chlorozinc species ($ZnCl_n^{2-n}$; n = 0 - 4) are stable, however, the stability of $ZnCl_3^-$ diminishes with increasing temperature (Ruaya and Seward, 1986). At low temperatures, low $\Sigma Cl^-$ and high $\Sigma S$ conditions, sulphide complexes predominate over chloride complexes, however, such fluids are not typical of those that result in significant zinc sulphide deposits (Hayashi et al., 1990).

Experiments by Anderson (1975) and Barrett and Anderson (1982) showed that solutions with $\Sigma Cl^- < 3m$, T < 150°C, and pH > 2 are unlikely to transport sufficient lead, zinc and reduced sulphur to form an economic deposit. Subsequent experiments by Ruaya and Seward (1986) and Barrett and Anderson (1988) showed that lead and zinc solubilities under conditions of $H_2S$ saturation are significantly increased at higher salinities. For example, a solution with pH = 4, 5m NaCl, $\Sigma S$ (as $H_2S$) = 0.001, and 150°C can transport 7.1 ppm Zn and 0.5 ppm Pb. These concentrations can increase to 50.1 and 4.37 ppm respectively at 200°C. Significantly more lead and zinc can be dissolved in low temperature, more oxidised brines (Anderson, 1973). The results of Anderson (1973) and Barrett and Anderson (1982, 1988) and Ruaya and Seward (1986) are consistent with the composition of lead - zinc-bearing, highly saline, low temperature (68 - 106°C) oil field brines which typically contain significantly higher concentrations of Zn compared to Pb and have $SO_4^{-2} > H_2S$ (Kharaka et al., 1987).

*Copper and iron*

The copper and iron chloride complexes $CuCl_{(aq)}$, $FeCl^+$ and $FeCl_{2(aq)}$ are probably the most abundant iron and copper complexes in most natural hydrothermal solutions with $\Sigma S$ between 0.1 - 1.0m, although bisulphide complexes may be important at low chloride concentrations and temperatures of less than 200°C (Crerar and Barnes, 1976; Ding and Seyfried, 1992; Heinrich and Seward, 1990; Walshe and Solomon, 1981). At lower

temperatures (ie ground waters) copper is probably in solution as the cupric ion ($Cu^{+}$), complexed with $OH^{-}$, $CO_3^{2-}$, $SO_4^{2-}$, $Cl^{-}$ and possibly organic complexes (Mann and Deutscher, 1977; Palmer and Baker, 1978; Rose, 1976). Experiments by Seyfried and Ding (1993) have shown that the solubilities of Cu and Fe co-existing with K-feldspar, muscovite and quartz increase with falling pH, increasing temperature and $Cl^{-}$ concentration, and that the solubility of Fe, and to a greater extent Cu, decrease and increase respectively with decreasing $fO_2$.

*Silver*

Based on experiments at 20°C, Schwarzenbach and Widmer (1966) determined that silver bisulphide complexes were the most important species for silver transport over a wide range of pH values in solutions devoid of Cl. Gammons and Barnes (1989) concluded that $Ag(HS)_2^{-}$ was the dominant species in near neutral to alkaline geothermal fluids with low $fO_2$, high $\sum S$ and temperatures < 300°C. In these fluids silver deposition occurred in response to either a decrease in $\sum S$ of the fluid, pH changes, or a decrease in the oxidation state of silver.

In NaCl-bearing solutions (5 x $10^{-5}$ to 3 molar NaCl; ie. most geothermal solutions) over the temperature range 100 - 353°C, $AgCl_n^{n-1}$ (n = 0, and 3) complexes are significantly more soluble than bisulphide complexes (Seward, 1976; Zotov et al., 1986; Gammons and Barnes, 1989; Gammons and William-Jones, 1995). With increasing temperature, the $AgCl_3^{-2}$ complex decreases in concentration and chlorosilver and dichlorosilver are prevalent, with the dichlorosilver species predominating in concentrated brines at temperatures above 200°C (Seward, 1976; Zotov et al., 1986). The solubility of silver chloride complexes are enhanced at higher temperatures and salinity, low pH and relatively oxidising conditions (Gammons and Barnes, 1989).

Silver is present in trace amounts as matildite in the Menninnie Dam deposit (range Ag = 0 - 900 ppm; Table 5.5) and has not been incorporated in thermodynamic models due the absence of reliable thermodynamic data for matildite, however, the conditions that favour transport of silver and lead and zinc are similar. Copper is present in minor amounts (range Cu = 0 - 6950 ppm) and has not been incorporated in models as it is unlikely to have been a significant component of the mineralising fluid.

## 11.3 Mineral deposition

Based on the interpretation of experimental Pb, Zn, Ag, Fe and Cu solubility data (Section 11.2), mechanisms likely to result in precipitation of sphalerite, pyrite, and galena include:

- For oxidised fluids, a reduction in the $fO_2$,
- drop in temperature,
- drop in pressure that may have promoted boiling and resulted in an increase in pH,

- decrease in the ligand concentration through dilution,
- increase in the content of dissolved reduced sulphur, and,
- changes in pH.

## 11.4 Hydrothermal modelling

Application of thermodynamic models to the interpretation of hydrothermal fluids and mineral deposits requires the following assumptions:

- the mineral paragenesis is known.
- physical and chemical attributes of the fluid are known, including; temperature, pressure, and the concentration of the chemical components, particularly $H^+$, $O_2$, $\Sigma S$, $\Sigma C$, $Na^+$, $Cl^-$, $Ca^{+2}$, and $K^+$, $Mg^{+2}$, and,
- equilibrium is attained between chemical species,
- thermodynamic data are reliable for the conditions being modelled,
- the speciation behaviour of the elements of interest are known,
- activity coefficients can be accurately estimated.

Equilibrium constants for the reactions listed in Appendix 11.1 were calculated using SUPCRT'92 (Johnson et al., 1992). Activity coefficients were calculated using the extended Debye-Huckel equation (Equation 1) and 'b' values of Helgeson (1969). 'A' and 'B' values are from Helgeson (1981) and å values for the specific ions are from Truesdell and Jones (1974).

$$-\log \gamma_i = ((Az_i^2\ I^{1/2}) \ /\ 1 + å_i\ BI^{1/2}) + bI \qquad \text{(Equation 11.1)}$$

Where $\gamma_i$ is the activity coefficient, z is the ionic charge, I is the ionic strength, A and B are temperature dependant constants, $å_i$ is the distance of closest approach for the specimen of interest, and b is the derivation function (varies between 0.03 and 0.05 up to 250°C, and is < 0.03 above 250°C)

The mineral paragenesis has been established in Chapter 5 and summarised in Figure 5.2. The physical and chemical attributes of the fluid have been constrained from fluid inclusion measurements, analyses of fluid inclusion decrepitates, carbon, oxygen and sulphur isotope analyses. Primary fluid inclusions have a range of trapping temperatures and salinities interpreted to have resulted from mixing between a higher salinity, lower temperature fluid (≈ 140°C and 27 wt.% NaCl equivalent) and a higher temperature, lower salinity fluid (≈ 180°C and 0 - 3 wt.% NaCl equivalent) with median trapping temperature of ≈ 154°C. An $fH_2$ ($fO_2$) versus pH diagram has been constructed for an assumed fluid composition of 25 wt.% NaCl equiv. and 150°C (Fig. 11.1). The molality of $Na^+$, $K^+$, $Cl^-$ and $Ca^+$ were calculated from fluid inclusion salinities and average K / Na and Ca / Na ratios of 0.041 and 0.155 respectively determined from analyses of fluid inclusion decrepitates (Table 9.5).

*Source of sulphur and concentration of the $\Sigma S$ content*

Interpretation of mixing between two fluids results in three possible sources of reduced sulphur:

- in-situ reduction of sulphate,
- reduced sulphur transported in a second fluid that locally mixed with the metal bearing fluid, and,
- reduced sulphur and the metals transported in the same fluid.

In-situ reduction of sulphate by biogenic or thermochemical means is not supported by interpretation of sulphur isotopes (Section 10.4.4.3). Mixing of a metal bearing fluid with a second fluid that contained reduced sulphur has been interpreted as a mechanism for the formation of some MVT deposits (Anderson, 1975; Beales, 1975; Sverjensky, 1981) and may have occurred at Menninnie Dam. Alternatively, reduced sulphur and chalcophile metals may have been transported in the same solution (Ruaya and Seward, 1986; Barrett and Anderson, 1988). Sulphur isotopes cannot be interpreted to distinguish between transportation of reduced sulphur in a second fluid, or co-transportation of sulphur and metals (Section 10.4.4.3). Co-transportation of metals and reduced sulphur is possible in a fluid with the physicochemical parameters interpreted for formation of the Menninnie Dam deposit (Ruaya and Seward, 1986; Barrett and Anderson, 1988), and is the simplest adequate explanation.

The $\Sigma S$ content of the fluid is unconstrained and has been estimated as 0.002 molal based on a review of the sulphur content of lower salinity terrestrial geothermal systems (eg. Wairakei) and high salinity terrestrial geothermal systems (eg. Salton Sea), sea-floor geothermal systems, Pb - Zn-bearing oil field brines, and Red Sea brines (Table 11.1).

Table 11.1. Total sulphur content of geothermal fluids.

| | $\Sigma S$ (molal) | Reference |
|---|---|---|
| Terrestrial geothermal systems | <0.00015 - 0.0067<br>typically 0.0005 - 0.003 | Hedenquist and Henley, 1985b; Krupp and Seward, 1987; Williams and McKibben, 1989. |
| Sea-floor geothermal systems | typically 0.004 - 0.009 | Von Damm, 1995. |
| Red Sea Brines (lower) | 0.01178 | Shanks and Bischoff, 1977. |
| Oil field brines | 0.00002 - 0.00578 | Kharaka et al., 1987; Carpenter et al., 1974; Sverjensky, 1984. |

Based on carbon and oxygen isotope modelling of fluid - rock interaction (Section 10.2.4.2), the molality of total carbon species ($\Sigma C$) was estimated as 0.01 and the dominant carbon bearing species in the fluid was interpreted to be $H_2CO_3$. The molality of $CO_2$ derived from isotopic modelling is a lower limit that encompasses all carbonate analyses (Figs. 10.3, 10.4). Most of the carbonates associated with mineralisation could have formed from a fluid with a higher $CO_2$ molality. An upper limit on the concentration of $CO_2$ can be

interpreted from fluid inclusion measurements. An immiscible $CO_2$ liquid phase was not observed in fluid inclusions at room temperature, although $CO_2$ clathrates were noted to have formed in a few fluid inclusions (Section 9.4).

The concentration of dissolved $CO_2$ may have been as high as 4.4 wt. % (1.026 molal for the fluid modelled in Figure 11.1) without formation of an immiscible $CO_2$ phase at room temperature (Hedenquist and Henley, 1985b). Low concentrations of $CO_2$ in geothermal fluids have been interpreted to result in formation of calc-silicate minerals rather than carbonates (Henley et al. 1984). Empirical observations of Wairakei and Broadlands geothermal systems, New Zealand, show that epidote and wairakite result from alteration of plagioclase at Wairakei (temp = 250°C, $CO_2$ = 0.01 molal), whereas chlorite and calcite result from alteration of plagioclase at Broadlands (temp = 260°C, $CO_2$ = 0.15 molal; Browne and Ellis, 1970; Henley et al. 1984). Although the temperature of the Menninnie Dam fluids are interpreted to have been too low for the formation of wairakite and epidote (Henley et al. 1984), low $CO_2$ concentrations may have favoured formation of Ca-bearing and zeolites such as laumontite, stilbite, heulandite and mordenite. Their absence, and the stability of carbonate minerals at Menninnie Dam is consistent with an estimated minimum $CO_2$ concentration of 0.01 molal.

## 11.5 Results and discussion

In this section the composition of the mineralising fluid is estimated, and the effects of variations in the concentration of dissolved sulphur are considered. Physical and chemical changes in the nature of the mineralising fluid that resulted in precipitation of sulphides, and how these may have affected the paragenesis of sphalerite and galena are considered. Based on interpretation of thermodynamic modelling, the paragenesis of sulphides and some gangue minerals in the Menninnie Dam deposit are reviewed.

### 11.5.1 Composition of the mineralising fluid

The stability fields for common iron oxides and sulphides, kaolinite, muscovite, K-feldspar, together with the solubility contours for dolomite, galena, sphalerite, and predominance fields for oxidised and reduced aqueous carbon and sulphur species are illustrated in Figure 11.1. The mineralogy of the galena - sphalerite stage at Menninnie Dam, and interpretation of carbon, oxygen and sulphur isotopes, can be used to constrain the log $fO_2$ and pH conditions of the mineralising fluid as follows:

- The carbonate replacement style of mineralisation constrains the fluid composition to the left and / or below the dolomite stability contours.
- Apart from trace amounts of hematite (<<1%), pyrite is the main iron-bearing mineral and constrains the fluids to the pyrite stability field.

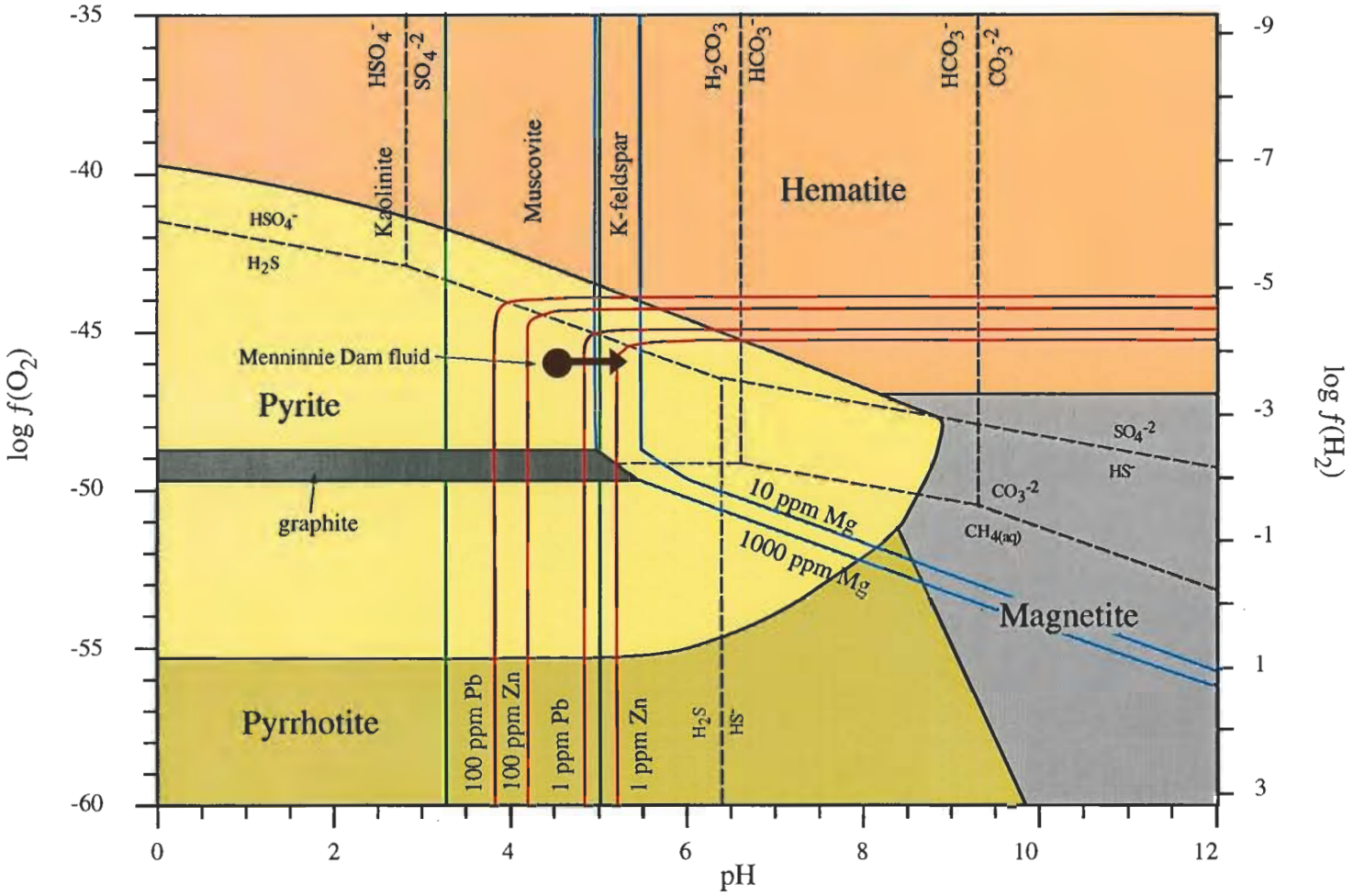


Fig. 11.1. Log $fO2$ - pH diagram for: temperature = 150°C, salinity = 25 wt.% NaCl equivalent, Na = 4.565 molal, K = 0.188 molal, Ca = 0.709 molal, Cl = 6.174 molal, $\Sigma S$ = 0.002 molal, $\Sigma C$ = 0.01 molal. The stability fields for Fe oxides, Fe sulphides, and graphite are shown as coloured fields. The stability field boundaries for K-feldspar, muscovite, and kaolinite are shown (vertical green lines). The 10 ppm, and 1000 ppm Mg solubility curves fluid in equilibrium with dolomite (blue lines). The predominance fields for aqueous carbon and sulphur-bearing species are delineated by dashed black lines. Solubility contours for 1 ppm and 100 ppm Pb and Zn in equilibrium with galena and sphalerite respectively are shown as red lines. The dark brown dot and arrow is the estimated composition and evolutionary trend of the mineralising fluid (ref. Appendix 11.1 for data used in calculations: Diagram calculated using an unpublished spreadsheet from Cooke et al., 1996:).

- Pre-existing microcline and adularia, formed during the latter stages of the early pyrite stage, were partially altered to sericite during the sphalerite - galena stage of mineralisation. The absence of kaolinite, presence of sericite, and partial dissolution of K-feldspar constrains the fluid to the muscovite stability field, probably close to the muscovite - K-feldspar boundary.
- The fluid is constrained to the $H_2CO_3$ predominance field above the graphite stability field based on interpretation of oxygen and carbon isotopes (Section 10.2.4.2), the absence of methane in fluid inclusions and the absence of hydrothermal graphite throughout the deposit.
- The absence of sulphate minerals and similar $\delta^{34}S$ values for different sulphide minerals was interpreted to have resulted from precipitation of sulphides from a $H_2S$-dominated fluid (Section 10.4.4.1) which constrains the fluid to the $H_2S$ predominance field.
- Barnes (1979) suggested that ore-forming solutions probably have a minimum Pb and Zn concentration of ≈ 10 ppm which is compatible with the levels of Pb and Zn in oil field brines (Kharaka et al., 1987; Carpenter et al., 1974), Red Sea brines (Shanks and Bischoff, 1977), Salton Sea geothermal field brines (Williams and McKibben, 1989) and sea floor geothermal vents (Von Damm, 1995). The solubility curves for 1 ppm and 100 ppm Pb and Zn are illustrated on Figure 11.1 and the initial Menninnie Dam mineralising fluid is interpreted to lie to the right (or above) the 1 ppm solubility contours for Pb and Zn.

When all of the constraints listed above are considered together, the mineralising fluid can be constrained to log $fO_2$ values between -44.5 and -48.5, and pH of 4.5 to 5.0 at 150°C. Trace amounts of hematite scattered throughout the sphalerite - galena stage of mineralisation are interpreted to indicate the mineralising fluid was probably near the higher $fO_2$ end of this 'window'. For the purposes of later calculations, the mineralising fluid is assumed to be pH = 4.6 and log $fO_2$ = -46, as shown by the brown spot on Figure 11.1.

### 11.5.2 Effects of variations in the ΣS content

The effect of changes in the concentration of reduced sulphur on the maximum solubility of lead and zinc for the Menninnie Dam-type fluid is illustrated in Figure 11.2. A molal concentration of 0.002 dissolved $H_2S$ (≈ 51.76 ppm) results in maximum solubilities of Zn and Pb of 14.86 ppm and 2.74 ppm respectively. At concentrations of $H_2S$ greater than 0.005 molal, the concentration of dissolved lead is less than 1 ppm which is lower than that interpreted to be necessary to form a significant lead deposit (Barnes, 1979). At $H_2S$ concentrations of less than 0.00117 molal, the maximum combined concentration of dissolved Pb and Zn (ie ≈ 25.47 ppm Zn and 4.71 ppm Pb) exceeds the concentration of dissolved $H_2S$ and some Pb and Zn will not be deposited.

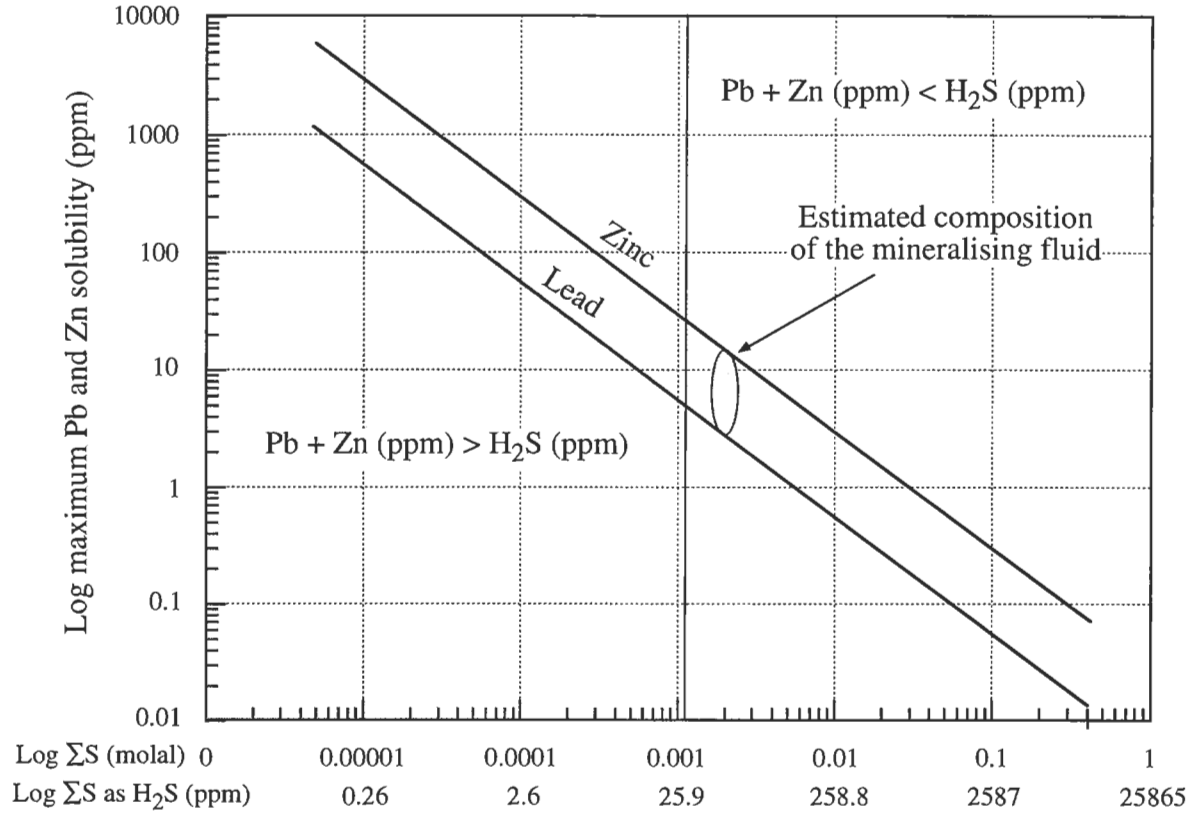


Fig. 11.2 Log maximum solubility of Pb and Zn versus log concentration of reduced sulphur for the mineralising fluid with 25wt.% NaCl equivalent, 150°C and log $fO_2$ = -46. The shaded area of the diagram corresponds to the field where the maximum solubility of Pb + Zn exceeds the concentration of reduced sulphur. Diagram calculated in the same manner as Fig. 11.1.

### 11.5.3 Deposition of sulphides at Menninnie Dam

Based on the assumed composition of the mineralising fluid (Figure 11.1) changes in $fO_2$ are not likely to have significant affect on sulphide deposition. Fluid inclusion measurements do not support decreases in temperature or pressure as mechanisms likely to have been important for deposition of sulphides at Menninnie Dam, and a temperature increase is interpreted based on fluid inclusion data (Section 9.6.3), through mixing of a Pb - Zn bearing fluid of ≈ 140°C and 27 wt.% NaCl equivalent with a fluid of ≈ 180°C and 0 - 3 wt.% NaCl equivalent.

The effect of a decrease in the ligand concentration (decrease in salinity) on the solubility of Pb and Zn for conditions applicable to Menninnie Dam has been evaluated by modelling fluid mixing of a 140°C and 27 wt.% NaCl equivalent brine with a 180°C and zero salinity heated water. The solubility of Pb and Zn have been calculated at 5°C intervals using the salinity, log K and $fO_2$ values listed in Appendix 11.1. Deposition of iron and copper sulphides occurred as minor amounts of FeS and chalcopyrite inclusions in sphalerite (Sections 5.2.3 and 5.5.2) and have not been included in calculations.

Results are illustrated in Figure 11.3 as solubility contours for 1, 10, and 100 ppm Pb and Zn in pH - temperature / salinity space. Also illustrated are the stability fields for K-feldspar, muscovite and kaolinite, and the estimated composition of the Menninnie Dam fluid. For conditions of gradual mixing, illustrated in Figure 11.3, a decrease in the ligand concentration through dilution is a possible depositional mechanism, although the interpreted fluid composition ('Path A'; Fig. 11.3), would have evolved at a shallow angle to the solubility contours for Pb and Zn. Catastrophic mixing would have resulted in rapid deposition and formation of finely crystalline sulphides, but is unlikely to have occurred as sphalerite crystals are locally up to 9 mm across (Fig 5.1c).

An increase in the content of dissolved reduced sulphur is not considered to be an important mechanism for sulphide deposition at Menninnie Dam. There is no significant local sulphur source in the host rocks and the only likely means of increasing the concentration of reduced sulphur would have been mixing of a metal-bearing fluid with a low reduced sulphur content with a second fluid that contained negligible dissolved metals but had a high reduced sulphur concentration.

If either a decrease in the ligand concentration, or an increase in the content of dissolved reduced sulphur was the *major* mechanism that resulted in sulphide precipitation, then mineralisation might be expected to occur in all rock types, however this is not the case and mineralisation is restricted to carbonate-bearing lithologies.

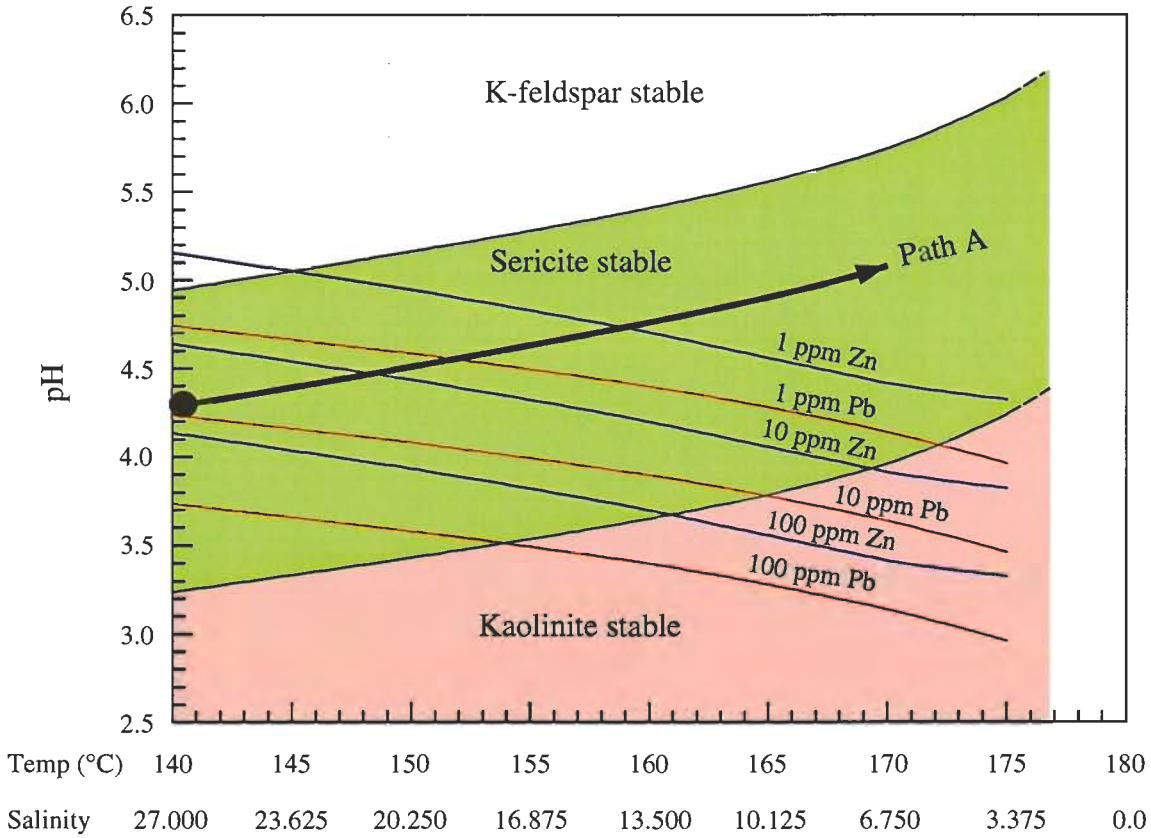


Fig. 11.3. Calculated solubility contours for Pb and Zn that would result from mixing of a 140°C, 27 wt.% NaCl equivalent fluid with a 180°C, 0 wt.% NaCl equivalent fluid. Also shown are the stability fields for kaolinite, muscovite and K-feldspar. The dark brown dot and arrow is the estimated composition of the Menninnie Dam mineralising fluid and the evolutionary path that would result from fluid mixing ('Path A').

An increase in pH at constant $fO_2$ is an effective mechanism for deposition of sulphides as the fluid composition would move at right angles to the Pb and Zn solubility contours illustrated in Figure 11.1. A increase in pH would be expected if a fluid of pH 4.6 encountered carbonate rock, illustrated by the following reactions;

$CaCO_3 + 2HCl \leftrightarrow CaCl_2 + H_2CO_{3(aq)}$ (Reaction 11.1)

$CaMg(CO_3)_2 + 4HCl \leftrightarrow CaCl_2 + MgCl_2 + 2H_2CO_3$ (Reaction 11.2)

The interpretation of an increase in pH as the *major* mechanism responsible for sulphide deposition is consistent with the carbonate replacement style of mineralisation (Section 5.2.3) and the rarity of mineralisation associated with other rock types.

### 11.5.4 Temporal zonation of Zn and Pb

Lead and zinc solubility contours for the conditions illustrated in Figure 11.1, show that Zn is consistently more soluble than Pb. The paragenetic relationship between sphalerite and galena precipitated from such a solution is dependant on the initial concentrations of Pb and Zn in solution, which will control which of the two minerals will reach saturation first (Barnes, 1979). For example; Huston and Large (1987) examined the Zn : Pb ratio (and 100Zn / Zn + Pb) of Cambrian massive sulphide deposits in western Tasmania, and concluded the Zn : Pb ratio was controlled more by the level of Zn and Pb saturation in the mineralising fluid than by the Zn and Pb content of the footwall volcanics or the process by which metals were leached from the source rocks. Deposits formed from fluids in which sphalerite reached saturation first might be expected to have a high Zn : Pb ratio.

The paragenetic sequence at Menninnie Dam shows that sphalerite 2 precipitated prior to galena 1, with intervening quartz 1 and Ca-Mn-Mg-Fe carbonate 1 (Fig. 5.2). The paragenesis is consistent throughout the northern and southern zones and cannot be attributed to 'zone refining', as has been suggested for some volcanic hosted massive sulphide deposits (Stanton, 1972; Braithwaite, 1974; Eldridge et al., 1983; Large, 1992). A Zn : Pb ratio of 5.6 : 1 is predicted from the solubility of Pb and Zn (both at saturation) in a fluid with 25 wt.% NaCl equivalent, 150°C and $\sum S = 0.002$ molal. However, the Zn : Pb ratio for the Menninnie Dam deposit is approximately 1.6 : 1 (Higgins et al. 1990). Given the consistent paragenesis of sphalerite precipitation followed by galena, the Pb : Zn ratio at Menninnie Dam cannot be adequately explained by variations in Zn and Pb concentration or variations due to mixing of a fluid at 140°C and with 27 wt.% NaCl with a fluid at 180°C and zero salinity (Fig. 11.3).

Possible explanations that may account for the Zn : Pb ratio and the paragenetic relationship of sphalerite and galena are:

- Dissolved lead was super saturated and did not attain equilibrium with galena during transport.
- The depositional mechanism was more efficient at depositing Pb than Zn and some of the Zn was lost from the system.
- An evolving fluid composition that was initially undersaturated in Pb and later undersaturated in Zn with $\Sigma S \geq \Sigma(Pb + Zn)$: or initially undersaturated in Pb with $\Sigma S < \Sigma(Zn + Pb)$ so that sulphur was consumed prior to galena saturation, and later solutions were saturated in Pb and because $\Sigma S < \Sigma(Pb + Zn)$, sulphur was consumed prior to sphalerite saturation.
- Low temperature kinetic effects may have favoured precipitation of sphalerite prior to galena.

The rate at which equilibrium is attained in low temperature solutions is not well known (eg. Ohmoto and Lasaga, 1982) and is beyond the scope of this study.

The possibility that some of the Zn may have been lost from the depositional site can be evaluated. Based on Figure 11.1, at log $fO_2 < -45.5$, the 1 ppm Pb solubility contour lies at pH = 4.82 whereas the 1 ppm Zn contour lies at pH = 5.20. The dolomite stability contour (for 1000 ppm Mg in solution) lies at pH 4.95 and if equilibrium was attained between the fluid and dolomite (with 1000 ppm dissolved Mg) the pH of the fluid would have remained near 4.95. At pH = 4.95, 3.12 ppm zinc and 0.58 ppm Pb could have remained in solution and possibly lost from the system. However, ignoring kinetic effects, the Zn : Pb ratio of precipitated sphalerite and galena would not be 1.6 if sphalerite was precipitated prior to galena.

Evolving oil field brine compositions have been proposed by Sverjensky (1984) and Burstein et al. (1993) to account for the common paragenesis of sphalerite prior to galena in many MVT deposits. An evolving fluid composition might relate to the concentration of Zn and Pb in the host rocks and the processes and rate by which trace amounts of Zn and Pb are leached from minerals such as biotite and K-feldspar (Hemley and Hunt, 1992; Graf, 1977; Cooke et al., in prep.). For example:

$$6nK^+ + 3Pb_nK_{1-2n}AlSi_3O_8 + 2H^+ \leftrightarrow KAl_3Si_3O_{10}(OH)_2 + 6SiO_2 + 3nPb^{+2} + 2K^+$$

(Pb in K-feldspar $\leftrightarrow$ muscovite + Pb; where $n \leq 0.5$)

$$n(Fe^{+2},Mg^{+2}) + KZn_n(Fe,Mg)_{3-n}AlSi_3O_{10}(OH)_2 \leftrightarrow K(Fe,Mg)_3AlSi_3O_{10}(OH)_2 + nZn^{+2}$$

(Zn in biotite $\leftrightarrow$ biotite + Zn; where $n \leq 1$)

Examination of the processes and rates (kinetic effects) at which Pb and Zn are leached from rock is not well known and beyond the scope of this study.

### 11.5.5 A review of the mineral paragenesis and fluid evolution

Using the fluid composition interpreted from thermodynamic modelling, the mechanisms responsible for the mineral paragenesis at Menninnie Dam can be postulated. The mineral paragenesis has previously been subdivided into three stages (Section 5.6.2):

- an early pyrite stage
- a sphalerite - galena stage, and,
- a late pyrite stage

The early pyrite stage resulted in dissolution of calcitic and dolomitic marbles due to the interaction with acid mineralising fluids. Both pH, and the $H_2CO_{3(aq)}$ component of the fluid would have increased through interaction of with carbonate rocks (Reactions 11.1 and 11.2, Section 11.5.3) and dependent on the concentration of Mg, Ca and $H_2CO_{3(aq)}$, equilibrium would have been attained with dolomite at ≈ pH 5.0 - 5.5. Dissolution of calcite may have continued to slightly higher pH and dolomite 1 may have been locally precipitated in zones of calcitic marble host rock. Minor amounts of talc, phlogopite and chlorite were locally precipitated. Although the controls on their precipitation have not been investigated, it is likely that increased $Mg^{+2}$ concentration due to dolomite dissolution favoured their precipitation (Kitto, 1994). As pH increased (Reactions 11.1 and 11.2, Section 11.5.3), pyrite would have reached saturation via the reactions:

$$FeCl^+ + 2H_2S_{(aq)} + 0.5O_{2(g)} \leftrightarrow Cl^- + 2H^+ + FeS_2 + H_2O$$

$$FeCl_2 + 2H_2S_{(aq)} + 0.5O_{2(g)} \leftrightarrow 2Cl^- + 2H^+ + FeS_2 + H_2O$$

Both of these reactions liberate protons and can locally lower the pH, which may account for local replacement of dolomite 1 by pyrite 1. As pyrite 1 was precipitated and pH increased through interaction with marble, K-feldspar became stable and adularia was precipitated.
The beginning of the sphalerite - galena stage is interpreted as a second pulse of Zn-rich, Pb-undersaturated fluid with pH ≈ 4.6 in which adularia was unstable and was partially altered to sericite:

$$3KAlSi_3O_8 + 2H^+ \leftrightarrow KAl_3Si_3O_{10}(OH)_2 + 6SiO_2 + 2K^+$$

As pH increased through fluid - marble interaction, sphalerite 1 and chalcopyrite 1 reached saturation and precipitated. As more fluid entered the system and pH was locally decreased, sphalerite 1 and chalcopyrite 1 underwent partial dissolution. An increase in pH due to fluid - marble interaction would promote saturation of Zn and formation of sphalerite 2 and chalcopyrite 2. As pH increased to ≈ pH 5.0 - 5.5, dissolved silica produced from the breakdown of diopside may have reached saturation and precipitated (Fournier, 1985). As

the pH increased through interaction of the fluid and the host marble, carbonate saturation was achieved leading to deposition of Ca-Mn-Mg-Fe carbonate 1. The fluid composition may have progressively evolved and the Pb : Zn ratio of the solution increased, Pb saturation was achieved leading to precipitation of galena. If the concentration of Pb in solution was close to 1 ppm, then it would not have attained saturation until the pH had increased to ≈ 4.8, and under such conditions, the rate of Ca-Mn-Mg-Fe carbonate 1 dissolution (if any) might be expected to be slow. As galena was precipitated and the pH increased, Ca-Mn-Mg-Fe carbonate 1 would have been stabilised and probably continued to precipitate. During galena precipitation, the concentration of dissolved sulphur may have dropped to the point where pyrite 1 started to dissolve, resulting in sulphide replacement textures.

The late pyrite stage is minor, and is interpreted to have resulted from a third fluid pulse that did not transport Pb or Zn but transported minor amounts of dissolved iron. Initiation of the late pyrite stage is marked by the appearance of sericite, indicative of a decrease in pH. Interaction of the fluids with the host marbles, and possibly Ca-Mn-Mg-Fe carbonate 1 would have resulted in an increase in pH, precipitation of pyrite 2, and Ca-Mn-Mg-Fe carbonate 2 as the pH increased above ≈ 5.0.

## 11.6 Conclusions

Based on interpretation of thermodynamic modelling, considerable concentrations of Pb and Zn can be transported in the low temperature (150°C) highly saline (≈ 6 molal), reduced sulphur-bearing brines inferred for the Menninnie Dam system. The chemical attributes of the mineralising fluid are predicted to have been: temperature ≈ 150°C, log $fO_2$ = -46, and pH = 4.6 based on thermodynamic modelling, and mineralogical, paragenetic, isotopic and fluid inclusion constraints. The molality of $\Sigma S$ and $\Sigma C$ chosen for construction of thermodynamic models are consistent with isotopic constraints, although the molality of $\Sigma C$ (0.01 molal) is considered to be a minimum value and the molality of $\Sigma S$ (0.002 molal) may be a maximum value. Dilution of the metal-bearing fluid by mixing with a low salinity but slightly hotter fluid was a possible depositional mechanism, however, the most effective depositional mechanism would have been an increase in pH due to fluid interaction with the host marbles which is consistent with the strata-bound nature of sulphides.

The three stages of mineralisation interpreted from petrographic observations are consistent with thermodynamic modelling, and are interpreted to have resulted from three pulses of fluid. The observations that sphalerite precipitated prior to galena, and that the Zn : Pb ratio of the deposit is 1.6 : 1 is problematic and is not easily explained by thermodynamic models. An evolving fluid composition, or low temperature kinetic effects, appear to be possible explanations.

# Chapter twelve
# Conclusions: A genetic model for the Menninnie Dam deposit and implications for exploration

## 12.1 Introduction

In this chapter, a genetic model for the Menninnie Dam Pb - Zn - Ag deposit is proposed, based on interpretation of the geological, geophysical, geochemical and isotopic constraints established in earlier chapters. This is followed by a comparison with features characteristic of igneous intrusion related carbonate replacement-style deposits. In the final section of this chapter, implications for exploration of similar Pb - Zn - Ag deposits in the Eyre Peninsula are discussed.

## 12.2 Genesis of the Menninnie Dam deposit

Pb - Zn - Ag mineralisation at Menninnie Dam is hosted by dolomitic and calcitic marbles, and diopside-rich calc-silicate lithologies (Fig. 3.1) which comprise the Katunga Dolomite, Lower Middleback Jaspilite, and lower units of the Cook Gap Schist of the Middleback Subgroup, a subdivision of the Lower Proterozoic Hutchison Group (≈ 1964 - 1845 Ma., Parker, 1993b; Fig. 2.3). Bedding in the Katunga Dolomite is not apparent, however, units of the Lower Middleback Jaspilite and Cook Gap Schist to the east strike NNE and have a steep westerly dip. The Katunga Dolomite is bound to the west by a north - south trending, steep easterly dipping shear zone (> 50m wide) that consists of protocataclasites, cataclasites and local mylonites, and caused juxtaposition of Cook Gap Schist against the lower part of the Katunga Dolomite (Fig. 3.2).

The Hutchison Group was metamorphosed to upper amphibolite facies (≈ 700°C and 7 kbars) during the early phases of the Kimban Orogeny (KM-$D_{1-2}$; 1843 - 1738 Ma., Mortimer et al., 1988; Fanning, 1987), followed by retrograde greenschist facies metamorphism (≈ 450 - 550°C and 1 - 2 kbars) during the final stage of the Kimban Orogeny (KM-$D_3$; 1740 - 1710 Ma., Parker, 1993a; Fanning, 1994; Fig. 3.9). The shear zone bounding the western margin of the Katunga Dolomite at Menninnie Dam was formed during KM-$D_3$, and is correlated with other major mylonite zones formed elsewhere in the Eyre Peninsula.

MD granite dykes were intruded into the shear zone, and to a lesser extent, into the Katunga Dolomite and Cook Gap Schist during KM-$D_3$. Deformation was then concentrated along the margins of MD granite dykes in response to 'reaction softening' due to hydrothermal alteration (White et al., 1980). Late tectonic pegmatite dykes were intruded into the Katunga Dolomite and Cook Gap Schist, where they produced localised, and more pervasive zones of metasomatic alteration, particularly in calcitic marbles near the base of the Cook Gap Schist.

At Menninnie Dam, the Katunga Dolomite and Lower Middleback Jaspilite contain minor magnetite, which produces a short wavelength, north-northeast trending magnetic high. Units to the east and west of the Menninnie Dam prospect are less magnetic, and are interpreted to mainly comprise Cook Gap Schist ± Yadnarie Schist ± Warrow Quartzite (Fig. 6.1). The Menninnie Dam magnetic feature lies on the north-western flank of a long wavelength, sub-circular, magnetic high of lower magnetic intensity, associated with a near-coincident, long wavelength, gravity low that results from a subsurface ≈ 20 km diameter Hiltaba Suite granite (MD granite) that intruded to within 3 km of the palaeosurface (Figs. 6.3 - 6.5 and 12.1a).

During intrusion of the MD granite an acidic, Na-Ca-K-Cl-rich metal -bearing magmatic brine was exsolved from the granite. Alternatively, circulating, heated meteoric water was mobilised, and may have leached metals and chlorine (and sulphur?) from the MD granite: oxygen isotopic exchange with the MD granite may then have produced the 'magmatic' isotopic signature. The role of mixed magmatic and meteoric waters, or meteoric waters alone, in formation of mineral deposits is a contentious issue that spans deposits types from MVT to porphyry coppers (Roedder, 1971; Sheppard et al. 1971; White, 1974; Cline and Vanko, 1995; Bajwah et al., 1995; Bodnar, 1995; Glig, 1995, Taylor et al., 1995; Walshe et al., in press). Resolution of this issue is beyond the scope of this study. Based on the available data, the metal-bearing brine interpreted for Menninnie Dam is assumed to have *exsolved* from the MD granite.

The magmatic brine extracted a significant proportion of lead (and by inference other metals) from the MD granite (Fig. 7.8) and ascended through Cook Gap schist towards the trap site, possibly within the shear zone that bounds the western margin of the Katunga Dolomite at the Menninnie Dam prospect. Reduced sulphur, with $\delta^{34}S$ values between 4 and 6‰, was dissolved in the magmatic brine ($\Sigma S$ = 0.002 molal; Fig. 11.1). Sulphur may have been derived from the MD granite or from hydration of disseminated pyrite within the shear zone ($\delta^{34}S_{shear\ zone}$ = 3.8 to 4.8‰) or surrounding country rock ($\delta^{34}S_{Cook\ Gap\ Schist}$ = 5.4 to 7.4‰; $\delta^{34}S_{Archaean\ basement}$ = 5.9 to 6.1‰; Figs. 10.10, 10.11). The magmatic brine probably leached metals, including lead, from the Cook Gap Schist. More radiogenic lead would be expected to have been leached more easily and may account for the mixing trend present in lead isotopes (Doe et al., 1972; Ludwig and Silver, 1977; Doe et al., 1979; Godwin et al., 1988).

Marbles units in the Katunga Dolomite were fundamental to the formation of the Menninnie Dam deposit, as they were the trap site for metal deposition. The magmatic brine traversed up to 3 km of Cook Gap Schist between the MD granite and the trap site. The rate of ascent and temperature of the host rocks would have contributed to the extent to which the brine cooled and attained an average temperature at the trap site of ≈ 140°C (Fig. 9.12).

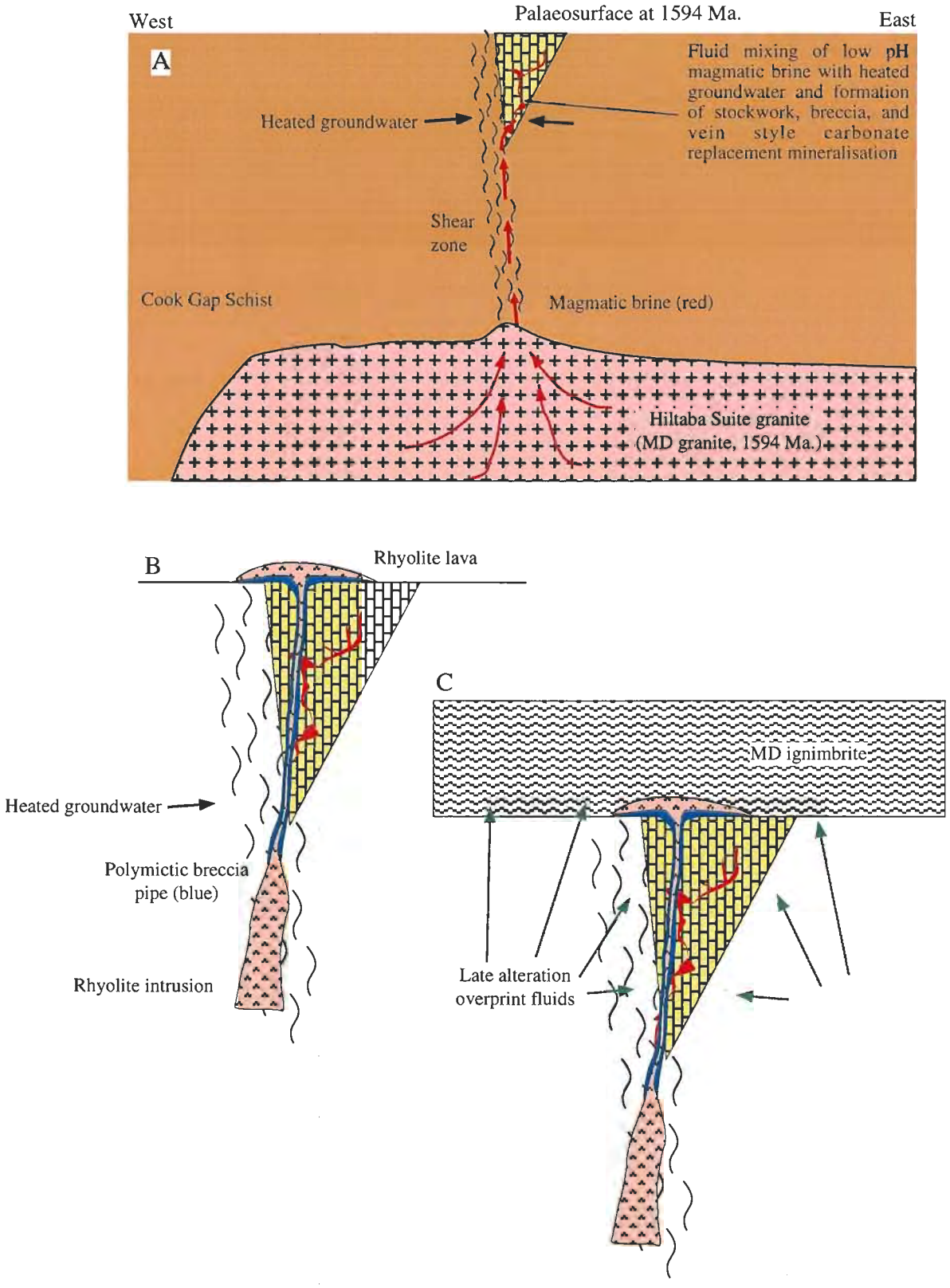


Fig. 12.1. Interpretative schematic model for the formation of the Menninnie Dam Pb - Zn - Ag deposit (not to scale). A: Intrusion of a Hiltaba Suite granite and exsolution of an acidic, magmatic brine that ascended and locally mixed with heated groundwaters within the Katunga Dolomite, and precipitated Pb - Zn - Ag carbonate replacement-style mineralisation. B: Rhyolite intruded dring the mineralising event and interacted with groundwater resulting in formation of polymictic breccia pipes. Rhyolite continued to intrude through the breccia pipe and locally erupted onto the palaeosurface forming a restricted flow or dome. C: Following cessation of the mineralising event, the MD ignimbrite was emplaced. After welding and cooling of the MD ignimbrite, circulation of heated groundwaters resulted in pervasive quartz - chlorite - carbonate calc-silicate alteration of the Hutchison Group, MD ignimbrite and polymictic breccias. Sulphide minerals were locally dissolved and reprecipitated by the late alteration overprint fluid.

At the site of sulphide deposition, the acidic brine (pH = 4.6 and ≈ 6 molal NaCl equivalent at 150°C) partially mixed with heated groundwater (≈ 180°C and near zero salinity). How groundwaters came to have a higher temperature than the magmatic brine is uncertain, and cannot be easily resolved from the data available. A possible explanation is that meteoric water was mobilised by an earlier, localised shallow-level intrusion derived from the MD granite. Both the magmatic brine and heated meteoric waters were subjected to lithostatic pressure and remained below the boiling point-depth curve, and those at greater depths generally had higher temperature (Fig. 9.11). Dilution through mixing with heated groundwater was a possible sulphide depositional mechanism, but less effective than the pH increase that resulted from dissolution of the host marbles (Figs. 11.1, 11.20).

Pb - Zn - Ag sulphide mineralisation occurs on a NNE trend over a 3 km strike length (Fig. 3.1). Sulphide and gangue minerals have replaced the marble and calc-silicate lithologies along a network of fractures and small faults (Figs. 5.1b - d). Marble dissolution resulted in formation of the central stockwork and breccia zone near the brine conduit, flanked by vein-style mineralisation to the north and south. Interaction between acidic brines and the host rock would have continually increased the size of fluid channelways, favouring ingress of heated meteoric fluids and resulting in local fluid mixing. Syn-mineralisation brittle faulting occurred and may have been important for permeability maintenance (Fig. 5.5e, f).

Sulphide and gangue minerals consist of a simple assemblage of pyrite, quartz, sphalerite, galena and Ca-Mn-Mg-Fe carbonate, together with minor chalcopyrite and chlorite, and trace amounts of adularia, sericite, fluorite, rhodonite, talc, phlogopite, dolomite, hematite and matildite. Primary sulphide textures are well preserved, and are consistent with sulphide and gangue deposition post-dating metamorphism, deformation and metasomatism. Three stages of hydrothermal activity are recognised to have occurred during the mineralising event (Fig. 5.2):

- an early pyrite stage,
- a sphalerite-galena stage, and
- a late pyrite stage

The onset of each stage was associated with dissolution of former minerals and / or deposition of sericite, indicative of acid fluids. Towards the end of each stage, adularia or carbonate was deposited, indicative of increased pH through interaction with the host marble. Plots of Pb, Zn, Cu, Ag, Au, Mn and Fe concentration versus northing have bell-shaped distributions (Fig. 5.25), and the highest metal concentrations correspond with the zone of stockwork and breccia mineralisation. Samples of vein style mineralisation to the north and south generally have lower metal concentrations. Lead isotope ratios have a similar spatial distribution, with the least radiogenic ratios associated with the zone of stockwork mineralisation, and more radiogenic ratios to the north and south (Fig. 7.9).

These distributions are consistent with a near-vertical fluid up-flow zone and deposition of most sulphide and gangue minerals proximal to the major fluid conduit.

The marble host rocks have a range of $\delta^{13}C$ and $\delta^{18}O$ values that incorporate values similar to those of modern marine carbonates; as well as lighter values that probably resulted from metamorphic and metasomatic processes (Fig. 10.2). The $\delta^{13}C$ and $\delta^{18}O$ host rock values are significantly heavier than those obtained form Ca-Mg-Mn-Fe carbonate associated with Pb - Zn -Ag mineralisation. The isotopic composition of Ca-Mg-Mn-Fe carbonate resulted from interaction between the mineralising fluid ($\delta^{13}C_{fluid}$ = -6.9‰; $\delta^{18}O_{fluid}$ = -2.0‰; $H_2CO_3$ -predominant), and the host rocks at temperatures between 125 and 200°C (Figs. 10.3, 10.4). Lower temperatures locally prevailed at host rock contacts, where $HCO_3^-$ may have been the predominant aqueous carbon-bearing species (Fig. 10.6). The carbon isotopic composition of the mineralising fluid is consistent with a magmatic carbon source. Based on analyses of talc, sericite, and phlogopite formed during the mineralising event at a temperature of ≈ 150°C, the mineralising fluid composition is calculated as $\delta D$ = -43 to -48 and $\delta^{18}O$ = 0.0 to -3.4‰, consistent with derivation from mixed magmatic and meteoric fluids (Fig. 10.8). Mineralised veins and breccia zones generally have sharp host rock contacts with a mineralogic and isotopic alteration halo that rarely extends for more than a few centimetres.

During the formation of the sphalerite-galena stage, and prior to the late pyrite stage, quartz- and feldspar-phyric rhyolite intruded the Hutchison Group in the southern part of the prospect (Figs. 3.1 and 12.1b). Rhyolites interacted explosively with (heated?) groundwaters contained in faults, resulting in fragmentation of the host rock and formation of fluidised polymictic breccia pipes (DP breccia). Some of the DP breccia pipes erupted onto the palaeosurface and formed near-vent facies polymictic breccia units (LP breccia) with local development of sub-horizontal layering, interpreted to have resulted from successive eruptions. Thinly bedded to thickly laminated muddy sandstone units were formed as a distal facies equivalent (Fig. 4.21).

Rhyolite intruded the DP breccia pipes, locally surrounding and incorporating domains of DP breccia, and forming peperite at the intrusion contacts. Some of the rhyolite intrusions erupted onto the palaeosurface through DP breccia vents and accumulations of LP breccia. Initial rhyolite ejecta was vesiculated, and formed mixed LP breccia and rhyolite pyroclasts in the near-vent facies, and pumice breccia units in more distal facies. The proportion of rhyolite pyroclasts increased with time, with a concurrent decrease in vesicularity and eventual eruption of coherent rhyolite, resulting in a restricted flow or dome (Fig. 4.21). DP breccia pipes and LP breccia units contain clasts of sulphide and gangue minerals that formed prior to the late pyrite stage of mineralisation. The matrix of DP breccias has been altered to an assemblage that includes minerals formed during the sphalerite-galena stage and the late

pyrite stage. U-Pb zircon dating of the rhyolite intrusions constrains the timing of granite emplacement and mineralisation to 1594 ± 7 Ma (Fig. 8.3). which is indistinguishable from that determined for the Hiltaba Suite granitoids and the co-magmatic Gawler Range Volcanics.

Soon after cessation of the mineralising event, the stratigraphy was mantled by a single cooling unit > 260m thick of lithic-rich welded ignimbrite (MD ignimbrite; Fig. 12.1c). Lithic clasts range in size from 2 mm to 20m diameter and comprise approximately 45% of the MD ignimbrite (Fig. 4.19). They are dispersed throughout the MD ignimbrite and are supported by densely welded juvenile pyroclasts. The thickness of the MD ignimbrite, abundance of lithic clasts, and shallow intrusion of a Hiltaba Suite granite are consistent with interpretation as an intracaldera ignimbrite. Emplacement of the MD ignimbrite probably occurred soon after eruption of rhyolite lava, resulting in preservation of unconsolidated LP breccia, muddy sandstone and pumice breccia units. Heat from the MD ignimbrite resulted in secondary welding of underlying pumice breccia units.

Some time after welding and cooling of the MD ignimbrite, the host rocks, mineralisation, LP breccia, and the basal 34 m of the MD ignimbrite in the southern zone of the Menninnie Dam deposit were partially altered to a texturally destructive chlorite - quartz - carbonate - calc-silicate hematite assemblage (late alteration overprint; 'LAO'; Fig. 12.1c). Existing Pb - Zn - Ag mineralisation was partially dissolved and re-deposited during this event, with no significant addition of Pb, Zn, Cu, Ag or sulphur. Fluid inclusions hosted by quartz 3 associated with the LAO have estimated trapping temperatures of 190 - 356°C and salinities between 0 - 5 wt.% NaCl equivalent, which is consistent with local formation of garnet. If the pressure correction applied to fluid inclusions associated with mineralisation is also applied to fluid inclusions associated with the LAO, the latter have similar trapping temperatures and salinities to the low salinity, higher temperature water that mixed with the metal-bearing brine, and an earlier phase of the LAO fluid may have been the heated groundwater involved in the mineralising event (Fig. 9.17).

The carbon isotopic composition of the LAO fluid ($\delta^{13}C_{fluid}$ = -1.4‰) is significantly heavier than that calculated for carbonate associated with Pb - Zn - Ag mineralisation. It is, however, similar to that of the host marbles ($\delta^{13}C$ = -0.5‰) and was probably inherited through fluid - rock interaction (Fig. 10.8). The $\delta D$ and $\delta^{18}O$ composition of the late alteration overprint fluid is indistinguishable from the isotopic composition determined for the mineralising fluid, and probably resulted from isotopic exchange with igneous rocks (Fig. 10.7).

The timing of the late alteration overprint is not known. It may be unrelated to the Pb - Zn - Ag mineralising event, or alternatively, it may be part of an evolving intrusion related system

as is commonly suggested for porphyry copper deposits (Lowell and Gilbert, 1970, Drummond and Godwin, 1976; Titley, 1982; Beane, 1982).

In summary, the Menninnie Dam Pb - Zn - Ag deposit is interpreted to be a carbonate replacement style of mineralisation genetically and temporally related to intrusion of a Hiltaba Suite granite at $\approx 1594 \pm 7$.

## 12.3 Comparison to other deposits carbonate hosted Pb - Zn - Ag deposits

Carbonate replacement Pb - Zn - Ag deposits interpreted to be genetically related to igneous intrusions have been referred to as distal skarns (Einaudi, 1981), manto and chimney deposits (Prescott, 1916, 1926; Beaty et al, 1990b) and high temperature carbonate replacement deposits (Titley 1993), and are well documented in the literature (eg. Emmons et al., 1927; Sawkins, 1964; Stacey et al., 1967; Atkinson and Einaudi, 1978; Erwood et al. 1979; Meinert, 1982; Sasaki et al., 1984; McLeroy et al., 1986; Megaw et al., 1988; Kalogeropoulos et al., 1989; Schneider and Toloza, 1990; Beaty et al., (eds.), 1990; Titley, 1990, 1993). Titley (1993) described the characteristics of high-temperature carbonate hosted massive sulphide ores in the United States, Mexico and Peru and emphasised the diversity of deposits. Some of the 'deposit-type' characteristics include:

- Most deposits lie above cratonic basement.
- Most deposits occur within basins, whereas MVT deposits commonly occur around basin margins.
- Deposits have an epigenetic relationship to the host carbonates, which comprise calcitic or dolomitic limestones or marbles.
- Mineralisation is strata-bound, and locally stratiform.
- Mineralisation is proximal to, and of similar age, to igneous intrusions.
- Mineralisation is not associated with a distinctive igneous rock type.
- Deposits vary widely in size, from a few hundred thousand tonnes to 37 million tonnes of ore at Santa Eulalia, Mexico.
- Mineralisation consists of various combinations of stockwork, vein and breccia styles.
- Mineralisation has knife-sharp sulphide - wall-rock contacts.
- The location of mineralised bodies is commonly structurally controlled.
- Ores are commonly massive and may be compositionally zoned on a deposit scale.
- Ores textures consist of compact masses, open space fill textures, compositionally zoned masses, and fragmental and brecciated textures.
- Ores generally comprise > 50% sulphides.
- Ores are pyritic, and contain lead and silver ± zinc with minor to significant copper and gold.

- Ag concentrations are generally > 50 ppm. The United States, Mexican, and Peruvian deposits listed by Titley (1993) have a mean Ag content of 197 ppm, whereas the mean for MVT deposits is 4.7 ppm.
- Deposits that occur high above basement in thick carbonate sequences are generally Pb- and Ag-rich.
- The alteration assemblage is generally devoid of calc-silicate minerals, and silicification is more common. Some deposits locally contain skarn minerals and deposits and were considered to be "*one end of a spectrum of carbonate-altered ores whose other pole is characterised by skarn-localised ores*" (Titley, 1993).
- A basement source for some of the lead is interpreted from isotope studies.
- Gangue minerals commonly comprise carbonate, silica, silicate minerals and locally fluorite.
- Ag is ubiquitous, Sn and W occur in some deposits and Mn is common.
- Mn-Fe-Mg-Ca carbonates occur in many deposits, locally in more distal regions.
- Magmatic fluids may be involved in base and precious metal deposition, although mixed fluid sources are invoked for some deposits.
- Fluids are commonly acidic, and in equilibrium with sericite or kaolinite.
- Sulphide deposition temperatures are generally in excess of 200°C

Megaw et al. (1988) provided a more detailed overview of Mexican high-temperature carbonate replacement deposits. They noted that many deposits have a range of fluid inclusion trapping temperatures (typically 200 to > 300°C) and salinities (typically 1 to > 25 wt.% NaCl equivalent), interpreted to have resulted from mixing between magmatic and meteoric fluids.

The Menninnie Dam Pb - Zn - Ag deposit has many features similar to high temperature carbonate replacement deposits. One of the few variants is that the temperature of the fluid from which most the Menninnie Dam mineralisation was precipitated is generally lower, and the Menninnie Dam deposit cannot be labelled 'high-temperature'. Temperatures of up to 240°C are interpreted from some of the Menninnie Dam fluid inclusions, and as previously suggested, temperatures appear to increase with depth. The lower precipitation temperature interpreted for the Menninnie Dam deposit may relate to the near-surface setting of mineralisation, and possibly from the greater distance from the heat source.

## 12.4 Implications for exploration of Pb - Zn - Ag deposits on the Eyre Peninsula of South Australia

The Menninnie Dam deposit is the most significant discovery of Pb - Zn - Ag mineralisation on the Eyre Peninsula of South Australia, and has previously been documented as a Broken Hill-type deposit. Based on the data presented in this thesis, the perceived potential for future discoveries of Broken Hill-type mineralisation on the Eyre Peninsula is down-graded.

However, recognition of the Menninnie Dam deposit as a carbonate-hosted replacement deposit associated with a Hiltaba Suite granite has significance for base metal explorers.

High-temperature carbonate-hosted Pb - Zn - Ag deposits commonly occur in carbonate host rocks adjacent to igneous centres. In most instances, Pb - Zn - Ag mineralisation has been interpreted as coeval with emplacement of felsic to intermediate intrusives or temporally related to volcanism and / or caldera collapse. High-temperature carbonate replacement deposits form an outer halo to porphyry copper style mineralisation at Bingham, Utah and Bisbee, Arizona (Atkinson and Einaudi, 1978; Bryant and Metz, 1966). The deposits at Leadville, Colorado, occur around the Breece Hill Stock which contains highly anomalous Cu (Beaty et al., 1990), although Thompson and Beaty (1990) suggested the Breece Hill Stock is significantly older than the spatially associated Pb - Zn - Ag mineralisation. Many of the Mexican deposits are mineralogically zoned, with increased copper and gold contents at depth. Some are associated with copper-rich skarns adjacent to intrusions of the same age (Megaw et al., 1988).

The key geological criteria recognised for Pb - Zn - Ag mineralisation at Menninnie Dam is the coincidence of several parameters:

- The presence of a Hiltaba Suite granite intruded to shallow crustal level.
- Presence of reactive carbonate rocks adjacent to the fluid conduit.
- Brittle structures in the marble which were important for fluid flow at the deposit scale.

Given the paucity of outcrop over much of the Eyre Peninsula and the depth of weathering (commonly > 50m), geophysical and geochemical exploration techniques are likely to be significant for base metal exploration. Many of the Hiltaba Suite granitoids have strong magnetic signatures and coincident gravity lows. Carbonate rocks of the Middleback Subgroup strike approximately north - south, and commonly contain magnetite, or lie stratigraphically above or below magnetic iron formations. Some of the attributes that may hamper successful exploration for high-temperature carbonate-hosted Pb - Zn - Ag deposits on the Eyre Peninsula are the common absence of magnetic ore or gangue minerals, the sharp contacts between mineralisation and the host carbonates, and the common absence of a geochemical or isotopic alteration halo. The irregular shape of many high-temperature carbonate replacement ore 'lenses' could result in difficult (and potentially small) drill targets. The shallow level of formation interpreted for the Menninnie Dam deposit (< 600 m) should be taken into account when considering the potential for porphyry copper (or copper-gold), or skarn-type mineralisation. It is worth noting that the Hiltaba Suite granites are exposed at varied levels of emplacement across the Eyre Peninsula. It is therefore possible that the right combination of a mineralised intrusion, emplaced at an appropriate depth and subjected to an appropriate level of erosion may exist.

The potential for other styles of mineralisation should be borne in mind. In many eroded caldera settings, base and precious metal veins are economically important, such as those associated with caldera forming cycles of the Tertiary Silverton, San Juan, Lake City, Uncompahgre and Creede Calderas and rhyolite intrusions in the Western San Juan mountains, Colorado (Bartos, 1993; Hayba et al., 1985).

In summary, although Menninnie Dam-style mineralisation may prove a challenging exploration target, its importance lies in that it is the first significant discovery of Pb - Zn - Ag mineralisation associated with the Hiltaba Suite.

# References


Allen, R.L., 1988. False pyroclastic textures in altered silicic lavas, with implications for volcanic-associated mineralisation. *Economic Geology*, v. **83**, p. 1424-1446.

Anderson, G.M., 1973. The hydrothermal transport and deposition of galena and sphalerite near 100°C. *Economic Geology*, v. **68**, p. 480-492.

Anderson, G.M., 1975. Precipitation of Mississippi Valley-type ores. *Economic Geology*, v. **70**, p. 937-942.

Anderson, J.E. Jr., 1969. Development of a snowflake texture in a welded tuff, Davis Mountains, Texas. *Geological Society of America Bulletin*, v. **80**, p. 2075-2080.

Andrew, A., 1992. Unpublished sulphur isotope data. Division of Exploration Geoscience, CSIRO, North Ryde, NSW.

Atkinson W.W. Jr., and Einaudi M.T., 1978. Skarn formation and Mineralisation in the Contact Aureole at Carr Fork, Bingham, Utah. *Economic Geology*, v. **73,** p. 1326-1365

Baes, C.F., Jr., and Mesmer, R.E., 1976. *The hydrolysis of cations,* New York: Wiley.

Baker, A.J., and Fallick, A.E., 1989. Evidence from Lewisian limestones for isotopically heavy carbon in two-thousand-million-year-old sea water. *Nature*, v. **337**, p. 352-354.

Baker, E.M., 1987. Brecciation, mineralisation and alteration of the Kidston gold deposit. In: Brennan, E. (convenor), *Pacific Rim Congress 87; an international congress on the geology, structure, mineralisation and economics of the Pacific Rim.*, Australasian Institute Mining and Metallurgy, p. 29-33.

Baker, E.M., 1988. The Kidston gold deposit. In: Morrison, G.W. (ed.), *Epithermal and porphyry style gold deposits in North Queensland*, Contributions of the Economic Geology Research Unit, James Cook University of North Queensland, Australia. v. **29**, p. 61-74.

Baker, E.M., Kirwin, D.J., and Taylor, R.G., 1986. Hydrothermal breccia pipes. *Contributions of the Economic Geology Research Unit.* James Cook University of North Queensland, Australia, v. **12**, 45p.

Ballance, P.F., 1984. Sheet-flow - dominated gravel fans of the non-marine middle Cenozoic Simmler Formation, central California. *Sedimentary Geology*, v. **38**, p. 337-359

Barnes, H.L., 1979. Solubilities of ore minerals. In Barnes, H.L., (ed.) *Geochemistry of hydrothermal ore deposits*, (second edition). John Wiley and Sons, New York, p. 404-460.

Barrett T.J., and Anderson, G.M., 1982. The solubility of sphalerite and galena in NaCl brines. *Economic Geology*, v. **77**, p. 1923-1933.

Barrett, T.J., and Anderson, G.M., 1988. The solubility of sphalerite and galena in 1 - 5 m NaCl solutions to 300°C. *Geochimica et Cosmochimica Acta,* v. **52**, p. 813-820.

Barton, P.B. Jr. 1978. Some ore textures involving sphalerite from the Furutobe Mine, Akita Prefecture, Japan. *Mining Geology*; v. **28**, p. 293-300.

Barton, P.B. Jr., and Bethke, P.M., 1987. Chalcopyrite disease in sphalerite: Pathology and epidemiology. *American Mineralogist*, v. **72**, p. 451-467.

Bateman, P.C. and Chappell, B.W., 1979. Crystallisation fractionation and solidification of the Toulumne intrusive series, CA. *Geological Society America Bulletin*, v. **90**, p . 465-482.

Beach, A., 1980. Retrogressive metamorphic processes in shear zones with special reference to the Lewisian complex. *Journal of Structural Geology*, v. **2**, p. 257-263.

Beales, F.W., 1975. Precipitation mechanisms for Mississippi Valley-type deposits. *Economic Geology*, v. **70**, p. 943-948

Beane, R.E., and Titley, S.R., 1981. Porphyry copper deposits. Part II. Hydrothermal alteration and mineralisation. In Skinner, B.J., (ed.) Seventy fifth anniversary volume, *Economic Geology monograph*, p. 235-269.

Beaty, D.W., and Landis, G.P., 1990. Part IV. Stable isotope geochemistry. In: Beaty, D.W. (ed.), Origin of the ore deposits at Gilman, Colorado. *Economic Geology, Monograph* **7**, p. 193-265.

Beaty, D.W., and Merchant, J.S., 1990. Origin of the ore deposits at Gilman, Part I. Introduction. In: Beaty, D.W., Landis, G.P., Thompson, T.B., Carbonate-hosted sulphide deposits of the Colorado mineral belt. *Economic Geology, Monograph* **7**, p. 198-202.

Beeson, R., 1990a. Broken Hill-type lead-zinc Deposits - an overview of their occurrence and geological setting. *Transactions Australian Institute of Mining and Metallurgy,* v. **99**, p. B163-B175.

Beeson, R., 1990b. 'The geochemical environment of the Wilcherry Hill base metal Mineralisation, South Australia': *Mineral Deposita* , v. **25**, p. 179-189.

Belkin, H.E., Cavarretta, G., De Vito, B., Tecce, F., 1988. Hydrothermal phlogopite and anhydrite from the SH2 well, Sabatini volcanic district, Latium, Italy: Fluid inclusion and mineral chemistry. *American Mineralogist*, v. **73**, p. 775-797.

Belperio, A.P., and Flint, R.B., 1993. The southeastern margin of the Gawler Craton. *Australian Journal of Earth Sciences*, v. **40**, p. 423-426.

Bente, K. and Doering, T., 1993. Solid-state diffusion in sphalerites: an experimental verification of the "chalcopyrite disease". *European Journal of Mineralogy*, v. **5**, p. 465-478.

Berman, R.G., 1990. Mixing properties of Ca-Mg-Fe-Mn garnets. *American Mineralogist*, v. **75**, p. 328-344.

Bethke, P.M., and Rye, R.O., 1979. Environment of ore deposition in the Creede Mining District, San Juan Mountains, Colorado: Part IV. Source of fluids from oxygen, hydrogen, and carbon isotope studies. *Economic Geology*, v. **74**, p. 1832-1851.

Bierwirth, P.N., 1982. Experimental welding of volcanic ash. Monash University, Victoria, Australia. B.Sc. Hons. thesis (unpublished).

Bird, M.I., Andrew, A.S., Chivas, A.R., and Lock, D.E., 1989. An isotopic study of surficial alunite in Australia: 1. Hydrogen and sulphur isotopes. *Geochemica et Cosmochemica Acta,* v. **53**, p. 3223-3237.

Blatt, H., Middelton, G. and Murray, R. C., 1980. *Origin of sedimentary rocks.* Prentice-Hall, Englewood Cliffs, New Jersey, U.S.A.

Blissett, A.H. and Radke, F., 1980. The Gawler Range Volcanics - a regional review. *Journal of the Geological Society of Australia,* v. **27**, p 51.

Blissett, A.H., 1975. Rock units of the Gawler Range Volcanics, South Australia. *Quarterly Geological Notes,* South Australia Geological Survey, v. **55**, p. 2-14

Blissett, A.H., 1985. *Gairdner, South Australia*, South Australia Geological Survey, 1:250,000 series - Explanatory notes , sheet SH53-15.

Blissett, A.H., 1986. Subdivision of the Gawler Range Volcanics in the Gawler ranges. South Australia Geological Survey. *Quarterly Geological Notes*, v. **97**, p. 2-11.

Blissett, A.H., Creaser, R.A., Daly, S.J., Flint, R.B., and Parker, A.J. Gawler Range Volcanics. In: Drexel, J.F., Preiss, W.V., and Parker, A.J., (eds), 1993, The geology of South Australia. v. 1, The Precambrian. *South Australian Geological Survey Bulletin,* v. **54**, p. 107-124.

Blissett, A.H., Parker, A.J., and Crooks, A.F., 1988. *Yardea map sheet.* 1:250,000 Geological Series. South Australian Department of Mines and Energy.

Bodnar, R.J., and Bethke, P.M., 1984. Systematics of stretching of fluid inclusions 1: Fluorite and sphalerite at 1 atmosphere confining pressure. *Economic Geology*, v. **79**, p. 141-161.

Bodnar, R.J., and Sterner, S.M., 1985. Applications of synthetic fluid inclusions in experimental geochemistry and petrology. In: Barnes, H.L., and Ulmer, G.C., (eds.).*Hydrothermal Experimental Techniques,* Wiley, New York.

Bodnar, R.J., Sterner, S.M., and Hall, D.L., 1989. Salty: A FORTRAN program to calculate compositions of fluid inclusions in the system NaCl - KCl - $H_2O$: *Computers and Geoscience*, v.**15**, p. 19-41.

Borisenko, A.S., 1977. Study of the salt composition of gas-liquid inclusions in minerals by the cryometric system. *Geologiya i Geofizika*, v. **18**, p. 16-27

Bortnikov, N.S., Genkin, A.D., Dobrovol'skaya, M.G., Muravitskaya, G.N. and Filimonova, A.A., 1991. The nature of chalcopyrite inclusions in sphalerite: exsolution, coprecipitation, or "disease"?. *Economic Geology*, v. **86**, p. 1070-1082.

Bottinga, Y., and Javoy, M., 1973. Comments on oxygen isotope geothermometry. *Earth and Planetary Science Letters*, v. **20**, p. 250-265.

Bourcier, W.L., and Barnes, H.L., 1987. Ore solution chemistry - VII. Stabilities of chloride and bisulphide complexes of zinc to 350°C. *Economic Geology*, v. **82**, p. 1839-1863.

Bozzo, A.T., Chen, H-S., Kass. J.R. and Barduhn, A.J., 1975. The properties of hydrates of chlorine and carbon dioxide. *Desalination*, v. **16**, p. 303-320.

Bradbury, J., 1988. The volcanic and shallow sub-volcanic component of the breccia hosted Olympic Dam U-Cu-Au deposit: implications for breccia pipe development. Monash University BSc. Hons thesis (unpublished), .

Bradley, G.M., 1980. Metamorphism of the Archean and Proterozoic basement at southern Eyre Peninsula, South Australia. *Journal of the Geological Society of Australia*, v. **27**, p. 50.

Braithwaite, R.L., 1974. The geology and origin of the Rosebery ore deposit, Tasmania. *Economic Geology*, v. **69**, p. 1086-1101.

Branch, C.D., 1978. Evolution of the Middle Proterozoic Chandabooka Caldera, Gawler Range acid volcano-plutonic province, South Australia. *Journal of the Geological Society of Australia*, v. **25**, p. 199-216.

Branney, M.J., and Kokelaar, B.P., 1992. A reappraisal of ignimbrite emplacement: progressive aggradation and changes from particulate to non-particulate flow during emplacement of high-grade ignimbrite. *Bulletin of Volcanology*, v. **54**, p. 504-520.

Branney, M.J., and Suthren, R.J., 1988. High-level peperitic sills in the English Lake District: Distinction from block lavas, and implications for Borrowdale Volcanic Group stratigraphy. *Geological Journal*, v. **23**, p. 171-187.

Branney, M.J., Kokelaar, B.P., and McConnell, B.J., 1992. The Bad Step Tuff: a lava-like rheomorphic ignimbrite in a calc-alkaline piecemeal caldera, English lake district. *Bulletin of Volcanology*, v. **53**, p. 187-199.

Brewster, G.W., 1980. Effect of chemical pretreatment on X-ray powder diffraction characteristics of clay minerals derived from volcanic ash. *Clays and Clay Minerals*, v. **28**, p. 303-310.

Brimhall, G.H., and Crerar, D.A., 1987. Ore fluids: magmatic to supergene. In: Carmichael, I.S.E. and Eugster, H.P., (eds.), Thermodynamic modelling of geological materials: Minerals, fluids and melts. Mineralogical Society of America, *Reviews in Mineralogy*, v.**17**, p. 235-322.

Brindley, G.W., and Brown, G., (eds.) 1980. Crystal structures of clay minerals and their X-ray identification. *Mineralogical Society Monograph,* **5**.

Brooks, E.R., 1995. Paleozoic fluidisation, folding, and peperite formation, northern Sierra Nevada, California. *Canadian Journal of Earth Science*, v. **32**, p. 314-324.

Brown, W.L., Macaudiere, J. and Ohnenstetter, M., 1980. Ductile shear zones in a meta-anorthosite from Harris, Scotland: textural and compositional changes in plagioclase. *Journal of Structural Geology*, **2**, p. 281-287.

Browne, P.R.L., and Ellis A.J., 1970. The Ohaki-Broadlands hydrothermal area, New Zealand; mineralogy and related geochemistry. *American Journal of Science,* v. **269** p. 97-131

Burnham, C.W., 1979. Magmas and hydrothermal fluids. In: Barnes, H.L., (ed.) *Geochemistry of hydrothermal ore deposits*. Second edition. New York: Wiley. p. 71-136.

Burnham, C.W., 1985. Energy release in Subvolcanic Environments: Implications for Breccia Formation, *Economic Geology,* v. **80:6**, p. 1515-1522.

Burstein, I.B., Shelton, K.L. Gregg, J.M. and Hagni, R.D., 1993. Complex, multiple ore fluids in the world class Southeast Missouri Pb - Zn - Cu deposits: Sulphur isotope evidence. In: Shelton, K.L. and Hagni, R.D., *Geology and geochemistry of Mississippi Valley-type ore deposits: Proceedings volume,* 27th annual meeting of the North-Central Section, Geological Society of America, University of Missouri-Rolla, Missouri.

Busby-Spera, C.J., and White, J.D.L., 1987. Variation in peperite textures associated with differing host-sediment properties. *Bulletin of Volcanology*, v. **49**, p. 765-775.

Campbell, E.M., and Twidale, C.R., 1991. The Gawler Ranges, South Australia: An unusual volcanic massif. *Australian Geographer* v. **22**(1) p.24-33.

Carpenter, A.B., Trout, M.L., and Pickett, E.E., 1974. Preliminary report on the origin and chemical evolution of lead- and zinc-rich oil field brines in Central Mississippi. *Economic Geology*, v. **69**, p. 1191-1206.

Carr, G.R. and Dean, J.A., 1990. Report to Aberfoyle Resources Ltd on the Pb isotopic compositions of samples from Menninnie Dam and the Gawler Range Volcanics, South Australia. *SIROTOPE report No.* **SR135.**

Carr, G.R., and Dean, J.A., 1991. Report to Aberfoyle Resources Limited on a Pb isotopic assessment of drill core samples from Menninnie Dam. SIROTOPE report No. SR155, (unpublished).

Carr, G.R., Gulson, B.L., and Dean, J.A., 1986. Report to Billiton Australia Pty. Ltd. on the significance of Lead isotopic compositions of samples from Menninnie Dam, South Australia. *SIROTOPE report No.* **SR028.**

Cas, R.A.F. and Wright, J.V., 1987. *Volcanic Successions modern and ancient.*. Chapman and Hall, London.

Cavarretta, G., Gianelli, G., Scandiffio, G., and Tecce, F., 1985. Evolution of the latera geothermal system 11: Metamorphic, hydrothermal mineral assemblages and fluid chemistry. *Journal of Volcanology and Geothermal Research*, v. **26**, p. 337-364.

Cerny, P., 1991a. Fertile granites of Precambrian rare-element pegmatite fields: is geochemistry controlled by tectonic setting or source lithologies? *Precambrian Research*, v. **51**, p. 429-468.

Cerny, P., 1991b. Rare-element granitic pegmatites. Part 1: anatomy and internal evolution of pegmatite deposits. *Geoscience Canada*, v. **18**, p. 49-67.

Christiansen, R.L., and Lipman, P.W., 1966. Emplacement and thermal history of a rhyolite lave flow near Fortymile Canyon, southern Nevada. *Geological Society of America Bulletin*, v. **77**, p. 671-684.

Circosta, G., and Gum, J., 1988. Geological investigation Mining Leases 5342 and 5361 Earea Dam, South Australia. South Australia Department of Mines and Energy, Open file envelope, **8062:79-133** (unpublished).

Clark, B.R., and Kelly, W.C., 1973. Sulphide deformation studies: I. Experimental deformation of pyrrhotite and sphalerite to 2000 bars and 500°C. *Economic Geology*, v. **68**, p. 332-352.

Clayton, R.N., and Mayeda, T.K., 1963. The use of pentaflouride in the extraction of oxygen from oxides and silicates for isotopic analysis. *Geochemica et Cosmochimica Acta*, v. **27**, p. 1296-1314.

Clynne, M.A., and Potter, R.W. II, 1977. Freezing point depression of synthetic brines. *Geological Society of America Abstracts with Programs*, v. **9**, p. 930

Cole, D.R., 1985. A preliminary evaluation of oxygen isotopic exchange between chlorite and water. *Geological Society of America Abstracts with Programs,* v. **17**, p. 550.

Collins, P.L.F., 1979. Gas hydrates in CO2-bearing fluid inclusions and the use of freezing data for the estimation of salinity. *Economic Geology*, v. **74**, p. 1435-1444.

Compston, W, Williams, I.S., and Meyer, C., 1984. U-Pb geochronology of zircons from lunar breccia 73217 using a sensitive high-resolution ion-microprobe. Proc., 14th Lunar Sci. Conf., *Journal of Geophysical Research.*, v. **89**, **B**, p. 525-534.

Compston, W., Kinny, P.D., Williams, I.S., and Foster, J., 1986. The age and Pb loss behaviour of zircons from the Isua supracrustal belt as determined by ion-microprobe. *Earth Planetary Science. Letters* v. **80**, p.71-81.

Compston, W., Williams, I.S., Kirschvink, J.L., Zhang Zichao., and Guogan, M.A., 1992. Zircon U-Pb ages for the Early Cambrian time-scale. *Journal of the Geological Society London*, v. **149**, p. 171-184.

Cooke, D.R., Bull, S.W., Donovan, S., and Rogers, J.R. K-metasomatism and base metal depletion in the Settlement Creek and Gold Creek Volcanics, McArthur Basin, Northern Territory - implications for base metal mineralisation. (in press, *Economic Geology*).

Coplen, T.B., Kendall, C., and Hopple, J., 1983. Comparison of stable isotope reference samples. *Nature*, v. **302**, p. 236-238.

Corbett, D., 1987. *Geology and scenery of South Australia,* Wakefield.

Cowan, D., 1990. Untitled petrological report No. DCA 90/10/2. David Cowan and Associates Pty. Ltd.

Cowley, W., and Fanning, C.M., 1991. Low-grade Archaean metavolcanics in the northern Gawler Craton. *Quarterly Geological Notes of the Geological Survey of South Australia*, v. **119**, p. 2-17.

Cowley, W.M., 1993. Cariewerloo Basin: Pandurra Formation. In: Drexel, J.F., Preiss, W.V., and Parker, A.J., (eds).The geology of South Australia. v. 1, The Precambrian. *South Australia Geological Survey Bulletin*, v. **54**, p139-142.

Cowley, W.M., and Flint, R.B., 1993. Gairdner Dyke Swarm. In: Drexel, J.F., Preiss, W.V. and Parker, A.J., (eds). The geology of South Australia. v. 1, The Precambrian. *South Australia Geological Survey Bulletin,* v. **54**. p. 142.

Cox, S.F., 1987. Flow mechanisms in sulphide minerals. *Ore Geology Reviews*, v. **2**, p. 133-171.

Craig, J.R., 1967. Phase relations and mineral equilibria in the Ag - Bi - Pb - S system. *Mineralium Deposita*, v. **1**, p. 278-306.

Crawford, M.L., 1981. Phase equilibria in aqueous fluid inclusions. In: Crawford, L.S. and Hollister, M.L., (eds.) *Short Course in Fluid Inclusions: Applications to Petrology*, , Calgary: Min. Soc. Canada, p. 75-100.

Creaser, R.A. and Cooper, J.A. 1993. U-Pb geochronology of Middle Proterozoic felsic magmatism surrounding the Olympic Dam Cu-U-Au-Ag deposits, South Australia. *Economic Geology,* v.**88**, p. 186-197.

Creaser, R.A., 1989. The geology and petrology of middle proterozoic felsic magmatism of the Stuart Shelf, South Australia: La Trobe University Melbourne, PhD thesis,(unpublished) 434p. In: Creaser R.A., and Cooper J.A., 1993, U-Pb geochronology of Middle Proterozoic felsic magmatism surrounding the Olympic Dam Cu-U-Au-Ag deposits, South Australia. *Economic Geology,* v. **88**, p. 186-197.

Creaser, R.A., 1995. Neodymium isotopic constraints for the origin of Mesoproterozoic felsic magmatism, Gawler Craton, South Australia. *Canadian Journal of Earth Sciences*, v. **32**, p. 460-471

Creaser, R.A., and Fanning, C.M., 1993. A U-Pb zircon study of the Mesoproterozoic Charleston Granite, Gawler Craton, South Australia. *Australian Journal of Earth Sciences*, v. **40**, p. 519-526.

Creaser, R.A., and White, A.J.R., 1991. Yardea Dacite– Large-volume, high temperature felsic volcanism from the Middle Proterozoic of South Australia. *Geology*, v. **19**, p. 49-51.

Crerar, D.A., and Barnes, H.L., 1976. Ore solution chemistry V. Solubilities of chalcopyrite and chalcocite assemblages in hydrothermal solution at 200° to 350°C. *Economic Geology*, v. **71**, p. 772-794.

Criss, R.E., and Taylor, H.P. (Jr.), 1986. Meteoric hydrothermal systems. In: Valley, J.W., Taylor, H.P. Jr. and O'Neil, J.R., (eds), Stable isotopes in high temperature geological processes. *Reviews in Mineralogy*, v. **16**, Mineralogical Society of America, p. 570.

Cross, K.C., 1993. Acropolis and Wirrda Well prospects. In: Drexel, J.F., Preiss, W.V., and Parker, A.J., (eds). The geology of South Australia. v. 1, The Precambrian. *South Australian Geological Survey Bulletin,* v. **54.** p. 138.

Cumming, G.L., and Richards, J.R., 1975. Ore lead isotope ratios in a continuously changing earth. *Earth and Planetary Science Letters*, v. **28**, p. 155-171.

Currie, K.L., 1971. The reaction 3 cordierite = 2 garnet + 4 sillimanite + 5 quartz as a geological thermometer in the Opinicon Lake region, Ontario. *Contributions to Mineralogy and Petrology*, v. **33**, p. 215-226.

Curtis, P.J., 1977. Mount Gunson Exploration. Pertography of LY2 DDH deep stratigraphic hole in Pandurra Formation. Report PMR 190/77, for Pacminex Pty Ltd. South Australia Department of Mines and Energy, open file envelope 3026 p. 345-435 (unpublished).

Dalgarno, C.R., Johnson, J.E., Forbes, B.G., and Thompson, B.P., 1968. Port Augusta map sheet. *South Australia Geological Survey. Geological Atlas 1:250,000 Series*, sheet **SI53-4**.

Daly, S.J., 1985. *Tarcoola map sheet.* South Australia Geological Survey, Geological Atlas 1:250,000 Series, sheet **SH53-10.**

Daly, S.J., 1993a. Corunna Conglomerate. In: Drexel, J.F., Preiss, W.V. and Parker, A.J., (eds). The geology of South Australia. v. 1, The Precambrian. *South Australia Geological Survey Bulletin,* v. **54**. p. 124-126.

Daly, S.J., 1993b. Tarcoola Formation. In: Drexel, J.F., Preiss, W.V., and Parker, A.J., (eds), 1993, The geology of South Australia. v. 1, The Precambrian. *South Australian Geological Survey Bulletin,* v. **54**, p. 68-69.

Daly, S.J., 1993c. Glenloth an Tarcoola Goldfields. In: Drexel, J.F., Preiss, W.V. and Parker, A.J., (eds). The geology of South Australia. v. 1, The Precambrian. *South Australia Geological Survey Bulletin,* v. **54**. p. 138-139.

Daly, S.J., and Fanning, C.M., 1990. Archaean geology of the Gawler Craton, South Australia. *Third Archaean Symposium Abstracts*, Perth.

Daly, S.J., and Fanning, C.M., 1993. Chapter 3, Archean. In: Drexel, J.F., Preiss, W.V., and Parker, A.J., (eds). The geology of South Australia. v. 1, The Precambrian. *South Australia Geological Survey Bulletin,* v. **54**, p. 33-50.

Daly, S.J., Horn, C.M., and Fradd, W.P., 1990. Tarcoola goldfields. In: Hughes, F.E. (ed.), Geology of the mineral deposits of Australia and Papua New Guinea. *The Australasian Institute of Mining and Metallurgy, Monograph Series*, v. **14**, p. 1049-1053.

Davidson, G.J., and Paterson, H.L., 1993. Oak Dam East: A prodigious, uranium-bearing massive iron-oxide body on the Stuart Shelf. *Geological Society of Australia, Abstracts* No. **34**, Specialist group in Economic Geology, 2nd. National Meeting Armidale, 4th - 5th February, 1993, p. 18-19.

Dean, J.A, 1991b. Preliminary report to Aberfoyle Resources Ltd. on lead isotopes from diamond drill holes PD0024, 25, 28 and 29, (unpublished).

Dean, J.A., 1991a. The metallogenic association of exploration samples from the Menninnie Dam area, Eyre Peninsula, South Australia, based on the Pb isptopic compositions of galena's - A report to Aberfoyle Resources Limited. SIROTOPE report No. SR199, (unpublished)

Dean, J.A., 1994. A metallogenic assessment of galena mineralisation at the Telephone Dam prospect, South Australia based on Pb isotopes. Exploration and mining report 73C, Sirotope report SR269. CSIRO, Division of Exploration and Mining, North Ryde, NSW (unpublished).

Dean, J.A., and Carr, G.R., 1990. Report to Aberfoyle Resources Limited on a Pb isotope study of exploration samples from the Eyre Penonsula, South Australia, Report SR 114. CSIRO, Division of Exploration and Mining, North Ryde, NSW (unpublished).

Decarreau, A., Mondesir, H., and Besson, G., 1988. Synthese etstabilite des stevensites, kerolites, talcs magnesiens et nickeliferesentre 80 et 240°C. *Comptes Rendus Hebdomadaires des Seances. Academie des Sciences (Pairs).*, **t. 308**, Serie 11, p. 301-306.

Deer, W.A., Howie, R.A., and Zussman, J., 1978. *An introduction to the rock-forming minerals.* Longman, London.

Deines, P., Langmuir, D., Harmon, R.S., 1974. Stable carbon isotope ratios and the existence of a gas phase in the evolution of carbonate ground waters. *Geochimica et Cosmochimica Acta*, v. **38**, p. 1147-1164.

Delany P.T., 1982. Rapid intrusion of magma into wet rock: Groundwater flow due to pore pressure increases, *Journal of Geophysical Research,* v. **87**, p. 7739-7756.

Ding, K., and Seyfried, W.E., Jr., 1992. Determination of Fe-Cl complexing in the low pressure supercritical region (NaCl fluid): Iron stability constraints on pH of seafloor hydrothermal fluids. *Geochimica et Cosmochimica Acta,* v. **56**, p. 3681-3692.

DME, 1993. *Aeromagnetic pixil map Area B4* (parts Port Augusta and Whyalla 1: 250,000 map sheets).

Doe, B.R., and Delevaux, M.H., 1972. Source of lead in southeast Missouri galena ores. *Economic Geology*, v. **67**, p. 409-425.

Doe, B.R., and Zartman, R.E., 1979. Plumbotectonics: In Barnes, H.L., (ed.), *Geochemistry of Hydrothermal Ore Deposits.* Wiley Interscience, New York. p. 20-70.

Doe, B.R., Steven, T.A., Delevaux, M.H., Stacey, J.S., Lipman, P.W., and Fisher, F.S., 1979. Genesis of ore deposits in the San Juan Volcanic Field, Southwestern Colorado - Lead isotope evidence. *Economic Geology*, v. **74**, p. 1-26.

Drexel, J.F., Preiss, W.V., and Parker, A.J., (eds),1993. The Geology of South Australia. v.**1**, The Precambrian. *South Australia Geological Survey. Bulletin*, **54**.

Droop, G.T.R., 1987. A general equation for estimating Fe3+-Mg concentrations in ferromagnesian silicates and oxides from microprobe analayses using stoichiometric criteria. *Mineralogical Magazine*, v. **51**, p. 431-435.

Druitt, T.H., and Sparks, R.S.J., 1982. A proximal ignimbrite breccia facies on Santorini, Greece. *Journal of Volcanology and geothermal Research*, v. **13**, p. 147-171

Dzurisin, D., Denlinger, R.P., and Rosenbaum, J.G., 1990. Cooling rate and thermal structure determined from progressive magnetism of the dacite dome at Mount St. Helens, Washington. *Journal of Geophysical Research*, v. **95**, p. 2763-2780.

Eichelberger, J.C., and Koch, F.G., 1979. Lithic fragments in the Bandelier Tuff, Jemez Mountains, New Mexico. *Journal of Volcanology and geothermal Research,* v. **5**: p. 115-134.

Eldridge, C.S., Barton, P.B., and Ohmoto, H., 1983. Mineral textures and their bearing on formation of the Kuroko ore bodies. In: Ohmoto, H., and Skinner, B.J., (eds.), The Kuroko and related volcanogenic massive sulphide deposits, *Economic Geology,* Monograph **5**, p. 241-281

Eldridge, C.S., Bourcier, W.L., Ohmoto, H., and Barnes, H.L.. 1988, Hydrothermal inoculation and incubation of the chalcopyrite disease in sphalerite. *Economic Geology* v. **83**, p. 978-989.

Enos, P., 1977. Flow regimes in debris flow. *Sedimentology,* v. **24**, p. 133-142.

Esdale, D.J., Pridmore, D.F., Coggon, J.H., Muir, P.M., Williams, P.K., and Fritz, F.P., 1987. Olympic Dam deposit - geophysical case history. *Bulletin of the Australian Society of Exploration Geophysics*, v. **18**, p. 47-49.

Evans, B.W., and Guggenheim, S., Talc, pyrophyllite, and related minerals. In: Bailey, S.W. (ed.), 1988. Hydrous Phyllosilicates (exclusive of micas), *Mineralogical Society of America, Reviews in Mineralogy*, v. **19**, p. 225-294

Exley, R.A., Mattey, D.P., Clague, D.A., and Pillinger, C.T., 1986. Carbon isotope systematics of a mantle 'hot-spot': a comparison of Loihi seamount and MORB glasses. *Earth and Planetary Science Letters*, v. **78**, p. 189-199.

Fanning, C.M., 1984. Rb-Sr geochronology of a pegmatite intrusive into the Kalinjala Mylonite Zone. Amdel report GS . **6102/ 84** (unpublished).

Fanning, C.M., 1987. U-Pb zircon geochronology of Broadview DDH1, Wangary Gneiss, Carpa Granite and Middle Camp Granite. Amdel report, G7155/88 (unpublished).

Fanning, C.M., 1988. Tarcoola Gold Mine: U-Pb and Pb isotope study. In: Flintoft, M.W. and Horn, C.M., 1989, Compilation of exploration data available on the Tarcoola Blocks Goldmine, Tarcoola, South Australia: *Mines and Energy, South Australia* , Report book No. **89/88.**

Fanning, C.M., 1990. Single grain U-Pb zircon dating of two tuffaceous horizons from Wilgena 1. PRISE geochronology report, 89-020 (unpublished). In: Daly, S.J., 1993, Tarcoola Formation. In: Drexel, J.F., Preiss, W.V. and Parker, A.J., (eds),1993, The geology of South Australia. Volume 1, The Precambrian. *South Australian Geological Survey Bulletin,* v. **54,** p. 68-69.

Fanning, C.M., 1993. Ion microprobe U-Pb Zircon dating of porphyritic felsic volcanic rocks from the Menninnie Dam prospect. Research School of Earth Sciences, The Australian National University. (unpublished).

Fanning, C.M., Blissett, A.H., Flint, R.B., Ludwig, K.R., and Parker, A.J., 1986. A refined geological history for the southern Gawler Craton through U-Pb zircon dating of acid volcanics, and correlations with northern Australia. *Australian Geological Society, Abstract* **15**, p. 67-68.

Fanning, C.M., Flint, R.B. and Preiss, W.V., 1983. Geochronology of the Pandurra Formation. *South Australia Geological Survey Quarterly Geological Notes*, v. **88**, p. 11-16.

Fanning, C.M., Flint, R.B., Parker, A.J., Ludwig, K.R. and Blissett, A.H., 1988. Refined Proterozoic evolution of the Gawler Craton, South Australia, through U-Pb zircon geochronology. *Precambrian Research,* v. **40/41**, p 363-386.

Fanning, C.M., Oliver, R.L., and Cooper, J.A., 1980. The Carnot Gneisses, a metamorphosed Archean supracrustal sequence in southern Eyre Peninsula. *Journal of the Geological Society of Australia,* v. **27**, p 47.

Faure, G., 1977. *Principals of isotope geology*. New York, John Wiley and Sons.

Ferry, J.M., (ed.), 1982. Characterisation of metamorphism through mineral equilibria. *Reviews in Mineralogy*, v. **10**, Mineralogical Society of America, Washington D.C.

Ferry, J.M., and Spear, F.S., 1978. Experimental calibration of the partitioning of Fe and Mg between biotite and garnet. *Contributions to Mineralogy and Petrology*, v. **66**, p. 113-117.

Fisher, R.V., 1960. Classification of volcanic breccias. *Geological Society of America Bulletin*, v. **71**, p. 973-982.

Fisher, R.V., and Schmincke, H-U, 1984. *Pyroclastic rocks*. Springer-Verlag, Berlin.

Fiske, R.S., and Tobisch, O.T., 1994. Middle Cretaceous ash-flow tuff and caldera-collapse deposit in the Minarets Caldera, east-central Sierra Nevada, California. *Geological Society of America Bulletin*, v. **106**, p. 582-593.

Flint, R.B., 1993a. Blue Range Beds. In: Drexel, J.F., Preiss, W.V., and Parker, A.J., (eds), 1993, The geology of South Australia. v. 1, The Precambrian. *South Australian Geological Survey Bulletin,* v. **54**, p. 142.

Flint, R.B., 1993b. Hiltaba Suite. In: Drexel, J.F., Preiss, W.V., and Parker, A.J., (eds), 1993, The geology of South Australia. v. 1, The Precambrian. *South Australian Geological Survey Bulletin,* v. **54**, p. 127-131.

Flint, R.B., and Rankin, L.R., 1989. *Kimba map sheet*. South Australia Geological Survey. Geological Atlas, 1:250,000 Series, sh. SI53-7.

Flint, R.B., Rankin, L.R., and Fanning, C.M., 1990. Definition of the Palaeoproterozoic St. Peters Suite of the Western Gawler Craton. *South Australia Geological Survey Quarterly Geological Notes*, v. **114**, p. 2-8.

Flintoff, M.W., and Horn, C.M., 1989. Compilation of exploration data available on the Tarcoola Blocks Goldmine, South Australia: Department of Mines and Energy, South Australia, Report book 89/88 (unpublished).

Fournier, R.O., 1985. The behavior of silica in hydrothermal solutions. In: Berger, B.P. and Bethke, P.M., (eds.) Geology and geochemistry of epithermal systems. *Reviews in Economic Geology*, v. **2**, p. 45-61.

Fradd, W.P., 1988. Earea Dam Goldfield, historical review and production records. *South Australia Department of Mines and Energy, Report Book*, v. **88/40**

Friedman, I., and O'Neil, J.R., 1977. Data of geochemistry. Compilation of stable isotope fractionation factors of geochemical interest. *U.S. Geological Survey Professional Paper*, **440-KK**.

Frost, B.R., and Tracey, R.J., 1991. P-T paths form zoned garnets: some minimum criteria. *American Journal of Science*, v. **291**, p. 917-939.

Gammons, C.H., and Barnes, H.L., 1989. The solubility of Ag2S in near neutral aqueous sulphide solutions at 25 to 300°C. *Geochimica et Cosomchimica Acta*, v. **53**, p. 279-290.

Gammons, C.H., and Williams-Jones, A.E., 1995. Hydrothermal geochemistry of electrum: Thermodynamic constraints. *Economic Geology*, v. **90**, p. 420-432.

Garner, A., 1996. Coarse lithic breccias of the Gawler Ranges Volcanic Province: Source, emplacement and significance. BSc (Hons.) thesis, Department of Geology, University of Tasmania, Hobart, Tasmania (unpublished).

Gerdes, R.A., 1972. A helicopter gravity survey of the Gawler Platform. *South Australia Mineral Resources Review*, v. **133**, p. 137-147

Giles, C.W., 1977. Rock units in the Gawler Range Volcanics, Lake Everard area, South Australia. *Quarterly Geological Notes, Geological Survey of South Australia*:, v. **61**, p. 7-16.

Giles, C.W., 1980. A comparative study of Archaean and Proterozoic felsic volcanic associations in southern Australia. University of Adelaide PhD thesis, (unpublished).

Giles, C.W., 1988. Petrogenesis of the Proterozoic Gawler Range Volcanics, South Australia. *Precambrian Research*, v. **40/41**, p. 407-427.

Giles, C.W., Goode, A.D.T., and Lemon, N.M., 1980. Middle Proterozoic volcanism and sedimentation in the Moonabie area. *Journal of the Geological Society of Australia,* v. **27**, p 53.

Godwin, C.I., Gabites, J.E., and Andrew, A, 1988. Lead table: a galena lead isotope base for the Canadian Cordillera, with a guide to its use by explorationists. *British Columbia Ministry of Energy, Mines and Petroleum Resources Paper,* **1988-4**.

Godwin, C.I., Sinclair, A.J., Ryan, B.D., 1982. Lead isotope models for the genesis of carbonate-hosted Zn-Pb, shale-hosted Ba-Zn-Pb, and silver-rich deposits in the Northern Canadian Cordillera. *Economic Geology*, v. **77**, p. 82-94.

Goff, F., 1983. Subsurface structure of Valles Caldera; a resurgent cauldron in northern New Mexico. 36th annual meeting, The Geological Society of America Rocky Mountain Section; 79th annual meeting, Cordilleran Section, Salt Lake City, UT, May 2-4, 1983, *Abstracts with Pograms Geological Society of America.*, v. **15** (**5**), p. 381

Gow, P.A., Wall, V.J. and Valenta, R.K., 1993. The regional geophysical response of the Stuart Shelf, South Australia. *Exploration Geophysics*, v. **24**, p. 513-520.

Graf, J.L., 1977. Rare earth elements as hydrothermal tracers during the formation of massive sulphide deposits in volcanic rocks. *Economic Geology,* v. **72**, p. 527-548.

Graham, C.M., Vilino, J.A., and Harmon, R.S., 1987. An experimental study of hydrogen isotope exchange between aluminous chlorite and water. *American Mineralogist*, v. **72**, p. 566-579.

Gregory, R.T., and Criss, R.E., 1986. Isotopic exchange in open and closed systems. In Valley, J.W., Taylor, H.P. and O'Neil, J.R., (eds.), *Stable isotopes in high temperature geological processes. Reviews in mineralogy*, v. **16**, Mineralogical Society of America, p. 91-128.

Gresens, R.L., 1967. Composition-volume relationships of metasomatism. *Chemical Geology*, v. **2**, p. 47-65.

Griggs, D.T., and Handlin, J., 1960. Rock deformation. *Geological Society of America Memoirs*, v. **79**, p. 21-39.

Gross, G.A., 1991. Genetic concepts for iron-formation and associated metalliferous sediments. *Economic Geology Monograph* , v. **8**, p. 51-81.

Gulson, B.L., 1986. Lead isotopes in mineral exploration. *Developments in economic geology,* v. **23**. Elsevier Science Publishing Co. Inc. NY.

Gulson, B.L., Large, R.R., and Porritt, P.M., 1987. Base metal exploration of the Mount Read Volcanics, Western Tasmania: Pt. III. Application of lead isotopes at Elliott Bay. *Economic Geology*, v. **82**, p. 308-327.

Haas, J.L., 1971. The effect of salinity on the maximum thermal gradient of a hydrothermal system at hydrostatic pressure. *Economic Geology*, v. **66**, p. 940-946.

Hanson, R.E., and Schweickert, R.A., 1982. Chilling and brecciation of a Devonian rhyolitic sill intruded into wet sediments, northern Sierra Nevada, California. *Journal of Geology*, v. **90**, p. 717-724.

Hanson, R.E., and Wilson, T.J., 1993. Large scale rhyolite peperites (Jurassic, southern Chile). *Journal of Volcanology and Geothermal Research,* v. **54,** p. 247-264.

Hayashi, K., Sugaki, A., and Kitakaze, A., 1990. Solubility of sphalerite in aqueous sulphide solutions at temperatures between 25 and 240°C. *Geochimica et Cosmochimica Acta,* v. **54**, p. 715-725.

Haynes, F.M., Sterner, S.M., and Bodnar, R.J., 1988. Synthetic fluid inclusions in natural quartz. IV. Chemical analyses by SEM/EDA: Evaluation of method. *Geochimica et Cosmochimica Acta*, v. **52**, p. 969-977.

Hazlitt, J.S., and Thompson, T.B., 1990. Breccia Bodies in the Leadville District, with Emphasis on Occurrences in the Black Cloud Mine, Lake County, Colorado. In: *Economic Geology, Monograph* , **7**, p. 180-192.

Heaton, T.H.E., and Sheppard, S.M.F., 1977. Hydrogen and oxygen isotope evidence for sea-water-hydrothermal alteration and ore deposition, Troodos complex, Cyprus, In: *Volcanic Processes in Ore Genesis, Special Paper*, **7**, Geological Society of London, p. 42-57,

Hedenquist, J. W., and Henley, R. W., 1985a. Hydrothermal eruptions in the Waiotapu geothermal system, New Zealand. Origin, breccia deposits and effect on precious-metal mineralisation. *Economic Geology*, v. **80**, p.1640-1668.

Hedenquist, J. W., and Henley, R. W., 1985b. The importance of CO2 on freezing point measurements of fluid inclusions: Evidence from active geothermal systems and implications for epithermal ore deposition. *Economic Geology,* v. **80**, p.1379-1406.

Heiken, G., and Wohletz, K., 1987. Tephra deposits associated with silicic domes and lava flows. *Geological Society of America Special Paper*, v. **212**, p. 55-76

Hein, K.A.A., Both, R.A. and Bone, Y., 1989. The geology and genesis of the Tarcoola gold deposits, South Australia. *Mineralium Deposita,* v. **29**, p 224-236.

Heinrich, C.A., and Seward, T.M., 1990. A spectrophotometric study of aqueous iron (II) chloride complexing from 25 to 200 degrees C. *Geochimica et Cosmochimica Acta*, v. **54**, p. 2207-2221.

Helgeson, H.C., 1967. Thermodynamics of complex dissociation in aqueous solution at elevated temperatures. *Journal of Physics and Chemistry*, v. **71**, p. 3121-3136.

Helgeson, H.C., 1969. Thermodynamics of hydrothermal systems at elevated temperatures and pressures. *American Journal of Science*, v. **267**, p. 729-804.

Helgeson, H.C., Kirkham, D.H., and Flowers, G.C., 1981. Theoretical prediction of the thermodynamic behavior of aqueous electrolytes at high pressures and temperatures: IV. Calculation of activity coefficients, osmotic coefficients, and appartent molal and standard and relative partial molal properties to 600°C and 5 Kb. *American Journal of Science*, v. **281**, p. 1249-1516.

Hellsten, K.J., 1985. Review of exploration results, 1980 - 1985, Wilcherry Hill, E.L. 1057, S.A. Report number 08.2850, v. 1, Billiton Australia Ltd, company report (unpublished).

Hemley, J.J and Hunt, J.P., 1992. Hydrothermal ore-forming processes in the light of studies in rock-buffered systems: I. Some general geologic applications. *Economic Geology*, v. **87**, p. 22-43.

Hemley, J.J., Cygan, G.L., Fein, J.B., Robinson, G.R., and D'Angelo, W.M., 1992. Hydrothermal ore-forming processes in the light of studies in rock-buffered systems: I. Iron - copper - zinc - lead sulphide solubility relations. *Economic Geology*, v. **87**, p. 1-22.

Henkel, H., 1976. Studies on density and magnetic properties from North Western Sweden. *Pure and Applied Geophysics*, v. **114**, p. 235-249.

Henley, R.W., and Ellis, A.J., 1983. Geothermal systems, ancient and modern: a geochemical review. *Earth Science Reviews*, v. **19**, p. 1-50.

Henley, R.W., and McNabb, A., 1978. Magmatic vapour plumes and ground-water interaction in porphyry copper emplacement. *Economic Geology,* v. **73**, p. 1-20.

Henley, R.W., Truesdell, A.H., Barton, P.B. Jr., and Whitney, J.A., 1984. Fluid-mineral equilibria in hydrothermal systems. *Reviews in Economic Geology*, v. **1**, 267p.

Higgins, M. L., Berg, R.C., and Hellsten, K.J., 1990. Menninnie Dam lead-zinc-silver prospect, Eyre Peninsula. In: Hughes, F.E., (ed.) *Geology of the Mineral Deposits of Australia and Papua New Guinea* .The Australasian Institute of Mining and Metallurgy: Melbourne, p. 1055-1058

Higgins, M.L., and Hellsten, K.J., 1986. The Menninnie Dam lead - zinc - silver prospect, South Australia. *Geological Society of Australia Abstracts*, **15**, p. 97-98.

Hodge, D.S., Harbin, M.A., Patterson, J.L., and Sweeney, J.F., 1982. Gravity studies of subsurface mass distributions of granitic rocks in Maine and New Hampshire. *American Journal of Science*, v. **282**, p. 1289-1324.

Hoefs, J., 1980. *Stable isotope geochemistry*, 2nd edition, New York, Heidelberg, Berlin, Springer-Verlag.

Hoisch, T.D., 1990. Empirical calibration of six geobarometers for the mineral assemblage quartz + muscovite + biotite + plagioclase + garnet. *Contributions to Mineralogy and Petrology*, v. **104**, p. 225-234.

Holdaway, M.J., 1971. Stability of andalusite and the aluminium silicate diagram. *American Journal of Science*, v. **271**, p. 97-131.

Holland, H.D., 1984. *The chemical evolution of the atmosphere and oceans* Princeton University Press.

Holser, W.T., 1984. Gradual and abrupt shifts in ocean chemistry during Phanerozoic time. In: Holland, H.D, Trendall, A.F, (eds.) *Patterns of change in Earth evolution.* Springer-Verlag. Berlin, p. 123-143.

Howells, M.F., Reedman, A.J., and Campbell, S.D.G., 1991. *Ordovician (Caradoc) marginal basin volcanism in Snowdonia (north-west Wales).* London: HMSO for the British Geological Survey.

Huon, S., Burkhard, M., and Hunziker, J., 1994. Mineralogical, K-Ar, stable isotope and Sr isotope systematics of K-white micas during very low grade metamorphism of limestones (Helvetic nappes, western Switzerland). *Chemical Geology (Isotope Geoscience Section)*, v. **113**, p. 347-376.

Huston, D.L., and Large, R.R., 1987. Genetic and exploration significance of the zinc ratio (100Zn/(Zn+Pb)) in massive sulphide systems. *Economic Geology*, v. **82**, p. 1521-1539.

Huston, D.L., Power, M., Gemmell, J.B., and Large, R.R., 1995. Design, calibration and geological application of the first operational Australian laser ablation sulphur isotope microprobe. *Australian Journal of Earth Sciences*, v. **42**, p. 549-556.

Hutton, D.W., 1982. A tectonic model for the emplacement of the main Donegal granite, NW Ireland. *Journal of the Geological Society of London*, v. **139**, p. 615-631.

Ikin, N.P., and Harmon, R.S., 1981. D/H and $^{18}O/^{16}O$ ratios and mineralogy of serpentinites from the highland boarder fracture zone, Scotland. *Bulletin of Mineralogy*, v. **104**, p. 795-800.

Ineson, P.R., 1989. *Introduction to practical ore microscopy.* Longman Scientific and Technical (Longman earth science series).

Ishihara, S., 1981. The granitoid series and mineralisation. In: Skinner, B.J. (ed.), *Economic Geology 75th Anniversary Volume*, The Economic Geology Publishing Company, El Paso, Texas.

Jackson, M.L., 1969. *Soil Chemical Analysis - Advanced Course*: 2nd Edition, published by the author, Madison, Wisconsin.

Jagodzinski, E., 1985. The geology of the Gawler Range Volcanics in the Toondoolya Bluff area, and U-Pb dating of the Yardea Dacite at Lake Acraman. University of Adelaide Honours thesis (unpublished).

James, H.L., 1954. Sedimentary facies of iron formation. *Economic Geology* ,v. **49**, p. 235-293.

John, D.A., 1995. Tilted middle Tertiary ash-flow calderas and subjcent granitic plutons, southern Stillwater Range, Nevada: Cross sections of an Oligocene igneous center. *Geological Society of America Bulletin*, v. **107**, p. 180-200.

Johnson, A.M., 1970. *Physical processes in geology.* San Francisco, Freeman, Cooper and Co., 557p.

Johnson, J.P. and Cross, K.C., 1991. Geochemical and Sm-Nd isotopic constraints on the genesis of the Olympic Dam Cu-U-Au-Ag deposit, South Australia. In: Pagel, M. and Leroy, J.L. (eds.), *Source transport and deposition of ore metals.* Balkema, Rotterdam, p. 395-400.

Johnson, J.P., and McCulloch, M., T 1995. Sources of mineralising fluids for the Olympic Dam Deposit (South Australia); Sm-Nd isotopic constraints. *Chemical-Geology*, v. **121**, p. 177-199.

Johnson, J.W., Oelkers, E.H., and Helgeson, H.C., 1992. *SUPCRT92*: A software package for calculating the standard molal thermodynamic properties of minerals, gases, aqueous species, and reactions from 1 to 5000 bars and 0° to 1000°C. *Computers and Geosciences*, v. **18**, p. 899-947.

Kamata, H., Suzuki-Kamata, K., and Bacon, C.R., 1993. Deformation of the Wineglass Welded Tuff and the timing of caldera collapse at Crater Lake, Oregon. *Journal of Volcanology and Geothermal Research*, v. **56**, p. 253-266.

Kanasewich, E.R., 1962. Approximate age of tectonic activity using lead isotopes. *Geophysical Journal*, v. **7**, p. 158.

Kanasewich, E.R., and Farquhar, R.M., 1965. Lead isotope ratios from the Cobolt-Noranda area, Canada. *Canadian Journal of Earth Sciences*, v. **2**, p. 361.

Kanaya, H., Nozawa, T., and Tainosho, Y., 1984. Study on the Ibaragi granite complex. Some physical properties. *Bulletin of the Geological Society of Japan*, v. **35**, p. 147-157.

Kharaka, Y.K., Maest, A.S., Carothers, W.W., Law, L.M., Lamothe, P.J., and Fries, T.L., 1987. Geochemistry of metal-rich brines from central Mississippi Salt Dome basin, U.S.A. *Applied Geochemistry*, v. **2**, p. 543-561.

Kienle, J., Kyle, P.R., Self, S., Motyka, R.J., and Lorenz, V., 1980. Ukinrek maars, Alaska, I. April 1977 eruption sequence, petrology and tectonic setting. *Journal of Volcanology and Geothermal Research*, v. **7**, p. 11-39.

Kitto, P.A., 1994. Structural and geochemical controls on mineralisation at Renison, Tasmania. PhD thesis, University of Tasmania (unpublished).

Kohn, M.J., and Spear, F.S., 1991a. Error propagation for barometers: 1. Accuracy and precision of experimentally located end-member reactions. *American Mineralogist*, v. **76**, p. 128-137

Kohn, M.J., and Spear, F.S., 1991b. Error propagation for barometers: 2. Application to rocks. *American Mineralogist*, v. **76**, p. 138-147.

Kojima, S., 1990. A coprecipitation experiment on intimate association of sphalerite and chalcopyrite and its bearing on the genesis of Kuroko ores. *Mining Geology*, v. **40**, p. 147-158.

Kojima, S., and Sugaki, A., 1987. An experimental study on chalcopyritization of sphalerite induced by hydrothermally metasomatic reactions. *Mining Geology*, v. **37**, p. 373-380.

Kokelaar, B.P., 1982. Fluidisation of wet sediments during the emplacement and cooling of various igneous bodies. *Journal of the Geological Society of London*, v. **139**, p. 21-33.

Kokelaar, P., Branney, M., Moore, I., and Howells, M., 1994. Processes and controls of caldera collapse and related ignimbrite emplacement in Snowdonia (Wales), the Lake District (England) and Glencoe (Scotland), United Kingdom, Field Guide. *I.A.V.C.E.I. Commission on Explosive Volcanism field workshop,* May 18-29, 1994.

Koziol, A.M., 1989. Reclalibration of the garnet - plagioclase - $Al_2SiO_5$ - quartz (GASP) geobarometer and applications to natural paragenesis. *EOS*, v. **70**, p. 493.

Kretz, R., 1994. *Metamorphic crystallisation.* John Wiley and Sons, Chichester, England, New York, U.S.A..

Krupp, R.E. and Seward, T.M., 1987. The Rotokawa geothermal system, New Zealand: An active epithermal gold-depositing environment. *Economic Geology*, v. **82**, p. 1109-1129.

Kuroda, Y., Suzuoki, T., Matsuo, S., and Shirozu, H., 1976. A preliminary study of D/H ratios of chlorites. *Contributions to Mineralogy and Petrology*, v. **57**, p. 223-225.

Kyser, T.K. (ed.), 1987. Short course in stable isotope geochemistry of low temperature fluids. *Mineralogical Association of Canada, Short course handbook*, v. **13,** 452p.

Lalor, J.H., 1986. Olympic Dam copper-uranium-gold-silver deposit, South Australia. In: Horn, M.K. (ed.), *4th Circum-Pacific Energy and Minerals Resources Conference, Singapore, 1986. Transactions*, p. 561-587.

Laouar, R., Boyce, A.J., Fallick, A.E., and Leake, B.E, 1990. A sulphur isotope study on selected Caledonian granites of Britain and Ireland. *Geological Journal*, v. **25**, p. 359-369.

Large, R.R., 1992. Australian volcanic-hosted massive sulphide deposits: Features, styles and genetic models. In: *Economic Geology*, v. **87**, p. 471-510.

Le Bas, M.J., Le Maitre, R.W., Streckeisen, A., and Zanettin, B., 1986. A chemical classification of volcanic rocks based on the Total Alkali-Silica diagram. *Journal of Petrology*, v. **27**, p. 745-750.

Le Maitre, R.W. (ed), 1989. *A classification of igneous rocks and glossary of terms.* International Union of Geological Sciences Subcommission on the Systematics of Igneous Rocks. Blackwell Scientific Publications, Victoria, Australia.

Leaman, D.E., 1994. Criteria for the evaluation of potential field interpretations. *First Break*, **12 (4)**, p. 181-191.

Lee, K., 1989. (unpublished data). In: Higgins, M. L., Berg, R. C. and Hellsten, K. J., 1990, Menninnie Dam lead-zinc-silver prospect, Eyre Peninsula. In: Hughes F.E., (ed.) *Geology of the Mineral Deposits of Australia and Papua New Guinea* , The Australasian Institute of Mining and Metallurgy: Melbourne, p. 1055-1058.

Lee, M.K., 1986. A new gravity survey of the Lake District and a three dimensional model of the granitic batholith. *Journal of the Geological Society of London*, v. **143**, p. 425-435.

Lemon, N.M., 1972. A sedimentological approach to the geology of the Corunna area, South Australia. University of Adelaide BSc. (Hons.) thesis (unpublished).

Lemon, N.M., 1980. The Middleback Subgroup. *Journal of the Geological Society of Australia*, v. **27**, p. 48.

Lemon, N.M., and Gostin, V.A., 1983. *Fluvial sedimentology field excursion, Whyalla-Corunna-Depot Creek area. 18th - 20th August, 1983.* Geological Society of Australia. Australasian Sedimentologists Group.

Lindgren, W., 1912. The nature of replacement. *Economic Geology*, v. **7**, p. 521-535.

Lipman, P.W., 1965. Chemical comparison of glassy and crystalline volcanic rocks. *Special Paper, Geological Society of America*, v. **81**, p. 260-261.

Lipman, P.W., 1976. Caldera-collapse breccias in the western San Juan Mountains, Colorado. *Geological Society. America Bulletin,* v. **87**: p. 1397-1410.

Lipman, P.W., 1984. The roots of ash flow calderas in Western North America: Windows into the tops of granitic batholiths. *Journal of Geophysical Research* v. **89**: No. **B10**, p. 8801-8841.

Lipman, P.W., and Christiansen, R.L., 1964. Zonal features of an ash-flow sheet in the Piapi Canyon Formation, southern Nevada, B74-8. *US Geological Survey Professional Paper,* No. **501B.**

Lipman, P.W., Bogatikov, O.A., Tsvetkov, A.A., Gazis, C., Gurbanov, A.G., Hon, K., Koronovsky, N.V., Kovalenko, V.I., Marchev, P., 1993. 2.8-Ma ash-flow caldera at Chegem River in the northern Caucasus Mountains (Russia), contemporaneous granites, and associated ore deposits. *Journal of Volcanology and geothermal Research.* v. **57**, p. 85-124.

Lipman, P.W., Christainsen, R.L., and Van Alstine, R.E., 1969. Retention of alkalis by calc-alkalic rhyolites during crystallisation and hydration. *American Mineralogist*, v. **54**, p. 286-291.

Lister, G.S., and Snoke, A.W., 1984. S - C mylonites. *Journal of Structural Geology*, v. **6**, p. 617-638.

Lofgren, G., 1971a. Spherulitic textures in glassy and crystalline rocks. *Journal of Geophysical Research,* v. **76**, p. 5635-5648.

Lofgren, G., 1971b. Experimentally produced devitrification textures in natural rhyolitic glass. *Geological Society of America Bulletin,* **82**, p. 111-124.

Lofgren, G., 1974. An experimental study of plagioclase crystal morphology: isothermal crystallisation. *American Journal of Science*, v. **274**, p. 243-273.

Logan, R.G., Murray, W.J., and Williams, N., 1990. HYC silver - lead - zinc deposit, McArthur River. In: Hughes, F.E., (ed.) *Geology of the mineral deposits of Australia and Papua New Guinea.* The Australasian Institute of Mining and Metallurgy: Melbourne, p. 907-911.

London, D., 1995. Geochemical features of peraluminous granites, pegmatites, and rhyolites as sources of lithophile metal deposits. In: Thompson, J.F.H, (ed.) Magmas, fluids, and ore deposits. *Mineralogical Association of Canada Short Course Series*, v. **23**, p. 175-202.

Lorenz, V., 1973. On the formation of maars. *Bulletin of Volcanology*, v. **37**, p. 1-22.

Lorenz, V., 1986. On the growth of maars and diatremes and its relevance to the formation of tuff rings. *Bulletin of Volcanology*, v. **48**, p. 265-274.

Ludwig, K.R., and Silver, l.T., 1977. Lead - isotope inhomogeneity in Precambrian igneous K - feldspars. *Geochemica et Cosmochemica Acta,* v. **41**, p. 1457 - 1471.

Luzhnaja, N.P., and Vereshtchetina, I.P., 1946. Sodium, calcium, magnesium chlorides in aqueous solutions at -57° to +125°C (polythermic solubility): *Zhurnl. Prikl. Khim.*, **v. 19**, p. 723-733.

Mann, A.W., and Deutscher, R.I., 1977. Solution chemistry of copper in water containing carbonate, sulphate, and chloride ions. *Chemical Geology*, v.**19**, p. 253-265.

Marumo, K., Nagasawa, K., and Kuroda, Y., 1980. Mineralogy and hydrogen isotope geochemistry of clay minerals in the Ohnuma Geothermal Area, Northeastern Japan. *Earth and Planetry Science Letters*, v. **47**, p. 255-262.

Mason, A.A.C., 1953. The Vulcan tin mine. In: Edwards, A.B., (ed.) *Geology of Australian ore deposits*, Australasian Institute of Mining and Metallurgy, Melbourne, Australia. p. 718-721.

Matsuhisa, Y., Goldsmith, J.R., and Clayton, R.N., 1979. Oxygen isotope fractionation in the system quartz-albite-anorthite-water. *Geochimica et Cosmochimica Acta*, v. **43**, p. 1131-1140.

McCallum M.E., 1985. Experimental Evidence for Fluidisation Processes in Breccia Pipe Formation': Economic Geology, v. **80:6**, p. 1523-1543.

McCrea, L.M., 1950. The isotope chemistry of carbonates and a palaeotemperature scale: *Journal of Chemistry and Physics*, v. **18**, p. 849-857.

McPhie, J., and Hunns, S.R., 1995. Secondary welding of submarine, pumice-lithic breccia at Mount Chalmers, Queensland, Australia. *Bulletin of Volcanology*, v. **57**, p. 170-178.

Mehnert, K.R., 1968. *Migmatites and the origin of granitic rocks*. Amsterdam, Elsevier.

Mellors, R.A., and Sparks, R.S.J., 1991. Spatter-rich pyroclastic flow deposits on Santorini, Greece. *Bulletin of Volcanology*, v. **53**, p. 327-342.

Metz, P., 1976. Experimental investigation of the metamorphism of siliceous dolomites, 3. *Contributions Mineralogy and Petrology*, v. **58**, p. 137-148.

Meyer, C., Shea, E.P., Goddard, C.C., Jr., and Staff., 1968. Ore deposits at Butte, Montana. In: Ridge, J.D., (ed.), *Ore deposits of the United States, 1933-1967.* American Institute of Mining and Metallurgy. Petroleum Engineers, v. **2**, p. 1373-1416.

Miguel, A., Miranda, G., and Megaw, P.K.M., 1986. Magmatic-hydrothermal breccias and certain silver - lead - zinc chimneys of the Potosi Mine, Santa Eulalia District, Chihuahua, Mexico. In: Clark, K.F., Megaw, P.K.M. and Ruiz, J., *Lead - zinc - silver carbonate-hosted deposits of Northern Mexico.* Guidebook for field and mine excursions, Nov. 13 - 17, 1986. Society of Economic Geologists.

Miller, R.B., and Paterson, S.R., 1994. The transition from magmatic to high-temperature solid-state deformation: implications from the Mount Stuart batholith, Washington. *Journal of Structural Geology*, v. **16**, p. 853-865.

Mondesir, H., 1987. *Le systeme Ni-Mg-Si-$H_2O$: Mesure des coefficients de partage solide / solution pour le couple Ni / Mg. Cristallochimie et stabilite des lizardites, talc, kerolite, et lizardite de synthese* [These en Sciences]: Orsay.

Mortimer, G.E., Cooper, J.A., and Oliver, R.L., 1980. Retrological and petrochemical evolution of the 1.82 b.y. Donington Granitoid Suite of the southeast Eyre Peninsula. *Journal of the Geological Society of Australia*, v. **27**, p. 50.

Mortimer, G.E., Cooper, J.A., and Oliver, R.L., 1986. The geochronological and geochemical evolution of the Proterozoic Lincoln Complex, Eyre Peninsula, South Australia. In: 8th Australian Geological Convention, Adelaide, 1986. *Geological Society of Australia Abstracts*, v. **15**, p. 140-141.

Mortimer, G.E., Cooper, J.A., Paterson, H.L., Cross, K., Hudson, G.R.T., and Uppill, R.K., 1988. Zircon U-Pb dating in the vicinity of the Olympic Dam Cu-U-Au deposit, Roxby Downs, South Australia: *Economic Geology*. v. **83**, p. 694-709.

Murphy, G.C., 1990. Lennard Shelf lead - zinc deposits. In: Hughes, F.E. (ed.) *Geology of the mineral deposits of Australia and Papua New Guinea*. The Australasian Institute of Mining and Metallurgy: Melbourne, p. 1103-1109.

Mustard, H.M., 1983. Breccia forming processes at the Kidston gold deposit. James Cook University of North Queensland B.Sc (Hons.) thesis, (unpublished).

Naumann, C.F., 1826. *Lehrbuch der Mineralogie*, Engelmann, Leipzig, p 209.

Newhall, C.G., and Melson, W.G., 1983. Explosive activity associated with the growth of volcanic domes. *Journal of Volcanology and Geothermal Research*, v. **17**, p. 111-131.

Norman, M.B.11, 1974. Improved techniques for selective staining of feldspar and other minerals using amaranth. *Journal of Research, U.S. Geological Survey*, v. **2**, p. 73-79.

Norrish, K., and Chappel, B.W., 1977. X-ray flourescence spectrometry. In: Hawkesworth, C.J., and Norry, M.J., (eds.) *Continental basa;ts and mantle xenoliths*, Shiva, Orpington (London), and Birkhauser Boston, p. 230-249.

Norrish, K., and Hutton, J.T., 1969. An accurate X-ray spectrographic method for the analysis of a wide range of geological samples. *Geochim. Cosomchim. Acta*, v. **33**, p. 431-453.

Novak, G.A., and Colville, A.A, 1989. A practical interactive least squares cell-parameter program using an electronic spreadsheet and a personal computer. *American Mineralogist*, v. **74**, p. 488-490.

O'Neil, J.R., 1986. Chapter 1. Theoretical and experimental aspects of isotopic fractionation. In: Valley, J.W., Taylor, H.P. Jr. and O'Neil, J.R., (eds.), Stable isotopes in high temperature geological processes. *Reviews in Mineralogy*, v. **16**, Mineralogical Society of America. p. 570.

O'Neil, J.R., and Taylor, H.P., 1967. The oxygen isotope and cation exchange chemistry of feldspars. *American Mineralogist*, v. **52**, p. 1414-1437.

O'Neil, J.R., Clayton, R.N., Mayeda, T.K., 1969. Oxygen isotope fractionation in divalent metal carbonates. *Journal of Chemistry and Physics*, v. **51**, p. 5547-5558.

O'Shea, P.D., 1982. ELs 935, 710, 713, lake Hart, Kangaroo Bluff, Fiddle Hill. Report on mapping of the Pandurra Formation. Report WY82.7, for Afmenco Pty. Ltd. South Australia Department of Mines and Energy, open file envelope 3992, p. 20-67 (unpublished).

Ohmoto, H., 1986. Chapter 14, Stable isotope geochemistry of ore deposits. In: Stable isotopes in high temperature geological processes. *Reviews in mineralogy*. v. **16**. Mineralogical Society of America.

Ohmoto, H., and Lasaga, A.C., 1982. Kinetics of reactions between aqueous sulphates and sulphides in hydrothermal systems. *Geochemica et Cosmochemica Acta*, v. **46**, p. 1727-1745.

Ohmoto, H., and Rye, R.O., 1979. Isotopes of sulphur and carbon. In: Barnes, H.L., (ed.) 1979, *Geochemistry of hydrothermal ore deposits*. Second edition. New York: Wiley.

Oreskes, N., and Einaudi, M.T., 1990. Origin of rare earth element enriched breccias at the Olympic Dam Cu-U-Au-Ag deposit, Roxby Downs, South Australia. *Economic Geology*, v. **85**, p. 1-28.

Oreskes, N., and Einaudi, M.T., 1992. Origin of hydrothermal fluids at Olympic Dam: preliminary results from fluid inclusions and stable isotopes. *Economic Geology*, v. **87**, p. 64-90.

Palmer, S.E., and Baker, E.W., 1978. Copper porphyrins in deep sea sediments: A possible indicator of oxidised terrestial organic matter. *Science*, v. **201**, p. 49-51.

Parker, A. J., Preiss, W. V. and Rankin, L. R.,1993. Geological framework. In: Drexel, J. F., Preiss, W. V. and Parker, A. J., (eds), *The geology of South Australia. volume 1, The Precambrian.*. South Australia Geological Survey Bulletin, **54**. p. 9-23.

Parker, A.J., 1978. Structural, stratigraphic and metamorphic geology of the Lower Proterozoic rocks in the Cowell/Cleve district, eastern Eyre Peninsula. University of Adelaide. PhD thesis (unpublished).

Parker, A.J., 1980a. Stratigraphic subdivision of the Hutchison Group on the northeastern Eyre Peninsula. *Journal of the Geological Society of Australia*, v. **27**, p 48.

Parker, A.J., 1980a. The Kalinjala Mylonite Zone, eastern Eyre Peninsula. *Quarterly Geological Notes, South Australia Geological Survey*, v. **76**, p. 6-11.

Parker, A.J., 1983. *Whyalla map sheet. South Australia.* Geological Survey. Geological atlas 1:250,000 series, sheet SI53-8.

Parker, A.J., 1989. Mafic dyke swarms in relation to extensional tectonics: A Proterozoic model. *Geological Society of Australia Abstracts*, v. **24**, p. 114-115.

Parker, A.J., 1993a. Kimban Orogeny. In: Drexel, J. F., Preiss, W. V. and Parker, A. J., (eds), The geology of South Australia. volume 1, The Precambrian. *South Australia Geological Survey Bulletin*, **54**, p. 71-82.

Parker, A.J., 1993b. Cleve and Moonta Subdomains. In: Drexel, J. F., Preiss, W. V. and Parker, A. J., (eds), The geology of South Australia. volume 1, The Precambrian. *South Australia Geological Survey Bulletin*, **54**, p. 51-68.

Parker, A.J., and Lemon, N.M., 1982. Reconstruction of the Early Proterozoic stratigraphy of the Gawler Craton, South Australia. *Geological Society of Australia Journal*, v. **29**, p. 221-238.

Parker, A.J., Fanning, C.M., and Flint, R.B., 1985. Geology. In: Twidale, C.R., Tyler, M.J., and Davies, M. (eds.), Natural history of the Eyre Peninsula. *Royal Society of South Australia. Occasional Publications*, v. **4**, p. 21-45.

Parker, A.J., Fanning, C.M., Flint, R.B., Martin, A.R., and Rankin, L.R., 1988. *Archean-Early Proterozoic granitoids, metasediments and mylonites of southern Eyre Peninsula, South Australia.* Specialist Group in Tectonics and Structural Geology Field Guide Series No. **2**. Geological Society of South Australia.

Parr, J.M., and Plimer, I.K., 1993. Models from Broken Hill Type lead - zinc - silver deposits. In: Kirkham, R.V., Sinclair, W.D., Thorpe, R.I., and Duke, J.M. (eds.) Mineral Deposit Modelling. *Geological Association of Canada Special Paper*, **40**, p. 253-288.

Paterson, E., Bunch, J.L., and Duthie, D.M.L., 1986. Note -Preparation of randomly-orientated samples for X-ray diffractometry. *Clay Minerals*, v. **21**, p. 101-106.

Paterson, H.L., and Muir, P.M., 1986. *Exploration Licence 1316*, relinquishment report, South Australian Department of Mines and Energy, Report **6562.**

Paterson, S.R., Vernon, R.H., and Tobisch, O.T., 1989. A review of criteria for the identification of magmatic and tectonic foliations in granitoids. *Journal of Structural Geology*, v. **11**, p. 349-363.

Perrotta, A., and Scarpati, C., 1994. The dynamics of the breccia at Meseo eruption (Campi Flegrei, Italy) and the significance of spatter clasts associated with lithic breccias. *Journal of Volcanology and Geothermal Research*, v. **59**, p. 335-355.

Potter, R.W., 1977. Pressure corrections for fluid-inclusion homogenisation temperatures based on the volumetric properties of the system NaCl - H2O. *Journal of Research, U.S. Geological Survey*, v. **5**, p603-607.

Potter, R.W., and Brown, D.L., 1977. The volumetric properties of aqueous sodium chloride solutions from 0° to 500°C at pressures of up to 2000 bars based on a regression of available data in the literature. *U.S. Geological Survey Bulletin* , **1421C**.

Preiss, W.V., (compiler), 1987. *The Adelaide Geosyncline - Late Proterozoic stratigraphy, sedimentation, palaeontology and tectonics.* South Australia Geological Survey Bulletin, v. **53**.

Rajagopalan, S., Zhiqun, S., and Major, R., 1993. Geophysical investigations of volcanic terrains: A case history from the Gawler range Volcanic Province, South Australia. *Exploration geophysics*, v. **24**, p. 769-778.

Ramdohr, P., 1969. *Ore minerals and their intergrowths.* Pergamon, Oxford, 1174p.

Ramsay, J.G. and Huber, M.I., 1987. *The techniques of modern structural geology*, v. *2: Folds and fractures.* Academic Press, London.

Rankin, L.R., Flint, R.B., and Fanning, C.M., 1988. The Bosanquet Formation of the Gawler Craton. South Australia. Geological Survey. *Quaterly Geological Notes*, v. **105**, p. 12-18.

Recio, C., Fallick, A.E., and Ugidos, J.M, 1991. Sulphur isotope systematics of granitoids and associated rocks from the Avila - La Alberca area (Western Sistema Central Spain). *Revisita De La Sociedad Geologica De Espana*, v. **4**, p. 371-381.

Reeve, J.S., 1990a. The discovery and evaluation of the Olympic Dam deposit. In: Glasson, K.R., Rattigan, J.M., Blaikie, A.H., and Woodcock, J.T., (eds.). *Geological aspects of the discovery of important minerals in Australia.* The Australian Institute of Mining and Metallurgy, Melbourne, p. 125-133.

Reeve, J.S., 1990b. The discovery of gold mineralisation within the Olympic Dam deposit, South Australia. In: Glasson, K.R., Rattigan, J.M., Blaikie, A.H., and Woodcock, J.T., (eds.). *Geological aspects of the discovery of important minerals in Australia.* The Australasian Institute of Mining and Metallurgy, Melbourne, p. 57-58.

Reeve, J.S., Cross, K.C., Smith, R.N., and Oreskes, N., 1990. Olympic Dam copper-uranium-gold-silver deposit. In: Hughes, F.E. (ed.). Geology of the mineral deposits of Australia and Papua New Guinea. *Australasian Institute of Mining and Metallurgy. Monograph Series*, **14**, p. 1009-1035.

Richard, K., and Courtright, J.H., 1959. Geology of Toquepala, Peru, *American Institute Mining and Engineering Trans.*, v. **10**, p. 262-266.

Riehle, J.R., 1973. Calculated compaction profile of rhyolitic ash-flow tuffs. *Geological Society of America Bulletin*, v. **84**, p. 2193-2216.

Riehle, J.R., Miller, T.F., and Bailey, R.A., 1995. Cooling, degassing and compaction of rhyolitic ash flow tuffs: a computational model. *Bulletin of Volcanology*, v. **57**, p. 319-336.

Roach, M.J., 1993. Model 2D, version 3.1, Interactive 2D gravity and magnetic modelling for IBM PC compatible computers. Available from; The Centre for Ore Deposits and Exploration Studies, University of Tasmania, PO Box 252C Hobart, Tasmania 7001, Australia.

Roache, M.W., and Fanning, C.M., 1994. Timing of mineralisation at the Menninnie Dam Pb-Zn-Ag deposit, Eyre Peninsula, South Australia. *Geological Society of Australia, Abstracts*, v. **37**, p. 376-377.

Roberts, D.E., and Hudson, G.R.T., 1983. The Olympic Dam copper-uranium-gold-deposit, Roxby Downs, South Australia. *Economic Geology*, v. **78**, p. 799-822.

Robertson, B.D., 1989. The geology, petrology and geochemistry of the volcanics in the Kakotha region, Gawler Ranges, South Australia. University of Adelaide Honours thesis (unpublished).

Rock, N.M.S, and Carroll, G.W., 1990. MINTAB: A general-purpose mineral recalculation and tabulation program for Macintosh microcomputers. *American Mineralogist*, v. 75, p. 424-430.

Roedder, E., 1984. Fluid inclusions. *Reviews in mineralogy,* v.**12**, Mineralogial Society of America.

Rollinson, H., 1993. *Using geochemical data: evaluation, presentation, interpretation.* Longman, Essex, England.

Rose, A.W., 1976. The effect of aqueous chloride complexes in the origin of red-bed copper and related deposits. *Economic Geology*, v. **71**, p. 1036-1048.

Ross, C.S., and Smith, R.L., 1961. Ash-flow tuffs: Their origin, geologic relations and identification. *USGS Professional Paper* v. **366**.

Rowan, I.S., 1970. Regional gravity survey of Kimba and Elliston 1:250,000 map areas. *South Australia Mineral Resources Review*, v. **128**, p. 26-32.

Ruaya, J.R., and Seward, T.M., 1986. The stability of chlorozinc (II) complexes in hydrothermal solutions up to 350°C. *Geochimica et Cosmochimica Acta*, v. **50**, p. 651-661.

Russell, R.D., and Farquhar, R.M., 1960. *Lead isotopes in geology.* New York, Interscience.

Rye, D.M., and Williams, N., 1981. Studies of the base metal sulphide at McArthur River, Northern Territory, Australia: III. The stable isotope geochemistry of the H.Y.C., Ridge, and Cooley deposits. *Economic Geology*, v. **76**, p. 1-26.

Rye, R.O., Schuiling, R.D., Rye, M.D., and Jansen, J.B.H., 1976. Carbon, hydrogen and oxygen isotope studies of the regional metamorphic complex at Naxos, Greece. *Geochimica et Cosmochimica Acta*, v. **40**, p. 1031-1049.

Sakai, H., and Tsutsumi, M., 1978. D/H fractionation between serpentine and water at 100° to 500°C and 2000bar water pressure, and the D/H ratios of natural serpentines. *Earth and Planetry Science Letters*, v. **40**, p. 231-242.

Savin, S.M., and Lee, M., 1988. Isotopic studies of phyllosilicates. In: *Reviews in Mineralogy*, v. **19**, Mineralogical Society of America, p. 189-223,

Sawkins, F.J., O'Neill, J.R., and Thompson, J.M., 1979. Fluid inclusion and geochemical studies of vein gold deposits, Baguio district, Philippines. *Economic Geology*, v. **74**, p. 1420-1434.

Sawyer, D.A., and Lipman, P.W., 1983. Silver Bell Mountains, Arizona: Porphyry copper mineralisation in a late Cretaceous caldera complex (abstract), *Eos. Transactions of the American Geophysical Union*, v. **64,** p. 874.

Schmincke, H-U., 1967. Fused tuff and peperites in south-central Washington. *Geological Society of America Bulletin*, v. **78**, p. 319-330.

Schul'gina, M.P., Karchuck, O.S., and Yanatieva, O.K., 1955. New solid phases in the system KCl-$K_2SO_4$-$H_2O$. Sekt. *Fiz. Khim. Anal., Obsch. Zn. Neorg. Khim., Akad. Nauk. S.S.S.R.*, v. **26**, p. 198-210.

Schwarzenbach, G., and Widmer, M., 1966. Die Loslichkeit von Metallsulpfiden: II Silbersulfid. *Helvetica Chimica Acta*, v. **49**, p. 111-123.

Scott, I.R., 1987. The development of an ore reserve methodology for the Olympic Dam copper-uranium-gold deposit. In: *Resources and Reserves Symposium, Sydney, 1987*, The Australian Institute of Mining and Metallurgy, Melbourne, p. 99-103.

Scott, K.M., Vallance, J.W., and Pringle, P.T., 1995. Sedimentology, behavior, and hazards of debris flows at Mount Rainier, Washington. *United States Geological Survey Professional Paper*, No. **1547**.

Scott, R.B., 1971. Alkali exchange during devitrification and hydration of glasses in ignimbrite cooling units. *Geology*, v. **79**, p. 100-110.

Self, S., and Wright, J.V., 1983. Large wave forms from the Fish Canyon Tuff, Colorado. *Geology*, v. **11**, p. 443-446.

Self, S., Kienle, J., and Huot, J., 1980. Ukinrek maars, Alaska, II. Deposits and formation of the 1977 craters. *Journal of Volcanology and Geothermal Research*, v. **7**, p. 39-65.

Seward, T.M., 1976, The solubility of chloride complexes of silver in hydrothermal solutions up to 300°C. *Geochimica et Cosomchimica Acta,* v. **40**, p. 1329-1341.

Seyfried, W.E (Jr.), and Ding, K., 1993. The effect of redox on the relative solubilities of copper and iron in Cl-bearing aqueous fluids at elevated temperatures and pressures: An experimental study with application to subseafloor hydrothermal systems. *Geochimica et Cosomchimica Acta*, v. **57**. p. 1905-1917.

Shand, S.J., 1927. *The eruptive rocks*. Wiley, New York.

Shanks, W.C., and Bischoff, J.L., 1977. Ore transport and deposition in the Red Sea geothermal system: A geochemical model. *Geochimica et Cosmochimica Acta*, v. **41**, p. 1507-1519.

Sharma, P.V., 1986. *Geophysical methods in geology*. Elsevier Science, New York.

Shawe, D.R., and Snyder, D.B., 1988. Ash-flow eruptive megabreccias of the Manhattan and Mount Jefferson calderas, Nye County, Nevada. *U.S. Geological Survey. Professional. Paper,* No. **1471**.

Shelton, K.L., 1983. Composition and origin of ore-forming fluids in a carbonate-hosted porphyry copper and skarn deposit: A fluid inclusion and stable isotope study of Mines Gaspe, Quebec. *Economic Geology*, v. **78**, p. 387-421.

Shepherd, T.J., Rankin, A.H., and Alderton, D.H.M., 1985. A practical guide to fluid inclusion studies. Blackie & Son. Glasgow, United Kingdom, p. 239.

Sheppard, S.M.F., 1977. The Cornubian batholith, SW England: D/H and 18O / 16O studies of kaolinite and other alteration minerals. *Journal of the Geological Society*, v. **133**, p. 573-591.

Sheppard, S.M.F., 1986. Characterisation and isotopic variations in natural waters. In: Valley, J.W., Taylor, H.P. (Jr.), and O'Neil, J.R., Stable isotopes in high temperature geological processes. *Reviews in Mineralogy*, v. **16**, p. 165-184.

Sheppard, S.M.F., and Gilg, H.A., 1996. Stable isotope geochemistry of clay minerals. *Clay Minerals*, v. **31**, p. 1-24.

Sheppard, S.M.F., and Schwartz, H.P., 1970. Fractionation of carbon and oxygen isotopes and magnesium between metamorphic calcite and dolomite. *Contributions to Mineralogy and Petrology*, v. **26**, p. 161-198.

Shimazaki, H., and Kusakabe, M., 1990. D/H ratios of sericites from the Kamioka Mining Area. *Mining Geology*, v. **40**, p. 385-388.

Sibson, R.H., 1977. Fault rocks and fault mechanisms. *Journal. Geological Society of London*, v. **133**, p. 191-213.

Sillitoe R. H., 1985. Ore Related Breccias in Volcanoplutonic Arcs: *Economic Geology* v. **80:6** p. 1467-1514.

Sillitoe, R.H., Baker, E.M., and Brooks, W.A., 1984. Gold deposits and hydrothermal eruption breccias assocaited with a maar volcano at Wau, Papua New Guinea. *Economic Geology*, v. **79**, p. 638-655.

Slaughter, J., Kerrick, D.M., and Wall, V.J., 1975. Experimental and thermodynamic study of equilibria in the system CaO-MgO-SiO2-H2O-CO2. *American Journal of Science*, v. **275**, p. 143-162.

Smith, G.A., 1986. Coarse-grained nonmarine volcaniclastic sediment: Terminology and depositional process. *Geological Society of America Bulletin*, v. **97**, p. 1-10.

Smith, R.B., Braile, L.W, 1994. The Yellowstone hotspot. *Journal of Volcanology and Geothermal Research*, v. **61**, p. 121-187.

Smith, R.L., 1960. Ash flows. *Geological Society of America Bulletin*, v. **71**, p. 795-842.

Smith, R.L., and Bailey, R.A., 1968. Resurgent Cauldrons. In: Studies in volcanology, *Memoirs, Geological Society of America,* v. **116**, p. 613-662.

Smith, R.M., and Martell, A.E., 1976. *Critical stability constants*: Volume 1: Amino acids, Volume 2: Amines, Volume 3: Other organic ligands,Volume 4: Inorganic complexes, New York: Plenum Press.

Smith, R.N., 1993. Olympic Dam: some developments in geological understanding over nearly two decades. In: *Australasian Institute of Mining and Metallurgy, Publication Series*, **2/93**, The Australasian Institute of Mining and Metallurgy Centenary Conference, Adelaide, 1993.

Sparks, R.S. J., Self, S., and Walker, G.P.L., 1973. Products of ignimbrite eruptions. *Geology* v. **1**, p. 115-118.

Sparks, R.S.J., Wilson, L., and Hulme, G., 1978. Theoretical modelling of the generation, movement, and emplacement of pyroclastic flows by column collapse. *Journal of Geophysical Research*, v. **83** No. **B4**, p. 1727-1739.

Spear, F.S., 1993. *Metamorphic phase equilibria and pressure - temperature - time paths*. Mineralogical Society of America, Washington, D. C.

Spear, F.S., and Cheney, J.T., 1989. A petrogenic grid for pelitic schists in the system SiO2 - Al2O3 - FeO - MgO - K2O - H2O. *Contributions to Mineralogy and Petrology*, v. **101,** p. 149-164.

Spear, F.S., and Peacock, S.M., 1990. *Metamorphic P-T-t paths, program manual and computer exercises for the calculation of metamorphic phase equilibria, pressure-temperature-time paths and thermal evolution of orogenic belts*. Rensselaer Polytech Institute, Troy, N.Y., U.S.A.

Spencer, E., 1937. The potash-soda-felspars; I, Thermal stability. *Mineralogical Magazine*, v. **24**, p. 53-494.

Stacey, J.S., and Kramer, J.D., 1975. Approximation of terrestrial lead isotope evolution by a two-stage model. *Earth and Planetary Science Letters*, v. **26**, p. 207-221.

Stanton, R.L., 1972. *Ore Petrology*. McGraw-Hill, New York.

Sterner, S.M., and Bodnar, R.J., 1984. Synthetic fluid inclusions in natural quartz. 1. Compositional types synthesized and applications to experimental geochemistry. *Geochimica et Cosmochimica Acta*, v. **48**, p. 2659-2668.

Stevenson, R.J., Briggs, R.M., and Hodder, P.W., 1993. Emplacement history of a low-viscosity, fountain-fed pantelleritic lava flow. *Journal of Volcanology and Geothermal Research*, v. **57**, p. 39-56.

Stewart, K., and Foden, J., 1990. The fundamental role of mantle derived magma in the production of a large volume felsic volcanic province, Gawler Ranges, South Australia. Seventh international conference on geochronology, cosmochronology and isotope geology, Canberra, *Geological Society of Australia, Abstracts*, v. **27**, p. 96.

Stewart, K.P., 1992. High temperature felsic volcanism and the role of mantle magmas in Proterozoic crustal growth: The Gawler Range Volcanic Province. University of Adelaide PhD thesis (unpublished).

Strauss, H., 1993. The sulphur isotopic record of Precambrian sulphates: new data and critical evaluation of the existing record. *Precambrian Research*, v. **63**, p. 225-246.

Sturt, B. A., 1962. The composition of garnets from pelitic schists in relation to the grade of regional metamorphism. *Journal of Petrology*, v. **3, part 2**, p. 181-191.

Sun, S.S., and Page, R., 1994. Lead-isotope-based stratigraphic correlations and ages of Proterozoic sediment-hosted Pb-Zn deposits in the Mount Isa Inlier. *AGSO Research Newsletter*, v. **20**, p. 1-2.

Suzuoki, T., and Epstein, S., 1976. Hydrogen isotope fractionation between OH-bearing minerals and water. *Geochemica et Cosmochemica Acta*, v. **40**, p. 1229-1240.

Sverjensky, D.A., 1981. Isotopic alteration of carbonate host rocks as a function of water to rock ratio - an example from the upper Mississippi Valley zinc - lead district. *Economic Geology*, v. **76**, p. 154-172.

Sverjensky, D.A., 1981. The origin of a Mississippi Valley-type desposit in the Viburnum Trend, Southeast Missouri. *Economic Geology*, v. **76**, p. 1848-1872.

Sverjensky, D.A., 1984. Oil field brines as ore-forming solutions. *Economic Geology*, v. **79**, p. 23-37.

Sverjensky, D.A., 1986. Genesis of Mississippi Valley-type lead - zinc desposits (sic). *Annual Review Earth and Planetary Science*, v. **14**, p. 177-199.

Talwani, M., 1965. Computation with the help of a digital computer of magnetic anaomlies caused by bodies of arbitary shape. *Geophysics*, v. **30**, p. 797-817.

Talwani, M., Worzel, J.L., and Landisman, M., 1959. Rapid gravity computations for two-dimensional bodies with application to Mendocino submarine fracture zone. *Journal of Geophysical Research*, v. **64 (1)**, p. 49-59.

Taylor, B.E. and Bucher-Nurminen, K., 1986. Oxygen and carbon isotope and cation geochemistry of metasomatic carbonates and fluids - Bergel aureole, Northern Italy. *Geochimica et Cosmochiica Acta*, v. **50**, p. 1267-1279.

Taylor, B.E., 1987. Stable isotope geochemistry of ore-forming fluids. In: Kyser, T.K., (ed.) *Short course in stable isotope geochemistry of low temperature fluids*. v. **13**, Mineralogical Association of Canada.

Taylor, H.P. (Jr.), 1974. The application of hydrogen and oxygen isotope studies to problems of hydrothermal alteration and ore deposition. *Economic Geology*, v. **69**, p. 843-883.

Taylor, H.P. (Jr.), 1979. Oxygen and hydrogen isotope relationships in hydrothermal mineral deposits. In: Barnes, H.L. (ed.), 1979, *Geochemistry of hydrothermal ore deposits*, (second edition). John Wiley and Sons, New York, Chichester, Brisbane, Toronto, p. 236-277.

Taylor, H.P., (Jr.), 1977. Water-rock interaction and the origin of H2O in granite batholiths. *Journal Geological Society of London*, v. **133**, p. 509-558.

Taylor, H.P., O'Neil, J.R., and Kaplan, I.R. (eds.), 1991. Stable isotope geochemistry: A tribute to Samuel Epstein. *The Geochemical Society, Special Publication* No. **3**. Trinity University, San Antonio, Texas.

Taylor, W.R., and Berry, R.F., 1990. Origin of the Proterozoic graphite deposits of the southern Eyre peninsula, South Australia - constraints from stable isotope geochemistry. Geological Society of Australia, Abstracts No. 25, *Gondwanna: terranes and Resources*. Tenth Australian Geological Convention, Hobart.

Terry, R.D., and Chilingar, G.V., 1955. Summary of "Concerning some additional aids in sedimentary formations", by M.S. Shevetsov. *Journal of Sedimentary Petrology*, v. **25**, p. 229-234.

Thompson, B.P., 1966. The lower boundary of the Adelaide System and older basement relationships in South Australia. *Journal of the Geological Society of Australia*, v. **13**, p. 216.

Thompson, B.P., 1969. Precambrian crystalline basement. In: Parkin, L.W., (ed.), *Handbook of South Australian geology*. Geological Survey of South Australia, p. 21-48.

Thompson, M.D., 1985. Evidence for a late Precambrian caldera Boston, Massachusetts. *Geology*: v. **13**, p. 641-643.

Thompson, T.B., and Beaty, D.W., 1990. Geology and the origin of the ore deposits in the Leadville District, Colorado: Part II. Oxygen, hydrogen, carbon, sulphur, and lead isotope data and development of a genetic model. *Economic Geology, Monograph* , v. **7,** p. 156-179.

Trommsdorff, V., 1966. Progressive metamorphose kieseliger Karbonatgesteine in den Zentralalpen zwischen Bernina und Simplon. *Schweizerische Mineralogische und Petrographische Mitteilungen,* v. **66**, p. 431-460.

Trommsdorff, V., 1972. Change in T-X during metamorphism of siliceous dolomitic rocks of the central Alps. *Schweizerische Mineralogische und Petrographische Mitteilungen.*, v. **52,** p. 1-4.

Truesdell, A.H., and Jones, B.F., 1974. WATEQ, a computer program for calculating chemical equilibria of natural waters. *Journal Research, U.S. Geological Survey*, v. **2**, p. 233-248.

Tucker, D.H., and Nelson, R.G., 1991. Interpretation and exploration significance of the 1988 Eyre Peninsula airborne magnetic survey, South Australia. *The Australian Society of Exploration geophysicists, 8th Conference and Exhibition, Sydney 1991. Abstracts* , No. **30,** p .31-33.

Turbeville, B.N., 1992. Tephra fountaining, rheomorphism, and spatter flow during emplacement of the Pitigliano Tuffs, Latera caldera, Italy. *Journal of Volcanology and Geothermal Research*, v. **53**, p. 309-327.

Turner, A.R., 1975. The petrology of the eastern Gawler Range Volcanic Complex. *Geological Survey of South Australia, Bulletin,* v. **45**. p. 7-9.

Turner, F.J., 1967. Thermodynamic appraisal of steps in progressive metamorphism of siliceous dolomitic limestones. *Neues Jahrbuch fuer Mineralogie. Monatshefte* , v. **1**, p. 1-22.

Turner, F.J., 1980. *Metamorphic petrology, mineralogical, field, and tectonic aspects*. New York, McGraw-Hill.

Valley, J.W., 1986. Stable isotope geochemistry of metamorphic rocks. In: *Stable isotopes in high temperature geological processes.*

Van Hook, H.J., 1960. The ternary system $Ag_2S$-$Bi_2S_8$-PbS. *Economic Geology*, v. **55**, p. 759-788.

Velde, B., 1965. Experimental determination of muscovite polymorph stabilities. *American Mineralogist*, v. **50**, p. 436.

Vigneresse, J.L., 1983. Enracinement des granites armoricains estime d'apres la gravimrtrie. *Bulletin de la Societe Geologique et miniere de Bretagne*, v. **15**C, p. 1-15.

Vigneresse, J.L., 1990. Use and misuse of geophysical data to determine the shape at depth of granitic intrusions. *Geological Journal*, v. **25**, p. 249-260.

Voight, B., Glicken, H., Janda, R.J. and Douglas, P.M., 1981. Catastrophic rock slide avalanche of May 18. In: Lipman, P.W., and Mullineaux, D.R.,(eds.) 1981, The 1980 eruptions of Mount St. Helens, Washington. *United States Geological Survey Professional Paper*, No. **1250**, p. 347-377.

Von Damm, K.L., 1995. Controls on the chemistry and temporal variability of seafloor hydrothermal fluids. In Humphris, S.E., Zierenberg, R.A., Mullineaux, L.S. and Thomson, R.E., (eds.), Seafloor hydrothermal systems, physical, chemical, biological, and geological interactions. American Geophysical Union, *Geophysical Monograph* v. **91**.

Walker, G.P.L., 1985. Origin of coarse lithic breccias near ignimbrite source vents. *Journal of Volcanology and Geothermal Research,*. v. **25**, p. 157-171.

Walshe, J.L., and Solomon, M., 1981. An investigation into the environment of formation of the volcanic-hosted Mt. Lyell copper deposits using geology, mineralogy, stable isotopes, and a six-component chlorite solid solution model. In: Solomon, M., Walshe, J.L., Eastoe, C.J., (eds.), A special issue on the geology and mineral deposits of Tasmania. *Economic Geology*, v. **76** p. 246-284

Walters, S.J., 1996. An overview of Broken Hill type deposits. In: Pongratz, J., and Davidson,G., *New Developments in Broken Hill-type deposits, CODES Special Publication,* **1**, University of Tasmania, Hobart, Tasmania, p. 1-10.

Watmuff, G., 1973a. Stratigraphy and petrology of the Gawler Range Volcanics. Field and laboratory studies of certain features of the Gawler Range Volcanics and associated rocks from Kokatha, Glenloth, Corunna and Lake Frome areas. Amdel progress report 7. South Australia. Department of Mines and Energy. Open file envelope, 2038, (unpublished).

Watmuff, G., 1973b. Stratigraphy and petrology of the Gawler Range Volcanics. petrographic examination of a suite of Gawler Range Volcanics and associated rocks from the Glenloth and Lake Everard areas. Amdel progress report 8. South Australia. Department of Mines and Energy. Open file envelope, 2038, (unpublished).

Webb, A.W., 1980. A geochronological investigation of the tectono-magmatic history of the Gawler Craton. *Journal of the Geological Society of Australia*, v. **27**, p. 45.

Webb, A.W., Thompson, B.P., Blissett, A.H., Daly, S.J., Flint, R.B., and Parker, A.J., 1986. Geochronology of the Gawler Craton, South Australia. *Australian Journal of Earth Sciences*, v. **33**, p. 119-143.

Wedepohl, K.H., 1978. Lead. In: Wedepohl, K.H., (ed.), *Handbook of geochemistry.* Berlin, Springer Verlag, v. **11/5**, p. 82-E-1 - 82-E-18.

Weissberg, B.G., 1969. Gold-silver ore-grade percipitates from New Zealand thermal waters. *Economic Geology*, v. **64**, p. 95-108.

Wenner, D.B., and Taylor, H.P. (Jr.), 1971. Temperatures of serpentinization of ultramafic rocks based on $O^{18}$ / $O^{16}$ fractionation between coexisting serpentine and magnetite. *Contributions to Mineralogy and Petrology*, v. **32**, p. 165-185.

Wenner, D.B., and Taylor, H.R., Jr., 1973. Oxygen and hydrogen isotope studies of the serpentinisation of ultramafic rocks in oceanic environments and continental ophiolites. *American Journal of Science*, v. **273**, p. 207-239.

Wenrich, K.J., 1985. Mineralisation of breccia pipes in Northern Arizona. *Economic Geology*, v. **80**, p. 1722-1735.

White, J.D.L., 1991. Maar-diatreme phreatomagmatism at Hopi, Buttes, Navajo Nation (Arizona), USA. *Bulletin of Volcanology*, v. **53**, p. 239-258.

White, S., 1976. The effects of strain on the microstructures, fabrics, and deformation mechanisms in quartzites. *Philosophical Transactions of the Royal Society of London*, v. **A283**, p. 69-86.

White, S.H., Burrows, S.E., Carreras, J., Shaw, N.D., Humphreys, F.J., 1980. On mylonites in ductile shear zones. *Journal of Structural Geology*, v. **2**, p. 175-187.

Willcox, J.B., and Stagg, H.M.J., 1990. Australia's southern margin: A product of oblique extension. *Tectonophysics*, v. **173**, p. 269-281.

Williams, A.E., and McKibben, M.A., 1989. A brine interface in the Salton Sea Geothermal System, California: Fluid geochemical and isotopic characteristics. *Geochimica et Cosmochimica Acta*, v. **53**, p. 1905-1920.

Williams, H., and McBirney, A.R., 1979. *Volcanology*. Freeman, Cooper and Company, San Francisco.

Williams, I.S., and Claesson, S., 1987. Isotopic evidence for the Precambrian provenance and Caledonian metamorphism of high grade paragneisses from the Seve Nappes, Scandinavian Caledonides. II. Ion microprobe zircon U-Th-Pb. *Contributions to Mineralogy and Petrology* , v. **97**, p. 205-217.

Winchester, J.A., and Floyd, P.A., 1977. Geochemical determination of different magma series and their dirrerentiation products using immobile trace elements. *Chemical Geology*, v. **20**, p. 325-343.

Winkler, H.G.F., 1976. *Petrogenesis of metamorphic rocks*. Springer Verlag, New York, 4th edition.

Wolfe, J.A., 1986. Breccias related to explosive volcanism. *Journal of Southeast Asian Earth Sciences*, v. **1**, p. 63-79.

Wood, S.A., Crerar, D.A., and Borcsik, M.P., 1987. Solubility of the assemblage pyrite - pyrrhotite - marcasite - sphalerite - galena - gold - stibnite - bismuthinite - argentite - molybdenite in $H_2O$ - NaCl - $CO_2$ solutions from 200° to 350°C. *Economic Geology*, v.**82**, p. 1864 - 1887.

Wright, F.E., 1915. Obsidian from Hraftntinnuhryggur, Iceland: Its lithophysae and surface markings. *Geological Society of American Bulletin*, v. **26**, p. 255-286.

Wright, J.V., and Walker, G.P.L., 1977. The Ignimbrite source problem: significance of a co-ignimbrite lag-fall deposit. *Geology*. v. **5.** p. 729-732.

Wright, J.V., and Walker, G.P.L., 1981. Eruption, transport and deposition of ignimbrite: a case study from Mexico. *Journal of Volcanology and Geothermal Research*. v. **9**. p. 111-131.

Wyborn, L.A.I., Wyborn, D., Warren, R.G., and Drummond, B.J., 1992. Proterozoic granite types in Australia: implications for lower crust composition, structure and evolution. *Transactions of the Royal Society of Edinburgh: Earth Sciences*, v. **83**, p. 201-209.

Yanatieva, O.K., 1946. Solubility polytherms in the system $CaCl_2$-$MgCl_2$-$H_2O$ and $CaCl_2$-NaCl-$H_2O$. *Zhurnal Prikladnoi Khimii,* v. **19**, p. 707-722

Yeates, G., 1990. Middleback Range iron ore deposits. In Hughes, F.E., (ed.), Geology of the mineral deposits of Australia and Papua New Guinea. *Australasian Institute of Mining and Metallurgy. Monograph Series*, v. **14**, p. 1045-1048.

Zartman, R.E., and Stacey, J.S., 1971. Lead isotopes and mineralisation ages in Belt Supergroup rocks, northwestern Montana and northern Idaho. *Economic Geology*, v. **66**, p. 849-860.

Zheng, Y-F., 1993. Calculation of oxygen isotope fractionation in hydroxyl-bearing silicates. *Earth and Planetary Science Letters*, v. **120**, p. 247-263.

Zheng, Y-F., and Hoefs, J., 1993. Carbon and oxygen isotopic covariations in hydrothermal calcites. Theoretical modeling on mixing processes and applications to Pb-Zn deposits in the Harz Mountains, Germany. *Mineralium Deposita*, v. **28**, p. 78-89.

Zotov, A.V., Levin, K.A., Khodakovskiy, I.L., and Kozlov, V.K., 1986. Thermodynamic parameters of Ag(I) chloride complexes in aqueous solution at 273 - 623°K. *Geochemistry International,* v. **23**, p. 103-116.

## Appendix 3.1

Summary drill logs and cross sections

## Accompanying notes

*Rock types*

The rock types are briefly described in the accompanying key and in more detail in Chapter 3 and 4. Units of less than one metre in thickness are not visible at this scale and where such units or contacts are considered to be important, they are dealt with in more detail in the main text. The upper percussion pre-collar of many holes was not logged as part of this study. Un-patterned or un-coloured zones below the start of drill core corresponds to zones of nil recovery. Rock types are displayed as a series of horizontally stacked units. In reality this is not the case, however it is not possible to show the angular relationships between units as drill core is mostly unorientated. A more realistic representation of the angular relationship between units is shown on the schematic interpretative cross sections. A graphical display of grain size is not applicable as clastic units have been substantially modified by upper amphibolite facies metamorphism.

*Structure*

Fault zones are shown as black bars. The thickness of each bar reflects the drill core intersection width of the structural feature. The orientation of structures cannot be determined due to the unorientated nature of the drill core.

*Alteration*

The intensity of alteration is subdivided into three categories: 1 = weak, 2 = moderate, and 3 = intense. Numerical values have not been applied to the intensity of alteration and subdivision was by visual estimation. Alteration has been subdivided into four different types as depicted in the key. Subdivision into these groups is on the basis of a combination of mineral assemblage, textural and temporal relationships and are more fully explained in the main text.

*Mineralisation*

The occurrence of sulphide minerals constitutes mineralisation. Mineralisation is displayed in bar form where the width of the bar reflects the length of drill core which has been mineralised and the length of the bar reflects a visual estimation of the intensity of mineralisation. The intensity of mineralisation is subdivided into three categories, 1 = trace to 5% total sulphides, 2 = 5-20% total sulphides and 3 = >20% total sulphides. Mineralisation is subdivided into three different types each represented by a different colour as depicted in the key. Subdivision into these groups is on the basis of mineralogy, texture and association with a particular style of alteration and is more fully explained in the main text.

**Appendix 3.1 cont.**

*Geochemistry*

The six elements presented are only elements which were routinely analysed. The geochemical data is a combination of three data sets.

1) Core grinds. A grind was taken along the length of almost all core with variable sample intervals of less than 1m to several metres.
2) Zones with visible mineralisation in diamond drill holes were resampled and quarter core was analysed.
3) Percussion holes and the pre-collar to diamond drill core were usually sampled as 2m composites and in some cases 10m composites (percussion holes have the prefix 'PE' or 'RP' followed by a four digit number).

Assay results are presented in bar graph form where the thickness of the bar reflects the width of the sample interval and the length of the bar reflects the assay value in accordance with the appropriate scale. Each bar graph is clipped at a maximum value, (eg. 2 wt % for zinc). Where the analysis exceeds the clip value, the analysis has been recorded at the end of the appropriate bar in the appropriate units (ie wt % for Zn, Pb, Fe and Mn and ppm for Cu and Ag.). Where assay values would have overwritten each other due to closely spaced high values, only the highest analysis is recorded.

# Key to drill hole logs

## Rock types

Tertiary and Quaternary sediments

Clays, dominantly kaolinitic with minor quartz and iron oxides

Menninnie Dam ignimbrite

Muddy sandstone and pumice breccia

Layered polymictic breccia pipes

Discordant polymictic breccia pipes

Rhyolite intrusions and lava

Quartz veins

Granite dykes

Amphibolite intrusions or flows

Graphitic schist.

Quartz-feldspar-biotite-muscovite-sillimanite-garnet schist.

Silicate, carbonate, and calc-silicate facies iron formations

Diopside - quartz rock.

Massive diopside

Diopside - marble rock

Marble

## Fault zones

Brittle fault zones

## Alteration

Texturally destructive quartz ± carbonate ± chlorite ± epidote ± garnet ± tremolite ± graphite ± rhodochrosite ± hematite ± serpentinite alteration associated with the late alteration overprint.

Quartz ± talc ± phlogopite ± sericite ± carbonate ± adularia ± chlorite ± rhodonite alteration associated with Pb - Zn - Ag mineralisation

Microcline ± sericite ± albite ± andradite ± grossular ± epidote ± tremolite ± sphene ± chlorite ± calcite ± hematite associated with metasomatic alteration

Sericite ± chlorite ± quartz alteration associated with deformation (KM-$D_3$ )

## Mineralisation

Disseminated and vein pyrite ± chalcopyrite ± galena ± sphalerite mineralisation associated with the late alteration overprint

Stockwork, breccia and vein carbonate replacement-style, sphalerite, galena and pyrite mineralisation. Chalcopyrite is present as chalcopyrite disease in sphalerite

Disseminated and rare vein pyrite generally associated with zones of deformation (KM-$D_3$ )

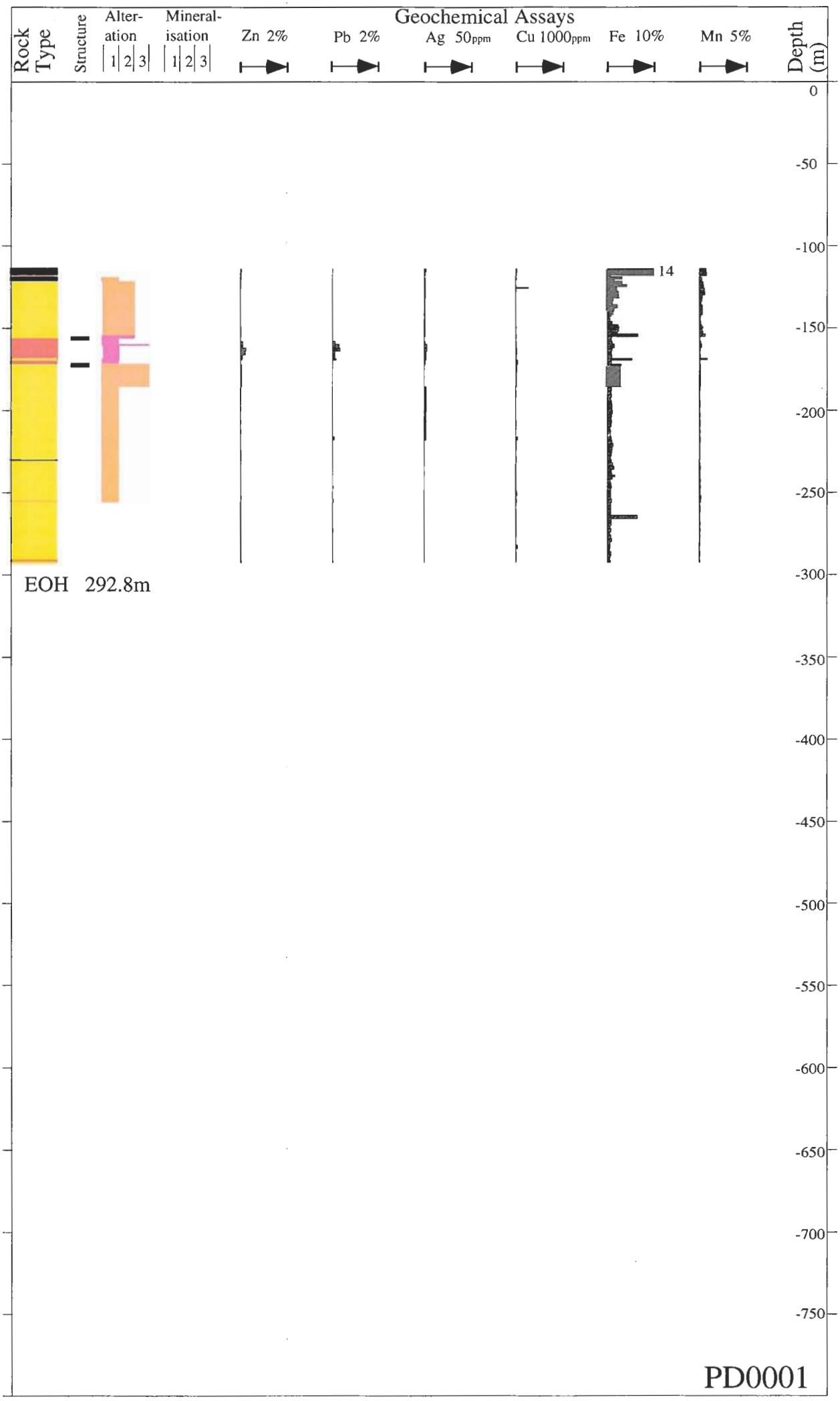
Rock Type
Structure
Alter-ation
1 2 3
Mineral-isation
1 2 3
Geochemical Assays
Zn 2%
Pb 2%
Ag 50ppm
Cu 1000ppm
Fe 10%
Mn 5%
Depth (m)
0
-50
-100
-150
-200
-250
-300
-350
-400
-450
-500
-550
-600
-650
-700
-750
14
EOH 292.8m
PD0001

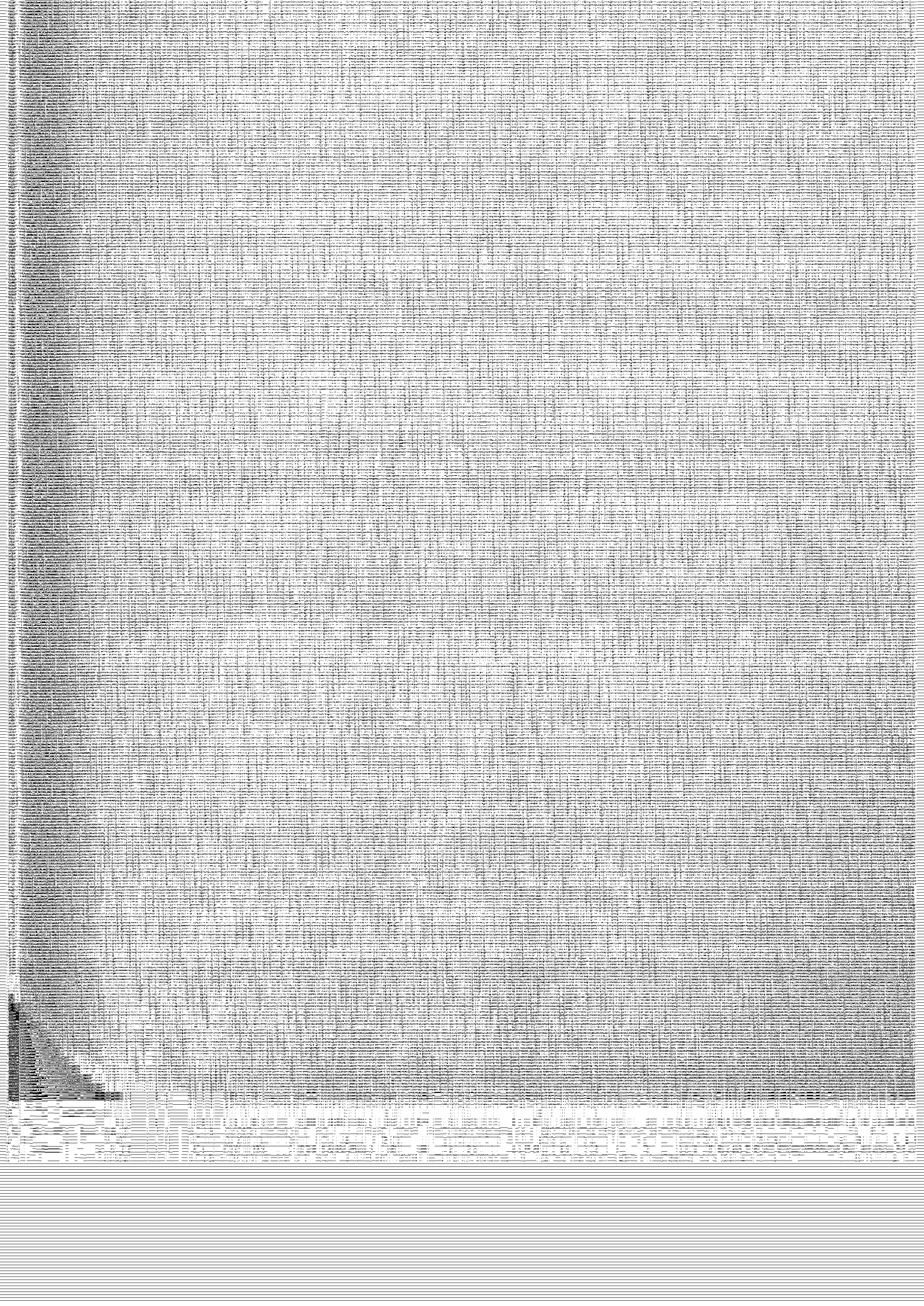

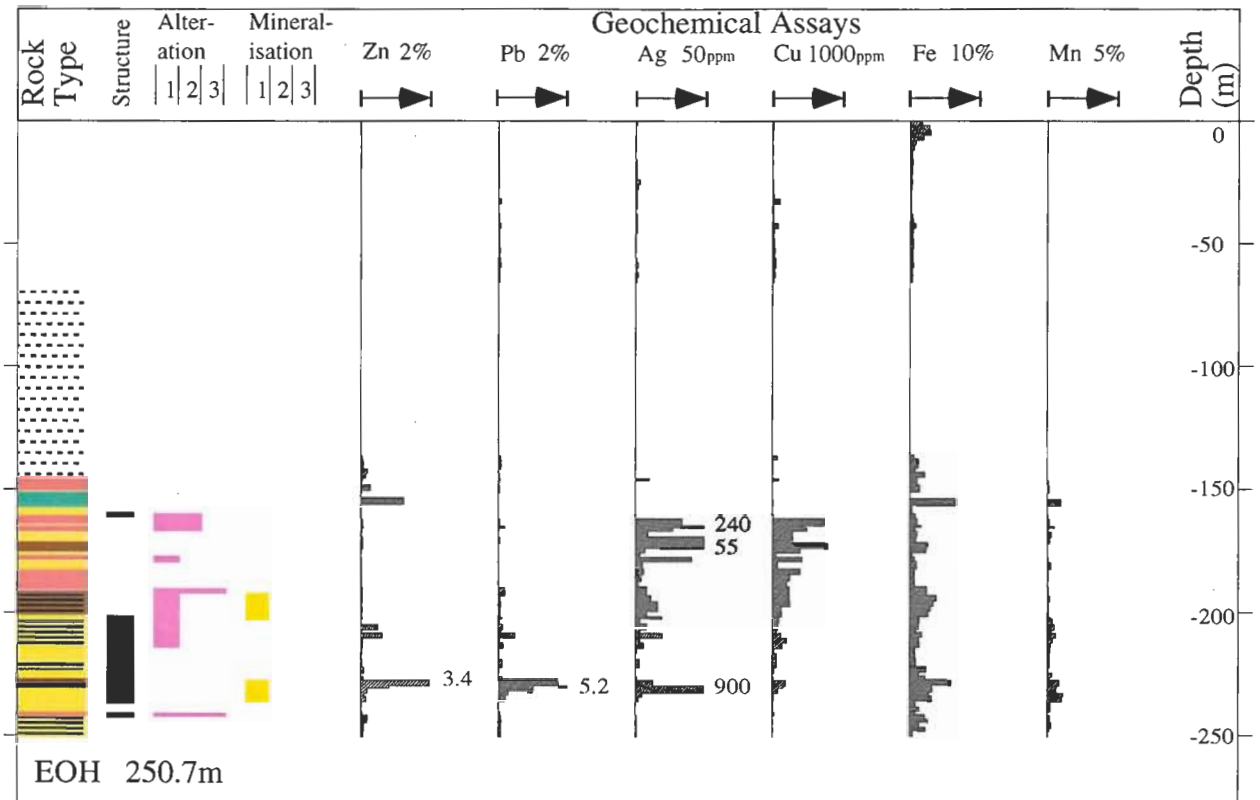


EOH 250.7m



PD0002

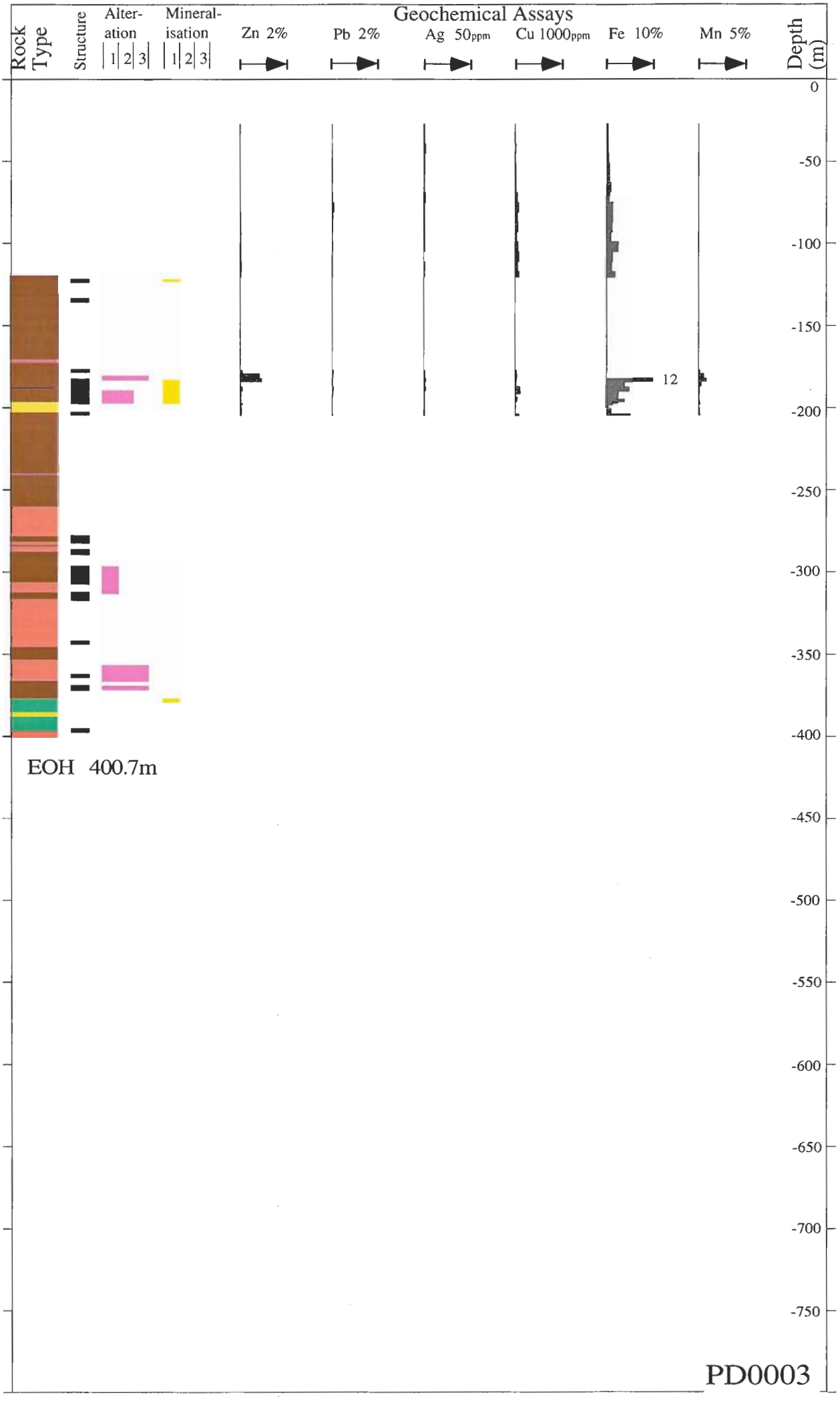
Rock Type
Structure
Alter-ation
1 2 3
Mineral-isation
1 2 3
Geochemical Assays
Zn 2%
Pb 2%
Ag 50ppm
Cu 1000ppm
Fe 10%
Mn 5%
Depth (m)
0
-50
-100
-150
-200
-250
-300
-350
-400
-450
-500
-550
-600
-650
-700
-750
12
EOH 400.7m
PD0003

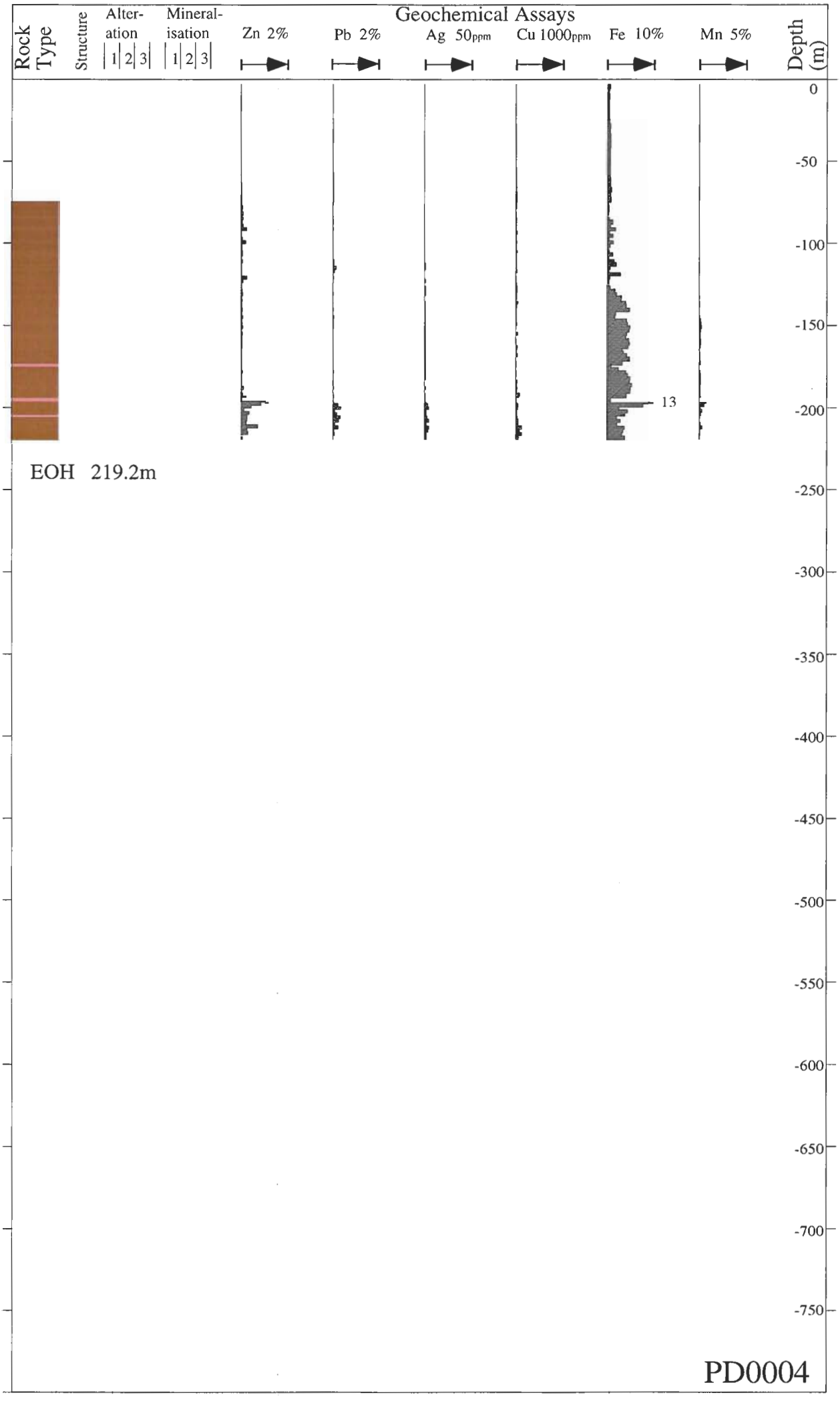
Geochemical Assays
Rock Type
Structure
Alter-ation
1 2 3
Mineral-isation
1 2 3
Zn 2%
Pb 2%
Ag 50ppm
Cu 1000ppm
Fe 10%
Mn 5%
Depth (m)
0
-50
-100
-150
-200
-250
-300
-350
-400
-450
-500
-550
-600
-650
-700
-750
13
EOH 219.2m
PD0004

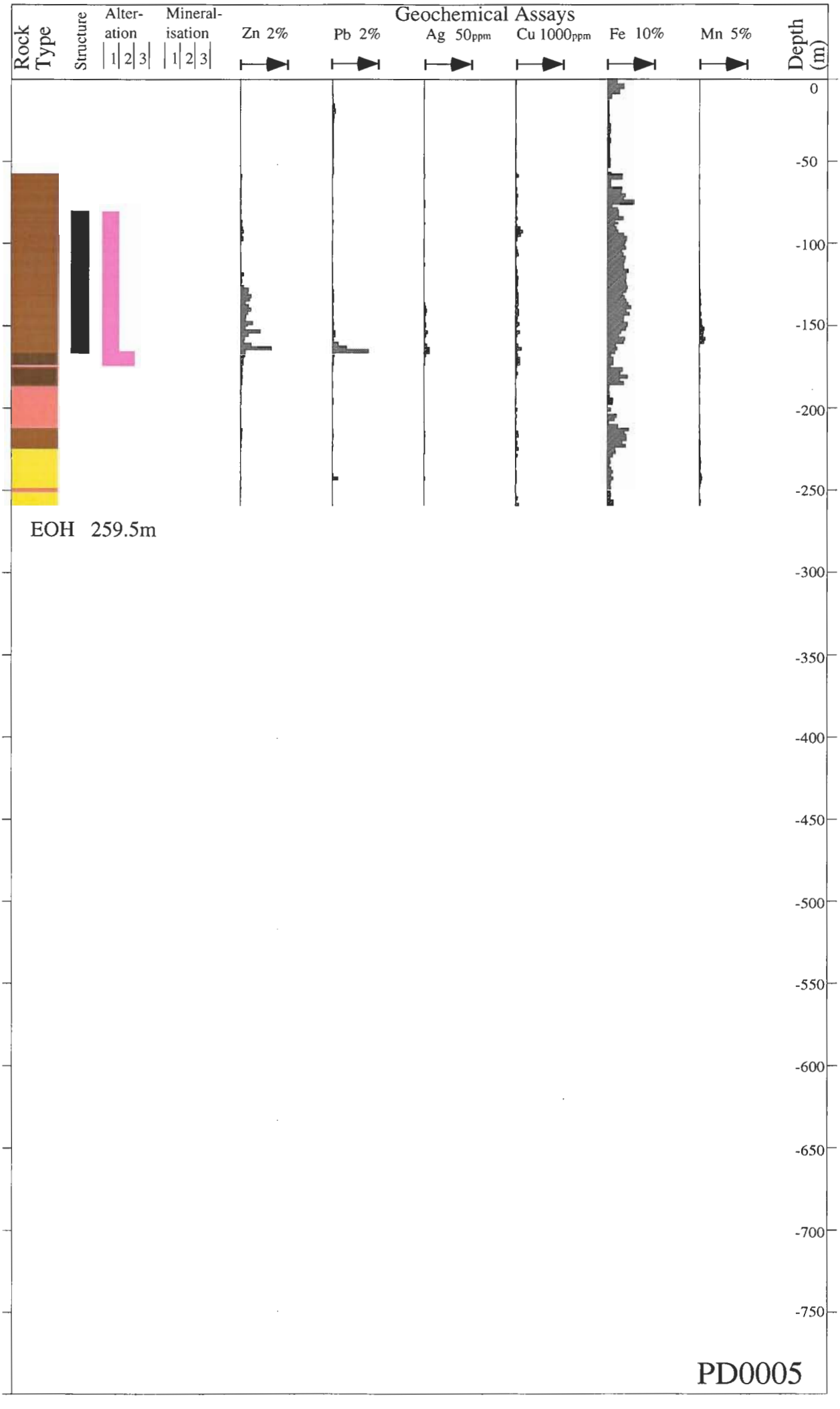
Rock Type
Structure
Alter-ation
1 2 3
Mineral-isation
1 2 3
Geochemical Assays
Zn 2%
Pb 2%
Ag 50ppm
Cu 1000ppm
Fe 10%
Mn 5%
Depth (m)
0
-50
-100
-150
-200
-250
-300
-350
-400
-450
-500
-550
-600
-650
-700
-750
EOH 259.5m
PD0005

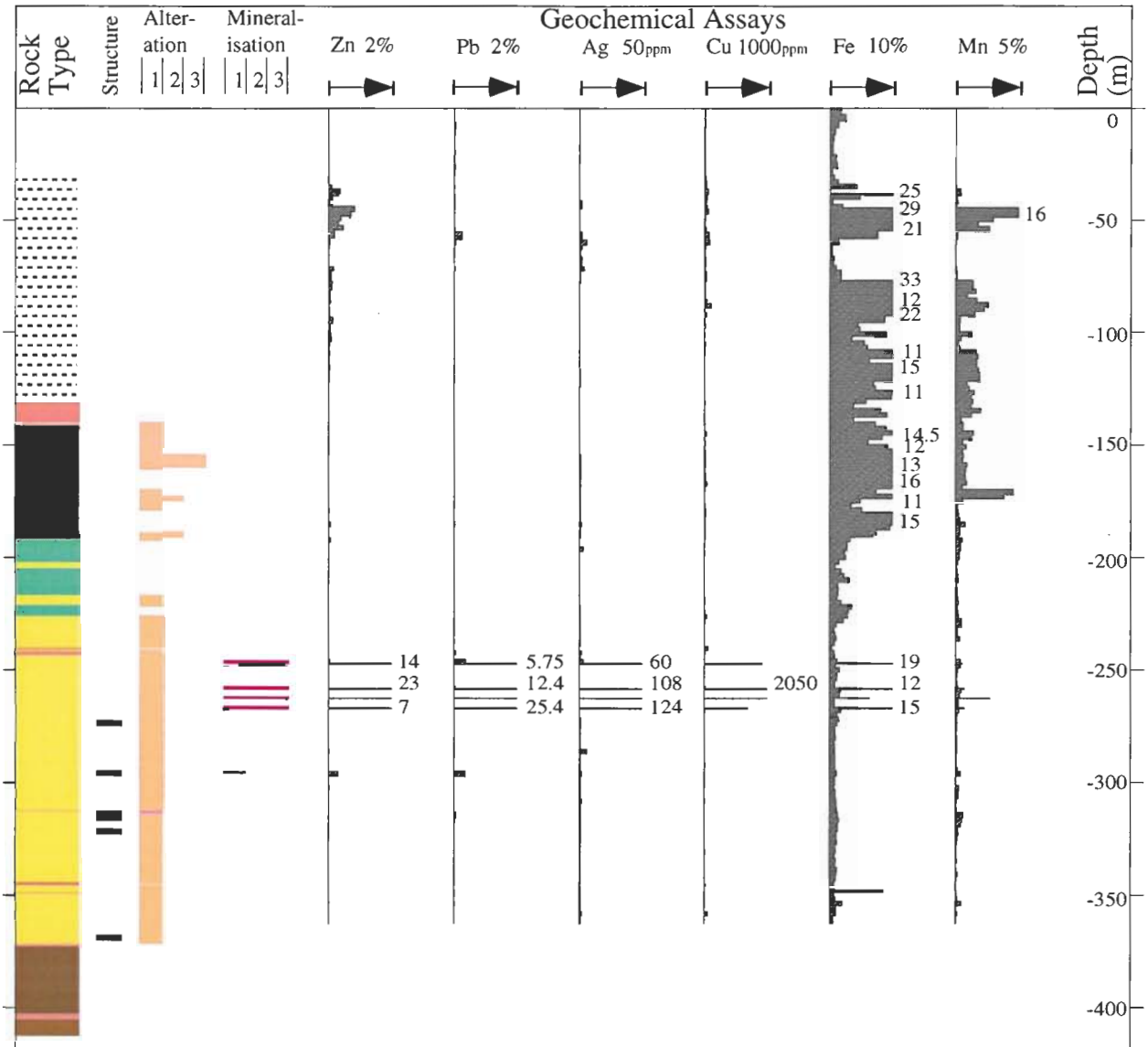


EOH 411.3m

PD0006

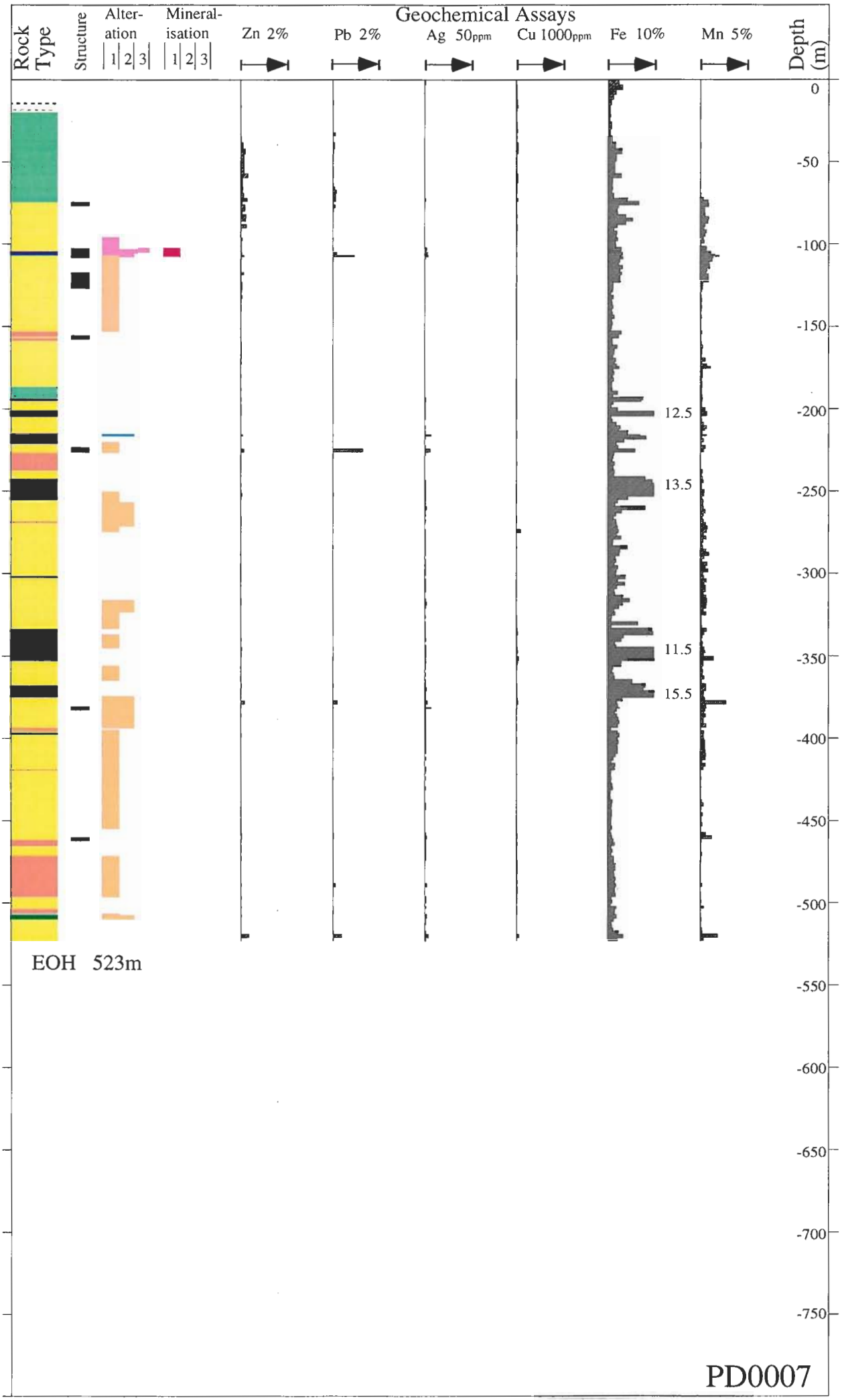
Rock Type
Structure
Alter-ation
1 2 3
Mineral-isation
1 2 3
Geochemical Assays
Zn 2%
Pb 2%
Ag 50ppm
Cu 1000ppm
Fe 10%
Mn 5%
Depth (m)
0
-50
-100
-150
-200
-250
-300
-350
-400
-450
-500
-550
-600
-650
-700
-750
12.5
13.5
11.5
15.5
EOH 523m
PD0007

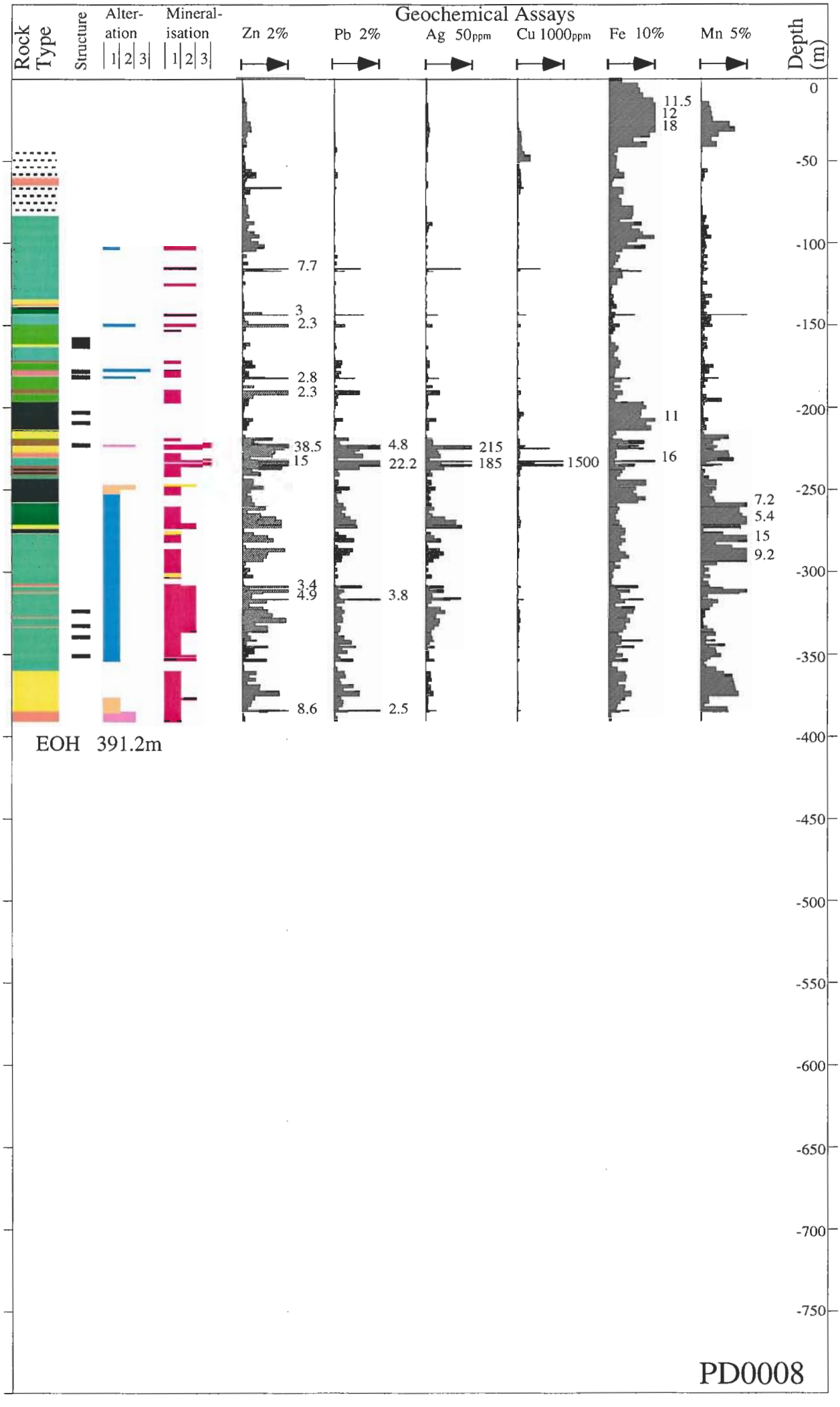
Rock Type
Structure
Alter-ation
1 2 3
Mineral-isation
1 2 3
Geochemical Assays
Zn 2%
Pb 2%
Ag 50ppm
Cu 1000ppm
Fe 10%
Mn 5%
Depth (m)
0
-50
-100
-150
-200
-250
-300
-350
-400
-450
-500
-550
-600
-650
-700
-750
7.7
3
2.3
2.8
2.3
38.5
15
3.4
4.9
8.6
4.8
22.2
3.8
2.5
215
185
1500
11.5
12
18
11
16
7.2
5.4
15
9.2
EOH 391.2m
PD0008

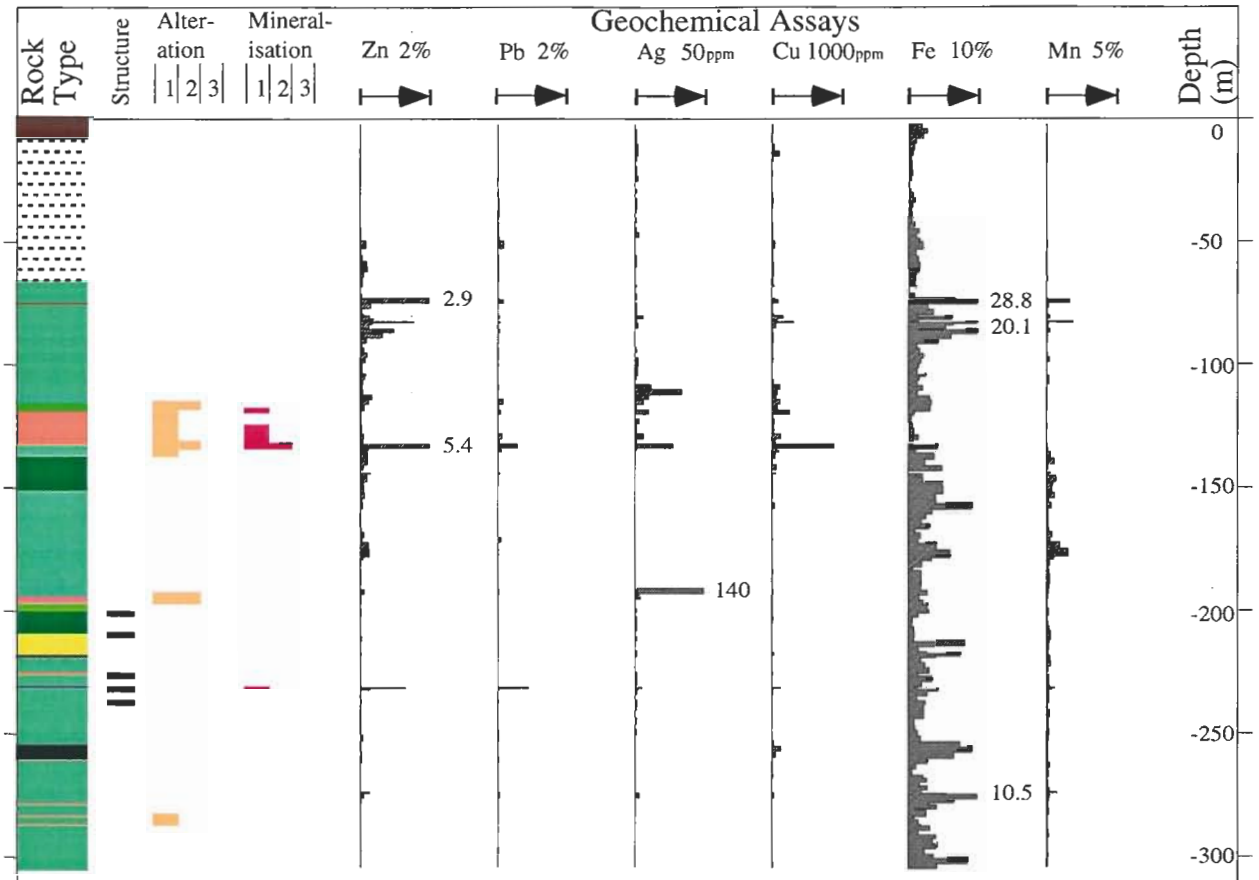


EOH 304m

-350
-400
-450
-500
-550
-600
-650
-700
-750

PD0009

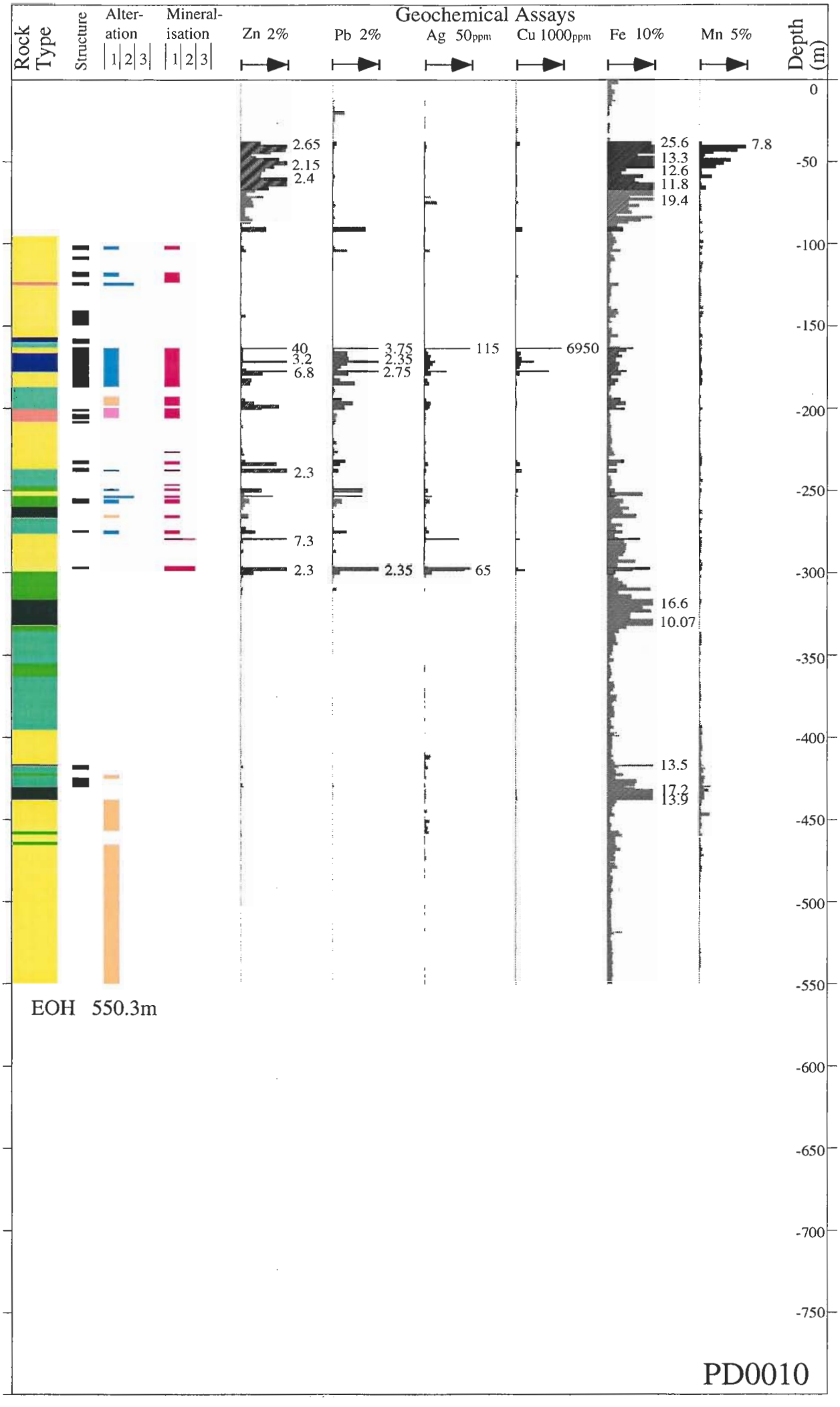
Rock Type
Structure
Alter-ation
1 2 3
Mineral-isation
1 2 3
Geochemical Assays
Zn 2%
Pb 2%
Ag 50ppm
Cu 1000ppm
Fe 10%
Mn 5%
Depth (m)
2.65
2.15
2.4
40
3.2
6.8
2.3
7.3
2.3
3.75
2.35
2.75
2.35
115
65
6950
25.6
13.3
12.6
11.8
19.4
16.6
10.07
13.5
17.2
13.9
7.8
0
-50
-100
-150
-200
-250
-300
-350
-400
-450
-500
-550
-600
-650
-700
-750
EOH 550.3m
PD0010

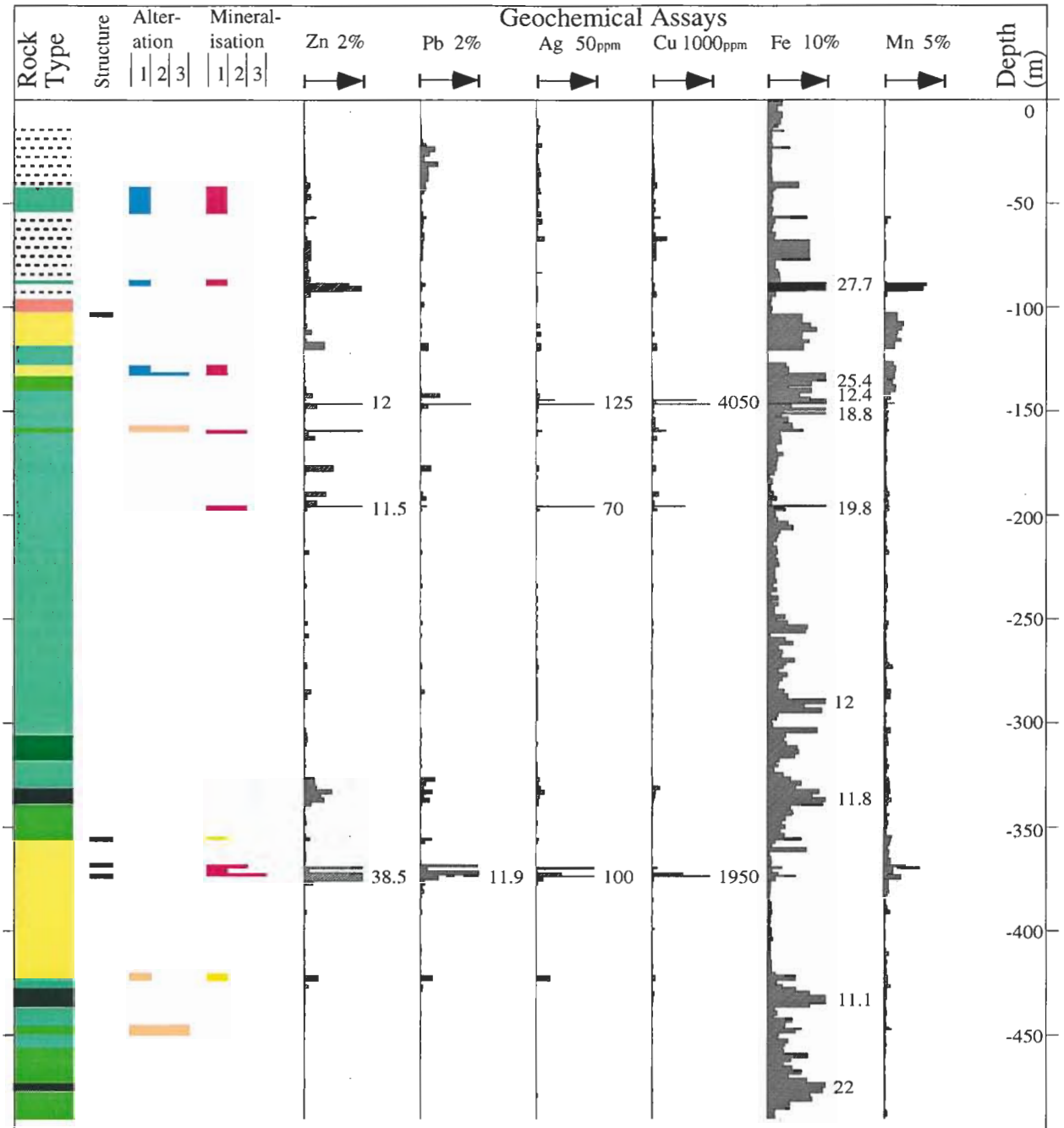
Rock Type
Structure
Alter-ation
1 2 3
Mineral-isation
1 2 3
Geochemical Assays
Zn 2%
Pb 2%
Ag 50ppm
Cu 1000ppm
Fe 10%
Mn 5%
Depth (m)
0
-50
-100
-150
-200
-250
-300
-350
-400
-450
-500
-550
-600
-650
-700
-750
12
11.5
38.5
11.9
125
70
100
4050
1950
27.7
25.4
12.4
18.8
19.8
12
11.8
11.1
22
EOH 490.3m
PD0011

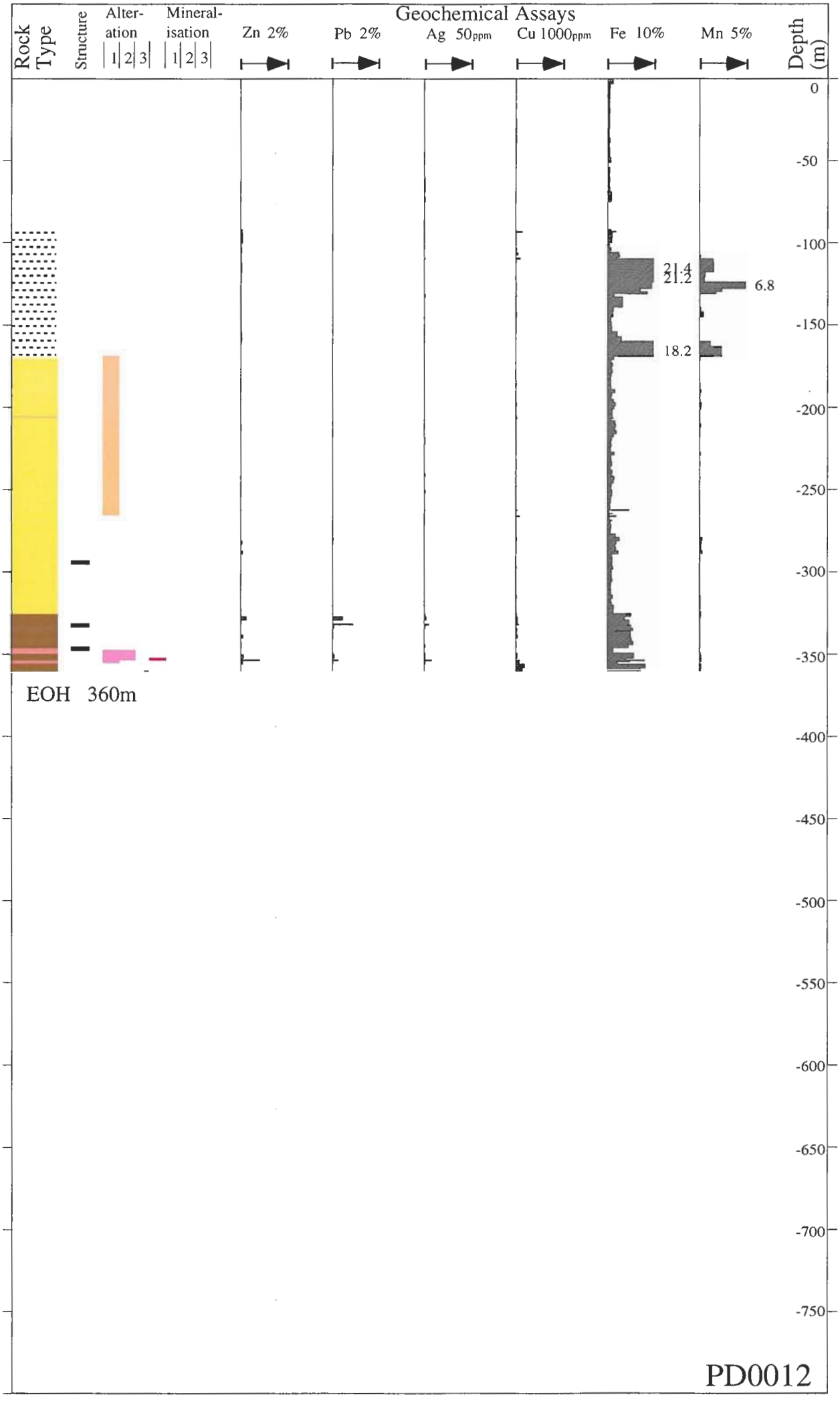
Rock Type
Structure
Alter-ation
1 2 3
Mineral-isation
1 2 3
Geochemical Assays
Zn 2%
Pb 2%
Ag 50ppm
Cu 1000ppm
Fe 10%
Mn 5%
Depth (m)
0
-50
-100
-150
-200
-250
-300
-350
-400
-450
-500
-550
-600
-650
-700
-750
21.4
21.2
6.8
18.2
EOH 360m

PD0012

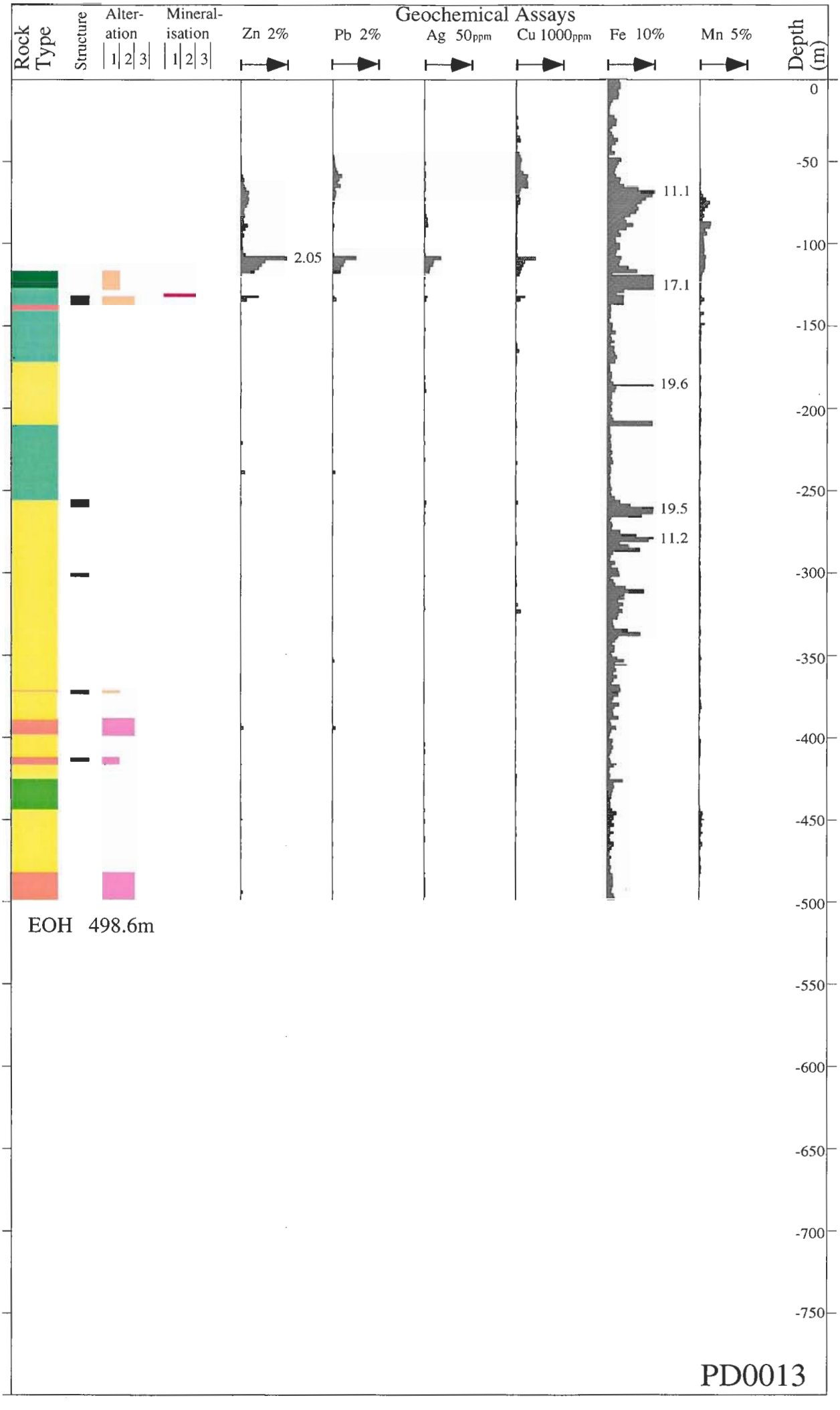
Rock Type
Structure
Alter-ation
1 2 3
Mineral-isation
1 2 3
Geochemical Assays
Zn 2%
Pb 2%
Ag 50ppm
Cu 1000ppm
Fe 10%
Mn 5%
Depth (m)
0
-50
-100
-150
-200
-250
-300
-350
-400
-450
-500
-550
-600
-650
-700
-750
2.05
11.1
17.1
19.6
19.5
11.2
EOH 498.6m
PD0013

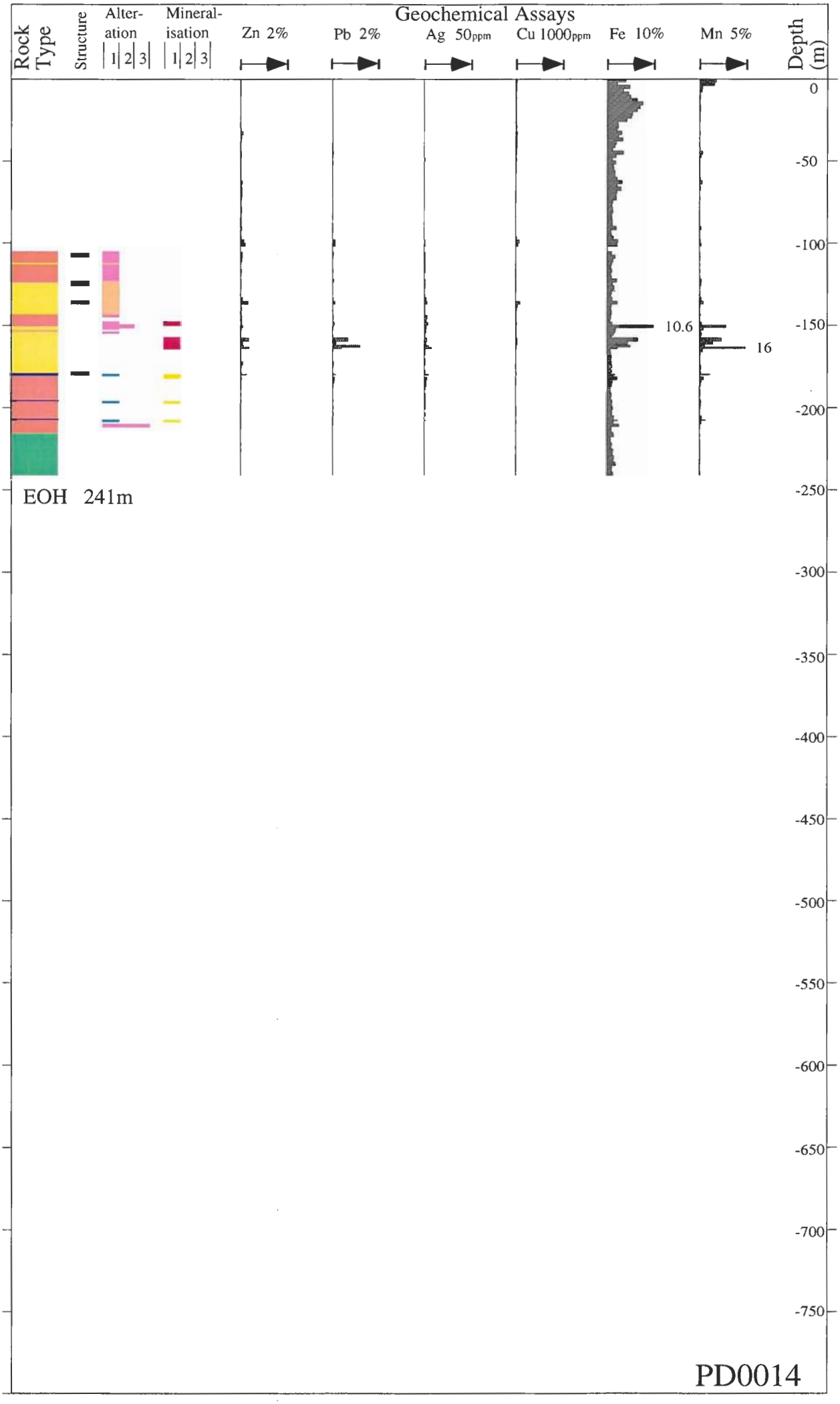
Rock Type
Structure
Alter-ation
1 2 3
Mineral-isation
1 2 3
Geochemical Assays
Zn 2%
Pb 2%
Ag 50ppm
Cu 1000ppm
Fe 10%
Mn 5%
Depth (m)
0
-50
-100
-150
-200
-250
-300
-350
-400
-450
-500
-550
-600
-650
-700
-750
10.6
16
EOH 241m
PD0014

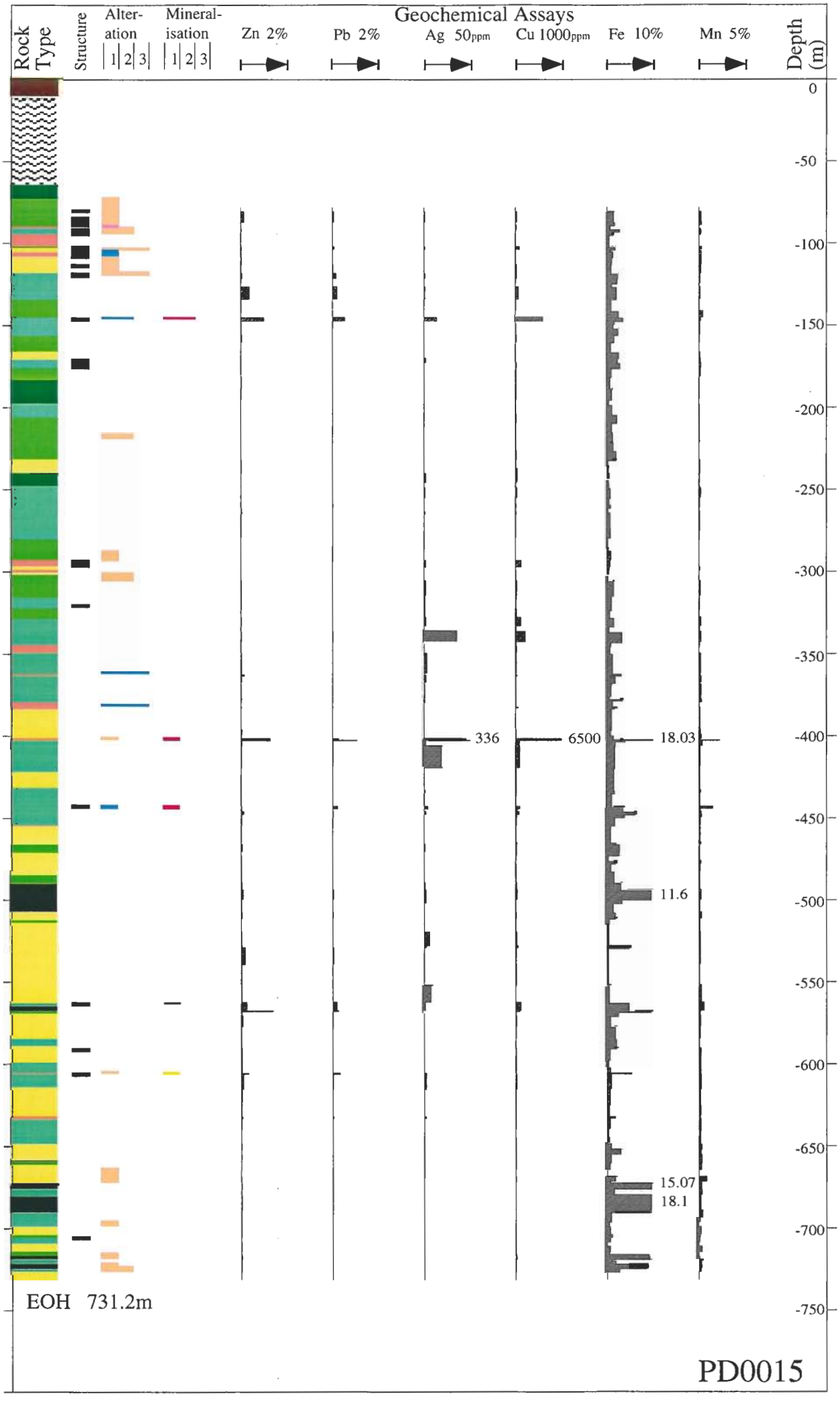
Rock Type
Structure
Alter-ation
1 2 3
Mineral-isation
1 2 3
Geochemical Assays
Zn 2%
Pb 2%
Ag 50ppm
Cu 1000ppm
Fe 10%
Mn 5%
Depth (m)
0
-50
-100
-150
-200
-250
-300
-350
-400
-450
-500
-550
-600
-650
-700
-750
336
6500
18.03
11.6
15.07
18.1
EOH 731.2m
PD0015

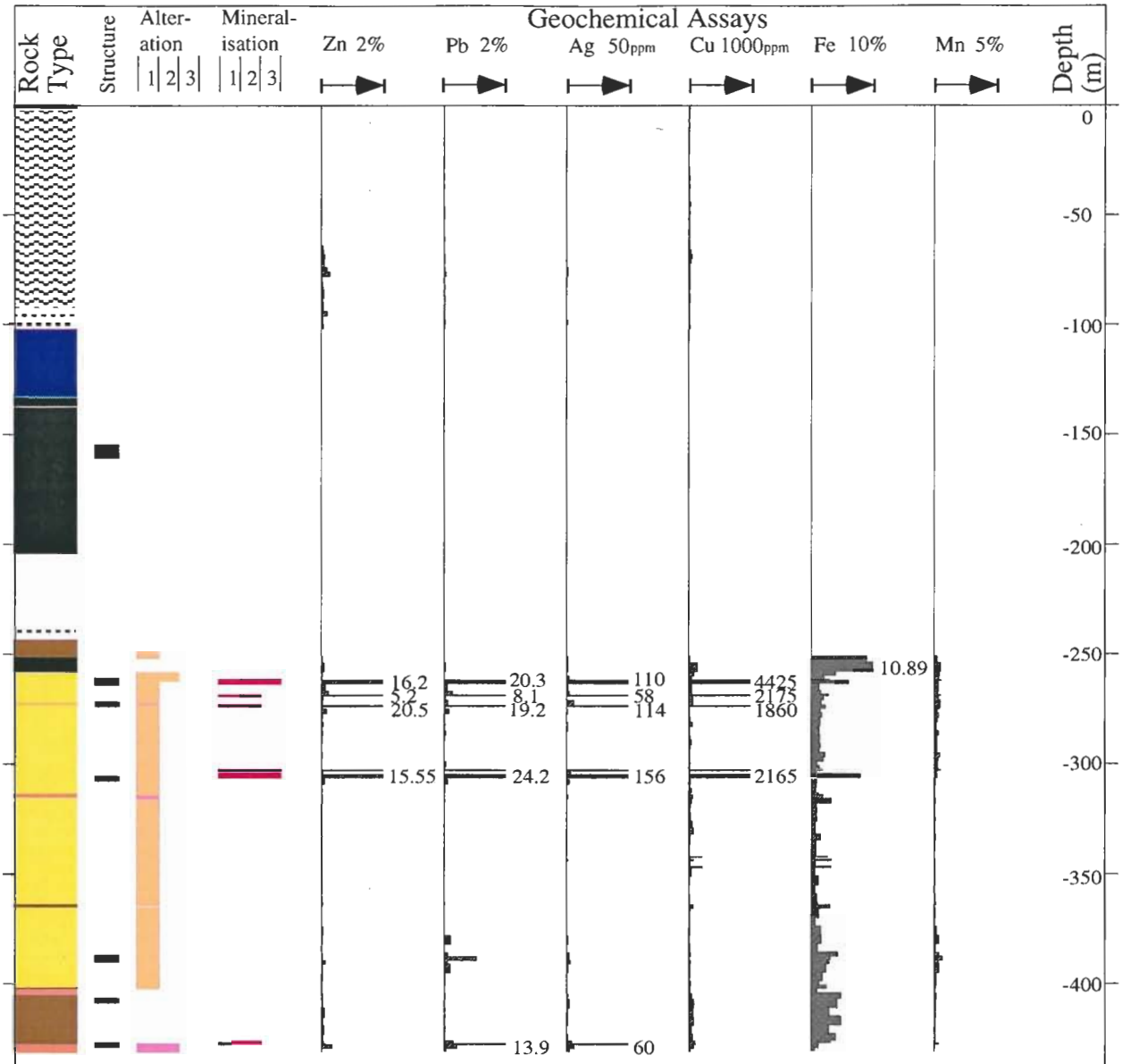
Rock Type
Structure
Alter-ation
1 2 3
Mineral-isation
1 2 3
Geochemical Assays
Zn 2%
Pb 2%
Ag 50ppm
Cu 1000ppm
Fe 10%
Mn 5%
Depth (m)
0
-50
-100
-150
-200
-250
-300
-350
-400
-450
-500
-550
-600
-650
-700
-750
16.2
5.2
20.5
15.55
20.3
8.1
19.2
24.2
13.9
110
58
114
156
60
4425
2175
1860
2165
10.89
EOH 430.8m

PD0016

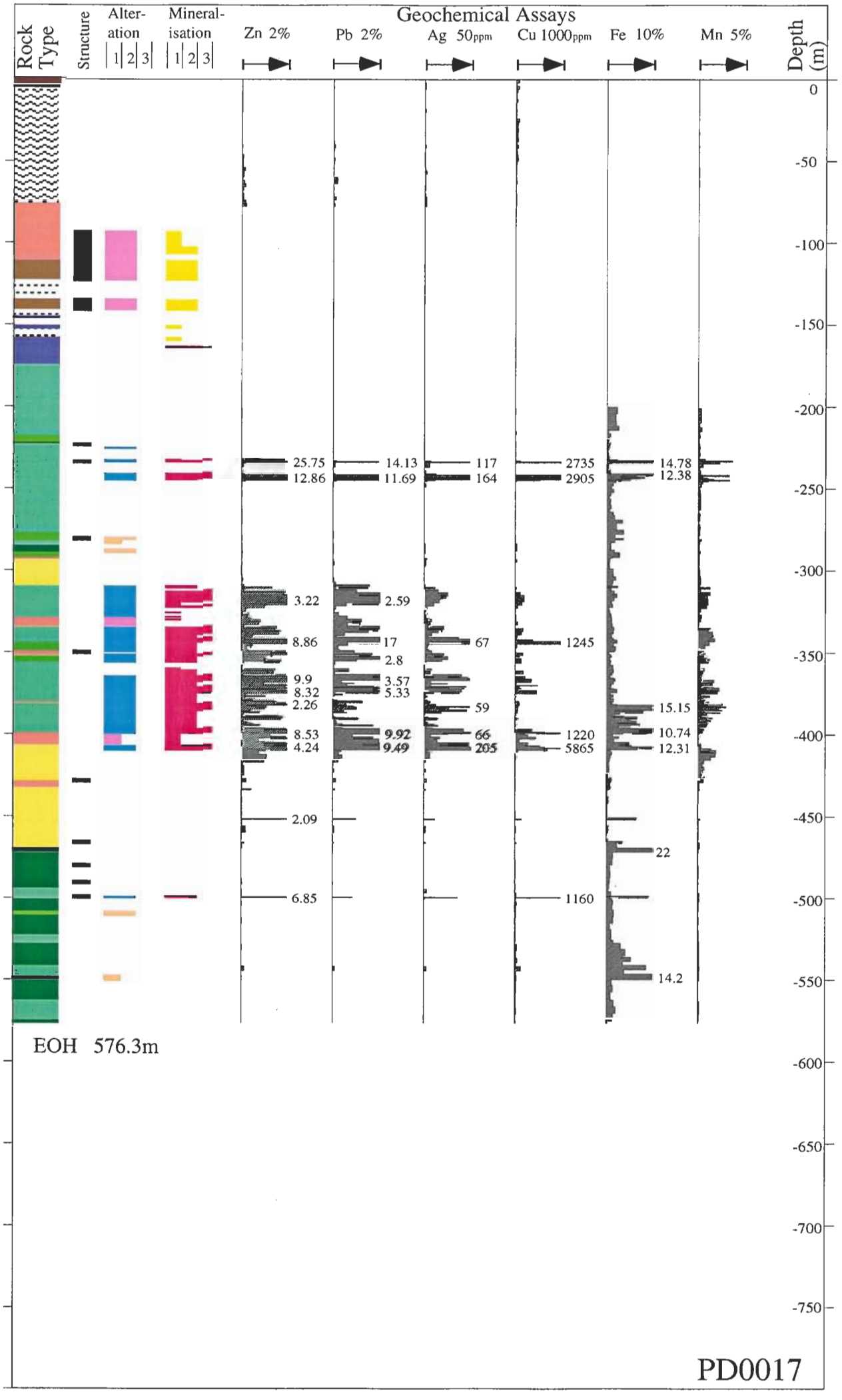
Rock Type
Structure
Alter-ation 1 2 3
Mineral-isation 1 2 3
Geochemical Assays
Zn 2%
Pb 2%
Ag 50ppm
Cu 1000ppm
Fe 10%
Mn 5%
Depth (m)
0
-50
-100
-150
-200
-250
-300
-350
-400
-450
-500
-550
-600
-650
-700
-750
25.75
12.86
3.22
8.86
9.9
8.32
2.26
8.53
4.24
2.09
6.85
14.13
11.69
2.59
17
2.8
3.57
5.33
9.92
9.49
117
164
67
59
66
205
2735
2905
1245
1220
5865
1160
14.78
12.38
15.15
10.74
12.31
22
14.2
EOH 576.3m
PD0017

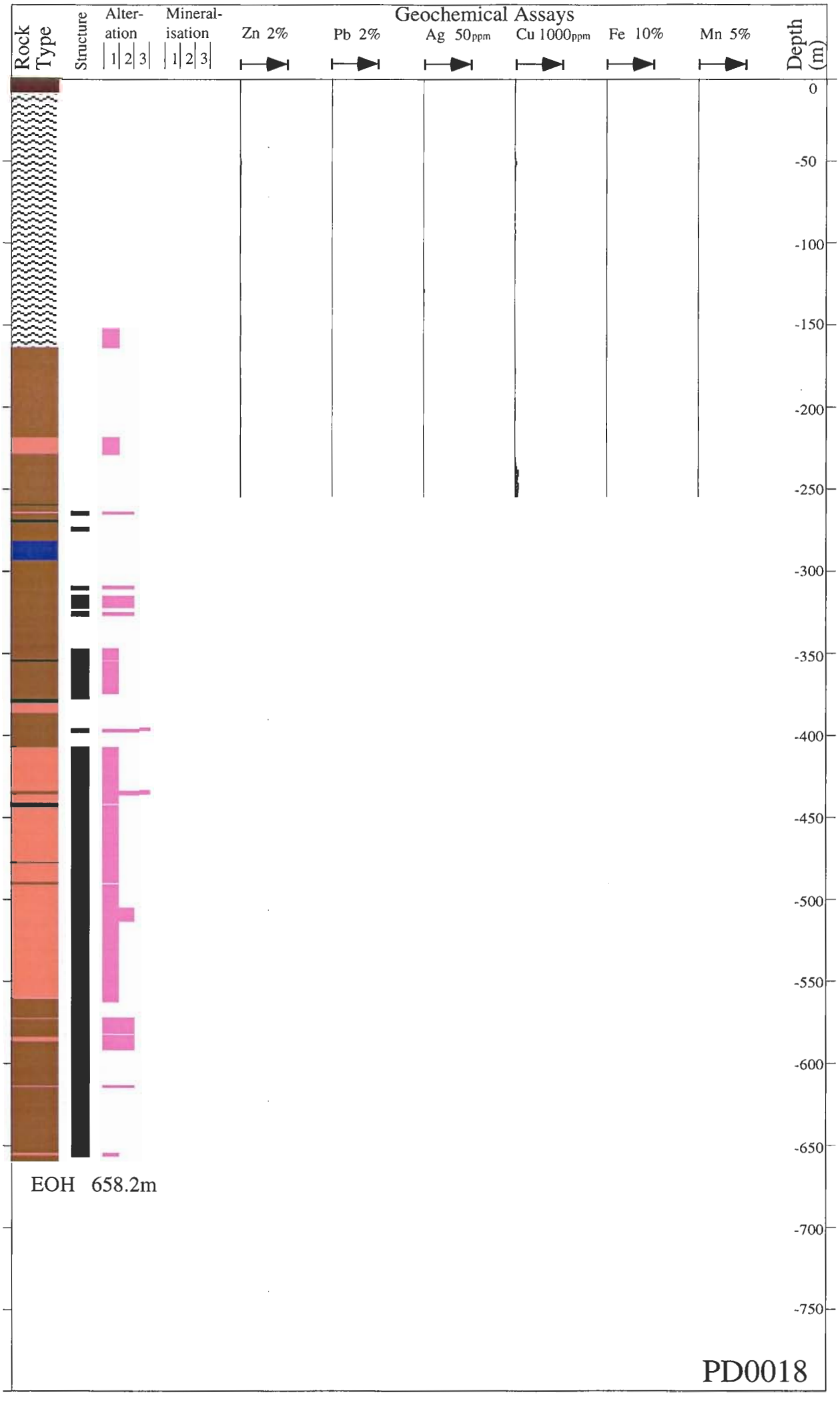
Rock Type
Structure
Alter-ation
1 2 3
Mineral-isation
1 2 3
Geochemical Assays
Zn 2%
Pb 2%
Ag 50ppm
Cu 1000ppm
Fe 10%
Mn 5%
Depth (m)
0
-50
-100
-150
-200
-250
-300
-350
-400
-450
-500
-550
-600
-650
-700
-750
EOH 658.2m
PD0018

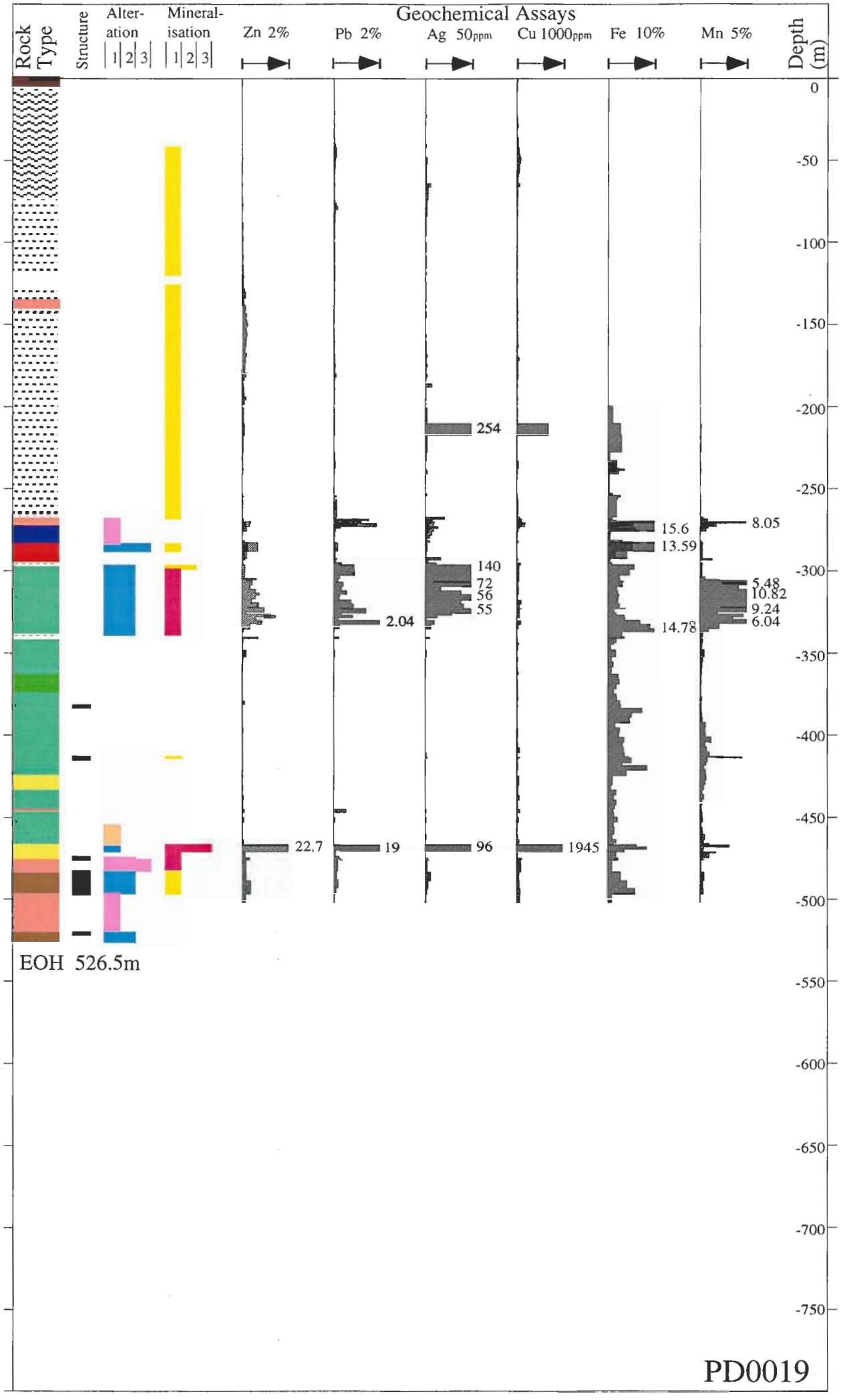
Rock Type
Structure
Alter-ation
1 2 3
Mineral-isation
1 2 3
Geochemical Assays
Zn 2%
Pb 2%
Ag 50ppm
Cu 1000ppm
Fe 10%
Mn 5%
Depth (m)
0
-50
-100
-150
-200
-250
-300
-350
-400
-450
-500
-550
-600
-650
-700
-750
254
140
72
56
55
2.04
22.7
19
96
1945
15.6
13.59
14.78
8.05
5.48
10.82
9.24
6.04
EOH 526.5m
PD0019

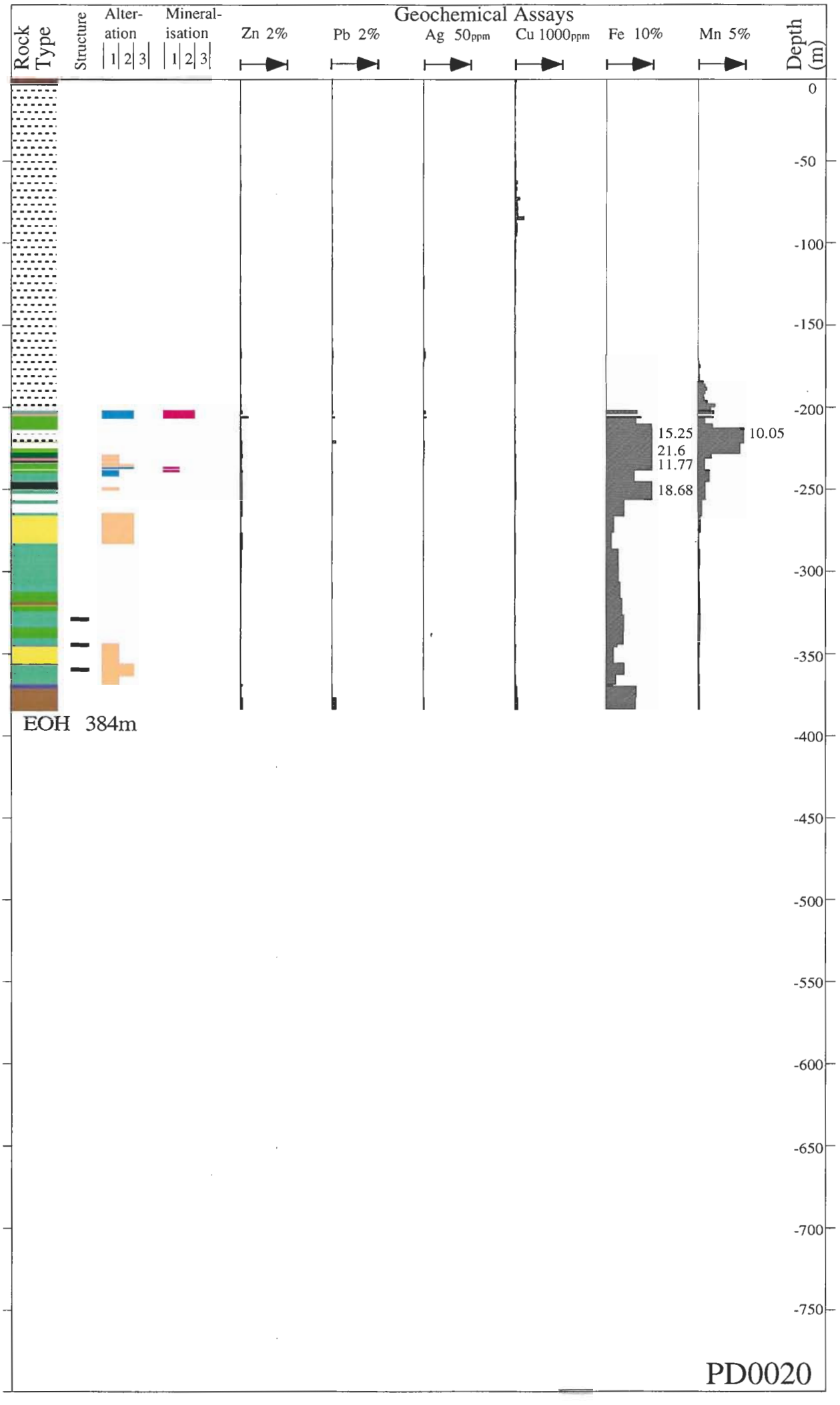
Rock Type
Structure
Alter-ation
1 2 3
Mineral-isation
1 2 3
Geochemical Assays
Zn 2%
Pb 2%
Ag 50ppm
Cu 1000ppm
Fe 10%
Mn 5%
Depth (m)
0
-50
-100
-150
-200
-250
-300
-350
-400
-450
-500
-550
-600
-650
-700
-750
15.25
21.6
11.77
18.68
10.05
EOH 384m
PD0020

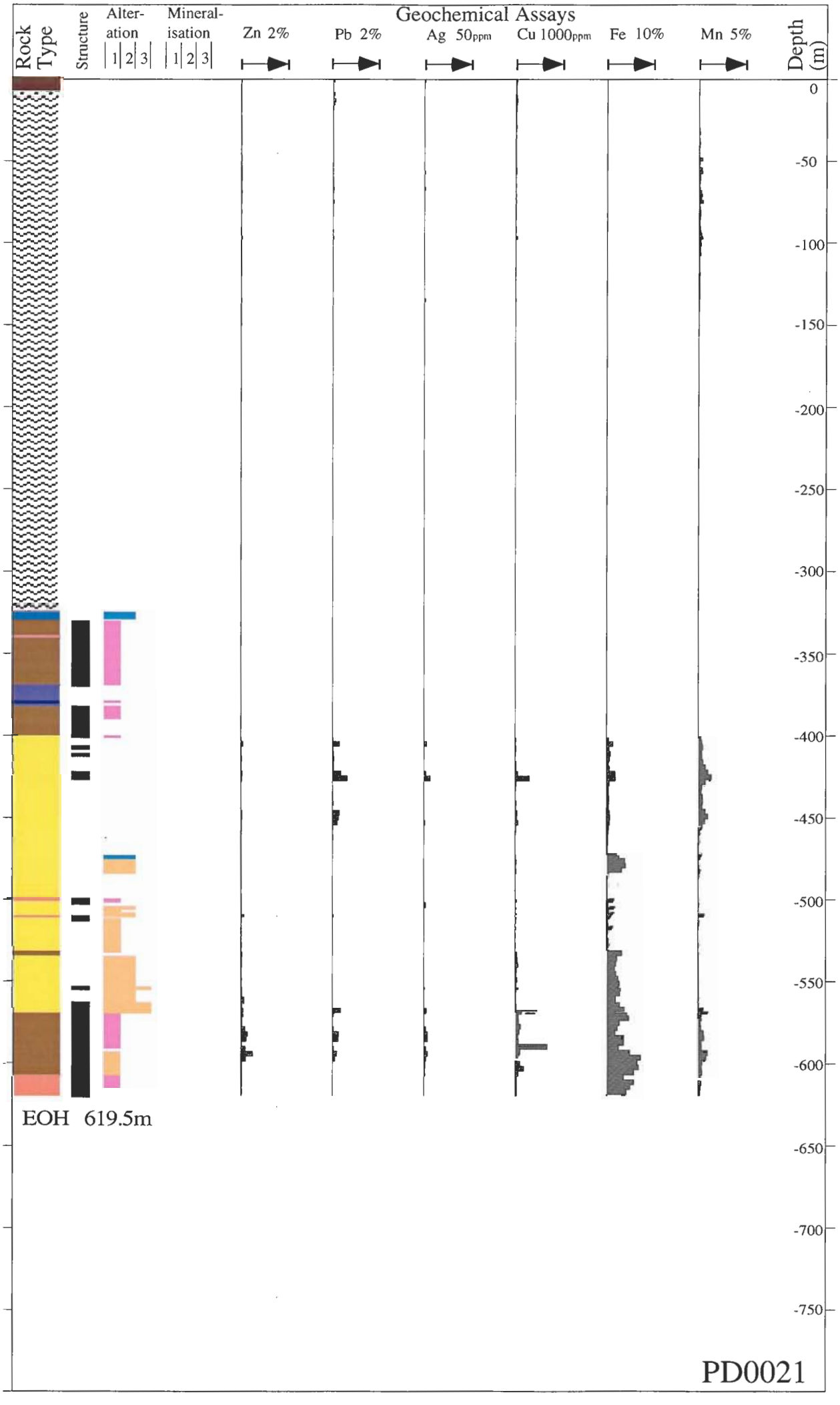
Rock Type
Structure
Alter-ation
1 2 3
Mineral-isation
1 2 3
Geochemical Assays
Zn 2%
Pb 2%
Ag 50ppm
Cu 1000ppm
Fe 10%
Mn 5%
Depth (m)
0
-50
-100
-150
-200
-250
-300
-350
-400
-450
-500
-550
-600
-650
-700
-750
EOH 619.5m
PD0021

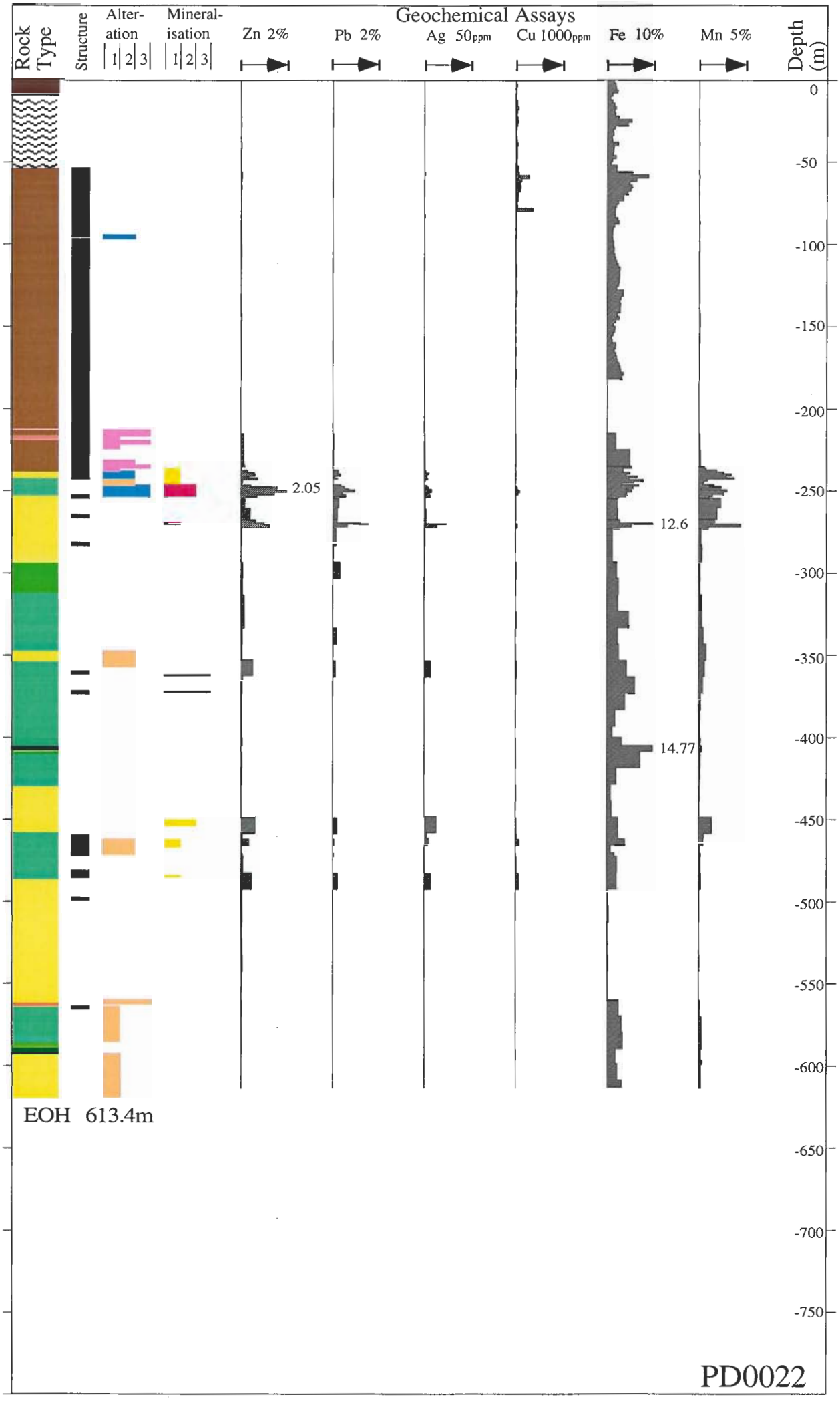
Rock Type
Structure
Alter-ation
1 2 3
Mineral-isation
1 2 3
Geochemical Assays
Zn 2%
Pb 2%
Ag 50ppm
Cu 1000ppm
Fe 10%
Mn 5%
Depth (m)
0
-50
-100
-150
-200
-250
-300
-350
-400
-450
-500
-550
-600
-650
-700
-750
2.05
12.6
14.77
EOH 613.4m
PD0022

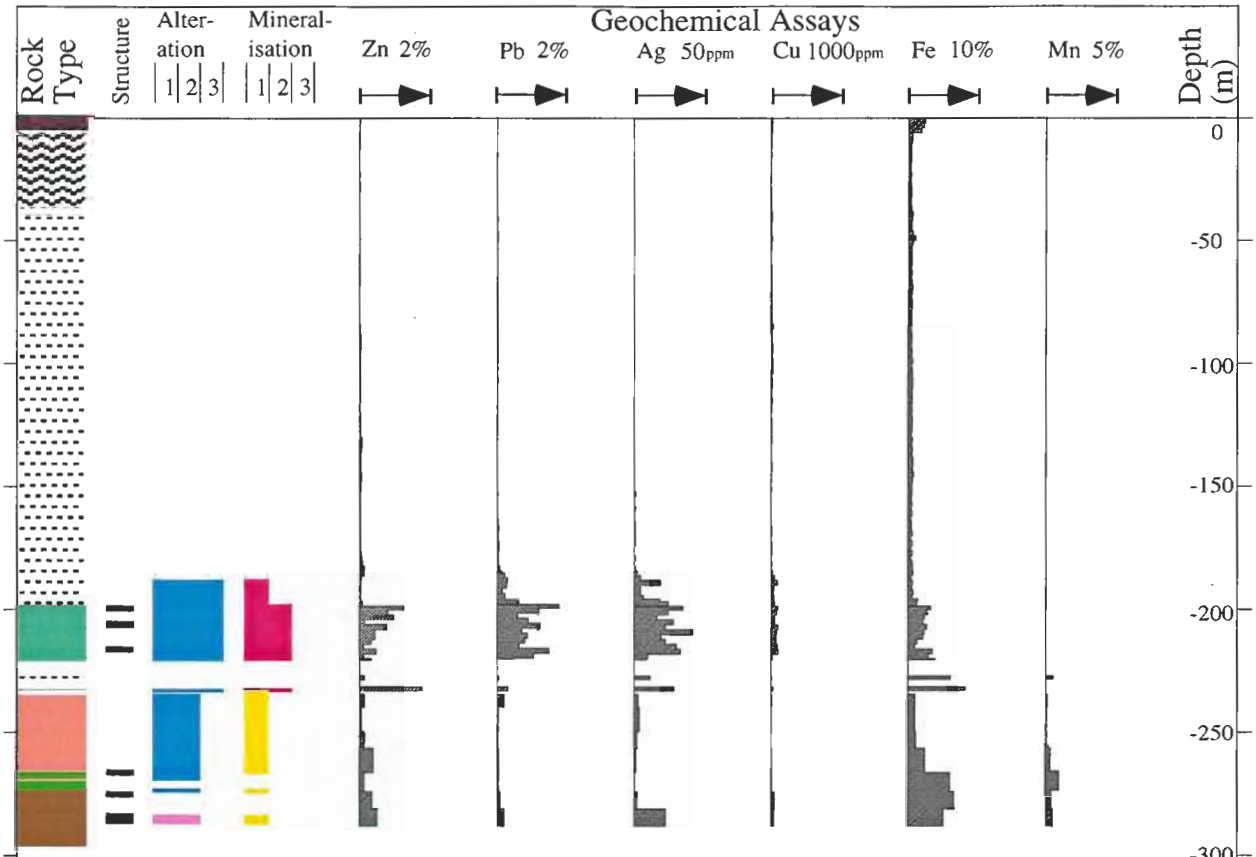


-350
-400
-450
-500
-550
-600
-650
-700
-750

PD0023

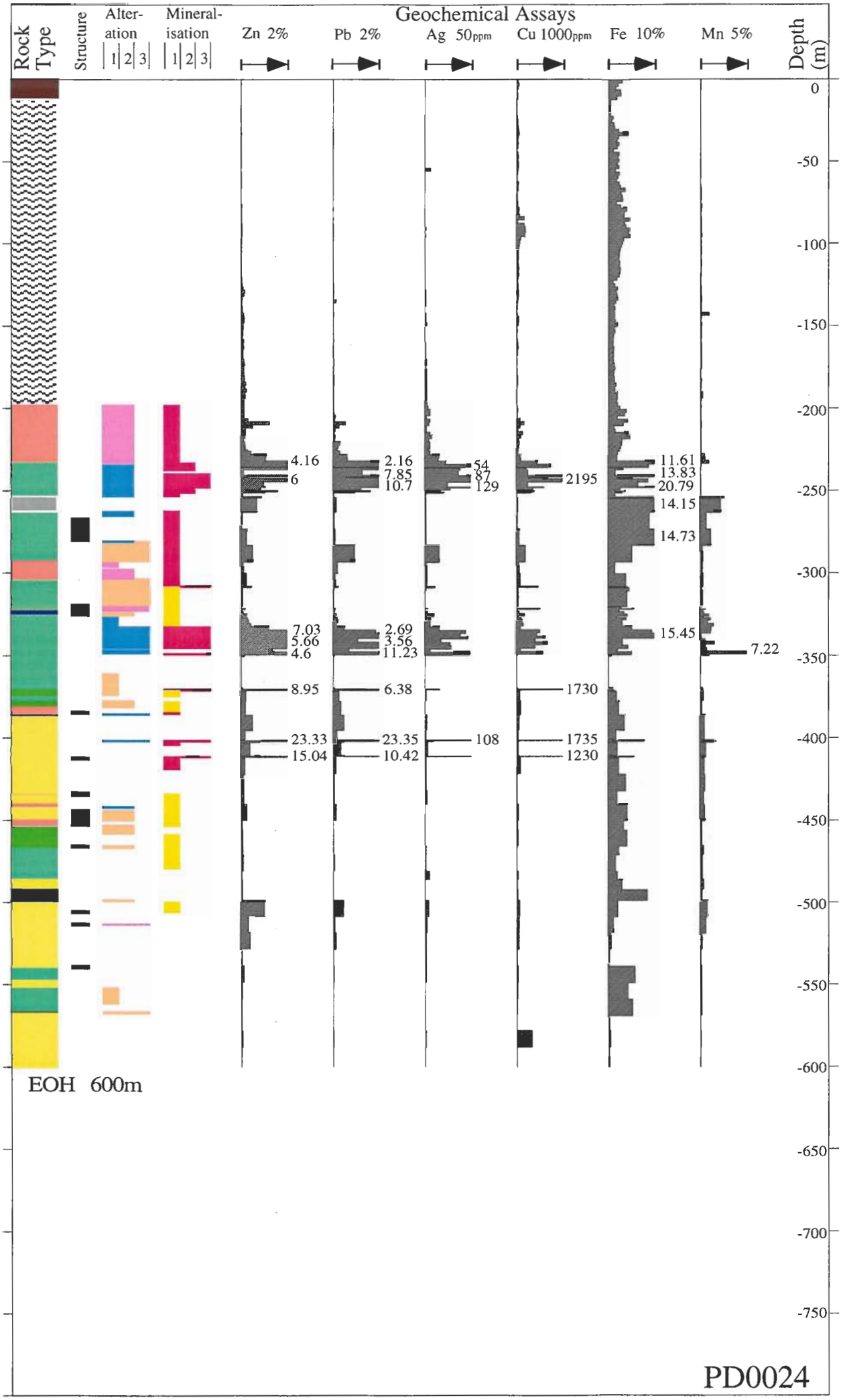
Rock Type
Structure
Alter-ation
1 2 3
Mineral-isation
1 2 3
Geochemical Assays
Zn 2%
Pb 2%
Ag 50ppm
Cu 1000ppm
Fe 10%
Mn 5%
Depth (m)
0
-50
-100
-150
-200
-250
-300
-350
-400
-450
-500
-550
-600
-650
-700
-750
4.16
6
7.03
5.66
4.6
8.95
23.33
15.04
2.16
7.85
10.7
2.69
3.56
11.23
6.38
23.35
10.42
54
87
129
108
2195
1730
1735
1230
11.61
13.83
20.79
14.15
14.73
15.45
7.22
EOH 600m
PD0024

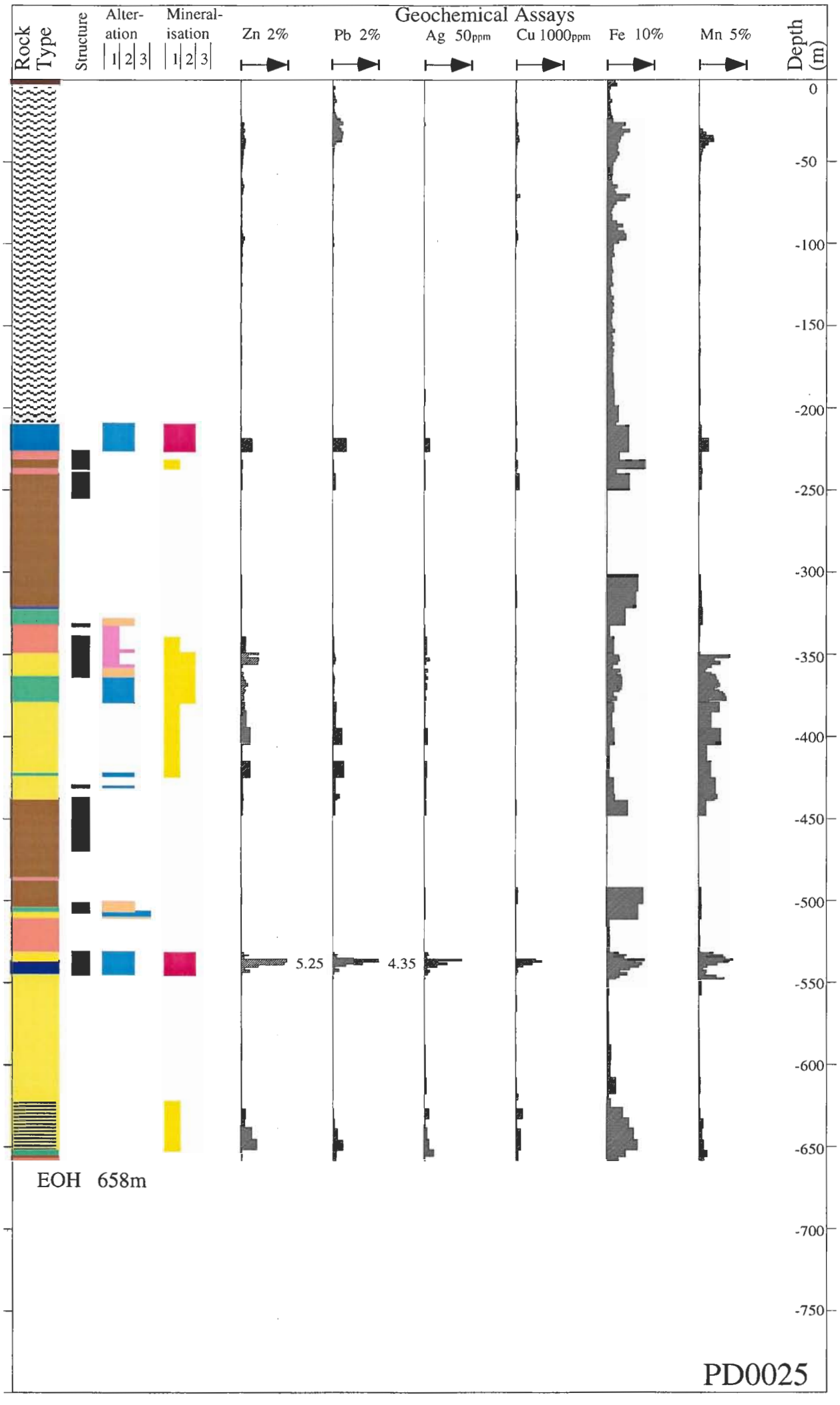
Geochemical Assays
Rock Type
Structure
Alter-ation
1 2 3
Mineral-isation
1 2 3
Zn 2%
Pb 2%
Ag 50ppm
Cu 1000ppm
Fe 10%
Mn 5%
Depth (m)
0
-50
-100
-150
-200
-250
-300
-350
-400
-450
-500
-550
-600
-650
-700
-750
5.25
4.35
EOH 658m
PD0025

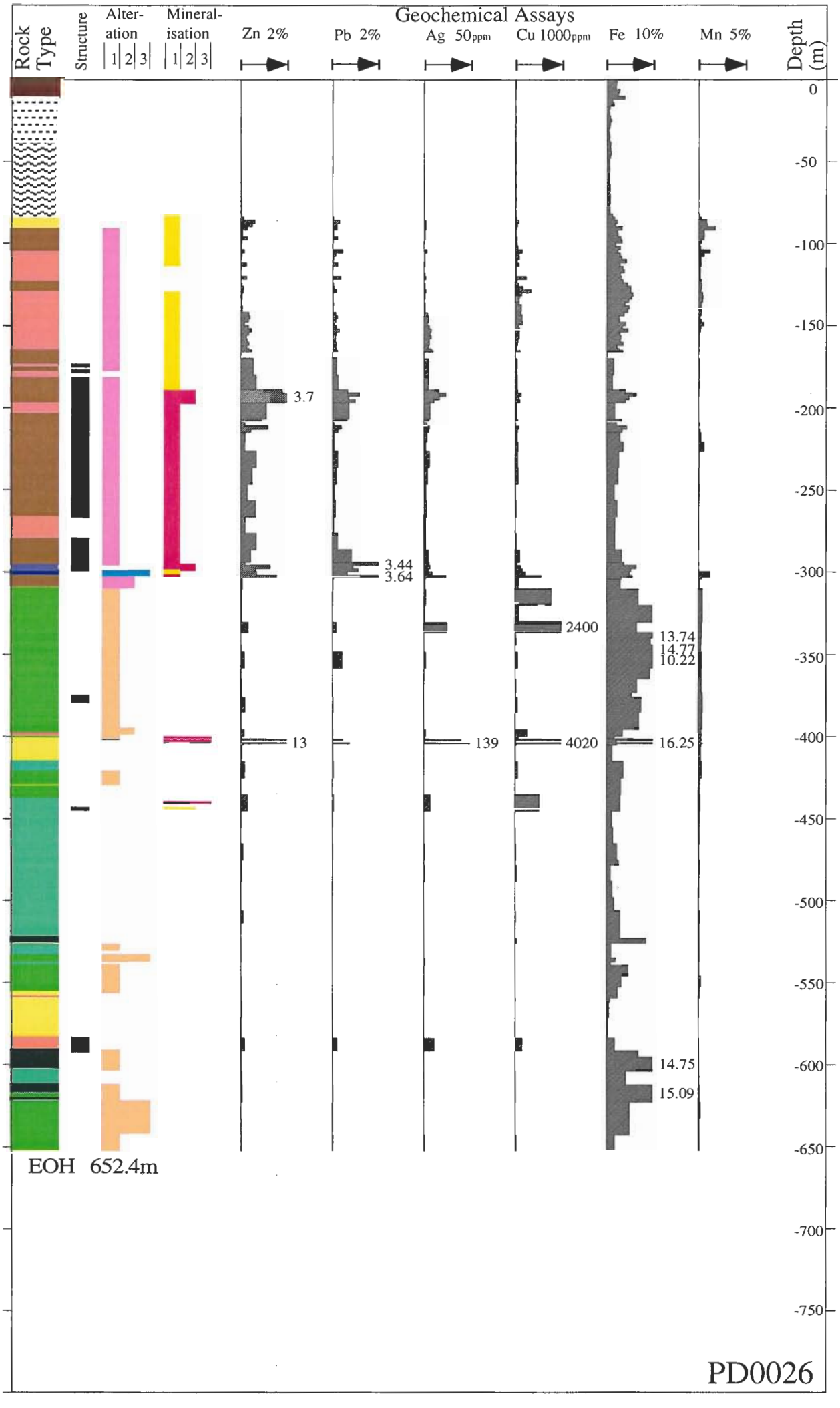
Rock Type
Structure
Alter-ation
1 2 3
Mineral-isation
1 2 3
Geochemical Assays
Zn 2%
Pb 2%
Ag 50ppm
Cu 1000ppm
Fe 10%
Mn 5%
Depth (m)
0
-50
-100
-150
-200
-250
-300
-350
-400
-450
-500
-550
-600
-650
-700
-750
3.7
13
3.44
3.64
139
2400
4020
13.74
14.77
10.22
16.25
14.75
15.09
EOH 652.4m
PD0026

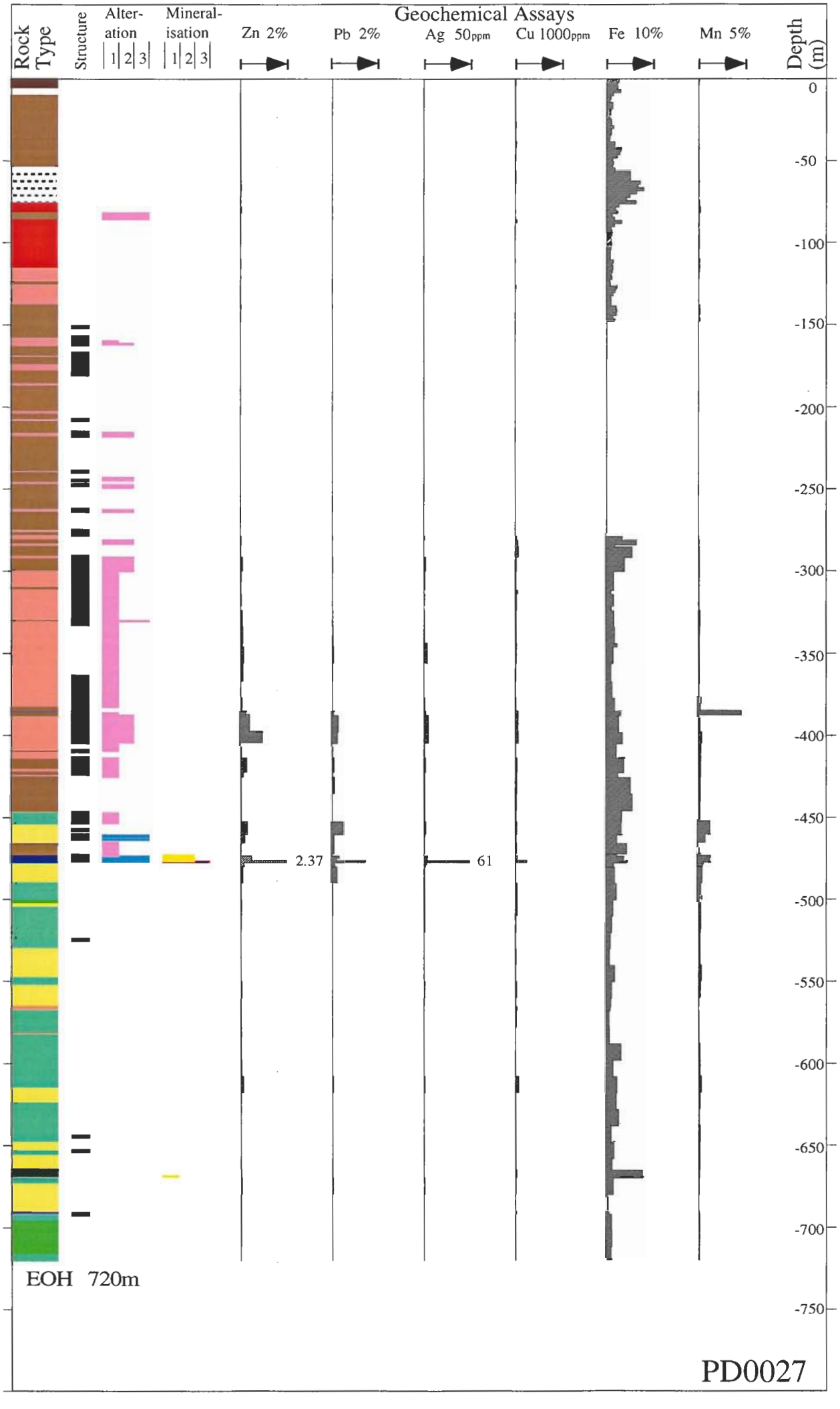
Rock Type
Structure
Alter-ation
1 2 3
Mineral-isation
1 2 3
Geochemical Assays
Zn 2%
Pb 2%
Ag 50ppm
Cu 1000ppm
Fe 10%
Mn 5%
Depth (m)
0
-50
-100
-150
-200
-250
-300
-350
-400
-450
-500
-550
-600
-650
-700
-750
2.37
61
EOH 720m
PD0027

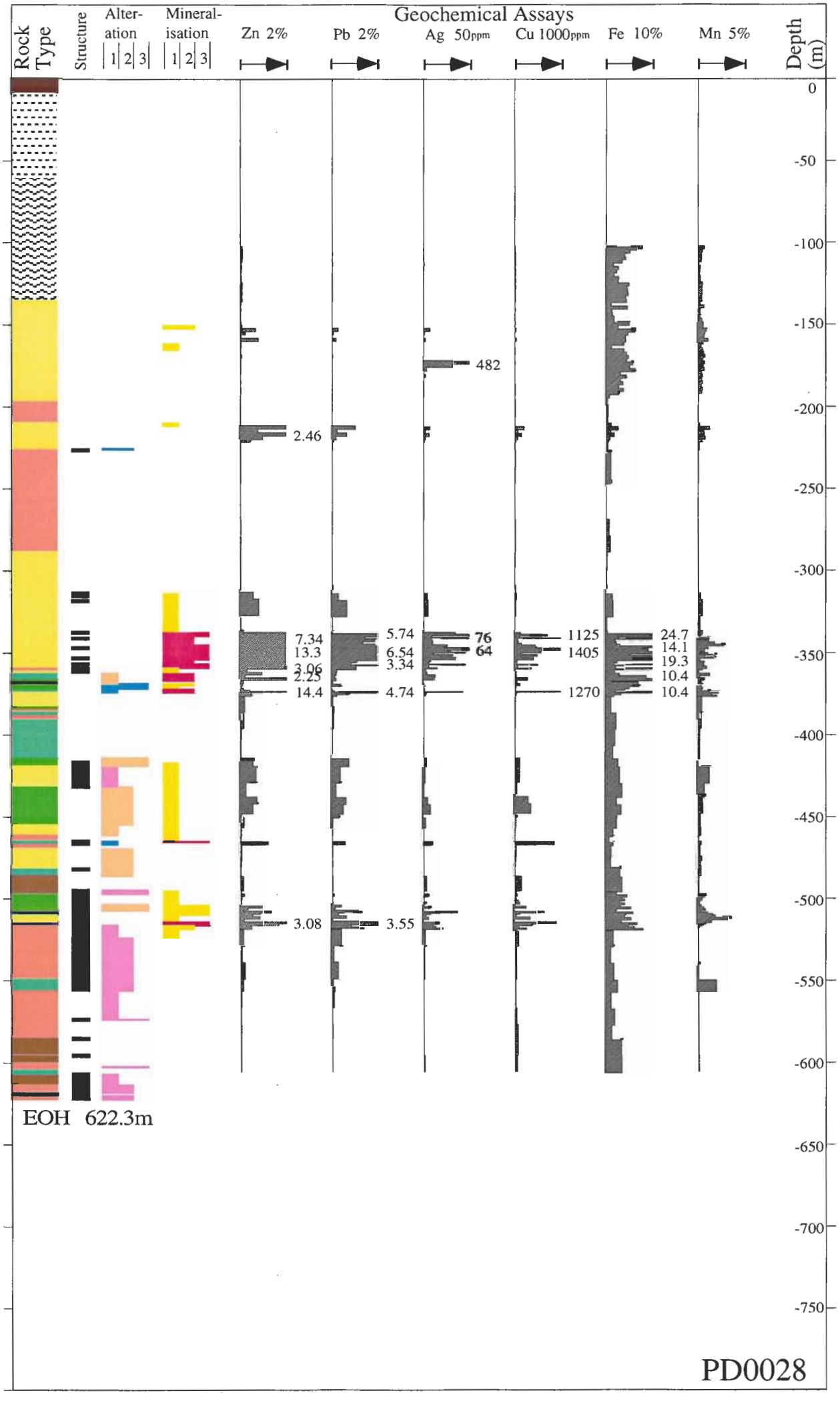
Rock Type
Structure
Alter-ation
1 2 3
Mineral-isation
1 2 3
Geochemical Assays
Zn 2%
Pb 2%
Ag 50ppm
Cu 1000ppm
Fe 10%
Mn 5%
Depth (m)
0
-50
-100
-150
-200
-250
-300
-350
-400
-450
-500
-550
-600
-650
-700
-750
482
2.46
7.34
13.3
3.06
2.25
14.4
3.08
5.74
6.54
3.34
4.74
3.55
76
64
1125
1405
1270
24.7
14.1
19.3
10.4
10.4
EOH 622.3m
PD0028

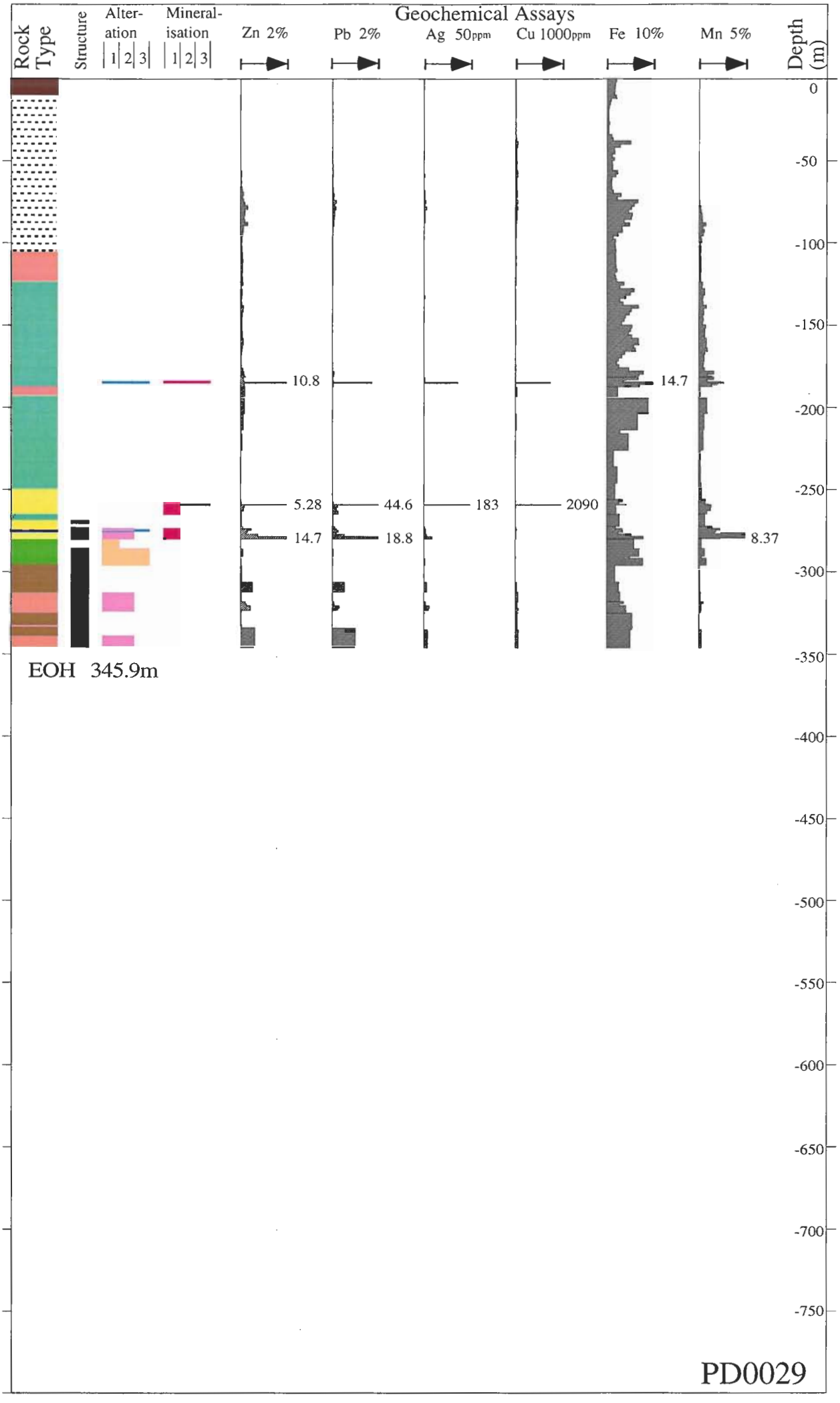
Rock Type
Structure
Alter-ation
1 2 3
Mineral-isation
1 2 3
Geochemical Assays
Zn 2%
Pb 2%
Ag 50ppm
Cu 1000ppm
Fe 10%
Mn 5%
Depth (m)
0
-50
-100
-150
-200
-250
-300
-350
-400
-450
-500
-550
-600
-650
-700
-750
10.8
5.28
14.7
44.6
18.8
183
2090
14.7
8.37
EOH 345.9m
PD0029

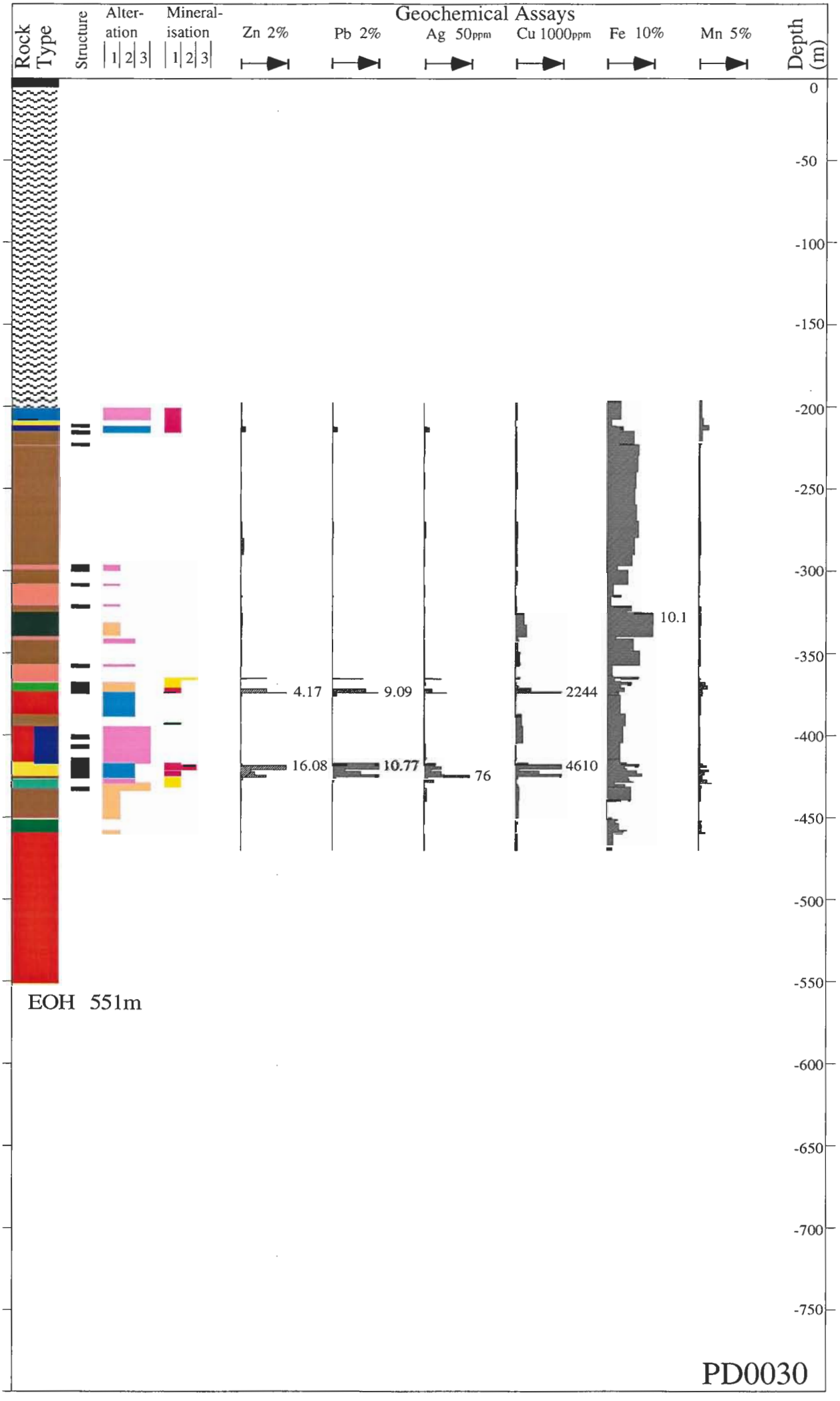
Rock Type
Structure
Alter-ation
1 2 3
Mineral-isation
1 2 3
Geochemical Assays
Zn 2%
Pb 2%
Ag 50ppm
Cu 1000ppm
Fe 10%
Mn 5%
Depth (m)
0
-50
-100
-150
-200
-250
-300
-350
-400
-450
-500
-550
-600
-650
-700
-750
4.17
16.08
9.09
10.77
76
2244
4610
10.1
EOH 551m
PD0030

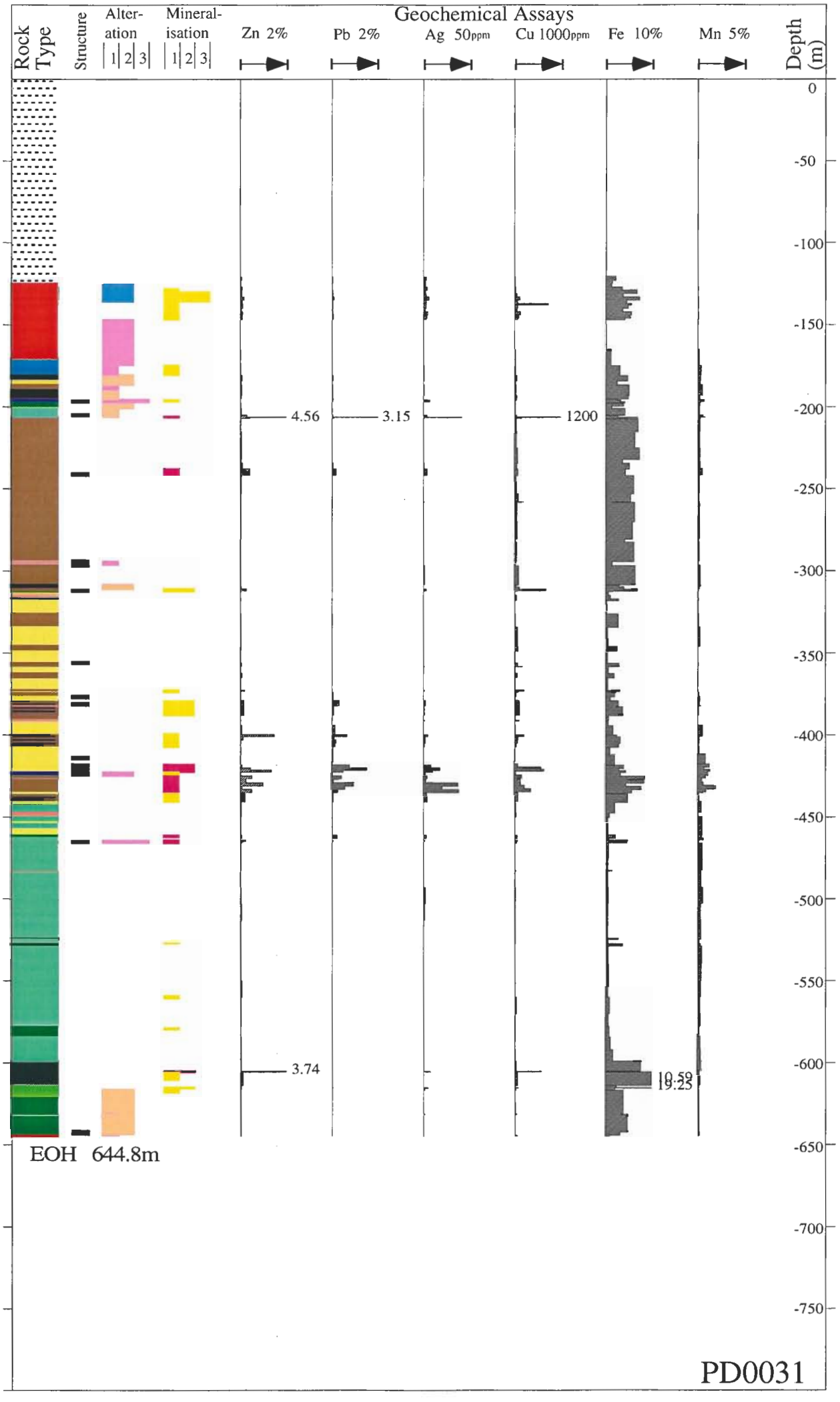
Geochemical Assays
Rock Type
Structure
Alter-ation
1 2 3
Mineral-isation
1 2 3
Zn 2%
Pb 2%
Ag 50ppm
Cu 1000ppm
Fe 10%
Mn 5%
Depth (m)
0
-50
-100
-150
-200
-250
-300
-350
-400
-450
-500
-550
-600
-650
-700
-750
4.56
3.15
1200
3.74
10.59
19.25
EOH 644.8m
PD0031

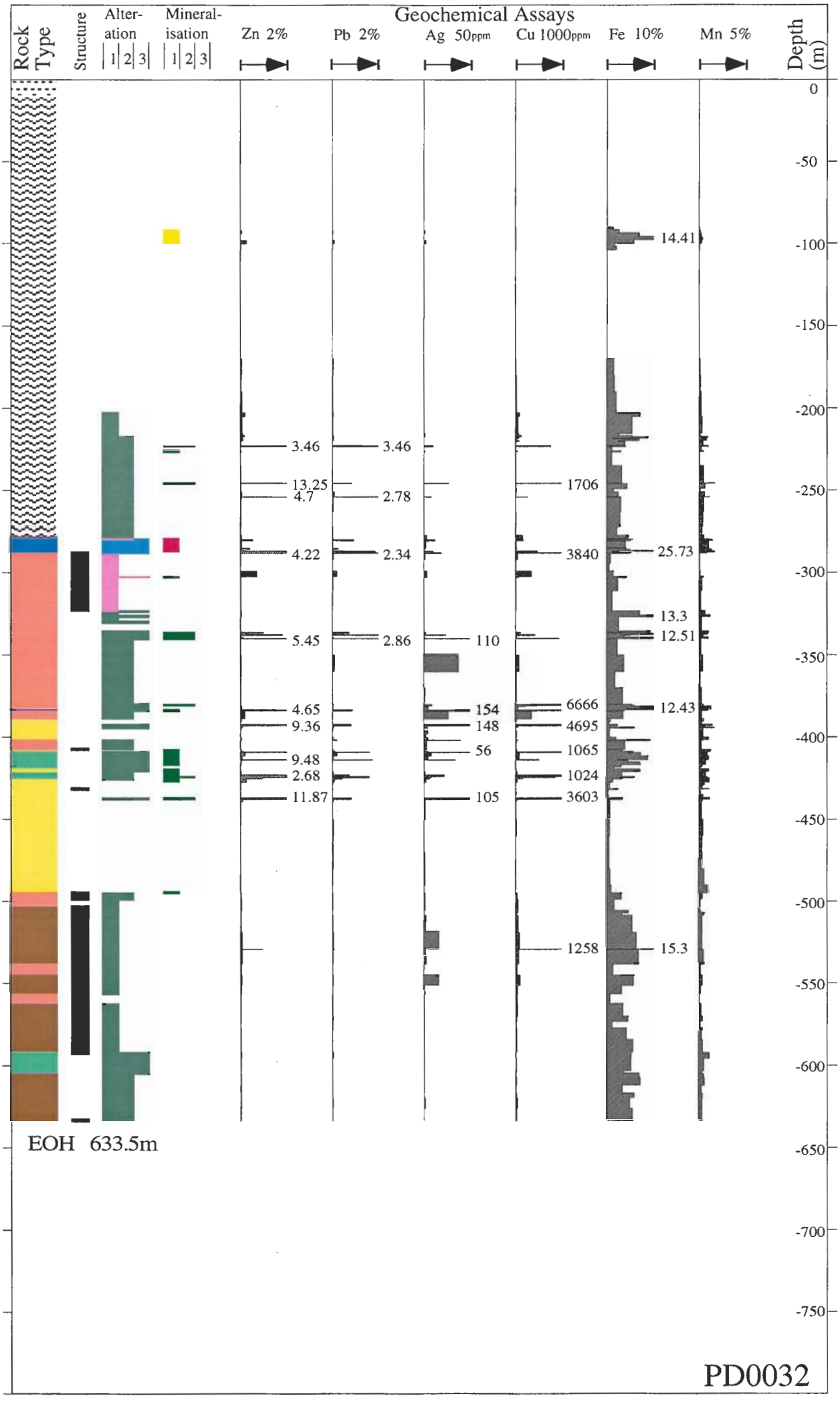
Rock Type
Structure
Alter-ation
1 2 3
Mineral-isation
1 2 3
Geochemical Assays
Zn 2%
Pb 2%
Ag 50ppm
Cu 1000ppm
Fe 10%
Mn 5%
Depth (m)
0
-50
-100
-150
-200
-250
-300
-350
-400
-450
-500
-550
-600
-650
-700
-750
3.46
13.25
4.7
4.22
5.45
4.65
9.36
9.48
2.68
11.87
3.46
2.78
2.34
2.86
110
154
148
56
105
1706
3840
6666
4695
1065
1024
3603
1258
14.41
25.73
13.3
12.51
12.43
15.3
EOH 633.5m
PD0032

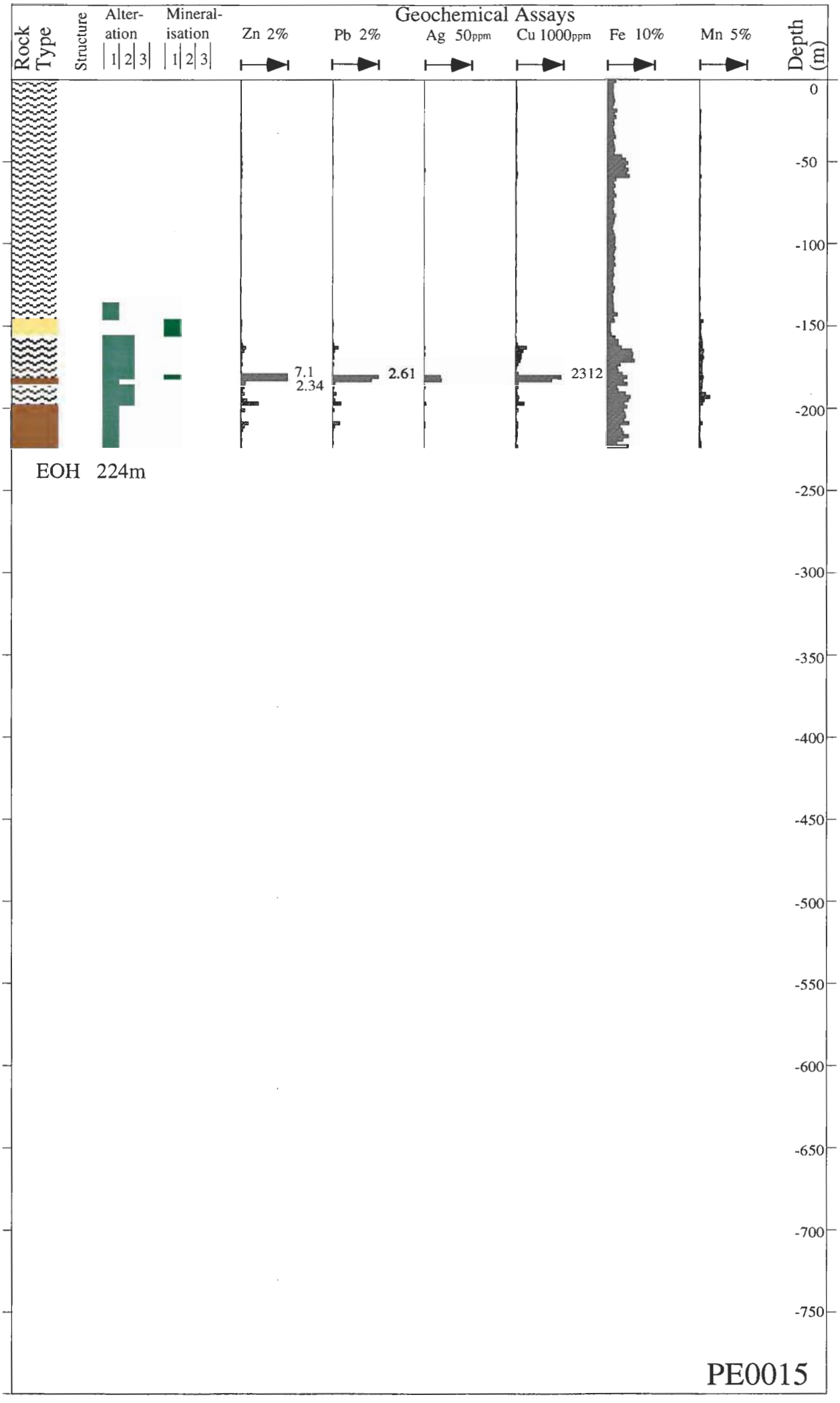
Rock Type
Structure
Alter-ation
1 2 3
Mineral-isation
1 2 3
Geochemical Assays
Zn 2%
Pb 2%
Ag 50ppm
Cu 1000ppm
Fe 10%
Mn 5%
Depth (m)
0
-50
-100
-150
-200
-250
-300
-350
-400
-450
-500
-550
-600
-650
-700
-750
7.1
2.34
2.61
2312
EOH 224m

PE0015

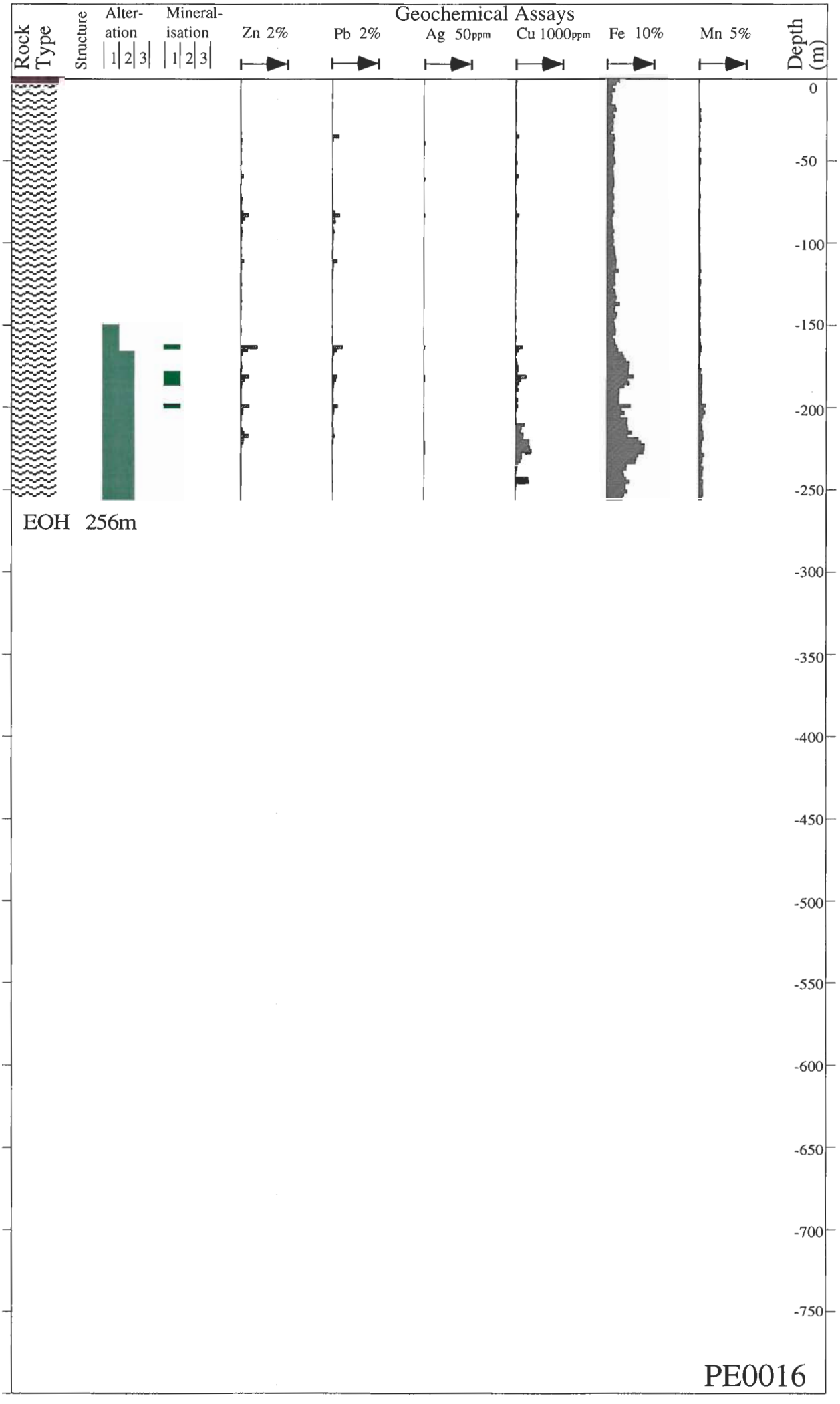
Rock Type
Structure
Alter-ation
1 2 3
Mineral-isation
1 2 3
Geochemical Assays
Zn 2%
Pb 2%
Ag 50ppm
Cu 1000ppm
Fe 10%
Mn 5%
Depth (m)
0
-50
-100
-150
-200
-250
-300
-350
-400
-450
-500
-550
-600
-650
-700
-750
EOH 256m
PE0016

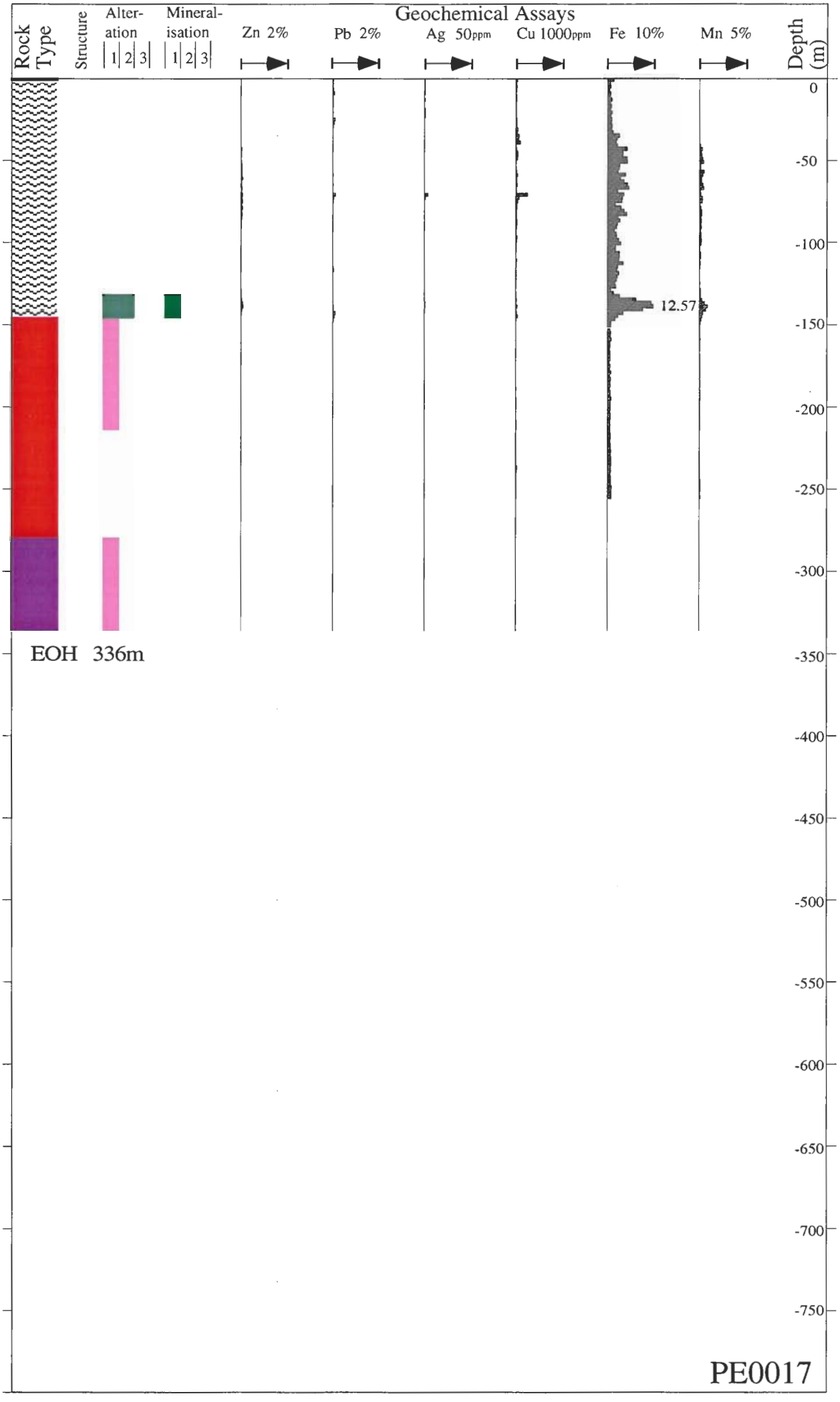
Rock Type
Structure
Alter-ation
1 2 3
Mineral-isation
1 2 3
Geochemical Assays
Zn 2%
Pb 2%
Ag 50ppm
Cu 1000ppm
Fe 10%
Mn 5%
Depth (m)
0
-50
-100
-150
-200
-250
-300
-350
-400
-450
-500
-550
-600
-650
-700
-750
12.57
EOH 336m

PE0017

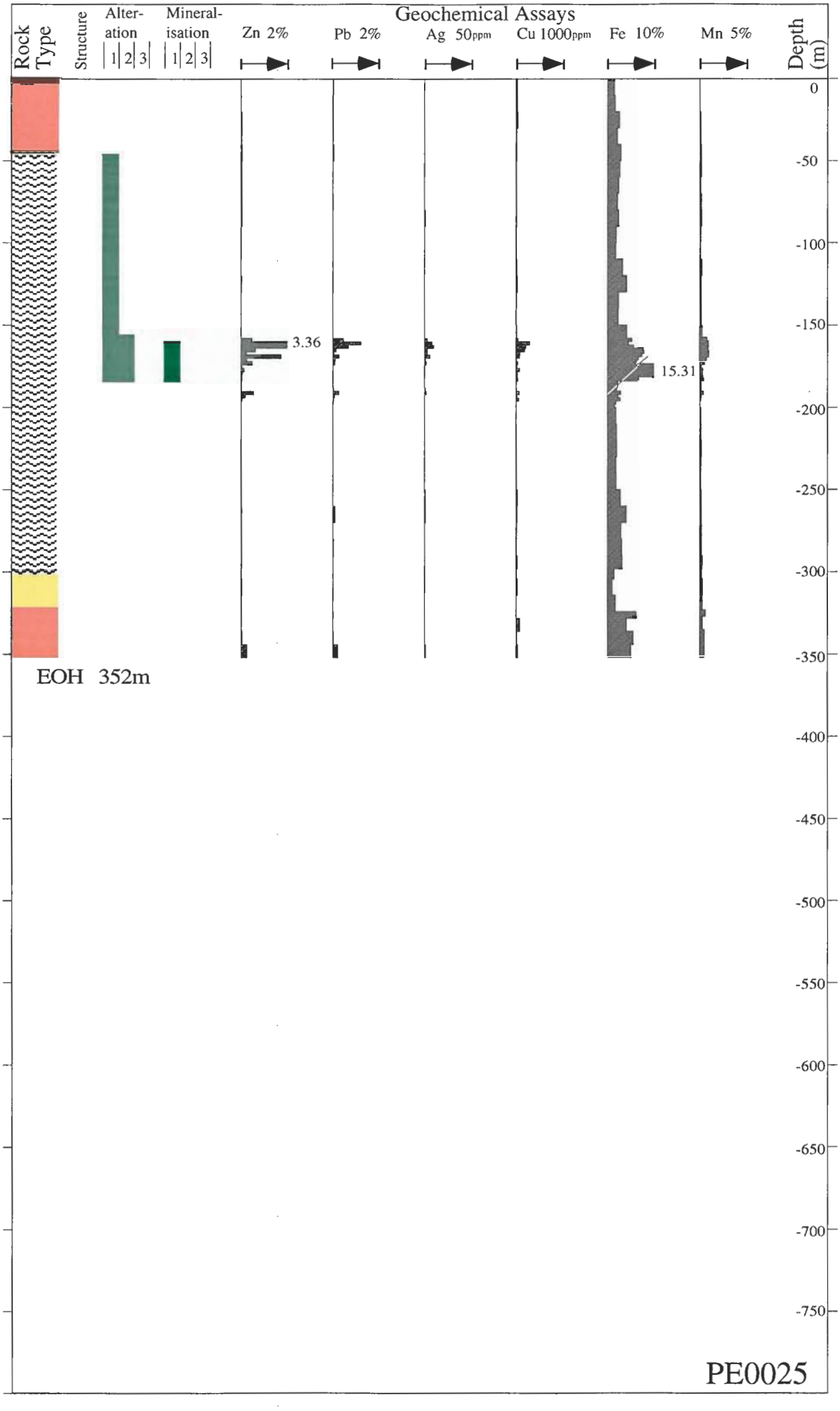
Rock Type
Structure
Alter-ation
1 2 3
Mineral-isation
1 2 3
Geochemical Assays
Zn 2%
Pb 2%
Ag 50ppm
Cu 1000ppm
Fe 10%
Mn 5%
Depth (m)
0
-50
-100
-150
-200
-250
-300
-350
-400
-450
-500
-550
-600
-650
-700
-750
3.36
15.31
EOH 352m

PE0025

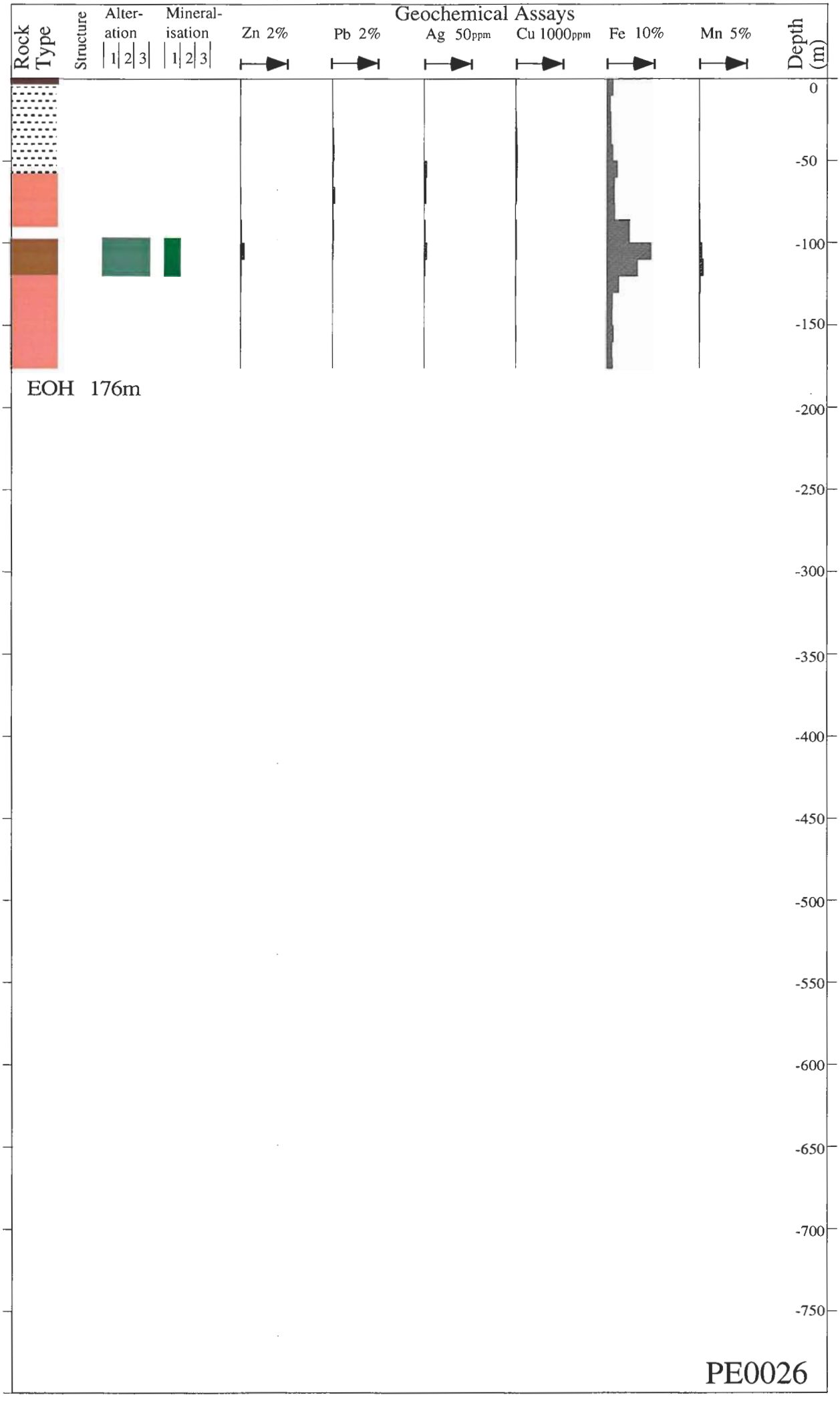
Rock Type
Structure
Alter-ation
1 2 3
Mineral-isation
1 2 3
Geochemical Assays
Zn 2%
Pb 2%
Ag 50ppm
Cu 1000ppm
Fe 10%
Mn 5%
Depth (m)
0
-50
-100
-150
EOH 176m
-200
-250
-300
-350
-400
-450
-500
-550
-600
-650
-700
-750

PE0026

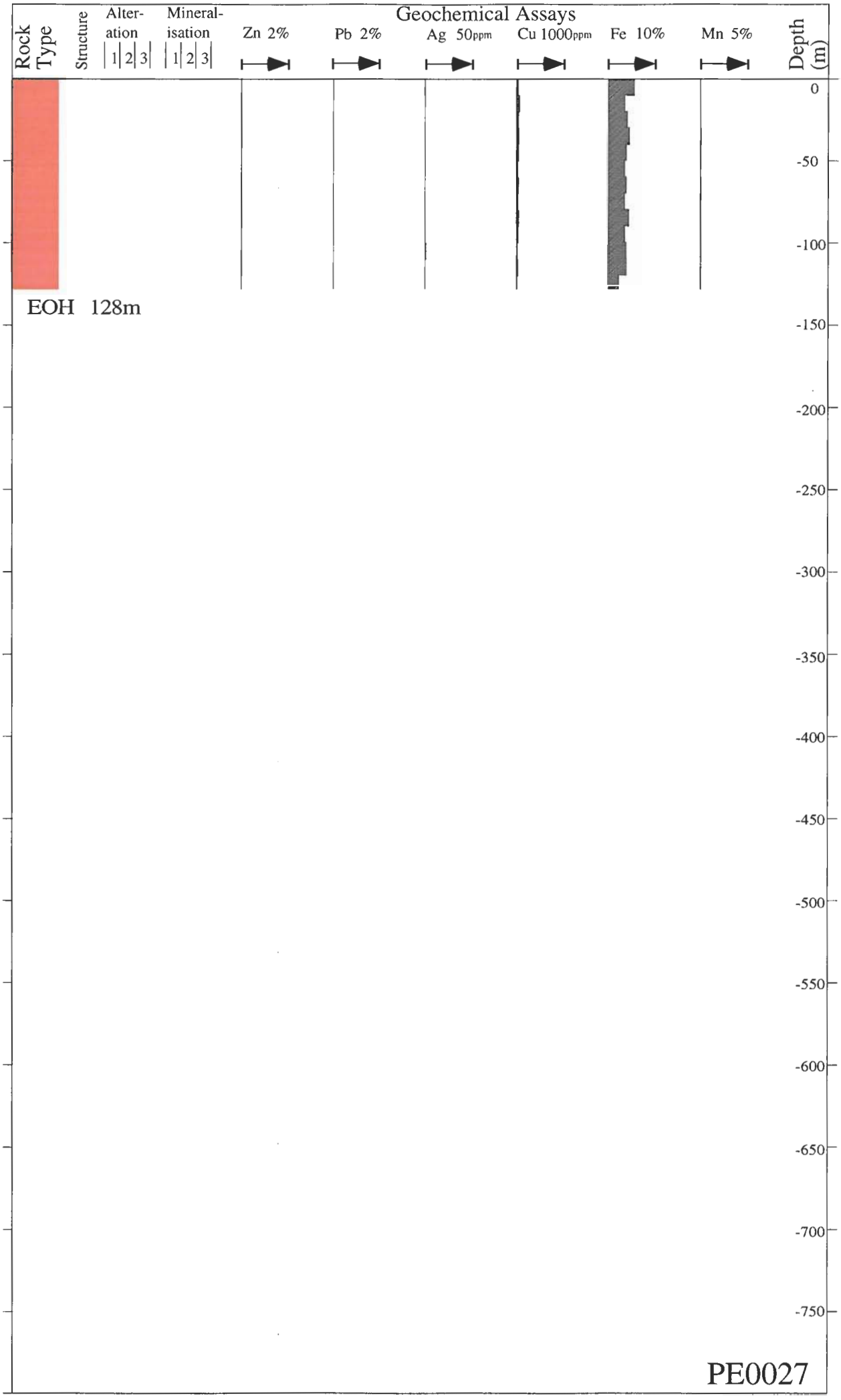
Rock Type
Structure
Alter-ation
1 2 3
Mineral-isation
1 2 3
Geochemical Assays
Zn 2%
Pb 2%
Ag 50ppm
Cu 1000ppm
Fe 10%
Mn 5%
Depth (m)
0
-50
-100
EOH 128m
-150
-200
-250
-300
-350
-400
-450
-500
-550
-600
-650
-700
-750
PE0027

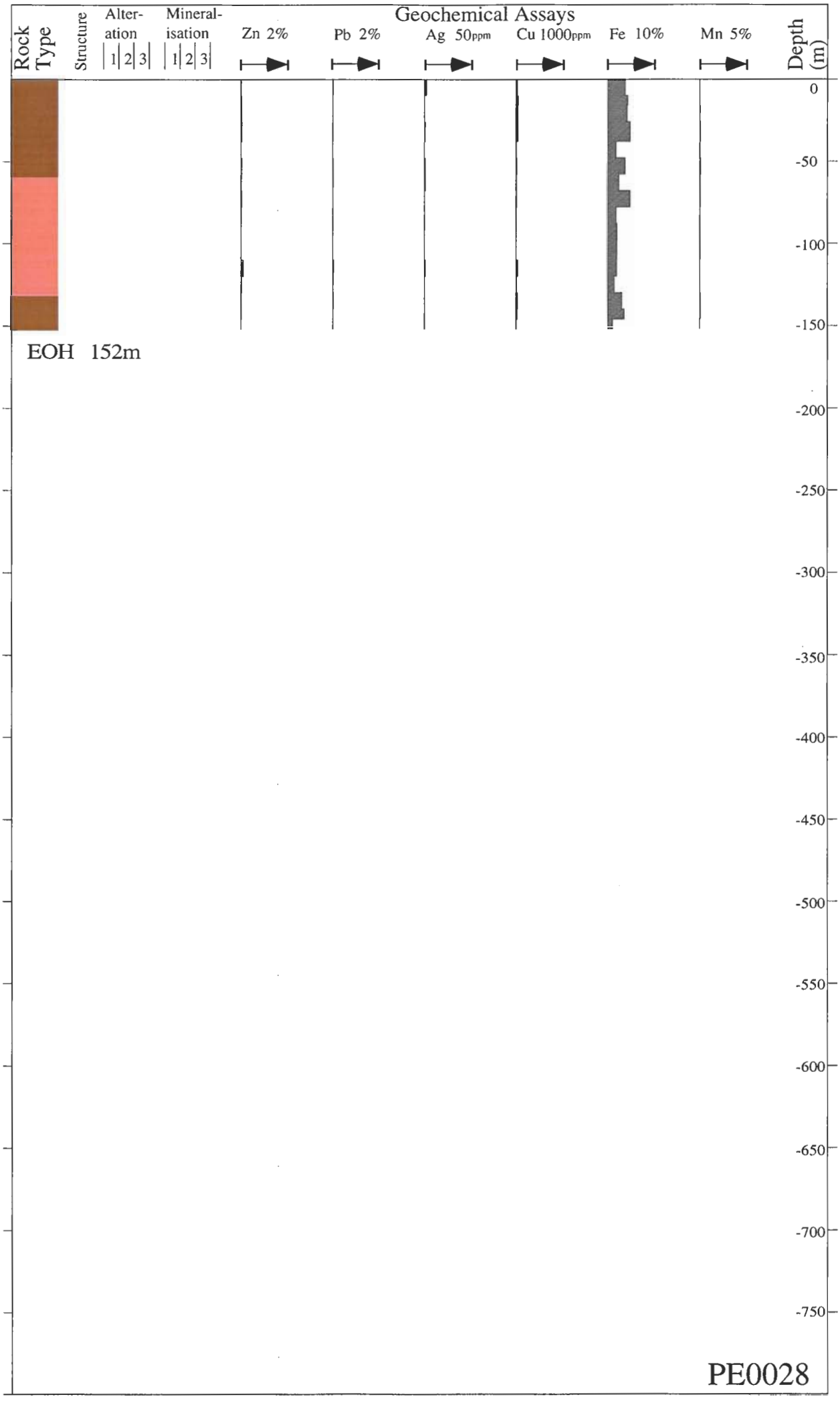
Rock Type
Structure
Alter-ation
1 2 3
Mineral-isation
1 2 3
Geochemical Assays
Zn 2%
Pb 2%
Ag 50ppm
Cu 1000ppm
Fe 10%
Mn 5%
Depth (m)
0
-50
-100
-150
EOH 152m
-200
-250
-300
-350
-400
-450
-500
-550
-600
-650
-700
-750

PE0028

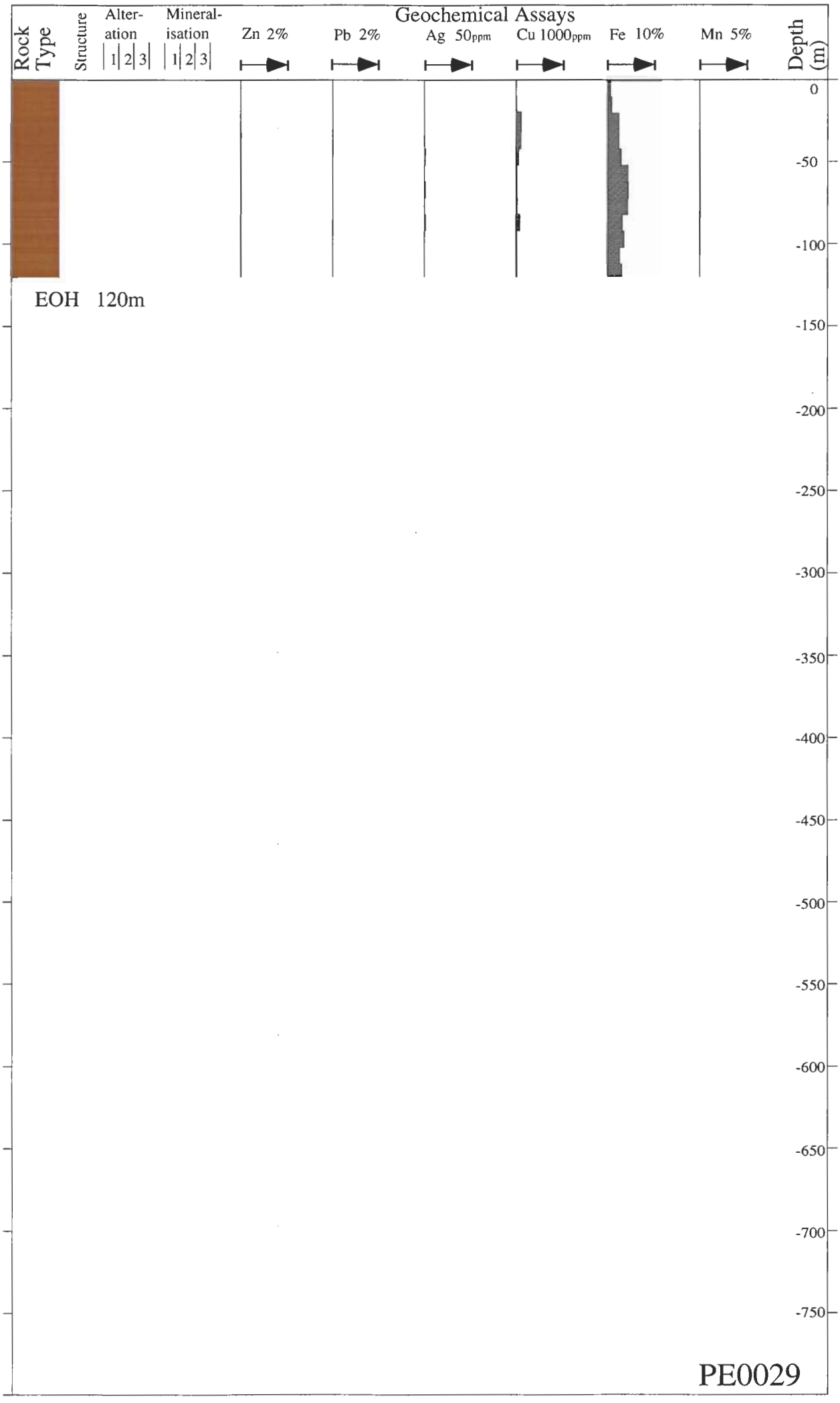
Rock Type
Structure
Alter-ation
1 2 3
Mineral-isation
1 2 3
Geochemical Assays
Zn 2%
Pb 2%
Ag 50ppm
Cu 1000ppm
Fe 10%
Mn 5%
Depth (m)
0
-50
-100
EOH 120m
-150
-200
-250
-300
-350
-400
-450
-500
-550
-600
-650
-700
-750

PE0029

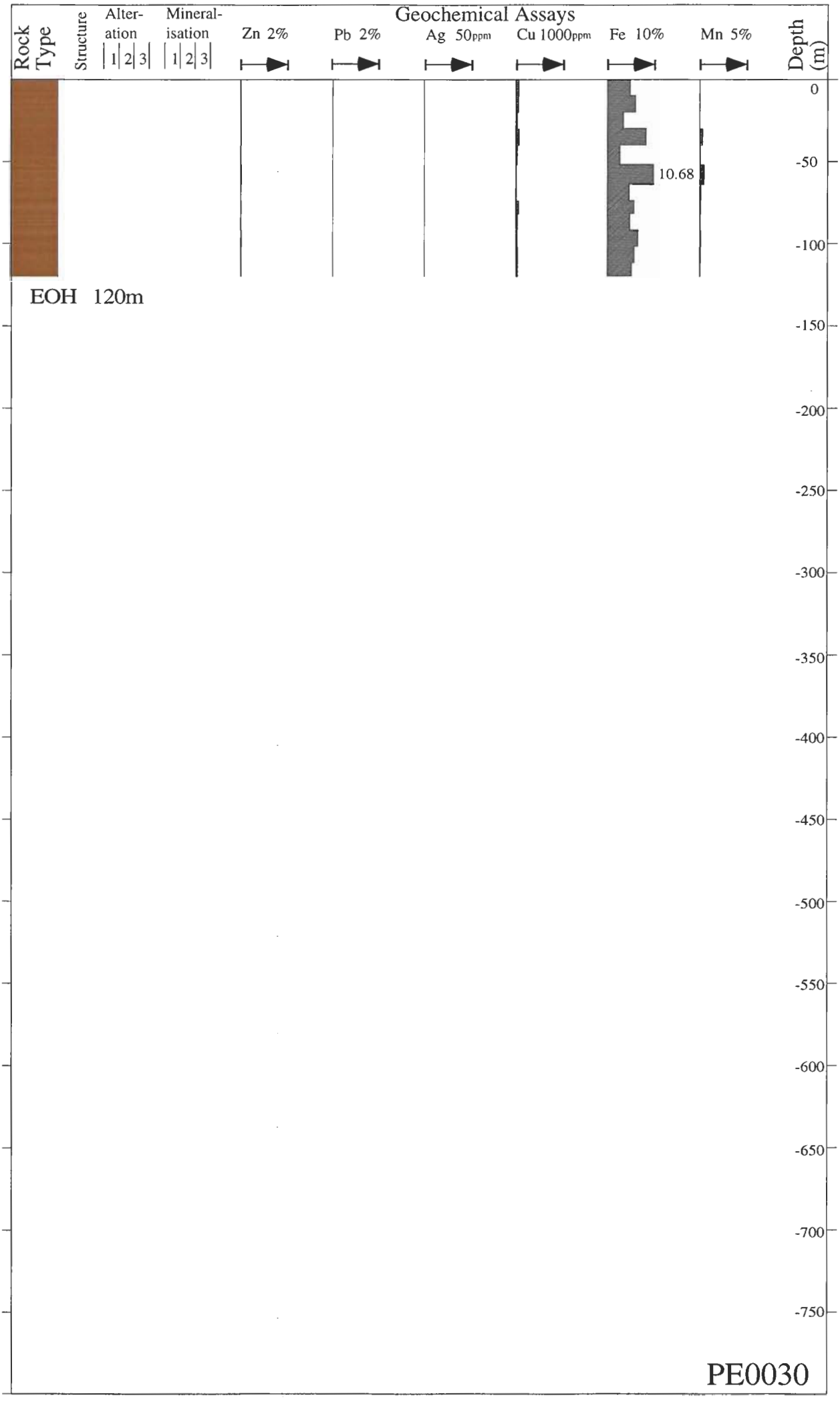
Rock Type
Structure
Alter-ation
1 2 3
Mineral-isation
1 2 3
Geochemical Assays
Zn 2%
Pb 2%
Ag 50ppm
Cu 1000ppm
Fe 10%
Mn 5%
Depth (m)
0
-50
-100
-150
-200
-250
-300
-350
-400
-450
-500
-550
-600
-650
-700
-750
10.68
EOH 120m

PE0030

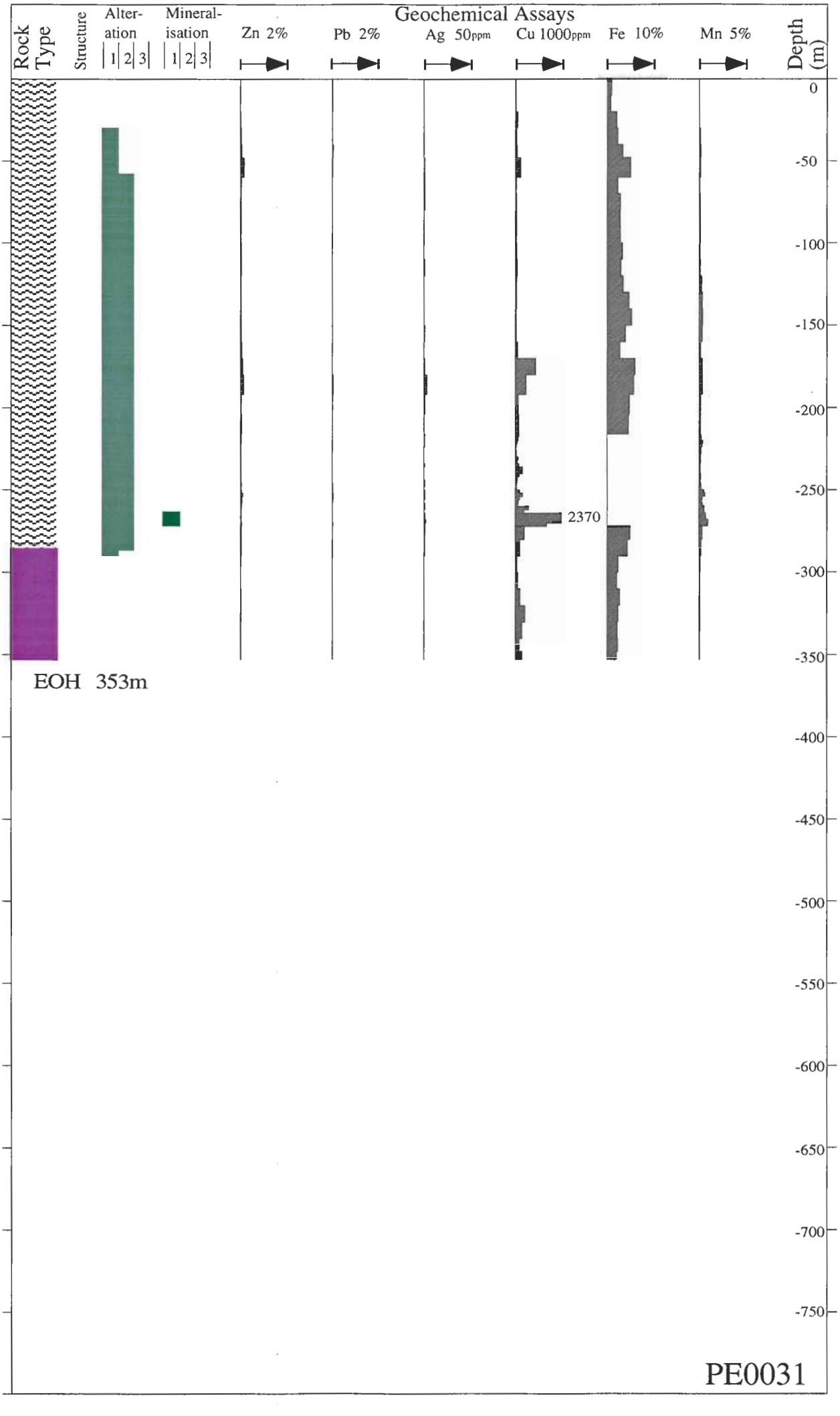
Rock Type
Structure
Alter-ation
1 2 3
Mineral-isation
1 2 3
Geochemical Assays
Zn 2%
Pb 2%
Ag 50ppm
Cu 1000ppm
Fe 10%
Mn 5%
Depth (m)
0
-50
-100
-150
-200
-250
-300
-350
-400
-450
-500
-550
-600
-650
-700
-750
2370
EOH 353m
PE0031

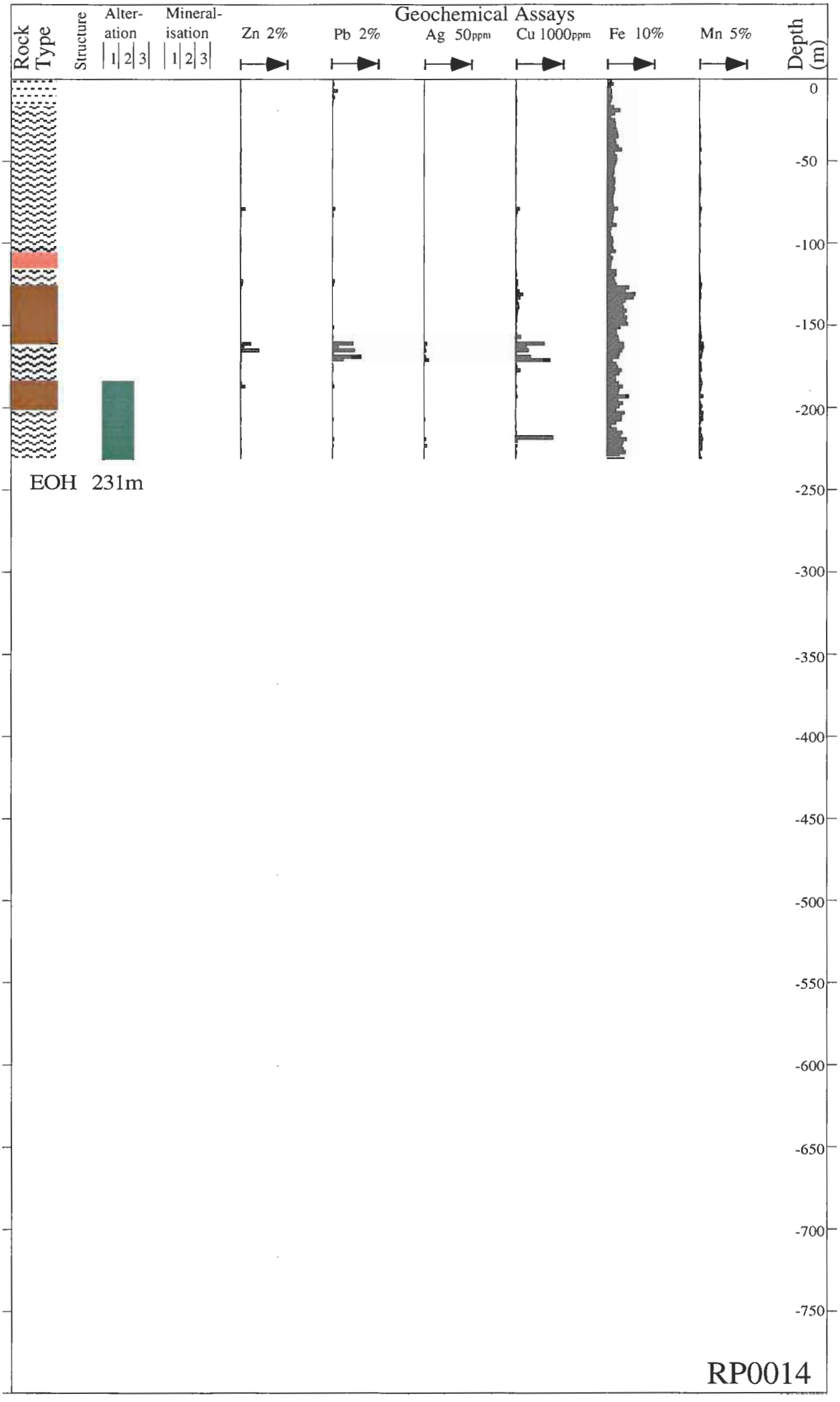
Rock Type
Structure
Alter-ation
1 2 3
Mineral-isation
1 2 3
Geochemical Assays
Zn 2%
Pb 2%
Ag 50ppm
Cu 1000ppm
Fe 10%
Mn 5%
Depth (m)
0
-50
-100
-150
-200
-250
-300
-350
-400
-450
-500
-550
-600
-650
-700
-750
EOH 231m
RP0014

## Key to cross sections

Tertiary and Quaternary sediments.

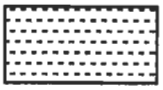
Dominantly kaolinitic clays.

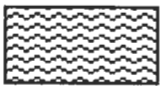
Menninnie Dam ignimbrite.

Muddy sandstone and pumice breccia units

Layered polymictic breccia units.

Discordant polymictic breccia pipes.

Rhyolitic intrusions and lava.

quartz vein .

Lincoln Complex Granite dykes.

Amphibolite intrusions or flows

Graphitic units.

Quartz - feldspar - biotite - garnet - sillimanite - muscovite schist.

Calcitic and dolomitic marble.

Iron Formations dominated by iron rich silicates and magnetite.

Quartz-diopside rock, massive diopside, diopside and dolomitic or calcitic marble rock.

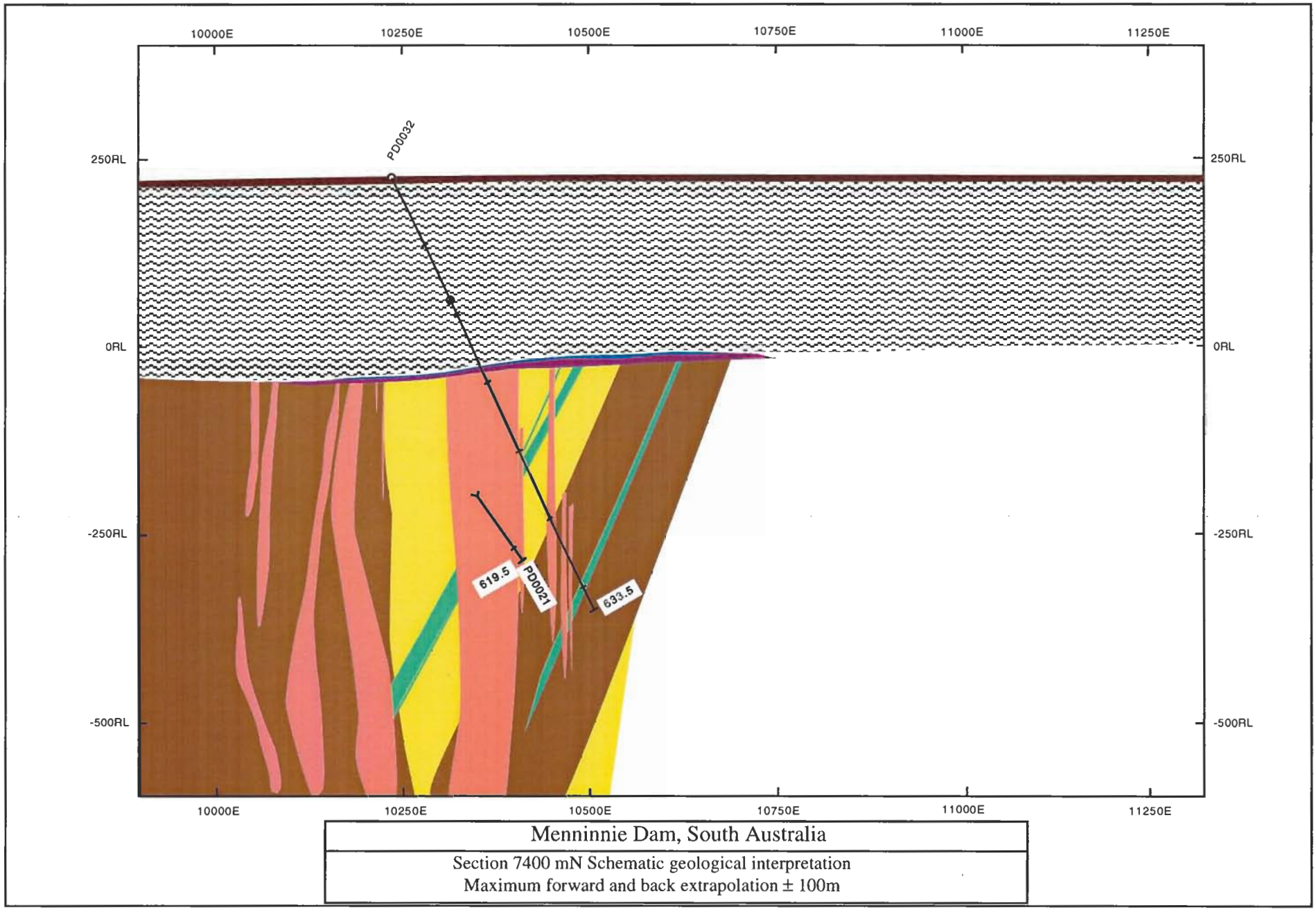


Menninnie Dam, South Australia

Section 7400 mN Schematic geological interpretation
Maximum forward and back extrapolation ± 100m

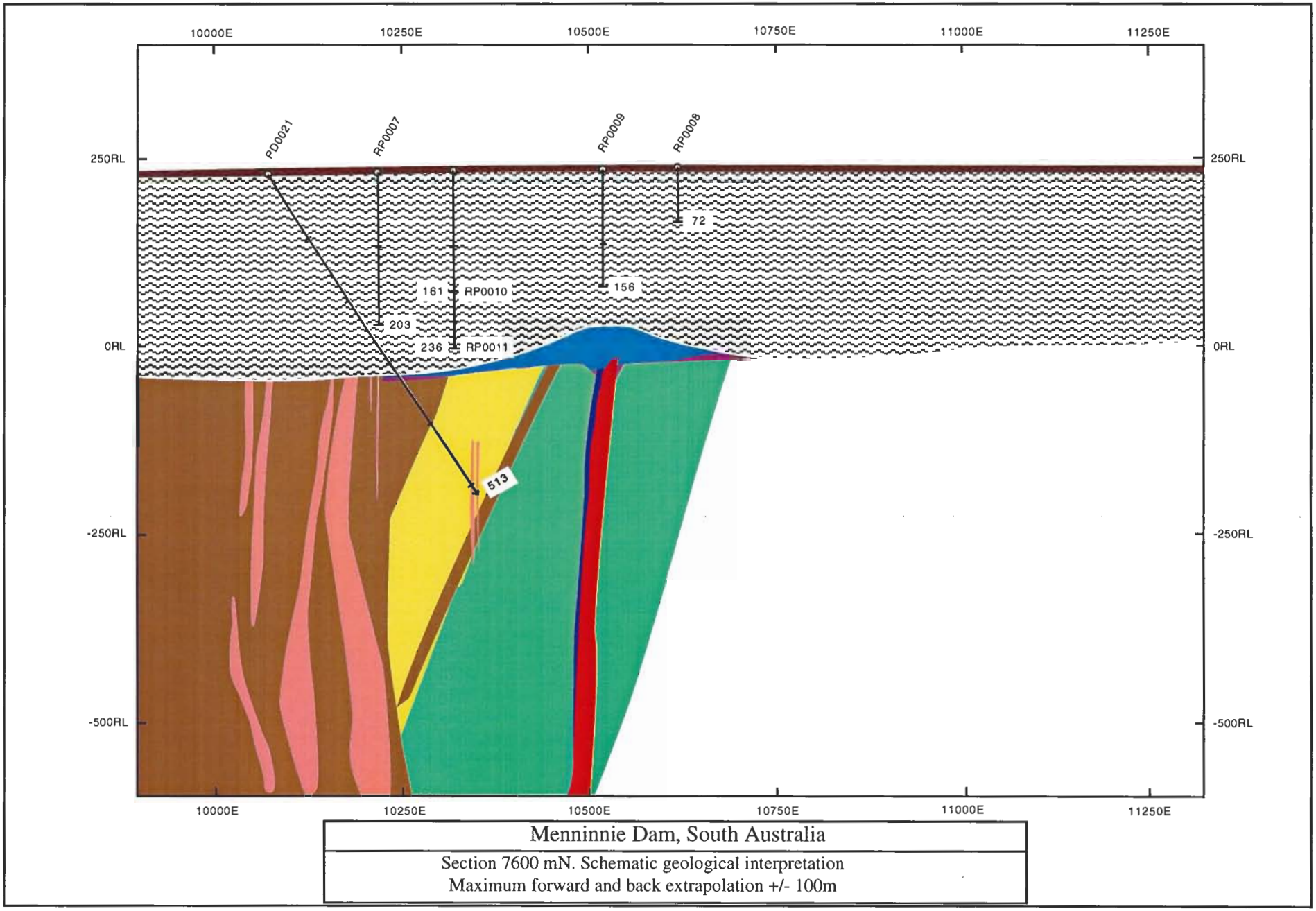


Menninnie Dam, South Australia

Section 7600 mN. Schematic geological interpretation
Maximum forward and back extrapolation +/- 100m

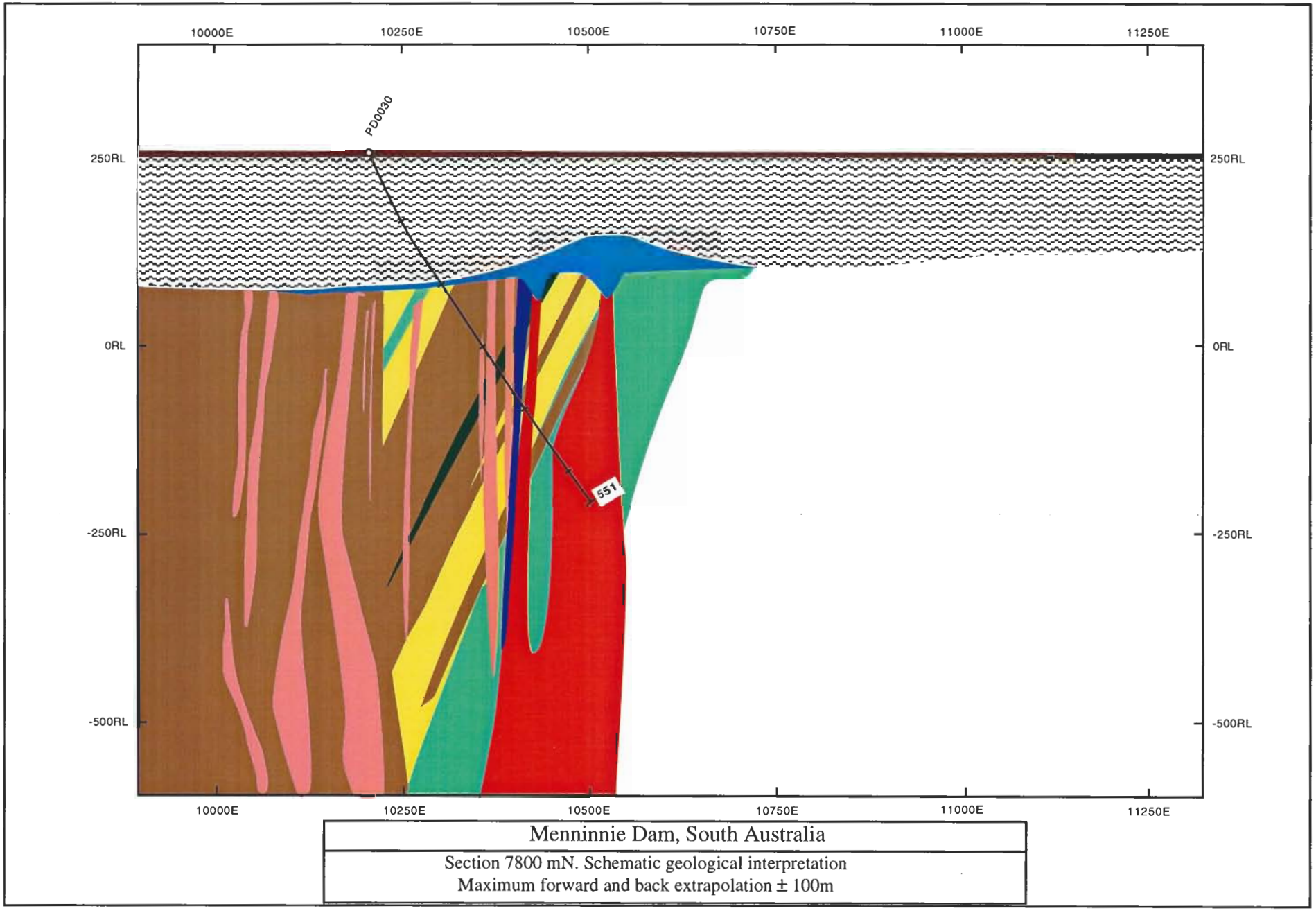


Menninnie Dam, South Australia

Section 7800 mN. Schematic geological interpretation
Maximum forward and back extrapolation ± 100m

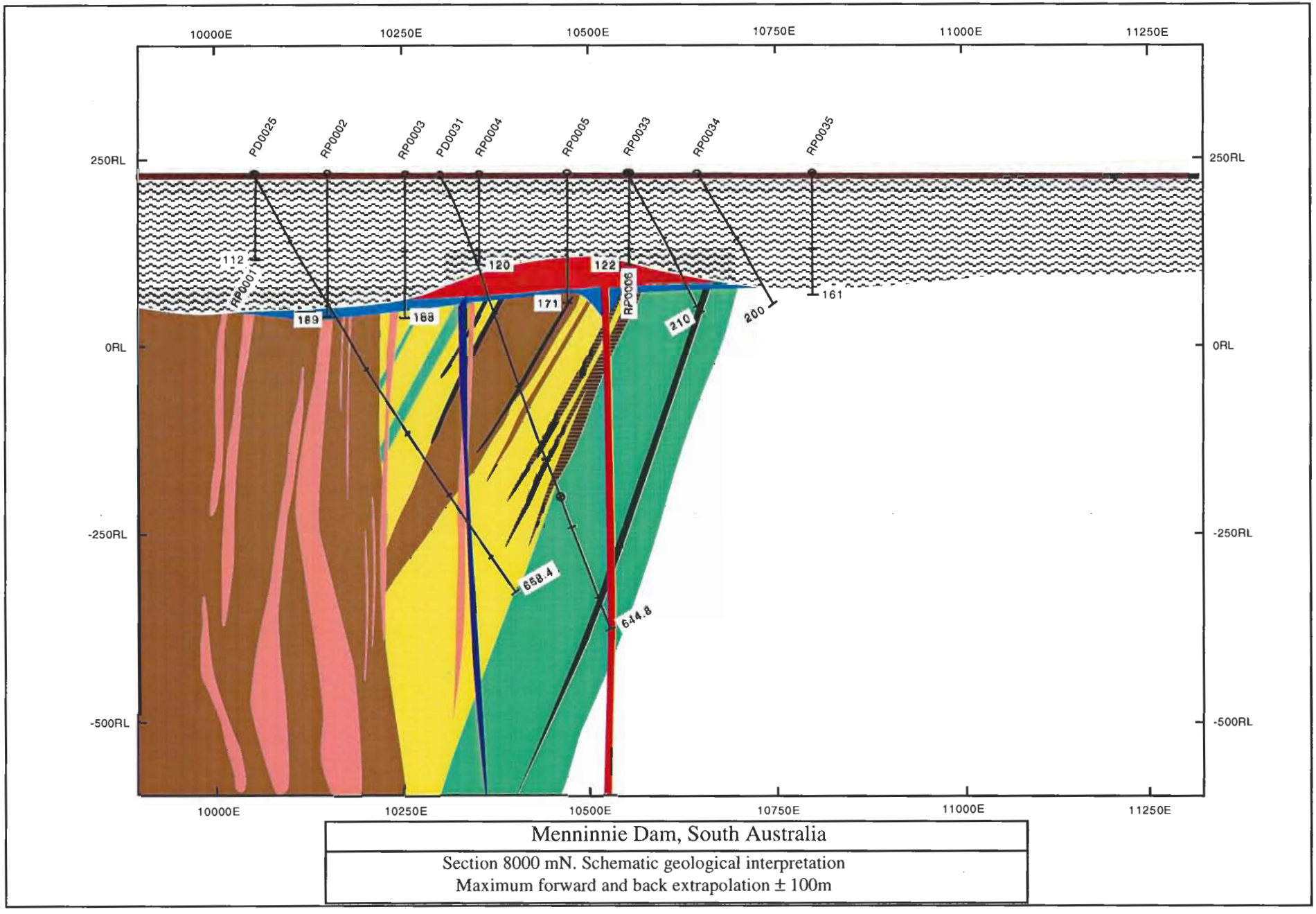


Menninnie Dam, South Australia

Section 8000 mN. Schematic geological interpretation
Maximum forward and back extrapolation ± 100m

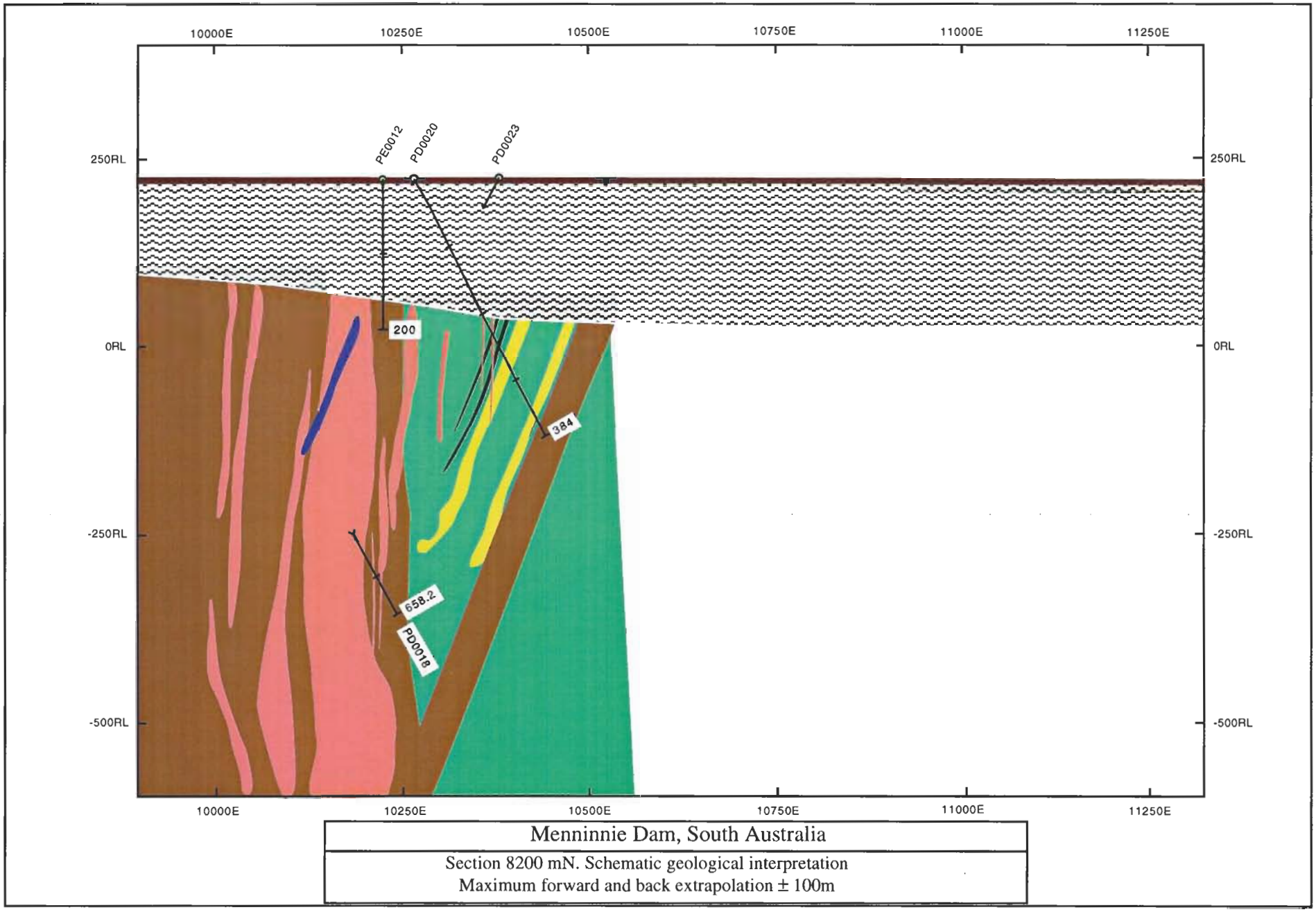


Menninnie Dam, South Australia

Section 8200 mN. Schematic geological interpretation
Maximum forward and back extrapolation ± 100m

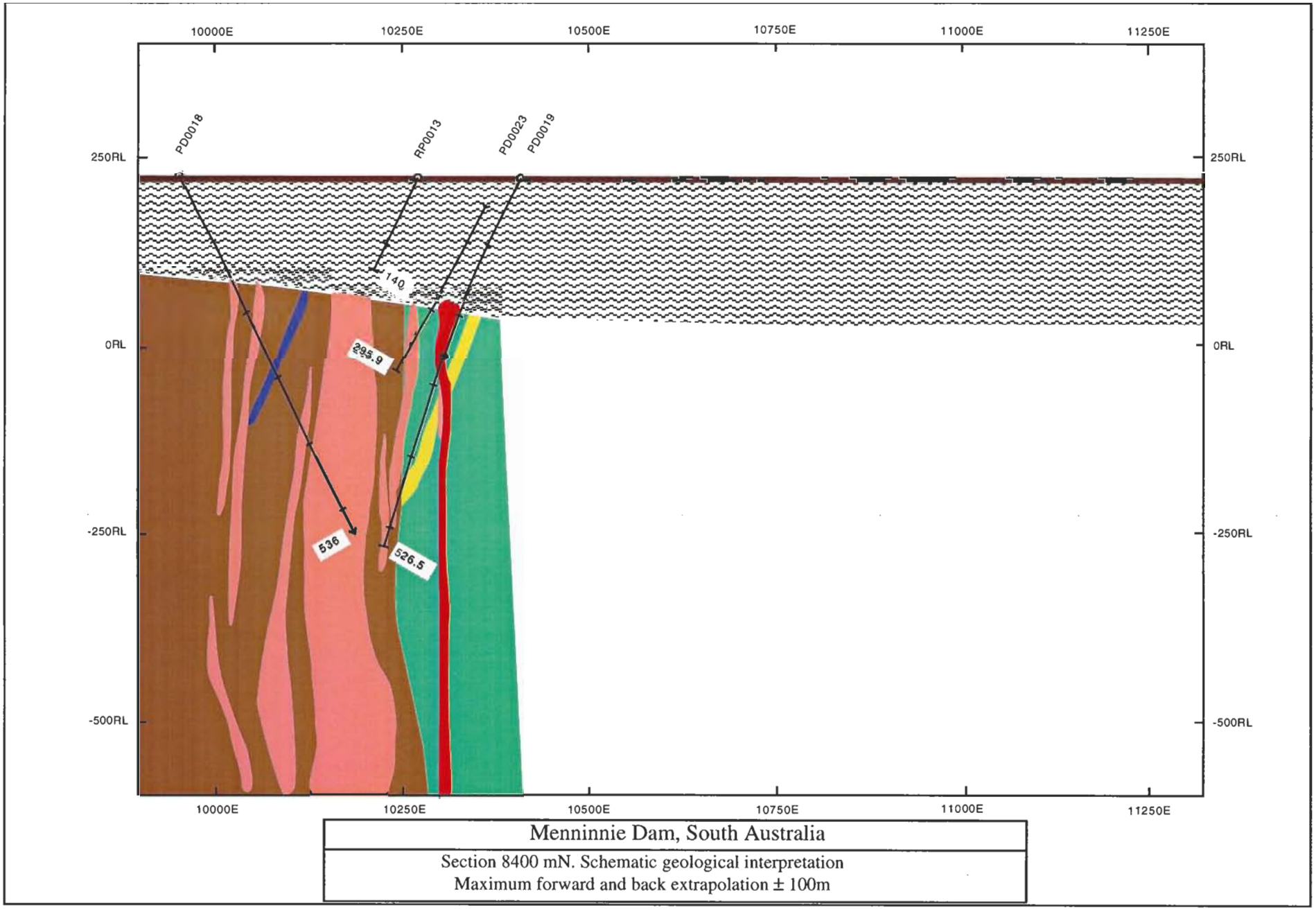


Menninnie Dam, South Australia

Section 8400 mN. Schematic geological interpretation
Maximum forward and back extrapolation ± 100m

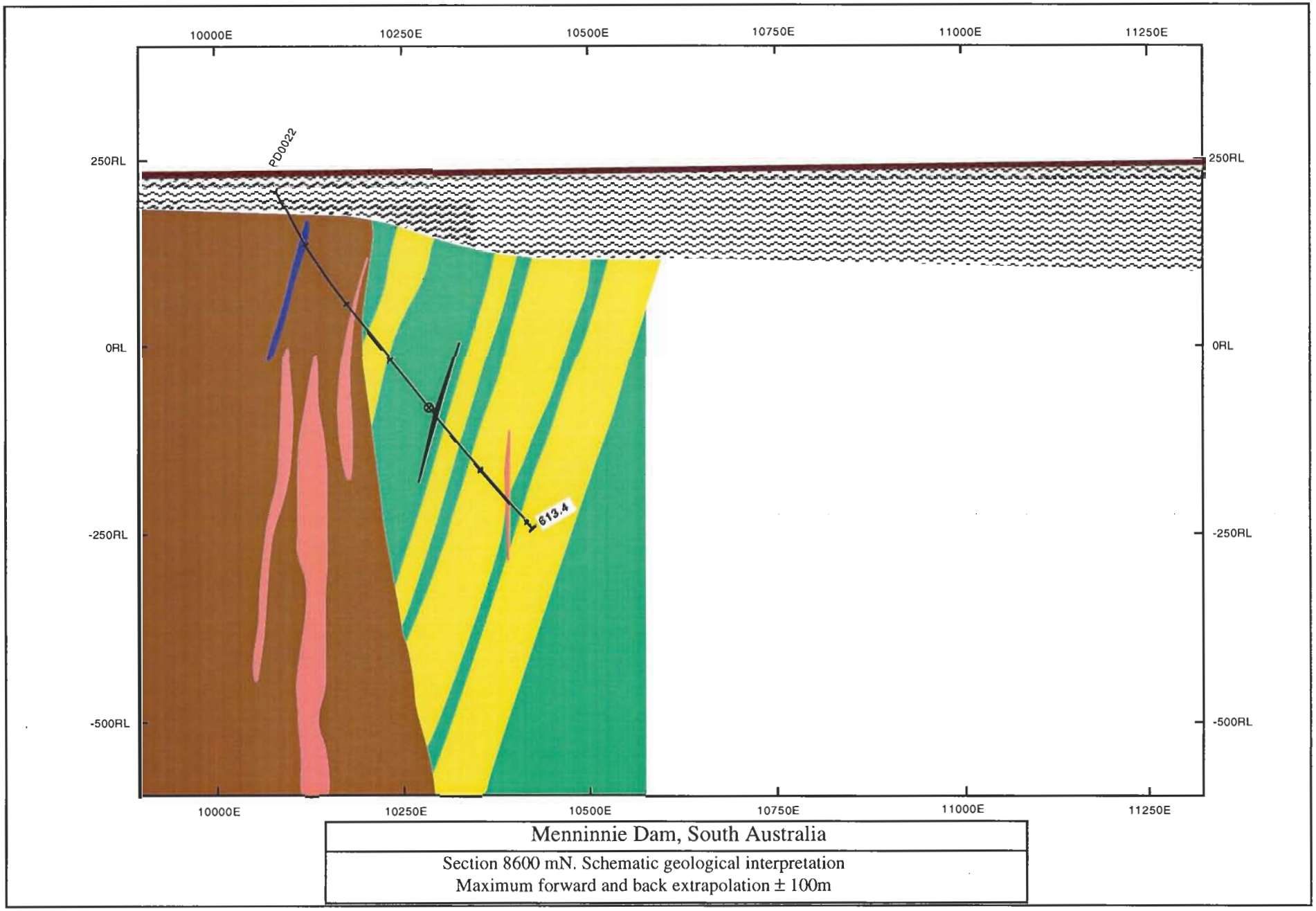


Menninnie Dam, South Australia

Section 8600 mN. Schematic geological interpretation
Maximum forward and back extrapolation ± 100m

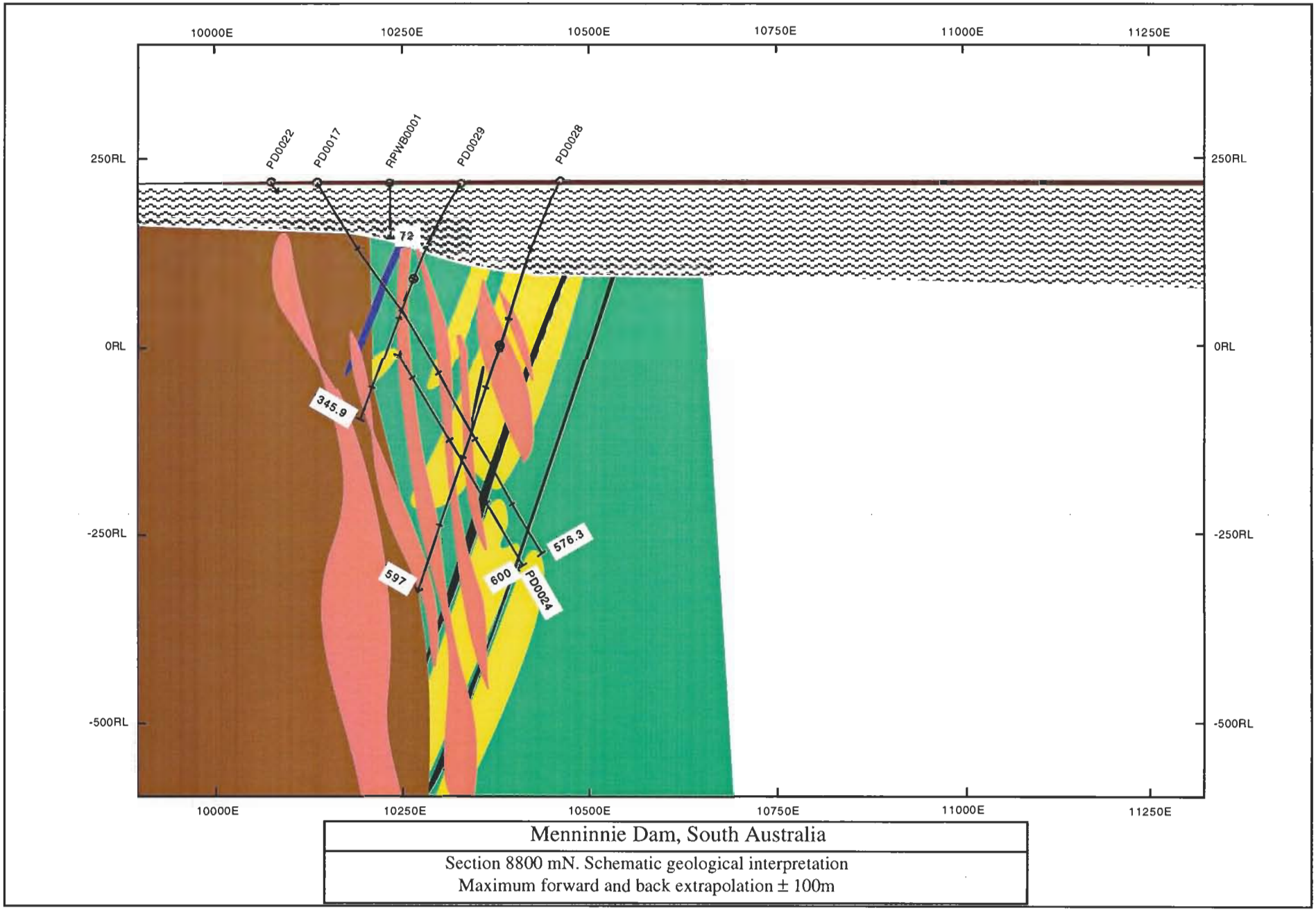


Menninnie Dam, South Australia

Section 8800 mN. Schematic geological interpretation
Maximum forward and back extrapolation ± 100m

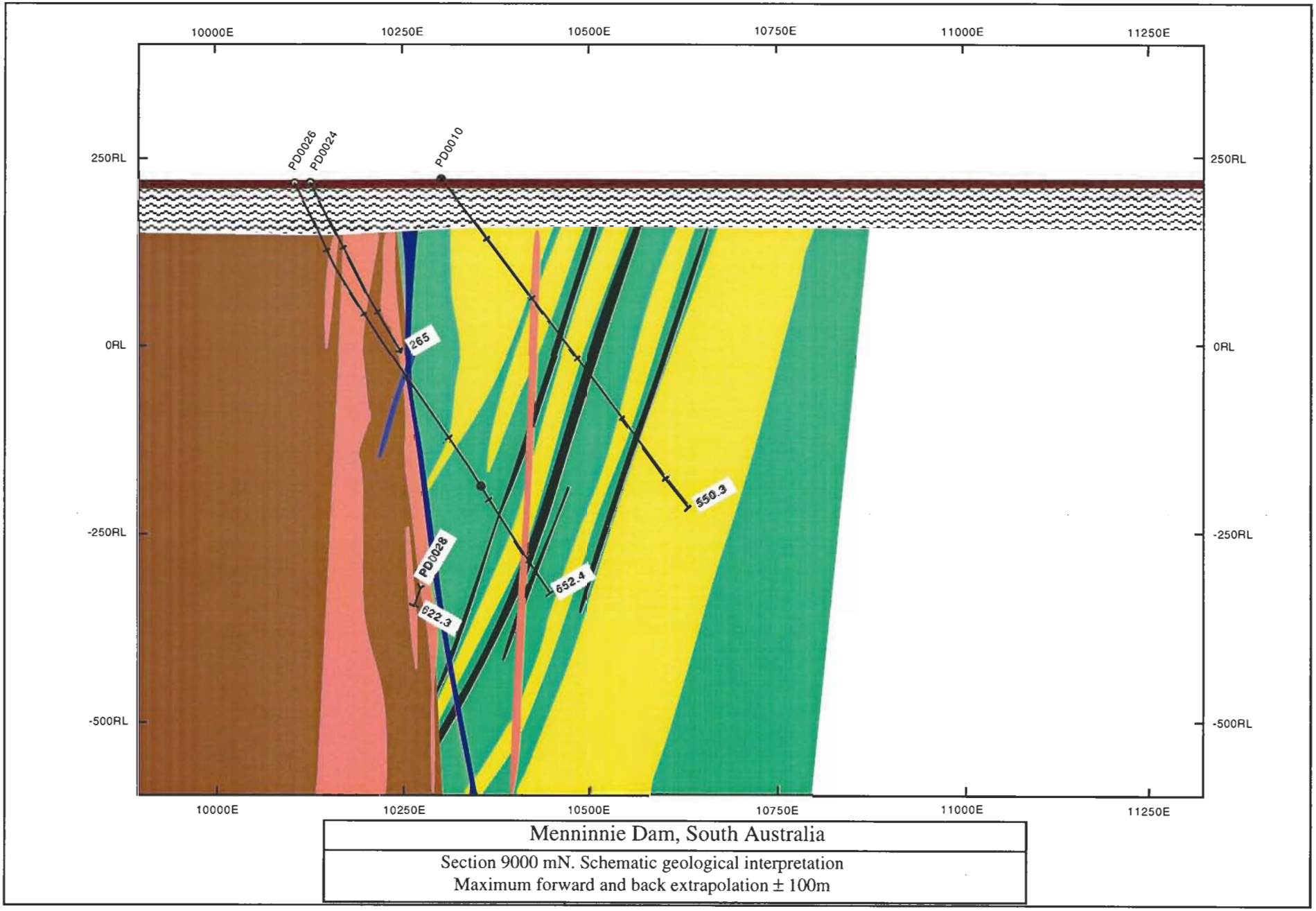


Menninnie Dam, South Australia

Section 9000 mN. Schematic geological interpretation
Maximum forward and back extrapolation ± 100m

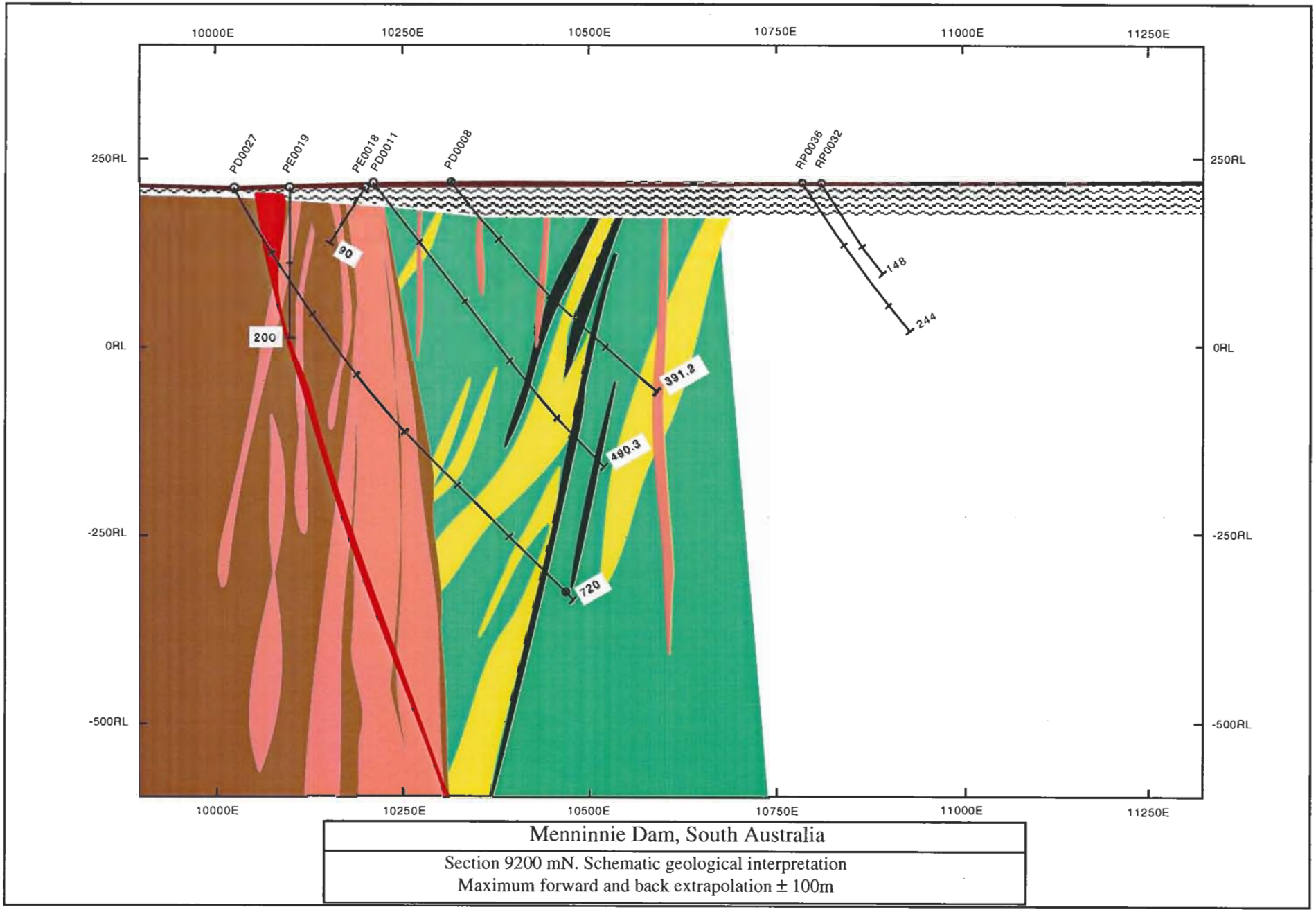


Menninnie Dam, South Australia

Section 9200 mN. Schematic geological interpretation
Maximum forward and back extrapolation ± 100m

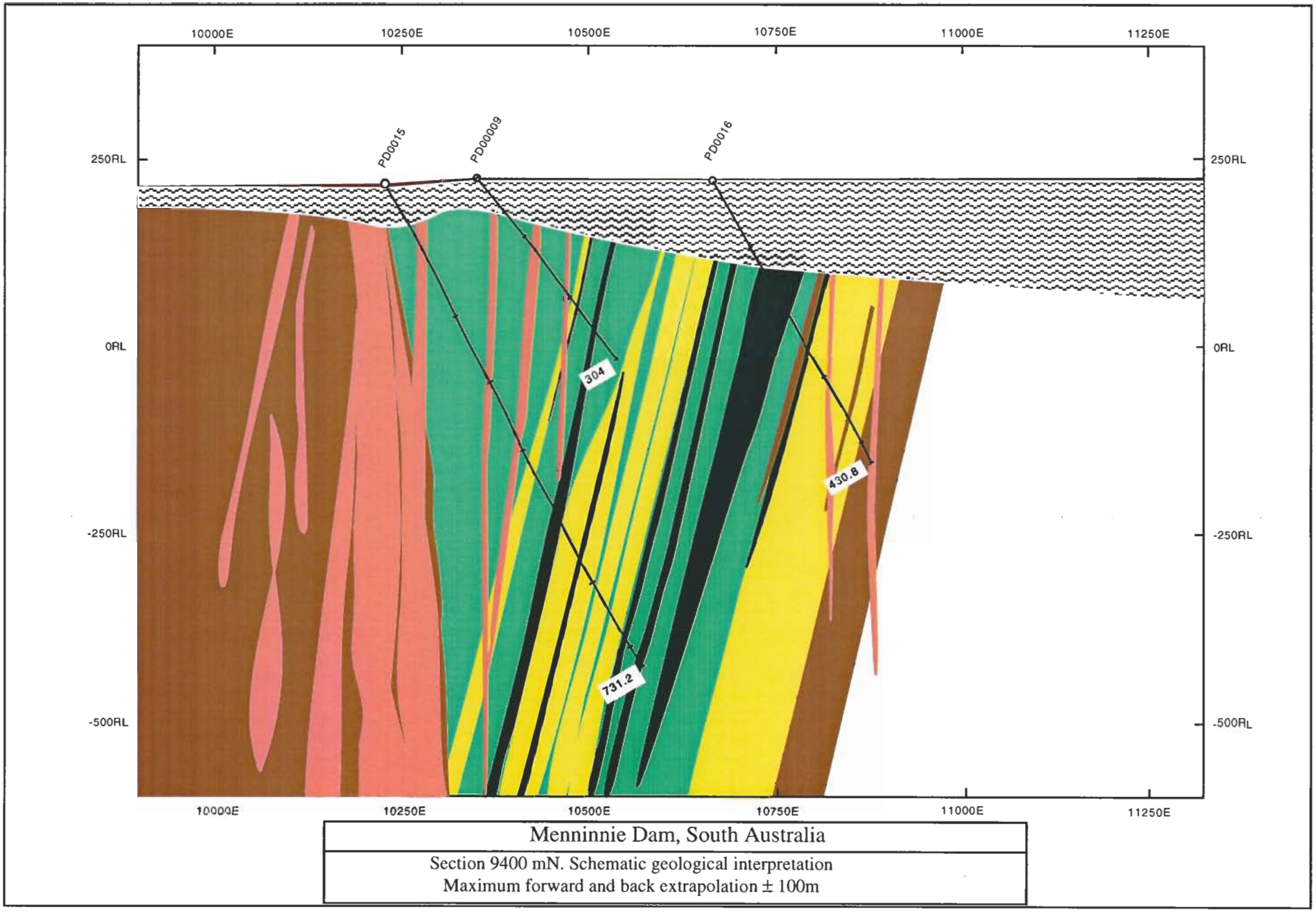


Menninnie Dam, South Australia

Section 9400 mN. Schematic geological interpretation
Maximum forward and back extrapolation ± 100m

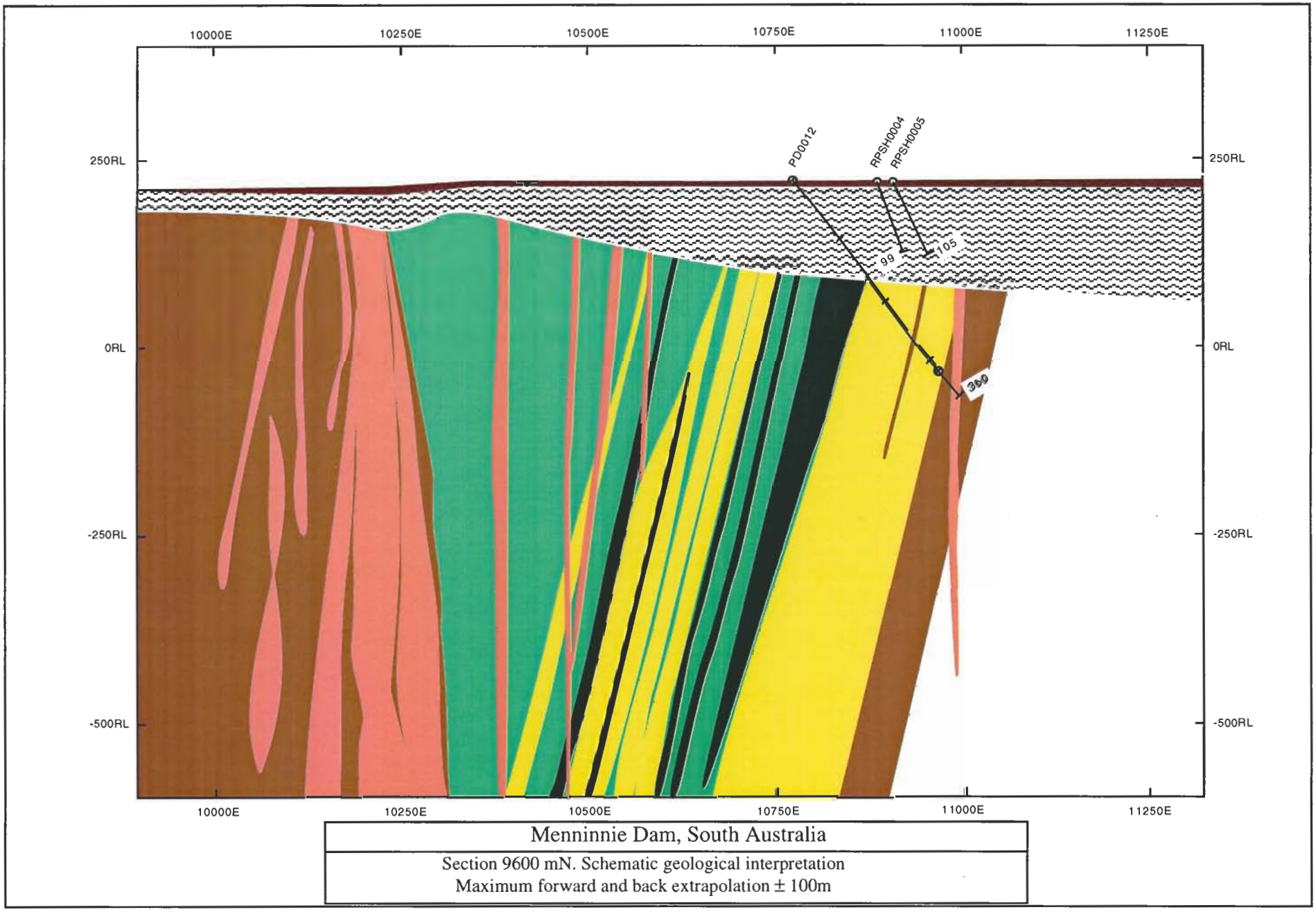


Menninnie Dam, South Australia

Section 9600 mN. Schematic geological interpretation
Maximum forward and back extrapolation ± 100m

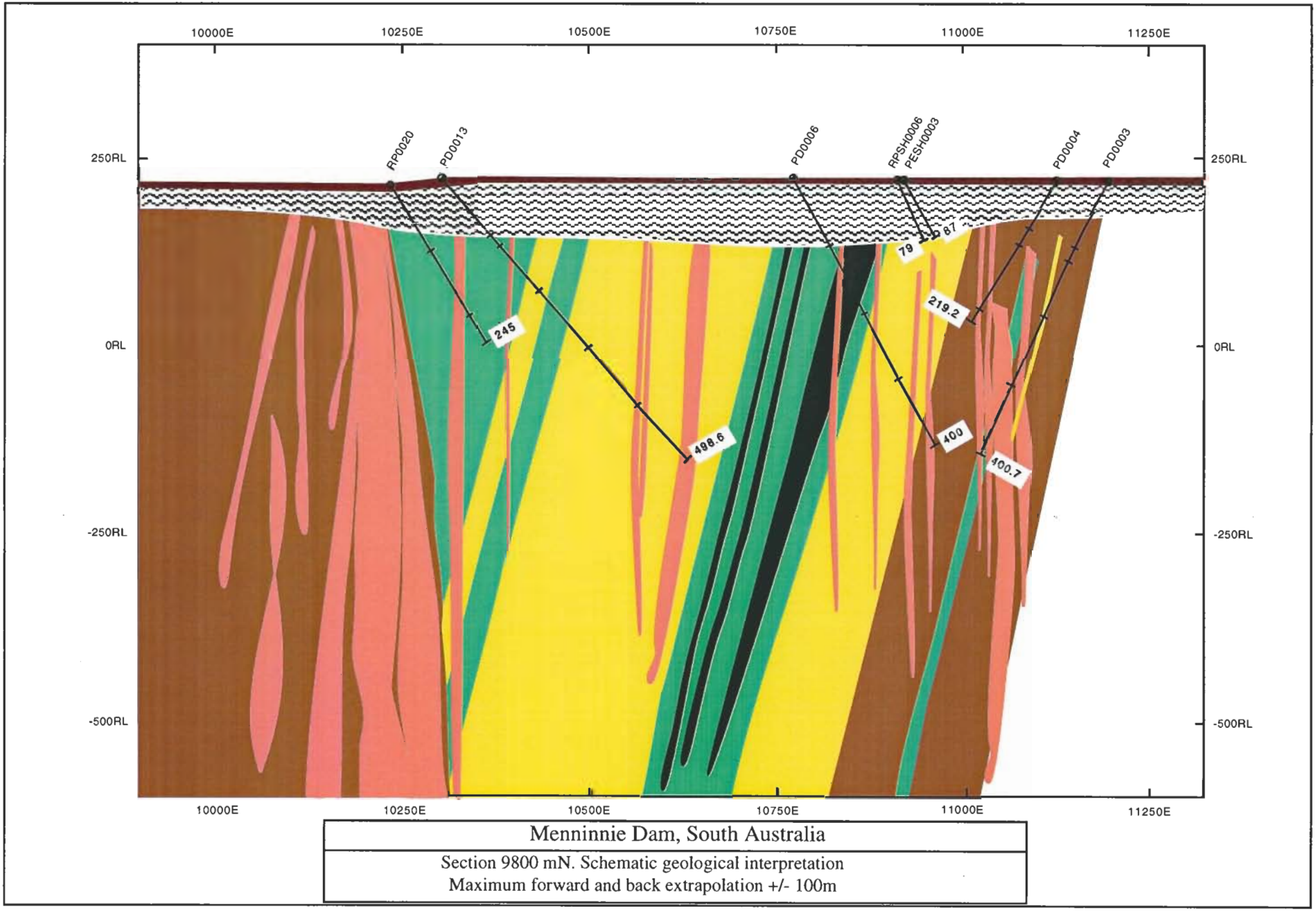


Menninnie Dam, South Australia

Section 9800 mN. Schematic geological interpretation
Maximum forward and back extrapolation +/- 100m

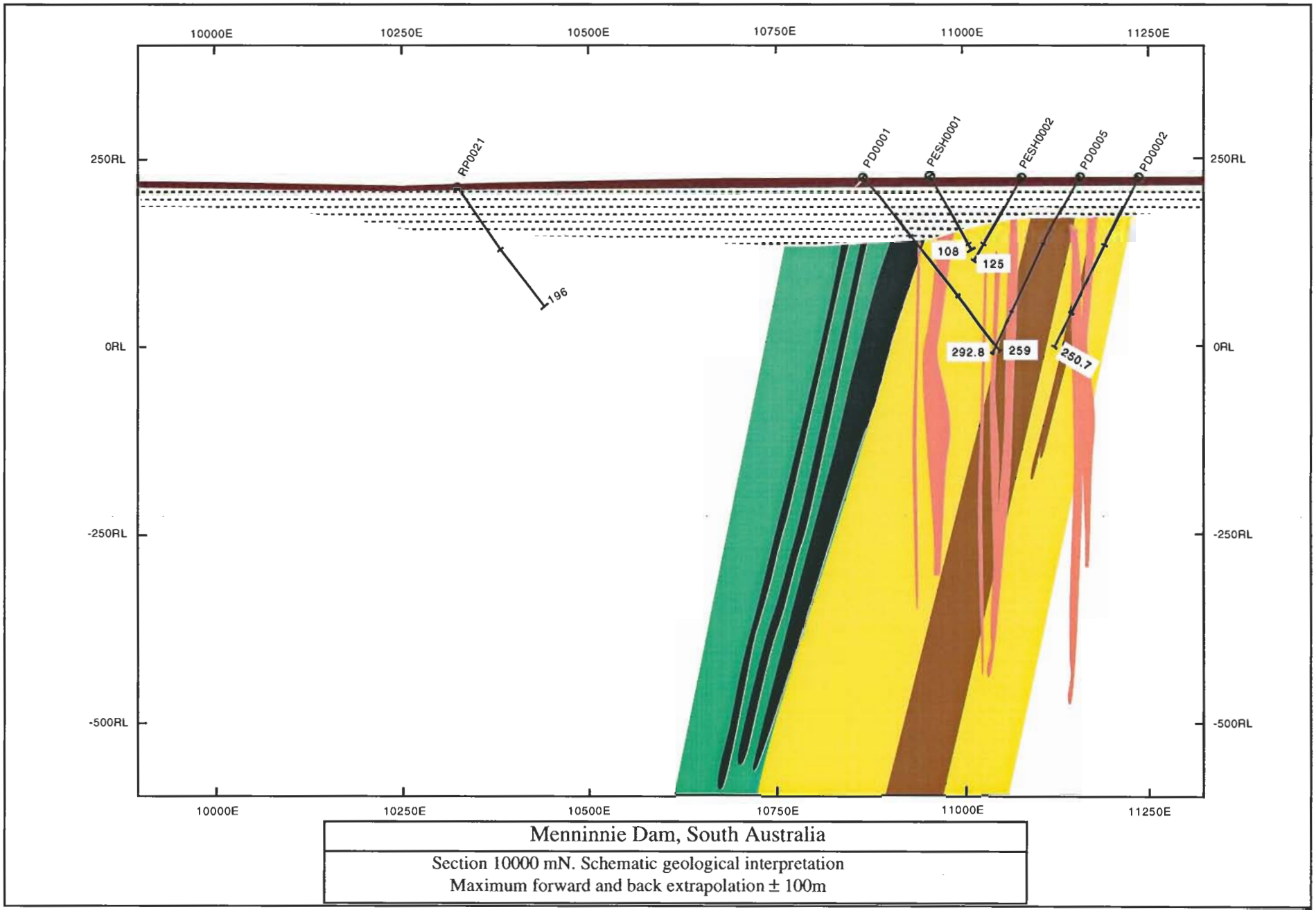


Menninnie Dam, South Australia

Section 10000 mN. Schematic geological interpretation
Maximum forward and back extrapolation ± 100m

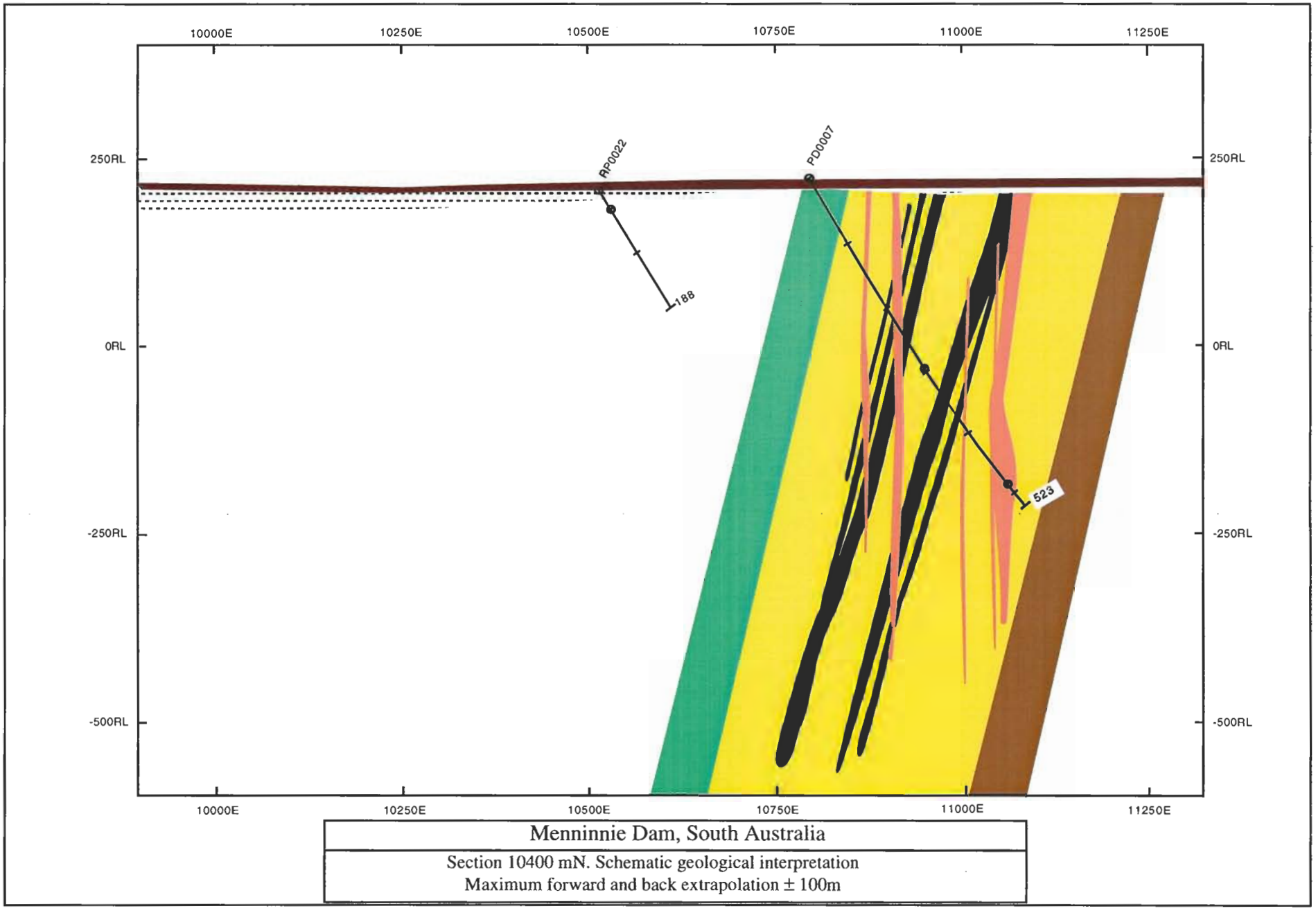


Menninnie Dam, South Australia

Section 10400 mN. Schematic geological interpretation
Maximum forward and back extrapolation ± 100m

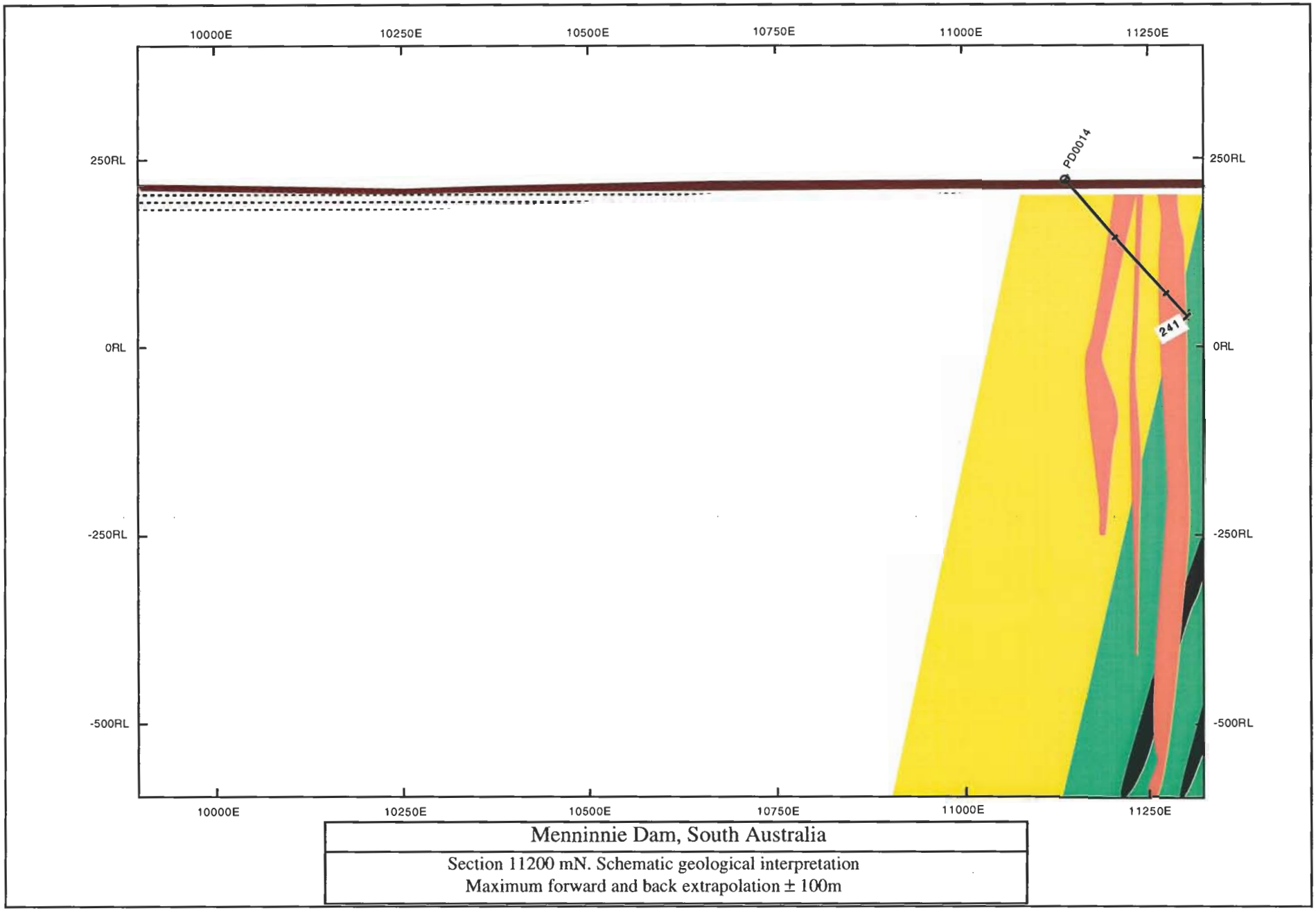


Menninnie Dam, South Australia

Section 11200 mN. Schematic geological interpretation
Maximum forward and back extrapolation ± 100m

## Appendix 3.2

XRF Analyses of Menninnie Dam samples; Machine settings and standards.

Approximately 1-2 kg of sample was crushed in a steel jaw-crusher to < 1 cm maximum size. The crushed rock was then split to obtain a 1 - 200 gm sub-sample. The sub-sample was ground to a powder in a chrome steel ring mill and a portion of the powder was fused into a glass disk using the technique of Norrish and Hutton (1969). A second portion of the powder was pressed to form a boric acid encased pellet using the technique of Norrish and Chappell (1977). Glass disks and pressed power pellets were analysed by XRF spectrometry using a Phillips PW1480 spectrometer at the Geology Department, University of Tasmania. Instrumental conditions are listed in Tables A and B. Trace element concentrations were determined using mass absorption coefficients calculated from major element analyses. Results were corrected against a number of international standards, specpure silica blanks, and the secondary standards, 'Tasbas' (basalt) and 'Tasgran' (granite) listed in Table C. On average, 2 - 3 standards, blanks, and one duplicate analyses was analysed for every 6 - 7 samples analysed.

Loss on ignition (L.O.I.) is the sum of $H_2O^+$, $H_2O^-$, and other gaseous phases measured on approximately 1 gram of powder held at 1000°C for 24 hours (powders were kept in a desiccator for several hours prior to weighing). Unless values for $Fe_2O_3$ and FeO are specified, the total iron content of analyses is expressed as $Fe_2O_3$.

Table A. Instrumental conditions for major elements analysed (expressed as oxides).

| Oxide | Line | Tube | kV | mA | Crystal | Counter | Collimator | Vacuum | Time (s) |
|---|---|---|---|---|---|---|---|---|---|
| $SiO_2$ | K alpha | ScMo | 40 | 70 | PE | Flow | Coarse | Yes | 50 |
| $TiO_2$ | K alpha | ScMo | 90 | 30 | LiF200 | Flow | Fine | Yes | 40 |
| $Al_2O_3$ | K alpha | ScMo | 40 | 70 | PE | Flow | Coarse | Yes | 40 |
| $Fe_2O_3$ | K alpha | ScMo | 90 | 30 | LiF200 | Flow | Fine | Yes | 10 |
| MnO | K alpha | ScMo | 90 | 30 | LiF200 | Flow | Fine | Yes | 20 |
| MgO | K alpha | ScMo | 40 | 70 | PX1 | Flow | Coarse | Yes | 50 |
| CaO | K alpha | ScMo | 40 | 70 | LiF200 | Flow | Fine | Yes | 10 |
| $Na_2O$ | K alpha | ScMo | 40 | 70 | PX1 | Flow | Coarse | Yes | 100 |
| $K_2O$ | K alpha | ScMo | 40 | 70 | LiF200 | Flow | Fine | Yes | 20 |
| $P_2O_5$ | K alpha | ScMo | 40 | 70 | GE | Flow | Coarse | Yes | 40 |

## Appendix 3.2 cont.

Table B. Instrumental conditions for trace elements analysed.

| Element | Line | Tube | kV | mA | Crystal | Counter | Colli - mator | Vacuum | Det$^{n}$ limit ppm | Precision |
|---|---|---|---|---|---|---|---|---|---|---|
| Sc | K alpha | Au | 40 | 70 | LiF200 | Flow | Fine | Yes | 2 | 10±1, 30±1 |
| V | K alpha | Au | 40 | 70 | LiF200 | Flow | Fine | Yes | 2 | 30±2, 100±1 |
| Cr | K alpha | Au | 40 | 70 | LiF200 | Flow | Fine | Yes | 1 | 10±2, 400±4 |
| Ni | K alpha | ScMo | 90 | 30 | LiF200 | Flow | Fine | Yes | 1 | 3±0.5, 20±0.5, 200±2 |
| Rb | K alpha | ScMo | 90 | 30 | LiF200 | Scintill | Fine | Yes | 1 | 10±1, 70±1, 170±2 |
| Sr | K alpha | Au | 80 | 35 | LiF200 | Scintill | Fine | Yes | 1 | 10±1, 200±2, 500±5 |
| Y | K alpha | ScMo | 90 | 30 | LiF200 | Scintill | Fine | Yes | 1 | 10±2, 20±1, 100±2 |
| Zr | K alpha | Au | 80 | 35 | LiF200 | Scintill | Fine | Yes | 1 | 100±2, 250±4, 500±10 |
| Nb | K alpha | Au | 80 | 35 | LiF200 | Scintill | Fine | Yes | 1 | 10±0.5, 20±1 |
| Ba | L alpha | Au | 40 | 70 | LiF200 | Flow | Fine | Yes | 4 | 500±5, 1200±5 |
| La | L alpha | Au | 40 | 70 | LiF200 | Flow | Fine | Yes | 2.5 | 20±1, 40±2, 100±2 |
| Ce | L beta | Au | 40 | 70 | LiF200 | Flow | Fine | Yes | 5 | 30±2, 80±3, 150±1 |
| Nd | L alpha | Au | 40 | 70 | LiF200 | Flow | Fine | Yes | 3 | 15±1, 30±2, 50±2 |
| Pb | L beta | ScMo | 40 | 70 | LiF200 | Scintill | Fine | Yes | 1.5 | 20±1, 50±1 |
| Th | L alpha | ScMo | 90 | 30 | LiF200 | Scintill | Fine | Yes | 1.5 | 25±1, 100±2 |
| U | L alpha | ScMo | 90 | 30 | LiF200 | Scintill | Fine | Yes | 1 | 5±1, 40±1 |

Table C. Chemical composition of Tasbas and Tasgran standards.

| | Tasbas | | | Tasgran | | |
|---|---|---|---|---|---|---|
| | wt.% | ±1 sigma | % sigma | wt.% | ±1 sigma | % sigma |
| $SiO_2$ | 44.56 | 0.23 | 0.5 | 72.6 | 0.17 | 0.2 |
| $TiO_2$ | 2.31 | 0.04 | 1.7 | 0.29 | 0.01 | 3.4 |
| $Al_2O_3$ | 14.14 | 0.10 | 0.7 | 13.65 | 0.08 | 0.6 |
| $Fe_2O_3$ | 12.65 | 0.09 | 0.8 | 2.29 | 0.03 | 1.3 |
| MnO | 0.17 | 0.01 | 5.1 | 0.04 | 0.003 | 7.5 |
| MgO | 8.16 | 0.11 | 1.3 | 0.59 | 0.04 | 6.8 |
| CaO | 7.81 | 0.06 | 0.8 | 1.87 | 0.02 | 1.1 |
| $Na_2O$ | 5.43 | 0.12 | 2.1 | 2.82 | 0.1 | 3.5 |
| $K_2O$ | 1.86 | 0.03 | 1.6 | 4.61 | 0.04 | 0.9 |
| $P_2O_5$ | 0.97 | 0.03 | 2.6 | 0.12 | 0.002 | 1.7 |
| LOI | 1.56 | 0.02 | 1.3 | 0.86 | 0.02 | 2.3 |
| Total | 99.62 | | | 99.74 | | |
| | ppm | | | ppm | | |
| Ba | 204 | 3.0 | 1.5 | 462 | 4.5 | 1.0 |
| Rb | 16.5 | 0.7 | 4.2 | 259 | 3.0 | 1.2 |
| Nb | 61.4 | 1.2 | 2.0 | 17 | 0.5 | 2.9 |
| La | 43.4 | 1.4 | 3.2 | 38.8 | 1.0 | 2.6 |
| Ce | 89 | 3.4 | 3.9 | 86.9 | 3.2 | 3.7 |
| Sr | 1025 | 11.2 | 1.1 | 152 | 1.5 | 1.0 |
| Nd | 41.2 | 2.4 | 5.8 | 37.4 | 1.8 | 4.8 |
| Zr | 260 | 4.3 | 1.7 | 157 | 2.5 | 1.6 |
| Y | 23.1 | 0.6 | 2.6 | 35 | 1.0 | 2.9 |
| Sc | 13.1 | 0.5 | 3.8 | 6.7 | 0.3 | 4.5 |
| V | 163 | 2.3 | 1.4 | 25.4 | 1.0 | 3.9 |
| Cr | 198 | 4.1 | 2.1 | 10 | 0.5 | 5.0 |
| Ni | 154 | 2.0 | 1.3 | 3.4 | 0.2 | 5.9 |
| Pb | 5.9 | 0.8 | 13.6 | 18.8 | 0.5 | 2.7 |
| Th | 4.7 | 0.4 | 8.5 | 26.8 | 1.3 | 4.9 |
| U | 1.5 | 0.5 | 33.3 | 4.1 | 0.7 | 17.1 |

**Appendix 3.3** Microprobe analysis of minerals used for thermobarometric calculations

Garnet compositions are calculated on the basis of 8 cations and 12 oxygens using Mintab version 1.1 software by Rock and Corroll (1990), which uses the proceedures of Droop (1987).

| Mineral | Location | Traverse dist. (μm) | MgO (wt.%) | Al2O3 (wt.%) | SiO2 (wt.%) | CaO (wt.%) | TiO2 (wt.%) | Cr2O3 (wt.%) | MnO (wt.%) | FeO (wt.%) | H2O (wt.%) | F (wt.%) | Na2O (wt.%) | Cl (wt.%) | K2O (wt.%) | Total (wt.%) |
|---|---|---|---|---|---|---|---|---|---|---|---|---|---|---|---|---|
| Biotite 2 | Margin | | 7.561 | 20.409 | 32.690 | 0.000 | 4.684 | | 0.393 | 17.790 | 3.594 | 0.505 | 0.191 | 0.000 | 8.863 | 96.472 |
| Biotite 2 | Margin | | 8.325 | 18.266 | 32.274 | 0.000 | 2.293 | | 0.263 | 21.445 | 3.508 | 0.415 | 0.108 | 0.034 | 8.276 | 95.023 |
| Biotite 2 | Margin | | 7.600 | 19.221 | 33.448 | 0.009 | 2.901 | | 0.300 | 19.290 | 3.587 | 0.435 | 0.130 | 0.017 | 9.780 | 96.530 |
| Biotite 3 | Margin | | 8.225 | 19.492 | 33.187 | 0.000 | 1.910 | | 0.284 | 19.979 | 3.525 | 0.498 | 0.204 | 0.101 | 9.123 | 96.295 |
| Biotite 8 | Margin | | 7.551 | 19.054 | 33.119 | 0.029 | 3.137 | | 0.205 | 19.398 | 3.529 | 0.470 | 0.118 | 0.101 | 9.649 | 96.139 |
| Biotite 10 | Core | | 7.797 | 19.793 | 34.383 | 0.005 | 2.448 | | 0.342 | 19.657 | 3.642 | 0.487 | 0.113 | 0.000 | 9.721 | 98.387 |
| Biotite 10 | Core | | 7.924 | 19.744 | 33.824 | 0.003 | 2.254 | | 0.443 | 20.117 | 3.703 | 0.267 | 0.168 | 0.067 | 9.389 | 97.775 |
| Biotite 10 | Core | | 7.907 | 19.418 | 33.791 | 0.000 | 2.323 | | 0.293 | 19.531 | 3.667 | 0.269 | 0.134 | 0.101 | 9.808 | 97.104 |
| Biotite 11 | Margin | | 8.150 | 19.402 | 33.460 | 0.009 | 2.163 | | 0.328 | 19.639 | 3.524 | 0.581 | 0.147 | 0.034 | 9.741 | 96.924 |
| Biotite 1A | Margin | -20 | 7.893 | 19.029 | 33.525 | 0.005 | 3.026 | | 0.323 | 20.849 | 3.508 | 0.704 | 0.178 | 0.014 | 9.700 | 98.754 |
| Garnet 1A | Margin | 0 | 1.900 | 20.606 | 35.232 | 1.010 | 0.024 | 0.006 | 12.274 | 27.309 | 0.000 | | | | | 98.361 |
| Garnet 1A | Traverse | 61 | 2.205 | 20.510 | 35.823 | 1.075 | 0.023 | 0.004 | 10.831 | 27.924 | 0.094 | | | | | 98.489 |
| Garnet 1A | Traverse | 117 | 2.300 | 20.431 | 35.869 | 1.270 | 0.035 | 0.021 | 10.380 | 27.837 | 0.161 | | | | | 98.304 |
| Garnet 1A | Traverse | 175 | 2.251 | 20.330 | 34.943 | 1.827 | 0.028 | 0.000 | 9.984 | 27.651 | 0.000 | | | | | 97.014 |
| Garnet 1A | Traverse | 233 | 2.231 | 20.419 | 35.123 | 2.343 | 0.006 | 0.010 | 9.713 | 27.158 | 0.000 | | | | | 97.003 |
| Garnet 1A | Traverse | 284 | 2.231 | 20.431 | 35.754 | 2.945 | 0.029 | 0.000 | 9.388 | 26.724 | 0.102 | | | | | 97.604 |
| Garnet 1A | Traverse | 342 | 2.168 | 20.593 | 35.305 | 3.236 | 0.015 | 0.010 | 9.075 | 27.058 | 0.000 | | | | | 97.460 |
| Garnet 1A | Traverse | 395 | 2.241 | 20.260 | 34.883 | 3.001 | 0.082 | 0.046 | 8.991 | 26.703 | 0.000 | | | | | 96.207 |
| Garnet 1A | Traverse | 450 | 2.238 | 20.350 | 35.407 | 3.129 | 0.152 | 0.006 | 8.982 | 26.662 | 0.000 | | | | | 96.926 |
| Garnet 1A | Traverse | 508 | 2.254 | 20.629 | 35.047 | 3.232 | 0.072 | 0.044 | 8.866 | 26.828 | 0.000 | | | | | 96.972 |
| Garnet 1A | Traverse | 573 | 2.358 | 20.476 | 35.520 | 2.523 | 0.028 | 0.033 | 9.102 | 27.598 | 0.000 | | | | | 97.638 |
| Garnet 1A | Traverse | 627 | 2.430 | 20.423 | 35.461 | 2.023 | 0.009 | 0.035 | 9.229 | 27.998 | 0.074 | | | | | 97.682 |
| Garnet 1A | Traverse | 685 | 2.497 | 20.490 | 35.313 | 2.102 | 0.076 | 0.021 | 8.965 | 28.134 | 0.000 | | | | | 97.598 |
| Garnet 1A | Traverse | 744 | 2.448 | 20.445 | 35.510 | 2.431 | 0.000 | 0.041 | 9.179 | 27.724 | 0.150 | | | | | 97.928 |
| Garnet 1A | Traverse | 804 | 2.430 | 20.384 | 35.191 | 2.549 | 0.243 | 0.023 | 8.798 | 28.372 | 0.021 | | | | | 98.011 |

**Appendix 3.3 cont.**

| Mineral | Location | Traverse dist. (μm) | MgO (wt.%) | Al2O3 (wt.%) | SiO2 (wt.%) | CaO (wt.%) | TiO2 (wt.%) | Cr2O3 (wt.%) | MnO (wt.%) | FeO (wt.%) | H2O (wt.%) | F (wt.%) | Na2O (wt.%) | Cl (wt.%) | K2O (wt.%) | Total (wt.%) |
|---|---|---|---|---|---|---|---|---|---|---|---|---|---|---|---|---|
| Garnet 1A | Traverse | 858 | 2.373 | 20.450 | 35.388 | 2.821 | 0.035 | 0.021 | 8.908 | 27.736 | 0.113 | | | | | 97.845 |
| Garnet 1A | Traverse | 917 | 2.377 | 20.522 | 35.781 | 3.000 | 0.124 | 0.001 | 8.672 | 27.811 | 0.133 | | | | | 98.421 |
| Garnet 1A | Traverse | 982 | 2.417 | 20.499 | 35.602 | 3.401 | 0.008 | 0.007 | 8.565 | 27.492 | 0.256 | | | | | 98.247 |
| Garnet 1A | Traverse | 1037 | 2.325 | 20.525 | 35.987 | 3.759 | 0.036 | 0.014 | 8.504 | 27.343 | 0.382 | | | | | 98.875 |
| Garnet 1A | Traverse | 1093 | 2.338 | 20.497 | 35.841 | 3.752 | 0.035 | 0.021 | 8.349 | 27.454 | 0.345 | | | | | 98.632 |
| Garnet 1A | Traverse | 1155 | 2.349 | 20.455 | 35.457 | 3.544 | 0.019 | 0.026 | 8.303 | 27.739 | 0.248 | | | | | 98.140 |
| Garnet 1A | Traverse | 1206 | 2.355 | 20.425 | 35.641 | 2.321 | 0.064 | 0.031 | 8.754 | 28.427 | 0.173 | | | | | 98.191 |
| Garnet 1A | Traverse | 1327 | 2.366 | 20.619 | 35.684 | 1.429 | 0.038 | 0.013 | 9.495 | 28.562 | 0.000 | | | | | 98.206 |
| Garnet 1A | Traverse | 1385 | 2.159 | 20.346 | 35.898 | 1.366 | 0.077 | 0.044 | 10.395 | 28.184 | 0.326 | | | | | 98.795 |
| Garnet 1A | Margin | 1423 | 1.952 | 20.688 | 35.269 | 1.030 | 0.014 | 0.023 | 11.934 | 27.670 | 0.000 | | | | | 98.580 |
| Biotite 1A | Margin | 1443 | 8.004 | 21.012 | 33.678 | 0.003 | 1.879 | | 0.304 | 19.673 | 3.556 | 0.615 | 0.122 | 0.038 | 8.507 | 97.391 |
| Biotite 1B | Margin | -20 | 8.445 | 19.811 | 33.811 | 0.000 | 2.457 | | 0.303 | 19.925 | 3.596 | 0.557 | 0.150 | 0.046 | 9.469 | 98.570 |
| Garnet 1B | Traverse | 0 | 1.882 | 20.599 | 35.256 | 1.136 | 0.015 | 0.000 | 12.237 | 27.207 | 0.000 | | | | | 98.332 |
| Garnet 1B | Traverse | 94 | 2.256 | 20.481 | 35.438 | 1.591 | 0.008 | 0.015 | 9.939 | 28.387 | 0.087 | | | | | 98.202 |
| Garnet 1B | Traverse | 177 | 2.400 | 20.546 | 35.837 | 1.703 | 0.099 | 0.000 | 9.137 | 28.888 | 0.118 | | | | | 98.728 |
| Garnet 1B | Traverse | 248 | 2.464 | 20.522 | 35.602 | 1.921 | 0.076 | 0.000 | 8.494 | 29.113 | 0.063 | | | | | 98.255 |
| Garnet 1B | Traverse | 332 | 2.535 | 20.500 | 35.824 | 2.098 | 0.036 | 0.012 | 8.259 | 29.156 | 0.283 | | | | | 98.703 |
| Garnet 1B | Traverse | 405 | 2.574 | 20.436 | 35.982 | 1.948 | 0.011 | 0.000 | 8.048 | 29.174 | 0.371 | | | | | 98.544 |
| Garnet 1B | Traverse | 495 | 2.567 | 20.363 | 35.729 | 1.574 | 0.024 | 0.006 | 8.637 | 29.088 | 0.361 | | | | | 98.349 |
| Garnet 1B | Traverse | 575 | 2.580 | 20.537 | 35.736 | 1.487 | 0.034 | 0.015 | 8.459 | 29.267 | 0.041 | | | | | 98.156 |
| Garnet 1B | Traverse | 700 | 2.613 | 20.472 | 35.595 | 1.725 | 0.037 | 0.008 | 8.600 | 29.115 | 0.215 | | | | | 98.380 |
| Garnet 1B | Traverse | 789 | 2.572 | 20.307 | 35.531 | 1.800 | 0.025 | 0.001 | 8.429 | 29.076 | 0.395 | | | | | 98.136 |
| Garnet 1B | Traverse | 864 | 2.561 | 20.545 | 35.474 | 1.832 | 0.021 | 0.011 | 8.610 | 29.270 | 0.138 | | | | | 98.462 |
| Garnet 1B | Traverse | 987 | 2.487 | 20.473 | 35.491 | 2.514 | 0.007 | 0.011 | 8.369 | 28.617 | 0.214 | | | | | 98.183 |
| Garnet 1B | Traverse | 1067 | 2.392 | 20.617 | 35.658 | 3.544 | 0.098 | 0.000 | 8.168 | 28.006 | 0.108 | | | | | 98.591 |
| Garnet 1B | Traverse | 1141 | 2.238 | 20.555 | 35.597 | 4.057 | 0.071 | 0.015 | 8.154 | 27.445 | 0.117 | | | | | 98.249 |
| Garnet 1B | Traverse | 1215 | 2.435 | 20.619 | 35.611 | 2.901 | 0.037 | 0.023 | 8.313 | 28.289 | 0.003 | | | | | 98.231 |

**Appendix 3.3 cont.**

| Mineral | Location | Traverse dist. (μm) | MgO (wt.%) | Al2O3 (wt.%) | SiO2 (wt.%) | CaO (wt.%) | TiO2 (wt.%) | Cr2O3 (wt.%) | MnO (wt.%) | FeO (wt.%) | H2O (wt.%) | F (wt.%) | Na2O (wt.%) | Cl (wt.%) | K2O (wt.%) | Total (wt.%) |
|---|---|---|---|---|---|---|---|---|---|---|---|---|---|---|---|---|
| Garnet 1B | Traverse | 1315 | 2.500 | 20.537 | 35.652 | 2.490 | 0.046 | 0.000 | 8.639 | 28.105 | 0.067 | | | | | 98.036 |
| Garnet 1B | Traverse | 1375 | 2.276 | 20.511 | 35.646 | 3.305 | 0.834 | 0.055 | 8.339 | 27.999 | 0.000 | | | | | 98.965 |
| Garnet 1B | Traverse | 1449 | 2.329 | 20.500 | 35.768 | 3.769 | 0.063 | 0.000 | 8.499 | 27.353 | 0.321 | | | | | 98.602 |
| Garnet 1B | Traverse | 1537 | 2.331 | 20.600 | 35.653 | 3.781 | 0.036 | 0.038 | 8.392 | 27.521 | 0.131 | | | | | 98.483 |
| Garnet 1B | Traverse | 1607 | 2.304 | 20.548 | 36.075 | 3.568 | 0.059 | 0.009 | 8.355 | 27.698 | 0.340 | | | | | 98.956 |
| Garnet 1B | Traverse | 1681 | 2.764 | 20.150 | 34.089 | 2.621 | 0.037 | 0.000 | 7.632 | 27.556 | 0.000 | | | | | 94.849 |
| Garnet 1B | Traverse | 1757 | 2.467 | 20.585 | 35.988 | 2.473 | 0.034 | 0.015 | 8.584 | 28.508 | 0.235 | | | | | 98.889 |
| Garnet 1B | Traverse | 1830 | 2.451 | 20.484 | 35.721 | 2.336 | 0.010 | 0.000 | 8.490 | 28.591 | 0.235 | | | | | 98.318 |
| Garnet 1B | Traverse | 1908 | 2.401 | 20.612 | 35.597 | 2.338 | 0.045 | 0.000 | 8.464 | 28.900 | 0.017 | | | | | 98.374 |
| Garnet 1B | Traverse | 1992 | 2.452 | 20.559 | 36.172 | 2.223 | 0.023 | 0.012 | 8.739 | 28.477 | 0.289 | | | | | 98.946 |
| Garnet 1B | Traverse | 2086 | 2.445 | 20.605 | 36.083 | 1.803 | 0.020 | 0.000 | 9.068 | 28.825 | 0.242 | | | | | 99.091 |
| Garnet 1B | Traverse | 2168 | 2.227 | 20.500 | 35.815 | 1.746 | 0.033 | 0.000 | 10.104 | 28.382 | 0.328 | | | | | 99.135 |
| Biotite 1B | Margin | 2188 | 8.038 | 19.296 | 34.390 | 0.018 | 3.156 | | 0.299 | 20.061 | 3.642 | 0.529 | 0.130 | 0.032 | 9.903 | 99.494 |
| Biotite 2 | Margin | -20 | 9.689 | 19.970 | 34.665 | 0.026 | 1.647 | | 0.388 | 18.783 | 3.614 | 0.651 | 0.200 | 0.020 | 9.847 | 99.500 |
| Garnet 2 | Margin | 20 | 1.845 | 20.449 | 35.869 | 0.912 | 0.000 | 0.020 | 12.814 | 27.011 | 0.305 | | | | | 99.225 |
| Biotite 3 | Margin | -20 | 8.517 | 19.855 | 34.489 | 0.000 | 1.917 | | 0.384 | 20.227 | 3.601 | 0.633 | 0.166 | 0.000 | 9.481 | 99.270 |
| Biotite 4 | Margin | -20 | 8.380 | 19.905 | 34.055 | 0.000 | 2.643 | | 0.278 | 19.683 | 3.660 | 0.476 | 0.197 | 0.036 | 9.809 | 99.122 |
| Garnet 4 | Margin | 20 | 2.120 | 20.479 | 35.644 | 1.347 | 0.048 | 0.012 | 11.026 | 27.784 | 0.123 | | | | | 98.583 |
| Garnet 4 | Margin | 20 | 2.061 | 20.449 | 35.371 | 1.343 | 0.028 | 0.004 | 10.999 | 28.252 | 0.200 | | | | | 98.707 |
| Garnet 4 | Traverse | 20 | 1.942 | 20.206 | 35.934 | 1.125 | 0.000 | 0.015 | 11.512 | 27.168 | 0.455 | | | | | 98.357 |
| Garnet 4 | Traverse | 53 | 2.101 | 20.383 | 36.093 | 1.204 | 0.024 | 0.031 | 10.629 | 27.599 | 0.178 | | | | | 98.242 |
| Garnet 4 | Traverse | 154 | 2.227 | 20.342 | 35.931 | 1.743 | 0.022 | 0.002 | 10.003 | 28.110 | 0.497 | | | | | 98.877 |
| Garnet 4 | Traverse | 204 | 2.132 | 20.485 | 35.964 | 2.085 | 0.043 | 0.027 | 9.709 | 28.260 | 0.285 | | | | | 98.990 |
| Garnet 4 | Traverse | 298 | 1.765 | 20.427 | 36.242 | 3.147 | 0.000 | 0.000 | 9.853 | 27.271 | 0.519 | | | | | 99.224 |
| Garnet 4 | Traverse | 342 | 1.457 | 20.329 | 36.108 | 3.895 | 0.082 | 0.000 | 9.927 | 26.303 | 0.353 | | | | | 98.454 |

**Appendix 3.3 cont.**

| Mineral | Location | Traverse dist. (μm) | MgO (wt.%) | Al2O3 (wt.%) | SiO2 (wt.%) | CaO (wt.%) | TiO2 (wt.%) | Cr2O3 (wt.%) | MnO (wt.%) | FeO (wt.%) | H2O (wt.%) | F (wt.%) | Na2O (wt.%) | Cl (wt.%) | K2O (wt.%) | Total (wt.%) |
|---|---|---|---|---|---|---|---|---|---|---|---|---|---|---|---|---|
| Garnet 4 | Traverse | 392 | 1.166 | 20.241 | 35.737 | 4.537 | 0.353 | 0.026 | 9.991 | 26.224 | 0.135 | | | | | 98.410 |
| Garnet 4 | Traverse | 453 | 1.125 | 20.267 | 36.040 | 4.543 | 0.045 | 0.014 | 10.380 | 25.988 | 0.584 | | | | | 98.986 |
| Garnet 4 | Traverse | 525 | 1.138 | 20.292 | 35.912 | 4.491 | 0.092 | 0.000 | 10.572 | 25.909 | 0.481 | | | | | 98.887 |
| Garnet 4 | Traverse | 580 | 1.158 | 20.425 | 36.112 | 4.418 | 0.032 | 0.007 | 10.620 | 26.135 | 0.494 | | | | | 99.401 |
| Garnet 4 | Traverse | 650 | 1.211 | 20.429 | 35.967 | 4.278 | 0.127 | 0.032 | 10.380 | 26.245 | 0.221 | | | | | 98.890 |
| Garnet 4 | Traverse | 691 | 1.202 | 20.311 | 36.040 | 4.251 | 0.043 | 0.075 | 10.237 | 26.234 | 0.401 | | | | | 98.794 |
| Garnet 4 | Traverse | 741 | 1.235 | 20.301 | 36.057 | 4.118 | 0.079 | 0.012 | 10.491 | 25.973 | 0.414 | | | | | 98.680 |
| Garnet 4 | Traverse | 792 | 1.283 | 20.234 | 36.022 | 3.926 | 0.040 | 0.005 | 10.186 | 26.013 | 0.389 | | | | | 98.098 |
| Garnet 4 | Traverse | 843 | 1.279 | 19.913 | 35.326 | 3.864 | 0.965 | 0.025 | 9.854 | 26.951 | 0.000 | | | | | 98.177 |
| Garnet 4 | Margin | 886 | 1.216 | 20.079 | 35.894 | 4.224 | 0.030 | 0.000 | 10.104 | 25.667 | 0.529 | | | | | 97.743 |
| Biotite 4 | Margin | 906 | 7.871 | 19.731 | 34.319 | 0.000 | 2.641 | | 0.275 | 19.570 | 3.599 | 0.561 | 0.132 | 0.033 | 9.647 | 98.379 |
| Biotite 4 | Margin | 906 | 7.958 | 19.629 | 34.056 | 0.000 | 2.514 | | 0.353 | 19.678 | 3.663 | 0.403 | 0.150 | 0.017 | 9.759 | 98.180 |
| Biotite 5 | Margin | -20 | 8.353 | 19.751 | 33.953 | 0.001 | 2.169 | | 0.263 | 20.585 | 3.559 | 0.621 | 0.130 | 0.067 | 9.264 | 98.716 |
| Garnet 5 | Margin | 20 | 1.878 | 20.193 | 35.589 | 1.512 | 0.446 | 0.000 | 11.567 | 27.234 | 0.079 | | | | | 98.498 |
| Garnet 6 | Margin | 20 | 2.099 | 20.580 | 36.042 | 1.293 | 0.000 | 0.030 | 10.826 | 27.989 | 0.131 | | | | | 98.990 |
| Garnet 6 | Margin | 20 | 2.122 | 20.615 | 35.883 | 1.151 | 0.004 | 0.000 | 11.078 | 27.968 | 0.067 | | | | | 98.888 |
| Garnet 6 | Margin | 20 | 1.725 | 20.584 | 35.719 | 1.045 | 0.011 | 0.034 | 11.909 | 27.380 | 0.000 | | | | | 98.407 |
| Plagioclase 1 | | | | 24.860 | 59.160 | 5.920 | | | | | | | 7.590 | | 0.490 | 98.020 |
| lagioclase 2 | | | | 25.690 | 58.320 | 6.870 | | | | | | | 7.380 | | 0.210 | 98.470 |
| Plagioclase 2 | | | | 25.370 | 59.340 | 6.430 | | | | | | | 7.440 | | 0.210 | 98.790 |
| Plagioclase 3 | | | | 24.830 | 59.840 | 5.880 | | | | | | | 7.800 | | 0.310 | 98.660 |
| Plagioclase 3 | | | | 25.360 | 59.300 | 6.460 | | | | | | | 7.540 | | 0.250 | 98.910 |
| Plagioclase 4 | | | | 25.340 | 58.700 | 6.680 | | | | | | | 7.410 | | 0.190 | 98.320 |
| Plagioclase 4 | | | | 25.240 | 58.850 | 6.020 | | | | | | | 7.460 | | 0.530 | 98.100 |
| Plagioclase 4 | | | | 25.190 | 59.260 | 6.330 | | | | | | | 7.660 | | 0.280 | 98.720 |

**Appendix 3.3 cont.**

| Mineral | Location | Traverse dist. (μm) | MgO (wt.%) | Al2O3 (wt.%) | SiO2 (wt.%) | CaO (wt.%) | TiO2 (wt.%) | Cr2O3 (wt.%) | MnO (wt.%) | FeO (wt.%) | H2O (wt.%) | F (wt.%) | Na2O (wt.%) | Cl (wt.%) | K2O (wt.%) | Total (wt.%) |
|---|---|---|---|---|---|---|---|---|---|---|---|---|---|---|---|---|
| K-feldspar 1 | Margin | | | 18.990 | 62.620 | 0.020 | | | | | | | 1.460 | | 14.620 | 97.710 |
| K-feldspar 1 | Core | | | 18.900 | 63.340 | 0.060 | | | | | | | 1.590 | | 14.290 | 98.180 |
| K-feldspar 1 | Core | | | 18.980 | 63.220 | 0.060 | | | | | | | 1.580 | | 14.200 | 98.040 |
| K-feldspar 1 | Margin | | | 19.030 | 62.740 | 0.000 | | | | | | | 0.960 | | 15.240 | 97.970 |
| K-feldspar 2 | Margin | | | 18.870 | 63.090 | 0.000 | | | | | | | 1.250 | | 14.970 | 98.180 |
| K-feldspar 2 | Core | | | 19.100 | 63.090 | 0.050 | | | | | | | 1.100 | | 15.240 | 98.580 |
| K-feldspar 3 | Core | | | 19.150 | 63.330 | 0.010 | | | | | | | 0.990 | | 15.250 | 98.730 |
| K-feldspar 4 | Core | | | 19.080 | 62.830 | 0.020 | | | | | | | 1.350 | | 14.910 | 98.190 |
| K-feldspar 4 | Margin | | | 18.860 | 62.240 | 0.020 | | | | | | | 1.070 | | 15.060 | 97.250 |
| Muscovite 1 | | | 0.480 | 36.320 | 43.860 | 0.000 | 0.600 | | 0.000 | 1.160 | 4.382 | 0.070 | 0.510 | 0.000 | 10.860 | 98.242 |
| Muscovite 1 | | | 0.440 | 36.260 | 44.040 | 0.000 | 0.570 | | 0.040 | 1.010 | 4.376 | 0.070 | 0.510 | 0.040 | 10.980 | 98.336 |
| Muscovite 1 | | | 0.650 | 36.110 | 43.140 | 0.000 | 0.680 | | 0.030 | 1.250 | 4.362 | 0.000 | 0.550 | 0.050 | 10.640 | 97.462 |
| Muscovite 1 | | | 0.480 | 36.320 | 44.510 | 0.000 | 0.670 | | 0.020 | 0.980 | 4.412 | 0.080 | 0.530 | 0.000 | 10.890 | 98.892 |
| Muscovite 1 | | | 0.970 | 35.400 | 44.060 | 0.000 | 0.430 | | 0.000 | 2.130 | 4.393 | 0.000 | 0.460 | 0.050 | 10.370 | 98.263 |
| Muscovite 1 | | | 0.610 | 35.140 | 43.860 | 0.010 | 0.860 | | 0.000 | 1.210 | 4.355 | 0.030 | 0.490 | 0.020 | 10.770 | 97.355 |
| Muscovite 1 | | | 0.510 | 35.620 | 44.780 | 0.000 | 0.760 | | 0.000 | 1.070 | 4.418 | 0.040 | 0.510 | 0.000 | 10.940 | 98.648 |
| Muscovite 2 | | | 0.550 | 35.250 | 44.010 | 0.000 | 0.820 | | 0.040 | 1.010 | 4.326 | 0.090 | 0.490 | 0.040 | 10.850 | 97.476 |
| Muscovite 2 | | | 0.550 | 35.490 | 43.400 | 0.000 | 0.850 | | 0.040 | 0.870 | 4.292 | 0.140 | 0.470 | 0.000 | 10.910 | 97.012 |
| Muscovite 2 | | | 0.510 | 35.530 | 44.180 | 0.000 | 0.890 | | 0.000 | 1.000 | 4.290 | 0.240 | 0.540 | 0.000 | 10.950 | 98.130 |
| Muscovite 2 | | | 0.530 | 35.430 | 43.560 | 0.020 | 0.820 | | 0.000 | 0.900 | 4.342 | 0.030 | 0.460 | 0.000 | 10.590 | 96.682 |
| Muscovite 2 | | | 0.520 | 35.800 | 42.990 | 0.020 | 0.560 | | 0.000 | 1.280 | 4.268 | 0.160 | 0.480 | 0.000 | 10.900 | 96.978 |
| Muscovite 3 | | | 0.540 | 35.400 | 43.810 | 0.000 | 0.710 | | 0.000 | 0.960 | 4.295 | 0.150 | 0.450 | 0.000 | 10.730 | 97.045 |
| Muscovite 3 | | | 0.590 | 35.470 | 43.680 | 0.000 | 0.530 | | 0.000 | 1.220 | 4.253 | 0.240 | 0.510 | 0.000 | 10.940 | 97.433 |
| Muscovite 4 | | | 0.540 | 35.390 | 43.030 | 0.000 | 0.660 | | 0.000 | 1.050 | 4.316 | 0.000 | 0.540 | 0.040 | 10.740 | 96.306 |
| Muscovite 4 | | | 0.510 | 35.380 | 43.630 | 0.000 | 0.790 | | 0.000 | 0.910 | 4.348 | 0.000 | 0.500 | 0.050 | 10.960 | 97.078 |
| Muscovite 4 | | | 0.600 | 35.220 | 44.090 | 0.000 | 0.890 | | 0.000 | 1.120 | 4.356 | 0.050 | 0.500 | 0.040 | 10.950 | 97.816 |
| Sillimanite 1 | | | 0.110 | 61.050 | 36.140 | | 0.030 | | | 0.550 | | | | | 0.100 | 97.980 |
| Sillimanite 2 | | | 0.400 | 58.420 | 36.210 | | 0.050 | | | 1.610 | | | | | 0.550 | 97.240 |

**Appendix 3. 4**

Granite dyke compositions for granite dykes from the Menninnie Dam prospect determined by XRF analysis, and representative compositions for Lincoln Complex Granites, St. Peters Suite Granites and Hiltaba Suite Granites. Total iron expressed as Fe2O3 unless otherwise indicated; n/a = not analysed.

References;1, Parker (1993a), 2, Flint (1993b), 3, this study.

| | 1 | 2 | 3 | 4 | 5 | 6 | 7 | 8 | 9 | 10 | 11 |
|---|---|---|---|---|---|---|---|---|---|---|---|
| SiO2 (wt.%) | 56.24 | 67.66 | 67.29 | 70.76 | 66.64 | 76.67 | 65.33 | 73.24 | 71.10 | 74.03 | 72.68 |
| TiO2 (wt.%) | 0.82 | 0.68 | 0.66 | 0.41 | 0.56 | 0.22 | 1.00 | 0.13 | 0.44 | 0.08 | 0.20 |
| Al2O3 (wt.%) | 14.53 | 14.78 | 15.12 | 14.37 | 15.30 | 11.96 | 14.87 | 14.63 | 14.17 | 14.39 | 8.03 |
| Fe2O3 (wt.%) | 9.90 | 4.72 | 4.47 | 3.67 | 3.35 | 1.49 | 6.01 | 1.19 | 3.53 | 1.35 | 0.78 |
| FeO (wt.%) | n/a | n/a | n/a | n/a | n/a | n/a | n/a | n/a | n/a | n/a | 1.14 |
| MnO (wt.%) | 0.15 | 0.06 | 0.05 | 0.06 | 0.04 | 0.01 | 0.07 | 0.01 | 0.06 | 0.07 | 0.03 |
| MgO (wt.%) | 5.80 | 1.01 | 0.94 | 1.42 | 1.40 | 0.11 | 1.27 | 0.27 | 0.50 | 0.32 | 0.24 |
| CaO (wt.%) | 6.72 | 2.79 | 2.80 | 1.95 | 2.33 | 0.59 | 3.22 | 0.76 | 1.47 | 0.59 | 0.74 |
| Na2O (wt.%) | 2.40 | 2.83 | 2.80 | 2.75 | 4.43 | 2.28 | 2.70 | 4.05 | 3.05 | 3.86 | 3.42 |
| K2O (wt.%) | 2.40 | 5.17 | 5.44 | 4.88 | 4.10 | 6.51 | 5.43 | 4.57 | 5.23 | 4.45 | 5.35 |
| P2O5 (wt.%) | 0.21 | 0.16 | 0.16 | 0.12 | 0.18 | 0.02 | 0.29 | 0.13 | 0.25 | 0.29 | 0.19 |
| H2O+ (wt.%) | n/a | n/a | n/a | n/a | n/a | n/a | n/a | n/a | 0.52 | 0.61 | 0.10 |
| H2O- (wt.%) | n/a | n/a | n/a | n/a | n/a | n/a | n/a | n/a | n/a | n/a | 0.62 |
| CO2 (wt.%) | n/a | n/a | n/a | n/a | n/a | n/a | n/a | n/a | n/a | n/a | n/a |
| LOI (wt.%) | n/a | n/a | n/a | 0.47 | 0.73 | n/a | n/a | 0.60 | n/a | 0.97 | 0.96 |
| Total (wt.%) | 99.17 | 99.86 | 99.73 | 100.86 | 99.06 | 99.86 | 100.19 | 99.58 | 100.32 | 101.01 | 94.48 |
| Ba (ppm) | 554 | 1015 | 1128 | 989 | 796 | 574 | 1113 | 319 | n/a | 355 | 210 |
| Ce (ppm) | n/a | n/a | n/a | n/a | 225 | n/a | n/a | 46 | n/a | 63 | 95 |
| Co (ppm) | n/a | n/a | n/a | 129 | 86 | n/a | n/a | 96 | n/a | 35 | 80 |
| Cr (ppm) | n/a | 13 | 14 | 65 | 48 | n/a | 8 | 19 | n/a | 5 | 20 |
| Cu (ppm) | n/a | n/a | n/a | 65 | 145 | n/a | n/a | 49 | n/a | 30 | 200 |
| La (ppm) | n/a | n/a | n/a | 53 | 160 | n/a | n/a | 20 | n/a | 50 | 60 |
| Li (ppm) | n/a | n/a | n/a | n/a | n/a | n/a | n/a | n/a | n/a | n/a | n/a |
| Nb (ppm) | 12 | 15 | 14 | 94 | 14 | 10 | 20 | 12 | n/a | 24 | 26 |
| Ni (ppm) | 106 | 20 | 19 | 7 | 34 | n/a | n/a | 14 | n/a | 13 | 40 |
| Pb (ppm) | n/a | n/a | n/a | 48 | 59 | n/a | n/a | 50 | n/a | 25 | 170 |
| Rb (ppm) | 105 | 208 | 179 | 51 | n/a | 284 | 210 | n/a | n/a | 270 | 420 |
| Sc (ppm) | n/a | n/a | n/a | n/a | n/a | n/a | n/a | n/a | n/a | n/a | n/a |
| Sr (ppm) | 226 | 155 | 165 | 136 | 332 | 46 | 172 | 94 | n/a | 28 | 50 |
| Th (ppm) | n/a | n/a | n/a | 166 | 53 | n/a | n/a | 14 | n/a | 13 | 36 |
| U (ppm) | n/a | n/a | n/a | 32 | 10 | n/a | n/a | 9 | n/a | 6 | 8 |
| V (ppm) | 160 | 45 | 53 | 5 | 74 | n/a | n/a | 34 | n/a | 10 | 20 |
| W (ppm) | n/a | n/a | n/a | 50 | 432 | n/a | n/a | 630 | n/a | n/a | 10 |
| Y (ppm) | 32 | 44 | 38 | 32 | 7 | 22 | 48 | 5 | n/a | 35 | 34 |
| Zn (ppm) | n/a | n/a | n/a | 75 | 54 | n/a | n/a | 34 | n/a | 28 | 80 |
| Zr (ppm) | 229 | 307 | 310 | 193 | 309 | 211 | 362 | 97 | n/a | 200 | 170 |
| Analyses | 3 | 7 | 3 | 8 | 5 | 3 | 3 | 7 | 5 | 9 | 2 |
| Reference | 1 | 1 | 1 | 1 | 1 | 1 | 1 | 1 | 1 | 1 | 1 |

| | | |
|---|---|---|
| 1 | Lincoln Complex | Quartz gabbronorite (Donnington Suite) |
| 2 | Lincoln Complex | Memory Cove Charnock(Donnington Suite) |
| 3 | Lincoln Complex | Megacrystic Granite(Donnington Suite) |
| 4 | Lincoln Complex | Minbrie Gneiss, Elbow Hill (Donnington Suite equiv.) |
| 5 | Lincoln Complex | Middle Camp Granite (Colbert Suite equivalent) |
| 6 | Lincoln Complex | Alkali Feldspar Granite (Colbert Suite) |
| 7 | Lincoln Complex | Hornblende Granite (Colbert Suite) |
| 8 | Lincoln Complex | Carpa Granite (Moody Suite) |
| 9 | Lincoln Complex | Granite Moody Tank (Moody Suite) |
| 10 | Lincoln Complex | Yunta Well Leucogranite, (Moody Suite) |
| 11 | Lincoln Complex | Carappee Granite (Moody Suite) |

**Appendix 3. 4 cont.**

| | 12 | 13 | 14 | 15 | 16 | 17 | 18 | 19 | 20 | 21 | 22 |
|---|---|---|---|---|---|---|---|---|---|---|---|
| SiO2 (wt.%) | 64.78 | 71.45 | 61.7 | 59.75 | 60.85 | 63.85 | 67.22 | 69.03 | 70.41 | 71.57 | 72.93 |
| TiO2 (wt.%) | 0.36 | 0.34 | 0.68 | 0.97 | 1.05 | 0.61 | 0.74 | 0.47 | 0.32 | 0.29 | 0.34 |
| Al2O3 (wt.%) | 16.02 | 13.45 | 17.53 | 14.93 | 16.13 | 16.9 | 13.53 | 13.19 | 13.89 | 13.41 | 12.87 |
| Fe2O3 (wt.%) | 4.09 | 2.29 | 5.86 | 4.12 | 3.07 | 4.37 | 2.77 | 4.53 | 1.58 | 1.26 | 2 |
| FeO (wt.%) | n/a | 1.07 | n/a | 2.73 | 2.84 | n/a | 1.99 | n/a | 1.2 | 1.16 | 1.5 |
| MnO (wt.%) | 0.09 | 0.07 | 0.19 | 0.07 | 0.1 | 0.05 | 0.02 | 0.05 | 0.02 | 0.04 | 0.06 |
| MgO (wt.%) | 1.07 | 0.83 | 1.84 | 3.2 | 1.66 | 1.37 | 1.23 | 0.7 | 0.74 | 0.54 | 0.38 |
| CaO (wt.%) | 2.29 | 1.61 | 3.87 | 2.52 | 2.76 | 1.73 | 1.11 | 0.84 | 0.58 | 0.78 | 1.26 |
| Na2O (wt.%) | 4.51 | 3.88 | 5.03 | 4.08 | 4.33 | 5.2 | 3.45 | 2.58 | 3.66 | 2.91 | 3.14 |
| K2O (wt.%) | 5.86 | 4.13 | 2.36 | 3.97 | 4.3 | 4.94 | 4.99 | 5.53 | 5.24 | 6.06 | 5.21 |
| P2O5 (wt.%) | 0.21 | 0.08 | 0.3 | 0.27 | 0.27 | 0.2 | 0.2 | 0.13 | 0.09 | 0.07 | 0.09 |
| H2O+ (wt.%) | n/a | n/a | n/a | 1.61 | 1.43 | n/a | 1.02 | n/a | 1.43 | 0.94 | 0.24 |
| H2O- (wt.%) | n/a | n/a | n/a | 0.4 | 0.36 | n/a | 0.41 | n/a | 0.45 | 0.36 | 0.25 |
| CO2 (wt.%) | n/a | n/a | n/a | 0.91 | 0.4 | n/a | 0.5 | n/a | 0.35 | 0.35 | 0.03 |
| LOI (wt.%) | 0.68 | 0.99 | 0.65 | n/a | n/a | 0.94 | n/a | 1.55 | n/a | n/a | 0.65 |
| Total (wt.%) | 99.96 | 100.19 | 100.01 | 99.53 | 99.55 | 100.16 | 99.18 | 98.60 | 99.96 | 99.74 | 100.95 |
| Ba (ppm) | 1737 | 945 | 1115 | 968 | 1368 | 3275 | 955 | 915 | 787 | 691 | 626 |
| Ce (ppm) | 200 | 73 | 140 | 137 | 134 | 335 | 247 | 126 | 116 | 169 | 142 |
| Co (ppm) | 27 | 126 | n/a | n/a | n/a | 40 | n/a | 7 | n/a | n/a | 102 |
| Cr (ppm) | 13 | 14 | n/a | 46 | 21 | n/a | 6 | 23 | 3 | 2 | 25 |
| Cu (ppm) | 7 | 19 | n/a | n/a | n/a | n/a | n/a | n/a | n/a | n/a | n/a |
| La (ppm) | 85 | 43 | 76 | n/a | n/a | n/a | n/a | n/a | n/a | n/a | n/a |
| Li (ppm) | n/a | n/a | n/a | n/a | n/a | n/a | n/a | 17 | n/a | n/a | n/a |
| Nb (ppm) | 26 | 15 | 14 | 21 | 21 | 13 | 38 | 15 | 25 | 30 | 22 |
| Ni (ppm) | 10 | 11 | n/a | 34 | 12 | 30 | 5 | 6 | 7 | 3 | n/a |
| Pb (ppm) | 66 | 5 | n/a | n/a | n/a | n/a | n/a | n/a | n/a | n/a | n/a |
| Rb (ppm) | 280 | 179 | 145 | 144 | 151 | 100 | 217 | 160 | 177 | 253 | n/a |
| Sc (ppm) | n/a | n/a | n/a | n/a | n/a | n/a | n/a | n/a | n/a | n/a | n/a |
| Sr (ppm) | 591 | 281 | 566 | 243 | 237 | 1225 | 100 | 90 | 138 | 73 | 120 |
| Th (ppm) | 93 | 11 | n/a | 36 | 30 | 8 | 63 | 20 | 105 | 58 | 70 |
| U (ppm) | 30 | 3 | n/a | 9 | 7 | n/a | 13 | 5 | 19 | 49 | 12 |
| V (ppm) | 50 | 25 | 74 | n/a | n/a | n/a | n/a | n/a | n/a | n/a | n/a |
| W (ppm) | n/a | n/a | n/a | n/a | n/a | n/a | n/a | n/a | n/a | n/a | n/a |
| Y (ppm) | 18 | 31 | 33 | 39 | 47 | 70 | 76 | 33 | 33 | 53 | 20 |
| Zn (ppm) | 54 | 58 | n/a | n/a | n/a | n/a | n/a | n/a | n/a | n/a | n/a |
| Zr (ppm) | 261 | 190 | 296 | 443 | 517 | 410 | 443 | 193 | 284 | 258 | 192 |
| Analyses | 6 | 4 | 11 | 9 | 10 | 2 | 4 | 10 | 2 | 7 | 8 |
| Reference | 1 | 1 | 1 | 2 | 2 | 2 | 2 | 2 | 2 | 2 | 2 |

| | | |
|---|---|---|
| 12 | Lincoln Complex | Burkitt Granite (Moody Suite) |
| 13 | St. Peters Suite | St. Peters Suite, granite-adamellite |
| 14 | St. Peters Suite | St. Peters Suite, granodiorite dykes |
| 15 | Hiltaba Suite | mafic granite, Andamooka |
| 16 | Hiltaba Suite | mafic granite, Olympic Dam |
| 17 | Hiltaba Suite | mafic granite, Kingoonya |
| 18 | Hiltaba Suite | adamellite, Moonta |
| 19 | Hiltaba Suite | granite, Tarcoola |
| 20 | Hiltaba Suite | felsic granitoid, Andamooka |
| 21 | Hiltaba Suite | felsic granite, Olympic Dam |
| 22 | Hiltaba Suite | Charleston Granite |

**Appendix 3. 4 cont.**

| | 23 | 24 | 25 | 26 | 27 | 28 | 29 | 30 | 31 | 32 | 33 |
|---|---|---|---|---|---|---|---|---|---|---|---|
| SiO2 (wt.%) | 74.57 | 74.93 | 74.94 | 75.56 | 75.62 | 76.49 | 76.6 | 77.6 | 73.84 | 76.17 | 72.23 |
| TiO2 (wt.%) | 0.26 | 0.22 | 0.27 | 0.19 | 0.12 | 0.16 | 0.16 | 0.21 | 0.12 | 0.21 | 0.05 |
| Al2O3 (wt.%) | 13.25 | 13.63 | 12.9 | 12.45 | 12.32 | 11.8 | 12.4 | 10.7 | 14.4 | 13.64 | 13.65 |
| Fe2O3 (wt.%) | 0.66 | 1.37 | 0.69 | 0.94 | 0.78 | 1.21 | 0.44 | 1.29 | 0.9 | 0.72 | 1.14 |
| FeO (wt.%) | 0.72 | n/a | 0.58 | 0.81 | n/a | 0.54 | 0.74 | n/a | n/a | n/a | n/a |
| MnO (wt.%) | 0.07 | 0.01 | 0.05 | 0.03 | 0.05 | 0.03 | 0.02 | 0.02 | 0.09 | 0.05 | 0.07 |
| MgO (wt.%) | 0.22 | 0.24 | 0.2 | 0.16 | 0.06 | 0.13 | 0.15 | 0.29 | 0.44 | 0.52 | 0.46 |
| CaO (wt.%) | 0.82 | 0.77 | 0.56 | 0.64 | 0.51 | 0.46 | 0.57 | 0.11 | 0.86 | 0.55 | 1.27 |
| Na2O (wt.%) | 3.12 | 3.85 | 3.59 | 3.02 | 3.59 | 3.2 | 3.15 | 2.32 | 6.92 | 6.85 | 2.63 |
| K2O (wt.%) | 5.64 | 4.6 | 5.42 | 5.29 | 4.83 | 5.44 | 5.22 | 6.65 | 1.09 | 0.61 | 5.93 |
| P2O5 (wt.%) | 0.04 | 0.06 | 0.04 | 0.03 | 0.08 | 0.03 | 0.02 | 0.04 | 0.16 | 0.13 | 0.17 |
| H2O+ (wt.%) | 0.29 | n/a | 0.47 | 0.52 | n/a | 0.28 | 0.29 | n/a | n/a | n/a | n/a |
| H2O- (wt.%) | 0.05 | n/a | 0.02 | 0.11 | n/a | 0.46 | 0.15 | n/a | n/a | n/a | n/a |
| CO2 (wt.%) | n/a | n/a | n/a | n/a | n/a | 0.01 | 0.04 | n/a | n/a | n/a | n/a |
| LOI (wt.%) | n/a | 0.91 | 0.55 | 0.62 | 0.46 | 0.61 | n/a | 0.78 | 1.4 | 0.97 | 1.94 |
| Total (wt.%) | 99.71 | 100.59 | 100.28 | 100.37 | 98.42 | 100.85 | 99.95 | 100.01 | 100.2 | 100.4 | 99.55 |
| Ba (ppm) | 308 | 1420 | 354 | 416 | 56 | 221 | n/a | 380 | 156 | 47 | 205 |
| Ce (ppm) | n/a | 85 | n/a | n/a | 74 | 152 | n/a | 60 | n/a | n/a | n/a |
| Co (ppm) | n/a | 63 | n/a | n/a | n/a | n/a | n/a | 45 | n/a | n/a | n/a |
| Cr (ppm) | n/a | n/a | n/a | n/a | n/a | n/a | n/a | n/a | n/a | n/a | n/a |
| Cu (ppm) | n/a | n/a | n/a | n/a | n/a | n/a | n/a | n/a | 4 | 2 | 3 |
| La (ppm) | n/a | n/a | n/a | n/a | n/a | n/a | n/a | n/a | n/a | n/a | n/a |
| Li (ppm) | 19 | n/a | 20 | 20 | 52 | 19 | n/a | n/a | n/a | n/a | n/a |
| Nb (ppm) | n/a | 10 | n/a | n/a | 28 | 22 | n/a | 38 | 19 | 12 | 10 |
| Ni (ppm) | n/a | 33 | n/a | n/a | n/a | n/a | n/a | n/a | 8 | 11 | 6 |
| Pb (ppm) | n/a | n/a | n/a | n/a | n/a | n/a | n/a | n/a | 37 | 24 | 80 |
| Rb (ppm) | 244 | 137 | 286 | 291 | 315 | 324 | n/a | 550 | 80 | 46 | 278 |
| Sc (ppm) | n/a | n/a | n/a | n/a | n/a | n/a | n/a | n/a | 3 | 3 | 3 |
| Sr (ppm) | 86 | 540 | 77 | 63 | 23 | 34 | n/a | 30 | 36 | 21 | 33 |
| Th (ppm) | 45 | 17 | 27 | 43 | 34 | 41 | n/a | 120 | 27 | 17 | 9 |
| U (ppm) | 7 | n/a | 7 | 9 | 7 | 9 | n/a | 22 | 17 | 9 | 13 |
| V (ppm) | n/a | n/a | n/a | n/a | n/a | n/a | n/a | n/a | 9 | 11 | 5 |
| W (ppm) | n/a | n/a | n/a | n/a | n/a | n/a | n/a | n/a | n/a | n/a | n/a |
| Y (ppm) | n/a | 23 | n/a | n/a | 26 | 31 | n/a | 40 | 10 | 12 | 8 |
| Zn (ppm) | n/a | n/a | n/a | n/a | n/a | n/a | n/a | n/a | 24 | 23 | 28 |
| Zr (ppm) | 236 | 220 | 322 | 244 | 112 | 197 | n/a | 200 | 73 | 244 | 38 |
| Analyses | 15 | 3 | 5 | 17 | 8 | 7 | 2 | 1 | 1 | 1 | 1 |
| Reference | 2 | 2 | 2 | 2 | 2 | 2 | 2 | 2 | 3 | 3 | 3 |

| | | |
|---|---|---|
| 23 | Hiltaba Suite | granite, Minnipa |
| 24 | Hiltaba Suite | felsic granite, Kingoonya |
| 25 | Hiltaba Suite | Calca Granite |
| 26 | Hiltaba Suite | granite, Kokatha |
| 27 | Hiltaba Suite | granite, Kychering Rocks |
| 28 | Hiltaba Suite | granite, Hiltaba |
| 29 | Hiltaba Suite | granite, Buckleboo |
| 30 | Hiltaba Suite | granite, Cultana |
| 31 | Menninnie Dam | Drill hole PD0032, 333.29m |
| 32 | Menninnie Dam | Drill hole PD0032, 290.71m |
| 33 | Menninnie Dam | Drill hole PD0007, 461.8m |

**Appendix 3. 4 cont.**

| | 34 | 35 | 36 | 37 | 38 | 39 | 40 | 41 | 42 | 43 | 44 |
|---|---|---|---|---|---|---|---|---|---|---|---|
| SiO2 (wt.%) | 72.02 | 73.31 | 74.43 | 72.51 | 71.72 | 70.73 | 73.53 | 72.82 | 63.84 | 70.15 | 74.44 |
| TiO2 (wt.%) | 0.05 | 0.18 | 0.09 | 0.09 | 0.04 | 0.08 | 0.12 | 0.08 | 0.52 | 0.19 | 0.09 |
| Al2O3 (wt.%) | 13.97 | 14.32 | 13.98 | 13.83 | 14.99 | 15.73 | 13.88 | 13.73 | 16.58 | 14.03 | 13.33 |
| Fe2O3 (wt.%) | 1.65 | 1.31 | 1.15 | 1.28 | 0.67 | 0.68 | 1.92 | 1.43 | 4.28 | 1.82 | 1.04 |
| FeO (wt.%) | n/a | n/a | n/a | n/a | n/a | n/a | n/a | n/a | n/a | n/a | n/a |
| MnO (wt.%) | 0.06 | 0.02 | 0.02 | 0.05 | 0.06 | 0.01 | 0.06 | 0.07 | 0.09 | 0.03 | 0.04 |
| MgO (wt.%) | 0.6 | 0.7 | 0.45 | 0.49 | 0.24 | 0.34 | 0.59 | 0.67 | 1.7 | 0.66 | 0.26 |
| CaO (wt.%) | 0.66 | 0.53 | 0.45 | 0.95 | 0.48 | 0.92 | 0.48 | 0.55 | 1.62 | 1.5 | 1.4 |
| Na2O (wt.%) | 1.85 | 3.15 | 3.4 | 2.43 | 3.21 | 4.58 | 3.15 | 2.4 | 3.65 | 2.96 | 5.48 |
| K2O (wt.%) | 6.93 | 5.44 | 5.27 | 5.94 | 7.3 | 6.18 | 5.29 | 6.16 | 4.99 | 6.01 | 2.04 |
| P2O5 (wt.%) | 0.14 | 0.15 | 0.18 | 0.13 | 0.16 | 0.03 | 0.22 | 0.14 | 0.2 | 0.12 | 0.23 |
| H2O+ (wt.%) | n/a | n/a | n/a | n/a | n/a | n/a | n/a | n/a | n/a | n/a | n/a |
| H2O- (wt.%) | n/a | n/a | n/a | n/a | n/a | n/a | n/a | n/a | n/a | n/a | n/a |
| CO2 (wt.%) | n/a | n/a | n/a | n/a | n/a | n/a | n/a | n/a | n/a | n/a | n/a |
| LOI (wt.%) | 1.75 | 1.48 | 0.9 | 1.82 | 0.87 | 0.88 | 1.09 | 1.8 | 1.73 | 2.39 | 1.08 |
| Total (wt.%) | 99.68 | 100.6 | 100.3 | 99.55 | 99.73 | 100.2 | 100.3 | 99.85 | 99.2 | 99.87 | 99.45 |
| Ba (ppm) | 181 | 361 | 164 | 380 | 372 | 232 | 196 | 353 | 976 | 550 | 170 |
| Ce (ppm) | n/a | n/a | n/a | n/a | n/a | n/a | n/a | n/a | n/a | n/a | n/a |
| Co (ppm) | n/a | n/a | n/a | n/a | n/a | n/a | n/a | n/a | n/a | n/a | n/a |
| Cr (ppm) | n/a | n/a | n/a | n/a | n/a | n/a | n/a | n/a | n/a | n/a | n/a |
| Cu (ppm) | 4 | 6 | 5 | 7 | 3 | 6 | 5 | 4 | 10 | 47 | 4 |
| La (ppm) | n/a | n/a | n/a | n/a | n/a | n/a | n/a | n/a | n/a | n/a | n/a |
| Li (ppm) | n/a | n/a | n/a | n/a | n/a | n/a | n/a | n/a | n/a | n/a | n/a |
| Nb (ppm) | 5 | 7 | 12 | 10 | 4 | 14 | 11 | 9 | 11 | 40 | 18 |
| Ni (ppm) | 5 | 6 | 8 | 8 | 5 | 8 | 11 | 5 | 7 | 8 | 8 |
| Pb (ppm) | 119 | 34 | 61 | 60 | 57 | 102 | 49 | 48 | 38 | 68 | 39 |
| Rb (ppm) | 326 | 162 | 201 | 173 | 281 | 232 | 208 | 246 | 158 | 367 | 98 |
| Sc (ppm) | 2 | 4 | 3 | 3 | 2 | 8 | 3 | 2 | 8 | 4 | 3 |
| Sr (ppm) | 26 | 52 | 41 | 57 | 61 | 107 | 48 | 29 | 394 | 88 | 144 |
| Th (ppm) | 8 | 30 | 11 | 19 | 11 | 8 | 11 | 15 | 32 | 60 | 17 |
| U (ppm) | 46 | 10 | 27 | 18 | 6 | 29 | 30 | 5 | 6 | 40 | 49 |
| V (ppm) | 3 | 10 | 8 | 7 | 5 | 4 | 10 | 4 | 48 | 11 | 7 |
| W (ppm) | n/a | n/a | n/a | n/a | n/a | n/a | n/a | n/a | n/a | n/a | n/a |
| Y (ppm) | 24 | 12 | 12 | 10 | 10 | 11 | 26 | 8 | 13 | 21 | 13 |
| Zn (ppm) | 53 | 28 | 29 | 42 | 47 | 36 | 52 | 36 | 74 | 50 | 28 |
| Zr (ppm) | 63 | 101 | 44 | 71 | 54 | 42 | 75 | 58 | 199 | 190 | 59 |
| Analyses | 1 | 1 | 1 | 1 | 1 | 1 | 1 | 1 | 1 | 1 | 1 |
| Reference | 3 | 3 | 3 | 3 | 3 | 3 | 3 | 3 | 3 | 3 | 3 |

| | | |
|---|---|---|
| 34 | Menninnie Dam | Drill hole PD0013, 485m |
| 35 | Menninnie Dam | Drill hole PD0018, 380.2)m |
| 36 | Menninnie Dam | Drill hole PD0018, 454.5m |
| 37 | Menninnie Dam | Drill hole PD0003, 370m |
| 38 | Menninnie Dam | Drill hole PD0005, 197.3m |
| 39 | Menninnie Dam | Drill hole PD0027, 567.03m |
| 40 | Menninnie Dam | Drill hole PD0032, 233.1m |
| 41 | Menninnie Dam | Drill hole PD0001, 156.8m |
| 42 | Menninnie Dam | Drill hole PD0007, 154.6m |
| 43 | Menninnie Dam | Drill hole PD0012, 206.37m |
| 44 | Menninnie Dam | Drill hole PD0013, 137.75m |

**Appendix 3. 4 cont.**

| | 45 | 46 | 47 | 48 | 49 | 50 | 51 | 52 |
|---|---|---|---|---|---|---|---|---|
| SiO2 (wt.%) | 70.74 | 73.95 | 64.53 | 73.96 | 73.47 | 73.15 | 77.03 | 71.72 |
| TiO2 (wt.%) | 0.06 | 0.07 | 0.91 | 0.12 | 0.12 | 0.12 | 0.13 | 0.12 |
| Al2O3 (wt.%) | 14.17 | 13.83 | 14.04 | 12.06 | 13.15 | 11.92 | 12.48 | 12.38 |
| Fe2O3 (wt.%) | 1.05 | 1.03 | 5.41 | 1.43 | 1.09 | 1.14 | 2.44 | 1.32 |
| FeO (wt.%) | n/a | n/a | n/a | | | | | |
| MnO (wt.%) | 0.03 | 0.03 | 0.1 | 0.07 | 0.04 | 0.14 | 0.07 | 0.26 |
| MgO (wt.%) | 1.1 | 0.31 | 1.47 | 0.72 | 0.36 | 0.69 | 1 | 1.19 |
| CaO (wt.%) | 0.82 | 0.3 | 1.83 | 1.41 | 1.05 | 2.75 | 0.23 | 1.75 |
| Na2O (wt.%) | 3.04 | 3.22 | 2.83 | 2.65 | 2.97 | 0.76 | 0.13 | 0.07 |
| K2O (wt.%) | 7.07 | 6.44 | 4.88 | 5.56 | 5.78 | 6.34 | 3.68 | 5.51 |
| P2O5 (wt.%) | 0.09 | 0.17 | 0.43 | 0.03 | 0.03 | 0.03 | 0.03 | 0.02 |
| H2O+ (wt.%) | n/a | n/a | n/a | n/a | n/a | n/a | n/a | n/a |
| H2O- (wt.%) | n/a | n/a | n/a | n/a | n/a | n/a | n/a | n/a |
| CO2 (wt.%) | n/a | n/a | n/a | n/a | n/a | n/a | n/a | n/a |
| LOI (wt.%) | 1.33 | 0.61 | 2.59 | 2.07 | 1.71 | 3.42 | 2.74 | 4.36 |
| Total (wt.%) | 99.5 | 99.35 | 96.43 | 100.1 | 99.77 | 100.5 | 99.96 | 98.7 |
| Ba (ppm) | 1131 | 261 | 2285 | 590 | 836 | 634 | 566 | 594 |
| Ce (ppm) | n/a | n/a | n/a | n/a | n/a | n/a | n/a | n/a |
| Co (ppm) | n/a | n/a | n/a | n/a | n/a | n/a | n/a | n/a |
| Cr (ppm) | n/a | n/a | n/a | n/a | n/a | n/a | n/a | n/a |
| Cu (ppm) | 4 | 5 | 19 | 8 | 4 | 7 | 5 | 4 |
| La (ppm) | n/a | n/a | n/a | n/a | n/a | n/a | n/a | n/a |
| Li (ppm) | n/a | n/a | n/a | n/a | n/a | n/a | n/a | n/a |
| Nb (ppm) | 4 | 13 | 53 | 13 | 15 | 12 | 12 | 16 |
| Ni (ppm) | 9 | 8 | 12 | 9 | 7 | 9 | 8 | 4 |
| Pb (ppm) | 99 | 65 | 74 | 14 | 7 | 18 | 4 | 7 |
| Rb (ppm) | 211 | 250 | 191 | 191 | 215 | 354 | 237 | 268 |
| Sc (ppm) | 2 | 2 | 7 | 3 | 4 | 3 | 2 | 4 |
| Sr (ppm) | 140 | 53 | 416 | 85 | 83 | 63 | 8 | 18 |
| Th (ppm) | 21 | 10 | 87 | 28 | 32 | 24 | 29 | 33 |
| U (ppm) | 17 | 13 | 14 | 4 | 5 | 4 | 5 | 6.5 |
| V (ppm) | 10 | 7 | 62 | 8 | 8 | 8 | 9 | 6 |
| W (ppm) | n/a | n/a | n/a | n/a | n/a | n/a | n/a | n/a |
| Y (ppm) | 7 | 12 | 24 | 18 | 23 | 20 | 19 | 25 |
| Zn (ppm) | 25 | 37 | 157 | 35 | 28 | 47 | 44 | 61 |
| Zr (ppm) | 55 | 63 | 495 | 119 | 132 | 117 | 117 | 126 |
| Analyses | 1 | 1 | 1 | 1 | 1 | 1 | 1 | 1 |
| Reference | 3 | 3 | 3 | 3 | 3 | 3 | 3 | 3 |

| | | |
|---|---|---|
| 45 | Menninnie Dam | Drill hole PD0009, 283.1m |
| 46 | Menninnie Dam | Drill hole PD0021, 169.66m |
| 47 | Menninnie Dam | Drill hole PD0021, 161.88m |
| 48 | Menninnie Dam | PD0030, 385.5, rhyolite component of peperite |
| 49 | Menninnie Dam | PD0030, 471m, weakly altered rhyolite intrusion |
| 50 | Menninnie Dam | PD0031, strongly altered rhyolite intrusion |
| 51 | Menninnie Dam | PD0030, 403m, strongly altered rhyolite intrusion |
| 52 | Menninnie Dam | PD0031, 157.5m, coherent rhyolite |

## Appendix 3.5

XRD mineral identification of metasomatised and non-metasomatised rocks from Menninnie Dam

### Equipment

All analyses were carried out at the laboratorities of Tasmanian Development and Resources, Hobart, Tasmania, by Mr. R.N. Woolley.
Samples were run on an automated Philips X-ray diffractometer system as follows:

PW 1729 generator
Nickel filtered copper K alpha radiation at 40kV and 30mA
PW 1050 goniometer
PW 1710 printing recorder and microprocessor
PW1752 graphite monochronometer
PW1711 sample spinner and a proportional detector

Samples were calibrated with the addition of an internal natural quartz standard.
Mineral identification was by a semiautomated search - match method using software developed by CSIRO.
The six strongest peaks of iron titanium oxides are used for cell dimension refinement using the Excel templates of Novak and Colville (1989).

### Results

| Drill hole | Depth | Rock description | Treatment | Minerals identified (decreasing abundance) |
|---|---|---|---|---|
| PD0006 | 382.25 | Non-metasomatised, banded, impure marble | HCl | cal / K-fel / amp / chl / mica / qz / cpx / plg(?) |
| PD0007 | 100.5 | Non-metasomatised, banded, impure marble | HCl | dol / mica / tlc / chl / cal |
| PD0001 | 127.5 | Metasomatically altered iron formation bands | HCl | cal / K-fel / plg / he / qz / amp / chl / mica / smectite(?) |
| PD0007 | 116.32 | Metasomatically altered impure marble | HCl | dol / K-fel / qz / chl / mica / sid / smectite(?) |
| PD0007 | 264.65 | Metasomatically altered impure marble | HCl | cal / kfel / mica / he / qz / plg / chl / smectite(?) |
| PD0002 | 171.42 | Metasomatically altered diopside? | HCl | qz / tlc / cal / opal / dol |
| PD0006 | 193.42 | Metasomatically altered diopside | HCl | K-fel / woll / gar (grossular?) / mica |
| PD0026 | 634.29 | Light brown, metasomatically altered rock | HCl | epi / cal / apatite (flouroapatite?) / gar / chl |
| PD0031 | 624.28 | Metasomatically altered marble and calc-silicates | HCl | cpx / K-fel / epi / cal / qz / chl |

### Key to minerals

cal = calcite, K-fel = K-felspar, plg = plagioclase, he = hematite, qz = quartz, amp = ampbibole, chl = chlorite,
cpx = diopside, tlc = talc, dol = dolomite, sid = siderite, woll = wollastinite, gar = garnet, epi = epidote

## Appendix 4.1

Estimated percentage of lithic clasts < 100 mm across in the MD ignimbrite

| Drill hole | Depth (m) down hole | Height above base (m) (vert) | % lithics < 100mm dia. |
|---|---|---|---|
| PD0032 | 116.00 | 142.08 | 20 |
| PD0032 | 126.00 | 133.34 | 25 |
| PD0032 | 131.80 | 128.27 | 25 |
| PD0032 | 151.20 | 111.32 | 30 |
| PD0032 | 154.30 | 108.61 | 40 |
| PD0032 | 170.30 | 94.62 | 30 |
| PD0032 | 181.00 | 85.27 | 35 |
| PD0032 | 183.00 | 83.52 | 80 |
| PD0032 | 196.35 | 71.85 | 40 |
| PD0032 | 201.80 | 67.09 | 35 |
| PD0032 | 221.70 | 49.69 | 40 |
| PD0032 | 241.00 | 32.82 | 42 |
| PD0032 | 255.00 | 20.58 | 42 |
| PD0032 | 270.00 | 7.47 | 60 |
| PD0021 | 151.30 | 141.94 | 18 |
| PD0021 | 157.70 | 136.69 | 22 |
| PD0021 | 161.00 | 133.98 | 30 |
| PD0021 | 181.60 | 117.08 | 30 |
| PD0021 | 184.00 | 115.11 | 27 |
| PD0021 | 188.50 | 111.42 | 40 |
| PD0021 | 197.16 | 104.31 | 40 |
| PD0021 | 199.50 | 102.39 | 80 |
| PD0021 | 203.18 | 99.37 | 40 |
| PD0021 | 204.55 | 98.25 | 37 |
| PD0021 | 206.14 | 96.94 | 30 |
| PD0021 | 212.92 | 91.38 | 30 |
| PD0021 | 218.30 | 86.96 | 35 |
| PD0021 | 226.15 | 80.52 | 40 |
| PD0021 | 234.60 | 73.59 | 45 |
| PD0021 | 238.00 | 70.80 | 40 |
| PD0021 | 254.50 | 57.26 | 40 |
| PD0021 | 262.50 | 50.69 | 40 |
| PD0021 | 276.80 | 38.96 | 12 |
| PD0021 | 279.50 | 36.74 | 12 |
| PD0021 | 279.55 | 36.70 | 20 |
| PD0021 | 283.90 | 33.13 | 25 |
| PD0021 | 286.18 | 31.26 | 25 |
| PD0021 | 290.07 | 28.07 | 10 |
| PD0021 | 292.50 | 26.07 | 30 |
| PD0021 | 302.00 | 18.28 | 32 |
| PD0021 | 311.50 | 10.48 | 27 |
| PD0021 | 324.27 | 0.00 | 33 |
| PD0025 | 170.00 | 33.97 | 20 |
| PD0025 | 176.00 | 28.92 | 20 |
| PD0025 | 178.50 | 26.82 | 20 |

**Appendix 4.1 cont.**

| Drill hole | Depth (m) down hole | Height above base (m) (vert) | % lithics < 100mm dia. |
|---|---|---|---|
| PD0025 | 181.30 | 24.46 | 35 |
| PD0025 | 183.52 | 22.60 | 27 |
| PD0025 | 187.80 | 19.00 | 25 |
| PD0025 | 194.90 | 13.03 | 37 |
| PD0025 | 196.40 | 11.77 | 37 |
| PD0025 | 198.70 | 9.83 | 35 |
| PD0025 | 209.10 | 1.09 | 37 |

**Appendix 4.1 cont.**
Lithic clasts of > 100mm across in the Menninnie Dam ignimbrite

| Drill hole | Top of clast (m) (down hole) | Base of clast (m) (down hole) | Base of clast (m) Above base (vert.) | Top of clast (m) Above base (vert.) | Thickness (m) (Vertical) | Clast lithology |
|---|---|---|---|---|---|---|
| PD0021 | 158.63 | 159.43 | 134.71 | 135.37 | 0.66 | foliated granite |
| PD0021 | 161.40 | 181.10 | 116.86 | 133.09 | 16.23 | foliated granite |
| PD0021 | 187.30 | 187.50 | 111.58 | 111.75 | 0.16 | schist |
| PD0021 | 191.90 | 194.02 | 106.21 | 107.96 | 1.75 | foliated granite |
| PD0021 | 194.20 | 195.75 | 104.78 | 106.06 | 1.28 | foliated granite |
| PD0021 | 197.31 | 198.16 | 102.80 | 103.50 | 0.70 | brecciated granite + schist |
| PD0021 | 200.17 | 202.66 | 99.09 | 101.14 | 2.05 | foliated granite |
| PD0021 | 203.28 | 203.66 | 98.26 | 98.58 | 0.31 | mylonitic schist |
| PD0021 | 203.92 | 204.22 | 97.80 | 98.05 | 0.25 | foliated granite |
| PD0021 | 206.92 | 208.75 | 94.07 | 95.58 | 1.51 | mylonitic schist |
| PD0021 | 209.66 | 210.00 | 93.04 | 93.32 | 0.28 | mylonitic schist |
| PD0021 | 210.15 | 212.74 | 90.78 | 92.92 | 2.13 | foliated granite |
| PD0021 | 224.50 | 224.77 | 80.87 | 81.09 | 0.22 | foliated granite |
| PD0021 | 226.33 | 233.62 | 73.57 | 79.58 | 6.01 | brecciated schist + granite |
| PD0021 | 235.17 | 237.30 | 70.54 | 72.30 | 1.76 | foliated granite |
| PD0021 | 239.80 | 242.72 | 66.07 | 68.48 | 2.41 | granite mylonite |
| PD0021 | 243.05 | 243.43 | 65.49 | 65.80 | 0.31 | granite and mylonite |
| PD0021 | 243.55 | 243.68 | 65.28 | 65.39 | 0.11 | foliated granite |
| PD0021 | 244.28 | 254.06 | 56.73 | 64.79 | 8.06 | brecciated schist and granite |
| PD0021 | 255.28 | 257.46 | 53.93 | 55.72 | 1.80 | brecciated schist and granite |
| PD0021 | 269.30 | 269.70 | 43.84 | 44.17 | 0.33 | brecciated schist and granite |
| PD0021 | 284.28 | 285.15 | 31.11 | 31.82 | 0.72 | brecciated schist and granite |
| PD0021 | 293.25 | 294.19 | 23.66 | 24.43 | 0.77 | foliated granite |
| PD0021 | 303.30 | 307.90 | 12.36 | 16.15 | 3.79 | brecciated foliated granite |
| PD0021 | 310.35 | 311.02 | 9.79 | 10.34 | 0.55 | brecciated foliated granite |
| PD0021 | 318.17 | 318.78 | 3.39 | 3.90 | 0.50 | brecciated foliated granite |
| PD0021 | 319.62 | 319.77 | 2.58 | 2.70 | 0.12 | brecciated foliated granite |
| PD0021 | 320.19 | 321.25 | 1.36 | 2.23 | 0.87 | brecciated diopside, marble and granite |
| PD0025 | 170.38 | 175.61 | 29.25 | 33.65 | 4.40 | foliated granite |

**Appendix 4.1 cont**

| Drill hole | Top of clast (m) (down hole) | Base of clast (m) (down hole) | Base of clast (m) Above base (vert.) | Top of clast (m) Above base (vert.) | Thickness (m) (Vertical) | Clast lithology |
|---|---|---|---|---|---|---|
| PD0025 | 183.12 | 183.23 | 22.84 | 22.93 | 0.09 | schist |
| PD0025 | 189.85 | 190.00 | 17.15 | 17.28 | 0.13 | schist |
| PD0025 | 198.02 | 198.45 | 10.04 | 10.40 | 0.36 | brecciated foliated granite |
| PD0025 | 199.20 | 208.92 | 1.24 | 9.41 | 8.17 | brecciated foliated granite |
| PD0032 | 114.00 | 115.00 | 139.26 | 140.16 | 0.91 | granite |
| PD0032 | 119.08 | 119.47 | 135.20 | 135.56 | 0.35 | granite |
| PD0032 | 120.30 | 121.21 | 133.63 | 134.45 | 0.82 | granite + marble |
| PD0032 | 122.90 | 123.90 | 131.19 | 132.10 | 0.91 | foliated granite |
| PD0032 | 124.05 | 124.22 | 130.90 | 131.05 | 0.15 | brecciated granite |
| PD0032 | 124.90 | 126.78 | 128.58 | 130.28 | 1.70 | foliated granite |
| PD0032 | 127.81 | 128.12 | 127.36 | 127.65 | 0.28 | foliated granite |
| PD0032 | 129.16 | 129.49 | 126.12 | 126.42 | 0.30 | brecciated granite |
| PD0032 | 130.21 | 131.70 | 124.12 | 125.47 | 1.35 | foliated granite |
| PD0032 | 135.16 | 136.40 | 119.86 | 120.98 | 1.12 | foliated granite |
| PD0032 | 136.99 | 137.10 | 119.23 | 119.33 | 0.10 | foliated granite |
| PD0032 | 138.30 | 140.75 | 115.92 | 118.14 | 2.22 | foliated granite |
| PD0032 | 142.86 | 144.60 | 112.43 | 114.01 | 1.58 | foliated granite |
| PD0032 | 145.61 | 146.20 | 110.98 | 111.51 | 0.53 | foliated granite |
| PD0032 | 146.79 | 147.31 | 109.97 | 110.44 | 0.47 | foliated granite |
| PD0032 | 153.19 | 153.45 | 104.41 | 104.64 | 0.24 | foliated granite |
| PD0032 | 160.61 | 161.48 | 97.13 | 97.92 | 0.79 | foliated granite |
| PD0032 | 179.76 | 180.93 | 79.50 | 80.56 | 1.06 | foliated granite |
| PD0032 | 183.34 | 183.60 | 77.08 | 77.32 | 0.24 | foliated granite |
| PD0032 | 198.20 | 199.27 | 62.88 | 63.85 | 0.97 | brecciated granite |
| PD0032 | 202.00 | 202.31 | 60.12 | 60.41 | 0.28 | brecciated granite |
| PD0032 | 202.67 | 220.30 | 43.82 | 59.80 | 15.98 | altered foliated granite |
| PD0032 | 220.78 | 221.20 | 43.01 | 43.39 | 0.38 | altered foliated granite |
| PD0032 | 221.22 | 221.46 | 42.77 | 42.99 | 0.22 | folaited granite |
| PD0032 | 223.20 | 226.34 | 38.35 | 41.19 | 2.85 | brecciated marble |
| PD0032 | 226.67 | 235.12 | 30.39 | 38.05 | 7.66 | foliated granite |
| PD0032 | 237.30 | 237.47 | 28.26 | 28.42 | 0.15 | foliated granite |

**Appendix 4.1 cont.**

| Drill hole | Top of clast (m) (down hole) | Base of clast (m) (down hole) | Base of clast (m) Above base (vert.) | Top of clast (m) Above base (vert.) | Thickness (m) (Vertical) | Clast lithology |
|---|---|---|---|---|---|---|
| PD0032 | 239.14 | 239.48 | 26.44 | 26.75 | 0.31 | foliated granite |
| PD0032 | 240.00 | 240.35 | 25.65 | 25.97 | 0.32 | schist |
| PD0032 | 248.91 | 251.02 | 15.98 | 17.89 | 1.91 | foliated granite |
| PD0032 | 251.50 | 251.88 | 15.20 | 15.55 | 0.34 | foliated granite and schist |

**Appendix 5.1.**
Compositions of adularia determined using a Cameca SX - 50 electron microprobe at the Central Science Laboratory, University of Tasmania.

| Drill Hole | Depth (m) | Na2O (wt.%) | MgO (wt.%) | Al2O3 (wt.%) | SiO2 (wt.%) | K2O (wt.%) | CaO (wt.%) | Cr2O3 (wt.%) | TiO2 (wt.%) | MnO (wt.%) | FeO* (wt.%) | SrO (wt.%) | BaO (wt.%) | total (wt.%) |
|---|---|---|---|---|---|---|---|---|---|---|---|---|---|---|
| PD0016 | 272.6 | 0.24 | 0.00 | 18.69 | 64.05 | 15.39 | 0.03 | 0.02 | 0.00 | 0.00 | 0.00 | 0.19 | 0.12 | 98.73 |
| PD0016 | 272.6 | 0.21 | 0.01 | 18.69 | 63.10 | 14.98 | 0.00 | 0.05 | 0.01 | 0.00 | 0.00 | 0.18 | 0.50 | 97.72 |
| PD0016 | 305.0 | 0.21 | 0.00 | 18.81 | 63.58 | 15.22 | 0.00 | 0.00 | 0.00 | 0.00 | 0.02 | 0.20 | 0.23 | 98.27 |
| PD0016 | 305.0 | 0.31 | 0.00 | 18.59 | 64.52 | 15.41 | 0.00 | 0.00 | 0.04 | 0.00 | 0.00 | 0.19 | 0.03 | 99.08 |
| PD0016 | 305.0 | 0.23 | 0.00 | 18.65 | 64.25 | 15.37 | 0.00 | 0.00 | 0.00 | 0.04 | 0.00 | 0.23 | 0.04 | 98.82 |
| PD0016 | 305.0 | 0.21 | 0.00 | 18.52 | 63.92 | 15.11 | 0.00 | 0.02 | 0.00 | 0.09 | 0.00 | 0.21 | 0.12 | 98.20 |
| PD0016 | 305.0 | 0.18 | 0.01 | 18.89 | 64.36 | 15.31 | 0.00 | 0.11 | 0.05 | 0.00 | 0.01 | 0.20 | 0.04 | 99.15 |
| PD0016 | 305.0 | 0.28 | 0.00 | 18.70 | 64.78 | 15.31 | 0.00 | 0.00 | 0.01 | 0.04 | 0.03 | 0.23 | 0.08 | 99.44 |
| PD0016 | 305.0 | 0.21 | 0.01 | 18.74 | 64.13 | 15.41 | 0.00 | 0.02 | 0.02 | 0.02 | 0.00 | 0.22 | 0.09 | 98.86 |
| PD0016 | 305.0 | 0.24 | 0.01 | 18.62 | 64.15 | 15.29 | 0.00 | 0.00 | 0.00 | 0.00 | 0.05 | 0.18 | 0.00 | 98.54 |
| PD0016 | 305.0 | 0.13 | 0.02 | 17.84 | 65.89 | 14.68 | 0.01 | 0.00 | 0.00 | 0.00 | 0.04 | 0.20 | 0.05 | 98.85 |
| PD0016 | 305.0 | 0.20 | 0.00 | 18.51 | 64.78 | 15.20 | 0.00 | 0.01 | 0.04 | 0.00 | 0.02 | 0.16 | 0.14 | 99.05 |
| PD0028 | 366.1 | 0.52 | 0.00 | 18.53 | 64.95 | 14.81 | 0.00 | 0.02 | 0.01 | 0.03 | 0.00 | 0.24 | 0.00 | 99.10 |
| PD0028 | 366.1 | 0.26 | 0.11 | 18.60 | 63.73 | 15.17 | 0.01 | 0.05 | 0.02 | 0.03 | 0.06 | 0.24 | 0.05 | 98.32 |
| PD0028 | 366.1 | 0.20 | 0.28 | 18.72 | 63.85 | 15.28 | 0.01 | 0.03 | 0.03 | 0.00 | 0.10 | 0.21 | 0.06 | 98.78 |
| PD0028 | 366.1 | 0.52 | 0.00 | 18.79 | 64.17 | 15.08 | 0.00 | 0.00 | 0.00 | 0.00 | 0.00 | 0.19 | 0.02 | 98.77 |
| PD0028 | 366.1 | 0.24 | 0.15 | 18.69 | 64.62 | 14.88 | 0.12 | 0.00 | 0.00 | 0.00 | 0.08 | 0.18 | 0.05 | 98.98 |
| PD0028 | 366.1 | 0.20 | 0.20 | 18.94 | 63.78 | 15.31 | 0.00 | 0.00 | 0.03 | 0.02 | 0.13 | 0.19 | 0.00 | 98.79 |
| PD0028 | 366.1 | 0.25 | 0.05 | 18.70 | 63.95 | 15.35 | 0.03 | 0.01 | 0.00 | 0.00 | 0.08 | 0.17 | 0.09 | 98.68 |
| PD0028 | 366.1 | 0.18 | 0.38 | 18.47 | 63.68 | 15.40 | 0.00 | 0.00 | 0.01 | 0.00 | 0.10 | 0.17 | 0.06 | 98.45 |
| PD0028 | 366.1 | 0.33 | 0.25 | 18.81 | 63.47 | 15.07 | 0.00 | 0.03 | 0.00 | 0.00 | 0.03 | 0.16 | 0.25 | 98.39 |

* Total iron expressed as FeO

## Appendix 5.2

Chemical analyses of mineralised zones below the base of weathering that contain greater than 1000 ppm Pb or Zn. The sample interval immediate above and below the mineralised zone is also included. Chemical analyses of whole rock inbetween mineralised zones have not been included.

| Drill hole | From (m) | To (m) | interval (m) | Zn (ppm) | Cu (ppm) | Pb (ppm) | Ag (ppm) | Mn (ppm) | Fe (ppm) | Au (ppm) | As (ppm) | Hg (ppm) | Sn (ppm) | W (ppm) | Ba (ppm) |
|---|---|---|---|---|---|---|---|---|---|---|---|---|---|---|---|
| PD0001 | 156 | 158 | 2 | 30 | 8 | 20 | 1 | 460 | 8500 | 0 | | | | | |
| PD0001 | 158 | 159.7 | 1.7 | 910 | 12 | 1150 | 1 | 1650 | 11000 | 0 | | | | | |
| PD0001 | 159.7 | 162 | 2.3 | 790 | 18 | 2800 | 3 | 2350 | 15000 | 0 | | | | | |
| PD0001 | 162 | 164 | 2 | 2350 | 22 | 3300 | 3 | 1300 | 10000 | 0 | | | | | |
| PD0001 | 164 | 166 | 2 | 1950 | 24 | 950 | 2 | 850 | 8500 | 0 | | | | | |
| PD0001 | 166 | 168.37 | 2.37 | 740 | 12 | 1000 | 2 | 1150 | 9500 | 0 | | | | | |
| PD0001 | 168.37 | 169.2 | 0.83 | 560 | 14 | 1600 | 2 | 8800 | 54000 | 0 | | | | | |
| PD0001 | 169.2 | 172 | 2.8 | 40 | 38 | 20 | 1 | 650 | 8500 | 0 | | | | | |
| PD0002 | 154.3 | 156.9 | 2.6 | 12000 | 10 | 70 | 0 | 10000 | 66000 | | | | | | |
| PD0002 | 156.9 | 158.6 | 1.7 | 65 | 4 | 12 | 0 | 150 | 3000 | | | | | | |
| PD0002 | 162.3 | 165.1 | 2.8 | 460 | 740 | 540 | 34 | 1700 | 11000 | | | | | | |
| PD0002 | 165.1 | 165.9 | 0.8 | 730 | 430 | 1900 | 240 | 5300 | 17000 | | | | | | |
| PD0002 | 165.9 | 167.3 | 1.4 | 310 | 500 | 105 | 27 | 1100 | 7500 | | | | | | |
| PD0002 | 187.5 | 190 | 2.5 | 220 | 210 | 110 | 2 | 550 | 7000 | | | | | | |
| PD0002 | 190 | 193.4 | 3.4 | 550 | 240 | 1900 | 8 | 900 | 25000 | | | | | | |
| PD0002 | 193.4 | 196 | 2.6 | 470 | 240 | 590 | 11 | 1750 | 39000 | | | | | | |
| PD0002 | 200 | 202.1 | 2.1 | 200 | 135 | 540 | 8 | 1100 | 27000 | | | | | | |
| PD0002 | 202.1 | 202.8 | 0.7 | 440 | 85 | 1100 | 19 | 2500 | 12000 | | | | | | |
| PD0002 | 202.8 | 205 | 2.2 | 110 | 90 | 320 | 3 | 4000 | 14000 | | | | | | |
| PD0002 | 205 | 207.2 | 2.2 | 5000 | 80 | 1300 | 8 | 5500 | 13000 | | | | | | |
| PD0002 | 207.2 | 208.5 | 1.3 | 250 | 60 | 790 | 3 | 3200 | 9000 | | | | | | |
| PD0002 | 208.5 | 210.5 | 2 | 6300 | 125 | 4900 | 20 | 6300 | 18000 | | | | | | |
| PD0002 | 210.5 | 212.5 | 2 | 610 | 210 | 400 | 3 | 3950 | 13000 | | | | | | |
| PD0002 | 212.5 | 214.7 | 2.2 | 540 | 150 | 1450 | 6 | 2350 | 14000 | | | | | | |
| PD0002 | 214.7 | 216.7 | 2 | 370 | 32 | 210 | 1 | 2100 | 7500 | | | | | | |
| PD0002 | 216.7 | 219.2 | 2.5 | 280 | 60 | 310 | 0 | 1650 | 8000 | | | | | | |
| PD0002 | 219.2 | 222.5 | 3.3 | 360 | 60 | 1200 | 3 | 1550 | 9000 | | | | | | |
| PD0002 | 222.5 | 224.7 | 2.2 | 1000 | 28 | 290 | 1 | 940 | 24000 | 0 | | | | | |
| PD0002 | 224.7 | 226.2 | 1.5 | 70 | 8 | 70 | 1 | 3500 | 13000 | 0 | | | | | |
| PD0002 | 226.2 | 227.8 | 1.6 | 700 | 16 | 1200 | 1 | 2150 | 23000 | 0 | | | | | |
| PD0002 | 227.8 | 230 | 2.2 | 34000 | 200 | 17000 | 13 | 9000 | 60000 | 0 | | | | | |

**Appendix 5.2 cont.**

| Drill hole | From (m) | To (m) | interval (m) | Zn (ppm) | Cu (ppm) | Pb (ppm) | Ag (ppm) | Mn (ppm) | Fe (ppm) | Au (ppm) | As (ppm) | Hg (ppm) | Sn (ppm) | W (ppm) | Ba (ppm) |
|---|---|---|---|---|---|---|---|---|---|---|---|---|---|---|---|
| PD0002 | 230 | 230.9 | 0.9 | 8200 | 160 | 52000 | 900 | 7000 | 32000 | 0 | | | | | |
| PD0002 | 230.9 | 232.9 | 2 | 1900 | 85 | 10000 | 440 | 6500 | 33000 | 0 | | | | | |
| PD0002 | 232.9 | 234.4 | 1.5 | 1050 | 16 | 2800 | 5 | 11500 | 28000 | 0 | | | | | |
| PD0002 | 234.4 | 236.4 | 2 | 1550 | 18 | 1950 | 2 | 10500 | 32000 | 0 | | | | | |
| PD0002 | 236.4 | 239 | 2.6 | 120 | 10 | 160 | 1 | 2400 | 8500 | 0 | | | | | |
| PD0002 | 240.6 | 242 | 1.4 | 480 | 30 | 520 | 0 | 530 | 8000 | | | | | | |
| PD0002 | 242 | 244 | 2 | 2000 | 6 | 670 | 1 | 1900 | 22000 | | | | | | |
| PD0002 | 244 | 245 | 1 | 1750 | 16 | 910 | 1 | 1800 | 26500 | | | | | | |
| PD0002 | 245 | 247.2 | 2.2 | 850 | 8 | 660 | 1 | 3100 | 14000 | | | | | | |
| PD0003 | 177 | 179.15 | 2.15 | 900 | 32 | 510 | 1 | 1350 | 4 | 0 | | | | | |
| PD0003 | 179.15 | 181.9 | 2.75 | 8400 | 36 | 260 | 1 | 5800 | 8 | 0 | | | | | |
| PD0003 | 181.9 | 184 | 2.1 | 9200 | 26 | 140 | 2 | 8300 | 120000 | 0 | | | | | |
| PD0003 | 184 | 187 | 3 | 110 | 22 | 75 | 1 | 2650 | 39000 | 0 | | | | | |
| PD0004 | 185 | 187 | 2 | 240 | 20 | 65 | 0 | 1200 | 53000 | | | | | | |
| PD0004 | 187 | 189 | 2 | 1150 | 28 | 290 | 1 | 1000 | 50000 | | | | | | |
| PD0004 | 189 | 191 | 2 | 210 | 20 | 50 | 0 | 1000 | 49000 | | | | | | |
| PD0004 | 191 | 193 | 2 | 700 | 80 | 210 | 1 | 1100 | 41000 | | | | | | |
| PD0004 | 193 | 193.8 | 0.8 | 2200 | 65 | 480 | 1 | 1500 | 41000 | | | | | | |
| PD0004 | 193.8 | 196.7 | 2.9 | 240 | 10 | 240 | 1 | 90 | 7000 | | | | | | |
| PD0004 | 196.7 | 197.4 | 0.7 | 12000 | 34 | 560 | 2 | 7500 | 130000 | | | | | | |
| PD0004 | 197.4 | 199.5 | 2.1 | 8300 | 50 | 2200 | 4 | 5500 | 77000 | | | | | | |
| PD0004 | 199.5 | 201 | 1.5 | 4100 | 44 | 3400 | 5 | 1200 | 25000 | | | | | | |
| PD0004 | 201 | 203 | 2 | 1000 | 24 | 770 | 2 | 2900 | 44000 | | | | | | |
| PD0004 | 203 | 204.9 | 1.9 | 3300 | 24 | 1750 | 2 | 1800 | 38000 | | | | | | |
| PD0004 | 204.9 | 206.75 | 1.85 | 2500 | 34 | 3300 | 3 | 620 | 20000 | | | | | | |
| PD0004 | 206.75 | 208.85 | 2.1 | 2400 | 55 | 2500 | 5 | 350 | 28000 | | | | | | |
| PD0004 | 208.85 | 211 | 2.15 | 2100 | 55 | 850 | 2 | 1250 | 21000 | | | | | | |
| PD0004 | 211 | 213 | 2 | 7000 | 130 | 2200 | 5 | 3000 | 37000 | | | | | | |
| PD0004 | 213 | 215 | 2 | 2500 | 80 | 500 | 4 | 1000 | 34000 | | | | | | |
| PD0004 | 215 | 217 | 2 | 2800 | 125 | 700 | 2 | 1100 | 31000 | | | | | | |
| PD0004 | 217 | 219.2 | 2.2 | 510 | 60 | 140 | 2 | 430 | 38000 | | | | | | |
| PD0005 | 90 | 92 | 2 | 930 | 100 | 150 | 0 | 120 | 19000 | | | | | | |
| PD0005 | 92 | 94 | 2 | 1400 | 155 | 250 | 0 | 180 | 23000 | | | | | | |
| PD0005 | 94 | 96 | 2 | 560 | 110 | 80 | 0 | 230 | 36000 | | | | | | |

**Appendix 5.2 cont.**

| Drill hole | From (m) | To (m) | interval (m) | Zn (ppm) | Cu (ppm) | Pb (ppm) | Ag (ppm) | Mn (ppm) | Fe (ppm) | Au (ppm) | As (ppm) | Hg (ppm) | Sn (ppm) | W (ppm) | Ba (ppm) |
|---|---|---|---|---|---|---|---|---|---|---|---|---|---|---|---|
| PD0005 | 96 | 98.8 | 2.8 | 1100 | 38 | 200 | 0 | 400 | 42000 | | | | | | |
| PD0005 | 98.8 | 100.4 | 1.6 | 160 | 8 | 44 | 0 | 350 | 39000 | | | | | | |
| PD0005 | 116 | 118 | 2 | 300 | 40 | 120 | 0 | 450 | 45000 | | | | | | |
| PD0005 | 118 | 120 | 2 | 1400 | 36 | 260 | 0 | 410 | 41000 | | | | | | |
| PD0005 | 120 | 122 | 2 | 440 | 60 | 120 | 0 | 560 | 41000 | | | | | | |
| PD0005 | 122 | 124 | 2 | 670 | 48 | 280 | 0 | 620 | 40000 | | | | | | |
| PD0005 | 124 | 126 | 2 | 360 | 50 | 65 | 0 | 620 | 41500 | | | | | | |
| PD0005 | 126 | 128 | 2 | 1150 | 34 | 180 | 0 | 580 | 43500 | | | | | | |
| PD0005 | 128 | 130 | 2 | 3300 | 42 | 460 | 0 | 1200 | 41000 | | | | | | |
| PD0005 | 130 | 132 | 2 | 3100 | 60 | 480 | 0 | 1250 | 33500 | | | | | | |
| PD0005 | 132 | 134 | 2 | 4500 | 55 | 590 | 0 | 1100 | 37000 | | | | | | |
| PD0005 | 134 | 136 | 2 | 3800 | 60 | 580 | 0 | 1700 | 41000 | | | | | | |
| PD0005 | 136 | 138 | 2 | 1950 | 68 | 320 | 1 | 1850 | 45000 | | | | | | |
| PD0005 | 138 | 140 | 2 | 3400 | 44 | 390 | 2 | 1350 | 51000 | | | | | | |
| PD0005 | 140 | 142 | 2 | 4400 | 70 | 410 | 3 | 1200 | 41000 | | | | | | |
| PD0005 | 142 | 144 | 2 | 3100 | 75 | 410 | 2 | 2300 | 48000 | | | | | | |
| PD0005 | 144 | 146 | 2 | 2200 | 48 | 270 | 1 | 1300 | 36000 | | | | | | |
| PD0005 | 146 | 148 | 2 | 2050 | 38 | 540 | 1 | 2500 | 35000 | | | | | | |
| PD0005 | 148 | 150 | 2 | 5100 | 80 | 560 | 2 | 2600 | 43500 | | | | | | |
| PD0005 | 150 | 151 | 1 | 2900 | 44 | 460 | 2 | 3800 | 43000 | | | | | | |
| PD0005 | 151 | 153 | 2 | 1950 | 20 | 360 | 1 | 5500 | 40000 | | | | | | |
| PD0005 | 153 | 155 | 2 | 8500 | 90 | 1250 | 4 | 4600 | 29500 | | | | | | |
| PD0005 | 155 | 157 | 2 | 3200 | 42 | 1200 | 2 | 3950 | 25000 | | | | | | |
| PD0005 | 157 | 159 | 2 | 1750 | 18 | 510 | 1 | 6500 | 38000 | | | | | | |
| PD0005 | 159 | 161 | 2 | 1350 | 20 | 420 | 1 | 5300 | 35000 | | | | | | |
| PD0005 | 161 | 163 | 2 | 4600 | 55 | 2400 | 3 | 620 | 18000 | | | | | | |
| PD0005 | 163 | 165 | 2 | 13500 | 130 | 6050 | 6 | 190 | 21000 | | | | | | |
| PD0005 | 165 | 167 | 2 | 2050 | 36 | 15500 | 6 | 340 | 16500 | | | | | | |
| PD0005 | 167 | 169 | 2 | 2000 | 48 | 950 | 2 | 620 | 7500 | | | | | | |
| PD0005 | 169 | 174 | 5 | 1250 | 100 | 490 | 1 | 770 | 12500 | | | | | | |
| PD0005 | 174 | 175.5 | 1.5 | 630 | 28 | 260 | 0 | 320 | 6500 | | | | | | |
| PD0005 | 240 | 242 | 2 | 90 | 24 | 330 | 0 | 2450 | 8000 | | | | | | |
| PD0005 | 242 | 244 | 2 | 250 | 26 | 2400 | 1 | 3300 | 12500 | | | | | | |
| PD0005 | 244 | 246 | 2 | 75 | 18 | 95 | 0 | 2450 | 7500 | | | | | | |

**Appendix 5.2 cont.**

| Drill hole | From (m) | To (m) | interval (m) | Zn (ppm) | Cu (ppm) | Pb (ppm) | Ag (ppm) | Mn (ppm) | Fe (ppm) | Au (ppm) | As (ppm) | Hg (ppm) | Sn (ppm) | W (ppm) | Ba (ppm) |
|---|---|---|---|---|---|---|---|---|---|---|---|---|---|---|---|
| PD0006 | 243 | 245 | 2 | 32 | 0 | 34 | 1 | 610 | 8500 | | | | | | |
| PD0006 | 245 | 246.7 | 1.7 | 460 | 8 | 3700 | 3 | 4000 | 12000 | | | | | | |
| PD0006 | 246.7 | 247.35 | 0.65 | 140000 | 930 | 57500 | 60 | 5500 | 190000 | 0.45 | | | | | |
| PD0006 | 247.35 | 249 | 1.65 | 40 | | 10 | 1 | 4050 | 10000 | | | | | | |
| PD0006 | 257 | 257.9 | 0.9 | 110 | 18 | 430 | 1 | 2100 | 8500 | | | | | | |
| PD0006 | 257.9 | 258.45 | 0.55 | 230000 | 2050 | 124000 | 108 | 7100 | 120000 | 0.4 | | | | | |
| PD0006 | 258.45 | 260 | 1.55 | 50 | 4 | 30 | 1 | 4700 | 17500 | | | | | | |
| PD0006 | 260 | 262.3 | 2.3 | 40 | 4 | 20 | 1 | 3400 | 16000 | | | | | | |
| PD0006 | 262.3 | 262.4 | 0.1 | 175000 | 1450 | 170000 | 104 | 27500 | 63000 | | | | | | |
| PD0006 | 262.4 | 266.6 | 4.2 | 70 | 4 | 60 | 1 | 2300 | 8000 | | | | | | |
| PD0006 | 266.6 | 267.23 | 0.63 | 70000 | 690 | 254000 | 124 | 7100 | 150000 | 0.3 | | | | | |
| PD0006 | 267.23 | 269 | 1.77 | 80 | 8 | 50 | 1 | 2700 | 18000 | | | | | | |
| PD0006 | 293 | 294.7 | 1.7 | 48 | 0 | 30 | 1 | 1600 | 9000 | | | | | | |
| PD0006 | 294.7 | 297 | 2.3 | 3100 | 6 | 3600 | 2 | 4000 | 11500 | | | | | | |
| PD0006 | 297 | 299 | 2 | 36 | 2 | 46 | 1 | 620 | 8500 | | | | | | |
| PD0007 | 84 | 86 | 2 | 2100 | 10 | 80 | 0 | 8900 | 53000 | | | | | | |
| PD0007 | 86 | 88 | 2 | 115 | 8 | 36 | 0 | 8100 | 39000 | | | | | | |
| PD0007 | 88 | 90 | 2 | 2500 | 26 | 200 | 0 | 5150 | 20000 | | | | | | |
| PD0007 | 90 | 92 | 2 | 200 | 20 | 34 | 0 | 3950 | 13000 | | | | | | |
| PD0007 | 105 | 106.8 | 1.8 | 480 | 20 | 1700 | 3 | 11000 | 31500 | | | | | | |
| PD0007 | 106.8 | 107.65 | 0.85 | 1400 | 22 | 9300 | 4 | 20000 | 27500 | | | | | | |
| PD0007 | 107.65 | 109 | 1.35 | 340 | 12 | 250 | 1 | 13500 | 32500 | | | | | | |
| PD0007 | 115 | 117 | 2 | 195 | 8 | 28 | 0 | 7600 | 26000 | | | | | | |
| PD0007 | 117 | 118.5 | 1.5 | 1250 | 10 | 30 | 0 | 6500 | 30000 | | | | | | |
| PD0007 | 118.5 | 123 | 4.5 | 230 | 16 | 26 | 0 | 8800 | 26000 | | | | | | |
| PD0007 | 222 | 224.1 | 2.1 | 36 | 4 | 50 | 1 | 5400 | 22000 | | | | | | |
| PD0007 | 224.1 | 225.95 | 1.85 | 1300 | 12 | 13000 | 6 | 3550 | 59000 | | | | | | |
| PD0007 | 225.95 | 228 | 2.05 | 42 | 8 | 155 | 1 | 370 | 13500 | | | | | | |
| PD0007 | 375 | 377 | 2 | 48 | 24 | 28 | 1 | 5200 | 31000 | | | | | | |
| PD0007 | 377 | 379 | 2 | 1600 | 36 | 2000 | 3 | 28000 | 20000 | | | | | | |
| PD0007 | 379 | 381.1 | 2.1 | 65 | 12 | 70 | 1 | 6200 | 22500 | | | | | | |
| PD0007 | 486 | 488 | 2 | 50 | 18 | 70 | 0 | 300 | 15000 | | | | | | |
| PD0007 | 488 | 490 | 2 | 70 | 16 | 1050 | 2 | 1950 | 17500 | | | | | | |
| PD0007 | 490 | 493 | 3 | 38 | 18 | 165 | 0 | 160 | 15000 | | | | | | |

**Appendix 5.2 cont.**

| Drill hole | From (m) | To (m) | interval (m) | Zn (ppm) | Cu (ppm) | Pb (ppm) | Ag (ppm) | Mn (ppm) | Fe (ppm) | Au (ppm) | As (ppm) | Hg (ppm) | Sn (ppm) | W (ppm) | Ba (ppm) |
|---|---|---|---|---|---|---|---|---|---|---|---|---|---|---|---|
| PD0007 | 517 | 519 | 2 | 80 | 12 | 155 | 1 | 2100 | 22500 | | | | | | |
| PD0007 | 519 | 521 | 2 | 3400 | 50 | 3700 | 4 | 18500 | 33000 | | | | | | |
| PD0007 | 521 | 523 | 2 | 80 | 10 | 165 | 1 | 3300 | 20000 | | | | | | |
| PD0008 | 106 | 108 | 2 | 260 | 14 | 60 | 0 | 3200 | 14000 | | | | | | |
| PD0008 | 108 | 109.7 | 1.7 | 1850 | 20 | 1300 | 1 | 7100 | 23000 | | | | | | |
| PD0008 | 109.7 | 112 | 2.3 | 220 | 12 | 44 | 0 | 2450 | 19000 | | | | | | |
| PD0008 | 112 | 114 | 2 | 2500 | 18 | 1100 | 1 | 5900 | 13000 | | | | | | |
| PD0008 | 114 | 115.95 | 1.95 | 200 | 6 | 50 | 0 | 3000 | 9000 | | | | | | |
| PD0008 | 115.95 | 116.05 | 0.1 | 520 | 10 | 190 | 0 | 5200 | 12500 | | | | | | |
| PD0008 | 116.05 | 116.6 | 0.55 | 77000 | 500 | 11500 | 38 | 7500 | 26000 | | | | | | |
| PD0008 | 116.6 | 117.25 | 0.65 | 1650 | 40 | 620 | 1 | 6100 | 22000 | | | | | | |
| PD0008 | 117.25 | 117.45 | 0.2 | 9000 | 70 | 540 | 2 | 4500 | 41000 | 0 | | | | | |
| PD0008 | 117.45 | 117.65 | 0.2 | 11000 | 46 | 1300 | 3 | 5300 | 24000 | 0 | | | | | |
| PD0008 | 117.65 | 117.8 | 0.15 | 17000 | 46 | 4500 | 8 | 5200 | 70000 | 0 | | | | | |
| PD0008 | 117.8 | 120 | 2.2 | 780 | 8 | 130 | 1 | 2300 | 28000 | | | | | | |
| PD0008 | 120 | 122 | 2 | 70 | 6 | 36 | 0 | 1250 | 29000 | | | | | | |
| PD0008 | 122 | 124 | 2 | 150 | 6 | 80 | 0 | 2150 | 17000 | | | | | | |
| PD0008 | 124 | 126 | 2 | 1250 | 12 | 630 | 1 | 6700 | 17000 | | | | | | |
| PD0008 | 126 | 128 | 2 | 160 | 4 | 28 | 0 | 1300 | 6000 | | | | | | |
| PD0008 | 140.4 | 142.7 | 2.3 | 470 | 4 | 350 | 0 | 2800 | 4000 | | | | | | |
| PD0008 | 142.7 | 144.15 | 1.45 | 8500 | 32 | 510 | 1 | 6100 | 13000 | 0 | | | | | |
| PD0008 | 144.15 | 144.3 | 0.15 | 30000 | 190 | 13000 | 13 | 50000 | 56000 | 0 | | | | | |
| PD0008 | 144.3 | 146 | 1.7 | 680 | 6 | 350 | 1 | 11000 | 11500 | | | | | | |
| PD0008 | 146 | 148 | 2 | 990 | 4 | 390 | 1 | 11000 | 8000 | | | | | | |
| PD0008 | 148 | 150 | 2 | 2500 | 10 | 700 | 1 | 9300 | 9000 | | | | | | |
| PD0008 | 150 | 151.6 | 1.6 | 23000 | 70 | 4600 | 7 | 12000 | 22000 | | | | | | |
| PD0008 | 151.6 | 154 | 2.4 | 1300 | 6 | 430 | 0 | 3700 | 12000 | | | | | | |
| PD0008 | 154 | 156 | 2 | 300 | 6 | 80 | 0 | 1500 | 9000 | | | | | | |
| PD0008 | 160 | 161.1 | 1.1 | 38 | 0 | 40 | 0 | 1500 | 4000 | | | | | | |
| PD0008 | 161.1 | 163 | 1.9 | 3200 | 40 | 470 | 0 | 5900 | 13500 | | | | | | |
| PD0008 | 163 | 165 | 2 | 1400 | 10 | 830 | 2 | 6800 | 20000 | | | | | | |
| PD0008 | 165 | 166.3 | 1.3 | 195 | 8 | 80 | 0 | 3050 | 17000 | | | | | | |
| PD0008 | 170 | 172 | 2 | 830 | 8 | 390 | 1 | 3000 | 19000 | | | | | | |
| PD0008 | 172 | 174.5 | 2.5 | 4300 | 28 | 3400 | 4 | 3900 | 25000 | | | | | | |

**Appendix 5.2 cont.**

| Drill hole | From (m) | To (m) | interval (m) | Zn (ppm) | Cu (ppm) | Pb (ppm) | Ag (ppm) | Mn (ppm) | Fe (ppm) | Au (ppm) | As (ppm) | Hg (ppm) | Sn (ppm) | W (ppm) | Ba (ppm) |
|---|---|---|---|---|---|---|---|---|---|---|---|---|---|---|---|
| PD0008 | 174.5 | 176.5 | 2 | 5500 | 10 | 2800 | 4 | 13500 | 22000 | | | | | | |
| PD0008 | 176.5 | 178.25 | 1.75 | 1100 | 4 | 690 | 1 | 8700 | 13500 | | | | | | |
| PD0008 | 178.25 | 180 | 1.75 | 2700 | 8 | 2900 | 1 | 8600 | 13000 | | | | | | |
| PD0008 | 180 | 182 | 2 | 2800 | 10 | 2000 | 2 | 3550 | 11500 | | | | | | |
| PD0008 | 182 | 182.45 | 0.45 | 9900 | 6 | 2200 | 3 | 1580 | 11000 | | | | | | |
| PD0008 | 182.45 | 182.9 | 0.45 | 28000 | 60 | 9000 | 14 | 19000 | 45000 | | | | | | |
| PD0008 | 182.9 | 185 | 2.1 | 940 | 6 | 490 | 2 | 7000 | 27000 | | | | | | |
| PD0008 | 185 | 187 | 2 | 110 | | 80 | 1 | 3000 | 10000 | | | | | | |
| PD0008 | 187 | 188.5 | 1.5 | 5000 | 20 | 1250 | 7 | 4700 | 24000 | | | | | | |
| PD0008 | 188.5 | 190.25 | 1.75 | 130 | 6 | 70 | 1 | 1600 | 10000 | | | | | | |
| PD0008 | 190.25 | 192.75 | 2.5 | 23000 | 70 | 11000 | 15 | 1350 | 29000 | | | | | | |
| PD0008 | 192.75 | 195 | 2.25 | 4600 | 18 | 1600 | 2 | 5900 | 17000 | | | | | | |
| PD0008 | 195 | 197.2 | 2.2 | 2800 | 4 | 860 | 2 | 22500 | 12500 | | | | | | |
| PD0008 | 197.2 | 199.2 | 2 | 2600 | 18 | 1400 | 3 | 3850 | 74000 | | | | | | |
| PD0008 | 199.2 | 201.2 | 2 | 1000 | 22 | 530 | 2 | 2000 | 80000 | | | | | | |
| PD0008 | 201.2 | 203.2 | 2 | 660 | 38 | 110 | 1 | 2500 | 70000 | | | | | | |
| PD0008 | 205.6 | 207 | 1.4 | 360 | 70 | 60 | 1 | 2300 | 67000 | | | | | | |
| PD0008 | 207 | 209 | 2 | 4500 | 36 | 3700 | 11 | 7500 | 110000 | | | | | | |
| PD0008 | 209 | 211.5 | 2.5 | 2800 | 18 | 850 | 3 | 3600 | 80000 | | | | | | |
| PD0008 | 211.5 | 214.2 | 2.7 | 2000 | 30 | 550 | 3 | 5900 | 91000 | | | | | | |
| PD0008 | 214.2 | 215.2 | 1 | 34 | 2 | 16 | 0 | 1100 | 13000 | | | | | | |
| PD0008 | 215.2 | 217.2 | 2 | 70 | 6 | 40 | 0 | 3150 | 15500 | | | | | | |
| PD0008 | 217.2 | 219.6 | 2.4 | 1200 | 8 | 640 | 1 | 30000 | 8000 | | | | | | |
| PD0008 | 219.6 | 220.6 | 1 | 13000 | 48 | 6200 | 7 | 21000 | 28000 | | | | | | |
| PD0008 | 220.6 | 222.6 | 2 | 5000 | 50 | 2300 | 8 | 13000 | 76000 | | | | | | |
| PD0008 | 222.6 | 223.45 | 0.85 | 6700 | 50 | 2600 | 7 | 5500 | 18000 | | | | | | |
| PD0008 | 223.45 | 223.75 | 0.3 | 73000 | 180 | 48000 | 115 | 14000 | 59000 | 0 | | | | | |
| PD0008 | 223.75 | 224.2 | 0.45 | 120000 | 160 | 46000 | 215 | 18000 | 64000 | 0.1 | | | | | |
| PD0008 | 224.2 | 224.95 | 0.75 | 11000 | 32 | 5800 | 20 | 17500 | 20000 | 0 | | | | | |
| PD0008 | 224.95 | 225.15 | 0.2 | 90000 | 160 | 49000 | 90 | 15500 | 47000 | 0.1 | | | | | |
| PD0008 | 225.15 | 225.7 | 0.55 | 385000 | 700 | 133000 | 180 | 6500 | 75000 | | | | | | |
| PD0008 | 225.7 | 227 | 1.3 | 18000 | 38 | 11000 | 12 | 14000 | 14000 | | | | | | |
| PD0008 | 227 | 228.8 | 1.8 | 14000 | 60 | 8900 | 14 | 30000 | 16000 | | | | | | |
| PD0008 | 228.8 | 231.2 | 2.4 | 13000 | 50 | 12500 | 16 | 31000 | 16000 | | | | | | |

**Appendix 5.2 cont.**

| Drill hole | From (m) | To (m) | interval (m) | Zn (ppm) | Cu (ppm) | Pb (ppm) | Ag (ppm) | Mn (ppm) | Fe (ppm) | Au (ppm) | As (ppm) | Hg (ppm) | Sn (ppm) | W (ppm) | Ba (ppm) |
|---|---|---|---|---|---|---|---|---|---|---|---|---|---|---|---|
| PD0008 | 231.2 | 231.3 | 0.1 | 3100 | 34 | 1800 | 3 | 19000 | 12000 | | | | | | |
| PD0008 | 231.3 | 232.95 | 1.65 | 3400 | 30 | 1400 | 4 | 35000 | 11500 | | | | | | |
| PD0008 | 232.95 | 233.45 | 0.5 | 150000 | 1400 | 101000 | 185 | 10000 | 160000 | 0.1 | | | | | |
| PD0008 | 233.45 | 235 | 1.55 | 20000 | 370 | 35000 | 17 | 5700 | 12000 | 0 | | | | | |
| PD0008 | 235 | 235.45 | 0.45 | 56000 | 1500 | 222000 | 140 | 23000 | 57000 | | | | | | |
| PD0008 | 235.45 | 235.85 | 0.4 | 9000 | 230 | 11000 | 16 | 14000 | 21000 | 0 | | | | | |
| PD0008 | 235.85 | 236.3 | 0.45 | 87000 | 1300 | 78500 | 78 | 11500 | 55000 | 0 | | | | | |
| PD0008 | 236.3 | 238.3 | 2 | 17000 | 90 | 11000 | 20 | 1200 | 34000 | | | | | | |
| PD0008 | 238.3 | 240.3 | 2 | 4200 | 50 | 1550 | 5 | 4000 | 28000 | | | | | | |
| PD0008 | 240.3 | 242.3 | 2 | 7800 | 55 | 2300 | 7 | 2700 | 24000 | | | | | | |
| PD0008 | 242.3 | 244.6 | 2.3 | 410 | 14 | 140 | 1 | 8400 | 16000 | | | | | | |
| PD0008 | 244.6 | 247.9 | 3.3 | 4700 | 24 | 1600 | 6 | 17000 | 80000 | | | | | | |
| PD0008 | 247.9 | 248.7 | 0.8 | 4300 | 16 | 830 | 2 | 2900 | 23000 | | | | | | |
| PD0008 | 248.7 | 250.7 | 2 | 9000 | 44 | 6600 | 10 | 16500 | 58000 | | | | | | |
| PD0008 | 250.7 | 252.7 | 2 | 3700 | 28 | 3000 | 5 | 12000 | 52000 | | | | | | |
| PD0008 | 252.7 | 254.7 | 2 | 2100 | 24 | 980 | 3 | 9400 | 60000 | | | | | | |
| PD0008 | 254.7 | 256.7 | 2 | 3900 | 26 | 1200 | 5 | 14000 | 79000 | | | | | | |
| PD0008 | 256.7 | 258.6 | 1.9 | 4100 | 28 | 1600 | 3 | 15500 | 63000 | | | | | | |
| PD0008 | 258.6 | 261 | 2.4 | 5300 | 24 | 3900 | 6 | 72000 | 17000 | | | | | | |
| PD0008 | 261 | 263 | 2 | 10000 | 20 | 5050 | 9 | 42000 | 22000 | | | | | | |
| PD0008 | 263 | 265 | 2 | 2100 | 30 | 3100 | 3 | 42000 | 18000 | | | | | | |
| PD0008 | 265 | 267 | 2 | 7900 | 28 | 4700 | 7 | 45000 | 14000 | | | | | | |
| PD0008 | 267 | 269 | 2 | 14500 | 46 | 7100 | 21 | 54000 | 15000 | | | | | | |
| PD0008 | 269 | 271.7 | 2.7 | 17000 | 70 | 9400 | 33 | 53000 | 22000 | | | | | | |
| PD0008 | 271.7 | 272.1 | 0.4 | 7100 | 28 | 2400 | 8 | 1600 | 9000 | | | | | | |
| PD0008 | 272.1 | 273.8 | 1.7 | 17000 | 60 | 10000 | 39 | 43000 | 27000 | | | | | | |
| PD0008 | 273.8 | 276.5 | 2.7 | 490 | 16 | 290 | 1 | 2800 | 35000 | | | | | | |
| PD0008 | 276.5 | 278.2 | 1.7 | 4800 | 26 | 1800 | 5 | 24000 | 34000 | | | | | | |
| PD0008 | 278.2 | 280.2 | 2 | 11000 | 34 | 5100 | 9 | 95000 | 25000 | | | | | | |
| PD0008 | 280.2 | 282.2 | 2 | 13500 | 28 | 8400 | 16 | 150000 | 35000 | | | | | | |
| PD0008 | 282.2 | 284.2 | 2 | 120 | 12 | 60 | 1 | 16000 | 27000 | | | | | | |
| PD0008 | 284.2 | 286.2 | 2 | 1400 | 14 | 1400 | 2 | 34000 | 20000 | | | | | | |
| PD0008 | 286.2 | 288.2 | 2 | 18500 | 40 | 8000 | 15 | 76000 | 23000 | | | | | | |
| PD0008 | 288.2 | 290.2 | 2 | 11000 | 30 | 6600 | 19 | 71000 | 36000 | | | | | | |

**Appendix 5.2 cont.**

| Drill hole | From (m) | To (m) | interval (m) | Zn (ppm) | Cu (ppm) | Pb (ppm) | Ag (ppm) | Mn (ppm) | Fe (ppm) | Au (ppm) | As (ppm) | Hg (ppm) | Sn (ppm) | W (ppm) | Ba (ppm) |
|---|---|---|---|---|---|---|---|---|---|---|---|---|---|---|---|
| PD0008 | 290.2 | 292.2 | 2 | 10500 | 28 | 3400 | 14 | 92000 | 43000 | | | | | | |
| PD0008 | 292.2 | 294.2 | 2 | 9100 | 16 | 3100 | 8 | 54000 | 25000 | | | | | | |
| PD0008 | 294.2 | 296.4 | 2.2 | 1400 | 8 | 700 | 2 | 17500 | 12500 | | | | | | |
| PD0008 | 296.4 | 298.1 | 1.7 | 690 | 8 | 190 | 0 | 3500 | 24000 | | | | | | |
| PD0008 | 298.1 | 300.1 | 2 | 3200 | 8 | 1200 | 2 | 8700 | 10000 | | | | | | |
| PD0008 | 300.1 | 302.1 | 2 | 1900 | 6 | 180 | 0 | 3800 | 6500 | | | | | | |
| PD0008 | 302.1 | 304.1 | 2 | 4500 | 10 | 1400 | 6 | 10000 | 9000 | | | | | | |
| PD0008 | 304.1 | 306.1 | 2 | 165 | 4 | 100 | 0 | 2200 | 5000 | | | | | | |
| PD0008 | 306.1 | 308.3 | 2.2 | 490 | 4 | 320 | 0 | 8000 | 5000 | | | | | | |
| PD0008 | 308.3 | 308.95 | 0.65 | 1050 | 8 | 620 | 2 | 9000 | 11000 | | | | | | |
| PD0008 | 308.95 | 310.1 | 1.15 | 34000 | 65 | 12000 | 19 | 10000 | 63000 | | | | | | |
| PD0008 | 310.1 | 311.2 | 1.1 | 3000 | 10 | 1400 | 4 | 24000 | 17000 | | | | | | |
| PD0008 | 311.2 | 312.8 | 1.6 | 21000 | 28 | 4300 | 19 | 50000 | 44000 | | | | | | |
| PD0008 | 312.8 | 313.7 | 0.9 | 8900 | 18 | 3000 | 6 | 42000 | 22000 | | | | | | |
| PD0008 | 313.7 | 316 | 2.3 | 4100 | 12 | 1900 | 7 | 7400 | 25000 | | | | | | |
| PD0008 | 316 | 316.9 | 0.9 | 3700 | 10 | 2600 | 38 | 1550 | 24000 | | | | | | |
| PD0008 | 316.9 | 317.35 | 0.45 | 49000 | 130 | 38000 | 26 | 12500 | 74000 | | | | | | |
| PD0008 | 317.35 | 319.4 | 2.05 | 10500 | 24 | 4400 | 6 | 18500 | 34000 | | | | | | |
| PD0008 | 319.4 | 321.6 | 2.2 | 3000 | 10 | 1000 | 2 | 12500 | 13000 | | | | | | |
| PD0008 | 321.6 | 323.6 | 2 | 9000 | 28 | 3300 | 16 | 9400 | 56000 | | | | | | |
| PD0008 | 323.6 | 325.6 | 2 | 11000 | 50 | 4400 | 21 | 4300 | 53000 | | | | | | |
| PD0008 | 325.6 | 328.05 | 2.45 | 13000 | 42 | 3200 | 11 | 4400 | 38500 | | | | | | |
| PD0008 | 328.05 | 328.55 | 0.5 | 8100 | 38 | 3800 | 9 | 1950 | 20000 | | | | | | |
| PD0008 | 328.55 | 331.2 | 2.65 | 19000 | 60 | 3700 | 15 | 1800 | 45000 | | | | | | |
| PD0008 | 331.2 | 333.2 | 2 | 5600 | 24 | 1200 | 14 | 2400 | 35000 | | | | | | |
| PD0008 | 333.2 | 335.2 | 2 | 11000 | 46 | 2700 | 9 | 7100 | 37000 | | | | | | |
| PD0008 | 335.2 | 336.9 | 1.7 | 11000 | 38 | 2400 | 6 | 13500 | 30000 | | | | | | |
| PD0008 | 336.9 | 339.2 | 2.3 | 2300 | 14 | 1600 | 6 | 16000 | 20000 | | | | | | |
| PD0008 | 339.2 | 341.8 | 2.6 | 3600 | 22 | 4300 | 7 | 6100 | 27000 | | | | | | |
| PD0008 | 341.8 | 342.5 | 0.7 | 6100 | 30 | 6900 | 9 | 15500 | 73000 | | | | | | |
| PD0008 | 342.5 | 344.4 | 1.9 | 1850 | 22 | 7600 | 4 | 5300 | 26000 | | | | | | |
| PD0008 | 344.4 | 345.5 | 1.1 | 1650 | 10 | 2100 | 1 | 26000 | 14000 | | | | | | |
| PD0008 | 345.5 | 346.5 | 1 | 11000 | 38 | 9200 | 9 | 8500 | 54000 | | | | | | |
| PD0008 | 346.5 | 348.1 | 1.6 | 5100 | 10 | 3400 | 2 | 16000 | 18000 | | | | | | |

**Appendix 5.2 cont.**

| Drill hole | From (m) | To (m) | interval (m) | Zn (ppm) | Cu (ppm) | Pb (ppm) | Ag (ppm) | Mn (ppm) | Fe (ppm) | Au (ppm) | As (ppm) | Hg (ppm) | Sn (ppm) | W (ppm) | Ba (ppm) |
|---|---|---|---|---|---|---|---|---|---|---|---|---|---|---|---|
| PD0008 | 348.1 | 350 | 1.9 | 5100 | 16 | 5700 | 3 | 17000 | 16000 | | | | | | |
| PD0008 | 350 | 352 | 2 | 2400 | 8 | 1500 | 3 | 22000 | 29000 | | | | | | |
| PD0008 | 352 | 353.4 | 1.4 | 1200 | 6 | 2600 | 3 | 10500 | 13000 | | | | | | |
| PD0008 | 353.4 | 354.7 | 1.3 | 10500 | 38 | 8100 | 9 | 6800 | 40000 | | | | | | |
| PD0008 | 354.7 | 356.7 | 2 | 210 | 4 | 260 | 0 | 3400 | 6000 | | | | | | |
| PD0008 | 356.7 | 358.2 | 1.5 | 500 | 4 | 370 | 0 | 6100 | 6000 | | | | | | |
| PD0008 | 358.2 | 360.9 | 2.7 | 560 | 4 | 1300 | 0 | 16500 | 18000 | | | | | | |
| PD0008 | 360.9 | 363 | 2.1 | 6100 | 16 | 4400 | 5 | 25000 | 35000 | | | | | | |
| PD0008 | 363 | 365 | 2 | 3000 | 10 | 4900 | 5 | 34000 | 38000 | | | | | | |
| PD0008 | 365 | 367 | 2 | 5800 | 12 | 2300 | 6 | 35000 | 36000 | | | | | | |
| PD0008 | 367 | 369 | 2 | 2100 | 8 | 2900 | 2 | 36000 | 19500 | | | | | | |
| PD0008 | 369 | 371 | 2 | 7600 | 10 | 8300 | 5 | 37000 | 35000 | | | | | | |
| PD0008 | 371 | 373 | 2 | 7400 | 10 | 3900 | 5 | 38000 | 33000 | | | | | | |
| PD0008 | 373 | 375.9 | 2.9 | 16000 | 20 | 11000 | 8 | 41000 | 48000 | | | | | | |
| PD0008 | 375.9 | 376.5 | 0.6 | 5000 | 8 | 1700 | 1 | 8100 | 36000 | | | | | | |
| PD0008 | 376.5 | 378.5 | 2 | 5500 | 20 | 2900 | 2 | 8600 | 34000 | | | | | | |
| PD0008 | 378.5 | 380.5 | 2 | 4100 | 30 | 4000 | 2 | 9000 | 25000 | | | | | | |
| PD0008 | 380.5 | 382.5 | 2 | 3700 | 20 | 3600 | 2 | 3600 | 18000 | | | | | | |
| PD0008 | 382.5 | 384.55 | 2.05 | 2300 | 8 | 1800 | 2 | 29000 | 16000 | | | | | | |
| PD0008 | 384.55 | 384.95 | 0.4 | 86000 | 65 | 25000 | 11 | 27000 | 43000 | | | | | | |
| PD0008 | 384.95 | 385.75 | 0.8 | 11000 | 16 | 5900 | 4 | 30000 | 24000 | | | | | | |
| PD0008 | 385.75 | 388.2 | 2.45 | 470 | 6 | 460 | 0 | 1100 | 4000 | | | | | | |
| PD0008 | 388.2 | 391.2 | 3 | 1100 | 8 | 1300 | 0 | 970 | 5000 | | | | | | |
| PD0009 | 130 | 132.1 | 2.1 | 750 | 48 | 430 | 1 | 220 | 6350 | | | | | | |
| PD0009 | 132.1 | 133.75 | 1.65 | 54000 | 910 | 5600 | 28 | 290 | 42000 | | | | | | |
| PD0009 | 132.1 | 133.75 | 1.65 | 54000 | 910 | 5600 | 28 | 290 | 42000 | | | | | | |
| PD0009 | 133.75 | 134.6 | 0.85 | 2400 | 65 | 830 | 1 | 900 | 11700 | | | | | | |
| PD0009 | 134.6 | 135.3 | 0.7 | 520 | 100 | 1000 | 0 | 165 | 8300 | | | | | | |
| PD0009 | 135.3 | 138 | 2.7 | 2100 | 48 | 120 | 0 | 2800 | 38000 | | | | | | |
| PD0009 | 138 | 140.5 | 2.5 | 2000 | 8 | 42 | 0 | 5550 | 24000 | | | | | | |
| PD0009 | 140.5 | 142.5 | 2 | 820 | 65 | 44 | 0 | 1100 | 49000 | | | | | | |
| PD0009 | 143.7 | 144.3 | 0.6 | 2900 | 55 | 560 | 0 | 2850 | 21000 | | | | | | |
| PD0009 | 144.3 | 145 | 0.7 | 370 | 8 | 60 | 0 | 860 | 11200 | | | | | | |
| PD0009 | 145 | 147.5 | 2.5 | 2000 | 10 | 170 | 0 | 6950 | 21500 | | | | | | |

**Appendix 5.2 cont.**

| Drill hole | From (m) | To (m) | interval (m) | Zn (ppm) | Cu (ppm) | Pb (ppm) | Ag (ppm) | Mn (ppm) | Fe (ppm) | Au (ppm) | As (ppm) | Hg (ppm) | Sn (ppm) | W (ppm) | Ba (ppm) |
|---|---|---|---|---|---|---|---|---|---|---|---|---|---|---|---|
| PD0009 | 147.5 | 148.8 | 1.3 | 790 | 10 | 90 | 0 | 4500 | 49500 | | | | | | |
| PD0009 | 148.8 | 151.9 | 3.1 | 1000 | 12 | 38 | 0 | 3900 | 50500 | | | | | | |
| PD0009 | 151.9 | 154 | 2.1 | 1200 | 8 | 50 | 0 | 5900 | 39500 | | | | | | |
| PD0009 | 154 | 156 | 2 | 500 | 6 | 32 | 0 | 1600 | 40000 | | | | | | |
| PD0009 | 170 | 172 | 2 | 500 | 8 | 760 | 0 | 2650 | 14300 | | | | | | |
| PD0009 | 172 | 174.6 | 2.6 | 2300 | 6 | 22 | 0 | 9650 | 40500 | | | | | | |
| PD0009 | 174.6 | 177.7 | 3.1 | 2500 | 4 | 75 | 0 | 15500 | 60500 | | | | | | |
| PD0009 | 177.7 | 179 | 1.3 | 700 | 4 | 22 | 0 | 5250 | 33500 | | | | | | |
| PD0009 | 189 | 191 | 2 | 28 | 6 | 20 | 0 | 1750 | 18100 | | | | | | |
| PD0009 | 191 | 193 | 2 | 1100 | 16 | 280 | 140 | 1200 | 27500 | | | | | | |
| PD0009 | 193 | 195 | 2 | 160 | 7 | 65 | 4 | 640 | 15900 | | | | | | |
| PD0009 | 230.25 | 231 | 0.75 | 145 | 5 | 85 | 0 | 2150 | 9950 | | | | | | |
| PD0009 | 231 | 231.4 | 0.4 | 13000 | 120 | 8950 | 5 | 5950 | 13700 | | | | | | |
| PD0009 | 231.4 | 232 | 0.6 | 2650 | 16 | 330 | 2 | 3850 | 43000 | | | | | | |
| PD0009 | 232 | 234 | 2 | 100 | 12 | 48 | 1 | 1450 | 27500 | | | | | | |
| PD0009 | 272.1 | 273.6 | 1.5 | 14 | 0 | 12 | 0 | 2000 | 19000 | | | | | | |
| PD0009 | 273.6 | 274 | 0.4 | 2600 | 18 | 490 | 0 | 7500 | 55000 | | | | | | |
| PD0009 | 274 | 276 | 2 | 910 | 26 | 460 | 3 | 2100 | 105000 | | | | | | |
| PD0010 | 35.6 | 37.9 | 2.3 | 145 | 26 | 430 | 0 | 46 | 5450 | | | | | | |
| PD0010 | 162.4 | 163.45 | 1.05 | 660 | 0 | 195 | 0 | 710 | 28000 | | | | | | |
| PD0010 | 163.45 | 163.58 | 0.13 | 400000 | 6950 | 37500 | 115 | 2800 | 55500 | | | | | | |
| PD0010 | 163.45 | 163.58 | 0.13 | 400000 | 6950 | 37500 | 115 | 2800 | 55500 | | | | | | |
| PD0010 | 163.58 | 165.6 | 2.02 | 290 | 26 | 610 | 2 | 1350 | 41000 | | | | | | |
| PD0010 | 163.58 | 165.6 | 2.02 | 920 | 26 | 610 | 2 | 1350 | 41000 | | | | | | |
| PD0010 | 165.6 | 167.6 | 2 | 820 | 105 | 6300 | 4 | 1150 | 24000 | | | | | | |
| PD0010 | 165.6 | 167.6 | 2 | 820 | 105 | 6300 | 4 | 1150 | 24000 | | | | | | |
| PD0010 | 167.6 | 169 | 1.4 | 810 | 70 | 6350 | 7 | 1900 | 31500 | | | | | | |
| PD0010 | 167.6 | 169 | 1.4 | 810 | 70 | 6350 | 7 | 1900 | 31500 | | | | | | |
| PD0010 | 169 | 171.07 | 2.07 | 920 | 120 | 6900 | 6 | 2500 | 17800 | | | | | | |
| PD0010 | 169 | 171.07 | 2.07 | 920 | 120 | 6900 | 6 | 2500 | 17800 | | | | | | |
| PD0010 | 171.07 | 172.07 | 1 | 32000 | 390 | 23500 | 12 | 2150 | 17500 | | | | | | |
| PD0010 | 171.07 | 172.07 | 1 | 32000 | 390 | 23500 | 12 | 2150 | 17500 | | | | | | |
| PD0010 | 172.07 | 174 | 1.93 | 610 | 105 | 6150 | 9 | 1350 | 26000 | | | | | | |
| PD0010 | 172.07 | 174 | 1.93 | 610 | 105 | 6150 | 9 | 1350 | 26000 | | | | | | |

**Appendix 5.2 cont.**

| Drill hole | From (m) | To (m) | interval (m) | Zn (ppm) | Cu (ppm) | Pb (ppm) | Ag (ppm) | Mn (ppm) | Fe (ppm) | Au (ppm) | As (ppm) | Hg (ppm) | Sn (ppm) | W (ppm) | Ba (ppm) |
|---|---|---|---|---|---|---|---|---|---|---|---|---|---|---|---|
| PD0010 | 174 | 176 | 2 | 490 | 75 | 3550 | 6 | 1300 | 23000 | | | | | | |
| PD0010 | 174 | 176 | 2 | 490 | 75 | 3550 | 6 | 1300 | 23000 | | | | | | |
| PD0010 | 176 | 177.11 | 1.11 | 2350 | 16 | 2000 | 4 | 2250 | 23000 | | | | | | |
| PD0010 | 176 | 177.11 | 1.11 | 2350 | 16 | 2000 | 4 | 2250 | 23000 | | | | | | |
| PD0010 | 177.11 | 177.76 | 0.65 | 68000 | 720 | 27500 | 24 | 3000 | 41000 | | | | | | |
| PD0010 | 177.11 | 177.76 | 0.65 | 68000 | 720 | 27500 | 24 | 3000 | 41000 | | | | | | |
| PD0010 | 177.76 | 180 | 2.24 | 9500 | 75 | 6650 | 7 | 3050 | 29000 | | | | | | |
| PD0010 | 177.76 | 180 | 2.24 | 9500 | 75 | 6650 | 7 | 3050 | 29000 | | | | | | |
| PD0010 | 180 | 182 | 2 | 520 | 2 | 460 | 0 | 1500 | 8150 | | | | | | |
| PD0010 | 180 | 182 | 2 | 520 | 2 | 460 | 1 | 1500 | 8150 | | | | | | |
| PD0010 | 182 | 184 | 2 | 4550 | 18 | 3100 | 3 | 3200 | 23000 | | | | | | |
| PD0010 | 182 | 184 | 2 | 4550 | 18 | 3100 | 3 | 3200 | 23000 | | | | | | |
| PD0010 | 184 | 186 | 2 | 4150 | 26 | 9500 | 5 | 2800 | 16600 | | | | | | |
| PD0010 | 184 | 186 | 2 | 4150 | 26 | 9500 | 5 | 2800 | 16600 | | | | | | |
| PD0010 | 186 | 188 | 2 | 670 | 7 | 470 | 0 | 940 | 8150 | | | | | | |
| PD0010 | 192 | 194 | 2 | 210 | 0 | 115 | 0 | 2100 | 9700 | | | | | | |
| PD0010 | 194 | 196 | 2 | 1800 | 16 | 3850 | 2 | 770 | 28000 | | | | | | |
| PD0010 | 194 | 196 | 2 | 1800 | 16 | 3850 | 2 | 70 | 28000 | | | | | | |
| PD0010 | 196 | 198 | 2 | 5700 | 26 | 8650 | 7 | 490 | 39500 | | | | | | |
| PD0010 | 196 | 198 | 2 | 5700 | 26 | 8650 | 7 | 490 | 39500 | | | | | | |
| PD0010 | 198 | 200 | 2 | 16500 | 14 | 5050 | 6 | 700 | 18300 | | | | | | |
| PD0010 | 198 | 200 | 2 | 16500 | 14 | 5050 | 6 | 700 | 18300 | | | | | | |
| PD0010 | 200 | 200.8 | 0.8 | 9050 | 5 | 5200 | 4 | 3150 | 37000 | | | | | | |
| PD0010 | 200 | 200.8 | 0.8 | 9050 | 5 | 5200 | 4 | 3150 | 37000 | | | | | | |
| PD0010 | 200.8 | 203 | 2.2 | 200 | 2 | 470 | 1 | 1500 | 5450 | | | | | | |
| PD0010 | 203 | 205 | 2 | 100 | 0 | 1950 | 2 | 1250 | 7650 | | | | | | |
| PD0010 | 205 | 207 | 2 | 70 | 0 | 1450 | 2 | 1150 | 6400 | | | | | | |
| PD0010 | 207 | 208.2 | 1.2 | 400 | 0 | 1450 | 1 | 2450 | 6250 | | | | | | |
| PD0010 | 208.2 | 210 | 1.8 | 195 | 0 | 1050 | 2 | 940 | 7350 | | | | | | |
| PD0010 | 210 | 212 | 2 | 970 | 2 | 140 | 0 | 1250 | 9350 | | | | | | |
| PD0010 | 218 | 220 | 2 | 400 | 0 | 520 | 1 | 1450 | 10900 | | | | | | |
| PD0010 | 220 | 222 | 2 | 540 | 5 | 1700 | 2 | 1800 | 10600 | | | | | | |
| PD0010 | 222 | 224 | 2 | 170 | 2 | 240 | 0 | 1250 | 7750 | | | | | | |
| PD0010 | 224 | 226 | 2 | 890 | 0 | 810 | 1 | 1150 | 11300 | | | | | | |

**Appendix 5.2 cont.**

| Drill hole | From (m) | To (m) | interval (m) | Zn (ppm) | Cu (ppm) | Pb (ppm) | Ag (ppm) | Mn (ppm) | Fe (ppm) | Au (ppm) | As (ppm) | Hg (ppm) | Sn (ppm) | W (ppm) | Ba (ppm) |
|---|---|---|---|---|---|---|---|---|---|---|---|---|---|---|---|
| PD0010 | 226 | 227.3 | 1.3 | 1000 | 7 | 2150 | 2 | 1600 | 14300 | | | | | | |
| PD0010 | 227.3 | 229 | 1.7 | 1550 | 7 | 810 | 1 | 2350 | 16500 | | | | | | |
| PD0010 | 229 | 231.5 | 2.5 | 320 | 2 | 165 | 1 | 3250 | 4700 | | | | | | |
| PD0010 | 231.5 | 233 | 1.5 | 2000 | 28 | 5400 | 1 | 2400 | 35000 | | | | | | |
| PD0010 | 231.5 | 233 | 1.5 | 2000 | 28 | 5400 | 1 | 2400 | 35000 | | | | | | |
| PD0010 | 233 | 235 | 2 | 15500 | 85 | 3050 | 4 | 2450 | 20500 | | | | | | |
| PD0010 | 233 | 235 | 2 | 15500 | 85 | 3050 | 4 | 2450 | 20500 | | | | | | |
| PD0010 | 235 | 237 | 2 | 410 | 0 | 145 | 1 | 950 | 2750 | | | | | | |
| PD0010 | 235 | 237 | 2 | 410 | 0 | 140 | 1 | 950 | 2750 | | | | | | |
| PD0010 | 237 | 239 | 2 | 23000 | 120 | 2350 | 2 | 980 | 20500 | | | | | | |
| PD0010 | 237 | 239 | 2 | 23000 | 120 | 2350 | 2 | 980 | 20500 | | | | | | |
| PD0010 | 239 | 241 | 2 | 320 | 0 | 25 | 1 | 1950 | 2000 | | | | | | |
| PD0010 | 247 | 249 | 2 | 550 | 5 | 550 | 1 | 510 | 6650 | | | | | | |
| PD0010 | 249 | 251 | 2 | 9050 | 38 | 12900 | 4 | 2000 | 16000 | | | | | | |
| PD0010 | 249 | 251 | 2 | 9050 | 38 | 12900 | 4 | 2000 | 16000 | | | | | | |
| PD0010 | 251 | 253.3 | 2.3 | 1400 | 6 | 540 | 1 | 790 | 76000 | | | | | | |
| PD0010 | 251 | 253.3 | 2.3 | 1400 | 6 | 540 | 1 | 790 | 7600 | | | | | | |
| PD0010 | 253.3 | 253.66 | 0.36 | 14000 | 50 | 12800 | 8 | 930 | 20500 | | | | | | |
| PD0010 | 253.3 | 253.66 | 0.36 | 14000 | 50 | 12800 | 8 | 930 | 20500 | | | | | | |
| PD0010 | 253.66 | 255.05 | 1.39 | 1300 | 4 | 690 | 1 | 1200 | 16200 | | | | | | |
| PD0010 | 255.05 | 257.9 | 2.85 | 3750 | 10 | 4000 | 6 | 590 | 35000 | | | | | | |
| PD0010 | 257.9 | 259.9 | 2 | 1600 | 4 | 1700 | 2 | 530 | 28000 | | | | | | |
| PD0010 | 259.9 | 261.7 | 1.8 | 970 | 3 | 300 | 1 | 550 | 46500 | | | | | | |
| PD0010 | 261.7 | 264.2 | 2.5 | 95 | 0 | 70 | 0 | 3300 | 34000 | | | | | | |
| PD0010 | 264.2 | 267 | 2.8 | 3300 | 12 | 880 | 2 | 540 | 63000 | | | | | | |
| PD0010 | 267 | 268.35 | 1.35 | 240 | 2 | 150 | 0 | 3350 | 10700 | | | | | | |
| PD0010 | 270 | 272 | 2 | 155 | 0 | 24 | 0 | 1350 | 32500 | | | | | | |
| PD0010 | 272 | 274.4 | 2.4 | 2250 | 3 | 650 | 3 | 770 | 19000 | | | | | | |
| PD0010 | 274.4 | 276.05 | 1.65 | 6300 | 5 | 5900 | 5 | 2600 | 32500 | | | | | | |
| PD0010 | 274.4 | 276.05 | 1.65 | 6300 | 5 | 5900 | 5 | 2600 | 32500 | | | | | | |
| PD0010 | 276.05 | 278.6 | 2.55 | 410 | 2 | 130 | 1 | 480 | 15600 | | | | | | |
| PD0010 | 278.6 | 279.25 | 0.65 | 250 | | 120 | 2 | 2800 | 23000 | | | | | | |
| PD0010 | 279.25 | 279.8 | 0.55 | 73000 | 85 | 520 | 38 | 1150 | 70500 | | | | | | |
| PD0010 | 279.25 | 279.8 | 0.55 | 73000 | 85 | 520 | 38 | 1150 | 70500 | | | | | | |

**Appendix 5.2 cont.**

| Drill hole | From (m) | To (m) | interval (m) | Zn (ppm) | Cu (ppm) | Pb (ppm) | Ag (ppm) | Mn (ppm) | Fe (ppm) | Au (ppm) | As (ppm) | Hg (ppm) | Sn (ppm) | W (ppm) | Ba (ppm) |
|---|---|---|---|---|---|---|---|---|---|---|---|---|---|---|---|
| PD0010 | 279.8 | 282 | 2.2 | 970 | 3 | 150 | 2 | 3050 | 37000 | | | | | | |
| PD0010 | 294 | 296 | 2 | 100 | 7 | 110 | 0 | 3900 | 23000 | | | | | | |
| PD0010 | 296 | 296.8 | 0.8 | 1250 | 6 | 1050 | 4 | 2650 | 23000 | | | | | | |
| PD0010 | 296.8 | 297.9 | 1.1 | 23000 | 48 | 23500 | 65 | 2750 | 92000 | | | | | | |
| PD0010 | 296.8 | 297.9 | 1.1 | 23000 | 48 | 23500 | 65 | 2750 | 92000 | | | | | | |
| PD0010 | 297.9 | 298.72 | 0.82 | 50000 | 200 | 30000 | 44 | 1850 | 54500 | | | | | | |
| PD0010 | 297.9 | 298.72 | 0.82 | 50000 | 200 | 30000 | 44 | 1850 | 54500 | | | | | | |
| PD0010 | 298.72 | 301 | 2.28 | 5500 | 18 | 3050 | 8 | 590 | 18900 | | | | | | |
| PD0010 | 298.72 | 301 | 2.28 | 5500 | 18 | 3050 | 8 | 590 | 15900 | | | | | | |
| PD0010 | 301 | 303 | 2 | 1200 | 9 | 690 | 2 | 2400 | 14900 | | | | | | |
| PD0010 | 303 | 305 | 2 | 360 | 5 | 250 | 0 | 1300 | 24500 | | | | | | |
| PD0010 | 307 | 309 | 2 | 70 | 6 | 46 | 0 | 1100 | 43000 | | | | | | |
| PD0010 | 309 | 311 | 2 | 780 | 8 | 1800 | 1 | 1050 | 94500 | | | | | | |
| PD0010 | 311 | 313 | 2 | 580 | 7 | 200 | 0 | 1500 | 24500 | | | | | | |
| PD0011 | 145.3 | 146.2 | 0.9 | 180 | 65 | 185 | 2 | 2300 | 104000 | | | | | | |
| PD0011 | 146.2 | 146.5 | 0.3 | 2150 | 85 | 1050 | 2 | 8900 | 52500 | | | | | | |
| PD0011 | 146.5 | 146.73 | 0.23 | 120000 | 4050 | 17400 | 125 | 490 | 14500 | | | | | | |
| PD0011 | 146.5 | 146.73 | 0.23 | 120000 | 4050 | 17400 | 125 | 490 | 145000 | | | | | | |
| PD0011 | 146.73 | 148.75 | 2.02 | 4400 | 36 | 2700 | 2 | 2600 | 41000 | | | | | | |
| PD0011 | 148.75 | 149.85 | 1.1 | 690 | 18 | 480 | 1 | 1300 | 148000 | | | | | | |
| PD0011 | 158 | 159 | 1 | 450 | 110 | 90 | 0 | 2450 | 43500 | | | | | | |
| PD0011 | 159 | 159.67 | 0.67 | 20000 | 240 | 290 | 5 | 3700 | 60500 | | | | | | |
| PD0011 | 159.67 | 162 | 2.33 | 1400 | 20 | 75 | 1 | 1900 | 22000 | | | | | | |
| PD0011 | 162 | 164 | 2 | 3800 | 85 | 70 | 0 | 1500 | 23000 | | | | | | |
| PD0011 | 164 | 166 | 2 | 95 | 20 | 70 | 0 | 1500 | 24000 | | | | | | |
| PD0011 | 174.1 | 176 | 1.9 | 55 | 4 | 32 | 0 | 1550 | 15700 | | | | | | |
| PD0011 | 176 | 178.85 | 2.85 | 10100 | 65 | 3800 | 2 | 1350 | 15300 | | | | | | |
| PD0011 | 178.85 | 180.8 | 1.95 | 580 | 12 | 230 | 0 | 1450 | 11300 | | | | | | |
| PD0011 | 187 | 188.7 | 1.7 | 75 | 6 | 44 | 0 | 2650 | 5200 | | | | | | |
| PD0011 | 188.7 | 191 | 2.3 | 7600 | 115 | 800 | 0 | 4300 | 9700 | | | | | | |
| PD0011 | 191 | 192.92 | 1.92 | 540 | 18 | 1950 | 0 | 2550 | 14800 | | | | | | |
| PD0011 | 192.92 | 195.43 | 2.51 | 4300 | 42 | 130 | 0 | 3850 | 7200 | | | | | | |
| PD0011 | 195.43 | 195.84 | 0.41 | 115000 | 570 | 2150 | 70 | 2400 | 198000 | | | | | | |
| PD0011 | 195.43 | 195.84 | 0.41 | 115000 | 570 | 2150 | 70 | 2400 | 198000 | | | | | | |

**Appendix 5.2 cont.**

| Drill hole | From (m) | To (m) | interval (m) | Zn (ppm) | Cu (ppm) | Pb (ppm) | Ag (ppm) | Mn (ppm) | Fe (ppm) | Au (ppm) | As (ppm) | Hg (ppm) | Sn (ppm) | W (ppm) | Ba (ppm) |
|---|---|---|---|---|---|---|---|---|---|---|---|---|---|---|---|
| PD0011 | 195.84 | 196.1 | 0.26 | 2400 | 22 | 210 | 1 | 4550 | 28000 | | | | | | |
| PD0011 | 196.1 | 196.86 | 0.76 | 410 | 26 | 80 | 0 | 2200 | 11800 | | | | | | |
| PD0011 | 196.86 | 197.9 | 1.04 | 1050 | 90 | 560 | 3 | 3950 | 30000 | | | | | | |
| PD0011 | 197.9 | 198.45 | 0.55 | 120 | 5 | 70 | 0 | 1900 | 11500 | | | | | | |
| PD0011 | 215 | 217 | 2 | 38 | 2 | 24 | 0 | 2150 | 16100 | | | | | | |
| PD0011 | 217 | 219 | 2 | 1650 | 24 | 590 | 0 | 3900 | 17300 | | | | | | |
| PD0011 | 219 | 221 | 2 | 44 | 3 | 42 | 0 | 1350 | 14400 | | | | | | |
| PD0011 | 255 | 257 | 2 | 95 | 22 | 44 | 0 | 1400 | 65500 | | | | | | |
| PD0011 | 257 | 259 | 2 | 1500 | 12 | 410 | 1 | 1700 | 5200 | | | | | | |
| PD0011 | 259 | 261 | 2 | 65 | 3 | 24 | 0 | 1200 | 30500 | | | | | | |
| PD0011 | 282 | 284 | 2 | 105 | 2 | 110 | 1 | 2200 | 18000 | | | | | | |
| PD0011 | 284 | 286 | 2 | 2350 | 6 | 1400 | 1 | 5700 | 28500 | | | | | | |
| PD0011 | 286 | 288.6 | 2.6 | 1150 | 6 | 310 | 1 | 5150 | 35500 | | | | | | |
| PD0011 | 288.6 | 291 | 2.4 | 120 | 3 | 30 | 1 | 1500 | 120000 | | | | | | |
| PD0011 | 324 | 326 | 2 | 130 | 5 | 55 | 1 | 1700 | 27500 | | | | | | |
| PD0011 | 326 | 328 | 2 | 3450 | 18 | 5050 | 3 | 4100 | 40000 | | | | | | |
| PD0011 | 328 | 330.1 | 2.1 | 3550 | 18 | 1900 | 2 | 4850 | 58500 | | | | | | |
| PD0011 | 330.1 | 331.95 | 1.85 | 4150 | 140 | 1100 | 4 | 4950 | 48500 | | | | | | |
| PD0011 | 331.95 | 334 | 2.05 | 9550 | 65 | 4200 | 7 | 5450 | 89000 | | | | | | |
| PD0011 | 334 | 336 | 2 | 5650 | 48 | 1100 | 3 | 3800 | 77000 | | | | | | |
| PD0011 | 336 | 338 | 2 | 6700 | 30 | 3250 | 2 | 6250 | 118000 | | | | | | |
| PD0011 | 338 | 339.7 | 1.7 | 2400 | 20 | 630 | 2 | 3500 | 94500 | | | | | | |
| PD0011 | 339.7 | 342 | 2.3 | 240 | 14 | 105 | 0 | 1950 | 39500 | | | | | | |
| PD0011 | 353 | 355.23 | 2.23 | 410 | 6 | 370 | 0 | 2050 | 29000 | | | | | | |
| PD0011 | 355.23 | 356.25 | 1.02 | 1850 | 14 | 3900 | 2 | 6650 | 57500 | | | | | | |
| PD0011 | 356.25 | 358 | 1.75 | 310 | 10 | 1550 | 1 | 5900 | 13400 | | | | | | |
| PD0011 | 368 | 369.25 | 1.25 | 185 | 4 | 140 | 0 | 5500 | 5800 | | | | | | |
| PD0011 | 369.25 | 370.15 | 0.9 | 37000 | 90 | 19600 | 85 | 30500 | 25000 | | | | | | |
| PD0011 | 370.15 | 372 | 1.85 | 1550 | 20 | 2500 | 1 | 7900 | 7500 | | | | | | |
| PD0011 | 372 | 373.38 | 1.38 | 49000 | 540 | 32000 | 22 | 7850 | 18300 | | | | | | |
| PD0011 | 373.38 | 373.8 | 0.42 | 385000 | 1950 | 119000 | 100 | 3500 | 48000 | | | | | | |
| PD0011 | 373.8 | 376 | 2.2 | 33000 | 34 | 6250 | 6 | 14500 | 13600 | | | | | | |
| PD0011 | 376 | 378 | 2 | 3000 | 12 | 1600 | 1 | 4050 | 6200 | | | | | | |
| PD0011 | 378 | 380 | 2 | 220 | 8 | 610 | 0 | 3950 | 5600 | | | | | | |

**Appendix 5.2 cont.**

| Drill hole | From (m) | To (m) | interval (m) | Zn (ppm) | Cu (ppm) | Pb (ppm) | Ag (ppm) | Mn (ppm) | Fe (ppm) | Au (ppm) | As (ppm) | Hg (ppm) | Sn (ppm) | W (ppm) | Ba (ppm) |
|---|---|---|---|---|---|---|---|---|---|---|---|---|---|---|---|
| PD0011 | 420 | 421.2 | 1.2 | 290 | 8 | 125 | 0 | 1950 | 13800 | | | | | | |
| PD0011 | 421.2 | 423.9 | 2.7 | 4800 | 60 | 4200 | 12 | 3350 | 48000 | | | | | | |
| PD0011 | 423.9 | 425.45 | 1.55 | 280 | 8 | 105 | 0 | 3050 | 16200 | | | | | | |
| PD0011 | 425.45 | 425.9 | 0.45 | 50 | 5 | 18 | 0 | 2150 | 13200 | | | | | | |
| PD0011 | 425.9 | 427.25 | 1.35 | 1500 | 14 | 900 | 0 | 5850 | 26500 | | | | | | |
| PD0011 | 427.25 | 429 | 1.75 | 360 | 14 | 690 | 0 | 2400 | 49000 | | | | | | |
| PD0012 | 325.18 | 327 | 1.82 | 185 | 20 | 170 | 1 | 1550 | 50500 | | | | | | |
| PD0012 | 327 | 329 | 2 | 2550 | 42 | 4500 | 2 | 1100 | 37500 | | | | | | |
| PD0012 | 329 | 331.45 | 2.45 | 115 | 40 | 130 | 0 | 1000 | 47500 | | | | | | |
| PD0012 | 331.45 | 332 | 0.55 | 46 | 65 | 8850 | 5 | 810 | 44500 | | | | | | |
| PD0012 | 332 | 334 | 2 | 44 | 18 | 580 | 1 | 1050 | 51500 | | | | | | |
| PD0012 | 348.9 | 350 | 1.1 | 165 | 28 | 230 | 1 | 1350 | 57500 | | | | | | |
| PD0012 | 350 | 352.15 | 2.15 | 1200 | 28 | 710 | 1 | 1700 | 57500 | | | | | | |
| PD0012 | 352.15 | 353.25 | 1.1 | 680 | 10 | 250 | 1 | 2150 | 40500 | | | | | | |
| PD0012 | 353.25 | 353.75 | 0.5 | 8200 | 90 | 2400 | 8 | 1000 | 81000 | | | | | | |
| PD0012 | 353.75 | 354.25 | 0.5 | 850 | 44 | 250 | 1 | 2400 | 49000 | | | | | | |
| PD0013 | 104 | 106 | 2 | 830 | 22 | 135 | 0 | 5100 | 19000 | | | | | | |
| PD0013 | 106 | 108 | 2 | 1950 | 42 | 490 | 1 | 4300 | 17600 | | | | | | |
| PD0013 | 108 | 110 | 2 | 20500 | 430 | 10100 | 18 | 6350 | 29500 | | | | | | |
| PD0013 | 110 | 112 | 2 | 10500 | 200 | 5150 | 10 | 5400 | 26500 | | | | | | |
| PD0013 | 112 | 114 | 2 | 9000 | 160 | 4700 | 9 | 5650 | 24500 | | | | | | |
| PD0013 | 114 | 116 | 2 | 7700 | 120 | 3550 | 6 | 5650 | 44500 | | | | | | |
| PD0013 | 116 | 118 | 2 | 5800 | 100 | 3200 | 5 | 4250 | 64000 | | | | | | |
| PD0013 | 118 | 119.5 | 1.5 | 380 | 75 | 90 | 0 | 2750 | 10000 | | | | | | |
| PD0013 | 130 | 131.6 | 1.6 | 44 | 8 | 18 | 0 | 1300 | 19700 | | | | | | |
| PD0013 | 131.6 | 132.75 | 1.15 | 7700 | 200 | 690 | 3 | 2250 | 35000 | | | | | | |
| PD0013 | 132.75 | 135 | 2.25 | 2450 | 95 | 1550 | 2 | 4950 | 34500 | | | | | | |
| PD0013 | 135 | 136.9 | 1.9 | 70 | 7 | 42 | 0 | 1700 | 34500 | | | | | | |
| PD0013 | 236 | 237.8 | 1.8 | 26 | 4 | 8 | 0 | 1000 | 8300 | | | | | | |
| PD0013 | 237.8 | 239.7 | 1.9 | 1700 | 18 | 1100 | 0 | 1550 | 7500 | | | | | | |
| PD0013 | 239.7 | 241.55 | 1.85 | 55 | 5 | 24 | 0 | 1100 | 4800 | | | | | | |
| PD0013 | 391 | 393 | 2 | 130 | 10 | 230 | 0 | 290 | 8400 | | | | | | |
| PD0013 | 393 | 395 | 2 | 1150 | 10 | 1250 | 0 | 490 | 19500 | | | | | | |
| PD0013 | 395 | 397 | 2 | 75 | 8 | 155 | 0 | 210 | 8800 | | | | | | |

**Appendix 5.2 cont.**

| Drill hole | From (m) | To (m) | interval (m) | Zn (ppm) | Cu (ppm) | Pb (ppm) | Ag (ppm) | Mn (ppm) | Fe (ppm) | Au (ppm) | As (ppm) | Hg (ppm) | Sn (ppm) | W (ppm) | Ba (ppm) |
|---|---|---|---|---|---|---|---|---|---|---|---|---|---|---|---|
| PD0014 | 133 | 135.27 | 2.27 | 850 | 7 | 370 | 2 | 2000 | 10800 | | | | | | |
| PD0014 | 135.27 | 137.07 | 1.8 | 3250 | 95 | 1050 | 3 | 4250 | 22000 | | | | | | |
| PD0014 | 137.07 | 139 | 1.93 | 190 | 42 | 55 | 1 | 880 | 8900 | | | | | | |
| PD0014 | 139 | 141 | 2 | 430 | 22 | 100 | 1 | 710 | 8300 | | | | | | |
| PD0014 | 141 | 143.27 | 2.27 | 170 | 12 | 65 | 1 | 650 | 9200 | | | | | | |
| PD0014 | 143.27 | 143.82 | 0.55 | 170 | 10 | 95 | 1 | 1250 | 6500 | | | | | | |
| PD0014 | 143.82 | 146 | 2.18 | 580 | 16 | 360 | 3 | 670 | 8600 | | | | | | |
| PD0014 | 146 | 148 | 2 | 560 | 12 | 350 | 2 | 540 | 6600 | | | | | | |
| PD0014 | 148 | 149.76 | 1.76 | 440 | 22 | 840 | 4 | 2150 | 10900 | | | | | | |
| PD0014 | 149.76 | 151.37 | 1.61 | 920 | 14 | 300 | 2 | 29000 | 106000 | | | | | | |
| PD0014 | 151.37 | 152.9 | 1.53 | 300 | 12 | 180 | 2 | 4100 | 18300 | | | | | | |
| PD0014 | 152.9 | 154.5 | 1.6 | 210 | 8 | 70 | 2 | 1600 | 17300 | | | | | | |
| PD0014 | 154.5 | 156 | 1.5 | 250 | 8 | 70 | 1 | 2400 | 14100 | | | | | | |
| PD0014 | 156 | 157.48 | 1.48 | 170 | 8 | 250 | 1 | 1550 | 9200 | | | | | | |
| PD0014 | 157.48 | 159.5 | 2.02 | 3550 | 30 | 6750 | 3 | 24000 | 65500 | | | | | | |
| PD0014 | 159.5 | 161.4 | 1.9 | 830 | 30 | 1550 | 2 | 14500 | 44500 | | | | | | |
| PD0014 | 161.4 | 161.95 | 0.55 | 290 | 24 | 145 | 2 | 5550 | 20000 | | | | | | |
| PD0014 | 161.95 | 163.1 | 1.15 | 1200 | 20 | 12000 | 5 | 5700 | 50000 | | | | | | |
| PD0014 | 163.1 | 164 | 0.9 | 3800 | 18 | 3950 | 8 | 160000 | 21500 | | | | | | |
| PD0014 | 164 | 166 | 2 | 150 | 9 | 230 | 1 | 3700 | 7200 | | | | | | |
| PD0014 | 178.42 | 179.63 | 1.21 | 430 | 14 | 240 | 1 | 1800 | 8100 | | | | | | |
| PD0014 | 179.63 | 180 | 0.37 | 2600 | 22 | 1350 | 5 | 11500 | 16400 | | | | | | |
| PD0014 | 180 | 181.2 | 1.2 | 115 | 6 | 75 | 0 | 1050 | 12300 | | | | | | |
| PD0015 | 124.28 | 126.33 | 2.05 | 75 | | 45 | 0 | 545 | 11300 | 0 | | | | | |
| PD0015 | 126.33 | 133.88 | 7.55 | 3710 | 65 | 1955 | 1 | 1390 | 22200 | | | | | | |
| PD0015 | 133.88 | 141 | 7.12 | 230 | 10 | 25 | 0 | 435 | 10600 | 0 | | | | | |
| PD0015 | 141 | 144.98 | 3.98 | 160 | | 45 | 0 | 4425 | 26500 | 0 | | | | | |
| PD0015 | 144.98 | 147.14 | 2.16 | 9965 | 605 | 5315 | 14 | 2080 | 36700 | | | | | | |
| PD0015 | 147.14 | 148.89 | 1.75 | 260 | 5 | 185 | 0 | 1065 | 17400 | | | | | | |
| PD0015 | 361.49 | 362.59 | 1.1 | 245 | 10 | 25 | 0 | 1515 | 33200 | | 0 | 0 | 3 | 24 | 791 |
| PD0015 | 362.59 | 363.37 | 0.78 | 1495 | 35 | 35 | 2 | 1320 | 10100 | | 0 | 0 | 0 | 57 | 358 |
| PD0015 | 363.37 | 367.02 | 3.65 | 330 | 15 | 50 | 2 | 2750 | 20000 | | 0 | 0 | 4 | 83 | 15 |
| PD0015 | 398.95 | 401.37 | 2.42 | 300 | 15 | 30 | 0 | 2755 | 15400 | | 3 | 0 | 4 | 12 | |
| PD0015 | 401.37 | 402.32 | 0.95 | 12700 | 4990 | 2560 | 46 | 1695 | 34700 | | 8 | 0 | 6 | 433 | 793 |

**Appendix 5.2 cont.**

| Drill hole | From (m) | To (m) | interval (m) | Zn (ppm) | Cu (ppm) | Pb (ppm) | Ag (ppm) | Mn (ppm) | Fe (ppm) | Au (ppm) | As (ppm) | Hg (ppm) | Sn (ppm) | W (ppm) | Ba (ppm) |
|---|---|---|---|---|---|---|---|---|---|---|---|---|---|---|---|
| PD0015 | 402.32 | 402.66 | 0.34 | 12700 | 6500 | 10600 | 336 | 22900 | 180300 | | 280 | 0 | 5 | 1400 | 38 |
| PD0015 | 402.66 | 405.83 | 3.17 | 405 | 85 | 160 | 3 | 3950 | 19100 | | 0 | 0 | 0 | 14 | 14 |
| PD0015 | 527.63 | 529.04 | 1.41 | 355 | 50 | 140 | 2 | 1700 | 52200 | | 35 | 0 | 3 | 20 | 408 |
| PD0015 | 529.04 | 539 | 9.96 | 1835 | 15 | 400 | 0 | 1585 | 3600 | | 0 | 0 | 0 | 54 | 14 |
| PD0015 | 539 | 551.52 | 12.52 | 195 | 20 | 60 | 0 | 965 | 3200 | | 0 | 0 | 0 | 17 | 35 |
| PD0015 | 551.52 | 562.15 | 10.63 | 320 | 5 | 185 | 9 | 2940 | 8800 | | 8 | 0 | 0 | 10 | 27 |
| PD0015 | 562.15 | 567.15 | 5 | 2540 | 115 | 1780 | 3 | 5795 | 51900 | | 193 | 0 | 8 | 10 | 126 |
| PD0015 | 567.15 | 567.8 | 0.65 | 13900 | 90 | 2500 | 0 | 2335 | 99900 | | 0 | 0 | 3 | 479 | 232 |
| PD0015 | 567.8 | 570.28 | 2.48 | 410 | 15 | 110 | 0 | 1430 | 28800 | | 0 | 0 | 6 | 28 | 82 |
| PD0015 | 596.81 | 605.3 | 8.49 | 300 | 10 | 50 | 0 | 2230 | 7700 | | 0 | 0 | 4 | 31 | 19 |
| PD0015 | 605.3 | 605.95 | 0.65 | 3255 | 15 | 3105 | 2 | 2170 | 53500 | | 0 | 0 | 22 | 160 | 527 |
| PD0015 | 605.95 | 615 | 9.05 | 940 | 25 | 245 | 2 | 2780 | 9300 | | 0 | 0 | 0 | 44 | 10 |
| PD0016 | 260 | 261.8 | 1.8 | 245 | 45 | 85 | 2 | 3785 | 21300 | | | | | | |
| PD0016 | 261.76 | 262.26 | 0.5 | 162000 | 4425 | 142000 | 58 | 5660 | 30100 | | | | | | |
| PD0016 | 261.8 | 263.5 | 1.7 | 162000 | 2300 | 203000 | 110 | 1745 | 24100 | | | | | | |
| PD0016 | 262.26 | 263.45 | 1.19 | 145200 | 1105 | 116000 | 48 | 3350 | 60600 | | | | | | |
| PD0016 | 263.5 | 267 | 3.5 | 1265 | 45 | 1020 | 1 | 3305 | 13000 | | | | | | |
| PD0016 | 267 | 268.6 | 1.6 | 2315 | 50 | 2600 | 2 | 2905 | 15800 | | | | | | |
| PD0016 | 268.6 | 269 | 0.4 | 52000 | 2175 | 81000 | 58 | 5110 | 27900 | | | | | | |
| PD0016 | 269 | 271 | 2 | 460 | 65 | 360 | 0 | 3405 | 20700 | | | | | | |
| PD0016 | 271 | 273.4 | 2.4 | 395 | 65 | 1180 | 6 | 4900 | 16100 | | | | | | |
| PD0016 | 273.4 | 273.75 | 0.35 | 205000 | 1860 | 192000 | 114 | 3365 | 22800 | | | | | | |
| PD0016 | 273.75 | 275 | 1.25 | 370 | 15 | 270 | 0 | 4680 | 23300 | | | | | | |
| PD0016 | 275 | 277 | 2 | 1655 | 15 | 1525 | 1 | 2790 | 15000 | | | | | | |
| PD0016 | 277 | 279 | 2 | 370 | 15 | 90 | 0 | 3715 | 17800 | | | | | | |
| PD0016 | 301 | 302.6 | 1.6 | 125 | 10 | 235 | 0 | 3080 | 13300 | | | | | | |
| PD0016 | 302.6 | 302.9 | 0.3 | 74000 | 2155 | 83000 | 53 | 5180 | 18300 | | | | | | |
| PD0016 | 302.9 | 304.65 | 1.75 | 370 | 20 | 93 | 3 | 1895 | 8600 | | | | | | |
| PD0016 | 304.65 | 306.1 | 1.45 | 150000 | 1760 | 200000 | 137 | 1075 | 33400 | | | | | | |
| PD0016 | 304.71 | 306.17 | 1.46 | 155500 | 2165 | 242000 | 156 | 2560 | 79300 | | | | | | |
| PD0016 | 306.1 | 307 | 0.9 | 985 | 20 | 665 | 0 | 1215 | 8200 | | | | | | |
| PD0016 | 307 | 309 | 2 | 995 | 25 | 1110 | 2 | 1170 | 8400 | | | | | | |
| PD0016 | 309 | 311 | 2 | 125 | 20 | 60 | 0 | 690 | 7300 | | | | | | |
| PD0016 | 374 | 378 | 4 | 360 | 15 | 25 | 0 | 2050 | 15500 | | | | | | |

**Appendix 5.2 cont.**

| Drill hole | From (m) | To (m) | interval (m) | Zn (ppm) | Cu (ppm) | Pb (ppm) | Ag (ppm) | Mn (ppm) | Fe (ppm) | Au (ppm) | As (ppm) | Hg (ppm) | Sn (ppm) | W (ppm) | Ba (ppm) |
|---|---|---|---|---|---|---|---|---|---|---|---|---|---|---|---|
| PD0016 | 378 | 382 | 4 | 195 | 10 | 2015 | 1 | 3500 | 16000 | | | | | | |
| PD0016 | 382 | 386 | 4 | 80 | 15 | 25 | 0 | 1105 | 10000 | | | | | | |
| PD0016 | 386 | 387.6 | 1.6 | 160 | 30 | 1115 | 2 | 3700 | 42900 | | | | | | |
| PD0016 | 387.6 | 389.35 | 1.75 | 270 | 5 | 10400 | 2 | 6690 | 30800 | | | | | | |
| PD0016 | 389.35 | 391 | 1.65 | 1220 | 25 | 930 | 3 | 3370 | 28600 | | | | | | |
| PD0016 | 391 | 395 | 4 | 255 | 15 | 1875 | 1 | 3820 | 24300 | | | | | | |
| PD0016 | 395 | 399 | 4 | 235 | 15 | 295 | 0 | 1805 | 18200 | | | | | | |
| PD0016 | 423 | 426 | 3 | 260 | 60 | 85 | 1 | 870 | 40100 | | | | | | |
| PD0016 | 426 | 427.1 | 1.1 | 495 | 95 | 2890 | 4 | 1205 | 31500 | | | | | | |
| PD0016 | 427.1 | 427.55 | 0.45 | 1090 | 100 | 139000 | 60 | 3715 | 11700 | | | | | | |
| PD0016 | 427.55 | 429.2 | 1.65 | 3360 | 75 | 4140 | 6 | 325 | 10500 | | | | | | |
| PD0016 | 429.2 | 430.8 | 1.6 | 50 | 20 | 580 | 2 | 205 | 5500 | | | | | | |
| PD0017 | 232 | 233.52 | 1.52 | 960 | 10 | 75 | 0 | 7570 | 6200 | 0 | | | | | |
| PD0017 | 233.06 | 233.56 | 0.5 | 7760 | 110 | 1590 | 7 | 0 | 0 | | | 0.015 | | | |
| PD0017 | 233.52 | 234.25 | 0.73 | 257500 | 2735 | 141300 | 186 | 5520 | 126900 | | | 0 | | | |
| PD0017 | 233.56 | 234.25 | 0.69 | 214300 | 2045 | 103400 | 117 | 8020 | 147800 | | | 0.225 | 7 | 3240 | |
| PD0017 | 234.25 | 237 | 2.75 | 725 | 5 | 940 | 6 | 5510 | 4200 | | | | | | |
| PD0017 | 234.25 | 234.75 | 0.5 | 1630 | 10 | 870 | 1 | 0 | 0 | | | 0.01 | | | |
| PD0017 | 237 | 239 | 2 | 90 | | 55 | 0 | 1835 | 3600 | 0 | | 0 | | | |
| PD0017 | 239 | 241.53 | 2.53 | 110 | | 20 | 2 | 2655 | 6800 | | | | | | |
| PD0017 | 241 | 241.53 | 0.53 | 1120 | 10 | 880 | 13 | 2800 | 7800 | | 31 | 0.01 | | | |
| PD0017 | 241.53 | 242.5 | 0.97 | 136500 | 1760 | 152700 | 115 | 34000 | 90700 | | | 0 | | | |
| PD0017 | 241.53 | 242.03 | 0.5 | 150500 | 1605 | 151700 | 100 | 31100 | 123800 | | | 0.018 | | 3070 | |
| PD0017 | 242.03 | 243.5 | 1.47 | 126900 | 2145 | 221400 | 116 | 3890 | 62900 | | | 0.1 | | 1880 | |
| PD0017 | 242.5 | 243.5 | 1 | 152200 | 3880 | 192400 | 125 | 5300 | 33800 | | | | | | |
| PD0017 | 243.5 | 244.6 | 1.1 | 160200 | 2820 | 272500 | 164 | 6705 | 81100 | | | 0 | | | |
| PD0017 | 243.5 | 244.15 | 0.65 | 1640 | 20 | 1370 | 2 | 0 | 0 | | | 0.175 | | | |
| PD0017 | 244.15 | 244.63 | 0.48 | 128600 | 2905 | 116900 | 64 | 17300 | 71800 | | | 0.155 | 13 | 1840 | |
| PD0017 | 244.6 | 245.2 | 0.6 | 28000 | 540 | 20900 | 12 | 34500 | 51300 | | | | | | |
| PD0017 | 244.63 | 245.16 | 0.53 | 18700 | 110 | 21500 | 11 | 24700 | 34700 | | 569 | 0.3 | 4 | 213 | |
| PD0017 | 245.16 | 245.66 | 0.5 | 1640 | 20 | 1370 | 3 | 0 | 0 | | | 0.005 | | | |
| PD0017 | 245.2 | 247 | 1.8 | 235 | | 115 | 0 | 5350 | 18600 | 0 | | 0 | | | |
| PD0017 | 308.5 | 310 | 1.5 | 970 | | 860 | 1 | 2175 | 11200 | | | 0 | | | |
| PD0017 | 310 | 311.1 | 1.1 | 3550 | 25 | 15400 | 9 | 13500 | 23700 | | | | | | |

**Appendix 5.2 cont.**

| Drill hole | From (m) | To (m) | interval (m) | Zn (ppm) | Cu (ppm) | Pb (ppm) | Ag (ppm) | Mn (ppm) | Fe (ppm) | Au (ppm) | As (ppm) | Hg (ppm) | Sn (ppm) | W (ppm) | Ba (ppm) |
|---|---|---|---|---|---|---|---|---|---|---|---|---|---|---|---|
| PD0017 | 310 | 311.1 | 1.1 | 13300 | 30 | 3600 | 12 | 7910 | 11400 | 0.03 | 54 | 0.05 | | 144 | 44 |
| PD0017 | 311.1 | 313.1 | 2 | 1030 | 10 | 910 | 0 | 3090 | 9100 | | 4 | 0.01 | | | |
| PD0017 | 313.1 | 315 | 1.9 | 18600 | 110 | 9900 | 14 | 13600 | 15400 | 0.045 | 73 | 0.025 | 9 | 193 | |
| PD0017 | 315 | 317 | 2 | 31500 | 200 | 23900 | 24 | 10500 | 21700 | 0.08 | 119 | 0.03 | | 341 | |
| PD0017 | 317 | 319 | 2 | 32200 | 200 | 25900 | 17 | 10900 | 15100 | 0.045 | 21 | 0.015 | | 309 | |
| PD0017 | 319 | 321 | 2 | 23500 | 150 | 24400 | 15 | 11300 | 9900 | 0.025 | | 0.03 | | 245 | |
| PD0017 | 321 | 323 | 2 | 10100 | 50 | 5500 | 9 | 0 | 0 | | | 0.005 | | | |
| PD0017 | 323 | 325 | 2 | 1830 | 10 | 940 | 2 | 2960 | 4600 | | 6 | | | | |
| PD0017 | 325 | 327 | 2 | 540 | 5 | 350 | 1 | 1720 | 6100 | | 8 | | 3 | | |
| PD0017 | 327 | 329 | 2 | 2560 | 25 | 2060 | 2 | 3990 | 8900 | | 7 | | | 27 | 15 |
| PD0017 | 329 | 331 | 2 | 3810 | 20 | 5800 | 4 | 3190 | 10600 | 0.015 | 15 | 0.01 | 5 | 35 | 361 |
| PD0017 | 331 | 333 | 2 | 7540 | 60 | 11900 | 7 | 0 | 0 | 0.015 | | 0.02 | | | |
| PD0017 | 333 | 335.2 | 2.2 | 1060 | 5 | 5980 | 4 | 950 | 11400 | | 11 | 0.005 | | | 521 |
| PD0017 | 335.2 | 337 | 1.8 | 14800 | 175 | 19800 | 20 | 12200 | 15200 | 0.04 | 22 | 0.045 | 7 | 146 | 20 |
| PD0017 | 337 | 339 | 2 | 16300 | 145 | 14900 | 14 | 10100 | 14000 | 0.035 | 37 | 0.035 | | 156 | |
| PD0017 | 339 | 341 | 2 | 4740 | 45 | 4710 | 7 | 0 | 0 | | | 0.015 | | | |
| PD0017 | 341 | 341.9 | 0.9 | 1460 | 25 | 1140 | 2 | 15300 | 10800 | 0.015 | 16 | 0.015 | 3 | | |
| PD0017 | 341.9 | 343 | 1.1 | 20600 | 385 | 99500 | 36 | 13700 | 14600 | 0.055 | 164 | 0.055 | | 150 | |
| PD0017 | 343 | 344.75 | 1.75 | 88600 | 1245 | 170000 | 67 | 16800 | 22400 | 0.185 | 494 | 0.16 | 6 | 1530 | |
| PD0017 | 344.75 | 347 | 2.25 | 4240 | 40 | 6140 | 4 | 10900 | 14400 | 0.025 | 43 | 0.005 | 5 | 38 | 213 |
| PD0017 | 347 | 349.2 | 2.2 | 1700 | 15 | 1950 | 2 | 6730 | 18600 | 0.015 | 46 | 0.005 | 7 | | 186 |
| PD0017 | 349.2 | 350.05 | 0.85 | 2340 | 20 | 2490 | 4 | 4100 | 16300 | 0.015 | 36 | 0.005 | 5 | | 323 |
| PD0017 | 350.05 | 351.57 | 1.52 | 20000 | 175 | 8910 | 7 | 0 | 0 | 0.02 | | 0.035 | | | |
| PD0017 | 351.57 | 352.53 | 0.96 | 13500 | 100 | 16700 | 20 | 6960 | 8000 | 0.045 | 193 | 0.025 | | 165 | 158 |
| PD0017 | 352.53 | 353.38 | 0.85 | 300 | | 210 | 1 | 2340 | 10300 | 0.04 | 11 | 0.005 | | | 11 |
| PD0017 | 353.38 | 355.4 | 2.02 | 10500 | 135 | 28000 | 24 | 8790 | 6500 | 0.04 | 87 | 0.025 | | 93 | |
| PD0017 | 355.4 | 356.43 | 1.03 | 16600 | 135 | 9890 | 18 | 11500 | 8700 | 0.035 | 91 | 0.045 | | 176 | |
| PD0017 | 356.43 | 358.5 | 2.07 | 530 | | 740 | 1 | 2260 | 7600 | | 9 | | 3 | | |
| PD0017 | 358.5 | 361 | 2.5 | 410 | | 210 | 1 | 2250 | 13400 | | 5 | | 7 | | |
| PD0017 | 361 | 363 | 2 | 14100 | 180 | 6690 | 7 | 0 | 0 | 0.02 | | 0.025 | | | |
| PD0017 | 363 | 364.35 | 1.35 | 750 | | 540 | 1 | 4410 | 11400 | | 4 | 0.01 | | | 19 |
| PD0017 | 364.35 | 366.1 | 1.75 | 54800 | 220 | 27300 | 39 | 3670 | 7000 | 0.04 | 109 | 0.235 | | 642 | 45 |
| PD0017 | 366.1 | 367 | 0.9 | 78600 | 365 | 35700 | 46 | 4270 | 15800 | 0.075 | 260 | 0.39 | | 1300 | 16 |
| PD0017 | 367 | 368.15 | 1.15 | 99000 | 355 | 34100 | 48 | 2940 | 18400 | 0.085 | 140 | 0.37 | | 1550 | |

**Appendix 5.2 cont.**

| Drill hole | From (m) | To (m) | interval (m) | Zn (ppm) | Cu (ppm) | Pb (ppm) | Ag (ppm) | Mn (ppm) | Fe (ppm) | Au (ppm) | As (ppm) | Hg (ppm) | Sn (ppm) | W (ppm) | Ba (ppm) |
|---|---|---|---|---|---|---|---|---|---|---|---|---|---|---|---|
| PD0017 | 368.15 | 369.85 | 1.7 | 9820 | 30 | 3500 | 6 | 0 | 0 | 0.02 | | 0.035 | | | |
| PD0017 | 369.85 | 370.2 | 0.35 | 64000 | 500 | 8840 | 24 | 5210 | 8300 | 0.045 | 31 | 0.12 | | 776 | 58 |
| PD0017 | 370.2 | 371.6 | 1.4 | 19100 | 100 | 5760 | 6 | 0 | 0 | 0.035 | | 0.03 | | | |
| PD0017 | 371.6 | 372.2 | 0.6 | 53000 | 135 | 27000 | 44 | 9670 | 8500 | | 70 | 0.016 | | 636 | |
| PD0017 | 372.2 | 372.58 | 0.38 | 760 | 5 | 350 | 1 | 5390 | 5200 | | 10 | 0.005 | 4 | | |
| PD0017 | 372.58 | 373 | 0.42 | 15200 | 65 | 19100 | 26 | 16000 | 15700 | 0.06 | 413 | 0.045 | | 125 | |
| PD0017 | 373 | 375.1 | 2.1 | 83200 | 470 | 53300 | 39 | 21500 | 22400 | 0.12 | 276 | 0.165 | | 1070 | |
| PD0017 | 375.1 | 376.5 | 1.4 | 1790 | | 710 | 2 | 3300 | 7600 | | 6 | 0.01 | | | |
| PD0017 | 376.5 | 377.1 | 0.6 | 10500 | 30 | 3980 | 4 | 0 | 0 | | | 0.045 | | | |
| PD0017 | 377.1 | 378.05 | 0.95 | 1530 | 5 | 490 | 2 | 6230 | 13700 | | 19 | 0.015 | | | 19 |
| PD0017 | 378.05 | 378.95 | 0.9 | 380 | | 150 | 0 | 3350 | 8400 | | 10 | 0.005 | | | |
| PD0017 | 378.95 | 379.5 | 0.55 | 5040 | 10 | 1990 | 4 | 0 | 0 | | | 0.045 | | | |
| PD0017 | 379.5 | 379.7 | 0.2 | 210 | 5 | 780 | 2 | 3330 | 14300 | | 10 | 0.015 | | | 212 |
| PD0017 | 379.7 | 380.8 | 1.1 | 14500 | 85 | 13100 | 7 | 0 | 0 | | | 0.035 | | | |
| PD0017 | 380.8 | 381.53 | 0.73 | 14500 | 100 | 5510 | 4 | 0 | 0 | | | 0.045 | | | |
| PD0017 | 381.53 | 382.32 | 0.79 | 22600 | 95 | 5900 | 13 | 10700 | 11500 | | 81 | 0.075 | | 184 | |
| PD0017 | 382.32 | 382.67 | 0.35 | 2300 | 10 | 260 | 2 | 0 | 0 | | | 0.01 | | | |
| PD0017 | 382.67 | 383.4 | 0.73 | 6440 | 70 | 9150 | 59 | 31000 | 151500 | | 291 | 0.035 | 3 | 62 | |
| PD0017 | 383.4 | 384.8 | 1.4 | 10200 | 60 | 10500 | 27 | 23100 | 97000 | | 208 | 0.065 | | 79 | |
| PD0017 | 384.8 | 385.85 | 1.05 | 3890 | 60 | 4850 | 47 | 6390 | 134400 | | 243 | 0.065 | 3 | 29 | |
| PD0017 | 385.85 | 386.5 | 0.65 | 580 | 10 | 1160 | 2 | 0 | 0 | | | 0.005 | | | |
| PD0017 | 386.5 | 387 | 0.5 | 7910 | 50 | 6160 | 19 | 24400 | 80200 | | 151 | 0.055 | 3 | 63 | 13 |
| PD0017 | 387 | 387.75 | 0.75 | 1000 | 10 | 260 | 1 | 0 | 0 | | | 0.035 | | | |
| PD0017 | 387.75 | 388.25 | 0.5 | 150 | 30 | 50 | 1 | 0 | 0 | | | 0.025 | | | |
| PD0017 | 388.25 | 389.33 | 1.08 | 470 | | 320 | 0 | 3930 | 17000 | 0.5 | 18 | | 8 | | 27 |
| PD0017 | 389.33 | 389.73 | 0.4 | 15500 | 20 | 1160 | 5 | 0 | 0 | | | 0.035 | | | |
| PD0017 | 389.73 | 390 | 0.27 | 1260 | | 320 | 1 | 3460 | 11600 | | 9 | | 8 | | |
| PD0017 | 390 | 391.15 | 1.15 | 17200 | 40 | 10800 | 14 | 9970 | 66200 | | 23 | 0.05 | | 198 | 36 |
| PD0017 | 391.15 | 391.95 | 0.8 | 850 | 5 | 650 | 2 | 14300 | 46600 | | 58 | | 11 | | 205 |
| PD0017 | 391.95 | 392.4 | 0.45 | 80 | | 40 | 0 | 0 | 0 | 0.5 | | 0.015 | | | |
| PD0017 | 392.4 | 393.55 | 1.15 | 2380 | 10 | 1180 | 4 | 9860 | 64300 | | 53 | | 6 | 28 | 14 |
| PD0017 | 393.55 | 394.1 | 0.55 | 190 | | 40 | 1 | 0 | 0 | | | 0.01 | | | |
| PD0017 | 394.1 | 394.8 | 0.7 | 4200 | 20 | 3680 | 10 | 10200 | 72400 | | 98 | | 7 | 32 | 18 |
| PD0017 | 394.8 | 395.5 | 0.7 | 7480 | 10 | 17200 | 14 | 8990 | 52600 | | | 0.02 | 3 | 66 | 18 |

**Appendix 5.2 cont.**

| Drill hole | From (m) | To (m) | interval (m) | Zn (ppm) | Cu (ppm) | Pb (ppm) | Ag (ppm) | Mn (ppm) | Fe (ppm) | Au (ppm) | As (ppm) | Hg (ppm) | Sn (ppm) | W (ppm) | Ba (ppm) |
|---|---|---|---|---|---|---|---|---|---|---|---|---|---|---|---|
| PD0017 | 395.5 | 396.35 | 0.85 | 100 | | 90 | 1 | 1950 | 24900 | | | | 7 | | |
| PD0017 | 396.35 | 396.95 | 0.6 | 510 | 10 | 3940 | 8 | 0 | 0 | | | 0.015 | | | |
| PD0017 | 396.95 | 398.95 | 2 | 43300 | 345 | 20100 | 42 | 5180 | 107400 | | 147 | 0.055 | 4 | 389 | 19 |
| PD0017 | 398.95 | 399.55 | 0.6 | 85300 | 1220 | 99200 | 66 | 1880 | 90300 | | | 0.065 | | 1510 | 399 |
| PD0017 | 399.55 | 399.8 | 0.25 | 7170 | 65 | 21600 | 20 | 1130 | 33700 | | | 0.02 | 5 | 53 | 754 |
| PD0017 | 399.8 | 400.35 | 0.55 | 4160 | 180 | 43200 | 25 | 870 | 34600 | | | 0.015 | | | 326 |
| PD0017 | 400.35 | 402 | 1.65 | 11900 | 250 | 8070 | 6 | 0 | 0 | | | 0.015 | | | |
| PD0017 | 402 | 402.9 | 0.9 | 29000 | 425 | 17200 | 16 | 1050 | 26600 | | | 0.05 | 9 | 388 | 317 |
| PD0017 | 402.9 | 403.3 | 0.4 | 9140 | 110 | 8640 | 10 | 490 | 16600 | | | 0.01 | 3 | 70 | 380 |
| PD0017 | 403.3 | 405.3 | 2 | 6810 | 60 | 19700 | 13 | 820 | 15700 | | | 0.015 | | 69 | 338 |
| PD0017 | 405.3 | 406.6 | 1.3 | 20600 | 255 | 40200 | 48 | 820 | 48900 | | | 0.055 | 3 | 177 | 314 |
| PD0017 | 406.6 | 407.25 | 0.65 | 14300 | 205 | 12900 | 16 | 1270 | 27800 | | | 0.02 | | 160 | 316 |
| PD0017 | 407.25 | 408.15 | 0.9 | 37600 | 520 | 26000 | 48 | 3100 | 54800 | | | 0.075 | 4 | 350 | 204 |
| PD0017 | 408.15 | 408.62 | 0.47 | 26800 | 5865 | 94900 | 205 | | 123100 | | | 0.065 | | 301 | 19 |
| PD0017 | 408.62 | 409.88 | 1.26 | 42400 | 705 | 93500 | 90 | 3710 | 67500 | | | 0.014 | | 467 | 33 |
| PD0017 | 409.88 | 411 | 1.12 | 9880 | 40 | 3300 | 2 | 13200 | 7800 | | | | | | |
| PD0017 | 411 | 413 | 2 | 6940 | 10 | 2075 | 5 | 18100 | 10800 | | | | | | |
| PD0017 | 413 | 415 | 2 | 10400 | 20 | 3580 | 5 | 17400 | 8000 | | | | | | |
| PD0017 | 415 | 417 | 2 | 10000 | 10 | 2445 | 2 | 12500 | 6000 | | | | | | |
| PD0017 | 417 | 419 | 2 | 735 | 5 | 305 | 0 | 5730 | 4600 | 0 | | | | | |
| PD0017 | 419 | 421 | 2 | 1185 | 5 | 140 | 0 | 3905 | 4800 | | | | | | |
| PD0017 | 421 | 423 | 2 | 1295 | 5 | 710 | 2 | 5785 | 5100 | | | | | | |
| PD0017 | 423 | 425 | 2 | 1180 | 5 | 200 | 0 | 4345 | 4300 | | | | | | |
| PD0017 | 425 | 427 | 2 | 245 | 5 | 100 | 0 | 3070 | 4300 | 0 | | | | | |
| PD0017 | 427 | 429.1 | 2.1 | 2155 | 10 | 1470 | 3 | 6390 | 10300 | | | | | | |
| PD0017 | 429.1 | 433.2 | 4.1 | 330 | 15 | 110 | 0 | 1940 | 8700 | 0 | | | | | |
| PD0017 | 433.2 | 434 | 0.8 | 4410 | 5 | 1035 | 2 | 2275 | 4200 | | | | | | |
| PD0017 | 434 | 438 | 4 | 180 | 5 | 30 | 0 | 755 | 2200 | 0 | | | | | |
| PD0017 | 447 | 451.35 | 4.35 | 210 | 10 | 35 | 0 | 450 | 2000 | 0 | | | | | |
| PD0017 | 451.35 | 451.9 | 0.55 | 20900 | 145 | 10200 | 12 | 2740 | 65200 | | | | | | |
| PD0017 | 451.9 | 456 | 4.1 | 350 | 5 | 110 | 0 | 735 | 1000 | 0 | | | | | |
| PD0017 | 456 | 460 | 4 | 1960 | 20 | 610 | 2 | 1120 | 4600 | | | | | | |
| PD0017 | 460 | 464 | 4 | 120 | 5 | 35 | 0 | 850 | 900 | | | | | | |
| PD0017 | 464 | 465.7 | 1.7 | 35 | 5 | 25 | 0 | 700 | 2600 | 0 | | | | | |

**Appendix 5.2 cont.**

| Drill hole | From (m) | To (m) | interval (m) | Zn (ppm) | Cu (ppm) | Pb (ppm) | Ag (ppm) | Mn (ppm) | Fe (ppm) | Au (ppm) | As (ppm) | Hg (ppm) | Sn (ppm) | W (ppm) | Ba (ppm) |
|---|---|---|---|---|---|---|---|---|---|---|---|---|---|---|---|
| PD0017 | 465.7 | 466.45 | 0.75 | 1285 | 35 | 500 | 2 | 2045 | 34600 | | | | | | |
| PD0017 | 466.45 | 469.45 | 3 | 285 | 5 | 40 | 0 | 2435 | 22200 | 0 | | | | | |
| PD0017 | 496.7 | 499.4 | 2.7 | 105 | 35 | 45 | 0 | 1915 | 9600 | 0 | | | | | |
| PD0017 | 499.4 | 499.75 | 0.35 | 68500 | 1160 | 8655 | 37 | 1465 | 90100 | | | | | | |
| PD0017 | 499.4 | 499.8 | 0.4 | 50200 | 700 | 6030 | 23 | 1300 | 92400 | | 141 | 0.235 | | 645 | 13 |
| PD0017 | 499.75 | 500.65 | 0.9 | 0 | 25 | 5 | 1 | 1775 | 7800 | | | | | | |
| PD0019 | 344.86 | 348.12 | 3.26 | 330 | 25 | 80 | 0 | 1870 | 5700 | | | | | | |
| PD0019 | 348.12 | 352.26 | 4.14 | 1710 | 5 | 525 | 1 | 4600 | 16500 | | | | | | |
| PD0019 | 352.26 | 355.3 | 3.04 | 415 | 25 | 35 | 0 | 3120 | 7100 | | | | | | |
| PD0019 | 442.5 | 445 | 2.5 | 290 | 30 | 10 | 0 | 1720 | 14300 | | | | | | |
| PD0019 | 445 | 446.98 | 1.98 | 995 | 70 | 5225 | 1 | 1940 | 10900 | | | | | | |
| PD0019 | 446.98 | 450 | 3.02 | 235 | 20 | 90 | 0 | 2150 | 12900 | | | | | | |
| PD0019 | 465.74 | 466.82 | 1.08 | 610 | 15 | 140 | 0 | 10100 | 10600 | | | | | | |
| PD0019 | 466.82 | 468.09 | 1.27 | 109000 | 1895 | 150000 | 76 | 32000 | 62000 | | | | | | |
| PD0019 | 468.09 | 469.5 | 1.41 | 227000 | 1275 | 188000 | 96 | 4300 | 84000 | | | | | | |
| PD0019 | 469.5 | 471.07 | 1.57 | 192000 | 1945 | 190000 | 95 | 3800 | 35300 | | | | | | |
| PD0019 | 471.08 | 471.78 | 0.7 | 570 | 25 | 465 | 0 | 17700 | 17800 | | | | | | |
| PD0019 | 471.78 | 474.68 | 2.9 | 1340 | 25 | 505 | 0 | 10100 | 17500 | | | | | | |
| PD0019 | 474.68 | 475.77 | 1.09 | 3230 | 115 | 1935 | 3 | 3370 | 21600 | | | | | | |
| PD0019 | 475.77 | 476.21 | 0.44 | 2895 | 20 | 3835 | 4 | 4720 | 20600 | | | | | | |
| PD0019 | 476.21 | 483.39 | 7.18 | 1565 | 90 | 1425 | 2 | 1175 | 8600 | | | | | | |
| PD0019 | 483.39 | 488.75 | 5.36 | 1670 | 50 | 985 | 6 | 4640 | 27100 | | | | | | |
| PD0019 | 488.75 | 493.5 | 4.75 | 3605 | 55 | 1605 | 3 | 3360 | 41600 | | | | | | |
| PD0019 | 493.5 | 496.9 | 3.4 | 3610 | 80 | 765 | 2 | 3670 | 58400 | | | | | | |
| PD0019 | 496.9 | 502 | 5.1 | 1485 | 70 | 180 | 1 | 380 | 7800 | | | | | | |
| PD0020 | 369.76 | 376.7 | 6.94 | 448 | 46 | 70 | 0 | 1865 | 66000 | | | | | | |
| PD0020 | 376.7 | 384 | 7.3 | 994 | 72 | 1835 | 1 | 1850 | 64400 | | | | | | |
| PD0021 | 0 | 2 | 2 | 240 | 30 | 740 | 1 | 285 | | | | | | | |
| PD0021 | 401.08 | 403.5 | 2.42 | 110 | 10 | 295 | 0 | 1970 | 4400 | | | | | | |
| PD0021 | 403.5 | 406.5 | 3 | 790 | 10 | 2930 | 3 | 3140 | 13800 | | | | | | |
| PD0021 | 406.5 | 409.5 | 3 | 165 | 15 | 255 | 0 | 4110 | 6100 | | | | | | |
| PD0021 | 418.5 | 421.5 | 3 | 105 | 15 | 550 | 0 | 6900 | 6700 | | | | | | |
| PD0021 | 421.5 | 424.5 | 3 | 530 | 60 | 3705 | 2 | 9700 | 18400 | | | | | | |
| PD0021 | 424.5 | 427.5 | 3 | 390 | 310 | 6460 | 7 | 13600 | 19500 | | | | | | |

**Appendix 5.2 cont.**

| Drill hole | From (m) | To (m) | interval (m) | Zn (ppm) | Cu (ppm) | Pb (ppm) | Ag (ppm) | Mn (ppm) | Fe (ppm) | Au (ppm) | As (ppm) | Hg (ppm) | Sn (ppm) | W (ppm) | Ba (ppm) |
|---|---|---|---|---|---|---|---|---|---|---|---|---|---|---|---|
| PD0021 | 427.5 | 430.5 | 3 | 90 | 25 | 50 | 0 | 6900 | 6100 | | | | | | |
| PD0021 | 442.5 | 445.5 | 3 | 60 | 10 | 50 | 0 | 3370 | 4600 | | | | | | |
| PD0021 | 445.5 | 448.5 | 3 | 340 | 45 | 2990 | 0 | 6800 | 7100 | | | | | | |
| PD0021 | 448.5 | 451.5 | 3 | 380 | 30 | 2665 | 0 | 9800 | 7300 | | | | | | |
| PD0021 | 451.5 | 454.5 | 3 | 250 | 65 | 2130 | 1 | 6600 | 6700 | | | | | | |
| PD0021 | 454.5 | 457.5 | 3 | 315 | 20 | 160 | 0 | 3530 | 4600 | | | | | | |
| PD0021 | 574.5 | 577.5 | 3 | 445 | 50 | 20 | 0 | 1630 | 26000 | | | | | | |
| PD0021 | 577.5 | 580.5 | 3 | 1785 | 90 | 495 | 2 | 2430 | 22000 | | | | | | |
| PD0021 | 580.5 | 583.5 | 3 | 2810 | 65 | 2555 | 4 | 5060 | 16600 | | | | | | |
| PD0021 | 583.5 | 586.5 | 3 | 2210 | 35 | 2485 | 4 | 5800 | 35900 | | | | | | |
| PD0021 | 586.5 | 589.5 | 3 | 310 | 50 | 90 | 0 | 2580 | 35600 | | | | | | |
| PD0021 | 589.5 | 592.5 | 3 | 1930 | 655 | 570 | 2 | 2770 | 24000 | | | | | | |
| PD0021 | 592.5 | 595.5 | 3 | 5130 | 80 | 1855 | 4 | 9500 | 49200 | | | | | | |
| PD0021 | 595.5 | 598.5 | 3 | 2080 | 35 | 1015 | 2 | 7800 | 72600 | | | | | | |
| PD0021 | 598.5 | 601.5 | 3 | 395 | 105 | 25 | 1 | 3520 | 64900 | | | | | | |
| PD0022 | 236.4 | 237.6 | 1.2 | 350 | 5 | 190 | 1 | 7880 | 35100 | | | | | | |
| PD0022 | 237.6 | 238.8 | 1.2 | 2900 | 20 | 2370 | 2 | 19700 | 35400 | | | | | | |
| PD0022 | 238.8 | 240 | 1.2 | 5690 | 10 | 2280 | 5 | 27300 | 50000 | | | | | | |
| PD0022 | 240 | 241.1 | 1.1 | 6030 | 15 | 3200 | 3 | 35400 | 42200 | | | | | | |
| PD0022 | 241.1 | 242.2 | 1.1 | 3150 | 5 | 790 | 3 | 29500 | 66900 | | | | | | |
| PD0022 | 242.2 | 243.3 | 1.1 | 7230 | 15 | 2030 | 4 | 38500 | 48000 | | | | | | |
| PD0022 | 243.3 | 244.4 | 1.1 | 600 | 5 | 160 | 1 | 9290 | 78900 | | | | | | |
| PD0022 | 245.5 | 246.5 | 1 | 270 | | 110 | 1 | 4360 | 32700 | | | | | | |
| PD0022 | 246.5 | 247.5 | 1 | 4130 | 10 | 3530 | 3 | 16500 | 69600 | | | | | | |
| PD0022 | 247.5 | 248.9 | 1.4 | 15700 | 40 | 5020 | 5 | 24200 | 57400 | | | | | | |
| PD0022 | 248.9 | 249.6 | 0.7 | 15500 | 50 | 6830 | 8 | 2450 | 43000 | | | | | | |
| PD0022 | 249.6 | 251 | 1.4 | 20500 | 95 | 9360 | 8 | 30900 | 54800 | | | | | | |
| PD0022 | 251 | 252.5 | 1.5 | 14500 | 50 | 4150 | 6 | 26900 | 43700 | | | | | | |
| PD0022 | 252.5 | 253.9 | 1.4 | 6910 | 10 | 5580 | 7 | 14800 | 42200 | | | | | | |
| PD0022 | 253.9 | 254.8 | 0.9 | 700 | 5 | 770 | 1 | 10900 | 25500 | | | | | | |
| PD0022 | 254.8 | 260.8 | 6 | 1730 | 10 | 2520 | 1 | 24000 | 22900 | | | | | | |
| PD0022 | 260.8 | 267.8 | 7 | 3965 | 12 | 1910 | 2 | 19900 | 23600 | | | | | | |
| PD0022 | 267.8 | 269.8 | 2 | 6290 | 5 | 1790 | 2 | 17700 | 28200 | | | | | | |
| PD0022 | 269.8 | 270.4 | 0.6 | 10200 | 35 | 15400 | 24 | 12700 | 126000 | | | | | | |

**Appendix 5.2 cont.**

| Drill hole | From (m) | To (m) | interval (m) | Zn (ppm) | Cu (ppm) | Pb (ppm) | Ag (ppm) | Mn (ppm) | Fe (ppm) | Au (ppm) | As (ppm) | Hg (ppm) | Sn (ppm) | W (ppm) | Ba (ppm) |
|---|---|---|---|---|---|---|---|---|---|---|---|---|---|---|---|
| PD0022 | 270.4 | 272.4 | 2 | 12500 | 45 | 6400 | 14 | 45500 | 53500 | | | | | | |
| PD0022 | 272.4 | 273.2 | 0.8 | 480 | 10 | 280 | 1 | 10500 | 28800 | | | | | | |
| PD0022 | 303.2 | 313.2 | 10 | 658 | 12 | 15 | 0 | 1470 | 25600 | | | | | | |
| PD0022 | 313.2 | 323.2 | 10 | 1480 | 2 | 30 | 0 | 2980 | 24200 | | | | | | |
| PD0022 | 323.2 | 333.2 | 10 | 1470 | 24 | 35 | 0 | 3155 | 47500 | | | | | | |
| PD0022 | 333.2 | 343.2 | 10 | 552 | 4 | 1665 | 0 | 5250 | 23700 | | | | | | |
| PD0022 | 343.2 | 353.2 | 10 | 550 | 8 | 155 | 0 | 8055 | 26200 | | | | | | |
| PD0022 | 353.2 | 363.2 | 10 | 4720 | 30 | 1160 | 7 | 6250 | 43000 | | | | | | |
| PD0022 | 363.2 | 373.2 | 10 | 646 | 16 | 145 | 0 | 4380 | 61000 | | | | | | |
| PD0022 | 438.6 | 448.6 | 10 | 204 | 0 | 50 | 0 | 400 | 10400 | | | | | | |
| PD0022 | 448.6 | 458.6 | 10 | 5976 | 18 | 1925 | 12 | 14300 | 25100 | | | | | | |
| PD0022 | 458.6 | 461.8 | 3.2 | 686 | 24 | 140 | 2 | 5660 | 25700 | | | | | | |
| PD0022 | 461.8 | 465.7 | 3.9 | 3548 | 80 | 650 | 4 | 4750 | 39500 | | | | | | |
| PD0022 | 465.7 | 470.3 | 4.6 | 322 | 4 | 25 | 0 | 1410 | 8400 | | | | | | |
| PD0022 | 472.5 | 482.5 | 10 | 870 | 20 | 120 | 0 | 1790 | 22100 | | | | | | |
| PD0022 | 482.5 | 492.5 | 10 | 4560 | 74 | 2100 | 7 | 2370 | 21400 | | | | | | |
| PD0022 | 492.5 | 502.5 | 10 | 578 | 2 | 65 | 0 | 520 | 2300 | | | | | | |
| PD0023 | 180 | 182 | 2 | 746 | 8 | 375 | 0 | 35 | 6300 | | | | | | |
| PD0023 | 274 | 281 | 7 | 3580 | 50 | 810 | 2 | 4200 | 67300 | | | | | | |
| PD0023 | 281 | 288 | 7 | 5100 | 38 | 1995 | 23 | 4950 | 51700 | | | | | | |
| PD0024 | 126 | 128 | 2 | 890 | 35 | 285 | 0 | 1020 | 20000 | | | | | | |
| PD0024 | 128 | 130 | 2 | 1565 | 40 | 370 | 1 | 985 | 17900 | | | | | | |
| PD0024 | 130 | 132 | 2 | 1240 | 40 | 285 | 1 | 1035 | 18800 | | | | | | |
| PD0024 | 132 | 134 | 2 | 520 | 40 | 155 | 1 | 1465 | 20600 | | | | | | |
| PD0024 | 134 | 136 | 2 | 400 | 25 | 1345 | 1 | 1275 | 16400 | | | | | | |
| PD0024 | 136 | 138 | 2 | 275 | 20 | 100 | 1 | 1110 | 13100 | | | | | | |
| PD0024 | 140 | 142 | 2 | 605 | 15 | 150 | 0 | 1280 | 13600 | | | | | | |
| PD0024 | 142 | 144 | 2 | 1095 | 20 | 320 | 1 | 9200 | 14200 | | | | | | |
| PD0024 | 144 | 146 | 2 | 1385 | 45 | 220 | 1 | 1080 | 14100 | | | | | | |
| PD0024 | 146 | 148 | 2 | 1335 | 45 | 220 | 1 | 895 | 15300 | | | | | | |
| PD0024 | 148 | 150 | 2 | 965 | 35 | 215 | 2 | 1640 | 19700 | | | | | | |
| PD0024 | 160 | 162 | 2 | 920 | 30 | 195 | 1 | 1085 | 10100 | | | | | | |
| PD0024 | 162 | 164 | 2 | 1205 | 35 | 230 | 1 | 1135 | 12000 | | | | | | |
| PD0024 | 164 | 166 | 2 | 790 | 20 | 170 | 1 | 1240 | 11500 | | | | | | |

**Appendix 5.2 cont.**

| Drill hole | From (m) | To (m) | interval (m) | Zn (ppm) | Cu (ppm) | Pb (ppm) | Ag (ppm) | Mn (ppm) | Fe (ppm) | Au (ppm) | As (ppm) | Hg (ppm) | Sn (ppm) | W (ppm) | Ba (ppm) |
|---|---|---|---|---|---|---|---|---|---|---|---|---|---|---|---|
| PD0024 | 166 | 168 | 2 | 720 | 20 | 215 | 1 | 1365 | 11600 | | | | | | |
| PD0024 | 168 | 170 | 2 | 755 | 10 | 205 | 1 | 1205 | 10500 | | | | | | |
| PD0024 | 170 | 172 | 2 | 1250 | 15 | 395 | 2 | 1365 | 11600 | | | | | | |
| PD0024 | 172 | 174 | 2 | 1475 | 15 | 420 | 2 | 1530 | 13600 | | | | | | |
| PD0024 | 174 | 176 | 2 | 1215 | 10 | 325 | 1 | 1250 | 14300 | | | | | | |
| PD0024 | 176 | 178 | 2 | 1110 | 15 | 340 | 2 | 590 | 12500 | | | | | | |
| PD0024 | 178 | 180 | 2 | 1065 | 15 | 330 | 2 | 455 | 11500 | | | | | | |
| PD0024 | 180 | 182 | 2 | 1465 | 20 | 375 | 2 | 400 | 13000 | | | | | | |
| PD0024 | 182 | 184 | 2 | 1460 | 20 | 420 | 2 | 1325 | 13500 | | | | | | |
| PD0024 | 184 | 186 | 2 | 2140 | 20 | 470 | 2 | 895 | 16900 | | | | | | |
| PD0024 | 186 | 188 | 2 | 1610 | 15 | 330 | 2 | 925 | 13900 | | | | | | |
| PD0024 | 188 | 190 | 2 | 2380 | 10 | 350 | 2 | 360 | 14500 | | | | | | |
| PD0024 | 190 | 192 | 2 | 1690 | 10 | 315 | 2 | 2365 | 19500 | | | | | | |
| PD0024 | 192 | 194 | 2 | 1740 | 10 | 330 | 2 | 2460 | 19700 | | | | | | |
| PD0024 | 194 | 196 | 2 | 1310 | 10 | 295 | 2 | 755 | 18000 | | | | | | |
| PD0024 | 196 | 198 | 2 | 1270 | 5 | 280 | 3 | 670 | 20400 | | | | | | |
| PD0024 | 198 | 200 | 2 | 1280 | 20 | 295 | 4 | 750 | 25300 | | | | | | |
| PD0024 | 200 | 202 | 2 | 1175 | 25 | 335 | 6 | 430 | 39600 | | | | | | |
| PD0024 | 202 | 204 | 2 | 1170 | 20 | 365 | 6 | 670 | 35100 | | | | | | |
| PD0024 | 204 | 206 | 2 | 1320 | 20 | 960 | 2 | 640 | 19000 | | | | | | |
| PD0024 | 206 | 208 | 2 | 2940 | 75 | 625 | 6 | 660 | 41500 | | | | | | |
| PD0024 | 208 | 210 | 2 | 12200 | 165 | 5340 | 5 | 1160 | 32500 | | | | | | |
| PD0024 | 210 | 212 | 2 | 5075 | 80 | 2460 | 2 | 1240 | 12600 | | | | | | |
| PD0024 | 212 | 214 | 2 | 1930 | 30 | 805 | 2 | 980 | 14800 | | | | | | |
| PD0024 | 214 | 216 | 2 | 1930 | 135 | 585 | 6 | 755 | 42600 | | | | | | |
| PD0024 | 216 | 218 | 2 | 1945 | 90 | 950 | 8 | 640 | 46800 | | | | | | |
| PD0024 | 218 | 220 | 2 | 1285 | 50 | 720 | 5 | 925 | 29400 | | | | | | |
| PD0024 | 220 | 222 | 2 | 1770 | 60 | 3180 | 6 | 985 | 28800 | | | | | | |
| PD0024 | 222 | 224 | 2 | 1970 | 50 | 2400 | 6 | 945 | 26700 | | | | | | |
| PD0024 | 224 | 225 | 1 | 2070 | 45 | 1850 | 4 | 780 | 22600 | | | | | | |
| PD0024 | 225 | 225.6 | 0.6 | 2905 | 50 | 2115 | 6 | 585 | 24700 | | | | | | |
| PD0024 | 225.6 | 227.6 | 2 | 4370 | 40 | 3110 | 6 | 805 | 20100 | | | | | | |
| PD0024 | 227.6 | 229.6 | 2 | 11000 | 90 | 6150 | 16 | 4505 | 19600 | | | | | | |
| PD0024 | 229.6 | 231.6 | 2 | 10800 | 105 | 6380 | 15 | 4890 | 19700 | | | | | | |

**Appendix 5.2 cont.**

| Drill hole | From (m) | To (m) | interval (m) | Zn (ppm) | Cu (ppm) | Pb (ppm) | Ag (ppm) | Mn (ppm) | Fe (ppm) | Au (ppm) | As (ppm) | Hg (ppm) | Sn (ppm) | W (ppm) | Ba (ppm) |
|---|---|---|---|---|---|---|---|---|---|---|---|---|---|---|---|
| PD0024 | 231.6 | 233.6 | 2 | 41600 | 460 | 21600 | 23 | 9080 | 116100 | | | | | | |
| PD0024 | 233.6 | 235.6 | 2 | 43800 | 745 | 52600 | 54 | 860 | 88000 | | | | | | |
| PD0024 | 235.6 | 237.1 | 1.5 | 48800 | 225 | 75000 | 39 | 130 | 32700 | | | | | | |
| PD0024 | 237.1 | 240.4 | 3.3 | 1230 | 255 | 12900 | 37 | 60 | 15600 | | | | | | |
| PD0024 | 240.4 | 241.4 | 1 | 49400 | 1555 | 78500 | 87 | 300 | 138300 | | | | | | |
| PD0024 | 241.4 | 241.8 | 0.4 | 1150 | 265 | 5680 | 49 | 140 | 21300 | | | | | | |
| PD0024 | 241.8 | 242.3 | 0.5 | 2610 | 700 | 59100 | 66 | 120 | 54300 | | | | | | |
| PD0024 | 242.3 | 242.5 | 0.2 | 7680 | 580 | 62900 | 89 | 120 | 20600 | | | | | | |
| PD0024 | 242.5 | 244.5 | 2 | 60000 | 2195 | 95700 | 97 | 480 | 87600 | | | | | | |
| PD0024 | 244.5 | 247.3 | 2.8 | 9670 | 250 | 66700 | 25 | 290 | 65100 | | | | | | |
| PD0024 | 247.3 | 247.9 | 0.6 | 10500 | 605 | 107000 | 129 | 260 | 207900 | | | | | | |
| PD0024 | 247.9 | 249.2 | 1.3 | 8550 | 365 | 12300 | 28 | 330 | 26600 | | | | | | |
| PD0024 | 249.2 | 249.9 | 0.7 | 1710 | 55 | 2710 | 4 | 370 | 15200 | | | | | | |
| PD0024 | 249.9 | 250.5 | 0.6 | 15900 | 390 | 16300 | 17 | 450 | 37000 | | | | | | |
| PD0024 | 250.5 | 250.8 | 0.3 | 3170 | 120 | 2360 | 8 | 300 | 16600 | | | | | | |
| PD0024 | 250.8 | 251.2 | 0.4 | 10500 | 325 | 9330 | 21 | 350 | 30400 | | | | | | |
| PD0024 | 251.2 | 253.4 | 2.2 | 530 | 10 | 200 | 1 | 420 | 15100 | | | | | | |
| PD0024 | 253.4 | 254.1 | 0.7 | 8870 | | 380 | 0 | 26400 | 99400 | | | | | | |
| PD0024 | 254.1 | 262.9 | 8.8 | 6962 | 24 | 1260 | 1 | 22500 | 141500 | | | | | | |
| PD0024 | 262.9 | 272.9 | 10 | 488 | 16 | 385 | 1 | 6990 | 89900 | | | | | | |
| PD0024 | 272.9 | 282.9 | 10 | 2556 | 66 | 755 | 1 | 11800 | 147300 | | | | | | |
| PD0024 | 282.9 | 292.9 | 10 | 5176 | 200 | 9420 | 16 | 2745 | 52100 | | | | | | |
| PD0024 | 292.9 | 299.9 | 7 | 972 | 60 | 2025 | 2 | 1940 | 15200 | | | | | | |
| PD0024 | 299.9 | 307.9 | 8 | 2254 | 74 | 985 | 2 | 2730 | 38800 | | | | | | |
| PD0024 | 307.9 | 308.4 | 0.5 | 4480 | 470 | 2210 | 11 | 2570 | 43600 | | | | | | |
| PD0024 | 308.4 | 310.4 | 2 | 574 | 34 | 280 | 1 | 1405 | 46100 | | | | | | |
| PD0024 | 310.4 | 320 | 9.6 | 580 | 38 | 160 | 0 | 2145 | 41600 | | | | | | |
| PD0024 | 320 | 321.2 | 1.2 | 80 | 5 | 100 | 0 | | 28800 | | | | | | |
| PD0024 | 321.2 | 321.6 | 0.4 | 1730 | 510 | 970 | 3 | 6310 | 55500 | | | | | | |
| PD0024 | 321.6 | 323 | 1.4 | 320 | 20 | 680 | 0 | 3450 | 24500 | | | | | | |
| PD0024 | 323 | 324.4 | 1.4 | 880 | 55 | 420 | 3 | 4170 | 34900 | | | | | | |
| PD0024 | 324.4 | 325.8 | 1.4 | 2550 | 175 | 1340 | 10 | 9840 | 42100 | | | | | | |
| PD0024 | 325.8 | 326.6 | 0.8 | 640 | 25 | 200 | 1 | 3050 | 18500 | | | | | | |
| PD0024 | 326.6 | 328 | 1.4 | 3040 | 95 | 1630 | 6 | 11500 | 40000 | | | | | | |

**Appendix 5.2 cont.**

| Drill hole | From (m) | To (m) | interval (m) | Zn (ppm) | Cu (ppm) | Pb (ppm) | Ag (ppm) | Mn (ppm) | Fe (ppm) | Au (ppm) | As (ppm) | Hg (ppm) | Sn (ppm) | W (ppm) | Ba (ppm) |
|---|---|---|---|---|---|---|---|---|---|---|---|---|---|---|---|
| PD0024 | 328 | 330 | 2 | 3410 | 130 | 2090 | 6 | 8650 | 30900 | | | | | | |
| PD0024 | 330 | 331.8 | 1.8 | 4390 | 160 | 1360 | 6 | 14900 | 31300 | | | | | | |
| PD0024 | 331.8 | 334 | 2.2 | 12100 | 90 | 5060 | 16 | 12200 | 51500 | | | | | | |
| PD0024 | 334 | 336 | 2 | 70300 | 515 | 18700 | 45 | 11600 | 95200 | | | | | | |
| PD0024 | 336 | 338 | 2 | 54800 | 450 | 26900 | 39 | 1580 | 154500 | | | | | | |
| PD0024 | 338 | 339.3 | 1.3 | 55000 | 625 | 27400 | 47 | 1970 | 123900 | | | | | | |
| PD0024 | 339.3 | 341.3 | 2 | 29400 | 415 | 10900 | 18 | 5500 | 31000 | | | | | | |
| PD0024 | 341.3 | 343.3 | 2 | 56600 | 670 | 35600 | 28 | 15200 | 31600 | | | | | | |
| PD0024 | 343.3 | 345.3 | 2 | 40400 | 410 | 33800 | 29 | 5500 | 43500 | | | | | | |
| PD0024 | 345.3 | 347.2 | 1.9 | 13600 | 90 | 7090 | 6 | 7050 | 21200 | | | | | | |
| PD0024 | 347.2 | 349.1 | 1.9 | 46000 | 570 | 112300 | 49 | 72200 | 50300 | | | | | | |
| PD0024 | 349.1 | 350.1 | 1 | 1550 | 15 | 560 | 0 | 9850 | 7100 | | | | | | |
| PD0024 | 369.4 | 370.3 | 0.9 | 580 | 20 | 580 | 0 | 2240 | 10400 | | | | | | |
| PD0024 | 370.3 | 370.9 | 0.6 | 89500 | 1730 | 63800 | 16 | 2680 | 11700 | | | | | | |
| PD0024 | 370.9 | 371.3 | 0.4 | 2350 | 90 | 2250 | 1 | 1380 | 16400 | | | | | | |
| PD0024 | 371.3 | 377.4 | 6.1 | 2174 | 68 | 2715 | 1 | 3135 | 18300 | | | | | | |
| PD0024 | 377.4 | 385.8 | 8.4 | 2004 | 88 | 3515 | 0 | 1510 | 23700 | | | | | | |
| PD0024 | 385.8 | 395 | 9.2 | 5054 | 54 | 4895 | 2 | 5450 | 35800 | | | | | | |
| PD0024 | 395 | 400.7 | 5.7 | 1858 | 38 | 1730 | 1 | 5395 | 17300 | | | | | | |
| PD0024 | 400.7 | 401.3 | 0.6 | 990 | | 780 | 0 | 14600 | 10300 | | | | | | |
| PD0024 | 401.3 | 401.7 | 0.4 | 233300 | 1735 | 233500 | 108 | 2860 | 78400 | | | | | | |
| PD0024 | 401.7 | 402.4 | 0.7 | 8090 | 50 | 4700 | 9 | 17100 | 19000 | | | | | | |
| PD0024 | 402.4 | 410.5 | 8.1 | 3978 | 32 | 3310 | 3 | 6845 | 20100 | | | | | | |
| PD0024 | 410.5 | 411.1 | 0.6 | 7910 | 50 | 4870 | 2 | 7000 | 16400 | | | | | | |
| PD0024 | 411.1 | 411.3 | 0.2 | 150400 | 1230 | 104200 | 50 | 2690 | 55800 | | | | | | |
| PD0024 | 411.3 | 411.7 | 0.4 | 1010 | 15 | 660 | 0 | 5610 | 14200 | | | | | | |
| PD0024 | 411.7 | 421.7 | 10 | 1798 | 84 | 1095 | 1 | 5075 | 23600 | | | | | | |
| PD0024 | 421.7 | 431.7 | 10 | 962 | 14 | 420 | 1 | 5805 | 38300 | | | | | | |
| PD0024 | 431.7 | 440.1 | 8.4 | 1094 | 8 | 470 | 2 | 4590 | 19300 | | | | | | |
| PD0024 | 440.1 | 449.9 | 9.8 | 2484 | 42 | 1330 | 0 | 5500 | 41500 | | | | | | |
| PD0024 | 449.9 | 455.6 | 5.7 | 278 | 18 | 50 | 0 | 1135 | 34100 | | | | | | |
| PD0024 | 492 | 498.6 | 6.6 | 306 | 26 | 65 | 0 | 1380 | 85700 | | | | | | |
| PD0024 | 498.6 | 508.6 | 10 | 10200 | 58 | 4435 | 4 | 8460 | 21400 | | | | | | |
| PD0024 | 508.6 | 518.6 | 10 | 3478 | 52 | 680 | 2 | 6765 | 11600 | | | | | | |

**Appendix 5.2 cont.**

| Drill hole | From (m) | To (m) | interval (m) | Zn (ppm) | Cu (ppm) | Pb (ppm) | Ag (ppm) | Mn (ppm) | Fe (ppm) | Au (ppm) | As (ppm) | Hg (ppm) | Sn (ppm) | W (ppm) | Ba (ppm) |
|---|---|---|---|---|---|---|---|---|---|---|---|---|---|---|---|
| PD0024 | 518.6 | 528.6 | 10 | 4152 | 50 | 1105 | 1 | 2070 | 6100 | | | | | | |
| PD0024 | 528.6 | 538.6 | 10 | 356 | 10 | 40 | 1 | 565 | 2200 | | | | | | |
| PD0025 | 94 | 96 | 2 | 832 | 56 | 240 | 0 | 890 | 41900 | | | | | | |
| PD0025 | 96 | 98 | 2 | 1608 | 50 | 365 | 0 | 995 | 41700 | | | | | | |
| PD0025 | 98 | 100 | 2 | 988 | 28 | 260 | 0 | 1030 | 25400 | | | | | | |
| PD0025 | 210.5 | 218.5 | 8 | 160 | 16 | 185 | 1 | 2845 | 47600 | | | | | | |
| PD0025 | 218.5 | 226.6 | 8.1 | 4864 | 32 | 5990 | 6 | 10800 | 47500 | | | | | | |
| PD0025 | 226.6 | 231.7 | 5.1 | 172 | 10 | 95 | 0 | 2770 | 27300 | | | | | | |
| PD0025 | 332.1 | 339.2 | 7.1 | 200 | 14 | 180 | 1 | 1300 | 7200 | | | | | | |
| PD0025 | 339.2 | 349 | 9.8 | 2056 | 12 | 525 | 3 | 625 | 15200 | | | | | | |
| PD0025 | 349 | 350.2 | 1.2 | 7660 | 15 | 710 | 3 | 1980 | 15100 | | | | | | |
| PD0025 | 350.2 | 352 | 1.8 | 3230 | 10 | 1030 | 1 | 34000 | 27200 | | | | | | |
| PD0025 | 352 | 354 | 2 | 7660 | 25 | 1450 | 6 | 17800 | 28000 | | | | | | |
| PD0025 | 354 | 356 | 2 | 7400 | 15 | 1040 | 2 | 24000 | 24000 | | | | | | |
| PD0025 | 356 | 358 | 2 | 720 | 5 | 190 | 1 | 14600 | 13600 | | | | | | |
| PD0025 | 362 | 363.5 | 1.5 | 750 | 10 | 560 | 2 | 18800 | 31400 | | | | | | |
| PD0025 | 363.5 | 365.5 | 2 | 1170 | 10 | 880 | 4 | 19700 | 33600 | | | | | | |
| PD0025 | 365.5 | 367.5 | 2 | 2000 | 5 | 830 | 1 | 22000 | 33500 | | | | | | |
| PD0025 | 367.5 | 369.5 | 2 | 2990 | 10 | 740 | 3 | 23700 | 33100 | | | | | | |
| PD0025 | 369.5 | 370.2 | 0.7 | 1730 | 5 | 570 | 3 | 21000 | 23400 | | | | | | |
| PD0025 | 370.2 | 371.4 | 1.2 | 1290 | 5 | 540 | 3 | 17400 | 32000 | | | | | | |
| PD0025 | 371.4 | 372.6 | 1.2 | 1990 | 10 | 660 | 1 | 22900 | 27700 | | | | | | |
| PD0025 | 372.6 | 373.6 | 1 | 1500 | 5 | 740 | 1 | 26800 | 13800 | | | | | | |
| PD0025 | 373.6 | 375.6 | 2 | 1100 | 5 | 390 | 1 | 29200 | 14500 | | | | | | |
| PD0025 | 375.6 | 377.9 | 2.3 | 1270 | 5 | 620 | 2 | 30700 | 21800 | | | | | | |
| PD0025 | 377.9 | 379 | 1.1 | 400 | 5 | 160 | 1 | 11600 | 9800 | | | | | | |
| PD0025 | 379 | 384.9 | 5.9 | 1512 | 8 | 1650 | 1 | 23200 | 15500 | | | | | | |
| PD0025 | 384.9 | 394.9 | 10 | 2366 | 10 | 1350 | 1 | 14300 | 11300 | | | | | | |
| PD0025 | 394.9 | 404.9 | 10 | 3988 | 8 | 4135 | 4 | 24400 | 16400 | | | | | | |
| PD0025 | 404.9 | 414.9 | 10 | 502 | 0 | 235 | 0 | 9530 | 5800 | | | | | | |
| PD0025 | 414.9 | 424.9 | 10 | 4038 | 4 | 4895 | 3 | 13800 | 5500 | | | | | | |
| PD0025 | 424.9 | 434.9 | 10 | 692 | 6 | 1220 | 2 | 18800 | 15000 | | | | | | |
| PD0025 | 434.9 | 437.8 | 2.9 | 914 | 4 | 2980 | 2 | 20700 | 17300 | | | | | | |
| PD0025 | 437.8 | 438.8 | 1 | 994 | 8 | 1845 | 1 | 17800 | 16700 | | | | | | |

**Appendix 5.2 cont.**

| Drill hole | From (m) | To (m) | interval (m) | Zn (ppm) | Cu (ppm) | Pb (ppm) | Ag (ppm) | Mn (ppm) | Fe (ppm) | Au (ppm) | As (ppm) | Hg (ppm) | Sn (ppm) | W (ppm) | Ba (ppm) |
|---|---|---|---|---|---|---|---|---|---|---|---|---|---|---|---|
| PD0025 | 438.8 | 448 | 9.2 | 676 | 24 | 1000 | 2 | 8420 | 45500 | | | | | | |
| PD0025 | 492 | 502 | 10 | 284 | 52 | 75 | 1 | 2555 | 79100 | | | | | | |
| PD0025 | 531 | 531.6 | 0.6 | 0 | 5 | 20 | 1 | 2460 | 7000 | | | | | | |
| PD0025 | 531.6 | 533 | 1.4 | 1080 | 5 | 710 | 4 | 15900 | 25200 | | | | | | |
| PD0025 | 533 | 533.7 | 0.7 | 3250 | 5 | 2050 | 5 | 27000 | 43000 | | | | | | |
| PD0025 | 533.7 | 534.3 | 0.6 | 660 | 5 | 390 | 1 | 9420 | 15300 | | | | | | |
| PD0025 | 534.3 | 535.7 | 1.4 | 1340 | 15 | 1640 | 3 | 29400 | 38000 | | | | | | |
| PD0025 | 535.7 | 536.7 | 1 | 52500 | 440 | 43500 | 41 | 37300 | 82200 | | | | | | |
| PD0025 | 536.7 | 537.7 | 1 | 33000 | 575 | 29500 | 15 | 32600 | 61300 | | | | | | |
| PD0025 | 537.7 | 539.2 | 1.5 | 18800 | 365 | 13100 | 25 | 20900 | 76400 | | | | | | |
| PD0025 | 539.2 | 540.7 | 1.5 | 7400 | 165 | 5640 | 14 | 9720 | 69800 | | | | | | |
| PD0025 | 540.7 | 542.2 | 1.5 | 1440 | 35 | 930 | 3 | 4970 | 49800 | | | | | | |
| PD0025 | 542.2 | 543.8 | 1.6 | 3780 | 50 | 2660 | 6 | 9050 | 28200 | | | | | | |
| PD0025 | 543.8 | 545.4 | 1.6 | 480 | 25 | 680 | 4 | 7760 | 44600 | | | | | | |
| PD0025 | 621.4 | 626.7 | 5.3 | 144 | 18 | 45 | 0 | 500 | 8900 | | | | | | |
| PD0025 | 626.7 | 633 | 6.3 | 1716 | 154 | 380 | 5 | 1580 | 34400 | | | | | | |
| PD0025 | 633 | 639 | 6 | 1406 | 28 | 640 | 1 | 4715 | 47700 | | | | | | |
| PD0025 | 639 | 646 | 7 | 4690 | 108 | 1980 | 3 | 3585 | 58100 | | | | | | |
| PD0025 | 646 | 652.2 | 6.2 | 6798 | 110 | 4395 | 5 | 5210 | 66200 | | | | | | |
| PD0025 | 652.2 | 656.2 | 4 | 406 | 48 | 1550 | 10 | 9205 | 40700 | | | | | | |
| PD0025 | 656.2 | 658.4 | 2.2 | 238 | 56 | 1320 | 1 | 5780 | 25100 | | | | | | |
| PD0026 | 82 | 84 | 2 | 334 | 20 | 110 | 0 | 860 | 12900 | | | | | | |
| PD0026 | 84 | 86 | 2 | 1286 | 26 | 505 | 0 | 2560 | 17200 | | | | | | |
| PD0026 | 86 | 88 | 2 | 6195 | 76 | 3030 | 2 | 8915 | 23400 | | | | | | |
| PD0026 | 88 | 90 | 2 | 4870 | 48 | 2050 | 2 | 9900 | 19500 | | | | | | |
| PD0026 | 90 | 92 | 2 | 2870 | 26 | 2000 | 2 | 18000 | 32900 | | | | | | |
| PD0026 | 92 | 94 | 2 | 700 | 22 | 360 | 1 | 6020 | 23700 | | | | | | |
| PD0026 | 94 | 96 | 2 | 800 | 20 | 380 | 1 | 6255 | 24300 | | | | | | |
| PD0026 | 96 | 98 | 2 | 2790 | 40 | 2200 | 1 | 5750 | 30300 | | | | | | |
| PD0026 | 98 | 100 | 2 | 376 | 36 | 245 | 0 | 3035 | 33100 | | | | | | |
| PD0026 | 102 | 104 | 2 | 106 | 56 | 70 | 0 | 2145 | 29900 | | | | | | |
| PD0026 | 104 | 106 | 2 | 1520 | 150 | 4305 | 3 | 12100 | 24600 | | | | | | |
| PD0026 | 106 | 108 | 2 | 478 | 80 | 1400 | 1 | 5920 | 29000 | | | | | | |
| PD0026 | 108 | 110 | 2 | 272 | 90 | 495 | 1 | 2440 | 32500 | | | | | | |

**Appendix 5.2 cont.**

| Drill hole | From (m) | To (m) | interval (m) | Zn (ppm) | Cu (ppm) | Pb (ppm) | Ag (ppm) | Mn (ppm) | Fe (ppm) | Au (ppm) | As (ppm) | Hg (ppm) | Sn (ppm) | W (ppm) | Ba (ppm) |
|---|---|---|---|---|---|---|---|---|---|---|---|---|---|---|---|
| PD0026 | 110 | 112 | 2 | 198 | 44 | 285 | 1 | 2465 | 42400 | | | | | | |
| PD0026 | 112 | 114 | 2 | 2450 | 78 | 2210 | 1 | 2500 | 29300 | | | | | | |
| PD0026 | 114 | 116 | 2 | 218 | 20 | 120 | 0 | 1825 | 36200 | | | | | | |
| PD0026 | 118 | 120 | 2 | 110 | 24 | 95 | 1 | 1680 | 29800 | | | | | | |
| PD0026 | 120 | 122 | 2 | 2560 | 238 | 3610 | 2 | 1580 | 32100 | | | | | | |
| PD0026 | 122 | 124 | 2 | 186 | 40 | 155 | 0 | 2745 | 35300 | | | | | | |
| PD0026 | 124 | 126 | 2 | 420 | 78 | 400 | 1 | 3760 | 45100 | | | | | | |
| PD0026 | 126 | 128 | 2 | 1270 | 166 | 700 | 1 | 3710 | 52900 | | | | | | |
| PD0026 | 128 | 130 | 2 | 1030 | 344 | 1700 | 2 | 2670 | 52400 | | | | | | |
| PD0026 | 130 | 132 | 2 | 608 | 142 | 330 | 1 | 4640 | 56900 | | | | | | |
| PD0026 | 140 | 142 | 2 | 552 | 120 | 315 | 1 | 3135 | 45600 | | | | | | |
| PD0026 | 142 | 144 | 2 | 3495 | 112 | 1475 | 4 | 2650 | 38000 | | | | | | |
| PD0026 | 144 | 146 | 2 | 3985 | 140 | 2090 | 5 | 1625 | 27000 | | | | | | |
| PD0026 | 146 | 148 | 2 | 3305 | 142 | 1375 | 5 | 2915 | 27900 | | | | | | |
| PD0026 | 148 | 150 | 2 | 1535 | 156 | 780 | 4 | 5980 | 41000 | | | | | | |
| PD0026 | 150 | 152 | 2 | 3305 | 68 | 1650 | 6 | 2250 | 33800 | | | | | | |
| PD0026 | 152 | 154 | 2 | 4545 | 88 | 2925 | 8 | 1935 | 46200 | | | | | | |
| PD0026 | 154 | 156 | 2 | 3420 | 88 | 1585 | 7 | 965 | 28700 | | | | | | |
| PD0026 | 156 | 158 | 2 | 2515 | 88 | 1355 | 8 | 825 | 31000 | | | | | | |
| PD0026 | 158 | 160 | 2 | 2800 | 56 | 1295 | 6 | 705 | 29500 | | | | | | |
| PD0026 | 160 | 162 | 2 | 3495 | 52 | 1625 | 6 | 935 | 35800 | | | | | | |
| PD0026 | 162 | 164 | 2 | 2740 | 34 | 1530 | 5 | 600 | 22500 | | | | | | |
| PD0026 | 164 | 165 | 1 | 3600 | 34 | 1610 | 8 | 465 | 27100 | | | | | | |
| PD0026 | 165 | 165.8 | 0.8 | 4728 | 106 | 2150 | 10 | 625 | 34700 | | | | | | |
| PD0026 | 170 | 180 | 10 | 5405 | 40 | 1730 | 5 | 770 | 14900 | | | | | | |
| PD0026 | 180 | 189 | 9 | 6700 | 44 | 2480 | 5 | 725 | 12700 | | | | | | |
| PD0026 | 189 | 191 | 2 | 18100 | 50 | 6650 | 16 | 430 | 40000 | | | | | | |
| PD0026 | 191 | 193 | 2 | 37000 | 135 | 11500 | 24 | 520 | 63500 | | | | | | |
| PD0026 | 193 | 195 | 2 | 31900 | 85 | 7060 | 17 | 230 | 48400 | | | | | | |
| PD0026 | 195 | 197 | 2 | 20100 | 100 | 9890 | 11 | 210 | 40600 | | | | | | |
| PD0026 | 197 | 207 | 10 | 11100 | 30 | 7235 | 7 | 215 | 17400 | | | | | | |
| PD0026 | 207 | 208 | 1 | 8910 | 50 | 6210 | 5 | 310 | 31900 | | | | | | |
| PD0026 | 209 | 211 | 2 | 1690 | 15 | 740 | 3 | 1230 | 21900 | | | | | | |
| PD0026 | 211 | 213 | 2 | 11700 | 75 | 3840 | 6 | 150 | 43900 | | | | | | |

**Appendix 5.2 cont.**

| Drill hole | From (m) | To (m) | interval (m) | Zn (ppm) | Cu (ppm) | Pb (ppm) | Ag (ppm) | Mn (ppm) | Fe (ppm) | Au (ppm) | As (ppm) | Hg (ppm) | Sn (ppm) | W (ppm) | Ba (ppm) |
|---|---|---|---|---|---|---|---|---|---|---|---|---|---|---|---|
| PD0026 | 213 | 215 | 2 | 4270 | 50 | 2360 | 5 | 1520 | 33500 | | | | | | |
| PD0026 | 215 | 220.7 | 5.7 | 1856 | 40 | 715 | 3 | 2570 | 28900 | | | | | | |
| PD0026 | 220.7 | 226.4 | 5.7 | 1750 | 62 | 680 | 2 | 5980 | 36400 | | | | | | |
| PD0026 | 226.4 | 236.4 | 10 | 6850 | 54 | 2200 | 6 | 1105 | 26600 | | | | | | |
| PD0026 | 236.4 | 246.4 | 10 | 4886 | 66 | 1690 | 4 | 535 | 24300 | | | | | | |
| PD0026 | 246.4 | 256.4 | 10 | 2844 | 14 | 760 | 2 | 975 | 16700 | | | | | | |
| PD0026 | 256.4 | 266.4 | 10 | 6480 | 24 | 1285 | 3 | 570 | 22600 | | | | | | |
| PD0026 | 266.4 | 276.4 | 10 | 1900 | 8 | 570 | 2 | 355 | 18300 | | | | | | |
| PD0026 | 276.4 | 286.4 | 10 | 6708 | 24 | 2180 | 2 | 430 | 17700 | | | | | | |
| PD0026 | 286.4 | 294 | 7.6 | 4350 | 98 | 8305 | 5 | 180 | 33000 | | | | | | |
| PD0026 | 294 | 295.9 | 1.9 | 1930 | 40 | 34400 | 6 | 440 | 37600 | | | | | | |
| PD0026 | 295.9 | 297.9 | 2 | 12900 | 115 | 8910 | 7 | 170 | 64400 | | | | | | |
| PD0026 | 297.9 | 299.8 | 1.9 | 6500 | 155 | 11300 | 5 | 420 | 53000 | | | | | | |
| PD0026 | 299.8 | 302 | 2.2 | 6910 | 210 | 6600 | 9 | 12400 | 49700 | | | | | | |
| PD0026 | 302 | 303.2 | 1.2 | 15600 | 565 | 36400 | 24 | 12300 | 55600 | | | | | | |
| PD0026 | 303.2 | 304.2 | 1 | 510 | 80 | 610 | 2 | 3370 | 32300 | | | | | | |
| PD0026 | 320.4 | 330.4 | 10 | 442 | 78 | 60 | 1 | 4345 | 99000 | | | | | | |
| PD0026 | 330.4 | 336.7 | 6.3 | 3138 | 2400 | 1650 | 25 | 3685 | 65100 | | | | | | |
| PD0026 | 336.7 | 340.1 | 3.4 | 86 | 12 | 20 | 0 | 3800 | 137400 | | | | | | |
| PD0026 | 344.2 | 348.5 | 4.3 | 210 | 4 | 30 | 0 | 2720 | 147700 | | | | | | |
| PD0026 | 348.5 | 358.5 | 10 | 1598 | 54 | 4250 | 2 | 3560 | 102200 | | | | | | |
| PD0026 | 358.5 | 365 | 6.5 | 236 | 2 | 30 | 0 | 3040 | 94600 | | | | | | |
| PD0026 | 373.2 | 376.3 | 3.1 | 640 | 12 | 170 | 0 | 4310 | 55100 | | | | | | |
| PD0026 | 376.3 | 385.3 | 9 | 2000 | 48 | 370 | 0 | 4500 | 75000 | | | | | | |
| PD0026 | 385.3 | 395.8 | 10.5 | 264 | 6 | 50 | 0 | 4045 | 70400 | | | | | | |
| PD0026 | 395.8 | 399.9 | 4.1 | 1468 | 258 | 180 | 2 | 3130 | 34800 | | | | | | |
| PD0026 | 399.9 | 401.5 | 1.6 | 494 | 72 | 50 | 1 | 2830 | 16900 | | | | | | |
| PD0026 | 401.5 | 402 | 0.5 | 11100 | 575 | 370 | 6 | 3620 | 58600 | | | | | | |
| PD0026 | 402 | 402.5 | 0.5 | 54700 | 1270 | 4460 | 41 | 3440 | 104700 | | | | | | |
| PD0026 | 402.5 | 404 | 1.5 | 240 | 20 | 120 | 1 | 2730 | 21600 | | | | | | |
| PD0026 | 404 | 404.5 | 0.5 | 130000 | 4020 | 7570 | 139 | 4680 | 162500 | | | | | | |
| PD0026 | 404.5 | 405.3 | 0.8 | 1150 | 30 | 250 | 0 | 3360 | 23100 | | | | | | |
| PD0026 | 405.3 | 415.3 | 10 | 394 | 10 | 310 | 0 | 2720 | 11800 | | | | | | |
| PD0026 | 415.3 | 425.3 | 10 | 1724 | 56 | 520 | 0 | 3560 | 36700 | | | | | | |

**Appendix 5.2 cont.**

| Drill hole | From (m) | To (m) | interval (m) | Zn (ppm) | Cu (ppm) | Pb (ppm) | Ag (ppm) | Mn (ppm) | Fe (ppm) | Au (ppm) | As (ppm) | Hg (ppm) | Sn (ppm) | W (ppm) | Ba (ppm) |
|---|---|---|---|---|---|---|---|---|---|---|---|---|---|---|---|
| PD0026 | 425.3 | 435.3 | 10 | 220 | 4 | 50 | 0 | 1745 | 31000 | | | | | | |
| PD0026 | 435.3 | 445.3 | 10 | 3080 | 518 | 530 | 7 | 1855 | 29700 | | | | | | |
| PD0026 | 445.3 | 455.3 | 10 | 348 | 4 | 110 | 0 | 1455 | 11700 | | | | | | |
| PD0026 | 455.3 | 465.3 | 10 | 148 | 8 | 40 | 0 | 1365 | 14200 | | | | | | |
| PD0026 | 580 | 583.9 | 3.9 | 122 | 0 | 30 | 0 | 335 | 2400 | | | | | | |
| PD0026 | 583.9 | 591.6 | 7.7 | 1606 | 150 | 2030 | 11 | 960 | 17700 | | | | | | |
| PD0026 | 591.6 | 595.4 | 3.8 | 116 | 0 | 20 | 0 | 925 | 69000 | | | | | | |
| PD0027 | 343.8 | 345.8 | 2 | 744 | 32 | 355 | 4 | 1105 | 25200 | | | | | | |
| PD0027 | 345.8 | 355.8 | 10 | 1398 | 28 | 615 | 4 | 1195 | 16400 | | | | | | |
| PD0027 | 355.8 | 367 | 11.2 | 1048 | 22 | 245 | 0 | 1195 | 11500 | | | | | | |
| PD0027 | 367 | 377 | 10 | 148 | 8 | 20 | 0 | 1035 | 13900 | | | | | | |
| PD0027 | 377 | 385 | 8 | 628 | 20 | 150 | 1 | 3145 | 19500 | | | | | | |
| PD0027 | 385 | 387.8 | 2.8 | 2574 | 64 | 965 | 2 | 47300 | 33000 | | | | | | |
| PD0027 | 387.8 | 397.8 | 10 | 4164 | 64 | 3020 | 5 | 1645 | 28000 | | | | | | |
| PD0027 | 397.8 | 404.8 | 7 | 9698 | 68 | 2620 | 5 | 3695 | 36300 | | | | | | |
| PD0027 | 404.8 | 413.6 | 8.8 | 418 | 16 | 210 | 1 | 2690 | 23100 | | | | | | |
| PD0027 | 413.6 | 422.4 | 8.8 | 2624 | 42 | 850 | 2 | 2630 | 39800 | | | | | | |
| PD0027 | 422.4 | 425.3 | 2.9 | 1110 | 36 | 285 | 1 | 2680 | 27100 | | | | | | |
| PD0027 | 425.3 | 435.3 | 10 | 222 | 34 | 965 | 1 | 1960 | 53900 | | | | | | |
| PD0027 | 435.3 | 445.5 | 10.2 | 294 | 28 | 95 | 1 | 1965 | 58000 | | | | | | |
| PD0027 | 445.5 | 452.4 | 6.9 | 222 | 18 | 25 | 1 | 1565 | 34600 | | | | | | |
| PD0027 | 452.4 | 460.3 | 7.9 | 2922 | 34 | 5100 | 2 | 13600 | 33600 | | | | | | |
| PD0027 | 460.3 | 465.5 | 5.2 | 1736 | 24 | 1220 | 1 | 8505 | 24300 | | | | | | |
| PD0027 | 465.5 | 472 | 6.5 | 296 | 36 | 1250 | 1 | 965 | 45600 | | | | | | |
| PD0027 | 472 | 473.3 | 1.3 | 90 | 10 | 450 | 1 | 2730 | 24100 | | | | | | |
| PD0027 | 473.3 | 474.7 | 1.4 | 4730 | 55 | 3490 | 4 | 14400 | 39700 | | | | | | |
| PD0027 | 474.7 | 476.1 | 1.4 | 4830 | 45 | 2340 | 4 | 13300 | 38600 | | | | | | |
| PD0027 | 476.1 | 477.4 | 1.3 | 23700 | 255 | 14500 | 61 | 13600 | 45300 | | | | | | |
| PD0027 | 477.4 | 478.7 | 1.3 | 1320 | 15 | 1230 | 3 | 6810 | 16800 | | | | | | |
| PD0027 | 478.7 | 480 | 1.3 | 1510 | 10 | 1670 | 2 | 5930 | 17400 | | | | | | |
| PD0027 | 480 | 490 | 10 | 922 | 16 | 2410 | 1 | 5545 | 19700 | | | | | | |
| PD0027 | 490 | 500 | 10 | 250 | 44 | 120 | 1 | 3990 | 23100 | | | | | | |
| PD0028 | 150 | 152 | 2 | 690 | | 85 | 0 | 6620 | 27600 | | | | | | |
| PD0028 | 152 | 154 | 2 | 6635 | 30 | 2660 | 7 | 9740 | 63300 | | | | | | |

**Appendix 5.2 cont.**

| Drill hole | From (m) | To (m) | interval (m) | Zn (ppm) | Cu (ppm) | Pb (ppm) | Ag (ppm) | Mn (ppm) | Fe (ppm) | Au (ppm) | As (ppm) | Hg (ppm) | Sn (ppm) | W (ppm) | Ba (ppm) |
|---|---|---|---|---|---|---|---|---|---|---|---|---|---|---|---|
| PD0028 | 154 | 156 | 2 | 2125 | | 580 | 1 | 7885 | 48600 | | | | | | |
| PD0028 | 156 | 158 | 2 | 320 | | 125 | 0 | 7475 | 43400 | | | | | | |
| PD0028 | 158 | 160 | 2 | 7810 | 35 | 1780 | 2 | 11400 | 43900 | | | | | | |
| PD0028 | 160 | 162 | 2 | 225 | | 80 | 0 | 5550 | 40100 | | | | | | |
| PD0028 | 210 | 212 | 2 | 80 | 5 | 20 | 0 | 1955 | 10500 | | | | | | |
| PD0028 | 212 | 214 | 2 | 24000 | 205 | 10200 | 7 | 12500 | 26000 | | | | | | |
| PD0028 | 214 | 216 | 2 | 7940 | 70 | 2500 | 2 | 6560 | 10000 | | | | | | |
| PD0028 | 216 | 218 | 2 | 24600 | 150 | 6535 | 6 | 7060 | 17500 | | | | | | |
| PD0028 | 218 | 220 | 2 | 10000 | 60 | 2030 | 2 | 7840 | 8200 | | | | | | |
| PD0028 | 220 | 221 | 1 | 4495 | 30 | 795 | 1 | 4320 | 5200 | | | | | | |
| PD0028 | 221 | 221.5 | 0.5 | 4080 | 25 | 595 | 1 | 4840 | 4400 | | | | | | |
| PD0028 | 221.5 | 226.4 | 4.9 | 176 | 6 | 110 | 0 | 1415 | 3300 | | | | | | |
| PD0028 | 308.6 | 313.4 | 4.8 | 190 | 24 | 400 | 0 | 735 | 1700 | | | | | | |
| PD0028 | 313.4 | 317.5 | 4.1 | 5972 | 34 | 3190 | 4 | 2995 | 15800 | | | | | | |
| PD0028 | 317.5 | 327.5 | 10 | 8352 | 20 | 6870 | 5 | 4595 | 17300 | | | | | | |
| PD0028 | 327.5 | 336 | 8.5 | 292 | 0 | 85 | 0 | 2160 | 3800 | | | | | | |
| PD0028 | 336 | 337.6 | 1.6 | 1460 | 5 | 650 | 1 | 6580 | 6100 | | | | | | |
| PD0028 | 337.6 | 338.7 | 1.1 | 32800 | 145 | 34000 | 36 | 5630 | 247000 | | | | | | |
| PD0028 | 338.7 | 339.8 | 1.1 | 180000 | 710 | 57400 | 60 | 3070 | 209000 | | | | | | |
| PD0028 | 339.8 | 340.8 | 1 | 34800 | 115 | 14800 | 10 | 14100 | 29500 | | | | | | |
| PD0028 | 340.8 | 341.1 | 0.3 | 178000 | 1125 | 74500 | 76 | 1320 | 137000 | | | | | | |
| PD0028 | 341.1 | 342.6 | 1.5 | 45500 | 75 | 19100 | 10 | 13500 | 22300 | | | | | | |
| PD0028 | 342.6 | 344 | 1.4 | 73400 | 90 | 13900 | 11 | 19800 | 25100 | | | | | | |
| PD0028 | 344 | 345 | 1 | 60800 | 160 | 19300 | 11 | 29800 | 33000 | | | | | | |
| PD0028 | 345 | 346.1 | 1.1 | 101000 | 465 | 53500 | 27 | 12000 | 141000 | | | | | | |
| PD0028 | 346.1 | 346.8 | 0.7 | 69000 | 495 | 26700 | 24 | 13100 | 81000 | | | | | | |
| PD0028 | 346.8 | 348.4 | 1.6 | 180000 | 1405 | 59500 | 64 | 9100 | 94200 | | | | | | |
| PD0028 | 348.4 | 348.9 | 0.5 | 94500 | 600 | 56600 | 27 | 4390 | 217000 | | | | | | |
| PD0028 | 348.9 | 349.4 | 0.5 | 133000 | 555 | 40600 | 31 | 12400 | 105000 | | | | | | |
| PD0028 | 349.4 | 350 | 0.6 | 150000 | 590 | 65400 | 46 | 3430 | 204000 | | | | | | |
| PD0028 | 350 | 350.8 | 0.8 | 65000 | 145 | 19500 | 12 | 20700 | 55200 | | | | | | |
| PD0028 | 350.8 | 352 | 1.2 | 117000 | 505 | 51900 | 33 | 8790 | 170000 | | | | | | |
| PD0028 | 352 | 352.6 | 0.6 | 95500 | 155 | 34300 | 20 | 19500 | 84300 | | | | | | |
| PD0028 | 352.6 | 354.2 | 1.6 | 91500 | 425 | 49000 | 36 | 3750 | 193000 | | | | | | |

**Appendix 5.2 cont.**

| Drill hole | From (m) | To (m) | interval (m) | Zn (ppm) | Cu (ppm) | Pb (ppm) | Ag (ppm) | Mn (ppm) | Fe (ppm) | Au (ppm) | As (ppm) | Hg (ppm) | Sn (ppm) | W (ppm) | Ba (ppm) |
|---|---|---|---|---|---|---|---|---|---|---|---|---|---|---|---|
| PD0028 | 354.2 | 355.4 | 1.2 | 36900 | 65 | 11300 | 9 | 8570 | 26600 | | | | | | |
| PD0028 | 355.4 | 356.6 | 1.2 | 29400 | 60 | 8650 | 7 | 7570 | 19100 | | | | | | |
| PD0028 | 356.6 | 357.3 | 0.7 | 42100 | 500 | 33400 | 46 | 8460 | 176000 | | | | | | |
| PD0028 | 357.3 | 358.9 | 1.6 | 27200 | 80 | 10900 | 7 | 11100 | 23000 | | | | | | |
| PD0028 | 358.9 | 359.6 | 0.7 | 30600 | 360 | 11000 | 16 | 6380 | 110000 | | | | | | |
| PD0028 | 359.6 | 361.6 | 2 | 3490 | 35 | 2470 | 4 | 2560 | 21200 | | | | | | |
| PD0028 | 361.6 | 363.1 | 1.5 | 9780 | 25 | 2190 | 5 | 14300 | 31000 | | | | | | |
| PD0028 | 363.1 | 364.8 | 1.7 | 2540 | 35 | 1690 | 14 | 3700 | 90100 | | | | | | |
| PD0028 | 364.8 | 366.5 | 1.7 | 22500 | 280 | 2210 | 12 | 7000 | 104000 | | | | | | |
| PD0028 | 366.5 | 366.8 | 0.3 | 170 | 10 | 80 | 1 | 1510 | 14900 | | | | | | |
| PD0028 | 366.8 | 368.4 | 1.6 | 1240 | 50 | 680 | 1 | 3210 | 72900 | | | | | | |
| PD0028 | 368.4 | 370 | 1.6 | 920 | 105 | 4300 | 2 | 5270 | 74100 | | | | | | |
| PD0028 | 370 | 371.2 | 1.2 | 340 | 30 | 240 | 1 | 6690 | 52800 | | | | | | |
| PD0028 | 371.2 | 372.3 | 1.1 | 1280 | 15 | 510 | 1 | 5510 | 42900 | | | | | | |
| PD0028 | 372.3 | 373.2 | 0.9 | 4030 | 15 | 1430 | 1 | 13900 | 22200 | | | | | | |
| PD0028 | 373.2 | 373.8 | 0.6 | 144000 | 1270 | 47400 | 43 | 23900 | 104000 | | | | | | |
| PD0028 | 373.8 | 375 | 1.2 | 5220 | 40 | 7620 | 3 | 16700 | 34800 | | | | | | |
| PD0028 | 375 | 376 | 1 | 5630 | 25 | 2550 | 2 | 22300 | 19700 | | | | | | |
| PD0028 | 376 | 386 | 10 | 2340 | 14 | 760 | 0 | 5815 | 12800 | | | | | | |
| PD0028 | 386 | 396 | 10 | 1302 | 8 | 675 | 0 | 3400 | 24300 | | | | | | |
| PD0028 | 406 | 413.9 | 7.9 | 216 | 0 | 75 | 0 | 1735 | 17000 | | | | | | |
| PD0028 | 413.9 | 418.8 | 4.9 | 6000 | 104 | 7755 | 3 | 1665 | 28000 | | | | | | |
| PD0028 | 418.8 | 428.8 | 10 | 7305 | 102 | 4050 | 3 | 13900 | 31300 | | | | | | |
| PD0028 | 428.8 | 437.4 | 8.6 | 2946 | 42 | 2065 | 2 | 8460 | 37200 | | | | | | |
| PD0028 | 437.4 | 441.8 | 4.4 | 7675 | 310 | 6560 | 6 | 4715 | 24900 | | | | | | |
| PD0028 | 441.8 | 447.8 | 6 | 5916 | 364 | 5270 | 9 | 5400 | 34600 | | | | | | |
| PD0028 | 447.8 | 450 | 2.2 | 978 | 52 | 3430 | 1 | 2620 | 25800 | | | | | | |
| PD0028 | 450 | 456.2 | 6.2 | 1415 | 24 | 840 | 4 | 2390 | 25200 | | | | | | |
| PD0028 | 456.2 | 461.3 | 5.1 | 400 | 0 | 130 | 0 | 2850 | 16900 | | | | | | |
| PD0028 | 461.3 | 464.7 | 3.4 | 152 | 0 | 35 | 0 | 765 | 8900 | | | | | | |
| PD0028 | 464.7 | 466.8 | 2.1 | 12100 | 862 | 5670 | 10 | 3525 | 17400 | | | | | | |
| PD0028 | 466.8 | 474 | 7.2 | 432 | 32 | 125 | 0 | 1955 | 12500 | | | | | | |
| PD0028 | 503 | 504.2 | 1.2 | 420 | 40 | 440 | 2 | 4780 | 33400 | | | | | | |
| PD0028 | 504.2 | 505.5 | 1.3 | 9800 | 270 | 4420 | 8 | 7900 | 56400 | | | | | | |

**Appendix 5.2 cont.**

| Drill hole | From (m) | To (m) | interval (m) | Zn (ppm) | Cu (ppm) | Pb (ppm) | Ag (ppm) | Mn (ppm) | Fe (ppm) | Au (ppm) | As (ppm) | Hg (ppm) | Sn (ppm) | W (ppm) | Ba (ppm) |
|---|---|---|---|---|---|---|---|---|---|---|---|---|---|---|---|
| PD0028 | 505.5 | 506.6 | 1.1 | 3670 | 15 | 2010 | 1 | 9800 | 24800 | | | | | | |
| PD0028 | 506.6 | 507.4 | 0.8 | 1570 | 35 | 1500 | 2 | 4080 | 22700 | | | | | | |
| PD0028 | 507.4 | 508.4 | 1 | 13400 | 635 | 13000 | 37 | 12300 | 60800 | | | | | | |
| PD0028 | 508.4 | 509.3 | 0.9 | 9320 | 150 | 5680 | 9 | 17500 | 45000 | | | | | | |
| PD0028 | 509.3 | 510.8 | 1.5 | 5770 | 65 | 3160 | 4 | 20400 | 42400 | | | | | | |
| PD0028 | 510.8 | 512.3 | 1.5 | 8920 | 360 | 6670 | 7 | 36200 | 56700 | | | | | | |
| PD0028 | 512.3 | 514 | 1.7 | 2090 | 30 | 840 | 1 | 16400 | 35600 | | | | | | |
| PD0028 | 514 | 515.1 | 1.1 | 30800 | 905 | 35500 | 17 | 9610 | 69500 | | | | | | |
| PD0028 | 515.1 | 516.2 | 1.1 | 16500 | 380 | 25800 | 12 | 5750 | 50200 | | | | | | |
| PD0028 | 516.2 | 517.5 | 1.3 | 5180 | 130 | 8680 | 15 | 1530 | 64200 | | | | | | |
| PD0028 | 517.5 | 518.5 | 1 | 5410 | 280 | 13700 | 21 | 620 | 82800 | | | | | | |
| PD0028 | 518.8 | 528.8 | 10 | 1730 | 80 | 4600 | 3 | 540 | 17400 | | | | | | |
| PD0028 | 528.8 | 538.8 | 10 | 496 | 28 | 1370 | 1 | 490 | 11900 | | | | | | |
| PD0028 | 538.8 | 549 | 10.2 | 1927 | 36 | 3300 | 1 | 2370 | 18600 | | | | | | |
| PD0028 | 549 | 556.4 | 7.4 | 1148 | 14 | 1190 | 0 | 21700 | 26800 | | | | | | |
| PD0028 | 556.4 | 566.4 | 10 | 400 | 18 | 835 | 0 | 1070 | 12700 | | | | | | |
| PD0029 | 174 | 176 | 2 | 420 | 10 | 110 | 0 | 4770 | 26600 | | | | | | |
| PD0029 | 176 | 178 | 2 | 1000 | 10 | 150 | 0 | 6485 | 47900 | | | | | | |
| PD0029 | 178 | 180 | 2 | 1495 | 10 | 765 | 0 | 16500 | 79300 | | | | | | |
| PD0029 | 180 | 181 | 1 | 1560 | 10 | 580 | 0 | 9530 | 70300 | | | | | | |
| PD0029 | 181 | 181.6 | 0.6 | 2130 | 10 | 420 | 0 | 14500 | 62400 | | | | | | |
| PD0029 | 181.6 | 183.1 | 1.5 | 1260 | 10 | 210 | 1 | 16400 | 68900 | | | | | | |
| PD0029 | 183.1 | 183.7 | 0.6 | 1190 | 5 | 340 | 1 | 8790 | 41200 | | | | | | |
| PD0029 | 183.7 | 184.6 | 0.9 | 1550 | 5 | 510 | 1 | 9320 | 35400 | | | | | | |
| PD0029 | 184.6 | 185.2 | 0.6 | 108000 | 760 | 17300 | 37 | 27000 | 147000 | | | | | | |
| PD0029 | 185.2 | 186 | 0.8 | 1550 | 5 | 200 | 1 | 20800 | 130000 | | | | | | |
| PD0029 | 186 | 187.5 | 1.5 | 1720 | 10 | 400 | 1 | 14500 | 70700 | | | | | | |
| PD0029 | 187.5 | 193.4 | 5.9 | 1844 | 34 | 135 | 0 | 1535 | 24200 | | | | | | |
| PD0029 | 194.5 | 203.8 | 9.3 | 1678 | 4 | 125 | 0 | 8880 | 89800 | | | | | | |
| PD0029 | 203.8 | 213.8 | 10 | 1140 | 22 | 55 | 0 | 5900 | 66700 | | | | | | |
| PD0029 | 213.8 | 216.1 | 2.3 | 240 | 4 | 60 | 0 | 4535 | 28500 | | | | | | |
| PD0029 | 257.5 | 258.9 | 1.4 | 260 | 5 | 420 | 1 | 7100 | 26300 | | | | | | |
| PD0029 | 258.9 | 259.4 | 0.5 | 52800 | 2090 | 446000 | 183 | 11000 | 41700 | | | | | | |
| PD0029 | 259.4 | 261 | 1.6 | 1690 | 15 | 2310 | 1 | 13900 | 19300 | | | | | | |

**Appendix 5.2 cont.**

| Drill hole | From (m) | To (m) | interval (m) | Zn (ppm) | Cu (ppm) | Pb (ppm) | Ag (ppm) | Mn (ppm) | Fe (ppm) | Au (ppm) | As (ppm) | Hg (ppm) | Sn (ppm) | W (ppm) | Ba (ppm) |
|---|---|---|---|---|---|---|---|---|---|---|---|---|---|---|---|
| PD0029 | 261 | 263 | 2 | 1230 | 5 | 1700 | 1 | 13200 | 20300 | | | | | | |
| PD0029 | 263 | 265 | 2 | 400 | 5 | 2550 | 1 | 9200 | 20700 | | | | | | |
| PD0029 | 272.5 | 273.8 | 1.3 | 970 | 10 | 1040 | 1 | 14500 | 19000 | | | | | | |
| PD0029 | 273.8 | 274.8 | 1 | 4650 | 30 | 1930 | 2 | 23400 | 33500 | | | | | | |
| PD0029 | 274.8 | 275.9 | 1.1 | 3040 | 10 | 2640 | 2 | 19000 | 34800 | | | | | | |
| PD0029 | 275.9 | 277 | 1.1 | 2460 | 10 | 1580 | 2 | 17700 | 24700 | | | | | | |
| PD0029 | 277 | 278.5 | 1.5 | 7490 | 15 | 5260 | 3 | 74900 | 52500 | | | | | | |
| PD0029 | 278.5 | 280 | 1.5 | 147000 | 15 | 188000 | 9 | 83700 | 79700 | | | | | | |
| PD0029 | 280 | 286 | 6 | 126 | 0 | 25 | 0 | 3100 | 59100 | | | | | | |
| PD0029 | 296.1 | 306.1 | 10 | 524 | 0 | 120 | 0 | 1160 | 17500 | | | | | | |
| PD0029 | 306.1 | 312.1 | 6 | 5212 | 30 | 5290 | 3 | 1090 | 25900 | | | | | | |
| PD0029 | 312.1 | 318 | 5.9 | 426 | 58 | 145 | 0 | 1990 | 28900 | | | | | | |
| PD0029 | 318 | 319.2 | 1.2 | 2150 | 45 | 730 | 2 | 5010 | 37200 | | | | | | |
| PD0029 | 319.2 | 320.5 | 1.3 | 2600 | 40 | 870 | 2 | 2640 | 27600 | | | | | | |
| PD0029 | 320.5 | 322 | 1.5 | 4200 | 45 | 3000 | 6 | 2720 | 42100 | | | | | | |
| PD0029 | 322 | 323.2 | 1.2 | 4400 | 70 | 2390 | 5 | 2800 | 40500 | | | | | | |
| PD0029 | 323.2 | 324.4 | 1.2 | 470 | 40 | 120 | 1 | 2220 | 42900 | | | | | | |
| PD0029 | 324.4 | 325 | 0.6 | 110 | 60 | 40 | 1 | 1120 | 41200 | | | | | | |
| PD0029 | 325 | 335 | 10 | 250 | 40 | 35 | 0 | 445 | 55300 | | | | | | |
| PD0029 | 335 | 345.9 | 10.9 | 5766 | 66 | 9820 | 4 | 3045 | 51000 | | | | | | |
| PD0030 | 197.5 | 208 | 10.5 | 362 | 46 | 255 | 0 | 2375 | 29400 | | | | | | |
| PD0030 | 208 | 212.1 | 4.1 | 572 | 6 | 350 | 0 | 3880 | 9000 | | | | | | |
| PD0030 | 212.1 | 212.5 | 0.4 | 2012 | 40 | 705 | 3 | 3740 | 18000 | | | | | | |
| PD0030 | 212.5 | 215.3 | 2.8 | 2002 | 30 | 2065 | 6 | 9680 | 34300 | | | | | | |
| PD0030 | 215.3 | 223 | 7.7 | 148 | 34 | 100 | 1 | 3040 | 58700 | | | | | | |
| PD0030 | 364 | 364.9 | 0.9 | 80 | 10 | 90 | 1 | 1030 | 11700 | | | | | | |
| PD0030 | 364.9 | 365.3 | 0.4 | 11300 | 92 | 3100 | 10 | 1310 | 67900 | 0.03 | | | | | |
| PD0030 | 365.3 | 365.5 | 0.2 | 2740 | 94 | 13500 | 19 | 2710 | 69400 | 0 | | | | | |
| PD0030 | 365.5 | 367.5 | 2 | 70 | 8 | 130 | 1 | 1410 | 15500 | 0 | | | | | |
| PD0030 | 369.5 | 371.5 | 2 | 80 | 62 | 90 | 1 | 10000 | 28600 | 0 | | | | | |
| PD0030 | 371.5 | 373.7 | 2.2 | 11500 | 334 | 14600 | 9 | 4080 | 37300 | 0 | | | | | |
| PD0030 | 373.7 | 373.9 | 0.2 | 41700 | 2244 | 90900 | 25 | 4770 | 19000 | 0.03 | | | | | |
| PD0030 | 373.9 | 376 | 2.1 | 640 | 30 | 1940 | 1 | 4300 | 25100 | 0 | | | | | |
| PD0030 | 415 | 417.1 | 2.1 | 60 | 10 | 100 | 1 | 2150 | 27700 | 0.03 | | | | | |

**Appendix 5.2 cont.**

| Drill hole | From (m) | To (m) | interval (m) | Zn (ppm) | Cu (ppm) | Pb (ppm) | Ag (ppm) | Mn (ppm) | Fe (ppm) | Au (ppm) | As (ppm) | Hg (ppm) | Sn (ppm) | W (ppm) | Ba (ppm) |
|---|---|---|---|---|---|---|---|---|---|---|---|---|---|---|---|
| PD0030 | 417.1 | 418.2 | 1.1 | 560 | 268 | 24400 | 12 | 4840 | 42200 | 0 | | | | | |
| PD0030 | 418.2 | 419.2 | 1 | 53300 | 3146 | 51700 | 11 | 9150 | 69200 | 0 | | | | | |
| PD0030 | 419.2 | 420.8 | 1.6 | 160800 | 4610 | 107700 | 18 | 1910 | 37500 | 0 | | | | | |
| PD0030 | 420.8 | 422.1 | 1.3 | 4470 | 74 | 5090 | 7 | 11200 | 42500 | 0 | | | | | |
| PD0030 | 422.1 | 424 | 1.9 | 6180 | 510 | 12000 | 18 | 6810 | 64200 | 0.06 | | | | | |
| PD0030 | 424 | 425.4 | 1.4 | 11100 | 2476 | 34200 | 76 | 4210 | 75000 | 0 | | | | | |
| PD0030 | 425.4 | 427 | 1.6 | 1000 | 48 | 1160 | 3 | 4190 | 44900 | 0 | | | | | |
| PD0030 | 427 | 428.4 | 1.4 | 140 | 16 | 710 | 11 | 9620 | 47600 | 0 | | | | | |
| PD0031 | 131 | 133 | 2 | 656 | 46 | 464 | 3 | 402 | 38000 | | | | | | |
| PD0031 | 133 | 135 | 2 | 1586 | 111 | 899 | 6 | 572 | 73600 | | | | | | |
| PD0031 | 135 | 137 | 2 | 887 | 67 | 415 | 3 | 562 | 45400 | | | | | | |
| PD0031 | 200.7 | 205 | 4.3 | 433 | 16 | 60 | 0 | 1654 | 41900 | | | | | | |
| PD0031 | 205 | 206.15 | 1.15 | 2860 | 47 | 470 | 4 | 5650 | 26900 | | | | | | |
| PD0031 | 206.15 | 206.3 | 0.15 | 45600 | 1200 | 31500 | 42 | 7960 | 69700 | 0.053 | | | | | |
| PD0031 | 206.3 | 207 | 0.7 | 4010 | 152 | 670 | 1 | 2150 | 46300 | | | | | | |
| PD0031 | 207 | 215 | 8 | 201 | 36 | 40 | 0 | 2610 | 70500 | | | | | | |
| PD0031 | 234.2 | 237.8 | 3.6 | 945 | 55 | 413 | 1 | 2385 | 51900 | | | | | | |
| PD0031 | 237.8 | 241.7 | 3.9 | 4174 | 80 | 1743 | 4 | 5210 | 43200 | | | | | | |
| PD0031 | 241.7 | 253 | 11.3 | 447 | 37 | 87 | 0 | 1600 | 61100 | | | | | | |
| PD0031 | 309.5 | 311 | 1.5 | 390 | 116 | 20 | 1 | 1850 | 40100 | | | | | | |
| PD0031 | 311 | 312 | 1 | 2610 | 681 | 170 | 3 | 680 | 68400 | 0.019 | | | | | |
| PD0031 | 312 | 312.5 | 0.5 | 230 | 58 | 100 | 1 | 920 | 14700 | | | | | | |
| PD0031 | 365 | 372.6 | 7.6 | 199 | 11 | 23 | 0 | 210 | 4600 | | | | | | |
| PD0031 | 372.6 | 373.3 | 0.7 | 1870 | 207 | 170 | 1 | 360 | 30400 | | | | | | |
| PD0031 | 373.3 | 374 | 0.7 | 178 | 78 | 17 | 0 | 336 | 21400 | | | | | | |
| PD0031 | 376.6 | 378.9 | 2.3 | 89 | 13 | 445 | 0 | 2435 | 10000 | | | | | | |
| PD0031 | 378.9 | 382.2 | 3.3 | 1540 | 104 | 3103 | 2 | 2002 | 27700 | | | | | | |
| PD0031 | 382.2 | 382.5 | 0.3 | 183 | 106 | 2026 | 1 | 3080 | 23500 | | | | | | |
| PD0031 | 382.5 | 388 | 5.5 | 1522 | 108 | 604 | 1 | 982 | 37200 | | | | | | |
| PD0031 | 388 | 390.9 | 2.9 | 110 | 19 | 60 | 0 | 171 | 6400 | | | | | | |
| PD0031 | 391.5 | 394 | 2.5 | 84 | 8 | 25 | 0 | 211 | 5600 | | | | | | |
| PD0031 | 394 | 399.7 | 5.7 | 534 | 18 | 1313 | 0 | 5424 | 15700 | | | | | | |
| PD0031 | 399.7 | 401 | 1.3 | 14800 | 203 | 6570 | 5 | 5030 | 24400 | | | | | | |
| PD0031 | 401 | 403 | 2 | 1100 | 77 | 1000 | 2 | 1630 | 31900 | | | | | | |

**Appendix 5.2 cont.**

| Drill hole | From (m) | To (m) | interval (m) | Zn (ppm) | Cu (ppm) | Pb (ppm) | Ag (ppm) | Mn (ppm) | Fe (ppm) | Au (ppm) | As (ppm) | Hg (ppm) | Sn (ppm) | W (ppm) | Ba (ppm) |
|---|---|---|---|---|---|---|---|---|---|---|---|---|---|---|---|
| PD0031 | 403 | 405 | 2 | 250 | 58 | 1720 | 2 | 1780 | 31100 | | | | | | |
| PD0031 | 405 | 407.2 | 2.2 | 120 | 35 | 1300 | 1 | 1140 | 28200 | | | | | | |
| PD0031 | 407.2 | 412 | 4.8 | 158 | 9 | 442 | 0 | 1390 | 9000 | | | | | | |
| PD0031 | 412 | 418.1 | 6.1 | 121 | 9 | 365 | 0 | 8485 | 19800 | | | | | | |
| PD0031 | 418.1 | 420 | 1.9 | 640 | 80 | 7850 | 8 | 12500 | 39600 | 0.155 | | | | | |
| PD0031 | 420 | 421.3 | 1.3 | 4410 | 570 | 15100 | 18 | 7280 | 29000 | 0.125 | | | | | |
| PD0031 | 421.3 | 422.5 | 1.2 | 13500 | 640 | 5160 | 10 | 13300 | 43500 | 0.085 | | | | | |
| PD0031 | 422.5 | 424.8 | 2.3 | 180 | 36 | 400 | 2 | 10900 | 32400 | | | | | | |
| PD0031 | 424.8 | 426.6 | 1.8 | 4940 | 165 | 4450 | 4 | 8770 | 85300 | | | | | | |
| PD0031 | 426.6 | 427 | 0.4 | 2250 | 62 | 2970 | 2 | 4730 | 48500 | | | | | | |
| PD0031 | 427 | 429 | 2 | 2310 | 138 | 810 | 3 | 4570 | 83600 | 0.009 | | | | | |
| PD0031 | 429 | 431 | 2 | 9860 | 142 | 9510 | 38 | 6210 | 44000 | 0.117 | | | | | |
| PD0031 | 431 | 433 | 2 | 780 | 218 | 5840 | 21 | 19700 | 77100 | 0.223 | | | | | |
| PD0031 | 433 | 435 | 2 | 4820 | 357 | 2430 | 39 | 9050 | 56600 | 0.06 | | | | | |
| PD0031 | 435 | 435.5 | 0.5 | 260 | 45 | 390 | 3 | 6070 | 37300 | | | | | | |
| PD0031 | 435.5 | 440.6 | 5.1 | 2015 | 86 | 416 | 4 | 1469 | 47700 | | | | | | |
| PD0031 | 440.6 | 447.2 | 6.6 | 375 | 24 | 95 | 0 | 3772 | 20000 | | | | | | |
| PD0031 | 463 | 464 | 1 | 30 | 3 | 40 | 1 | 6290 | 5700 | | | | | | |
| PD0031 | 464 | 464.8 | 0.8 | 2370 | 58 | 420 | 1 | 1140 | 46900 | | | | | | |
| PD0031 | 464.8 | 465 | 0.2 | 160 | 9 | 60 | 1 | 630 | 9100 | | | | | | |
| PD0031 | 598.9 | 605.1 | 6.2 | 318 | 30 | 11 | 0 | 3725 | 76600 | | | | | | |
| PD0031 | 605.1 | 605.5 | 0.4 | 37400 | 576 | 190 | 7 | 950 | 55000 | 0.031 | | | | | |
| PD0031 | 605.5 | 613.8 | 8.3 | 1043 | 61 | 20 | 0 | 2235 | 105900 | | | | | | |
| PD0032 | 96 | 98 | 2 | 91 | 7 | 23 | 0 | 3635 | 144100 | | | | | | |
| PD0032 | 98 | 100 | 2 | 2590 | 16 | 941 | 2 | 2568 | 58000 | | | | | | |
| PD0032 | 100 | 102 | 2 | 166 | 12 | 29 | 0 | 975 | 17300 | | | | | | |
| PD0032 | 190 | 202.7 | 12.7 | 650 | 26 | 238 | 0 | 2222 | 20500 | | | | | | |
| PD0032 | 202.7 | 204.9 | 2.2 | 2041 | 85 | 437 | 0 | 2453 | 71300 | | | | | | |
| PD0032 | 204.9 | 215.3 | 10.4 | 625 | 54 | 190 | 0 | 3101 | 55000 | | | | | | |
| PD0032 | 215.3 | 216.5 | 1.2 | 984 | 74 | 290 | 1 | 996 | 26500 | | | | | | |
| PD0032 | 216.5 | 217.4 | 0.9 | 1750 | 128 | 376 | 1 | 1856 | 55900 | | | | | | |
| PD0032 | 217.4 | 218.2 | 0.8 | 845 | 74 | 556 | 0 | 9846 | 89000 | | | | | | |
| PD0032 | 220.3 | 222.7 | 2.4 | 254 | 12 | 41 | 0 | 4510 | 39900 | | | | | | |
| PD0032 | 222.7 | 223.5 | 0.8 | 34600 | 769 | 34600 | 10 | 10200 | 41200 | | | | | | |

**Appendix 5.2 cont.**

| Drill hole | From (m) | To (m) | interval (m) | Zn (ppm) | Cu (ppm) | Pb (ppm) | Ag (ppm) | Mn (ppm) | Fe (ppm) | Au (ppm) | As (ppm) | Hg (ppm) | Sn (ppm) | W (ppm) | Ba (ppm) |
|---|---|---|---|---|---|---|---|---|---|---|---|---|---|---|---|
| PD0032 | 223.5 | 226 | 2.5 | 117 | 6 | 32 | 0 | 2683 | 11300 | | | | | | |
| PD0032 | 235 | 245.6 | 10.6 | 253 | 15 | 50 | 0 | 4927 | 32800 | | | | | | |
| PD0032 | 245.6 | 245.8 | 0.2 | 132500 | 1706 | 8350 | 27 | 17300 | 22000 | | | | | | |
| PD0032 | 245.8 | 248.9 | 3.1 | 268 | 10 | 53 | 0 | 6465 | 44400 | | | | | | |
| PD0032 | 251 | 253.9 | 2.9 | 628 | 12 | 890 | 0 | 6110 | 25000 | | | | | | |
| PD0032 | 253.9 | 254 | 0.1 | 47000 | 260 | 27800 | 8 | 11400 | 17100 | | | | | | |
| PD0032 | 254 | 263 | 9 | 372 | 9 | 380 | 0 | 5132 | 30600 | | | | | | |
| PD0032 | 279.6 | 279.9 | 0.3 | 420 | 10 | 470 | 3 | 10900 | 55200 | | | | | | |
| PD0032 | 279.9 | 280.65 | 0.75 | 5390 | 175 | 9280 | 12 | 14700 | 50800 | | | | | | |
| PD0032 | 280.65 | 285.1 | 4.45 | 533 | 13 | 250 | 2 | 10300 | 41000 | | | | | | |
| PD0032 | 285.1 | 285.8 | 0.7 | 4150 | 29 | 2560 | 1 | 10800 | 42800 | | | | | | |
| PD0032 | 285.8 | 286.6 | 0.8 | 300 | 3 | 80 | 1 | 13900 | 51000 | | | | | | |
| PD0032 | 286.6 | 286.8 | 0.2 | 2670 | 12 | 2610 | 1 | 9000 | 257300 | | | | | | |
| PD0032 | 286.8 | 287.7 | 0.9 | 31700 | 476 | 18700 | 10 | 16800 | 25500 | | | | | | |
| PD0032 | 287.7 | 288.2 | 0.5 | 42200 | 3840 | 23400 | 19 | 8450 | 52200 | | | | | | |
| PD0032 | 288.2 | 292 | 3.8 | 178 | 46 | 378 | 1 | 874 | 7800 | | | | | | |
| PD0032 | 292 | 294.2 | 2.2 | 95 | 12 | 36 | 0 | 677 | 8000 | | | | | | |
| PD0032 | 294.2 | 299 | 4.8 | 135 | 11 | 30 | 0 | 763 | 5200 | | | | | | |
| PD0032 | 299 | 302.3 | 3.3 | 7184 | 349 | 1900 | 3 | 1619 | 14200 | | | | | | |
| PD0032 | 302.3 | 302.8 | 0.5 | 360 | 68 | 255 | 3 | 5064 | 42700 | | | | | | |
| PD0032 | 335.3 | 336.15 | 0.85 | 323 | 10 | 30 | 0 | 10700 | 93900 | | | | | | |
| PD0032 | 336.15 | 336.9 | 0.75 | 9980 | 111 | 7340 | 2 | 9920 | 31000 | | | | | | |
| PD0032 | 336.9 | 337.6 | 0.7 | 2330 | 30 | 420 | 1 | 9280 | 111900 | | | | | | |
| PD0032 | 337.6 | 337.95 | 0.35 | 18100 | 426 | 20300 | 24 | 1910 | 51500 | | | | | | |
| PD0032 | 337.95 | 339.1 | 1.15 | 240 | 20 | 80 | 1 | 4290 | 38000 | | | | | | |
| PD0032 | 339.1 | 339.95 | 0.85 | 1190 | 34 | 450 | 1 | 10300 | 125100 | | | | | | |
| PD0032 | 339.95 | 340.05 | 0.1 | 54500 | 953 | 28600 | 110 | 5150 | 53600 | | | | | | |
| PD0032 | 340.05 | 350 | 9.95 | 162 | 9 | 39 | 0 | 1990 | 23100 | | | | | | |
| PD0032 | 381.2 | 383.2 | 2 | 570 | 63 | 230 | 5 | 13100 | 124300 | | | | | | |
| PD0032 | 383.2 | 384 | 0.8 | 46500 | 5470 | 8760 | 154 | 9800 | 38700 | | | | | | |
| PD0032 | 384 | 388.7 | 4.7 | 1860 | 360 | 110 | 27 | 2700 | 35300 | | | | | | |
| PD0032 | 388.7 | 390.5 | 1.8 | 340 | 34 | 80 | 1 | 5030 | 7800 | | | | | | |
| PD0032 | 390.5 | 392.25 | 1.75 | 120 | 5 | 80 | 1 | 2970 | 4900 | | | | | | |
| PD0032 | 392.25 | 393.15 | 0.9 | 93600 | 4695 | 8200 | 148 | 14300 | 23700 | 0.036 | | | | | |

**Appendix 5.2 cont.**

| Drill hole | From (m) | To (m) | interval (m) | Zn (ppm) | Cu (ppm) | Pb (ppm) | Ag (ppm) | Mn (ppm) | Fe (ppm) | Au (ppm) | As (ppm) | Hg (ppm) | Sn (ppm) | W (ppm) | Ba (ppm) |
|---|---|---|---|---|---|---|---|---|---|---|---|---|---|---|---|
| PD0032 | 393.15 | 394 | 0.85 | 1040 | 49 | 500 | 3 | 6870 | 7000 | | | | | | |
| PD0032 | 394 | 394.5 | 0.5 | 550 | 13 | 530 | 4 | 16600 | 59000 | | | | | | |
| PD0032 | 407.4 | 408.6 | 1.2 | 410 | 30 | 360 | 1 | 13100 | 34100 | | | | | | |
| PD0032 | 408.6 | 409 | 0.4 | 1420 | 22 | 1090 | 4 | 11400 | 58300 | 0.01 | | | | | |
| PD0032 | 409 | 409.3 | 0.3 | 38800 | 1065 | 16200 | 56 | 7590 | 45900 | | | | | | |
| PD0032 | 409.3 | 411.4 | 2.1 | 2050 | 86 | 2050 | 8 | 9070 | 74300 | | | | | | |
| PD0032 | 411.4 | 413.6 | 2.2 | 750 | 82 | 360 | 4 | 10300 | 89900 | | | | | | |
| PD0032 | 413.6 | 413.85 | 0.25 | 94800 | 512 | 17400 | 34 | 9220 | 24400 | | | | | | |
| PD0032 | 413.85 | 415 | 1.15 | 460 | 4 | 180 | 1 | 7220 | 46300 | | | | | | |
| PD0032 | 421 | 422.7 | 1.7 | 270 | 36 | 270 | 1 | 7440 | 33200 | | | | | | |
| PD0032 | 422.7 | 423.9 | 1.2 | 26800 | 1024 | 7410 | 22 | 6800 | 33100 | | | | | | |
| PD0032 | 423.9 | 424.6 | 0.7 | 38500 | 863 | 16100 | 8 | 8500 | 59100 | | | | | | |
| PD0032 | 424.6 | 425.3 | 0.7 | 9360 | 154 | 4350 | 6 | 11300 | 33100 | | | | | | |
| PD0032 | 425.3 | 427.3 | 2 | 2550 | 43 | 910 | 2 | 11100 | 13500 | | | | | | |
| PD0032 | 427.3 | 429.3 | 2 | 110 | 6 | 120 | 1 | 5500 | 6700 | | | | | | |
| PD0032 | 435 | 436.75 | 1.75 | 140 | 4 | 50 | 1 | 4200 | 4200 | | | | | | |
| PD0032 | 436.75 | 437.7 | 0.95 | 118700 | 3603 | 8210 | 105 | 11700 | 33400 | 0.021 | | | | | |
| PD0032 | 437.7 | 439 | 1.3 | 860 | 28 | 400 | 1 | 3520 | 4900 | | | | | | |
| PD0032 | 519 | 529.1 | 10.1 | 676 | 82 | 415 | 16 | 3814 | 64000 | | | | | | |
| PD0032 | 529.1 | 529.2 | 0.1 | 9530 | 1258 | 810 | 4 | 4410 | 153000 | | | | | | |
| PD0032 | 529.2 | 538.2 | 9 | 613 | 64 | 185 | 2 | 5397 | 68500 | | | | | | |
| PE0015 | 160 | 162 | 2 | 800 | 46 | 630 | 1 | 3540 | 24200 | | | | | | |
| PE0015 | 162 | 164 | 2 | 2154 | 244 | 2500 | 1 | 3835 | 31200 | | | | | | |
| PE0015 | 164 | 166 | 2 | 1484 | 168 | 920 | 1 | 5160 | 53400 | | | | | | |
| PE0015 | 166 | 168 | 2 | 620 | 132 | 415 | 1 | 3940 | 56800 | | | | | | |
| PE0015 | 178 | 180 | 2 | 202 | 68 | 100 | 1 | 3535 | 33000 | | | | | | |
| PE0015 | 180 | 182 | 2 | 71000 | 2312 | 26100 | 18 | 4485 | 43400 | | | | | | |
| PE0015 | 182 | 184 | 2 | 23400 | 798 | 17000 | 19 | 4045 | 35700 | | | | | | |
| PE0015 | 184 | 186 | 2 | 1822 | 64 | 980 | 1 | 3285 | 43900 | | | | | | |
| PE0015 | 186 | 188 | 2 | 1582 | 58 | 710 | 1 | 3555 | 21500 | | | | | | |
| PE0015 | 188 | 190 | 2 | 706 | 28 | 370 | 1 | 2505 | 24200 | | | | | | |
| PE0015 | 190 | 192 | 2 | 1560 | 42 | 1585 | 1 | 7460 | 39600 | | | | | | |
| PE0015 | 192 | 194 | 2 | 578 | 70 | 470 | 1 | 11900 | 50300 | | | | | | |
| PE0015 | 194 | 196 | 2 | 2652 | 60 | 1110 | 1 | 6085 | 46900 | | | | | | |

**Appendix 5.2 cont.**

| Drill hole | From (m) | To (m) | interval (m) | Zn (ppm) | Cu (ppm) | Pb (ppm) | Ag (ppm) | Mn (ppm) | Fe (ppm) | Au (ppm) | As (ppm) | Hg (ppm) | Sn (ppm) | W (ppm) | Ba (ppm) |
|---|---|---|---|---|---|---|---|---|---|---|---|---|---|---|---|
| PE0015 | 196 | 198 | 2 | 7678 | 192 | 3750 | 2 | 4005 | 37700 | | | | | | |
| PE0015 | 198 | 200 | 2 | 236 | 28 | 60 | 1 | 1275 | 43500 | | | | | | |
| PE0015 | 200 | 202 | 2 | 1896 | 66 | 820 | 1 | 1275 | 36000 | | | | | | |
| PE0015 | 202 | 204 | 2 | 178 | 20 | 55 | 1 | 920 | 39000 | | | | | | |
| PE0015 | 206 | 208 | 2 | 380 | 24 | 90 | 1 | 1375 | 36800 | | | | | | |
| PE0015 | 208 | 210 | 2 | 3330 | 54 | 3245 | 1 | 3820 | 47600 | | | | | | |
| PE0015 | 210 | 212 | 2 | 1560 | 50 | 1015 | 1 | 1570 | 28300 | | | | | | |
| PE0015 | 212 | 214 | 2 | 870 | 36 | 310 | 1 | 1510 | 32300 | | | | | | |
| PE0016 | 32 | 34 | 2 | 204 | 20 | 110 | 1 | 930 | 7900 | | | | | | |
| PE0016 | 34 | 36 | 2 | 190 | 68 | 2870 | 1 | 710 | 15000 | | | | | | |
| PE0016 | 36 | 38 | 2 | 626 | 28 | 325 | 1 | 1360 | 16900 | | | | | | |
| PE0016 | 56 | 58 | 2 | 174 | 14 | 60 | 1 | 925 | 13600 | | | | | | |
| PE0016 | 58 | 60 | 2 | 1234 | 56 | 70 | 1 | 1165 | 13900 | | | | | | |
| PE0016 | 60 | 62 | 2 | 400 | 32 | 170 | 1 | 1675 | 14900 | | | | | | |
| PE0016 | 78 | 80 | 2 | 266 | 8 | 80 | 1 | 1045 | 13000 | | | | | | |
| PE0016 | 80 | 82 | 2 | 1030 | 26 | 1100 | 1 | 1325 | 15500 | | | | | | |
| PE0016 | 82 | 84 | 2 | 3360 | 78 | 3240 | 1 | 800 | 13500 | | | | | | |
| PE0016 | 84 | 86 | 2 | 1706 | 44 | 1225 | 1 | 780 | 10600 | | | | | | |
| PE0016 | 86 | 88 | 2 | 736 | 26 | 1255 | 1 | 1085 | 11700 | | | | | | |
| PE0016 | 88 | 90 | 2 | 256 | 10 | 145 | 1 | 1070 | 11600 | | | | | | |
| PE0016 | 108 | 110 | 2 | 326 | 10 | 175 | 1 | 1680 | 18800 | | | | | | |
| PE0016 | 110 | 112 | 2 | 1290 | 38 | 2070 | 1 | 1655 | 20600 | | | | | | |
| PE0016 | 112 | 114 | 2 | 486 | 28 | 630 | 1 | 1660 | 19800 | | | | | | |
| PE0016 | 160 | 162 | 2 | 150 | 10 | 30 | 1 | 1955 | 18100 | | | | | | |
| PE0016 | 162 | 164 | 2 | 7180 | 154 | 4400 | 1 | 2945 | 22700 | | | | | | |
| PE0016 | 164 | 166 | 2 | 3020 | 72 | 1915 | 1 | 2460 | 24400 | | | | | | |
| PE0016 | 166 | 168 | 2 | 890 | 36 | 790 | 1 | 1725 | 33700 | | | | | | |
| PE0016 | 178 | 180 | 2 | 344 | 40 | 100 | 1 | 1790 | 46500 | | | | | | |
| PE0016 | 180 | 182 | 2 | 3644 | 236 | 2140 | 1 | 3410 | 57600 | | | | | | |
| PE0016 | 182 | 184 | 2 | 1512 | 122 | 1555 | 1 | 3265 | 44500 | | | | | | |
| PE0016 | 184 | 186 | 2 | 782 | 82 | 755 | 1 | 3375 | 48600 | | | | | | |
| PE0016 | 196 | 198 | 2 | 304 | 42 | 315 | 1 | 2975 | 26200 | | | | | | |
| PE0016 | 198 | 200 | 2 | 3610 | 56 | 2345 | 1 | 7730 | 51400 | | | | | | |
| PE0016 | 200 | 202 | 2 | 1010 | 28 | 860 | 1 | 5240 | 31700 | | | | | | |

**Appendix 5.2 cont.**

| Drill hole | From (m) | To (m) | interval (m) | Zn (ppm) | Cu (ppm) | Pb (ppm) | Ag (ppm) | Mn (ppm) | Fe (ppm) | Au (ppm) | As (ppm) | Hg (ppm) | Sn (ppm) | W (ppm) | Ba (ppm) |
|---|---|---|---|---|---|---|---|---|---|---|---|---|---|---|---|
| PE0016 | 202 | 204 | 2 | 896 | 12 | 650 | 1 | 6900 | 38500 | | | | | | |
| PE0016 | 212 | 214 | 2 | 780 | 120 | 460 | 1 | 3340 | 45800 | | | | | | |
| PE0016 | 214 | 216 | 2 | 1434 | 100 | 530 | 1 | 4540 | 53900 | | | | | | |
| PE0016 | 216 | 218 | 2 | 3486 | 158 | 990 | 1 | 4420 | 45200 | | | | | | |
| PE0016 | 218 | 220 | 2 | 1390 | 150 | 305 | 1 | 4950 | 67800 | | | | | | |
| PE0016 | 220 | 222 | 2 | 1130 | 278 | 265 | 1 | 3025 | 74100 | | | | | | |
| PE0016 | 222 | 224 | 2 | 444 | 280 | 100 | 1 | 3125 | 81500 | | | | | | |
| PE0017 | 22 | 24 | 2 | 28 | 12 | 160 | 1 | 15 | 7900 | | | | | | |
| PE0017 | 24 | 26 | 2 | 26 | 26 | 1055 | 1 | 20 | 9700 | | | | | | |
| PE0017 | 26 | 28 | 2 | 32 | 28 | 630 | 1 | 15 | 8500 | | | | | | |
| PE0017 | 68 | 70 | 2 | 372 | 20 | 90 | 1 | 1260 | 22000 | | | | | | |
| PE0017 | 70 | 72 | 2 | 832 | 256 | 1265 | 4 | 1600 | 36000 | | | | | | |
| PE0017 | 72 | 74 | 2 | 488 | 74 | 465 | 1 | 3320 | 33000 | | | | | | |
| PE0017 | 140 | 142 | 2 | 486 | 12 | 215 | 1 | 7020 | 77100 | | | | | | |
| PE0017 | 142 | 144 | 2 | 252 | 24 | 1065 | 1 | 3840 | 33700 | | | | | | |
| PE0017 | 144 | 146 | 2 | 178 | 44 | 825 | 1 | 3000 | 22500 | | | | | | |
| PE0025 | 150 | 158 | 8 | 164 | 18 | 30 | | 2850 | 42200 | | | | | | |
| PE0025 | 158 | 160 | 2 | 4706 | 44 | 4615 | 3 | 8025 | 53000 | | | | | | |
| PE0025 | 160 | 162 | 2 | 33600 | 302 | 12300 | 8 | 9360 | 45500 | | | | | | |
| PE0025 | 162 | 164 | 2 | 23600 | 210 | 6840 | 10 | 9500 | 57200 | | | | | | |
| PE0025 | 164 | 166 | 2 | 6262 | 192 | 1475 | 3 | 9015 | 77600 | | | | | | |
| PE0025 | 166 | 168 | 2 | 2332 | 86 | 370 | 3 | 10000 | 79600 | | | | | | |
| PE0025 | 168 | 170 | 2 | 17400 | 78 | 2680 | 6 | 9960 | 75100 | | | | | | |
| PE0025 | 170 | 172 | 2 | 2540 | 10 | 1090 | 1 | 7410 | 68200 | | | | | | |
| PE0025 | 172 | 174 | 2 | 4780 | 42 | 800 | 2 | 5560 | 61600 | | | | | | |
| PE0025 | 174 | 176 | 2 | 406 | 22 | 45 | | 1700 | 101600 | | | | | | |
| PE0025 | 176 | 178 | 2 | 1245 | 76 | 125 | | 3130 | 153100 | | | | | | |
| PE0025 | 178 | 180 | 2 | 548 | 32 | 115 | | 3005 | 112300 | | | | | | |
| PE0025 | 188 | 190 | 2 | 180 | 16 | 325 | 1 | 1570 | 20600 | | | | | | |
| PE0025 | 190 | 192 | 2 | 5420 | 74 | 2555 | 2 | 4020 | 28500 | | | | | | |
| PE0025 | 192 | 194 | 2 | 1796 | 20 | 650 | | 1870 | 23400 | | | | | | |
| PE0025 | 194 | 196 | 2 | 516 | 60 | 420 | | 1465 | 27900 | | | | | | |
| PE0025 | 336 | 344 | 8 | 394 | 20 | 160 | | 5120 | 55800 | | | | | | |
| PE0025 | 344 | 352 | 8 | 2536 | 36 | 1985 | 1 | 4920 | 51300 | | | | | | |

**Appendix 5.2 cont.**

| Drill hole | From (m) | To (m) | interval (m) | Zn (ppm) | Cu (ppm) | Pb (ppm) | Ag (ppm) | Mn (ppm) | Fe (ppm) | Au (ppm) | As (ppm) | Hg (ppm) | Sn (ppm) | W (ppm) | Ba (ppm) |
|---|---|---|---|---|---|---|---|---|---|---|---|---|---|---|---|
| PE0026 | 0 | 10 | 10 | 54 | 12 | 140 | | 170 | 12500 | | | | | | |
| PE0026 | 86 | 100 | 14 | 472 | 24 | 420 | 1 | 1070 | 48500 | | | | | | |
| PE0026 | 100 | 110 | 10 | 1590 | 24 | 235 | 3 | 2900 | 95600 | | | | | | |
| PE0026 | 110 | 120 | 10 | 266 | 8 | 85 | 1 | 4150 | 65800 | | | | | | |
| PE0028 | 98 | 110 | 12 | 86 | 6 | 25 | | 280 | 19900 | | | | | | |
| PE0028 | 110 | 120 | 10 | 1024 | 36 | 285 | 1 | 240 | 19000 | | | | | | |
| PE0028 | 120 | 130 | 10 | 260 | 22 | 90 | | 230 | 14000 | | | | | | |
| PE0031 | 40 | 48 | 8 | 618 | 36 | 400 | | 1620 | 33800 | | | | | | |
| PE0031 | 48 | 60 | 12 | 1578 | 112 | 115 | 1 | 1280 | 50800 | | | | | | |
| PE0031 | 60 | 70 | 10 | 360 | 22 | 80 | 1 | 735 | 23100 | | | | | | |
| PE0031 | 170 | 180 | 10 | 910 | 442 | 80 | 1 | 3385 | 60600 | | | | | | |
| PE0031 | 180 | 192 | 12 | 1338 | 230 | 300 | 3 | 3630 | 58000 | | | | | | |
| PE0031 | 192 | 204 | 12 | 428 | 60 | 115 | 1 | 1685 | 48400 | | | | | | |

**Appendix 5.3**

Trace element compositions of galena determined using the Cameca SX - 50 electron microprobe at the Central Science Laboratory, University of Tasmania

| Drill hole | Depth (m) | Zone | Mineral | Ag (ppm) | Bi (ppm) | Sb (ppm) |
|---|---|---|---|---|---|---|
| PD0008 | 116 | C | Galena 1 | n/a | n/a | n/a |
| PD0008 | 116 | C | Galena 1 | 485 | 2809 | n/a |
| PD0008 | 116 | C | Galena 1 | 557 | 2738 | n/a |
| PD0008 | 116 | C | Galena 1 | 593 | 3253 | n/a |
| PD0008 | 116 | C | Galena 1 | 639 | 3006 | n/a |
| PD0008 | 225.65 | C | Galena 1 | 353 | 1762 | n/a |
| PD0016 | 305 | N | Galena 1 | 312 | 1312 | n/a |
| PD0016 | 305 | N | Galena 1 | n/a | n/a | n/a |
| PD0016 | 305 | N | Galena 1 | n/a | n/a | n/a |
| PD0016 | 305 | N | Galena 1 | 211 | 1857 | n/a |
| PD0016 | 305 | N | Galena 1 | n/a | n/a | n/a |
| PD0016 | 305 | N | Galena 1 | n/a | n/a | n/a |
| PD0016 | 305 | N | Galena 1 | 215 | 1456 | n/a |
| PD0016 | 305 | N | Galena 1 | 199 | 1961 | n/a |
| PD0017 | 234.15 | C | Galena 1 | 330 | 0 | 10 |
| PD0017 | 234.15 | C | Galena 1 | 480 | 0 | 0 |
| PD0017 | 234.15 | C | Galena 1 | 160 | 0 | 0 |
| PD0017 | 234.15 | C | Galena 1 | 160 | 0 | 240 |
| PD0017 | 234.15 | C | Galena 1 | 46 | 811 | 0 |
| PD0017 | 234.15 | C | Galena 1 | 238 | 582 | 70 |
| PD0017 | 234.15 | C | Galena 1 | 212 | 2516 | 0 |
| PD0017 | 234.15 | C | Galena 1 | 198 | 0 | 194 |
| PD0032 | 223.2 | S | Galena 1 | 91 | 1695 | n/a |
| PD0032 | 223.2 | S | Galena 1 | 92 | 1880 | n/a |
| PD0032 | 223.2 | S | Galena 1 | 68 | 1586 | n/a |
| PD0032 | 223.2 | S | Galena 1 | 142 | 1810 | n/a |
| PD0032 | 245.7 | S | Galena 1 | 203 | 2136 | 0 |
| PD0032 | 245.7 | S | Galena 1 | 0 | 651 | 0 |
| PD0032 | 245.7 | S | Galena 1 | 0 | 1944 | 0 |
| PD0032 | 245.7 | S | Galena 2 | 93 | 1674 | 0 |
| PD0032 | 245.7 | S | Galena 2 | 128 | 1331 | 0 |
| PD0032 | 245.7 | S | Galena 2 | 214 | 1505 | 0 |
| PD0032 | 245.7 | S | Galena 2 | 120 | 2316 | 0 |
| PD0032 | 245.7 | S | Galena 2 | 75 | 1883 | 0 |

N = northern zone; C = central zone; S = southern zone; n/a = not analysed

**Appendix 5.4**

Sphalerite compositions determined using the Cameca SX - 50 electron microprobe at the Central Science Laboratory, University of Tasmania

| Drill hole | Depth | Zone | Mineral | MnO (ppm) | Cd (ppm) | S (wt.%) | Fe* (wt.%) | Zn (wt.%) | Total (wt.%) |
|---|---|---|---|---|---|---|---|---|---|
| PD0008 | 116 | C | SP2 | n/a | 1433 | n/a | n/a | n/a | n/a |
| PD0008 | 116 | C | SP2 | n/a | 1394 | n/a | n/a | n/a | n/a |
| PD0008 | 116 | C | SP2 | n/a | 1637 | n/a | n/a | n/a | n/a |
| PD0008 | 225.65 | C | SP2 | n/a | 1894 | n/a | n/a | n/a | n/a |
| PD0016 | 263 | N | SP2 | 1110 | 1510 | 33.37 | 2.90 | 63.48 | 99.91 |
| PD0016 | 263 | N | SP2 | 2650 | 1760 | 33.23 | 3.91 | 62.04 | 99.65 |
| PD0016 | 263 | N | SP2 | 4070 | 1810 | 33.18 | 4.14 | 61.36 | 99.30 |
| PD0016 | 263 | N | SP2 | 5270 | 1660 | 33.19 | 4.32 | 61.87 | 100.14 |
| PD0016 | 263 | N | SP2 | 4660 | 1390 | 33.02 | 4.24 | 61.85 | 99.73 |
| PD0016 | 263 | N | SP2 | 3930 | 1300 | 32.99 | 4.08 | 61.93 | 99.52 |
| PD0016 | 263 | N | SP2 | 2570 | 1670 | 33.40 | 3.90 | 62.55 | 100.40 |
| PD0016 | 263 | N | SP2 | 3060 | 1950 | 33.04 | 4.18 | 62.22 | 100.00 |
| PD0016 | 263 | N | SP2 | 3590 | 1160 | 33.01 | 4.24 | 61.93 | 99.87 |
| PD0016 | 263 | N | SP2 | 3130 | 1710 | 33.13 | 4.24 | 61.80 | 99.68 |
| PD0016 | 263 | N | SP2 | 2990 | 2310 | 32.94 | 4.22 | 61.78 | 99.50 |
| PD0016 | 263 | N | SP2 | 2930 | 1760 | 32.95 | 4.02 | 61.84 | 99.64 |
| PD0016 | 263 | N | SP2 | n/a | n/a | 33.27 | 2.90 | 63.48 | 99.91 |
| PD0016 | 263 | N | SP2 | n/a | n/a | 33.23 | 3.91 | 62.04 | 99.66 |
| PD0016 | 263 | N | SP2 | n/a | n/a | 33.18 | 4.14 | 61.36 | 99.30 |
| PD0016 | 263 | N | SP2 | n/a | n/a | 33.19 | 4.32 | 61.87 | 100.14 |
| PD0016 | 263 | N | SP2 | n/a | n/a | 32.99 | 4.08 | 61.93 | 99.52 |
| PD0016 | 263 | N | SP2 | n/a | n/a | 33.02 | 4.24 | 61.85 | 99.73 |
| PD0016 | 263 | N | SP2 | n/a | n/a | 33.40 | 3.90 | 62.55 | 100.40 |
| PD0016 | 263 | N | SP2 | n/a | n/a | 33.01 | 4.24 | 61.93 | 99.87 |
| PD0016 | 263 | N | SP2 | n/a | n/a | 33.04 | 4.13 | 62.22 | 100.00 |
| PD0016 | 263 | N | SP2 | n/a | n/a | 33.13 | 4.24 | 61.80 | 99.68 |
| PD0016 | 263 | N | SP2 | 2930 | 1760 | 32.95 | 4.02 | 61.84 | 99.64 |
| PD0016 | 263 | N | SP2 | n/a | n/a | 32.94 | 4.22 | 61.78 | 99.50 |
| PD0016 | 263 | N | SP2 | 2320 | 1820 | 32.82 | 3.90 | 62.06 | 99.48 |
| PD0016 | 305 | N | SP2 | 470 | 1970 | 32.14 | 1.14 | 62.29 | 95.92 |
| PD0016 | 305 | N | SP2 | 1610 | 1940 | 33.14 | 1.59 | 65.30 | 100.46 |
| PD0016 | 305 | N | SP2 | n/a | 2436 | n/a | n/a | n/a | n/a |
| PD0016 | 305 | N | SP2 | 3119 | 1633 | n/a | n/a | n/a | n/a |
| PD0016 | 305 | N | SP2 | 6449 | 1593 | n/a | n/a | n/a | n/a |
| PD0016 | 305 | N | SP2 | 4356 | 1795 | n/a | n/a | n/a | n/a |
| PD0016 | 305 | N | SP2 | 1820 | 1890 | 33.02 | 1.74 | 64.99 | 100.61 |
| PD0016 | 305 | N | SP2 | 410 | 1830 | 32.92 | 2.41 | 63.64 | 99.37 |
| PD0032 | 223.2 | S | SP2 | 3703 | 2237 | n/a | n/a | n/a | n/a |
| PD0032 | 223.2 | S | SP2 | 2635 | 2162 | n/a | n/a | n/a | n/a |
| PD0032 | 223.2 | S | SP2 | 2019 | 1953 | n/a | n/a | n/a | n/a |
| PD0032 | 223.2 | S | SP2 | 2811 | 1769 | n/a | n/a | n/a | n/a |

N = northern zone; C = central zone; S = southern zone; SP2 = sphalerite 2; n/a = not analysed

*Iron and sulphur have been corrected for inclusions of chalcopyrite 2 that may have been incorporated in the sample spot by deducting the appropriate amount of iron and sulphur corresponding to the formula for chalcopyrite.

**Appendix 5.5**

Carbonate compositions determined using the Cameca SX - 50 electron microprobe at the Central Science Laboratory, University of Tasmania

| Drill hole | Depth (m) | Zone* | Mineral | MgCO3 (wt.%) | CaCO3 (wt.%) | MnCO3 (wt.%) | FeCO3 (wt.%) | ZnCO3 (wt.%) | SrCO3 (wt.%) | BaCO3 (wt.%) | Total (wt.%) |
|---|---|---|---|---|---|---|---|---|---|---|---|
| PD0028 | 366.1 | C | Late calcite vein | 0.00 | 99.89 | 0.00 | 0.03 | 0.04 | 0.06 | 0.02 | 100.03 |
| PD0028 | 366.1 | C | Late calcite vein | 0.00 | 99.81 | 0.00 | 0.00 | 0.04 | 0.04 | 0.00 | 99.89 |
| PD0016 | 272.6 | N | Late calcite vein | 0.27 | 94.35 | 4.47 | 0.92 | 0.00 | 0.00 | 0.00 | 100.00 |
| PD0016 | 272.6 | N | Late calcite vein | 0.35 | 97.71 | 1.11 | 0.73 | 0.00 | 0.09 | 0.01 | 100.00 |
| PD0016 | 272.6 | N | Late calcite vein | 0.83 | 96.51 | 1.52 | 0.72 | 0.00 | 0.30 | 0.01 | 99.89 |
| PD0016 | 305 | N | Dolomite | 49.86 | 47.95 | 0.57 | 1.56 | 0.00 | 0.05 | 0.01 | 100.00 |
| PD0016 | 305 | N | Dolomite | 50.27 | 47.92 | 0.61 | 1.14 | 0.05 | 0.00 | 0.00 | 99.99 |
| PD0016 | 305 | N | Dolomite | 50.33 | 47.08 | 0.80 | 1.74 | 0.02 | 0.02 | 0.01 | 99.99 |
| PD0016 | 305 | N | Dolomite | 47.15 | 48.77 | 1.24 | 2.71 | 0.01 | 0.04 | 0.08 | 99.99 |
| PD0016 | 305 | N | Dolomite | 44.14 | 51.87 | 1.27 | 2.67 | 0.00 | 0.04 | 0.00 | 99.99 |
| PD0032 | 245.7 | S | Ca-Mn-Mg-Fe carbonate 2 | 31.57 | 51.35 | 11.22 | 7.15 | 0.02 | 0.00 | 0.00 | 101.32 |
| PD0032 | 245.7 | S | Ca-Mn-Mg-Fe carbonate 2 | 20.10 | 51.10 | 10.64 | 19.72 | 0.25 | 0.00 | 0.02 | 101.83 |
| PD0032 | 245.7 | S | Ca-Mn-Mg-Fe carbonate 2 | 17.65 | 49.36 | 13.46 | 15.48 | 0.49 | 0.16 | 0.01 | 96.60 |
| PD0032 | 245.7 | S | Ca-Mn-Mg-Fe carbonate 2 | 24.42 | 51.15 | 19.50 | 6.77 | 0.08 | 0.00 | 0.00 | 101.91 |
| PD0032 | 245.7 | S | Ca-Mn-Mg-Fe carbonate 2 | 32.88 | 51.16 | 12.62 | 4.37 | 0.09 | 0.00 | 0.02 | 101.14 |
| PD0032 | 245.7 | S | Ca-Mn-Mg-Fe carbonate 2 | 32.88 | 48.08 | 11.27 | 7.72 | 0.13 | 0.00 | 0.05 | 100.86 |
| PD0032 | 245.7 | S | Ca-Mn-Mg-Fe carbonate 2 | 33.48 | 51.39 | 11.46 | 5.00 | 0.02 | 0.00 | 0.00 | 101.36 |
| PD0032 | 245.7 | S | Ca-Mn-Mg-Fe carbonate 2 | 31.12 | 41.86 | 11.99 | 14.13 | 0.12 | 0.00 | 0.00 | 99.22 |
| PD0017 | 234.15 | C | Ca-Mn-Mg-Fe carbonate 2 | 0.33 | 79.59 | 21.49 | 0.00 | 0.04 | 0.00 | 0.02 | 101.46 |
| PD0017 | 234.15 | C | Ca-Mn-Mg-Fe carbonate 2 | 9.56 | 47.23 | 43.17 | 0.00 | 0.03 | 0.00 | 0.01 | 100.00 |
| PD0017 | 234.15 | C | Ca-Mn-Mg-Fe carbonate 2 | 5.06 | 48.96 | 45.96 | 0.00 | 0.02 | 0.00 | 0.00 | 100.00 |
| PD0017 | 234.15 | C | Ca-Mn-Mg-Fe carbonate 2 | 17.23 | 50.13 | 32.57 | 0.00 | 0.03 | 0.00 | 0.05 | 100.00 |
| PD0017 | 234.15 | C | Ca-Mn-Mg-Fe carbonate 2 | 5.88 | 46.78 | 47.34 | 0.00 | 0.00 | 0.00 | 0.00 | 100.00 |
| PD0032 | 245.7 | S | Ca-Mn-Mg-Fe carbonate 2 | 32.85 | 51.11 | 11.64 | 4.33 | 0.07 | 0.00 | 0.00 | 100.00 |
| PD0032 | 245.7 | S | Ca-Mn-Mg-Fe carbonate 2 | 32.50 | 51.26 | 12.10 | 3.91 | 0.23 | 0.00 | 0.00 | 100.00 |
| PD0032 | 245.7 | S | Ca-Mn-Mg-Fe carbonate 2 | 31.64 | 51.11 | 12.55 | 4.34 | 0.36 | 0.00 | 0.00 | 100.00 |

*N = northern zone; C = central zone; S = southern zone

**Appendix 6.1.**
Field parameters used during acquisition of aeromagnetic data:

| Parameter | West of Menninnie Dam. Data acquired for Billiton Australia Ltd. | East of Menninnie Dam. Data acquired for the DME. |
|---|---|---|
| Flown | Sept. 1983 | Apr. - May 1993 |
| Aircraft | Rockwell Shrike Commander | Rockwell Shrike Commander |
| Line spacing | 300m | 400m |
| Line orientation | east - west | east - west |
| Tie line spacing | 3000m | 4000m |
| Tie line orientation | north - south | north - south |
| Mean terrain clearance | 70m | 80m |
| Navigation | Geocam 35mm tracking camera: Sperry Stars radar altimeter | Ashtech X11 GPS receiver |
| Magnetometer | Optically pumped Caesium vapour: GSM-8B p.m. base station | Scintrex VIW 2321-H8 Caesium vapour |
| Resolution | 0.04 nT | 0.001 nT |
| Sample rate | 0.2 sec (1 per 14m) | 0.1 sec |
| Installation | Tail stinger | Tail stinger |
| Passive compensation | | Applied; Noise envelope of raw magnetic data 0.2 nT |
| Active compensation | Peak to peak noise envelope for raw magnetic data = 2.49 nT | RMS AADC; Real time; Bandwidth DC to 0.9Hz; Effective noise envelope mostly less than 0.05 nT; NS,SN,EW,WE noise envelope difference 25% max. Output sample rate 0.1 sec. |

Processing of data acquired to the east of Menninnie Dam for DME.
The magnetic data have been corrected for regional gradient by subtraction of I.G.R.F. model 1985 and secular variation model 1985 - 1990. Diurnal magnetic variations have been removed. System parallax has been removed. Microlevelling has been applied. Inclination and declination have been computed continuously over the whole area using I.G.R.F. model 1990 computed at year 1991. Inclination for map centre = -65.47°. Declination for map centre = 7.05°. Gridding parameters: bicubic spline algorithm with mesh size of 100m by 100m.

Processing of data acquired to the west of Menninnie Dam for Billiton Australia Ltd.
The magnetic data have been corrected for regional gradient by subtraction of I.G.R.F model 1980 and addition of a datum of 2000nT. Diurnal magnetic variations have been removed. System parallax not applied and estimated as < 1 sample interval (0.2 sec). Levelling by tie lines only. Gridding parameters: gaussian filter af 125m radius.

**Appendix 6.2**

Bouguer gravity (mGal) and magnetic data (nT) for transect lines.

| | Line C - C' | | Line B - B' | | Line A - A' | | Line D - D' | |
|---|---|---|---|---|---|---|---|---|
| (km) | gravity | magnetics | gravity | magnetics | gravity | magnetics | gravity | magnetics |
| 0 | -12.5 | 1565 | -6.5 | 1772 | -26 | 1700 | -26.5 | 1645 |
| 1 | | 1467 | | 1797 | | 1635 | | 1558 |
| 2 | | 1529 | | 1780 | | 1732 | | 1564 |
| 3 | -12 | 1726 | -8 | 1772 | -25 | 1636 | -25.6 | 1548 |
| 4 | | 1678 | | 1764 | | 1627 | | 1551 |
| 5 | | 1544 | | 1688 | | 1590 | | 1570 |
| 6 | -10.5 | 1759 | -10 | 1632 | -23 | 1579 | -23 | 1528 |
| 7 | | 1735 | | 1605 | | 1559 | | 1491 |
| 8 | | 1589 | | 1587 | | 1540 | | 1482 |
| 9 | -7 | 1642 | -11 | 1549 | -22 | 1506 | -21.3 | 1473 |
| 10 | | 1654 | | 1516 | | 1493 | | 1463 |
| 11 | | 1699 | | 1642 | | 1477 | | 1476 |
| 12 | -6 | 1565 | -11 | 1789 | -20.5 | 1449 | -21.1 | 1494 |
| 13 | | 1559 | | 1709 | | 1420 | | 1505 |
| 14 | | 1565 | | 1747 | | 1418 | | 1524 |
| 15 | -9 | 1562 | -11.5 | 1800 | -19 | 1420 | -21.6 | 1535 |
| 16 | | 1568 | | 1777 | | 1436 | | 1551 |
| 17 | | 1580 | | 1831 | | 1448 | | 1581 |
| 18 | -11.5 | 1619 | -12 | 1684 | -18 | 1450 | -22.2 | 1642 |
| 19 | | 1604 | | 1764 | | 1453 | | 1854 |
| 20 | | 1613 | | 1797 | | 1500 | | 1984 |
| 21 | -14 | 1979 | -11.5 | 1705 | -17 | 1771 | -24 | 2052 |
| 22 | | 3200 | | 1713 | | 1543 | | 2120 |
| 23 | | 1436 | | 1717 | | 1534 | | 2067 |
| 24 | -17 | 1517 | -12 | 1887 | -17.5 | 1563 | -26 | 1908 |
| 25 | | 1458 | | 1759 | | 1534 | | 1980 |
| 26 | | 1490 | | 1503 | | 1596 | | 1847 |
| 27 | -19.5 | 1613 | -12 | 1579 | -19 | 1555 | -27.4 | 1687 |
| 28 | | 1541 | | 2041 | | 1560 | | 1554 |
| 29 | | 1663 | | 1608 | | 1588 | | 1535 |
| 30 | -21 | 1404 | -13.5 | 1637 | -20 | 1582 | -27.3 | 1368 |
| 31 | | 1538 | | 1618 | | 1567 | | 1520 |
| 32 | | 1768 | | 1536 | | 1539 | | 1513 |
| 33 | -21.5 | 1592 | -16 | 1503 | -20.5 | 1559 | -24.5 | 1467 |
| 34 | | 1565 | | 1566 | | 1560 | | |
| 35 | | 1565 | | 1995 | | 1380 | | |
| 36 | -20 | 1520 | -19 | 1415 | -21 | 1419 | -25.5 | |
| 37 | | 1476 | | 1494 | | 1587 | | |
| 38 | | 1437 | | 1524 | | 1542 | | |
| 39 | -18.5 | 1458 | -20.5 | 1524 | -21 | 1523 | | |
| 40 | | 1431 | | 1517 | | 1520 | | |
| 41 | | 1422 | | 1523 | | 1630 | | |
| 42 | -16.5 | 1422 | -21.5 | 1804 | -20 | 1620 | | |
| 43 | | 1428 | | 1809 | | 1533 | | |
| 44 | | 1452 | | 1650 | | 1542 | | |
| 45 | -16 | 1437 | -21 | 1609 | -18 | 1573 | | |
| 46 | | 1478 | | 1579 | | 1628 | | |
| 47 | | 1613 | | 1612 | | 1562 | | |
| 48 | -15 | 1577 | -19.5 | 1579 | -15.5 | 1642 | | |
| 49 | | 1529 | | 1519 | | 1570 | | |
| 50 | | 1565 | | 1459 | | 1517 | | |

**Appendix 6.2 cont.**

| | Line C - C' | | Line B - B' | | Line A - A' | | Line D - D' | |
|---|---|---|---|---|---|---|---|---|
| (km) | gravity | magnetics | gravity | magnetics | gravity | magnetics | gravity | magnetics |
| 51 | -17 | 1532 | -18 | 1432 | -12 | 1482 | | |
| 52 | | 1622 | | 1387 | | 1473 | | |
| 53 | | 1806 | | 1340 | | 1400 | | |
| 54 | -19.5 | 1961 | -17 | 1305 | -8.5 | 1370 | | |
| 55 | | 2152 | | 1307 | | 1398 | | |
| 56 | | 2083 | | 1332 | | 1352 | | |
| 57 | -23 | 2006 | -17 | 1341 | -6 | 1279 | | |
| 58 | | 1988 | | 1343 | | | | |
| 59 | | 1970 | | 1472 | | | | |
| 60 | -27.5 | 1905 | -17.5 | 1309 | | | | |
| 61 | | 1875 | | 1293 | | | | |
| 62 | | 1857 | | 1587 | | | | |
| 63 | -30 | 1842 | -19.5 | 1423 | | | | |
| 64 | | 1899 | | 1385 | | | | |
| 64.5 | | 1899 | | | | | | |
| 65 | | 1870 | | 1398 | | | | |
| 66 | -30 | 1850 | -23 | 1412 | | | | |
| 67 | | 1840 | | 1408 | | | | |
| 68 | | 1820 | | 1431 | | | | |
| 69 | -29 | 1810 | -26 | 1423 | | | | |
| 70 | | 1795 | | 1414 | | | | |
| 71 | | 1780 | | | | | | |
| 72 | -27.5 | 1800 | | | | | | |
| 73 | | 1840 | | | | | | |
| 74 | | 1420 | | | | | | |
| 75 | -24 | 1480 | | | | | | |

**Appendix 6.3**

Density measurements of samples from rock units used for two dimensional gravity modelling.

| Rock Type | location details | No. of samples | Average density | Reference |
|---|---|---|---|---|
| Hiltaba Suite Granite | Minnipa granite quarry | 1 | 2.610 | Amatek Ltd (testing by AMDEL) |
| Hiltaba Suite Granite | Cultana Complex | 4 | 2.649 | Gow (pers. comm.) |
| Hiltaba Suite Granite | Pildappa Rock | 6 | 2.651 | Gow (pers. comm.) |
| Hiltaba Suite Granite | Willauka Hill | 4 | 2.654 | Gow (pers. comm.) |
| Hiltaba Suite Granite | Willauka Hill | 3 | 2.579 | Gow (pers. comm.) |
| Hiltaba Suite Granite | Streaky Bay granite quarry | 1 | 2.610 | SADME (testing by AMDEL) |
| Hiltaba Suite Granite | Minnipa Granite. 600239mE, 6371658mN | 5 | 2.607 | This study |
| Hiltaba Suite Granite | Minnipa Granite. 600024mE, 6370327mN | 7 | 2.588 | This study |
| Hiltaba Suite Granite | Buckleboo Granite. 620891mE, 6358235mN | 4 | 2.606 | This study |
| Hiltaba Suite Granite | Charleston Granite. 704000mE, 6314400mN | 2 | 2.613 | This study |
| G.R.V. | Eucarro Dacite 629522mE, 6386938mN | 3 | 2.534 | This study |
| G.R.V. | Nonning Rhyodacite | 2 | 2.558 | This study |
| G.R.V. | Black Yardea Dacite | 2 | 2.646 | This study |
| G.R.V. | Red Yardea Dacite | 2 | 2.608 | This study |
| Lincoln Suite Granite | Wilcherry Hill. 636697mE, 6374601mN | 2 | 2.553 | This study |
| Lincoln Suite Granite | Poornamookinie Creek 638200mE, 6272100mN | 1 | 2.608 | This study |
| Lincoln Suite Granite | Menninnie Dam drill hole PD0021, 169m | 2 | 2.609 | This study |
| Lincoln Suite Granite | Wilcherry Hill. 640786mE, 6378899mN | 1 | 2.620 | This study |
| Lincoln Suite Granite | Sleaford Bay | 1 | 2.625 | This study |
| Lincoln Suite Granite | Wilcherry Hill. 637113mE, 6376976mN | 2 | 2.628 | This study |
| Lincoln Suite Granite | Carappee Hill. 618400mE, 6301700mN | 1 | 2.637 | This study |
| Lincoln Suite Granite | Arcoona, drill hole ASD1, 986-1027m | ? | 2.640 | Paterson and Muir (1986) |
| Lincoln Suite Granite | Burkitt Granite 137°2'30"E, 32°41'N | 2 | 2.640 | This study |
| Lincoln Suite Granite | Wilcherry Hill. 631710E, 6376070N | 2 | 2.653 | This study |
| Lincoln Suite Granite | Saddle Hill drill hole SHD1, 829-965m | ? | 2.680 | Paterson and Muir (1986) |
| Lincoln Suite Granite | Dromedary Dam drill hole DRD1, 1067-1192m | ? | 2.700 | Paterson and Muir (1986) |
| Lincoln Suite Granite | Arcoona drill hole ASD1, 946-975m | ? | 2.700 | Paterson and Muir (1986) |
| Lincoln Suite Granite | Refuge Rocks | 2 | 2.733 | Gow (pers. comm.) |
| Lincoln Suite Granite | Heaton Hill drill hole HHD1, 1132-1186m | ? | 2.760 | Paterson and Muir (1986) |
| Lincoln Suite Granite | Wertigo Granite | 4 | 2.819 | Gow (pers. comm.) |

**Appendix 6.3 cont.**

| Rock Type | location details | No. of samples | Average density | Reference |
|---|---|---|---|---|
| Warrow Quartzite | Poornamookinie Creek 638200mE, 6272100mN | 3 | 2.631 | This study |
| Warrow Quartzite | Caralue Bluff 610000mE, 6316500mN | 2 | 2.636 | This study |
| Warrow Quartzite | Range Road lookout 650900mE, 6274300mN | 1 | 2.655 | This study |
| Marble | Menninnie Dam drill hole PD0015, 509.49-.72m | 1 | 2.708 | This study |
| Cook Gap Schist | Wangaraleednie area 650800mE, 6273350mN | 1 | 2.727 | This study |
| Yadnarie Schist | Poolalalie Creek 633620mE, 6277000mN | 1 | 2.745 | This study |
| Marble | Menninnie Dam drill hole PD0026, 485.65-.8m | 1 | 2.762 | This study |
| Marble | Menninnie Dam drill hole PD0010, 229.91-230.1m | 1 | 2.769 | This study |
| Iron Formation | Menninnie Dam drill hole PD0006, 189.34-.56m | 1 | 2.785 | This study |
| Calc-silicate | Menninnie Dam drill hole PD0011, 170.6-.8m | 1 | 2.904 | This study |
| Iron Formation | Menninnie Dam drill hole PD0008, 277.0-.2m | 1 | 2.970 | This study |
| Marble | Menninnie Dam drill hole PD0006, 193.35-.5m | 1 | 3.087 | This study |
| Marble | Menninnie Dam drill hole PD0026, 462.3-.5m | 1 | 3.089 | This study |
| Marble | Menninnie Dam drill hole PD0014, 217.8-218.0m | 1 | 3.128 | This study |
| Calc-silicate | Menninnie Dam drill hole PD0020, 360.3-.53m | 1 | 3.221 | This study |
| Calc-silicate | Menninnie Dam drill hole PD0017, 482.6-.7m | 1 | 3.270 | This study |
| Calc-silicate | Menninnie Dam drill hole PD0026, 441.95m | 1 | 3.375 | This study |
| Sleaford Complex | 603500mE, 6355550mN | 6 | 2.761 | This study |

## Appendix 7.1

Sample preparation and analytical techniques used for Pb isotope determinations.

The following is a summary of techniques outlined in reports by Carr and Dean (1990); Carr, Gulson and Dean (1986); Carr and Dean (1991); Dean (1991); Fanning (1988).

### Sample preparation

*Pb isotope determinations from galena*

Galena was hand picked and dissolved in concentrated nitric acid. Lead was purified by micro-electrodeposition techniques onto platinum electrodes.

*Pb isotope determinations from whole rock samples*

Between 30 and 80 mg of the pulverised whole rock sample was digested in a teflon beaker using a 1 : 1 mixture of 7N HCl and 7N $HNO_3$. Lead was separated in anion exchange columns in dilute HBr solutions prior to final purification by micro-electrodeposition techniques onto platinum electrodes.

*Pb isotope determinations from feldspar*

The separation technique used to collect feldspar from the Charleston Granite is not known. A sample of the 'Cunyarie Granite' was crushed and sieved to give a 1 mm - 0.5 mm separate. Feldspar grains were then hand separated under a 25 power microscope. The feldspar was first washed with cold HCl and the leachate was separated and discarded. The sample was then subject to three more leaches; firstly with HCl, then with HCl + $HNO_3$, and finally total dissolution with HF. Each of the three leachates was retained and analysed.

*Sample of eastern suite schist*

The sample of the eastern suite schist from 410.6m in drill hole PD0006 underwent the same series of leaches described above for feldspars and each of the four leachates was retained and analysed.

With the exception of the feldspar sample from the Tarcoola Granite, all isotopic ratios were determined on a VG ISOMASS 54E thermal ionisation mass spectrometer run in fully automated mode at the SIROTOPE laboratory, CSIRO, North Ryde, NSW, Australia. Results have been normalised to the accepted value of international standard NBS 981 by applying a correction factor of +0.08% per atomic mass unit.

**Appendix 7.1 cont.**

*Feldspar from the Tarcoola Granite*

Feldspar samples from the Tarcoola Granite were crushed to -36 BSS mesh, deslimed and separated in tetrabromoethane (s.g. 2.6). The lighter fraction was sieved to give a -75 + 150 BSS mesh sub-fraction and potassium feldspar concentrates prepared using a combination of Frantz isodynamic and density column separators. The feldspar was acid washed with 1N HCl in an ultrasonic for 15 minutes then rinsed three times with nanopure $H_2O$ and rinsed again in an ultrasonic with nanopure $H_2O$ for a further 15 minutes. The samples were dried with distilled acetone in a clean air environment. The feldspars were then dissolved in an HF - $HNO_3$ mixture in open FEP teflon beakers, allowed to stand cold overnight, then dried and treated with 6N HCl then 1.5N HBr. Isotopic ratios were determined using a Finnigan MAT 261 multicollector mass spectrometer at the Australian National University with data collected in the static mode. The NBS common lead standard SRM981 was run in conjunction with the samples and gave the following means for three separate analyses:

$^{208}Pb / ^{206}Pb$ 2.1610 ± 0.02%

$^{207}Pb / ^{206}Pb$ 0.9133 ± 0.02%

$^{206}Pb / ^{204}Pb$ 16.886 ± 0.03%

**Sample details (ref. Appendix 7.2)**

Each sample in Appendix 7.2 is designated as 'gn', 'wr' or 'fel', dependant on whether the Pb isotope ratios were determined from galena, whole rock or feldspar samples respectively. In a number of instances, more than one set of results are presented for the same sample. These have resulted from either repeat analyses of the same sub-sample in which case the sample type has the suffix '/r', or, analyses of a new sub-sample, in which case samples have the suffix '/1, 2 etc. For galena analyses, the new sub-sample was derived from a different section of the initial rock - mineral specimen. For whole rock and feldspar analyses, the new sub-sample was derived from the same initial specimen that had undergone a different leach process. Leaches were sequential and Pb isotope determinations of sequential leaches have a numerical suffix ('/1, 2 etc). All repeat analyses lie within analytical precision of each other. Analyses of new galena sub-samples may not lie within the precision ellipse and indicate heterogeneity between galena grains on a hand specimen scale. Variance between analyses of new whole rock or feldspar sub-samples results from the efficiency of sequential leaches in extracting lead from different mineral species.

## Appendix 7.2
Lead isotope determinations

| Northing (mN) | Easting (mN) | Drill hole | Depth (m) | Zone | Sample description | Sample type | Assay Interval | Lead assay (wt.%) | U (ppm) | Th (ppm) | 208Pb /206Pb | 207Pb /206Pb | 206Pb /204Pb | 207Pb /204Pb | 208Pb /204Pb | Pb content (wt.%) | Ref. |
|---|---|---|---|---|---|---|---|---|---|---|---|---|---|---|---|---|---|
| 10000 | 10868.5 | PD0001 | 162 | N | ser alt gnd | wr | 162-164 | 0.3300 | 0.00 | 18.00 | 2.1679 | 0.9232 | 16.811 | 15.519 | 36.443 | 0.28 | 3 |
| 10000 | 10868.5 | PD0001 | 163.3 | N | ser alt gnd | wr | 162-164 | 0.3300 | 10.00 | 24.00 | 2.0932 | 0.8905 | 17.524 | 15.606 | 36.681 | 0.33 | 3 |
| 10000 | 10868.5 | PD0001 | 168.9 | N | ser alt gnd | wr | 168.37-169.2 | 0.1600 | 4.00 | 8.00 | 2.1638 | 0.9212 | 16.845 | 15.518 | 36.451 | 0.16 | 3 |
| 10000 | 11234.5 | PD0002 | 229.1 | N | gra sch | wr | 227.8-230 | 1.7000 | 18.00 | 0.00 | 2.1897 | 0.9360 | 16.584 | 15.523 | 36.313 | 1.7 | 3 |
| 10000 | 11234.5 | PD0002 | 230.8 | N | F | wr | 230-230.9 | 5.2000 | 50.00 | 0.00 | 2.1895 | 0.9357 | 16.593 | 15.527 | 36.330 | 5.2 | 3 |
| 10000 | 11234.5 | PD0002 | 231.1 | N | sh mar | wr | 230.9-232.9 | 1.0000 | 0.00 | 6.00 | 2.1852 | 0.9334 | 16.630 | 15.523 | 36.340 | 1 | 3 |
| 9800 | 11194.5 | PD0003 | 176.4 | N | sch | wr | 177-179.15 | 0.0510 | 6.00 | 18.00 | 2.0100 | 0.8280 | 19.053 | 15.775 | 38.297 | 0.051 | 3 |
| 9800 | 11194.5 | PD0003 | 185 | N | fzb | wr | 184-187 | 0.0075 | 14.00 | 26.00 | 2.1345 | 0.8984 | 17.333 | 15.572 | 36.996 | 0.057 | 3 |
| 9800 | 11194.5 | PD0003 | 186 | N | fzb | wr | 184-187 | 0.0075 | 10.00 | 26.00 | 2.1177 | 0.8709 | 17.901 | 15.589 | 37.908 | 0.057 | 3 |
| 9800 | 11124.6 | PD0004 | 208.2 | N | alt gnd | gn | 206.75-208.85 | 0.2500 | 0.00 | 0.00 | 2.1853 | 0.9243 | 16.817 | 15.544 | 36.750 | 86.6 | 3 |
| 10000 | 11155 | PD0005 | 163.6 | N | ser alt sch | gn | 163-165 | 0.6050 | 0.00 | 0.00 | 2.2199 | 0.9518 | 16.228 | 15.446 | 36.025 | 86.6 | 3 |
| 10000 | 11155 | PD0005 | 164.5 | N | ser alt sch | gn | 163-165 | 0.6050 | 0.00 | 0.00 | 2.1848 | 0.9220 | 16.846 | 15.532 | 36.805 | 86.6 | 3 |
| 9800 | 10769 | PD0006 | 247.35 | N | sul | gn | 246.7-247.35 | 5.7500 | 0.00 | 0.00 | 2.2338 | 0.9604 | 16.051 | 15.415 | 35.855 | 86.6 | 4 |
| 9800 | 10769 | PD0006 | 247.35 | N | sul | wr | 246.7-247.35 | 5.7500 | 0.00 | 0.00 | 2.2349 | 0.9605 | 16.074 | 15.439 | 35.924 | 5.75 | 4 |
| 9800 | 10769 | PD0006 | 258.45 | N | sul | wr | 257.9-258.45 | 12.4000 | 0.00 | 0.00 | 2.2363 | 0.9610 | 16.052 | 15.426 | 35.897 | 12.4 | 4 |
| 9800 | 10769 | PD0006 | 258.45 | N | sul | gn | 257.9-258.45 | 12.4000 | 0.00 | 0.00 | 2.2379 | 0.9607 | 16.054 | 15.423 | 35.927 | 86.6 | 4 |
| 9800 | 10769 | PD0006 | 258.45 | N | sul | gn/r | 257.9-258.45 | 12.4000 | 0.00 | 0.00 | 2.2365 | 0.9610 | 16.065 | 15.438 | 35.929 | 86.6 | 4 |
| 9800 | 10769 | PD0006 | 258.45 | N | sul | wr/r | 257.9-258.45 | 12.4000 | 0.00 | 0.00 | 2.2385 | 0.9615 | 16.081 | 15.462 | 35.997 | 12.4 | 4 |
| 9800 | 10769 | PD0006 | 267.23 | N | sul | gn/r | 266.6-267.23 | 25.4000 | 0.00 | 0.00 | 2.2375 | 0.9615 | 16.053 | 15.435 | 35.919 | 86.6 | 4 |
| 9800 | 10769 | PD0006 | 267.23 | N | sul | wr | 266.6-267.23 | 25.4000 | 0.00 | 0.00 | 2.2371 | 0.9613 | 16.056 | 15.435 | 35.919 | 25.4 | 4 |
| 9800 | 10769 | PD0006 | 267.23 | N | sul | gn | 266.6-267.23 | 25.4000 | 0.00 | 0.00 | 2.2343 | 0.9604 | 16.059 | 15.423 | 35.881 | 86.6 | 4 |
| 9800 | 10769 | PD0006 | 410.6 | N | sch. cold HCl leach 1 | wr | | | | | 2.2142 | 0.9449 | 16.358 | 15.456 | 36.219 | 0.00191 | 7 |
| 9800 | 10769 | PD0006 | 410.6 | N | sch. cold HCl leach 2 | wr | | | | | 2.1964 | 0.9298 | 16.701 | 15.528 | 36.681 | 0.000674 | 7 |
| 9800 | 10769 | PD0006 | 410.6 | N | sch. HCl/HNO3 leach 3 | wr | | | | | 2.2015 | 0.9306 | 16.769 | 15.605 | 36.916 | 0.00328 | 7 |
| 9800 | 10769 | PD0006 | 410.6 | N | sch. HF/HNO3 leach 4 | wr | | | | | 2.2262 | 0.8593 | 18.298 | 15.724 | 40.734 | 0.00145 | 7 |
| 9800 | 10769 | PD0006 | 410.6 | N | sch. HF/HNO3 leach 4 | wr | | | | | 2.2278 | 0.8593 | 18.336 | 15.755 | 40.850 | 0.0015 | 7 |
| 10400 | 10791.5 | PD0007 | 109 | N | met alt mar | wr | 107.65-109 | 0.0250 | 0.00 | 0.00 | 2.1515 | 0.8977 | 17.376 | 15.598 | 37.384 | 0.93 | 4 |
| 9200 | 10314 | PD0008 | 116.6 | C | sul | wr | 116-116.6 | 1.1500 | 0.00 | 30.00 | 2.2335 | 0.9600 | 16.067 | 15.424 | 35.886 | 1.15 | 4 |
| 9200 | 10314 | PD0008 | 144.3 | C | sul | wr | 144.15-144.3 | 1.3000 | 0.00 | 20.00 | 2.2360 | 0.9604 | 16.089 | 15.452 | 35.975 | 1.3 | 4 |
| 9200 | 10314 | PD0008 | 179.45 | C | gnd | fel/1 | 178.25-180 | 0.2900 | | | 2.1869 | 0.9403 | 16.455 | 15.473 | 35.986 | 0.0002 | 8 |
| 9200 | 10314 | PD0008 | 179.45 | C | gnd | fel/2 | 178.25-180 | 0.2900 | | | 2.1043 | 0.9028 | 17.197 | 15.525 | 36.188 | 0.0002 | 8 |
| 9200 | 10314 | PD0008 | 226 | C | sul | wr | 224.95-225.15 | 4.9000 | 0.00 | 180.00 | 2.2393 | 0.9616 | 16.075 | 15.458 | 35.997 | 4.9 | 4 |

**Appendix 7.2 cont.**

| Northing (mN) | Easting (mN) | Drill hole | Depth (m) | Zone | Sample description | Sample type | Assay Interval | Lead assay (wt.%) | U (ppm) | Th (ppm) | 208Pb /206Pb | 207Pb /206Pb | 206Pb /204Pb | 207Pb /204Pb | 208Pb /204Pb | Pb content (wt.%) | Ref. |
|---|---|---|---|---|---|---|---|---|---|---|---|---|---|---|---|---|---|
| 9200 | 10314 | PD0008 | 236 | C | sul | wr | 235.85-236.3 | 7.8500 | 0.00 | 40.00 | 2.2335 | 0.9604 | 16.051 | 15.415 | 35.850 | 7.85 | 4 |
| 9200 | 10314 | PD0008 | 282 | C | sul | wr | 280.2-282.2 | 0.8400 | 10.00 | 36.00 | 2.2227 | 0.9555 | 16.169 | 15.449 | 35.939 | 0.84 | 4 |
| 9200 | 10314 | PD0008 | 317.35 | C | sul | wr | 316.9-317.35 | 3.8000 | 50.00 | 180.00 | 2.2346 | 0.9599 | 16.108 | 15.462 | 35.995 | 3.8 | 4 |
| 9400 | 10350 | PD0009 | 133.75 | N | alt gnd / mar contact | wr | 132.1-133.75 | 0.5600 | 4.00 | 40.00 | 2.2043 | 0.9475 | 16.304 | 15.449 | 35.939 | 0.62 | 4 |
| 9000 | 10300 | PD0010 | 38 | C | wea, cly | wr | 37.9-40 | 0.1600 | 16.00 | 8.00 | 2.2070 | 0.9484 | 16.284 | 15.444 | 35.938 | 0.0866 | 4 |
| 9000 | 10300 | PD0010 | 62.5 | C | wea, cly | wr | 60-62.5 | 0.0220 | 12.00 | 10.00 | 2.1317 | 0.9162 | 16.940 | 15.521 | 36.112 | 0.075 | 4 |
| 9000 | 10300 | PD0010 | 163 | C | sul | wr | 163.45-163.58 | 3.7500 | 12.00 | 100.00 | 2.2326 | 0.9602 | 16.034 | 15.396 | 35.798 | 1.95 | 4 |
| 9000 | 10300 | PD0010 | 175.6 | C | sul | gn | 174-176 | 0.3550 | | | 2.2349 | 0.9609 | 16.050 | 15.422 | 35.869 | 86.6 | 8 |
| 9000 | 10300 | PD0010 | 177.76 | C | sul | wr | 177.11-177.76 | 2.7500 | 6.00 | 80.00 | 2.2284 | 0.9585 | 16.080 | 15.412 | 35.832 | 3 | 4 |
| 9000 | 10300 | PD0010 | 279.8 | C | sul | wr | 279.25-279.8 | 0.0520 | 4.00 | 20.00 | 2.2137 | 0.9521 | 16.260 | 15.482 | 35.995 | 0.11 | 4 |
| 9000 | 10300 | PD0010 | 298.72 | C | sul | wr | 297.9-298.72 | 3.0000 | 0.00 | 0.00 | 2.2321 | 0.9597 | 16.066 | 15.419 | 35.862 | 1.32 | 4 |
| 9200 | 10210 | PD0011 | 146 | C | sul | wr | 146.5-146.73 | 1.7400 | 4.00 | 200.00 | 2.2332 | 0.9603 | 16.060 | 15.422 | 35.865 | 16.4 | 4 |
| 9200 | 10210 | PD0011A | 160 | C | sul | wr | 159.67-162 | 0.0075 | 0.00 | 24.00 | 2.2182 | 0.9539 | 16.178 | 15.433 | 35.887 | 15.4 | 4 |
| 9200 | 10210 | PD0011A | 373.8 | C | sul | wr | 372-373.38 | 3.2000 | 0.00 | 0.00 | 2.2269 | 0.9578 | 16.103 | 15.423 | 35.859 | 0.23 | 4 |
| 9600 | 10775 | PD0012 | 353.75 | N | sul | wr | 353.25-353.75 | 0.2400 | 4.00 | 200.00 | 2.2194 | 0.9518 | 16.220 | 15.438 | 36.000 | 18.4 | 4 |
| 9800 | 10300 | PD0013 | 108 | N | wea | wr | 108-110 | 1.0100 | | | 2.2308 | 0.9598 | 16.032 | 15.388 | 35.764 | | 3 |
| 11200 | 11140 | PD0014 | 157.5 | N | sul | gn/1 | 157.48-159.5 | 0.6750 | | | 2.1983 | 0.9420 | 16.456 | 15.502 | 36.174 | 86.6 | 3 |
| 11200 | 11140 | PD0014 | 157.5 | N | sul | gn/2 | 157.48-159.5 | 0.6750 | | | 2.1971 | 0.9413 | 16.469 | 15.501 | 36.183 | 86.6 | 3 |
| 11200 | 11140 | PD0014 | 157.5 | N | sul | gn/3 | 157.48-159.5 | 0.6750 | | | 2.1941 | 0.9393 | 16.515 | 15.513 | 36.236 | 86.6 | 3 |
| 11200 | 11140 | PD0014 | 162 | N | sul | gn/1 | 161.95-163.1 | 1.2000 | | | 2.1882 | 0.9338 | 16.616 | 15.517 | 36.359 | 86.6 | 3 |
| 11200 | 11140 | PD0014 | 162 | N | sul | gn/2 | 161.95-163.1 | 1.2000 | | | 2.1852 | 0.9319 | 16.660 | 15.525 | 36.405 | 86.6 | 3 |
| 9390.7 | 10226.9 | PD0015 | 402.2 | N | gnd | fel | 401.37-402.32 | 0.2560 | | | 1.4069 | 0.5738 | 27.537 | 15.801 | 38.741 | 0.0002 | 8 |
| 9390.7 | 10226.9 | PD0015 | 402.5 | N | sul | wr | 402.32-402.66 | 1.0600 | | | 2.2184 | 0.9544 | 16.191 | 15.453 | 35.919 | 5 | 1 |
| 9390.7 | 10226.9 | PD0015 | 653.2 | N | sul | gn | 651.9-655.11 | 0.0030 | | | 2.2094 | 0.9487 | 16.348 | 15.509 | 36.120 | 86.6 | 1 |
| 9390.7 | 10226.9 | PD0015 | 653.2 | N | sul | gn/r | 651.9-655.11 | 0.0030 | | | 2.2102 | 0.9490 | 16.357 | 15.522 | 36.152 | 86.6 | 1 |
| 9390.7 | 10226.9 | PD0015 | 730.03 | N | sul | gn | not assayed | | | | 2.2353 | 0.9611 | 16.028 | 15.405 | 35.828 | 86.6 | 1 |
| 9391.9 | 10663.3 | PD0016 | 262.11 | N | sul | gn | 261.76-262.26 | 14.2000 | | | 2.2343 | 0.9608 | 16.040 | 15.412 | 35.839 | 86.6 | 1 |
| 9391.9 | 10663.3 | PD0016 | 262.11 | N | sul | gn/r | 261.76-262.26 | 14.2000 | | | 2.2355 | 0.9609 | 16.045 | 15.419 | 35.870 | 86.6 | 1 |
| 9391.9 | 10663.3 | PD0016 | 262.25 | N | sul | gn | 261.76-262.26 | 14.2000 | | | 2.2354 | 0.9610 | 16.041 | 15.415 | 35.857 | 86.6 | 1 |
| 9391.9 | 10663.3 | PD0016 | 268.23 | N | sul | gn | 268.6-269 | 8.1000 | | | 2.2357 | 0.9611 | 16.049 | 15.425 | 35.881 | 86.6 | 1 |
| 9391.9 | 10663.3 | PD0016 | 268.23 | N | sul | gn | 268.6-269 | 8.1000 | | | 2.2364 | 0.9613 | 16.049 | 15.427 | 35.891 | 86.6 | 1 |
| 9391.9 | 10663.3 | PD0016 | 268.23 | N | sul | gn | 268.6-269 | 8.1000 | | | 2.2366 | 0.9612 | 16.049 | 15.427 | 35.895 | 86.6 | 1 |
| 9391.9 | 10663.3 | PD0016 | 305.6 | N | sul | gn | 304.71-306.17 | 24.2000 | | | 2.2350 | 0.9611 | 16.027 | 15.404 | 35.821 | 86.6 | 1 |
| 8780.8 | 10136.2 | PD0017 | 164.2 | C | wea sul | gn | not assayed | no assay | | | 2.2302 | 0.9587 | 16.097 | 15.433 | 35.900 | 86.6 | 1 |

## Appendix 7.2 cont.

| Northing (mN) | Easting (mN) | Drill hole | Depth (m) | Zone | Sample description | Sample type | Assay Interval | Lead assay (wt.%) | U (ppm) | Th (ppm) | 208Pb /206Pb | 207Pb /206Pb | 206Pb /204Pb | 207Pb /204Pb | 208Pb /204Pb | Pb content (wt.%) | Ref. |
|---|---|---|---|---|---|---|---|---|---|---|---|---|---|---|---|---|---|
| 8780.8 | 10136.2 | PD0017 | 164.2 | C | wea sul | gn | not assayed | no assay | | | 2.2280 | 0.9575 | 16.123 | 15.437 | 35.921 | 86.6 | 1 |
| 8780.8 | 10136.2 | PD0017 | 233.81 | C | sul | gn | 233.56-234.25 | 10.3400 | | | 2.2337 | 0.9606 | 16.037 | 15.406 | 35.822 | 86.6 | 1 |
| 8780.8 | 10136.2 | PD0017 | 234.15 | C | sul | gn | 233.56-234.25 | 10.3400 | | | 2.2344 | 0.9608 | 16.035 | 15.407 | 35.829 | 86.6 | 1 |
| 8780.8 | 10136.2 | PD0017 | 241.7 | C | sul | gn | 241.53-242.03 | 15.1700 | | | 2.2339 | 0.9606 | 16.035 | 15.404 | 35.820 | 86.6 | 1 |
| 8780.8 | 10136.2 | PD0017 | 242.1 | C | sul | gn | 242.03-243.5 | 22.1400 | | | 2.2344 | 0.9608 | 16.037 | 15.408 | 35.833 | 86.6 | 1 |
| 8780.8 | 10136.2 | PD0017 | 243.18 | C | sul | gn | 242.03-243.5 | 22.1400 | | | 2.2362 | 0.9613 | 16.034 | 15.414 | 35.855 | 86.6 | 1 |
| 8780.8 | 10136.2 | PD0017 | 313.2 | C | sul | gn | 313.1-315 | 0.9900 | | | 2.2342 | 0.9608 | 16.029 | 15.401 | 35.812 | 86.6 | 1 |
| 8780.8 | 10136.2 | PD0017 | 319.3 | C | sul | gn | 319-321 | 2.4400 | | | 2.2364 | 0.9612 | 16.047 | 15.424 | 35.887 | 86.6 | 1 |
| 8780.8 | 10136.2 | PD0017 | 333.38 | C | ser + sul alt gnd | gn | 333-335.2 | 0.5980 | | | 2.2306 | 0.9593 | 16.056 | 15.402 | 35.815 | 86.6 | 1 |
| 8780.8 | 10136.2 | PD0017 | 333.38 | C | ser + sul alt gnd | gn | 333-335.2 | 0.5980 | | | 2.2296 | 0.9586 | 16.085 | 15.418 | 35.862 | 86.6 | 1 |
| 8780.8 | 10136.2 | PD0017 | 343.3 | C | sul | gn | 343-344.75 | 17.0000 | | | 2.2373 | 0.9614 | 16.056 | 15.437 | 35.922 | 86.6 | 1 |
| 8780.8 | 10136.2 | PD0017 | 366.4 | C | sul | gn | 366.1-367 | 3.5700 | | | 2.2325 | 0.9598 | 16.065 | 15.420 | 35.865 | 86.6 | 1 |
| 8780.8 | 10136.2 | PD0017 | 384.9 | C | sul | gn | 384.8-385.85 | 0.4850 | | | 2.2281 | 0.9579 | 16.142 | 15.462 | 35.966 | 86.6 | 1 |
| 8780.8 | 10136.2 | PD0017 | 398.7 | C | sul | gn | 396.95-398.95 | 2.0100 | | | 2.2305 | 0.9592 | 16.068 | 15.413 | 35.838 | 86.6 | 1 |
| 8780.8 | 10136.2 | PD0017 | 409.15 | C | sul | gn | 408.62-409.88 | 9.3500 | | | 2.2360 | 0.9610 | 16.046 | 15.420 | 35.880 | 86.6 | 1 |
| 8379.7 | 9953.4 | PD0018 | 507.85 | C | sul vn in ser alt gnd | gn | not assayed | no assay | | | 2.1496 | 0.9212 | 16.894 | 15.562 | 36.314 | 86.6 | 2 |
| 8380.9 | 10408.4 | PD0019 | 271.7 | C | wea | wr | 271-273 | 1.8700 | | | 2.2040 | 0.9455 | 16.358 | 15.466 | 36.053 | 0.08 | 2 |
| 8380.9 | 10408.4 | PD0019 | 271.7 | C | wea | wr | 271-273 | 1.8700 | | | 2.2041 | 0.9455 | 16.362 | 15.471 | 36.064 | 0.0733 | 2 |
| 8380.9 | 10408.4 | PD0019 | 300.5 | C | wea | gn | 299.15-302.65 | 0.9030 | | | 2.2215 | 0.9556 | 16.169 | 15.452 | 35.920 | 86.6 | 2 |
| 8380.9 | 10408.4 | PD0019 | 324.2 | C | wea | wr | 322.9-325.6 | 1.4100 | | | 2.2279 | 0.9579 | 16.093 | 15.416 | 35.853 | 0.35 | 2 |
| 8380.9 | 10408.4 | PD0019 | 324.2 | C | wea | wr | 322.9-325.6 | 1.4100 | | | 2.2282 | 0.9583 | 16.093 | 15.422 | 35.860 | 0.35 | 2 |
| 8380.9 | 10408.4 | PD0019 | 467.5 | C | sul | gn | 466.82-468.09 | 15.0000 | | | 2.2331 | 0.9603 | 16.037 | 15.401 | 35.812 | 86.6 | 2 |
| 8380.9 | 10408.4 | PD0019 | 469.15 | C | sul | gn | 468.09-469.5 | 18.8000 | | | 2.2330 | 0.9603 | 16.036 | 15.398 | 35.808 | 86.6 | 2 |
| 8380.9 | 10408.4 | PD0019 | 470.95 | C | sul | gn | 469.5-471.07 | 19.0000 | | | 2.2345 | 0.9605 | 16.067 | 15.432 | 35.901 | 86.6 | 2 |
| 7564 | 10073.7 | PD0021 | 167.3 | C | alt gnd clast in MD ig | fel/2 | not assayed | no assay | | | 2.1993 | 0.9339 | 16.410 | 15.325 | 36.090 | 0.0008 | 8 |
| 7564 | 10073.7 | PD0021 | 167.3 | C | alt gnd clast in MD ig | fel/3 | not assayed | no assay | | | 2.1891 | 0.9296 | 16.449 | 15.291 | 36.008 | 0.0011 | 8 |
| 7564 | 10073.7 | PD0021 | 167.3 | C | alt gnd clast in MD ig | fel/1 | not assayed | no assay | | | 2.1724 | 0.9183 | 16.674 | 15.312 | 36.223 | 0.0015 | 8 |
| 7564 | 10073.7 | PD0021 | 321.15 | C | sul clast in MD ig | gn | not assayed | no assay | | | 2.2311 | 0.9592 | 16.075 | 15.419 | 35.865 | 86.6 | 2 |
| 7564 | 10073.7 | PD0021 | 403.59 | C | sul | gn | 403.5-406.5 | 0.2930 | | | 2.1900 | 0.9372 | 16.563 | 15.523 | 36.274 | 86.6 | 2 |
| 7564 | 10073.7 | PD0021 | 427.05 | C | sul | gn | 424.5-427.5 | 0.6460 | | | 2.1631 | 0.9205 | 16.914 | 15.569 | 36.588 | 86.6 | 2 |
| 7564 | 10073.7 | PD0021 | 441.32 | C | sul | gn | 439.5-442.5 | 0.0245 | | | 2.1491 | 0.9150 | 17.001 | 15.556 | 36.536 | 86.6 | 2 |
| 7564 | 10073.7 | PD0021 | 619.4 | C | gnd | fel/1 | 616.5-619.5 | 0.0005 | | | 2.1328 | 0.9161 | 16.897 | 15.480 | 36.038 | 0.0003 | 8 |
| 7564 | 10073.7 | PD0021 | 619.4 | C | gnd | fel/3 | 616.5-619.5 | 0.0005 | | | 2.1277 | 0.9116 | 16.984 | 15.483 | 36.136 | 0.0003 | 8 |
| 8960.9 | 10125.4 | PD0024 | 241.1 | C | sul | gn | 240.4-241.4 | 7.8500 | | | 2.2370 | 0.9612 | 16.057 | 15.434 | 35.919 | 86.6 | 8 |

## Appendix 7.2 cont.

| Northing (mN) | Easting (mN) | Drill hole | Depth (m) | Zone | Sample description | Sample type | Assay Interval | Lead assay (wt.%) | U (ppm) | Th (ppm) | 208Pb /206Pb | 207Pb /206Pb | 206Pb /204Pb | 207Pb /204Pb | 208Pb /204Pb | Pb content (wt.%) | Ref. |
|---|---|---|---|---|---|---|---|---|---|---|---|---|---|---|---|---|---|
| 8960.9 | 10125.4 | PD0024 | 336.7 | C | sul | gn/3 | 336-338 | 2.6900 | | | 2.2316 | 0.9599 | 16.054 | 15.410 | 35.825 | 86.6 | 8 |
| 8960.9 | 10125.4 | PD0024 | 336.7 | C | sul | gn/2 | 336-338 | 2.6900 | | | 2.2319 | 0.9597 | 16.065 | 15.419 | 35.856 | 86.6 | 8 |
| 8960.9 | 10125.4 | PD0024 | 336.7 | C | sul | gn/1r | 336-338 | 2.6900 | | | 2.2334 | 0.9601 | 16.080 | 15.438 | 35.913 | 86.6 | 8 |
| 8960.9 | 10125.4 | PD0024 | 336.7 | C | sul | gn/1 | 336-338 | 2.6900 | | | 2.2352 | 0.9604 | 16.082 | 15.445 | 35.946 | 86.6 | 8 |
| 8960.9 | 10125.4 | PD0024 | 341.4 | C | sul | gn | 341.3-343.3 | 3.5600 | | | 2.2344 | 0.9605 | 16.061 | 15.427 | 35.887 | 86.6 | 8 |
| 7956.7 | 10051.6 | PD0025 | 218.8 | C | sul clast in LP | wr/4 | 218.5-226.6 | 0.599 | | | 2.1997 | 0.9422 | 16.413 | 15.464 | 36.104 | 0.4 | 8 |
| 7956.7 | 10051.6 | PD0025 | 218.8 | C | sul clast in LP | wr/3 | 218.5-226.6 | 0.599 | | | 2.2108 | 0.9459 | 16.414 | 15.525 | 36.288 | 0.5 | 8 |
| 7956.7 | 10051.6 | PD0025 | 218.8 | C | sul clast in LP | wr/2 | 218.5-226.6 | 0.599 | | | 2.1955 | 0.9396 | 16.477 | 15.481 | 36.174 | 0.4 | 8 |
| 7956.7 | 10051.6 | PD0025 | 218.8 | C | sul clast in LP | wr/1 | 218.5-226.6 | 0.599 | | | 2.1914 | 0.9365 | 16.571 | 15.518 | 36.313 | 1.3 | 8 |
| 7956.7 | 10051.6 | PD0025 | 218.8 | C | sul clast in LP | wr/1r | 218.5-226.6 | 0.599 | | | 2.1872 | 0.9341 | 16.617 | 15.522 | 36.344 | 1.3 | 8 |
| 7956.7 | 10051.6 | PD0025 | 218.8 | C | sul clast in LP | wr/5r | 218.5-226.6 | 0.599 | | | 2.1907 | 0.9354 | 16.620 | 15.546 | 36.408 | 0.4 | 8 |
| 7956.7 | 10051.6 | PD0025 | 218.8 | C | sul clast in LP | wr/5 | 218.5-226.6 | 0.599 | | | 2.1872 | 0.9335 | 16.650 | 15.543 | 36.417 | 0.4 | 8 |
| 7956.7 | 10051.6 | PD0025 | 226.1 | C | sul clast in LP | gn/1 | 218.5-226.6 | 0.5990 | | | 2.2339 | 0.9603 | 16.049 | 15.411 | 35.852 | 86.6 | 8 |
| 7956.7 | 10051.6 | PD0025 | 226.1 | C | sul clast in LP | gn/2 | 218.5-226.6 | 0.5990 | | | 2.2358 | 0.9607 | 16.057 | 15.426 | 35.901 | 86.6 | 8 |
| 7956.7 | 10051.6 | PD0025 | 226.1 | C | sul clast in LP | gn/3 | 218.5-226.6 | 0.5990 | | | 2.2275 | 0.9572 | 16.108 | 15.419 | 35.880 | 86.6 | 8 |
| 8746 | 10461.3 | PD0028 | 339 | C | sul | gn | not assayed | no assay | | | 2.2336 | 0.9606 | 16.035 | 15.404 | 35.815 | 86.6 | 8 |
| 8746 | 10461.3 | PD0028 | 354.4 | C | sul | gn | 352.6-354.2 | 4.9000 | | | 2.2319 | 0.9595 | 16.055 | 15.404 | 35.834 | 86.6 | 8 |
| 8746 | 10461.3 | PD0028 | 363.3 | C | sul | gn/1r | 363.1-364.8 | 0.1690 | | | 2.2304 | 0.9590 | 16.074 | 15.415 | 35.852 | 86.6 | 8 |
| 8746 | 10461.3 | PD0028 | 363.3 | C | sul | gn/2 | 363.1-364.8 | 0.1690 | | | 2.2284 | 0.9581 | 16.080 | 15.405 | 35.832 | 86.6 | 8 |
| 8746 | 10461.3 | PD0028 | 363.3 | C | sul | gn/1 | 363.1-364.8 | 0.1690 | | | 2.2329 | 0.9595 | 16.101 | 15.449 | 35.952 | 86.6 | 8 |
| 8746 | 10461.3 | PD0028 | 373.5 | C | sul | gn | 373.2-373.8 | 4.7400 | | | 2.2322 | 0.9600 | 16.048 | 15.406 | 35.832 | 86.6 | 8 |
| 8746 | 10461.3 | PD0028 | 508.3 | C | sul in DP | gn/1r | 507.4-508.4 | 1.3000 | | | 2.2319 | 0.9600 | 16.042 | 15.401 | 35.804 | 86.6 | 8 |
| 8746 | 10461.3 | PD0028 | 508.3 | C | sul in DP | gn/3 | 507.4-508.4 | 1.3000 | | | 2.2326 | 0.9598 | 16.066 | 15.420 | 35.869 | 86.6 | 8 |
| 8746 | 10461.3 | PD0028 | 508.3 | C | sul in DP | gn/2r | 507.4-508.4 | 1.3000 | | | 2.2296 | 0.9588 | 16.082 | 15.419 | 35.855 | 86.6 | 8 |
| 8746 | 10461.3 | PD0028 | 508.3 | C | sul in DP | gn/4 | 507.4-508.4 | 1.3000 | | | 2.2292 | 0.9585 | 16.082 | 15.415 | 35.851 | 86.6 | 8 |
| 8746 | 10461.3 | PD0028 | 508.3 | C | sul in DP | gn/4r | 507.4-508.4 | 1.3000 | | | 2.2292 | 0.9585 | 16.099 | 15.431 | 35.888 | 86.6 | 8 |
| 8746 | 10461.3 | PD0028 | 508.5 | C | sul in DP | gn/2 | 507.4-508.4 | 1.3000 | | | 2.2288 | 0.9584 | 16.081 | 15.412 | 35.841 | 86.6 | 8 |
| 8776.6 | 10329 | PD0029 | 259.1 | C | sul | gn | 258.9-259.4 | 44.6000 | | | 2.2330 | 0.9603 | 16.036 | 15.398 | 35.807 | 86.6 | 8 |
| 8776.6 | 10329 | PD0029 | 279.4 | C | sul | gn/2 | 270-280 | 0.0390 | | | 2.2308 | 0.9592 | 16.069 | 15.414 | 35.848 | 86.6 | 8 |
| 8776.6 | 10329 | PD0029 | 279.4 | C | sul | gn/1 | 270-280 | 0.0390 | | | 2.2323 | 0.9595 | 16.085 | 15.434 | 35.908 | 86.6 | 8 |
| 7764 | 10250 | PD0030 | 486.6 | C | weakly alt rhy int | wr | not assayed | no assay | | | 2.0304 | 0.7828 | 20.082 | 15.721 | 40.776 | 0.0003 | 8 |
| 8023 | 10300 | PD0031 | 178.9 | C | sul clast in LP | gn | 174.7-180.7 | 0.0110 | | | 2.2349 | 0.9607 | 16.042 | 15.411 | 35.852 | 86.6 | 8 |
| 8023 | 10300 | PD0031 | 206.2 | C | sul | gn | 206.15-206.3 | 3.1500 | | | 2.2309 | 0.9590 | 16.080 | 15.421 | 35.874 | 86.6 | 8 |
| 7406 | 10235 | PD0032 | 126.4 | S | MD ig | wr | not assayed | no assay | | | 2.1314 | 0.9202 | 17.135 | 15.768 | 36.522 | 0.0059 | 8 |

**Appendix 7.2 cont.**

| Northing (mN) | Easting (mN) | Drill hole | Depth (m) | Zone | Sample description | Sample type | Assay Interval | Lead assay (wt.%) | U (ppm) | Th (ppm) | 208Pb /206Pb | 207Pb /206Pb | 206Pb /204Pb | 207Pb /204Pb | 208Pb /204Pb | Pb content (wt.%) | Ref. |
|---|---|---|---|---|---|---|---|---|---|---|---|---|---|---|---|---|---|
| 7406 | 10235 | PD0032 | 126.4 | S | MD ig | wr | not assayed | no assay | | | 2.1308 | 0.9203 | 17.139 | 15.772 | 36.519 | 0.0059 | 8 |
| 7406 | 10235 | PD0032 | 245.7 | S | sul clast in MD ig | gn | 245.6-245.8 | 0.8350 | | | 2.2072 | 0.9449 | 16.417 | 15.512 | 36.235 | 86.6 | 8 |
| 7406 | 10235 | PD0032 | 383.25 | S | vn | gn | 383.2-384 | 0.8760 | | | 2.1829 | 0.9346 | 16.608 | 15.521 | 36.252 | 86.6 | 8 |
| 7406 | 10235 | PD0032 | 437.3 | S | vn | gn | 436.75-437.7 | 0.8210 | | | 2.2131 | 0.9505 | 16.293 | 15.488 | 36.057 | 86.6 | 8 |
| 10000 | 11080 | PDHMD2 | 76 | N | wea | wr | 74-76 | 1.5000 | 4.00 | 26.00 | 2.2371 | 0.9610 | 16.083 | 15.455 | 35.980 | 1.5000 | 3 |
| 10000 | 11080 | PDHMD2 | 76 | N | wea | wr | 74-76 | 1.5000 | 4.00 | 26.00 | 2.2374 | 0.9611 | 16.085 | 15.459 | 35.990 | 1.5000 | 3 |
| 10000 | 11080 | PDHMD2 | 78 | N | wea | wr | 76-78 | 1.5000 | 14.00 | 28.00 | 2.2343 | 0.9603 | 16.050 | 15.412 | 35.860 | 1.5000 | 3 |
| 10000 | 11080 | PDHMD2 | 78 | N | wea | wr | 76-78 | 1.5000 | 14.00 | 28.00 | 2.2389 | 0.9614 | 16.084 | 15.463 | 36.011 | 1.5000 | 3 |
| 9800 | 10920 | PDHMD3 | 80 | N | wea | gn | 78-80 | 5.1000 | 0.00 | 0.00 | 2.2357 | 0.9609 | 16.050 | 15.422 | 35.883 | 86.6 | 3 |
| 9800 | 10920 | PDHMD3 | 80 | N | wea | gn | 78-80 | 5.1000 | 0.00 | 0.00 | 2.2353 | 0.9607 | 16.060 | 15.429 | 35.899 | 86.6 | 3 |
| 9800 | 10920 | PDHMD3 | 80 | N | wea | gn | 78-80 | 5.1000 | 0.00 | 0.00 | 2.2364 | 0.9610 | 16.063 | 15.437 | 35.923 | 86.6 | 3 |
| 9800 | 10920 | PDHMD3 | 81 | N | wea | gn | 80-81 | 3.7000 | 0.00 | 0.00 | 2.2346 | 0.9604 | 16.071 | 15.435 | 35.912 | 86.6 | 3 |
| 9800 | 10920 | PDHMD3 | 81 | N | wea | gn | 80-81 | 3.7000 | 0.00 | 0.00 | 2.2350 | 0.9605 | 16.077 | 15.442 | 35.932 | 86.6 | 3 |
| 9800 | 10920 | PDHMD3 | 81 | N | wea | gn | 80-81 | 3.7000 | 0.00 | 0.00 | 2.2365 | 0.9607 | 16.080 | 15.448 | 35.963 | 86.6 | 3 |
| 9800 | 10920 | PDHMD3 | 82 | N | wea | gn | 81-82 | 2.5500 | 0.00 | 0.00 | 2.2347 | 0.9605 | 16.060 | 15.426 | 35.889 | 86.6 | 3 |
| 9800 | 10920 | PDHMD3 | 82 | N | wea | gn | 81-82 | 2.5500 | 0.00 | 0.00 | 2.2363 | 0.9608 | 16.082 | 15.452 | 35.964 | 86.6 | 3 |
| 6700 | 10600 | PE0025 | 169 | S | sul in MD ig | gn | 168-170 | 0.2680 | | | 2.2158 | 0.9508 | 16.293 | 15.492 | 36.101 | 86.6 | 5 |
| 6700 | 10600 | PE0025 | 191 | S | sul in MD ig | gn | 190-192 | 0.2555 | | | 2.1944 | 0.9398 | 16.506 | 15.512 | 36.220 | 86.6 | 5 |
| 5700 | 11200 | PE0026 | 71 | S | sul in MD ig | gn | 66-76 | 0.0985 | | | 2.1500 | 0.9222 | 16.860 | 15.548 | 36.249 | 86.6 | 5 |
| 10400 | 11240 | RMD109 | 34 | N | wea | wr | 32-34 | 0.1300 | 0.00 | 20.00 | 2.1356 | 0.8961 | 17.408 | 15.599 | 37.177 | 0.1300 | 3 |
| 10400 | 11240 | RMD109 | 58 | N | wea | wr | 56-58 | 0.1300 | 12.00 | 24.00 | 2.1457 | 0.8989 | 17.335 | 15.583 | 37.195 | 0.1300 | 3 |
| 10400 | 11240 | RMD109 | 58 | N | wea | wr | 56-58 | 0.1300 | 12.00 | 24.00 | 2.1480 | 0.8995 | 17.339 | 15.596 | 37.244 | 0.1300 | 3 |
| 10400 | 11240 | RMD109 | 70 | N | wea | wr | 68-70 | 0.4100 | 16.00 | 26.00 | 2.1509 | 0.9023 | 17.288 | 15.598 | 37.185 | 0.4100 | 3 |
| 11200 | 11295 | RMD116 | 12 | N | wea | wr | 10.0-12 | 0.1000 | 0.00 | 24.00 | 2.2174 | 0.9505 | 16.264 | 15.459 | 36.064 | 0.1000 | 3 |
| 11200 | 11295 | RMD116 | 36 | N | mar / cs | wr | 34-36 | 0.2000 | 36.00 | 0.00 | 2.2288 | 0.9584 | 16.070 | 15.402 | 35.817 | 0.2000 | 3 |
| 11200 | 11295 | RMD116 | 36 | N | mar / cs | wr | 34-36 | 0.2000 | 36.00 | 0.00 | 2.2312 | 0.9588 | 16.090 | 15.427 | 35.900 | 0.2000 | 3 |
| 11200 | 11295 | RMD116 | 42 | N | mar / cs | wr | 40-42 | 1.5000 | 12.00 | 70.00 | 2.2334 | 0.9595 | 16.105 | 15.453 | 35.968 | 1.5000 | 3 |
| 10400 | 10920 | RMD12 | 18 | N | wea | wr | 16-18 | 0.1700 | 0.00 | 0.00 | 2.1720 | 0.9152 | 16.985 | 15.544 | 36.891 | 0.1700 | 3 |
| 10400 | 10920 | RMD12 | 36 | N | wea | wr | 34-36 | 0.1350 | 0.00 | 0.00 | 2.1711 | 0.9153 | 16.972 | 15.534 | 36.846 | 0.1350 | 3 |
| 10800 | 11035 | RMD120 | 30 | N | wea | wr | 28-30 | 0.4300 | 8.00 | 32.00 | 2.1781 | 0.9224 | 16.836 | 15.529 | 36.670 | 0.4300 | 3 |
| 10400 | 11395 | RMD124 | 22 | N | wea | wr | 20-22 | 0.1300 | 0.00 | 26.00 | 2.1568 | 0.9158 | 17.004 | 15.571 | 36.674 | 0.1300 | 3 |
| 10400 | 11395 | RMD124 | 62 | N | wea | wr | 60-62 | 0.2300 | 18.00 | 14.00 | 2.1472 | 0.9088 | 17.145 | 15.582 | 36.814 | 0.2300 | 3 |
| 10200 | 11100 | RMD136 | 34 | N | wea | wr | 32-34 | 1.6000 | 34.00 | 18.00 | 2.2235 | 0.9517 | 16.260 | 15.474 | 36.155 | 1.6000 | 3 |
| 8400 | 10250 | RMD141 | 76 | C | wea | wr | 74-76 | 0.1250 | 76.00 | 14.00 | 2.1813 | 0.9355 | 16.602 | 15.531 | 36.214 | 0.1250 | 3 |

**Appendix 7.2 cont.**

| Northing (mN) | Easting (mN) | Drill hole | Depth (m) | Zone | Sample description | Sample type | Assay Interval | Lead assay (wt.%) | U (ppm) | Th (ppm) | 208Pb /206Pb | 207Pb /206Pb | 206Pb /204Pb | 207Pb /204Pb | 208Pb /204Pb | Pb content (wt.%) | Ref. |
|---|---|---|---|---|---|---|---|---|---|---|---|---|---|---|---|---|---|
| 8400 | 10150 | RMD143 | 20 | C | wea | wr | 18-20 | 0.2200 | 4.00 | 95.00 | 2.1896 | 0.9378 | 16.552 | 15.522 | 36.242 | 0.2200 | 3 |
| 8800 | 10205 | RMD144 | 48 | C | wea | wr | 46-48 | 0.2350 | 60.00 | 55.00 | 2.2093 | 0.9483 | 16.338 | 15.493 | 36.096 | 0.2350 | 3 |
| 10400 | 10865 | RMD15 | 34 | N | wea | wr | 32-34 | 0.5550 | 12.00 | 100.00 | 2.1662 | 0.9087 | 17.135 | 15.571 | 37.118 | 0.5550 | 3 |
| 10000 | 11265 | RMD152 | 44 | N | wea | wr | 42-44 | 0.2400 | 6.00 | 32.00 | 2.1255 | 0.8853 | 17.654 | 15.629 | 37.522 | 0.2400 | 3 |
| 10000 | 11265 | RMD152 | 44 | N | wea | wr | 42-44 | 0.2400 | 6.00 | 32.00 | 2.1288 | 0.8860 | 17.676 | 15.661 | 37.628 | 0.2400 | 3 |
| 8800 | 10360 | RMD153 | 76 | C | wea | wr | 74-76 | 0.0460 | 26.00 | 80.00 | 2.1706 | 0.9295 | 16.658 | 15.484 | 36.158 | 0.0460 | 3 |
| 9600 | 10420 | RMD156 | 18 | N | wea | wr | 16-18 | 0.6200 | 20.00 | 24.00 | 2.2231 | 0.9546 | 16.162 | 15.428 | 35.930 | 0.6200 | 3 |
| 9600 | 10420 | RMD156 | 48 | N | mar / cs | wr | 46-48 | 0.3500 | 14.00 | 22.00 | 2.2254 | 0.9568 | 16.118 | 15.421 | 35.868 | 0.3500 | 3 |
| 9600 | 10420 | RMD156 |  | N | wea | wr | not assayed | no assay |  |  | 2.2203 | 0.9546 | 16.159 | 15.425 | 35.878 | no assay | 3 |
| 9800 | 10975 | RMD162 | 66 | N | wea | wr | 64-66 | 2.0000 | 16.00 | 85.00 | 2.2284 | 0.9586 | 16.071 | 15.404 | 35.812 | 2.0000 | 3 |
| 9600 | 10415 | RMD167 | 18 | N | wea | wr | 16-18 | 0.1050 | 0.00 | 4.00 | 2.2033 | 0.9419 | 16.399 | 15.446 | 36.132 | 0.1050 | 3 |
| 9800 | 11195 | RMD172 | 24 | N | wea | wr | 22-24 | 0.5100 | 6.00 | 30.00 | 2.1618 | 0.9123 | 17.071 | 15.575 | 36.904 | 0.5100 | 3 |
| 9800 | 11195 | RMD172 | 24 | N | wea | wr | 22-24 | 0.5100 | 6.00 | 30.00 | 2.1557 | 0.9087 | 17.136 | 15.571 | 36.940 | 0.5100 | 3 |
| 9800 | 11195 | RMD172 | 48 | N | wea | wr | 46-48 | 0.2100 | 14.00 | 44.00 | 2.1842 | 0.9294 | 16.725 | 15.544 | 36.530 | 0.2100 | 3 |
| 10400 | 10720 | RMD18 | 24 | N | wea | wr | 22-24 | 0.1800 | 0.00 | 30.00 | 2.1320 | 0.8993 | 17.371 | 15.622 | 37.035 | 0.1800 | 3 |
| 10800 | 10710 | RMD205 | 26 | N | wea | wr | 24-26 | 0.0910 | 14.00 | 80.00 | 2.1330 | 0.8997 | 17.355 | 15.614 | 37.018 | 0.0910 | 3 |
| 10400 | 10615 | RMD21 | 26 | N | wea | wr | 24-26 | 0.1200 | 0.00 | 8.00 | 2.1415 | 0.9107 | 17.114 | 15.586 | 36.650 | 0.1200 | 3 |
| 10400 | 10615 | RMD21 | 26 | N | wea | wr/r | 24-26 | 0.1050 | 0.00 | 8.00 | 2.1421 | 0.9108 | 17.118 | 15.591 | 36.668 | 0.1050 | 3 |
| 10800 | 10510 | RMD215 | 48 | N | wea | wr | 46-48 | 0.0230 | 4.00 | 28.00 | 2.0779 | 0.8614 | 18.224 | 15.698 | 37.868 | 0.0230 | 3 |
| 10000 | 10635 | RMD26 | 26 | N | wea | wr | 24-26 | 0.9000 | 4.00 | 40.00 | 2.2027 | 0.9376 | 16.529 | 15.498 | 36.408 | 0.9000 | 3 |
| 10000 | 11025 | RMD31 | 42 | N | wea sul | wr | 40-42 | 1.6000 | 0.00 | 0.00 | 2.2335 | 0.9599 | 16.065 | 15.421 | 35.881 | 1.6000 | 3 |
| 10000 | 11025 | RMD31 | 42 | N | wea sul | wr/r | 40-42 | 1.6000 | 0.00 | 0.00 | 2.2341 | 0.9599 | 16.075 | 15.431 | 35.913 | 1.6000 | 3 |
| 10000 | 11025 | RMD31 | 46 | N | wea sul | wr | 44-46 | 19.0000 | 0.00 | 0.00 | 2.2325 | 0.9600 | 16.043 | 15.401 | 35.817 | 19.0000 | 3 |
| 10000 | 11025 | RMD31 | 46 | N | wea sul | wr | 44-46 | 19.0000 | 0.00 | 0.00 | 2.2353 | 0.9608 | 16.051 | 15.422 | 35.879 | 19.0000 | 3 |
| 10000 | 11025 | RMD31 | 50 | N | wea sul | wr | 48-50 | 4.6000 | 0.00 | 0.00 | 2.2367 | 0.9613 | 16.050 | 15.428 | 35.898 | 4.6000 | 3 |
| 10000 | 11025 | RMD31 | 50 | N | wea sul | wr | 48-50 | 4.6000 | 0.00 | 0.00 | 2.2365 | 0.9612 | 16.054 | 15.430 | 35.905 | 4.6000 | 3 |
| 10000 | 11025 | RMD31 | 50 | N | wea sul | wr | 48-50 | 4.6000 | 0.00 | 0.00 | 2.2351 | 0.9609 | 16.055 | 15.427 | 35.884 | 4.6000 | 3 |
| 10000 | 11025 | RMD31 | 51 | N | wea sul | wr | 50-51 | 7.8000 | 0.00 | 0.00 | 2.2347 | 0.9608 | 16.039 | 15.411 | 35.842 | 7.8000 | 3 |
| 10000 | 11025 | RMD31 | 51 | N | wea sul | wr | 50-51 | 7.8000 | 0.00 | 0.00 | 2.2345 | 0.9607 | 16.040 | 15.409 | 35.841 | 7.8000 | 3 |
| 10000 | 11025 | RMD31 | 51 | N | wea sul | wr | 50-51 | 7.8000 | 0.00 | 0.00 | 2.2351 | 0.9609 | 16.049 | 15.421 | 35.870 | 7.8000 | 3 |
| 9600 | 10515 | RMD45 | 30 | N | wea | wr | 28-30 | 1.5000 | 6.00 | 70.00 | 2.2117 | 0.9473 | 16.239 | 15.383 | 35.915 | 1.5000 | 3 |
| 9600 | 10515 | RMD45 | 32 | N | wea | wr | 30-32 | 1.0000 | 4.00 | 28.00 | 2.2093 | 0.9456 | 16.364 | 15.474 | 36.152 | 1.0000 | 3 |
| 10000 | 11010 | RMD60 | 36 | N | wea | wr | 34-36 | 0.1350 | 0.00 | 0.00 | 2.2171 | 0.9492 | 16.253 | 15.427 | 36.034 | 0.1350 | 3 |
| 10000 | 11010 | RMD60 | 36 | N | wea | wr | 34-36 | 0.1350 | 0.00 | 0.00 | 2.2185 | 0.9494 | 16.269 | 15.446 | 36.092 | 0.1350 | 3 |

## Appendix 7.2 cont.

| Northing (mN) | Easting (mN) | Drill hole | Depth (m) | Zone | Sample description | Sample type | Assay Interval | Lead assay (wt.%) | U (ppm) | Th (ppm) | 208Pb /206Pb | 207Pb /206Pb | 206Pb /204Pb | 207Pb /204Pb | 208Pb /204Pb | Pb content (wt.%) | Ref. |
|---|---|---|---|---|---|---|---|---|---|---|---|---|---|---|---|---|---|
| 10000 | 11010 | RMD60 | 36 | N | wea | wr | 34-36 | 0.1350 | 0.00 | 0.00 | 2.2196 | 0.9497 | 16.271 | 15.453 | 36.115 | 0.1350 | 3 |
| 10000 | 11040 | RMD61 | 54 | N | wea sul | wr | 52-54 | 3.2500 | 0.00 | 0.00 | 2.2337 | 0.9602 | 16.059 | 15.420 | 35.872 | 3.2500 | 3 |
| 10000 | 10690 | RMD65 | 12 | N | wea | wr | 10.0-12 | 2.0000 | 0.00 | 105.00 | 2.2160 | 0.9496 | 16.280 | 15.459 | 36.075 | 2.0000 | 3 |
| 10000 | 10690 | RMD65 | 14 | N | wea | wr | 12.0-14 | 2.1000 | 6.00 | 165.00 | 2.2134 | 0.9487 | 16.278 | 15.443 | 36.030 | 2.1000 | 3 |
| 10000 | 10635 | RMD66 | 36 | N | wea | wr | 34-36 | 0.2500 | 12.00 | 100.00 | 2.1940 | 0.9367 | 16.562 | 15.514 | 36.337 | 0.2500 | 3 |
| 9200 | 10520 | RMD69 | 28 | C | wea | wr | 36-28 | 0.3300 | 0.00 | 36.00 | 2.2081 | 0.9480 | 16.315 | 15.467 | 36.025 | 0.3300 | 3 |
| 9600 | 11055 | RMD86 | 52 | N | | wr | 50-52 | 0.5200 | 8.00 | 46.00 | 2.1642 | 0.9123 | 17.066 | 15.570 | 36.935 | 0.5200 | 3 |
| 8400 | 10505 | RMD94 | 54 | C | wea | wr | 52-54 | 0.4100 | 65.00 | 48.00 | 2.1700 | 0.9232 | 16.854 | 15.560 | 36.573 | 0.4100 | 3 |
| 7971.4 | 10149.9 | RPM0002 | 179 | C | LP? | wr | 178-180 | 0.2120 | | | 2.2219 | 0.9532 | 16.220 | 15.460 | 36.039 | 0.3 | 1 |
| 7972.8 | 10252.2 | RPM0003 | 109 | C | vn in MD ig | gn | 108-110 | 0.0045 | | | 2.1417 | 0.9100 | 17.128 | 15.587 | 36.683 | 86.6 | 1 |
| 7972.1 | 10552.9 | RPM0006 | 113 | C | sul in clast in MD ig | gn | 112-114 | 0.3675 | | | 2.1541 | 0.9079 | 17.159 | 15.579 | 36.962 | 86.6 | 1 |
| 7972.1 | 10552.9 | RPM0006 | 121 | C | sul in clast in MD ig | wr | 120-122 | 0.0865 | | | 2.1319 | 0.8929 | 17.496 | 15.623 | 37.301 | 0.057 | 1 |
| 7559.2 | 10220.1 | RPM0007 | 157 | C | sul in clast in MD ig | wr | 156-158 | 0.1055 | | | 2.1729 | 0.9290 | 16.712 | 15.525 | 36.312 | 1 | 1 |
| 7566.7 | 10319.8 | RPM0010 | 87 | C | sul in clast in MD ig | gn | not assayed | no assay | | | 2.1695 | 0.9221 | 16.891 | 15.576 | 36.646 | 86.6 | 1 |
| 7580 | 10320.9 | RPM0011 | 83 | C | sul in clast in MD ig | gn | 82-84 | 3.6400 | | | 2.1833 | 0.9317 | 16.679 | 15.540 | 36.415 | 86.6 | 1 |
| 7580 | 10320.9 | RPM0011 | 219 | C | sul vn in MD ig | gn | 218-220 | 4.9800 | | | 2.2144 | 0.9505 | 16.301 | 15.494 | 36.095 | 86.6 | 2 |
| 7580 | 10320.9 | RPM0011 | 236 | C | LP? | gn | 234-236 | 5.6100 | | | 2.1841 | 0.9294 | 16.731 | 15.550 | 36.541 | 86.6 | 2 |
| 7580 | 10320.9 | RPM0011 | 236 | C | LP? | gn | 234-236 | 5.6100 | | | 2.1724 | 0.9232 | 16.822 | 15.529 | 36.543 | 86.6 | 2 |
| 10100 | 10420 | RRP15/1 | 46 | N | mar / cs | wr | 44-46 | 1.2000 | 90.00 | 0.00 | 2.1146 | 0.8912 | 17.519 | 15.613 | 37.046 | 1.2 | 3 |
| 10100 | 10420 | RRP15/1 | 54 | N | mar / cs | wr | 52-54 | 0.2200 | 70.00 | 0.00 | 2.1729 | 0.9264 | 16.780 | 15.545 | 36.461 | 0.22 | 4 |
| 10100 | 10420 | RRP15/1 | 54 | N | mar / cs | wr/r | 52-54 | 0.2200 | 70.00 | 0.00 | 2.1725 | 0.9263 | 16.797 | 15.559 | 36.491 | 0.22 | 4 |
| | | TD1 | 60 | | Tarcoola Granite | fel | 60.39-60.59 | 0.0041 | 0.28 | | | | 15.858 | 15.341 | 35.616 | 0.0041 | 6 |
| | | TD1 | 60 | | Tarcoola Granite | fel/r | 60.39-60.59 | 0.0041 | 0.28 | | | | 15.879 | 15.361 | 35.679 | 0.0041 | 6 |
| | | TD2 | 50 | | Tarcoola Granite | fel | 50.02-50.25 | 0.0038 | 0.10 | | | | 15.863 | 15.343 | 35.633 | 0.0038 | 6 |
| | | TD2 | 50 | | Tarcoola Granite | fel/r | 50.02-50.25 | 0.0038 | 0.10 | | | | 15.864 | 15.356 | 35.670 | 0.0038 | 6 |
| 8820 | 10250 | Waterbore | 70 | C | sul | gn | 68-70 | 1.7500 | | | 2.2349 | 0.9607 | 16.050 | 15.420 | 35.871 | 86.6 | 1 |
| | | | | | Cunyarie Granite' | fel | | 0.0022 | | | | | 16.441 | 15.413 | 36.124 | 0.0022 | 7 |
| | | | | | Charleston Granite | fel/1 | | 0.0019 | | | 2.1742 | 0.8941 | 17.364 | 15.525 | 37.752 | 0.0019 | 8 |
| | | | | | Charleston Granite | fel/2 | | 0.0023 | | | 2.2348 | 0.9498 | 16.194 | 15.381 | 36.190 | 0.0023 | 8 |
| | | | | | Charleston Granite | fel/3 | | 0.0020 | | | 2.2405 | 0.9538 | 16.112 | 15.369 | 36.100 | 0.002 | 8 |
| | | | | | Charleston Granite | fel/4 | | 0.0014 | | | 2.2346 | 0.9494 | 16.206 | 15.386 | 36.214 | 0.0014 | 8 |

Abbreviations: alt = altered
C = central
cly = clay

## Appendix 7.2 cont.

Abbreviations:

cs = calc-silicate lithology
DP = Discordant polymictic breccia
fel = felspar
fzb = fault zone breccia
gn = galena
gnd = granite dyke
gra = graphitic
int = intrusion
LP = Layered polymictic breccia
mar = marble
MD ig = Menninnie Dam ignimbrite
met = metasomatic
N = northern
PD = diamond drill hole with percussion pre-collar.
PE = percussion drill hole.
r = repeat
rhy = rhyolite
RMD and RPM = rotary air blast drill hole.
S = southern
sch = schist
ser = sericite
sh = sheared
sul = sulphide
wea = weathered
wr = whole rock
vn = vein

References:

1 = Carr, G.R. and Dean, J.A. (1990). Report SR135
2 = Carr, G.R. and Dean, J.A., (1991). SR155
3 = Carr, G.R., Gulson, B.L. and Dean, J.A., 1986. SR028
4 = Davidson, G.J., 1985. Review of Pb-isotope sampling on the Eyre Peninsula
5 = Dean, J.A., 1991. SR199
6 = Fanning, M., 1988. Tarcoola Goled Mine: U-Pb isotope study
7 = This study
8 = Unpublished CSIRO data

**Appendix 8.1**

Summary of U - Pb zircon ion micropbrobe analyses of weakly altered, and strongly altered, rhyolite dykes.

Weakly altered rhyolite dyke

| Grain . spot | U (ppm) | Th (ppm) | Th / U | Pb (ppm) | 204/206* | % f206 | 206/238 | ± | 207/235 | ± | 207/206 | ± | Ages (Ma.) 206/238 | 207/235 | 207/206 | ± | % CONC |
|---|---|---|---|---|---|---|---|---|---|---|---|---|---|---|---|---|---|
| 1.1 | 115 | 102 | 0.88 | 39 | - | <0.01 | 0.2900 | 0.0086 | 3.944 | 0.133 | 0.0986 | 0.0013 | 1641 | 1623 | 1599 | 24 | 103 |
| 2.1 | 2982 | 2648 | 0.89 | 1048 | - | <0.01 | 0.2721 | 0.0186 | 3.783 | 0.270 | 0.1008 | 0.0014 | 1552 | 1589 | 1639 | 26 | 95 |
| 3.1 | 227 | 812 | 3.59 | 61 | 0.000157 | 0.25 | 0.2063 | 0.0062 | 2.686 | 0.096 | 0.0944 | 0.0015 | 1209 | 1325 | 1516 | 31 | 80 |
| 4.1 | 127 | 204 | 1.60 | 50 | 0.000054 | 0.09 | 0.2895 | 0.0086 | 3.925 | 0.133 | 0.0983 | 0.0013 | 1639 | 1619 | 1593 | 25 | 103 |
| 5.1 | 99 | 122 | 1.23 | 36 | - | <0.01 | 0.2855 | 0.0089 | 3.939 | 0.145 | 0.1001 | 0.0016 | 1619 | 1622 | 1626 | 30 | 100 |
| 6.1 | 122 | 259 | 2.12 | 53 | - | <0.01 | 0.2881 | 0.0094 | 4.011 | 0.147 | 0.1010 | 0.0013 | 1632 | 1636 | 1642 | 25 | 99 |
| 7.1 | 62 | 129 | 2.07 | 27 | 0.000359 | 0.57 | 0.2948 | 0.0102 | 3.821 | 0.231 | 0.0940 | 0.0043 | 1666 | 1597 | 1508 | 89 | 110 |
| 8.1 | 183 | 179 | 0.98 | 63 | - | <0.01 | 0.2859 | 0.0083 | 3.888 | 0.123 | 0.0987 | 0.0010 | 1621 | 1611 | 1599 | 18 | 101 |
| 9.1 | 140 | 258 | 1.84 | 46 | 0.000171 | 0.27 | 0.2771 | 0.0087 | 3.655 | 0.141 | 0.0957 | 0.0018 | 1577 | 1562 | 1542 | 36 | 102 |
| 10.1 | 102 | 204 | 2.00 | 32 | 0.000295 | 0.47 | 0.2235 | 0.0076 | 2.883 | 0.139 | 0.0935 | 0.0028 | 1301 | 1377 | 1499 | 58 | 87 |
| 11.1 | 54 | 83 | 1.54 | 21 | - | <0.01 | 0.2966 | 0.0119 | 4.050 | 0.194 | 0.0990 | 0.0022 | 1674 | 1644 | 1606 | 41 | 104 |
| 12.1 | 61 | 91 | 1.48 | 25 | - | <0.01 | 0.3129 | 0.0112 | 4.128 | 0.171 | 0.0957 | 0.0016 | 1755 | 1660 | 1541 | 32 | 114 |
| 13.1 | 539 | 1078 | 2.00 | 198 | 0.000230 | 0.37 | 0.2561 | 0.0072 | 3.447 | 0.108 | 0.0976 | 0.0011 | 1470 | 1515 | 1579 | 21 | 93 |
| 14.1 | 134 | 259 | 1.94 | 55 | 0.000048 | 0.08 | 0.2883 | 0.0089 | 4.002 | 0.145 | 0.1007 | 0.0016 | 1633 | 1635 | 1637 | 29 | 100 |
| 15.1 | 270 | 527 | 1.95 | 71 | 0.000131 | 0.21 | 0.2154 | 0.0061 | 2.874 | 0.092 | 0.0968 | 0.0012 | 1258 | 1375 | 1563 | 23 | 81 |
| 16.1 | 170 | 383 | 2.25 | 60 | 0.000025 | 0.04 | 0.2506 | 0.0072 | 3.419 | 0.104 | 0.0990 | 0.0008 | 1442 | 1509 | 1604 | 15 | 90 |
| 17.1 | 649 | 760 | 1.17 | 215 | 0.000072 | 0.11 | 0.2719 | 0.0079 | 3.689 | 0.110 | 0.0984 | 0.0004 | 1550 | 1569 | 1594 | 7 | 97 |
| 18.1 | 279 | 813 | 2.91 | 95 | 0.000002 | <0.01 | 0.1914 | 0.0055 | 2.560 | 0.078 | 0.0970 | 0.0007 | 1129 | 1289 | 1567 | 14 | 72 |
| 19.1 | 201 | 668 | 3.32 | 81 | 0.000065 | 0.10 | 0.2455 | 0.0071 | 3.310 | 0.102 | 0.0978 | 0.0008 | 1415 | 1483 | 1582 | 15 | 89 |

Strongly altered rhyolite dyke

| Grain . spot | U (ppm) | Th (ppm) | Th / U | Pb (ppm) | 204/206* | % f206 | 206/238 | ± | 207/235 | ± | 207/206 | ± | Ages (Ma.) 206/238 | 207/235 | 207/206 | ± | % CONC |
|---|---|---|---|---|---|---|---|---|---|---|---|---|---|---|---|---|---|
| 1.1 | 74 | 111 | 1.49 | 29 | - | <0.01 | 0.2942 | 0.0123 | 3.956 | 0.183 | 0.0975 | 0.0015 | 1662 | 1625 | 1577 | 29 | 105 |
| 2.1 | 95 | 131 | 1.38 | 36 | 0.000015 | 0.02 | 0.2865 | 0.0114 | 4.015 | 0.187 | 0.1017 | 0.0020 | 1624 | 1637 | 1654 | 37 | 98 |
| 3.1 | 185 | 274 | 1.48 | 72 | - | <0.01 | 0.2992 | 0.0103 | 4.023 | 0.158 | 0.0975 | 0.0014 | 1687 | 1639 | 1577 | 28 | 107 |
| 4.1 | 87 | 194 | 2.22 | 38 | - | <0.01 | 0.2811 | 0.0097 | 3.925 | 0.160 | 0.1013 | 0.0018 | 1597 | 1619 | 1647 | 33 | 97 |
| 4.2 | 69 | 156 | 2.28 | 28 | 0.000077 | 0.12 | 0.2665 | 0.0080 | 3.633 | 0.135 | 0.0989 | 0.0018 | 1523 | 1557 | 1603 | 35 | 95 |
| 5.1 | 44 | 78 | 1.76 | 19 | - | <0.01 | 0.3100 | 0.0129 | 4.213 | 0.218 | 0.0986 | 0.0026 | 1741 | 1677 | 1597 | 49 | 109 |
| 5.2 | 30 | 45 | 1.53 | 11 | 0.000205 | 0.33 | 0.2746 | 0.0117 | 3.729 | 0.192 | 0.0985 | 0.0024 | 1564 | 1578 | 1595 | 45 | 98 |

## Appendix 8.1 cont.

| Grain . spot | U (ppm) | Th (ppm) | Th / U | Pb* (ppm) | 204/206 | % f206 | 206/238 | ± | 207/235 | ± | 207/206 | ± | Ages (Ma.) 206/238 | 207/235 | 207/206 | ± | % CONC |
|---|---|---|---|---|---|---|---|---|---|---|---|---|---|---|---|---|---|
| 6.1 | 177 | 243 | 1.37 | 57 | - | <0.01 | 0.2718 | 0.0073 | 3.747 | 0.115 | 0.1000 | 0.0012 | 1550 | 1581 | 1623 | 23 | 96 |
| 7.1 | 72 | 26 | 0.36 | 28 | 0.000286 | 0.46 | 0.3684 | 0.0113 | 6.141 | 0.213 | 0.1209 | 0.0016 | 2022 | 1996 | 1969 | 23 | 103 |
| 8.1 | 48 | 72 | 1.49 | 17 | - | <0.01 | 0.2635 | 0.0084 | 3.620 | 0.123 | 0.0996 | 0.0009 | 1508 | 1554 | 1617 | 16 | 93 |
| 9.1 | 124 | 221 | 1.78 | 48 | - | <0.01 | 0.2749 | 0.0085 | 3.754 | 0.121 | 0.0991 | 0.0007 | 1566 | 1583 | 1606 | 13 | 98 |
| 10.1 | 276 | 672 | 2.44 | 117 | - | <0.01 | 0.2699 | 0.0078 | 3.648 | 0.110 | 0.0980 | 0.0005 | 1540 | 1560 | 1587 | 10 | 97 |
| 11.1 | 89 | 129 | 1.45 | 32 | 0.000009 | 0.02 | 0.2771 | 0.0081 | 3.770 | 0.121 | 0.0987 | 0.0010 | 1576 | 1586 | 1599 | 18 | 99 |
| 12.1 | 103 | 162 | 1.58 | 37 | 0.000116 | 0.19 | 0.2674 | 0.0081 | 3.599 | 0.126 | 0.0976 | 0.0014 | 1528 | 1549 | 1579 | 27 | 97 |
| 13.1 | 156 | 280 | 1.80 | 45 | 0.000021 | 0.03 | 0.2273 | 0.0066 | 3.106 | 0.096 | 0.0991 | 0.0008 | 1320 | 1434 | 1607 | 15 | 82 |

Notes : * - denotes no 204Pb detected.
Uncertainties given at the one sigma level.

**Appendix 9.1**
Fluid inclusion data

| Zone | East (m) | North (m) | Drill hole | Depth (m) | Host min | FI type | FI area (µm) | % fill | Tm 1 (°C) | freeze colour | Tm 2 (°C) | Tm 3 (°C) | Salinity | Tm 4 (°C) | Th 1 (°C) | Th 2 (°C) | Min 1 | Area1 (µm2) | Td 1 (°C) | Min 2 | Area2 (µm2) | Td 2 (°C) | Min 3 | Area3 (µm2) |
|---|---|---|---|---|---|---|---|---|---|---|---|---|---|---|---|---|---|---|---|---|---|---|---|---|
| C | 10250 | 7764 | PD0030 | 403 | qz ph | S2 | 12.6 | 96 | | | | -11.9 | 15.86 | | 163.0 | 169.0 | | | | | | | | |
| C | 10250 | 7764 | PD0030 | 403 | qz ph | S2 | 15.7 | 98 | | | | | | | 142.3 | 148.3 | | | | | | | | |
| C | 10250 | 7764 | PD0030 | 403 | qz ph | S2 | 18.8 | 97 | | | | | | | 150.6 | 156.6 | | | | | | | | |
| C | 10250 | 7764 | PD0030 | 403 | qz ph | S2 | 18.8 | 97 | | | | | | | 150.6 | 156.6 | | | | | | | | |
| C | 10250 | 7764 | PD0030 | 403 | qz ph | S2 | 39.3 | 93 | -45.9 | | -24.4 | -20.9 | 22.98 | | 150.8 | 156.8 | | | | | | | | |
| C | 10250 | 7764 | PD0030 | 403 | qz ph | S2 | 4.7 | 85 | | | | -18.8 | 21.54 | | 154.4 | 160.4 | | | | | | | | |
| C | 10250 | 7764 | PD0030 | 403 | qz ph | S2 | 7.1 | 95 | | | | -16.8 | 20.07 | | 156.2 | 162.2 | | | | | | | | |
| C | 10250 | 7764 | PD0030 | 403 | qz ph | S2 | 47.1 | 94 | -45.9 | | | -9.4 | 13.29 | | 165.3 | 171.3 | | | | | | | | |
| C | 10250 | 7764 | PD0030 | 403 | qz ph | S2 | 7.1 | 95 | | | | | | | 172.3 | 178.3 | | | | | | | | |
| C | 10250 | 7764 | PD0030 | 403 | qz ph | S2 | 23.6 | 95 | | | | -2.1 | 3.55 | | 175.5 | 181.5 | | | | | | | | |
| C | 10250 | 7764 | PD0030 | 403 | qz ph | S2 | | | | | | | | | 179.8 | 185.8 | | | | | | | | |
| C | 10250 | 7764 | PD0030 | 403 | qz ph | S2 | 9.4 | 90 | | | | -13.3 | 17.17 | | 184.4 | 190.4 | | | | | | | | |
| C | 10250 | 7764 | PD0030 | 403 | qz ph | S2 | 9.4 | 97 | | | | | | | 184.7 | 190.7 | | | | | | | | |
| C | 10250 | 7764 | PD0030 | 403 | qz ph | S2 | 23.6 | 93 | | | | | | | 190.0 | 196.0 | | | | | | | | |
| C | 10250 | 7764 | PD0030 | 403 | qz ph | S2 | 6.3 | 85 | | | | | | | 192.7 | 198.7 | | | | | | | | |
| C | 10250 | 7764 | PD0030 | 403 | qz ph | S2 | 6.3 | 85 | | | | | | | 192.7 | 198.7 | | | | | | | | |
| C | 10250 | 7764 | PD0030 | 403 | qz ph | S2 | 14.1 | 90 | | | | -6.4 | 9.73 | | 193.8 | 199.8 | | | | | | | | |
| C | 10250 | 7764 | PD0030 | 403 | qz ph | S2 | 39.3 | 93 | | | | | | | 197.3 | 203.3 | | | | | | | | |
| C | 10250 | 7764 | PD0030 | 403 | qz ph | S2 | 18.8 | 94 | | | | -5.8 | 8.95 | | 203.4 | 209.4 | | | | | | | | |
| C | 10250 | 7764 | PD0030 | 403 | qz ph | S2 | 12.6 | 92 | | | | -0.5 | 0.88 | | 215.0 | 221.0 | | | | | | | | |
| C | 10250 | 7764 | PD0030 | 403 | qz ph | S2 | 7.1 | 93 | | | | | | | 226.2 | 232.2 | | | | | | | | |
| C | 10250 | 7764 | PD0030 | 403 | qz ph | S2 | 39.3 | 88 | | | | | | | 276.1 | 282.1 | | | | | | | | |
| C | 10250 | 7764 | PD0030 | 403 | qz ph | S2 | 9.4 | 93 | | | | -3.4 | 5.56 | | | | | | | | | | | |
| C | 10250 | 7764 | PD0030 | 403 | qz ph | S2 | 7.1 | 93 | | | | -7.5 | 11.10 | | | | | | | | | | | |
| C | 10250 | 7764 | PD0030 | 403 | qz ph | S2 | 14.1 | 94 | | | | -11.9 | 15.86 | | | | | | | | | | | |
| C | 10250 | 7764 | PD0030 | 403 | qz ph | S2 | 14.1 | 94 | | | | -11.9 | 15.86 | | | | | | | | | | | |
| C | 10250 | 7764 | PD0030 | 403 | qz ph | S2 | 23.6 | 96 | | brown | | -23.8 | 24.84 | | | | | | | | | | | |
| C | 10250 | 7764 | PD0030 | 403 | qz ph | S2 | 9.4 | 90 | | | | | | | | | | | | | | | | |
| C | 10250 | 7764 | PD0030 | 403 | qz ph | S2 | 27.5 | 65 | | | | | | | | | | | | | | | | |
| C | 10250 | 7764 | PD0030 | 403 | qz ph | S3 | 25.1 | 97 | -49.9 | brown | -35.7 | | | | 137.0 | 143.0 | ? | 4.0 | | | | | | |
| C | 10250 | 7764 | PD0030 | 403 | qz ph | S3 | 42.4 | 96 | | brown | -26.7 | -24.9 | 25.52 | | 140.7 | 146.7 | ? | 0.25 | | | | | | |
| C | 10250 | 7764 | PD0030 | 403 | qz ph | S3 | 37.7 | 95 | -50.2 | brown | -24.3 | -23.3 | 24.52 | | 153.9 | 159.9 | ? | 0.25 | | | | | | |

**Appendix 9.1 cont.**

| Zone | East (m) | North (m) | Drill hole | Depth (m) | Host min | FI type | FI area (µm) | % fill | Tm 1 (°C) | freeze colour | Tm 2 (°C) | Tm 3 (°C) | Salinity | Tm 4 (°C) | Th 1 (°C) | Th 2 (°C) | Min 1 | Area1 (µm2) | Td 1 (°C) | Min 2 | Area2 (µm2) | Td 2 (°C) | Min 3 | Area3 (µm2) |
|---|---|---|---|---|---|---|---|---|---|---|---|---|---|---|---|---|---|---|---|---|---|---|---|---|
| C | 10250 | 7764 | PD0030 | 403 | qz ph | S3 | 28.3 | 95 | -45.0 | brown | -23.6 | -15.9 | 19.37 | | 160.5 | 166.5 | ? | 0.25 | | | | | | |
| C | 10250 | 7764 | PD0030 | 403 | qz ph | S3 | 37.7 | 92 | | | | -16.7 | 19.99 | | 239.6 | 245.6 | ? | 1.0 | | | | | | |
| C | 10250 | 7764 | PD0030 | 403 | qz ph | S3 | 37.7 | 95 | | | | -16.1 | 19.53 | | 291.6 | 297.6 | ? | 0.25 | | op | 4.0 | | | |
| C | 10250 | 7764 | PD0030 | 403 | qz ph | S3 | 37.7 | 97 | | brown | -25.0 | -15.0 | 18.63 | | | | carb | 4.0 | | | | | | |
| C | 10250 | 7764 | PD0030 | 403 | qz ph | S3 | 19.6 | 90 | | | | -12.0 | 15.96 | | 230.0 | 236.0 | carb | 1.0 | | | | | | |
| C | 10250 | 7764 | PD0030 | 403 | qz ph | S3 | 9.4 | 93 | | | | -2.1 | 3.55 | | | | carb | 0.25 | | | | | | |
| C | 10250 | 7764 | PD0030 | 403 | qz ph | S3 | 18.8 | 96 | | | -23.4 | -19.6 | 22.10 | | 128.3 | 134.3 | carb | 0.25 | | hal | 0.5 | | | |
| C | 10250 | 7764 | PD0030 | 403 | qz ph | S3 | 9.4 | 96 | | | | -12.0 | 15.96 | | 148.0 | 154.0 | carb | 0.25 | | | | | | |
| C | 10250 | 7764 | PD0030 | 403 | qz ph | S3 | 21.2 | 96 | | | | -10.7 | 14.67 | | 151.4 | 157.4 | carb | 0.25 | | | | | | |
| C | 10250 | 7764 | PD0030 | 403 | qz ph | S3 | 14.1 | 95 | | | | -23.3 | 24.52 | | 153.0 | 159.0 | carb | 0.25 | | | | | | |
| C | 10250 | 7764 | PD0030 | 403 | qz ph | S3 | 31.4 | 94 | | | | | | | 153.4 | 159.4 | carb | 0.25 | | | | | | |
| C | 10250 | 7764 | PD0030 | 403 | qz ph | S3 | 31.4 | 94 | | | | -10.2 | 14.15 | | 154.1 | 160.1 | carb | 1.0 | | hal | 0.5 | | | |
| C | 10250 | 7764 | PD0030 | 403 | qz ph | S3 | 22.0 | 95 | | | | -14.0 | 17.79 | | 155.9 | 161.9 | carb | 0.25 | | | | | | |
| C | 10250 | 7764 | PD0030 | 403 | qz ph | S3 | 25.1 | 94 | | | -23.4 | -16.0 | 19.45 | | 157.3 | 163.3 | carb | 1.0 | | | | | | |
| C | 10250 | 7764 | PD0030 | 403 | qz ph | S3 | 25.1 | 96 | | brown | -26.8 | -15.9 | 19.37 | | 159.3 | 165.3 | carb | 0.25 | | | | | | |
| C | 10250 | 7764 | PD0030 | 403 | qz ph | S3 | 18.8 | 97 | | | | | | | 160.8 | 166.8 | carb | 0.25 | | | | | | |
| C | 10250 | 7764 | PD0030 | 403 | qz ph | S3 | 12.6 | 96 | | | | -11.9 | 15.86 | | 163.0 | 169.0 | carb | 0.25 | | | | | | |
| C | 10250 | 7764 | PD0030 | 403 | qz ph | S3 | 9.4 | 96 | | | | -11.8 | 15.76 | | 166.5 | 172.5 | carb | 0.25 | | | | | | |
| C | 10250 | 7764 | PD0030 | 403 | qz ph | S3 | 15.7 | 95 | | | -22.9 | -11.4 | 15.37 | | 167.0 | 173.0 | carb | 0.25 | | | | | | |
| C | 10250 | 7764 | PD0030 | 403 | qz ph | S3 | 15.7 | 97 | | | -22.8 | -11.9 | 15.86 | | 167.0 | 173.0 | carb | 0.25 | | | | | | |
| C | 10250 | 7764 | PD0030 | 403 | qz ph | S3 | 9.4 | 95 | | | | -11.9 | 15.86 | | 167.3 | 173.3 | carb | 0.25 | | | | | | |
| C | 10250 | 7764 | PD0030 | 403 | qz ph | S3 | 7.9 | 94 | | | | -12.9 | 16.80 | | 222.2 | 228.2 | carb | 0.25 | | | | | | |
| C | 10250 | 7764 | PD0030 | 403 | qz ph | S3 | 14.1 | 93 | | | | -13.3 | 17.17 | | 285.8 | 291.8 | carb | 0.25 | | hal | 0.5 | | | |
| C | 10250 | 7764 | PD0030 | 403 | qz ph | S3 | 9.4 | 93 | | | | -2.1 | 3.55 | | | | carb | 0.25 | | | | | | |
| C | 10250 | 7764 | PD0030 | 403 | qz ph | S3 | 23.6 | 60 | | | | -15.1 | 18.72 | | | | carb | 0.25 | | | | | | |
| C | 10250 | 7764 | PD0030 | 403 | qz ph | S3 | 7.1 | 95 | | | | | | | 155.8 | 161.8 | hal | 0.25 | | | | | | |
| C | 10250 | 7764 | PD0030 | 403 | qz ph | S3 | 9.4 | 96 | | | | | | | 165.8 | 171.8 | hal | 0.25 | | | | | | |
| C | 10250 | 7764 | PD0030 | 403 | qz ph | S3 | 23.6 | 95 | | | | -9.5 | 13.40 | | 178.1 | 184.1 | hal | 0.25 | | | | | | |
| C | 10250 | 7764 | PD0030 | 403 | qz ph | S3 | 35.3 | 94 | | brown | | -12.9 | 16.80 | | 166.8 | 172.8 | op | 8.0 | | carb | 1.0 | | | |
| C | 10250 | 7764 | PD0030 | 403 | qz ph | S3 | 15.7 | 93 | | | | -2.1 | 3.55 | | | | op | 0.1 | | | | | | |
| C | 10250 | 7764 | PD0030 | 403 | qz ph | S3 | 15.7 | 93 | | | | -2.1 | 3.55 | | | | op | 0.1 | | | | | | |
| C | 10074 | 7564 | PD0021 | 451.87 | qz1 | P1 | 55.0 | 100 | | | | -12.9 | 16.80 | | | | | | | | | | | |
| C | 10210 | 9200 | PD0011 | 146.52 | qz1 | P2 | 6.3 | 96 | | | | -0.7 | 1.22 | | 147.8 | 151.0 | | | | | | | | |
| C | 10210 | 9200 | PD0011 | 146.52 | qz1 | P2 | 31.4 | 96 | | | | -1.0 | 1.74 | | 156.0 | 159.2 | | | | | | | | |

**Appendix 9.1 cont.**

| Zone | East (m) | North (m) | Drill hole | Depth (m) | Host min | FI type | FI area (µm) | % fill | Tm 1 (°C) | freeze colour | Tm 2 (°C) | Tm 3 (°C) | Salinity | Tm 4 (°C) | Th 1 (°C) | Th 2 (°C) | Min 1 | Area1 (µm2) | Td 1 (°C) | Min 2 | Area2 (µm2) | Td 2 (°C) | Min 3 | Area3 (µm2) |
|---|---|---|---|---|---|---|---|---|---|---|---|---|---|---|---|---|---|---|---|---|---|---|---|---|
| C | 10210 | 9200 | PD0011 | 146.52 | qz1 | P2 | 7.1 | 95 | | | | -1.0 | 1.74 | | 170.9 | 174.1 | | | | | | | | |
| C | 10210 | 9200 | PD0011 | 146.52 | qz1 | P2 | 18.8 | 96 | | | | -0.7 | 1.22 | | 175.8 | 179.0 | | | | | | | | |
| C | 10210 | 9200 | PD0011 | 146.52 | qz1 | P2 | 18.8 | 95 | | | | -1.0 | 1.74 | | 181.2 | 184.4 | | | | | | | | |
| C | 10210 | 9200 | PD0011 | 146.52 | qz1 | P2 | 39.3 | 95 | | | | -1.1 | 1.91 | | 197.2 | 200.4 | | | | | | | | |
| C | 10210 | 9200 | PD0011 | 146.52 | qz1 | P2 | 11.0 | 95 | | | | | | | 219.8 | 223.0 | | | | | | | | |
| C | 10210 | 9200 | PD0011 | 146.52 | qz1 | P2 | 14.1 | 93 | | | | | | | 224.4 | 227.6 | | | | | | | | |
| C | 10210 | 9200 | PD0011 | 146.52 | qz1 | P2 | 22.0 | 94 | | | | -0.7 | 1.22 | | 233.7 | 236.9 | | | | | | | | |
| C | 10210 | 9200 | PD0011 | 146.52 | qz1 | P2 | 23.6 | 90 | | | | -1.1 | 1.91 | | | | | | | | | | | |
| C | 10210 | 9200 | PD0011 | 146.52 | qz1 | P2 | 27.5 | 90 | | | | -1.1 | 1.91 | | | | | | | | | | | |
| C | 10210 | 9200 | PD0011 | 146.52 | qz1 | P2 | 14.1 | 88 | | | | -1.0 | 1.74 | | | | | | | | | | | |
| C | 10210 | 9200 | PD0011 | 146.52 | qz1 | P2 | 4.7 | 93 | | | | -0.7 | 1.22 | | | | | | | | | | | |
| C | 10210 | 9200 | PD0011 | 146.52 | qz1 | P2 | 14.1 | 90 | | | | -0.7 | 1.22 | | | | | | | | | | | |
| C | 10210 | 9200 | PD0011 | 146.52 | qz1 | P2 | 31.4 | 50 | | | | -0.7 | 1.22 | | | | | | | | | | | |
| C | 10210 | 9200 | PD0011 | 146.52 | qz1 | P2 | 18.8 | 90 | | | | -0.6 | 1.05 | | | | | | | | | | | |
| N | 10663 | 9391.9 | PD0017 | 164.2 | qz1 | P2 | 66.0 | 94 | | | | -1.1 | 1.91 | | 180.2 | 183.4 | | | | | | | | |
| N | 10663 | 9391.9 | PD0017 | 164.2 | qz1 | P2 | 37.7 | 60 | | | | | | | | | | | | | | | | |
| C | 10074 | 7564 | PD0021 | 451.87 | qz1 | P2 | | | | | | -23.2 | 24.46 | | 121.8 | 125.0 | | | | | | | | |
| C | 10074 | 7564 | PD0021 | 451.87 | qz1 | P2 | | | | | | -23.2 | 24.46 | | 125.9 | 129.1 | | | | | | | | |
| C | 10074 | 7564 | PD0021 | 451.87 | qz1 | P2 | 47.1 | 95 | | brown | | -23.0 | 24.34 | | 148.8 | 152.0 | | | | | | | | |
| C | 10074 | 7564 | PD0021 | 451.87 | qz1 | P2 | 47.1 | 96 | | brown | -23.8 | -23.2 | 24.46 | | 151.4 | 154.6 | | | | | | | | |
| C | 10074 | 7564 | PD0021 | 451.87 | qz1 | P2 | 706.9 | 95 | | brown | | -14.6 | 18.30 | | 163.4 | 166.6 | | | | | | | | |
| C | 10074 | 7564 | PD0021 | 451.87 | qz1 | P2 | 113.1 | 98 | | brown | -23.8 | -20.6 | 22.78 | | | | | | | | | | | |
| C | 10074 | 7564 | PD0021 | 451.87 | qz1 | P2 | 47.1 | 75 | | | | -12.0 | 15.96 | | | | | | | | | | | |
| C | 10074 | 7564 | PD0021 | 451.87 | qz1 | P2 | 4.7 | 97 | | | | -11.5 | 15.47 | | | | | | | | | | | |
| C | 10074 | 7564 | PD0021 | 451.87 | qz1 | P2 | 31.4 | 98 | | | | -10.5 | 14.46 | | | | | | | | | | | |
| C | 10125 | 8960.9 | PD0024 | 338.32 | qz1 | P2 | 11.8 | 90 | | | | -20.6 | | | 193.4 | 196.6 | | | | | | | | |
| C | 10125 | 8960.9 | PD0024 | 338.32 | qz1 | P2 | 11.8 | 90 | | | | | | | 207.1 | 210.3 | | | | | | | | |
| C | 10125 | 8960.9 | PD0024 | 338.32 | qz1 | P2 | 4.7 | 95 | | | | | | | 223.2 | 226.4 | | | | | | | | |
| C | 10074 | 7564 | PD0021 | 451.87 | qz1 | P3 | 259.2 | 97 | | | | -23.1 | 13.49 | 1.8 | 147.8 | 149.4 | ? | 0.16 | | | | | | |
| C | 10074 | 7564 | PD0021 | 451.87 | qz1 | P3 | 110.0 | 96 | | brown | -25.4 | -21.6 | 23.44 | | 153.1 | 156.3 | op | 25.0 | | | 4.0 | | | |
| C | 10074 | 7564 | PD0021 | 451.87 | qz1 | P3 | 1178.1 | 95 | | brown | -23.4 | -23.1 | 24.40 | | 153.3 | 156.5 | op(3) | 4.0 | | ? | 4.0 | | | |
| C | 10074 | 7564 | PD0021 | 451.87 | qz1 | P3 | 282.7 | 96 | | | -23.6 | -17.3 | 20.45 | | 156.1 | 159.3 | op | 9.0 | | | | | | |
| C | 10074 | 7564 | PD0021 | 451.87 | qz1 | P3 | 157.1 | 94 | | | | -10.2 | 14.15 | | | | op(2) | 9.0 | | ? | 9.0 | | | |
| S | 10235 | 7406 | PD0032 | 386.36 | qz3 | P2 | 56.5 | 98 | | | | -2.4 | 4.03 | | 157.2 | 199.2 | | | | | | | | |

**Appendix 9.1 cont.**

| Zone | East (m) | North (m) | Drill hole | Depth (m) | Host min | FI type | FI area (µm) | % fill | Tm 1 (°C) | freeze colour | Tm 2 (°C) | Tm 3 (°C) | Salinity | Tm 4 (°C) | Th 1 (°C) | Th 2 (°C) | Min 1 | Area1 (µm2) | Td 1 (°C) | Min 2 | Area2 (µm2) | Td 2 (°C) | Min 3 | Area3 (µm2) |
|---|---|---|---|---|---|---|---|---|---|---|---|---|---|---|---|---|---|---|---|---|---|---|---|---|
| S | 10235 | 7406 | PD0032 | 386.36 | qz3 | P2 | 56.5 | 98 | | | | -1.1 | 1.91 | | 158.4 | 200.4 | | | | | | | | |
| S | 10235 | 7406 | PD0032 | 386.36 | qz3 | P2 | 14.1 | 97 | | | | -0.6 | 1.05 | | 160.3 | 202.3 | | | | | | | | |
| S | 10235 | 7406 | PD0032 | 386.36 | qz3 | P2 | 14.1 | 97 | | | | -2.3 | 3.87 | | 162.6 | 204.6 | | | | | | | | |
| S | 10235 | 7406 | PD0032 | 386.36 | qz3 | P2 | 31.4 | 97 | | | | -2.2 | 3.71 | | 157.5 | 199.5 | | | | | | | | |
| S | 10235 | 7406 | PD0032 | 386.36 | qz3 | P2 | 25.1 | 97 | | | | -1.3 | 2.24 | | 154.9 | 196.9 | | | | | | | | |
| S | 10235 | 7406 | PD0032 | 386.36 | qz3 | P2 | 35.3 | 97 | | | | -2.1 | 3.55 | | 155.6 | 197.6 | | | | | | | | |
| S | 10235 | 7406 | PD0032 | 386.36 | qz3 | P2 | 56.5 | 97 | | | | -2.8 | 4.65 | | 153.9 | 195.9 | | | | | | | | |
| S | 10235 | 7406 | PD0032 | 386.36 | qz3 | P2 | 150.8 | 97 | | | | -3.0 | 4.96 | | | | | | | | | | | |
| S | 10235 | 7406 | PD0032 | 386.36 | qz3 | P2 | 141.4 | 97 | | | | -1.8 | 3.06 | | 160.8 | 202.8 | | | | | | | | |
| S | 10235 | 7406 | PD0032 | 386.36 | qz3 | P2 | 157.1 | 97 | | | | -1.2 | 2.07 | | 161.1 | 203.1 | | | | | | | | |
| S | 10235 | 7406 | PD0032 | 258.05 | qz3 | P2 | 7.1 | 96 | | | | -1.7 | 2.90 | | | | | | | | | | | |
| S | 10235 | 7406 | PD0032 | 386.36 | qz3 | P2 | 7.1 | 96 | | | | -2.4 | 4.03 | | 178.7 | 220.7 | | | | | | | | |
| S | 10235 | 7406 | PD0032 | 170 | qz3 | P2 | 11.8 | 96 | | | | -2.2 | 3.71 | | 159.4 | 201.4 | | | | | | | | |
| S | 10235 | 7406 | PD0032 | 386.36 | qz3 | P2 | 18.8 | 96 | | | | -2.8 | 4.65 | | 156.4 | 198.4 | | | | | | | | |
| S | 10235 | 7406 | PD0032 | 386.36 | qz3 | P2 | 28.3 | 96 | | | | -1.5 | 2.57 | | 168.9 | 210.9 | | | | | | | | |
| S | 10235 | 7406 | PD0032 | 386.36 | qz3 | P2 | 22.0 | 96 | | | | -3.2 | 5.26 | | 159.8 | 201.8 | | | | | | | | |
| S | 10235 | 7406 | PD0032 | 386.36 | qz3 | P2 | 25.1 | 96 | | | | -0.6 | 1.05 | | | | | | | | | | | |
| S | 10235 | 7406 | PD0032 | 386.36 | qz3 | P2 | 37.7 | 96 | | | | -3.2 | 5.26 | | 158.5 | 200.5 | | | | | | | | |
| S | 10235 | 7406 | PD0032 | 386.36 | qz3 | P2 | 50.3 | 96 | | | | ≈ 0.0 | | | 157.1 | 199.1 | | | | | | | | |
| S | 10235 | 7406 | PD0032 | 386.36 | qz3 | P2 | 50.3 | 96 | | | | -2.8 | 4.65 | | 159.9 | 201.9 | | | | | | | | |
| S | 10235 | 7406 | PD0032 | 386.36 | qz3 | P2 | 25.1 | 96 | | | | -1.7 | 2.90 | | 158.5 | 200.5 | | | | | | | | |
| S | 10235 | 7406 | PD0032 | 386.36 | qz3 | P2 | 25.1 | 96 | | | | -2.9 | 4.80 | | 158.6 | 200.6 | | | | | | | | |
| S | 10235 | 7406 | PD0032 | 386.36 | qz3 | P2 | 25.1 | 96 | | | | -1.5 | 2.57 | | 153.6 | 195.6 | | | | | | | | |
| S | 10235 | 7406 | PD0032 | 386.36 | qz3 | P2 | 50.3 | 96 | | | | -3.0 | 4.96 | | 179.6 | 221.6 | | | | | | | | |
| S | 10235 | 7406 | PD0032 | 386.36 | qz3 | P2 | 37.7 | 96 | | | | -1.6 | 2.74 | | 166.1 | 208.1 | | | | | | | | |
| S | 10235 | 7406 | PD0032 | 258.05 | qz3 | P2 | 21.2 | 96 | | | | ≈ 0.0 | | | 200.2 | 242.2 | | | | | | | | |
| S | 10235 | 7406 | PD0032 | 386.36 | qz3 | P2 | 28.3 | 96 | | | | -3.0 | 4.96 | | 185.2 | 227.2 | | | | | | | | |
| S | 10235 | 7406 | PD0032 | 386.36 | qz3 | P2 | 94.2 | 96 | | | | -1.0 | 1.74 | | 152.8 | 194.8 | | | | | | | | |
| S | 10235 | 7406 | PD0032 | 386.36 | qz3 | P2 | 84.8 | 96 | | | | -1.2 | 2.07 | | 151.1 | 193.1 | | | | | | | | |
| S | 10235 | 7406 | PD0032 | 223.33 | qz3 | P2 | 153.9 | 96 | | | | -1.6 | 2.74 | | 200.4 | 242.4 | | | | | | | | |
| S | 10235 | 7406 | PD0032 | 386.36 | qz3 | P2 | 88.0 | 96 | | | | -1.2 | 2.07 | | 158.3 | 200.3 | | | | | | | | |
| S | 10235 | 7406 | PD0032 | 386.36 | qz3 | P2 | 188.5 | 96 | | | | -1.1 | 1.91 | | 157.5 | 199.5 | | | | | | | | |
| S | 10235 | 7406 | PD0032 | 386.36 | qz3 | P2 | 380.1 | 96 | | | | -1.2 | 2.07 | | 163.7 | 205.7 | | | | | | | | |
| S | 10235 | 7406 | PD0032 | 386.36 | qz3 | P2 | 207.3 | 96 | | | | -2.0 | 3.39 | | 154.6 | 196.6 | | | | | | | | |

**Appendix 9.1 cont.**

| Zone | East (m) | North (m) | Drill hole | Depth (m) | Host min | FI type | FI area (µm) | % fill | Tm 1 (°C) | freeze colour | Tm 2 (°C) | Tm 3 (°C) | Salinity | Tm 4 (°C) | Th 1 (°C) | Th 2 (°C) | Min 1 | Area1 (µm2) | Td 1 (°C) | Min 2 | Area2 (µm2) | Td 2 (°C) | Min 3 | Area3 (µm2) |
|---|---|---|---|---|---|---|---|---|---|---|---|---|---|---|---|---|---|---|---|---|---|---|---|---|
| S | 10235 | 7406 | PD0032 | 386.36 | qz3 | P2 | 4.7 | 95 | | | | -2.0 | 3.39 | | 158.5 | 200.5 | | | | | | | | |
| S | 10235 | 7406 | PD0032 | 386.36 | qz3 | P2 | 4.7 | 95 | | | | -2.0 | 3.39 | | 154.7 | 196.7 | | | | | | | | |
| S | 10235 | 7406 | PD0032 | 386.36 | qz3 | P2 | 4.7 | 95 | | | | -1.2 | 2.07 | | 171.8 | 213.8 | | | | | | | | |
| S | 10235 | 7406 | PD0032 | 223.33 | qz3 | P2 | 12.6 | 95 | | | | -1.6 | 2.74 | | 204.3 | 246.3 | | | | | | | | |
| S | 10235 | 7406 | PD0032 | 258.05 | qz3 | P2 | 6.3 | 95 | | | | ≈ 0.0 | | | 240.2 | 282.2 | | | | | | | | |
| S | 10235 | 7406 | PD0032 | 386.36 | qz3 | P2 | 9.4 | 95 | | | | -2.0 | 3.39 | | 157.2 | 199.2 | | | | | | | | |
| S | 10235 | 7406 | PD0032 | 386.36 | qz3 | P2 | 9.4 | 95 | | | | -1.2 | 2.07 | | 171.5 | 213.5 | | | | | | | | |
| S | 10235 | 7406 | PD0032 | 386.36 | qz3 | P2 | 6.3 | 95 | | | | -3.6 | 5.86 | | 180.9 | 222.9 | | | | | | | | |
| S | 10235 | 7406 | PD0032 | 170 | qz3 | P2 | 11.8 | 95 | | | | -2.2 | 3.71 | | 163.0 | 205.0 | | | | | | | | |
| S | 10235 | 7406 | PD0032 | 386.36 | qz3 | P2 | 14.1 | 95 | | | | -2.0 | 3.39 | | 156.2 | 198.2 | | | | | | | | |
| S | 10235 | 7406 | PD0032 | 386.36 | qz3 | P2 | 14.1 | 95 | | | | -2.1 | 3.55 | | 165.9 | 207.9 | | | | | | | | |
| S | 10235 | 7406 | PD0032 | 386.36 | qz3 | P2 | 14.1 | 95 | | | | -0.6 | 1.05 | | 178.5 | 220.5 | | | | | | | | |
| S | 10235 | 7406 | PD0032 | 386.36 | qz3 | P2 | 28.3 | 95 | | | | -0.7 | 1.22 | | 159.3 | 201.3 | | | | | | | | |
| S | 10235 | 7406 | PD0032 | 258.05 | qz3 | P2 | 16.5 | 95 | | | | ≈ 0.0 | | | 195.9 | 237.9 | | | | | | | | |
| S | 10235 | 7406 | PD0032 | 386.36 | qz3 | P2 | 33.0 | 95 | | | | -2.0 | 3.39 | | 170.1 | 212.1 | | | | | | | | |
| S | 10235 | 7406 | PD0032 | 170 | qz3 | P2 | 18.8 | 95 | | | | ≈ 0.0 | | | 176.6 | 218.6 | | | | | | | | |
| S | 10235 | 7406 | PD0032 | 386.36 | qz3 | P2 | 25.1 | 95 | | | | -2.0 | 3.39 | | 158.8 | 200.8 | | | | | | | | |
| S | 10235 | 7406 | PD0032 | 386.36 | qz3 | P2 | 37.7 | 95 | | | | -1.2 | 2.07 | | 184.7 | 226.7 | | | | | | | | |
| S | 10235 | 7406 | PD0032 | 386.36 | qz3 | P2 | 62.8 | 95 | | | | -6.6 | 9.98 | | 160.7 | 202.7 | | | | | | | | |
| S | 10235 | 7406 | PD0032 | 386.36 | qz3 | P2 | 47.1 | 95 | | | | -3.6 | 5.86 | | 178.0 | 220.0 | | | | | | | | |
| S | 10235 | 7406 | PD0032 | 380 | qz3 | P2 | 56.5 | 95 | | | | -1.0 | 1.74 | | 188.9 | 230.9 | | | | | | | | |
| S | 10235 | 7406 | PD0032 | 386.36 | qz3 | P2 | 75.4 | 95 | | | | -2.0 | 3.39 | | 184.1 | 226.1 | | | | | | | | |
| S | 10235 | 7406 | PD0032 | 386.36 | qz3 | P2 | 58.9 | 95 | | | | -1.8 | 3.06 | | | | | | | | | | | |
| S | 10235 | 7406 | PD0032 | 386.36 | qz3 | P2 | 157.1 | 95 | | | | -1.2 | 2.07 | | 162.4 | 204.4 | | | | | | | | |
| S | 10235 | 7406 | PD0032 | 386.36 | qz3 | P2 | 94.2 | 95 | | | | -3.8 | 6.16 | | 190.7 | 232.7 | | | | | | | | |
| S | 10235 | 7406 | PD0032 | 386.36 | qz3 | P2 | 311.0 | 95 | | | | -1.2 | 2.07 | | 171.4 | 213.4 | | | | | | | | |
| S | 10235 | 7406 | PD0032 | 386.36 | qz3 | P2 | 235.6 | 95 | | | | -2.8 | 4.65 | | 163.2 | 205.2 | | | | | | | | |
| S | 10235 | 7406 | PD0032 | 170 | qz3 | P2 | 4.7 | 94 | | | | -2.0 | 3.39 | | 176.0 | 218.0 | | | | | | | | |
| S | 10235 | 7406 | PD0032 | 170 | qz3 | P2 | 12.6 | 94 | | | | ≈ 0.0 | | | 177.2 | 219.2 | | | | | | | | |
| S | 10235 | 7406 | PD0032 | 170 | qz3 | P2 | 12.6 | 94 | | | | -1.2 | 2.07 | | 169.0 | 211.0 | | | | | | | | |
| S | 10235 | 7406 | PD0032 | 386.36 | qz3 | P2 | 9.4 | 94 | | | | -2.0 | 3.39 | | 155.4 | 197.4 | | | | | | | | |
| S | 10235 | 7406 | PD0032 | 386.36 | qz3 | P2 | 6.3 | 94 | | | | -1.7 | 2.90 | | 158.9 | 200.9 | | | | | | | | |
| S | 10235 | 7406 | PD0032 | 386.36 | qz3 | P2 | 6.3 | 94 | | | | -2.4 | 4.03 | | | | | | | | | | | |
| S | 10235 | 7406 | PD0032 | 386.36 | qz3 | P2 | 19.6 | 94 | | | | -0.8 | 1.40 | | 163.5 | 205.5 | | | | | | | | |

**Appendix 9.1 cont.**

| Zone | East (m) | North (m) | Drill hole | Depth (m) | Host min | FI type | FI area (µm) | % fill | Tm 1 (°C) | freeze colour | Tm 2 (°C) | Tm 3 (°C) | Salinity | Tm 4 (°C) | Th 1 (°C) | Th 2 (°C) | Min 1 | Area1 (µm2) | Td 1 (°C) | Min 2 | Area2 (µm2) | Td 2 (°C) | Min 3 | Area3 (µm2) |
|---|---|---|---|---|---|---|---|---|---|---|---|---|---|---|---|---|---|---|---|---|---|---|---|---|
| S | 10235 | 7406 | PD0032 | 170 | qz3 | P2 | 28.3 | 94 | | | | -2.2 | 3.71 | | | | | | | | | | | |
| S | 10235 | 7406 | PD0032 | 386.36 | qz3 | P2 | 31.4 | 94 | | | | -1.8 | 3.06 | | 192.6 | 234.6 | | | | | | | | |
| S | 10235 | 7406 | PD0032 | 386.36 | qz3 | P2 | 35.3 | 94 | | | | -0.6 | 1.05 | | 175.2 | 217.2 | | | | | | | | |
| S | 10235 | 7406 | PD0032 | 170 | qz3 | P2 | 12.6 | 93 | | | | -2.4 | 4.03 | | 187.3 | 229.3 | | | | | | | | |
| S | 10235 | 7406 | PD0032 | 170 | qz3 | P2 | 9.4 | 93 | | | | -2.5 | 4.18 | | | | | | | | | | | |
| S | 10235 | 7406 | PD0032 | 170 | qz3 | P2 | 12.6 | 93 | | | | -1.8 | 3.06 | | | | | | | | | | | |
| S | 10235 | 7406 | PD0032 | 170 | qz3 | P2 | 9.4 | 93 | | | | -1.2 | 2.07 | | | | | | | | | | | |
| S | 10235 | 7406 | PD0032 | 170 | qz3 | P2 | 28.3 | 93 | | | | -2.0 | 3.39 | | 178.1 | 220.1 | | | | | | | | |
| S | 10235 | 7406 | PD0032 | 386.36 | qz3 | P2 | 18.8 | 93 | | | | -3.5 | 5.71 | | 152.9 | 194.9 | | | | | | | | |
| S | 10235 | 7406 | PD0032 | 170 | qz3 | P2 | 25.1 | 93 | | | | -1.6 | 2.74 | | 171.3 | 213.3 | | | | | | | | |
| S | 10235 | 7406 | PD0032 | 386.36 | qz3 | P2 | 37.7 | 93 | | | | -2.2 | 3.71 | | 201.6 | 243.6 | | | | | | | | |
| S | 10235 | 7406 | PD0032 | 386.36 | qz3 | P2 | 37.7 | 93 | | | | -3.2 | 5.26 | | 161.5 | 203.5 | | | | | | | | |
| S | 10235 | 7406 | PD0032 | 386.36 | qz3 | P2 | 37.7 | 93 | | | | -2.1 | 3.55 | | | | | | | | | | | |
| S | 10235 | 7406 | PD0032 | 386.36 | qz3 | P2 | 42.4 | 93 | | | | -1.5 | 2.57 | | 172.1 | 214.1 | | | | | | | | |
| S | 10235 | 7406 | PD0032 | 386.36 | qz3 | P2 | 77.8 | 93 | | | | -2.8 | 4.65 | | 179.2 | 221.2 | | | | | | | | |
| S | 10235 | 7406 | PD0032 | 386.36 | qz3 | P2 | 94.2 | 93 | | | | -2.0 | 3.39 | | 176.6 | 218.6 | | | | | | | | |
| S | 10235 | 7406 | PD0032 | 258.05 | qz3 | P2 | 55.0 | 93 | | | | ≈0.0 | | | 192.3 | 234.3 | | | | | | | | |
| S | 10235 | 7406 | PD0032 | 386.36 | qz3 | P2 | 66.0 | 93 | | | | -2.3 | 3.87 | | 153.8 | 195.8 | | | | | | | | |
| S | 10235 | 7406 | PD0032 | 386.36 | qz3 | P2 | 175.9 | 93 | | | | -2.0 | 3.39 | | 186.2 | 228.2 | | | | | | | | |
| S | 10235 | 7406 | PD0032 | 386.36 | qz3 | P2 | 188.5 | 93 | -48.0 | brown | | -1.7 | 2.90 | | 193.5 | 235.5 | | | | | | | | |
| S | 10235 | 7406 | PD0032 | 386.36 | qz3 | P2 | 9.4 | 92 | | | | -3.8 | 6.16 | | 209.0 | 251.0 | | | | | | | | |
| S | 10235 | 7406 | PD0032 | 386.36 | qz3 | P2 | 11.8 | 92 | | | | -2.4 | 4.03 | | | | | | | | | | | |
| S | 10235 | 7406 | PD0032 | 386.36 | qz3 | P2 | 15.7 | 92 | | | | -2.5 | 4.18 | | | | | | | | | | | |
| S | 10235 | 7406 | PD0032 | 170 | qz3 | P2 | 18.8 | 92 | | | | -1.7 | 2.90 | | 165.0 | 207.0 | | | | | | | | |
| S | 10235 | 7406 | PD0032 | 380 | qz3 | P2 | 14.1 | 92 | | | | -1.1 | 1.91 | | 202.3 | 244.3 | | | | | | | | |
| S | 10235 | 7406 | PD0032 | 386.36 | qz3 | P2 | 18.8 | 92 | | | | -2.5 | 4.18 | | 191.5 | 233.5 | | | | | | | | |
| S | 10235 | 7406 | PD0032 | 170 | qz3 | P2 | 37.7 | 92 | | | | -2.4 | 4.03 | | 178.1 | 220.1 | | | | | | | | |
| S | 10235 | 7406 | PD0032 | 170 | qz3 | P2 | 25.1 | 92 | | | | -2.0 | 3.39 | | | | | | | | | | | |
| S | 10235 | 7406 | PD0032 | 386.36 | qz3 | P2 | 37.7 | 92 | | | | -2.3 | 3.87 | | 213.7 | 255.7 | | | | | | | | |
| S | 10235 | 7406 | PD0032 | 386.36 | qz3 | P2 | 63.6 | 92 | -48.0 | brown | | -2.8 | 4.65 | | 194.9 | 236.9 | | | | | | | | |
| S | 10235 | 7406 | PD0032 | 386.36 | qz3 | P2 | 63.6 | 92 | | | | -1.2 | 2.07 | | 196.7 | 238.7 | | | | | | | | |
| S | 10235 | 7406 | PD0032 | 386.36 | qz3 | P2 | 56.5 | 92 | -48.0 | brown | | -1.7 | 2.90 | | | | | | | | | | | |
| S | 10235 | 7406 | PD0032 | 386.36 | qz3 | P2 | 75.4 | 92 | | | | -2.0 | 3.39 | | | | | | | | | | | |
| S | 10235 | 7406 | PD0032 | 386.36 | qz3 | P2 | 110.0 | 92 | | | | -2.4 | 4.03 | | | | | | | | | | | |

**Appendix 9.1 cont.**

| Zone | East (m) | North (m) | Drill hole | Depth (m) | Host min | FI type | FI area (µm) | % fill | Tm 1 (°C) | freeze colour | Tm 2 (°C) | Tm 3 (°C) | Salinity | Tm 4 (°C) | Th 1 (°C) | Th 2 (°C) | Min 1 | Area1 (µm2) | Td 1 (°C) | Min 2 | Area2 (µm2) | Td 2 (°C) | Min 3 | Area3 (µm2) |
|---|---|---|---|---|---|---|---|---|---|---|---|---|---|---|---|---|---|---|---|---|---|---|---|---|
| S | 10235 | 7406 | PD0032 | 386.36 | qz3 | P2 | 110.0 | 92 | | | | -2.2 | 3.71 | | | | | | | | | | | |
| S | 10235 | 7406 | PD0032 | 386.36 | qz3 | P2 | 4.7 | 91 | | | | -2.4 | 4.03 | | | | | | | | | | | |
| S | 10235 | 7406 | PD0032 | 386.36 | qz3 | P2 | 12.6 | 91 | | | | -2.1 | 3.55 | | 193.0 | 235.0 | | | | | | | | |
| S | 10235 | 7406 | PD0032 | 386.36 | qz3 | P2 | 6.3 | 91 | | | | -2.4 | 4.03 | | 208.7 | 250.7 | | | | | | | | |
| S | 10235 | 7406 | PD0032 | 386.36 | qz3 | P2 | 47.1 | 91 | | | | -1.7 | 2.90 | | | | | | | | | | | |
| S | 10235 | 7406 | PD0032 | 386.36 | qz3 | P2 | 62.8 | 91 | | | | -2.4 | 4.03 | | 195.8 | 237.8 | | | | | | | | |
| S | 10235 | 7406 | PD0032 | 386.36 | qz3 | P2 | 7.1 | 90 | | | | -2.4 | 4.03 | | 206.9 | 248.9 | | | | | | | | |
| S | 10235 | 7406 | PD0032 | 386.36 | qz3 | P2 | 19.6 | 90 | | | | -2.2 | 3.71 | | | | | | | | | | | |
| S | 10235 | 7406 | PD0032 | 380 | qz3 | P2 | 14.1 | 90 | | | | -1.0 | 1.74 | | 193.6 | 235.6 | | | | | | | | |
| S | 10235 | 7406 | PD0032 | 386.36 | qz3 | P2 | 31.4 | 90 | | | | -2.4 | 4.03 | | 220.4 | 262.4 | | | | | | | | |
| S | 10235 | 7406 | PD0032 | 170 | qz3 | P2 | 66.0 | 90 | | | | -2.2 | 3.71 | | 185.5 | 227.5 | | | | | | | | |
| S | 10235 | 7406 | PD0032 | 258.05 | qz3 | P2 | 7.1 | 88 | | | | -1.0 | 1.74 | | 271.6 | 313.6 | | | | | | | | |
| S | 10235 | 7406 | PD0032 | 386.36 | qz3 | P2 | 33.0 | 88 | | | | -2.0 | 3.39 | | | | | | | | | | | |
| S | 10235 | 7406 | PD0032 | 386.36 | qz3 | P2 | 7.1 | 85 | | | | -0.8 | 1.40 | | | | | | | | | | | |
| S | 10235 | 7406 | PD0032 | 386.36 | qz3 | P2 | 7.1 | 85 | | | | -2.4 | 4.03 | | | | | | | | | | | |
| S | 10235 | 7406 | PD0032 | 258.05 | qz3 | P2 | 7.9 | 85 | | | | -1.4 | 2.41 | | | | | | | | | | | |
| S | 10235 | 7406 | PD0032 | 258.05 | qz3 | P2 | 15.7 | 85 | | | | -1.5 | 2.57 | | 314.3 | 356.3 | | | | | | | | |
| S | 10235 | 7406 | PD0032 | 258.05 | qz3 | P2 | 18.8 | 85 | | | | -1.8 | 3.06 | | | | | | | | | | | |
| S | 10235 | 7406 | PD0032 | 386.36 | qz3 | P2 | 62.8 | 85 | | | | -2.6 | 4.34 | | | | | | | | | | | |
| S | 10235 | 7406 | PD0032 | 386.36 | qz3 | P2 | 25.1 | 83 | | | | -2.4 | 4.03 | | | | | | | | | | | |
| S | 10235 | 7406 | PD0032 | 380 | qz3 | P2 | 6.3 | 80 | | | | -1.4 | 2.41 | | | | | | | | | | | |
| S | 10235 | 7406 | PD0032 | 386.36 | qz3 | P2 | 6.3 | 80 | | | | -1.2 | 2.07 | | | | | | | | | | | |
| S | 10235 | 7406 | PD0032 | 386.36 | qz3 | P2 | 18.8 | 80 | | | | -2.2 | 3.71 | | 245.7 | 287.7 | | | | | | | | |
| S | 10235 | 7406 | PD0032 | 258.05 | qz3 | P2 | 47.1 | 75 | | | | -1.0 | 1.74 | | | | | | | | | | | |
| S | 10235 | 7406 | PD0032 | 258.05 | qz3 | P2 | 7.1 | 70 | | | | ≈ 0.0 | | | | | | | | | | | | |
| S | 10235 | 7406 | PD0032 | 258.05 | qz3 | P2 | 16.5 | 65 | | | | ≈ 0.0 | | | 308.5 | 350.5 | | | | | | | | |
| S | 10235 | 7406 | PD0032 | 258.05 | qz3 | P2 | 11.8 | 45 | | | | ≈ 0.0 | | | | | | | | | | | | |
| S | 10235 | 7406 | PD0032 | 223.33 | qz3 | P2 | | | | | | -0.6 | 1.05 | | 168.7 | 210.7 | | | | | | | | |
| S | 10235 | 7406 | PD0032 | 223.33 | qz3 | P2 | | | | | | -0.6 | 1.05 | | 173.7 | 215.7 | | | | | | | | |
| S | 10235 | 7406 | PD0032 | 223.33 | qz3 | P2 | | | | | | -0.6 | 1.05 | | 186.8 | 228.8 | | | | | | | | |
| S | 10235 | 7406 | PD0032 | 223.33 | qz3 | P2 | | | | | | -0.6 | 1.05 | | 176.7 | 218.7 | | | | | | | | |
| S | 10235 | 7406 | PD0032 | 223.33 | qz3 | P2 | | | | | | -0.6 | 1.05 | | 189.8 | 231.8 | | | | | | | | |
| S | 10235 | 7406 | PD0032 | 223.33 | qz3 | P2 | | | | | | -0.8 | 1.40 | | | | | | | | | | | |
| S | 10235 | 7406 | PD0032 | 223.33 | qz3 | P2 | | | | | | -0.8 | 1.40 | | 189.3 | 231.3 | | | | | | | | |

**Appendix 9.1 cont.**

| Zone | East (m) | North (m) | Drill hole | Depth (m) | Host min | FI type | FI area (µm) | % fill | Tm 1 (°C) | freeze colour | Tm 2 (°C) | Tm 3 (°C) | Salinity | Tm 4 (°C) | Th 1 (°C) | Th 2 (°C) | Min 1 | Area1 (µm2) | Td 1 (°C) | Min 2 | Area2 (µm2) | Td 2 (°C) | Min 3 | Area3 (µm2) |
|---|---|---|---|---|---|---|---|---|---|---|---|---|---|---|---|---|---|---|---|---|---|---|---|---|
| S | 10235 | 7406 | PD0032 | 223.33 | qz3 | P2 | | | | | | -0.8 | 1.40 | | | | | | | | | | | |
| S | 10235 | 7406 | PD0032 | 223.33 | qz3 | P2 | | | | | | -0.8 | 1.40 | | | | | | | | | | | |
| S | 10235 | 7406 | PD0032 | 223.33 | qz3 | P2 | | | | | | -0.8 | 1.40 | | 253.4 | 295.4 | | | | | | | | |
| S | 10235 | 7406 | PD0032 | 223.33 | qz3 | P2 | | | | | | -0.8 | 1.40 | | | | | | | | | | | |
| S | 10235 | 7406 | PD0032 | 223.33 | qz3 | P2 | | | | | | -0.6 | 1.05 | | 203.7 | 245.7 | | | | | | | | |
| S | 10235 | 7406 | PD0032 | 223.33 | qz3 | P2 | | | | | | -1.0 | 1.74 | | | | | | | | | | | |
| S | 10235 | 7406 | PD0032 | 223.33 | qz3 | P2 | | | | | | -1.0 | 1.74 | | 212.2 | 254.2 | | | | | | | | |
| S | 10235 | 7406 | PD0032 | 223.33 | qz3 | P2 | | | | | | -1.0 | 1.74 | | | | | | | | | | | |
| S | 10235 | 7406 | PD0032 | 223.33 | qz3 | P2 | | | | | | -1.0 | 1.74 | | 194.0 | 236.0 | | | | | | | | |
| S | 10235 | 7406 | PD0032 | 386.36 | qz3 | P3 | 12.6 | 95 | | | | -0.6 | 1.05 | | 176.2 | 218.2 | carb | 0.25 | | | | | | |
| S | 10235 | 7406 | PD0032 | 386.36 | qz3 | P3 | 226.2 | 90 | | | | -2.8 | 4.65 | | 194.8 | 236.8 | carb | 0.25 | | | | | | |
| S | 10235 | 7406 | PD0032 | 380 | qz3 | P3 | 127.2 | 90 | | | | -1.3 | 2.24 | | 187.9 | 229.9 | chl | 5.0 | | | | | | |
| S | 10235 | 7406 | PD0032 | 386.36 | qz3 | P3 | 37.7 | 96 | | | | -0.8 | 1.40 | | 154.8 | 196.8 | op | 0.25 | | | | | | |
| S | 10235 | 7406 | PD0032 | 386.36 | qz3 | P3 | 4.7 | 96 | | | | -1.5 | 2.57 | | 169.5 | 211.5 | trem | 0.25 | | | | | | |
| S | 10235 | 7406 | PD0032 | 386.36 | qz3 | P3 | 19.6 | 96 | | | | -2.0 | 3.39 | | 153.4 | 195.4 | trem | 1.0 | | | | | | |
| S | 10235 | 7406 | PD0032 | 386.36 | qz3 | P3 | 127.2 | 96 | | | | -1.3 | 2.24 | | 154.8 | 196.8 | trem | 4.0 | | | | | | |
| S | 10235 | 7406 | PD0032 | 386.36 | qz3 | P3 | 6.3 | 95 | | | | -1.5 | 2.57 | | 175.6 | 217.6 | trem | 0.25 | | | | | | |
| S | 10235 | 7406 | PD0032 | 386.36 | qz3 | P3 | 28.3 | 95 | | | | -2.0 | 3.39 | | 161.6 | 203.6 | trem | 0.25 | | | | | | |
| S | 10235 | 7406 | PD0032 | 170 | qz3 | P3 | 22.0 | 95 | | | | -1.8 | 3.06 | | 163.2 | 205.2 | trem | 4.0 | | | | | | |
| S | 10235 | 7406 | PD0032 | 386.36 | qz3 | P3 | 16.5 | 95 | | | | -0.6 | 1.05 | | 158.9 | 200.9 | trem | 1.0 | | | | | | |
| S | 10235 | 7406 | PD0032 | 386.36 | qz3 | P3 | 44.0 | 95 | | | | -0.6 | 1.05 | | 164.0 | 206.0 | trem | 5.0 | | | | | | |
| S | 10235 | 7406 | PD0032 | 386.36 | qz3 | P3 | 6.3 | 95 | | | | -2.4 | 4.03 | | | | trem | 0.25 | | | | | | |
| S | 10235 | 7406 | PD0032 | 386.36 | qz3 | P3 | 18.8 | 95 | | | | -0.8 | 1.40 | | 173.5 | 215.5 | trem | 0.25 | | | | | | |
| S | 10235 | 7406 | PD0032 | 386.36 | qz3 | P3 | 18.8 | 94 | | | | -2.0 | 3.39 | | 158.8 | 200.8 | trem | 1.0 | | | | | | |
| S | 10235 | 7406 | PD0032 | 386.36 | qz3 | P3 | 78.5 | 94 | | | | -1.4 | 2.41 | | 180.9 | 222.9 | trem | 0.25 | | | | | | |
| S | 10235 | 7406 | PD0032 | 170 | qz3 | P3 | 22.0 | 93 | | | | -1.6 | 2.74 | | 174.0 | 216.0 | trem | 1.0 | | | | | | |
| S | 10235 | 7406 | PD0032 | 386.36 | qz3 | P3 | 6.3 | 92 | | | | -3.8 | 6.16 | | 202.9 | 244.9 | trem | 0.25 | | | | | | |
| S | 10235 | 7406 | PD0032 | 386.36 | qz3 | P3 | 28.3 | 90 | | | | -2.5 | 4.18 | | | | trem | 1.0 | | | | | | |
| N | 10769 | 9800 | PD0006 | 258.2 | sp2 | P2 | 201.1 | 97 | | | | -1.9 | 3.2 | | 143.4 | 151.8 | | | | | | | | |
| N | 10769 | 9800 | PD0006 | 258.2 | sp2 | P2 | 44.0 | 95 | | | -23.7 | -8.1 | 11.8 | | 148.2 | 156.6 | | | | | | | | |
| N | 10769 | 9800 | PD0006 | 258.2 | sp2 | P2 | 37.7 | 97 | | | | -1.9 | 3.2 | | 149.0 | 157.4 | | | | | | | | |
| N | 10769 | 9800 | PD0006 | 258.2 | sp2 | P2 | 27.5 | 95 | | | -26.2 | -25.2 | 25.7 | | 156.5 | 164.9 | | | | | | | | |
| N | 10769 | 9800 | PD0006 | 258.2 | sp2 | P2 | 27.5 | 98 | | | | -1.9 | 3.2 | | 159.5 | 167.9 | | | | | | | | |
| N | 10769 | 9800 | PD0006 | 258.2 | sp2 | P2 | 103.7 | 97 | | | | -0.6 | 1.1 | | 160.0 | 168.4 | | | | | | | | |

**Appendix 9.1 cont.**

| Zone | East (m) | North (m) | Drill hole | Depth (m) | Host min | FI type | FI area (µm) | % fill | Tm 1 (°C) | freeze colour | Tm 2 (°C) | Tm 3 (°C) | Salinity | Tm 4 (°C) | Th 1 (°C) | Th 2 (°C) | Min 1 | Area1 (µm2) | Td 1 (°C) | Min 2 | Area2 (µm2) | Td 2 (°C) | Min 3 | Area3 (µm2) |
|---|---|---|---|---|---|---|---|---|---|---|---|---|---|---|---|---|---|---|---|---|---|---|---|---|
| N | 10769 | 9800 | PD0006 | 258.2 | sp2 | P2 | 37.7 | 97 | | | | -1.2 | 2.1 | | 165.0 | 173.4 | | | | | | | | |
| N | 10769 | 9800 | PD0006 | 258.2 | sp2 | P2 | 141.4 | 94 | | brown | -25.2 | -16.7 | 20.0 | | 173.7 | 182.1 | | | | | | | | |
| N | 10769 | 9800 | PD0006 | 258.2 | sp2 | P2 | 110.0 | | | | | | | | 174.8 | 183.2 | | | | | | | | |
| N | 10769 | 9800 | PD0006 | 258.2 | sp2 | P2 | 31.4 | 98 | | | | -1.9 | 3.2 | | 175.0 | 183.4 | | | | | | | | |
| N | 10769 | 9800 | PD0006 | 258.2 | sp2 | P2 | 37.7 | 93 | | | | -7.2 | 10.7 | | 176.3 | 184.7 | | | | | | | | |
| N | 10769 | 9800 | PD0006 | 258.2 | sp2 | P2 | 70.7 | 95 | | | | -5.8 | 8.9 | | 179.4 | 187.8 | | | | | | | | |
| N | 10769 | 9800 | PD0006 | 258.2 | sp2 | P2 | 4.7 | 90 | | | | | | | 193.0 | 201.4 | | | | | | | | |
| N | 10769 | 9800 | PD0006 | 258.2 | sp2 | P2 | 78.5 | 90 | | brown | | -11.1 | 15.1 | | 218.6 | 227.0 | | | | | | | | |
| N | 10769 | 9800 | PD0006 | 258.2 | sp2 | P2 | | | | | | -14.5 | 18.2 | | | | | | | | | | | |
| N | 10769 | 9800 | PD0006 | 258.2 | sp2 | P2 | 63.6 | 90 | | | | -11.1 | 15.1 | | | | | | | | | | | |
| N | 10769 | 9800 | PD0006 | 258.2 | sp2 | P2 | 169.6 | 98 | | | | -5.3 | 8.3 | | | | | | | | | | | |
| N | 10769 | 9800 | PD0006 | 258.2 | sp2 | P2 | 78.5 | 98 | | | -23.2 | -4.6 | 7.3 | | | | | | | | | | | |
| N | 10769 | 9800 | PD0006 | 258.2 | sp2 | P2 | 62.8 | 85 | | | | -4.0 | 6.4 | | | | | | | | | | | |
| N | 10769 | 9800 | PD0006 | 258.2 | sp2 | P2 | | | | | | -3.9 | 6.3 | | | | | | | | | | | |
| N | 10769 | 9800 | PD0006 | 258.2 | sp2 | P2 | 28.3 | 96 | | | | -1.9 | 3.2 | | | | | | | | | | | |
| N | 10769 | 9800 | PD0006 | 258.2 | sp2 | P2 | 37.7 | 95 | | | | -1.9 | 3.2 | | | | | | | | | | | |
| N | 10769 | 9800 | PD0006 | 258.2 | sp2 | P2 | 47.1 | 98 | | | | -1.9 | 3.2 | | | | | | | | | | | |
| N | 10769 | 9800 | PD0006 | 258.2 | sp2 | P2 | 204.2 | 96 | | | | -0.9 | 1.6 | | | | | | | | | | | |
| N | 10769 | 9800 | PD0006 | 258.2 | sp2 | P2 | 35.3 | 70 | | | | -0.6 | 1.1 | | | | | | | | | | | |
| N | 10769 | 9800 | PD0006 | 258.2 | sp2 | P2 | 47.1 | 94 | | | | -0.3 | 0.5 | | | | | | | | | | | |
| N | 10769 | 9800 | PD0006 | 258.2 | sp2 | P2 | 62.8 | 96 | | | | -0.3 | 0.5 | | | | | | | | | | | |
| N | 10769 | 9800 | PD0006 | 258.2 | sp2 | P2 | 94.2 | 96 | | | | -0.3 | 0.5 | | | | | | | | | | | |
| N | 10769 | 9800 | PD0006 | 258.2 | sp2 | P2 | 55.0 | 96 | | brown | -29.9 | | | | | | | | | | | | | |
| C | 10314 | 9200 | PD0008 | 150.3 | sp2 | P2 | 125.7 | 96 | -51.0 | brown | -25.2 | -22.5 | 24.0 | | 127.5 | 131.4 | | | | | | | | |
| C | 10314 | 9200 | PD0008 | 150.3 | sp2 | P2 | 282.7 | 97 | | | -26.2 | | 6.10 | 6.8 | 130.5 | 134.4 | | | | | | | | |
| C | 10314 | 9200 | PD0008 | 150.3 | sp2 | P2 | 78.5 | 96 | -50.6 | brown | -22.8 | -13.6 | 17.4 | | 138.4 | 142.3 | | | | | | | | |
| C | 10314 | 9200 | PD0008 | 150.3 | sp2 | P2 | 38.5 | 98 | | | -25.2 | | | | 151.8 | 155.7 | | | | | | | | |
| C | 10314 | 9200 | PD0008 | 116 | sp2 | P2 | 38.5 | 95 | | | | -1.3 | 2.2 | | 160.0 | 162.4 | | | | | | | | |
| C | 10300 | 9000 | PD0010 | 163.45 | sp2 | P2 | 56.5 | 96 | | | | | | | 132.2 | 136.6 | | | | | | | | |
| C | 10300 | 9000 | PD0010 | 163.45 | sp2 | P2 | 63.6 | 97 | | brown | -24.4 | -20.4 | 22.6 | | 138.6 | 143.0 | | | | | | | | |
| C | 10300 | 9000 | PD0010 | 163.45 | sp2 | P2 | | | | | | -4.4 | 7.0 | | 145.8 | 150.2 | | | | | | | | |
| C | 10300 | 9000 | PD0010 | 163.45 | sp2 | P2 | | | | | | | | | 158.8 | 163.2 | | | | | | | | |
| C | 10300 | 9000 | PD0010 | 163.45 | sp2 | P2 | 62.8 | 98 | | | | | | | 187.3 | 191.7 | | | | | | | | |
| C | 10300 | 9000 | PD0010 | 163.45 | sp2 | P2 | | 96 | | | | -14.1 | 17.9 | | | | | | | | | | | |

**Appendix 9.1 cont.**

| Zone | East (m) | North (m) | Drill hole | Depth (m) | Host min | FI type | FI area (µm) | % fill | Tm 1 (°C) | freeze colour | Tm 2 (°C) | Tm 3 (°C) | Salinity | Tm 4 (°C) | Th 1 (°C) | Th 2 (°C) | Min 1 | Area1 (µm2) | Td 1 (°C) | Min 2 | Area2 (µm2) | Td 2 (°C) | Min 3 | Area3 (µm2) |
|---|---|---|---|---|---|---|---|---|---|---|---|---|---|---|---|---|---|---|---|---|---|---|---|---|
| C | 10300 | 9000 | PD0010 | 163.45 | sp2 | P2 | 75.4 | 97 | | | -24.4 | -14.0 | 18.50 | -3.6 | | | | | | | | | | |
| C | 10300 | 9000 | PD0010 | 163.45 | sp2 | P2 | | 95 | | | | -14.0 | 17.8 | | | | | | | | | | | |
| C | 10300 | 9000 | PD0010 | 163.45 | sp2 | P2 | 23.6 | 97 | | | -22.0 | -13.6 | 17.4 | | | | | | | | | | | |
| C | 10210 | 9200 | PD0011 | 146.52 | sp2 | P2 | | | | | | -11.5 | 15.5 | | 123.1 | 126.8 | | | | | | | | |
| C | 10210 | 9200 | PD0011 | 146.52 | sp2 | P2 | | | | | -22.5 | -13.4 | 17.3 | | | | | | | | | | | |
| C | 10210 | 9200 | PD0011 | 146.52 | sp2 | P2 | | 96 | | | | -13.4 | 17.3 | | | | | | | | | | | |
| C | 10210 | 9200 | PD0011 | 146.52 | sp2 | P2 | | | | | -24.5 | -11.9 | 15.9 | | | | | | | | | | | |
| C | 10210 | 9200 | PD0011 | 146.52 | sp2 | P2 | | | | | | -11.6 | 15.6 | | | | | | | | | | | |
| N | 10663 | 9391.9 | PD0016 | 273.4 | sp2 | P2 | 113.1 | >99 | | | | -1.2 | 2.1 | | 114.6 | 122.2 | | | | | | | | |
| N | 10663 | 9391.9 | PD0016 | 262.77 | sp2 | P2 | | | | | | -4.4 | 7.0 | | 115.5 | 122.7 | | | | | | | | |
| N | 10663 | 9391.9 | PD0016 | 262.77 | sp2 | P2 | 62.8 | 98 | | | -24.3 | -24.1 | 25.0 | | 124.8 | 132.0 | | | | | | | | |
| N | 10663 | 9391.9 | PD0016 | 262.77 | sp2 | P2 | 63.6 | 99 | | | -24.6 | -19.3 | 21.9 | | 125.0 | 132.2 | | | | | | | | |
| N | 10663 | 9391.9 | PD0016 | 262.77 | sp2 | P2 | 62.8 | 98 | | | -24.3 | -23.3 | 24.5 | | 126.0 | 133.2 | | | | | | | | |
| N | 10663 | 9391.9 | PD0016 | 262.77 | sp2 | P2 | 25.1 | 99 | | | | | | | 130.5 | 137.7 | | | | | | | | |
| N | 10663 | 9391.9 | PD0016 | 262.77 | sp2 | P2 | 50.3 | 97 | | | | -13.8 | 17.6 | | 131.0 | 138.2 | | | | | | | | |
| N | 10663 | 9391.9 | PD0016 | 305.6 | sp2 | P2 | 78.5 | 97 | | | | -0.4 | 0.7 | | 136.0 | 145.0 | | | | | | | | |
| N | 10663 | 9391.9 | PD0016 | 305.6 | sp2 | P2 | 25.1 | 98 | | | | | | | 139.5 | 148.5 | | | | | | | | |
| N | 10663 | 9391.9 | PD0016 | 305.6 | sp2 | P2 | 44.0 | 97 | | | | -2.0 | 3.4 | | 140.1 | 149.1 | | | | | | | | |
| N | 10663 | 9391.9 | PD0016 | 273.4 | sp2 | P2 | 18.8 | 98 | | | | | | | 143.0 | 150.6 | | | | | | | | |
| N | 10663 | 9391.9 | PD0016 | 305.6 | sp2 | P2 | | | | | | -1.7 | 2.9 | | 143.1 | 152.1 | | | | | | | | |
| N | 10663 | 9391.9 | PD0016 | 305.6 | sp2 | P2 | 7.1 | 97 | | | | | | | 144.0 | 153.0 | | | | | | | | |
| N | 10663 | 9391.9 | PD0016 | 305.6 | sp2 | P2 | 4.7 | 97 | | | | | | | 144.2 | 153.2 | | | | | | | | |
| N | 10663 | 9391.9 | PD0016 | 305.6 | sp2 | P2 | 3.1 | 97 | | | | | | | 144.8 | 153.8 | | | | | | | | |
| N | 10663 | 9391.9 | PD0016 | 305.6 | sp2 | P2 | | | | | -21.6 | -1.5 | 2.6 | | 146.0 | 155.0 | | | | | | | | |
| N | 10663 | 9391.9 | PD0016 | 305.6 | sp2 | P2 | 3.1 | 97 | | | | -0.4 | 0.7 | | 147.8 | 156.8 | | | | | | | | |
| N | 10663 | 9391.9 | PD0016 | 305.6 | sp2 | P2 | 49.5 | 97 | | | | -2.0 | 3.4 | | 151.2 | 160.2 | | | | | | | | |
| N | 10663 | 9391.9 | PD0016 | 305.6 | sp2 | P2 | 19.6 | 96 | | | | -0.4 | 0.7 | | 153.3 | 162.3 | | | | | | | | |
| N | 10663 | 9391.9 | PD0016 | 305.6 | sp2 | P2 | | | | | -26.4 | | | | 154.5 | 163.5 | | | | | | | | |
| N | 10663 | 9391.9 | PD0016 | 262.77 | sp2 | P2 | 981.7 | 97 | | brown | -25.7 | -23.1 | 24.4 | | | | | | | | | | | |
| N | 10663 | 9391.9 | PD0016 | 262.77 | sp2 | P2 | | | | | -24.0 | -23.0 | 24.3 | | | | | | | | | | | |
| N | 10663 | 9391.9 | PD0016 | 262.77 | sp2 | P2 | 86.4 | 99 | | | -24.6 | -22.7 | 24.1 | | | | | | | | | | | |
| N | 10663 | 9391.9 | PD0016 | 262.77 | sp2 | P2 | 37.7 | 99 | | | | -17.6 | 20.7 | | | | | | | | | | | |
| N | 10663 | 9391.9 | PD0016 | 262.77 | sp2 | P2 | 38.5 | 99 | | | | -13.4 | 17.3 | | | | | | | | | | | |
| N | 10663 | 9391.9 | PD0016 | 262.77 | sp2 | P2 | 106.0 | 95 | | | -24.6 | -9.1 | 13.0 | | | | | | | | | | | |

**Appendix 9.1 cont.**

| Zone | East (m) | North (m) | Drill hole | Depth (m) | Host min | FI type | FI area (µm) | % fill | Tm 1 (°C) | freeze colour | Tm 2 (°C) | Tm 3 (°C) | Salinity | Tm 4 (°C) | Th 1 (°C) | Th 2 (°C) | Min 1 | Area1 (µm2) | Td 1 (°C) | Min 2 | Area2 (µm2) | Td 2 (°C) | Min 3 | Area3 (µm2) |
|---|---|---|---|---|---|---|---|---|---|---|---|---|---|---|---|---|---|---|---|---|---|---|---|---|
| N | 10663 | 9391.9 | PD0016 | 273.4 | sp2 | P2 | 1570.8 | >99 | | | | -7.0 | 10.5 | | | | | | | | | | | |
| N | 10663 | 9391.9 | PD0016 | 262.77 | sp2 | P2 | 125.7 | 98 | | | | -5.7 | 8.8 | | | | | | | | | | | |
| N | 10663 | 9391.9 | PD0016 | 262.77 | sp2 | P2 | 62.8 | 99 | | | | -2.0 | 3.4 | | | | | | | | | | | |
| N | 10663 | 9391.9 | PD0016 | 305.6 | sp2 | P2 | 44.0 | 97 | | | | -0.4 | 0.7 | | | | | | | | | | | |
| N | 10663 | 9391.9 | PD0016 | 305.6 | sp2 | P2 | 51.8 | 97 | | | | -0.4 | 0.7 | | | | | | | | | | | |
| N | 10663 | 9391.9 | PD0016 | 305.6 | sp2 | P2 | 62.8 | 97 | | | | -0.4 | 0.7 | | | | | | | | | | | |
| N | 10663 | 9391.9 | PD0016 | 305.6 | sp2 | P2 | 23.6 | 96 | | | | -0.2 | 0.4 | | | | | | | | | | | |
| C | 10136 | 8780.8 | PD0017 | 343.36 | sp2 | P2 | | | | | | | | | 111.8 | 123.3 | | | | | | | | |
| C | 10136 | 8780.8 | PD0017 | 343.36 | sp2 | P2 | 432.0 | 97 | | | | -5.9 | 9.1 | | 117.2 | 128.7 | | | | | | | | |
| C | 10136 | 8780.8 | PD0017 | 223.95 | sp2 | P2 | | 97 | | | -20.4 | -5.8 | 12.22 | 2.8 | 129.5 | 136.1 | | | | | | | | |
| C | 10136 | 8780.8 | PD0017 | 223.95 | sp2 | P2 | | 90 | | | | | | | 132.5 | 139.1 | | | | | | | | |
| C | 10136 | 8780.8 | PD0017 | 233.95 | sp2 | P2 | 94.2 | 95 | | | | | | | 132.1 | 139.1 | | | | | | | | |
| C | 10136 | 8780.8 | PD0017 | 343.36 | sp2 | P2 | | | | | | | | | 129.0 | 140.5 | | | | | | | | |
| C | 10136 | 8780.8 | PD0017 | 223.95 | sp2 | P2 | 33.0 | 98 | | | | | | | 140.0 | 146.6 | | | | | | | | |
| C | 10136 | 8780.8 | PD0017 | 233.95 | sp2 | P2 | 35.3 | 95 | | | | -0.7 | 1.2 | | 140.7 | 147.7 | | | | | | | | |
| C | 10136 | 8780.8 | PD0017 | 343.36 | sp2 | P2 | 145.3 | 97 | | | -23.0 | -9.0 | 12.8 | | 137.0 | 148.5 | | | | | | | | |
| C | 10136 | 8780.8 | PD0017 | 406.1 | sp2 | P2 | 82.5 | 94 | | | -21.7 | -5.2 | 8.1 | | 139.4 | 153.6 | | | | | | | | |
| C | 10136 | 8780.8 | PD0017 | 343.36 | sp2 | P2 | 70.7 | 97 | | | | | | | 142.7 | 154.2 | | | | | | | | |
| C | 10136 | 8780.8 | PD0017 | 233.95 | sp2 | P2 | 117.8 | 85 | | | | -1.0 | 1.7 | | 150.6 | 157.6 | | | | | | | | |
| C | 10136 | 8780.8 | PD0017 | 223.95 | sp2 | P2 | 37.7 | 96 | | | | -7.3 | 10.9 | | 151.3 | 157.9 | | | | | | | | |
| C | 10136 | 8780.8 | PD0017 | 223.95 | sp2 | P2 | | 97 | | | | | | | 151.5 | 158.1 | | | | | | | | |
| C | 10136 | 8780.8 | PD0017 | 233.95 | sp2 | P2 | 412.3 | 93 | | | | -0.1 | 0.2 | | 151.8 | 158.8 | | | | | | | | |
| C | 10136 | 8780.8 | PD0017 | 223.95 | sp2 | P2 | | 95 | -50.2 | brown | -23.8 | | | | 152.5 | 159.1 | | | | | | | | |
| C | 10136 | 8780.8 | PD0017 | 223.95 | sp2 | P2 | | | | | | -7.3 | 10.9 | | 155.8 | 162.4 | | | | | | | | |
| C | 10136 | 8780.8 | PD0017 | 233.95 | sp2 | P2 | 56.5 | 95 | | | | -0.8 | 1.4 | | 160.5 | 167.5 | | | | | | | | |
| C | 10136 | 8780.8 | PD0017 | 233.95 | sp2 | P2 | 23.6 | 93 | | | | -0.7 | 1.2 | | 160.5 | 167.5 | | | | | | | | |
| C | 10136 | 8780.8 | PD0017 | 223.95 | sp2 | P2 | | | | | | -4.2 | 6.7 | | 161.4 | 168.0 | | | | | | | | |
| C | 10136 | 8780.8 | PD0017 | 233.95 | sp2 | P2 | 28.3 | | | | | -0.5 | 0.9 | | 162.0 | 169.0 | | | | | | | | |
| C | 10136 | 8780.8 | PD0017 | 233.95 | sp2 | P2 | 70.7 | 88 | | | | | | | 164.2 | 171.2 | | | | | | | | |
| C | 10136 | 8780.8 | PD0017 | 223.95 | sp2 | P2 | | | | | | -3.9 | 6.3 | | 166.2 | 172.8 | | | | | | | | |
| C | 10136 | 8780.8 | PD0017 | 406.1 | sp2 | P2 | 88.0 | 96 | | | -21.6 | -5.2 | 8.1 | | 187.5 | 201.7 | | | | | | | | |
| C | 10136 | 8780.8 | PD0017 | 406.1 | sp2 | P2 | 88.0 | 96 | | | -21.6 | -5.2 | 8.1 | | 187.5 | 201.7 | | | | | | | | |
| C | 10136 | 8780.8 | PD0017 | 223.95 | sp2 | P2 | | 95 | | | | -0.1 | 0.2 | | 199.8 | 206.4 | | | | | | | | |
| C | 10136 | 8780.8 | PD0017 | 223.95 | sp2 | P2 | | 95 | | | | -0.8 | 1.4 | | 201.6 | 208.2 | | | | | | | | |

**Appendix 9.1 cont.**

| Zone | East (m) | North (m) | Drill hole | Depth (m) | Host min | FI type | FI area (µm) | % fill | Tm 1 (°C) | freeze colour | Tm 2 (°C) | Tm 3 (°C) | Salinity | Tm 4 (°C) | Th 1 (°C) | Th 2 (°C) | Min 1 | Area1 (µm2) | Td 1 (°C) | Min 2 | Area2 (µm2) | Td 2 (°C) | Min 3 | Area3 (µm2) |
|---|---|---|---|---|---|---|---|---|---|---|---|---|---|---|---|---|---|---|---|---|---|---|---|---|
| C | 10136 | 8780.8 | PD0017 | 406.1 | sp2 | P2 | 157.1 | 93 | | | -22.9 | -7.3 | 10.9 | | 252.6 | 266.8 | | | | | | | | |
| C | 10136 | 8780.8 | PD0017 | 223.95 | sp2 | P2 | 125.7 | 97 | | | -22.1 | -18.6 | 21.4 | | | | | | | | | | | |
| C | 10136 | 8780.8 | PD0017 | 223.95 | sp2 | P2 | 131.9 | 97 | | | -24.5 | -17.5 | 20.6 | | | | | | | | | | | |
| C | 10136 | 8780.8 | PD0017 | 223.95 | sp2 | P2 | | | | | | -12.2 | 16.1 | | | | | | | | | | | |
| C | 10136 | 8780.8 | PD0017 | 223.95 | sp2 | P2 | 37.7 | 97 | | | | -6.0 | 9.2 | | | | | | | | | | | |
| C | 10136 | 8780.8 | PD0017 | 223.95 | sp2 | P2 | 294.5 | 96 | | | -28.3 | -5.0 | 9.83 | 4.5 | | | | | | | | | | |
| C | 10136 | 8780.8 | PD0017 | 343.36 | sp2 | P2 | 84.8 | 97 | | | | -2.3 | 3.9 | | | | | | | | | | | |
| C | 10136 | 8780.8 | PD0017 | 223.95 | sp2 | P2 | | 98 | | | | -0.9 | 1.6 | | | | | | | | | | | |
| C | 10136 | 8780.8 | PD0017 | 233.95 | sp2 | P2 | 35.3 | 90 | | | | -0.7 | 1.2 | | | | | | | | | | | |
| C | 10136 | 8780.8 | PD0017 | 233.95 | sp2 | P2 | 16.5 | 95 | | | | -0.5 | 0.9 | | | | | | | | | | | |
| C | 10136 | 8780.8 | PD0017 | 233.95 | sp2 | P2 | 23.6 | 93 | | | | -0.5 | 0.9 | | | | | | | | | | | |
| C | 10136 | 8780.8 | PD0017 | 223.95 | sp2 | P2 | 141.4 | 95 | | | | | 9.83 | 4.5 | | | | | | | | | | |
| C | 10136 | 8780.8 | PD0017 | 223.95 | sp2 | P2 | 1099.6 | 96 | | brown | | | | | | | | | | | | | | |
| C | 10125 | 8960.9 | PD0024 | 241.1 | sp2 | P2 | 94.2 | 98 | | | | -11.5 | 15.5 | | 154.3 | 157.2 | | | | | | | | |
| C | 10125 | 8960.9 | PD0024 | 241.1 | sp2 | P2 | 157.1 | 96 | | | | -0.4 | 0.7 | | 183.1 | 186.0 | | | | | | | | |
| C | 10125 | 8960.9 | PD0024 | 241.1 | sp2 | P2 | 1413.7 | 96 | | | | -13.2 | 17.1 | | | | | | | | | | | |
| C | 10125 | 8960.9 | PD0024 | 241.1 | sp2 | P2 | 219.9 | 96 | | | | -12.8 | 16.7 | | | | | | | | | | | |
| C | 10125 | 8960.9 | PD0024 | 241.1 | sp2 | P2 | 235.6 | 95 | | | | -9.7 | 13.6 | | | | | | | | | | | |
| C | 10125 | 8960.9 | PD0024 | 241.1 | sp2 | P2 | 235.6 | 97 | | | | -8.9 | 12.7 | | | | | | | | | | | |
| C | 10026 | 9293.6 | PD0027 | 184.7 | sp2 | P2 | 28.3 | 96 | | | | -0.5 | 0.9 | | 135.0 | 140.3 | | | | | | | | |
| C | 10026 | 9293.6 | PD0027 | 184.7 | sp2 | P2 | 106.8 | 96 | | | | -0.4 | 0.7 | | 136.2 | 141.5 | | | | | | | | |
| C | 10026 | 9293.6 | PD0027 | 184.7 | sp2 | P2 | 84.8 | 96 | | | | -0.7 | 1.2 | | 138.5 | 143.8 | | | | | | | | |
| C | 10026 | 9293.6 | PD0027 | 184.7 | sp2 | P2 | 37.7 | 95 | | | | -3.5 | 5.7 | | 142.6 | 147.9 | | | | | | | | |
| C | 10026 | 9293.6 | PD0027 | 184.7 | sp2 | P2 | 50.3 | 96 | | | | -0.4 | 0.7 | | 143.3 | 148.6 | | | | | | | | |
| C | 10026 | 9293.6 | PD0027 | 184.7 | sp2 | P2 | 62.8 | 97 | | | | -7.0 | 10.5 | | 143.6 | 148.9 | | | | | | | | |
| C | 10026 | 9293.6 | PD0027 | 184.7 | sp2 | P2 | 103.7 | | | | | -0.1 | 0.2 | | 146.0 | 151.3 | | | | | | | | |
| C | 10026 | 9293.6 | PD0027 | 184.7 | sp2 | P2 | 39.3 | 96 | | | | -5.0 | 7.9 | | 148.7 | 154.0 | | | | | | | | |
| C | 10026 | 9293.6 | PD0027 | 184.7 | sp2 | P2 | 942.5 | 97 | | | | -0.3 | 0.5 | | 149.7 | 155.0 | | | | | | | | |
| C | 10026 | 9293.6 | PD0027 | 184.7 | sp2 | P2 | 954.3 | 97 | | | | -0.2 | 0.4 | | 151.0 | 156.3 | | | | | | | | |
| C | 10026 | 9293.6 | PD0027 | 184.7 | sp2 | P2 | 39.3 | 98 | | | | -5.0 | 7.9 | | 152.8 | 158.1 | | | | | | | | |
| C | 10026 | 9293.6 | PD0027 | 184.7 | sp2 | P2 | 23.6 | 96 | | | | -4.6 | 7.3 | | 161.5 | 166.8 | | | | | | | | |
| C | 10026 | 9293.6 | PD0027 | 184.7 | sp2 | P2 | 283.5 | 97 | | | -25.5 | -8.7 | 12.5 | | | | | | | | | | | |
| C | 10026 | 9293.6 | PD0027 | 184.7 | sp2 | P2 | 483.8 | 97 | | | | -8.5 | 12.3 | | | | | | | | | | | |
| C | 10026 | 9293.6 | PD0027 | 184.7 | sp2 | P2 | 212.1 | | | | | -1.0 | 1.7 | | | | | | | | | | | |

**Appendix 9.1 cont.**

| Zone | East (m) | North (m) | Drill hole | Depth (m) | Host min | FI type | FI area (µm) | % fill | Tm 1 (°C) | freeze colour | Tm 2 (°C) | Tm 3 (°C) | Salinity | Tm 4 (°C) | Th 1 (°C) | Th 2 (°C) | Min 1 | Area1 (µm2) | Td 1 (°C) | Min 2 | Area2 (µm2) | Td 2 (°C) | Min 3 | Area3 (µm2) |
|---|---|---|---|---|---|---|---|---|---|---|---|---|---|---|---|---|---|---|---|---|---|---|---|---|
| C | 10026 | 9293.6 | PD0027 | 184.7 | sp2 | P2 | 2356.2 | 97 | | | | -0.4 | 0.7 | | | | | | | | | | | |
| C | 10026 | 9293.6 | PD0027 | 184.7 | sp2 | P2 | 28.3 | 95 | | | | -0.2 | 0.4 | | | | | | | | | | | |
| C | 10026 | 9293.6 | PD0027 | 184.7 | sp2 | P2 | 157.1 | 97 | | | | -0.1 | 0.2 | | | | | | | | | | | |
| C | 10461 | 8746 | PD0028 | 347.38 | sp2 | P2 | | | | | | -2.1 | 3.5 | | 171.2 | 182.4 | | | | | | | | |
| C | 10461 | 8746 | PD0028 | 347.38 | sp2 | P2 | | | | | | -1.3 | 2.2 | | 194.8 | 206.0 | | | | | | | | |
| C | 10461 | 8746 | PD0028 | 347.38 | sp2 | P2 | | | | | | -1.6 | 2.7 | | 209.8 | 221.0 | | | | | | | | |
| C | 10461 | 8746 | PD0028 | 347.38 | sp2 | P2 | | | | | | -1.3 | 2.2 | | 218.3 | 229.5 | | | | | | | | |
| C | 10461 | 8746 | PD0028 | 347.38 | sp2 | P2 | | | | | | -1.6 | 2.7 | | 219.0 | 230.2 | | | | | | | | |
| C | 10461 | 8746 | PD0028 | 347.38 | sp2 | P2 | | | | | | -2.1 | 3.5 | | 230.4 | 241.6 | | | | | | | | |
| C | 10461 | 8746 | PD0028 | 347.38 | sp2 | P2 | | | | | | -1.7 | 2.9 | | | | | | | | | | | |
| S | 10235 | 7406 | PD0032 | 223.33 | sp2 | P2 | 196.3 | 96 | | | | -0.4 | 0.7 | | 153.0 | 159.9 | | | | | | | | |
| S | 10235 | 7406 | PD0032 | 223.33 | sp2 | P2 | 141.4 | 95 | | | | -0.9 | 1.6 | | 186.5 | 193.4 | | | | | | | | |
| S | 10235 | 7406 | PD0032 | 223.33 | sp2 | P2 | 377.0 | 98 | | | -24.3 | -9.7 | 13.6 | | | | | | | | | | | |
| S | 10235 | 7406 | PD0032 | 223.33 | sp2 | P2 | 117.8 | 98 | | | | -8.8 | 12.6 | | | | | | | | | | | |
| S | 10235 | 7406 | PD0032 | 223.33 | sp2 | P2 | 78.5 | 97 | | | | -7.5 | 11.1 | | | | | | | | | | | |
| S | 10235 | 7406 | PD0032 | 223.33 | sp2 | P2 | 1570.8 | 98 | | brown | | -1.3 | 2.2 | | | | | | | | | | | |
| S | 10235 | 7406 | PD0032 | 223.33 | sp2 | P2 | 66.0 | 90 | | | | -0.6 | 1.1 | | | | | | | | | | | |
| S | 10235 | 7406 | PD0032 | 223.33 | sp2 | P2 | 94.2 | 97 | | | | -0.4 | 0.7 | | | | | | | | | | | |
| S | 10235 | 7406 | PD0032 | 223.33 | sp2 | P2 | 66.0 | 85 | | | | -0.3 | 0.5 | | | | | | | | | | | |
| N | 10663 | 9391.9 | PD0016 | 262.77 | sp2 | S2 | 188.5 | | | brown | -25.6 | -9.5 | 13.4 | | | | carb | 4.0 | | | | | | |
| N | 10769 | 9800 | PD0006 | 258.2 | sp2 | P3 | 77.8 | 98 | | brown | | -16.3 | 19.7 | | 95.7 | 104.1 | carb | 1.0 | | | | | | |
| N | 10769 | 9800 | PD0006 | 258.2 | sp2 | P3 | 47.1 | 96 | | | -24.4 | -19.5 | 22.0 | | 155.5 | 163.9 | carb | 1.0 | | | | | | |
| N | 10769 | 9800 | PD0006 | 258.2 | sp2 | P3 | 131.9 | 95 | | | | -0.3 | 0.5 | | 167.5 | 175.9 | carb | 30.0 | | | | | | |
| N | 10769 | 9800 | PD0006 | 258.2 | sp2 | P3 | 66.0 | 95 | | | | -5.4 | 8.75 | 5.2 | 183.5 | 191.9 | carb | 6.0 | | | | | | |
| N | 10769 | 9800 | PD0006 | 258.2 | sp2 | P3 | 15.7 | 98 | | | | -1.4 | 2.4 | | | | carb | 1.0 | | | | | | |
| C | 10314 | 9200 | PD0008 | 150.3 | sp2 | P3 | | 96 | | | -24.6 | -20.4 | 22.6 | | 141.4 | 145.3 | carb | 2.0 | | | | | | |
| C | 10210 | 9200 | PD0011 | 146.52 | sp2 | P3 | 235.6 | 97 | | | -24.5 | -11.9 | 15.9 | | 124.5 | 128.2 | carb | 1.0 | | | | | | |
| C | 10210 | 9200 | PD0011 | 146.52 | sp2 | P3 | | | -52.1 | brown | -24.5 | | | | 124.5 | 128.2 | carb | 0.25 | | | | | | |
| C | 10210 | 9200 | PD0011 | 146.52 | sp2 | P3 | | | -51.0 | brown | -24.5 | -13.8 | 17.6 | | | | carb | 0.25 | | | | | | |
| N | 10663 | 9391.9 | PD0016 | 262.77 | sp2 | P3 | 37.7 | >99 | | brown | -29.6 | | | 11.1 | 125.6 | 132.8 | carb | 1.0 | | | | | | |
| N | 10663 | 9391.9 | PD0016 | 262.77 | sp2 | P3 | 628.3 | 95 | -51.2 | brown | -32.5 | -23.8 | 9.68 | 4.6 | 127.5 | 134.7 | carb | 81.0 | | ? | 12.0 | | | |
| N | 10663 | 9391.9 | PD0016 | 262.77 | sp2 | P3 | 50.3 | 99 | | | -24.3 | -22.8 | 24.2 | | 129.0 | 136.2 | ? | 0.25 | | | | | | |
| N | 10663 | 9391.9 | PD0016 | 262.77 | sp2 | P3 | 62.8 | 98 | | | | -6.4 | 9.7 | | 141.2 | 148.4 | carb | 9.0 | | | | | | |
| N | 10663 | 9391.9 | PD0016 | 262.77 | sp2 | P3 | 37.7 | 99 | | | | | | | 141.4 | 148.6 | carb | 1.0 | | | | | | |

**Appendix 9.1 cont.**

| Zone | East (m) | North (m) | Drill hole | Depth (m) | Host min | FI type | FI area (µm) | % fill | Tm 1 (°C) | freeze colour | Tm 2 (°C) | Tm 3 (°C) | Salinity | Tm 4 (°C) | Th 1 (°C) | Th 2 (°C) | Min 1 | Area1 (µm2) | Td 1 (°C) | Min 2 | Area2 (µm2) | Td 2 (°C) | Min 3 | Area3 (µm2) |
|---|---|---|---|---|---|---|---|---|---|---|---|---|---|---|---|---|---|---|---|---|---|---|---|---|
| C | 10136 | 8780.8 | PD0017 | 233.95 | sp2 | P3 | 235.6 | 93 | | | | -0.5 | 0.9 | | 126.1 | 133.1 | carb | 16.0 | | | | | | |
| C | 10136 | 8780.8 | PD0017 | 233.95 | sp2 | P3 | 157.1 | 95 | | | | | | | 135.6 | 142.6 | carb | 9.0 | | ? | 9.0 | | | |
| C | 10136 | 8780.8 | PD0017 | 233.95 | sp2 | P3 | 37.7 | 95 | | | | -0.5 | 0.9 | | 143.9 | 150.9 | carb | 1.0 | | | | | | |
| C | 10136 | 8780.8 | PD0017 | 233.95 | sp2 | P3 | 282.7 | 93 | | | | -0.6 | 1.1 | | 151.7 | 158.7 | carb | 8.0 | | | | | | |
| C | 10136 | 8780.8 | PD0017 | 223.95 | sp2 | P3 | 157.1 | 97 | | | | -5.1 | 9.83 | 4.5 | | | carb | 4.0 | | | | | | |
| C | 10136 | 8780.8 | PD0017 | 233.95 | sp2 | P3 | 22.0 | 94 | | | | -0.6 | 1.1 | | | | carb | 1.0 | | | | | | |
| C | 10136 | 8780.8 | PD0017 | 233.95 | sp2 | P3 | 282.7 | 93 | | | | -0.4 | 0.7 | | | | carb | 6.0 | | | | | | |
| C | 10136 | 8780.8 | PD0017 | 233.95 | sp2 | P3 | 44.0 | 88 | | | | -0.8 | 1.4 | | | | carb | 4.0 | | | | | | |
| N | 10663 | 9391.9 | PD0016 | 262.77 | sp2 | S2 | 94.2 | 100 | | | | -20.7 | 22.8 | | | | carb | 6.0 | | | | | | |
| N | 10769 | 9800 | PD0006 | 258.2 | sp2 | P3 | 207.3 | 95 | | | -22.7 | -2.5 | 4.2 | | 147.0 | 155.4 | carb | 6.0 | | | | | | |
| N | 10769 | 9800 | PD0006 | 258.2 | sp2 | P3 | 62.8 | 94 | | | | -7.8 | 11.5 | | 154.3 | 162.7 | carb | 1.0 | | | | | | |
| N | 10769 | 9800 | PD0006 | 258.2 | sp2 | P3 | 56.5 | 95 | | | | -1.9 | 3.2 | | 161.0 | 169.4 | carb | 1.0 | | | | | | |
| N | 10769 | 9800 | PD0006 | 258.2 | sp2 | P3 | 353.4 | 96 | | | -23.8 | -7.2 | 10.7 | | 171.9 | 180.3 | carb | 12.0 | | | | | | |
| N | 10769 | 9800 | PD0006 | 258.2 | sp2 | P3 | 99.0 | 97 | | | | | | | 182.8 | 191.2 | carb | 2.0 | | | | | | |
| N | 10769 | 9800 | PD0006 | 258.2 | sp2 | P3 | 62.8 | 94 | | | | -2.0 | 3.4 | | 184.6 | 193.0 | carb | 2.0 | | | | | | |
| N | 10769 | 9800 | PD0006 | 258.2 | sp2 | P3 | 78.5 | 96 | | | | -0.3 | 0.5 | | | | carb | 4.0 | | | | | | |
| N | 10769 | 9800 | PD0006 | 258.2 | sp2 | P3 | 84.8 | 93 | -55.0 | brown | -25.2 | -8.6 | 12.4 | | | | carb | 1.0 | | | | | | |
| C | 10314 | 9200 | PD0008 | 150.3 | sp2 | P3 | 37.7 | 96 | -50.5 | brown | -23.0 | -13.7 | 17.5 | | 134.4 | 138.3 | carb | 1.0 | | | | | | |
| C | 10314 | 9200 | PD0008 | 150.3 | sp2 | P3 | 33.0 | 96 | | | -24.7 | -18.8 | 21.5 | | | | carb | 1.0 | | | | | | |
| C | 10300 | 9000 | PD0010 | 163.45 | sp2 | P3 | 125.7 | 97 | | | | | 19.30 | -5.0 | 170.0 | 174.4 | carb | 0.25 | | | | | | |
| C | 10210 | 9200 | PD0011 | 146.52 | sp2 | P3 | | | | | | -12.0 | 16.0 | | 123.1 | 126.8 | carb | 0.25 | | | | | | |
| N | 10663 | 9391.9 | PD0016 | 262.77 | sp2 | P3 | 39.3 | 99 | | | | | | | 115.0 | 122.2 | carb | 0.25 | | | | | | |
| N | 10663 | 9391.9 | PD0016 | 262.77 | sp2 | P3 | 117.8 | 98 | | brown | -24.4 | -9.6 | 13.5 | | 119.5 | 126.7 | carb | 8.0 | | | | | | |
| N | 10663 | 9391.9 | PD0016 | 262.77 | sp2 | P3 | 1178.1 | 97 | -72.8 | | -25.2 | -11.0 | 15.0 | | 124.5 | 131.7 | carb | 25.0 | | | | | | |
| N | 10663 | 9391.9 | PD0016 | 262.77 | sp2 | P3 | 28.3 | 98 | | | | -23.3 | 24.5 | | 128.4 | 135.6 | carb | 0.25 | | | | | | |
| N | 10663 | 9391.9 | PD0016 | 262.77 | sp2 | P3 | 47.1 | 99 | | | | -6.4 | 9.7 | | 128.8 | 136.0 | carb | 0.25 | | | | | | |
| N | 10663 | 9391.9 | PD0016 | 262.77 | sp2 | P3 | 169.6 | 98 | | | | | | | 129.8 | 137.0 | carb | 4.0 | | | | | | |
| N | 10663 | 9391.9 | PD0016 | 273.4 | sp2 | P3 | 75.4 | 95 | | | | -1.2 | 2.1 | | 129.4 | 137.0 | carb | 1.0 | | | | | | |
| N | 10663 | 9391.9 | PD0016 | 262.77 | sp2 | P3 | 106.0 | >99 | | | | -6.5 | 9.9 | | 133.2 | 140.4 | carb | 4.0 | | | | | | |
| N | 10663 | 9391.9 | PD0016 | 262.77 | sp2 | P3 | 141.4 | 97 | | | | -6.4 | 9.7 | | 135.5 | 142.7 | carb | 25.0 | | | | | | |
| N | 10663 | 9391.9 | PD0016 | 262.77 | sp2 | P3 | 28.3 | 99 | | | -26.2 | -23.3 | 24.5 | | | | carb | 4.0 | | | | | | |
| N | 10663 | 9391.9 | PD0016 | 262.77 | sp2 | P3 | 137.4 | 99 | | | | -1.2 | 2.1 | | | | carb | 4.0 | | | | | | |
| N | 10663 | 9391.9 | PD0016 | 262.77 | sp2 | P3 | 27.5 | >99 | | | | -6.5 | 9.9 | | | | carb | 0.25 | | | | | | |
| N | 10663 | 9391.9 | PD0016 | 305.6 | sp2 | P3 | | | | brown | -24.9 | -22.0 | 23.7 | | | | carb | 16.0 | | | | | | |

**Appendix 9.1 cont.**

| Zone | East (m) | North (m) | Drill hole | Depth (m) | Host min | FI type | FI area (µm) | % fill | Tm 1 (°C) | freeze colour | Tm 2 (°C) | Tm 3 (°C) | Salinity | Tm 4 (°C) | Th 1 (°C) | Th 2 (°C) | Min 1 | Area1 (µm2) | Td 1 (°C) | Min 2 | Area2 (µm2) | Td 2 (°C) | Min 3 | Area3 (µm2) |
|---|---|---|---|---|---|---|---|---|---|---|---|---|---|---|---|---|---|---|---|---|---|---|---|---|
| N | 10663 | 9391.9 | PD0016 | 305.6 | sp2 | P3 | | | -52.6 | brown | -31.3 | | | | | | carb | 4.0 | | | | | | |
| C | 10136 | 8780.8 | PD0017 | 343.36 | sp2 | P3 | 1963.5 | 95 | | | -22.6 | -15.1 | 18.7 | | 108.6 | 120.1 | carb | 100 | | | | | | |
| C | 10136 | 8780.8 | PD0017 | 223.95 | sp2 | P3 | 138.2 | 95 | | | -23.1 | -20.0 | 22.4 | | 127.6 | 134.2 | carb | 1.0 | | | | | | |
| C | 10136 | 8780.8 | PD0017 | 233.95 | sp2 | P3 | 1413.7 | 96 | -53.3 | brown | -26.2 | -13.2 | | 19.8 | 133.0 | 140.0 | carb | 56.0 | | hal | 36.0 | 66.2 | | |
| C | 10136 | 8780.8 | PD0017 | 233.95 | sp2 | P3 | 131.9 | 95 | | | | -0.4 | 0.7 | | 134.9 | 141.9 | carb | 25.0 | | | | | | |
| C | 10136 | 8780.8 | PD0017 | 233.95 | sp2 | P3 | 37.7 | 94 | -53.4 | brown | -24.4 | -12.1 | 16.1 | | 137.0 | 144.0 | carb | 4.0 | | ? | 1.0 | | | |
| C | 10136 | 8780.8 | PD0017 | 233.95 | sp2 | P3 | | 93 | | | | | | | 140.5 | 147.5 | carb | 1.0 | | ? | 1.0 | | | |
| C | 10136 | 8780.8 | PD0017 | 233.95 | sp2 | P3 | 47.1 | 90 | | | | -0.4 | 0.7 | | 143.8 | 150.8 | carb | 9.0 | | | | | | |
| C | 10136 | 8780.8 | PD0017 | 233.95 | sp2 | P3 | 58.9 | 90 | | | | -1.2 | 2.1 | | 143.8 | 150.8 | carb | 9.0 | | | | | | |
| C | 10136 | 8780.8 | PD0017 | 223.95 | sp2 | P3 | | 93 | | brown | -25.1 | -20.1 | 22.4 | | 149.3 | 155.9 | carb | 2.0 | | | | | | |
| C | 10136 | 8780.8 | PD0017 | 233.95 | sp2 | P3 | 18.8 | 90 | | | | -1.1 | 1.9 | | 150.1 | 157.1 | carb | 1.0 | | | | | | |
| C | 10136 | 8780.8 | PD0017 | 233.95 | sp2 | P3 | 50.3 | 93 | | | | -0.4 | 0.7 | | 151.9 | 158.9 | carb | 4.0 | | | | | | |
| C | 10136 | 8780.8 | PD0017 | 233.95 | sp2 | P3 | 235.6 | 93 | | | | -0.4 | 0.7 | | 154.1 | 161.1 | carb | 18.0 | | | | | | |
| C | 10136 | 8780.8 | PD0017 | 233.95 | sp2 | P3 | 55.0 | 88 | | | | -0.3 | 0.5 | | 157.5 | 164.5 | carb | 9.0 | | | | | | |
| C | 10136 | 8780.8 | PD0017 | 233.95 | sp2 | P3 | 33.0 | | | | | -0.4 | 0.7 | | 157.5 | 164.5 | carb | 16.0 | | | | | | |
| C | 10136 | 8780.8 | PD0017 | 233.95 | sp2 | P3 | 18.8 | 93 | -53.4 | brown | -24.4 | -12.6 | 16.5 | | 158.2 | 165.2 | carb | 1.0 | | ? | 1.0 | | | |
| C | 10136 | 8780.8 | PD0017 | 233.95 | sp2 | P3 | 176.7 | 90 | | | | -0.6 | 1.1 | | 158.3 | 165.3 | carb | 16.0 | | | | | | |
| C | 10136 | 8780.8 | PD0017 | 233.95 | sp2 | P3 | 150.8 | 92 | | | | -0.4 | 0.7 | | 158.5 | 165.5 | carb | 25.0 | | | | | | |
| C | 10136 | 8780.8 | PD0017 | 233.95 | sp2 | P3 | 58.9 | 90 | | | | -0.4 | 0.7 | | 159.2 | 166.2 | carb | 9.0 | | | | | | |
| C | 10136 | 8780.8 | PD0017 | 233.95 | sp2 | P3 | 353.4 | 92 | | | | -0.9 | 1.6 | | 160.6 | 167.6 | carb | 49.0 | | | | | | |
| C | 10136 | 8780.8 | PD0017 | 233.95 | sp2 | P3 | 39.3 | 95 | | | | -0.4 | 0.7 | | 161.0 | 168.0 | carb | 4.0 | | | | | | |
| C | 10136 | 8780.8 | PD0017 | 233.95 | sp2 | P3 | 61.3 | 90 | | | | -0.4 | 0.7 | | 161.5 | 168.5 | carb | 4.0 | | | | | | |
| C | 10136 | 8780.8 | PD0017 | 233.95 | sp2 | P3 | 23.6 | 88 | | | | -0.3 | 0.5 | | 161.6 | 168.6 | carb | 4.0 | | | | | | |
| C | 10136 | 8780.8 | PD0017 | 233.95 | sp2 | P3 | 44.0 | 88 | | | | -0.5 | 0.9 | | 164.8 | 171.8 | carb | | | | | | | |
| C | 10136 | 8780.8 | PD0017 | 233.95 | sp2 | P3 | 70.7 | 90 | | | | -0.4 | 0.7 | | 170.0 | 177.0 | carb | 4.0 | | | | | | |
| C | 10136 | 8780.8 | PD0017 | 233.95 | sp2 | P3 | 25.1 | 93 | | | | -1.6 | 2.7 | | 170.1 | 177.1 | carb | 1.0 | | | | | | |
| C | 10136 | 8780.8 | PD0017 | 343.36 | sp2 | P3 | 56.5 | 95 | | | -25.0 | -16.8 | 20.1 | | | | carb | 1.0 | | | | | | |
| C | 10136 | 8780.8 | PD0017 | 233.95 | sp2 | P3 | 125.7 | 95 | | | | -0.6 | 1.1 | | | | carb | 9.0 | | | | | | |
| C | 10136 | 8780.8 | PD0017 | 233.95 | sp2 | P3 | 31.4 | 94 | | | | -1.1 | 1.9 | | | | carb | 9.0 | | | | | | |
| C | 10136 | 8780.8 | PD0017 | 233.95 | sp2 | P3 | 196.3 | 90 | | | | -0.6 | 1.1 | | | | carb | 18.0 | | | | | | |
| C | 10461 | 8746 | PD0028 | 347.38 | sp2 | P3 | 628.3 | 98 | | | -26.4 | -4.7 | 7.4 | | | | carb | 48.0 | | | | | | |
| N | 10769 | 9800 | PD0006 | 258.2 | sp2 | P3 | 432.0 | 97 | | brown | -25.5 | -5.1 | 8.0 | | 105.4 | 113.8 | carb | 35.0 | | | | | | |
| N | 10769 | 9800 | PD0006 | 258.2 | sp2 | P3 | 62.8 | 98 | | brown | | -6.5 | 9.9 | | 114.2 | 122.6 | carb | 4.0 | | | | | | |
| N | 10769 | 9800 | PD0006 | 258.2 | sp2 | P3 | 113.1 | 97 | | | -25.5 | | | | | | carb | 6.0 | | | | | | |

## Appendix 9.1 cont.

| Zone | East (m) | North (m) | Drill hole | Depth (m) | Host min | FI type | FI area (µm) | % fill | Tm 1 (°C) | freeze colour | Tm 2 (°C) | Tm 3 (°C) | Salinity | Tm 4 (°C) | Th 1 (°C) | Th 2 (°C) | Min 1 | Area1 (µm2) | Td 1 (°C) | Min 2 | Area2 (µm2) | Td 2 (°C) | Min 3 | Area3 (µm2) |
|---|---|---|---|---|---|---|---|---|---|---|---|---|---|---|---|---|---|---|---|---|---|---|---|---|
| N | 10663 | 9391.9 | PD0016 | 262.77 | sp2 | P3 | 471.2 | 99 | | | | | | | 139.0 | 146.2 | hem | 25.0 | | carb | 35.0 | | | |
| N | 10663 | 9391.9 | PD0016 | 262.77 | sp2 | P3 | 314.2 | 97 | | brown | -29.6 | -14.1 | 9.68 | 4.6 | 123.3 | 130.5 | hal | 4.0 | 63.5 | carb | 49.0 | | op | <1 |
| N | 10663 | 9391.9 | PD0016 | 262.77 | sp2 | P3 | 75.4 | 99 | | brown | -25.6 | -10.7 | 26.3 | | 125.4 | 132.6 | hal | 4.0 | 1.7 | | | | | |
| C | 10136 | 8780.8 | PD0017 | 223.95 | sp2 | P3 | | 95 | | | -24.8 | -9.0 | 12.8 | | 127.5 | 134.1 | op | 4.0 | | | | | | |
| N | 10769 | 9800 | PD0006 | 258.2 | sp2 | P3 | 122.5 | >99 | | | | -7.4 | 11.0 | | 113.5 | 121.9 | ser | 24.0 | | | | | | |

Zone: N = northern, C = central, S = southern

East: Local grid, easting coordinate of drill hole collar

North: Local grid, northing coordinate of drill hole collar

Host min: (fluid inclusion host mineral), qz1 = quartz 1, sp2 = sphalerite 2, qz3 = quartz 3, qz ph = quartz phenocrysts in the strongly altered rhyolite intrusion

FI area: Fluid inclusion area calculated as an ellipse by estimatating the maximum length and maximum width of each fluid inclusion.

% fill: Estimated volume % liquid in the fluid inclusion (Shepherd et al., 1985)

Tm 1: First melting phenomenon

freeze colour: Colour of the fluid inclusion upon freezing

Tm 2: Final melting temperature of hydrohalite

Tm 3: Final ice melting temperature

Salinity: wt.% NaCl equivalent

Tm 4: Final clathrate melting temperature

Th 1: Liquid - vapour homogenisation temperature

Th 2: Pressure corrected liquid - vapour homogenisation temperature.

Min 1: Mineral inclusion; op = opaque, op(2) = 2 opaque inclusions, op(3) = 3 opaque inclusions, carb = carbonate, trem = tremolite, hem = hematite, ser = sericite, chl = chlorite, hal = halite, ? = unknown non-opaque mineral

Area 1: Area of mineral inclusion 1 calculated assuming a square shape

Td 1: Temperature of dissolution for mineral inclusion 1

Min 2: Mineral inclusion

Area 2: Area of mineral inclusion 2 calculated assuming a square shape

Td 2: Temperature of dissolution for mineral inclusion 2

Min 3: Mineral inclusion

Area 3: Area of mineral inclusion 3 calculated assuming a square shape

## Appendix 10.1

Oxygen isotope data for carbonate minerals

| Description | Drill hole | Depth (m) | North (m) | East (m) | ∂13C V-SMOW | ∂18O V-SMOW | Fluid temp °C | *∂18O | **∂13C |
|---|---|---|---|---|---|---|---|---|---|
| DP breccia matrix | PD0025 | 538.7 | 7956.7 | 10051.6 | -4.24 | 7.74 | 154 | -4.61 | -5.57 |
| DP breccia matrix | PD0028 | 345.32 | 8746 | 10461.3 | -3.95 | 12.65 | 154 | 0.31 | -5.29 |
| DP breccia matrix | PD0028 | 507.55 | 8746 | 10461.3 | -2.79 | 9.67 | 154 | -2.68 | -4.13 |
| DP breccia matrix | PD0010 | 171.34 | 9000 | 10300 | -2.27 | 14.16 | 154 | 1.81 | -3.61 |
| DP breccia matrix | PD0027 | 476.2 | 9293.6 | 10025.5 | -2.20 | 10.85 | 154 | -1.50 | -3.54 |
| DP breccia matrix | PD0024 | 385.53 | 8960.9 | 10125.4 | -2.05 | 8.10 | 154 | -4.24 | -3.39 |
| DP breccia matrix | PD0026 | 300.99 | 9060.3 | 10104.3 | -1.87 | 13.38 | 154 | 1.03 | -3.21 |
| Late alt overprint | PD0032 | 285.3 | 7406 | 10235 | -2.56 | 5.19 | 243 | -2.36 | -1.38 |
| Late alt overprint | PD0032 | 252.07 | 7406 | 10235 | -2.94 | 4.09 | 282 | -2.04 | -1.15 |
| Late alt overprint | PD0032 | 386.71 | 7406 | 10235 | -1.79 | 7.23 | 205 | -2.04 | -1.47 |
| Late alt overprint | PD0032 | 120.65 | 7406 | 10235 | -1.58 | 8.41 | 200 | -1.12 | -1.39 |
| Late alt overprint | PD0032 | 223.3 | 7406 | 10235 | -0.55 | 8.18 | 231 | 0.13 | 0.39 |
| Marble | PD0007 | 100.4 | 10400 | 10791.5 | -0.39 | 19.89 | | | |
| Marble | PD0010 | 173.64 | 9000 | 10300 | -0.65 | 19.97 | | | |
| Marble | PD0010 | 217.63 | 9000 | 10300 | -1.08 | 19.01 | | | |
| Marble | PD0010 | 407.77 | 9000 | 10300 | 1.02 | 19.46 | | | |
| Marble | PD0011A | 381.25 | 9200 | 10210 | 0.46 | 19.37 | | | |
| Marble | PD0013 | 449.16 | 9800 | 10300 | 0.57 | 20.42 | | | |
| Marble | PD0015 | 478.4 | 9390.7 | 10226.9 | 1.22 | 20.73 | | | |
| Marble | PD0017 | 423.7 | 8780.8 | 10136.2 | 0.54 | 18.14 | | | |
| Marble | PD0017 | 461.15 | 8780.8 | 10136.2 | 1.08 | 20.69 | | | |
| Marble | PD0021 | 479.1 | 7564 | 10073.7 | 1.09 | 19.96 | | | |
| Marble | PD0022 | 267.06 | 8703.7 | 10075 | -0.16 | 19.98 | | | |
| Marble | PD0022 | 523.09 | 8703.7 | 10075 | 1.63 | 19.38 | | | |
| Marble | PD0024 | 399.67 | 8960.9 | 10125.4 | -0.19 | 16.05 | | | |
| Marble | PD0024 | 522.2 | 8960.9 | 10125.4 | -0.09 | 20.92 | | | |
| Marble | PD0024 | 522.4 | 8960.9 | 10125.4 | 0.34 | 19.14 | | | |
| Marble | PD0024 | 596.48 | 8960.9 | 10125.4 | 1.32 | 19.20 | | | |
| Marble | PD0025 | 603.37 | 7956.7 | 10051.6 | 0.60 | 16.26 | | | |
| Marble | PD0026 | 569.56 | 9060.3 | 10104.3 | 0.99 | 21.09 | | | |
| Marble | PD0027 | 483.33 | 9293.6 | 10025.5 | 0.32 | 19.75 | | | |
| Marble | PD0027 | 678.62 | 9293.6 | 10025.5 | 0.18 | 15.52 | | | |
| Marble | PD0028 | 291.22 | 8746 | 10461.3 | 0.93 | 18.82 | | | |
| Marble | PD0028 | 381.25 | 8746 | 10461.3 | 0.64 | 19.71 | | | |
| Marble | PD0029 | 250.2 | 8776.6 | 10329 | -0.09 | 19.02 | | | |
| Marble | PD0031 | 340.42 | 8023 | 10300 | 0.52 | 17.15 | | | |
| Marble | PD0031 | 531.81 | 8023 | 10300 | 0.70 | 17.34 | | | |
| Impure marble | PD0006 | 179.2 | 9800 | 10769 | -4.21 | 13.97 | | | |
| Impure marble | PD0006 | 382 | 9800 | 10769 | -1.01 | 13.94 | | | |
| Impure marble | PD0007 | 255.2 | 10400 | 10791.5 | -2.25 | 17.45 | | | |
| Impure marble | PD0008 | 116.26 | 9200 | 10314 | 0.20 | 15.34 | | | |
| Impure marble | PD0008 | 266.3 | 9200 | 10314 | -0.44 | 16.14 | | | |
| Impure marble | PD0008 | 277 | 9200 | 10314 | -1.71 | 13.00 | | | |
| Impure marble | PD0010 | 229.91 | 9000 | 10300 | -0.99 | 9.65 | | | |
| Impure marble | PD0013 | 153.5 | 9800 | 10300 | -0.88 | 17.25 | | | |
| Impure marble | PD0013 | 286 | 9800 | 10300 | -0.64 | 14.36 | | | |
| Impure marble | PD0015 | 523.8 | 9390.7 | 10226.9 | 0.37 | 17.73 | | | |
| Impure marble | PD0016 | 385.3 | 9391.9 | 10663.3 | -2.09 | 10.87 | | | |
| Impure marble | PD0031 | 416.07 | 8023 | 10300 | 0.48 | 14.89 | | | |
| Metasomatic marble | PD0001 | 127.45 | 10000 | 10868.5 | -0.06 | 17.03 | | | |
| Metasomatic marble | PD0001 | 227.84 | 10000 | 10868.5 | 0.34 | 18.01 | | | |
| Metasomatic marble | PD0001 | 291.3 | 10000 | 10868.5 | -0.58 | 12.79 | | | |
| Metasomatic marble | PD0006 | 218.3 | 9800 | 10769 | -0.12 | 17.04 | | | |
| Metasomatic marble | PD0006 | 368.85 | 9800 | 10769 | 0.06 | 16.56 | | | |
| Metasomatic marble | PD0006 | 380 | 9800 | 10769 | -1.15 | 14.46 | | | |
| Metasomatic marble | PD0007 | 116.2 | 10400 | 10791.5 | 0.24 | 16.77 | | | |

## Appendix 10.1 cont.

| Description | Drill hole | Depth (m) | North (m) | East (m) | ∂13C V-SMOW | ∂18O V-SMOW | Fluid temp °C | *∂18O calc-H2O | **∂13C calc-H2O |
|---|---|---|---|---|---|---|---|---|---|
| Metasomatic marble | PD0007 | 257.04 | 10400 | 10791.5 | 0.68 | 16.09 | | | |
| Metasomatic marble | PD0007 | 261.3 | 10400 | 10791.5 | -0.37 | 17.89 | | | |
| Metasomatic marble | PD0010 | 469.68 | 9000 | 10300 | -0.16 | 11.21 | | | |
| Metasomatic marble | PD0010 | 502.21 | 9000 | 10300 | 0.01 | 15.48 | | | |
| Metasomatic marble | PD0012 | 187.7 | 9600 | 10775 | 0.24 | 17.61 | | | |
| Metasomatic marble | PD0012 | 251.25 | 9600 | 10775 | -0.24 | 15.06 | | | |
| Metasomatic marble | PD0014 | 171.8 | 11200 | 11140 | -0.15 | 11.41 | | | |
| Metasomatic marble | PD0015 | 509.72 | 9390.7 | 10226.9 | -1.80 | 10.80 | | | |
| Metasomatic marble | PD0015 | 669.72 | 9390.7 | 10226.9 | 0.16 | 14.25 | | | |
| Metasomatic marble | PD0020 | 273.7 | 8275.7 | 10266.4 | -0.19 | 10.30 | | | |
| Metasomatic marble | PD0020 | 282.61 | 8275.7 | 10266.4 | -0.27 | 9.42 | | | |
| Metasomatic marble | PD0028 | 478.88 | 8746 | 10461.3 | -0.70 | 7.77 | | | |
| Margin carbonates | PD0024 | 401.28 | 8960.9 | 10125.4 | -0.92 | 14.23 | 154 | 1.88 | -2.26 |
| Margin carbonates | PD0021 | 451.87 | 7564 | 10073.7 | -1.37 | 14.61 | 154 | 2.27 | -2.71 |
| Margin carbonates | PD0006 | 247.27 | 9800 | 10769 | 0.68 | 14.69 | 154 | 2.35 | -0.66 |
| Margin carbonates | PD0008 | 150.6 | 9200 | 10314 | -3.77 | 14.87 | 154 | 2.52 | -5.11 |
| Intra-mineralisation | PD0028 | 367.28 | 8746 | 10461.3 | -5.56 | 8.68 | 154 | -3.67 | -6.90 |
| Intra-mineralisation | PD0015 | 731.12 | 9390.7 | 10226.9 | -1.43 | 9.22 | 154 | -3.13 | -2.77 |
| Intra-mineralisation | PD0019 | 467.12 | 8380.9 | 10408.4 | -2.56 | 9.34 | 154 | -3.01 | -3.90 |
| Intra-mineralisation | PD0013 | 131.6 | 9800 | 10300 | -4.87 | 9.55 | 154 | -2.79 | -6.21 |
| Intra-mineralisation | PD0026 | 365.62 | 9060.3 | 10104.3 | -4.24 | 9.67 | 154 | -2.68 | -5.58 |
| Intra-mineralisation | PD0016 | 273.68 | 9391.9 | 10663.3 | -1.62 | 9.92 | 154 | -2.43 | -2.96 |
| Intra-mineralisation | PD0008 | 322.4 | 9200 | 10314 | -4.82 | 10.07 | 154 | -2.28 | -6.16 |
| Intra-mineralisation | PD0016 | 261.8 | 9391.9 | 10663.3 | -1.81 | 10.35 | 154 | -1.99 | -3.15 |
| Intra-mineralisation | PD0008 | 117.5 | 9200 | 10314 | -5.56 | 10.37 | 154 | -1.98 | -6.90 |
| Intra-mineralisation | PD0008 | 115.92 | 9200 | 10314 | -3.07 | 10.48 | 154 | -1.87 | -4.41 |
| Intra-mineralisation | PD0008 | 247.62 | 9200 | 10314 | -1.34 | 10.61 | 154 | -1.73 | -2.67 |
| Intra-mineralisation | PD0008 | 235.39 | 9200 | 10314 | -2.53 | 10.69 | 154 | -1.66 | -3.87 |
| Intra-mineralisation | PD0016 | 273.54 | 9391.9 | 10663.3 | -0.38 | 10.98 | 154 | -1.37 | -1.72 |
| Intra-mineralisation | PD0028 | 366.22 | 8746 | 10461.3 | -3.33 | 11.44 | 154 | -0.91 | -4.67 |
| Intra-mineralisation | PD0011A | 369.36 | 9200 | 10210 | -3.95 | 11.49 | 154 | -0.86 | -5.29 |
| Intra-mineralisation | PD0025 | 351.98 | 7956.7 | 10051.6 | -3.72 | 11.56 | 154 | -0.79 | -5.06 |
| Intra-mineralisation | PD0008 | 235.05 | 9200 | 10314 | -3.28 | 11.56 | 154 | -0.79 | -4.62 |
| Intra-mineralisation | PD0008 | 289.83 | 9200 | 10314 | -4.20 | 11.59 | 154 | -0.76 | -5.54 |
| Intra-mineralisation | PD0027 | 463.81 | 9293.6 | 10025.5 | -3.17 | 11.98 | 154 | -0.37 | -4.51 |
| Intra-mineralisation | PD0022 | 241 | 8703.7 | 10075 | -4.25 | 12.32 | 154 | -0.02 | -5.59 |
| Intra-mineralisation | PD0017 | 343.36 | 8780.8 | 10136.2 | -4.17 | 12.54 | 154 | 0.19 | -5.51 |
| Halo. 12cm from vein | PD0006 | 246.545 | 9800 | 10769 | -0.16 | 14.85 | | | |
| Halo. 16cm from vein | PD0006 | 246.46 | 9800 | 10769 | -0.18 | 14.90 | | | |
| Halo. 20.5cm from vein | PD0006 | 246.41 | 9800 | 10769 | -0.16 | 14.88 | | | |
| Halo. 25.5cm from vein | PD0006 | 246.36 | 9800 | 10769 | 0.23 | 14.61 | | | |
| Halo. 5cm from contact. | PD0006 | 246.62 | 9800 | 10769 | -0.09 | 15.82 | | | |
| Halo. 8.5cm from vein. | PD0006 | 246.585 | 9800 | 10769 | -0.21 | 15.58 | | | |
| Halo.1cm from veint. | PD0006 | 246.67 | 9800 | 10769 | -5.46 | 15.23 | | | |

*∂18O calcite - H2O (Friedman and O'Neil, 1977

**∂13C calcite - H2O (Ohmoto and Rye, 1979)

## Appendix 10.2

X-ray diffractograms of silicate minerals used for hydrogen and oxygen isotope analyses. Samples were analysed by X-ray diffraction prior to treatment with Na-acetate to remove carbonate minerals (ref. Section 10.3.2).

Key to mineral abbreviations used in diffractograms

| | | |
|---|---|---|
| MS | = | Muscovite |
| CH | = | Chlorite |
| AB | = | Albite |
| M | = | Microcline |
| Q | = | Quartz |
| C | = | Calcite |
| D | = | Dolomite |
| A | = | Ankerite |
| PH | = | Phlogopite |
| PY? | = | Pyrite (uncertain) |
| T | = | Talc |

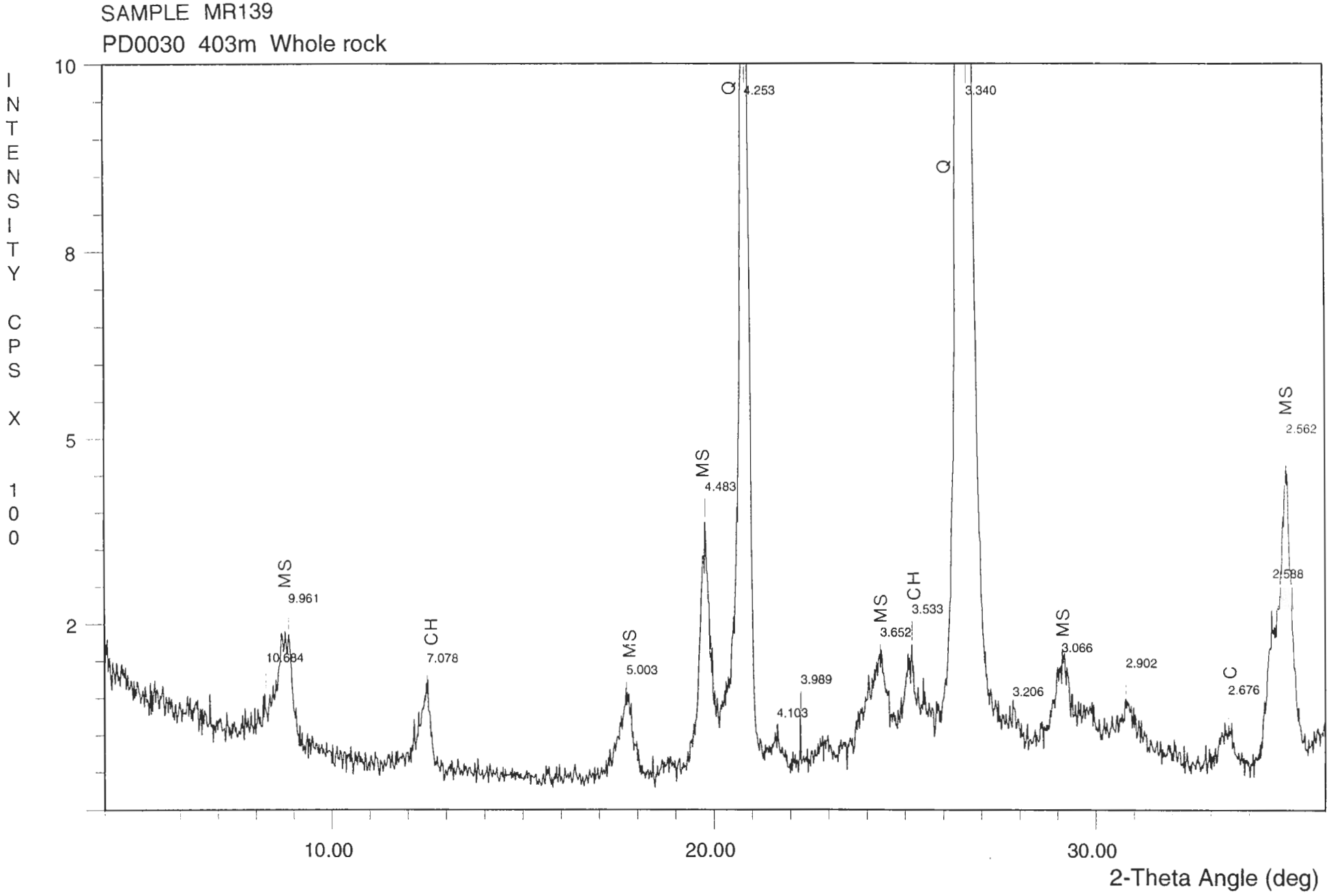
SAMPLE MR139
PD0030 403m Whole rock
INTENSITY CPS X 100
10
8
5
2
MS
9.961
10.684
CH
7.078
MS
5.003
MS
4.483
Q
4.253
4.103
3.989
MS
3.652
CH
3.533
Q
3.340
3.206
MS
3.066
2.902
C
2.676
MS
2.562
2.588
10.00
20.00
30.00
2-Theta Angle (deg)

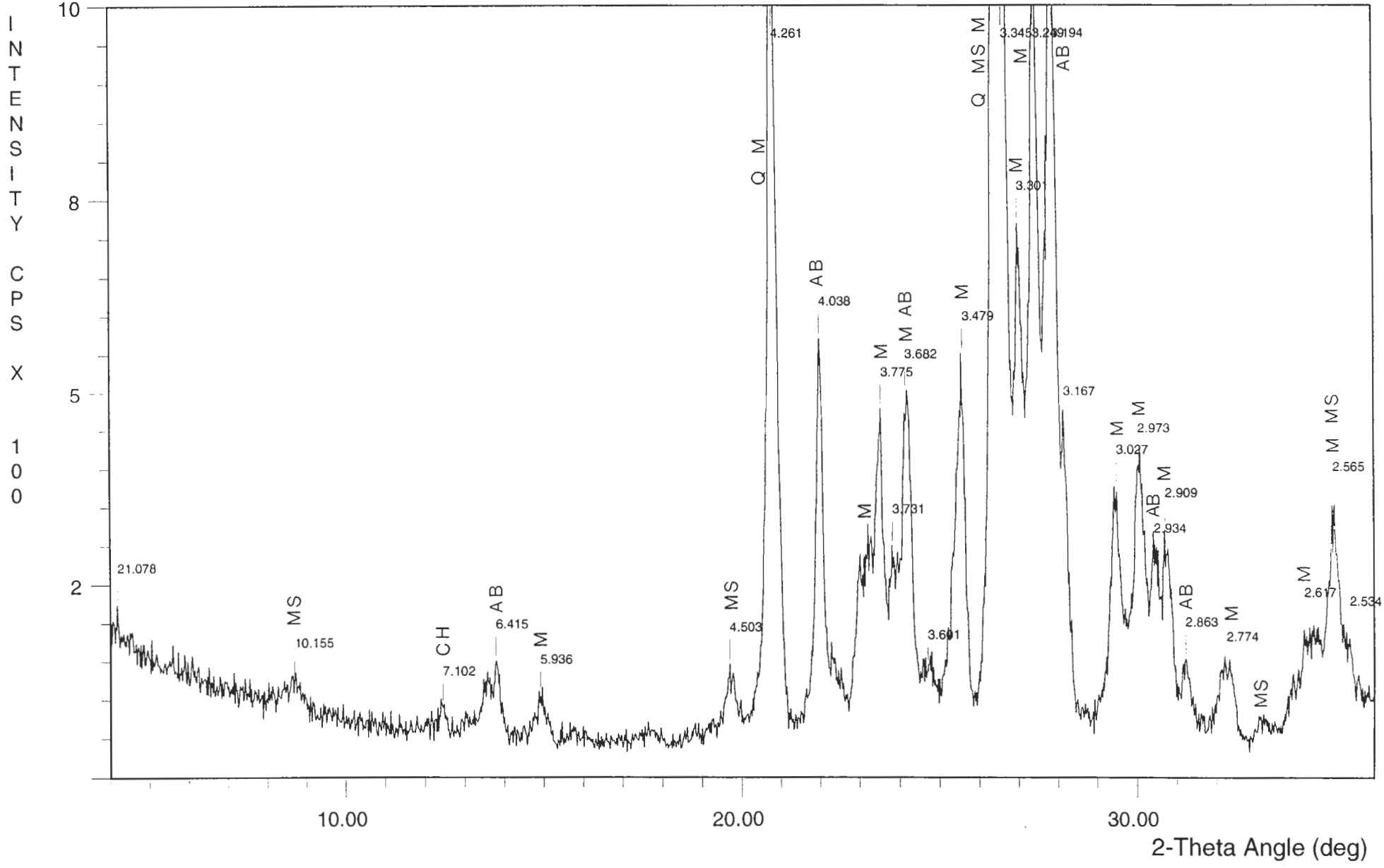
SAMPLE MR141
PD0030 471m Whole rock
INTENSITY CPS X 100
10
8
5
2
21.078
MS
10.155
CH
7.102
AB
6.415
M
5.936
MS
4.503
Q M
4.261
AB
4.038
M
3.775
M AB
3.682
3.731
3.691
M
3.479
Q MS M
3.345
M
3.301
3.249
3.194
AB
3.167
M
3.027
M
2.973
AB
2.934
M
2.909
AB
2.863
M
2.774
MS
M
2.617
M MS
2.565
2.534
10.00
20.00
30.00
2-Theta Angle (deg)

SAMPLE MR144

PD0032 245m Chlorite

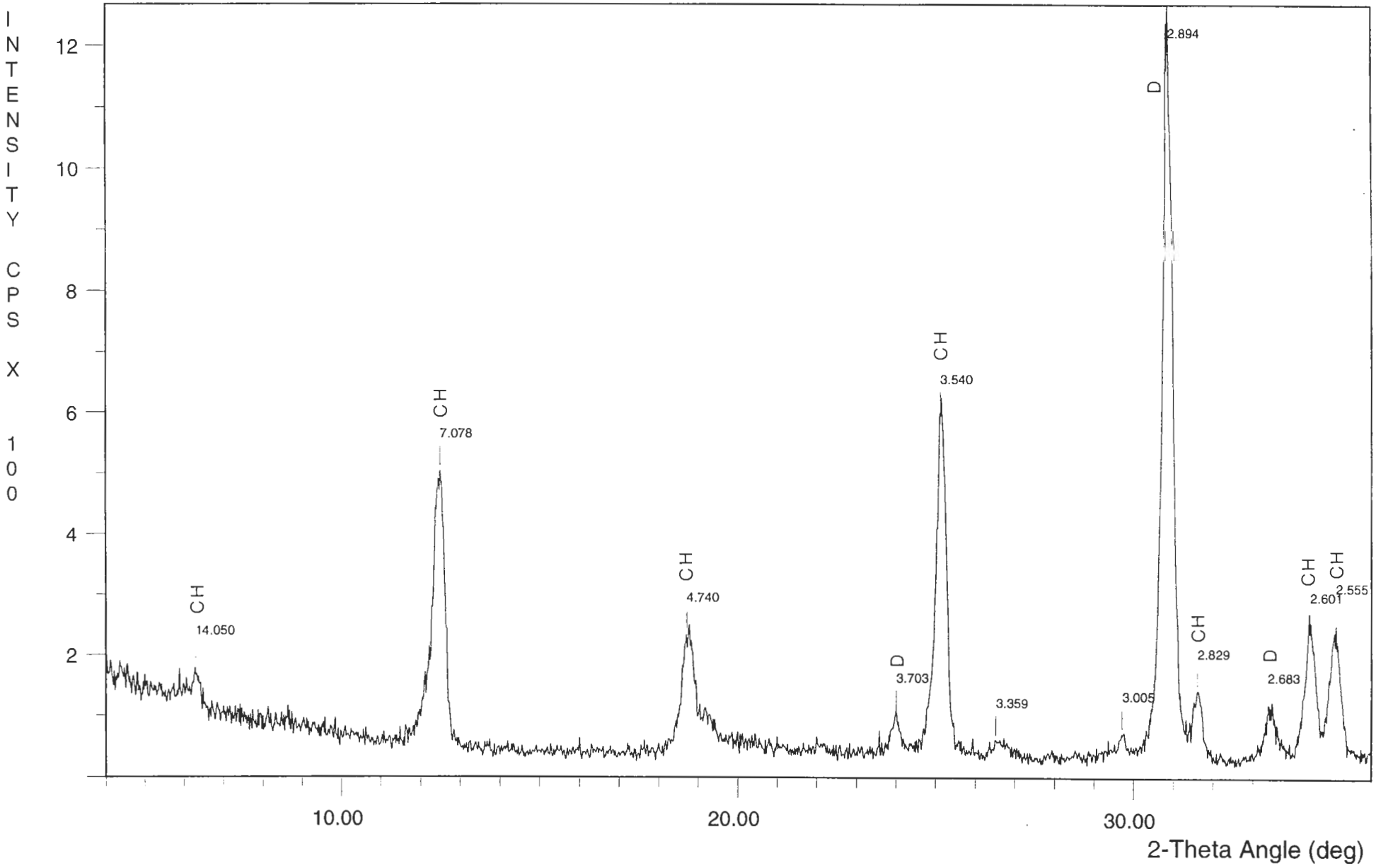

SAMPLE MR145

PD0032 380m : chlorite

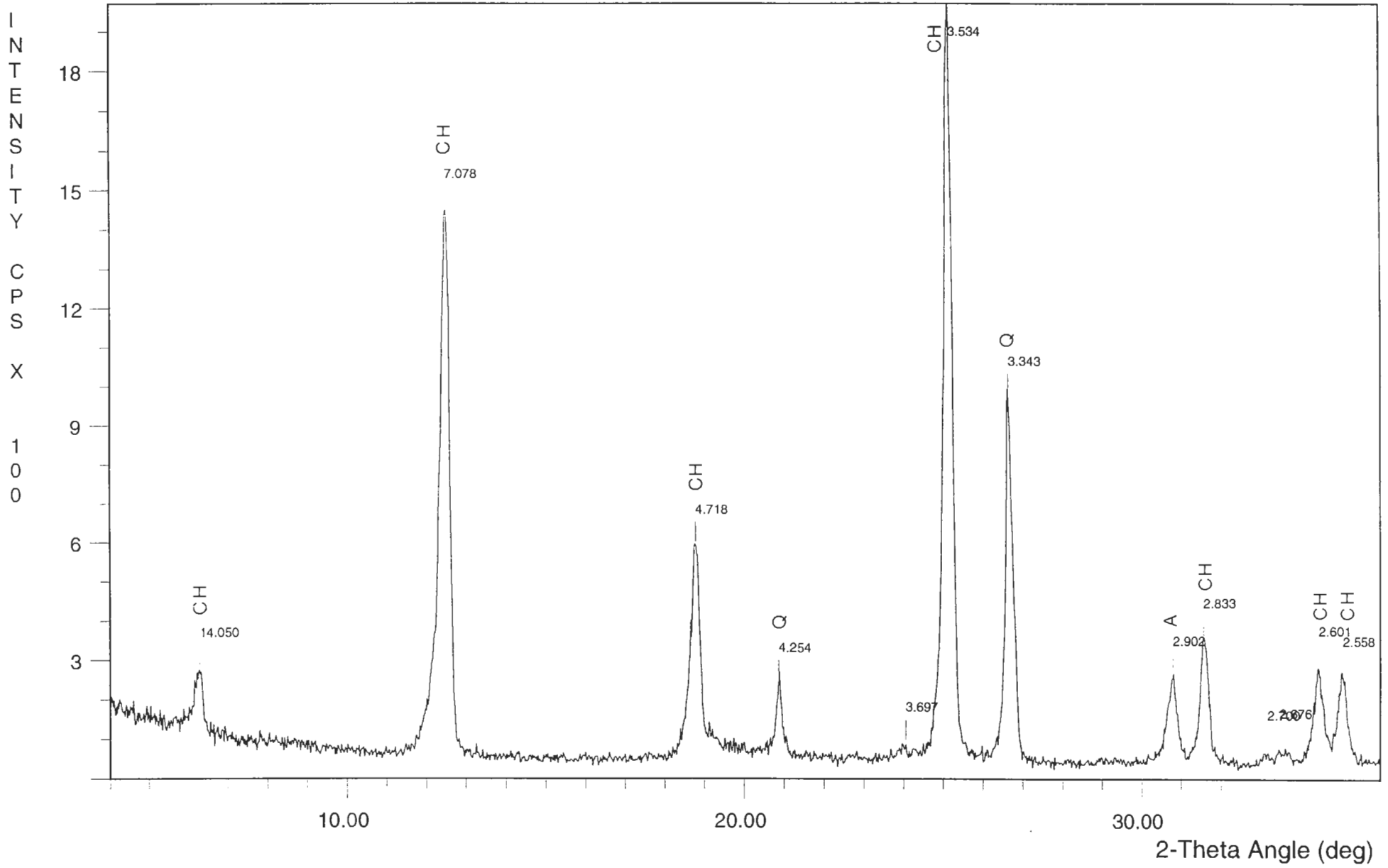

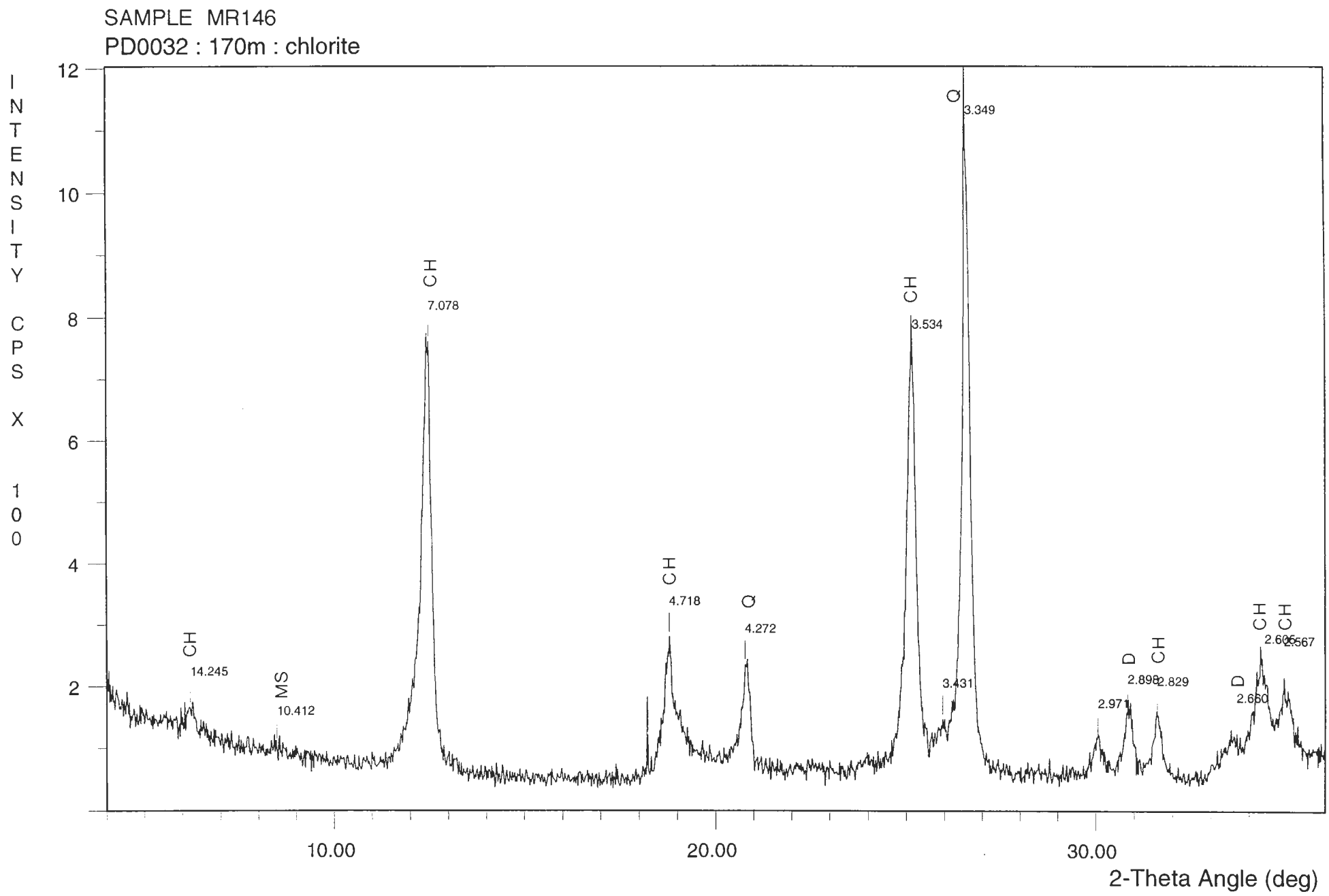
SAMPLE MR146
PD0032 : 170m : chlorite
INTENSITY CPS X 100
12
10
8
6
4
2
CH
14.245
MS
10.412
CH
7.078
CH
4.718
Q
4.272
CH
3.534
Q
3.349
3.431
2.97
D
2.898
CH
2.829
D
2.660
CH
2.606
CH
2.567
10.00
20.00
30.00
2-Theta Angle (deg)

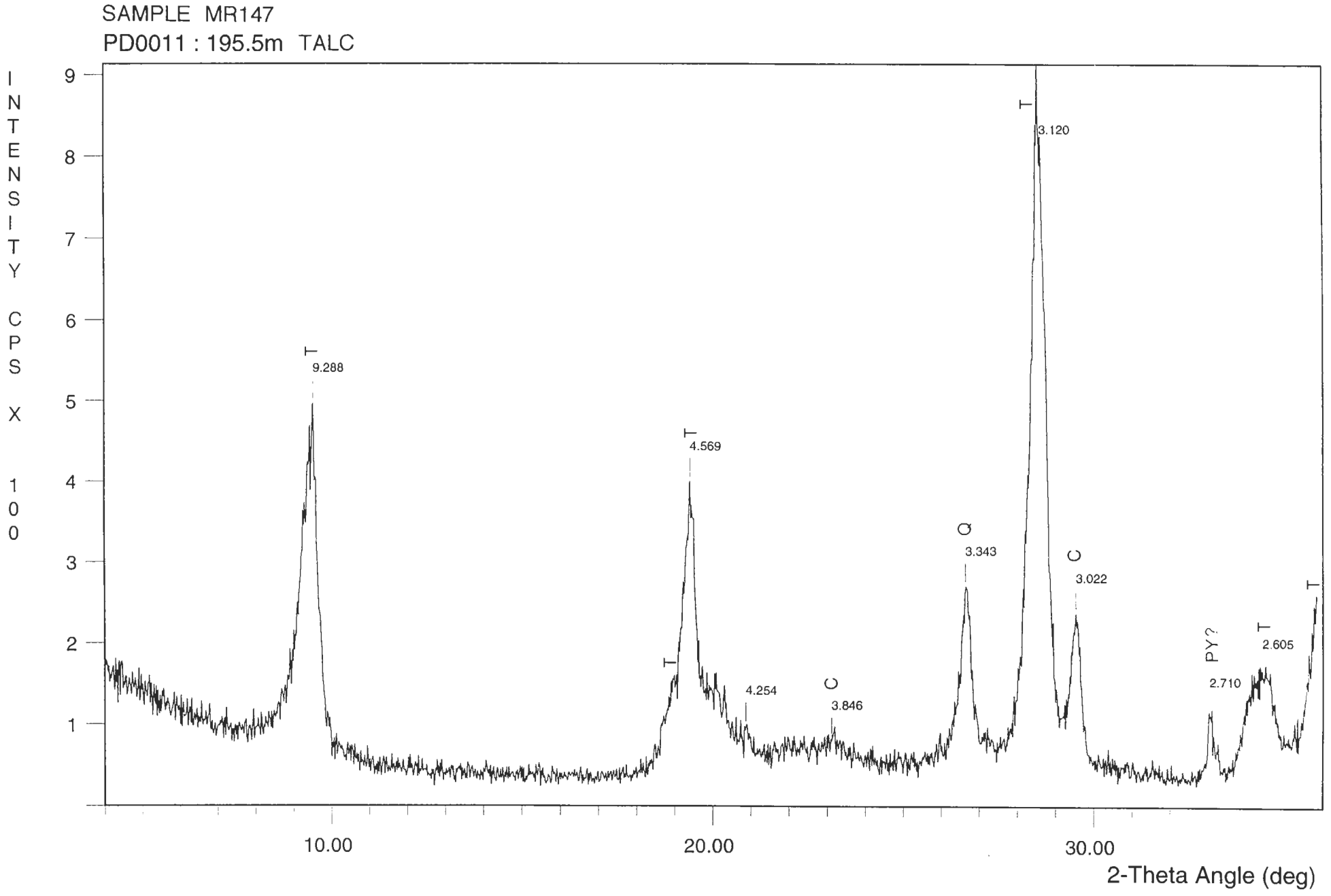
SAMPLE MR147
PD0011 : 195.5m TALC
INTENSITY CPS X 100
9
8
7
6
5
4
3
2
1
T
9.288
T
4.569
T
3.120
Q
3.343
C
3.022
T
2.605
PY?
2.710
T
C
3.846
4.254
10.00
20.00
30.00
2-Theta Angle (deg)

SAMPLE MR148

PD0016 : 273 : sericite

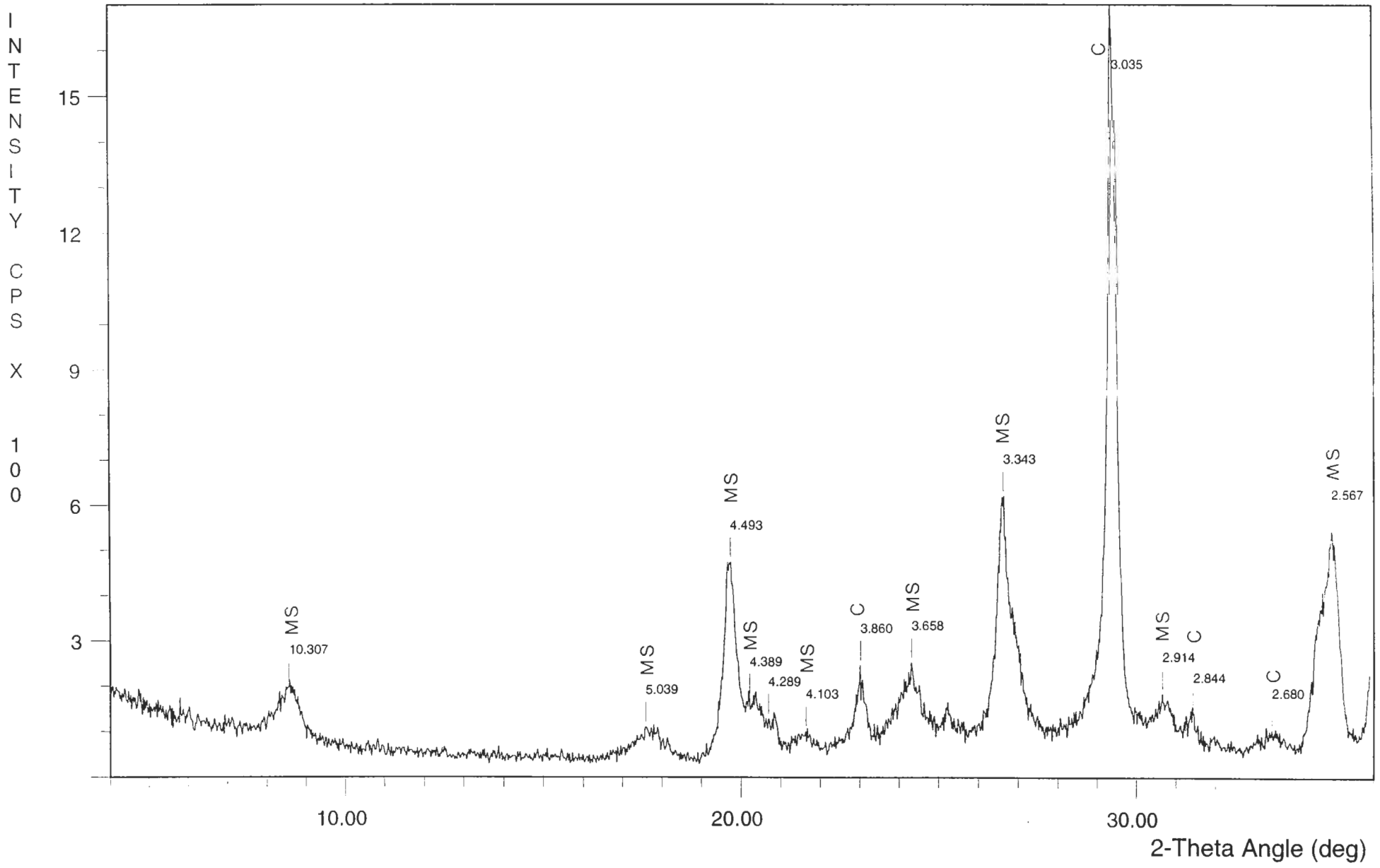

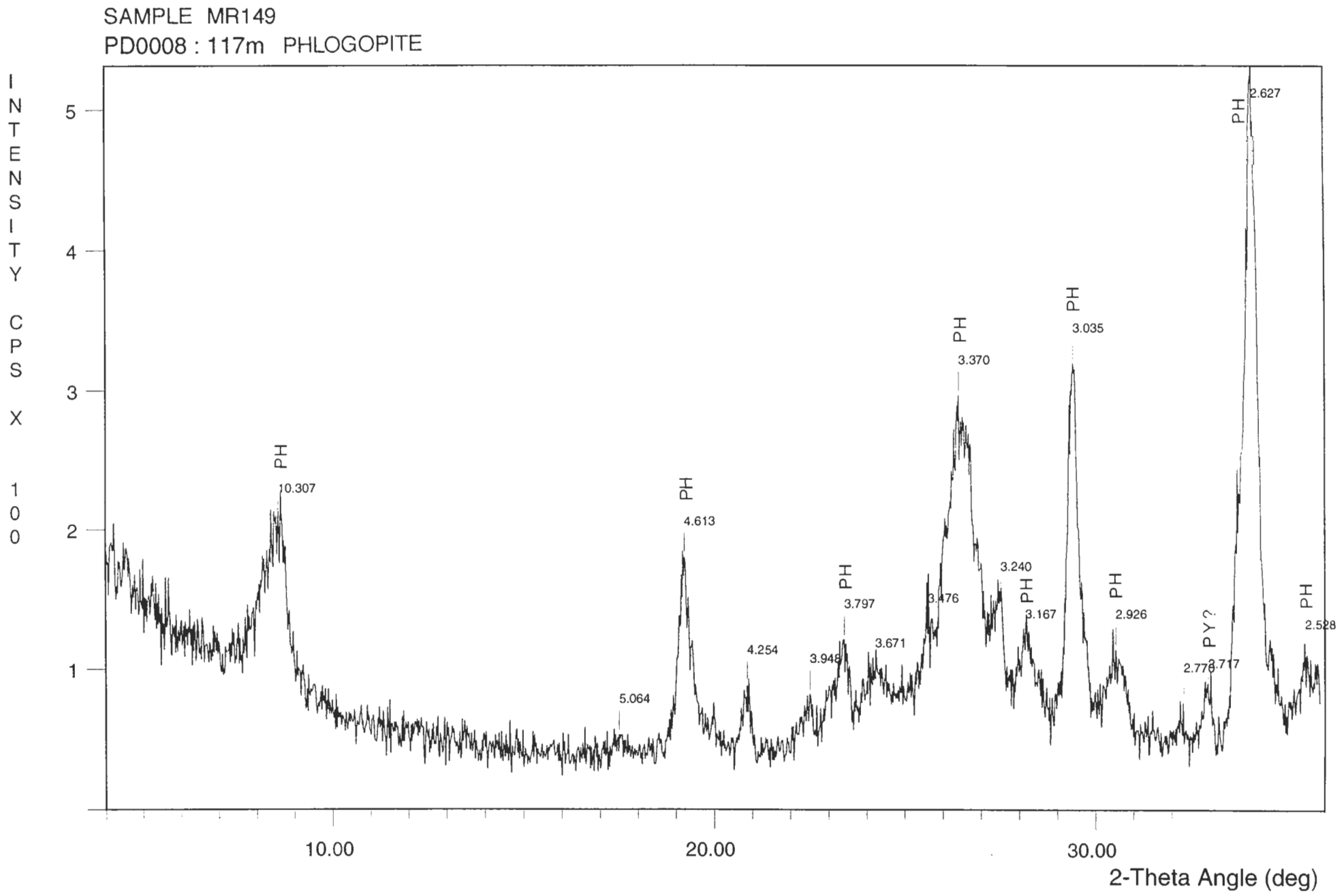
SAMPLE MR149
PD0008 : 117m PHLOGOPITE
INTENSITY CPS X 100
5
4
3
2
1
PH
10.307
PH
4.613
5.064
4.254
PH
3.797
3.948
3.671
3.476
PH
3.370
3.240
PH
3.167
PH
3.035
PH
2.926
PY?
2.778
2.717
PH
2.627
PH
2.528
10.00
20.00
30.00
2-Theta Angle (deg)

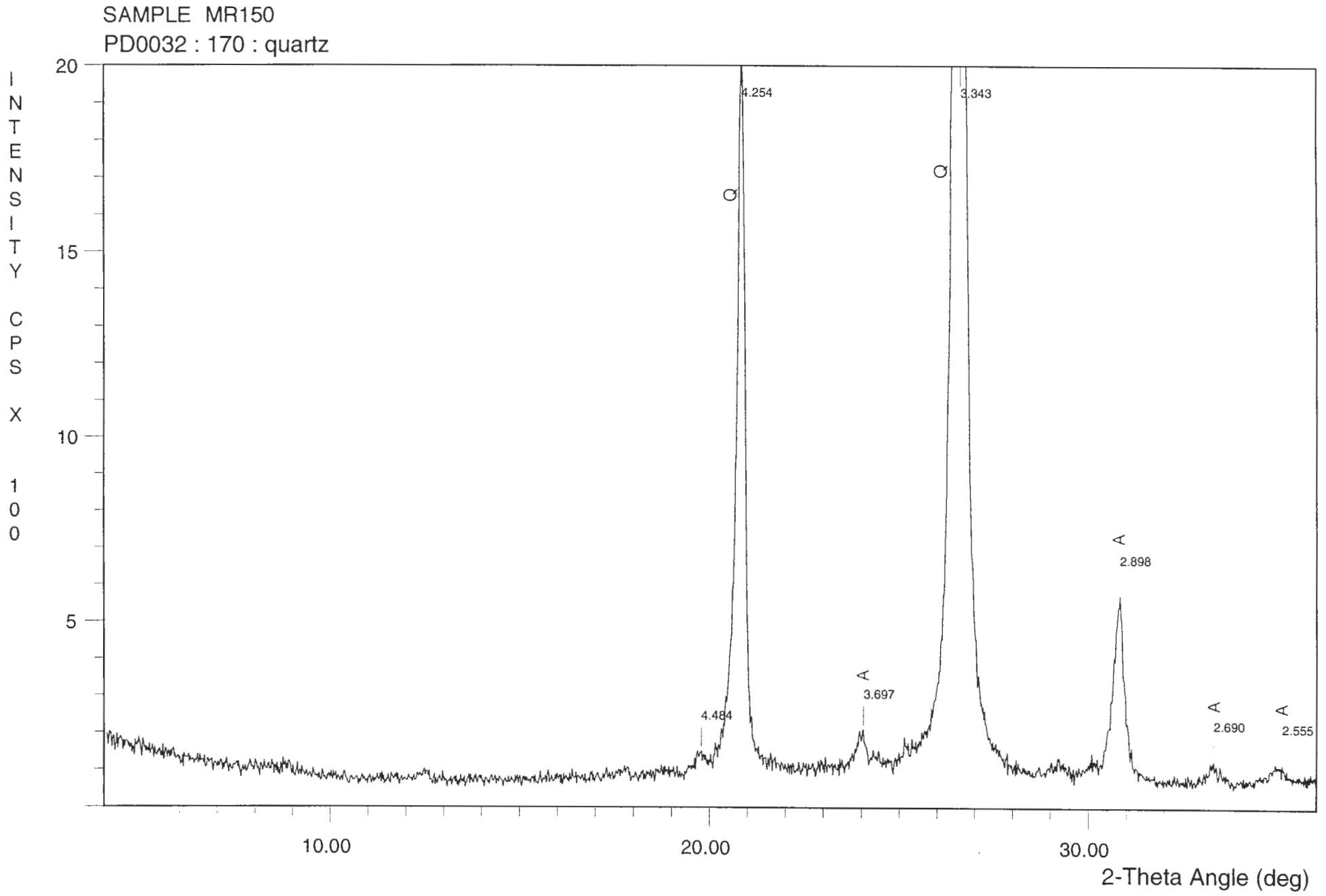
SAMPLE MR150
PD0032 : 170 : quartz
INTENSITY CPS X 100
20
15
10
5
4.254
3.343
Q
Q
A
3.697
4.484
A
2.898
A
2.690
A
2.555
10.00
20.00
30.00
2-Theta Angle (deg)

## Appendix 10.3

Sulphur isotope data

| Zone | Drill Hole | Depth (m) | Northing (m) | Easting (m) | Method | Py1 ∂34S | Py1* ∂34S | Py2 ∂34S | Py2* ∂34S | Py3 ∂34S | Py3* ∂34S | Sp2 ∂34S | Sp2* ∂34S | Gn1 ∂34S | Gn1* ∂34S | Cpy3 ∂34S | Cpy3* ∂34S | Cpy4 ∂34S | Cpy4* ∂34S |
|---|---|---|---|---|---|---|---|---|---|---|---|---|---|---|---|---|---|---|---|
| Northern | PD0006 | 258.20 | 9800.0 | 10769.0 | L | 4.864 | 0.026 | | | | | 0.678 | 0.005 | 1.748 | 0.025 | | | | |
| Central | PD0008 | 115.97 | 9200.0 | 10314.0 | L | 4.316 | 0.009 | | | | | 5.165 | 0.007 | 3.597 | 0.017 | | | | |
| Central | PD0008 | 223.40 | 9200.0 | 10314.0 | L | 5.683 | 0.010 | | | | | | | 4.861 | 0.019 | | | | |
| Central | PD0008 | 223.40 | 9200.0 | 10314.0 | L | | | 4.963 | 0.010 | | | | | | | | | | |
| Central | PD0008 | 236.30 | 9200.0 | 10314.0 | C | 5.500 | | | | | | | | 5.600 | | | | | |
| Central | PD0008 | 241 | 9200.0 | 10314.0 | L | 3.923 | 0.039 | | | | | | | | | | | | |
| Central | PD0008 | 241 | 9200.0 | 10314.0 | L | 4.130 | 0.065 | | | | | | | | | | | | |
| Central | PD0008 | 247.62 | 9200.0 | 10314.0 | L | 3.281 | 0.016 | | | | | | | 4.462 | 0.044 | | | | |
| Central | PD0011 | 146.52 | 9200.0 | 10210.0 | L | 5.629 | 0.034 | | | | | 6.014 | 0.026 | 5.887 | 0.009 | 5.415 | 0.008 | | |
| Central | PD0011A | 369.36 | 9200.0 | 10210.0 | L | 4.339 | 0.005 | | | | | 3.729 | 0.029 | 3.222 | 0.069 | | | | |
| Northern | PD0012 | 353.25 | 9600.0 | 10775.0 | C | 3.400 | | | | | | | | | | | | | |
| Central | PD0015 | 731.12 | 9390.7 | 10226.9 | L | 4.328 | 0.016 | | | | | 3.120 | 0.048 | 2.379 | 0.105 | | | | |
| Northern | PD0016 | 261.76 | 9391.9 | 10663.3 | C | 5.000 | | | | | | 5.100 | | 3.000 | | | | | |
| Northern | PD0016 | 262.57 | 9391.9 | 10663.3 | L | 3.499 | 0.008 | | | | | 3.775 | 0.028 | 3.753 | 0.012 | | | | |
| Northern | PD0016 | 262.90 | 9391.9 | 10663.3 | L | 4.235 | 0.018 | | | | | 4.654 | 0.008 | 4.782 | 0.011 | | | | |
| Northern | PD0016 | 272.43 | 9391.9 | 10663.3 | L | 5.565 | 0.048 | | | | | | | | | | | | |
| Northern | PD0016 | 272.43 | 9391.9 | 10663.3 | L | 6.530 | 0.007 | | | | | | | 7.526 | 0.010 | 8.232 | 0.045 | | |
| Northern | PD0016 | 305.60 | 9391.9 | 10663.3 | L | 5.686 | 0.010 | | | | | 2.699 | 0.020 | 3.453 | 0.025 | | | | |
| Central | PD0017 | 151.15 | 8780.8 | 10136.2 | L | 3.093 | 0.020 | | | | | | | | | | | | |
| Central | PD0017 | 233.95 | 8780.8 | 10136.2 | L | 3.175 | 0.013 | | | | | 5.383 | 0.043 | 4.953 | 0.006 | | | | |
| Central | PD0017 | 396.95 | 8780.8 | 10136.2 | C | 4.800 | | | | | | 3.500 | | 3.000 | | | | | |
| Central | PD0017 | 406.45 | 8780.8 | 10136.2 | L | 6.335 | 0.010 | | | | | 5.398 | 0.029 | | | | | | |
| Central | PD0017 | 406.45 | 8780.8 | 10136.2 | L | | | | | | | 5.980 | 0.037 | 6.759 | 0.083 | | | | |
| Central | PD0019 | 296.42 | 8380.9 | 10408.4 | C | -2.000 | | | | | | | | -0.100 | | | | | |
| Central | PD0019 | 298.20 | 8380.9 | 10408.4 | L | 0.434 | 0.010 | | | | | | | 1.426 | 0.022 | | | | |
| Central | PD0019 | 466.82 | 8380.9 | 10408.4 | C | 4.500 | | | | | | | | 3.600 | | | | | |
| Central | PD0021 | 321.15 | 7564.0 | 10073.7 | C | 5.100 | | | | | | | | -1.600 | | | | | |
| Central | PD0021 | 403.99 | 7564.0 | 10073.7 | C | | | | | | | | | 3.800 | | | | | |
| Central | PD0021 | 451.87 | 7564.0 | 10073.7 | L | 3.441 | 0.029 | | | | | | | | | | | | |
| Central | PD0021 | 451.87 | 7564.0 | 10073.7 | L | 5.037 | 0.023 | | | | | | | | | | | | |
| Central | PD0022 | 240.87 | 8703.7 | 10075.0 | L | 4.391 | 0.123 | | | | | 5.112 | 0.059 | | | | | | |
| Central | PD0022 | 240.87 | 8703.7 | 10075.0 | L | 7.218 | 0.019 | | | | | | | | | | | | |

## Appendix 10.3 cont.

| Zone | Drill Hole | Depth (m) | Northing (m) | Easting (m) | Method | Py1 ∂34S | Py1* ∂34S | Py2 ∂34S | Py2* ∂34S | Py3 ∂34S | Py3* ∂34S | Sp2 ∂34S | Sp2* ∂34S | Gn1 ∂34S | Gn1* ∂34S | Cpy3 ∂34S | Cpy3* ∂34S | Cpy4 ∂34S | Cpy4* ∂34S |
|---|---|---|---|---|---|---|---|---|---|---|---|---|---|---|---|---|---|---|---|
| Central | PD0024 | 236.85 | 8960.9 | 10125.4 | L | 4.509 | 0.028 | | | | | | | | | | | | |
| Central | PD0024 | 241.10 | 8960.9 | 10125.4 | L | 5.614 | 0.010 | | | | | 5.054 | 0.010 | 4.371 | 0.005 | | | | |
| Central | PD0024 | 241.10 | 8960.9 | 10125.4 | L | | | | | | | 4.610 | 0.019 | | | | | | |
| Central | PD0024 | 401.31 | 8960.9 | 10125.4 | L | 6.348 | 0.003 | | | | | 5.067 | 0.021 | 4.104 | 0.012 | | | | |
| Central | PD0025 | 226.10 | 7956.7 | 10051.6 | C | | | | | | | | | -1.200 | | | | | |
| Central | PD0026 | 197.20 | 9060.3 | 10104.3 | L | -0.475 | 0.023 | | | | | 0.857 | 0.045 | 0.233 | 0.011 | | | | |
| Central | PD0028 | 338.08 | 8746.0 | 10461.3 | L | 5.707 | 0.008 | | | | | 4.797 | 0.017 | 4.943 | 0.019 | | | | |
| Central | PD0028 | 345.10 | 8746.0 | 10461.3 | C | 4.200 | | | | | | 4.000 | | 3.000 | | | | | |
| Central | PD0028 | 347.38 | 8746.0 | 10461.3 | L | 5.221 | 0.018 | | | | | 3.363 | 0.006 | 3.027 | 0.010 | | | | |
| Central | PD0028 | 373.20 | 8746.0 | 10461.3 | C | 3.200 | | | | | | 4.200 | | 2.700 | | | | | |
| Central | PD0028 | 508.30 | 8746.0 | 10461.3 | C | 3.500 | | | | | | | | 3.800 | | | | | |
| Central | PD0029 | 184.70 | 8776.6 | 10329.0 | L | 4.128 | 0.013 | | | | | | | | | | | | |
| Central | PD0029 | 258.90 | 8776.6 | 10329.0 | L | 3.761 | 0.003 | | | | | 6.803 | 0.021 | 4.974 | 0.022 | | | | |
| Central | PD0030 | 419.20 | 7764.0 | 10250.0 | C | 2.540 | | | | | | 3.100 | | -2.200 | | | | | |
| Central | PD0030 | 422.10 | 7764.0 | 10250.0 | L | -3.036 | 0.012 | | | | | | | | | | | | |
| Central | PD0030 | 424.00 | 7764.0 | 10250.0 | C | 2.600 | | | | | | | | 2.700 | | 3.600 | | | |
| Central | PD0031 | 178.96 | 8023.0 | 10300.0 | L | 3.307 | 0.009 | | | | | | | | | | | | |
| Central | PD0031 | 178.96 | 8023.0 | 10300.0 | L | 3.325 | 0.011 | | | | | | | | | | | | |
| Central | PD0031 | 178.96 | 8023.0 | 10300.0 | L | 4.884 | 0.013 | | | | | 2.997 | 0.048 | 2.298 | 0.012 | | | | |
| Central | PD0031 | 196.00 | 8023.0 | 10300.0 | L | | | 5.814 | 0.013 | | | | | | | | | | |
| Central | PD0031 | 196.00 | 8023.0 | 10300.0 | L | | | 3.958 | 0.035 | | | | | | | | | | |
| Central | PD0031 | 206.24 | 8023.0 | 10300.0 | L | 5.203 | 0.005 | | | | | 5.083 | 0.033 | 3.443 | 0.008 | | | | |
| Southern | PD0032 | 120.65 | 7406.0 | 10235.0 | L | | | | | 5.597 | 0.012 | | | | | | | | |
| Southern | PD0032 | 223.30 | 7406.0 | 10235.0 | L | 5.738 | 0.018 | | | | | 4.410 | 0.062 | 3.351 | 0.019 | | | | |
| Southern | PD0032 | 223.30 | 7406.0 | 10235.0 | L | 6.069 | 0.008 | | | | | | | | | | | | |
| Southern | PD0032 | 245.58 | 7406.0 | 10235.0 | L | | | | | | | 2.288 | 0.320 | 4.813 | 0.112 | | | | |
| Southern | PD0032 | 245.58 | 7406.0 | 10235.0 | L | | | | | | | 2.891 | 0.320 | | | | | | |
| Southern | PD0032 | 258.08 | 7406.0 | 10235.0 | L | 4.790 | 0.005 | | | | | | | 3.762 | 0.022 | | | | |
| Southern | PD0032 | 380.12 | 7406.0 | 10235.0 | L | | | | | | | 1.870 | 0.063 | | | | | 2.871 | 0.013 |
| Southern | PD0032 | 380.12 | 7406.0 | 10235.0 | L | | | | | 2.984 | 0.007 | | | | | | | 3.996 | 0.012 |
| Southern | PD0032 | 380.12 | 7406.0 | 10235.0 | L | | | | | 3.413 | 0.012 | | | | | | | 4.991 | 0.009 |
| Southern | PD0032 | 380.12 | 7406.0 | 10235.0 | L | | | | | 3.402 | 0.011 | | | | | | | | |
| Southern | PD0032 | 380.12 | 7406.0 | 10235.0 | L | | | | | 6.423 | 0.021 | | | | | | | | |
| Southern | PD0032 | 380.12 | 7406.0 | 10235.0 | L | | | | | 6.524 | 0.012 | | | | | | | | |

## Appendix 10.3 cont.

| Zone | Drill Hole | Depth (m) | Northing (m) | Easting (m) | Method | Py1 ∂34S | Py1* ∂34S | Py2 ∂34S | Py2* ∂34S | Py3 ∂34S | Py3* ∂34S | Sp2 ∂34S | Sp2* ∂34S | Gn1 ∂34S | Gn1* ∂34S | Cpy3 ∂34S | Cpy3* ∂34S | Cpy4 ∂34S | Cpy4* ∂34S |
|---|---|---|---|---|---|---|---|---|---|---|---|---|---|---|---|---|---|---|---|
| Southern | PD0032 | 380.12 | 7406.0 | 10235.0 | L | | | | | 6.536 | 0.034 | | | | | | | | |
| Southern | PD0032 | 392.95 | 7406.0 | 10235.0 | L | | | | | | | 0.679 | 0.151 | | | | | 4.030 | 0.065 |
| Southern | PD0032 | 392.95 | 7406.0 | 10235.0 | L | | | | | | | 4.416 | 0.045 | -2.297 | 0.008 | | | 4.517 | 0.013 |
| Southern | PD0032 | 423.92 | 7406.0 | 10235.0 | L | | | | | 5.131 | 0.012 | 6.302 | 0.022 | 6.195 | 0.057 | | | | |
| ES Py | PD0006 | 410.62 | 9800.0 | 10769.0 | L | 7.376 | 0.008 | | | | | | | | | | | | |
| ES Py | PD0006 | 410.62 | 9800.0 | 10769.0 | L | 7.205 | 0.035 | | | | | | | | | | | | |
| ES Py | PD0006 | 410.62 | 9800.0 | 10769.0 | L | 5.878 | 0.004 | | | | | | | | | | | | |
| ES Py | PD0006 | 410.62 | 9800.0 | 10769.0 | L | 5.432 | 0.010 | | | | | | | | | | | | |
| KM-D3 Py | PD0018 | 435.00 | 8379.7 | 9953.4 | L | 4.787 | 0.016 | | | | | | | | | | | | |
| KM-D3 Py | PD0018 | 435.00 | 8379.7 | 9953.4 | L | 3.824 | 0.018 | | | | | | | | | | | | |
| Metsom Py | PD0013 | 119.18 | 9800.0 | 10300.0 | L | 12.759 | 0.021 | | | | | | | | | | | | |
| Metsom Py | PD0013 | 119.18 | 9800.0 | 10300.0 | L | 10.865 | 0.031 | | | | | | | | | | | | |
| Sleaford Py | | | | | | 6.1 | | | | | | | | | | | | | |
| Sleaford Py | | | | | | 5.9 | | | | | | | | | | | | | |

Zone: ES Py = pyrite from the eastern suite schist.
KM-D3 Py = pyrite from the shear zone separating the eastern and central suites.
Metsom Py = pyrite associated with metasomatism.
Sleaford Py = ∂34S values reported by Bird et al. (1989).

Method: L = laser analysis, C = conventional analysis

* measure of the precision at 2 sigma

**Appendix 11.1.** Parameters used for modelling of the solubility of Pb and Zn that would result from mixing of a fluid at 140°C, 27 wt.% NaCl equiv. with a fluid of 180°C and 0 wt.% equiv. Equilibrium constants were calculated using SUPCRT'92 (Johnson et al., 1992). Activity coefficients were calculated using the extended Debye-Huckel equation and 'A' and 'B' values from Helgeson (1969). Na, K, Ca, and Cl were determined from from fluid inclusions. $\Sigma S$, $\Sigma C$ and $fO2$ values are explained in the text (Chapter 11).

| **Temp °C** | **140** | **145** | **150** | **155** | **160** | **165** | **170** | **175** | **180** | **150*** |
|---|---|---|---|---|---|---|---|---|---|---|
| salinity (wt% NaCl equiv.) | 27.00 | 23.63 | 20.25 | 16.88 | 13.50 | 10.13 | 6.75 | 3.38 | 0.00 | 25.00 |
| Na (ppm) | 83361 | 72941 | 62520 | 52100 | 41680 | 31260 | 20840 | 10420 | 0 | 77186 |
| K (ppm) | 5835 | 5106 | 4376 | 3647 | 2917 | 2188 | 1459 | 729 | 0 | 5403 |
| Ca (ppm) | 22570 | 19749 | 16927 | 14106 | 11285 | 8464 | 5642 | 2821 | 0 | 20898 |
| Cl (ppm) | 173772 | 152050 | 130329 | 108607 | 86886 | 65164 | 43443 | 21721 | 0 | 160900 |
| $\Sigma S$ (molality) | 0.00222 | 0.00185 | 0.00151 | 0.00121 | 0.00092 | 0.00067 | 0.00043 | 0.00021 | 0 | 0.00200 |
| $\Sigma C$ (molality) | 0.01112 | 0.00927 | 0.00758 | 0.00604 | 0.00463 | 0.00334 | 0.00214 | 0.00103 | 0 | 0.01000 |
| log $fO_2$ | -47.380 | -46.683 | -46.000 | -45.332 | -44.677 | -44.036 | -43.407 | -42.790 | -42.185 | -46.000 |
| A parameter for Debye-Huckel equation | 0.670 | 0.680 | 0.6898 | 0.700 | 0.711 | 0.722 | 0.734 | 0.745 | 0.758 | 0.6898 |
| B parameter for Debye-Huckel equation | 0.351 | 0.352 | 0.3533 | 0.355 | 0.356 | 0.357 | 0.358 | 0.359 | 0.361 | 0.3533 |
| | | | | | | | | | | |
| Log K value of the reaction.... | | | | | | | | | | |
| $C + 2H_2O \leftrightarrow CH_{4(aq)} + O_{2(g)}$ | 53.21 | 52.46 | 51.73 | 51.02 | 50.32 | 49.64 | 48.97 | 48.31 | 47.67 | 51.73 |
| $C + O_{2(g)} + H_2O \leftrightarrow HCO_3^- + H^+$ | -41.21 | -40.58 | -39.95 | -39.34 | -38.74 | -38.16 | -37.58 | -37.02 | -36.47 | -39.95 |
| $C + O_{2(g)} + H_2O \leftrightarrow H_2CO_{3(aq)}$ | -47.86 | -47.26 | -46.68 | -46.11 | -45.55 | -45.01 | -44.48 | -43.97 | -43.46 | -46.68 |
| $CaMg(CO_3)_2 + 4H^+ \leftrightarrow Ca^{+2} + Mg^{+2} + 2H_2O + 2C_{(s)} + 2O_{2(g)}$ | -83.49 | -82.36 | -81.25 | -80.17 | -79.12 | -78.09 | -77.09 | -76.10 | -75.14 | -81.25 |
| $CaMg(CO_3)_2 + 4H^+ \leftrightarrow Ca^{+2} + Mg^{+2} + 2H_2CO_{3(aq)}$ | 12.22 | 12.16 | 12.10 | 12.04 | 11.98 | 11.93 | 11.88 | 11.83 | 11.79 | 12.10 |
| $CaMg(CO_3)_2 + 4H^+ + 2H_2O \leftrightarrow Ca^{+2} + Mg^{+2} + 4O_{2(g)} + 2CH_{4(aq)}$ | -189.91 | -187.29 | -184.72 | -182.21 | -179.76 | -177.36 | -175.02 | -172.73 | -170.49 | -184.72 |
| $CH_{4(aq)} + 2O_{2(g)} \leftrightarrow HCO_3^- + H^+ + H_2O$ | 94.43 | 93.04 | 91.68 | 90.36 | 89.06 | 87.80 | 86.55 | 85.34 | 84.15 | 91.68 |
| $CH_{4(aq)} + 2O_2 \leftrightarrow CO_3^{-2} + H_2O + H^+$ | 84.26 | 82.86 | 81.48 | 80.14 | 78.82 | 77.53 | 76.26 | 75.02 | 73.80 | 81.48 |
| $CH_{4(aq)} + 2O_{2(g)} \leftrightarrow H_2CO_{3(aq)} + H_2O$ | 101.07 | 99.72 | 98.41 | 97.13 | 95.87 | 94.65 | 93.45 | 92.28 | 91.14 | 98.41 |
| $CO_3^{-2} + H^+ \leftrightarrow HCO_3^-$ | 10.16 | 10.18 | 10.20 | 10.22 | 10.24 | 10.27 | 10.29 | 10.32 | 10.34 | 10.20 |
| $3Fe_2O_3 \leftrightarrow 2Fe_3O_4 + 0.5O_{2(g)}$ | -24.18 | -23.81 | -23.45 | -23.09 | -22.75 | -22.41 | -22.08 | -21.76 | -21.44 | -23.45 |
| $Fe_2O_3 + 4SO_4^{-2} + 8H^+ \leftrightarrow 2FeS_2 + 4H_2O + 7.5O_{2(g)}$ | -281.11 | -276.35 | -271.69 | -267.13 | -262.66 | -258.28 | -253.98 | -249.77 | -245.64 | -271.69 |
| $Fe_2O_3 + 4HSO_4^- + 4H^+ \leftrightarrow 2FeS_2 + 4H_2O + 7.5O_{2(g)}$ | -295.42 | -290.95 | -286.58 | -282.31 | -278.14 | -274.05 | -270.05 | -266.14 | -262.31 | -286.58 |
| $Fe_3O_4 + 6SO_4^{-2} + 12H^+ \leftrightarrow 3FeS_2 + 6H_2O + 11O_{2(g)}$ | -409.57 | -402.62 | -395.81 | -389.14 | -382.61 | -376.21 | -369.93 | -363.78 | -357.74 | -395.81 |

**Appendix 11.1 cont.**

| Temp °C | 140 | 145 | 150 | 155 | 160 | 165 | 170 | 175 | 180 | 150* |
|---|---|---|---|---|---|---|---|---|---|---|
| $Fe_3O_4 + 6HS^- + 6H^+ + O_{2(g)} \leftrightarrow 3FeS_2 + 6H_2O$ | -121.16 | -119.80 | -118.48 | -117.20 | -115.95 | -114.75 | -113.58 | -112.44 | -111.34 | -118.48 |
| $Fe_3O_4 + 6H_2S_{(aq)} + O_{2(g)} \leftrightarrow 3FeS_2 + 6H_2O$ | -82.29 | -80.88 | -79.50 | -78.15 | -76.82 | -75.53 | -74.26 | -73.02 | -71.80 | -79.50 |
| $Fe_3O_4 + 3HS^- + 3H^+ \leftrightarrow 3FeS + 3H_2O + 0.5O_2$ | -7.73 | -7.85 | -7.96 | -8.08 | -8.20 | -8.33 | -8.45 | -8.58 | -8.71 | -7.96 |
| $Fe_3O_4 + 3H_2S_{(aq)} \leftrightarrow 3FeS + 3H_2O + 0.5O_{2(g)}$ | -11.70 | -11.61 | -11.52 | -11.44 | -11.36 | -11.28 | -11.21 | -11.14 | -11.07 | -11.52 |
| $FeS_2 + H_2O \leftrightarrow FeS + H^+ + HS^- + 0.5O_{2(g)}$ | -37.81 | -37.32 | -36.84 | -36.37 | -35.92 | -35.47 | -35.04 | -34.62 | -34.21 | -36.84 |
| $FeS_2 + H_2O \leftrightarrow FeS + H_2S_{(aq)} + 0.5O_{2(g)}$ | -31.33 | -30.83 | -30.34 | -29.86 | -29.40 | -28.94 | -28.49 | -28.05 | -27.62 | -30.34 |
| $H_2CO_{3(aq)} \leftrightarrow H^+ + HCO_3^-$ | -6.64 | -6.68 | -6.72 | -6.77 | -6.81 | -6.85 | -6.90 | -6.95 | -6.99 | -6.72 |
| $H_2S_{(aq)} + 2O_{2(g)} \leftrightarrow 2H^+ + SO_4^{-2}$ | 81.98 | 80.58 | 79.22 | 77.88 | 76.57 | 75.29 | 74.03 | 72.80 | 71.59 | 79.22 |
| $H_2S_{(aq)} + 2O_{2(g)} \leftrightarrow H^+ + HSO_4^-$ | 85.56 | 84.23 | 82.94 | 81.68 | 80.44 | 79.23 | 78.05 | 76.89 | 75.76 | 82.94 |
| $H_2S_{(aq)} \leftrightarrow H^+ + HS^-$ | -6.48 | -6.49 | -6.50 | -6.51 | -6.52 | -6.54 | -6.55 | -6.57 | -6.59 | -6.50 |
| $HS^- + 2O_{2(g)} \leftrightarrow H^+ + SO_4^{-2}$ | 88.46 | 87.07 | 85.72 | 84.39 | 83.09 | 81.83 | 80.59 | 79.37 | 78.18 | 85.72 |
| $HSO_4^- \leftrightarrow H^+ + SO_4^{-2}$ | -3.58 | -3.65 | -3.72 | -3.80 | -3.87 | -3.94 | -4.02 | -4.09 | -4.17 | -3.72 |
| $PbS + 2H^+ + 2Cl^- \leftrightarrow PbCl_2 + H_2S_{(aq)}$ | 1.64 | 1.47 | 1.31 | 1.14 | 0.98 | 0.81 | 0.65 | 0.48 | 0.32 | 1.31 |
| $PbS + 2H^+ + 3Cl^- \leftrightarrow PbCl_3^- + H_2S_{(aq)}$ | 1.82 | 1.64 | 1.46 | 1.29 | 1.11 | 0.93 | 0.76 | 0.58 | 0.40 | 1.46 |
| $PbS + 2H^+ + 4Cl^- \leftrightarrow PbCl_4^{-2} + H_2S_{(aq)}$ | 2.33 | 2.15 | 1.97 | 1.78 | 1.60 | 1.42 | 1.23 | 1.05 | 0.86 | 1.97 |
| $PbS + 2H^+ + Cl^- \leftrightarrow PbCl^+ + H_2S_{(aq)}$ | 2.64 | 2.50 | 2.35 | 2.21 | 2.07 | 1.94 | 1.80 | 1.66 | 1.53 | 2.35 |
| $PbS + 2H^+ \leftrightarrow Pb^{+2} + H_2S_{(aq)}$ | 4.74 | 4.64 | 4.54 | 4.44 | 4.34 | 4.25 | 4.16 | 4.07 | 3.98 | 4.54 |
| $ZnS + 2H^+ + 2Cl^- \leftrightarrow ZnCl_2 + H_2S_{(aq)}$ | 0.82 | 0.67 | 0.51 | 0.36 | 0.20 | 0.05 | -0.11 | -0.26 | -0.42 | 0.51 |
| $ZnS + 2H^+ + 3Cl^- \leftrightarrow ZnCl_3^- + H_2S_{(aq)}$ | 1.73 | 1.59 | 1.44 | 1.30 | 1.15 | 1.01 | 0.86 | 0.71 | 0.56 | 1.44 |
| $ZnS + 2H^+ + 4Cl^- \leftrightarrow ZnCl_4^{-2} + H_2S_{(aq)}$ | 0.99 | 0.85 | 0.70 | 0.55 | 0.39 | 0.24 | 0.08 | -0.08 | -0.23 | 0.70 |
| $ZnS + 2H^+ + Cl^- \leftrightarrow ZnCl^+ + H_2S_{(aq)}$ | 0.73 | 0.59 | 0.45 | 0.31 | 0.17 | 0.03 | -0.10 | -0.24 | -0.38 | 0.45 |
| $ZnS + 2H^+ \leftrightarrow Zn^{+2} + H_2S_{(aq)}$ | 3.60 | 3.57 | 3.53 | 3.50 | 3.47 | 3.44 | 3.41 | 3.37 | 3.34 | 3.53 |
| $2KAl_2AlSi_3O_{10}(OH)_2 + 2H^+_{(aq)} + 3H_2O \leftrightarrow 3Al_2Si_2O_5(OH)_4 + 2K^+_{(aq)}$ | 4.98 | 4.92 | 4.85 | 4.79 | 4.73 | 4.67 | 4.61 | 4.55 | 4.50 | 4.85 |
| $3KAlSi_3O_8 + 2H^+ \leftrightarrow KAl_2AlSi_3O_{10}(OH)_2 + 6SiO_2 + 2K^+$ | 8.39 | 8.35 | 8.31 | 8.28 | 8.24 | 8.21 | 8.18 | 8.14 | 8.11 | 8.31 |

* Used for construction of Figure 11.1